

Conference of Indian Aerosol Science and Technology Association 2018

“Aerosol Impacts: Human Health to Climate Change”

26-28 November 2018
IIT Delhi
New Delhi, India

Organized by:
Centre for Atmospheric Sciences
Indian Institute of Technology Delhi

SPONSORING AGENCIES



सत्यमेव जयते

Government of India
Department of Science & Technology
Ministry of Science & Technology



सत्यमेव जयते

Ministry of Environment,
Forest and Climate Change

Government of India



सत्यमेव जयते

MINISTRY OF EARTH SCIENCES



UNDERSTANDING,
ACCELERATED

TSI Instruments India Private Ltd.

Tel: 080 - 67877200 Web : www.tsi.com

3rd Floor , #447, Sri Sai Heights

17th Cross, 17th Main, Sector - 4

HSR Layout, Bangalore 560102

Email id: rama.ramisetty@tsi.com

TSI – GLOBAL LEADER IN PARTICLE MEASUREMENT TECHNOLOGY

50+ years of experience, continuous designing and developing novel instruments in aerosol science and technology in close association with aerosol research community.

INTRODUCING QUARTZ CRYSTAL MICROBALANCE MICROORIFICE UNIFORM DEPOSITION IMPACTOR (QCM-MOUDI)

Mass in real-time, True-mass detection,
PM2.5 in 6 stages, 45 nm -6 μ m aerodynamic diameter



Real Time Particle Mass, Number and Size measurement Instruments and Solutions

- + Atmospheric Aerosol (Ultrafine to super-micron) monitoring
- + Indoor and Outdoor Airquality monitoring
- + Engine Exhaust Particle characterization
- + Filter Testing
- + Aerosol Generators



UNDERSTANDING,
ACCELERATED

TSI Instruments India Private Ltd.
3rd Floor, #447, Sri Sai Heights
17th Cross, 17th Main, Sector - 4
HSR Layout, Bangalore 560102

Tel: 080 - 67877200
Web : www.tsi.com
Email id: rama.ramisetty@tsi.com

GRIMM  **AEROSOL
TECHNIK**

 *AlfaTech Services*



[AlfaTech Services](#)

[the environment people](#)

3rd Floor Mohit House, D-3
Shopping Centre II, Mansarovar
Garden,
New Delhi – 110015

Tel: +91 11 2544 6275 / 2544 6276
Mob: +91 98101 46294 / +91 98103 98050
Fax: +91 11 2544 6277

E-mail: alfatech@alfatechservices.com

Website: www.alfatechservices.com

www.grimm-aerosol.com

GRIMM Aerosol Technik Ainring GmbH & Co. KG
Dorfstrasse 9, 83404 Ainring, Germany



PORTABLE AEROSOL SPECTROMETER 'DUST DECODER' 11-D *(New)*

- TSP, PM₁₀, PM₄, PM_{2.5}, PM₁ & PM_{coarse}
- Inhalable, Thoracic & Respirable
- Particle Size Range: 0.25 to 35 microns
- 31 equidistant size channels
- Up to 3 million particle/litre
- Up to 1,00,000 micrograms/m³
- > 97% reproducibility
- light scattering at single particles with diode laser
- Time resolution: 6 sec for 31 channels and 1 sec for 16 channels
- 8 – 10 hours battery operation
- Automated altitude correction of flow rate up to 5000 meter altitude



TRANSPORTABLE AIR QUALITY MONITORING STATION EDM 164

- Real-Time Monitoring Of PM Values (PM₁₀, PM_{2.5}, PM₁) and Particle Number
- Additional Information On Particle Size And Mass Distribution
- 11 Size Channels < 1 μm For Precise Submicron Detection
- Compact And Mobile Weather Housing
- Short And Long-Term Continuous Monitoring Of Dust Pollution
- Upgrade for Meteorological sensors
- Versatile Data Acquisition & Communication (Data Logger With GSM Via Internet)



MINI WIDE RANGE AEROSOL SPECTROMETER MiniWRAS 1371

- 10 nm – 35 μm (10 – 193 nm Electrical, 0.253 – 35 μm Optical)
- 41 Size Channels (10 Electrical and 31 Optical)
- Dust Fractions Acc. To En 481 (Inhalable, Thoracic, Respirable)
- PM-10, PM-2.5, PM-1
- Li-Ion Battery, 14.4 VDC, 4.8 AH For 8 Hr Operation
- Total Weight: 7.6 kg (16.8 lbs)



SCANNING MOBILITY PARTICLE SIZER WITH CONDENSATION PARTICLE COUNTER

- Particle Size Distribution from 5 – 1094 Nm
- Anti-Spill CPC Saturator Design
- Neutralizers: Am-241, aDBD, Soft X-Ray, Ni-63
- Reproducibility: > 95% For Single Count Mode
and > 90% For Photometric Mode
- Size Range: 5 – 350 Nm (M - DMA); 10 - 1094 Nm (L - DMA)
- Size Resolution: Stepping Mode: 45 - 255 Channels
Scanning Mode: 64 Channels Per Decade;
Logarithmic Spacing



WIDE RANGE AEROSOL SPECTROMETER EDM 665

(Outdoor continuous 24/7 operation)

- combines two technologies for particle counting and classifying in one
 - (a) the Scanning Mobility Particle Sizer (SMPS+C) with the butanol condensation particle counter for nanoparticles and
 - (b) the approved EDM 180 for the larger fraction.
- Designed and specifically built for atmospheric monitoring.
- Particle size range from 5 nm to 32 µm in 71 particle size channels.
- Fully automatic 24/7 monitoring system.
- Sampling with isothermal drying system (nafion).
- Versatile data acquisition and communication (data logger with GSM via internet).
- Meteorological sensors for wind speed and direction, precipitation, pressure, temperature and relative humidity.
- Data reproducibility > 95% (SMPS) and >97% (EDM).
- Interfaces: data logger, USB, GSM with SIM card for mobile network.



THE STANDARD FOR ALL-WEATHER ENVIRONMENTAL MONITORING #199

Stand-Alone Air-Conditioned Environmental Weather Protection Housing For 19" Rack Instruments.

- The 199 is suitable for all weather conditions from Tropical heat to arctic cold.
- Operating temperatures: -20°C to +60°C
- Weight: 125 kgs. Including air-conditioner



AlfaTech Services

the environment people

3rd Floor Mohit House, D-3 Shopping Centre II,
Mansarovar Garden, New Delhi – 110015

Tel: +91 11 2544 6275 / 2544 6276 Mob: +91 98101 46294 / +91 98103 98050

Fax: +91 11 2544 6277

E-mail: alfatech@alfatechservices.com Website: www.alfatechservices.com

OTHER EXHIBITORS



MARS Bioanalytical Pvt Ltd
201-203 Atlantic Plaza,
DDA LSC, Mayur Vihar Ph-1Ex
Delhi-110091



501, Zenith Complex, 28/2,
Near Agriculture College,
Shivaji Nagar, Pune,
Maharashtra 411005



Metrohm India Limited
Origin Sri Towers, 3&4, Fourrts Avenue
Annai Indira Nagar, Thoraipakkam
Chennai - 600097



Tesscorn AeroFluid Inc.
1285, 5th Main, 17th Cross ,
HSR Sector 7,
Bangalore 560102



GG-1, 139- C,
PVR Road, Vikaspuri,
New Delhi - 110018.

Contents

Sl No	Abstract No	Title	Author	Page No
1	A1	Performance evaluation of beta attenuation monitor under Indian ambient conditions	Shukla & Aggarwal	1
2	A2	Certified reference material for particulate matter	Agarwal <i>et al</i>	4
3	A3	A new approach for highly-efficient, concentrated sampling of aerosol particles from 10 nm to 10 μ m: bioaerosol applications	Savage <i>et al</i>	7
4	A4	Outdoor and indoor sources of 1.1 – 4.0 nm particles	Vakeva <i>et al</i>	11
5	A5	Improving airborne nanoparticle and cluster detection with the butanol based laminar flow condensation nuclei counters grimm 5.403 and 5.412.	Steiner <i>et al</i>	15
6	A6	Smart air quality network, the measurement network for the future	Ziegler <i>et al</i>	18
7	A7	Summer-time aerosol pollution over two contrasting environments	Devara <i>et al</i>	23
8	A8	Dust morphology over Panchgaon, Haryana	Devara <i>et al</i>	26
9	A9	First results of aerosol characterization using a polar nephelometer at Auh, Gurgaon	Devara <i>et al</i>	29
10	A10	Influence of blue moon phenomenon on the temporal variation of atmospheric pollutants in an NCR outskirts locality; a gis approach	Yadav <i>et al</i>	32
11	A11	Spatial and temporal variation of Particulate matter and gaseous pollutants In Delhi for 2018 year	Tiwari <i>et al</i>	34
12	A12	Gradients in PM _{2.5} and its relation with modis aod over Indian mega cities	Mahesh <i>et al</i>	37
13	A13	Studies on carbonaceous aerosols from a high altitude site in the central Himalayas	Srivastava <i>et al</i>	38
14	A14	Fossil fuel VS wood burning black carbon components in Southern Delhi outskirts	Dumka <i>et al</i>	42
15	A15	Aerosol and pollutant assessment wintertime in Delhi : The WIFEX Campaign	Dumka <i>et al</i>	44
16	A16	Impact of urban terrain on simulation of air-pollutants	Nishi Srivastava	46
17	A17	Evaluation of aerosol optical thickness and its impact over coal mining region using ground-based sunphotometer observations	Kumar <i>et al</i>	50
18	A18	Preliminary investigation of PM ₁ variation at Bengaluru, Karnataka state	Manjunatha <i>et al</i>	55
19	A19	Comparison of aerosol angstrom exponent with AOTat 555 nm for a South Indian city Bengaluru, Karnataka using satellite data	Ganesh <i>et al</i>	60
20	A20	Chemical characterization of atmospheric aerosols over Varanasi	Pratap <i>et al</i>	65
21	A21	Impacts of severe dust storms on aerosol characteristics over Kanpur	Kumar <i>et al</i>	68
22	A23	Variability of PM _{2.5} and PM ₁₀ and the optical properties of aerosols over Varanasi	Kumar <i>et al</i>	72
23	A24	Concentration of indoor radon, thoron and their daughter products in and around Kolar gold fields, Kolar district, Karnataka, India	Reddy <i>et al</i>	76

24	A25	Dependence of aerosol removal on initial concentration using two group model	Anand <i>et al</i>	81
25	A26	Study of ultrafine particle exposure using multi-compartment model	Krishan <i>et al</i>	85
26	A27	Study of deposition of radon progeny aerosols at different air velocities	Mishra <i>et al</i>	89
27	A28	Identification and quantification of microplastics associated with inhalable aerosol fraction (PM ₁₀)	Tiwari <i>et al</i>	93
28	A29	Photo-degradation behaviour of brown carbon generated from biomass combustion under UV light exposure	Rathod <i>et al</i>	97
29	A30	Radiative forcing estimation of aerosols at four locations in India and Pakistan using ground-based remote sensing measurements	Soni <i>et al</i>	101
30	A31	Efficency of rainfall in scavenging differnt types of aerosols over eastern Himalayan	Dutta <i>et al</i>	105
31	A32	Evaluation of single-layer warm clouds and aerosol optical depth from MODIS onboard TERRA satellite	Banerjee & Ghosh	108
32	A33	Long-term measurement of cloud condensation nuclei over a high altitude hill station over eastern Himalaya	Roy <i>et al</i>	111
33	A34	Urban emissions load from passenger transportation to the atmosphere	Choudhary <i>et al</i>	113
34	A35	Quantification of dust transport to eastern Arabian Sea during storm period using satellite and ground based data.	Aswini & Kumar	116
35	A36	Characteristics and distribution of carbonaceous species over Bay of Bengal during winter monsoon outflow.	Nayak <i>et al</i>	120
36	A37	A preliminary study on ozone precursor-NMVOCs at an urban site of Delhi during monsoon	Kumar <i>et al</i>	123
37	A38	Effect of atmospheric aerosols on surface UV radiation	Singh <i>et al</i>	127
38	A39	Comparative study of aerosol particle size distribution and new particle formation events during summer and winter seasons at Delhi.	Jose <i>et al</i>	130
39	A40	Emission of PM _{2.5} during traditional cooking process - a case study	Masiwal <i>et al</i>	134
40	A41	Variation of aerosol optical properties over Delhi: a study on 2016 and 2017 Diwali episode	Singh <i>et al</i>	137
41	A42	Study of air pollutants alongside major roadways in Agra	Singh <i>et al</i>	142
42	A43	PM _{2.5} bound carbonaceous aerosols: Assessment during hazy and non-hazy days	Satsangi <i>et al</i>	145
43	A44	Mass concentration, enrichment and health risk assessment through ingestion, dermal and inhalation exposure pathways posed by heavy metals in PM _{2.5}	Sah <i>et al</i>	150
44	A45	Atmospheric gas and particulate phase distribution of parent polycyclic aromatic hydrocarbons and their nitro-derivative and their variation with NOX	Verma <i>et al</i>	156
45	A46	Chemical characterizarion and source apportionment of PM ₁ at a sub-urban site of Agra	Mangal <i>et al</i>	161
46	A47	Ambient particulate matter and ozone levels at a suburban site of India: influence of biomass burning and dust storm	Kumari <i>et al</i>	167
47	A48	Estimation of carbonaceous aerosols at indoor environment of Cafeteria during winter season in Delhi, India	Mandal <i>et al</i>	172
48	A49	Impact of environmental bio-aerosol pollution on human	Balyan <i>et al</i>	176

		health: a “follow up study” on exacerbation of COPD		
49	A50	Potential of urban vegetation in attenuating atmospheric particulate pollution	Sharma & Ghosh	178
50	A51	Estimation of radiative forcing due to carbonaceous aerosols: their climate feedback	P Ajay <i>et al</i>	182
51	A52	Estimation of aerosol radiative forcing: a synthesis of hybrid analysis	Subba <i>et al</i>	186
52	A53	Distribution of volatile organic compounds over Indian subcontinent during winter: WRF-Chem simulations versus observations	Chutia <i>et al</i>	191
53	A54	Occurrence of single and multiple aerosol layers over the sub Himalayan region of India	Dahutia <i>et al</i>	196
54	A55	Characterization of bioaerosols in post-monsoon season at various locations of an educational institute in Northeast India	Khataniar <i>et al</i>	201
55	A56	Aerosol number concentration and inhaled particle number in an educational institution located in the lower Himalayas, India	Prabhu <i>et al</i>	204
56	A57	Concentration and size segregated distribution of fungal bioaerosols in an open landfill site in Dehradun, India	Sandeep & Vijay	207
57	A58	Aerosol dynamics in the Indian sector of southern ocean and coastal Antarctic region during austral summer- its implication on local climate.	Shaikh <i>et al</i>	211
58	A59	Impact of surface layer energy and flux exchanges on the near surface black carbon aerosols over a tropical coastal region Goa	Salim <i>et al</i>	215
59	A60	Aerosol characterization in the subtropical humid region of Northern India	Singh <i>et al</i>	220
60	A61	Studies on seasonal variation of indoor radon, thoron and progeny concentrations around Hemavathi river basin, Karnataka, India	Niranjan & Ningappa	224
61	A62	Identification of source regions and type of aerosols during High aerosols events over Gujarat	Vaghmaria & James	229
62	A63	Levels of btex during transitional period of summer and winter along a roadside area of east Delhi	Garg & Gupta	231
63	A64	Generation of nanoaerosols through automobiles and estimation of their effects on human health: an investigatory case study in Delhi /NCR	Joshi & Kachhawa	234
64	A65	Indoor phthalates and potential health risks: a critical review	Kaur <i>et al</i>	237
65	A66	Short-chain saturated dicarboxylicacids (C ₂ -C ₄) in aerosols collected at bellary station in South India	Boreddy <i>et al</i>	239
66	A67	Study of size-segregated atmospheric aerosol over Raipur, Chhattisgarh, India	Nirmalkar <i>et al</i>	241
67	A68	Summertime black and brown carbon (BC and BRC) in the Eastern Indo-Gangetic plain	Rana & Sarkar	244
68	A69	Regional sulfate drives long-term rise in AOD over megacity Kolkata, India	Rawat & Sarkar	249

69	A70	Gravimetric and real time measurement of indoor PM _{2.5} , BC and PN concentration during cooking in biomass cookstoves	Sarika <i>et al</i>	254
70	A71	Absorption properties of brown carbon in freshly emitted and aged ambient aerosol over an urban site in Mumbai	Sarkar <i>et al</i>	258
71	A72	Health risks of PM-bound trace metals in Mumbai slums	Anand <i>et al</i>	264
72	A73	Characterization of water soluble organic carbon and related functional groups by H ¹ NMR at suburban Mumbai	S. Yadav <i>et al</i>	265
73	A74	Influence of aerosol radiative effects on atmospheric thermal structure and dynamical response over India in the ECHAM6-HAM2 gcm	Muduchuru & Venkataraman	269
74	A75	Influence of recent changes in aerosol abundance on temperature response and snow cover fraction over the Himalayan region	Sharma & Venkataraman	273
75	A76	Mitigation of absorbing aerosols and their climate impacts over India: influence of sectoral interventions.	Tibrewal & Venkataraman	276
76	A77	An observational analysis of aerosol cloud interaction over India	Das <i>et al</i>	279
77	A78	Different metrics used in site selection for air quality	Lekinwala <i>et al</i>	283
78	A79	Emissions from open-field burning of agricultural residue in Vadodara, Gujarat	Kapoor <i>et al</i>	287
79	A80	Re-estimating on-road vehicles and travel characteristics of Delhi city: a vehicle survey approach	Khan <i>et al</i>	291
80	A81	Complexity of short-lived climate forcers (SLCFS) in rural India: Variability and chemistry of black and brown carbon and ozone interplay at a unique biomass-burning hotspot of global significance in the Indo Gangetic plains (IGP)	Prakash <i>et al</i>	295
81	A82	Emissions of particle-bound elements from on-road vehicle emission: an assessment of potential health risk	Prakash & Habib	299
82	A83	Chemical characterization of ambient PM _{2.5} at Ghaziabad, most polluted industrial city in India.	Gupta <i>et al</i>	305
83	A84	Air quality simulations over Delhi using WRF-CHEM: influences of local emissions and dynamics	K. Shukla <i>et al</i>	310
84	A85	Ultrafine and fine aerosol exposure and effect on heart rate of healthy adults: a case study at IIT Delhi	Baig <i>et al</i>	311
85	A86	Health effects of outdoor PM _{2.5} in Lucknow in the high risk months of October- January	Tripathi <i>et al</i>	313
86	A87	GIS-based emission inventory of air pollutants and green house gases in three cities of Uttar Pradesh and development of web-based tool for air quality management	Pathak <i>et al</i>	316
87	A88	Transformation and evolution of organic aerosol (OA) during fog processing	Mandariya <i>et al</i>	319
88	A89	Development and experimental validation of coupled flow-aerosol dynamics model for a glowing wire	Ghosh <i>et al</i>	322
89	A90	Seasonal variation of carbonaceous and water-soluble inorganic constituents of PM _{2.5} aerosols over a megacity, New Delhi	Bhowmik <i>et al</i>	326

90	A91	Aerosol particle number size distribution study in Delhi NCR	Mishra <i>et al</i>	330
91	A92	Bioaerosol load inventory at central IGP region, IIT Kanpur	Gupta <i>et al</i>	333
92	A93	Experimental and analytical study on aerosol behavior in piping assembly under varying flow conditions	Dwivedi <i>et al</i>	335
93	A94	A study on hygroscopic growth of CSI and CSOH particles	Mishra <i>et al</i>	342
94	A95	Design of a novel eccentric impactor PM sampler: an approach to reduce particle bounce off in single stage inertial impactor	Biswas & Gupta	348
95	A96	Carbonaceous and mineralogical composition of aerosol during EL-NIÑO influenced Indian summer monsoon	Rajeev <i>et al</i>	351
96	A97	Influence of cooking fuel on PM _{2.5} bound PAHS emission and associated health risk	Ola <i>et al</i>	355
97	A98	Characterization of ambient aerosols and their sources through carbon stable isotope measurements	Singh <i>et al</i>	359
98	A99	Comparison of indoor and outdoor bioaerosol concentration and composition at Indo Gangetic plains and their effect on human health	Srivastava <i>et al</i>	362
99	A100	Deposition modeling of ambient aerosols in human respiratory system: a 1-y long record from Kanpur in Indo-Gangetic plain	Rajput <i>et al</i>	367
100	A101	A field survey based case study assessing the impacts of rural cooking practices and ventilation conditions on human health	Singh <i>et al</i>	372
101	A102	Impacts of air masses on fog water chemical composition and contribution In the Indo Gangetic plain	Izhar <i>et al</i>	376
102	A103	Relationship between air pollutants and meteorological parameters and examination of possible inter-dependence of pollutant levels in two major Indian cities with varying climatic conditions	Rathi <i>et al</i>	381
103	A104	Preliminary approach of monitoring possible linkage between health effects and outdoor PM _{2.5} from a polluted urban environment	Tripathi <i>et al</i>	385
104	A105	Impact of fog processing on light absorption properties of brown carbon aerosols in Indo-Gangetic plain	Choudhary <i>et al</i>	389
105	A106	Assessment of fine particle profile in surface mine using an artificial neural network model	Dhuliya <i>et al</i>	394
106	A107	Evaluating the estimated concentration and optical properties of aerosol component from the aero-opt (matlab package)	Verma <i>et al</i>	399
107	A108	Sources and implication of black carbon (BC) aerosols simulated over Hindukush-Himalayan (HKH) region on glacier snowmelt runoff	Santra <i>et al</i>	404
108	A109	Chemical signatures of urban, open burning and dust transportation in a tropical urban environment over eastern Indian region	Priyadharshini <i>et al</i>	408
109	A110	Seasonal variation in black carbon burden simulated with WRF-CHIMERE model over Indian subcontinent	Ghosh <i>et al</i>	412
110	A111	Potential of simulated atmospheric black carbon (BC) burden and its radiative response to the emission strength efficacy over the Indian region in a chemical transport model (CHIMERE)	Ghosh <i>et al</i>	416

111	A112	Spatio-temporal variations of PM _{2.5} mass over India using regional climate model	Srivastava <i>et al</i>	420
112	A113	Identification of source region of secondary aerosol during fog evolution in the urban atmosphere "Delhi" India during 2016-17	Tiwari <i>et al</i>	423
113	A114	Evaluation of the skynet calibration methodologies for direct and diffuse solar irradiance	Ningombam <i>et al</i>	428
114	A115	Mobility analysis as a tool for characterization of non-spherical nanoparticles	Thajudeen <i>et al</i>	434
115	A116	Physical and chemical properties of atmospheric aerosol at Alaknanda valley (Srinagar) in the central Himalaya region	Bisht <i>et al</i>	437
116	A117	Long-term assessment of near-surface air pollutants at an urban station in Indo-Gangetic basin	Srivastava <i>et al</i>	443
117	A118	Long term variability and trend analysis of black carbon over ny-ålesund, arctic	Sonbawne <i>et al</i>	447
118	A119	Chemical characterization of fine particulate during fog and non-fog period of the winter season of 2017-18 at Delhi	Acharja & Ali	451
119	A120	Role of winds on sink mechanism of fine mode aerosols	Yang & Pandithurai	455
120	A121	New particle formation: influence of planetary boundary layer and air mass	Singla <i>et al</i>	459
121	A122	The black carbon oscillation (BCO) mode detected in the caipeex measurements	P R C Rahul <i>et al</i>	465
122	A123	Estimation of nitrate in organic and inorganic form at a high altitude site in Western ghats	Mukherjee <i>et al</i>	468
123	A124	On the measurement of ice nuclei characteristics over a high altitude station in the Indian region	Kumar <i>et al</i>	473
124	A125	Evaluation of simulated PM concentrations using WRF-CHEM over India during a pre-monsoon month	Maji & Beig	477
125	A126	Characteristic features of organic and elemental carbon: Estimation of sources over a high altitude station	Raju <i>et al</i>	483
126	A127	Sodium Aerosol charging and concentration decay under unipolar ion field in closed chamber	Pujala <i>et al</i>	489
127	A128	Determination of deposition velocity of mixed aerosols by chemical techniques	Pujala <i>et al</i>	494
128	A129	Sodium aerosol leakage through concrete specimens	P N Sujatha <i>et al</i>	498
129	A130	Studies on chemical behavior of sodium fire aerosol in closed and open environment	Subramanian <i>et al</i>	503
130	A131	Comparison of sodium metal aerosol characteristics in inert gas	Kumar <i>et al</i>	509
131	A132	Analysis of mixed NAK aerosols by ion chromatography	Ananthanarayanan <i>et al</i>	514
132	A133	Physical and chemical characterization of sodium combustion aerosols	Pradeep <i>et al</i>	519
133	A134	Heavy metal enrichment on indoor fine particulate matter in different socio-economic zones of Delhi	Garg & Ghosh	526
134	A135	Dust storm over the Arabian Sea during the summer season- The July 2016 Case	Kaskaoutis <i>et al</i>	533
135	A136	Long-term (2007-2017) measurements of aerosol characteristics at urban stations Delhi and Lucknow	Kumar <i>et al</i>	537

136	A138	Winter aerosol characterization at an urban coastal site (Bhubaneswar) located in the downwind of Indo-Gangetic plains	Panda <i>et al</i>	543
137	A139	The sub-daily variability in aerosols and its radiative effect inferred from ground and satellite measurements	Mukherjee & Vinoj	549
138	A140	Long term trend in PM10 associated metal concentration in an institutional area of Delhi	Yadav <i>et al</i>	558
139	A141	Variation of nh ₃ concentration from agricultural activities in relation with meteorological parameters	Sudesh & Kulshrestha	563
140	A142	Personal exposure to fine and coarse mode particle in various transport modes in Delhi	Singh & Srivastava	566
141	A143	Spatial variation of BTEX in a sensitive environment of the Delhi	Mehta <i>et al</i>	571
142	A144	Reactive nitrogen chemistry during winter season along the urban transect of NCR, Delhi	Tiwari & Kulshrestha	575
143	A145	Water soluble organic carbon and its association with other carbonaceous aerosol species at urban and rural sites In Indo-Gangetic plains	Mishra & Kulshrestha	580
144	A146	Impact of direct radiative effect of atmospheric brown clouds on atmospheric stability over Indian core monsoon region	Jangid <i>et al</i>	585
145	A147	Atmospheric reactive nitrogen fluxes and scavenging through wet and dry deposition in western Himalayas (India)	Sharma & Kulshrestha	589
146	A148	Biogenic and anthropogenic isoprene emissions in the ambient air of Delhi	Kashyap & Kumar	595
147	A149	Control of emissions of reactive nitrogen in rural household through soft approach	Verma & Kulshrestha	600
148	A150	Sources and characteristics of aerosols over a smart city Bhubaneswar in summer and winter	Kumar & Sushree	603
149	A151	Distinct influence of long range transport on the seasonal inhomogeneties in aerosol properties and air pollutants over Udaipur in Western India	Vyas & Gogof	606
150	A152	Aerosol optical depth and carbonaceous aerosol over a semi-arid location in southern India: temporal and source characteristics	Rajeshkumar <i>et al</i>	613
151	A153	Assessment of indoor air pollution during construction activities	Vachhani <i>et al</i>	619
152	A154	Long-term observations of black carbon aerosol over a rural location in southern peninsular India: role of dynamics and meteorology	Ravi Kiran <i>et al</i>	627
153	A155	Contribution of non-exhaust particulate matter emissions from road traffic in Delhi	Biswal <i>et al</i>	631
154	A156	Chemical characterisation of PM 2.5 collected at a tropical rural site Gadanki	Jain <i>et al</i>	636
155	A157	Role of dynamics and meteorology in the formation and maintenance of elevated aerosol layers over Indian region	Venkat ratnam <i>et al</i>	642
156	A158	Modelling study of regional transport on particulate matter concentration during a pollution episode in Delhi	Singh <i>et al</i>	647
157	A159	Temporal trends in rain water PH and ION composition over India	Singh & Singh	653

158	A160	Design and calibration of led based broadband integrating nephelometer	Ramachandran <i>et al</i>	657
159	A161	Distributions, sources, and health risks of atmospheric PM _{2.5} - bound polycyclic aromatic hydrocarbons in rural Jamshedpur, India	Kumar <i>et al</i>	662
160	A162	Assessment of particulate matter variation over world heritage site and steel city of India	Gogikar & Tyagi	668
161	A163	A satellite observation based study on aerosol-cloud-precipitation interaction over two smart cities of Odisha during pre-monsoon season	Kant & Panda	675
162	A164	A satellite based decision support tool for monitoring and forecasting air quality over India	Patadia & Noojipady	678
163	A165	Radiation forcing of special events over the urban environment of Ahmedabad city	Gharekhan <i>et al</i>	682
164	A166	Air pollution and health: inflammation and reactive oxygen species induced by particulate matter from Hyderabad city	Gangamma <i>et al</i>	687
165	A167	Smokers aerosols and health: lung adenocarcinoma TCGA gene expression analysis among	Gangamma & Pradhan	689
166	A168	Role of outgoing longwave radiation on cloud fraction over India	Shah & Srivastava	691
167	A169	A long term satellite based study of aerosol effects on visibility over the capital city of Assam, Guwahati	Biswas & Dahutia	694
168	A170	Evolution and characteristics of organic aerosol in the urban atmosphere through highly time resolved measurements	Singh <i>et al</i>	700
169	A171	Reactive oxygen species generation capability of ambient +aerosol over the Arabian sea	Patel & Rastogi	703
170	A172	Neutralization of aerosol acidity by ambient ammonia: implication to aqueous phase SO ₂ oxidation	A. K. Sudheer	705
171	A173	Black carbon mixing state characterisation of climatically relevant size aerosols	Sarangi <i>et al</i>	709
172	A174	Diurnal variability in characteristics of water-soluble brown carbon through online measurements over New Delhi	Rastogi <i>et al</i>	712
173	A175	Cloud detection using image processing	P. Malaidevan <i>et al</i>	716
174	A176	Impacts of dust-ice-cloud interactions on precipitation variability	Patel <i>et al</i>	719
175	A177	Long term trends in aerosol optical depth over Bay of Bengal	Rajesh T. A. & Dhaker	724
176	A178	Spatial distribution of black carbon aerosol: road campaign experiment in western India	Rajesh T. A. <i>et al</i>	729
177	A179	Ionic effect on cloud formation and electric field of thunderclouds	M. Chandra	733
178	A180	Simultaneous measurements of number, mass and chemical compositional characteristics of aerosol emissions during fireworks	Joshi <i>et al</i>	735
179	A181	Size differentiated atmospheric aerosols during firecrackers burning at Raipur	Mahilang <i>et al</i>	738
180	A182	Short term perturbation in aerosol characteristics over North western part of India: case study during a severe dust storm	Bansal & Singh	742
181	A183	Measurement of carbonaceous aerosol with high time resolution: Equivalence of TC-BC and OC/EC	Rigler <i>et al</i>	746

182	A184	Measurement of carbonaceous aerosol: high time resolution measurement and source apportionment of TC, BC and OC, EC	Rigler <i>et al</i>	748
183	A185	Study of relationship between dust storms and aerosol concentration over Thar desert region of India using satellite imageries	Sujitha <i>et al</i>	750
184	A186	Study of atmospheric aerosol over semi-arid urban region Rajkot using multi-wavelength solar radiometer	Godhani <i>et al</i>	754
185	A187	Absorbing aerosols over a semi arid rain shadow location in India	Soyam <i>et al</i>	759
186	A188	Seasonal variability of suspended particulate matter in ambient atmosphere over Sikkim Himalaya, India	Sharma & Ranjan	763
187	A189	Analysis of surface ozone (O ₃) and its chemistry at a semi-arid region, Anantapur, southern India	Elijabetthamma <i>et al</i>	765
188	A190	Variations in scattering properties of surface aerosols during monsoon season at semi-arid region, Anantapur, southern India.	Manjunatha <i>et al</i>	770
189	A191	Aerosol black carbon: its characteristics over semi-arid region, Anantapur	Reddy <i>et al</i>	775
190	A192	Investigating the characteristics of mineral dust over Arabian sea through modis observations	Rao <i>et al</i>	779
191	A193	Variability of surface energy balance over semi-arid station Anantapur using gldas model data	Reddy <i>et al</i>	785
192	A194	Comparision of AOD over Ahmedabad city using satellite and ground data	Sen <i>et al</i>	790
193	A195	A framework for exposure assessment in rural Indian households: a case study of Rajasthan	Tigala <i>et al</i>	794
194	A196	Observed relation between aerosol optical properties with relative humidity	Paul <i>et al</i>	795
195	A198	Sources and origin of aerosols at a receptor site in the world's most polluted megacity	Bhandari <i>et al</i>	799
196	A199	Improved diffusion loss correction down to 1 nm particles for SMPS measurements	Scheckman <i>et al</i>	802
197	A200	A quartz crystal cascade impactor for real-time ambient measurement	Chen <i>et al</i>	803
198	A201	Impact of California fires on local and regional air quality: the role of a low-cost sensor network and satellite observations	Gupta <i>et al</i>	806
199	A202	The use of a size scanning nephelometer to constrain particle size-distribution and their scattering properites	Martins <i>et al</i>	808
200	A203	Seasonal variability of aerosol and its impact on cloud properties over Gangetic West Bengal	Sarkar <i>et al</i>	812
201	A204	Spatio - temporal variability of cloud and aerosol properties associated with inter - annual variation of summer monsoon onset over Gangetic West Bengal	Khan <i>et al</i>	816
202	A205	Ground based and space borne lidar remote sensing of the intense forest fire at Seshachala forest range during march 2014: a case study	Rojaraman <i>et al</i>	820
203	A206	Long-term climatology of aerosols over Tirupati: a study using Satellite and model simulations	Vijayakumar <i>et al</i>	824
204	A207	One-decade pre-monsoon and post-monsoon trends of aerosol optical depth in relation to meteorological parameters over Indian subcontinent	Barik & Acharya	829

205	A208	Effect of aerosol chemistry on temperature pattern in north-western India during rice and wheat crop residue burning	Acharya <i>et al</i>	832
206	A209	Source apportionment of black carbon over Agartala in the North eastern India	Kaur <i>et al</i>	835
207	A210	Summertime aerosol characteristics at a free-tropospheric site Himansh (4080 m a.s.l) in the western Himalayas	Arun <i>et al</i>	838
208	A211	Characterization of the 'aerosol humidograph instrument' for aerosol optical growth studies	Vaishya <i>et al</i>	841
209	A212	Diurnal variability of integrated water vapour content (IWC) in the atmospheric boundary layer (ABL) and its transport to the free troposphere during fair weather and cloudy conditions	Davis & Raju	845
210	A213	Characteristics of carbonaceous aerosols over a tropical coastal location in southern peninsular India	Aswini <i>et al</i>	849
211	A214	Vertical structure of optical and radiative effects of aerosols across the Indo-Gangetic plain	Vaishya <i>et al</i>	853
212	A215	Sources and transport of aerosol species contributing to aerosol optical depth measured over the Bay of Bengal and the Arabian sea from source and receptor oriented modelling approaches	Santra <i>et al</i>	857
213	A216	Estimation of short-wave aerosol direct radiative forcing over a semi-arid region-Kadapa, Andhra Pradesh.	Vachaspati <i>et al</i>	861
214	A217	Aerosol and pollutant assessment during winter time in delhi: The WIFEX Campaign	Dumka <i>et al</i>	865
215	A218	Mass distribution of size segregated particulate matter at different traffic sites of agra region	Tiwari <i>et al</i>	868
216	A219	Response of Indian summer monsoon rainfall to dust aerosols of west Asian origin at climatological scale	Singh <i>et al</i>	871
217	A220	Aerosol vertical transport studies during the pre-monsoon of 2011 over Kanpur	Sethi <i>et al</i>	876
218	A221	Polycyclic aromatic hydrocarbons (PAHS): characterization, distribution and source markers for Agra (Taj city), U.P., India	Dubey <i>et al</i>	880
219	A222	Simulation of an extreme dust episode using WRF-CHEM	Choudhury <i>et al</i>	885
220	A223	Analysis of a dust storm originated over west Asia using NWP model	Singh <i>et al</i>	892
221	A224	Finding the possible facts of spatio-temporal variation of AOD over the lower part of Ganges plain of West Bengal, India	Dutta <i>et al</i>	899
222	A225	Diurnal variation of PM _{2.5} over the Indian region using merra-2 reanalysis dataset	Bali & Dey	903
223	A226	Build-up of ambient PM _{2.5} in Delhi NCT using high resolution satellite dataset	Chowdhury <i>et al</i>	906
224	A227	Quantification of health benefits due to reduction in anthropogenic PM _{2.5} resulting from mitigation of key emitting sectors through chemical transport model	Upadhyay <i>et al</i>	910
225	A228	Ice nucleating particle properties of aerosols in the Himalayan region	Yadav <i>et al</i>	913
226	A229	Aerosol associated water soluble inorganic ions in the Dhauladhar region of north-western Himalaya: seasonal variation in concentration, sources and processes	Kaushal <i>et al</i>	917

227	A230	Spatial and temporal variation aspects of aerosol black carbon concentration over India	Kumar <i>et al</i>	921
228	A231	Effect of aerosol coagulation on homogeneity in a reaction chamber	Khan <i>et al</i>	923
229	A232	Effect of solute strength and chemical nature of atomised aerosol particles on charge size distributions	Mariam <i>et al</i>	926
230	A233	Dead time estimation of LICEL transient digitizer of Raman lidar system	Jaswant <i>et al</i>	931
231	A234	Simulation of volatile organic compounds and secondary organic aerosols over the Indian region by the CAM4-CHEM model using CMIP5 and CMIP6 emissions	Vats <i>et al</i>	934
232	A236	Effect of heat and cold waves on all-cause mortality in an urban pollution hotspot over central Indo-Gangetic basin: implications of PM ₁₀ exposure	Singh <i>et al</i>	941
233	A237	Improvements in the simulation of aerosols over the Indian region using CAM5 model and the smog-India (speciated multipollutant generator) emissions inventory developed as part of the NCAP-coalesce project compared to CMIP6 emissions	Sharma & Ganguly	948
234	A238	Fog droplets and aerosols interaction: characterization of trace elements and secondary organic aerosols	Chakraborty <i>et al</i>	952
235	A239	Air quality modelling of co using aermოდ: contribution of various sources in the city of Varanasi	Katiyar <i>et al</i>	956
236	A240	Aerosol indirect radiative forcing on marine clouds over Indian Ocean	Rao & Dey	960

PERFORMANCE EVALUATION OF BETA ATTENUATION MONITOR UNDER INDIAN AMBIENT CONDITIONS

KRITIKA SHUKLA^{1,2}, SHANKAR G. AGGARWAL^{2,*}

¹Academy of Scientific and Innovative Research (AcSIR), CSIR- National Physical Laboratory Campus, New Delhi – 110012, India

²Environmental Sciences and Biomedical Metrology Division, CSIR- National Physical Laboratory, New Delhi – 110012, India

(*Correspondence at aggarwalsg@nplindia.org)

KEYWORDS: β -ray absorption method, Gravimetric method, Water content, Relative humidity

ABSTRACT

There are several measurement methods for the mass concentration of particulate matter in the ambient air. Gravimetric method is a direct method in the determination of the mass concentration and considered as the most reliable one. The most commonly used real-time techniques for measuring particulate matter are Tapered- Element Oscillating Microbalance (TOEM) and Beta Attenuation Monitor (BAM) method. These indirect methods have been widely used as they require less laboratory work than gravimetric method. Among these real-time techniques BAM is one of the most commonly used techniques for PM_{2.5} measurements in India. However, its performance is reported to be dependent on the ambient conditions such as humidity, high particle mass loading, water content of the particle surface, i.e. chemical composition of aerosol. These factors have been reported and evaluated in this paper. Understanding of these parameters can ensure optimal application of BAM and accurate interpretation of the result.

INTRODUCTION

Continuous exposure to elevated concentration of airborne particulate matter (PM) with the aerodynamic diameter less than 2.5 micrometers can lead to adverse health effects including respiratory, cardiovascular and circulatory diseases. The documented detrimental effects of particulate matter pollution to human health have drawn attention to the need for integrated mitigation strategies, including the establishment of air quality guidelines, continuous and accurate monitoring of PM concentrations and effective control of population exposure. The use of near real-time PM monitors has been supported over the past decades mainly due to their ability to provide continuous measurements with minimal human intervention. The most commonly used near real-time techniques for measuring PM are the Tapered-Element Oscillating Microbalance (TEOM) and Beta Attenuation Monitor (BAM) method. Continuous PM monitoring is valuable for providing short-term information on ambient concentrations. Beta attenuation monitoring is a widely used real-time air monitoring technique in India. Some studies have pointed out reliability problem of its measurement results. There are some factors affecting its performance such as relative humidity, high mass loading, chemical composition of particulate matter which governs the water content, etc. In India, the relative humidity varies from 40% to more than 90% depending on the location and season. Particulate matter concentration also varies in rural and urban sites. BAM's linearity of the PM mass measurement has been reported only up to 100 $\mu\text{g}/\text{m}^3$ in most of the manual of instrument. Beyond which BAM has never been tested under such conditions rather it is used in majority. In addition, chemical composition of PM consisting of secondary particles leads to overestimation of mass measurements in BAM due to hygroscopic nature of these particles. On the other hand, soot particles are non-hygroscopic and can retain considerable amount of water on their surfaces. Reliability of the measurement of PM is an important issue because measurement data is used to establish a policy. Therefore, performance of BAM is required to be tested under different Indian ambient conditions.

NEED FOR PERFORMANCE EVALUATION OF BAM

Several studies have compared indirect/near real-time BAM with direct GM particle mass concentration measurements and identified a number of parameters that lead to over or under estimation of the mass concentration (e.g., Chang et al., 2001; Lazaridis et al., 2008; Shin et al., 2011). These differences often depend on meteorological conditions and therefore exhibit seasonal variability (Gebicki and Szymanska,

2012). Variations in the aerosol chemical composition affects the water content of particles and thus also induce differences between BAM and GM measurements.

BAM provide continuous hourly measurements of particulate matter concentrations using the relationship between attenuation of beta particles and particle deposition on a glass filter tape. The mass determination by beta attenuation method (BAM) depends on the exponential decrease in the number of beta particles (electrons) transmitted through a thin deposit of particulate sample as the deposit thickness is increased. This relationship between the attenuation of beta ray and the particle deposit on the filter tape is described as (Jaklevic et al., 1981)

$$I = I_0 e^{-\mu x}$$

where, I and I₀ are the attenuated and un-attenuated beta ray intensities (count s⁻¹), respectively, μ is the mass absorption coefficient (m² kg⁻¹) and x is the mass areal density of particle deposit (kg m⁻²).

Beta-ray attenuation monitors consist of size selective inlet (cyclone or impaction), a beta source usually C₁₄, a beta ray detector and an inlet heater along with a temperature controller for conditioning of the sampling air. Mostly all the beta-ray attenuation monitors currently present in the market come with the heating assembly for the temperature management. An inlet heater helps in eliminating the condensation effects on the filter which tends to increase the value of the mass concentration but the disadvantage associated with this is that it evaporates the semi-volatile components such as NH₄NO₃, etc. which eventually bias the mass concentration value when compared with reference method like gravimetric method. These differences in measurement conditions between the BAM and the GM method can significantly affect quantitative agreement between the two methods. Therefore, there is a need to explore these areas and find a solution to overcome bias measurements of BAM. We are working on the calibration and performance evaluation of BAM in Indian conditions to make it more reliable and effective technique.

POTENTIAL BIASES / PERFORMANCE LIMITING FACTORS OF BAM

BAM is the standard method approved by US EPA, 1999 for real time monitoring of particulate matter. The reliability of BAM measurements has been questioned by many researchers and documented in literature. There are potential factors contributing to the mass concentration differences in BAM when compared with the reference method. The major contributing factors are RH, water content of aerosols and chemical composition of particulate matter. Water content of aerosols depends on the ability of the particles to hold water under given RH conditions, i.e. their hygroscopicity which mainly depends on their chemical composition, e.g. inorganic particles are more hygroscopic whereas organic particles can comparatively take up lower amounts of water. Therefore, water content of the aerosols is mainly governed by the relative abundance of inorganic salts in aerosols with a possible influence by water soluble organic matter at low RH of 50% (Aggarwal et al., 2007). This lead to overestimation of mass measurements. This also indicates that ambient RH is another major factor of concern. Soot particles also important even though they are non-hygroscopic in nature. Operation protocol of BAM usually specify the heating of inlet line before the sample reaches the filter tape at a temperature approximately 30°C in order to reduce the relative humidity to below 60%. This method minimizes the particle-bound water helping in getting good results but it may also tends to loss many volatile particulate matter present in the ambient air sample. But when the ambient RH is very high (60% - 90%), the temperature of the heating inlet is not enough for water in aerosols to evaporate sufficiently (Shin et al., 2012). The absolute humidity remains the same irrespective of the air temperature change. This results in high mass measurements.

PROGRESS AT CSIR-NPL

We are working on the calibration and performance evaluation of BAM in Indian conditions to make it more reliable and effective technique. Currently, we are comparing BAM measurements under different ambient conditions with Gravimetric method. We have reference FRM to run parallel with BAM for mass measurement comparison. We are evaluation the effect of above discussed parameter on BAM performances.

CONCLUSION

Beta-ray attenuation method is one of the most commonly used technique for real-time PM_{2.5} measurement all over the world. This method has advantage of simplicity and ease of automation for large-scale applications. However, its performance is reported to be dependent on the meteorological conditions as well as systemic errors which lead to over or under estimation of mass concentration of particulate matter. BAM suffers from positive sampling artifacts (absorption and adsorption of water and other gaseous compounds on sampled particles and filter media) and from negative sampling artifacts (the loss of semi-volatile material during sampling). Therefore a detailed understanding of the parameters that affect the measurements in Indian conditions is necessary to ensure optimal application of the instrument and accurate interpretation of the result.

ACKNOWLEDGEMENTS

The authors acknowledge the support of KENTEK Environment Technology, Korea for helping us in the setting up the instrumental facility.

REFERENCES

- Aggarwal, S.G., Mochida, M., Kitamori, Y., Kawamura, K., 2007. Chemical closure study on hygroscopic properties of urban aerosol particle in Sapporo, Japan. *Environment Science and technology* 41, 6920-6925.
- Chang, C. T., Tsai, C. J., Lee, C. T., Chang, S. Y., Cheng, M. T., & Chein, H. M., 2001. Differences in PM10 concentrations measured by β -gauge monitor and hi-vol sampler. *Atmospheric Environment*, 35(33), 5741-5748
- EC, 2010. Guide to the Demonstration of Equivalence of Ambient Air Monitoring Methods. Retrieved February 10, 2014 from <http://ec.europa.eu/environment/air/quality/legislation/pdf/equivalence.pdf>
- Gebicki, J., Szymańska, K., 2012. Comparative field test for measurement of PM10 dust in atmospheric air using gravimetric (reference) method and β -absorption method (eberline FH 62-1). *Atmos. Environ.* 54, 18e24.
- Jacklevic, J.M., Gatti, R.C., Goulding, f.s., Loo, B.W., 1981. A β -gauge method applied to aerosol samples. *Environmental Science and Technology* 15, 680-686.
- Lazaridis, M., Spyridak, A., Solberg, S., Smolik, J., Zdimal, V., Eleftheriadis, K., Aleksanropoulou, V., Hov, O., Georgopoulos, P.G., 2005. Mesoscale modeling of combined aerosol and photo-oxidant processes in the Eastern Mediterranean. *Atmos. Chem. Phys.* 5, 927e940.
- Shin, S.E., Jung, C.H., Kim, Y.P., 2011. Analysis of the measurement difference for the PM10 concentrations between beta-ray absorption and gravimetric methods at Gosan. *Aerosol Air Qual. Res.* 11, 846e853.
- Shin, S.E., Jung, ChH., Kim, Y.P., 2012. Estimation of the optimal heated inlet air temperature for the beta-ray absorption method: analysis of the PM10 concentration difference by different methods in coastal areas. *Adv. Environ. Res.* 1 (1), 69e82
- U.S. Environmental Protection Agency, 1999. Ambient Air Monitoring Reference and Equivalent Methods, Code of Federal Regulations (CFR) Title 40, Part 53. US-EPA, Washington, DC (revised July 1999)

CERTIFIED REFERENCE MATERIAL FOR PARTICULATE MATTER

RISHU AGARWAL^{1,2}, SHANKAR G. AGGARWAL^{2,*}, PRASHANT PATEL^{1,2}, KHEM SINGH²,
DAYA SONI² AND PRABHA JOHRI

¹Academy of Scientific & Innovative Research (AcSIR), CSIR-National Physical Laboratory Campus,
New Delhi, 110012

²Environmental Sciences & Biomedical Metrology Division, CSIR-National Physical Laboratory, New
Delhi 110012

(*Correspondence at aggarwalsg@nplindia.org)

KEYWORDS: Certified Reference Material (CRM), Particulate Matter, National Metrology Institute (NMI)

INTRODUCTION

Air quality has gathered much attention in the recent decades especially after the repercussions of industrialization have become significant and noticeable. Particulate matter forms a major part of the air pollutants, especially in a country like India where developmental activities are on a peak at present. Various agencies such as central and state pollution control boards monitor the air quality at different stations across the country. The accuracy of such measurements is a critical issue as there have been reports of several health problems (e.g. asthma) being aggravated by the air pollutants such as particulate matter of size <2.5 μm . The methods used in these measurements (sampling to analysis) should be traceable to SI units through an institute called National Metrology Institute (NMI) of the respective country to have comparable results and thus a better monitoring process. This will help in formulating the appropriate pollution control and abatement policies at the regional and national levels.

Certified Reference Materials (CRMs) are required to ensure the quality, reliability and inter-comparability of the analytical data generated (Aggarwal et al., 2013, Mori et al., 2008). CRMs also hold great importance for the validation of the analytical methods and the instrument performance. Several CRMs are available for particulate matter developed by NMIs of different countries, such as CRM 1648a by National Institute of Standards and Technology (NIST), USA; NIES CRM 28 by National Institute of Environmental Studies (NIES), Japan; ERM CZ100 and ERM CZ120 by Institute for Reference Materials and Measurements (IRMM), Belgium. However, only three NMIs (NIST, NIES, IRMM) of the world have produced such CRMs till date. Majority of the CRMs developed so far for atmospheric particulate matter are representative of the urban atmospheres and traffic junctions. One of the prime reasons of selecting urban sites to collect the bulk particulate matter is the heavy pollution in these areas as compared to the rural sites. India, being ranked as one of the polluted countries in terms of air quality has however not developed any CRM for particulate matter as of now or any other air pollutant as a matter of fact.

Most of the CRMs developed so far have certified the values for elemental composition of the particulate matter (Aggarwal et al., 2013). Only a few have been certified for polycyclic aromatic hydrocarbons (PAHs), nitrated polycyclic aromatic hydrocarbons (Nitro-PAHs) and polychlorinated biphenyls (PCBs). For example, SRM 2786 and SRM 2787 by NIST and ERM CZ100 and ERM CZ120 by IRMM have been characterized for PAHs and nitro-PAHs (Schantz et al., 2016). The RM 8785 developed by NIST is the only filter-based reference material available which is certified for total carbon and elemental carbon. Also, the urban dust SRM 1649a has been certified for isotopic (^{14}C), elemental, total and organic carbon in addition to the PAHs (Currie et al., 2002). The limited availability of CRMs for black carbon and organic carbon is because of the difficulty or sophisticated methods required to produce it with acceptable stability and homogeneity. Maintaining homogeneity in filter-based CRM is one of the most challenging tasks. For production of RM 8785, a sophisticated dust generation and collection system was used to deposit the fine fraction of particulate matter on filters simultaneously under similar flow conditions (Klouda et al., 2005). Another approach of producing filter-based CRM used is loading of air particulate material onto the filters through the deposition of aliquots from liquid suspension via vacuum filtration (Zeisler et al., 1998).

NEED FOR PARTICULATE MATTER CRMS

The development of reference materials is necessary in many ways. Since, the international reports of air pollution in Indian cities is on a rise in recent times, debates have arisen on the reliability of measurements because the ground reality seems different. Also, within our country's system, different organizations

monitoring air quality in the same city report varied results which create a lot of ambiguity for public and policy makers as well. The problem could lie either in their monitoring systems or in their protocols. Such monitoring data lead to the misleading reports from international agencies as they base their studies on these secondary data published. One of the solutions to this issue can be the use of calibrated instruments in monitoring and CRMs in analytical process to ensure the quality of data generated from measurements. The use of CRM is necessary since the environmental issues like air quality hold crucial importance both at public and policy makers domain. Although particulate matter CRMs developed by other countries like USA, Japan and Europe can be used but the environmental conditions of our country are different from them. Therefore, if India also produces its own particulate matter CRM, it will be beneficial both technically as well as economically in ensuring the quality of air quality data generated.

CHALLENGES IN DEVELOPING PARTICULATE MATTER CRMS

The production of particulate matter CRM is a challenging task as compared to any other material standard. The foremost challenge is to collect a bulk amount of material. The collection of starting material will take a long time and the seasonal variations in the composition of material might cause a problem in homogeneity, and thus certification of the material. Therefore, almost all the available standards were collected from some exhaust systems of the public services like road tunnel over a shorter period. The CRMs available from NIST have been derived from a single material that was collected somewhere during 1960s. Since then, they have used the same material to produce different type of particulate matter CRM (both filter-based and powder form). It took 10 years to collect 3 kg of material by NIES, Japan to develop NIES CRM 28 (Mori et al., 2008). This explains the difficult task of collecting starting material in bulk. Another challenge in developing particulate matter CRM is maintaining the stability and homogeneity of material over the years and if it is a filter based one, then for whole lot it is more difficult to maintain the homogeneity on the entire surface area of the filter. Although, development of CRM is a tedious process, but it is important to develop it especially for a country like India where the air quality issues are on a rise and measurement accuracy should be a prime concern.

PROGRESS AT CSIR-NPL

At CSIR-National Physical Laboratory, we have developed a facility for collection of particulate matter. The facility is functional since November 2017. The instrument used is designed such that it can collect the particulate matter in powder form with a flow rate of 1200 lpm. It is based on the principle of impaction and cyclone both. The instrument consists of an inlet, a cyclone assembly, backup filter holder, flow meter, pump and a control unit. The inlet has a provision of attaching an impaction surface to segregate the coarse ($>2.5 \mu\text{m}$) and fine ($<2.5 \mu\text{m}$) fraction of particles. The impaction surface can be removed to collect TSP (Total Suspended Particulate Matter). The particles separated by centrifugal force in the cyclone assembly are collected in the attached container at the bottom. The air stream then travels through a backup assembly where a filter is placed to collect any remaining ultrafine fraction of the particulate matter. The instrument has high collection efficiency, however, the amount of material collected depends on the prevailing environmental conditions.

CONCLUSION

Air quality has become one of the prime concerns in the recent past because of its visible impacts on human health. However, much attention has not been paid on the accuracy of the measurements declaring the state of air quality as poor. To deal with these concerns and help policy makers draft suitable policies to curb air pollution, the measurements need to be accurate and precise. CRMs are a way to ensure the accuracy and reliability of the data obtained from air monitoring measurements. So far, our country does not own a reference material for particulate matter, however looking at the current scenario of ambiguity in air quality monitoring data, it is even more important to develop a reference material for this purpose. Also, the use of standard and traceable protocols should be advocated and the data originating from such measurements should only be used to improve the data quality.

ACKNOWLEDGEMENT

The authors acknowledge Prof. Tomoaki Okuda of Keio University, Japan for his help in setting up the collection facility. RA thanks University Grant Commission (UGC) for granting the fellowship (Ref. No. 23196/ (NET-DEC.2015)).

REFERENCES

- Aggarwal, S. G., Kumar, S., Mandal, P., Sarangi, B., Singh, K., Pokhariyal, J., Mishra, S. K., Agarwal, S., Sinha, D., Singh S., Sharma C. and Gupta P.K. (2013). Traceability issue in PM 2.5 and PM 10 measurements. *Mapan*, 28(3), 153-166.
- Currie, L. A., Benner Jr, B. A., Kessler, J. D., Klinedinst, D. B., Klouda, G. A., Marolf, J. V., ... and Chow, J. C. (2002). A critical evaluation of interlaboratory data on total, elemental, and isotopic carbon in the carbonaceous particle reference material, NIST SRM 1649a. *Journal of Research of the National Institute of Standards and Technology*, 107(3), 279.
- Heller-Zeisler, S. F., Fajgelj, A., Bernasconi, G., Tajani, A., and Zeisler, R. (1998). Examination of a procedure for the production of a simulated filter-based air particulate matter reference material. *Fresenius' journal of analytical chemistry*, 360(3-4), 435-438.
- Klouda, G. A., Filliben, J. J., Parish, H. J., Chow, J. C., Watson, J. G., and Cary, R. A. (2005). Reference material 8785: Air particulate matter on filter media. *Aerosol science and technology*, 39(2), 173-183.
- Mori, I., Sun, Z., Ukachi, M., Nagano, K., McLeod, C. W., Cox, A. G., and Nishikawa, M. (2008). Development and certification of the new NIES CRM 28: urban aerosols for the determination of multielements. *Analytical and bioanalytical chemistry*, 391(6), 1997-2003.
- Schantz, M. M., Cleveland, D., Heckert, N. A., Kucklick, J. R., Leigh, S. D., Long, S. E., and Porter, B. J. (2016). Development of two fine particulate matter standard reference materials (<4 μm and <10 μm) for the determination of organic and inorganic constituents. *Analytical and bioanalytical chemistry*, 408(16), 4257-4266.

A NEW APPROACH FOR HIGHLY-EFFICIENT, CONCENTRATED SAMPLING OF AEROSOL PARTICLES FROM 10 NM TO 10 μ M: BIOAEROSOL APPLICATIONS

N. SAVAGE¹, M. NIETO-CABALLERO², M. HERNANDEZ², P. KEADY¹ AND S. HERING^{1,3}

¹ Aerosol Devices Inc., Fort Collins, CO USA

²University of Colorado at Boulder, Boulder, CO USA

³Aerosol Dynamics Inc., Berkley, CA USA

KEYWORDS: Aerosol particles, condensation growth tube collector, bioaerosol, aerosol instrumentation.

INTRODUCTION

Airborne bacteria, fungi and viruses are part of ambient particulate matter either as very small individual particles, aggregates or bound to other airborne particles. Thus, their airborne size distribution varies from a few nanometers to several micrometers. They are an important source of human and animal infection and pose a contamination risk to pharmaceutical and food processing operations. However, regular monitoring of bioaerosols are a difficult challenge. Current bioaerosol sampling methods are limited resulting in a lack of quality information about the airborne nature and effects of bioaerosols.

Active sampling methods are common tools for monitoring in hospitals and pharmaceutical facilities as well as for the collection of bioaerosols in outdoor and indoor environments. However, most active air sampling instruments have strong particle size dependencies for their collection efficiency. The three main types of active samplers are impingers, impactors and filters. Liquid impingers are the least destructive and the liquid collection can be later cultured to identify microorganisms with semi-quantitative results. However, their effective physical collection efficiency is limited to particles >0.5 micrometer, with reported sampling efficiencies $<10\%$ for particles between 30 and 100 nm (Hogan et al 2005) which is the size of most bare viral particles. Other disadvantages include the difficulty capturing hydrophobic particles, re-aerosolization, and cell multiplication during the long collection periods required. Impactors collect bioaerosols onto solid surfaces. They are commonly used for size segregation. They also have better physical collection efficiencies than impingers, exceeding 90% (Burton and Reponen 2007). Among their disadvantages, low humidity during collection can cause cells to dry and break apart, and their infectivity may be damaged by stress during the collection. Filtration methods can collect particles with high efficiency, but particle extraction from the filter media is variable and inefficient. They are used for their convenience as they can be easily deployed in the field and be programmed to collect time-resolved samples. Like impactors, filtration sampling causes mechanical stress and desiccation that can damage and kill the organisms. All three collection methods require multiple sample preparation steps for analysis, are prone to contamination and produce dilute samples limit analysis sensitivity.

Even though there is a wide variety of liquid collectors, impactors, and filter samplers available, there is a need for a new sampling approach capable of providing high physical collection efficiency over a wide range of particles sizes (from 10 nm to 10 μ m) and high biological recovery efficiency. The Spot SamplerTM instrument we present in this paper provides a new alternative for more efficient collection of bioaerosols down to 10nm both as concentrated spots on solid surfaces or concentrated suspensions into liquid for biological characterization (Eiguren Fernandez et al. 2014b). We also present a new collection technique that instantly preserves microbial genetic material upon capture. This innovative collection platform is directly compatible with subsequent molecular biology analyses including, but not limited to quantitative PCR (qPCR), targeted genomic amplifications, metagenomic DNA sequencing, RNA sequencing as well as targeted biopolymer analyses (e.g. allergens) and proteomics.

METHODS

The Spot Sampler particle collector uses a three-stage, moderated laminar-flow condensation approach to enlarge airborne particles as small as 5 nm at moderate temperatures (Figure 1). The aerosol enters into a cold section (conditioner) followed by a warm-, wet-walled growth region where the air becomes supersaturated and particle growth activation occurs (initiator). The third stage (moderator) provides the distance needed for continued particle condensation growth into $\sim 3\mu$ m droplets, while simultaneously reducing water vapor in the sample stream to prevent condensation on the walls downstream of the

collection site. The droplets are delivered to the collection matrix through a low-velocity jet impactor. The high humidity of the sample flow and the warm water blanket encapsulating the particles is advantageous for viable microorganism collection. Bioaerosols can be collected dry for microscopic or molecular analysis, or as a suspension into liquid, (i.e. water or nutrient broth) for molecular and biological assays. The sampler flow rate is 1.0-1.5 L/min. The system is capable of time-resolved, sequential collection into a multi-well plate for dry samples, and can be run unattended for several days when the aim of the collection is the characterization of the chemical properties of the aerosols (Eiguren Fernandez, et al. 2014a).

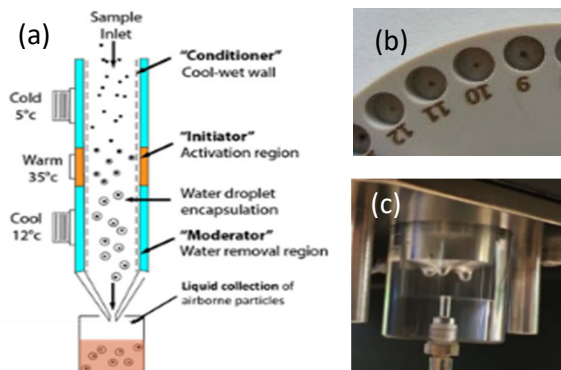


Figure 1. (a) Three-stage water condensation growth approach (b) dry collection into a multi-well sample plate, (c) liquid collection.

VIRUS APPLICATIONS

Researchers studying the capture of live laboratory-generated virus particles tested a prototype high-flow condensation growth sampler and compared the results to commonly used liquid impingers (Pan et al., 2016, Lednickly et al, 2016 and Walls et al., 2016). The test bioaerosols were MS2 bacteriophage and H1N1 influenza particles. The collected virions presence and infectivity were measured by culturing, qPCR, and a variety of bioassays. The physical collection efficiency of the MS2 particles (28 - 45 nm) was measured using a condensation particle counter, optical particle counter, and differential mobility analyzer to determine concentration and size distribution.

BACTERIA AND YEAST APPLICATIONS

Laboratory generated aerosols of *E.coli* (bacteria) and *S. kudriavezii* (yeast) were collected by a prototype high-flow condensation growth sampler and compared the results to commonly used liquid impingers (Pan et al., 2018). Viability of the aerosolized microorganisms was observed on a few different media types: 1) PBS for both *E.coli* and *S. kudriavezii*, 2) nutrient broth for *E. coli* and 3) Yeast Tryptone Glucose broth for *S. kudriavezii*. The physical collection efficiency of the bacteria and yeast particles was measured using an optical particle counter to determine concentration and size distribution. Culturing techniques and collection efficiency was used to evaluate the overall performance of each collector.

GENOMIC PRESERVATION TECHNIQUES

Different solid phase substrates were pre-treated with genomic preservative and tested for their ability to efficiently collect airborne biological particles and instantly preserve their genetic material. Coupons (5 mm disks) of the following materials were placed in a multi-well plate: glass microfibers, paper and quartz fibers. With each of these solid substrates, the recovery of known bioaerosol quantities (*Bacillus subtilis*; bacteria) were determined and compared to identical amounts added to liquid preservative in condensation growth collector reservoirs. Aerosol cytometry and qPCR methods were used to compare the preservation of genetic material, both sampling directly into liquid preservative or onto pre-treated substrates.

RESULTS & DISCUSSIONS

VIRUS APPLICATIONS

The physical collection efficiency of the MS2 particles, as indicated from the particle counter measurements, was > 90% for a prototype high-flow condensation growth sampler, as compared to < 10% for the commonly used SKC BioSampler, for an order of magnitude improvement (Pan et al., 2016). Walls et al., (2016) confirmed the >90% physical collection efficiency for MS2 particles, independent of particle size. Pan showed the fraction of MS2 particles that remained viable after capture averaged 45 times greater for the condensation growth sampler, when using water as the collection medium. MS2 recovery was enhanced to more than 100 times greater than the BioSampler with tryptone yeast extract broth as the collection medium. Walls showed a collection efficiency of infectious MS2 virions to be 20 times greater compared to the AGI-4 sampler. Collection of the infectious H1N1 influenza virus particles was 74% with the condensation growth sampler, which was 13 times higher than the BioSampler (5.6%, Lednickly et al, 2016). In the same study, Lednickly showed that the condensation growth sampler allows the collection of viable virus at much lower airborne concentrations than the BioSampler. The true capture recovery may be higher as they did not take into account transport losses or inactivation from the aerosolization process.

BACTERIA AND YEAST APPLICATIONS

The performance of the condensation growth tube for the collection of viable bacteria and yeast was compared against the commonly used SKC BioSampler. Results showed that the collection efficiency of viable *E. coli* was similar or better than the SKC BioSampler, depending on the collection media used. However, regardless of the media used for the collection of *S. kudriavezii*, the condensation growth tube out-performed the SKC BioSampler for the collection of viable yeast. In fact, the condensation growth tube had a detection limit lower than one order of magnitude for the observed yeast aerosol compared to the SKC Biosampler.

GENOMIC PRESERVATION TECHNIQUES

Polymerase chain reaction along with aerosol cytometry of the bioaerosols collected by the condensation growth tube, either on solid collector surfaces or directly into liquid preservatives, confirmed that bioaerosol concentration and preservation was compatible with modern genomic analyses of DNA (quantitation and sequencing). Compared to liquid recovery, quartz coupons had the highest and most consistent recovery efficacy with the least variation.

CONCLUSIONS

Sampling techniques for the collection of bioaerosols have improved over the years; however, none of the available samplers offer both good physical collection efficiency and adequate recovery efficiency of viable samples. The new approach used by our condensation growth technology provides an alternative to the conventional impingers, impactors or filter collections. The fully-integrated, portable commercial sampler and its quiet operation is advantageous for routine monitoring in indoor environments. The sampler collection efficiency is >90% for both solid and liquid collection for particle sizes from 10 nm to 10 µm. Studies show that the water-condensation growth technology provides a powerful method for more accurate assessment of infectious airborne microbe transmission and health threats than the existing bioaerosol samplers can offer.

ACKNOWLEDGEMENTS

We gratefully acknowledge the support from the National Institutes of Health (RC3 ES019081-01), and the National Science Foundation (1721940).

REFERENCES

Burton, N.C., S.A. Grinshpun, and T. Reponen. Physical collection efficiency of filter materials for bacteria and viruses. *Ann. Occup. Hyg.*, 2007, 51:143-151.

Eiguren Fernandez, A., G.S. Lewis, S. Spielman, Time-resolved characterization of particle associated polycyclic aromatic hydrocarbons using a newly-developed sequential spot sampler with automated extraction and analysis. *Atmos. Environ.* 2014a, 96:125-134.

Eiguren Fernandez, A., G.S. Lewis, and S.V. Hering. Design and Laboratory Evaluation of a Spot Sampler for Time-Resolved Measurement of Airborne Particle Composition. *Aerosol Science and Technology* 2014b, 48(6):655-663.

Lednický, J., M. Pan, J. Loeb, H. Hsieh, A. Eiguren-Fernandez, S. Hering, Z.H. Fan and C.-Y. Wu, Highly efficient collection of infectious pandemic Influenza H1N1 virus (2009) through laminar-flow water based condensation. *Aerosol Sci. Tech.*, 2016, [DOI: 10.1080/02786826.2016.1179254](https://doi.org/10.1080/02786826.2016.1179254).

Pan, M., A. Eiguren-Fernandez, H. Hsieh, N. Afshar-Mohajer, S.V. Hering, J. Lednický, Z. H. Fan and C.-Y. Wu. Efficient collection of viable virus aerosol through laminar-flow, water-based condensational particle growth, *J. Appl. Microbiol.*, 2016, 120: 805–815.

Pan, Maohua & Carol, Leah & Lednický, John & Eiguren-Fernandez, Arantzazu & Hering, Susanne & Fan, Z & Wu, Chang-Yu. (2018). Collection of airborne bacteria and yeast through water-based condensational growth. *Aerobiologia*. 10.1007/s10453-018-9517-7.

Walls, H.J., D.S. Ensor, L.A. Harvey, J.H. Kim, R.T. Chartier, S.V. Hering, S.R. Spielman and G.S. Lewis: Generation and sampling of nanoscale infectious viral aerosols, *Aerosol Sci. Tech.*, 2016, DOI:10.1080/02786826.2016.1191617.

OUTDOOR AND INDOOR SOURCES OF 1.1 – 4.0 NM PARTICLES

M. VÄKEVÄ, J. VANHANEN, E. MIETTINEN, P. SALO

Airmodus Ltd, Erik Palménin aukio 1, 00560 Helsinki, Finland

KEYWORDS: Nca, nucleation, exposure, nano particles, sources

INTRODUCTION

Atmospheric nucleation processes generate large numbers of nano sized aerosol particles (Kulmala *et al.*, 2013; Kontkanen *et al.*, 2017). All combustion sources generate single digit nano aerosol. Rönkkö and his colleagues (Rönkkö *et al.*, 2017) report how traffic, and engines in general, are a remarkable source of sub 3 nm particles, which they have named nano cluster aerosol (NCA). Rönkkö *et al.* estimate that in an urban environment the lifetime of the NCA is about 20 minutes. Since the reported number concentrations in the vicinity of traffic are high (Rönkkö *et al.*, 2017; Carnerero *et al.*, 2017) people in densely populated areas with a lot of traffic breath in NCA whenever outdoors.

Indoor air aerosol is a combination of particles and gases from outdoor and indoor sources. Due to high losses on any surfaces, single digit nano aerosol particles are often considered to have indoor origin rather than having been transported through HVAC system or infiltration. The observed outdoor numbers are, however, so high, that this might not be the case if the air intakes are close to traffic or if there is a possibility for infiltration through the building envelope. Indoor sources of sub 3 nm can be SOA formation, but based on recent studies about car brakes (Nosko *et al.*, 2016) we anticipated that also e.g. many renovation efforts may produce sub 3 nm particles. The indoor concentrations of NCA have not been studied very widely (measurements are reported e.g. by Ahonen *et al.*, 2017 for indoor air in a semiconductor processing area) thus not much information is available on the indoor sources of NCA.

To study NCA sources outdoors and indoors, we reviewed reported NCA concentrations outdoors and measured NCA concentrations indoors during different activities.

METHODS

To learn more about indoor nano particles, we measured the sizes of nano particles in the air of our laboratory under normal operation and while renovation work was conducted next room. Indoor particle number size distribution of 1.1 to 4 nm and total number of 4-1000 nm particles were measured using the Airmodus A11 nCNC system in a laboratory room.

The Airmodus A11 nano Condensation Nucleus Counter (nCNC) system consists of a Particle Size Magnifier (PSM) and a CPC (Airmodus model A20). The used PSM model was first introduced by Vanhanen *et al.*, 2011. PSM is a pre-conditioner, which is used to grow aerosol particles as small as 1 nm in mobility diameter by condensing diethylene glycol onto them. The single digit nano particles in the sample grow up to about 90 nm. Since the supersaturation inside the PSM can be changed through changing the mixing ratio of the sample and saturator flow rates, the size of the particles that are activated can be changed, and further a size distribution for 1-4 nm particles determined. The counting of particles is performed with a normal CPC. This approach allows the detection of both neutral and charged aerosol particles, which makes the system very sensitive for particles < 4 nm, as opposed to e.g. SMPS systems due to the low charging efficiency of such small particles.

The measurements were conducted in a laboratory that is operated in lower pressure than the adjacent rooms. The pressure difference is maintained in order to isolate the R&D lab, i.e. to prevent any (though normally none exist) nanoparticles or fumes in the lab air from escaping to other premises. The instruments measured laboratory air on one of the lab tables; the air entered the room via air supply units and from surrounding rooms through the gaps below the doors, moved past the instruments and on to the local ventilation exhaust units on the other side of the instruments. The HVAC ductwork in the corridor next to the lab was renovated: the air supply to our offices was cut off at about 9 am and the renovation work started. Exhaust units were still operating. The work included cutting metal air and water ducts, and draining and water vacuum cleaning water supply ducts (part of chilled beams system). The vacuum cleaner contained no filters (the filters are removed when water vacuuming). The work area was not covered or isolated. At the time of the renovation efforts, due to lack of supply air, all measured air was from adjacent rooms. At 3 pm the work was finished and supply air was switched back on.

RESULTS & DISCUSSIONS

Most of the time the number concentrations of ultrafine particles measured were fairly low, i.e. the air in our laboratory is well filtered.

Particle number concentration measurement results are presented in Figure 1a and 1b. On the first night of the measurements presented in the figure, the supply air rate was lower than on the second night due to adjustments of the HVAC system. During night and morning hours the concentrations of $>4\text{nm}$ particles were low; only 200-400 $\#/cc$ with limited air supply, and even lower when air supply rate was according to design specifications. The concentrations of 1.1-4nm particles were higher, 500-1500 $\#/cc$, and of the same order of magnitude than reported for indoor and ambient air ions by Kolarz *et al.*, 2009 and Hirsikko *et al.*, 2011. Except during the renovation work, the number of 1-4 nm was higher than the number of 4-1000 nm. During the renovation work a clear increase of all particle sizes was observed. The biggest increase was in the particles with diameter larger than 4 nm, which is likely due to abundance of condensable vapors that readily grow the nano cluster aerosol particles into larger sizes. Renovation work exposes both the workers and people in the vicinity of the activities to nano particles in remarkable concentrations.

We also observed a likely SOA event, or the effect of nearby traffic, with clear particle growth, in the morning before the renovation started.

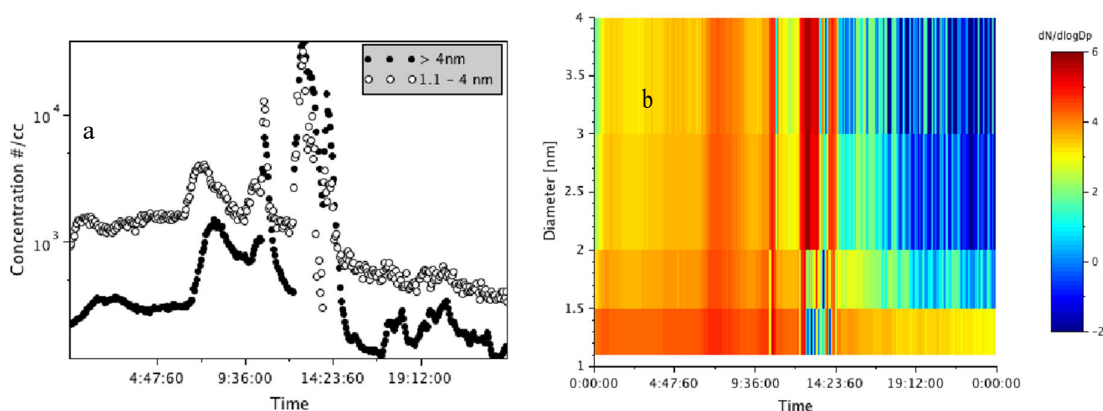


Figure 1. Particle number concentrations in Airmodus laboratory air: on the left 4-1000 nm compared to $<4\text{nm}$; on the right four different size ranges below 4 nm

CONCLUSIONS

Indoor sources of nano cluster aerosol can produce concentrations comparable to ambient observations. Renovation work that included cutting metal ducts is a likely source of nano aerosol, even nano cluster aerosol. Renovation work exposes both the people conducting the work and in the vicinity of the activities to nano particles in remarkable concentrations.

Single digit nano aerosol are present in all environments, and often in remarkably high concentrations. The numbers can be high both indoors and outdoors. The health effect of such small particles should be studied in more detail

ACKNOWLEDGEMENTS

We would like to acknowledge the work of all the researchers we used as references.

REFERENCES

Ahonen, L.R., J. Kangasluoma, J. Lammi, K. Lehtipalo, K. Hämeri, T. Petäjä & M. Kulmala (2017) *First measurements of the number size distribution of 1–2 nm aerosol particles released from manufacturing processes in a cleanroom environment*, *Aerosol Science and Technology*, 51:6, 685-693, DOI: 10.1080/02786826.2017.1292347

Carnerero, C., Pérez, N., Reche, C., Ealo, M., Titos, G., Lee, H.-K., Eun, H.-R., Park, Y.-H., Dada, L., Paasonen, P., Kerminen, V.-M., Mantilla, E., Escudero, M., Gómez-Moreno, F. J., Alonso-Blanco, E., Coz, E., Saiz-Lopez, A., Temime-Roussel, B., Marchand, N., Beddows, D. C. S., Harrison, R. M., Petäjä, T., Kulmala, M., Ahn, K.-H., Alastuey, A., Querol, X. *Vertical and horizontal distribution of regional new particle formation events in Madrid*. *Atmos. Chem. Phys. Discuss.*, <https://doi.org/10.5194/acp-2018-173>, in review, 2018.

Hirsikko, A., Nieminen, T., Gagné, S., Lehtipalo, K., Manninen, H. E., Ehn, M., Hörrak, U., Kerminen, V.-M., Laakso, L., McMurry, P. H., Mirme, A., Mirme, S., Petäjä, T., Tammet, H., Vakkari, V., Vana, M., and Kulmala, M.: *Atmospheric ions and nucleation: a review of observations*, *Atmos. Chem. Phys.*, 11, 767-798, <https://doi.org/10.5194/acp-11-767-2011>, 2011

Kolarža, P.M., D.M.Filipović, B.P.Marinković, *Daily variations of indoor air-ion and radon concentrations*, *Applied Radiation and Isotopes*, Volume 67, Issue 11, 2009

Kontkanen, J., Lehtipalo, K., Ahonen, L., Kangasluoma, J., Manninen, H.E., Hakala, J., Rose, C., Sellegri, K., Xiao, S., Wang, L., Qi, X., Nie, W., Ding, A., Yu, H., Lee, S., Kerminen, V.-M., Petäjä, T., Kulmala, M. *Measurements of sub-3 nm particles using a particle size magnifier in different environments: from clean mountain top to polluted megacities*. *Atmos. Chem. Phys.*, 17, 2017

Kulmala, M., Kontkanen, J., Junninen, H., Lehtipalo, K., Manninen, H.E., Nieminen, T., Petäjä, T., Sipilä, M., Schobesberger, S., Rantala, P., Franchin, A., Jokinen, T., Järvinen, E., Äijälä, M., Kangasluoma, J., Hakala, J., Aalto, P.P, Paasonen, P., Mikkilä, J., Vanhanen, J., Aalto, J., Hakola, H., Makkonen, U., Ruuskanen, T., Mauldin, R.L., Duplissy, J., Vehkamäki, H., Bäck, J., Kortelainen, A., Riipinen, I., Kürten,

T., Johnston, M.V. Smith, J.N., Ehn, M., Mentel, T.F., Lehtinen, K.E.J., Laaksonen, A., Keminien, V.-M., and Worsnop, D.: *Direct observations of atmospheric aerosol nucleation*. Science, 339, 943-946, 2013.
Nosko O., J. Vanhanen, U. Olofsson (2017) Emission of 1.3–10 nm airborne particles from brake materials, Aerosol Science and Technology, 51:1, 91-96, DOI: 10.1080/02786826.2016.1255713

Rönkkö, T., Kuuluvainen, H., Karjalainen, P., Keskinen, J., Hillamo, R., Niemi, J. V., Pirjola, L., Timonen, H. J., Saarikoski, S., Saukko, E., Järvinen, A., Silvennoinen, H., Rostedt, A., Olin, M., Yli-Ojanperä, J., Nousiainen, P., Kousa, A., Dal Maso, M. *Traffic is a major source of atmospheric nanocluster aerosol*. Proc. Natl. Acad. Sci. U.S.A., 2017. doi:10.1073/pnas.1700830114

Vanhanen, J., Mikkilä, J., Lehtipalo, K., Sipilä, M., Manninen, H. E., Siivola, E., Petäjä, T., Kulmala, M. *Particle Size Magnifier for Nano-CN Detection*, Aerosol Sci. Technol., 45: 4, 533-542, 2011

IMPROVING AIRBORNE NANOPARTICLE AND CLUSTER DETECTION WITH THE BUTANOL BASED LAMINAR FLOW CONDENSATION NUCLEI COUNTERS GRIMM 5.403 AND 5.412.

G. STEINER^{1,2,3}; M. ORZAN¹; I. NAGLER¹; E. PETRAKAKIS¹; M. SELIMOVIC¹;
C. TAUBER¹; S. BRILKE¹; P. WLASITS¹; F. TETTICH³

¹ University of Vienna, Faculty of Physics, Boltzmanngasse 5, 1090 Wien, Austria

² University of Innsbruck, Ion Physics and Applied Physics, Technikerstr. 25, 6020 Innsbruck, Austria

³ Grimm Aerosol Technik Ainring GmbH & Co. KG, Dorfstrasse 9, 83404 Ainring, Germany

KEYWORDS: CPC, counting efficiency, nanoparticles, molecular clusters.

INTRODUCTION

Over the last years, the size range of airborne molecular clusters (< 3nm) has become of highest importance in the field of aerosol sciences since it covers the initial steps of new particle formation in the atmosphere (e.g. Kulmala et al. 2013); therefore, having a major climate relevant impact. Also, it was recently shown that a major fraction of traffic produced particles contributes to the sub 3nm size range (Rönkkö et al. 2017). Evidently, also the development of new instrumentation for the classification and detection of sub 3nm particles and clusters is an extremely emerging field.

The detection of charged aerosols and clusters in the size range below 3nm was already investigated at the turn of the 19th to the 20th century (as reviewed e.g. by Flagan, 1998). However, the detection of electrically neutral aerosols in this size range is by far more challenging and was, most probably, first made possible in the 1960's by the development of a mixing type particle size magnifier (PSM) by Kogan & Burnasheva (1960).

METHODS

Here we present experiments with two n-butanol based CPCs (Grimm 5403 and 5412) that were operated with modified settings of their internal temperatures. At standard settings, the saturator temperatures are 35°C (model 5403) and 36° (model 5412) and the condenser temperature is 10°C for both models (Figure 1). Temperature settings and vapor pressure conditions for these temperatures were used as input parameters to a finite element model. By solving the partial differential equations for heat- and mass-transfer in the condenser section of the CPCs, we were able to determine the saturation ratio profiles in the condenser. Changing the input parameters, enabled us to find settings for an improved CPC performance.

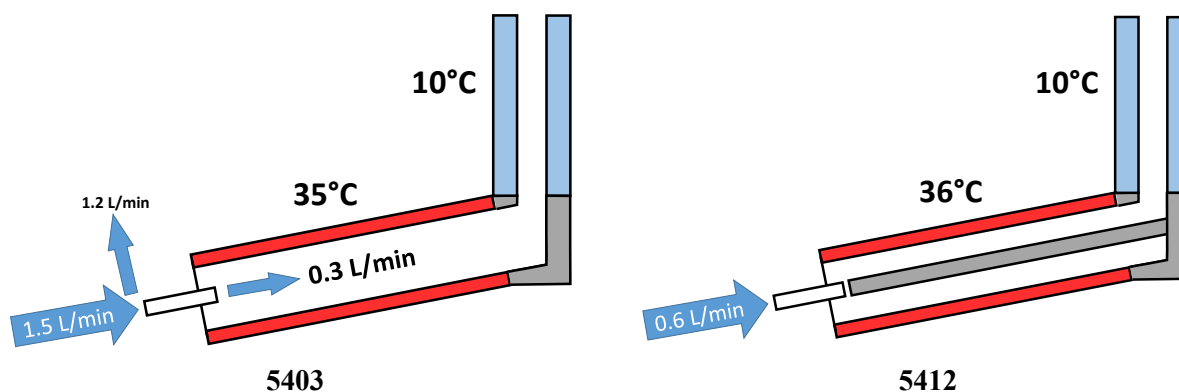


Figure 1. Flow path and standard temperature settings of saturator (red) and condenser (blue) section of Grimm CPCs models 5403 and 5412.

RESULTS & DISCUSSIONS

We will show the results of measurements determining the CPC counting efficiency with seed aerosols of different size and chemical composition and demonstrate an improved detection of molecular clusters down to sizes of 1.28 nm (TBA+; tetrabutylammonium ion) or 1.43 nm (THA+; tetraheptylammonium ion).

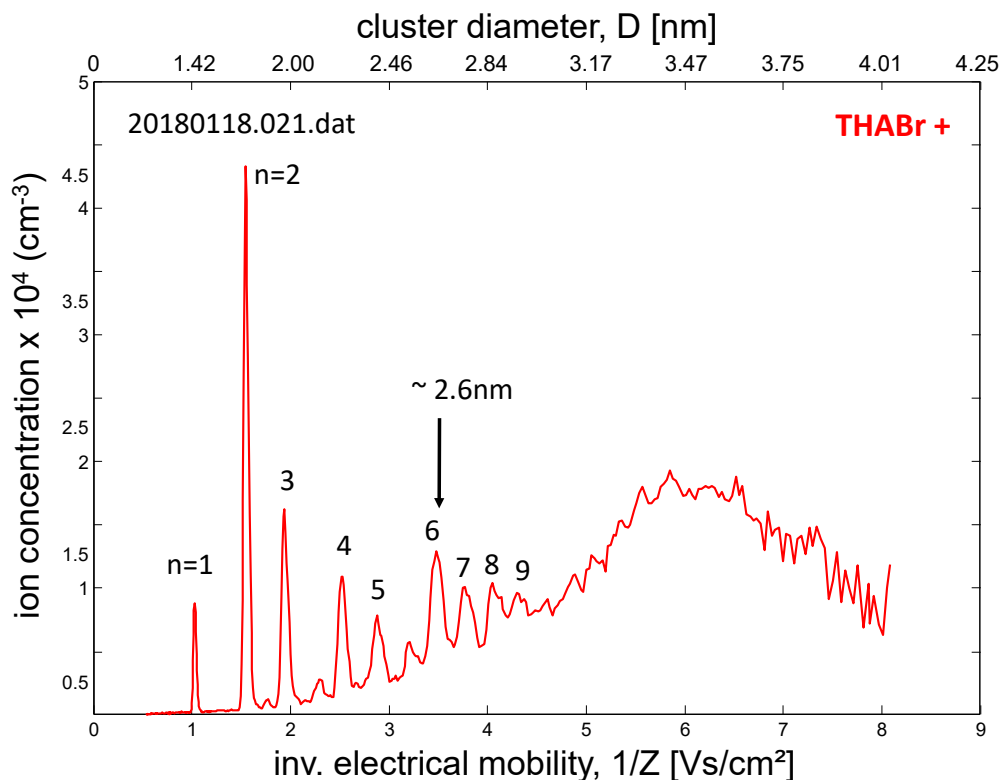


Figure 2. Mobility (Size) spectrum of clusters generated by electro spraying a solution of the salt tetraheptylammonium bromide in ethanol. The spectrum was recorded with a tuned Grimm 5403 CPC that achieves an improved counting efficiency down to cluster diameters < 2 nm

ACKNOWLEDGEMENTS

This work was supported by the Austrian Science Fund, FWF (project no. P27295-N20), the Tiroler Wissenschaftsfonds (nanoTOF-ICE) and the University of Innsbruck promotion grant for young researchers.

REFERENCES

- Kulmala et al. (2013) Direct Observations of Atmospheric Aerosol Nucleation. *Science*, 339, 943
- Rönkkö et al. (2017) Traffic is a major source of atmospheric nanocluster aerosol. *PNAS*, 114 (29) 7549-7554
- Flagan (1998) History of Electrical Aerosol Measurements. *Aerosol Sci. Technol.* 28:4, 301-380
- Kogan & Burnasheva (1960) *Phys. Chem. Moscow* 34:2630.
- Kuang et al. (2012) Modification of Laminar Flow Ultrafine Condensation Particle Counters for the Enhanced Detection of 1 nm Condensation Nuclei. *Aerosol Sci. Technol.* 46:309-315.

Vanhanen et al. (2011) Particle Size Magnifier for Nano-CN Detection. *Aerosol Sci. Technol.*, 45:4, 533-542

Winkler et al. (2008) Heterogeneous nucleation experiments bridging the scale from molecular ion clusters to nanoparticles. *Science*, 319, 1374-1377

Pinterich et al. (2016) The versatile analyzing nuclei counter (vSANC). *Aerosol Sci. Technol.* 50, 947-958 (2016)

Kangasluoma et al. (2015) Sub-3nm Particle Detection with Commercial TSI 3772 and Airmodus A20 Fine Condensation Particle Counters. *Aerosol Sci. Technol.*, 49:8, 674-681

SMART AIR QUALITY NETWORK, THE MEASUREMENT NETWORK FOR THE FUTURE

V. ZIEGLER ¹, M. PESCH ¹, M. HANK ¹, M. BUDDE ², M. BEIGL ², T. RIEDEL ², J. RIESTERER ², K. SCHÄFER ³, S. EMEIS ⁴, D. YOUNG ⁴, J. CYRYS ⁵, M. KOWALSKI ⁵, J. SCHNELLE-KREIS ⁶, A. PHILIPP ⁷, E. PETERSEN ⁷, J. REDELSTEIN ⁷, H. GRIMM ⁸, S. HINTERREITER ⁸, T. GRATZA ⁹

¹ Grimm Aerosol Technik Ainring GmbH & CO.KG, Germany;

² Karlsruhe Institute of Technology, Institute of Telematics, Chair for Pervasive Computing Systems / TECO, Germany;

³ Atmospheric Physics Consultant, Germany;

⁴ Karlsruhe Institute of Technology, Institute of Meteorology and Climate Research, Department Atmospheric Environmental Research, (IMK-IFU);

⁵ German Research Center for Environmental Health - Helmholtz Zentrum München (HMGU), Institute of Epidemiology, Germany;

⁶ German Research Center for Environmental Health - Helmholtz Zentrum München (HMGU), Cooperation Group of Comprehensive Molecular Analytics, Germany;

⁷ University of Augsburg, Institute of Geography, Chair for Physical Geography and Quantitative Methods, Germany;

⁸ Aerosol Akademie, e.V, Germany;

⁹ Stadt Augsburg, Umweltamt, Germany

(*Correspondence at volker.ziegler@grimm.durag.com)

KEYWORDS: Alternative measurement network, instrumentation, low cost sensor, algorithm, modelling, air quality, environmental sensing, source apportionment.

INTRODUCTION

A pragmatic, data driven approach, which for the first time combines existing in situ and remote sensing data sets with a networked mobile air pollutant measurement strategy in the urban space is an objective of the Smart Air Quality Network (SmartAQnet) project. It aims to implement an intelligent, reproducible, finely-tuned (spatial, temporal), yet cost-effective air quality measuring network, initially in the model region of Augsburg, Germany. Central to this is the development and utilization of partial, already existing (but not yet combined) data on the one hand and the collection and integration of relevant missing data on the other hand. Unmanned aerial vehicles (UAV) with low-weight meteorological sensors and particle counter are used to monitor the three-dimensional dynamics of the lower atmosphere. Ground-based remote sensing by ceilometer for mixing layer height detection as well as a Radio-Acoustic Sounding System (RASS) for temperature and wind profile measurements at the University of Augsburg campus complete the new network architecture and UAV height profiling of atmospheric parameters. Introduction was given by Budde et al. (2017a)¹

The SmartAQnet research initiative focuses on the subject of data access and data-based applications. Such complex monitoring provides the basis for deeper process understanding of air pollution exposure. The network architecture is shown and first results about spatial variation of meteorological influences upon air pollution exposure is presented using ceilometer, UAV and the existing monitoring network data.

METHODS

The Smart Air Quality Network is a pragmatic and data driven concept, in which all available data (from the high precision measurements to the low-cost sensors) are for the first time combined with the mobile

measurements into an integrated measurement strategy. The following information will be integrated for modelling and forecast:

- meteorological data and city development plans; emission cadasters
- sensors in buildings for the control of HVAC- systems or shading systems
- remote sensing data (aerial photography, satellite observation, etc.)
- new mobile measurement concepts (public traffic + ultra-low-cost-sensors)
- use of Scientific Scouts (Indicative Ambient Particulate Monitors) and existing stationary AQMS
- measurements with UAV; traffic counting sensors



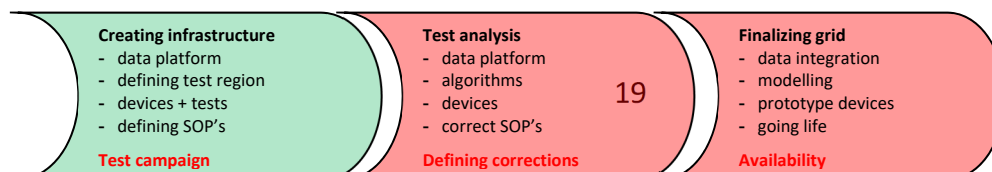
Figure 1+2: different sources are put together in IOT-platform

Ground-based remote sensing by ceilometer for mixing layer height (equivalent boundary layer height (BLH) is used here) detection (see Emeis et al. (2003)², Wiegner et al. (2014)³) as well as a Radio-Acoustic Sounding System (RASS) for temperature and wind profile measurements (see Emeis et al. (2009)⁴, Emeis et al. (2012)⁵) at the university campus complete the new network and UAV height profiling of atmospheric parameters. Such complex monitoring provides the basis for deeper process understanding of air pollution and evaluation data for small-scale chemistry-transport modelling (see Schäfer et al. (2005)⁶, Schäfer et al. (2006)⁷, Schäfer et al. (2011)⁸, Schäfer et al. (2016)⁹, Wagnier, Schäfer (2017)¹⁰).

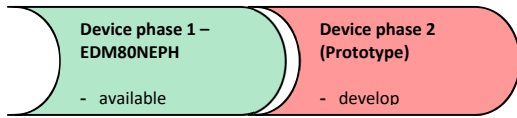


Figure 3. Location for the fixed-wing UAV (left, spiral rise) and copter (right, straight rise) height profiling at the campus of the University of Augsburg.

PROJECT PHASES



GRIMM HAS THE TASK TO DEVELOP A SUITABLE, RELIABLE AND SMART INDICATIVE AMBIENT PARTICULATE MONITOR:



SETUP FOR FIELD TEST AT THREE DIFFERENT LOCATIONS:

In order to have the right base for inter comparison of sensor/sensor as well as sensor/reference we made a setup with 5 Scientific Scouts + 1 EDM164 reference. All devices are equipped with humidity and temperature sensors. Target was to develop an ambient algorithm as well as to compare reproducibility of sensor to sensor, as well as traceability sensor to reference.

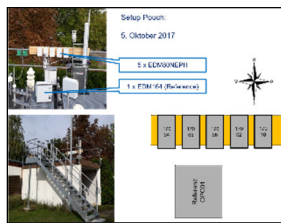


Figure 4: Pouch (GER) very low readings



Figure 5: Augsburg (GER) higher readings



Figure 6: Chengdu (CN) high readings

FIRST RESULTS & DISCUSSIONS FOR DEVICE DEVELOPEMENT

These results are mainly focussed on the device development. Most of the market available sensors are nephelometer cells, which are not able to distinguish particle size information. They are very sensitive towards temperature, humidity and dust contamination, which leads to significant drift behaviour. The lower detection limits are mostly above 15 to 20 $\mu\text{g} / \text{m}^3$, so in consequence the readings below the detections limits are very noisy. Originally, they have been developed for indoor use where these influences are of minor importance. During our long-term tests, we achieved the following results:

- with the developed algorithm and technology, we significantly decreased the detection limit down to 3-5 μg for the used measurement cell. We are now able to compensate the influence of humidity and temperature
- with the e-filter we are able to extend life-time of the sensors regarding service and calibration
- under changing aerosol conditions, a new local calibration is necessary in ambient air!
- depending on the local dust concentration, a local recalibration is mandatory at least every two weeks
- the closer the measurements are located to hotspots, the higher must be the density of reference units/sensor

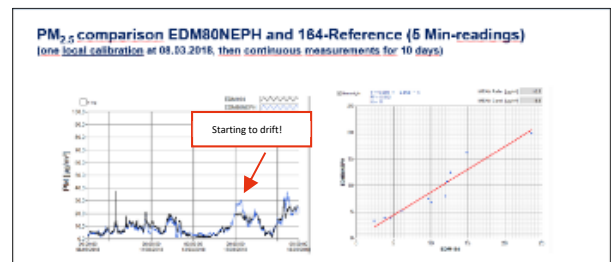
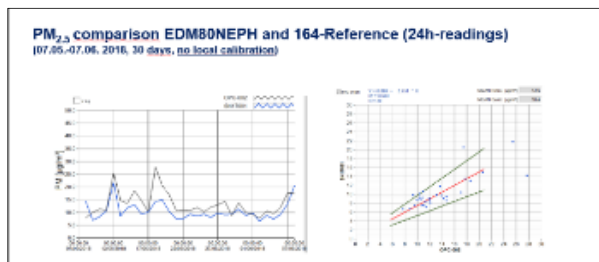


Figure 7. Difference between local calibration and no local calibration

CONCLUSIONS & OUTLOOK

- 1.) Our test showed, that a periodical and local recalibration is mandatory in order to keep the drift of the sensors under control. Calibration has to be done under ambient air conditions (since laboratory aerosols are stable, often artificial aerosols and therefore behaving different to ambient air conditions).
- 2.) The use of an E-filter for auto-zero function and for rinsing the measurement cell extends the service-life of a low-cost sensor. Nevertheless, it is not enough to reach the target of minimum 1- year service interval.
- 3.) With a commonly available photometric cell it is not possible to determine different PM-values (PM_1 , $PM_{2.5}$, PM_4 and PM_{10}) under changing aerosol conditions. Other technical solutions like OPC (optical particle counting) or hybrid solutions (OPC/Photometer) are needed.

ACKNOWLEDGEMENTS

- Project SmartAQnet is funded by the German Federal Ministry of Transport and Digital Infrastructure - Bundesministerium für Verkehr und Digitale Infrastruktur (BMVI) under grant no. 19F2003B.
- Thanks to the project team for the excellent, interdisciplinary cooperation.
<http://www.smartaqnet.com>
- Special thanks to our partner Chengdu University of Information Technology, School of Atmospheric Sciences, Chengdu, China (Prof. Shigong Wang, Prof. Xiaoling Zhang, Dr. Ping Kang)



REFERENCES & PICTURES

GRIMM Aerosol Ainring GmbH & CO.KG, Wikimedia Commons, University of Augsburg, KIT-TECO, Open Street Map, World Air Quality

Budde, M., Riedel, T., Beigl, M., Schäfer, K., Emeis, S., Cyrys, J., Schnelle-Kreis, J., Philipp, A., Ziegler, V., Grimm, H., Gratza, T., “SmartAQnet – Remote and In-Situ Sensing of Urban Air Quality.” Proc. SPIE 10424, 104240C-1–104240C-8 (2017a).

Emeis, S., Münkel, C., Vogt, S., Müller, W., Schäfer, K., “Determination of mixing-layer height.” Atmos. Environ., 38, 2, 273-286 (2004).

Wiegner, M., Madonna, F., Biniotoglou, I., Forkel, R., Gasteiger, J., Geiß, A., Pappalardo, G., Schäfer, K., Thomas, W., “What is the benefit of ceilometers for aerosol remote sensing? An answer from EARLINET.” Atmos. Meas. Techn., 7, 1979–1997 (2014).

Emeis, S., Schäfer, K., Münkel, C., “Observation of the structure of the urban boundary layer with different ceilometers and validation by RASS data.” Meteorol. Z., 18, 2, 149-154 (2009).

Emeis, S., Schäfer, K., Münkel, C., Friedl, R., Suppan, P., “Evaluation of the interpretation of ceilometer data with RASS and radiosonde data.” *Bound.-Lay. Meteorol.*, 143, 25–35 (2012).

Schäfer, K., Emeis, S., Hoffmann, H., Jahn, C., Müller, W., Heits, B., Haase, D., Drunkenmölle, W.-D., Bächlin, W., Schlünzen, H., Leitl, B., Pascheke, F., Schatzmann, M., “Field measurements within a quarter of a city including a street canyon to produce a validation data set.” *Int. J. Environ. Pollut.*, 25, 1/2/3/4, 201-216 (2005).

Schäfer, K., Emeis, S., Hoffmann, H., Jahn, C., “Influence of mixing layer height upon air pollution in urban and sub-urban area.” *Meteorol. Z.*, 15, 647-658 (2006).

Schäfer, K., Emeis, S., Schrader, S., Török, S., Alföldy, B., Osan, J., Pitz, M., Münkel, C., Cyrys, J., Peters, A., Sarigiannis, D., Suppan, P., “A measurement based analysis of the spatial distribution, temporal variation and chemical composition of particulate matter in Munich and Augsburg.” *Meteorol. Z.*, 21, 1, 47-57 (2011).

Schäfer, K., Elsasser, M., Arteaga-Salas, J.M., Gu, J.W., Pitz, M., Schnelle-Kreis, J., Cyrys, J., Emeis, S., Prévôt, A.S.H., Zimmermann, R., “Impact of meteorological conditions on airborne fine particle composition and secondary pollutant characteristics in urban area during winter-time.” *Meteorol. Z.*, 25, 3, 267-279 (2016).

Wagner, P., Schäfer, K., “Influences of meteorological parameters and mixing layer height upon air pollutant concentrations in urban area.” *Urban Climate*, 22, 64–79 (2017).

SUMMER-TIME AEROSOL POLLUTION OVER TWO CONTRASTING ENVIRONMENTS

P.C.S. DEVARA¹, P.B. SHARMA¹, P.P. DAS¹, Y. NEENU¹, G. KALPANA¹, U.C. DUMKA² AND SURESH TIWARI³

¹Amity Centre for Ocean Atmospheric Science and Technology (ACOAST) & Amity Centre for Environmental Science and Health (ACESH), Amity University Haryana (AUH), Gurgaon 122413, India.

²Aryabhata Research Institute for Observational Sciences (ARIES), Nainital 263002, India.

³Indian Institute of Tropical Meteorology-Delhi Unit (IITM-DU), New Delhi 110060, India.

KEYWORDS: Aerosols, Air Quality, Urban, Rural, Meteorological Episodes.

INTRODUCTION

The increase in pollution level, consequently an increase in aerosol loading, has direct impact on health, energy, water and climate. The abatement of air pollution and climate impacts has generally been treated separately. Now there is growing consensus among scientists that the problems of air quality and climate impacts need to be treated together to achieve sustainable development and a low carbon society. The quantification of various pollutant concentration levels requires knowledge of pollution level over a background or a rural site. Albeit, both the rural and urban sites, considered in the present study, are separated by an aerial distance of about 40 km; the difference in their station altitude as well as that in the surroundings make it interesting to study PM_{2.5} over these sites, amongst other constituents, in view of its potential impact on human health. The results of the experiments conducted during April 13-30, 2016 (~ 2 weeks) over the above two locations, one is representative of rural and the other is urban, are reported with plausible attribution to the findings, in this communication.

STUDY REGIONS & INSTRUMENTATION

The study regions considered in the present investigations are (i) Amity University Campus in Panchgaon (28.31 deg N, 76.90 deg E, 285 m above mean sea level) and (ii) the locations of Delhi NCR (23.28 deg N, 77.13 deg E, 218 m above mean sea level). The Panchgaon site is situated in a rural village, with a few scattered hamlets with a very meagre population. This study region is enclosed by Aravalli hillocks of average elevation of about 200 m. This site receives pollution from the neighbouring industrial locations (Manesar and Gurgaon). More details on this study site can be found in Devara *et al.* (2016). The megacity Delhi and the surrounding area, generally known as the National Capital Region (NCR), which is one of the most polluted urban regions in the world (Lodhi *et al.*, 2013). This site is a densely populated urban location with heavy traffic. The Delhi's air pollution is a combination of factors including industries, power plants, domestic combustion of coal and biomass, and transport (direct vehicle exhaust and indirect road dust) (Gurjar *et al.*, 2004; Kumar and Foster, 2007; Pandithurai *et al.*, 2008).

A suit of instruments (Aerodynamic Particle Sizer; Microtops II; Aethalometer; Weather and Environmental Monitor; Palm-size Air Quality Monitor, and Three-wavelength Nephelometer), have been operated simultaneously during the summer period. Of all, except the passive remote sensing instrument, Microtops II, which uses Sun as the source, all other instruments were operated round-the-clock. All the instruments, except the Palm-size Air Quality (PM_{2.5}) Monitor, have been operated in the University campus site. These data sets archived at one-minute interval have been used to investigate the day-to-day variations in the PM₁, PM_{2.5} and PM₁₀ mass concentrations. The Palm-size Air Quality Monitor (AirBeam) has been used for making mobile observations (from 0800h to 2000h) of air quality at pre-designed locations of pollution in the Delhi NCR during the study period.

RESULTS & DISCUSSION

The PM_{2.5} mass concentration was found to vary from 34 µg/m³ on 15 April 2016 to about 10 µg/m³ (a reduction of about one-third). It is also noted that there was dust- / sand-storm interference with local pollution on 19 and 27 April 2016, which made the PM₁₀ and PM_{2.5} concentrations to increase up to 136 µg/m³ and 30 µg/m³, respectively. Thus, the results clearly indicate that the measurements are significantly affected by the local meteorology as well as long-range transport process of air pollutants, induced by both land and marine processes. Drastic reduction in the visibility on the stormy days (19th & 27th April 2016) is also noted. The BC mass concentration, mainly generated by the transport activity due to incomplete combustion of fuel, showed high concentration (~15 µg/m³) at the beginning of the study period and subsequent decrease from 5.51 to 2.30 µg/m³. This continuous reduction in BC mass concentration suggests that the dust rise due to convection-driven circulation may be more responsible for the observed higher PM concentration. This is consistent with the results of the presence of abundant fine-mode particles in the BC mass concentrations, reported in the literature (for example, Safai *et al.*, 2014). The daily average column-integrated aerosol optical depth (extinction or attenuation of solar radiation) measured at five wavelengths (380, 500, 675, 870 and 1020 nm) showed monotonic increase during the study period.

CONCLUSIONS

The significant results of the study include (i) prominent role of local and long-range pollution sources and underlying meteorological processes in the undulations of pollutant concentrations, (ii) momentous reduction in pollution level of PM_{2.5} and total scattering coefficient (implying increase in visibility) during first half period and enhancement in second half, (iii) noteworthy influence of dust- / sand-storms on local pollution, (iv) drop in BC mass concentration from 5.5 micrograms per cubic meter to 1.1 microgram per cubic meter, (v) increasing trend in columnar AOD, mainly due to dust- / sand-storms during the study period, (vi) enhancement in Angstrom exponent, indicating abundance of fine-mode particles as compared to coarse-mode particles on the days of dust- / sand-storm activity and (vii) significant variations in PM_{2.5} mass concentration at different locations in Delhi.

ACKNOWLEDGEMENTS

The authors are highly grateful to the authorities of AUH, Gurugram. Thanks, are also due to S. Jain, M. P. Alam, T. Paul, S. Tiwari of AUH and A.K. Srivastava and D.S. Bisht of IITM-D (MoES), New Delhi.

REFERENCES

- Devara, P.C.S., M.P. Alam, U.C. Dumka, S. Tiwari and A.K. Srivastava (2017). Anomalous features of black carbon aerosols observed over a rural station during Diwali festival of 2015. In Text Book Series "Water Science and Technology" (Chapter 24), 77, Springer Nature (In Press).
- Gurjar, B.R., J.A. van Aardenne, J. Lelieveld and M. Mohan (2004). Emission estimates and trends (1990–2000) for megacity Delhi and implications. *Atmos. Environ.*, **38**, 5663.
- Kumar, N., A. Chu, and A. Foster. (2007). An Empirical Relationship between PM_{2.5} and Aerosol Optical Depth in Delhi Metropolitan. *Atmos. Environ.* **41**, 4492.
- Lodhi, N. K., S. N. Begum, S. Singh, and K. Kumar (2013). Aerosol Climatology at Delhi in the Western Indo-Gangetic Plain: Microphysics, Long-Term Trends, and Source Strengths." *J. Geophys. Res.*, **118**, 1.

Pandithurai, G., S. Dipu, K.K. Dani, S. Tiwari, D.S. Bisht, P.C.S. Devara, and R.T. Pinker (2008). Aerosol Radiative Forcing during Dust Events over New Delhi, India. *J. Geophys. Res.* **113**, D13209, doi: 10.1029/2008JD009804.

Safai, P.D., P.C.S. Devara, M.P. Raju, K. Vijayakumar and P.S.P. Rao (2014). Relationship between black carbon and associated optical, physical and radiative properties of aerosols over two contrasting environments. *Atmos. Res.*, **149**, 292.

DUST MORPHOLOGY OVER PANCHGAON, HARYANA

P.C.S. DEVARA¹, T. PAUL¹, D.M. GILES², G. BEIG³, P.P. DAS¹, Y. NEENU¹ AND G. KALPANA¹.

¹Amity Centre for Ocean Atmospheric Science and Technology (ACOAST) & Amity Centre for Environmental Science and Health (ACESH), Amity University Haryana (AUH), Gurgaon-122413, India.

²Science Systems and Applications, Inc., NASA Godard Space Flight Center, MD-20771, USA.

³Indian Institute of Tropical Meteorology, Dr. Homi Bhabha Road, Pashan, Pune-411008, India.

KEYWORDS: Aeronet, Mapan, Dust, Aerosols, Calipso.

INTRODUCTION

Dust storm is a natural phenomenon, which refers to erosion, transportation and deposition of dust particles in the atmosphere by strong wind currents. Dust can carry irritate spores, bacteria, viruses, and persistent organic pollutants (Gharai, 2013) which can cause severe health issues when inhaled by human beings. The Inter-governmental Panel on Climate Change (IPCC) and World Meteorological organization (WMO) have recognised dust as one of the major components of atmospheric aerosol, which plays an important role in climate variability. The dust particles usually scatter and absorb the incoming shortwave radiation while they absorb and emit the outgoing longwave radiation. Using the recently installed MAPAN (Monitoring of Air Pollution and Networking) and AERONET (Aerosol Robotic Network) systems have been used to capture a dust event on 21 May 2017. The morphological aspects such as PM₁, PM_{2.5} and PM₁₀ mass concentrations from MAPAN system and Aerosol Optical, microphysical and radiative parameters from AERONET have been analysed. The concurrent observation from MODIS, OMI and CALIPSO satellite have also been used. The results from NAPPS (Naval Aerosol) have also been used to support the inference.

EXPERIMENTAL SITE, DATA AND ANALYSIS

The experimental location, Panchgaon (28.39°N, 76.90°E, 285 m above mean sea level), located in Haryana State, made up of five villages, is a rural station surrounded by Aravalli hillocks. The environment in and around the experimental location is influenced by the Thar desert located in the north-east direction and receives dust through long range transport process associated with complex wind pattern induced by the orography of the surrounding region. It is about 35 km from the capital city, New Delhi and 5 km from the Delhi-Jaipur national highway (NH 8). Although it is a rural station with sparse residential buildings and population, it poses sporadic pollution due to the slow movement of heavy vehicles in the highway. The experimental facilities applied in the present study include (i) AERONET-Multi-Filter Sun-Sky Radiometer, a collaborative project between AUH and NASA, and (ii) MAPAN-Mapping of Air Pollution and Network, a collaborative project between AUH and IITM (MoES). The data from these instruments were used to record the dust storm event, which are then verified with concurrent satellite observations. Complete details of the AERONET and MAPAN systems are available in the literature (Holben *et al.*, 1998; Yadav *et al.*, 2014). The data collected at 15 min interval in the case of AERONET while at 1 min interval in the case of MAPAN have been used in the study. The coincident satellite (MODIS) data have been used to support the observed dust features.

RESULTS & DISCUSSION

The particulate portion of an aerosol is referred to as Particulate Matter or PM, generated from dust sources, can transport over thousands of kms and affect the residents in a vast area even rather far from main sources (Goudie, 2009). Figure 1A displays the daily mean variations of PM₁, PM_{2.5} and PM₁₀, and Figure 1B depicts AOD, observed from 17-25 May 2017. The interesting feature that can be observed from the plots

is that a significant increase in the PM mass concentration and AOD on May 21 may be due to occurrence of a dust storm over the experimental station.

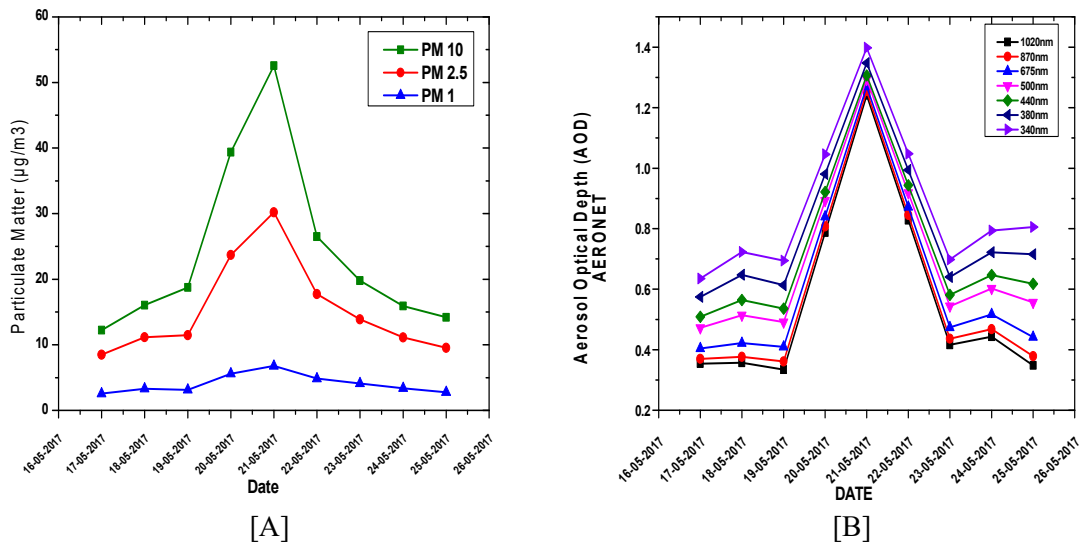


Figure 1: Daily mean variations in MAPAN-PM and AERONET-AOD from 17 through 25, 2017.

CONCLUSIONS

Using the recently installed MAPAN (Monitoring of Air Pollution and Networking) and AERONET (Aerosol Robotic Network) systems have been used to capture a dust event on 21 May 2017. The morphological aspects such as PM_{10} , $PM_{2.5}$, and PM_1 mass concentrations from MAPAN system and Aerosol Optical, microphysical and radiative parameters from AERONET have been analysed. The concurrent observation from MODIS, OMI and CALIPSO satellite have also been used. The results from NAPPS (Naval Aerosol) have also been used to support the inference. The results indicate (i) higher Aerosol Optical Depths (AOD), Particulate Mass Concentration on the dusty day as compared to the neighbouring days, (ii) mono-model volume size distribution on dusty day against bi-model distribution prior and post dusty days, (iii) lower Angstrom Exponent indicating coarse mode dominance and lower SSA values, exhibiting absorbing aerosols, (iv) more perceptible water content, supporting Aerosol growth, (v) larger asymmetry factor, suggesting, delineating more non-sphericity, positive radiative forcing in the atmosphere and also at Top of Atmosphere, exhibiting warming and (vi) long range transport of dust and higher dust mass concentration from HYSPLIT and NAPPS models, respectively.

ACKNOWLEDGEMENTS

This work was supported by the AERONET and MAPAN for which the authors are thankful to NASA, GSFC, USA and IITM, MoES, New Delhi. The authors are also grateful to the authorities of AUH for their constant encouragement and support throughout the work reported in this communication.

REFERENCES

- Biswadip, G. et al. (2013). Monitoring intense dust storms over the Indian region using satellite data- a case study, *Intl. J. Remote Sens.*, **34**, 7038.
- Goude, A.S. (2009). Dust storms: recent developments, *J. Environ Manage.*, **90**, 89.

Holben, B.N. et al. (1998). A federated instrument network and data archive for aerosol characterization, *Remote Sens. Environ.*, **66**, 1.

Yadav, R. et al. (2014). Distributions of ozone and related trace gases at an urban site in western India, L. *Atmos. Chem.*, **71**, 125.

FIRST RESULTS OF AEROSOL CHARACTERIZATION USING A POLAR NEPHELOMETER AT AUH, GURGAON

P.C.S. DEVARA¹, D.S. NICHOLAS², M. KUMAR², T. PAUL¹, P.P. DAS¹, Y. NEENU¹ AND G. KALPANA¹

¹Amity Centre for Ocean Atmospheric Science and Technology (ACOAST) & Amity Centre for Environmental Science and Health (ACESH), Amity University Haryana (AUH), Gurgaon-122413, India.

²Ecotech Pty Ltd., Knoxfield, VIC 3180, Melbourne, Australia.

KEYWORDS: Polar Nephelometer, Multiwavelength, Scattering Coefficient, Horizontal Visibility.

INTRODUCTION

Aerosols over any location is due to a combination of local sources and long-range transport which can result in a variety of mixing (both internal and external) states. Through their scattering and absorption properties, aerosol particles also affect visibility, air quality (Horvath,1995) and human health (Nadadur and Hollingsworth, 2015). Integrating Nephelometers offer a direct method of measuring light scattering by airborne particles, but they have angular integration limitations (Muller *et al.*, 2005). Moreover, nephelometers occupy an important position in monitoring climate-related aerosol properties, that is, spectral total, backward and forward scattering coefficients (Rama Gopal *et al.*, 2014). Aerosol characterization experiments, employing an Ecotech Model Aurora 4000 Integrating Polar Nephelometer with a backscatter-attachment, have been in progress since 2017 at Amity University Haryana, Gurgaon, India. The environment in and around the site is rural, and the sampling site is enveloped by Aravalli hillocks, making the terrain a valley. Thus, results reported in this paper are unique from the terrain-induced boundary layer in a changing rural environment and associated local circulation-affected pollution. In the present paper, we report and discuss some of the interesting aspects such as (i) space-time-spectral variations of aerosol total and backscattering coefficients, (ii) asymmetry parameter, (iii) relationship with local meteorological parameters, PM_{2.5} and PM₁₀ mass concentrations, (iv) horizontal visibility, and (v) comparison between weekdays and weekend scattering coefficients from the measurements made on some typical days in 2017.

INSTRUMENTATION & DATA

Aerosol characterization experiments have been conducted over the Amity University Haryana (AUH), Gurgaon, employing an Ecotech model Aurora 4000 Polar three-wavelengths (450nm Blue, 525nm Green and 635nm Red) integrating nephelometer with an embedded backscatter attachment. These features allow a greater range of light scattering measurements beyond what simple backscatter can give. The Aurora will measure, continuously and in real-time, light scattering in a sample of ambient air due to the presence of particulate matter (specifically, the scattering coefficient σ_{sp}) at three wavelengths. The polar nephelometer is unique in the sense that it has a backscatter shutter that can be set to any angle from 10° through 90° at up to 17 different positions. When the backscatter shutter is positioned at a specific angle the nephelometer measures the light scattering from that angle, through to 170°. In the present study, the hourly and daily mean variations of the scattering and related properties of atmospheric aerosols on some typical days during 2017 over the site More details can be found in Ecotech Technical Report (2015).

RESULTS & DISCUSSION

A typical plot of diurnal variation of total aerosol extinction at three wavelengths, observed on 13 September 2017 is shown in Figure 1. This plot clearly depicts an initial increase, gradual decrease as the

day progresses, minimum during noon hours. This may be attributed to the lifting of atmospheric boundary layer and resulting ventilation of pollutants and decrease in aerosol scattering coefficient.

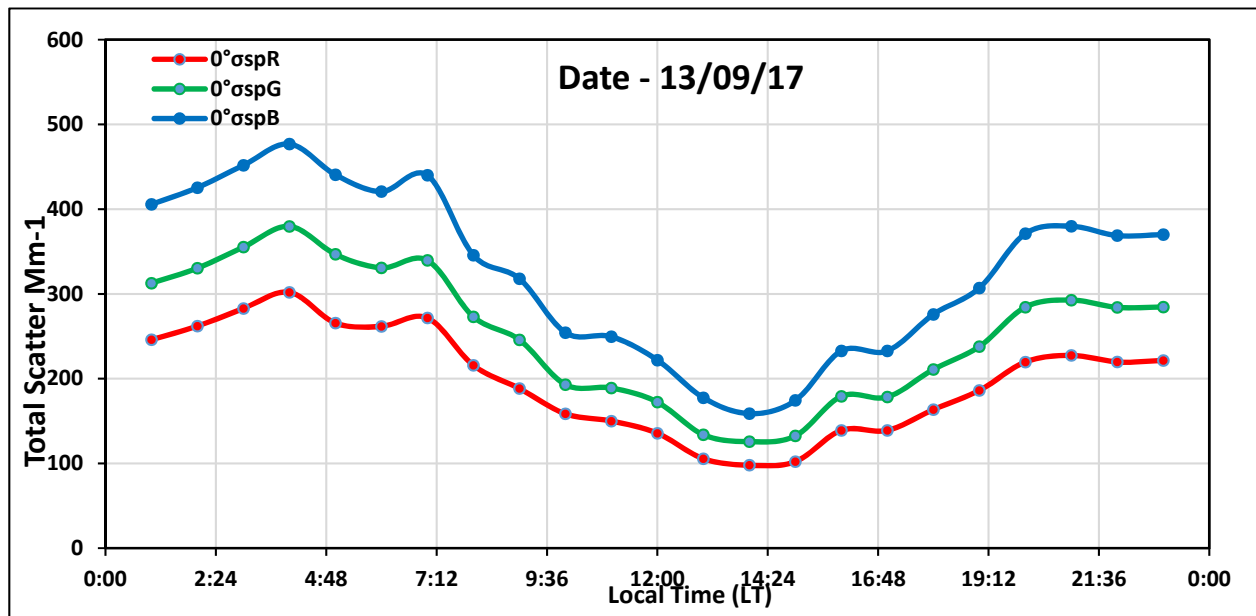


Figure 1: Spectral-time variation of aerosol scatter observed on 13 September 2017, a clear-sky day.

CONCLUSIONS

For the first time, a tri-wavelength polar nephelometer has been operated over the AUH region. The significant results obtained on some typical experimental days in 2017 are presented. The time variation of scattering coefficient revealed a deep minimum around noon hours while the linear visibility showed opposite variation. The mean variation in the scattering coefficient (signature of air pollution) is found to be more on weekdays and less on weekends, which is consistent.

ACKNOWLEDGEMENTS

This work was supported by an India-Australia Collaborative Research Project, for which the authors are thankful to AUH and Ecotech. The authors are also grateful to the authorities of AUH for their constant encouragement and support throughout the work reported in this communication.

REFERENCES

- Ecotech Technical Report (2015). <https://www.ecotech.com/wp-content/uploads/2015/.../Aurora-4000-User-Manual.pdf>
- Horvath, H. (1995). Estimation of the average visibility in Central Europe. *Atmos. Environ.*, **29**, 241.
- Müller, T., A. Nowak, A. Wiedensohler, P. Sheridan, M. Laborde, D. S. Covert, A. Marinoni, K. Imre, B. Henzing, J-C Roger, S. M. Santos, R. Wilhelm, Y-Q Wang and G. Leeuw (2009). Angular illumination and truncation of three different integrating nephelometers: Implications for empirical, size-based corrections. *Aerosol Sci. Tech.*, **43**, 581.

Nadadur, S. S. and Hollingsworth, J. W. (Eds.). (2015). *Air Pollution Health Effects*, Springer London, 439p.

Rama Gopal, K., A.P. Lingaswamy, M.A. Shaik and S.S. Babu (2014). *In-situ* measurements of atmospheric aerosols by using integrating nephelometer over a semi-arid station, South India. *Atmos. Environ.*, **86**, 228.

INFLUENCE OF BLUE MOON PHENOMENON ON THE TEMPORAL VARIATION OF ATMOSPHERIC POLLUTANTS IN AN NCR OUTSKIRT LOCALITY; A GIS APPROACH

NEENU YADAV¹, KALPANA GARSA¹, P. P. DAS^{1*}, P.C.S. DEVARA¹

¹Amity University Haryana, Gurgaon – 122 413, India

(*Correspondence at: prabhuprasaddas@gmail.com)

INTRODUCTION

Atmospheric turbidity exists in atmosphere with atmospheric aerosol load. Aerosols are solid, liquid and gaseous particles suspended in the atmosphere having size ranging from 10^{-3} μm to 10^{-2} μm . These particles are either emitted from natural sources (such as volcanic eruptions, dust storms, forest and grassland fires, sea spray, etc.) or of anthropogenic origin (such as the burning of fossil fuels). Gaseous pollutants such as CO, NO₂, SO₂ and particulate matter (PM) from both of the above sources significantly affect human welfare and the case of the National Capital Region (NCR) of India is no different with pronounced air pollution being witnessed for the past couple of years. While the effect of various atmospheric processes such as dust storms etc. has been investigated by environmental researchers, studies on the effect of astronomical phenomena on air pollution particularly the interrelationship between these events and gaseous pollutants as well as PM is very scarce.

The present study investigated the effect of blue moon occurrence on the activity of gaseous air pollutants including CO, NO₂, SO₂ and PM in a suburban NCR region. at Amity University Haryana campus (AUH), Panchgaon. (latitude=28°32'North, longitude=76°55'East, station level=285 m above mean sea level). The site is about 60 km from Delhi and comes within the NCR. It is surrounded by fields from three sides and on fourth side there are hillocks (Aravali hills) of average height 50 m. Site is located in outskirts of Gurgaon (north –east direction) which is densely populated. Pollution from this area is moderated by hillocks.

KEYWORDS: Aerosol, Turbidity, Blue moon, GIS, DEM

METHODS

The concentration of gaseous pollutants and PM were collected in Air Quality Monitoring Station (AQMS) situated at AUH. The collection belongs to a real time observation of 15minute resolution. For the present study 30 days of data (15 days each before and after the occurrence of blue moon on 31st January 2018) was analyzed. The concentration of the gaseous pollutants for every 15minute were interpolated in geographic information system (GIS) to create digital elevation models (DEMs) where the elevation is represented by pollutant concentration. Thus, the research involved the interpretation of 180 DEMs involving CO, NO₂, SO₂, PM₁, PM_{2.5}, PM₁₀ activity to find out the effect of blue moon on air gaseous pollution.

RESULT AND DISCUSSION

Analysis of the modelled surfaces portray a noteworthy influence of blue moon on pre-occurrence air pollution. Data indicates a significant higher diurnal concentration from 15th January to 24th January. However, the activity was more pronounced for night time from 24th to 30th January just before the occurrence of the phenomenon on 31st January 2018. However, the diurnal pollution predominates that of the night time once the phenomena was over. This distinct shift of pollutant activity during night time close

to the occurrence of the event indicates a noteworthy influence of moon's radiation (presumably more longer wavelength radiation) on air pollutants.

CONCLUSION

While significant knowledge has been gained on the influence of atmospheric processes on air pollution, that of astronomical phenomena on air pollution is scarce. Present study investigates the blue moon astronomical phenomena on air pollutants in a suburban region of NCR. The results indicate a distinct shift of night time pollution from that of day time just before the occurrence of the phenomena. The observation may be attributed to the increasing longer wavelength radiation influence on air pollutants.

ACKNOWLEDGEMENTS

The authors sincerely acknowledge the support provided by the ACOAST, AUH for the present research.

SPATIAL AND TEMPORAL VARIATION OF PARTICULATE MATTER AND GASEOUS POLLUTANTS IN DELHI FOR 2018 YEAR

SHASHI TIWARI¹, SAGNIK DEY² AND SADIQA ABBAS¹

^{*1}Manav Rachna international institute of research and studies, Faridabad, India

^{*2}Center of Atmospheric Science, Indian Institute of Technology, Delhi, India

KEYWORDS: PM_{2.5}, in-situ data, Satellite, Delhi, GWR

ABSTRACT

High-resolution temporal and spatial air pollution data are imperative to understand the physical and chemical processes affecting air quality. The data were collected for this analysis is especially of 2018 since many monitoring sites had not been established before 2018. The data of PM_{2.5}, PM₁₀, SO₂, CO, NO₂, and O₃ at 36 stations during January 2018 to October 2018 were collected to uncover the spatial and temporal variation of the pollutants in Delhi. The mean concentrations of PM_{2.5} exceeded the permissible limit for Ambient Air Quality for 87% of the Delhi areas in winter while it decreased to 17% in the monsoon season. Whereas the O₃ level increased dramatically during summer season but surprisingly not at all the sites of Delhi. During the autumn and winter months, million tons of crop residues are burnt, and winds blow from India's north and northwest towards east, this could be the reason of frequently Observed high pollution days in the east region of Delhi. During summer season in the month of June the pollutant concentration again goes high compared to March that is justified by seeing fire count data in Delhi and nearby during last days of May and June months. Pearson correlation analysis indicated that all of the pollutants exhibited significant correlation one another. PM₁₀ was a major pollutant affecting the air quality of Delhi in all of the seasons, 86% of Delhi areas are polluted in even monsoon season having the least concentration. Both SO₂ and NO₂ exerted significantly adverse effects on the air quality in spring and autumn, but CO pollutant behavior is difficult to understand since it is highly varying with stations irrespective of season. O₃ was found to be the dominant species among the pollutants affecting the air quality in summer, showing unexpectedly very high concentration at Punjabi Bagh and RK Puram. The in-situ data for various pollutants is compared with respect to satellite data for air pollution. However Pearson correlation analysis and grey correlation analysis could not be utilized to investigate the spatial correlation of AQI and the pollutant levels. Thus geographical weight regression model (GWR) was used to produce the coefficient of determination (R²) and local regression coefficients for each area mapped to show the spatial variability.

INTRODUCTION

High-resolution temporal and spatial air pollution data are imperative to understand the physical and chemical processes affecting air quality. Apart from the effects of PM, gaseous pollutants also play significant roles on human health and environment. For example, the accumulation of many gaseous pollutants including CO, SO₂, NO₂, and O₃ increased the susceptibility to respiratory diseases and reduced the lung fraction, thereby leading to hematological problems and cancer. The in-situ data for various pollutants is compared with respect to satellite data for air pollution. The aim of this study is (1) to understand the correlation of six pollutants and determine the dominant factor for the air quality index, (2) to decipher the seasonal variation of six pollutants and identify key factors, To the best of our knowledge, hardly any studies have concerned about ambient pollutants covered the data of multi observation stations and assessed the spatial variation of the pollutants in Delhi through spatial interpolation methods.

METHODS

The real-time hourly concentrations of PM_{2.5}, PM₁₀, CO, SO₂, NO₂, and 8-h O₃ at 37 stations were downloaded from the website of central pollution control board. The data of six criteria pollutants at 37 cities from January 2018 to October 2018 were collected because many monitoring sites had not been established before 2018. The mean concentrations of the species were calculated on the basis of the data supplied by the monitoring sites at each station. The accuracy, consistency, and validity of the data have been checked based on some methods, as well as comparison with the previous data. Moreover, at least 30 daily mean concentrations except in February were applied to calculate monthly mean concentration of six criteria pollutants. Pearson correlation analysis was used to decipher the relationships between AQI and the concentrations of six criteria pollutants. Grey correlation analysis (GCA) was used to determine the predominant factor affecting air quality in Delhi. However, Pearson correlation analysis and grey correlation analysis could not be utilized to investigate the spatial correlation of AQI and the pollutant levels. Thus, geographical weight regression (GWR) model was used to produce the coefficient of determination (R²) and local regression coefficients for each city of the study areas, which were then mapped to show the spatial variability. Thus, IDW interpolation method was selected to generate spatially continuous values to explore the spatial distribution of the pollutants. All of the statistical analysis and figures shown herein were performed by the ArcGIS 10.4 for Windows.

RESULTS AND DISCUSSION

The Monthly average concentrations of PM_{2.5} ranged from 288 µg/m³ (DTU) in the month of January to 27 µg/m³ (Najafgarh) in the month of September. The monthly mean concentrations of PM₁₀ varied between 430 µg/m³ (at Anand Vihar) in the month of January and 77 µg/m³ (at Najafgarh) in the month of September. The mean concentrations of NO₂ ranged from 131 µg/m³ (at Anand Vihar) in the month of January to 10 µg/m³ (at Bawana) in the month of September. However, O₃ was a major pollutant in summer, implying that the pollution was promoted by the photochemical processes due to the strong solar radiation. For PM₁₀ Rohini, Jahangirpuri, Ashok Vihar, Mandir Marg, Anand Vihar, Sonia Vihar, are the most polluted areas among all having concentration above 300 µg/m³ in the month of January and February. The PM₁₀ concentration from February month to March goes down. Surprisingly again in the month of April pollutant concentration increased suddenly. Again from July to August month PM₁₀ concentration goes high. One thing to be noticed here in map for PM₁₀ concentration Punjabi Bagh was at minimum. While for PM_{2.5} and NO₂ concentration, Punjabi Bagh is second highest after Anand vihar while lowest concentration is at Lodhi road. At Narela station PM₁₀ concentration were high while for NO₂ these areas concentration is low, same with more nearby stations. This indicates North West area is more prone to dust pollution. During the autumn and winter months, million tons of crop residues are burnt, and winds blow from India's north and northwest towards east, this could be the reason of frequently Observed high pollution days in the east region of Delhi. In the month of June NO₂ concentration goes down to significant value. All the stations except RK Puram, ITO, Punjabi bagh has concentration under 50. In July month all stations has concentration under 50. The reason of lowest concentration of pollutant PM₁₀ and PM_{2.5} in monsoon season may be due to particulate matter wash off or any other chemical reaction involved. CO has no clear trend month wise. The reason could be the vehicular emission is different at different stations. Ozone concentration is highest at all stations either in the month of April or May. Interestingly, Punjabi

Bagh and RK Puram station has shown very high concentration, it is also to be noticed that these mentioned stations has very low PM₁₀ concentration. Weak sunlight in winter could inhibit the formation of O₃ because the formation of O₃ depended on the intensity of solar radiation. Furthermore, high temperature and strong solar radiation tended to generate large amount of OH radical, resulting in the formation of O₃ through the reaction of VOC and OH radical.

CONCLUSIONS

PM_{2.5} at 84% stations has exceeded the permissible limit in winter season this percentage has decreased to 78% to 17% for season summer and monsoon consecutively. NO₂ at 27% stations has exceeded the permissible limit in winter season. PM₁₀ concentration at all stations has exceeded the permissible limit throughout year. Fortunately the mean concentrations of SO₂ and CO are below the permissible limit throughout all months at all stations. However, the O₃ concentration peaked in spring and summer, which was associated with the strong stratosphere troposphere exchange process and solar radiation. SO₂ and NO₂, exerted significantly adverse effects on the air quality in winter and autumn. O₃ displayed high level in summer, inferring the impacts promoted by photochemical process. Coal combustion, biomass burning, crop burning (November-December is time for post-harvest period of the monsoon crop of paddy— when farmers burn crop residue), Low temperature, less boundary height, weaker winds may be the reason for winter high concentration. During summer season in the month of June the pollutant concentration again goes high compared to March that is justified by seeing fire count data in Delhi and nearby during last days of May and June months. In 2018 during last days of April fire count data has increased by 42% compared to March month. The PM_{2.5} & NO₂ concentration trend is somewhat alike for few stations, but not for all showing the pollutant sources are different for PM_{2.5} & NO₂ at many places.

ACKNOWLEDGEMENTS

This work was supported by CPCB.

REFERENCES:

- Rui Li, Lulu Cui , Junlin Li , An Zhao , Hongbo Fu , Yu Wu ,2017. Spatial and temporal variation of particulate matter and gaseous pollutants in China during 2014-2016. *Atmospheric Environment* 161 (2017) 235-246.
- Salvi, S. et al., 2018 "The burden of chronic respiratory diseases and their heterogeneity across the states of India", *The Lancet Global Health*.

GRADIENTS IN PM_{2.5} AND ITS RELATION WITH MODIS AOD OVER INDIAN MEGA CITIES

B.MAHESH¹, K.NIRANJAN¹ and V.SREEKANTH¹

¹Department of Physics, Andhra University, Visakhapatnam-530003

KEYWORDS: Aerosols, Air Pollution, Human Health, Aod, Pm_{2.5}

ABSTRACT:

Keeping in view the growing interest in the air pollution attributed morbidity and mortality, this study investigates the levels of ambient fine particulate matter and empirical relations between Aerosol Optical Depth (AOD) and PM_{2.5} mass concentrations established over five Indian mega cities. over the rapidly developing and agglomerating Indian cities. Despite several measures and pollution mitigation strategies being implemented over Delhi, it recorded the highest PM_{2.5} among all the study cities, across all the seasons, in all the times of the day. The annual mean (\pm standard deviation) PM_{2.5} is found to be $\sim 37 \pm 17$, 51 ± 23 , 54 ± 36 , 80 ± 67 , 114 ± 86 over the cities of Chennai, Hyderabad, Mumbai, Kolkata and Delhi respectively. Winter season is the most hazardous among others, with almost all of its days exceeding the WHO threshold for daily mean PM_{2.5}. Based on the annual and seasonal segregation of the daily mean PM_{2.5}, a clear northward increasing trend is observed in i) mean PM_{2.5}, ii) median PM_{2.5}, iii) spread in the PM_{2.5} distribution, iv) skewness in the PM_{2.5} distributions, v) percentage number of days when PM_{2.5} exceeding the WHO and Indian NAAQS. Similarly, based on the annual and seasonal mean diurnal variations, it was found that the i) number of polluted hours in a day ii) departure of hourly PM_{2.5} concentrations from WHO and Indian air quality thresholds iii) difference between the maximum and minimum hourly PM_{2.5} concentrations increase as we move from CHN in the south to DEL in the north. In colder seasons (PMON and WIN), over MUM, KOL, DEL the rush hour traffic peak PM_{2.5} concentrations are comparable to that of mid-night highs. On the other hand, the diurnal variations over CHN and HYD are characterized by two well-developed peaks. Over all the study cities, MON season recorded the lowest PM_{2.5} concentrations and no clear diurnal pattern is observed over this season. Weekday and weekend daily mean PM_{2.5} distributions are similar, statistics are comparable; MUM and KOL exhibiting a small decrease in concentrations during weekends. The demographic factors influencing the concentrations and the modulations by weather and other natural phenomena were thoroughly discussed.

The relations (linear and quadratic) are sought to predict the surface PM_{2.5} mass concentrations from high resolution columnar AOD datasets. Current study utilizes multi-city public domain PM_{2.5} data (from US Consulate and Embassy's air monitoring program) and MODIS AOD, spanning for almost four years. PM_{2.5} is found to be positively correlated with AOD. Station-wise linear regression analysis has shown spatially varying regression coefficients. Similar analysis has been repeated by eliminating data from the elevated aerosol prone seasons, which has improved the correlation coefficient. The impact of the day to day variability in the local meteorological conditions on the AOD-PM_{2.5} relationship has been explored by performing a multiple regression analysis. A cross-validation approach for the multiple regression analysis considering three years of data as training dataset and one-year data as validation dataset yielded an R value of ~ 0.63 . The study was concluded by discussing the factors which can improve the relationship.

The statistics and analysis presented in the manuscript are highly useful for the policy makers to strategize their region-specific mitigation efforts.

STUDIES ON CARBONACEOUS AEROSOLS FROM A HIGH ALTITUDE SITE IN THE CENTRAL HIMALAYAS

PRIYANKA SRIVASTAVA¹, MANISH NAJA¹, RAJESH KUMAR², HEMA JOSHI³, U C DUMKA¹, MUKUNDA M GOGOI⁴, S. SURESH BABU⁴

¹ Aryabhata Research Institute of Observational Sciences (ARIES), Nainital, India

² National Center for Atmospheric Research (NCAR), Boulder, USA

³ Indian Institute of Technology Kanpur (IIT Kanpur), Kanpur

⁴ Space Physics Laboratory (SPL), VSSC, ISRO, Trivandrum

KEYWORDS: Carbonaceous Aerosols, Bc, Ec, Oc, Co, CO₂, CH₄

INTRODUCTION

Carbonaceous aerosols are very important due to their direct effects on health, radiation budget and their indirect effect in altering cloud properties, thus acting as short term climate forcers. Simultaneous measurements of BC, CO, CH₄ and CO₂ have particular importance in terms of radiation budget, constraining emission sources and tropospheric chemistry. In this reference, extensive observations of aerosols and trace gases (CO, CO₂ and CH₄) are carried at ARIES, Manora Peak, (29.4°N, 79.5°E, 1958 m amsl). Temporal variations of these species are discussed here. A five particles back-air trajectory analysis from HYSPLIT utilizing residence time of air masses over the defined region of Northern India has been used to correlate simultaneously elevated levels of these trace gases and aerosols. Longitudinal spread of these air masses over different seasons has also been studied. Observations of CO along with BC have also been used to identify the role of different emissions sources. Some episodic events have also been identified and analysed over the period of study. Source identification (mainly wood burning and fossil fuel combustion) using various statistical and chemical methods has also been extensively conducted. More details of this work will be presented.

METHODS

BC observations: BC measurements were made using Aethalometer, which measures the mass concentration based on the optical attenuation of light beam at seven wavelengths with a time resolution of 2 min for a period 2014-2017. Pressure, temperature, multiple scattering and loading corrections were applied to remove the artifacts associated in the measurements.

OC-EC observations: The abundances of carbonaceous species (OC and EC) were measured by a EC-OC analyzer (Sunset Lab, USA) using a thermo-optical transmittance (TOT) protocol. The instrument apportions OC and EC utilizing thermal, chemical and optical properties.

CO₂, CO and CH₄ observations: For the simultaneous measurements of CO, CH₄ and CO₂, a Cavity Ring-Down Spectroscopy based Picarro G2401 analyzer (Picarro Inc., CA, USA) is used. The CRDS technique deploys an optical cavity with highly reflective mirrors where the optical absorbance of the gases is determined by the light dissipation rate in the optical cavity.

RESULTS & DISCUSSIONS

Temporal Variations in BC, EC-OC, CO₂, CH₄, CO

Strong seasonal and diurnal variations were observed in averaged total carbon (TC=EC+OC) during 2014-2017 period. In general, total annual average of BC concentration at the site is about 1000 ng/m^3 with the highest concentrations during winter season (DJF).

Seasonal average is about 1360 ng/m^3 in winter period. BC concentration shows a drastic decrease to average of only about 750 in monsoon season (JJA), with the seasonal mean BC falling to less than half

the value that prevail in other seasons (Fig 1). Extensive monsoon rainfall (totalling to 68% of the annual, occurring at the site and might be responsible for such washout of BC aerosols which suggest strong wet scavenging.

EC-OC, CO show higher levels during the day and the diurnal variations are of similar pattern to that of BC but have opposite pattern when compared with those of CO₂. Such a pattern in CO is associated with upslope winds that bring relatively polluted air from the low-altitude areas to the mountaintop. The daily average CO levels are observed to be higher occasionally (550 ppbv and more) during spring. CO₂ and CH₄ also show unimodal diurnal variations and are mostly anti-correlated. While CH₄ peaked during the mid-noon, due to the increased consumption by photosynthesis CO₂ -showed a dip around the same period every season.

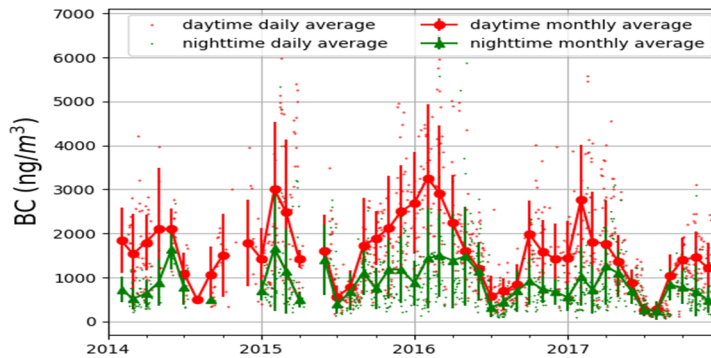


Fig 1. Variations in day and night time black carbon during 2014–2017 period at Nainital.

Influence of Air Mass Transport

Correlation of seasonal BC concentration with the seasonal residence time of these air masses was carried to see the contribution of different air masses to BC concentration as shown in Fig 2.

Highest correlation was found for the winter season indicating maximum BC contribution from NW direction, most likely due to stagnated air mass at lower altitudes in winter. Spring and autumn had intermediate coefficient values due to relatively faster air masses. Lowest correlation was observed during summer-monsoon and could be due to origin of these air masses from the oceanic regions which are poor in BC and also leads to dilution of continental emissions after it reaches the site. This method of evaluating BC contribution from different air masses is consistent with the cluster weighted analysis of trajectories.

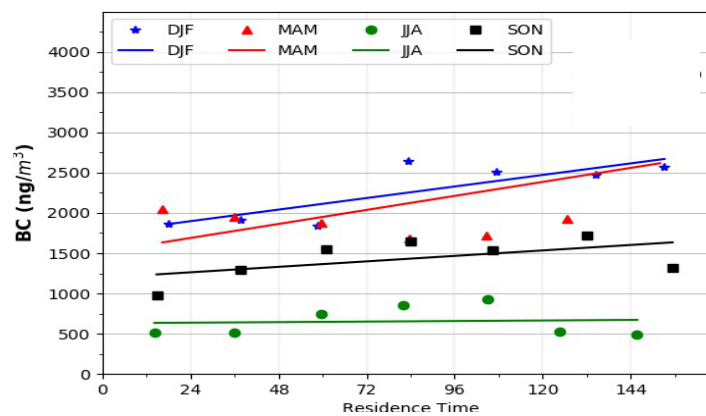


Fig 2. Scatterplot showing correlations between BC and residence time in four seasons for 2014-2017 period.

BC-CO Correlation

BC and CO correlation showed a stronger positive correlation during the winter, when compared with spring or autumn. It seems to be largely due to significant contribution of local sources. Additionally, the boundary layer processes could be playing an important role in winter. Lifetime of CO is much higher than BC and hence, long-distance travel by BC in other seasons (e.g. influence of the marine air-mass or other regional air-masses) might have greater dilution/loss thereby poorer correlation. Slope obtained also indicate variable seasonal combustion efficiencies.

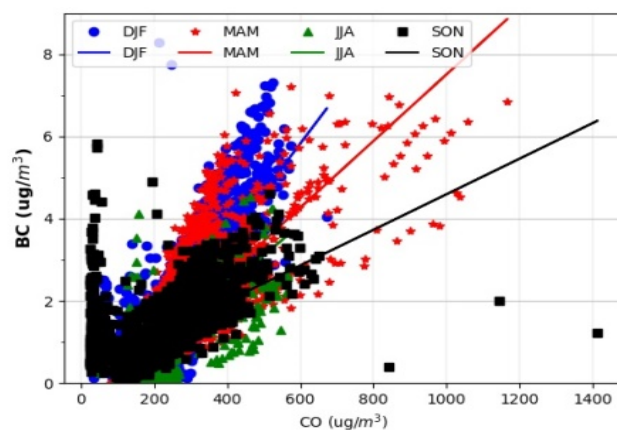


Fig 3. Scatterplot showing correlations between BC and CO in four seasons for 2014-2017.

Source Identification

Emissions of aerosols in this region are mainly from wood burning and fossil fuel combustion. Since both these sources have variable absorption in different wavelengths, angstrom exponent for 370–520nm and 660–950 nm was used to provide a better description of the wavelength dependence from the UV- to the near-IR region. Angstrom exponent was minimum in monsoon and varied from about 0.4 to about 1.3 on an average for the whole period. The light absorption at the lowest and highest wavelengths showed clearly distinct diurnal cycles. Also the biomass burning and fossil components were separated and dominance of fossil fuel component was noticed. Distinct diurnal and seasonal cycles were found for both the components. This method was also validated using measured OC/EC ratio and had consistent result with lower OC/EC ratio.

CONCLUSIONS

1. BC, EC/OC, CO, CO₂ and CH₄ all show unimodal seasonal variations with only CO₂ having lower concentration in day time while all other parameters have a daytime peak. This could mainly be due to increased biogenic photosynthesis which is a major CO₂ sink. On the other hand, other parameters are strongly associated with the evolutions of atmospheric boundary layer dynamics.
2. Seasonal variation of BC, EC/OC aerosols and CO showed high concentration during the dry winter seasons and low concentration during the monsoon seasons. CO however has maxima in spring and a broader elevated structure than BC in summer monsoon showing greater wet scavenging efficiency of BC than CO.
3. Correlation of seasonal mean BC mass concentrations CO indicates the influence of fresh emissions and common combustion sources mainly in winter/spring.
4. It is inferred from trajectory analysis that the long-range transport from North and North West (Africa

and Europe) might also influence BC concentration at the site apart from the influence of regional pollution and transports from the IGP region.

5. Angstrom exponent and absorption of BC in UV and IR channels show influence of different sources at the site. OC/EC ratio and wavelength based statistical source segregation show dominance of fossil fuel based sources.

ACKNOWLEDGEMENTS

Authors are thankful to the support provided by ISRO-ARFI, ISRO-ATCTM and ARIES for this project.

FOSSIL FUEL VS WOOD BURNING BLACK CARBON COMPONENTS IN SOUTHERN DELHI OUTSKIRTS

U. C. DUMKA¹, P.C.S. DEVARA², D. G. KASKAOUTIS³, R. KUMAR⁴, S. KUMAR¹, and S. TIWARI⁵

¹Aryabhata Research Institute of Observational Sciences, Nainital, 263 001, India

²Amity Centre for Ocean-Atmospheric Science and Technology, University of Haryana, Gurgaon 122413, India

³Institute for Environmental Research and Sustainable Development, National Observatory of Athens, 118 10, Athens, Greece

⁴Indian Metrological Department, Lodhi Road, New Delhi – 110 003, India

⁵Indian Institute of Tropical Meteorology, Pune – 411 008, India

⁵Indian Institute of Tropical Meteorology, New Delhi Branch, New Delhi -110 060, India

KEYWORDS: Black Carbon, Aethalometer Model, Fossil-Fuel Combustion, Wood Burning.

INTRODUCTION

Due to the rapidly increasing economic growth, energy demands, industrialization/urbanization, traffic, coal-based thermal power plants, brick-kilns, house-hold biofuel combustion for heating and cooking purposes and agricultural crop residue burning over India, large amounts of black carbon (BC) aerosols have been accumulated, particularly over the Indo-Gangetic Plains. In this study, we analyse year-long (April 2015 to March 2016) measurements of real time BC mass concentrations, carried out via a seven wavelength portable Aethalometer at a rural site in southern Delhi outskirts (~50 km away from the city center). We present the temporal variation of BC mass concentration and assess the contribution of BC_{ff} and BC_{wb} (fossil-fuel and wood burning components of BC) to the total BC mass on daily, monthly and seasonal basis.

EXPERIMENTAL SITE AND MEASUREMENTS DETAILS

The BC measurements were carried out at Panchgaon, a village located ~50 km from the Delhi center in the Indian state of Haryana. Two major cities namely Gurgaon and Manesar that host several small and large scale industries are located northeast of the observational site. Furthermore, the site is influenced by dust aerosols mostly in the pre-monsoon and monsoon seasons through long-range transport from Thar Desert, located about 200 km away in southwest. Further details about the measuring sites can be found in Devara et al. (2016). The BC mass concentration measurements were carried out from April 2015 to March 2016 using a seven channel portable Aethalometer (AE-42, Magee Scientific, USA) at a sampling interval of 5 min (10 m above the ground level) and a standard flow rate of 5 liters per min.

RESULTS & DISCUSSIONS

The temporal variations of daily mean BC, BC_{ff} and BC_{wb} for the study period are shown in Fig 1. The total BC mass concentration shows a distinct seasonal pattern with low values ($4.6 \pm 0.2 \mu\text{g m}^{-3}$) in summer (June-July-August) and high ($9.3 \pm 0.7 \mu\text{g m}^{-3}$) in winter (December-January-February). The annual mean BC at 880 nm is $7.2 \pm 0.3 \mu\text{g m}^{-3}$ (range of 0.09 – 38.6 $\mu\text{g m}^{-3}$). The high values (above 15 $\mu\text{g m}^{-3}$) during November and December are mostly attributed to the influence of transported smoke plumes from the agricultural residue burning in northwest India (Kaskaoutis et al., 2014). Further, we estimated the fossil fuel and wood/biomass burning components of the BC mass using the “Aethalometer Model” approach. The estimated BC_{ff} mass concentration accounts for 81% of the total BC mass on annual basis, whereas the BC_{wb} ranges from $0.55 \pm 0.06 \mu\text{g m}^{-3}$ in July to $2.7 \pm 0.2 \mu\text{g m}^{-3}$ in December. The highest BC_{ff}/BC fraction

was observed in April-June (~86 - 87% at 880 nm), while the BC_{wb}/BC peaks in October - December (23 - 29% at 880 nm).

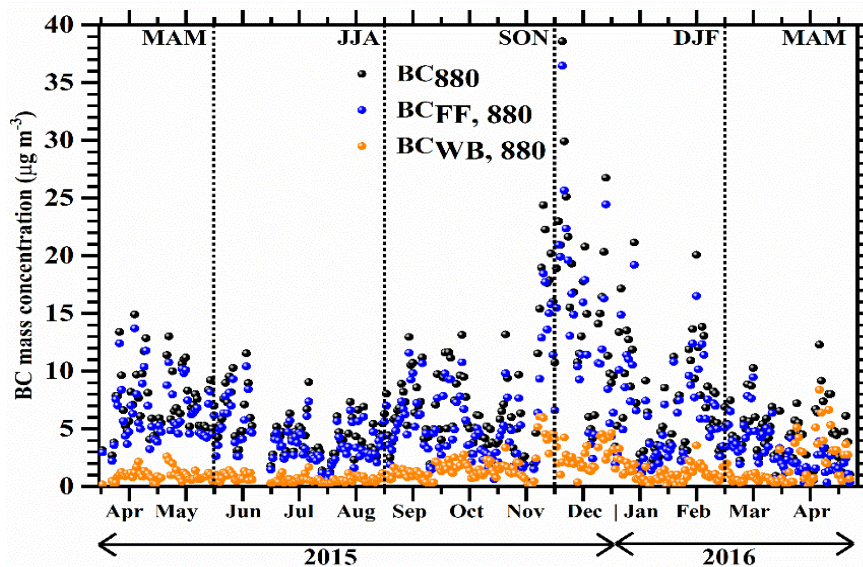


Figure 1: Temporal variation of BC, BC_{ff} and BC_{wb} mass concentration during the study period.

CONCLUSIONS

The main findings of this research are summarized as follows:

1. The BC emitted from the fossil-fuels (BC_{ff}) contributes 81% (annually) to the total BC concentration.
2. A larger fraction of BC from wood/biomass burning (BC_{wb}) was observed during the evening and night hours in the winter season.

ACKNOWLEDGEMENTS

Authors gratefully acknowledge the Director ARIES and Vice-Chancellor Amity University Haryana for providing all kind of infrastructure and supports for the measurements.

REFERENCES

Devara, P.C.S., Alam, M.P., Dumka, U.C., Tiwari S., Srivastava A.K., (2016). Anomalous features of black carbon and particulate matter observed over a rural station during Diwali festival of 2015. In Text Book Series “*Water Science and Technology*”, Springer (in Press).

Kaskaoutis, D.G., Kumar S., Sharma D., Singh R.P., Kharol S.K., Sharma M., Singh A.K., Singh S., Singh A., Singh D., (2014). Effects of crop residue burning on aerosol properties, plume characteristics and long-range transport over northern India. *J. Geophys. Res.* 119, 5424-5444, doi: 10.1002/2013JD021357.

AEROSOL AND POLLUTANT ASSESSMENT WINTERTIME IN DELHI : THE WIFEX CAMPAIGN

U. C. DUMKA¹, SURESH TIWARI², D. G. KASKAOUTIS³, S.D. ATTRI⁴, V. K. SONI⁴, P.D. SAFAI⁵
AND NARENDRA SINGH¹

¹Aryabhata Research Institute of Observational Sciences, Nainital, 263 001, India

²Indian Institute of Tropical Meteorology, New Delhi Branch, New Delhi -110 060, India

³Institute for Environmental Research and Sustainable Development, National Observatory of Athens, 118 10, Athens, Greece

⁴Indian Metrological Department, Lodhi Road, New Delhi – 110 003, India

⁵Indian Institute of Tropical Meteorology, Pune – 411 008, India

KEYWORDS: Black Carbon, Delhi, Boundary-Layer Dynamics, Aethalometer Model.

INTRODUCTION

During the last decades, the carbonaceous aerosol [such as elemental carbon, (EC); black carbon (BC); organic carbon, (OC)] emissions exhibit an increasing trend over the globe, particularly in the developing south and east Asian countries, pointing out the need for detailed assessment of the levels and source apportionment close to the source. In the present work, we analyse experimental datasets consisted of continuous measurements of BC mass concentration, scattering, absorption and extinction aerosol coefficients, along with intensive aerosol properties [e.g single scattering albedo (SSA), extinction and absorption Ångström exponents (SAE and AAE, respectively)], air pollutants (CO, NO_x, O₃) and meteorological observations carried out during the winter fog experiment (WIFEX) that had been taken place in Delhi during wintertime (December 2015 to February 2016).

EXPERIMENTAL SITE AND MEASUREMENT DETAILS

The measurement sites were located in the greater Delhi region, with a total population of ~17 million, which is among the most polluted cities over the globe due to very high emissions from industries, automobiles, power plants, brick-kilns, domestic heating and cooking, open biomass burning and transported plumes of dust and agricultural burning. Except for the high emission rates from various sources, the aerosol and pollution levels in Delhi are strongly impacted by the local and regional meteorology and, especially during winter, the dry conditions, calm winds and shallow mixing layer favor very large concentrations near the ground. Therefore, the current campaign took place during wintertime to assess the sources of the BC mass concentration along with aerosol properties and several other pollutants. Further details of the experimental site and measurements protocol for the WIFEX is presented elsewhere (Bisht et al., 2016; Guide et al., 2017)

RESULTS & DISCUSSIONS

The temporal variation of Aethalometer (AE-33; Magee Scientific USA) measured BC, BC_{ff}, BC_{wb} (fossil-fuel and wood burning components of BC, respectively), along with the monochromatic Photoacoustic Extinctionmeter (PAX; Droplet Measurement Technologies, Inc., CO, USA) measurements of the extinction, scattering, absorption and single scattering albedo, PM₁₀ and PM_{2.5} mass concentrations and trace gas pollutants such as NO_x, CO and O₃ are analysed. High values of PM₁₀ ($245.5 \pm 109.8 \mu\text{g m}^{-3}$) and PM_{2.5} ($145.5 \pm 69.5 \mu\text{g m}^{-3}$) concentrations were recorded during the campaign (Figure 1a), composed of a large (~10% to PM₁₀ and ~17% to PM_{2.5}) BC fraction. During the same period, the daily BC mass concentrations varied from 3 to 60 $\mu\text{g m}^{-3}$ (with mean of $24.4 \pm 12.2 \mu\text{g m}^{-3}$), mostly affected by changes in meteorological conditions, in mixing layer height and dispersion, and by differences in carbonaceous emission rates, with highest concentrations during night and early morning hours (Figure 1b). The fossil-fuel combustions from

traffic, industries and domestic use of natural gas dominated when compared to burning of wood, waste material, dung cakes and agricultural crop residue. The BC_{ff}/BC was found to be 73% at 880 nm and 56% at 370 nm, exhibiting large daily and diurnal variability, while the relative contributions of BC_{ff} and BC_{wb} depend on wavelength. Furthermore, the average NO , NO_2 , O_3 and CO concentrations were found to be 7.9 ± 2.3 ppb, 12.9 ± 1.9 ppb, 31.3 ± 18.4 ppb and 1.7 ± 0.5 ppm, respectively, while high levels of b_{sca} and b_{abs} coefficients were also recorded. Nearly all the examined parameters exhibited more or less prominent peaks around 08:00 - 09:00 LST indicating the influence of the morning rush-traffic emissions associated with a generally low MLH. The aerosol and primary air-pollutant concentrations were progressively decreasing towards midday, closely following the increase in MLH, thus allowing for vertical mixing and dilution processes. The increase in the concentrations after $\sim 17:00$ LST was coinciding with the increased domestic cooking and gradual formation of a surface inversion prohibiting vertical mixing. Later on, the evening traffic rush hour and open fires of waste material in the roads for heating purposes (especially in the slams) further increased the PM and BC concentrations and maintained them at high levels throughout the night. BC_{ff} and BC_{wb} were found to be strongly related to CO and NO emissions indicating common local sources of primary combustions, while the BC_{ff}/BC_{wb} ratio was not found to be related to CO/NO_x.

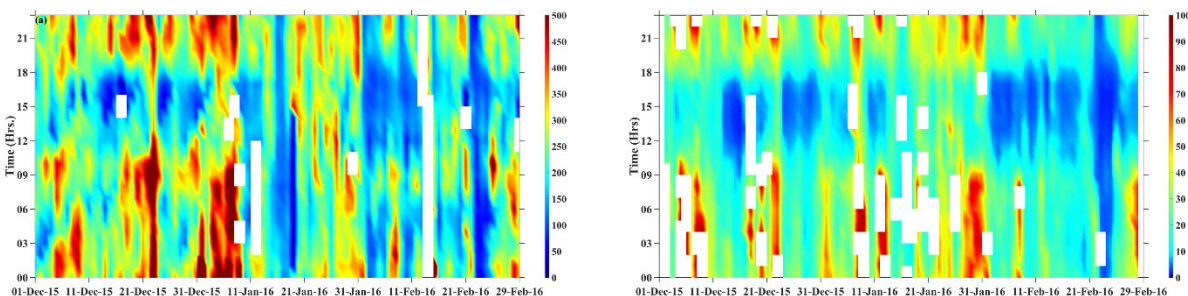


Figure 1: Temporal variation of PM_{10} (a) and BC (b) mass concentration during the whole campaign period.

CONCLUSIONS

The main findings from the analysis can be summarized in the following:

1. Very high pollution levels were recorded over Delhi during wintertime.
2. A large BC variation (3 to $60 \mu\text{g m}^{-3}$ on daily basis) was observed.
3. The BC_{ff}/BC was found to be 73% at 880 nm and 56% at 370 nm.
4. The boundary layer dynamics control the diurnal variations of BC, PM and trace gas concentrations.

ACKNOWLEDGEMENTS

The authors are grateful to Director IITM Pune, Director General IMD, Secretary MoES, Govt. of India and Director IARI, New Delhi for their constant encouragement and continuous support for carrying the Fog Experiment over Delhi.

REFERENCES

Bisht, D.S., Tiwari, S., Dumka, U.C. et al., (2016). Tethered balloon-born and ground-based measurements of black carbon and particulate profiles within the lower troposphere during the foggy period in Delhi, India. *Sci. Total Environ.*, 573, 894-905.

Ghude, S.D., Chate, D.M., Jena, C., et al., (2016). Premature mortality in India due to $PM_{2.5}$ and ozone exposure. *Geophys. Res. Lett.* 43, 4650 – 4658.

IMPACT OF URBAN TERRAIN ON SIMULATION OF AIR-POLLUTANTS

NISHI SRIVASTAVA

Department of Physics B.I.T.-Mesra Ranchi-Jharkhand, India

KEYWORDS: Air Pollution, Urban heat island, parameterization

INTRODUCTION:

About half of the world population residing in the urban area which is expected to get extended about 70% in near future by 2030. Fast develop of urban areas caused population movement from rural area to urban area and it is still continuing. Increase in urbanization/industrialization along with very high density of population in cities has caused severe problems and captured the attention of scientist worldwide. Adverse effects of urbanization could be seen on the environment primarily in form of pollution, modification in the physical and chemical properties of the atmosphere and henceforth the climate. Urban Heat Island effect is the cumulative effect of these impacts on the urban climate (Taha 1997; Zhao et al., 2014). It is defined as: “An Urban Heat Island (UHI) is an urban area or metropolitan area that is significantly warmer than its surrounding rural areas due to human activities.” The temperature of the surrounding rural area is much lower than its urban neighborhood.

The Urban Heat Island (UHI) is a phenomenon whereby urban regions experience warmer temperature than their rural, undeveloped surroundings. The heat island is defined on the basis of temperature differences between urban and rural stations, and the isothermal patterns of near-surface air temperatures resemble the contours of an island. Though heat islands phenomenon could be noticed on any area (rural/urban) and may vary on its spatial scale of occurrence but buildup areas i.e. cities are more favorable for occurrence of this phenomenon. Concrete surface or paved surface makes urban areas more prone to be heated and release large amount of heat as compared to land/field area (Grimmond, 2007). UHI have negative impacts on the inhabitants of the cities but these effects are not only limited till UHI area. It also affects the surrounding areas eco-system and also affects weather away from cities also. UHI contribute indirectly to the climate change because to their contribution to green house effects and ultimately to global warming.

Urban climate differs significantly from rural climate and the magnitudes of this difference are governed by various factors. Modification in the energy balance due to various consequences of urbanization of cities affects the urban thermal environment and results in urban heat island effect (UHI); thereby urban areas often experience difference in temperature from surrounding rural areas. Greenhouse gases and pollutants, urban terrain modification, removal of vegetation, alteration in radiation budget due to aerosols, anthropogenic heating, geographical location and wind flow pattern are major reasons causing UHI (Oke 2002; Voogt & Oke, 2013; Feizizadeh, 2013). There are several reasons also which contributes to UHI. The factors add to and enhance the UHI are as:

1. Dimension of the City: Aerodynamic behavior of the cities/urban areas is quite different from the rural, undeveloped and vegetated areas.
2. Urban Desert: Urban areas could be considered as desert owing to no or very less vegetation; and reduced efficiency to absorb the rain water.
3. Urban Canopy: Urban canopy act very differently than vegetated area canopy. Tall building roof and walls absorb the radiation more than vegetated area and as a consequence emitted more than it.
4. Humidity Effects: Urban development affects the relative humidity of its environment prominently as in urban areas air is warmer than rural area.
5. Urban Haze: Urban areas are suffering for severe air pollution now a days and the haze or smog form due to air pollution can trap the outgoing thermal radiation and prevent escaping of heat to the atmosphere.

6. Anthropogenic Heat: Another cause to raise the urban environment is burning of fossil fuels. Heat get released because of burning of fossil fuel and this contributes in enhancement of the urban temperature i.e. contribute to UHI.
7. Air Pollution: Air pollutants and UHI both have positive feedback effect on each other; i.e. presence of one causes enhancement in other.

Connection between UHI and Air Pollution

- UHI and urban air pollution have complementary effect on one another.
 - UHI exacerbates problem of urban air pollution by placing additional needs on the cooling systems throughout the city leading to more air pollution.
8. Air pollutants (aerosols/gaseous pollutants) are also found to enhance the UHI effects. They can absorb and emit the longwave radiation and thus has potential to increase the longwave radiation energy received at the urban land surface.

As aforementioned that along with other parameters, air pollutants concentrations are also observed significantly higher than that of rural clean atmosphere. In this work we have be focused on air pollutants and UHI connections. Air pollution and UHI are inter-related to each other (Sarrat et al., 2006; J. Fallmann et al, 2016). In this work we explored the relation in between the UHI and air pollutants concentration with modeling approach. In general chemical transport model does not incorporate the impact of urban terrain but in this work we have explore the impact of urban terrain on the distribution of air pollutants. We attempted to answer the question: How the specific context of a city contributes to local and regional air pollution?

METHODS:

In this work we have attempted to answer the questions which address increase in UHI and its connection with local and regional air pollution as climate change may get affected with local urban heat island. In this process we have used a chemical transport model.

Chemical transport modeling is the need of the day for developing countries like India because it is difficult to have a dense network of ground based observatories in developing nation. At the same time ground based observations have low spatial and temporal resolution. When simulations are performed over very small resolution to incorporate effect of urbanization then it is mandatory to consider the small scale dynamics which affects the fluxes of energy and momentum. Inside the grid of the representation of urban terrain is a challenging task. But it is a crucial step for the exact estimation of air pollution as dynamics of urban atmosphere highly gets affected depending on the terrain of urban area i.e. impact of UHI on the atmospheric dynamics. Thus it is very essential to represent the urban terrain structure properly in the air pollution model.

Urban climate differs significantly from rural climate and the magnitudes of this difference are governed by various factors. Along with other parameters, air pollutants concentrations are also observed significantly higher than that of rural clean atmosphere. The prime objective of proposed work was to develop an atmospheric modeling system focused on urban areas. Thus we worked on a modeling system which is expected to simulate the air pollution taken into account the complex heterogeneity of the urban areas. Indeed, while urban areas are of great social interest, research scientists have to face to a number of scientific challenges in order to represent the high heterogeneity of the urban surfaces and objects (buildings, parks, trees, etc.) in numerical models. At the same time this heterogeneity affects significantly the processes determining the interactions between a city and the atmosphere.

Atmospheric motions are generated on various scales and models are developed to evaluate these scales properly. Efficient models exist which can explore the UHI effects very efficiently. But urban climate model does not incorporate the current air pollution scenario and details about gaseous/aerosol pollutants. Thus studies finding connection between CTM models with urban climate model is still sparse.

In the present work we have worked on an interface between urban climate model and chemical transport model. For this work we have selected a state of art chemical transport model “CHIMERE”. This model can give simulation from hemispherical scale to urban scale with varying resolution from 1-2Km to 200Km. This model is very powerful research tool for verification of parameterization and hypotheses. This model requires the meteorological input to start its simulation for the projection of air pollutants. In present study WRF model has been used to provide meteorological input to the model. This model is flexible, state of art, atmospheric simulation system that is portable, and very efficient with parallel computing platforms. WRF model is suitable for simulation on various temporal ranging from few meters to thousands of Kms, i.e. from urban scale to regional scales. In WRF model urban parameterization schemes such as UCM, BEP and BEM are available. To introduce the ideas of urbanization in CHIMERE, we utilized these available urban schemes in CHIMERE to introduce the effects of buildings. Introduction of these schemes in the CHIMERE, helped the system to compute the fluxes of momentum and heat on a higher resolved vertical grid than the one initially define by the user to produce its regional simulation. These fluxes are used as new sources or sinks of momentum and heat at the surface level. In these schemes though building are not precisely describe but their effect is parameterized. Thus linking of these two model increased the efficiency of the both the model significantly. Over Indian domain which is suffering from severe air degradation and urban heating, these model simulation result will help the policy maker in framing the mitigation strategies.

CONCLUSIONS

In this work we dealt with two type of models i.e. meso-scale model chemical transport model. Both of the models have huge difference in the physics and dynamics as both models deals with different aspects of meteorology and thus huge difference exists in the physical and chemical processes taken into account. Thus in order to use information from one model in other a suitable connects/interface is need and in present work, we have used the meteorological model information successfully in the chemical transport model by implementing the urban parameterization scheme in the meso-scale model. The objective of the work primarily focused on finding the connection in between the UHI and air pollution.

Climate change is serious issue worldwide and over Indian continent severity of air pollution cannot be ignore especially in the winter season. Along with the air pollution, heating i.e. notable temperature rise in cities has been recorded; which is due to various reasons along with UHI. Thus in Indian continent proper evaluation of UHI and air pollution is need of the day for its mitigation. Our simulation relation can be useful for reduction air pollutants. The simulation results from present work are useful to design alarming system and to provide pollution alerts to the public.

In this work we have developed an interface between existing urban climate model and chemical transport model. Our objective was to couple WRF with its urban parameterization (called WRF-BEP-BEM) with a chemical transport model (CHIMERE). With the use of urban parameterization in WRF model we could introduce the effects of buildings in CHIMERE model simulations. WRF-BEP-BEM computes the effect of buildings on radiation and turbulence. The system computes the fluxes of momentum and heat on a higher resolved vertical grid than the one initially define by the user to produce its regional simulation. By implantation of urban parameterization schemes in the chemical transport model we can avail information about the

We have simulated the concentration of air pollutants without urban parameterization scheme and with parameterization schemes in the WRF model. We studied various air pollutants and temperature patterns in these simulations and notable changes have been noticed in the different parameters owing to use of urban parameterization. These changes occurred due to change in energy flux associated with building and urban structures. These information provide an opportunity for the urban planner to implement energy saving strategies in the context of climate change and the building designing sustainable cities.

These information are also useful to understand the interaction between the urban structures, urban climate in context of climate change.

These model simulation results could be useful for the policy maker in framing the mitigation strategies. Though the urban climate models and chemical transport models are existing but still the connection between these models are lacking. Urbanization and air pollution as separate problem but both are interrelated with each other and significantly influences each other. Thus in this work we moved one step ahead in the modeling field which will be useful for scientific society to development the UHI and air pollution scenario with more accuracy.

ACKNOWLEDGEMENTS:

Author acknowledges the SERB for SERB overseas post doctoral fellowship-2016.

REFERENCES

Bakhtiar Feizizadeh and Thomas Blaschke, Examining Urban Heat Island Relations to Land Use and Air Pollution: Multiple End member Spectral Mixture Analysis for Thermal Remote Sensing, IEEE Journal of Selected Topics in Applied Earth Observations and Remote Sensing, VOL. 6, NO. 3, June 2013

Grimmond, S., Urbanization and global environmental change: local effects of urban warming. Geogr. J. 173, 83–88, 2007.

Joachim Fallmann, Renate Forkel, Stefan Emeis, Secondary effects of urban heat island mitigation measures on air quality, Atmospheric Environment 125, 199–211, 2016.

Oke, T. R. Boundary Layer Climates (Routledge, 2002).

Sarrat C., A. Lemonsu, V. Masson, D. Guedalia, Impact of urban heat island on regional atmospheric pollution, Atmospheric Environment 40, 1743–1758, 2006.

Taha, H. Urban climates and heat islands: albedo, evapo-transpiration, and anthropogenic heat. Energy Build. 25, 99–103, 1997.

Voogt, J. A. & Oke, T. R. Thermal remote sensing of urban climates. Remote Sens. Environ. 86, 370–384, 2013.

Zhao, L., Lee, X., Smith, R. B. & Oleson, K. Strong contributions of local background climate to urban heat islands. Nature 511, 216–219, 2014.

EVALUATION OF AEROSOL OPTICAL THICKNESS AND ITS IMPACT OVER COAL MINING REGION USING GROUND-BASED SUNPHOTOMETER OBSERVATIONS

AKSHAY KUMAR^{1*} AND AKHOURI PRAMOD KRISHNA¹

¹Department of Remote Sensing, Birla Institute of Technology, Mesra, Ranchi, Jharkhand-835215, India

(*Correspondence at: akshay61296@gmail.com)

KEYWORDS: Aerosol Optical Thickness (Aot); Coal Mining; Proximity Analysis; Gis

INTRODUCTION

Monitoring of aerosol concentration around coal mining region becomes a prior step to assess atmospheric pollution in the area. Anthropogenic activities, industries, coal mine fire, overburden dumping, transportation and other mining operations are primary sources for increasing pollution in the area. The aerosols are described as tiny particles found in either solid or liquid state of matter, suspended in the air (excluding cloud particles) with an extensive combination of sizes, ranging from $10^{-2}\mu\text{m}$ to $10^2\mu\text{m}$ (Ranjan et al., 2007; Kumar and Krishna, 2017). Aerosol optical depth (AOD) also called aerosol optical thickness (AOT) is very imperative physical parameters for studying the characteristic of atmospheric aerosol that is related to direct solar radiation by scattering the absorption process (Ranjan et al., 2007). South Karanpura is one of the most productive coalfields of the Jharkhand state employing both sub-surface and opencast mining techniques. Such a large-scale mining practice has led to significantly more environmental pollution, particularly deterioration in air quality by dust and gaseous pollutants (Armstrong et al., 1980; Kumar and Krishna, 2017). Air pollution problem is not only within the mining area but also in the surrounding locations. The relationship between coal mining activities and aerosol concentration were also investigated by several researchers (Chadwick et al., 1987; Munroe et al., 2008). They found that biomass burning and mining-related activities (blasting, transportation, dumping) are responsible for air pollution in the region. Wavelength dependence of scattering and absorption effects of aerosols is illustrated by Ångström wavelength exponent (α) and Ångström turbidity (β) formula (Ångström 1964). In recent past, several studies have been conducted on various aspects of Ångström exponents (O'Neill et al., 2001; Kalapureddy and Devara, 2008). They described Ångström exponents as a tool to estimate particle size distribution, extrapolating AOT throughout the broad spectral region to distinguish the different aerosol types (Kumar and Krishna, 2017). The relationship between the wavelength (α) and turbidity (β) follows a power law called Ångström power law. It seems to be a good representation of aerosol that has a wide variety of origins and compositions (McCartney, 1976). In the present study, MICROTUPS-II Sunphotometer instrument was used to collect Aerosol optical thickness (AOT) data during winter season over South Karanpura Coalfield region, Jharkhand, India. The pattern of measured AOT concentration (at five different wavelengths 340, 500, 870, 936 and 1020 nm) was spatially analyzed in a GIS to assess environmental condition in the area.

METHODS

Ground-based AOT data along with temperature and PWV content was recorded using MICROTUPS II Sunphotometer (with an accuracy ± 0.03) during January 2014. At each site, five samples were collected and their average values were used. All the observations were recorded during clear sky conditions which imply cloud-free days or proper sunshine (during 10:00 to 16:00 h). The recorded values of AOT, temperature and PWV at observation sites interpolated in a GIS environment after importing the geographic locations of sampling points from the GPS. The spatial pattern of AOT, temperature and PWV concentrations were analyzed after interpolation through inverse distance weightage (IDW) technique. This method applies spatial correlation of variables and predicts the values of variables at unobserved locations

based on those of observed locations (Guofeng et al., 2010; Kumar and Krishna, 2017). Ångström exponent (α) and turbidity coefficient (β) are other two important parameters for studying the atmospheric aerosol properties along with AOT. The Ångström exponent (α) provides the aerosol particle size which can be easily obtained by the Ångström power law (Ångström, 1964). The exponent ' α ' denotes the relatively high proportion of small particles to large particles (Latha and Badrinath, 2004). In simple terms, when the aerosol particle size equals the size of air molecules, the value of ' α ' approaches 4 whereas, when the size of an aerosol particle is large, the value of ' α ' approaches 0. Thus, large values of ' α ' indicate relatively small size particles. The turbidity coefficient ' β ' on the other hand, estimates the aerosol loading over the site (Ranjan et al., 2007).

RESULTS & DISCUSSIONS

Aerosol optical thickness concentration

The concentration of AOT was measured at 42 locations in SKCR during the winter period of January 2014. The spatial pattern of AOT distribution analyzed using geographical information system (GIS), revealed variations in the AOT concentration at all five wavelengths ranging from 340 to 1020 nm (Figure 1). The spatial distribution map of all wavelengths for SKCR indicates that the value of AOT concentration for shorter wavelength (340 nm) is higher as compared to longer wavelength (1020 nm). It shows that the regions were indicating the dominance of finer size particles over larger size in the atmosphere. The concentration of AOT over SKCR between 0.077-3.333 with mean value of 1.113 and standard deviation is 0.783. The statistics of aerosol concentration for all wavelengths (340-1020 nm) are shown in Table 1.

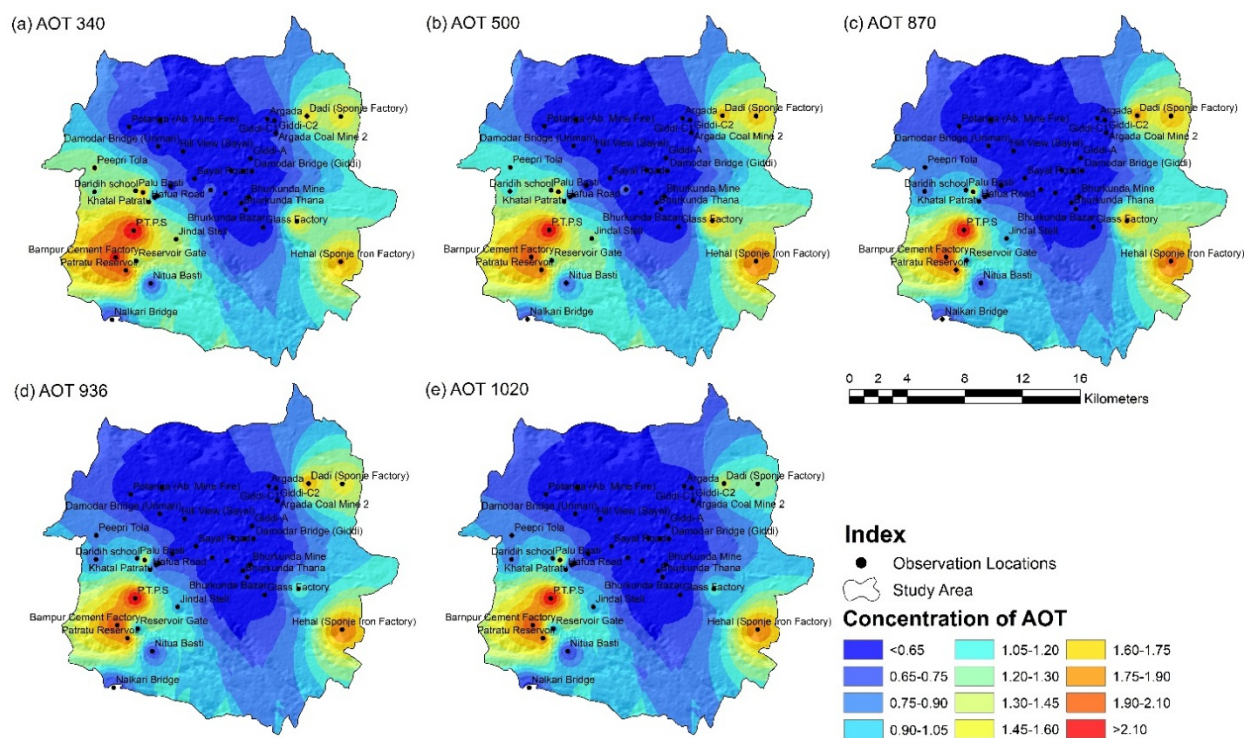


Figure 1: Map showing a variation of AOT at different wavelengths over South Karanpura Coalfield region during the year 2014.

In SKCR, the AOT (340-1020 nm) concentration has been found to be greater at industrial zones (P.T.P.S., J.S.P.L., Bhurkunda, Chaingada, Dari and Hehal), followed by mining areas such as Potanga, Railgada, Sayal, Saunda, Sirka, Giddi-C and Bhurkunda colliery. Such trends may be due to the high

frequency of transportation activities, loading/ unloading of coal and smoke emissions from coal-based industries causing high dispersions of dust particles into the atmosphere whereas, it is lower in the residential areas. A high value of AOT at lower wavelengths shows that at both the observation sites, the small size particles are dominant. The gradual decrease of AOT with increasing wavelengths suggests that the aerosol size distribution of this site is according to the Junge’s inverse power law distribution (Ranjan et al., 2007):

$$\frac{dn}{dr} = Cr^{-v} \quad (1)$$

Where, C represents a constant depending on the total number of particles. The average AOT concentration has been analyzed, and it indicates that small size particles are dominated by coarser size, over SKCR. The concentration of finer size particles in coalfield region mostly originate from thermal power plants and allied industries.

Wavelengths/ Parameters	Min	Max	Mean	Median	Mode	Std. deviation
AOT 340	0.511	3.333	1.113	0.693	0.593	0.783
AOT 500	0.213	2.999	0.787	0.375	0.289	0.766
AOT 870	0.077	2.555	0.503	0.192	0.114	0.654
AOT 936	0.104	2.565	0.505	0.231	0.139	0.615
AOT 1020	0.102	2.574	0.526	0.258	0.193	0.605
Angstrom Exponent ($\alpha_{340-870}$)	0.472	2.593	1.49	1.42	2.46	0.64
Turbidity Coefficient (β_{340})	0.031	1.923	0.388	0.15	0.07	0.506

Table 1. Statistics of AOT and Angstrom parameters over South Karanpura coalfield region (SKCR) during January 2014.

Size characteristics of aerosols

To determine aerosol size distribution and total columnar aerosol loading over South Karanpura Coalfield, the ‘ α ’ and ‘ β ’ are calculated and plotted for the wavelength pair 340 and 870 nm (Figure 2). The high value of ‘ α ’ implies the dominance of smaller size aerosol particles and vice versa. The value of $\alpha_{340-870}$ lies between 0.472 and 2.593 with a mean of 1.490 and standard deviation of 0.640 (Table 1). This indicates that different sizes of aerosols are present in the atmosphere of South Karanpura Coalfield region owing to various sources of origin and weather parameters.

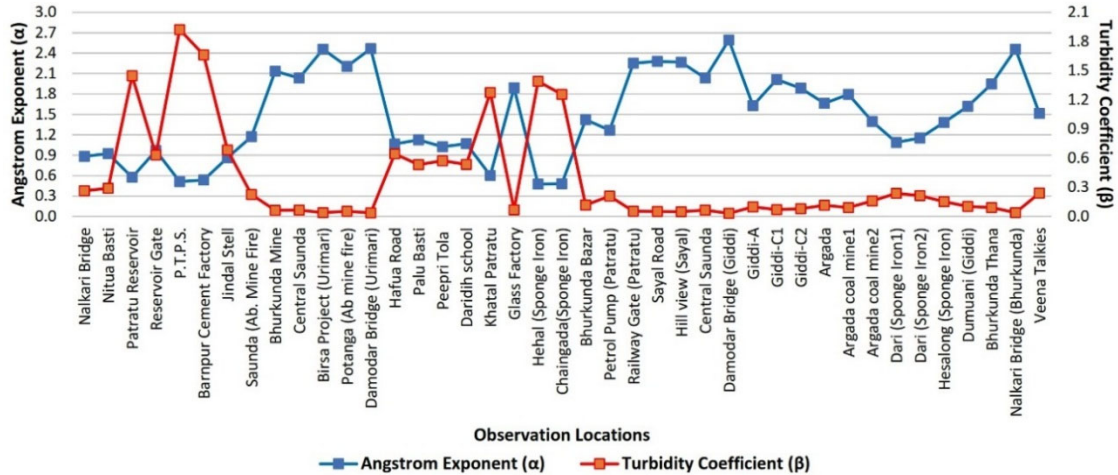


Figure 2. Variation of Ångström exponent (α) and Turbidity coefficient (β) over South Karanpura Coalfield region.

CONCLUSIONS

Aerosol concentration and their size characteristics over South Karanpura Coalfield region have been studied. The maximum level (>3.0) is observed near the industries (P.T.P.S., Hehal, Chaingada, Bhurkunda, etc.) followed by coal mining area (Potanga, Railgada, Sirka and Giddi-C). Lower AOT concentration (<1.0) is noted near forest areas and planned residential area, followed by settlement and waterbodies. Ångström parameters (α , β) values extend between 0.031-1.923 over study area indicates the presence of different particle sizes of aerosols (mostly fine-mode particles). Aerosols influence and its impact may be useful in better visualizing the spatio-temporal variations in the mining region investigated in the present study. The outcome of this study provides a quantitative assessment of the environmental conditions over coal mining region and can help in the formulation of environmental development policy.

ACKNOWLEDGEMENTS

This work was supported by Birla Institute of Technology, Mesra, Ranchi, under the Institute research fellowship for Ph.D. programme.

REFERENCES

- Armstrong, J.A., Russel, P.A. and D.C. Darmel (1980). Particle From Surface Mining, Part I - Vertical Measurements, Report No. EPA-600/9-80-041 (Research Triangle Park, NC: USEPA, Industrial Environmental Research Laboratory).
- Chadwick, M.J., Highton, N.H. and N. Lindman (1987). *Environmental Impacts of Coal Mining and Utilisation*. A Complete Revision of Environmental Implications of Expanded Coal Utilization. Pergamon Press, England.
- Guofeng, W., Leeuw, J., Skidmore, A.K., Yaolin, L. and H.H.T. Prins (2010). Comparison of extrapolation and interpolation methods for estimating daily photo synthetically active radiation (PAR)-a case study of the Poyang lake national nature reserve, China. *Geo-spatial Information Science*, **13**, 235-242.
- Kalapureddy, M.C.R. and P.C.S. Devara (2008). Characterization of aerosols over oceanic regions around India during pre-monsoon 2006. *Atmos. Environ.* **42**, 6816–6827.

Kumar, A. and A. P. Krishna A. P. (2017). Winter seasons assessment of atmospheric aerosol over Coalfield region of India using geoinformatics. *Urban climate*, **20**, 94-119.

Latha, K.M. and K.V.S. Badrinath (2004). Association of aerosol optical depth with near surface aerosol properties in urban environment. *Indian J. Radio & Space Phys.* **33**, 256-259.

McCartney, E.J. (1976). *Optics of the Atmosphere: Scattering by Molecules and Particles*. John Wiley & Sons, New York, 421.

Munroe, D.K., Wolfenbarger, S.R., Calder, C.A., Shi, T., Xiao, N., Lam, C.Q. and D. Li (2008). The relationships between biomass burning, landcover/use change, and the distribution of carbonaceous aerosols in mainland Southeast Asia: a review and synthesis. *Journal of Land Use Science* **3**, 161-183.

O'Neill, N.T., Eck, T.F., Holben, B.N., Smirnov, A., Dubovik, O. and Royer, A. (2001). Bimodal Size Distribution Influences on the Variation of Angstrom Derivatives in Spectral and Optical Depth Space, *Journal of Geophysical Research: Atmospheres*, **106**, 9787-9806.

Ranjan, R.R., Joshi, H.P. and K.N. Iyer (2007). Spectral variation of total column aerosol optical depth over Rajkot: a tropical semi-arid Indian station. *Aerosol Air Qual. Res.* **7**, 33-45.

PRELIMINARY INVESTIGATION OF PM₁ VARIATION AT BENGALURU, KARNATAKA STATE

A S MANJUNATHA, K E GANESH, LATHA KUMARI, T S PRANESH

Department of Physics, B.M.S. College of Engineering, Bull Temple Road, Bengaluru-560019, India

KEY WORDS: Pm₁, Fluorine, Aerosol

INTRODUCTION

Atmospheric particulate matter (PM) consists of minuscule particles of solid or liquid matter, with diameters ranging from 0.001 μm to 100 μm . The time for which PM is suspended in the atmosphere ranges from a few hours to a few weeks. Smaller the particle is, longer it will stay in the air. Particles in air are either directly emitted when fuel is burnt and when dust is carried by wind or indirectly formed, when gaseous pollutants previously emitted to air turn into particulate matter. The air quality in urban areas with regard to PM concentrations is receiving more attention as an increasing share of the world's population lives in urban centre [UNO, 2003]. The traffic-generated emissions are accounting more than 50% of the total PM emissions in the urban areas [Worbel *et al.*, 2000]. Based on size, particulate matter is often divided into two main groups. The coarse fraction contains the larger particles with a size ranging from 2.5 to 10 μm (PM_{2.5}-PM₁₀). The fine fraction contains the smaller ones with a size up to 2.5 μm (PM_{2.5}).

The particles in the fine fraction which are smaller than 0.1 μm are called ultrafine particles. Most of the total mass of airborne particulate matter is usually made up of fine particles ranging from 0.1 to 2.5 μm . Ultrafine particles often contribute only a few percent to the total mass, though they are the most numerous, representing over 90% of the number of particles [Pfeiffer *et al.*, 2005].

The main sources for ambient PM concentrations at urban roadways are vehicle exhausts, emissions from tyre and brake wear and re-suspension of road dust. During recent years, India is experiencing unprecedented economy growth rate and rapid urbanization. This resulted in expansion of city, increase in urban population, vehicular population, traffic congestion, large scale construction activity and unsystematic land usage [Sumana Datta *et al.*, 2006]. Coarse PM can come down to earth by rain washout or by gravity settling. The case of fine and ultrafine PM with size one micrometre and below is different. Primarily they can get into the respiratory track very easily once inhaled by the human being.

The present study has been conducted in covering the objectives of the mass concentration of PM, chemical composition and morphology of the collected sample at two different locations of Bengaluru.

DETAILS ABOUT THE STUDY REGION

Bengaluru lies in the southeast of the South Indian state of Karnataka. It is in the heart of the Mysore Plateau (a region of the larger Precambrian Deccan Plateau) at an average elevation of 920 m. It is positioned at 12.97°N 77.56°E and covers an area of 1741 km². The majority of the city of Bengaluru lies in the Bengaluru Urban district of Karnataka and the surrounding rural areas are a part of the Bengaluru rural district. The region comprising the Bengaluru Urban and Rural districts is known as the Bengaluru (region). Being the capital city of Karnataka, majority of IT establishments, health institutes, education institutes, industries are located in Bengaluru which in turn attracts talented minds to establish them in the city as well as increases the extent of anthropogenic activity.

METHOD OF STUDY AND ANALYSIS

The particles were collected onto a polytetrafluoroethylene of size 1 μm or less than that (47mm filter paper) using PM₁ particulate sampler (ENVIROTECH APM 577 IITK-KNOWHOW) equipped with impactors

of different filters. A 25mm of filter paper is used to remove the particulate size more than 1µm. Sample were collected for 24hr starting from 6AM at a rate of 10 litres per minute. The filter paper used for collection of particulate matter of diameter 1µm or less than that were weighed before and after sampling. After use the filter paper is incubated for 24hr until further analysis.

Table 1

ELEMENT	WEIGHT%	ATOMIC%
C K	30.72	41.15
O K	1.21	1.21
F K	68.07	57.64

Table 2

ELEMENT	WEIGHT%	ATOMIC%
C K	32.32	42.95
O K	1.36	1.36
F K	66.25	55.65
P K	0.07	0.03

RESULTS AND DISCUSSION

Mass concentration

The mass concentration of PM₁ whose diameter is 1µm or less than that were collected at two different locations of Bengaluru. The sample collected at Basavangudi was incubated for 24hr and the mass concentration is found to be 50µg/m³. Whereas sample collected at Hosur road was also incubated for 24hr and the mass concentration found to be 212µg/m³ which is four times than at Basavangudi. The reason for high concentration at Hosur road is may be due to industries located close to the observation site, high traffic flow and construction activities.

SEM-EDAX analysis

Scanning electron microscope (SEM) is used to study the morphology and Energy Dispersive Analysis X ray (EDAX) is used to study the chemical composition in the collected sample. The collected two samples were subjected to SEM and EDAX for 30 min of exposure. Based on their morphology and chemical analysis, two main classes were detected, natural and anthropogenic [Talbi *et al.*, 2018]. The natural particles have irregular shapes and rough surfaces and sometimes form aggregates with irregular shapes and sizes. The anthropogenic particles emitted by combustion process were essentially spherical and rounded with a smooth surface [Mirjana *et al.*, 2006]. In our SEM images also, we have observed the regular shape as well as irregular shapes of PM corresponding to natural and anthropogenic source of PM [Fig1 and Fig 2]. The EDAX Spectra of the sample collected at Basavangudi confirms the presence of Fluorine, Carbon, Oxygen [Fig 3] but the sample collected at Hosur road shows the presence of Fluorine, Carbon, Oxygen with Phosphorus [Fig 4]. Table 1 and Table 2 shows the composition of elements in PM₁ collected in filter paper.

The major components present in the dust collected at two locations in Bengaluru city are Carbon and Fluorine. The weight percentages of Carbon and Flourine is 30.72% and 68.07% at Basavangudi and 32.32% and 66.25% at Hosur road respectively.

The weight percentage of Oxygen and Phosporus is very less compared to Carbon and Flourine. The presence of high concentration of Flourine may be due to of natural origin through weathering and dissolution of minerals. The principal anthropogenic sources may include aluminium smelters, fertilizer factories and industrial activities such as brick, tile, pottery, cement works and ceramic industries [Barbara

et al 2013]. The sources of Fluorine also may be from copper and nickel production, phosphate ore processing, phosphate fertilizer production, ceramic manufacturing, glue and adhesive production and glass manufacture [WHO., 2002].

Carbonaceous combustion aerosol is emitted directly into the atmosphere as a by-product of incomplete combustion occurring in fossil fuel, bio fuels and bio mass burning [Reddington *et al.*, 2013]. Carbonaceous aerosol account for a large fraction of PM. It includes the aerosol constituents that are based on carbon, organic carbon (OC), elemental carbon (EC) and carbonate minerals. Carbon aerosol of fine particles with diameter 300nm are likely to be from combustion and secondary [Sahan *et al.*, 2008]

Fig 1. SEM image of PM₁ at Hosur Road

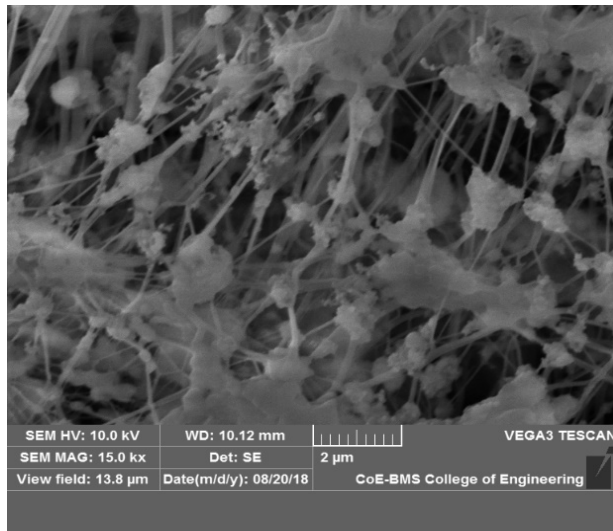


Fig 2. SEM image of PM₁ at Basavangudi

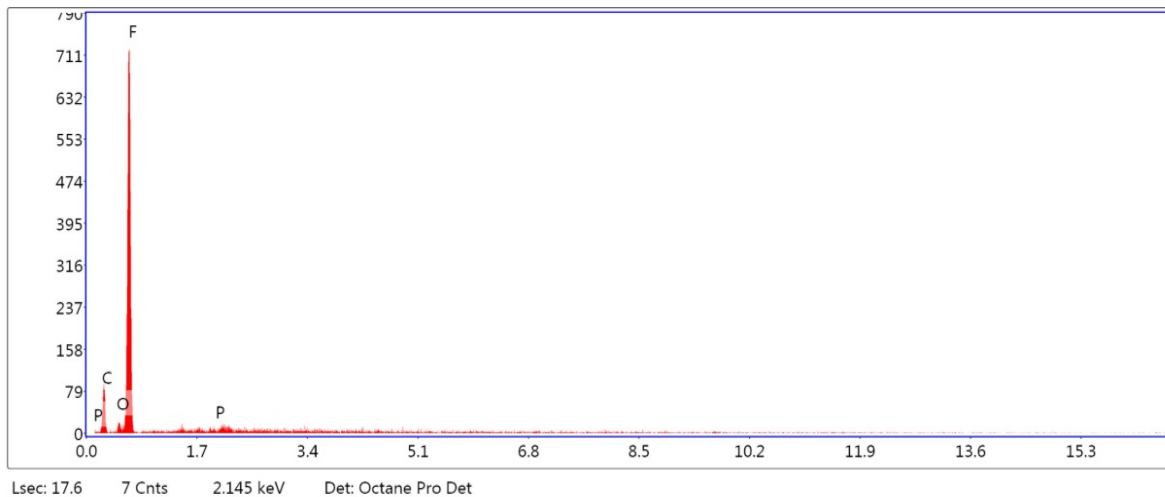
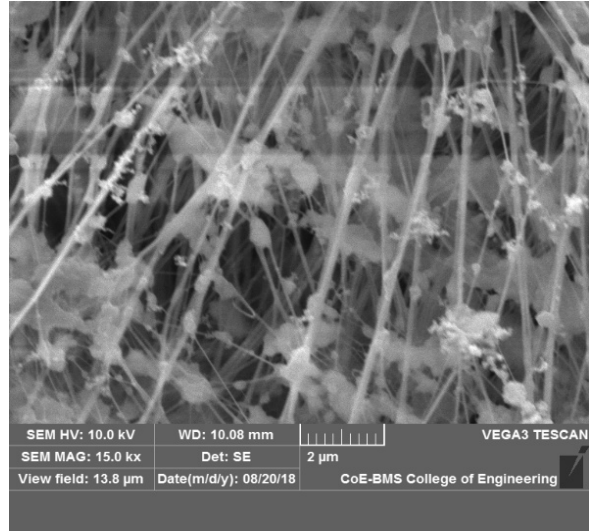


Fig 3. EDAX spectra of sample collected at Hosur Road

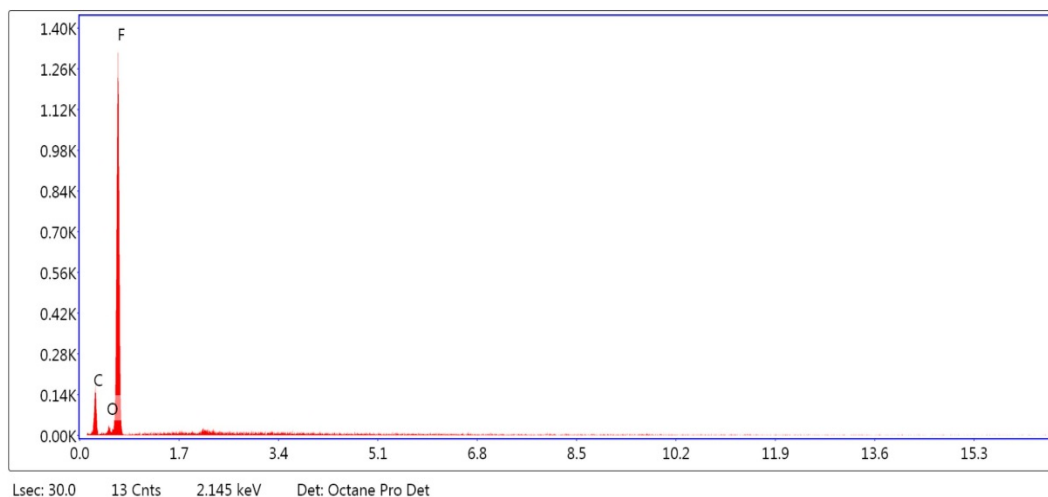


Fig 4. EDAX spectra of sample collected at Basavangudi

Meteorological Parameters

The average temperature, humidity, wind speed, wind direction parameter on the days of sampling at two different location of Bengaluru is recorded and is show in the below table.

Parameters	Basavangudi	Hosur Road
Temperature (°C)	25	21
Humidity (%)	86	90
Wind Speed (Km/hr)	19	6
Wind Direction	WSW	WSW

CONCLUSION

The mass concentration PM with diameter of 1 μ m and less than that at two locations of Bengaluru is found to be 50 μ g/m³ and 212 μ g/m³ respectively. The SEM-EDAX analysis shows the presence of Fluorine and Carbon as major components of PM₁ in the atmosphere.

For the samples collected at two locations of Bengaluru city, the observed high concentration of Fluorine and Carbon may be due to from the industries of aluminium, steel situated at the place of sampling as well as from the combustion of fossil fuels. For a through understanding more number of sampling is required which we will be completing in the coming days.

REFERENCES

Abdelhamid Talbi, Yacine Kerchich, Rabah Kerbachi, Menouer Boughedaoui.; “Assessment of annual air pollution level with PM₁, PM_{2.5}, PM₁₀ and associated heavy metals in Algiers, Algeria”; Environmental pollution,2018,232,252-263.

Andrzej Wrobel,;“Beta activity: a carrier for visual attention”; Act neurobiol. Exp, 2000,60, pp.547- 260.

Barbara Walna & Iwona Kurzyca & Ewa Bednorz & Leszek Kolendowicz,; “Fluoride pollution of atmospheric precipitation and its relationship with air circulation and weather patterns”, Environ Monit Assess, 2013, 185,5497–5514.

C. L. Reddington, G. McMeeking, G. W. Mann, H. Coe, M. G. Frontoso, D. Liu, M. Flynn, D. V. Spracklen and K. S. Carslaw, “The mass and number size distributions of black carbon aerosol over Europe”, 2013, Atmos. Chem. Phys, 13, 4917–4939.

E. Sahan, H.M. Ten Brink, E.P. Weijers,; “Carbon in Atmospheric Particulate Matter”, 2008, ECN-E-08-060.

Mirjana Tasic, Branislava Duric-Stanojevic, Salvica Rajsic, Zoran Mijic, Velibr Novakovic,; “Physico-Chemical Characterization of PM₁₀-PM_{2.5} in the Belgrade Urban Area”; Acta Chim. Slov. 2006, 53, 401-405.

Sumana Datta ,Michael Pierce, Milton W. Datta,;“ Perlecan Signaling : Helping hedgehog stimulate prostate cancer growth”; [The International Journal of Biochemistry & Cell Biology](#),2006,38(11),1855-1861.

R. L. Pfeiffer. “Sampling for PM₁₀ and PM_{2.5} Particulates”,2005, USDA-ARS-NSTL,

The world organization prospects: The 2003 Revision, united nation publication. Sales No. E.04.XIII.6 ISBN 92-1-141396-0

WHO Report (2002). Report Environmental Health Criteria: 227 Fluoride. World Health Organization. <http://www.inchem.org/documents/ehc/ehc/ehc227.htm>. Accessed March 2012

COMPARISON OF AEROSOL ANGSTROM EXPONENT WITH AOT AT 555 nm FOR A SOUTH INDIAN CITY BENGALURU, KARNATAKA USING SATELLITE DATA

K. E. GANESH¹, A.S. MANJUNATHA¹, G. DHANYA¹, M. SHIVKUMAR², T. S. PRANESHA¹

¹Department of Physics

²Department of Electronics and Communication Engineering

B.M.S College of Engineering, Bull Temple Road, Bengaluru - 560 019, India

KEYWORDS: Angstrom exponent, AOT, satellite data,

INTRODUCTION

Tiny suspended particles in the atmosphere are known as atmospheric aerosols. Particulates are being added to the atmosphere constantly by many ways at every moment. Monitoring the concentration of these particulates in the atmosphere is very important in view of radiation balance and public health. We know that particulates have been classified as fine or small (<0.1 μ m), large (between 0.1-1 μ m) and coarse particles (>0.1 μ m). Large and coarse sized particles can deposit to Earth's surface by gravity settling, but the fine particles tend to remain in the atmosphere relatively longer time. Various particulates, so called the aerosol types have a different effect on the sign and magnitude of the aerosol radiative forcing [Satheesh and Krishna Moorthy, 2005].

The population density in fast growing cities and the related human activities (e.g., construction, transportation, energy generation, industrial production, etc.) pose serious challenge to the ecological environment [Glasow et al., 2013 and Sekovski et al., 2012]. For example, air and water pollutions associated with human activities have become one of the most forthcoming environmental issues of fast growing cities in recent decades [Kanakidou et al., 2011], especially in the developing countries where limited resources are available for addressing the pollution issues. Bengaluru, being the fast growing city of India is not free from air and water pollution problems.

The Aerosol Optical Thickness (AOT) which is a measure of the spectral solar extinction gives fair idea about the columnar particulate load in the atmosphere. Extinction by aerosol due to scattering or absorption or by both combined, is a continuous function of wavelength without selective bands or lines. Since attenuation effects of scattering and absorption by dust are difficult to separate, Angstrom (1929) suggested an empirical formula relating the aerosol optical thickness ($\tau_{p\lambda}$) with the wavelength (λ) generally known as Angstrom's turbidity formula, given by

$$\tau_{p\lambda} = \beta\lambda^{-\alpha}$$

In this formula, the index α is the wavelength exponent, β is turbidity coefficient and the wavelength λ is in μ m. Aerosol Angstrom exponent is an index which is a measure of the ratio of small to large particles in the atmosphere. Higher this ratio, larger will be the concentration of small sized particles and vice versa.

An attempt has been made in this paper to correlate the Aerosol Optical Thickness (AOT) value at 555 nm with Aerosol Angstrom exponent (Alpha) for eleven years (2000 to 2010) obtained from Giovanni satellite data.

GEOGRAPHY OF BENGALURU

Bengaluru is the capital of the Indian state of Karnataka. It has a population of over ten million as per the recent census (<http://www.indiaonlinepages.com/population/bangalore-population.html>). It is one of the fastest growing cities in India and is branded as the '*Silicon Valley of India*' for fostering the growth of Information Technology (IT) based industries in the country. Its elevation is over 900 m above sea level and is positioned at 12.97° N, 77.56° E which covers an area of 2,190 km². Being the capital city of Karnataka, majority of IT establishments, health institutes, education institutes, industries are located in Bengaluru which in turn attracts talented minds to establish them in the city. Increase in population therefore increases the extent of anthropogenic activity and pollution related problems.

METHOD OF DATA COLLECTION AND ANALYSIS

The Aerosol Optical Thickness (AOT) satellite data at 555 nm and Aerosol Angstrom exponent (Alpha) have been collected from the Giovanni site developed by NASA. Giovanni is a short form for the Goddard Earth Sciences Data and Information Services Center (GES DISC) Interactive Online Visualization ANd aNalysis Infrastructure. It is a web-based application developed by the NASA GES DISC and it is easy to use. There is no need to learn data formats, programming, or to download large amounts of data. We will get customized data analyses and visualizations with ease [Ganesh et al, 2018]. Visualization of AOT plot on time scale graph have been generated for the location Bengaluru for each year from 2000 to 2010. From the graph, average AOT at 555 nm and the Aerosol Angstrom exponent (Alpha) have been worked out for every month of each year (<http://giovanni.gsfc.nasa.gov/giovanni/>).

RESULT

An attempt has been made in this paper to understand the dependency between AOT @ 555 nm and Alpha for a period of eleven years starting from 2000 to 2010. The result analysis is presented in Tables 1&2 and Figures 1&2.

As we know already that aerosol Angstrom exponent (Alpha) gives us the measure of the ratio of small to large particles in the atmosphere and higher value of alpha indicates higher concentration of small size particles and vice versa. It is clear from figure 2 that there is a gradual increase in the small size particulate load in the atmosphere from year 2000 to 2010. From tables 1&2, a rough estimate shows that there is about 41% increase in small sized particles and about 7% increase in AOT from the year 2000 to 2010. Small sized particle undergo changes in size. They grow in the presence of water vapour, agglomerate leading to increase in size, settle down under gravity or removed by scavenging. The trend between Alpha and AOT follows almost reverse pattern as is evident from figure 1, that is, whenever Alpha value is high, AOT showed low value and vice versa. The growth of small sized particles sustains up to one threshold level. After a particular threshold level because of the influence of gravity, small particles settle down. This removal of small particles in the atmosphere results in low value of AOT. On the other hand, low value of Alpha and high value of AOT may be because of particles having size higher than small or fine particles. One of the reasons for increase in the concentration of fine particles (<0.1 μ m) is due to increase in anthropogenic activities. The largest values of AOT are associated with small values of Alpha which is characteristic of the presence of dust (Holben et al., 2001). As per the latest report from the transport department, the total vehicles registered as on January 2018 in Bengaluru is 73,07,812 (http://transport.karnataka.gov.in/uploads/editor_images/1520940902_BenJan18.pdf). Bengaluru has no major polluting industries, hence the fossil fuel burning from the vehicles contributes considerably towards the increase of fine particles in the atmosphere. The study made by Tata Energy Research Institute identifies that about 50% of particulate load is from transport sector (TERI, 2010).

CONCLUSIONS

This work gives a fair idea about the impact of urbanization and increased anthropogenic activities in the city of Bengaluru. Since the satellite data through Giovanni web site is available only at 500 nm & 555 nm, a clear picture of AOT at other wavelengths is not available at present. AOT values at many wavelengths will give a clear cut idea about Alpha & Beta and their possible relation to anthropogenic activities.

ACKNOWLEDGEMENTS

The authors wish to thank the Management and Principal of the college for providing the facility. Special thanks to the Giovanni team members for providing the data sets.

REFERENCES

- Angstrom A (1929). On the atmospheric transmission of sun radiation and on dust in the air. *Geografis Annal*, **2**, page 156.
- Ganesh K. E, G. Dhanya, M. Shivkumar, T. S. Pranesha (2018). A study on long term variation in particulate matter and black carbon aerosol optical thickness over Mysuru, India : a satellite data approach, *MAUSAM*, **69**, 2 (April 2018), 331-334.
- Glasow von R, T. D. Jickells, A. Baklanov (2013). Megacities and large urban agglomerations in the coastal zone: interactions between atmosphere, land, and marine ecosystems, *Ambio*, vol. 42, no. 1, pp. 13–28.
- Holben, B. N., D. Tanre, A. Smirnov, T. F. Eck, Slutsker, N. Abuhassan, W. W. Newcomb, J. S. Schafer, B. Chatenet, F. Lavenu, Y. J. Kaufman, J. Vande Castle, A. Setzer, B. Markham, D. Clark, R. Frouin, R. Halthore, A. Karneli, N. T. O'Neill, C. Pietras, R. T. Pinker, K. Voss, and G. Zibordi (2001). An emerging ground-based aerosol climatology: Aerosol optical depth from AERONET *Journal of Geophysical Research* Vol. 106, Pages 12,067-12,097.
- Kanakidou M., N. Mihalopoulos, T. Kindap et al (2011). Megacities as hot spots of air pollution in the east mediterranean, *Atmospheric Environment*, vol. 45, no. 6, pp. 1223–1235.
- Satheesh, S. K. and Krishna Moorthy, K (2005). Radiative effects of natural aerosols: A review, *Atmos. Envir.*, **35**, pp.2089–2110.
- Sekovski I, A. Newton, and W. C. Dennison (2012). Megacities in the coastal zone: using a driver-pressure-state-impact-response framework to address complex environmental problems, *Estuarine, Coastal and Shelf Science*, vol. 96, no. 1, pp. 48–59.
- TERI (2010). Air quality assessment, emission inventory and source apportionment study for Bangalore city. Final report, New Delhi: the energy and Resources Institute. 186 pp. [Project report No.2004 FF 28].

	Jan	Feb	Mar	Apr	May	June	July	Aug	Sep	Oct	Nov	Dec	Avg AOT
2000	***	***	0.242	0.279	0.226	***	***	***	***	0.141	0.194	0.112	0.199
2001	0.178	0.19	0.258	0.145	0.191	***	***	***	0.167	0.105	0.203	0.061	0.166
2002	0.203	0.109	0.236	0.211	0.264	***	***	***	0.185	***	0.119	0.107	0.179
2003	0.158	0.282	0.250	0.198	0.262	0.360	0.473	***	***	0.368	0.107	0.109	0.256
2004	0.145	0.232	0.242	0.241	***	0.204	0.103	***	***	***	0.094	0.090	0.168
2005	0.254	0.120	0.219	0.190	0.244	0.219	***	***	***	0.265	0.067	0.141	0.191
2006	0.099	0.097	0.272	0.309	0.247	***	***	0.331	0.185	0.094	0.156	0.152	0.194
2007	0.138	0.174	0.291	0.267	0.225	0.085	***	***	***	0.218	0.101	0.164	0.184
2008	0.091	0.176	0.166	0.236	0.250	0.296	***	***	0.091	***	0.158	0.125	0.176
2009	0.154	0.268	0.308	0.227	0.242	0.147	***	***	0.190	0.283	0.189	0.259	0.226
2010	***	0.176	0.275	0.291	0.305	0.170	***	***	0.196	***	***	0.086	0.214

*** indicates non availability of data

Table1: Average values of AOT at 555nm for eleven years

	Jan	Feb	Mar	Apr	May	June	July	Aug	Sep	Oct	Nov	Dec	Avg Alpha
2000	1.005	0.926	1.016	0.999	1.043	***	***	***	***	0.756	0.982	1.004	0.972
2001	1.115	1.010	1.037	***	1.082	***	***	***	***	***	***	1.097	1.068
2002	1.029	0.990	0.984	1.005	0.887	***	***	***	***	***	***	1.187	1.013
2003	1.104	0.971	0.936	0.967	0.976	0.947	***	***	***	***	0.876	0.991	0.971
2004	1.000	0.980	0.928	0.898	***	***	***	***	***	***	1.040	1.045	0.981
2005	1.008	0.990	0.923	***	1.143	***	***	***	***	***	0.946	1.008	1.003
2006	0.986	0.989	1.111	0.926	1.178	***	***	***	***	***	***	1.096	1.047
2007	1.016	0.967	0.941	1.008	1.262	***	***	***	***	***	1.199	1.555	1.135
2008	***	***	***	1.052	1.098	***	***	***	***	1.592	1.649	1.240	1.326
2009	1.271	1.226	1.540	1.076	***	***	***	***	***	***	***	1.807	1.384
2010	2.008	1.202	1.427	1.961	***	***	***	***	***	***	***	***	1.649

*** indicates non availability of data

Table 2: Average values of Aerosol Angstrom exponent (Alpha) for eleven years

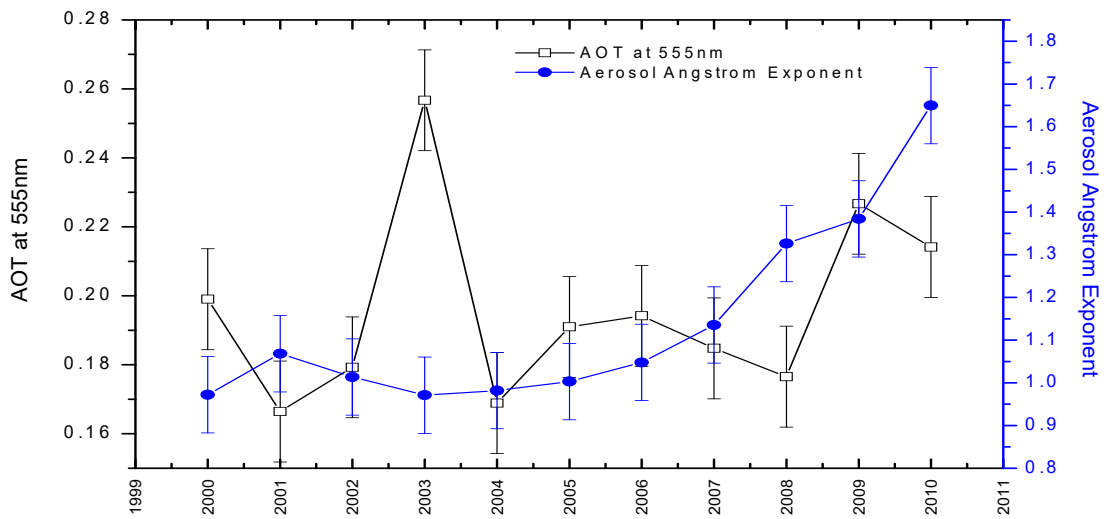


Figure 1: Mutual dependency between average AOT at 555 nm and Aerosol Angstrom Exponent for eleven years

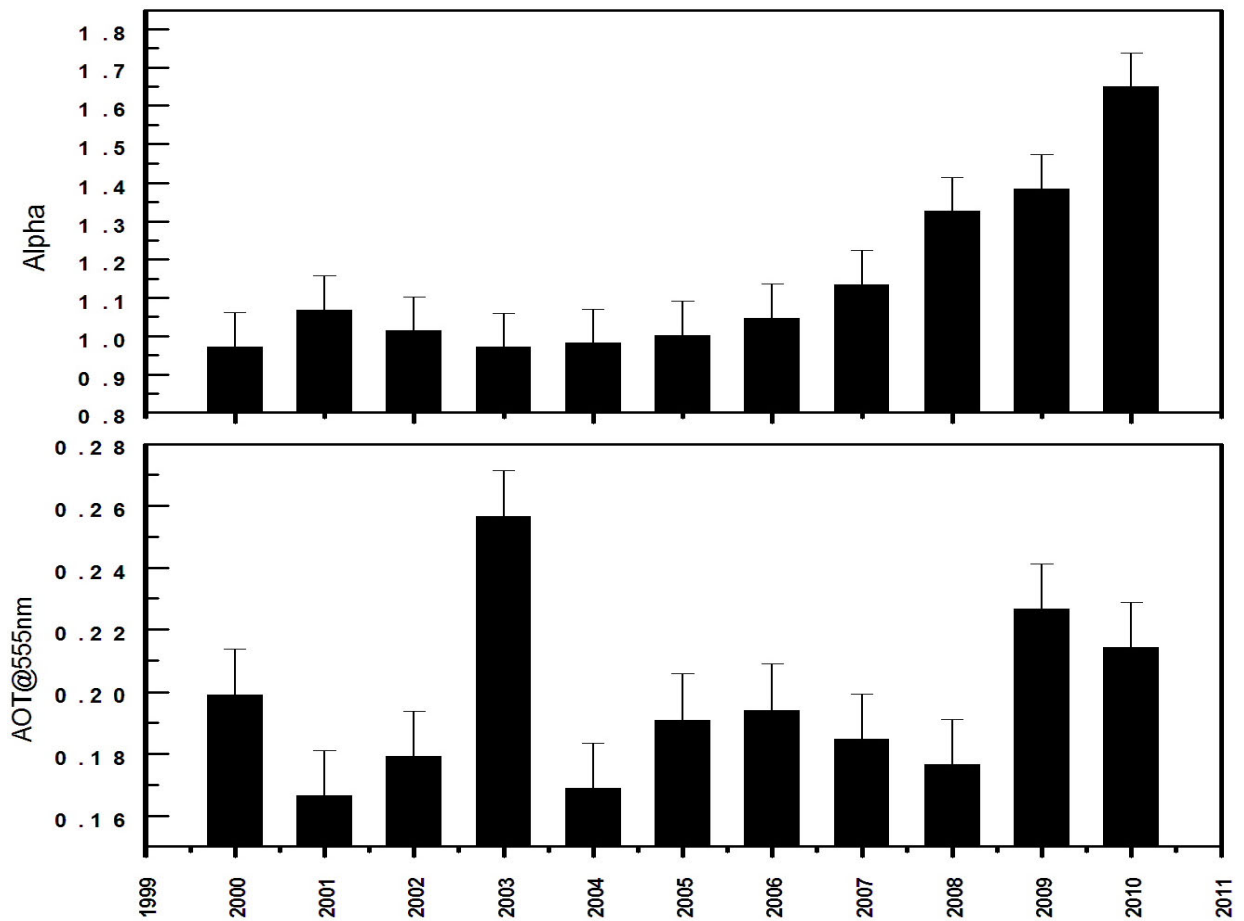


Figure 2: Variation of Average AOT at 555nm and Aerosol Angstrom Exponent for eleven years

CHEMICAL CHARACTERIZATION OF ATMOSPHERIC AEROSOLS OVER VARANASI

V. PRATAP, S. TIWARI, A. KUMAR, P. KUMAR, A. K. SINGH

Department of Physics, Institute of Science, Banaras Hindu University, Varanasi 221005

KEYWORDS: Aerosols, Sem-Edx, Ion Chromatography, PM_{10} , $PM_{2.5}$.

INTRODUCTION

Atmospheric aerosols are consequences of both anthropogenic and natural means as well, which play a vital role in climate change by modulating microphysical properties of clouds and altering the earth's radiation budget through its direct or indirect effect. Water soluble ions and heavy metals constitute major proportion of particulate matters found in the atmosphere. Particles of diameter $\leq 10\mu\text{m}$ (PM_{10}) and $\leq 2.5\mu\text{m}$ ($PM_{2.5}$) both prevail in the atmosphere and causes serious health issues to the humans (Pope and Dockery 2006). Adverse effects caused to the humans due to these particulates drives to have better understanding about their physical and chemical properties associated with them. Scanning Electron Microscopy coupled with Energy dispersive spectroscopy (SEM-EDX) and Ion chromatography (IC) are very important techniques to have better understanding of chemical characteristics of these aerosols (Srivastava et al., 2009; Pachauri et al., 2013). SEM-EDX gives elemental composition whereas IC gives information about ionic content of such particulate matters. In the present study we have attempted to investigate chemical composition and also ionic contents of aerosols over Varanasi region, which lies in the eastern part of the Indo-Gangetic plain. High Volume Samplers are deployed at our campus in order to collect data for both types of particulate matters which runs twice a week.

METHODS

The Sampling of the aerosols was carried out at height of approx. 10 metres on terrace of the Department of Physics, BHU which is a lush green campus and is devoid of any industrial activity which can influence the sampling site. The study has been carried out for the period of 3 months from November 2016 to January 2017. Aerosols were collected using two Respirable Dust Sampler one for $PM_{2.5}$ samples and other for PM_{10} , manufactured by Envirotech pvt. Ltd. Samples were collected on Whatmann filter papers. The flow rate was kept at $1\text{ m}^3/\text{hr}$. The sampling duration was 24 hours. Both Prior to the sampling and after the sampling samples were kept in Dessicator for 24 hrs in order to eliminate humidity from it and then these filters papers were weighed using high resolution electronic microbalance.

RESULTS AND DISCUSSIONS

Figure 1 shows variation of mass concentrations of particulate matters for the months from November 2016 to January 2017. From this we can easily observed high concentrations of both PM_{10} and $PM_{2.5}$ particulates as stipulated by National Ambient Air Quality Standard (NAAQS) $60\mu\text{g}/\text{m}^3$ for PM_{10} and $40\mu\text{g}/\text{m}^3$ for $PM_{2.5}$ for the period of 24 hrs. High concentrations of particulates is attributed to stable meteorological conditions and in winter season and also enhanced biomass burning in this season. SEM-EDS analysis shows dominance of carbon and oxygen for all the days of observation and other elements like Sodium, Silicon, Aluminum, Magnesium, Sulphur, Potassium and Calcium were also found in small amount in to these samples. In Figure 2 scanning electron micrographs are shown which suggests morphology of these samples and EDS spectrum is also shown which depicts elemental composition of samples collected. Ion Chromatography result shows dominance of sulphate and Nitrate ions and other

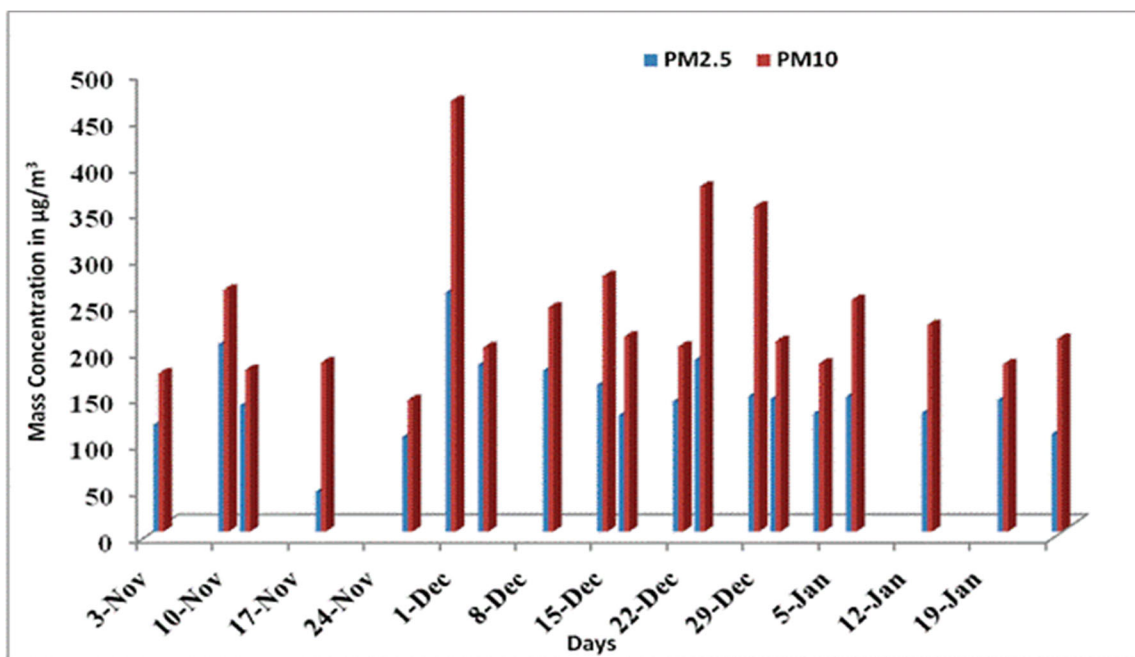


Figure 1. Variation of mass concentrations of PM₁₀ and PM_{2.5}.

ions detected are Fluoride, chloride and cations found are Potassium, Sodium, Calcium, Magnesium and Lithium. Large concentrations of SO₄²⁻ can be attributed to oxidation of Sulphur dioxide emitted as a result of burning of fossil fuels and vehicular emission (Sharma et al., 2010). Concentration of NO₃⁻ is also higher pertaining to vehicular emission and fertilizer used in agricultural farms. Similarly Mg²⁺ concentration is attributed to cement dust as numerous infrastructure activities are being carried out in the city across the year. Potassium is also known as biomass tracer and its high concentration confirms biomass burning in this season which is an obvious fact as people practice burning of woods in order to warm themselves in this winter season (Singh et al., 2014). Na⁺ ions are result of transport of sea salt to this region. Presence of Cl⁻ may be due to local activities being performed in the city like in saree industries fabric bleaching is done as Varanasi is hub of 'Saree' industries.

Table 1. Percentage Contribution of each element as obtained from EDS Spectra of different samples at Varanasi city.

Date	C	O	Al	Si	S	Cl	K	Zn	Mg	Na	Ca	Ba
3/11/2016	38.8	36.5	2.3	12.7	1.9	0.5	2.5	---	0.1	4.7	---	---
9/11/2016	44.6	34.3	1.5	7.5	2.3	0.4	4.2	---	0.1	3.5	---	1.5
11/11/2016	37	38.1	3.1	10.2	1.9	0.2	2.6	---	0.3	2.2	3.6	---
18/11/2016	36.1	38.1	2.3	10.8	2.7	0.2	2.7	---	0.2	5.7	---	1.2
26/11/2016	33.6	40.1	3.1	12.1	2.3	---	2.5	---	0.4	3.6	2.4	---
3/12/2016	33.8	38.3	2.1	15.1	0.2	---	1.5	1.8	---	4.7	---	2.4
9/12/2016	39.2	34.7	3.5	15.7	0.4	---	1.8	---	---	4.5	---	---
16/12/2016	47.7	14.8	2.7	0.3	0.6	0.6	0.4	---	---	1.4	---	---
29/12/2016	23.4	39.3	2.2	18.7	---	---	2	3.1	---	6.8	1	3.4
6/1/2017	36.8	33.7	2	14.6	---	0.8	2	2.2	---	3.9	1.1	2.9
13/01/2017	49	33	1.1	9	0.8	0.9	1.3	---	---	3.9	1	---
20/01/17	46.2	37.6	2.3	11.8	2.9	0.3	2.1	---	---	3.3	1.1	---
25/01/2017	38.4	36	2.9	10.6	4.2	---	2.5	---	---	3.2	2.1	---

CONCLUSIONS

The chemical composition and ionic contents of aerosols over Varanasi region were carried out in Department of Physics, BHU, Varanasi. Average concentrations of PM₁₀ and PM_{2.5} were found to be high as $144 \pm 44 \mu\text{g m}^{-3}$ and $236 \pm 80 \mu\text{g m}^{-3}$ respectively. Enhanced concentrations of different ions like sulfate, Nitrate, Fluoride, Bromide, Chlorine, Potassium, Sodium, Lithium were found as a result of different industrial activities and vehicular emissions in the city. SEM-EDS analysis also revealed presence of trace metals in to the atmosphere during the study period at the sampling site.

ACKNOWLEDGEMENTS

This work is partially supported through UGC, New Delhi under MRP Program and partially by ISRO-ARFI Program.

REFERENCES

- Pachauri, T., Singla, V., Satsangi, A., Lakhani, A. and Kumari, K. M. (2013). SEM-EDX Characterization of Individual Coarse Particles in Agra, India. *Aerosol and Air Quality Research*, **13**, 523.
- Pope, C.A., Dockery D.W. (2006). Health effects of fine particulate air pollution: lines that connect. *Journal of Air and Waste Management Association*, **56**, 709.
- Singh, A.K., Srivastava, M. K., Singh, M., Srivastava, A., Kumar, Sarvan, Tiwari, Shani. Singh, B. P., Bisht, D. S. and Tiwari, Suresh (2014), Characterisation of Atmospheric Aerosol by SEM-EDX and Ion Chromatography Techniques for Eastern Indo-Gangetic Plain Location, Varanasi, India, *International Journal of Advances in Earth Sciences*, **3 (2)**, 41.
- Sharma, S.K, Datta, A., Saud, T., Saxena, M., Mandal, T.K., Ahammed Y.N., Arya, B.C. (2010), Seasonal variability of ambient NH₃, NO, NO₂ and SO₂ over Delhi. *J. Environ SCI (China)*, **22 (7)**, 579.
- Srivastava, A., Jain, V.K., Srivastava, A. (2009). SEM-EDX analysis of various sizes aerosols in Delhi India. *Environmental Monitoring and Assessment*, **150**, 405.

IMPACTS OF SEVERE DUST STORMS ON AEROSOL CHARACTERISTICS OVER KANPUR

AKHILESH KUMAR, SHANI TIWARI, VINEET PRATAP, A.K. SINGH

Atmospheric Research Lab., Department of Physics, Banaras Hindu University,
Varanasi - 221005, India.

KEYWORDS: Dust Storm, Aod, Modis, Aeronet, Igb.

INTRODUCTION

Indo – Gangetic Basin (IGB) experience a frequent and intense dust storm during the pre-monsoon season (April, May, June). Mineral dusts are attributed as major component of aerosol loading in the troposphere that affects the aerosol optical properties, radiative forcing, climate system, monsoon, and hydrological cycle. These dust particles have size greater than $1\mu\text{m}$ which generally consist of quartz, mica and clay minerals generated by the natural weathering that breaks the rock. Energy balance can be modified by the atmospheric aerosols through scattering and absorption of light (Sokolik and Toon, 1996). Health of people exposed during dust event is found to be affected due to disturbed air quality of the urban and rural areas lying along the track of dust storm (Dey et al., 2004). The Thar desert centred in western India and Eastern Pakistan is the major source of dust in the Indian subcontinent (Washington et al., 2003). Due to large influx from long range transport of mineral dust aerosol from the western arid regions, highest aerosol loading over the IG plains during pre-monsoon season is found (El-Askary., 2015). The OPAC model suggests that Delhi aerosol is the best example of mixture of urban and desert aerosol type (Singh et al., 2005). Due to higher loading of aerosol during dust storm an enhanced level of water vapour is found which can affect the glob of climate modelling and rainfall pattern as well over the region. In this paper we have analysed two major dust storm events arisen during 2018 pre- monsoon season 14-June, 2018. Impact of dust storm on aerosol optical and physical properties has been studied.

METHODS

To study the properties of atmospheric aerosols we have used satellite as well as ground based measurement. AERONET is ground –based remote sensing aerosol network established by NASA. Measurement of the direct sun and diffuse sky radiances within the spectral range 340-1020 nm using CIMEL sun/sky radiometers is taken (Holben et al., 1998). AERONET provides data at three levels: level 1.0 (unscreened), level 1.5 (cloud screened) and level 2.0 (cloud screened and quality assured). All the properties of aerosols can be accessed from the AERONET website (<http://aeronet.gsfc.nasa.gov/measurement>). Water vapour content is calculated at 936 nm between the spectral range 870-1020 nm. In spite of limited spatial coverage of such ground-based aerosol remote sensing, reliable and continuous data on aerosol optical properties at particular locations is being provided.

The MODIS is a payload scientific instrument built by Santa Barbara Remote Sensing that was launched into the earth orbit by NASA in 1999 on board the Terra (EOS) satellite. It covers the entire earth every 1 to 2 days. MODIS covers large spectral range varying from $0.4\mu\text{m}$ to $14.4\mu\text{m}$ (36 channels). The channels between 0.4 to $2.1\mu\text{m}$ are important for studying aerosol properties and five channels near infrared (0.865 , 0.905 , 0.936 , 0.940 and $1.24\mu\text{m}$) are important for remote sensing to water vapour (Remer et al., 2005). The retrieval algorithm and accuracy of the aerosol products (AOD and Angstrom exponent) are well explained *and uncertainty in MODIS AOD measurement over the land is found to be $\pm (0.05 \pm 0.15 \tau)$* . Images of dust storms are downloaded from site (<https://lance-modis.eosdis.nasa.gov/cgi-bin/imagery/realtime.cgi>).

RESULTS & DISCUSSIONS

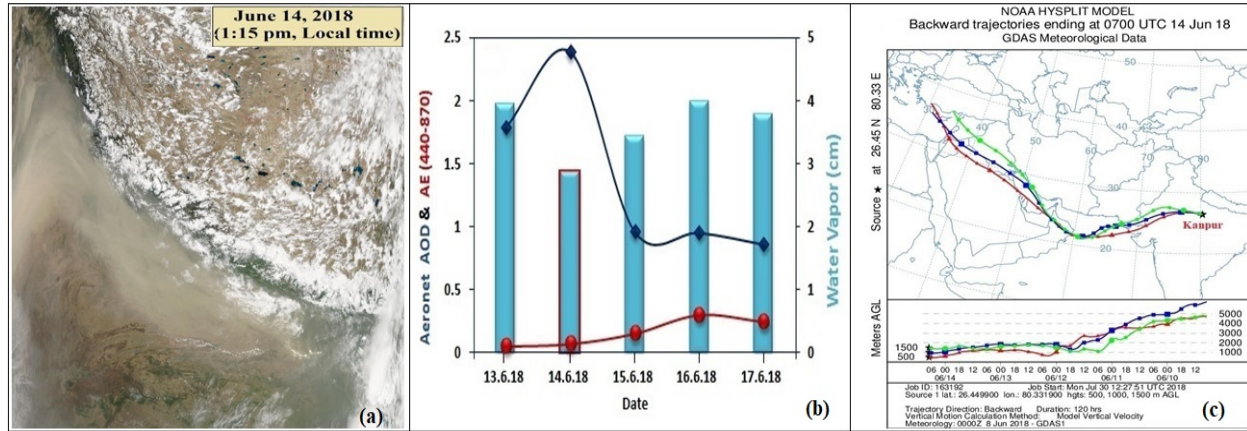


Figure 1. (a) MODIS AQUA images showing long range transport of dust storms. The white colour exhibits clouds. The dust is shown in pale beige colour. (b) Variation of AOD, Angstrom Exponent (AE) and water vapour during the dust storm event. (c) Five days back-trajectory at Kanpur using HYSPLIT model during the dust storm.

Aerosol Optical Depth (AOD) is an important parameter to characterize the atmospheric aerosols and with the help of AOD we can also get the information about solar radiation by scattering and absorption process (Ranjana et al., 2007). Along with AOD, Angstrom Exponent is another important parameter which gives size distribution of aerosol. AOD (τ) and AE(α) follow the Angstrom's power law, given by $\tau(\lambda) = \beta\lambda^{-\alpha}$. In figure 1(b) variation in AOD₅₀₀ (τ), AE (α) and water vapour observed by AERONET level 1.5 data during the dust storms for 2018 are shown. Generally AOD does not exceed value >1 until there is some special events present like haze, cloudy weather, dust storms and others. Average value of τ during non-dusty days is generally found in the range of 0.4–0.6 (Prasad and Singh, 2007). During the Delhi dust storm (Apr–June, 2003), AE value is found to be decreased drastically (Singh et al., 2005) and in case of Saharan dust as well. On the storm day (14 June 2018) value of AOD is found to be approximately 2.5 times greater than monthly average AOD. Corresponding lower values of Angstrom Exponents is found ($\alpha \sim 0.6$).

With the help of HYSPLIT back trajectory model, source and path followed by the dust storm can be predicted. Image of this trajectory can be extracted from the site NOAA HYSPLIT (<http://www.arl.noaa.gov/>). In figure 1(c) air mass back trajectory, during the dust storm, at three heights has shown. For the dust storm occurred on 14th June, it is taken at heights 500, 1000, 1500 m respectively. HYSPLIT back trajectory directly gives the information about transportation of dust particles e.g. whether the dust storms are passing through over the sea surface or only they cover the desert or mid arid regions. The dust storm event of 14 June, 2018 is mainly originated from Middle East, covering the gulf regions which affect the Indo- Gangetic Basin. Difference in AOD can be clearly seen due to the change in trajectory of the dust storms, which follow different paths for dust event on 14 June. This large difference is due to the contribution of Thar Desert, because dust storm (for all three levels) from source region is passing through the Thar. Major changes in the optical properties have been observed due to slight change of dust storm trajectory. It may be due to the intense dust storm at the end of pre-monsoon season or major contribution of Thar Desert.

Precipitable water vapour (PWV) can be defined as the total amount of water vapour contained in a vertical column from the ground to the specified height in the troposphere (Turner et al., 2002). Water Vapor is the most abundant greenhouse gas and much important component of the atmosphere (Solomon et al., 2010).

Water vapour is very sensitive to the onset of monsoon. In figure 1(b) variation of water vapour along with AOD and AE is shown. Water vapour after the dust storm event is found to be enhanced as the dust passing through the Arabian Sea. Dust particles absorb moisture from the Arabian Sea before entering the IG Basin which cause enhancement in water vapour. Water vapour on the event day of 14 June is found to be enhanced up to 3 cm and 4 cm respectively.

CONCLUSIONS

During the dust storm event significant changes in aerosol optical properties are found. AOD values is found to be increased drastically ($\tau \sim 2.4$) with corresponding lower exponent value ($\alpha \sim 0.06$). Enhancement of water vapour content is found due to the moisture transportation from Arabian Sea along with dust aerosols. MODIS images, synoptic meteorological condition, air mass back trajectory and AERONET analysis clearly suggest that the dust storm originated from the Middle East, reached over Indian subcontinent through long range transportation and covered entire IGB.

ACKNOWLEDGEMENTS

AK is thankful to DST New Delhi for financial support under Inspire-JRF program. We are also thankful to NASA for providing satellite (MODIS) data (MOD 08-D3, <http://modis-atmos.gsfc.nasa.gov/>). The work is partially supported by ISRO Bangalore under ISRO-SSPS to BHU.

REFERENCES

- Dey, S., Tripathi, S.N., Singh, R.P., Holben, B.N. (2004). Influence of dust storms on the aerosol optical properties over the Indo-Gangetic basin. *Journal of Geophysical Research D: Atmospheres* **109**, 1.
- El-Askary, H., 2015. On the Detection and Monitoring of the Transport of an Asian Dust Storm Using Multi-Sensor Satellite Remote Sensing. *Journal of Environmental Informatics* **25**, 99–116.
- Prasad, A.K., Singh, R.P. (2007). Changes in aerosol parameters during major dust storm events (2001-2005) over the Indo-Gangetic Plains using AERONET and MODIS data. *Journal of Geophysical Research Atmospheres* **112**.
- Ranjan, R.R., Joshi, H.P., Iyer, K.N. (2007). Spectral Variation of Total Column Aerosol Optical Depth over Rajkot: A Tropical Semi-arid Indian Station. *Aerosol and Air Quality Research* **7**, 33.
- Remer, L.A., Kaufman, Y.J., Tanré, D., Mattoo, S., Chu, D.A., Martins, J. V., Li, R.-R., Ichoku, C., Levy, R.C., Kleidman, R.G., Eck, T.F., Vermote, E., Holben, B.N. (2005). The MODIS Aerosol Algorithm, Products, and Validation. *Journal of the Atmospheric Sciences* **62**, 947.
- Singh, S., Nath, S., Kohli, R., Singh, R. (2005). Aerosols over Delhi during pre-monsoon months: Characteristics and effects on surface radiation forcing. *Geophysical Research Letters* **32**, 1.
- Sokolik, I.N., Toon, O.B. (1996). Direct radiative forcing by anthropogenic airborne mineral aerosols. *Nature* **381**, 681.
- Solomon, S., Rosenlof, K.H., Portmann, R.W., Daniel, J.S., Davis, S.M., Sanford, T.J., Plattner, G.K. (2010). Contributions of stratospheric water vapor to decadal changes in the rate of global warming. *Science* **327**, 1219.
- Turner, D.D., Ferrare, R.A., Heilman Brasseur, L.A., Feltz, W.F., Tooman, T.P. (2002). Automated

retrievals of water vapor and aerosol profiles from an operational raman lidar. *Journal of Atmospheric and Oceanic Technology* **19**, 37.

Washington, R., Todd, M., Middleton, N.J., Goudie, A.S. (2003). Dust-storm source areas determined by the total ozone monitoring spectrometer and surface observations. *Annals of the Association of American Geographers*.

VARIABILITY OF PM_{2.5} AND PM₁₀ AND THE OPTICAL PROPERTIES OF AEROSOLS OVER VARANASI

P. KUMAR¹, A. CHOUDHARY², V. PRATAP¹, A. K. SINGH¹ AND A. SHUKLA²

¹Department of Physics, Institute of Science, Banaras Hindu University, Varanasi, India.

²Transport Planning and Environment Division, CSIR-Central Road Research Institute, New Delhi, India.

KEYWORDS: Pm_{2.5}, Pm₁₀, Aerosols, Modis Aod, Ae, Hysplit.

INTRODUCTION

Atmospheric aerosols are the major constituents of the Earth's atmosphere which have a significant impact on regional as well as on the global climate change (Satheesh *et al.*, 2006). High natural and anthropogenic sources all over world have significantly increased the aerosol loading of the Earth's atmosphere. Indo-Gangetic Plain is one of the largest river bases in the world which is highly populated and experiences strong intra-seasonal and inter-annual aerosol variability (Tiwari *et al.*, 2015). The sources of atmospheric aerosols over Indian landmasses are found highly variable and have distinct features (Verma *et al.*, 2015). During pre-monsoon season the northern India is dominated mostly by the loading of dust particles (Gautam *et al.*, 2011). Aerosol optical properties such as aerosol optical depth (AOD) and angstrom exponent (AE) are the key factors for climate change research. In the present study, on the daily basis PM_{2.5}, PM₁₀, using high volume samplers and the MODIS Aqua AOD and AE satellite data were collected and analyzed to study the variability of PM_{2.5}, PM₁₀, and the optical properties of aerosols over Varanasi, situated at Indo-Gangetic basin.

METHODS

The experimental setup using two high volume air samplers was made in the Department of physics, Banaras Hindu University, Varanasi (latitude 25.2677° N and longitude 82.9913° E) for the collection of PM_{2.5} and PM₁₀ particles on daily basis. The PM_{2.5} particles were collected with the help of Fine particulate sampler (Envirotech APM550) and PM₁₀ samples was collected using Respirable dust sampler (Envirotech APM 460NL). The samples collection was done ~24 hrs for PM_{2.5} and for PM₁₀ particles. The mass concentrations of PM_{2.5} and PM₁₀ as well as MODIS Aqua AOD and AE during January 2017 to December 2017 were analysed. The MODIS Aqua AOD at 550nm and AE at 0.412-0.47µm values were collected from the Giovanni site (<http://giovanni.gsfc.nasa.gov/giovanni/>). To find the different sources of the aerosols HYSPLIT air mass back trajectories has been analyzed.

RESULTS & DISCUSSIONS

The monthly mean mass concentrations of PM_{2.5} and PM₁₀ during January 2017–December 2017 are shown in Figure 1 along with their standard deviations. The maximum monthly mean concentrations of PM_{2.5} and PM₁₀ were found to be 167.48±25.64µg/m³ and 264.46±65.34µg/m³ respectively in the month of December 2017. However the minimum monthly mean concentrations of PM_{2.5} and PM₁₀ were found to be 25.47±16.95µg/m³ in the month of April 2017 and 115.67±78.94µg/m³ in the month of October respectively. The maximum PM_{2.5} and PM₁₀ concentrations were observed during the winter season mostly in the month of December 2017 due to biomass burning and other anthropogenic activities. The PM_{2.5} and PM₁₀ concentrations were observed to be highest during winter followed with summer season. The annual mean of PM₁₀ is about nearly three times higher than the standard set by NAAQ (60µg/m³) for PM₁₀. However, PM_{2.5} is twice higher than the annual standard (40µg/m³) set by NAAQ for PM_{2.5}.

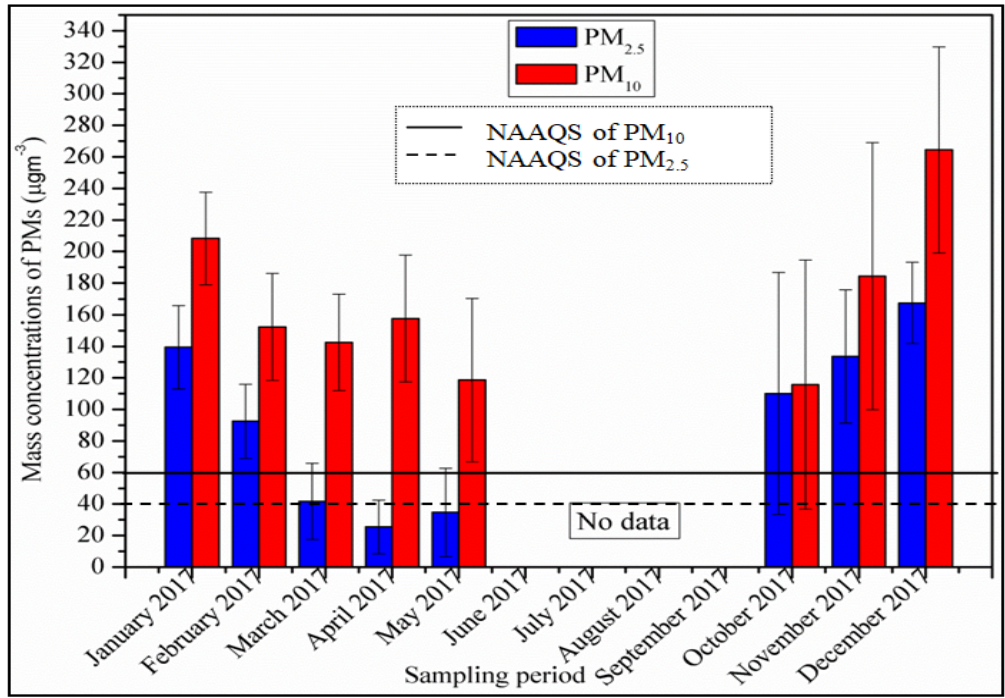


Figure 1. The monthly mean mass concentrations and standard deviations of PM_{2.5} and PM₁₀ for year 2017.

It is observed that monthly mean average AODs are fairly high in the month of December 2017 (1.11 ± 0.66) in the winter season. The production of small size particles is mainly because of anthropogenic activities in the winter season in Varanasi. Figure 2 shows the monthly mean and standard deviations of AOD at 500nm and AE at 412-470nm during January 2017–December 2017.

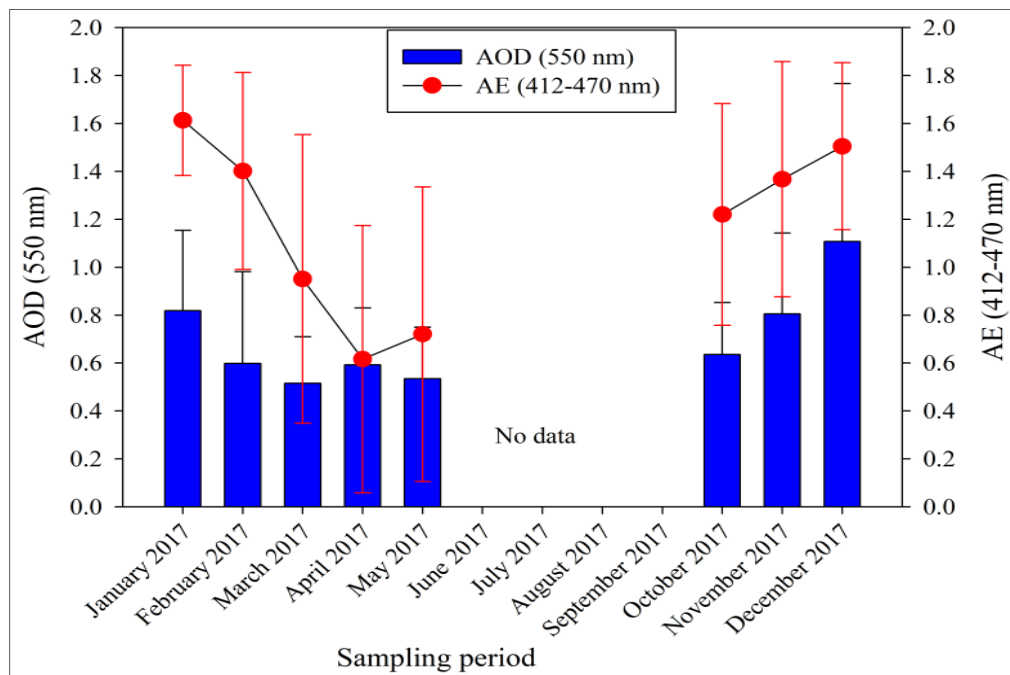


Figure 2. The monthly mean and standard deviations of AOD at 500nm and AE at 412-470nm during the year 2017.

The air mass back trajectories originating from Northern India during the winter are carrying a large amount of biomass-burning and continental aerosols over the study area (Reddy *et al.*, 2016). Figure 3 (a) and (b) shows the seven days backward trajectory for the December 8, 2017 and for the May 5, 2017 respectively.

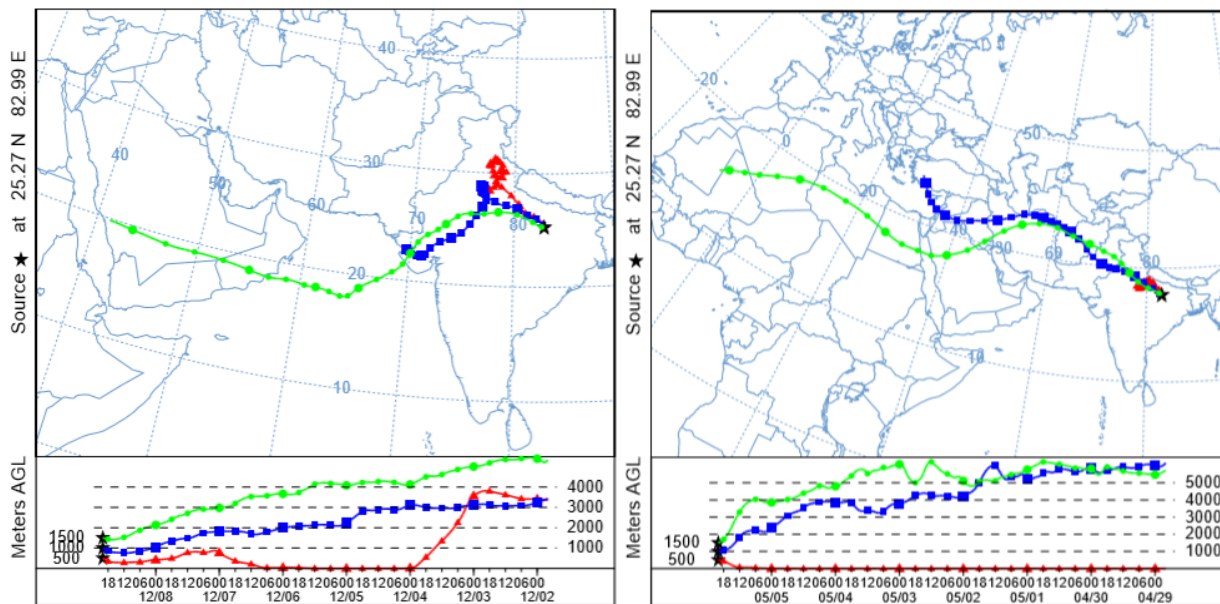


Figure 3 (a), (b). The seven days backward trajectory analysis for the month of December 8, 2017 and for May 5, 2017 respectively.

The AOD observed with minimum value of 0.22 in March month due to air mass transition time. The high values of MODIS Aqua AOD during summer months could be attributed to the increased concentration of continental aerosol loading due to high temperatures. However in the present study, same as the other sources such as long-range transport of dust from north-western India are also the major concerns (Badrinath *et al.*, 2007). The $AE > 1$ values indicate the fine mode particles dominate while $AE < 1$ values suggest the dominance of coarse mode particles (Eck *et al.*, 2010). The maximum daily mean values of AE are found to be 1.61 ± 0.23 during month of January 2017 and minimum daily mean values of AE 0.62 ± 0.56 during month of April 2017, respectively. Higher the values of AE during winter are mainly due to the biomass/bio fuel burning enhancement, which produces higher quantities of fine mode and absorbing aerosols in the atmosphere. The lower values of AE in summer season are due to dust activity in the downwind direction of the dust outflows (Prasad *et al.*, 2007).

CONCLUSIONS

In the present study, the concentrations of $PM_{2.5}$, PM_{10} , MODIS AOD and AE are studied in Varanasi. The concentration of $PM_{2.5}$ is found dominated in the winter months whereas PM_{10} is found to be dominated in the summer months. The AE values are found to be high in winter and low during summer months. The maximum monthly mean AOD in winter season is associated with large AE values indicative of fine mode particles. The high value of AOD occurs in the SW direction indicates pollutants are mainly from dust and agricultural residues burning over the study area. The seven days back trajectories analyses show that the arid regions of the Thar Desert, Afghanistan, Middle East and the Africa (Saharan Desert) have been found

to be major contributors of the mineral dust over Varanasi during the summer and biomass burning during winter season.

ACKNOWLEDGEMENTS

This work is supported by the SERB-DST, New Delhi, India, under the scheme of SERB National Post-Doctoral Fellowship (PDF/2017/001898). The work is partially supported by UGC under MRP program. The back-trajectories used in this study were obtained from website <https://www.ready.noaa.gov/HYSPLIT.php>. Authors are also thankful to MODIS team and NASA (<https://giovanni.gsfc.nasa.gov/giovanni/>) for providing satellite data.

REFERENCES

- Badarinath, K.V.S., Shailesh Kumar, K., Kaskaoutis, D.G., Kambezidis, H.D., (2007). Influence of atmospheric aerosols on solar spectral irradiance in an urban area. *J. Atmos. Sol.-Terr. Phy.* **69**, 589–599.
- Eck, T.F., Holben, B.N., Sinyuk, A., Pinker, R.T., Goloub, P., Chen, H., Chatenet, B., Li, Z., Singh, R.P., Tripathi, S.N., Reid, J.S., Giles, D.M., Dubovik, O., O'Neill, N.T., Smirnov, A., Wang, P., Xia, X. (2010). Climatological aspects of the optical properties of fine/coarse mode aerosol mixtures. *J. Geophys. Res.* **115**, D19205.
- Gautam, R., Hsu, N.C., Tsay, S.C., Lau, K.M., Holben, B., Bell, S., Smirnov, A., Li, C., Hansell, R., Ji, Q., Payra, S., Aryal, D., Kayastha, R., Kim, K.M. (2011). Accumulation of aerosols over the Indo-Gangetic plains and southern slopes of the Himalayas: distribution, properties and radiative effects during the 2009 pre-monsoon season. *Atmos. Chem. Phys.*, **11**, 12841–12863.
- Prasad, A. K., R.P. Singh and Ashbindu Singh (2007). Seasonal climatology of aerosol optical depth over the Indian subcontinent: trend and departures in recent years, *Int. J. Rem. Sen.* **27**, 2323.
- Reddy, K.R.O., G. Balakrishnaiah, K. Rama Gopal, N.S.K. Reddy, T. Chakradhar Rao, L.T. Reddy, Reddy, N.S. M.V. Hussain Reddy, R. R. Reddy, S.K.R. Boreddy and S. Babu (2016). Long term (2007 – 2013) observations of columnar aerosol optical properties and retrieved size distributions over Anantapur, India using Multi Wavelength solar Radiometer. *Atmos. Environ.* **142**, 238–250.
- Satheesh SK, Moorthy KK, Kaufman YJ, Takemura T (2006). Aerosol optical depth, physical properties and radiative forcing over the Arabian Sea. *Meteorog. Atmos. Phys.* **91**, 45–62.
- Tiwari S, Srivastava AK, Singh AK, Singh S (2015). Identification of aerosol types over IndoGangetic Basin: implications to optical properties and associated radiative forcing. *Environ. Sci. Pollut. Res.*, **22**, 12246-12260.
- Verma, S., D. Prakash, P. Ricaud, S. Payara, J. Attie, and M. Soni (2015). A new classification of aerosol sources and types as measured over Jaipur, India, *Aerosol Air Qual. res.* **15**, 985-993.

CONCENTRATION OF INDOOR RADON, THORON AND THEIR DAUGHTER PRODUCTS IN AND AROUND KOLAR GOLD FIELDS, KOLAR DISTRICT, KARNATAKA, INDIA

K. UMESHA REDDY¹, C. NINGAPPA², E. SRINIVASA³ AND J. SANNAPPA⁴

¹Research and Development centre, Bharathiar University, Coimbatore- 641 046, Tamil Nadu, India.

²Dept. of Physics & VTU RC, Vidya Vikas Institute of Engg. and Tech., Mysuru- 570028, India.

³Department of Physics, IDSG Govt. College, Chickamagaluru, Karnataka, India.

⁴Department of Studies in Physics, Kuvempu University, Shimoga-577451, India.

(*Correspondence at ningappacvvi@gmail.com)

KEYWORDS: Radon, Thoron, dosimeter, KGF.

INTRODUCTION

Radon have three naturally arising radioactive isotopes namely ^{220}Rn (thoron), with half-life of 55.6 s, ^{219}Rn (Actinon) with half-life of 3.96 s and ^{222}Rn with half-life of 3.825 days (Mukesh Kumar *et al.*, 2014). More than 50 % (1.26 mSv) of the annual effective dose is due to inhalation of ^{222}Rn , ^{220}Rn and their decay products. Out of which, 1.15 mSv is received from ^{222}Rn and its decay products, while 0.11 mSv is from ^{220}Rn and its products (Rosaline Mishra andMayya 2008).

The main aim of the present work is to determine indoor concentration of radon, thoron their progenies using single entry pinhole dosimeter and DRPS (Direct Radon Progeny Sensor) and DTPS (Direct Thoron Progeny Sensor), developed by BARC, Mumbai. Measurement have been carried out at 30 different places of the study area in three different seasons of the year. Study area is around Kolar Gold Fields (KGF) –a world famous gold mine, Kolar district, Karnataka. No such research work related this type of study as carried out in this area and hence, this study is very important.

The geology of the study area consists of closepet granite, hornblende gneiss, champion gneiss, quartzite, metabasalt, metagabbro, dolerite dyke, amphibolite, grey granite, ferruginous and fuchsite quartzite. Major portion of the study area is covered by hornblende gneiss and closepet granite. Geological map of the study area with selected locations is as shown in Figure 1. From the obtained data, equilibrium factor between radon, thoron and their progeny and annual effective dose received due to radon and thoron were also estimated and compared with the world average safe values.

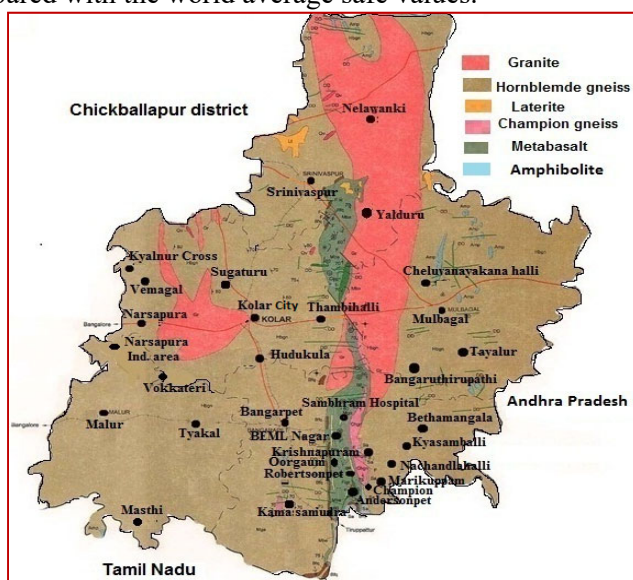


Figure 1. Geological map of study area with locations.

METHODS

The instrument used is pin-hole-based radon–thoron dosimeter consists of two separated compartments. Each compartment has a length of 4.1 cm and a radius of 3.1 cm (Sahoo *et al.*, 2013). Schematic diagram of Pin-hole dosimeter is shown in Figure 2. In the first compartment, named as radon + thoron chamber, both radon and thoron enter through a glass fibre filter paper (pore size 0.7 mm), and the air containing radon and thoron from this compartment diffuses to the second compartment, named as radon chamber, through pin hole which acts as a diffuse barrier that cut off the entry of thoron into this chamber due to its short half-life (55.8 s). Hence, only radon enters into this compartment (Prabhjot Singh *et al.*, 2015).

For progeny measurements, deposition-based direct radon and thoron progeny sensors (DTPS/DRPS) were used as shown in Figure 3. After the exposure time, the LR-115 films retrieved, etched in 2.5 NaOH solutions at a temperature of 60⁰ C for a period of 90 min at constant temperature water bath. Then the films were washed and dried. The track density was obtained by using a standard spark counter with operating voltage (500 V) and also a pre-sparking voltage (900 V) of spark (Rosaline Mishra and Mayya 2008). By using different equations, concentration of radon, thoron and their progeny, inhalation dose due to radon, thoron and their progeny and equilibrium factors of radon and thoron are calculated.

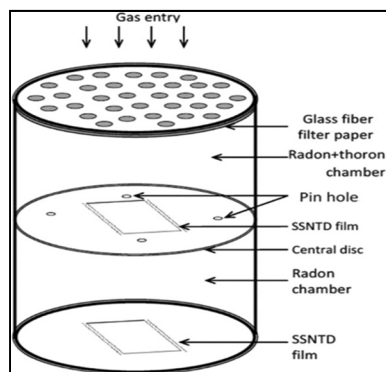


Figure 2. Schematic diagram of Pin-hole dosimeter.

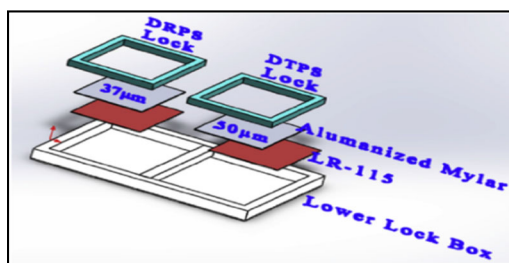


Figure 3. Direct Radon and Thoron progeny sensors.

RESULTS & DISCUSSIONS

The measured values of average indoor radon, thoron and their progeny concentrations, inhalation dose and equilibrium factors of radon and thoron at different places of the study area during summer, winter and rainy seasons of a year have been summarised in Table 1. The dwellings selected for indoor study are randomly chosen at different places of the study area constructed by using bricks and cement with different types of floorings in ground floor. It is observed that the large variation of radon and thoron concentration from one place to another and average radon concentration is higher than thoron concentration. In some places, thoron concentration is higher than the radon concentration. This is due to various factors like

variation in activity of radium and thorium in soil, rocks, building materials used for construction of houses, ventilation condition, radon in water, local geology and meteorological parameters etc., (Ningappa *et al.*, 2008, Sannappa *et al.*, 2010).

The Equilibrium Equivalent Radon Concentration (EERC) and Equilibrium Equivalent Thoron Concentration (EETC) are measured using Direct Radon Progeny Sensors (DRPS) and Direct Thoron Progeny Sensors (DTPS) respectively. At all the places, obtained annual inhalation dose values are within the action level of 3-10 mSv.y⁻¹ as recommended by ICRP (ICRP 1993) and the average is lesser than the global average value of 2.4 mSv.y⁻¹ (UNSCEAR 1998).

The Equilibrium Factor (EF) is the measure of the degree of radioactive equilibrium between radon, thoron, and its short-lived radioactive decay products, and is important to determine the dose accurately. The average value of radon is lesser than the UNSCEAR reported values of 0.4 for radon (UNSCEAR 2000) and for thoron higher than the reported value of 0.03 for thoron (UNSCEAR 2008).

Seasonal variation of radon and thoron and their progeny concentration are shown in Figures 4 and 5, respectively. The results show that the higher concentration of radon, thoron and their progeny are observed during winter season when compared to summer and rainy seasons which mainly depend on ventilation conditions.

Parameter	Range	Average
Radon Conc.	24.9-125.9 (Bq.m ⁻³)	64.3 (Bq.m ⁻³)
Thoron Conc.	20.0-128.3 (Bq.m ⁻³)	58.7 (Bq.m ⁻³)
EERC	6.5-22.5 (Bq.m ⁻³)	15.4 (Bq.m ⁻³)
EETC	0.9-7.4 (Bq.m ⁻³)	4.3 (Bq.m ⁻³)
Inhalation dose	0.77-3.68 (mSv.y ⁻¹)	2.31 (mSv.y ⁻¹)
Radon Equilibrium Factor	0.17-0.42	0.25
Thoron Equilibrium Factor	0.03-0.13	0.08

Table 1. The range of different parameters with average values measured across the study area.

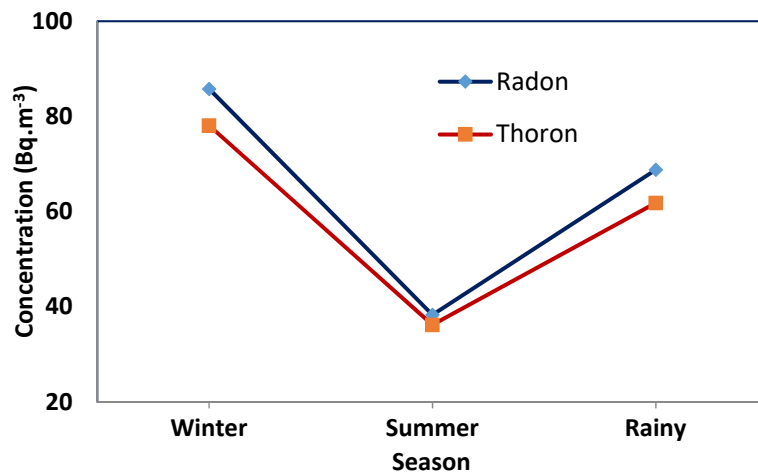


Figure 4. Seasonal variation of average concentration of indoor radon and thoron.

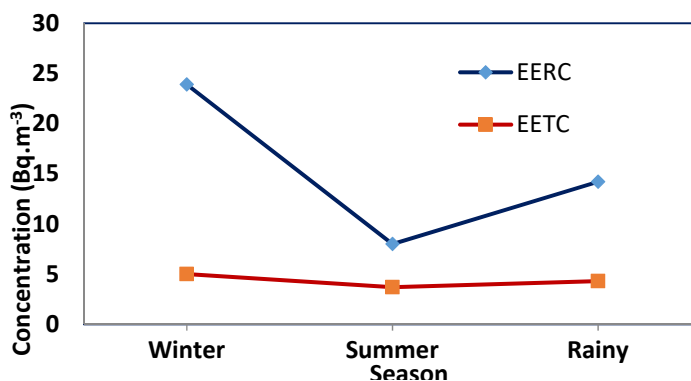


Figure 5. Seasonal variation of average indoor radon and thoron progeny concentration.

CONCLUSIONS

The average indoor concentration of radon value in the present study is 64.3 Bq.m^{-3} which is higher than the world average value of 40 Bq.m^{-3} for dwellings and national average of 42 Bq.m^{-3} recommended by UNSCEAR 2000, and lower than the action level of 100 Bq.m^{-3} recommended by WHO. The average indoor concentration of thoron value in the present study is 58.7 Bq.m^{-3} which is higher than the world average value of 10 Bq.m^{-3} for dwellings and national average of 12.2 Bq.m^{-3} recommended by UNSCEAR 2000. The higher values of indoor radon, thoron and their progeny concentration are observed at the places having granitic rocks which have higher activity of radionuclides. It also depends on type of building materials, ventilation condition and local geology.

Higher concentration of radon, thoron and their progeny and annual inhalation dose in indoor environments has been observed in winter season compared to summer and rainy seasons. Compared to summer season, in rainy season slightly higher values have been observed.

REFERENCES

B. K. Sahoo, B. K. Sapra, S. D. Kanse, J. J. Gaware, Y. S. Mayya (2013). A new pin-hole discriminated $^{222}\text{Rn}/^{220}\text{Rn}$ passive measurement device with single entry face. *Radiat Meas*, 58, 52.

International Commission on Radiological Protection (ICRP) (1993); Protection against radon-222 at home and at work. ICRP Publication 65, Pergamon Press, Oxford.

Mukesh Kumar, Anshu Agarwal, Rajesh Kumar (2014). Study of radon, thoron and their progeny levels in indoor environment of Firozabad city in U.P., India, *J Radioanal Nucl Chem*, 302(3), 1475.

Ningappa, C., Sannappa, J., Chandrashekara, M. S., and Paramesh, L., (2008). Concentrations of radon and its daughter Products in and around bangalore city. *Radiation Protection Dosimetry* (2008), Vol. 130, No. 4, pp. 459–465.

Prabhjot Singh, Parminder Singh, Surinder Singh, B. K. Sahoo, B. S. Bajwa (2015). A study of indoor radon, thoron and their progeny measurement in Tosham region Haryana, India. *J Radiat Res Appl Sci* 8(2), 226.

Rosaline Mishra & Mayya Y S (2008). Study of a deposition-based direct thoron progeny sensor (DTPS) technique for estimating equilibrium equivalent thoron concentration (EETC) in indoor environment. *Radiat Meas*, 43(8), 1408.

Sannappa J, Ningappa C, NarasimhaPrakash KN (2010).Natural radioactivity levels in granite regions of Karnataka State.Ind. J. Pure Appl. Phys. 48(11), 817.

United Nations Scientific Committee on the Effects of Atomic Radiation (UNSCEAR) (2000).Sources and effects of ionizing radiation.Report to the General Assembly with Scientific Annexes. Vol. 1, Annex B: Exposure from natural radiation sources. United Nations.

United Nations Scientific Committee on the Effects of Atomic Radiation (UNSCEAR) (1998).Sources and effects of ionizing radiation.Report to the General Assembly with Scientific Annexes. Vol. 1, Annex B: Exposure from natural radiation sources. United Nations.

United Nations Scientific Committee on the Effects of Atomic Radiation (UNSCEAR) (2008).Sources and effects of ionizing radiation.Report to the General Assembly with Scientific Annexes. Vol. 1, Annex B: Exposure from natural radiation sources, United Nations.

DEPENDENCE OF AEROSOL REMOVAL ON INITIAL CONCENTRATION USING TWO GROUP MODEL

S Anand^{1,2}, Tanmay Sarkar¹, Jayant Krishan¹, Kapil Deo Singh¹, R M Tripathi^{1,2}, Y S Mayya³

¹Bhabha Atomic Research Centre, Mumbai - 400085, India

²Homi Bhabha National Institute, Mumbai - 400094 India

³Dept of Chemical Engineering, IIT, Mumbai, India

KEYWORDS: Aerosol, two group model, removal of aerosol, air cleaning.

INTRODUCTION

Aerosols are produced in various industries manufacturing chemicals, medicine, paint, etc. under controlled conditions. Various fuels burned in houses also generate large number of aerosol particles. In the context of nuclear fuel cycle, large release of radioactive aerosols is possible only during the accidental conditions. These large releases are removed in the reactor containment system along with engineered safety features. The study of evolution of aerosol characteristics in these systems is important to minimize the environmental impact. Hence, large number of theoretical as well as experimental works are carried out to understand the evolution of aerosol metrics. In the present study, the dependency of ventilation controlled removal of aerosols from containment on their initial concentration is studied using two-group model.

METHODOLOGY

Primary aerosol particles released undergo microphysical processes such as coagulation and get depleted due to ventilation and depletion. These processes lead to a distribution in size of the aerosol particles, which are distributed in different size bins, each of them referred to as a mode. For each of these modes, the distribution function is assumed and the equations are solved to obtain the aerosol properties.

In the present study, the primary particles (group 1) coagulate to form secondary particles (group 2). Hence, two modes exist in the system i.e. the system consist of particles represented by two size groups. Volume of the primary and coagulated particles are assumed to be V_1 and V_2 respectively. The loss of two particles in group 1 leads to increment of a particle in group 2. Hence, the gain to second group is, $\left(\frac{1}{2}\right) K_{11} n_1^2$.

Therefore, two-group equation is expressed as:

$$\frac{dn_1}{dt} = S - K_{11}n_1^2 - K_{12}n_1n_2 - (\lambda_0 + \lambda_1)n_1 \quad (1)$$

$$\frac{dn_2}{dt} = \frac{1}{2}K_{11}n_1^2 - \frac{1}{2}K_{22}n_2^2 - \{\lambda_0 + \lambda_2\}n_2 \quad (2)$$

where, n_1 and n_2 are number concentration of primary (Group1) and secondary particles (Group 2) respectively. $S(t)$ is the source emission rate of aerosols. K_{11} , K_{12} and K_{22} are coagulation kernel representing coagulation of two primary particles, a primary and a secondary particle and two secondary particles respectively. λ_0 is the ventilation rate, and λ_1 and λ_2 are removal of primary and secondary particles respectively due to deposition.

The mass balance equation is given by,

$$\frac{1}{\rho} \frac{dw}{dt} = SV_1 - (\lambda_0 + \lambda_1)n_1V_1 - \{\lambda_0 + \lambda_2\}V_2n_2 \quad (3)$$

where, $\frac{dw}{dt}$ is the rate of change of total aerosol mass in the chamber, and ρ is the particle density. The first term on the RHS of Eq.(3) represents addition of primary aerosol source, second term on the RHS is the removal of primary particles due to ventilation and deposition, and third term is removal of secondary particles.

Conservation of mass law relates volume of the secondary particles in terms of primary particles and can be written as (assuming $\rho = 1$):

$$V_2(t) = \frac{w(t) - n_1 V_1}{n_2(t)} \quad (4)$$

The general removal rate is obtained from the following equation (a minimum value of removal rate has been considered):

$$\lambda(V) = \frac{\lambda_{min}}{\alpha + \beta} \left\{ \beta \left(\frac{V}{V_{min}} \right)^{-\alpha} + \alpha \left(\frac{V}{V_{min}} \right)^{\beta} \right\} \quad (5)$$

where, λ_{min} , and V_{min} represent the minimum value of removal rate and the particle volume at which it occurs. Monomer removal rate for primary and secondary particles is then given by:

$$\lambda_1 = \frac{\lambda_{min}}{\alpha + \beta} \left\{ \beta \left(\frac{V_1}{V_{min}} \right)^{-\alpha} + \alpha \left(\frac{V_1}{V_{min}} \right)^{\beta} \right\} \quad (6)$$

$$\lambda_2(t) = \frac{\lambda_{min}}{\alpha + \beta} \left\{ \beta \left(\frac{V_2(t)}{V_{min}} \right)^{-\alpha} + \alpha \left(\frac{V_2(t)}{V_{min}} \right)^{\beta} \right\} \quad (7)$$

The coupled system of Eqs.(1) and (2) is solved by making a transformation in terms of characteristic variables and solving the dimensionless equations obtained. Let characteristic volume, number concentration, mass and time be V_c , n_c , w_c and t_c respectively.

Let $V_c = V_1$, the particle volume is scaled in terms of primary particle volume.

$$\begin{aligned} U_1 &= \frac{V_1}{V_1} = 1; & U_2 &= \frac{V_2}{V_1}; & U_{min} &= \frac{V_{min}}{V_1} \\ t_c &= \frac{1}{\lambda_{min}}; & \tau &= \frac{t}{t_c}; & n_c &= \frac{1}{K_{11} t_c} \\ w_c &= V_c n_c; & w^* &= \frac{w}{w_c} \\ C_1 &= \frac{n_1}{n_c}; & C_2(t) &= \frac{n_2(t)}{n_c} \end{aligned} \quad (8)$$

where, U_1 and U_2 are scaled primary and secondary group particle volume respectively, τ is scaled time, w^* is scaled mass, C_1 and C_2 are scaled primary and secondary group particle concentration respectively.

In terms of dimensionless parameters, Eqs.(1 – 7) can be written as:

$$\frac{dC_1}{d\tau} = S^*(\tau) - C_1^2 - \frac{K_{12}(\tau)}{K_{11}} C_1 C_2 - \frac{(\lambda_0 + \lambda_1)}{\lambda_{min}} C_1 \quad (9)$$

$$\frac{dC_2}{d\tau} = \frac{1}{2} C_1^2 - \frac{1}{2} \frac{K_{22}(\tau)}{K_{11}} C_2^2 - \frac{\lambda_0 + \lambda_2(\tau)}{\lambda_{min}} C_2 \quad (10)$$

$$\frac{dw^*}{d\tau} = S^*(\tau) - \frac{(\lambda_0 + \lambda_1)}{\lambda_{min}} C_1 - \frac{\lambda_0 + \lambda_2(\tau)}{\lambda_{min}} U_2(\tau) C_2 \quad (11)$$

$$U_2(\tau) = \frac{w^*(\tau) - C_1}{C_2(\tau)} \quad (12)$$

$$\lambda_1 = \frac{\lambda_{min}}{\alpha + \beta} \left\{ \beta \left(\frac{1}{U_{min}} \right)^{-\alpha} + \alpha \left(\frac{1}{U_{min}} \right)^{\beta} \right\} \quad (13)$$

$$\lambda_2(\tau) = \frac{\lambda_{min}}{\alpha + \beta} \left\{ \beta \left(\frac{U_2(\tau)}{U_{min}} \right)^{-\alpha} + \alpha \left(\frac{U_2(\tau)}{U_{min}} \right)^{\beta} \right\} \quad (14)$$

α and β are constants and typical values of these exponents are, $\alpha = 2$, $\beta = 2$. Eqs.(9-14) are coupled system of equations and must be solved together.

RESULTS AND DISCUSSION

The numerical solutions of Eqs.(9-14) are obtained using Mathematica (Wolfram Inc, 2005) for two different U_{min} . U_{min} is evaluated using the expression, $d_{p,min} = d_{p,1} (u_{min})^{\frac{1}{3}}$, is the diameter where the V-shaped deposition velocity curve possesses a minimum and $d_{p,1}$ is the primary particle diameter. λ_{min} is evaluated from the size dependent deposition rate curve (Fig.1). From Fig.1, $\lambda_{min} \approx 0.3 \text{ h}^{-1}$.

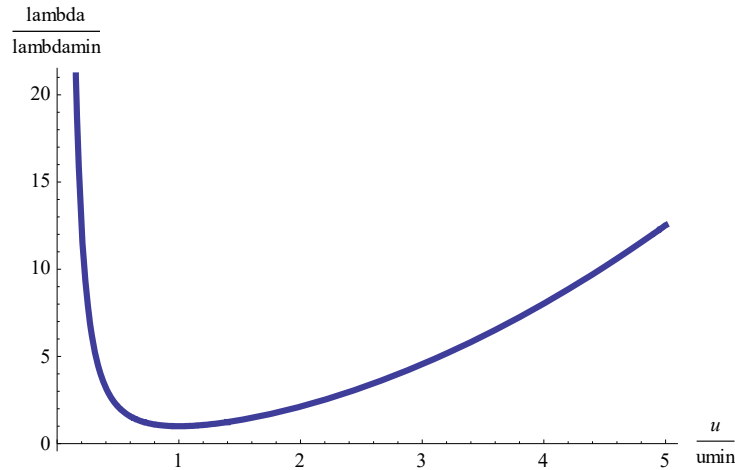


Fig.1. Scaled size-dependent deposition rate

Fuchs kernel has been used in the study to account for coagulation due to Brownian motion. A typical primary particle size of 50 nm with density of 2000 kg/m³ is considered in this study. Numerical solutions are obtained for $U_{min} = 100$ & 10. For this given system, $t_c = 1.08 \times 10^4$ s and $n_c = 10^{11}$ # m⁻³. The initial condition of $C_1(0) = 100$ will correspond to an initial primary particle concentration of 10^{13} # m⁻³ and mass concentration of 10^{-6} kg m⁻³.

From Fig.2a, it is observed that the airborne mass concentration (w^*) at $\tau \sim 7.5$ are 10^{-5} , 5×10^{-5} and 0.5 for initial concentration ($C_1(0)$) values of 10^4 (blue curve), 10^2 (red curve), 10^3 (black curve) respectively. An important observation is that higher initial concentration leads to lower airborne mass. For example, the mass concentration for the case of $C_1(0) = 10000$ cross-over the mass concentration curve of $C_1(0) = 1000$ at $\tau \sim 2$. However, cross-over between $C_1(0) = 100$ and $C_1(0) = 1000$ does not occur and it shows existence of a critical value of initial concentration beyond which the cross-over takes place. This is due to the fact that for small increase in concentration, coagulation increases the size and hence lowering the removal rate. For crossover to happen, the change in size due to coagulation should go beyond the minimum size. Similar observations are noticed for $U_{min} = 10$ (Fig.2b), i.e., cross-over between two different $C_1(0)$ and existence of critical value of $C_1(0)$.

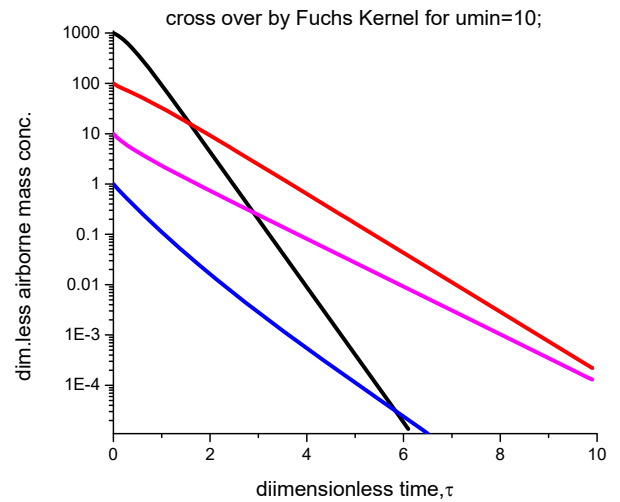
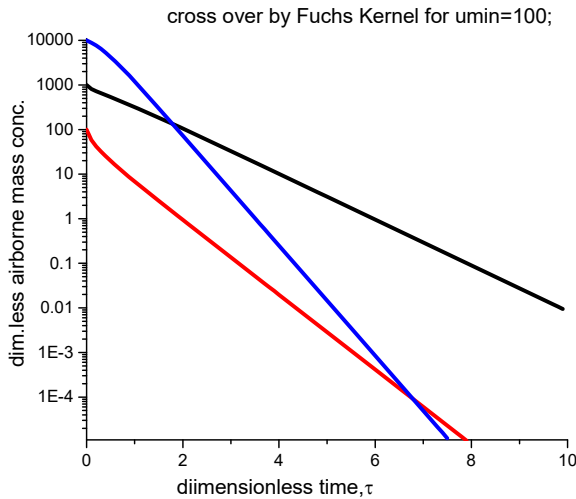


Fig.2. Temporal evolution of dimensionless airborne mass concentration, a) $U_{min} = 100$ & b) $U_{min} = 10$

CONCLUSION

The effect of initial aerosol concentration on the complex evolution of aerosol metrics is studied using relatively simple two-group model. Lower asymptotic mass concentration for a given high initial concentration is mainly due to the interplay of coagulation and removal processes in the system. Such initial high concentration releases are only possible during the accidental conditions, volcanic releases and forest fires. Although similar theoretical observations were made in the past in terms of number concentration for high number emission rate (continuous) sources, it is noteworthy to examine in terms of mass concentration in future.

STUDY OF ULTRAFINE PARTICLE EXPOSURE USING MULTI-COMPARTMENT MODEL

JAYANT KRISHAN¹, S. ANAND^{1,2}, KAPIL DEO SINGH¹, R M TRIPATHI^{1,2} AND Y.S. MAYYA³

¹Health Physics Division, Bhabha Atomic Research Centre, Mumbai - 400085, India

²Homi Bhabha National Institute-BARC, Mumbai - 400094 India

³Department of Chemical Engineering, IIT, Mumbai, India

KEYWORDS: Ultrafine particles, Exposure, Coagulation, Compartment model.

INTRODUCTION

The ultrafine particles (particle size < 100 nm) are produced at domestic and industrial levels in large scale through various activities such as cooking, heating, nanoparticles production, paint industry, pharmaceuticals, etc. Ultrafine particles (UFPs) pose risk of causing inhalation health hazards. Concentrations of these UFPs in terms of mass are well established but the mass concentration does not give true idea about the number concentration. A smaller number of larger mass particles may skew the distribution function. Therefore, it may happen that the information about large number of smaller mass particles is lost. To quantify the potential health risks, exposure due to ultrafine particles must be evaluated using number concentration. In the present study, single compartment and multi-compartment models are used along with the concept of effective coagulation kernel to estimate the number concentration of particles in the working environment.

METHODOLOGY

Single Compartment Model

In this approach, mono-disperse particles emitted from a source S at a constant rate undergo coagulation, removal due to ventilation (Air Exchange Rate (AER)) and dispersion in a given volume. These newly formed particles are distributed uniformly in the volume given volume V (Fig 1).

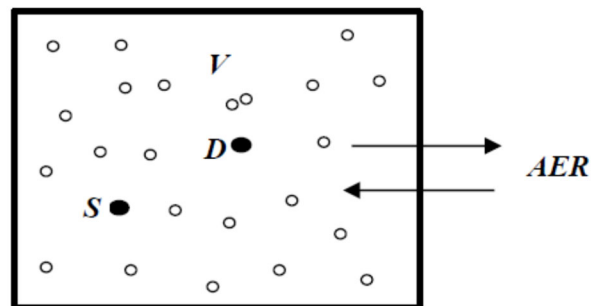


Figure1. Uniform distribution of particles in a volume V using single compartment model (S – Source, D – Measurement position)

Multi-compartment Model

Multi-compartment models are developed where the regions in a given working area are separated based on the dynamics of the processes and the ventilation rate. Each of the compartments has different dispersion and removal properties. A two compartment model assumes that the compartments are separated either by a physical boundary or different ventilation characteristics, i.e., concentration, ventilation rate inside a particular region is same but is different from the other compartment in the system. In the present study,

we use two compartment model to illustrate for a typical continuous release scenario in an indoor environment.

In general, the rate of change of number concentration in i^{th} compartment is given by,

$$\frac{V_i dN_i}{dt} = S \delta_{i1} V_i + \sum_{j:j \neq i} \lambda_j V_j N_j - \lambda_i V_i N_i - k_{eff} V_i N_i^2 - \lambda_{dep_i} V_i N_i \quad (1a)$$

where, N_i is the total number concentration (m^{-3}), λ_i is the ventilation rate in compartment i , λ_{dep_i} is the depletion of the number concentration due to deposition in the i^{th} compartment. For a two compartment model number concentration in first and second compartment are given by following equations 1b and 1c respectively.

$$\frac{V_1 dN_1}{dt} = S V_1 - \lambda_1 V_1 N_1 - k_{eff} V_1 N_1^2 - \lambda_{dep_1} V_1 N_1 \quad (1b)$$

$$\frac{V_2 dN_2}{dt} = \lambda_1 V_1 N_1 - \lambda_2 V_2 N_2 - k_{eff} V_2 N_2^2 - \lambda_{dep_2} V_2 N_2 \quad (1c)$$

S is the source emission rate ($\text{m}^{-3}\text{s}^{-1}$) estimated using the relation (Anand et al., 2016),

$$S = 0.5 k_{eff} (N_0, \lambda) N_0^2 + \lambda N_0 \quad (2)$$

k_{eff} is the effective coagulation coefficient (m^3s^{-1}) evaluated using the relationship (Anand et al., 2016),

$$k_{eff} = A2 + \frac{(A1-A2)}{1 + \left(\frac{\beta}{x_0}\right)^p} \quad (3)$$

where, $\beta = \frac{\lambda}{N}$ is the ratio of ventilation rate to the steady-state total number concentration, $A1$, $A2$, x_0 and p are the fitting constants depends on the primary particle size given in Table 1 below:

Table 1. Effective Coagulation Constant Data

Size (nm)	A1	A2	X0	P
10	4.91×10^{-15}	1.96×10^{-15}	5.44×10^{-17}	0.64
20	3.95×10^{-15}	2.38×10^{-15}	4.61×10^{-17}	0.62
30	3.20×10^{-15}	2.34×10^{-15}	6.97×10^{-17}	1.09

The size in above table represents the initial particle diameter emitted from the source. This effective coagulation kernel accounts for the change in the size distribution from the source to measurement location. Delta function in the first term of RHS of Eq.(1) represents that the source is zero in the first compartment. Second term in equation 1 represents the source in any compartment due to exchange of particles due to interaction with other compartments. Although λ_{dep_i} is a function of surface area of the compartment and particle size, a constant value of 10^{-5} s is assumed in the present study. Hence, for a given steady-state number concentration in a compartment, source term is estimated using Eq.(2) and then the concentration in any compartment is evaluated using Eq.(3).

This proposed model is then used to estimate the near-field and far-field concentrations in a test environment, and the results are compared with the measured and model values of number concentration (Jensen et al., 2018). For the estimation of source emission rate, near-field concentration values ($\sim 0.7 \text{ m}$ away from the actual source location) from Jensen et al. (2018) is considered. With a concentration value of $4 \times 10^{10} \text{ m}^{-3}$ and AER = 3.5 and 10 h^{-1} , S is estimated as 4.05×10^7 and 1.13×10^8 respectively $\text{m}^{-3}\text{s}^{-1}$ from Eq.(2); it is also found that the effect of AER on S is minimal. The ventilation rate considered in 2-compartment model calculations for two case studies are given in Table 2.

Table 2. Ventilation rate for the two compartments

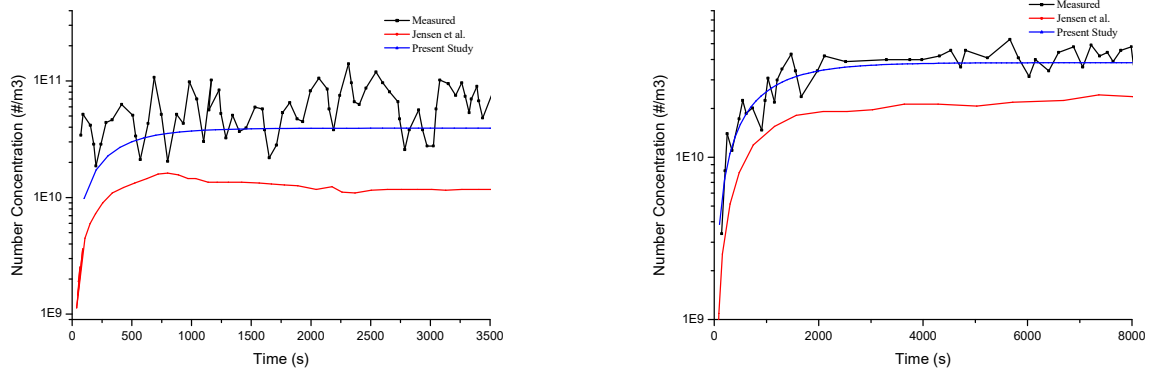
	AER, h^{-1}	
	Compartment 1 \leftrightarrow 2	Compartment 2 \leftrightarrow Outside
Case 1	10	0.10
Case 2	3.5	0.35

\leftrightarrow Represents the bi-directional air flow between the two compartments.

RESULTS & DISCUSSIONS

Number concentration for single compartment model corresponding to high air exchange rate (10 h^{-1}) and low air exchange rate (3.5 h^{-1}) are presented in figure 1. From Figure 1, it is observed that near field number

concentration estimated using the present model is in close agreement with the measured and predicted values (Jensen et al.). In case of single compartment model, our methodology assumes uniform distribution of particles, therefore, the number concentration value obtained at near field and far field are same.

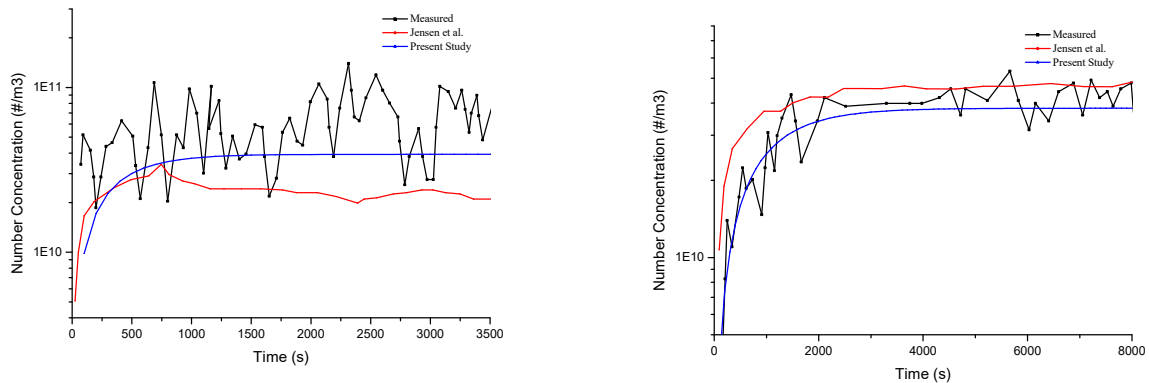


High Flow Rate

Low flow Rate

Figure 1. Number concentration using single compartment model at near field location

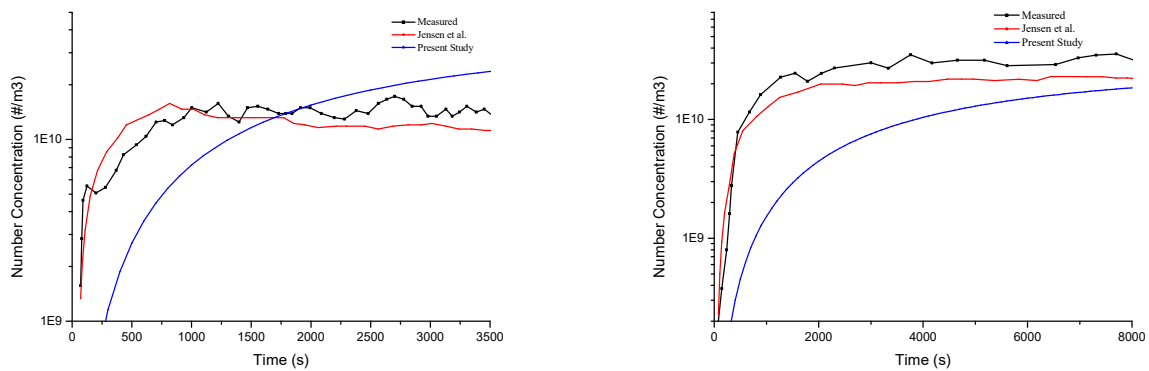
In case of two compartment model, the concentration is evaluated at near-field and far-field locations and results are given in Figure 2 and 3 respectively.



High flow rate

Low flow rate

Figure 2. Number concentration using 2 compartment model at near field location



High flow rate

Low flow rate

Figure 3. Number concentration using 2 compartment model at far field location

From Figure 2 and 3, it is observed that the number concentration at near field location can be predicted more accurately once the source estimation is done precisely. At far field location, rate of increase of number concentration is lower than the measured and value predicted by Jensen et al. (2018). However, the saturation value reached converges to the measured concentration value. Number concentration obtained at near and far field is very sensitive to the ratio of ventilation rate between the two compartments. It is observed that with increase in ventilation rate (keeping the ratio same), UFPs number concentration increases faster and tends to follow the trend observed in measured values. Hence, if information about ventilation rate is known precisely, concentration profile of UFPs can be predicted more accurately.

CONCLUSIONS

The number concentration of UFPs using single and multi-compartment model proposed in the present study and the measurements are in close agreement. It is observed that the concentration of UFPs is a strong function of ventilation rate. It is also observed that a higher ventilation rate does not guarantee lower number concentration of UFPs in the chamber. Therefore, the ventilation parameter has to be optimized so as to ensure minimum exposure of UFPs in the working environment.

REFERENCES

Jensen A, Maso M D, Koivisto A J, Belut E, Meyer A, Tongeren M V, Jimenez A S, Tuinma I, Domat M, Toftum J and I. K. Koponen (2018). Comparison of Geometrical Layouts for a Multi-Compartment Aerosol Model from a Single-Chamber Dispersion Study, *Environments* **5**, 52.

Anand, S., B. Sreekanth and Y.S. Mayya (2016), Effective Coagulation Coefficient Approach for Estimating Particle Number Emission Rates for Strong Emission Sources, *Aerosol and Air Quality Research*, **16**, 1541-1547.

Anand S., Jayant Krishan and Y.S. Mayya (2018). Study of residential exposure due to ultrafine aerosol particles using a simple indoor model, *AT2018, Aerosol Technology*, Bilbao – Spain, **WM3-03**, 239.

STUDY OF DEPOSITION OF RADON PROGENY AEROSOLS AT DIFFERENT AIR VELOCITIES

ROSALINE MISHRA¹, RAMA PRAJITH¹, SAMIM MOLLA², RAJESWARI P. ROUT¹, S. JALALUDDIN S.¹ AND B.K.SAPRA¹

¹Radiological Physics and Advisory Division, Bhabha Atomic Research Centre, Mumbai 400094

²Health Physics Division, Bhabha Atomic Research Centre, Mumbai 400085

KEYWORDS: Radon Progeny, Unattached Fraction, Air Velocity, Deposition

INTRODUCTION

The inhalation of radon (²²²Rn), thoron (²²⁰Rn) and its progeny contribute to a major fraction (55%) of the natural background radiation dose to humans (UNSCEAR, 2000). Essentially the progeny of radon and thoron, which are the radioisotopes of polonium (Z = 84), bismuth (Z = 83) and lead (Z = 82), deposit in the respiratory tract once inhaled and contribute to the inhalation dose.

Besides the fast reactions of neutralization and cluster formation, the decay products of ²²²Rn and ²²⁰Rn participate in normal atmospheric kinetics and attach to existing particles of airborne aerosol. Consequently, they deposit on any available surface in direct contact to indoor air. In view of their radiolytic nature and concurrent hazard to human health, their deposition indoors is of considerable importance. It may be noted that deposition is a positive phenomenon, as it is responsible for lowering the progeny concentration from the indoor environment. Surface-deposition supplements ventilation as a means of reducing human exposure to progeny.

In the environment these progeny particles exist in two states one in the size range 0.5 nm to 5 nm with a mean around 1 nm, which are not attached to aerosols are termed as fine/unattached fraction. These unattached fraction when attach themselves to the aerosol particles, they are referred to as attached fraction. They are in the size range of 10 nm to 1 micron with mean size of about 200 nm.

The unattached fraction in the environment depends on the aerosol concentration, air velocity in the environment and the air exchange rate. It is known that as the aerosol concentration is increased the unattached fraction will be reduced, and with a higher air exchange rate the accumulation of progeny is reduced in the concerned environment, hence reducing the inhalation dose. In the present work, the effect of air velocity or the friction velocity on progeny deposition on the surface has been studied. It is essential to study this deposition behavior of progeny not only for an enclosed environment but also it has implication on the progeny deposition in the respiratory tract.

METHODS

The measurements were carried out in the 0.5 m³ chamber using radon and thoron mixed powder source. Deposited flux were measured by Direct Radon and Thoron progeny sensors (DRPS and DTPS). These are deposition based direct passive progeny sensing techniques (Mishra et al., 2009a). Measurements were carried out in two conditions, first one at no air movement condition, and the second one at a friction velocity of 6cm/s. The friction velocity in the chamber was calculated from fan parameters (Mishra et al., 2009). For each condition 10 DTPS and 10 DRPSs were placed on each surface (all four inside walls, ceiling and floor) in the inside of the chamber. The exposure was carried out for a period of 48 hours. After exposure, the DRPS and DTPSs were retrieved and chemical analysis and alpha track counting was carried out.

Field measurements were carried out in a uranium mine, wherein effect of air velocity on the unattached fraction and radon progeny deposition velocity was studied. The unattached fraction was measured by integrated sampler (Mishra et al., 2010). It consists of a wire-mesh and a filter-paper arranged in an array, with DRPS facing each of them. The sampling was carried out at 2 lpm for 15 minutes, followed by chemical processing of the DRPS. The air velocity measurements was carried out using hot-wire anemometer. The attached fraction progeny deposition velocity was measured as a ratio of deposited atom

flux on wire-mesh capped DRPS (Mayya et al., 2010) to the attached fraction atom concentration in the air measured using integrated sampler (Mishra et al., 2009b).

RESULTS & DISCUSSIONS

The deposited thoron progeny atom flux and radon progeny atom flux obtained under no air movement condition and under a friction velocity of 6.25 cm/s on all the surface inside the chamber is tabulated in Table. 1.

Chamber Inner surface	Friction velocity	Thoron progeny Deposited atom flux (atoms/cm ² /s)	Thoron progeny Deposited atom flux (atoms/cm ² /s)
Front wall	0	13795±391	9443±545
	6.25	18627±223	13150±212
Back wall	0	11428±408	7643±361
	6.25	14765±261	14579±273
Left wall	0	12428±504	6264±446
	6.25	16940±315	16843±242
Right wall	0	12968±504	8739±522
	6.25	16940±315	12757±437
Ceiling	0	8455±356	7814±656
	6.25	15645±503	16836±792
Floor	0	25012±521	13811±512
	6.25	20596±486	15121±372

Table 1. Deposited thoron progeny and radon progeny atom flux on different wall surfaces of the chamber in two air velocity conditions

In the first case, where no air movement was there, maximum deposited flux for both radon progeny and thoron progeny was obtained on the floor of the chamber. In the case of thoron progeny the ratio of deposited flux on floor to the walls was measured to be 2, whereas that to the ceiling was 3. In the case of radon progeny the deposited flux ratio on floor to walls, and floor to ceiling was measured to be 2.

At a friction velocity of 6.25 cm/s, an uniform mixing was observed due to which the ratio of deposited flux on floors to wall and floors to ceiling, both in case of radon progeny and thoron progeny were found to be 1. This implies an equal deposited flux on all surfaces because of uniform mixing.

The effect of air velocity on the unattached fraction in Uranium mines is shown in Fig.1. It was observed that the unattached fraction increased as the air velocity was increased.

As the progeny deposition velocity is a direct function of unattached fraction in the environment, it will increase with increase in unattached fraction. The attached fraction deposition velocity measured using wire-mesh capped DRPS at different locations with different air velocities is given in Table. 2. It was observed that the attached fraction deposition velocity remained almost constant even when the air velocity is changed.

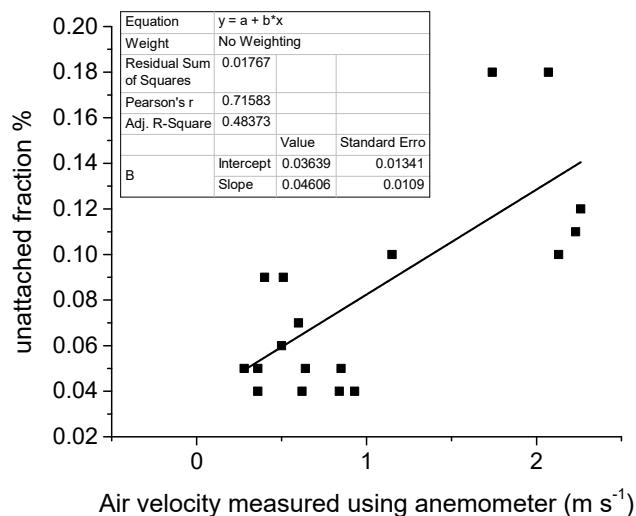


Figure 1. Radon progeny unattached fraction versus air velocity in Uranium mine.

Air velocity (m/s)	Radon progeny deposition velocity (Attached) (m/h)
0.1-0.5	0.028
0.5-1.0	0.041
1.0-1.5	0.033
1.5-2.0	0.038
2.0-2.5	0.031
Average	0.034±0.005

Table 2. Attached fraction radon progeny deposition velocity measured at different air velocities in Uranium mines.

CONCLUSIONS

Effect of air movement in terms of friction velocity and air velocity on the deposition behavior of radon progeny and thoron progeny was studied. It was observed that the increase in air velocity causes uniform mixing and leads to uniform and increased surface deposition on the walls. This will also hold good in mine atmosphere wherein air velocity is introduced to decrease the inhalation doses of the occupational workers. Further, it was observed that air velocity increase in mines increases the unattached fraction, but it has least effect on the attached fraction deposition velocity. This implies that the attached fraction deposition velocity remains almost constant against change in environmental parameters.

REFERENCES

Mayya Y.S., Mishra Rosaline, Prajith Rama, Sapra B.K. and Kushwaha H.S. (2010) Wire-mesh capped deposition sensors: Novel passive tool for coarse fraction flux estimation of radon thoron progeny in indoor environments. *Science of Total Environment*, **409**(2), 378-383.

Mishra Rosaline, Mayya Y. S., Kushwaha H. S. (2009a) Measurement of $^{220}\text{Rn}/^{222}\text{Rn}$ progeny deposition velocities on surfaces and their comparison with theoretical models. *Journal of Aerosol Science*, **40**, 1-15.

Mishra Rosaline, Sapra B.K., Mayya Y.S. (2009b) Development of an integrated sampler based on direct $^{222}\text{Rn}/^{220}\text{Rn}$ progeny sensors in flow-mode for estimating unattached/attached progeny concentration. *Nuclear Instrumentation and Methods in Physics Research*, **B 267**, 3574–3579.

Mishra Rosaline, Y. S. Mayya, and L. Tommasino. (2012) Mimicking lung dose by wire-mesh capped deposition sensors: a new dosimetric strategy of radon (thoron) decay products. *Radiat. Prot. Dos.*, 1-8.

IDENTIFICATION AND QUANTIFICATION OF MICROPLASTICS ASSOCIATED WITH INHALABLE AEROSOL FRACTION (PM₁₀)

M. TIWARI¹, T.D. RATHOD^{1,2}, P.Y. AJMAL¹, R.C. BHANGRE¹ AND S. K. SAHU*^{1,2}

¹Environmental Monitoring and Assessment Section, Health Safety and Environmental Group, Bhabha Atomic Research Centre, Mumbai- 400 085 India

²Homi Bhabha National Institute, Anushakti Nagar Mumbai– 400 094, India.

(*Correspondence at: sksahu@barc.gov.in, Tel:0222-5592375)

KEYWORDS: Microplastic, Pm₁₀, Fluorescence Microscopy, Nile Red.

INTRODUCTION

There is a large amount of plastic used in packaging, furniture, textile, etc., of which we get exposed in our daily life. Once plastics are discarded and released in environment, over time these material may degrade in to micron and submicron sizes plastics. Microplastics are a widespread particular contaminant originating from the breakdown of larger plastic debris (secondary) or directly manufactured submillimetric size (primary) (Cole et al., 2011). These plastics have been defined as particles with the largest dimension smaller than 5 mm; a recent study detected the presence of these man-made fibers in the atmospheric fallout in the Parisian agglomeration (Dris et al., 2016). It suggests that the atmospheric phase contains fibers that lead to human exposure. This exposure raises concern as they are observed in human lungs with a microscope. It was showed that 87% of the studied lungs (n = 114) contained fibers. Cellulosic and plastic fibers were both observed (Pauly et al. 1998). The key aim of this study is to identify and quantify (number wise) microplastic associated with ambient aerosols with inhalable fraction (PM₁₀).

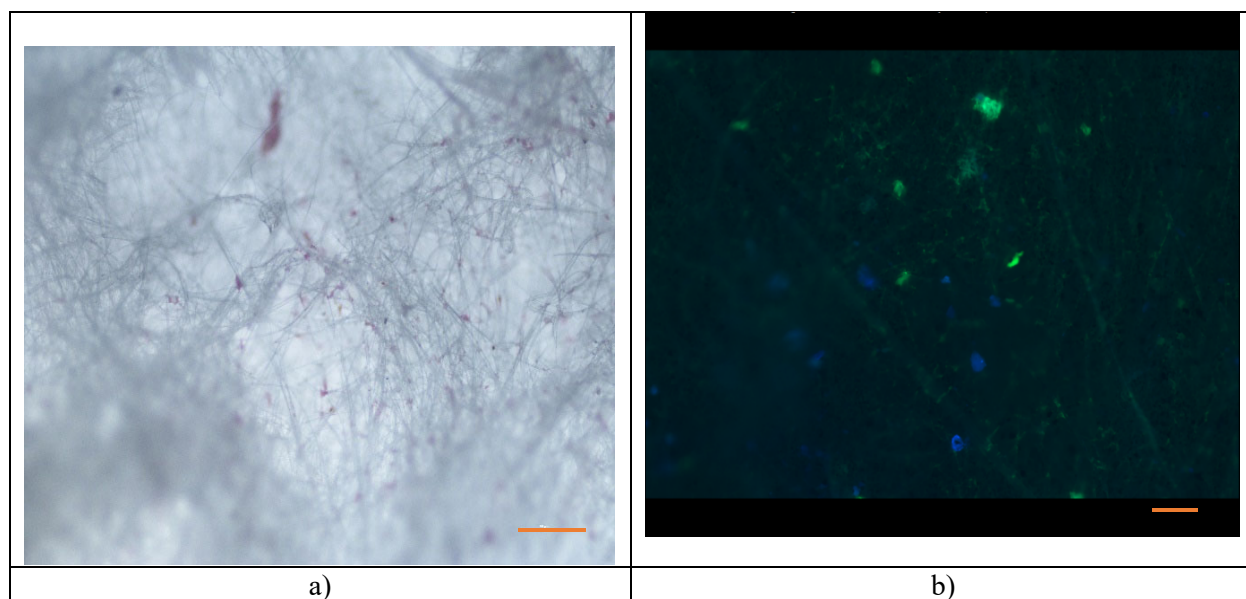


Fig 1. a) optical microscopic images of filter paper laden with microplastic after staining (scale bar is of 100 μ m), b) fluorescence microscopic images (scale bar represents 10 μ m).

METHODS

PM₁₀ samples were collected at BARC, Trombay Mumbai during November 2017 using APM 460 NL (Envirotech Instruments Pvt. Ltd.) sampler. Sampling duration for individual sample was 24 h which was equivalent to 1600 m³ air at a sampling flow rate of 1.12 m³ min⁻¹. Mass loading on filter papers were

determined gravimetrically. Collected air filter samples were treated with H₂O₂ and alkaline KOH solution to reduce the organic component in sample prior to staining with suitable dye (Hurley et al., 2018). Staining of filter papers was carried out using Nile Red (NR) dye with concentration of 10 µg mL⁻¹ (in Acetone) with an exposure time of 30 min. Each NR-stained microplastic was tested with excitation wavelength of blue light and emission wavelengths were processed using FITC filter under a fluorescent microscope (Carl Zeiss AXIO, Imager M1). The dye adsorbs onto plastic surfaces and renders them fluorescent (green or blue colour) when irradiated with blue light. Image analysis allows fluorescent particle to be identified and counted (Shim et al., 2016; Maes et al., 2017). Typical optical and fluorescent microscopic images for air filter sample are shown in Fig 1. Microplastics were counted at multiple areas (1.3 mm²) of filter paper and integrated for overall deposition on the filter. Microplastics number concentrations were calculated by dividing the total number of microplastic by sampled volume in m³.

RESULTS & DISCUSSIONS

Mass concentrations of PM₁₀ at BARC, Mumbai were found to be vary between 31.3 to 55.5 µg m⁻³ with a mean value of 41.3 µg m⁻³ during sampling period. Average concentration of microplastics and their variation in air samples are presented in Fig 2 I). Average number concentration of microplastics varies from 480 to 3335 # m⁻³ during sampling period. Observed values are two to three magnitude higher than a study, where indoor concentrations were reported between 1.0 and 60.0 fibersm⁻³ and Outdoor concentrations are significantly lower as they range between 0.3 and 1.5 fibersm⁻³ (Dris et al., 2016). This variation is due to analysis of MP in different size range for Dris et al., 2016 has reported the size of plastics more than 50µm, while this study is focused on particle associated with PM₁₀. There were no data in literature to compare with this study, at our knowledge. We have also try to find out the correlation between mass concentration of PM₁₀ and number concentration of microplastic. It is observed that these two factor are poorly correlated Fig. 2 II).

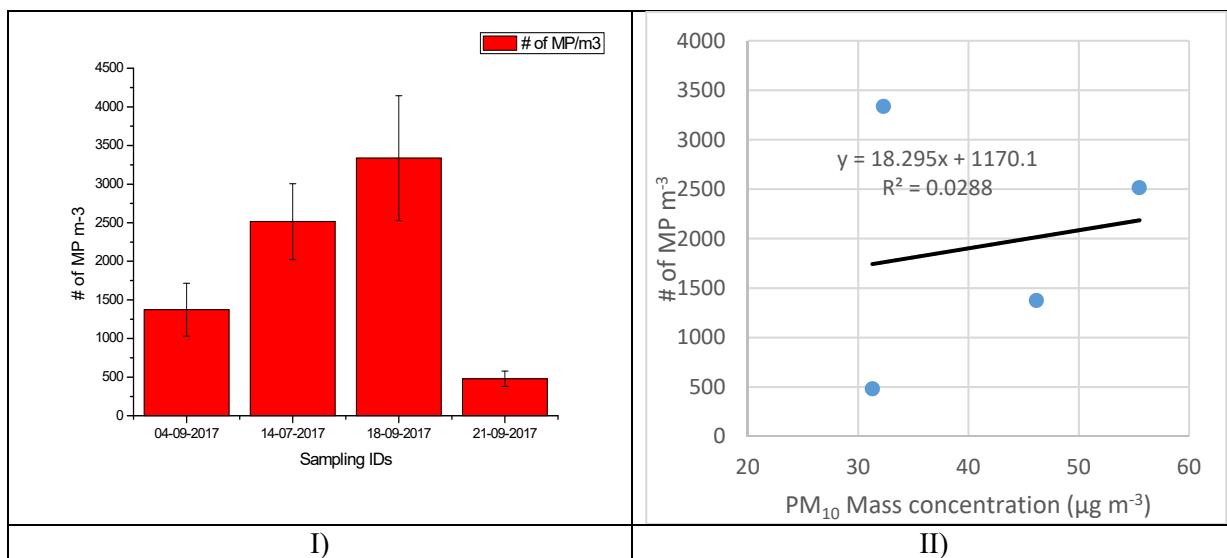


Fig 2: I) Number concentration variation of microplastics associated with PM₁₀ II) Correlation between PM₁₀ mass concentration and microplastic concentration.

Abundance of microplastics with different sizes from 1 to 10 µm is shown in Fig. 3. It can be observed from the Fig. 3 that MP were equally distributed in all size ranges and peak values are at 4 and 10µm. Particles less than 1µm were not reported, as their fluorescence yield is not significant to distinguished with background non plastic item in the sample.

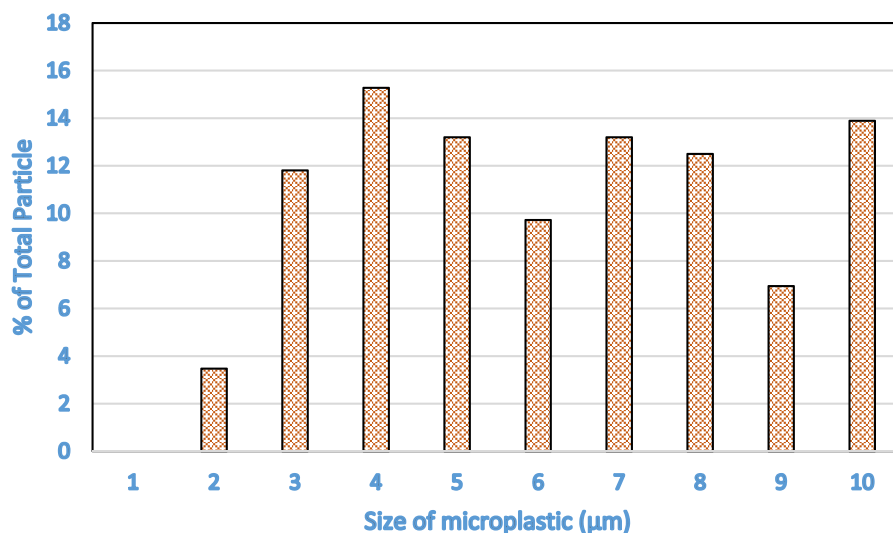


Fig 3:Size distribution of microplastic particle associated with PM₁₀.

CONCLUSIONS

This study provides an approach to identify air born microplastic. Fluorescent microscopy was recognized to detect microplastics and obtain their abundance in PM₁₀, but it was not suitable for particle below 1µm. This study is the first report microplastics associated with PM₁₀, in best of our knowledge. Further investigations are still needed to estimate microplastics relative contribution in inhalation. These air born microplastic may settle down in indoor environment, can be ingested, particularly by young children due to their frequent hand-to-mouth contacts other than inhalation. Additional analytical tools like IR-microscope can provide information regarding polymer type, which can be further useful in source apportionment and toxicity assessment of microplastic in air.

ACKNOWLEDGEMENTS

Authors would like to declare there is no financial and personal conflict associated with this study.

REFERENCES

- Cole, M., Lindeque, P., Halsband, C., Galloway, T.S., (2011) Microplastics as contaminants in the marine environment: a review. *Mar. Pollut. Bull.* **62**, 2588–2597.
- Dris, R., Gasperi, J., Saad, M., Mirande, C., Tassin, B., (2016) Synthetic fibers in atmospheric fallout: A source of microplastics in the environment? *Marine Pollution Bulletin* **104**, 290–293.
- Hurley, R.R., Lusher, A.L., Olsen, M. and Nizzetto, L. (2018) Validation of a Method for Extracting Microplastics from Complex, Organic-Rich, Environmental Matrices. *Environ. Sci. Technol.* **52**, 7409–7417.
- Maes, T., Jessop, R., Wellner, N., Haupt, K., Mayes, A.G. (2017) A rapid-screening approach to detect and quantify microplastics based on fluorescent tagging with Nile Red. *Scientific Report* **7**, 44501.
- Pauly, J.L., Stegmeier, S.J., Allaart, H.A., Cheney, R.T., Zhang, P.J., Mayer, A.G., Streck, R.J., (1998) Inhaled cellulosic and plastic fibers found in human lung tissue. *Cancer Epidemiol. Biomarkers Prev.* **7**, 419-428.

Shim, W. J., Song, Y. K., Hong, S. H., Jang, M (2016) Identification and quantification of microplastics using Nile Red staining. *Marine Pollution Bulletin* **113**, 469–476.

PHOTO-DEGRADATION BEHAVIOUR OF BROWN CARBON GENERATED FROM BIOMASS COMBUSTION UNDER UV LIGHT EXPOSURE

T.D. RATHOD^{1,2}, S. K. SAHU*^{1,2}, M. TIWARI¹, P.Y. AJMAL¹ AND R.C. BHANGRE¹

¹Environmental Monitoring and Assessment Section, Health Safety and Environmental Group, Bhabha Atomic Research Centre, Mumbai- 400085 India

²Homi Bhabha National Institute, Anushakti Nagar Mumbai– 400094, India.

KEYWORDS: Brown Carbon, Biomass Combustion, Photodegradation, Uv

INTRODUCTION

Biomass combustion is one of the major sources of carbonaceous aerosols injection in the atmosphere. The major share of the primary Black carbon (BC) and primary organic carbon (OC) are emitted globally from biomass burning (Bond et al., 2004). The amount of impact these carbonaceous species can have on climate depends upon their optical properties. The BC material has weak (λ^{-1}) spectral dependence of the absorption coefficient (Bond et al., 2006; Lack et al., 2013). Certain types of OC absorb radiation efficiently in near-UV visible ranges. This class of compounds together is termed as brown carbon (Laskin et al., 2015). In contrast to BC, the light-absorption coefficient of BrC has strong wavelength dependence ($\lambda^{-2}-\lambda^{-6}$) with absorption increasing sharply from the visible to the UV range (Lack et al., 2013; Moosmueller et al., 2011). This extensive range is inherent to the chemical variability of BrC constituents and implies that no single AAE value can be selected as an intrinsic parameter describing BrC in models (Laskin et al., 2015). The complexity of light-absorbing organic compounds and variations in their relative concentrations make it difficult to characterize the molecular composition and determine which types of molecules or molecular aggregates dictate the optical properties of BrC.

The condensed secondary organic phase is subjected to aging process in the environment (George C et al., 2015). It is found that condensed-phase photochemical reactions may not only change the organic aerosol composition, but also change the volatility distribution of the organic compounds resulting from photo induced fragmentation. The laboratories based experiment suggests that there can be loss of mass in organic aerosol and decrease in particle size due to UV irradiation (Epstein S. A. et al., 2014, Wong, J. P. et al., 2015, Daumit, K. E. et al., 2016 and Kroll, J. H. et al., 2006). In order to selectively study condensed-phase photochemical aging, the experiments with bulk organic material after driving away the volatile constituents have been carried out (Kurtis T. Malechaand and Sergey A. Nizkorodov, 2016). It was estimated that the secondary organic aerosol particles lose at least 1% of their mass per day under representative atmospheric conditions. The primary BrC emissions as well belong to condense organic phase in atmosphere. Thus its photochemical aging can be considered to be inevitable. It needs to be studied for robust attribution of organic aerosol properties studied at source emissions. In present paper, photochemical degradation of water soluble (WSBrC) under UV exposure is discussed.

METHODS

The pyrolytic aerosols generated from wood combustion were collected via laboratory scale experiment. The details regarding the experimental set up are discussed elsewhere (Rathod et al., 2017). The angstrom exponent for the generated aerosols was greater than 2 indicating the presence of BrC (Rathod et al., 2017). The sampled BrC was extracted using deionised water to obtain WSBrC. After extraction process, the solvents were stored in conical flask which was wrapped with aluminium foil to prevent light exposure. Out of 20 ml of extracted solvents, 3ml of each solvent were used for further analysis. The extracted solvent was taken into quartz crucible and OC/Inorganic carbon (IC)/ Elemental carbon (EC) was determined with TCTN Analyser (Primacs^{SNC-100}, Skalar Analytical). The DIN method was calibrated and used for simultaneous measurement of OC, EC and IC. The DIN analysis, which is initiated by the Deutsches Institut für Normung, differentiates between the organic, elemental and inorganic form of carbon. The

sample is heated at increasing temperatures from 400 °C, 600 °C and 900 °C at which respectively the OC, EC and IC combust. The OC concentration obtained in TC analyser corresponds to WSBrC for our experiments. The photo degradation of WSBrC under UV exposure was optimised by sequential sets of experiments. Several aliquots of extracted solvent (1 ml) were formed in quartz crucible. One batch of aliquots were used for DIN analysis to provide OC/EC/IC data for samples before exposure to UV light. The other batch was exposed to 370 nm UV wavelength for 10, 30, 45, 60, 80, 100, and 120 minutes respectively. An enclosed chamber was used to selectively expose the sample to 370 nm. The Xenon lamp and grating arrangement was used for desired UV light exposure. Each aliquot was then further analysed in TCTN analyser for its OC, EC and IC contents.

RESULTS & DISCUSSIONS

It was observed that in WSBrC showed a gradual decrease in its concentration with increase in exposure time. The WSBrC achieved equilibrium concentration after 60 min of UV light exposure as shown in figure 1 (a). The degradation behaviour of WSBrC under UV exposure observed in our experiment was used to determine its relaxation time, defined as the time required reaching its stable concentration. The graph of log (% concentration) w.r.t. time was fitted with exponential function of the form,

$$y = A_1 e^{\left(\frac{-t}{l}\right)} + y_0 \quad \text{eq. 1}$$

The values of the fitted parameter are given in figure 1. Using the exponential fit the degradation rate constant (r_c) of BrC under UV exposure was determined to be 0.0096 min^{-1} . The degradation rate constant was used to estimate relaxation time (l) of BrC under UV exposure as,

$$l = \frac{1}{r_c} \quad \text{eq. 2}$$

This gives relaxation time of WSBrC as $104 \pm 8 \text{ min}$. Thus it indicates the photo degradation process of BrC starts as soon as they get emitted in atmosphere via biomass combustion. This photochemical loss in primary WSBrC entering atmosphere can potentially alter its column burden and radiative forcing estimates. There was no change observed in the EC and IC concentration under UV exposure as shown in figure 2. The net change in WSBrC was estimated to be about 58% after sufficient UV exposure ($t = 120 \text{ min}$)

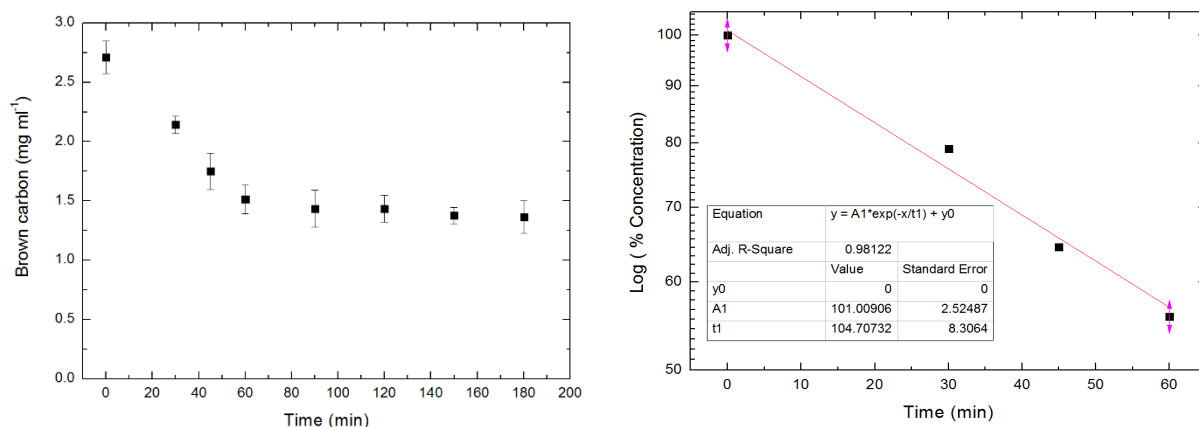


Figure 1 a) The variation of water soluble brown carbon concentration w.r.t. time of UV (370 nm) exposure.

b) The exponential fitting of log (% concentration) Vs Time to determine the relaxation time for OC under UV exposure

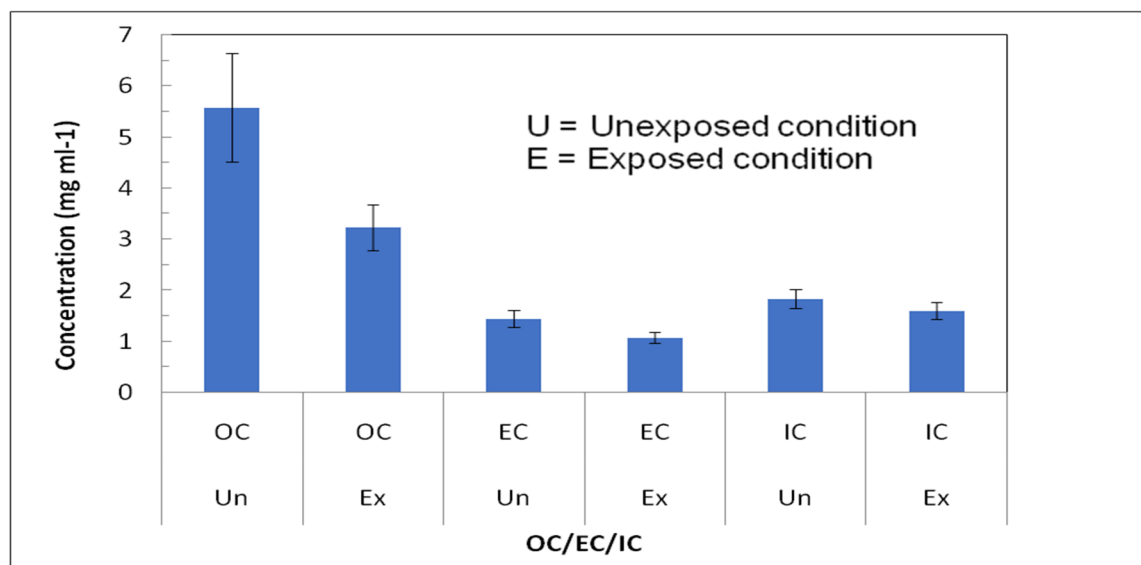


Figure 2 OC/EC/IC concentration values for samples under different condition of UV exposure

CONCLUSIONS

The BrC generated from wood combustion was sampled and extracted using deionised water to obtain WSBrc. The photo degradation behaviour of WSBrc was studied under UV (370 nm) exposure. It was observed that up to 58 % WSBrc underwent photo degradation during UV exposure. The degradation constant was estimated to be 0.0096 min^{-1} with relaxation time of 104 min. There was no effect of UV on EC and IC content of the samples. The photo degradation of primary WSBrc can be an important phenomenon to consider while estimating its optical properties at source emissions.

ACKNOWLEDGEMENTS

Authors would like to declare there is no financial and personal conflict associated with this study.

REFERENCES

- Bond, T. C., Streets, D. G., Yarber, K. F., Nelson, S. M., Woo, J. H., & Klimont, Z. (2004). A technology-based global inventory of black and organic carbon emissions from combustion. *Journal of Geophysical Research: Atmospheres*, 109 (D14).
- Bond, T. C., and Bergstrom, R. W.: Light absorption by carbonaceous particles: An investigative review, *Aerosol Science and Technology*, 40, 27-67, 10.1080/02786820500421521, 2006.
- Daumit, K. E.; Carrasquillo, A. J.; Sugrue, R. A.; Kroll, J. H. Effects of condensed-phase oxidants on secondary organic aerosol formation. *J. Phys. Chem. A* 2016, 120 (9), 1386–94.
- Epstein, S. A.; Blair, S. L.; Nizkorodov, S. A. Direct photolysis of α -pinene ozonolysis secondary organic aerosol: effect on particle mass and peroxide content. *Environ. Sci. Technol.* 2014, 48 (19), 11251–8.
- George, C.; Ammann, M.; D'Anna, B.; Donaldson, D. J.; Nizkorodov, S. A. Heterogeneous photochemistry in the atmosphere. *Chem. Rev.* 2015, 115 (10), 4218–58.
- Kroll, J. H.; Ng, N. L.; Murphy, S. M.; Flagan, R. C.; Seinfeld, J. H. Secondary organic aerosol formation from isoprene photooxidation. *Environ. Sci. Technol.* 2006, 40 (6), 1869–77.

Laskin, A., Laskin, J., & Nizkorodov, S. A. (2015). Chemistry of atmospheric brown carbon. *Chemical reviews*, 115(10), 4335-4382.

Lack, D. A., & Langridge, J. M. (2013). On the attribution of black and brown carbon light absorption using the Ångström exponent. *Atmospheric Chemistry and Physics*, 13(20), 10535-10543.

Malecha, K. T., & Nizkorodov, S. A. (2016). Photodegradation of secondary organic aerosol particles as a source of small, oxygenated volatile organic compounds. *Environmental science & technology*, 50(18), 9990-9997.

Moosmüller, H., Chakrabarty, R. K., Ehlers, K. M., & Arnott, W. P. (2011). Absorption Ångström coefficient, brown carbon, and aerosols: basic concepts, bulk matter, and spherical particles. *Atmospheric Chemistry and Physics*, 11(3), 1217-1225.

Rathod, T., Sahu, S. K., Tiwari, M., Yousaf, A., Bhangare, R. C., & Pandit, G. G. (2017). Light Absorbing Properties of Brown Carbon Generated from Pyrolytic Combustion of Household Biofuels. *Aerosol and Air Quality Research*, 17(1), 108-116.

Wong, J. P.; Zhou, S.; Abbatt, J. P. Changes in secondary organic aerosol composition and mass due to photolysis: relative humidity dependence. *J. Phys. Chem. A* 2015, 119 (19), 4309–16.

RADIATIVE FORCING ESTIMATION OF AEROSOLS AT FOUR LOCATIONS IN INDIA AND PAKISTAN USING GROUND-BASED REMOTE SENSING MEASUREMENTS

MANISH SONI¹, SWAGATA PAYRA^{1,*} AND SUNITA VERMA²

¹Department of Physics, Birla Institute of Technology Mesra, Jaipur Campus, 27 Malviya Industrial Area, Jaipur, 302017, India.

²Department of Environment and Sustainable Development (ESD), Banaras Hindu University (BHU), Varanasi, 22105, UP, India.

KEYWORDS: Radiation Budget, Sbdart ,Aeronet ,Aerosol.

INTRODUCTION

Uncertainty in estimation of radiative climate forcing is mainly caused by aerosols due to our poor understanding of aerosols cloud interactions as well as scarcity (IPCC, 2007, 2013). This radiative forcing primarily depends upon size distribution, chemical composition and abundance of aerosols. Due to the various types the impact of aerosols on atmosphere is different (Verma *et al.*, 2006; Kaskaoustis *et al.*, 2007). Scattering Aerosols like sea salt sulphate etc usually generates negative forcing (cooling) in the atmosphere. Absorbing aerosols like mineral dust, black carbon produces positive forcing (warming). This forcing also depends upon source location. The focus of present study is to quantify the radiation budget of aerosols over Jaipur, Kanpur (Both India), Lahore and Karachi (Pakistan) from April 2010 to March 2015. These sites differ in topography and climate. The Aerosol radiative forcing (ARF) has been determined for shortwave spectrum (0.3–3.0 μm) individually for the top of the atmosphere (TOA), bottom of the atmosphere (BOA) and within the atmosphere (ATM) over study region. Santa Barbara DISORT Atmospheric Radiative Transfer model (SBDART) is used to simulate the aerosols radiative effect. For this level 1.5 Aerosol Robotic Network (AERONET) data is acquired for the study period i.e April 2010 to May 2015.

SITE DESCRIPTION and METHODS

For this paper, SBDART (Ricchiazzi *et al.*, 1998) model is used. This is a FORTRAN computer code designed specifically for the analysis to calculate the radiative properties of a particular location when optical properties are known. Optical Properties of Aerosols and Clouds (OPAC, Hess *et al.*, 1998) along with ground-based sunphotometer is collected at a part of AERONET project. Usually eight radiation streams are used for the radiative forcing calculations in shortwave region (0.3–3.0 μm). The TOA and the surface downward and upward fluxes are calculated at the 1-hr interval for a 24-hr period with and without aerosol conditions separately. The diurnally averaged radiative forcing at the TOA and BOA (Bottom of Atmosphere or surface) is obtained as difference between the net flux (down - up) with and without aerosols. Further, the resultant net atmospheric forcing (ATM) is calculated using the difference between TOA and BOA. The aerosol produces a cooling effect if the sign of radiative forcing comes negative and warming effect for positive forcing. For these daily averaged values are used to obtain monthly averages and so on.

Four sites namely Jaipur, Kanpur, Lahore and Karachi is used in this paper where AERONET cimel sunphotometer is installed. Jaipur is a semi-arid region and is moderately polluted generally. Kanpur is a heavy industrial site and one of the polluted cities of India lies in Indo-Gangetic Plain. More detailed description can be found elsewhere (Payra *et al.*, 2015; Soni *et al.*, 2018) .Lahore is second most populated and one of the polluted city of Pakistan. It experiences a semi-arid climate. It lies in the north-eastern end of Pakistan's Punjab province. Karachi is a coastal and sixth most populated city in Pakistan. It experiences arid climate.

RESULTS & DISCUSSIONS

Variation in Radiative Forcing (Monthly and Annual)

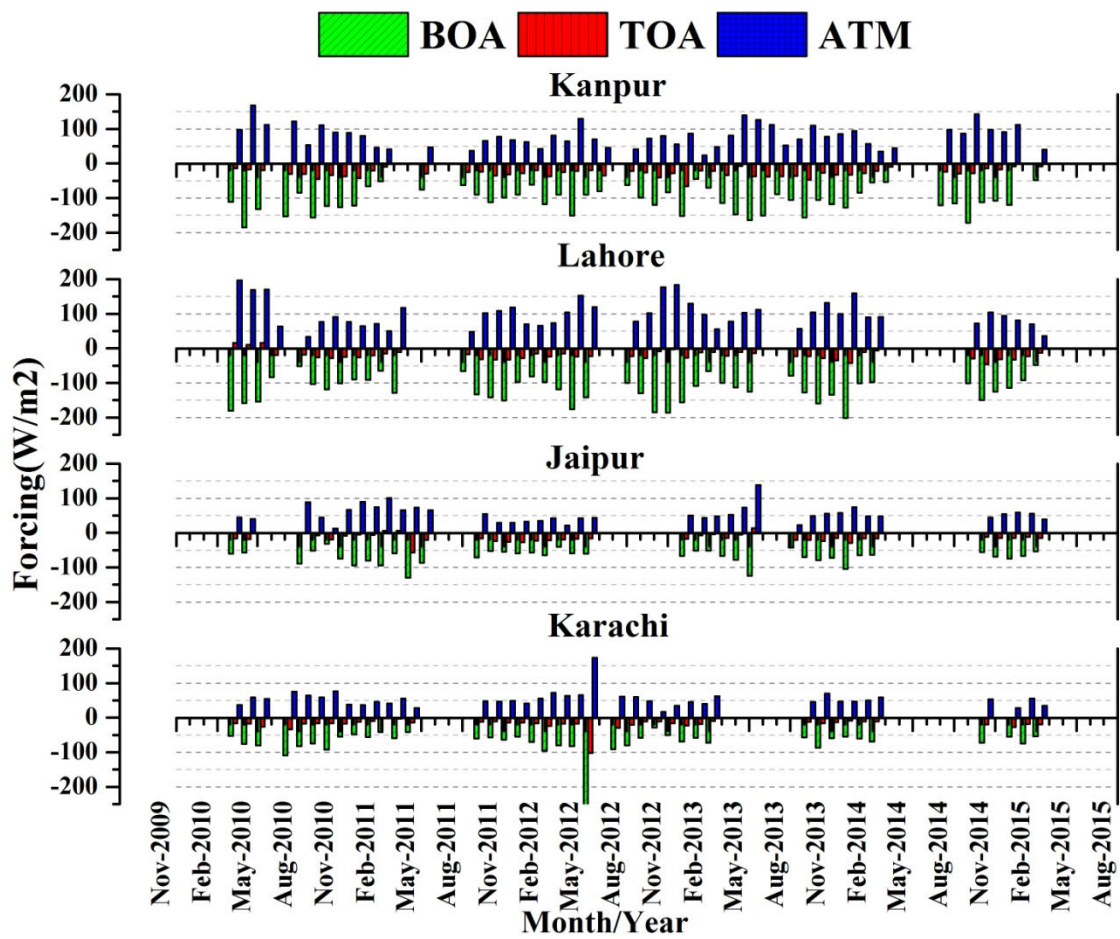


Figure 1. Monthly Variation of Aerosol Radiative Forcing at Jaipur, Kanpur, Lahore and Karachi.

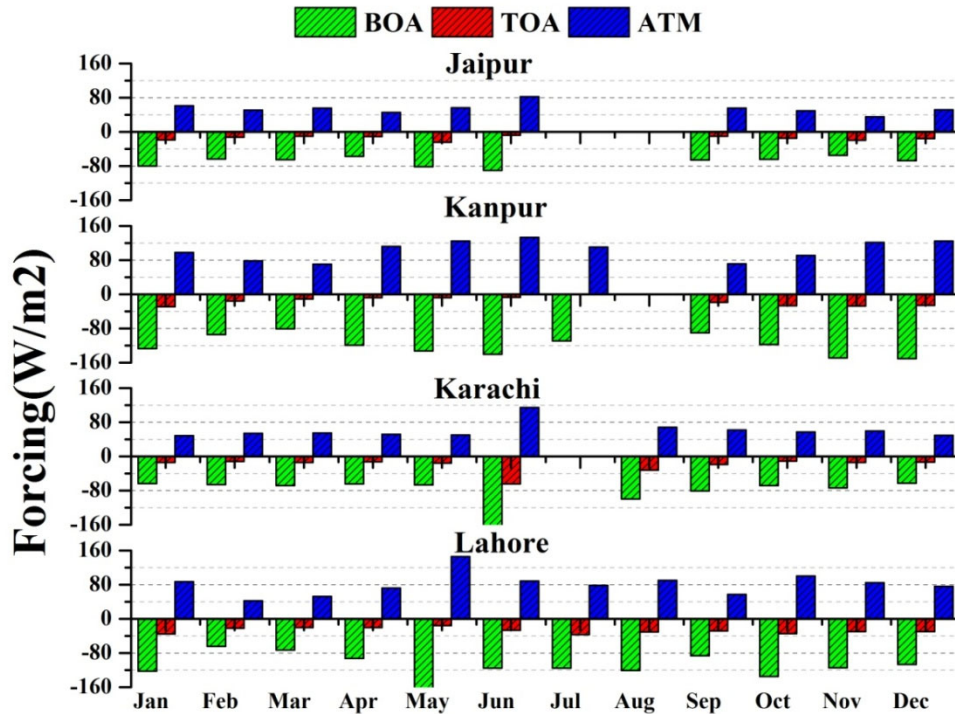


Figure 2. The inter-annual variation in shortwave aerosol radiative forcing at BOA, TOA and ATM during study period.

The monthly mean and inter-annual variation of ARF at TOA, BOA, and ATM during April 2010 to March 2015 is shown in Fig.1 and 2. The BOA and TOA forcing is mostly negative (Fig. 1,2) during all months which indicating cooling effect. The ATM forcing is positive during all months indicative of heating of the atmosphere. The ATM forcing is more prominent during pre-monsoon months (April–June). For all the four sites the radiative forcing at BOA and ATM found higher during pre-monsoon months of the year. Kanpur and Lahore are heavy industrial and polluted sites and also due to presence of dust particles in the atmosphere during the pre-monsoon months, the magnitude of BOA and ATM is more. The magnitude of Jaipur and Karachi site is much lesser then these two sites.

CONCLUSIONS

The inter-annual monthly averaged min-max of ARF at TOA for Jaipur during 2010–2015 is found between -24.43 to -7.93 Wm^{-2} , while the ARF at BOA is found to be between -90.18 to -55.01 Wm^{-2} . Likewise, the ARF within the atmosphere (ATM) comes in the range of 35.29 to 82.25 Wm^{-2} over Jaipur. The inter annual monthly average min-max of ARF at TOA, BOA and ATM come in the ranges of -29.20 to -1.04 Wm^{-2} , -150.31 to -81.17 Wm^{-2} , and 70.51 to 133.44 Wm^{-2} respectively over Kanpur. The inter annual monthly average of ARF at TOA, BOA and ATM come in the ranges of -36.71 to -15.37 Wm^{-2} , -160.93 to -64.16 Wm^{-2} , and 42.01 to 145.56 Wm^{-2} respectively for Lahore. The inter annual monthly average of ARF at TOA, BOA and ATM come in the ranges of -64.17 to -11.5 Wm^{-2} , -178.31 to -63.12 Wm^{-2} , and 49.09 to 114.14 Wm^{-2} respectively for Karachi. Monthly Mean Average shows that the ATM is more pronounced during the pre-monsoon period which indicates heating of the atmosphere. The total averaged ATM during the pre-monsoon for Jaipur, Kanpur, Lahore and Karachi is 61.88 , 123.22 , 102.12 and 72.19 Wm^{-2} respectively. Pre-monsoon shows higher values of ATM due to the presence of dust particles in the atmosphere.

ACKNOWLEDGEMENTS

We acknowledge Giovanni online data system, AERONET group associated NASA personnel for the production of the data used in this research effort. We would also like to thanks for partial support grant which is obtained from MOES sponsored project, New Delhi India.

REFERENCES

Hess, M., Keopke, P. and Schult, I. (1998). Optical properties of aerosols and clouds: The software package OPAC. *Bull. Am. Meteorol. Soc.* 79: 831–844.

IPCC (Intergovernmental Panel on Climate Change) (2007) Climate Change, 2007: The Physical Science Basis. Contribution of Working Group I to the Fourth Assessment Report of the Intergovernmental Panel on Climate Change, Cambridge University Press, Cambridge,USA.

IPCC, 2013: Climate Change 2013: The Physical Science Basis. Contribution of Working Group I to the Fifth Assessment Report of the Intergovernmental Panel on Climate Change, Cambridge University Press, Cambridge,USA.

Kaskaoutis, D.G., Kambezidis, H.D., Hatzianastassiou, N., Kosmopoulos, P.G. and Badarinath, K.V.S. (2007).Aerosol climatology: On the discrimination of aerosol types over four AERONET sites. *Atmos. Chem. Phys. Discuss.* 7: 6357–6411.

Payra, S., Soni, M., Kumar, A., Prakash, D., Verma, S. (2015). Intercomparison of aerosol optical thickness derived from MODIS and in situ ground datasets over Jaipur, a semiarid zone in India. *Environ. Sci. Tech.* 49 (15), 9237–9246,doi: 10.1021/acs.est.5b02225.

Ricchiazzi, P., Yang, S., Gautier, C. and Sowle, D. (1998). SBDART: A research and teaching software tool for plane-parallel radiative transfer in the Earth's atmosphere. *Bull. Am. Meteorol. Soc.* 79: 2101–2114.

Soni, M., Payra, S., & Verma, S. (2018). Particulate matter estimation over a semi arid region Jaipur, India using satellite AOD and meteorological parameters. *Atmos. Poll. Res.*, Volume 9 Issue 5, doi: 10.1016/j.apr.2018.03.001.

Verma, S., Boucher, O., Upadhyaya, H.C. andd Sharma,O.P. (2006). Sulfate aerosols forcing: An estimate using a three-dimensional interactive chemistry scheme.*Atmos. Environ.* 40: 7953–7962.

EFFICENCY OF RAINFALL IN SCAVANGING DIFFERENT TYPES OF AEROSOLS OVER EASTERN HIMALAYAN

M DUTTA¹, A CHATTERJEE^{1,2}, A ROY¹, A GHOSH¹, S.K DAS¹, S.K GHOSH^{2,3}, S RAHA^{1,2,3}

¹Environmental Sciences Section, Bose Institute, P1/12 CIT Scheme VII-M, Kolkata 700054, India

²National Facility on Astroparticle Physics and Space Science, Bose Institute, 16 A J C Bose Road, Darjeeling 734101, India

³Center for Astroparticle Physics and Space Science, Bose Institute, Block-EN, Sector-V, Kolkata 700091, India

KEYWORDS: Aerosols, below-cloud scavenging, in- cloud scavenging, rainfall

INTRODUCTION

Wet scavenging is the major removal pathway for the aerosol wash out from the atmosphere. Aerosols when scavenged within the cloud is called the in-cloud scavenging whereas the aerosols are washed out below the cloud after interacting with the rain drops and called the below-cloud scavenging. Most of the atmospheric aerosols get deposited to the Earth's surface through the later process. The factors associated with the rain like rain intensity, rain-drop size distribution, duration of the rain etc as well as the factors associated with the aerosols like aerosol size and the pollution level governs the aerosol below-cloud scavenging. The degree of aerosol-rain interaction and hence the scavenging governs the acidity of the rain water and thus it in turns affects the regional biogeochemical cycles. Here in this study we have conducted an extensive sampling program on the scavenging of different types of aerosols like sea-salt and anthropogenic of different sizes due to rain as well as how their degree of the regeneration varies after the rain. To do this, we have collected size segregated (fine and coarse) aerosols before, during and after the rain and chemically analyzed the aerosol samples in terms of various major water soluble ionic species for sea-salt and anthropogenic components. The study is mainly focused to investigate the wet scavenging and regeneration of sea-salt and anthropogenic size-segregated aerosols and the controlling factors behind them.

METHODS

For the collection of respirable dust sample of aerodynamic diameter less than 10 micron (model APM 460BL) and aerodynamic diameter less than 2.5 micron was measured by fine dust sample of (model APM 550) manufactured by Envirotec Instrument Pvt Ltd, India was used. The respirable dust sampler and fine mode sampler collected the samples with a flow rate of $1.4\text{m}^3 \text{min}^{-1}$ and $1\text{m}^3\text{hr}^{-1}$ respectively. Total respirable particulate matter was collected on the filter paper (EPM 2000 filter paper from Whatman of 8"x10" dimension) and fine mode particles were collected on a PTFE filter paper of 47 mm diameter. Each sampling was started at 1000hrs (local time) and run for ~24 hrs. Both the sampler was placed on the terrace of a three- storied building (~15m above ground level) on our institute premises at Darjeeling. The aerosol mass (μg) was determined by the differences between initial and final weight of the filter paper and the concentration μgm^{-3} was determined by dividing the aerosol mass by total volume of air (m^3).

For the analysis of water soluble ions, Ion chromatography separation method was used. The major ions, namely anions (Cl^- , NO_3^- and SO_4^{2-}) and cations (Na^+ , NH_4^+ , K^+ , Ca^{2+} and Mg^{2+}) were analysed by Ion chromatography (861 Advanced Compact IC, Metrohm, Switserzerland) using analytical column IonPac[®] AS15 with micro-membrane suppressor ASRS ultra II 2mm, 38 nM. KOH as eluent and triple distilled water as regenerator for anions was used. Similarly CSRS ultra II 2mm, 6mM methan sulfonic acid as eluent and triple distilled water as regenerator were used for cations. Data was collected on all the rainy days and corresponding dry (before day of rain) and wet day (post day of rain) data were also obtained. The anthropogenic, sea salt and dust aerosols were calculated as follows:

$$[\text{Anthropogenic aerosol}] = [\text{non-seaSO}_4^{2-}] + [\text{NO}_3^-] + [\text{NH}_4^+] + [\text{K}^+]$$

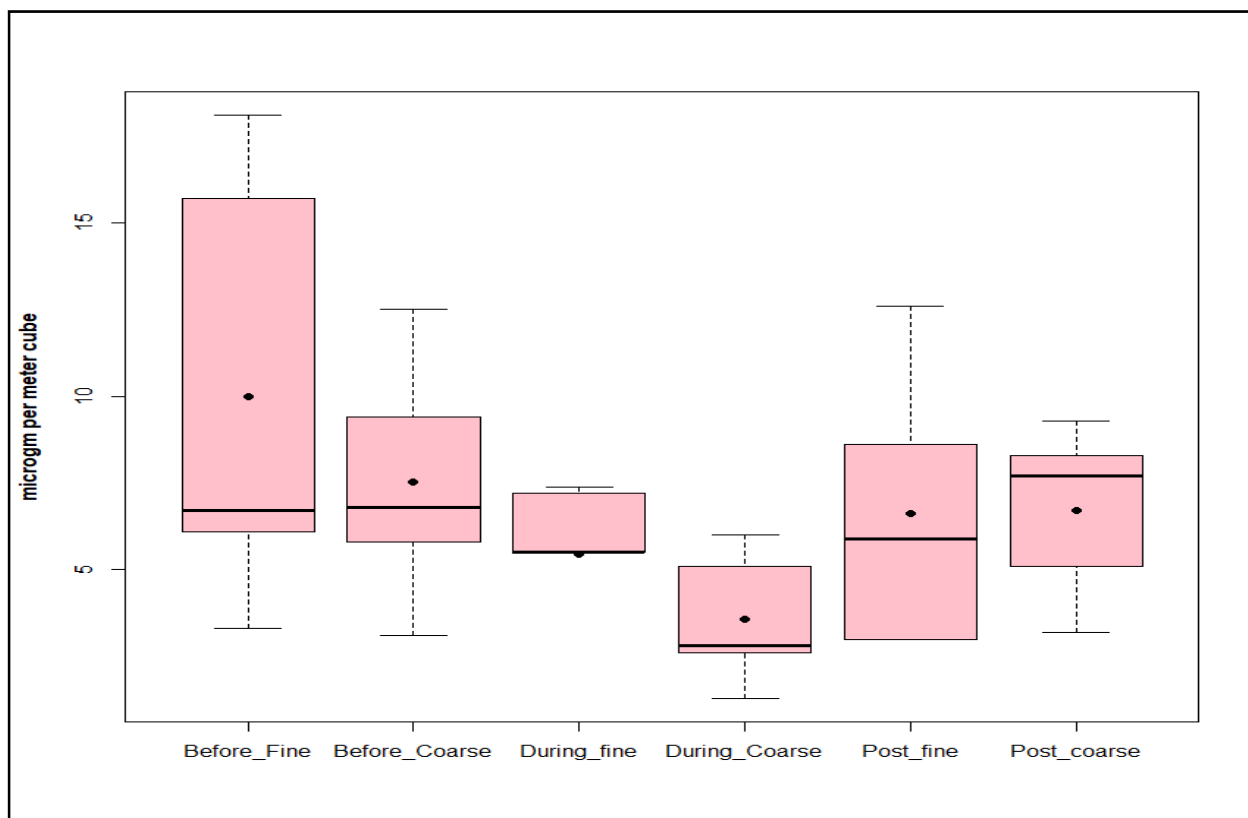
$$[\text{Seal salt aerosol}] = [\text{Na}^+] + [\text{Cl}^-] + [\text{seaSO}_4^{2-}] + [\text{seaMg}^{2+}] + [\text{seaCa}^{2+}]$$

$$[\text{Dust aerosol}] = [\text{non-sea Ca}^{2+}] + [\text{non-sea Mg}^{2+}]$$

RESULTS AND DISCUSSION

The study was carried out over a high altitude station Darjeeling (27.01°N, 88.15°E, ~2200m amsl) in monsoon season in the year 2016. It is found that fine mode and coarse mode aerosols ranges from 1.7 to 18.1 $\mu\text{g}\text{m}^{-3}$ and 1.3 to 12.5 $\mu\text{g}\text{m}^{-3}$ respectively during the entire study period. The mean concentration of fine and coarse mode was found to be $7.3 \pm 4.4 \mu\text{g}\text{m}^{-3}$ and $5.9 \pm 2.8 \mu\text{g}\text{m}^{-3}$ respectively. The total concentration of coarse mode aerosol was found to be less compared to fine mode aerosol. Percentage of scavenging of coarse mode aerosol is more compared to fine mode where as the regeneration of coarse mode is much higher than the fine mode aerosol. It has been observed that aerosol concentration both in fine and coarse mode decrease significantly on the rainy day and then increased slightly on the post-rainy day. It was observed that fine mode anthropogenic and coarse mode sea salt aerosol was scavenged the least. Regeneration was found in all the sampling events and the highest was observed in coarse mode sea-salt aerosols. The scavenging of coarse mode sea salt aerosol was very small and the regeneration was extremely high which implies that there was a continuous supply of air mass loaded with coarse mode sea salt aerosol during the entire sampling period. The total anthropogenic aerosol concentration was found nearly four times less compared to total sea salt aerosol concentration and no contribution from dust aerosols was found in monsoon season in fine mode. In coarse mode we find contribution from dust Figure 1: Concentration (μm^3) of fine and coarse mode aerosol before, during and post rainfall events in the monsoon season.

mode aerosols however the concentration was very less compared to sea salt and anthropogenic aerosol.



This implies that mineral dust and anthropogenic aerosols are scavenged much more than sea salt aerosols in coarse mode.

CONCLUSIONS

The concentration of fine mode aerosol was found more compared to coarse mode in monsoon season. Percentage of coarse mode aerosol scavenging was higher than fine mode where reverse phenomena was observed in case of regeneration.

ACKNOWLEDGEMENT

Authors would like to thank Department of Science & Technology (DST) Strategic Programmes, Large Initiatives and Coordinated Action Enabler (SPLICE) climate Change programme, Government of India for their funding.

REFERENCES

Chatterjee A, Adak A, Singh AK, Srivastava MK, Ghosh SK, et al. (2010) Aerosol Chemistry over a High Altitude Station at Northeastern Himalayas, India. PLoS ONE 5(6): e11122. doi:10.1371/journal.pone.0011122.

IPCC: Climate Change 2007: The Physical Science Basis. Contribution of Working Group I to the Fourth Assessment Report of the Intergovernmental Panel on Climate Change, Cambridge University Press, Cambridge, United Kingdom and New York, NY, USA, 2007.

Sarkar C, Chatterjee A, Singh AK, Ghosh SK, Raha S, 2015. Characterization of black carbon aerosols over Darjeeling-a high altitude Himalayan Station in Eastern India. Aerosol Air Qual. Res. 15, 465–478.

EVALUATION OF SINGLE-LAYER WARM CLOUDS AND AEROSOL OPTICAL DEPTH FROM MODIS ONBOARD TERRA SATELLITE

SUBHASIS BANERJEE AND SANJAY K GHOSH

Center for Astroparticle Physics and Space Science, Bose institute, India

INTRODUCTION

Satellite retrievals of cloud properties play a very important role in understanding the impact of cloud system on earth's radiation budget and on climate systems (Painemal et al., 2011). Cloud effective radius and cloud optical thickness estimated from non-absorbing and absorbing wave lengths are the two most important independent variables retrieved from sensors on-board many satellites including Earth Observing System (EOS) satellites Terra and Aqua. From cloud effective radius and cloud optical thickness other properties can be derived like cloud liquid water path, droplet number concentration etc. In this study MODIS level-2 cloud product from Terra have been used to assess micro-physical properties of low-height, single-layer warm clouds over entire landmass of India and compared with AOD also obtained from MODIS Terra.

METHODOLOGY

In this study, MODIS level-2 cloud product from Terra have been used to assess micro-physical properties of low-height, single layer warm clouds over entire landmass of India. Cloud top pressure has been set greater than 850 hPa (to ensure low-height cloud scenes) whereas cloud top temperature was set greater than 5°C. Such cloud scenes of an entire year have been filtered out to study cloud effective radius, cloud optical thickness, cloud droplet number concentration and cloud liquid water path. Data points retrieved for a whole year (2017) over entire landmass of India. Data pixels averaged over 0.2 x 0.2 degree grid for latitude 10 to 30 and longitude 70 to 90. Comparative analyses of these properties also carried out for the whole year to that of only monsoon season. Aerosol Optical Depth data obtained in 1 x 1 degree grid for the same year and presented here to evaluate the influence of the same on cloud micro-physical properties.

RESULTS & DISCUSSIONS

Cloud effective radius was found to be higher in Indo-Gangetic region (14-16 micron) during monsoon season, however for whole year western coastal area and part of eastern coast showed higher values. North western part of India which is arid region showed much smaller values throughout the year (6-8 micron). Average cloud droplet number concentration in this region is much higher than any other part of the country (Figure 2). This part of the country being close to desert must be a source of dust aerosol which cloud serve as potential source of cloud condensation nuclei (CCN). Abundance of CCN could lead to higher droplet concentration. In the same time, lesser amount of available atmospheric moisture could lead to smaller drop sizes. Excepting this region Indo-Gangetic plane showed much higher values than the rest part of the country as far as cloud droplet number concentration is concerned. Indo-Gangetic region including north-western part of the country being the region of highest AOD could impact cloud micro-physical properties at least up to some extent. However further studies should be carried out with longer time data for conclusive analyses.

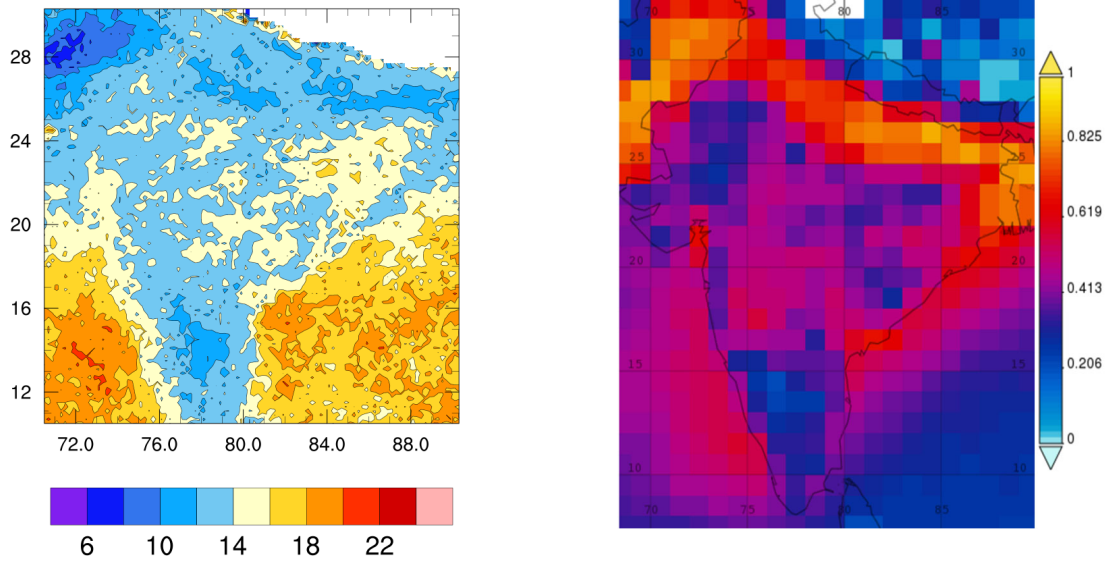


Figure 1: Cloud effective radius(micron) and AOD over Indian landmass for the year 2017

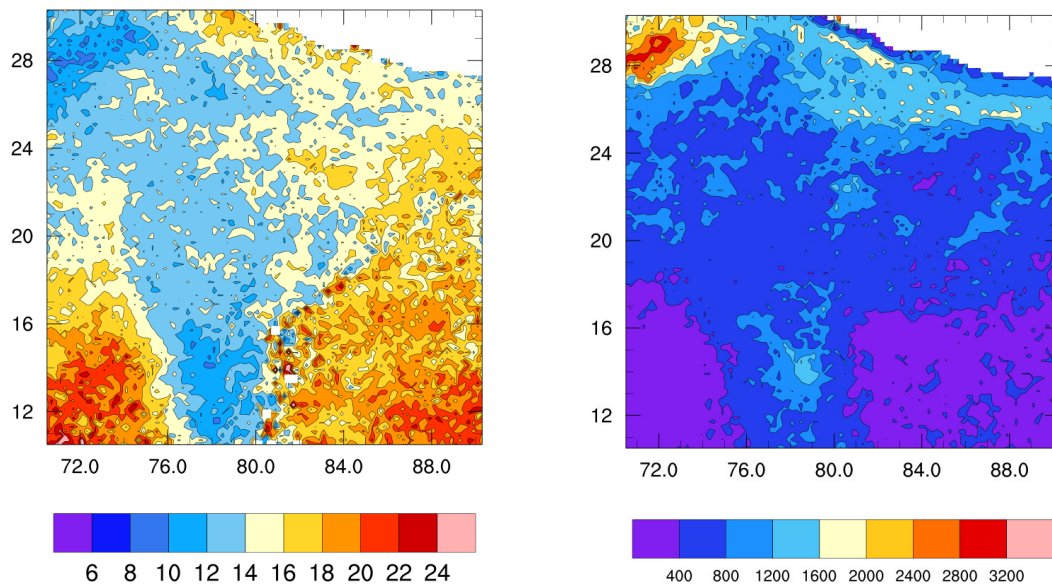


Figure 2: Cloud effective radius(micron) during monsoon season(JJAS) and Cloud droplet number concentration(per cc) averaged for the entire year over Indian landmass

ACKNOWLEDGEMENT

The MODIS/Terra Clouds 5-Min L2 Swath 1km and 5km datasets were acquired from the Level-1 and Atmosphere Archive & Distribution System (LAADS) Distributed Active Archive Center (DAAC), located in the Goddard Space Flight Center in Greenbelt, Maryland (<https://ladsweb.modaps.eosdis.nasa.gov/>).

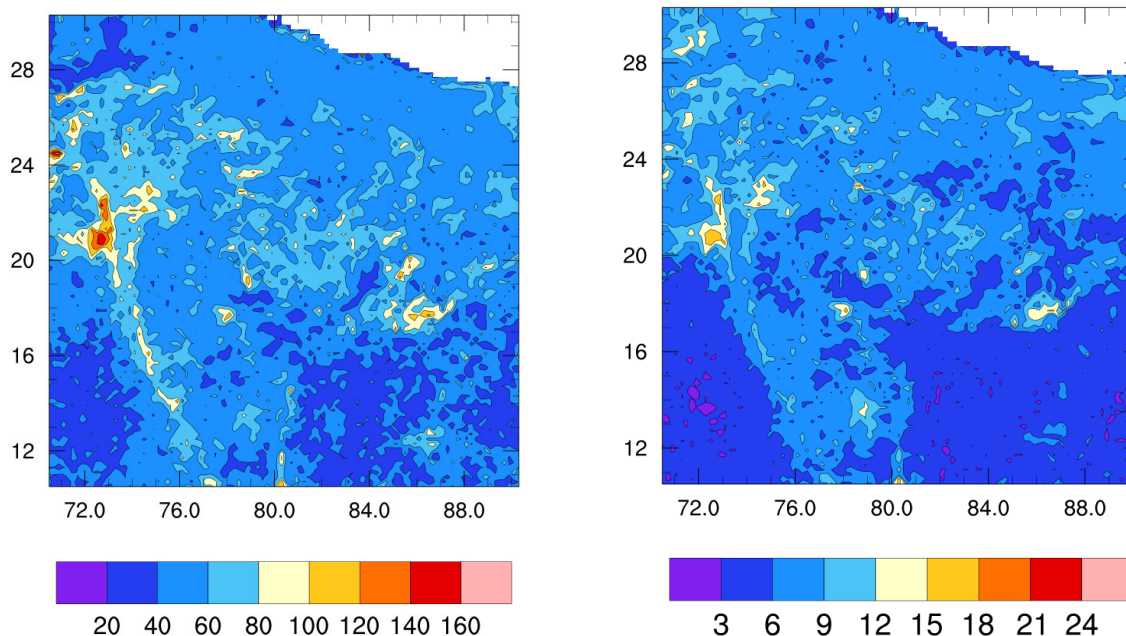


Figure 3: Cloud water path (gm/m^2) and Cloud optical thickness averaged for the whole year.

REFERENCES

Ahmed, I. et al. (2013). Long-term measurements of cloud droplet concentrations and aerosol-cloud interaction in continental boundary layer clouds, *Tellus B*, 65, 20138.

Painemal, D. and Zuidema, P. (2011). Assessment of MODIS cloud effective radius and optical thickness retrievals over the south Pacific with VOCALS-Rex in situ measurements, *Journal of geophysical Research*, vol. 116, D24206.

Platnick, S., Ackerman, S., King, M., et al., (2015). MODIS Atmosphere L2 Cloud Product (06_L2). NASA MODIS Adaptive Processing System, Goddard Space Flight Center, USA: http://dx.doi.org/10.5067/MODIS/MOD06_L2.061

Prabha, T. V. et al. (2012), Spectral width of pre-monsoon and monsoon clouds over Indo-Gangetic valley, *Journal of geophysical Research*, Vol. 117, D20205.

Zeng, S. Et al. (2014). Study of global cloud droplet number concentration with A-Train satellites, *Atmos. Chem. Phys.*, 14, 7125-7134.

LONG-TERM MEASUREMENT OF CLOUD CONDENSATION NUCLEI OVER A HIGH ALTITUDE HILL STATION OVER EASTERN HIMALAYA

ARINDAM ROY¹, ABHIJIT CHATTERJEE^{1,2}, ABHINANDAN GHOSH¹, SANAT KUMAR DAS¹,
SANJAY KUMAR GHOSH^{2,3}, SIBAJI RAHA^{1,2,3}

¹Environmental Sciences Section, Bose Institute, Kolkata, India

²National Facility on Astroparticle Physics and Space Science, Darjeeling, India

³Center for Astroparticle Physics and Space Science, Bose Institute, Kolkata, India

KEYWORDS: Cloud Condensation Nuclei, Eastern Himalaya

INTRODUCTION

Cloud droplets are formed due to the condensation of water vapour on the surface of submicron aerosol particles (also called condensation nuclei or CN) under certain atmospheric super saturation (SS) condition ([Andreae and Rosenfeld, 2008](#)). The condensation process depends on both the size and chemical nature of the aerosol particles. The aerosol particles having the ability to form the growth of cloud droplets at atmospheric SS are called cloud condensation nuclei (CCN). Aerosol particles which are highly hydrophobic in nature like black carbon, dust etc. could also act as CCN if they get well mixed or coated with soluble parts of aerosols or gases. CCN has a great ability to perturb cloud albedo, cloud lifetime, cloud height and other microphysical properties of the cloud. Role of aerosols in CCN activity has been investigated over a few Indian stations, but Eastern part of Himalaya remain unexplored. This study is an attempt to understand long-term interaction between aerosol and CCN over a high altitude observation site in the eastern Himalayas.

METHODS

We have measured condensation nuclei (CN) and cloud condensation nuclei (CCN) over Darjeeling (27.03°N, 88.26° E), a high altitude hill station over eastern Himalaya (~2200 amsl) during dry seasons of 2015-2018. The number concentration of condensation nuclei (N_{CN}) was measured by water based Condensation Particle Counter (CPC; TSI Model 3783), which measures N_{CN} in diameter range 7.0 nm – 3.0 μ m whereas CCN concentration was measured by a continuous-flow thermal-gradient diffusion chamber (DMT-CCN counter – 100). Aerosol samples have been drawn inside a 50-cm tall column of CCN-100. For this study, we have measured the concentration of N_{CCN} at 0.1 to 1% supersaturation (SS) with an interval of 0.1%. The instrument was configured to sample the particles every second and to complete one SS cycle in an hour.

RESULTS & DISCUSSIONS

Seasonal variation of N_{CN} and N_{CCN} shows a higher concentration of CN and CCN during premonsoon followed by winter and post-monsoon. The average concentrations of CN and CCN during premonsoon (7220 ± 1988 and 1998 ± 862 cm^{-3}) were almost double of postmonsoon (4498 ± 1341 and 887 ± 295 cm^{-3}). The concentration of CN and CCN in winter was found to be 5917 ± 1683 and 1652 ± 694 cm^{-3} respectively. The up-slope valley wind and tourist activity played major roles in enhancing CN and CCN concentration during pre-monsoon. On the other hand, night-time biomass burning enhances CN and CCN concentrations in winter. The mean value of AR (0.5% SS) over Darjeeling was found to be almost equal in winter (0.32 ± 0.05) and premonsoon (0.3 ± 0.07) and higher than a postmonsoon season (0.24 ± 0.07).

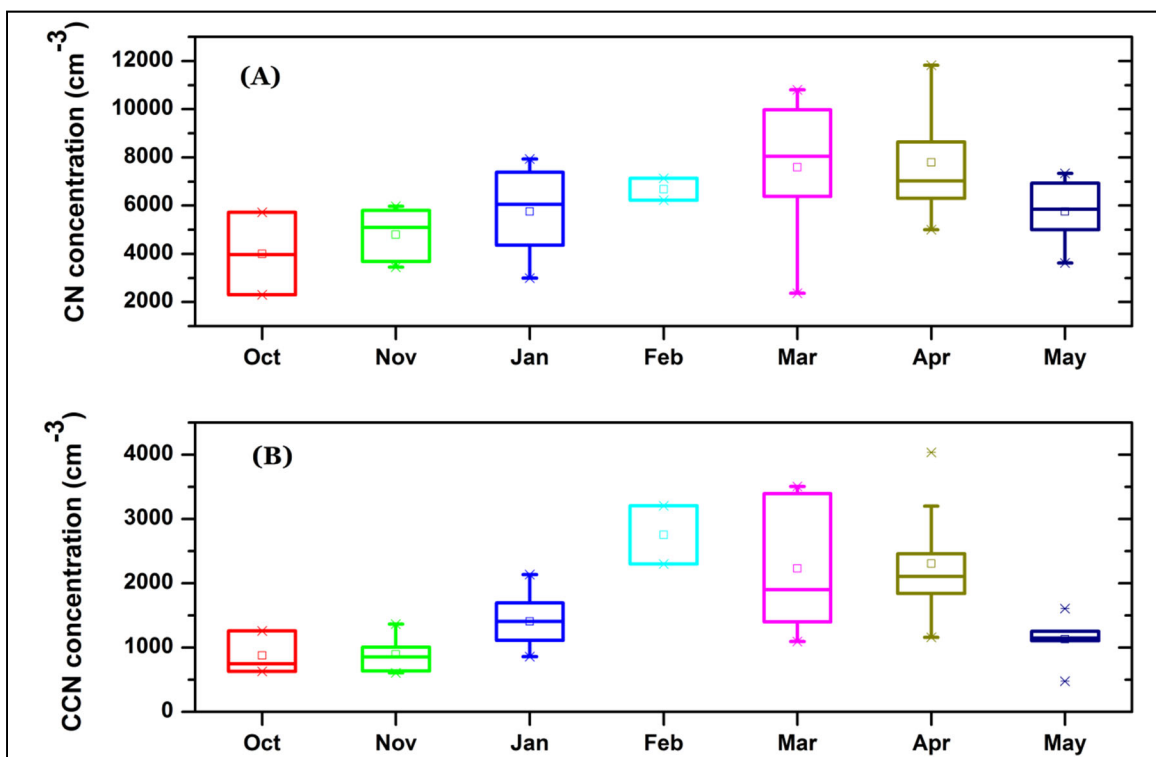


Fig 1 : Box-whisker plot of monthly CCN and CN concentration during the entire study period

CONCLUSIONS

We observed that submicron aerosols became more hygroscopic during their transport by external mixing during pre-monsoon. Whereas during winter aerosols from biomass burning became larger in size due to the coating of organic aerosols, trace gasses and other soluble inorganic species which in turn activated to CCN.

ACKNOWLEDGEMENTS

Authors would like to thank Science and Engineering Council, Department of Science and Technology, Government of India for supporting the study under IRHPA (Intensification of Research in High Priority Areas, Grant No. - [IR/S2/PF-01/2011](#))

REFERENCES

Andreae, M. O., & Rosenfeld, D. (2008). Aerosol–cloud–precipitation interactions. Part 1. The nature and sources of cloud-active aerosols. *Earth-Science Reviews*, 89(1-2), 13-41.

URBAN EMISSIONS LOAD FROM PASSENGER TRANSPORTATION TO THE ATMOSPHERE

A. CHOUDHARY¹, P. KUMAR², A. SHUKLA¹ A. K. SINGH² and S. TIWARI³

¹Transport Planning and Environment Division, CSIR-Central Road Research Institute, New Delhi, India.

²Department of Physics, Institute of Science, Banaras Hindu University, Varanasi, India.

³Environment Monitoring and Research Centre, Indian Meteorological Department, New Delhi, India.

KEYWORDS: Tail-Pipe Emission, Ambient Emission, Carbonaceous Pollutants

INTRODUCTION

Transport crisis in cities is characterized by congestion, degree of noise and air pollution, traffic fatalities and injuries (Pucher et al., 2007). The excessive growth in vehicular population significantly increases air pollution and related health issues (Nagpure et al., 2014;). On-road traffic is the major contributor in the rise of air pollution in cities like Delhi as compared to other sources like industry, residential, and thermal power plants (Jain et al., 2014; Kumar et al., 2015). The increase in urban road transportation has significantly increased vehicular emissions. Several studies have shown that vehicular emissions are a major culprit for the air quality degradation in Indian cities (Nagpure et al., 2014). In developing countries mix of both motorized and non-motorized vehicles (heterogeneous traffic) traveling at different speeds are the causes of frequent interruption and congestion. The situation is exacerbated by the rapid growth of cities, urbanization, in adequate transport infrastructure, rampant suburban sprawl, rising motor vehicle ownership and use, insufficient public transport, and inadequate as well as uncoordinated land use and transport planning (Pucher et al., 2007). Several policies have been initiated to improve urban mobility in Indian cities.

Transport sector is a major contributor of carbonaceous emission globally, contributes around 23% of CO₂, of which road traffic is responsible for almost three-quarters (Van der Hoeven, 2012). According to Unger et al. (2010) motor vehicles have emerged as the largest contributor to atmospheric warming. India is the fourth largest emitter of greenhouse gases globally, following China, the United States, and the European Union (Beermann et al., 2016).

RESEARCH METHODOLOGY

Highly-trafficked stretch of urban traffic corridors was selected for the real world emission measurement in Guwahati and Delhi. Two month old to 16 year old vehicles of different mileages passenger cars and auto-rickshaws fuelled with CNG and gasoline were selected and their driving and emission profile were measured by the instruments V-Box (driving profile), five gas analyser and Kane auto-plus emission analyser. The survey of test route were also done with driver and owner of passenger cars and auto-rickshaws for vehicle kilometre travelled per day, inspection/maintenance and use of public transport/week to know the carbon footprint associated with day to day activities of passenger transportation.

Besides the on road measurement of tail-pipe emission ambient concentration of CO and CO₂ were also measured (from CO & CO₂ analyser) for whole year 2017 at a main red light, near CRRI gate which is highly trafficked. The meteorological variables were also measured at the site.

RESULTS AND DISCUSSION

The study characterized the carbonaceous emission of passenger transportation from the source as well as the ambient atmosphere at local scale in urban atmosphere. Figure 1 show the passenger cars tail pipe emission trend of CO (ppm) concentration. It is clearly depicting with increasing the mileage emission rate increases significantly. The 16 year old vehicle has maximum emission rate, ranges from 1000 to 23000 ppm, as compared to the new vehicle (ranges within 1000 ppm) having lower mileage. Some high emission peaks for different mileage vehicles are also visible in Figure1, indicative of stop-and-go events with sharp

emission peaks (Choudhary and Gokhale, 2016). This highlights the contribution of per vehicle carbonaceous emission from the older vehicle is significantly high to the local atmosphere.

Figure 2 show daily ambient concentration of carbonaceous pollutants CO and CO₂ near highly trafficked road. The local near ground concentration of CO and CO₂ ranges of 0.5 to 2.5 ppm and 275 to 450 ppm. This signifies that on an average up to 2.5ppm CO and 275 to 450 ppm CO₂ is daily contributed to the local urban atmosphere at a single trafficked point in Delhi.

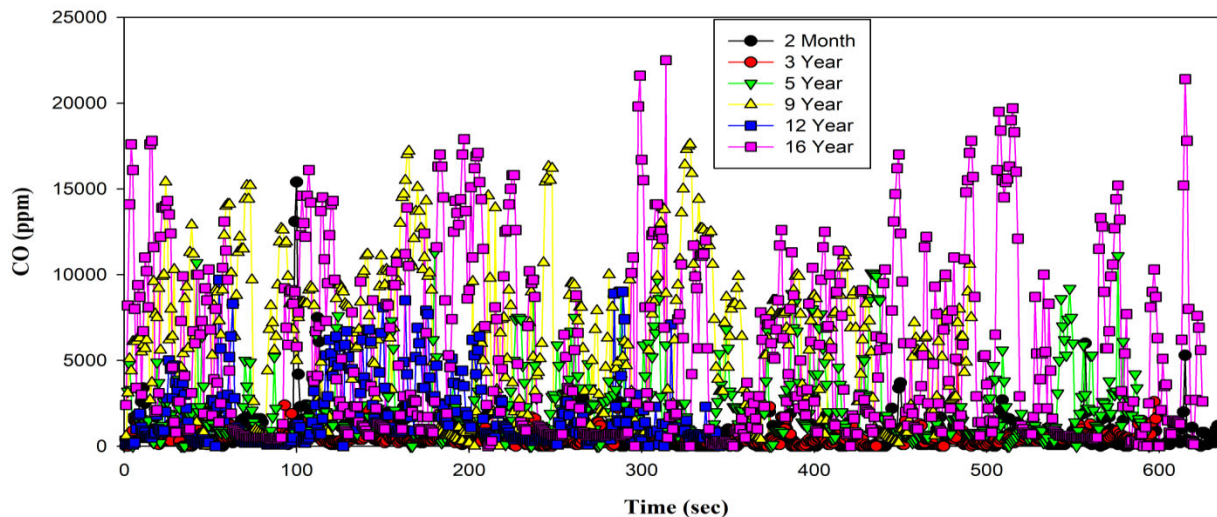


Figure 1. Carbonaceous emission from the tail-pipe for different mileage test vehicles

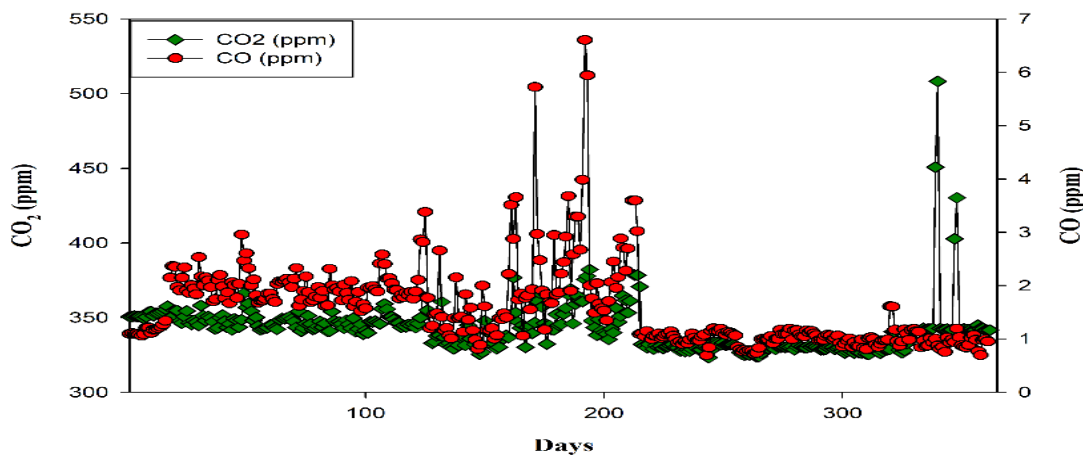


Figure 2. Carbonaceous emission at a highly trafficked road at main red light point in Delhi

CONCLUSION

The results are demonstrating that both individual level and source level carbonaceous emission are in alarming stage. Especially the higher mileage vehicles have several time more emission rate. Analysis especially defined the per vehicle carbonaceous emission and per day carbonaceous emission to a highly for trafficked road to the urban atmosphere at local scale.

ACKNOWLEDGEMENT

Arti Choudhary thankfully acknowledges the financial assistance provided by SERB-DST, New Delhi, India, under the scheme of SERB National Post-Doctoral Fellowship (PDF/2017/001284). Authors also acknowledge the Indian Meteorological Department, New Delhi for providing.

REFERENCES

- Beermann, J., Damodaran, A., Jörgensen, K., Schreurs, M.A. (2016). Climate action in Indian cities: an emerging new research area. *Journal of Integrative Environmental Sciences*, 1-12.
- Choudhary A, Gokhale S. 2016. Urban real-world driving traffic emissions during interruption and congestion. *Transportation Research Part D: Transport and Environment* 43: 59-70.
- Jain, M., Mohan, S., Pal, A. (2014). Motor vehicle exhaust emissions in Delhi. *International Journal of Current Engineering and Technology* 4, 2693-2696.
- Kumar, P., Khare, M., Harrison, R.M., Bloss, W.J., Lewis, A.C., Coe, H., Morawska, L. (2015). New directions: Air pollution challenges for developing megacities like Delhi. *Atmospheric Environment* 122, 657-661.
- Nagpure, A.S., Gurjar, B.R., Martel, J. (2014). Human health risks in national capital territory of Delhi due to air pollution. *Atmospheric Pollution Research* 5.
- Pucher, J., Peng, Z. R., Mittal, N., Zhu, Y., and Korattyswaroopam, N. (2007). Urban transport trends and policies in China and India: impacts of rapid economic growth. *Transport Reviews*, 27(4), 379-410.
- Unger, N., Bond, T.C., Wang, J.S., Koch, D.M. Menon, S., Shindell, D.T. and Bauer, S. (2010). Attribution of climate forcing to economic sectors. *Proceedings of the National Academy of Sciences* 107, 3382-3387.
- Van der Hoeven, M. (2012). CO2 emissions from fuel combustion: highlights. Paris: Organisation for Economic Co-operation and Development. *International Energy Agency (OECD/IEA)*.

QUANTIFICATION OF DUST TRANSPORT TO EASTERN ARABIAN SEA DURING STORM PERIOD USING SATELLITE AND GROUND BASED DATA.

M. A. ASWINI¹, ASHWINI KUMAR^{1*}

Geological Oceanography Division, CSIR-National Institute of Oceanography, Dona Paula, Goa – 403004

KEYWORDS: Dust aerosols, Monitoring, Remote sensing, Arabian Sea, Calipso, Lidar.

INTRODUCTION

Aeolian dust is one of the major component in the atmospheric aerosol budget, plays a significant role in the atmospheric, oceanic, terrestrial processes (Dentener et al., 1996; Arimoto, 2001; Jickells et al., 2005). These dust particles can undergo long-range transport ranging from regional to intercontinental scales. Chemical composition of mineral dust undergo modification during long range transport, which can significantly contribute to regional as well as global radiative budget (Tegen et al., 1996; Arimoto, 2001). Seasonality in the wind system modifies the temporal and spatial distribution of dust, its amount of deposition and chemical properties. A large amount of dust gets in to the atmosphere during dust storms, which can undergo transcontinental transport. Quantification of the dust supply to receptor region (e.g. Surface Ocean) is crucial to understand the biogeochemical cycling of mineral dust. In this study we have attempted to quantify amount of dust transported from Arabian Peninsula to Eastern Arabian Sea during a dust storm event using satellite and ground based observation.

METHODS

The cross transport and the amount dust present in the atmospheric column is calculated using the CALIPSO (Cloud-Aerosol Lidar and Infrared Pathfinder Satellite Observations) profiles. It measure vertical profiles of atmospheric particles at 532 and 1064 nm near nadir during both day and night. The primary products are the calibrated and geo-located LIDAR profiles of 532- and 1064-nm total attenuated backscatters depolarization ratio, which is computed from the two polarization components of the attenuated backscatter. The CALIPSO level 2 data version 4.10 standard profile data are used. The cloud presence removed using the cloud aerosol discrimination score -20 and -100 (Yu et al., 2010) and quality check has been done using the extinction quality control flag to remove false retrieval (Winker et al., 2013). The attenuated dust backscatter and extinction are calculated using total aerosol backscatter, then converted the dust extinction to concentration using mass extinction efficiency (Yu et al., 2015). CALIPSO profile was compared with the ground based micro pulse LIDAR (MPL) profiles retrieved at Goa (a coastal city on Eastern Arabian Sea; 15.4° N, 73.8° E), where 4 km extended thick layer is observed for more than 20 days. Profile of normalized backscatter data and depolarization ratio of MPL (from 01-23 Apr 2015) is used during and after the dust storm period. The amount of dust quantified from CALIPSO profile is validated from ground based high volume sampler collected aerosol mass loading at Goa. Mass loading is calculated from the difference weight between the filter paper before and after sampling and normalizing it with volume of air pumped for collection which is expressed in $\mu\text{g m}^{-3}$. Atmospheric aerosols were typically collected for 24 hour duration. Samples collected during 04-22 Apr 2018 samples are used in the present study.

RESULTS & DISCUSSIONS

A dust storm is generated in the Arabian region mainly in the Qatar Peninsula (25°N, 51° E) and Rub Al Khali (21° N, 48° E) on 02 April 2015 and its formation is identified using the daily satellite images of MODIS (moderate resolution imaging spectroradiometer) Aqua. Dust storm spread towards northern Arabian Sea and Indian subcontinent within a week, mainly dictated by the prevailing wind regime. Trade winds and strong westerly's modulate the direction and transport of the dust storm. Higher level dust travels

towards the Pakistan, Afghanistan, and northern Indian region in the direction of strong westerly wind. Daily CALIPSO profiles were classified in to three categories near to source region (S), near to the sampling region Goa (G) and Central Arabian Sea (C). In the profile, Longitude of S is taken from 40- 55 °E, for C is 55-72 °E and for G 72-80 °E with similar latitude (5-40 °N) for all category. The selected profiles for S, C and G during 02-10 April 2015 is shown in Fig. 1. Only night time profiles are used for the study to avoid the background noises.

The evolution and spreading of mineral dust during storm period is shown in Fig. 1, where the abundance of dust at 3 different locations (S, C, and G) is highlighted. On 02 April, dust near the source region, where thick dust layer can be seen from 14-24 °N as evident from high scattering coefficient in the lower part (>2km). The spatial dissipation of dust layer found to extend horizontally in 10-28 °N belt and vertically at higher altitude (>6km). In the open ocean, similar spread is observed. The vertical profile near Goa shows a vertically extended layer at 4.5km with scattering coefficient >0.02 Sr/km⁻¹.

Micro pulse LIDAR (MPL) installed in the receptor region shows the similar pattern like CALIPSO profiles of G. Normalized Relative Backscattering (NRB) shows the scattering due the atmospheric particle and clouds whereas depolarization ratio (DR) represents the non-sphericity of the particle. From 4th April, MPL profile shows 4 km vertically extended dust layer with high NRB (5 counts km²/ μs μj) and DR(0.1-1.0) which clearly shows the signature of Arabian dust presents in the Goa region.

Using CALIPSO retrieval the amount of dust quantified for 12 aerosol profile of S, C and G. About 1200 μg m⁻³ dust raised in the near source region profiles, where maximum dust showing in the in the 25-30 °N belt. About 200 μg m⁻³ dust concentration calculated in the near Goa (G) which is comparable with the mass loading values estimated from HVS collection.

CONCLUSIONS

Dust storm generated on the 02 April in the Arabian Peninsula and dispersed towards the northern southern and western side of source area. Dust concentration calculated from the CALIPSO profiles shows that 1200 μg m³ is raised from the source region and 200 μgm⁻³ measured in receptor region. The signature of dust storm derived at Arabia is observed at Goa (receptor region) by MPL observations and quantity of dust measured by HVS compares well with the dust estimated from CALIPSO profile.

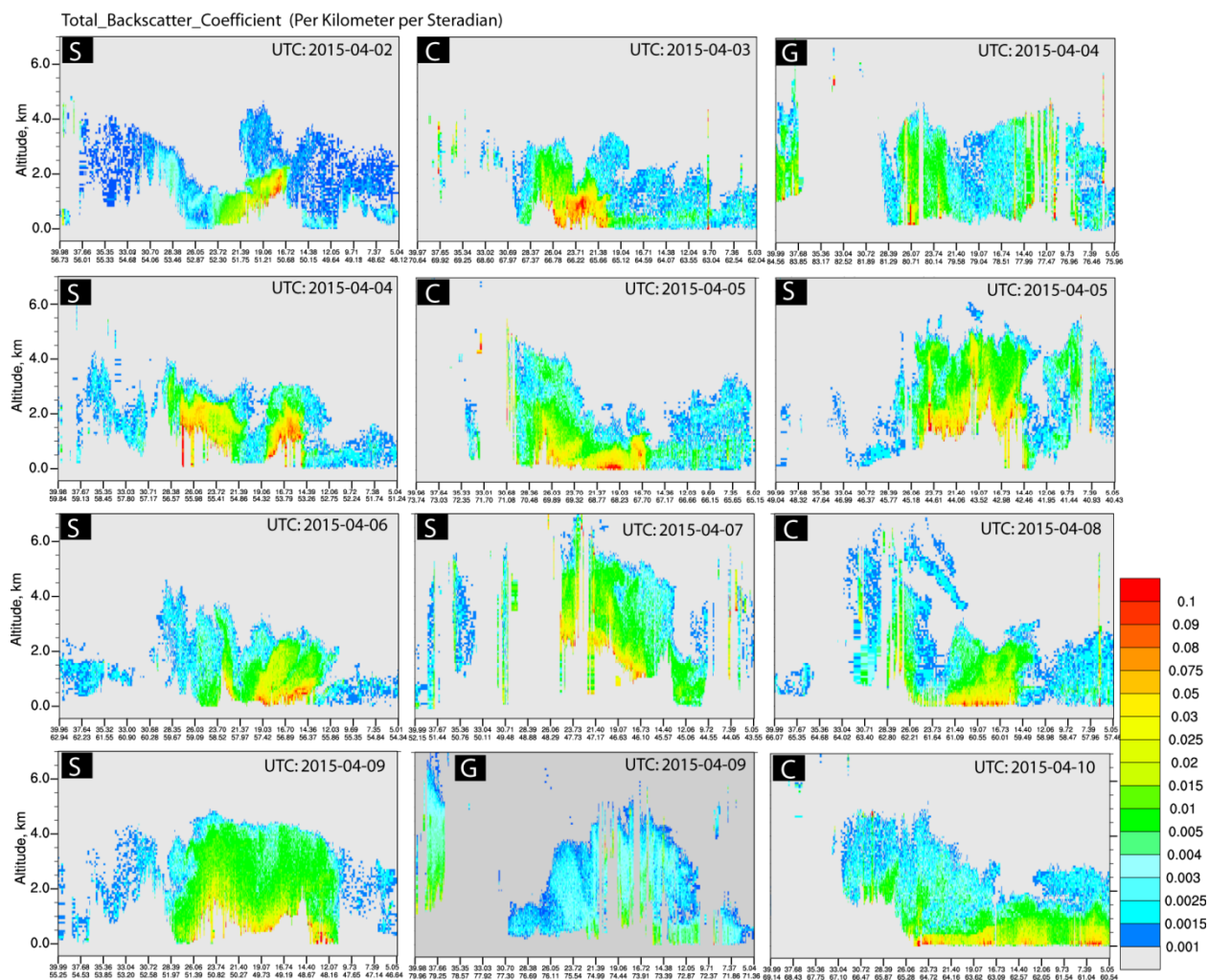


Fig. 1 Total backscatter coefficient at 532 nm from CALIPSO satellite during the dust storm period (from 02 – 10 April, 2015) over the study region, where S, C and G represents the profiles near the source, over ocean and near the Goa respectively.

ACKNOWLEDGEMENTS

We would like to thank Director, CSIR-National Institute of Oceanography for support and encouragement during this study. A. K thanks Department of Science and Technology, Govt. of India for providing financial support under the INSPIRE programme (INSPIRE Faculty scheme; IFA13-EAS-13).

REFERENCES

- Arimoto, R. (2001). Eolian dust and climate: relationships to sources, Tropospheric chemistry, transport and deposition. *Earth-Science Reviews* Vol.54, 29–42. Doi:10.1016/S0012-8252(01)00040-X.
- Dentener, et al., (1996). Role of mineral aerosol as reactive surface in the global troposphere. *Journal of Geophysical Research*, 101 (D17), 22689–22889.
- Jickells T. D., et al., (2005). Global Iron Connections between Desert Dust, Ocean Biogeochemistry, and Climate. *Science*, 308 (5718), 67-71. doi: 10.1126/science.1105959.

Tegen I., A, Lacis I, Fung, 1990. The Influence of mineral aerosols from disturbed soils on climate forcing, *Nature*, 380, 419-422. Ginoux, Paul, 2017: Atmospheric chemistry: Warming or cooling dust? *Nature Geoscience*, 10(4), DOI:10.1038/ngeo2923

Winker, D. M., W. H. Hunt, and M. J. McGill (2007), Initial performance assessment of CALIOP, *Geophys. Res. Lett.*, 34, L19803, doi:10.1029/2007GL030135.

Yu H., et al., (2010) Global view of aerosol vertical distributions from CALIPSO lidar Measurements and GOCART simulations: Regional and seasonal variations *Journal of Geophys. Res.*, VOL. 115, D00H30, doi:10.1029/2009JD013364.

Yu H., et al., (2015). Quantification of trans-Atlantic dust transport from seven-year (2007–2013) record of CALIPSO lidar measurements, *Remote Sensing of Environment* 159 (2015) 232–249.

CHARACTERISTICS AND DISTRIBUTION OF CARBONACEOUS SPECIES OVER BAY OF BENGAL DURING WINTER MONSOON OUTFLOW.

GOURAV NAYAK¹, ASHWINI KUMAR^{1*}, TUHIN K. MANDAL², SUDHIR K SHARMA²

¹Geological Oceanography Division, CSIR-National Institute of Oceanography, Dona Paula, Goa - 403004

²Department of Atmospheric Science and Metrology, CSIR-National Physical Laboratory, New Delhi- 110012

KEYWORDS: Carbonaceous Aerosols, Elemental and Organic Carbon, Secondary Organic Carbon, Bay of Bengal

INTRODUCTION:

Bay of Bengal (BoB) is surrounded on the three sides by a densely populated land mass with anthropogenic as well as natural sources of aerosols. During wintertime, north-easterly winds at the surface level bring polluted air masses from continental regions to the remote atmosphere of BoB. These pollutants can significantly impact the surface ocean biogeochemical processes. Carbonaceous species are one of the important constituent among these pollutants which are sensitive to incoming radiation as well as plays a vital role in controlling the atmospheric processes within marine boundary layer of Bay of Bengal. The impact of carbonaceous aerosol depend strongly on its physical and chemical properties, as well as on its residence time and distribution in the atmosphere, it is thus important to understand their properties as well as their abundance in the marine region. In this context, aerosol samples were collected during two cruises on board ORV Sindhu Sadhana (SSD-14 and SSD-19) at the beginning of Winter Monsoon (October, 2015) and at the end of Winter Monsoon (February, 2016) and concentration and distribution of carbonaceous aerosols were quantified over BoB.

METHODS:

Atmospheric aerosols were collected in BoB, during two cruises following the cruise track shown in Fig. 1. During SSD-14, relatively weak winds were observed (mainly due to transition in wind regime from south-west to north-east) compared to strong north-east winds during SSD-19 (February). The cruise track during October 2015 was mostly confined to coastal region covering a latitudinal stretch between 13° to 21° N. However, the February, 2016 cruise covered a larger area in open oceanic region of Bay of Bengal between 13°-21° N and 80°-90° E (**Error! Reference source not found.**).

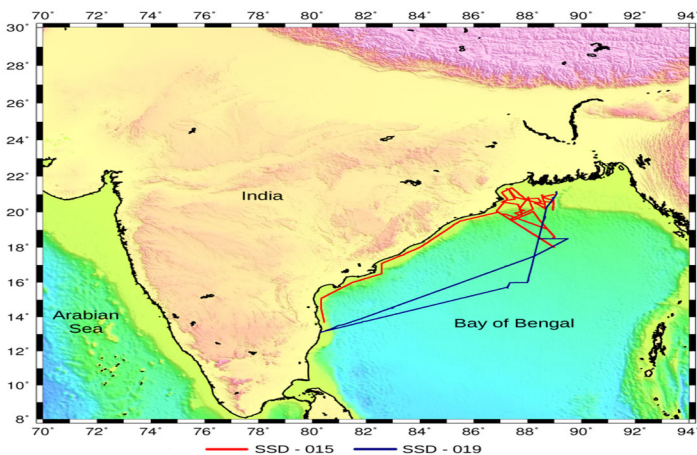


Figure 1 Cruise track of SSD-014 and SSD-019 during October 2015 and February 2016, respectively in Bay of Bengal.

A total of 22 aerosol samples (Bulk and PM10) were collected on board using high volume samplers (Envirotech, HVS-430) and PALLFLEX™ tissue quartz filters (20×25cm²; pre-combusted at 200°C). The samplers were installed on the top deck of the ship, ~25 m above the sea surface. Each sample was collected for time period ranging from 22-24 h at a flow rate of 1.1m³ min⁻¹. The samples were collected only when the ship was cruising at a speed of about 8-10 knots h⁻¹, ensuring that the winds were from the foreside of the ship and contamination from the ship's exhaust did not affect the sampling. 1 cm² cross-section was taken from the sample under a clean laminar flow for carbonaceous species analysis. Elemental carbon (EC) and organic carbon (OC) concentrations were measured on Thermal/Optical Carbon Analyzer using IMPROVE A Total Optical Reflection (TOR) technique (Chow et al., 2007). Along with samples, blanks were also analyzed, and the mass concentration of EC and OC were corrected for blanks. In addition, water-soluble organic carbon and ionic species were also measured in the aerosol samples (Kumar et al., 2016)

RESULTS AND DISCUSSION:

The data has been classified and analyzed depending on the dominant source contribution to the aerosol loadings. All 22 samples were treated as one dataset and divided into three classes, Coastal Air Parcel (CAP); Marine Air Parcel (MAP) and; Coastal and Marine Air Parcel (CAP+MAP) based on the origin of the air parcel and the time air parcel had spent while reaching the sampling point. Mass concentration of EC, OC and WSOC in the samples affected by MAP shows relatively lower variability compared to those affected by CAP and CAP+MAP. The maximum, minimum, and average (\pm std. dev.) concentration of EC, OC and WSOC is summarized in Table 1.

	CAP (n=7)				MAP (n=5)				CAP+MAP (n=10)			
	Min	Max	AM	SD	Min	Max	AM	SD	Min	Max	AM	SD
OC	1.26	6.25	3.18	1.89	0.82	4.24	2.58	1.33	0.46	4.75	2.60	1.64
EC	0.91	2.60	1.71	0.71	0.82	2.59	1.53	0.67	0.49	2.15	1.39	0.53
WSOC	0.67	3.97	1.83	1.31	0.39	1.60	1.01	0.47	0.16	3.00	1.47	1.05
nss-K⁺	0.28	1.60	0.78	0.54	0.42	1.27	0.87	0.30	0.29	1.33	0.81	0.39
OC/EC	1.20	2.41	1.76	0.45	1.00	2.19	1.63	0.42	0.95	2.76	1.70	0.64

Table 1: Minimum, maximum, average (\pm std dev) of carbonaceous species, OC/EC and nss-K⁺ in aerosol samples affected by CAP, MAP, CAP+MAP (in $\mu\text{g m}^{-3}$).

Organic carbon is the dominant fraction among carbonaceous species due to its abundant sources. Conspicuously, OC concentration is higher in CAP than in MAP and CAP+MAP. This is because during long-range transportation, a fraction of OC undergoes oxidation and thus primary OC concentration gets reduced over time. Since CAP measurements are somewhat closer to the source region, we would expect higher OC concentration in CAP samples. However, the average concentration of MAP and CAP+MAP didn't vary very much. Elemental carbon followed similar trend as that of OC. The average concentration of EC remained more or less same in all three domains. Relative concentrations of EC and OC are of immense importance for direct radiative forcing calculations in climate dynamics and are detailed by OC/EC ratios. The average value of OC/EC is about ~1.7 in all the three cases. Low OC/EC values are typically a characteristic of continental anthropogenic fossil-fuel emissions. The observed ratio is in contrast with previous studies over BoB, where very high ratios (more than 6.0) were reported during several campaign (Sudheer and Sarin, 2008; Srinivas and Sarin, 2014). Further, OC is extremely well correlated with EC for CAP, MAP, and CAP+MAP ($R^2=0.87, 0.83$ and 0.79 respectively), indicating the common source of emission. WSOC/OC also followed the similar trend as that of OC/EC and remained

about the same for all the regimes (about ~0.5). Significant correlations ($R^2=0.83$, 0.86 and 0.95 respectively) are observed between WSOC and OC irrespective of the origin of the air parcels. OC/EC ratio along with tracers like nss-K⁺ concentration and nss-K⁺/OC ratios has been used for source identification (Kumar et al., 2016). CAP and CAP+MAP samples show good correlation between OC and nss-K⁺ ($R^2=0.59$ and 0.74) while MAP samples show an insignificant correlation ($R^2=-0.02$). This is expected owing to the fact that nss-K⁺ is a proxy for biomass burning and MAP samples are devoid of these due to absence of biomass burning source in marine region. It is interesting to note here that OC/EC ratio does not support biomass burning contribution which is contradictory from nss-K⁺ versus OC correlation. This suggest more diagnostic ratios need to be analyzed to make a firm conclusion related to source of carbonaceous species We also analyzed secondary organic carbon (SOC) formation using EC-Tracer method and found that SOC has a good correlation with water soluble organic carbon (WSOC; $R^2 = 0.65$, 0.62 , 0.92 respectively for CAP, MAP and CAP+MAP) implying similar chemical nature of SOC and WSOC during the study period over BoB.

CONCLUSIONS:

The distribution of carbonaceous species were quantified during winter outflow over Bay of Bengal. A large variability is observed in the mass concentration of carbonaceous species which were affected by air-mass derived from continents (CAP and CAP+MAP) compared to those which are affected by marine air masses (MAP). The OC/EC values shows the dominance of fossil-fuel emission sources in this study which is in contrast with the values reported previously from this region which largely indicate dominance of Biomass burning emissions over Bay of Bengal. More diagnostic ratios or tracers need to be invoked to make firm conclusion related to source identification of carbonaceous species

ACKNOWLEDGEMENTS

We would like to thank Director, CSIR-National Institute of Oceanography for support and encouragement during this study. G.N. and A. K thanks Department of Science and Technology, Govt. of India for providing financial support under the INSPIRE programme (INSPIRE Fellowship and INSPIRE Faculty scheme; IFA13-EAS-13). We thank Captain and crew member of SSD-14 and 19 for the support during sample collection. The authors gratefully acknowledge the NOAA Air Resources Laboratory (ARL) for the provision of the HYSPLIT transport and dispersion model (<http://www.ready.noaa.gov>) used in this study.

REFERENCES:

- Chow, J. C., Watson, J. G., Chen, L.-W. A., Chang, M.-C. O., Robinson, N. F., Trimble, D. L., and Kohl, S. D. (2007). The IMPROVE_A temperature protocol for thermal/optical carbon analysis: Maintaining consistency with a long-term database, *J. Air Waste Manage. Assoc.*, **57**, 1014 – 1023.
- Kumar, Ashwini, Ram, K., Ojha, N. (2016) Variations in carbonaceous species at a high-altitude site in western India: Role of synoptic scale transport, *Atmospheric Environment* **125**, 371 – 382.
- Sudheer, A. K., Sarin, M. M., (2008), Carbonaceous aerosols in MABL of Bay of Bengal: Influence of continental outflow, *Atmospheric Environment* **42**, 4089 – 4100.
- Srinivas, B., Sarin, M. M., (2014) PM_{2.5}, EC and OC in atmospheric outflow from the Indo-Gangetic Plain: Temporal variability and aerosol organic carbon-to-organic mass conversion factor, *Science of the Total Environment* **487**, 196 – 205.

A PRELIMINARY STUDY ON OZONE PRECURSOR-NMVOCs AT AN URBAN SITE OF DELHI DURING MONSOON

M. KUMAR^{1,2}, T.K. MANDAL^{1,2}, and S.K. SHARMA^{1,2}

¹Environmental Sciences and Biomedical Metrology Division, CSIR-National Physical Laboratory, New Delhi-110012, India

²Academy of Scientific & Innovative Research (AcSIR), CSIR- National Physical Laboratory Campus, New Delhi-110012, India

KEYWORDS: BTEX, VOCs, Ozone, Monsoon

INTRODUCTION

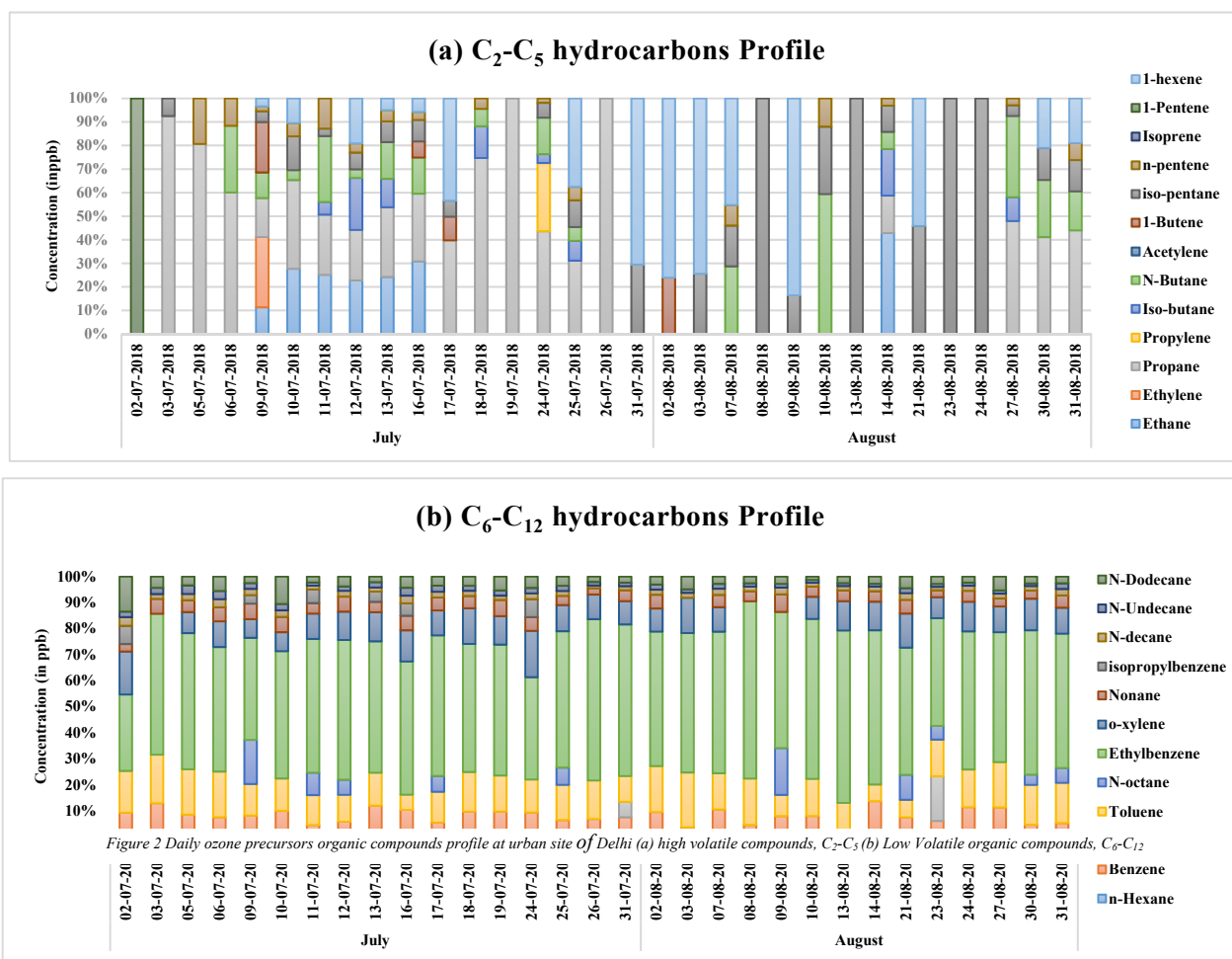
Tropospheric ozone (O₃) being a secondary air pollutant comes under the list of criteria pollutant whose monitoring and reduction in ambient air has been made mandatory through clean air act (CAA) in 1970. Further amendments in CAA extended the measurements of air pollutant in ambient air to include volatile organic compounds (VOCs) which contribute in the formation of ground level O₃. VOCs are any carbon containing compounds which is present in vapour phase in the ambient air at normal atmospheric conditions. Increased rate of fossil fuel consumption, rapid industrialisation and higher vehicular growth in urban areas have led to the emission of several hazardous air pollutants in ambient air which also include VOCs. Apart from tropospheric O₃ formation these compounds are also responsible for the formation of secondary organic aerosol (SOA) which accounts for nearly 50-60 % in fine particulate composition and also affect human health. Some studies have correlated volatile organics like BTEX (benzene, toluene, ethylbenzene and xylene) to be the carcinogenic in nature (Dutta *et al.* 2009; Zhang *et al.* 2012). Owing to this important role in atmospheric chemistry US-Environmental Protection Agency (US-EPA) gave the list of 55 ozone-precursor target species with each compounds varying in their volatilities and ozone forming potential. In the present study we have determined 25 such organic compounds (having C₂-C₁₂ carbon) in the ambient air of Delhi at an urban site during monsoon months in 2018. Monsoon season is considered as the cleanest season having low concentration of almost every air pollutant because of its cleansing action. Hence, information about individual species in ambient air will give us an understanding of their reactivity in this season and influence of anthropogenic sources in ambient level.

METHODS

Air samples were collected at CSIR-National Physical Laboratory (CSIR-NPL) (28°38' N, 77°10' E; 218 m mean sea level), New Delhi during July-August 2018 using 1-L cleaned and passivated canister through active sampling. Three samples per day were collected during morning (0900-1200), afternoon (1200-1500) and evening (1500-1800) period. Air samples before analysis on GC were first passed through inline-particulate filter (0.2 µm Make: Swagelok) and Nafion[®] dryer for removal of any sort of particles and moisture respectively. All the samples were analyzed immediately after sampling using GC-FID (Make: Perkin Elmer, Model- Clarus 580) equipped with alumina PLOT column (for highly volatile compounds; 50 m x 0.32 mm) and 100 % dimethyl siloxane column (for less volatile compounds; 50 m x 0.22 x 1 µm) in attachment with thermal desorption unit (Make: Perkin Elmer, Model- TurboMatrix 300). Each sample is first transferred to TurboMatrix TD peltier-cooled trap (at -30 °C) for retaining all the analytes which eliminates the use of liquid cryogen. Afterwards, trap is rapidly heated upto 325 °C and the desorbed vapors are then fed into the GC columns through transfer line where GC oven is programmed as follows: 46 °C for 15 min, then 5 °C/min to 170 °C, then 15 °C/min to 200 °C and hold for 6 min. Analytes concentration is detected through dual flame ionization detector at 250 °C. The instrument was calibrated using NIST traceable standard calibration gas mixture of 25 compounds having ±10 % analytical accuracy. Data handling is performed using TotalChrom and TurboMatrix control software.

RESULTS AND DISCUSSIONS

Total NMVOCs concentration during monsoon months varied from 42.79 – 256.48 ppbv with average of 108.11 ± 52.93 ppbv. Figure 1 shows the profile of C₂-C₅ (a) and C₆-C₁₂ (b) hydrocarbons at NPL during monsoon months. The no. of low volatile compounds detected were higher as comparison to high volatile compounds. The concentration varied from 4.21 – 52.92 ppbv for C₂-C₅ hydrocarbon and 1.13 – 30.09 ppbv for C₆-C₁₂ hydrocarbons, respectively. Aromatic compounds like BTEX accounts for the major portion in TVOCs, in this study it holds nearly ~ 50 % share in total VOCs and can be considered as an indicator of



road traffic emissions (Hoque *et al.*, 2008). Lee *et al.* 2002 has also showed the contribution of BTEX in TNVOC to be about 50-70%. A good correlation among BTEX species suggest contribution of vehicular emission in the ambient air of Delhi (Table 1). Averaged concentration of Ethylbenzene (30.09 ± 13.24 ppb) was the highest among BTEX followed by toluene (7.67 ± 3.31 ppb), benzene (4.52 ± 1.82 ppb) and o-xylene (6.35 ± 2.50 ppb). In urban areas, ratios of T/B less than 2.0 is an indication of the influence from mobile source emission (Elbir *et al.*, 2007) and in this study, the T/B ratio was found to be 1.69. Among the lower carbon compounds propane, iso-butane, n-butane and iso-pentane were the majorly detected hydrocarbons which indicates emission from unburned gasoline, evaporative gasoline, (Arsene *et al.*, 2009). Less volatile compounds (C₉ or more) like decane, undecane and dodecane are emitted from the liquids having higher viscosity like diesel or aviation fuel.

	Benzene	Toluene	Ethylbenzene	o-xylene
Benzene	1			
Toluene	0.50	1		
Ethylbenzene	0.53	0.79	1	
o-xylene	0.59	0.61	0.68	1

Table 2 BTEX inter-species correlation

CONCLUSION

The concentration of O₃ precursors hydrocarbons (C₂-C₁₂) were determined at an urban site in Delhi, India during monsoon season. It was observed that at present site higher carbon compounds were detected more in number than lower carbon compounds. The presence of high volatile compounds in the ambient air like n-butane, propane, ethane, iso-pentane, iso-butane could be explained through the vicinity of the sampling site to fuel station selling petrol and diesel. Ethane is mostly found in compressed natural gas (CNG) which explains its presence in current site because the site is nearby to the gas filling station. The significant amount of BTEX found at the site could be explained by its nearness to moving road side traffic (less than 100 m). Due to the effectiveness of O₃ formation and health risks associated with various VOCs species is dissimilar, it becomes important to study and investigate concentration of individual VOC species at different microenvironment settings.

ACKNOWLEDGMENT

Authors are thankful to Director, CSIR-National Physical Laboratory and Head, Environmental Sciences and Biomedical Metrology Division, CSIR-NPL, New Delhi for their constant encouragement and valuable support. Authors thankfully acknowledge the ISRO-GBP, Bangalore for financial support under the AT-CTM program (GAP-114732). One-of the authors, - M. Kumar is thankful to the University Grant Commission (UGC) for providing the fellowship and also acknowledge the Academy of Scientific and Innovative Research (AcSIR) for facilitating him as Ph.D. student.

REFERENCES

- Dutta, C., Som, D., Chatterjee, A., Mukherjee, A. K., Jana, T. K., & Sen, S. (2009). Mixing ratios of carbonyls and BTEX in ambient air of Kolkata, India and their associated health risk. *Environmental Monitoring and Assessment*, 148(1-4), 97-107.
- Zhang, Y., Mu, Y., Liu, J., & Mellouki, A. (2012). Levels, sources and health risks of carbonyls and BTEX in the ambient air of Beijing, China. *Journal of Environmental Sciences*, 24, 124-130.
- Lee, S. C., Chiu, M. Y., Ho, K. F., Zou, S. C., & Wang, X. (2002). Volatile organic compounds (VOCs) in urban atmosphere of Hong Kong. *Chemosphere*, 48(3), 375-382.
- Hoque, R. R., Khillare, P. S., Agarwal, T., Shridhar, V., & Balachandran, S. (2008). Spatial and temporal variation of BTEX in the urban atmosphere of Delhi, India. *Science of the total environment*, 392(1), 30-40.
- Arsene, C., Bougatioti, A., & Mihalopoulos, N. (2009). Sources and variability of non-methane hydrocarbons in the Eastern Mediterranean. *Global NEST Journal*, 11(3), 333-340.

Elbir, T., Cetin, B., Cetin, E., Bayram, A., & Odabasi, M. (2007). Characterization of volatile organic compounds (VOCs) and their sources in the air of Izmir, Turkey. *Environmental monitoring and assessment*, 133(1-3), 149-160.

EFFECT OF ATMOSPHERIC AEROSOLS ON SURFACE UV RADIATION
**SACHCHIDANAND SINGH^{*A,B}, SANDHYA JOSE^{A,B}, AMIT KUMAR MISHRA^C, NEELESH K
LODHI^D**

^aEnvironmental Sciences and Biomedical Metrology Division, CSIR-National Physical Laboratory, New Delhi-110012, India.

^bAcademy of Scientific and Innovative Research (AcSIR), CSIR-National Physical Laboratory Campus, New Delhi-110012, India

^cSchool of Environmental Sciences, Jawaharlal Nehru University, New Delhi 110067, India

^dCentre for Environment Science and Climate Resilient Agriculture (CESCRA), ICAR–Indian Agricultural Research Institute, New Delhi 110012, India

(*Correspondence at ssingh@nplindia.org)

KEYWORDS: Atmospheric aerosols, UVB and UVA flux, Vitamin D

INTRODUCTION

Particulate air pollutants or atmospheric aerosol is not only a potential health hazard but it is also known to affect the Earth's radiation budget and hydrological cycle. It reduces the solar radiation reaching the Earth's surface leading to global cooling. Although, the reduction in solar flux due to aerosols is more pronounced in the shortwave (Visible and Near Infra Red) region of the solar spectrum, its impact in UVB and UVA flux can also be quite significant. The continuous increase in atmospheric particulate pollutants due to biomass burning, industrialization and urban development coupled with deforestation and dust storms in Indian and other Asian regions is likely to have an adverse effect on the amount of UV radiation being available at the Earth surface, particularly in the high polluted regions. Although, the amount of UV radiation at the surface is affected by several factors such as solar zenith angle, ozone column, atmospheric aerosols, amount of clouds and surface albedo (Foster, 1995), it is possible to delineate the effect of other parameters to see the effect of aerosols on the surface UV radiation.

In the present study we are trying to see the association between the long term trend in aerosol optical depth (AOD) and reduction in the surface UVA and UVB radiation during different season at Delhi. The study becomes important particularly in the light of the recent report by ASSOCHAM (The Associated Chambers of Commerce & Industry of India) Healthcare Committee which says that about 88% of Delhi's population suffers from Vitamin D deficiency (<http:// ASSOCHAM.org/newsdetail.php?id=6793>). It is to be noted that UVB is the major source of Vitamin D in humans (Holick and Chen, 2008).

DATA & METHODOLOGY

We have used the satellite-based Clouds and Earth's Radiant Energy System (CERES) data products to retrieve the daily mean global all-sky UVA (315-400 nm) and UVB (280-315 nm) flux at the surface centered at Delhi (28.50⁰N, 77.50⁰ E) with a 1°x1° spatial scales during October 2012 to September 2015. These data were compared with the observations of UVA and UVB done at the CSIR-National Physical Laboratory (NPL) using Kipp & Zonen Radiometer models UVS-A-T and UVS-B-T, respectively. Once the confidence in CERES derived UVA and UVB flux was established, we used the long term CERES data for further study to see the impact of aerosols on these flux. CERES data product is also used for aerosol optical depth (AOD), cloud optical depth (COD), ozone (O₃) etc.

As the UV radiation is affected by solar geometry, clouds and ozone apart from the aerosol, it is difficult to get rid of other effects completely, particularly through observations. In order to do so 17 years (March 2000 to Feb 2016) of daily data from satellite measurements have been used to derive AOD vs UV correlation under different solar zenith angle, clouds and ozone concentration. To reduce the solar geometry effect on UV the analyses was done for each month separately. Further, the analysis was done using data slicing by cloud optical depth (COD) and columnar ozone concentration to get the AOD vs UV correlation.

The data slicing is done for four percentile regimes (<25%, 25-50%, 50-75%, >75%) of COD and ozone to reduce cloud and ozone effect on UV radiation, separately. More details about the methodology can be seen in Singh et al (2018).

RESULTS & CONCLUSIONS

The CERES derived UVA and UVB measurements showed very good agreement with the measurements done at NPL during October 2012 to September 2015. The two data (CERES retrieved and the observed) showed a very good correlations that were significant at 99% confidence levels (CL, $p < 0.0001$). The Pearson's correlation coefficient (r) for UVA and UVB radiation between the two were ~ 0.92 and ~ 0.93 , respectively. The mean bias errors for UVA and UVB with respect to NPL-measured UV fluxes are about -1% and 9% , respectively. In general a negative correlation between UV fluxes and AOD was observed over Delhi during all seasons. The trend analysis of UVA and UVB surface fluxes over Delhi was done using 17 years (March 2000 – Feb 2016) of monthly CERES-derived observations. It showed that UVA and UVB are decreasing at the rate of $\sim 0.07 \text{ Wm}^{-2} \text{ yr}^{-1}$ and $0.003 \text{ Wm}^{-2} \text{ yr}^{-1}$ respectively with 0.005 yr^{-1} AOD increase over Delhi, which are statistically significant at 90% confidence level ($p < 0.1$) as revealed by Mann-Kendall (M-K) test.

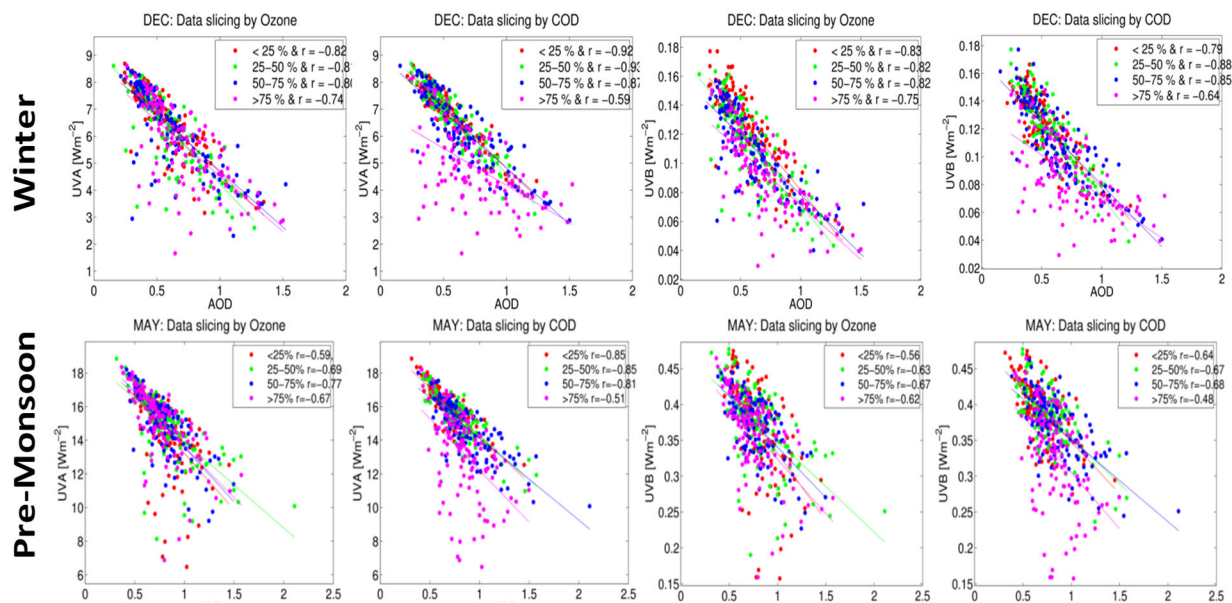


Fig. 1 Association between particulate air pollutants [used aerosol optical depth (AOD) as proxy] and surface UVA/UVB radiation during winter and Pre-monsoon (each month are taken as representative for that particular season). The legends show different slicing criterion for ozone and COD data with Pearson's correlation coefficients (r).

The UVA and UVB flux vs AOD (at 550nm) correlation was studied for the daily CERES data obtained during 2000-2016 using data slicing by cloud optical depth (COD) and columnar ozone concentration for all the four seasons (a) winter, (b) summer, (c) monsoon, and (d) post-monsoon and is shown in figure 1 and 2. Figure 1 shows this correlation during winter and Pre-monsoon for the representative months of december for winter and May for the pre monsoon. The different slicing criterion for ozone and COD data with Pearson's correlation coefficients (r) is shown in the legend. Similarly, figure 2 shows the correlation studies during monsoon and post monsoon season with representative months July and October respectively. The data slicing is done for four percentile regimes (<25%, 25-50%, 50-75%, >75%) of COD and ozone to reduce cloud and ozone effect on UV radiation, separately.

The Figs. 1 and 2 show a decrease in UVA and UVB flux with increase in AOD. The negative correlations exist in all four ozone regimes and COD regime with highest negative correlation coefficients (r) for COD slicing category (<25%) as compared to ozone slicing category. This indicates that clouds affect UV radiation more as compared to ozone in respective months. The significant decrease in r values in highest

COD regimes (>75%) as compared to lowest COD regimes (<25%) again show the importance of cloud optical depth in assessing AOD vs UV relation. We found almost similar r values in all four ozone regimes. It shows about 4-5 Wm^{-2} decrease in UVA radiation per unit increase in AOD in almost all seasons for all different slicing techniques. The decrease in UVB is about 0.09 – 0.14 Wm^{-2} per unit AOD. However, the differences in slopes in different seasons may be attributed to the seasonality in aerosol properties (size, shape and chemistry).

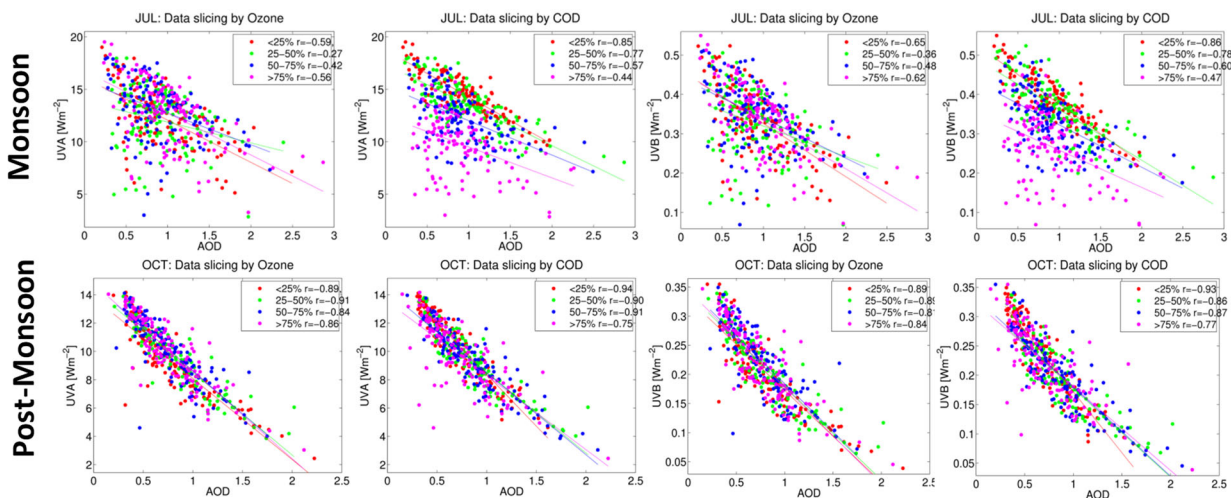


Fig. 2 Association between particulate air pollutants [used aerosol optical depth (AOD) as proxy] and surface UVA/UVB radiation during monsoon and post-monsoon (each month are taken as representative for that particular season). The legends show different slicing criterion for ozone and COD data with Pearson's correlation coefficients (r).

ACKNOWLEDGEMENT

One of the authors (SJ) would like to acknowledge the Department of Science and Technology, Government of India for providing financial support as a DST INSPIRE Fellow (IF160279). NKL gratefully thanks to acknowledge financial support from SERB (Science and Engineering Research Board) for National Post-Doctoral Fellowship. A part of this research was funded by Indian Council of Medical Research (ICMR) under Global environment Change & Health.

REFERENCES:

- Holick, M.F. and Chen, T.C., 2008. Vitamin D deficiency: a worldwide problem with health consequences–. *The American journal of clinical nutrition*, 87(4), pp.1080S-1086S.
- Forster, P. M. de F., 1995. Modeling ultraviolet radiation at the Earth's surface. Part I: The sensitivity of ultraviolet irradiances to atmospheric changes, *J. Appl. Meteorol.*, 34, 2412 – 2425.
- Singh, S., Lodhi, N.K., Mishra, A.K., Jose, S., Kumar, S.N. and Kotnala, R.K., 2018. Assessment of satellite-retrieved surface UVA and UVB radiation by comparison with ground-measurements and trends over Mega-city Delhi. *Atmospheric Environment*, 188, 60-70.

COMPARATIVE STUDY OF AEROSOL PARTICLE SIZE DISTRIBUTION AND NEW PARTICLE FORMATION EVENTS DURING SUMMER AND WINTER SEASONS AT DELHI

SANDHYA JOSE^{A,B}, HUMAIRA GHAYAS^{A,B}, AMIT KUMAR MISHRA^C, SACHCHIDANAND SINGH^{A,B}

^a Environmental and Biomedical Metrology Division, CSIR-National Physical Laboratory, New Delhi-110012, India.

^b Academy of Scientific and Innovative Research, CSIR-National Physical Laboratory Campus, New Delhi-110012, India.

^c School of Environmental Sciences, Jawaharlal Nehru University, New Delhi-110067, India.

(*Correspondence at sandhya.kalluvilayil@gmail.com)

KEYWORDS: Aerosol, Aerosol Particle Size Distribution, New Particle Formation, Winter, Summer

INTRODUCTION

Aerosol are known to affect the climate system directly by interacting with radiation and indirectly by acting as cloud condensation nuclei (CCN) (Twomey et al, 1977). Aerosol size distribution is one of the main factors determining the effect of aerosol on the atmosphere. Up to a size of 10 microns, aerosol size distribution could adversely affect both, the health and climate. Due to its distinctive geography, climate, industry and transport Delhi shows a high concentration of pollutants nearly throughout the year. The pronounced seasonal variations in atmospheric/weather conditions over Delhi, also affects the aerosol properties including the size distribution (Bisht et al., 2015). Hence it is important to specifically characterize the aerosol size distribution over the region during different season. In this paper we try to analyze the characteristic difference of the aerosol size distribution over Delhi for the two major season, winter and summer. Along with it we also try to analyse the New Particle Formation (NPF) events. NPF events are basically gas to particle conversion occurring in the atmosphere leading to secondary aerosol formation. These NPF events can act as potential source for the CCN and impact the cloud dynamics and thereby alter the climate system.

DATA AND METHODOLOGY

Aerosol Particle Size Distribution (APSD) has been measured using the GRIMM-Wide Range Aerosol Spectrometer (WRAS) mounted at the rooftop of CSIR- National Physical Laboratory, Delhi (28.64° N, 77.17° E) one of the most polluted megacities of the world. WRAS gives the aerosol particle size distribution over 70 channels from 5nm to 32µm at a span of 5 minutes' interval. The GRIMM-WRAS system is integrated with Scanning Mobility Particle counter (SMPS) containing Condensation Particle Counter (CPC) along with Optical Particle Counter (OPC). The detailed description of the instrument is described elsewhere (Grimm and Eatough, 2009). The meteorological parameters like temperature, relative humidity, wind speed and wind direction are also given by the instrument. There is an overlapping region from 250nm to 350nm due to the integration of SMPC and OPC, here we take the average number concentration for the analysis.

The continuous measurement was done from 1st December 2011 to 24th December 2011 for winter and 1st April 2012 to 30th April 2012 for summer. Any discrepancy in the data has been noted and eliminated. The particle size distribution has been categorized into 3 modes, Nucleation mode (5 nm-30 nm), Aitken Mode (30 nm-100 nm) and Accumulation Mode (100 nm- 1000 nm). NPF events are identified by the criteria defined by Kulmala et al (2008). One-month aerosol size particle size distribution has been analysed for both the seasons and the results have been studied and reported below.

RESULTS AND DISCUSSIONS

Summer and winter season Aerosol Particle Size Distribution (APSD) have been studied. A total of 48 days data have been analysed for the work. Temporal variation of APSD is shown in the figure 1 for both the seasons along with the data gaps. The total number concentration decreased significantly as the season changed from winter to summer. Winter reported an average total number concentration of about $17.5 \times 10^3 \text{ cm}^{-3}$ while summer reported $9.36 \times 10^3 \text{ cm}^{-3}$ aerosol particle concentration. A shift in the mode of the particles could also be seen during the transition period of both the season. Most of the winter particles were comprised of Aitken and Accumulation mode particles whereas summer particles were comprised of fine and Aitken mode particles. The mode wise particle number concentration analysis is shown in figure 2. Aitken mode dominated in both the seasons, however the concentration differed considerably. The mode wise diurnal variation of mean aerosol particle concentration has also been studied. Bimodal pattern has been observed for both seasons with peak values during the morning and evening hours. This high particle concentration during the morning and evening hours is associated with the high rush of traffic during these hours. Among the two peaks, evening peak has been seen more prominent owing to the boundary layer dynamics connected to the daily meteorology

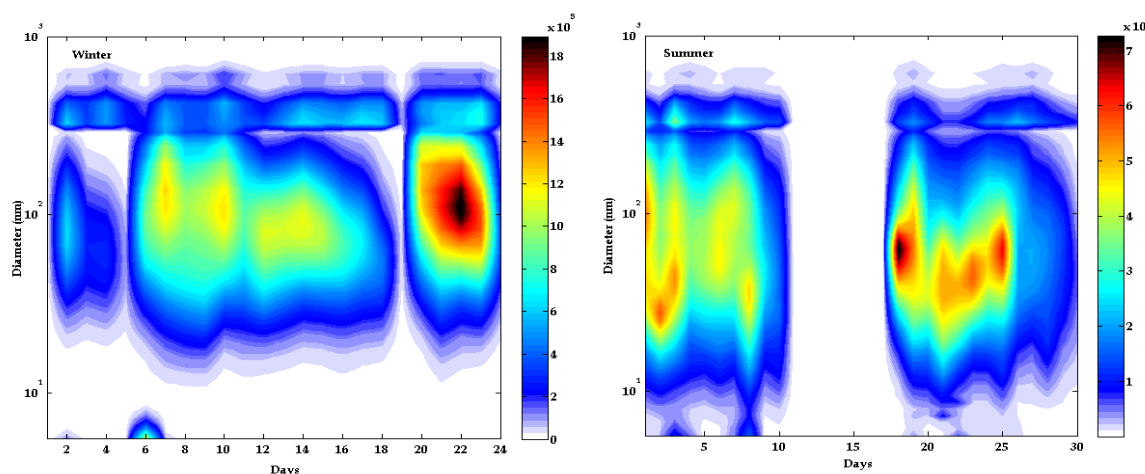


Fig 1 Contour plots of Average aerosol particle size distribution during winter and summer seasons

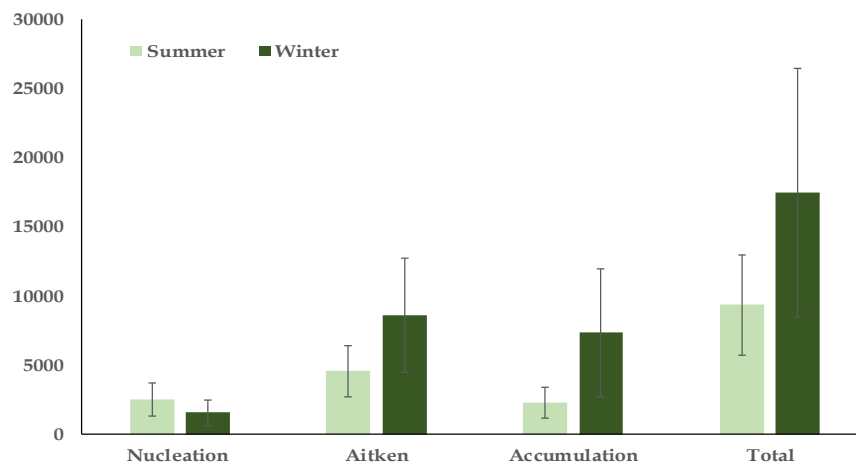


Fig 2: Mode wise aerosol particle concentration for winter and summer seasons.

New Particle Formation (NPF) events have also been observed during the observation period. A typical NPF event is shown in the figure 3. The burst of nucleation mode particle around the midday could be

clearly seen in the representative figure for summer although for winter NPF events, this burst of particle could be seen in late evening time. The mode diameter plunges to nucleation range during the initial stages of the NPF event. Significant changes in the NPF event characteristics were also observed in both the seasons. Summer events were daytime events whereas winter events were nocturnal events. Despite the high pollution scenarios during winter period, reported NPF events are less during this period of the year, whereas more events are reported during summer.

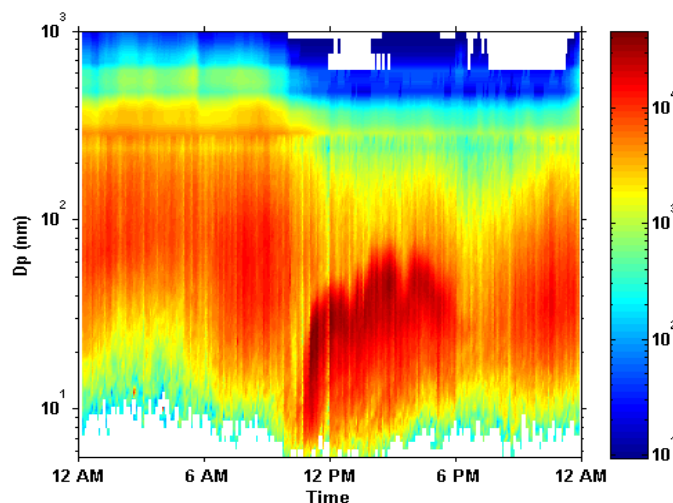


Fig 3 Contour plot showing the summer NPF event (20/04/2012)

CONCLUSIONS

A comparative study of aerosol size distribution for summer and winter season has been done for Delhi. 48 days data has been analysed and following conclusions have been reasoned.

- Aerosol particle number concentration is more during winter than summer owing to the high pollution episodes owing to the meteorological conditions observed during this time of the year.
- Winter reported a mean total number concentration of $17.5 \times 10^3 \text{ cm}^{-3}$ while summer reported $9.36 \times 10^3 \text{ cm}^{-3}$ aerosol particle concentration.
- Aitken mode particle dominated for both the seasons.
- Diurnal variation of number concentration showed bimodal pattern with peak values during morning and evening traffic hours
- NPF events are observed during both the seasons.
- Nocturnal NPF events are reported during winter.

ACKNOWLEDGMENTS

One of the authors (SJ) would like to acknowledge the Department of Science and Technology, Government of India for providing financial support as a DST INSPIRE Fellow (IF160279). A part of this work was sponsored by ISRO-GBP (Indian Space Research Organisation – Geosphere Biosphere Programme) under ARFI (Aerosol Radiative Forcing over India) project.

REFERENCES

Twomey, S., 1977. The influence of pollution on the shortwave albedo of clouds. *Journal of the atmospheric sciences*, 34(7), pp.1149-1152.

Bisht, D.S., et al., (2015). Carbonaceous aerosols and pollutants over Delhi urban environment: Temporal evolution, source apportionment and radiative forcing. *Science of the Total Environment*, 521, 431-445.

Grimm, H. and Eatough, D.J., 2009. Aerosol measurement: the use of optical light scattering for the determination of particulate size distribution, and particulate mass, including the semi-volatile fraction. *Journal of the Air & Waste Management Association*, 59, 101-107.

Kulmala, M., Laakso, L., Lehtinen, K.E.J., Riipinen, I., Maso, M.D., Anttila, T., Kerminen, V.M., Horrak, U., Vana, M. and Tammet, H., 2004. Initial steps of aerosol growth. *Atmospheric Chemistry and Physics*, 4, 2553-2560.

EMISSION OF PM_{2.5} DURING TRADITIONAL COOKING PROCESS - A CASE STUDY

R. MASIWAL^{1,2}, R. SAWLANI^{1,2}, R. SINGH¹, D.K. SHUKLA¹, C. SHARMA^{1,2},

¹ Environmental Sciences & Biomedical Metrology Division, CSIR - National Physical Laboratory, Dr. K. S. Krishnan Road, New Delhi -110012, India.

² Academy of Scientific and Innovative Research (AcSIR), CSIR - National Physical Laboratory Campus, New Delhi - 110012, India.

KEYWORDS: Indoor air pollution, Kitchen emission, Biomass burning, PM_{2.5}

INTRODUCTION

Biomass burning has an impact over local, regional and global air quality. Nearly 3 billion people around the globe use solid fuel to cook their food and warm their houses (WHO, 2014). Nearly 0.2 billion people use bio-fuel to cook and warm their houses in India. As per India's census report, out of the total populations, 49% depends upon firewood, 28.6% on Liquid Petroleum Gas (LPG), 9% on crop residue, 8.9% on dung cake, 2.9% on kerosene, 1.5% on coal, 0.1% on electricity, 0.4% on biogas while 0.5% use other mean (Census, 2011). As per WHO report, fuel choice is depended upon many factors such as income of a household, education, energy market structure, socio-cultural choices and geographical location (WHO, 2014). The indoor air pollutants level of a household depend upon the several factors such as fuel type, stove design, household design, family size, fuel quantity, location of cooking, time duration of the day and ventilation (WHO,2014 & Barnes et al., 2005). The type of fuel consumed by the people of an area is majorly influenced by the local energy market and the economy. The indoor air pollutants' concentration can vary from 10 to 100 times in those households which have poor ventilation conditions.

The use of biomass fuel (wood, cow dung and crop residue) to cook the food is very common in the rural India. When, the biomass fuel is burned using a traditional stove, the indoor air pollutant level enhances many folds. The traditional chullahs have very poor design as these can utilize only about 5-10% of generated energy. The uncontrolled air supply is the one of the most important factor that reduces the efficiency of the chullahs and enhances the level of emitted pollutants. Nearly 4.3 million deaths have been attributed to indoor burning of bio fuel during 2012 (WHO, 2014).

METHODOLOGY

An 8 days campaign in May, 2018 was conducted in a small village of Uttarakhand known as Masi, to measure the concentrations of emitted PM_{2.5} in the rural household kitchens during cooking process. The PM_{2.5} samples were collected over the pre-weighted quartz 47mm filter paper using the microwol100 low flow air sampler (M/s Ecotech). The indoor air was drawn using the sampler with a fix flow rate of 3 litre/min for 8 hours. The concentrations of PM_{2.5} were calculated using gravimetric method. The inlet was placed 1m above the surface level of the kitchen.

RESULTS & DISCUSSIONS

The burning of wood as a fuel emitted particulate matter and numerous other gases. In this study the particulate matter (PM_{2.5}) released during the indoor cooking process were collected on a filter paper and used for analysis. A household having separate kitchen with one window for ventilation was chosen as the monitoring site (Fig.1). The kitchen of the house has one attached storage room with a window. The kitchen has low lying ceilings resulting in accumulation of dense smoke. The PM_{2.5} low flow air sampler was fixed in a place just adjacent to the cook stove



Figure 1. The picture shows the use of biomass as cooking fuel and the exposure of the person

The PM_{2.5} samplings were carried out continuously for 8 days. The sampling period covered all the three time cooking process during a day. During the cooking process the visibility inside the kitchen get reduced, the person who was cooking and who were assisting reported irritation in their eyes. The time period of cooking process were varied from 30 to 45 minutes, and the variations were dependent upon the factors like number of individual for whom food was cooked, time period of the day and, food items which were cooked.

During the 8 days campaign the variations in the concentrations of PM_{2.5} were observed. The highest concentration was recorded during the day-2 followed by day-8 and day-1. The averaged concentration of PM_{2.5} is recorded as 3.2±1.1 mg/m³. No trend was observed in the change of PM_{2.5} concentration. Fig.2 shows the daily variation the concentration of PM_{2.5}.

The household is located inside the forest on a hilly terrain so, mostly wood was used for cooking because of its easy availability. Sometime crop residues were also used to ignite the fire but the major fuel used was the dried branches of trees. The selection of wood was not specific, the household members collected the wood from the region which is dominated by 4 to 5 varieties of trees. The wood is stored in the open before use.

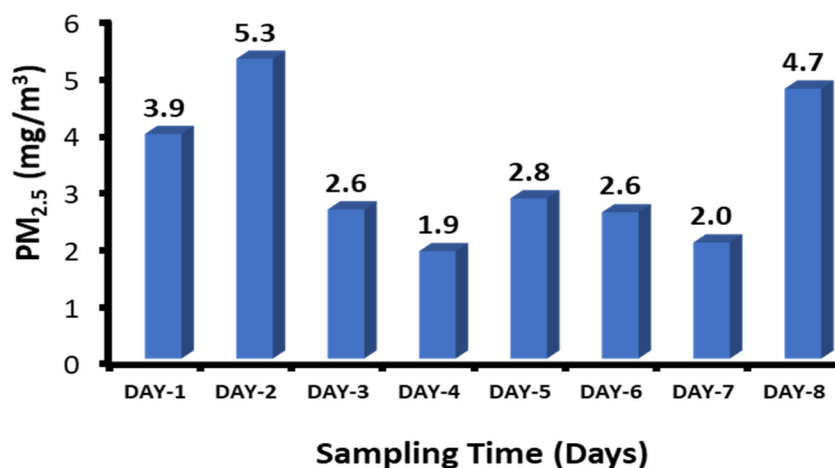


Figure 2. The graph illustrate the level of PM_{2.5} concentration inside the Kitchen

CONCLUSIONS

The study revealed the high concentrations of PM_{2.5} in the rural kitchen using the wood and crop residue for cooking in traditional chullahas in an Uttarakhand village. The consumption of bio fuel high in this area. As the villagers used hot water for their household work and bathing purposes besides cooking. Replacing the use of fuel wood species having high emissions of CO, NO_x and suspended particulate matter with the fuel wood of species having low emissions could be a way to reduce indoor pollution. The use of improved chullahs having chimney will reduce the indoor air pollution and will reduce the harmful health impacts. Adequate ventilation is required in the Kitchen. In newly constructing houses, the major focus should be given to proper ventilation. In the long term villagers will be able to access the clean fuel as the financial barrier will get reduce with time.

ACKNOWLEDGEMENTS

Authors thankfully acknowledge the Director, CSIR-National Physical Laboratory, New Delhi and Head, Environmental Sciences & Biomedical Metrology Division, CSIR-NPL, New Delhi, India for their constant encouragement and support. Renu Masiwal is thankful to UGC for providing her the Junior Research Fellowship.

REFERENCES

Barnes, B., Mathee, A., & Moilola, K. (2005). Assessing child time-activity patterns in relation to indoor cooking fires in developing countries: a methodological comparison. *International journal of hygiene and environmental health*, 208(3), 219-225.

Census, 2011. <http://www.census2011.co.in/data/village/51863-masi-uttarakhand.html>.

WHO, Household Fuel Combustion, 2014. www.who.int/about/licensing/copyright_form/en/index.html.

VARIATION OF AEROSOL OPTICAL PROPERTIES OVER DELHI: A STUDY ON 2016 and 2017 DIWALI EPISODE

SHISHIR KUMAR SINGH, JASWANT, RADHAKRISHNAN S.R., DEVESH KUMAR SHUKLA, and C. SHARMA

CSIR-National Physical Laboratory, Dr. K.S. Krishnan Marg, New Delhi-110012

KEYWORDS: Aerosols, Aerosols Optical Properties, Aerosol Optical Depth, Sun photometer, MODIS

INTRODUCTION

Aerosols play a crucial role in the Earth's radiation budget through direct, indirect and semi direct effects. Distribution of aerosols is an important factor that affects the weather and climate of the Earth-atmosphere system in many ways (Vaghmaria et al. 2018). The megacity Delhi situated in the western part of the Indo-Gangetic Plane (IGP) region is a hotspot of aerosols. Due to the rapid industrialization and population growth, degrading air quality is observed throughout the year and it becomes even worse during Diwali time due to the occurrence of SMOG and Haze (Sati et al. 2014). Diwali, the festival of lights, is celebrated by lightening oil lamps along with the burning of fireworks in the north Indian region. Due to these activities, a lot of pollutants are released in the air which impacts human health, air visibility and environment (Mukherjee et al. 2018). This work reports the study of the aerosol optical properties such as Aerosol Optical depth (AOD), Angstrom Exponent and Turbidity Coefficient during the Diwali episodes of 2016 and 2017.

DATA AND METHODS

The measurements were carried out in the campus of the National Physical Laboratory, New Delhi (28.25° N, 77.55° E and ~230 m above mean sea level). The measurements were taken using hand held and portable multiband Sunphotometer MICROTUPS-II which is developed by Solar Light Company. It measures solar intensity at five different wavelengths (380, 500, 870, 936 and 1020 nm) and provides the corresponding AOD. This works on the principle of extension of solar radiation intensity at a certain wavelength and calculates the corresponding optical depth by using the knowledge of the solar intensity at the top of the atmosphere (Tiwari et al. 2013). The data was collected using MICROTUPS-II at every one hour throughout the whole week of Diwali in 2016 and 2017.

In this study, the variation of aerosol optical properties during Diwali event (on 25th Oct–7th Nov 2016 and 16th Oct–27th Oct 2017) over the observation site is investigated, which shows the impact of Diwali festival to the increased concentration of aerosols in ambient air in comparison with the pre-diwali days. The aerosol loading (AOD) is mostly high over Delhi during Diwali and it leads to substantial air pollution and degradation of visibility (Sateesh et al. 2018).

Satellite based Moderate Resolution Imaging Spectroradiometer (MODIS) is available with good spatial and temporal coverage and are widely used to understand atmospheric processes and climate variability. AOD data for Delhi was obtained from MODIS Terra (MOD08_D3 v6.1) satellite as a daily mean gridded average in 1° × 1° spatial resolutions and is downloaded from the website <https://giovanni.gsfc.nasa.gov/giovanni/> (Acker et al. 2007).

RESULTS & DISCUSSIONS

Figure 1 shows the daily variation of AOD at 500 nm over the observation site measured by MICROTUPS-II sunphotometer during the Diwali events of the years 2016 and 2017. The daily mean of AOD over the site lies between 0.36 to 1.89 and 0.51 to 1.82 in the years 2016 and 2017 respectively. The

aerosol loading is found to be high in both the years after Diwali day. The AOD at 500 nm (AOD₅₀₀) was high over CSIR-NPL, varying from 1.07 and 1.11 during the study period.

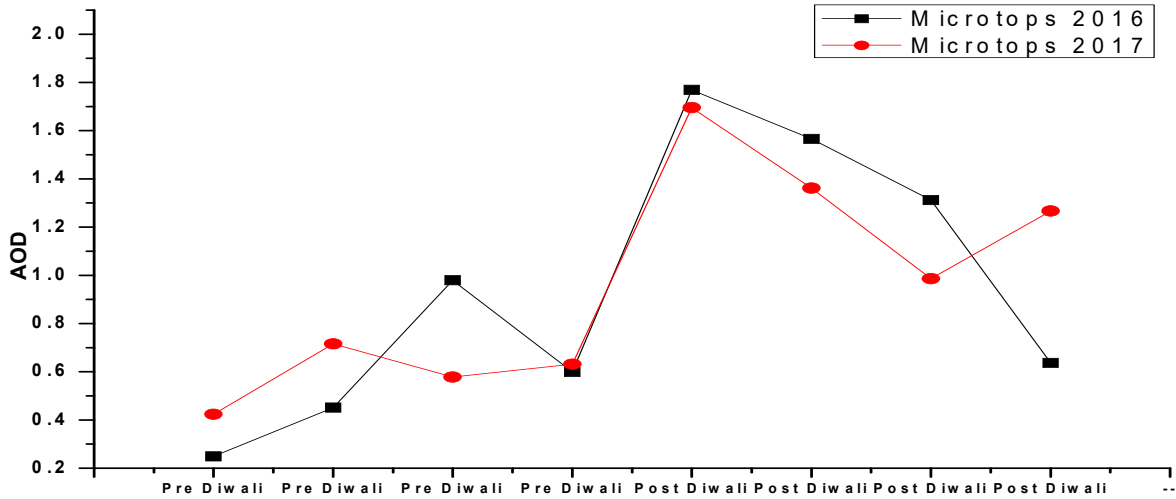


Fig 1: Variation of daily mean AOD over CSIR-NPL using MICROTUPS-II at wavelength 500 nm during Diwali 2016-17

The daily mean spectral variation of AOD at five different wavelengths 380, 500, 870, 936 and 1020nm measured from MICROTUPS-II sunphotometer is shown in figure 2. The AODs values were high at shorter wavelengths while they are relatively low at longer wavelengths which show the presence of fine-to-coarse mode particles.

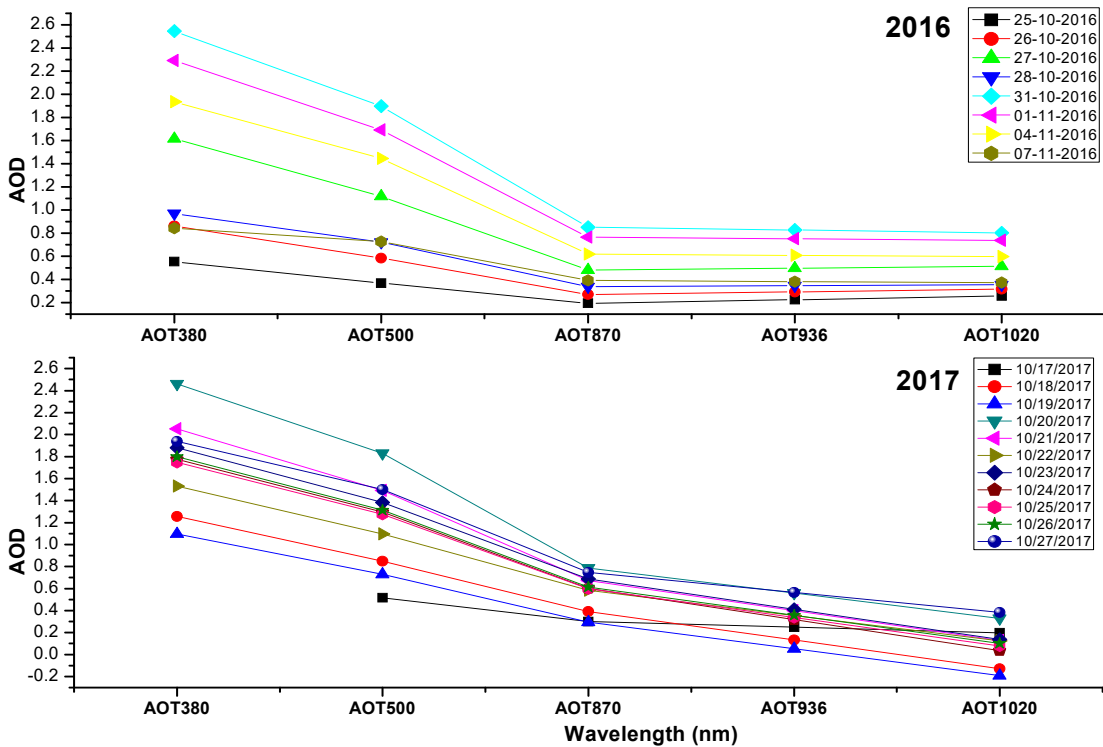


Fig 2: Spectral Variation of AOD at different wavelength 380, 500, 870, 936 and 1020 nm over the observation site during Diwali in the years 2016 and 2017

In figure 3, Angstrom exponent (α) and Turbidity coefficient (β) are computed for wavelength pair 380–870 nm using MICROTUPS-II data and plotted against the week of Diwali 2016 and 2017 for the

determination of aerosol size distribution and total columnar aerosol loading over the site. α is an indicator of the presence of fine mode particles ($\alpha > 1 \mu\text{m}$) to coarse-mode particles ($\alpha < 1 \mu\text{m}$). The value of α lies from 0.95 to 1.46 and 0.97 to 1.59 in 2016 and 2017 respectively, indicate the dominance of fine mode particles over the observation site. The variation of Turbidity coefficient (β) values lie from 0.16 to 0.71 and 0.23 to 0.65 during 2016 and 2017 respectively which shows the nature of variation of AOD.

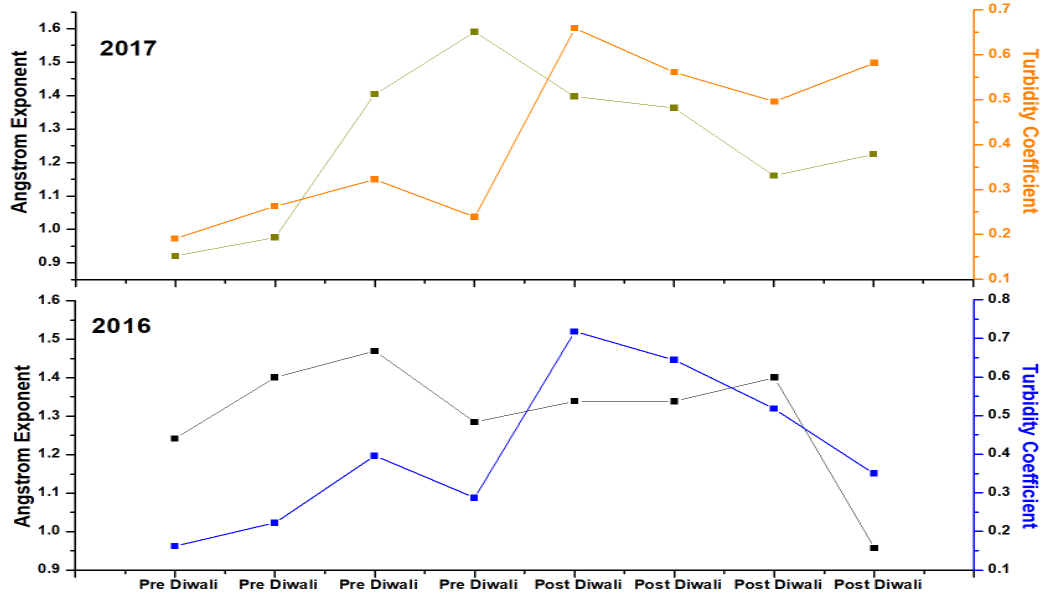


Fig. 3. Variation of Angstrom exponent (α) & Turbidity coefficient (β) over CSIR-NPL during Diwali 2016-17

For validation of Microtops sunphotometer AOD data, we used MODIS derived AOD data. MODIS AODs are derived at 550nm while Microtops AODs are derived at 500 nm. The Figure 4 depicts the variation of daily AODs at 550nm calculated from Microtops and MODIS level 3 data during the week of Diwali 2016 and 2017.

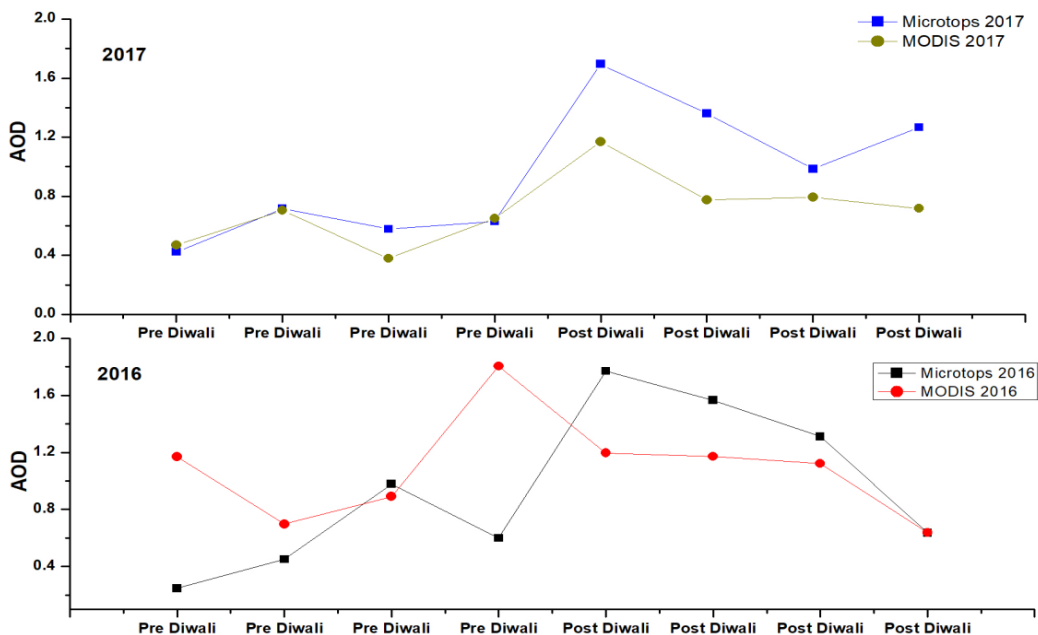


Fig 4: Comparison of AOD at 550 nm with the MODIS & MICROTUPS-II over Delhi during Diwali 2016-17

The figure 5 shows the 4 days backward trajectories derived from HYSPLIT (Hybrid Single Particle Lagrangian Integrated Trajectory) model having 3 different events of aerosol loading on 29th Oct (Pre-Diwali), 2nd Nov (Diwali) and 6th Nov (Post-Diwali) for 2016 and 19th Oct (Pre-Diwali), 23rd Oct (Diwali) and 27th Oct (Post -Diwali) for 2017. The red dots are representing the fire counts taken place during the diwali event. It can be seen that most of the aerosol loading is due to bursting of firecrackers and regional anthropogenic emissions.

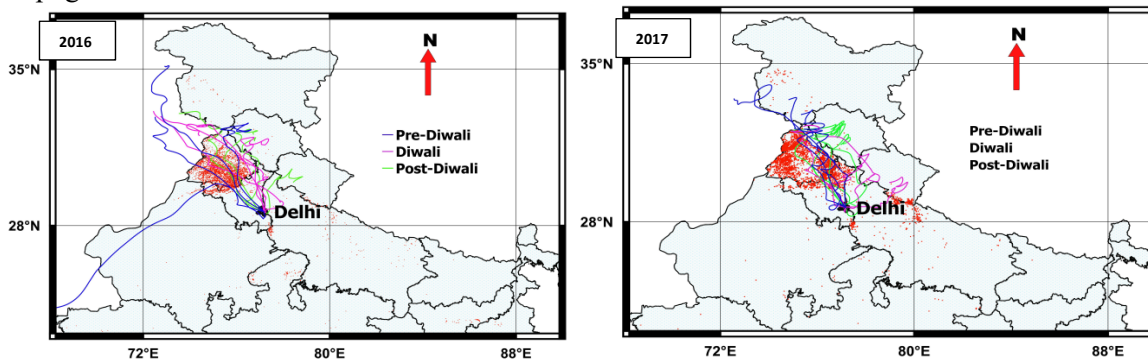


Figure 5: Four Days Backward HYSPLIT Trajectories for Diwali 2016-17

CONCLUSION

In this work the variation of aerosol optical properties over Delhi during Diwali in the years 2016 and 2017 is studied using ground and satellite-based measurements. The AOD derived from MODIS Terra satellite and ground based MICROTOPS-II sunphotometer are compared. The main conclusion drawn from the study is:

1. The aerosol loading is found to be enhanced after Diwali day.
2. The spectral variation of AOD clearly states that AODs are high at shorter wavelengths and relatively low at longer wavelengths show the presence of fine-to-coarse mode particles.
3. The AOD derived from MICROTOPS-II and MODIS have 62% correlation.
4. The back trajectory of HYSPLIT model analysis shows the aerosol loading during Diwali might be due to bursting of firecrackers and anthropogenic emissions.

REFERENCE

Acker, J. G. and Leptoukh, G. (2007), Online Analysis Enhances Use of NASA Earth Science Data. Eos, Trans. AGU, Vol. 88, No. 2, pp 14-17.

Mukherjee, T., Asutosh, A., Pandey, S.K., Yang, L., Gogoi, P.P., Panwar, A. and Vinoj, V. (2018). Increasing Potential for Air Pollution over Megacity New Delhi: A Study Based on 2016 Diwali Episode. Aerosol and Air Quality Research, 18: 2510–2518, 2018.

Sateesh, M., Soni, V. K. and Raju, P.V.S. (2018). Effect of Diwali Firecrackers on Air Quality and Aerosol Optical Properties over Mega City (Delhi) in India. Earth Systems and Environment (2018). <https://doi.org/10.1007/s41748-018-0054-x>.

Sati, A.P. and Mohan, M. (2014). Analysis of air pollution during a severe smog episode of November 2012 and the Diwali Festival over Delhi, India. International Journal of Remote Sensing, 2014, Vol. 35, No. 19, 6940–6954.

Tiwari, S. and Singh, A.K. (2013). Variability of Aerosol Parameters Derived from Ground and Satellite Measurements over Varanasi Located in the Indo-Gangetic Basin. Aerosol and Air Quality Research, 13(2), 627–638.

Vaghmaria, N., Mevada, N. and Maliakal, J. (2018). Impact of Diwali Festival on Aerosol Optical Properties over an Urban City, Ahmedabad (India). *Aerosol and Air Quality Research*, 18: 522–532, 2018.

STUDY OF AIR POLLUTANTS ALONGSIDE MAJOR ROADWAYS IN AGRA

SHALENDRA PRATAP SINGH¹, RANJIT KUMAR² AND ASHOK JANGID¹

¹Department of Physics and Computer Science, Dayalbagh Educational Institute (*Deemed University*)
Dayalbagh, Agra – 282005, India.

²Department of Chemistry, Dayalbagh Educational Institute (*Deemed University*) Dayalbagh, Agra –
282005, India.

KEYWORDS: PM_{2.5}, PM₁₀, CO₂ and Particle-number-concentration (PNC).

INTRODUCTION

Atmospheric particulate materials are particles of solid or liquid phase dispersed in the atmosphere. These are produced either by the mechanical disintegration processes occurring over land (e.g., lift up of dust) and ocean (e.g., sea-spray) or by chemical reactions occurring in the atmosphere (e.g., conversion of sulphur dioxide to sulphuric acid droplets) (Prospero et al., 1983). Particulate matters are often carried to locations far away from their sources through transportation systems. Most of the PM sources are located near the Earth's surface and hence their concentration (mass per unit volume) is larger near the surface. Particulate matters are present throughout the boundary layer, at number concentrations depending upon factors such as location, atmospheric conditions, annual and diurnal cycles and presence of local sources. The highest concentrations are usually found in urban areas, reaching up to 10⁸ and 10⁹ particles per cm³ (Seinfeld and Pandis, 1998).

Ambient concentrations of many air pollutants are elevated near roadways (Houston et al., 2004). A rigorous examination of personal exposures to these pollutants requires that close attention be given to the time that people spend alongside major roadways. The present study also revolves around the same issue, but with the new perspective in order to search the effect of concentration of particulate matter alongside major roadways in the Agra. The reason for the selection of the site is that a high concentration of particulate matter is observed throughout the year. Besides this, Agra is famous for world monuments and cultural heritage and known as city of Taj which attracts tourist from all over the world and at the same time Agra is also one of the highly polluted cities in India. So, it is obvious to study quality of air index in order to make roadmap for the future investigations related to it.

METHODS

Site Description

The geographical location of Agra is (27°10' N, 78°05' E) over Indo-Gangetic plain which is 200 km south-east from Delhi. Two third of its peripheral boundaries are surrounded by Thar Desert of Rajasthan. The climate and weather of Agra is extreme and tropical.

Routes Description

In present work, air quality over the two busiest routes of the Agra region has been studied. The first route started from Bhagat Halwai to Agra Cantt and Agra Cantt to Bhagat Halwai and the second route from Rambagh to Sikandra. The points covered in the first route were Bhagat Halwai, Bhagwan Talkies, Nagar Nigam, Hari Parwat, St. John's, Sai ki Takiya, Sadar and Agra Cantt. The second route comprises of Rambagh, Water Works, Sultanganj Ki Puliya, Bhagwan Talkies, Khandari, Transport Nagar and Sikandra. PM_{2.5} level, PM₁₀ level, CO₂ level, relative humidity and temperature were measured on each route for 6-h periods per day (8:00-11:00 and 14:00-18:00) and 10 minutes stoppage at every point between April and September 2017. The readings were collected by the instrument which is placed on the motorbike which runs along with the constant speed of 20 km/h.

Monitoring procedures

A low cost indigenous portable monitor IAQ 3007R manufactured by (Rave Innovations) was used for measuring air quality, with the capability to simultaneously monitor CO₂, Particle Concentration, Temperature and Relative Humidity. The working is based on the principle of light scattering (Particulates PM_{2.5}, PM₁₀) and NDIR (CO₂).

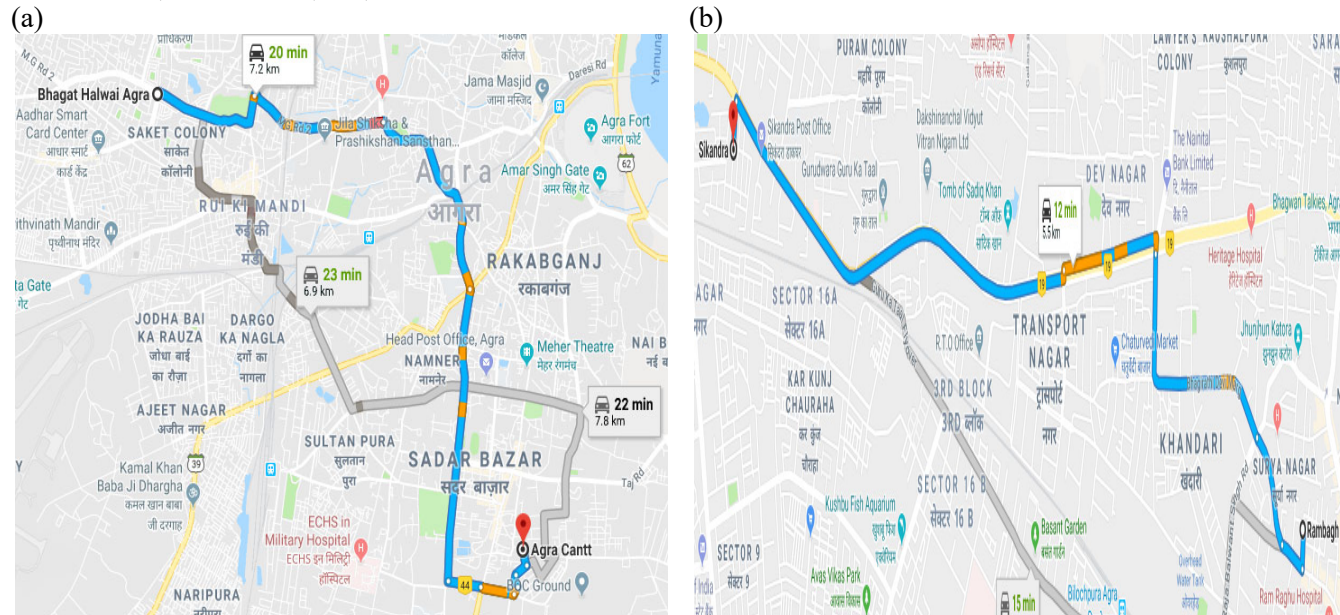


Figure. 1 Two routes shows on Google maps: (a) Bhagat Halwai to Agra Cantt and (b) Rambagh To Sikandra

RESULTS & DISCUSSIONS

The PM_{2.5}, PM₁₀, CO₂ relative humidity and temperature readings obtained on the Bhagat to Agra Cantt and Rambagh to Sikandra routes. The overall average concentration of PM_{2.5} ranged from 8.03 to 353.03 $\mu\text{g}/\text{m}^3$. The highest PM_{2.5} level was 353.03 $\mu\text{g}/\text{m}^3$ on the route of Bhagat Halwai to Agra Cantt in evening time. The PM₁₀ readings obtained on the Bhagat to Agra Cantt and Rambagh to Sikandra routes. The overall average concentration of PM₁₀ ranged from 18.9 to 987 $\mu\text{g}/\text{m}^3$. The highest PM₁₀ level was 987 $\mu\text{g}/\text{m}^3$ found on the route of Agra Cantt to Bhagat Halwai (Backward) in morning time. The relative humidity readings obtained on the Bhagat to Agra Cantt and Rambagh to Sikandra routes. The overall average concentration of relative humidity (RH)% ranged from 19 to 79. The highest relative humidity level was 79 on the route of Rambagh to Sikandra in Morning session. The CO₂ readings obtained on the Bhagat Halwai to Agra Cantt and Rambagh to Sikandra routes. The overall average concentration of CO₂ ranged from 730 to 4572 ppm. The highest CO₂ level was 4572 ppm found on the Sikandra to Rambagh in evening session.

CONCLUSIONS

In present study, air pollutants PM_{2.5}, PM₁₀, CO₂ relative humidity and temperature are measured alongside major roadways in Agra. It was found that parameters studied are exceed IAQ and/or WHO standards on most of the lines under study.

REFERENCES

Houston D., Wu J., Ong P., and Winer. (2004) A. Structural disparities of urban traffic in Southern California: implications for vehicle-related air pollution exposure in minority and high-poverty neighborhoods. *J Urban Aff*: 26, 565–592.

Seinfeld, J.H., and S.N. Pandis (1998) *Atmospheric Chemistry and Physics: From air pollution to climate change*. Wiley-Inter Science: United States.

Prospero, J.M., R.J. Charlson, B. Mohnen, R Jaenicke, A.C. Delany, J. Mayers, W Zoller and K. Rahn.(1983.) The atmospheric aerosol system - an overview, *Rev. Geophys. Space Phys.*, 21, 1607-1629

PM_{2.5} BOUND CARBONACEOUS AEROSOLS: ASSESSMENT DURING HAZY AND NON-HAZY DAYS

APARNA SATSANGI¹, ANITA LAKHANI¹ AND K. MAHARAJ KUMARI¹

¹Department of Chemistry, Faculty of Science, Dayalbagh Educational Institute,
Dayalbagh, Agra-282005, India

KEYWORDS: Relative Humidity, Hazy Days, Secondary Organic Aerosol, Back Trajectories

INTRODUCTION

Haze pollution is a typical synoptic phenomenon which has severe adverse effects on cloud formation, human health, visibility and climate forcing. It is characterized by elevated levels of fine particles, which influences the chemical composition and lifetime in the atmosphere (Hou et al., 2011). Haze generally results from high levels of air particles emitted by anthropogenic sources and gas-to-particle conversion. During such events visibility is very low (less than 1 km) and relative humidity is high (more than 90%) (Tan et al., 2009; Ram et al., 2012; Huang et al., 2014; Zhu et al., 2016; Li et al., 2017; Ding et al., 2018). An important fraction of atmospheric aerosols which influence haze formation are carbonaceous aerosols, contributing 20–70% of particulate matter (Fuzzi et al., 2006; Ram and Sarin, 2011; Ram and Sarin, 2015). Despite the increasing interest of the scientific world in carbonaceous aerosol developed in the recent years, our understanding of the sources and formation mechanisms of this component and its role in haze formation and climate change is still limited (Cesari et al., 2018). The present study is an attempt to understand the role of carbonaceous aerosols from origin to its transport and vertical distribution so that a complete picture may be attained. Thus, PM_{2.5} bound carbonaceous aerosols were collected and assessed. The study of meteorological parameters along with chemical composition would provide a holistic view in understanding the origin and transport of aerosol for middle Indo-Gangetic Plain (IGP).

METHODS

Location of Sampling Site

The study was carried out at Sikandarpur Mustkil (27.26° N, 78.00° E; a rural), a village in the North Central region of India. It is situated in a densely populated and one of the most polluted state; Uttar Pradesh, which lies in the Indo-Gangetic plains of Northern India. Most of its area is used for agricultural activities where mainly rice, wheat and seasonal vegetables are cultivated. This region is a semi-arid zone adjacent to the Thar Desert with subtropical type of climate. In this region, winters are chilly (during December to February, temperature varies from 3 to 15 °C). The season frequently experiences heavy fog and haze which disturbs daily life and hinders visibility.

Sampling: PM_{2.5} samples were collected from mid-November 2016 to February 2017 on the roof of a house in Sikandarpur at about 12 m above the ground level. For sample collection, quartz fiber filters (QFF, 47 mm, Pallflex) were weighed and placed in Fine Particulate Sampler (Model: APM 550EL; Make: M/s Envirotech Instruments Private Limited) for 24 hours at a flow rate of 1.0 m³ hr⁻¹.

Determination of Particulate Mass Concentration: PM_{2.5} mass concentration was determined by the gravimetric analysis of exposed filters using electronic microbalance. Each filter was stabilized at constant temperature (25±1°C) and relative humidity (50±1%) for 48 hours before and after sampling.

Analysis of Carbonaceous aerosol

The aerosol samples were analyzed for concentrations of OC and EC using DRI Model 2001 (Thermal/Optical Carbon Analyzer). This instrument follows IMPROVE thermal/optical reflectance (TOR)

protocol. The analyzer was calibrated with known quantities of CH₄ every day. Replicate analyses were performed at the rate of one per group of 10 samples. Blank filters were also analyzed and the sample results were corrected for blank concentrations, which were 1.0 and 0.5 μgC m⁻³ for OC and EC, respectively. The detection limits for EC and OC were below 1.0 μgC m⁻³. **Meteorological Parameters**

Meteorological parameters were reported from www.wunderground.com. Aerosol optical depth (AOD) was simulated from <https://neo.sci.gsfc.nasa.gov>. During the study period, average temperature (Temp, °C) varied from 4.0 to 18.0°C. It showed inverse correlation with relative humidity (RH, %) varying from 62.0% to 98.0%. In winter, wind speed was low and varied from 0.1 to 2.2 m sec⁻¹. Mostly the wind speed was very low but, if present, it was from northwestern (320° to 360°) direction. Visibility was reduced during winter due to the occurrence of fog and haze. Barometric pressure value (740 to 760 mm Hg) was high indicative of thermal lows. Figure 1 shows meteorological parameters of hazy and non-hazy days during the month of December.

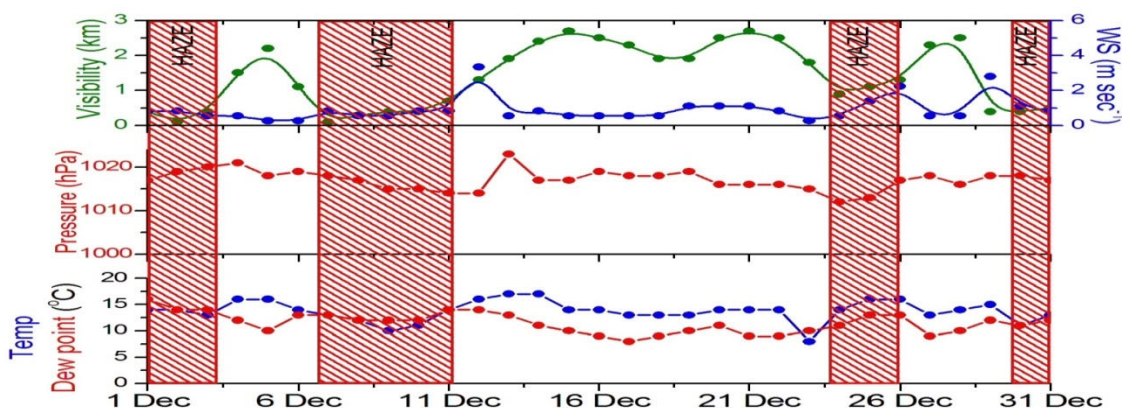


Figure 1: Meteorological conditions during Haze formation

Identification of Haze Events and Influence of meteorological parameters

In winter season, decreased boundary layer height led to accumulation of aerosol particles (high aerosol loadings). On certain days, due to low temperature, low solar intensity, low wind speed (<1.0 m sec⁻¹) but very high relative humidity (>90%), there is too much reduction in visibility (becomes less than 500 m). Such atmospheric occurrence may be termed as ‘haze’ and the days are ‘hazy’ days. Contrarily, many days are such that though temperature and wind speed are low but relative humidity is less than 90%, such days do not observe any reduction in visibility or haze formation. These were ‘clear’ or ‘non-hazy’ days. The emissions of pollutants and the stagnant conditions favour haze formation which alters the composition of the aerosols through aqueous-phase reactions (Tan et al., 2009).

RESULTS & DISCUSSION:

Aerosol Optical Depth (AOD)

On 7 and 15, 30 December, no haze occurred and low AOD was recorded as 0.63 0.58 0.56, respectively while when haze formed, AOD enhanced and was 0.85, 1.0 and 0.94 on 25, 26 and 28 December, respectively.

Variation in PM_{2.5} mass concentrations

During winter, clear (non-hazy) days have PM_{2.5} concentrations 93.1±17.9 μg m⁻³. This was different from very high PM_{2.5} mass concentrations (288.2±57.9 μg m⁻³) recorded during the occurrence of haze event. This shows that PM_{2.5} concentrations rise to more than three times during haze formation. Severe haze

occurred in the month of December. Relative humidity drastically varied from 35% to 99%. PM_{2.5} mass concentrations showed negative correlation with RH, as RH increased and wind speed (WS) lowered, PM_{2.5} increased and vice-versa. This led to stagnation of atmospheric particles during haze formation as compared to dispersion during clear/non-hazy days. Thus, haze persisted till WS was strong enough to blow away the suspended particles leading to increased visibility.

Variation in Carbonaceous aerosol concentration

The average mass concentrations of OC and EC during winter season was $32.7 \pm 24.0 \mu\text{g m}^{-3}$ and $7.6 \pm 5.4 \mu\text{g m}^{-3}$, respectively while the concentrations were highly enhanced during the occurrence of haze (OC=72.3 $\mu\text{g m}^{-3}$ and EC=20.0 $\mu\text{g m}^{-3}$, respectively). EC particles mainly originate from the combustion of coal. As EC particles are hydrophobic species (Wang et al., 2014; Li et al., 2017); their concentrations are enhanced during haze due to the accumulation of these particles ultimately leading to enhancement in PM_{2.5} mass concentrations also. This is the platform for heterogeneous reactions which become predominant as RH rises. During winter season, total carbon (TC=OC+EC) accounted for 51% of the PM_{2.5} concentration, with OC (40%) and EC (11%) indicating that carbonaceous aerosols were one of the key components of fine particles in Sikandarpur. Good correlations ($r = 0.64$) were observed between TC and PM_{2.5} mass concentrations suggesting that both TC and PM_{2.5} had similar sources and formation processes. OC/EC ratios were lower during non-hazy days (2.5 to 3.0) while during hazy days, higher ratios were reported (3.6 to 3.9) suggesting secondary organic aerosol (SOA) formation. Total carbonaceous aerosol (TCA) was also recorded to be higher in haze (180 $\mu\text{g m}^{-3}$) as compared to the days when the weather was clear (82 $\mu\text{g m}^{-3}$). SOC was estimated by EC tracer method which is based on the estimation of $(\text{OC}/\text{EC})_{\text{min}}$. SOC was calculated to be 20% of OC during non-hazy days which rose to 28% of OC during haze formation. This may be due to very low wind speed during the occurrence of haze which suggests localized contribution.

Variation of OC Fractions

Eight carbon fractions have also been used to identify the source of carbonaceous aerosol (Kim et al., 2004). OC1 is abundant during biomass burning. OC2 is high during coal combustion while OC3 and EC1-OP are high during agricultural activities. Figure 2 shows the variation of OC fractions during haze and non-haze/clear days. It is observed that burning activities are enhanced during winter. Hence, OC1, OC2, OC3, EC1 and EC1-OP show enhanced concentrations. During haze these concentrations were high. This confirms major carbonaceous sources to be burning of biomass and coal; and agricultural practices.

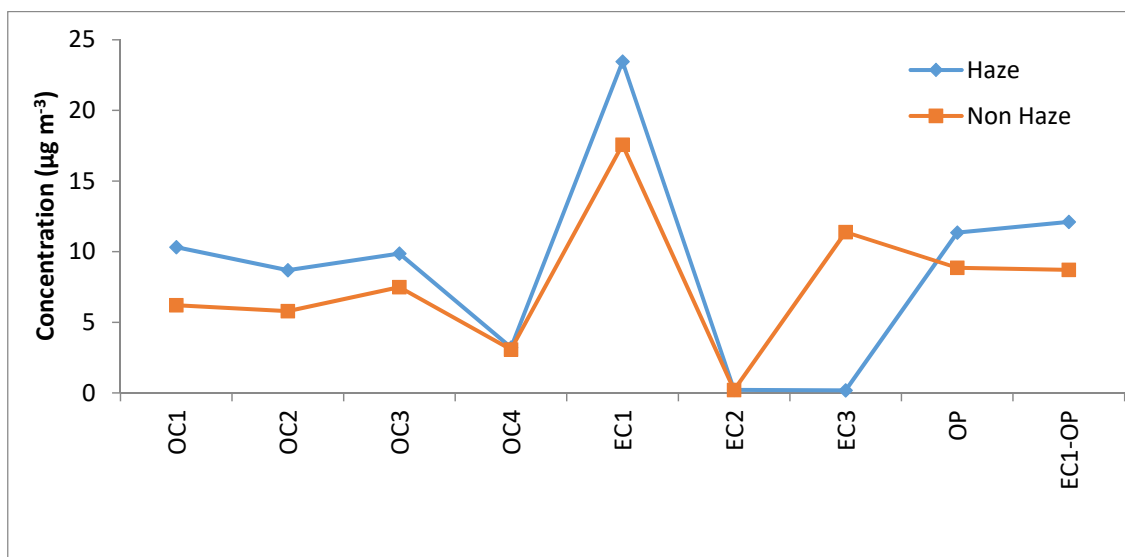


Figure 2: Variation of OC Fractions

Chuang et al. (2014), stated that $EC1-OP = Char-EC$ and $EC2+EC3 = Soot-EC$. Similar to OC/EC ratios, Char-EC/Soot-EC ratio is also an effective indicator for source identification of carbonaceous aerosols as it may be affected by SOA formation. Char-EC is favourably formed at low combustion temperatures from biomass activity (characteristic of winter season), whereas soot-EC is formed at high combustion temperatures from coal combustion. Chuang et al. (2014) have reported that these ratios generally vary from 0.6 (coal or vehicular emissions) to 22.6 (biomass burning). At the present site also Char-EC/Soot-EC ratios (18.0 ± 1.5) were also similar. Very high ratios (31.0 ± 1.1) were recorded during haze formation which indicates biomass and agricultural practices along with coal combustion to be the major sources of carbonaceous aerosols in Sikandarpur.

Air mass Back trajectories Analysis

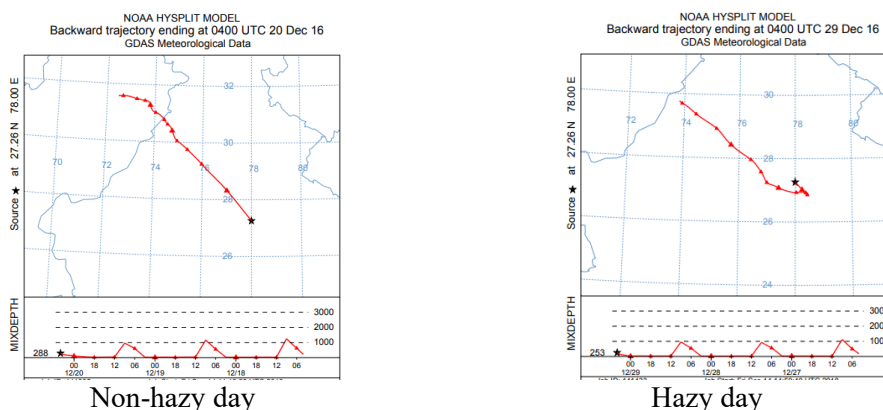


Figure 3: Air mass back trajectories from HYSPLIT Model

Air mass back trajectories simulated for the region during this time also confirm the presence of local contribution (Figure 3). As the distance between 2 longitudes is 111.3 km, it is noticed that the distance travelled by air masses is less (around 500 km). This localized air mass indicates stagnation in atmospheric conditions resulting in the formation of secondary aerosol formation from pre-existing aerosols due to accumulation and aging. The rise in carbonaceous concentrations is also due to enhanced burning activities which lead to increase in atmospheric particles. Coal and biomass burning is a common practice in the region to combat cold (Satsangi et al., 2012).

CONCLUSIONS

$PM_{2.5}$ concentrations ($288.2 \mu\text{g m}^{-3}$) increased to more than three times during haze formation. Similarly, OC and EC concentrations were also enhanced. High OC/EC ratios suggested conversion of pollutants to secondary aerosols due to their prolonged existence. This is probably due to stagnant synoptic conditions during haze events which are supported by localized contribution shown by air mass back trajectories. Char-EC/Soot-EC ratio also suggests biomass and agricultural practices along with coal combustion to be the significant contributors of carbonaceous aerosols.

ACKNOWLEDGEMENTS

This work is financially supported by Women Scientist Scheme (SR/WOS-A/AS-04/2013, WOS A Project, Department of Science and Technology), India. The authors gratefully acknowledge Director, Dayalbagh Educational Institute and Head, Department of Chemistry for providing necessary facilities.

REFERENCES

- Cesari, D., Merico, E., Dinoi, A., Marinoni, A., Bonasoni, P. and Contini, D. (2018) Seasonal variability of carbonaceous aerosols in an urban background area in Southern Italy. *Atmospheric Research* **200** 97-108.
- Chuang, M.T., Lee, C.T., Chou, C.C.K., Lin, N.H., Sheu, G.R., Wang, J.L., Chang, S.C., Wang, S.H., Chi, K.H., Young, C.Y. and Huang, H. (2014) Carbonaceous aerosols in the air masses transported from Indochina to Taiwan: Long-term observation at Mt. Lulin. *Atmospheric Environment* **89** 507-516.
- Ding, J., Zhang, Y., Han, S., Xiao, Z., Wang, J. and Feng, Y. (2018) Chemical, optical and radiative characteristics of aerosols during haze episodes of winter in the North China Plain. *Atmospheric Environment* **181** 164-176.
- Hou, B., Zhuang, G., Zhang, R., Liu, T., Guo, Z. and Chen, Y. (2011) The implication of carbonaceous aerosol to the formation of haze: Revealed from the characteristics and sources of OC/EC over a mega-city in China. *Journal of hazardous materials*, **190** 529-536.
- Huang, R.J., Zhang, Y., Bozzetti, C., Ho, K.F., Cao, J.J., Han, Y., Daellenbach, K.R., Slowik, J.G., Platt, S.M., Canonaco, F. and Zotter, P., 2014. High secondary aerosol contribution to particulate pollution during haze events in China. *Nature*, **514** 218.
- Kim, E., Hopke, P.K. and Edgerton, E.S. (2004) Improving source identification of Atlanta aerosol using temperature resolved carbon fractions in positive matrix factorization. *Atmospheric Environment*, **38** 3349-3362.
- Li, R., Hu, Y., Li, L., Fu, H. and Chen, J. (2017) Real-time aerosol optical properties, morphology and mixing states under clear, haze and fog episodes in the summer of urban Beijing. *Atmospheric Chemistry and Physics*, **17** 5079-5093.
- Ram, K. and Sarin, M.M. (2011) Day–night variability of EC, OC, WSOC and inorganic ions in urban environment of Indo-Gangetic Plain: implications to secondary aerosol formation. *Atmospheric Environment*, **45** 460-468.
- Ram, K., Sarin, M.M., Sudheer, A.K. and Rengarajan, R. (2012) Carbonaceous and secondary inorganic aerosols during wintertime fog and haze over urban sites in the Indo-Gangetic Plain. *Aerosol Air Quality Research*, **12** 359-370.
- Ram, K. and Sarin, M.M. (2015) Atmospheric carbonaceous aerosols from Indo-Gangetic Plain and Central Himalaya: Impact of anthropogenic sources. *Journal of Environmental Management*, **148** 153-163.
- Satsangi, A., Pachauri, T., Singla, V., Lakhani, A. and Kumari, K.M. (2012) Organic and elemental carbon aerosols at a suburban site. *Atmospheric Research*, **113** 13-21.
- Tan, J.H., Duan, J.C., Chen, D.H., Wang, X.H., Guo, S.J., Bi, X.H., Sheng, G.Y., He, K.B. and Fu, J.M., 2009. Chemical characteristics of haze during summer and winter in Guangzhou. *Atmospheric Research*, **94** 238-245.
- Zhu, C.S., Cao, J.J., Tsai, C.J., Shen, Z.X., Liu, S.X., Huang, R.J., Zhang, N.N. and Wang, P. (2016) The rural carbonaceous aerosols in coarse, fine, and ultrafine particles during haze pollution in northwestern China. *Environmental Science and Pollution Research*, **23** 4569-4575.

MASS CONCENTRATION, ENRICHMENT AND HEALTH RISK ASSESSMENT THROUGH INGESTION, DERMAL AND INHALATION EXPOSURE PATHWAYS POSED BY HEAVY METALS IN PM_{2.5}

DINESH SAH, PUNEET KUMAR VERMA, K. MAHARAJ KUMARI AND ANITA LAKHANI*

Department of Chemistry, Dayalbagh Educational Institute, Agra, U.P., India-282005

(*Correspondence at anita.lakhani01@gmail.com)

KEYWORDS: Urban area, PM_{2.5}, Heavy metals, Enrichment factor, Health risk assessment

INTRODUCTION

Fine particulate matter with an aerodynamic particle diameter of $\leq 2.5 \mu\text{m}$ (PM_{2.5}) has been of great concern due to its adverse health effects (Sun et al., 2006; Jiao et al., 2012). These PMs come from road dust, agriculture dust, construction, mining operations, and other activities (Juda-Rezler et al., 2011). It can reduce visibility, acidity of soil and climate change (Amanollahi et al., 2013). Globally, more than two million deaths are estimated each year as a direct effect of air pollution through damage to the lungs and the respiratory system (Shah et al., 2013). PM_{2.5} has high concentrations of many toxic metals that can be incorporated into the human body through ingestion, dermal contact and inhalation and have adverse physiological effects (Mohanraj et al., 2004). Transition metals like Fe, Ni, V, Cu, Cr and Zn have been considered to be toxic on the basis of their ability to support electron exchange and generate reactive oxygen species (ROS) in biological tissues (Ghio et al., 1996). ROS such as hydroxyl radicals (OH[•]), superoxide and hydrogen peroxide can produce oxidative stress as they deplete cells and are considered to be genotoxic and carcinogenic (Knaapen et al., 2004). As, Ni, Cd, and Cr are class I carcinogen; Pb is class II(B) carcinogen, and Cu, Zn, and Mn are non-carcinogen (IARC, 2017). Heavy metals in the human body can cause serious allergic respiratory disease and have a higher excess cancer risk to the exposed population (Taner et al., 2013). The main objectives of this study were to investigate the concentration of heavy metals (Cr, Mn, Fe, Co, Ni, Cu, Zn, As, Cd and Pb) in PM_{2.5} collected from an urban area of Agra, India, and to evaluate the human health risk via ingestion, dermal contact and inhalation exposure pathways.

MATERIALS AND METHODS

SAMPLE COLLECTION

Atmospheric aerosol samples were collected from the urban site. Bhagwan Talkies Crossing was selected to the best in regard to the ambient PM concentration at urban site in Agra. It is one of the busiest places in Agra and traffic flow is very high with about 10^5 average traffic loads of vehicles per day in all four directions. PM_{2.5} samples (N = 24) were collected on pre-combusted (600 °C, 4 h) 47 mm quartz fiber filters (Pallflex, Tissuquartz) using Fine Particulate Sampler (Envirotech APM 550) operated at a constant flow of 16.6 L min^{-1} . Before and after sampling, each filter paper was equilibrated in a desiccator for 24 h and then weighed by electronic microbalance (Mettler Toledo). Finally each sample was stored in a dedicated filter container and preserved in a refrigerator (-10 °C) until analysis. Samples were collected from January to June 2017.

ANALYSIS OF HEAVY METALS

One half of the exposed filter was cut into small pieces and then dissolved in HNO₃ (9 mL, 65%) and HClO₄ (3 mL, 70%). The solution was heated on a hot plate nearly to evaporate. After cooling at room temperature, the residue was dissolved with 10 mL of 6.5% HNO₃ and diluted in a 25 mL flask with distilled water. Then, the diluted solutions were transferred to polyethylene bottles and stored until

analysis. Heavy metals (Cr, Mn, Fe, Co, Ni, Cu, Zn, As, Cd and Pb) were analyzed using an inductively coupled plasma optical emission spectrometer (ICP-OES; iCAP 6300, Thermo Scientific).

ENRICHMENT FACTORS (EF)

It is based on the normalization of a tested metal against a conservative reference metal (Han et al., 2006) and used to differentiate between anthropogenic influences and natural background levels of heavy metals in PM_{2.5}. EF values were calculated with respect to Fe according to the following algorithm:

$$EF = (C_n/C_{ref})_{aerosol}/(B_n/B_{ref})_{background}$$

where, $(C_n/C_{ref})_{aerosol}$ and $(B_n/B_{ref})_{background}$ refer to the concentration ratio of a target metal and the reference metal Fe in PM_{2.5} samples and in the background topsoil, respectively. $EF < 10$ indicated the metal was minimally enriched, $10 < EF < 100$ indicated the metal was moderately enriched, and $EF > 100$ indicated the metal was highly enriched.

HUMAN EXPOSURE AND HEALTH RISK ASSESSMENT

The health effect to humans can occur through three exposure pathways: (a) ingestion of atmospheric particulates due to their deposition (b) dermal absorption of heavy metals in particles adhered to exposed skin and (c) direct inhalation of atmospheric particulates through mouth and nose. The average daily exposure dose of heavy metals through ingestion (ADD_{ing}), average daily exposure dose through dermal contact (ADD_{derm}) and average daily exposure dose through inhalation (ADD_{inh}) were calculated as follows:

$$ADD_{ing} = (C \times IngR \times EF \times ED \times CF)/(BW \times AT)$$

$$ADD_{derm} = (C \times SA \times AF \times EV \times ABS \times EF \times ED \times CF)/(BW \times AT)$$

$$ADD_{inh} = (C \times InhR \times EF \times ED)/(PEF \times BW \times AT)$$

The hazard quotient (HQ) is used to estimate the non-carcinogenic effect of heavy metals. The hazard index (HI) is equal to the sum of HQ of multiple routes (US EPA, 2009).

HQ and HI were estimated by the following equation:

$$HQ = ADD/RfD$$

$$HI = \Sigma HQ$$

HI value greater than 1 indicates there is a chance of non-carcinogenic effects. Greater the HI value, higher is the probability of non-carcinogenic effects.

Carcinogenic risk is the probability of an individual developing any type of cancer from lifetime exposure to carcinogenic hazards. Cancer risk (CR) value below 10^{-6} - 10^{-4} has been judged to be acceptable for regulatory purposes (US EPA, 2011).

$$CR = ADD_{inh} \times CSF_{inh}$$

Where, ADD is the average daily exposure dose through the ingestion, dermal contact and inhalation pathways, RfD is the reference dose, and CSF is the cancer slope factor. All the parameters used in non-cancer and cancer risk were taken by USEPA methods (US EPA, 2011).

RESULTS AND DISCUSSION

MASS CONCENTRATIONS OF PM_{2.5}

The daily concentrations of PM_{2.5} are shown in Figure 1. The mean PM_{2.5} concentrations were $110.4 \pm 39 \mu\text{g m}^{-3}$ (range 63.7 - $195.3 \mu\text{g m}^{-3}$). The concentrations of almost all the PM_{2.5} samples exceeded the NAAQS limit of $60 \mu\text{g m}^{-3}$.

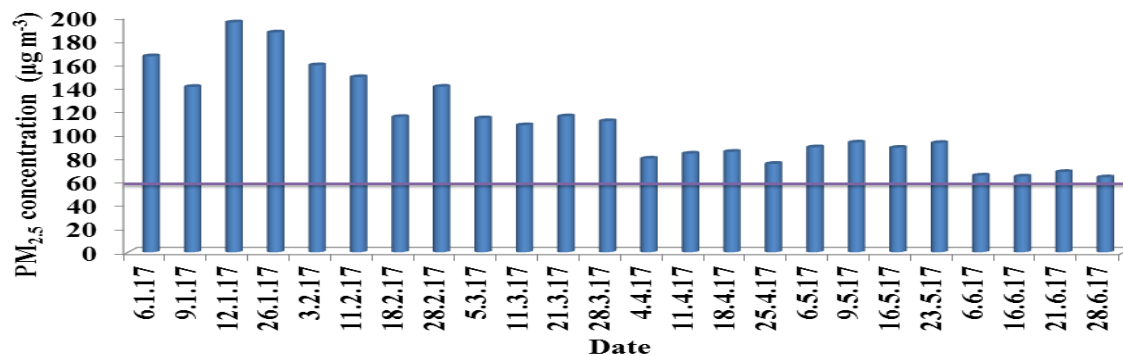


Figure 1. PM_{2.5} concentrations during the sampling period. The purple line shows the 60 µg m⁻³ 24 h standard set by NAAQS in India.

CONCENTRATION OF HEAVY METALS IN PM_{2.5}

As shown in Figure 2, the orders of concentrations of heavy metals were listed as follows: Fe > Zn > Pb > Cu > Mn > Cr > Ni > As > Cd > Co. Central Pollution Control Board, India (CPCB) establishes National Ambient Air Quality Standards (NAAQS, 2009) only for Pb, As and Ni. These standards are 1000, 6 and 20 ng m⁻³ for Pb, As and Ni, respectively. In the present study, As concentration exceeded to 1.6 times while Pb and Ni concentrations were below the limit. The limits set by the World Health Organization (WHO, 2006) are 6.6, 5, 500, 25, 150 and 0.25 ng m⁻³ for As, Cd, Pb, Ni, Mn and Cr, respectively. The Cr and As concentration exceeded the WHO limit. The Pb, Mn and Ni concentrations were below the WHO limit. As shown in Figure 3, the enrichment factor (EF) values decreased in the following order: Cd > Pb > Zn > As > Cu > Cr > Ni > Co > Mn > Fe. Mn, Fe, Co and Ni had EF values <10 can be considered as minimally enriched and to originate mainly from the natural sources. Cr was moderately enriched (10 < EF < 100). Cu, Zn, As, Cd and Pb had very high EF values (>100) and were considered greatly enriched.

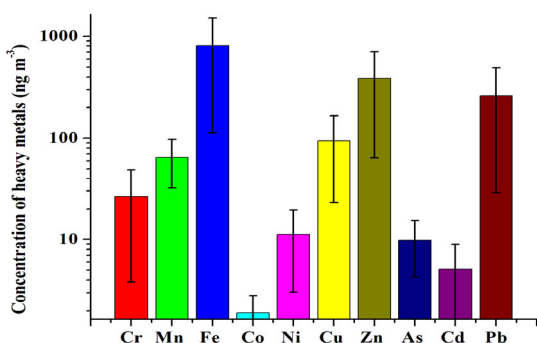


Figure 2. Concentration of heavy metals in PM_{2.5}.

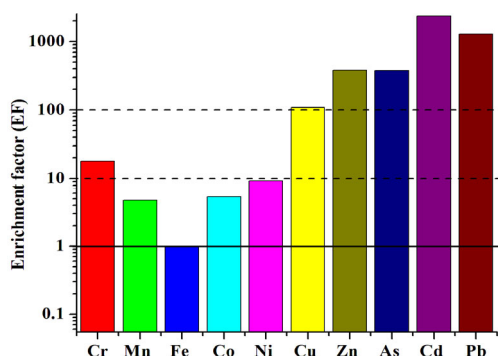


Figure 3. EF of different metals in PM_{2.5}.

NON-CARCINOGENIC AND CARCINOGENIC HEALTH RISK ASSESSMENT

The average daily dose (ADD) for all metals through inhalation, ingestion and dermal exposure are shown in Figure 4. The average daily dose for both children and adults follow the trend, ADD_{ing} > ADD_{der} > ADD_{inh}. The ingestion exposure pathway is higher than dermal and inhalation exposure. Among all the metals Zn had maximum and Cr had minimum average daily dose for all the respective pathways. The average daily dose for children is higher than adults through three exposure pathways.

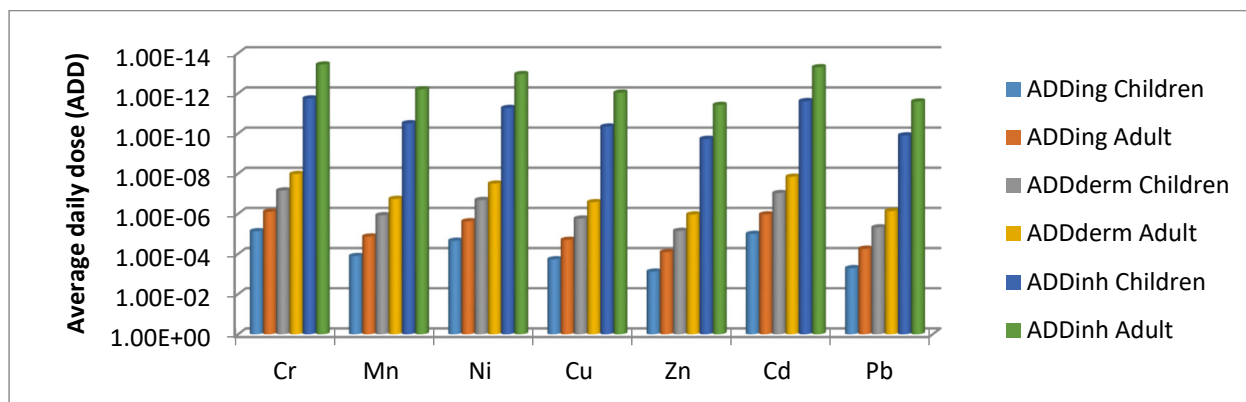


Figure 4. Average daily dose of metals in PM_{2.5} for multiple exposure pathways for children and adults.

The values of HQ and HI are shown in Figure 5. Children and adults follow similar decreasing order for Hazard Quotient (HQ) for Ni, Cu and Pb, $HQ_{ing} > HQ_{der} > HQ_{inh}$ except Cr, Mn and Cd. The HQ values for all heavy metals were below 1. HI values of metals for children and adults followed the order: Pb > Mn > Cd > Cr > Cu > Zn > Ni. HI values for children were greater than HI values for adults. HI values for all metals were under the safe limit ($HI < 1$) for both children and adults. The prevailing concentrations have no non-carcinogenic adverse effects to both children and adults residing in this area. Carcinogenic risk of heavy metals through inhalation exposure pathway has been shown in Figure 5. The decreasing order of carcinogenic risk (CR) for the heavy metals follows the similar trend for both children and adults: Cr(VI) > Cd > Ni. The carcinogenic risk of Cr(VI), Cd and Ni for both children and adults are under permissible limit ($<10^{-6}$). The cancer risk value for children is higher than those for adults.

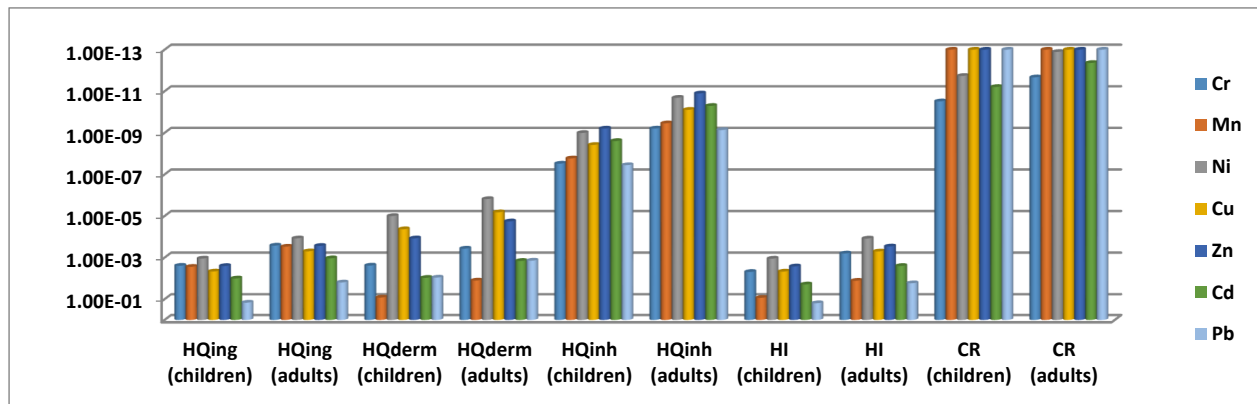


Figure 5. Risk characterization of heavy metals in PM_{2.5}.

CONCLUSIONS

PM_{2.5} samples were collected during January to June, 2017 in an urban area in Agra, India. PM_{2.5} concentrations exceeded the 24 h limit set by the NAAQS in India and WHO limit. The mean metal concentrations decreased in the following order: Fe > Zn > Pb > Cu > Mn > Cr > Ni > As > Cd > Co. The concentrations of Cr, As and Cd were above the WHO limits, whereas those for Mn, Ni and Pb were below the WHO limits. The concentrations of As were above the NAAQS limit, while those for Ni and Pb were below the NAAQS limit. The enrichment factor of the metals was in the following order: Cd > Pb > Zn > As > Cu > Cr > Ni > Co > Mn > Fe. The metals which have a high degree of enrichment originate from anthropogenic sources. Ingestion was the main exposure pathway which showed the highest level of risk to children and adults followed by dermal contact and inhalation exposure. Health risk analysis exhibited that all the metals had HI values lower than 1 for both children and adults indicating no non-carcinogenic risks from heavy metals to both children and adults. The carcinogenic risk

of heavy metals followed the order for both children and adults, Cr(VI) > Cd > Ni. The carcinogenic risks were found to be below the acceptable level (10^{-4} - 10^{-6}) for both children and adults.

ACKNOWLEDGEMENTS

We are grateful to Dr. Tarun Gupta and Mr. Amit Kumar Singh, IIT Kanpur for their help in analyzing samples by ICP-OES. We are thankful to Director and Head, Department of Chemistry, Dayalbagh Educational Institute, Agra, for providing us the necessary facilities.

REFERENCES

- Amanollahi, J., C. Tzanis, A.M. Abdullah, M.F. Ramli and S. Pirasteh (2013). Development of the models to estimate particulate matter from thermal infrared band of Landsat Enhanced Thematic Mapper. *Int. J. Environ. Sci. Technol* 10, 1245-1254.
- Ghio, A.J., R.J. Pritchard, J.R. Lehmann, D.W. Winsett and G.E. Hatch (1996). Lung inflammation after exposure to nonfibrous silicates increases with chelatable $[Fe^{3+}]$. *J. Toxicol. Environ. Health* 49 (1), 11-28.
- International Agency for Research on Cancer (IARC) (2017). Agents Classified by the IARC Monographs, Vol. 1-120. Available online: <http://monographs.iarc.fr/ENG/Classification/ClassificationsAlphaOrder.pdf> (assessed on 27 October 2017).
- Jiao, W., H.C. Frey and Y. Cao (2012). Assessment of inter-individual, geographic, and seasonal variability in estimated human exposure to fine particles. *Environ. Sci. Technol* 46 (22), 12519-12526.
- Juda-Rezler, K., M. Reizer and J.P. Oudinet (2011). Determination and analysis of PM₁₀ source apportionment during episodes of air pollution in Central Eastern European urban areas. The case of wintertime 45, 6557-6566.
- Knaapen, A.M., P.J. Borm, C. Albrecht and R.P. Schins (2004). Inhaled particles and lung cancer. Part A: mechanisms. *Int. J. Cancer* 109 (6), 799-809.
- Mohanraj, R., P.A. Azeez and T. Priscilla (2004). Heavy metal in airborne particulate matter of urban Coimbatore. *Environ. Contam. Toxicol* 47, 162-167.
- NAAQS (2009). The Gazette of India: Extraordinary Part II, Section 3 on 16 November 2009. Available on Website http://www.cpcb.nic.in/upload/Latest/Latest_49_MoEF_Notification.pdf.
- Shah, A.S.V., J.P. Langrish, H. Nair, D.A. McAllister, A.L. Hunter and K. Donaldson (2013). Global association of air pollution and heart failure: a systematic review and meta-analysis. *The Lancet* 382, 1039-1048.
- Sun, Y., G. Zhuang, A.A. Tang, Y. Wang and Z. An (2006). Chemical characteristics of PM_{2.5} and PM₁₀ in haze-fog episodes in Beijing. *Environ. Sci. Technol* 40 (10), 3148-3155.
- Taner, S., B. Pekey and H. Pekey (2013). Fine particulate matter in the indoor air of barbeque restaurants: Elemental compositions, sources and health risks. *Sci. Total Environ* 454-455, 79-87.
- U.S. EPA (U.S. Environmental Protection Agency), 2009. Risk Assessment Guidance for

Superfund Volume I: Human Health Evaluation Manual (Part F, Supplemental Guidance for Inhalation Risk Assessment). Office of Superfund Remediation and Technology Innovation, Washington, D.C.

US EPA, 2011. Risk Assessment Guidance for Superfund. In: Part, A. (Ed.), Human Health Evaluation Manual; Part E, Supplemental Guidance for Dermal Risk Assessment; Part F, Supplemental Guidance for Inhalation Risk Assessment, I.

World Health Organization (WHO) (2006). Health Risks of Particulate Matter from Longrange Transboundary Air Pollution. WHO Regional Office for Europe.

ATMOSPHERIC GAS AND PARTICULATE PHASE DISTRIBUTION OF PARENT POLYCYCLIC AROMATIC HYDROCARBONS AND THEIR NITRO-DERIVATIVE AND THEIR VARIATION WITH NO_x

P. K. VERMA¹, D. SAH¹, R. V. SATISH², N. RASTOGI², K. M. KUMARI¹ AND A. LAKHANI^{1*}

¹Department of Chemistry, Dayalbagh Educational Institute, Agra 282005, India

²Geosciences Division, Physical Research Laboratory, Ahmedabad 380009, India

(*Correspondence at anita.lakhani01@gmail.com)

KEYWORDS: Polycyclic Aromatic Hydrocarbons (PAHs), Nitro-PAHs, NO_x, Gas-particle partitioning

INTRODUCTION

Polycyclic Aromatic Hydrocarbons (PAHs) are ubiquitous, semi-volatile organic pollutants formed during incomplete combustion. They are highly carcinogenic and mutagenic in nature (Kameda et al. 2005). Atmospheric PAHs have received attention during the past decades because they can enter easily into human respiratory tract through inhalation and cause various health issues. PAHs can be partitioned between both the gas and particulate phase in atmosphere when exposed to temperatures at and above the standard temperature (Xie et al. 2014). Once PAHs enter into the air, they undergo through various atmospheric processes like gas-particle partitioning and heterogeneous reactions including photo-oxidation (Pitts B. F., and Pitts, J. N. 2000). The gas-particle partitioning of PAHs depends on the molecular weight of the compounds as well as temperature, humidity and other meteorological parameters (Birgul et al. 2011). Due to complexity of aerosol properties, their interaction with various atmospheric pollutants, atmospheric gas and particulate phase PAHs with respect to meteorological conditions has yet to be understood. Earlier studies report on PAH photolysis for various different sources like diesel exhaust, wood soot, silica gel and effect of meteorological conditions on particulate PAHs (Ozaki et al. 2005, Panther et al. 1999; Fang et al. 2004). However, very less attention has been given towards the interaction of gas and particulate phase PAHs with other atmospheric pollutants, especially those that could easily react with gas and particulate phase PAHs and form more carcinogenic and mutagenic derivatives. NO_x and Ozone can easily react with PAHs in the ambient air via nitration and ozonolysis respectively, giving products that are more potent than the parent compounds (Pitts B. F., and Pitts, J. N. 2000). Hence this study aims to determine the gas-particle partitioning of PAHs and to assess formation of Nitro-PAHs by reaction of parent PAHs with NO_x and NO₂.

METHODS

Atmospheric gas and particulate phase PAHs samples were collected from Bhagwan talkies crossing from November 2015 to February 2016. It is a crossing on the National Highway- 2 and observes mixed vehicular traffic throughout the day and night. Sampler was placed at the roof of double storey building. Samples were collected on Quartz fiber filters (QFFs) and on Poly-urethane foam (PUF) plugs for the particulate phase and gas phase respectively by High Volume Sampler Model TE-1000X (TISCH International, USA) at a flow rate of 0.2 m³ min⁻¹ for 24 hours. Prior to sampling, QFFs were kept at 750 °C overnight in a muffle furnace to eliminate any background contamination and packed in aluminum foil packages until sampling. The deposited mass was determined by weighing the QFF's both before and after sampling. Prior to sampling, PUFs were also pre-cleaned in Dichloromethane (DCM) (HPLC grade) by Soxhlet extraction. Cleaned PUFs were wrapped in aluminum foil and baked in an oven at 70 °C for 40 minutes to remove excessive DCM and transported to the field in zip locked bags without allowing exposure to ambient air. After sampling QFFs and PUFs were stored at -20°C until extraction.

QFFs were cut in small pieces and extracted at room temperature by ultrasonication for 60 min in a mixture of DCM and n-hexane (4:1 ratio), while the PUFs were Soxhlet extracted for 8 hours in DCM and n-hexane mixture. Both the gas and particulate phase extracts were cleaned by employing a silica gel column and concentrated to 1.5 mL by rotavapor (BUCHI) and stored at -20°C in glass vials until analysis.

2 parent PAHs {Fluoranthene (Fla) and Pyrene (Pyr)} and their nitro derivatives {3-Nitro Fluoranthene (3-NFla) and 1-Nitro Pyrene (1-NPyr)} were analyzed in selected ion monitoring mode according to their m/z ratio by Gas Chromatograph-Mass Spectrometer (GC-MS, BRUKER SCION SQ). Separation was achieved on Rtx-5 MS capillary column. Helium was used as carrier gas at a flow rate of 1 ml m⁻¹. The temperature of oven was set at 60°C for 4 minutes, it was increased to 290 °C at a rate of 8°C min⁻¹ and held for 30 min. The temperature of injector was maintained at 270 °C. The mass scanning ranged between 50 and 500. For each analysis 1 µl sample was injected in GC-MS.

Concentration of NO_x and NO₂ for the same period was monitored by online analyzer (Thermo scientific 42i) while the meteorological parameters like temperature, solar intensity, relative humidity, wind speed and wind direction will be recorded by weather station (WM 271).

RESULTS & DISCUSSIONS

The mean TSP concentration during the sampling period at the sampling site was 528.31 ± 109.3 µg m⁻³, it ranged from 356.2 to 733.7 µg m⁻³ during the sampling period. The mean ± standard deviation (S.D.), for the particulate and gas phase concentrations of PAHs and nitro-PAHs are given in table 1. The daily variation of particulate and gas phase parent PAHs and their derivatives along with NO_x, NO₂ and meteorological parameters (Temperature and Relative Humidity) are shown in figure 1. The average concentration of parent PAHs during the sampling period was approximately three times higher than their nitro-derivatives. The average concentration of NO_x and NO₂ on sampling events was 13.6 ± 7.4 ppb and 11.6 ± 7.3 ppb respectively and its average daily variation is shown in figure 1.

PAHs & N-PAHs	Gas phase ± S.D. (ng m ⁻³)	Particulate phase ± S.D. (ng m ⁻³)	Gas + Particulate phase (ng m ⁻³)	Φ
Fla	30.90 ± 27.4	31.25 ± 22.9	62.15	50.3
Pyr	60.24 ± 27.8	72.16 ± 25.2	132.40	54.5
3-N Fla	9.29 ± 7.5	13.79 ± 6.6	23.08	59.7
1-NPyr	17.73 ± 12.9	17.24 ± 9.3	34.97	49.3

Table 1. Atmospheric concentrations of PAHs and their nitro derivatives.

The distribution of PAHs and their nitro derivatives between both the gas and particulate phase was calculated using gas-particle partitioning coefficient (K_p , m³ µg⁻¹), which can be expressed as

$$K_p = (C_{\text{particulate}} / \text{TSP}) / C_{\text{gas}} \quad (1)$$

Where TSP is ambient concentration of Total Suspended Particulate Matter (µg m⁻³), $C_{\text{particulate}}$ and C_{gas} are PAHs concentration (ng m⁻³) in particulate and gas phase respectively. Particulate phase fraction (Φ) of PAHs and nitro-PAHs was also calculated using the following equation

$$\Phi = [(K_p \times \text{TSP}) / (1 + K_p \times \text{TSP})] \times 100 \quad (2)$$

It can be observed from the value of Φ, that Fla, Pyr and their Nitro-derivatives distribute equally between both the phase as shown in table 1. Extent of adsorption and absorption partitioning of Fla is determined by correlating its K_p with its subcooled liquid vapor pressure (P_i^o) ($\log K_p = m \log P_i^o + b$) and octanol-air partitioning coefficient (K_{OA}) ($\log K_p = \log K_{OA} + \log f_{OM} * 11.91$, f_{OM} is fraction of organic matter which is approximately 20 % of TSP) respectively. For adsorption, under equilibrium condition the slope for $\log K_p$ vs $\log P_i^o$ should be close to -1 and whereas for absorption mechanism the slope for $\log K_p$ vs $\log K_{OA} + \log f_{OM} * 11.91$ should be close to +1. Fla shows approximate equilibrium condition for absorption mechanism as its slope found close to +1 ($m = 0.94$, $b = -1.11$ $r^2 = 0.89$). Hence, the

dominance of absorption mechanism was observed during the sampling period and the partitioning of Fla between both the gas and particulate phase is governed by the concentration of organic carbon present on TSP surface.

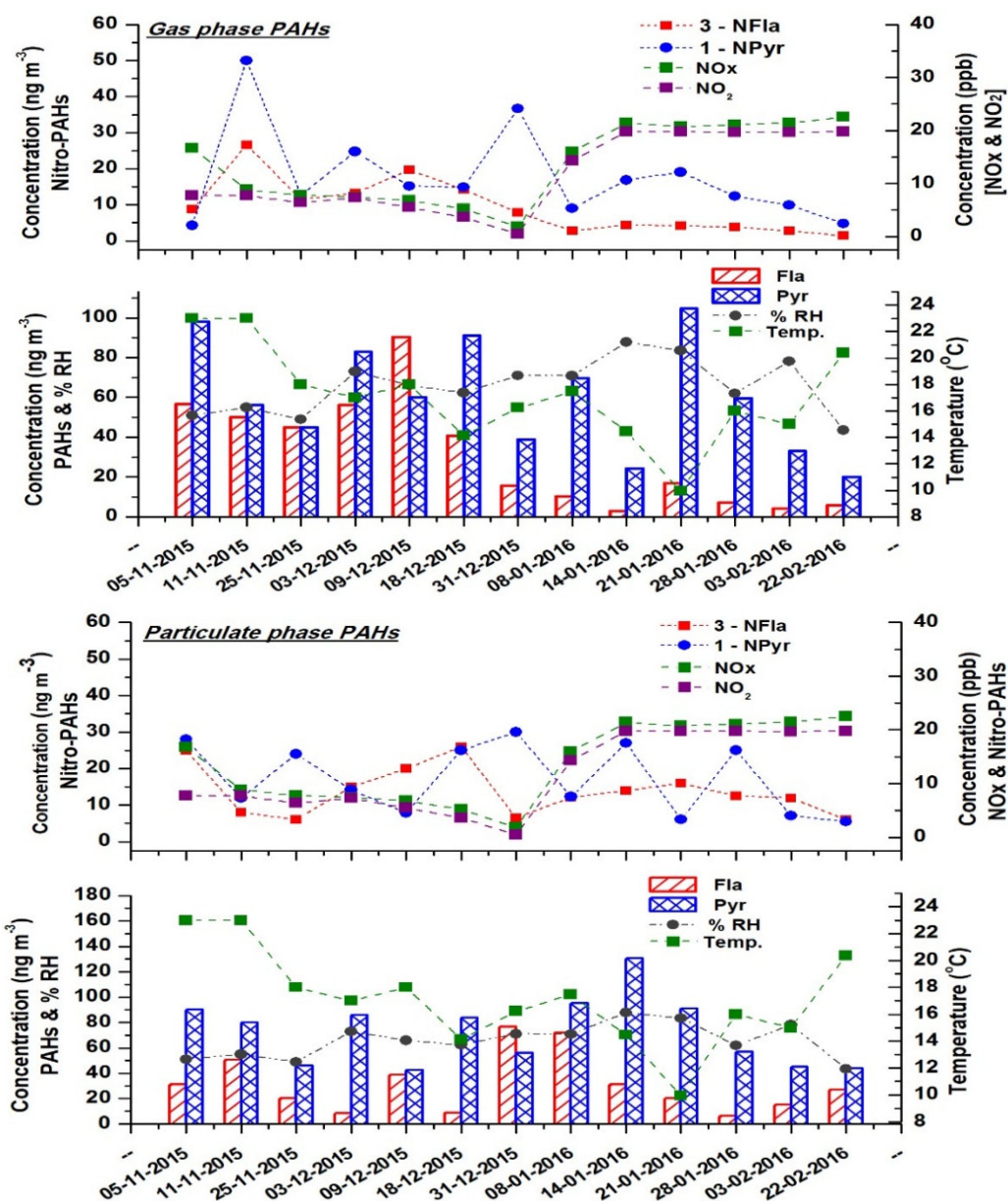


Figure 1. Variation in the concentration of PAHs, Nitro-PAHs, NO_x, NO₂ with Meteorological parameters.

Nitro-PAHs are emitted in the atmosphere either from the primary sources or formed via atmospheric reactions of their parent PAHs (Arey, 1998). Hence, the variation of gas and particulate phase concentration of PAHs and Nitro-PAHs was correlated with the ambient concentration of NO_x, NO₂ and various meteorological parameters. It can be observed from figure 1, that PAHs and Nitro-PAHs concentration in ambient air not only depend on NO_x and NO₂ but also depends on meteorological parameters. Strong negative correlation between NO_x and NO₂ with the gas phase concentration of 3-NFla and 1-NPyr was observed ($r = -0.69$ to -0.42). During the entire sampling period the concentration of Nitro-PAHs was inversely proportional to the concentration of NO_x and NO₂. In December 2015, the concentration of 3-NFla and 1-NPyr was higher and NO_x and NO₂ was found less in the ambient air but

in January 2016, the trend gets reversed which indicates that the gas phase concentration of Nitro-PAHs depends on NO_x and NO₂, and gas-phase radical-initiated reactions of parent PAHs with NO_x and NO₂ may be responsible for the formation of nitro-PAHs in ambient air (Zimmermann et al., 2013). On the other hand, for particulate phase Nitro-PAHs less significant negative correlation was obtained ($r = -0.32$ to -0.13), which indicates towards the emission from traffic sources and very less amount of parent PAHs in the particulate phase reacts with ambient NO_x and NO₂ to form its nitro-derivatives.

CONCLUSIONS

Gas-particle distribution shows that Fla, Pyr and their Nitro-derivatives distributes equally in both the gas and particulate phase. Absorption partitioning mechanism dominates for Fla and its concentration in atmospheric gas and particulate phase is governed by organic carbon present on TSP surface. Gas phase concentration of Nitro PAHs depends the atmospheric reaction between parent PAHs, NO_x and NO₂ whereas Nitro-PAHs concentration in the particulate phase mainly depends on primary emissions.

ACKNOWLEDGEMENT

The authors are grateful to the Director, Dayalbagh Educational Institute Agra; Head, Department of Chemistry for providing necessary help; and Department of Science and Technology, DST project No.: SB/S4/AS-150/2014, New Delhi, for financial assistance.

REFERENCES

- Arey, J. (1998). Atmospheric reactions of PAHs including formation of nitroarenes. In *PAHs and related compounds* (pp. 347-385). Springer, Berlin, Heidelberg.
- Birgöl, A., Tasdemir, Y., & Cindoruk, S. S. (2011). Atmospheric wet and dry deposition of polycyclic aromatic hydrocarbons (PAHs) determined using a modified sampler. *Atmospheric research*, *101*(1-2), 341-353.
- Fang, G. C., Wu, Y. S., Chen, M. H., Ho, T. T., Huang, S. H., & Rau, J. Y. (2004). Polycyclic aromatic hydrocarbons study in Taichung, Taiwan, during 2002–2003. *Atmospheric Environment*, *38*(21), 3385-3391.
- Kameda, Y., Shirai, J., Komai, T., Nakanishi, J., & Masunaga, S. (2005). Atmospheric polycyclic aromatic hydrocarbons: size distribution, estimation of their risk and their depositions to the human respiratory tract. *Science of the Total Environment*, *340*(1-3), 71-80.
- Ozaki, M., Wada-Katsumata, A., Fujikawa, K., Iwasaki, M., Yokohari, F., Satoji, Y., ... & Yamaoka, R. (2005). Ant-nestmate and non-nestmate discrimination by a chemosensory sensillum. *Science*, *309*(5732), 311-314.
- Panther, B. C., Hooper, M. A., & Tapper, N. J. (1999). A comparison of air particulate matter and associated polycyclic aromatic hydrocarbons in some tropical and temperate urban environments. *Atmospheric Environment*, *33*(24-25), 4087-4099.
- Pitts, B. F., & Pitts, J. N. (2000). Chemistry of the upper and lower atmosphere: Theory, experiments and applications. *Academic, US*.
- Xie, M., Hannigan, M. P., & Barsanti, K. C. (2014). Gas/particle partitioning of n-alkanes, PAHs and oxygenated PAHs in urban Denver. *Atmospheric environment*, *95*, 355-362.

Zimmermann, K., Jariyasopit, N., Massey Simonich, S. L., Tao, S., Atkinson, R., & Arey, J. (2013). Formation of nitro-PAHs from the heterogeneous reaction of ambient particle-bound PAHs with N₂O₅/NO₃/NO₂. *Environmental science & technology*, 47(15), 8434-8442.

CHEMICAL CHARACTERIZATION AND SOURCE APPORTIONMENT OF PM₁ AT A SUB-URBAN SITE OF AGRA

ANKITA MANGAL¹, ANITA LAKHANI, K. MAHARAJ KUMARI*

Department of Chemistry, Faculty of Science, Dayalbagh Educational Institute, Dayalbagh, Agra 282005, India

(*Correspondence at maharajkumari.k@rediffmail.com)

KEYWORDS: PM₁; Chemical Characterization; Source Apportionment

INTRODUCTION

Currently, a number of studies have focused on the submicron particulate matter (PM₁) fraction (particles with an aerodynamic diameter of less than 1 μm) since there is increased evidence of the association between exposure to submicron particles and different respiratory and cardiovascular diseases, cancer, and mortality (Yubero *et al.*, 2015; Franck *et al.*, 2011). The toxicity of these particles seems to be linked with the presence of specific components, such as water soluble ions, metals and PAHs which are more abundant in the submicron particle size range. Primary submicron aerosols mainly arise from combustion processes (vehicle exhaust, industry and biomass burning). However, a large portion of the PM₁ fraction is formed by secondary particles, both organic and inorganic, generated by atmospheric reactions of primary pollutants (Tao *et al.*, 2012). Secondary organic aerosols are produced by photochemical oxidation of volatile and semi-volatile organic compounds. The main secondary inorganic species (ammonium sulfate and ammonium nitrate) are generated from the oxidation of sulphur dioxide and nitrogen oxides to sulfuric acid and nitric acid, respectively and subsequent neutralization with gaseous ammonia. SO₂ and NO_x are mostly emitted from fossil fuel combustion, while the dominant sources of NH₃ are livestock waste decomposition and agricultural fields (Hellsten *et al.*, 2008). Metals are non-volatile in nature and are therefore less prone to chemical reaction and transformation. They remain in their original form even after going through long range atmospheric transformation and metals like Pb, Cd, Zn, Cr, etc. are persistent in environment (Zheng *et al.*, 2013).

There is a limited extent of information on physico-chemical analysis and source apportionment of submicron particles present in ambient air. In this work, data from suburban site in Agra during a year (April 2016-March 2017) their chemical characterization and source apportionment is presented.

METHODS

Site description

Agra (27°10' N, 78°05' E) is located at the north central part of India. It is bounded by the Thar Desert of Rajasthan on its South East, West and North West peripheries and therefore, it is a semiarid area. For the present study the sampling site was Dayalbagh Educational Institute. It is about 10 km away from the industrial sector of the city. The institute campus lies by the side of the road that carries mixed vehicular traffic on the order of 10⁴. Industrial area of the city is about 6 km away from the site. The major industrial activities of the city are metal casting and rubber processing (Verma *et al.*, 2016).

Sample collection

Airborne particulate samples were collected on a pre-weighed 47 mm quartz fiber filter (QM-A) using PM₁ Particulate sampler (Envirotech APM 577) operated at a flow rate of 10 L min⁻¹ from April 2016-March 2017.

Analysis of trace metals

For metal analysis, one-fourth filter paper was digested with Nitric acid (69%, Merck) for 2 hours. After digestion, the solution was filtered through microporous membrane filter paper (Sartorius 393) and analyzed for metals by Inductively Coupled Plasma-Mass Spectrometry (ICP-MS Thermo Scientific)

Analysis of water soluble ions

For water soluble ions (cations and anions) analysis, one-fourth filter paper was cut and extracted ultrasonically for 30 minutes in deionized water (resistivity 18 MΩ cm). After ultrasonication, the extracts were filtered through microporous membrane filter paper (Sartorius 393) and analysed by ion chromatography (IC), Dionex ICS 1100.

RESULTS AND DISCUSSION

The average mass concentration of PM₁ was 52.8±6µg/m³ and 98±24µg/m³ during summer and winter respectively. This level was lower than those observed at IIT Kanpur, IIT Delhi (102.4/m³; Izhar *et al.*, 2016, 163.9±35.1µg/m³; Prakash *et al.*, 2016). PM₁ concentration observed in summer (52.8±6µg/m³) was lower than those observed for PM₁ at Chhattisgarh and Raipur (64.7±36.9µg/m³; Deshmukh *et al.*, 2011a and 72.1±39; Deshmukh *et al.*, 2011b) but higher during winter (98±24µg/m³) than those observed for PM₁ at Chhattisgarh and Raipur (64.7±36.9µg/m³; Deshmukh *et al.*, 2011a and 72.1±39; Deshmukh *et al.*, 2011b) but higher during winter (98±24µg/m³).

PM ₁	Summer		Winter	
	Average	SD ^c	Average	SD ^c
Mass	52.8 ^a	6	98 ^a	24
SO ₄ ²⁻	3.2 ^a	1	10 ^a	4.9
NO ₃ ⁻	2.3 ^a	0.9	9.1 ^a	4.1
Cl ⁻	2.1 ^a	1.1	7.5 ^a	3.2
F ⁻	0.5 ^a	0.1	0.6 ^a	0.3
Na ⁺	0.98 ^a	0.1	2.4 ^a	1.2
NH ₄ ⁺	2.28 ^a	1	8.0 ^a	2.9
K ⁺	1.5 ^a	0.9	4.7 ^a	1.9
Mg ²⁺	0.5 ^a	0.1	0.8 ^a	0.2
Ca ²⁺	1 ^a	0.4	2.4 ^a	0.8
V	20 ^b	1.4	38 ^b	4.7
Cr	60 ^b	26	80 ^b	20
Mn	40 ^b	16	60 ^b	95
Fe	878 ^b	304	1822 ^b	790
Ni	46 ^b	7	46 ^b	9.8
Cu	36 ^b	18	42 ^b	20
Zn	377 ^b	31	615 ^b	49
As	1.9 ^b	8*10 ⁻⁴	6 ^b	0.28
Cd	4 ^b	0.1	9 ^b	4
Pb	84 ^b	15	269 ^b	180

Table 1. Statistical summary of PM₁ analysis during summer and winter

^aConc in µg/m³

^bConc in ng/m³

SD^c Standard Deviation

Water soluble ions and metals

On average major anions, major cations and metals contributes 15%, 12% and 3% of PM₁ mass during summer and 20%, 15% and 4% during winter, respectively (figure 1). Table 1 show that, SO₄²⁻ (3.2±1.1µg/m³ and 10.6±6.9µg/m³) was the major PM₁ ion, followed by NO₃⁻ (2.3±0.9µg/m³ and 9.1±4.1µg/m³), NH₄⁺ (2.28±1.1µg/m³ and 8.0±2.9µg/m³) and Cl⁻ (2.1±1.1µg/m³ and 7.5±3.2µg/m³). Other water soluble ions were low in abundance: Na⁺ (0.98±0.1µg/m³ and 2.4±1.2µg/m³), K⁺ (1.5±0.9µg/m³ and 4.7±1.9µg/m³), Ca²⁺ (1.0±0.4µg/m³ and 2.4±0.8µg/m³), Mg²⁺ (0.5±0.1µg/m³ and 0.8±0.2µg/m³) and F⁻ (0.5±0.1µg/m³ and 0.6±0.3µg/m³) during summer and winter respectively. Metals show variation in concentration: Fe was the most abundant metal (878±304ng/m³ and 1822±790ng/m³) during summer and winter respectively, followed by Pb (84±16ng/m³ and 269±ng/m³) and Zn (377±31ng/m³ and 615±49ng/m³). Trace metals (V, Cr, Mn, Ni, Cu, As, Cd) were in the range 1.9±0.0008-60±16ng/m³ during summer and 8.5±0.28-80±20ng/m³ during winter.

Source Apportionment Analysis

Principle Component Analysis (PCA) was performed for source apportionment using SPSS 16.0 during summer and winter respectively. Table 2 and 3 shows the results of PCA during summer and winter, respectively. Three factors were generated during summer that accounted for 96% of total variance and four factors were generated during winter that accounted for 97% of the cumulative percent variance.

During summer, Factor 1 accounted for 40% of variance and was loaded with Cl⁻, V, Cr, Mn, Fe, Ni, Cu and As which may be attributed to industrial emissions. Industrial area is located about 8 km from the sampling area. Factor 2 accounted for 27% of total variance and was loaded with K⁺, Mg²⁺, Ca²⁺, Na⁺ Cd, Zn and Pb and indicates re-suspended soil (Satsangi *et al.*, 2013; Singh and Gupta, 2016; Agarwal *et al.*, 2017). Enrichment of metals increases with decreasing particle size. 80% of vehicular emissions contain particles in the ultrafine to fine (0.01–2.8µm) range (Singh and Gupta, 2016). Factor 3 accounted for 29% of total variance and was loaded with SO₄²⁻, NO₃⁻ and NH₄⁺ representing secondary formation (Satsangi *et al.*, 2013).

During winter, Factor 1 accounted for 42% of variance and was loaded with SO₄²⁻, NO₃⁻ and NH₄⁺ representing secondary formation (Satsangi *et al.*, 2013). Factor 2 accounted for 23% of total variance and was loaded with Cl⁻ and K⁺. High loadings of these metals in Factor 2 may be mainly attributed to biomass and coal burning activities. Biomass burning and coal combustion are considered as sources for PM₁ during winter time. Presence of K⁺ in this factor indicates biomass burning and coal burning, which is a common activity to combat cold at this site during the winter season. Factor 3 accounted for 17% of total variance and was loaded with Na⁺, Mg²⁺, Ca²⁺, Zn, Cd and Pb. High loadings of these species in factor 3 attributed to resuspended dust. The National Highway-2 (NH-2) (which connects New Delhi to Kolkata has a vehicular density of about 10⁶ vehicles per day) is about 2 km from the sampling site and may contribute to Zn emissions, a tracer of tyre wear (Singh and Gupta, 2016). Factor 4 accounted for 14% of total variance and was loaded with V, Cr, Ni, Mn, Fe, As and Cu representing influence of industrial emission at the present site.

Table 2. PCA analysis for PM₁ during summer

Species	Factor 1	Factor 2	Factor 3
Cl	0.820	-	-
NO ₃	-	-	0.874
SO ₄	-	-	0.855
Na	-	0.802	-
NH ₄	-	-	0.971
K	-	0.823	-
Mg	-	0.811	-
Ca	-	0.933	-
V	0.960	-	-
Cr	0.784	-	-
Mn	0.863	-	-
Fe	0.885	-	-
Ni	0.853	-	-
Cu	0.729	-	-
Zn	-	0.995	-
As	0.79	-	-
Cd	-	0.996	-
Pb	-	0.941	-
Sources	Industrial and vehicular	Resuspended soil	Secondary Formation

Table 3. PCA analysis for PM₁ during winter

Species	Factor 1	Factor 2	Factor 3	Factor 4
Cl	-	0.991	-	-
NO ₃	0.977	-	-	-
SO ₄	0.970	-	-	-
Na	-	-	0.957	-
NH ₄	0.989	-	-	-
K	-	0.971	-	-
Mg	-	-	0.935	-
Ca	-	-	0.978	-
V	-	-	-	0.643
Cr	-	-	-	0.910
Mn	-	-	-	0.874
Fe	-	-	-	0.866
Ni	-	-	-	0.874
Cu	-	-	-	0.947
Zn	-	-	0.898	-
As	-	-	-	0.715
Cd	-	-	0.817	-
Pb	-	-	0.819	-
Sources	Secondary Formation	Coal and Biomass Burning	Resuspended soil	Industrial and Vehicular

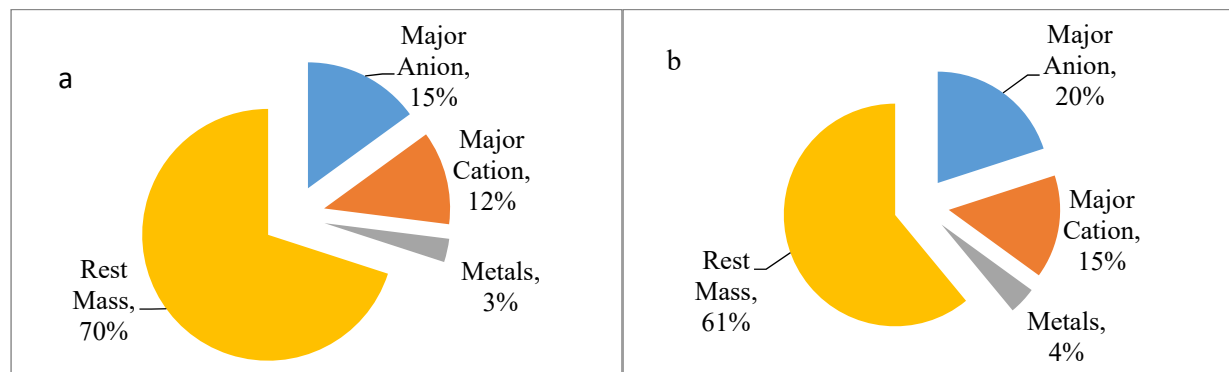


Figure 1. Mass percentage of major anions, major cations, metals and rest mass during (a) summer and (b) winter

CONCLUSIONS

PM₁ concentration at a suburban site of Agra was found to be 52.8±8µg/m³ during summer and 98±24µg/m³ during winter and characterized for water soluble ions and metals. Among water soluble ions: SO₄²⁻ was the most abundant ion followed by NO₃⁻, NH₄⁺ and Cl⁻ during summer and winter respectively. Among metals: Fe was the most abundant metal followed by Pb and Zn both during summer and winter. Major anions and major cations accounted for 15% and 12% during summer and 20% and 15% of PM₁ mass during winter. Metals accounted for 3% and 4% of PM₁ mass during summer and winter respectively. Factor analysis resolved three components during summer: industrial emissions, secondary formation and resuspended soil dust and four components during winter: industrial emissions, secondary formation, biomass and coal burning and resuspended soil dust.

ACKNOWLEDGEMENT

The authors are thankful to the Director, Dayalbagh Educational Institute, Agra and the Head, Department of Chemistry for necessary help. Authors gratefully acknowledge the financial support for this work which is provided by Department of Science and Technology (EMR/2016/001255).

REFERENCES

- Agarwal, A., A. Mangal, A. Satsangi, A. Lakhani and K.M. Kumari (2017). Characterization, sources and health risk analysis of PM_{2.5} bound metals during foggy and non-foggy days in sub-urban atmosphere of Agra. *Atmos Res*, **197**, 121-131.
- Deshmukh, D. K., M.K. Deb, Y.I. Tsai and S.L. Mkoma, (2011). Water soluble ions in PM_{2.5} and PM₁ aerosols in Durg city, Chhattisgarh, India. *Aerosol Air Qual. Res*, **11**, 696-708.
- Deshmukh, D. K., M.K. Deb, Y.I. Tsai and S.L. Mkoma, (2010). Atmospheric ionic species in PM_{2.5} and PM₁ aerosols in the ambient air of eastern central India. *Journal of atmospheric chemistry*, **66(1-2)**, 81.
- Franck, U., O. Herbarth, S. Röder, U. Schlink, M. Borte, U. Diez, and I. Lehmann (2011). Respiratory effects of indoor particles in young children are size dependent. *Sci Total Environ*, **409(9)**, 1621-1631.
- Hellsten, S., U. Dragosits, C. J. Place, M. Vieno, A. J. Dore, T. H. Misselbrook, Y.S. Tang and M. A. Sutton (2008). Modelling the spatial distribution of ammonia emissions in the UK. *Environ Pollut*, **154(3)**, 370-379.
- Izhar, S., A. Goel, A. Chakraborty and Tarun Gupta (2016). Annual trends in occurrence of submicron particles in ambient air and health risk posed by particle bound metals. *Chemosphere* **146**, 582-590.
- Satsangi, A., T. Pachauri, V. Singla, A. Lakhani and K.M. Kumari (2013). Water soluble ionic species in atmospheric aerosols: Concentrations and sources at Agra in the Indo-Gangetic Plain (IGP). *Aerosol Air Qual. Res*, **13**, 1877-1889.
- Singh, D.K. and T. Gupta (2016). Source apportionment and risk assessment of PM₁ bound trace metals collected during foggy and non-foggy episodes at a representative site in the Indo-Gangetic plain. *Sci Total Environ*, **550**, 80-94.
- Tao, J., Z. Shen, C. Zhu, J. Yue, J. Cao, S. Liu, Z. Lihua, and R. Zhang, (2012). Seasonal variations and chemical characteristics of sub-micrometer particles (PM₁) in Guangzhou, China. *Atmos Res*, **118**, 222-231.

Yubero, E., N. Galindo, J.F. Nicolás, J. Crespo, G. Calzolari and F. Lucarelli (2015). Temporal variations of PM₁ major components in an urban street canyon. *Environ Sci Pollut Res*, **22**(17), 13328-13335.

Zheng, J., K.H. Chen, X. Yan, S.J. Chen, G.C. Hu, X.W. Peng and Z.Y. Yang (2013). Heavy metals in food, house dust, and water from an e-waste recycling area in South China and the potential risk to human health. *Ecotoxicology and environmental safety*, **96**, 205-212.

AMBIENT PARTICULATE MATTER AND OZONE LEVELS AT A SUBURBAN SITE OF INDIA: INFLUENCE OF BIOMASS BURNING AND DUST STORM

SONAL KUMARI, ANITA LAKHANI, K. MAHARAJ KUMARI*

Department of Chemistry, Faculty of Science, Dayalbagh Educational Institute, Dayalbagh, Agra 282005, India

(*Correspondence at maharajkumari.k@rediffmail.com)

KEYWORDS: Pm_{2.5}, Ozone, Dust, Modis.

INTRODUCTION

Aerosols are important atmospheric pollutants that significantly influence the Earth's radiation budget by scattering as well as absorbing solar radiation (Ramanathan *et al.*, 2001). Dust is considered to be one of the major sources of tropospheric aerosol loading, and constitutes an important key parameter in climate aerosol-forcing studies (Kaufman *et al.*, 2002). Dust aerosols can influence atmospheric chemistry by affecting the photolysis rate coefficients through interaction with incoming solar radiation and by providing surface area for heterogeneous chemistry and deposition of different trace gases. Heterogeneous reactions on dust surfaces generally reduce the concentration of key atmospheric trace gases such as ozone (O₃), nitrogen oxides (NO_x), sulfur oxides and hydrogen oxides (Zhu *et al.*, 2010). Dust storms are major climate phenomena over India frequently originating in the north-western (NW) region of the Thar Desert, which has long been recognized as a primary source of atmospheric soil dust (Prasad and Singh, 2007). In Indo-Gangetic Plain (IGP) dust activity generally starts in March–April and peaks in May, i.e., prior to the onset of monsoon with strong pre-monsoon westerly winds transporting dust particles into the IGP region. Modeling studies have reported that heterogeneous chemistry on dust aerosol surface can reduce surface O₃ by 4-10% over northern Indian region (Baur *et al.*, 2004).

Every year, after harvest period large-scale burning of wheat residue is observed during April-May in the NW-IGP especially in the states of Punjab, Haryana, and western Uttar Pradesh, resulting in large-scale emission of aerosols and trace gases (Venkataraman *et al.*, 2006). Previous studies have reported that O₃ levels at downwind sites are affected by long range transport of O₃-rich air masses and/or long-range transport of O₃ precursors from fire active regions (Shan *et al.*, 2009).

In the present study, levels of PM_{2.5}, O₃, carbon monoxide (CO) and NO_x along with meteorological parameters are monitored to study the influence of a biomass burning and dust event over a suburban site of Agra.

METHODOLOGY

Measurements for the present study were carried out at a suburban site of Agra, Dayalbagh Educational Institute (27.16° N, 78.08° E) which is situated in the North-central part of India. Agra is surrounded by the Thar Desert on two-third of its periphery and has a semi-arid climate. Surface O₃, NO_x and CO were measured by continuously operating trace gas analyzers. O₃ levels were recorded using ultraviolet photometric O₃ analyzer (Thermo Scientific 49i) which functions on the absorption of UV radiation at 254 nm. NO_x analyzer (Thermo Scientific 42i) operates on the principle of chemiluminescence. The CO analyzer (Teledyne T300) operates on the principle of infrared (IR) absorption at 4.67 μm vibration-rotation band of CO. Meteorological parameters viz. wind direction, wind speed, temperature, relative humidity and

solar radiation were recorded at the sampling site using the Automatic Weather Station WM271 Data Logger at 1-h interval (Kumari *et al.*, 2018).

The fire count data was retrieved from MODIS instrument onboard Aqua and Terra satellites. The fire counts which have confidence value $\geq 80\%$ were selected to eliminate the chances of false fire detection (Giglio *et al.*, 2003).

Three-day (72 h) air-mass back trajectories for each hour at 100 m above ground level (AGL) were drawn using Geographical Information System (GIS) based Trajstat software (Wang *et al.*, 2009). The meteorological files for running the model were extracted from GDAS archive derived from NCEP global data assimilation system ($1 \times 1^\circ$). In addition, continuous measurement of $PM_{2.5}$ mass concentration was performed using a GRIMM-11C laser spectrometer. The instrument determines the particle matter level in 31 different grain size channels from 0.25 to 32 μm .

RESULT

The hourly time series plots of $PM_{2.5}$, O_3 , CO and NO_x during 5th-12th May, 2018 are shown in Fig. 1. During the study period, the average concentration of O_3 , CO, NO_x and $PM_{2.5}$ were 42.9 ± 23.3 ppb, 264.7 ± 226.4 ppb, 30.9 ± 23.1 ppb and 77.2 ± 28.7 $\mu g/m^3$. In the study period, two events with $PM_{2.5}$ levels above national ambient air quality standard (NAAQS) i.e $60 \mu g/m^3$ for 24 hours were observed. On 7th May (event 1) levels of $PM_{2.5}$ reached $173.2 \mu g/m^3$ (19.5% enhancement in peak value from previous day). Similarly, on 11th and 12th May $PM_{2.5}$ peak values reached $135 \mu g/m^3$. However, peak value of O_3 showed a decrease of 21.2 % on 8th May as compared to previous day while on 11th and 12th May O_3 values were higher (above 70 ppb during daytime). CO and NO_x levels on 8th May did not show any increasing trend, however, on 11th and 12th May higher values of both were observed.

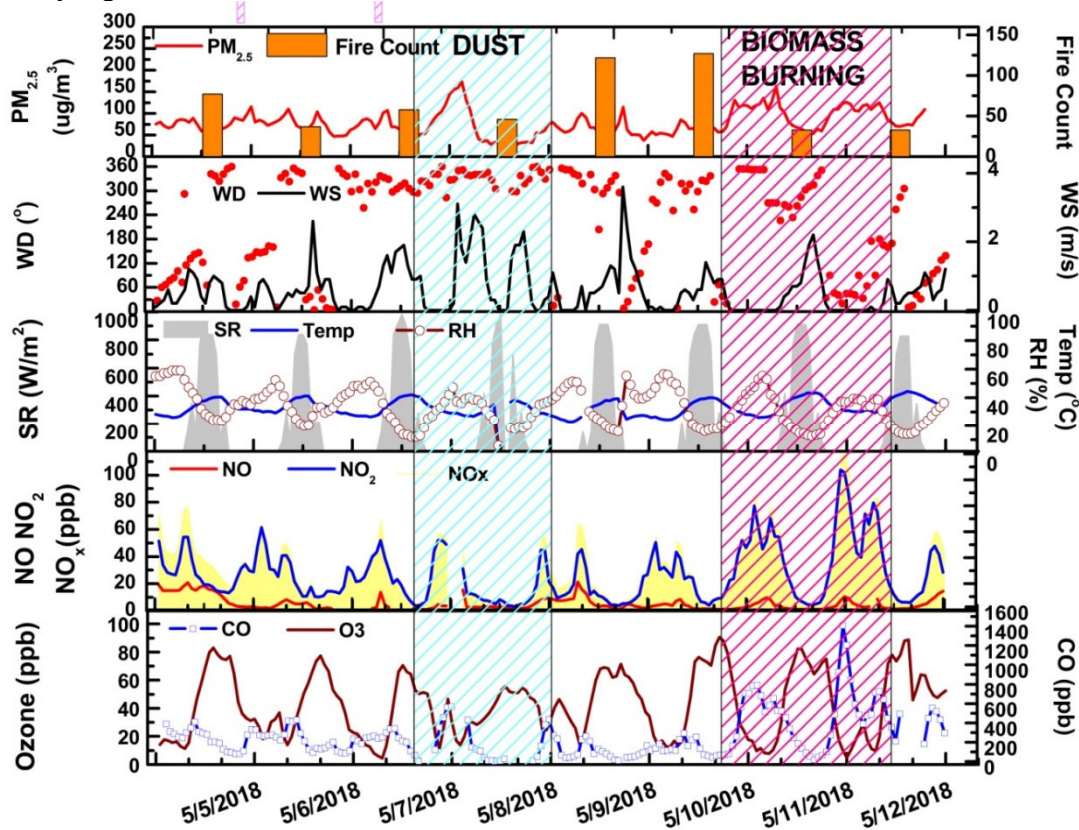


Figure 1. Hourly average mixing ratios of O_3 , CO, NO_x , $PM_{2.5}$, windspeed (WS), wind-direction (WD), solar radiation (SR), temperature (Temp), relative humidity (RH) and fire count at Agra. Shaded region represents the dust and biomass burning event.

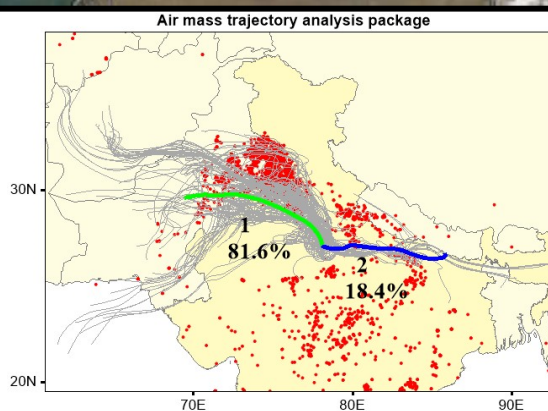
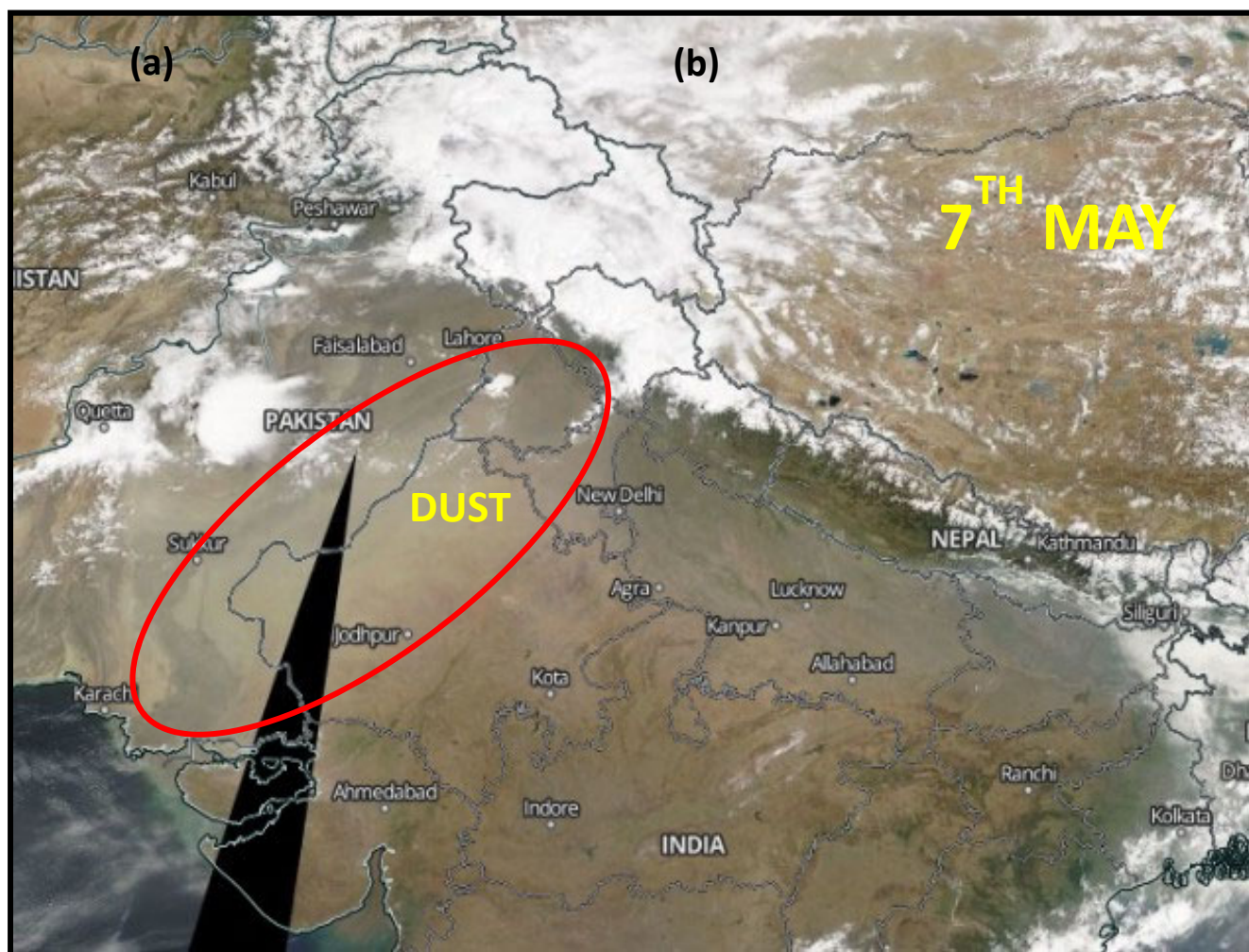


Figure 2. (a) True colour image observed over North India by MODIS on 7th May, 2018, (b) Three-day back-air trajectories during the study period at Agra and fire counts detected by MODIS

As meteorological parameters play an important role in trace gas levels (Ojha *et al.*, 2012), therefore, solar radiation, temperature, wind speed, wind direction, and relative humidity were monitored during the study period (Fig. 1). The average levels of relative humidity, temperature and wind speed were $35.8 \pm 4.9\%$, $32.6 \pm 1.6\text{ }^\circ\text{C}$ and $0.6 \pm 0.2\text{ m/s}$, respectively. During the study period, the predominant wind direction was NW. Similar to O_3 levels, a drop in solar radiation and relative humidity was observed on 8th May.

In order to investigate the variability of O₃ levels and the influence of long-range transport of air masses, 72 h backward trajectories at 1h interval were computed for the study period (Fig.2b). The trajectories arriving at the study site were classified into different clusters on the basis of change in TSV (total spatial variance). During the study period, the highest frequency of trajectories was observed in cluster-1 (81.6%) in which air masses predominantly originated from the NW-IGP while 18.4 % trajectories arrive from north-east region of the study site. The trajectories from NW-IGP reach the study site after travelling over Thar Desert, the potential source of dust. MODIS on 7th May recorded a dust event over Northern India (Fig. 2a). In the study period, several crop-residue burning activities were observed by MODIS over NW-IGP region. During the study period, the daily distribution of MODIS fire counts in the NW-IGP (26–33° N, 72–80° E) was considered (Fig.1). In the study region, 500 fire counts were detected during the study period with intense fire activities on 9th and 10th May. This suggests that the level of air pollutants at the study site can be affected by biomass burning activities and dust event.

Aerosol can affect O₃ concentration by absorbing or scattering solar radiation which causes change in photolysis rates, and also aerosols can influence the trace gas chemistry by providing surface for heterogeneous chemical reactions (Jacobson, 1998). A sudden drop in O₃ levels on 8th May after a dust event was observed. This suggests that high concentrations of coarse mineral aerosol in the atmosphere may lead to significant heterogeneous O₃ destruction on the particle surface, thereby affecting the O₃ concentrations even in areas very far away from the dust regions. Biomass burning can produce various chemical species such as CO, CO₂, hydrocarbons, aldehyde, aerosols and organic acids which can be transported to downwind sites and can influence the O₃ levels (Andreae, 1991; Sharma *et al.*, 2010). CO is considered as a biomass burning tracer which can be transported from fire active region to distant sites due to its long lifetime (~2 months). During event 2, high CO levels along with high levels of O₃, NO_x and PM_{2.5} were observed. Thus, high O₃ levels on 11th and 12th May can be attributed by fire activities observed on 9th and 10th May in NW-IGP.

CONCLUSION

The variations in ambient concentrations of O₃, PM_{2.5}, NO_x and CO were examined at a suburban site of Agra during 5th-12th May, 2018. Biomass burning and long-range transport of air pollutants contributed significantly to high O₃ levels during the study period. In addition to this, effect of a windblown dust was observed on O₃ levels resulting into reduction of 21.2% O₃ peak value.

ACKNOWLEDGEMENT

The authors are thankful to the Director, Dayalbagh Educational Institute, Agra and the Head, Department of Chemistry for necessary help. The authors gratefully acknowledge the financial support for this work which was provided by ISRO GBP under AT-CTM project.

REFERENCES

- Andreae, M.O. (1991). Biomass burning: its history, use, and distribution and its impact on environmental quality and global climate. In: Levine JS (ed) Global biomass burning, atmospheric, climatic, and biospheric implications. MIT Press, Cambridge, MA, 3–21.
- Bauer, S.E., Y. Balkanski, M. Schulz, D.A. Hauglustaine and F. Dentener (2004). Global modeling of heterogeneous chemistry on mineral aerosol surfaces: Influence on tropospheric ozone chemistry and comparison to observations, *J. Geophys. Res.*, 109, D02304, doi:10.1029/2003JD003868.
- Giglio, L., J. Descloitres, C.O. Justice and Y.J. Kaufman (2003). An enhanced contextual fire detection algorithm for MODIS. *Remote Sens Environ.*, 87(2):273–282.

Jacobson, M.Z. (1998). Studying the effects of aerosols on vertical photolysis rate coefficient and temperature profiles over an urban airshed, *J Geophys Res*, **103** 10593–10604.

Kaufman, Y.J., D. Tanrè and O. Boucher (2002). A satellite view of aerosols in the climate system. *Nature* 419, 215–223.

Kumari, S., N. Verma, A. Lakhani, S. Tiwari and K.M. Kandikonda, (2018). Tropospheric ozone enhancement during post-harvest crop-residue fires at two downwind sites of the Indo-Gangetic Plain. *Environ Sci Pollut Res*, 1-15.

Ojha, N., M. Naja, K.P. Singh, T. Sarangi, R. Kumar, S. Lal, M.G. Lawrence, T.M. Butler, H.C. Chandola (2012). Variabilities in ozone at a semiurban site in the Indo-Gangetic Plain region: association with the meteorology and regional processes. *J Geophys Res*, D20:117.

Prasad, A. K., and R. P. Singh (2007). Changes in aerosol parameters during major dust storm events (2001-2005) over the Indo-Gangetic Plains using AERONET and MODIS data, *J Geophys Res*, 112, D09208, doi:10.1029/2006JD007778.

Ramanathan, V., P.J. Crutzen, J. Lelieveld, A.P. Mitra, D. Althausen, J. Anderson, M.O. Andreae, W. Cantrell, G.R. Cass, C.E. Chung, and A.D. Clarke, (2001). Indian Ocean Experiment: An integrated analysis of the climate forcing and effects of the great Indo-Asian haze. *J Geophys Res*, 106(D22), pp.28371-28398.

Shan, W., Y. Yin, H. Lu, and H. Liang S (2009). A meteorological analysis of ozone episodes using HYSPLIT model and surface data. *Atmos Res* 93(4): 767–776.

Sharma, A.R., S.K. Kharol, K.V. Badarinath and D. Singh (2010). Impact of agriculture crop residue burning on atmospheric aerosol loading—a study over Punjab State, India. *Ann Geophys: Atmos Hydrospheres Space Sci* 28(2):367–379.

Venkataraman, C., G. Habib, D. Kadamba, M. Shrivastava, J.F. Leon, B. Crouzille, O. Boucher and D.G. Streets, (2006). Emissions from open biomass burning in India: integrating the inventory approach with high-resolution moderate resolution imaging spectroradiometer (MODIS) active-fire and land cover data. *Glob Biogeochem Cycles* 1(2):20.

Wang, Y.Q., X.Y. Zhang and Draxler Roland R, (2009). TrajStat: GIS-based software that uses various trajectory statistical analysis methods to identify potential sources from long-term air pollution measurement data. *Environ Model Softw* 24:938–939.

Zhu, S., T. Butler, R. Sander, J. Ma and M.G. Lawrence, (2010). Impact of dust on tropospheric chemistry over polluted regions: a case study of the Beijing megacity, *Atmos Chem Phys*, 10, 3855– 3873.

ESTIMATION OF CARBONACEOUS AEROSOLS AT INDOOR ENVIRONMENT OF CAFETERIA DURING WINTER SEASON IN DELHI, INDIA

P. MANDAL¹, SRI NAGESH M², A. MANDAL²

¹CSIR – National Environmental Engineering Research Institute, Delhi Zonal Centre, Naraina Industrial Area, New Delhi -110028, India

²Department of Environmental Engineering, Delhi Technological University, Shahbad Daulatpur Village, Rohini, Delhi-110042

KEYWORDS: Aerosol, Indoor Air Pollution, Particulate Matter,

Delhi INTRODUCTION

Despite arduous efforts put in research, the predominant sources contributing to indoor air pollution remained debatable. This is because, unlike other dining restaurants, cooking is carried out throughout the day in cafeteria. It is evident from this study that inflated concentrations of particulate matter (PM₁₀), primary organic carbon (OC) and elemental carbon (EC) prevailed in Cafeteria. The OC, a submicron particle (L M Castro, 1999) of combustion, and EC, an essential primary pollutant (Kripa Ram, 2008) emitted by incomplete combustion of fossil fuels (Abdus Salam, 2003), are the significant contributors to particulate matter (Di Ye, 2007). Yearlong observation of concentration of OC and EC by various researchers revealed a trend in indoor air pollution which is particularly high during winter season and low during the monsoon season. Traditionally, studies were carried out at outdoor environment and in classrooms (semi-outdoor environment), but people who spend their maximum time indoors (such as in offices, cafeterias and houses) are exposed to greater concentrations of pollutants in urban areas (K F Ho, 2004). Effort was made to put-forth the scenario of PM₁₀ (particulate matter 10 micrometers or less in diameter) and total carbon (carbonaceous aerosol) that comprised OC and EC during the winter season at cafeteria located in Rohini West in North-West district of Delhi.

METHODS

The cafeteria is located at the ground level, faced to major arterial roads. The sampling of PM₁₀ was carried out inside the cafeteria during the winter season (December 2014 to February 2015). The precautionary measures were taken not to expose the sampler directly to the outdoor environment. The sampler was placed at the juncture of dining and kitchen activities, within the premises of the cafeteria. The sampling location is shown in Figure 1.

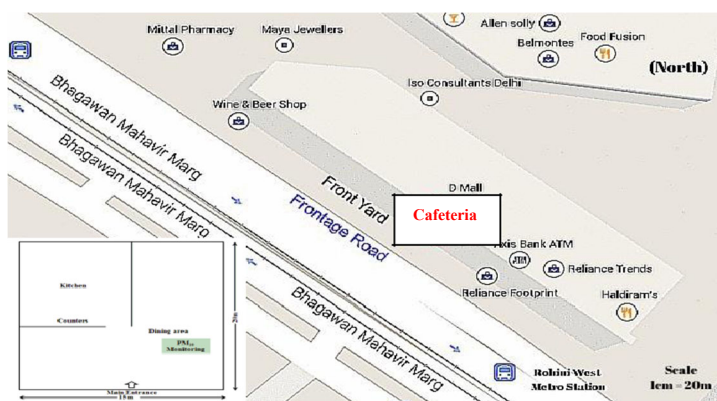


Figure 1. Sampling location of PM₁₀ monitoring at Cafeteria (Rohini, West).

PM₁₀ samples were collected on Whatman and Micro fiber quartz filter papers during the peak hours (1:00 p.m. to 4:00 p.m.) claimed by the cafeteria manager at a flow rate variation of 2.4 lpm to 3.0 lpm using APM 800 sampler (make Envirotech Pvt. Ltd., Delhi, India) both weekdays and weekends of the study period. The filter papers were pre-baked in a muffle furnace at 550°C for 6 hours only to remove organic impurities. They were also pre-desiccated and post-desiccated for 24 hours. The concentrations of PM₁₀ (µg/m³) were measured by gravimetric method using Sartorius Microbalance with accuracy till six decimals. OC and EC analyses were carried through Carbon Analyzer by Interagency Monitoring of Protected Visual Environment (IMPROVE) TOR (Thermal Optical Reflectance) protocol (The DRI Model 2001). The basic principle of the analyzer is to oxidize OC and EC at different temperatures to get their respective fractions. Analysis sequence of the IMPROVE protocol is OC, pyrolyzed carbon fraction (PY) and EC. OC is further divided into OC1, OC2, OC3, and OC4 at temperatures 140°C, 280°C, 480°C and 580°C respectively; and EC is further divided into EC1, EC2 and EC3 at temperatures 580°C, 740°C and 840°C respectively and analyzed. Predefined OC by the IMPROVE protocol is: OC = OC1 + OC2 + OC3 + OC4 + PY. Similarly, EC is predefined as: EC = EC1 + EC2 + EC3 – PY (Seung S Park, 2002 and Judith C Chow, 2012).

Meteorological parameters (such as temperature, wind speed, wind direction, relative humidity, etc.) were collected from the India Meteorological Department and from the Bhuvan Panchayat developed by NRSC – ISRO (2014). During the monitoring period (December 2014 to February 2015), the minimum and maximum temperatures varied between 2°C and 29°C respectively. During this period the average temperature of Delhi was 13°C, the average relative humidity was 60%, the wind speed was 4.00 knots and the prevailing wind directions were west and north-west in directions. The Wind Rose Plot over Delhi during the sampling period (December 2014 to February 2015) is shown in Figure 2.

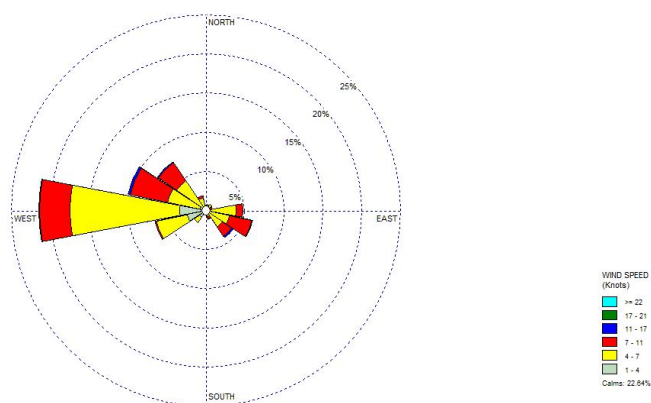


Figure 2. The Wind Rose Plot over Delhi (December 2014 to February 2015).

RESULTS & DISCUSSIONS

The collected samples were analyzed for PM₁₀, OC, EC and TC for both weekdays and weekends of the study period, to compare the maximum concentrations of indoor air pollution at cafeteria during the winter season. The maximum concentration of particulate matter (PM₁₀=3448 µg/m³), organic carbon (OC = 461µg/m³), elemental carbon (EC=114 µg/m³) and total carbon (TC=534µg/m³) respectively were observed during the winter period (December 2014 to February 2015). The concentrations of PM₁₀ were beyond the permissible limit (150µg/m³) of National Ambient Air Quality Standards (NAAQS) formulated by United States Environmental Protection Agency (USEPA, 2014). No standards or guidelines were established till date in India to control the increasing PM₁₀ concentration at indoor environment. A few studies have been carried out in India regarding the concentrations of air pollutants with respect to PM₁₀, and its correlation with carbonaceous aerosols. Till date no standard has been

formulated for the parameters of carbonaceous aerosols (OC, EC and TC). The statistics of concentrations of PM₁₀, OC, EC and TC at cafeteria, during the study period is shown in Table.1.

Days	PM ₁₀ (µg/m ³)	OC (µg/m ³)	EC (µg/m ³)	TC (µg/m ³)
Weekdays				
Min	2132	68	14	82
Max	3278	461	73	534
Average	2725	175	36	211
Weekends				
Min	1792	74	15	89
Max	3448	194	114	308
Average	2740	147	46	193

Total Sampling days N = 20 Days

Table 1. The statistics of concentrations of PM₁₀, OC, EC and TC at cafeteria, Rohini during during the study period (December 2014 to February 2015).

It was observed that meteorological parameter like wind speed and wind direction were the influential parameters to increase indoor concentration of PM₁₀, OC, EC and TC, due to frequent opening of doors on that particular day to accommodate maximum customers. OC was always the dominating component in TC than EC. PM₁₀ and EC concentrations were maximum in weekends days as compared to weekdays where as OC and TC concentrations were maximum in weekdays as compared to weekends observed during the study period. Impact of OC concentration both indoor and outdoor environment might be influenced by biomass combustion, traffic movement and long range transportation of air pollutants (Saarikoski, 2008), whereas, concentration of EC in atmosphere due to incomplete combustion of fossil fuels and industrial activities (Sziadat, 2008). The percentage of OC in TC, and EC in TC and TC in PM₁₀ were varied from 63 to 86%, 14 to 37% and 4 to 16% respectively.

CONCLUSIONS

The study revealed that following conclusion

Carbonaceous aerosols with respect to organic carbon (OC), elemental carbon (EC) and total carbon (TC) in particulate matter (PM₁₀) were the important constituents at indoor environment of cafeteria.

Indoor Air Pollution with respect to PM₁₀ concentrations is the severe problem of cafeteria especially at road side area.

The concentrations of carbonaceous aerosols influenced by meteorological parameters (wind speed and wind directions) and human interference or the guest count in the cafeteria

ACKNOWLEDGEMENTS

This work was supported by the Director, CSIR-NEERI, Nagpur.

REFERENCES

- Bhuvan Panchayats – Space based Information Support for Decentralized Planning (SIS – DP) <http://bhuvan-panchayat.nrsc.gov.in>. Accessed December 18, 2015.
- Castro, L.M and , Pio, C.A (1999). *Carbonaceous aerosol in urban and rural European atmospheres: estimation of secondary organic carbon concentrations*, (Atmospheric Environment 33: 2771-2781)
- Chow, J. C., Watson J.G (2012) *The IMPROVE_A temperature protocol for thermal/optical carbon analysis: maintaining consistency with a long-term database*, (Journal of the Air and Waste Management Association 57:9, 1014-1023).
- Ho, K.F, Cao, J.J (2004). *Indoor/outdoor relationships of organic carbon (OC) and elemental carbon (EC) in PM_{2.5} in roadside environment of Hong Kong*, (Atmospheric Environment 38: 6327-6335).
- Park, S. S. and Kim. Y.J (2002). *PM_{2.5} carbon measurements in two urban areas: Seoul and Kwangju, Kore.* (Atmospheric Environment 36: 1287-1297).
- Ram, K. and Sarin, M.M (2008). *Atmospheric abundances of primary and secondary carbonaceous species at two high-altitude sites in India: sources and temporal variability*, (Atmospheric Environment 42: 6785-6796).
- Saarikoski, S., Timonen H., Saarnio K., Aurela M., Jarvi L., Keronen, P., Kerminen, V. M. and Hillamo, R (2008). *Sources of organic carbon in fine particulate matter in northern European urban air*, (Atmospheric Chemistry and Physics, 8, 6281 – 6295).
- Salam, A. and Bauer, H (2003). *Aerosol chemical characteristics of a mega-city in Southeast Asia (Dhaka–Bangladesh)*, (Atmospheric Environment 37: 2517-2528).
- Szidat. S. and Ruff M (2009). *Fossil and non-fossil sources of organic carbon (OC) and elemental carbon (EC) in Goteborg, Sweden*, (Atmospheric Chemistry and Physics 9: 1521-1535).
- Ye. Di and Zhao, Qi (2007). *Characteristics of elemental Carbon and organic carbon in PM₁₀ during spring and autumn in Chongqing, China*, (China Particuology 5: 255-260).

IMPACT OF ENVIRONMENTAL BIO-AEROSOL POLLUTION ON HUMAN HEALTH: A “FOLLOW UP STUDY” ON EXACERBATION OF COPD

PALAK BALYAN^{1*}, CHIRASHREE GHOSH¹, ARUN KUMAR SHARMA², RAJNISH AWASTHI³ &
B. D. BANERJEE⁴

¹Environmental Pollution Laboratory, Department of Environmental Studies, University of Delhi.

²Department of Community Medicine, University College of Medical Sciences (UCMS), University of Delhi.

³Department of Pulmonary Medicine, University College of Medical Sciences (UCMS), University of Delhi.

⁴Department of Biochemistry, University College of Medical Sciences (UCMS), University of Delhi.

KEYWORDS: Bio-aerosol, Human health, COPD, Exacerbation & Follow-up study.

INTRODUCTION

Health manifestation of bioaerosols exposure remained limited to identification of symptoms and effect of bioaerosols exposure on pulmonary capacities at conventionally established high bioaerosols emission sites like compost site, dumping sites, sewer drains etc. Detailed information on the effect of exposure of bioaerosols on human respiratory dysfunction is yet to be explored and documented (Kampen *et al.*, 2014). Although several studies have been already shown air as most common and putative route of transmission of respiratory microbes but it is still not conclusively established that aerosolised bacterial exposure causes deterioration in COPD (Pusz *et al.*, 2015). The present study examines the role of bioaerosol exposure in the occurrence of exacerbations of COPD.

METHODOLOGY

A cohort of 50 COPD patients were recruited and followed for a period of one year. Location of residence of patients geocoded on a digital map of study area using a GPS device. The patients were grouped into five clusters based on proximity. Each patient was contacted by a personal visit once in a fortnight to record an episode of acute exacerbation of COPD and indoor and outdoor bioaerosol levels were measured fortnightly for each grid. In this manner data collection was carried out for 1 year. Data in relation to weather parameters like temperature and relative humidity and count of aerosolised bacteria and fungi were collected simultaneously for each cluster. Similarly, air pollution data on PM were obtained from DPCC and IBHAS monitoring station. The number of COPD exacerbation in cohort was measured and their incidence density was also calculated, beside this spatio-temporal extent and variability were analysed using heat maps.

RESULT

Spatial extent and incidence density of COPD exacerbation increases with rise in aerosolized bacteria and PM_{2.5} concentration and also with fall in temperature. Relative humidity and aerosolized fungal exposure were recorded not to be associated with COPD exacerbation. Parsimonious regression model was generated for all studied variables, aerosolized bacteria and decrease in temperature were found to significantly increase the probability of occurrence of COPD exacerbation. The effect of PM_{2.5} was nearly significant. The generalised estimated equation showed no significant association between other socio-economic covariates and episodes of COPD, thus suggesting the possibility of confounding the effects of these variables.

CONCLUSION

The COPD exacerbation episodes increase with the rise in aerosolised bacteria count, PM_{2.5} and fall in temperature. The relationship was non-conclusive with relative humidity and aerosolised fungal count. Thus, the intervention leading to a fall in the count of aerosolised bacteria may lead to decrease in COPD exacerbation episodes, especially during winter season and hence, will improve quality of life of COPD

patients. Further, long duration research with large sample should be designed and conducted to understand the long-term sequelae of bioaerosols exposure on patients with respiratory morbidities to generate further evidence for advocating measures to reduce bioaerosols exposure.

ACKNOWLEDGEMENT

Authors are thankful to Ministry of Environment, Forest and Climate change (MoEF), Govt. of India for supporting the research work financially.

REFERENCES

Kampen V, Sander I, Liebers V, Deckert A, Neumann HD, Buxtrup M, Willer E, Felten C, Jäckel U, Klug K, Brüning T. Concentration of bioaerosols in composting plants using different quantification methods. *Annals of occupational hygiene*. 2014;58(6):693-706.

Pusz W, Płaskowska E, Weber R, Kita W. Assessment of the abundance of airborne fungi in cattle barn of dairy farm. *Polish Journal of Environmental Studies*. 2015;24(1):241-8.

POTENTIAL OF URBAN VEGETATION IN ATTENUATING ATMOSPHERIC PARTICULATE POLLUTION

P. SHARMA AND C.GHOSH

Environmental Pollution Laboratory, Department of Environmental Studies, University of Delhi, Delhi

KEYWORDS: Particulate Matter, Attenuation, Deposition, Vegetation Etc.

INTRODUCTION

Urban areas are experiencing greater environmental stress because of increasing population and vehicular growth, which is transforming local air quality and making it unfit for human health. Several studies have been recorded and established that urban vegetation has significant potential in mitigating air pollutants and improving air quality (Setala *et al.*, 2013, Rai *et al.*, 2015). A well planned urban green space is a cost effective clean development method to control air pollution. In urban areas trees along road side and vegetated areas acts as an important receptor of atmospheric particulate pollutants and plays an efficient role as a filter for remediation of air pollutants. The foliar surface of such tree species deposit atmospheric particles, however, the particulate retention capacity on the leaf surface depends on particle size, deposition rate and texture of leaf surface (Harrison and Yin, 2000). The present study aims to evaluate the potential of selected tree species in depositing atmospheric particulate matter on their foliar surface and to analyse the role of a naturalized vegetation cover in attenuating particulate pollution.

METHODS

For studying the potential of urban vegetation in attenuating the atmospheric particulate matter the vegetated area of Northern ridge (the smallest segment of Delhi's ridge) was selected as the model study site. Northern ridge spread in an area of 87 hectares and has a close proximity to ring road which has a heavy traffic density with approximately 79 ± 14 vehicles per minute.

Particle Deposition Capacity of Selected Tree Species

Naturalized and common evergreen tree species were identified and selected for the study and total of three replicates for each of the selected tree species were maintained (Table 1). Dust capturing capacity by the foliar surface of selected tree species was calculated using the method of Prusty *et al.* (2005).

Table 1: Description of Selected Tree Species

S.No	Common Name	Scientific Name	Family
1	Banyan	<i>Ficus benghalensis</i>	Moraceae
2	Putranjiva	<i>Putranjiva roxburghii</i>	Putranjivaceae
3	Jamun	<i>Syzygium cumini</i>	Myrtaceae
4	Ashok	<i>Polyalthia longifolia</i>	Annonacea

Attenuation of Particulate matter by urban green cover

Taking ring road as a major source of pollution near Northern ridge green zone, the pollution attenuation was calculated at two distances, i.e., 50m away and 100m away from the source inside the vegetated ridge area.

The PM monitoring was done thrice a month **at the Source**, 50 m and 100 m **away from the source** during peak traffic hour from 9:00 am – 11:00 am using Dust (PM) Analyzer (Grimm – 11A, Germany), which recorded reading at every 1 minute interval for different particle sizes, PM₁₀, PM_{2.5}, PM₁ and PM_{0.25}.

Monitoring was conducted during summer (May and June) and Monsoon months (July and August) and attenuation factor of green areas was calculated based on the method given by Islam *et al.*, 2012.

RESULT AND DISCUSSION:

Particle Deposition capacity of selected tree species

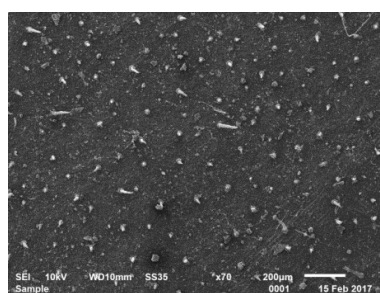
Variation observed in the dust capturing capacity of the selected species showed that Banyan had the highest dust capturing capacity (1.27 mg/cm²) followed by Jamun (0.73 mg/cm²), Putranjiva (0.39 mg/cm²), and the least capacity was reported for Ashok (0.38 mg/cm²) (table 2)

Table 2: Dust Capturing Capacity of the Selected Tree Species

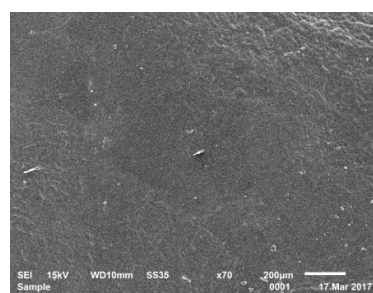
	<i>Ficus benghalensis</i> (Banyan)	<i>Putranjiva roxburghii</i> (Putranjiva)	<i>Syzygium cumini</i> (Jamun)	<i>Polyalthia longifolia</i> (Ashok)
Dust Capturing Capacity (mg/cm²)	1.27 ^a	0.39 ^b	0.73 ^{a b}	0.38 ^b

a and b are significantly different concentration at 0.05 level of significance

The outcome of the study showed that even in similar micro climatic conditions different tree species can have different potential to capture atmospheric particulate matter. Plant species differ in their ability to scavenge dust-laden air depending on several factors including canopy type, leaf and branch density, and specially leaf morphology like shape, size, structure, roughness, trichomes and stickiness of foliar surface (Prajapati and Tripathi, 2007; Sgrigna *et al.*, 2015). It was interesting to observe that trees like *Ficus benghalensis* (Banyan) with rough foliar was better in trapping particulate pollutant compared to smooth foliar surface trees like *Polyalthia longifolia* (Ashok). The Scanning electron microscopy study depicts that foliar surface of *Ficus benghalensis* was rich with trichomes where as *Polyalthia longifolia* exhibited smooth surface (Figure 1).



Ficus benghalensis



Polyalthia longifolia

Figure 1: SEM images of Ventral (Front) side of the foliar surface of selected plant species.

Attenuation of Particulate matter by urban green cover

Attenuation factor calculated for the vegetated area at 50m and 100m away from the source for different size particles showed that during summer months negative attenuation factor for PM₁₀ was reported at 50m away inside green area whereas, all other fine size particles (PM_{2.5}, PM₁ and PM_{0.25}) showed positive attenuation at 50m and 100m distance away from the source site. The probable reason for such observation could be that during summer month the higher coarse particle are generated from soil due to dust re-

suspension in vegetated area under the influence of high wind movement. Interestingly it was also observed that attenuation of particulate matter increases with distance away from the source and was reported to be more at 100m away from the source, which was predominant for fine particles as they can travel longer distance with air; contrary to coarser particle which settle quickly because of their large size.

Table 3: Seasonal Attenuation Factor

	Summer		Monsoon	
	50m	100m	50m	100m
PM ₁₀	-2.50	3.68	17.44	11.34
PM _{2.5}	9.45	10.72	11.05	11.86
PM ₁	8.96	10.56	12.99	18.81
PM _{0.25}	9.57	12.22	10.05	13.61

Beside this seasonal attenuation factor depicted to be more in monsoon as compared to summer months (Table 3). The probable reason for such observation is that during monsoon season dispersion rates are lower as compared to deposition rate because of condensation and hygroscopic growth of particles which increases with relative humidity (Rissler *et al.*, 2006). The increased attenuation factor during monsoon month was also attributed to the increased vegetation density after rainfall, as lot of trees flourish during that time; this increases the rate of particle deposition and attenuation by plant species. Coceal and Belcher, (2005) stated that the flourished leaves and branches and the dense greenbelt structure with shrubs and large trees slow down the airflow and trap the particulate matters.

CONCLUSION

The study depicts that naturalized tree species in an urban area plays an important role in depositing particulate matter on their foliar surface, however different tree species differ in their dust deposition potential owing to foliar morphological traits. Also, it could be inferred from the study that natural urban green areas significantly attenuate atmospheric particulate matter however, the particle deposition and attenuation is influenced by seasonal meteorological factors.

ACKNOWLEDGEMENT

The authors would like to acknowledge MOES and UGC for funding the work.

REFERENCES

- Coceal, O., & Belcher, S. E. (2005). Mean winds through an inhomogeneous urban canopy. *Boundary-Layer Meteorology*, 115(1), 47-68.
- Harrison, R. M., & Yin, J. (2000). Particulate matter in the atmosphere: which particle properties are important for its effects on health?. *Science of the total environment*, 249(1-3), 85-101.
- Islam, M. N., Rahman, K. S., Bahar, M. M., Habib, M. A., Ando, K., & Hattori, N. (2012). Pollution attenuation by roadside greenbelt in and around urban areas. *Urban Forestry & Urban Greening*, 11(4), 460-464.
- Prajapati SK, Tripathi BD (2007) Biomonitoring trace elements levels in PM10 released from vehicles using leaves of Saracaindica and Lantana Camara. *Ambio* 36:704–705
- Prusty, B. A. K., Mishra, P. C., & Azeez, P. A. (2005). Dust accumulation and leaf pigment content in vegetation near the national highway at Sambalpur, Orissa, India. *Ecotoxicology and Environmental Safety*, 60(2), 228-235.

- Rai, P. K. (2016). Biodiversity of roadside plants and their response to air pollution in an Indo-Burma hotspot region: implications for urban ecosystem restoration. *Journal of Asia-Pacific Biodiversity*, 9(1), 47-55.
- Rissler, J., Vestin, A., Swietlicki, E., Fisch, G., Zhou, J., Artaxo, P., & Andreae, M. O. (2006). Size distribution and hygroscopic properties of aerosol particles from dry-season biomass burning in Amazonia. *Atmospheric Chemistry and Physics*, 6(2), 471-491.
- Setälä, H., Viippola, V., Rantalainen, A. L., Pennanen, A., & Yli-Pelkonen, V. (2013). Does urban vegetation mitigate air pollution in northern conditions? *Environmental Pollution*, 183, 104-112.
- Sgrigna, G., Sæbø, A., Gawronski, S., Popek, R., & Calfapietra, C. (2015). Particulate Matter deposition on *Quercus ilex* leaves in an industrial city of central Italy. *Environmental pollution*, 197, 187-194.

ESTIMATION OF RADIATIVE FORCING DUE TO CARBONACEOUS AEROSOLS: THEIR CLIMATE FEEDBACK

AJAY P.¹, B. PATHAK^{1,2}, T. SUBBA¹, V. S. NAIR³, P.K. BHUYAN¹

¹Centre for Atmospheric Studies, Dibrugarh University, Dibrugarh 786004, India

²Department of Physics, Dibrugarh University, Dibrugarh 786004, India

³Space Physics Laboratory, Vikram Sarabhai Space Centre, Thiruvananthapuram 695022, India

KEYWORDS: Regcm, Black Carbon, Organic Carbon, Radiative Forcing, Cloud Liquid Water Path

INTRODUCTION

Carbonaceous aerosols are significant component of atmospheric aerosols, as they are potentially capable of regional climate change. Organic Carbon (OC) and Black Carbon (BC) are the two fractions of carbonaceous aerosols with antagonistic radiative properties. BC displays high absorbing characteristics whereas OC mainly contributes to surface cooling. Climatic significance of both BC and OC is very high both in regional and global scales. Along with that their reduction can also expect to enhance the health conditions considerably. Exact impacts of BC and OC over climate effects are not yet well understood initiating several observational and modeling studies globally.

In this study, we simulate the distribution of carbonaceous aerosols over Indian subcontinent with and without feedback to model meteorology using a high-resolution regional climate model (RCM), RegCM4.4. The Radiative effect of composite and constituent carbonaceous aerosols is also estimated to reveal the perturbation in solar radiation flux.

DATA AND METHODOLOGY

An upgraded version of Fourth generation regional climate model RegCM4 (Giorgi et al., 2012) of International Centre for Theoretical Physics (ICTP), RegCM 4.4 is used for the study. Regional emission inventory, REAS (Ohara et al., 2007) is used for the present study as it was reported RegCM simulations with REAS perform better over South Asia as reported by earlier studies (Nair et al., 2012). The simulation domain follows the Coordinated Regional Downscaling Experiment (CORDEX) project over South Asia with 160×216 grid points over North to South and West to East directions respectively. All the simulations follow a horizontal grid spacing of 50 km with 18 vertical sigma-pressure levels. Mercator-rotated projection is used for the simulations driven by ERA-Interim reanalysis (EIN 75) providing six hourly data. We carried out three simulations with RegCM 4.4 for the period 1st January 2008 to 1st January 2011 where the first year simulation is considered as spin-up period and hence not included for analysis. Details of all simulations along with the purpose are listed in Table 1.

Table 1: RegCM 4.4 Simulations and experimental descriptions

Simulation	Description
CONT	Control run to evaluate basic climatic evaluation without aerosol effect
OC+BC	Simulation of carbonaceous aerosols (OC and BC) allowing feedbacks on radiative, thermodynamic and dynamic fields.
BC	Simulation of only Black Carbon (BC) allowing feedbacks on radiative, thermodynamic and dynamic fields.

RESULTS & DISCUSSIONS

Distribution of carbonaceous aerosols

In Fig. 1 the mean BC and OC distribution during the years, 2009 and 2010 acquired from OC+BC simulation are shown. Fig. 4a shows that largest surface concentration of BC occurred over Indo- Gangetic Plains (IGP) region, which is reported earlier as a BC hot spot region. The maximum value of BC ranges around $3 \mu\text{g}/\text{m}^3$ over the IGP region.

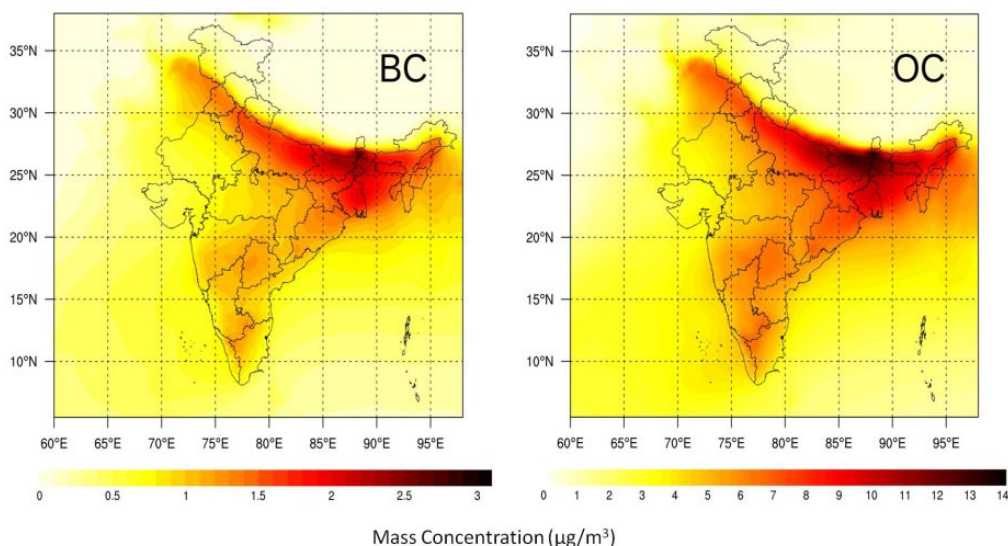


Figure. 1 Annual spatial variation of BC (left panel) and OC (right panel) distribution over the Indian sub-continent..

Concentration over North East India (NEI) is within $0.5 - 2 \mu\text{g}/\text{m}^3$. With left part opened to extremely polluted IGP region and remaining main land, aerosols can easily get transported to the NEI which has been studied and reported earlier (Pathak et al. 2016). Over the main land, the concentration exceeds $1 \mu\text{g}/\text{m}^3$ where as in oceanic region concentration remains less than $1 \mu\text{g}/\text{m}^3$. From the Fig 4b showing the concentration of OC it is evident that its distribution is similar to that of BC over the region but with very high concentration than its co-emission which is reported by previous studies (Ohara et al., 2007). The highest OC concentration is also around the IGP region with value peaking around $13 \mu\text{g}/\text{m}^3$. The OC concentration over other regions are as: NEI ($7 \mu\text{g}/\text{m}^3 - 9 \mu\text{g}/\text{m}^3$), mainland ($5 \mu\text{g}/\text{m}^3 - 8 \mu\text{g}/\text{m}^3$) and oceanic region ($< 5 \mu\text{g}/\text{m}^3$).

Radiative forcing due to carbonaceous aerosols

Fig. 2 shows correlation between the gridded radiative forcing against aerosol optical depth averaged over the monsoon period. Left/right panel represents the BC/BC+OC forcing respectively at the top of the atmosphere (TOA), in the atmosphere (ATM) and at the surface (SUR). The radiative forcing at ATM and TOA follows the opposite response, providing a reverse action upon the surface forcing which increases (less negative) as the AOD increases. Correlation between AOD and radiative frequency is reasonable (0.70) with better correlation in case of SUR (0.8). The lower middle atmosphere experiences significant warming in the presence of BC. Observing the lower figure carefully, we see that BC significantly influences the radiative forcing at TOA. Some of these comprise regions where there is high loading of BC (IGP). With the inclusion of OC along with BC, the OC fraction seems to enhance the surface cooling (more negative). The highest grid surface cooling changes from -22 Wm^{-2} to -38 Wm^{-2} as the aerosol

environment changes from BC to BC+OC respectively. This has significant impact at the TOA where, we see the uplift of the ATM heating stretching its value up to $+30 \text{ Wm}^{-2}$ in the locations where there is abundance of BC and BC+OC. However, due to the addition of OC fraction the atmospheric warming and surface cooling subsidizes the impact of BC along the TOA. The slope of TOA forcing is lowered in case of OC+BC with 35% of the values along the positive side. However, the correlation between the radiative forcing at TOA and the AOD in this case is much lower (~ 0.55). The positive values of the TOA forcing are seen at the places where there is abundance of OC+BC. The enhancement of the surface cooling is much higher in case of OC+BC, which allows the values at TOA to be much lower (less positive). This shows that the strong TOA cooling due to BC is offset by the OC fraction in the OC+BC aerosol environment.

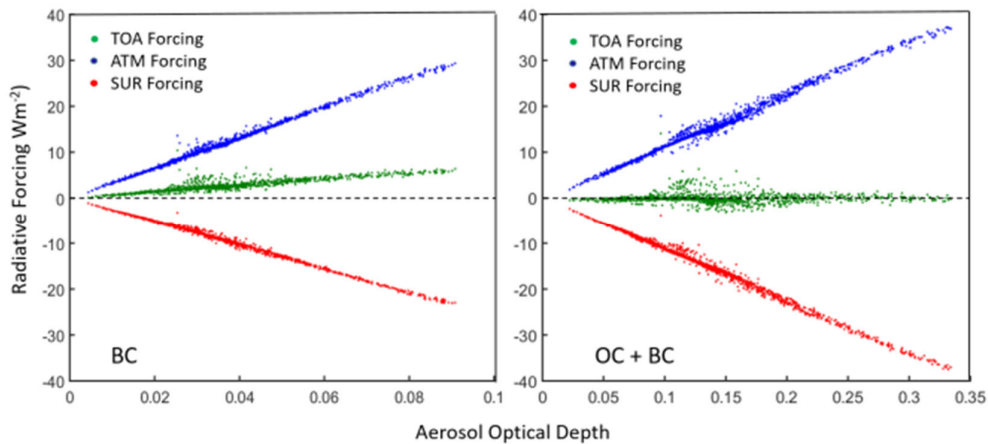


Figure 2. Correlation plot of AOD with (a) BC and (b) OC+BC induced ATM, SUR and TOA forcing during JJA

The bias distribution of cloud water path integrated from 1000 to 500 hPa for Control, BC and BC+OC simulations during the summer monsoon are studied (figure not shown). High reduction in cloud water path ($\sim 12 \text{ g m}^{-2}$) occurs mainly over the IGP region abundant with carbonaceous aerosols extending to the NE India. Besides the high carbonaceous aerosols concentrate regions, cloud reduction is experienced over oceanic region adjacent to south western coastal India and Southern BOB. The radiative effects of transportation of natural and anthropogenic aerosols from the landmasses (Nair et al., 2016) perturb cloud formation even over oceanic region. An increase in cloud water path is experienced over Central India and Northern BOB. High cloud formation occurs mainly over Western India and IGP in the OC+BC simulation than by only BC simulation. The change in cloud liquid water path due to the aerosols can modify the rainfall pattern.

CONCLUSIONS

- The main conclusions from the study are listed below:
- The model also performs reasonably well in terms of simulated BC and simulated OC surface distribution.
- TOA forcing by net carbonaceous aerosols(OC+BC) shows that this positive forcing is cancelled out by the cooling nature of OC aerosols making it negative almost all over the domain.
- In response to the radiative forcing of carbonaceous aerosols, a tendency in change of cloud liquid water path has been found.

- Carbonaceous aerosols are further found to have significant role modification of the rainfall pattern.

ACKNOWLEDGEMENTS

Authors are thankful to ISRO-GBP-ARFI for providing the financial support to carry out this work. BP is thankful to ICTP, Italy for providing access to the HPC.

REFERENCES

Giorgi F, Coppola E, Solmon F, Mariotti L, Sylla MB, Bi X, Elguindi N, Diro GY, Nair V, Giuliani G, Turuncoglu UU, Cozzini S, Guttler I, O'Brien TA, Tawfik AB, Shalaby A, Zakey AS, Steiner F, Stordal F, Sloan LC, Brankovic C (2012) RegCM4: model description and preliminary tests over multiple CORDEX domains. *Clim Res* 52:7–29. <https://doi.org/10.3354/cr01018>

Nair, S.V., Babu, S.S., Manoj, R.M., Moorthy, K.K., Chin, M., 2016. Direct radiative effects of aerosols over South Asia from observations and modelling. *Clim. Dyn.* <http://dx.doi.org/10.1007/s00382-016-3384-0>

Nair, V. S., F. Solmon, F. Giorgi, L. Mariotti, S. S. Babu and K. K. Moorthy (2012). Simulation of South Asian aerosols for regional climate studies. *J. Geophys. Res. Atmos.* 117.

Ohara T, Akimoto H, Kurokawa J, Horii N, Yamaji K, Yan X, Hayasaka T (2007) An Asian emission inventory of anthropogenic emission sources for the period 1980–2020. *Atmos Chem Phys* 7:4419–4444. <https://doi.org/10.5194/acp-7-4419-2007>, 2007

Pathak B, Subba T, Dahutia P, Bhuyan PK, Moorthy KK, Gogoi MM, Babu SS, Chutia L, Ajay P, Biswas J, Bharali C, Borgohain A, Dhar P, Guha A, De BK, Banik T, Chakraborty M, Kundu SS, Sudhakar S, Singh SB (2016) Aerosol characteristics in north-east India using ARFINET spectral optical depth measurements. *Atmos Environ* 125:461-473. <https://doi.org/10.1016/j.atmosenv.2015.07.038>

ESTIMATION OF AEROSOL RADIATIVE FORCING: A SYNTHESIS OF HYBRID ANALYSIS

T. SUBBA¹, M. M. GOGOI³, B. PATHAK^{1,2}, P. K. BHUYAN¹, S. S. BABU³

¹Centre for Atmospheric Studies, Dibrugarh University, Dibrugarh 786004, India

²Department of Physics, Dibrugarh University, Dibrugarh 786004, India

³Space Physics Laboratory, Vikram Sarabhai Space Centre, Thiruvananthapuram 695022, India

KEYWORDS: Shortwave Solar Radiation, Aerosol Optical Depth, Radiative Forcing, Fire Radiative Power

INTRODUCTION

Understanding of changes in past climates, as well as accurately forecasting possible future climates, relies upon knowledge of both natural and anthropogenic processes that alter the energy budget, including those related to aerosols. By the time of Fifth Assessment Report (IPCC 2013), aerosols and aerosol-related processes had emerged as contributing the maximum uncertainty to estimates of energy budget of the Earth. Reducing these uncertainties will require aerosol data sets with improved accuracies in quantification of their composition, optical properties and temporal and spatial coverage. On the other hand, modelling solar radiation to produce accurate estimates of surface reaching irradiance is challenging on clear-sky (cloud-free) days because of the presence of atmospheric aerosols with varying optical depths, as well as sizes and composition hence optical properties.

It is important to note that estimation of aerosol radiative forcing (ARF) is less accurate if the simulated (using radiative transfer or regional climate models) radiation fluxes are not validated against measurements. ARF estimation deviates further if the information of surface albedo is not accurately fed into the radiative transfer models. At this juncture, it is important to combine measurement and retrieval of aerosol properties with forward modelling of their impact on aerosol radiative forcing (ARF) to ensure consistency of aerosol products with the radiation field while also lending more credibility to the aerosol products themselves. One-dimensional radiative transfer models used to ensure consistency between observed surface irradiances and those computed with measured and retrieved aerosol properties have a second application; they can be used to estimate aerosol radiative forcing at the surface (MARF_{SUR}; Subba *et al.*, 2018). In Subba *et al.* (2018) ARF is estimated at a single site in Dibrugarh, India. In the present study this approach is expanded to estimate MARF_{SUR} at nine different ARFINET stations across the Indian subcontinent. These nine stations fall within five distinct geographic locations with different land use land cover patterns. Aerosol loading study and the impact of the burning activities has been further discussed. In addition, the review on the aerosol radiative forcing over the south Asian domain using previous studies have been included.

DATA AND METHODOLOGY

The Indian subcontinent is divided into various regions according to their geographic coordinates and regional features. We use ARFINET data from nine of these regions in this study. Included in these data are measured shortwave irradiances using CNR4 net-radiometer, several measured aerosol parameters using Multiwavelength Radiometer (MWR), Moderate Resolution Imaging Spectro-radiometer (MODIS) retrievals, Aethalometer and Nephelometer and retrieved aerosol parameters using the software packaged called Optical Properties of Aerosols and Clouds (OPAC; Hess *et al.*, 1998). These parameters are subsequently used in ARF calculations at the nine stations.

In the present study, we used the Santa Barbara Discrete Ordinate Radiative Transfer (SBDART) model developed by Ricchiazzi *et al.* (1998) to compute aerosol direct radiative forcing at various levels in the atmosphere by feeding the required inputs of aerosol properties into the model. This radiative transfer model computes plane parallel radiative transfer both in clear and aerosol conditions within the Earth's atmosphere

and at the surface (Ricchiuzzi et al., 1998; Kedia et al., 2010; Pathak et al., 2010). Key input parameters for SBDART are obtained from OPAC, which include AOD, SSA and asymmetry parameter values across the entire shortwave spectral region. Difference in the net solar irradiances ($F\downarrow\uparrow$, incoming - outgoing) in $W m^{-2}$, with and without aerosols, is defined as aerosol radiative forcing at the top of the atmosphere (ARF_{TOA}). That is,

$$ARF_{TOA} = (F\downarrow\uparrow_{with\ aerosol})_{TOA} - (F\downarrow\uparrow_{no\ aerosol})_{TOA} \quad (1)$$

Subba *et al.* (2018) explains the hybrid approach in details. In the hybrid approach surface irradiances for the ‘with aerosol’ conditions are obtained from CNR4 measurements, whereas SBDART is used to produce estimates of surface irradiances for the ‘no aerosol’ conditions in order to obtain the measured ARF at the surface ($MARF_{SUR}$). Unlike $MARF_{SUR}$ which uses measurements to obtain the surface irradiances for the ‘with aerosol’ conditions, both ARF_{ATM} and ARF_{TOA} estimates are based on SBDART computations for both the ‘with aerosol’ and ‘without aerosol’ conditions. $MARF_{SUR}$ and ARF_{SUR} agree to 3-4%, which is not unexpected given instrumental uncertainties, assumptions in the aerosol retrievals (Subba *et al.*, 2018). Hence, we can assume that $MARF_{SUR}$ is close to ARF_{SUR} . The difference between the radiative forcing at the top of the atmosphere and the surface gives the atmospheric forcing (ARF_{ATM}):

$$ARF_{ATM} = ARF_{TOA} - ARF_{SUR} \quad (2)$$

Considering the fact that biomass burning is one of the most important contributor to aerosol loading over south Asia, figuring persistency and annual scenario of the fire activities is vital. Average daily values of MODIS fire radiative power FRP ($1^\circ \times 1^\circ$) have been used in the present study.

RESULTS

Assessment of simulated radiation flux and aerosol radiative forcing

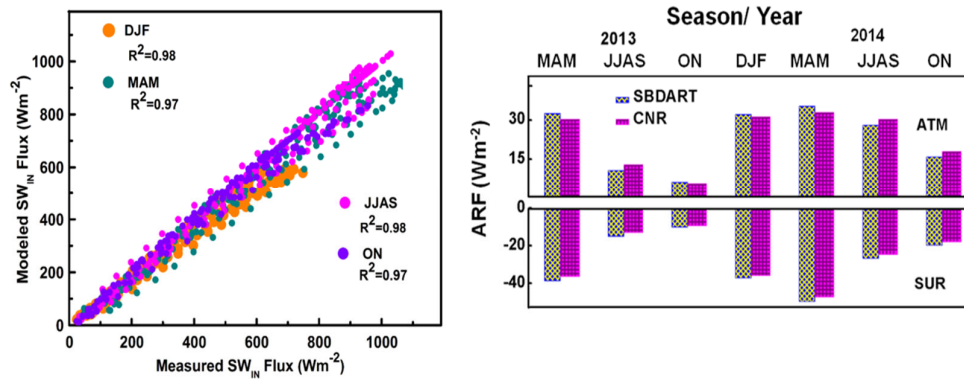


Figure. 1. Simulated downward SW flux at the surface using SBDART as a function of the incoming SW flux measured by CNR4 net-radiometer (left panel). Comparison of the seasonal SW aerosol radiative forcing estimation between model and field based estimations in the atmosphere and at the surface over Dibrugarh from MAM 2013–ON 2014 (right panel).

Modelled values of SW_{IN} using SBDART against respective net-radiometer measurements shows a very good agreement having correlation coefficient of $R^2 \sim 0.97$ in dry ON (retreating monsoon) and $R^2 \sim 0.98$ in DJF (winter). The mean bias error (MBE) between the two ranges from $-40 Wm^{-2}$ to $+7 Wm^{-2}$, equating to a percentage difference of 2 to 3%. Small bias in modelled values from the measurements can be attributed to the underestimation or overestimation of OPAC derived AOD that is used as an input in SBDART. According to the sensitivity analysis, $AOD \sim \pm 0.2$ can produce an alteration of flux by ± 20 to $40 Wm^{-2}$. The slight discrepancy can also be attributed to the instrumental and model uncertainties and the tentative nature of the parameters related to the aerosols. However, the very good agreement between the model and the observation of radiations, within 3% of disparity indicates that the input parameters of

SBDART (i.e., AOD, SSA, g) are appropriate in terms of spectral dependence. Similar approach has been followed for the estimation of ARF over eight other ARFINET locations.

Aerosol radiative forcing over south Asia: a review

Several dedicated field observations, satellite data processing and efficient modelling have been made in recent years in order to study the climatic impact of aerosols over Asian regions. These include the Indian Ocean Experiment (INDOEX), Asian Atmospheric Particle Environment (APEX), Sky Radiometer (SKYNET), the Asian Pacific Regional Aerosol characterization Experiment (ACE-Asia), Pacific Exploration of Asian Continent Emission (PEACE), the East Asian study of Tropospheric aerosols: an International Regional Experiment (EAST-AIRE), Integrated Campaign of aerosols, gases and Radiation Budget (ICARB), Regional Aerosol warming experiment (RAWEX), Seven South-East Asian Studies Program (7SEAS) etc. In addition, there are efforts from regular ground based measurements, such as Aerosol Radiative forcing over India Network (ARFINET, Moorthy et al., 2013, Babu et al., 2013), Aerosol Robotic Network (AERONET, Holben et al., 1998), and many more collaborated regional studies. A short review has been done on the estimations of ARF so far over south Asia. Regional assessment of ARF from the present and past studies over south, south-east and south-west Asia shows highest surface dimming ($\sim 70 \text{ Wm}^{-2}$) in west-Asia where the dust storms are prevalent followed by IGP and west-India ($\sim 40 \text{ Wm}^{-2}$). Surface cooling over NER is comparable to south-India ($\sim 31 \text{ Wm}^{-2}$) which is still higher than that over the oceanic and Himalayan regions ($\sim 23 \text{ Wm}^{-2}$). It is vital to estimate ARF using the hybrid approach considering the uncertainty in the impact of aerosol loading on the radiation budget over the south Asian domain which falls under the primary scope of current work.

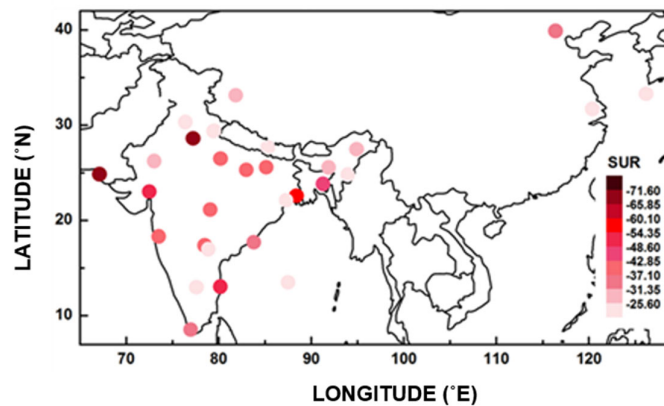


Figure. 2. Spatial variability of climatological average surface (SUR) ARFs over south Asia.

CONCLUSIONS

- Measured and simulated clear-sky solar radiations are compared and the climatological direct aerosol radiative forcing and aerosol radiative forcing efficiency are examined. The conclusions drawn from the present study has been summarized below.
- SBDART modelled ground reaching shortwave solar flux, MODIS retrieved surface reflectance along with the SBDART simulated ARF magnitude has been validated with the measurement with good correlation of $R^2 \sim 0.98$ (3-4 % of disparity), which gives the assurance of the reliability of these models in the absence of measurements.
- Sensitivity analysis of the surface radiation to aerosols indicated that the optical path length is reduced by ~ 0.15 during atmospheric transmission through aerosol laden atmosphere which would be ~ 0.74 in the absence of aerosols.

- We noticed typical TOA forcing dependence on SSA. The intrinsic scattering property of aerosols results in lower forcing at the TOA for higher SSA i.e. $-12.60 \text{ Wm}^{-2}\omega^{-1}$ which would be $+16.91 \text{ Wm}^{-2}\tau^{-1}$ in the presence of black carbon (BC) (only).
- Regional assessment of ARF from the present and past studies over south, south-east and south-west Asia shows highest surface dimming ($\sim 70 \text{ Wm}^{-2}$) in west-Asia where the dust storms are prevalent followed by IGP and west-India ($\sim 40 \text{ Wm}^{-2}$). Surface cooling over NER is comparable to south-India ($\sim 31 \text{ Wm}^{-2}$) which is still higher than that over the oceanic and Himalayan regions ($\sim 23 \text{ Wm}^{-2}$).
- Annual average of FRP values range from $\sim 14 \text{ W m}^{-2}$ to 126 W m^{-2} over the Indian subcontinent. However, at peak time of burning FRP values reach $\sim 2000 \text{ W m}^{-2}$ in highly biomass burning prevalent areas. Annual mean FRP values over eastern India ($\sim 30 \text{ MW}$) is maximum followed by central India ($\sim 24 \text{ MW}$), South India/ West India ($\sim 19 \text{ MW}$) and North India ($\sim 15 \text{ MW}$). The burning events are more prevalent during the afternoon hours of the local time which is well captured by Aqua satellite (13:00 hrs) over the Indian subcontinent.

ACKNOWLEDGEMENT

T.S. is thankful to Aerosol Radiative Forcing Network over India network under ISRO-GBP-(ARFI fellowship) at Dibrugarh University, India and Fulbright Kalam-Climate Fellowship (2017-2018). This work is also supported by FAST TRACK Project provided to B.P. by Department of Science and Technology, Govt. of India, ID No. SR/FTP/ES-1/2012. B.P is also thankful to ICTP for providing her associateship. Authors also thank MODIS science team.

REFERENCES

- Babu, S.S., Manoj, M.R., Moorthy, K.K., Gogoi, M.M., Nair, V.S., Kompalli, S.K., Satheesh, S.K., Niranjana, K., Ramagopal, K., Bhuyan, P.K., Singh, D., 2013. Trends in aerosol optical depth over Indian region: potential causes and impact indicators. *J. Geophys. Res. Atmos.* **118**, 11,794e11,806. <http://dx.doi.org/10.1002/2013JD020507>.
- Hess, M., P. Koepke and I. Schultz (1998). Optical properties of aerosols and clouds: the software package OPAC, *Bulletin American Meteorological Society* **79**, 831-844.
- Holben, B.N., Eck, T.F., Skitsker, I., Tanre, D., Bziis, J.P., Setzer, A., Vermote, E., Reagan, J.A., Kazilfnzan, Y.J., Nnknjima, T., Lauemi, F., Jankozoin, I., Smimov, A., 1998. AERONETda federated instrument network and data archive for aerosol characterization. *Remote Sens. Environ.* **66**, 1-16.
- IPCC, 2013. Climate Change 2013, Working group I contribution to the fifth assessment report of the Intergovernmental Panel on Climate Change, *Cambridge University press*.
- Kedia, S., Ramachandran, S., Kumar, A., and Sarin, M.M., 2010. Spatiotemporal gradients in aerosol radiative forcing and heating rate over Bay of Bengal and Arabian Sea derived on the basis of optical, physical, and chemical properties, *J. Geophys. Res.*, **115**, D07205, doi:10.1029/2009JD013136.
- Moorthy, K.K., Babu, S.S., Manoj, M.R., Satheesh, S.K., 2013. Buildup of aerosols over the Indian region. *Geophys. Res. Lett.* **40**, 1011-1014. <http://dx.doi.org/10.1029/2012GL054876>.
- Pathak, B., Kalita, G., Bhuyan, K., Bhuyan, P.K., Moorthy, K.K., 2010. Aerosol temporal characteristics and the resulting impact on radiative forcing at a location in the northeast India. *J. Geophys. Res.* **115**: D19204.

Ricchiuzzi, P., S. Yang, C. Gautier, and D. Soble (1998). SBDART: A research and teaching software tool for plane-parallel radiative transfer in the Earth's atmosphere, *Bull. Ame. Met. Soc.* **79**, 2101–2114.

Subba, T., Gogoi, M.M., Pathak, B., P. Ajay, Bhuyan, P.K., 2018. Assessment of 1D and 3D model simulated radiation flux based on surface measurements and estimation of aerosol forcing and their climatological aspects. *Atmos. Res.*, <https://doi.org/10.1016/j.atmosres.2018.01.012>.

DISTRIBUTION OF VOLATILE ORGANIC COMPOUNDS OVER INDIAN SUBCONTINENT DURING WINTER: WRF-CHEM SIMULATIONS VERSUS OBSERVATIONS

L. CHUTIA¹, N. OJHA², I. GIRACH³ AND B. PATHAK¹

¹Centre for Atmospheric Studies, Dibrugarh University, Dibrugarh-786004, Assam, India

²Space and Atmospheric Sciences Division, Physical Research Laboratory, Ahmedabad, Gujarat 380009, India

³Space Physics Laboratory, Vikram Sarabhai Space Centre, ISRO, Thiruvananthapuram - 695 022, India

KEYWORDS: Vocs, Nmhcs, Wrf-Chem, Radm2, South Asia

INTRODUCTION

Volatile Organic Compounds (VOCs) from both natural and anthropogenic sources have gained much attention over the last two decades due to their impacts on human health, air quality and climate. VOCs contribute significantly in the formation of aerosols through gas-to-particle conversion. VOCs include a variety of species such as non-methane hydrocarbons (NMHCs) and oxygenated VOCs which usually vary from few parts per trillion to several parts per billion. India among the Asian countries, is the second largest contributor to the emission of non-methane VOCs (NMVOCs) (32.8 Tg (+17 %) after China (Kurokawa *et al.* 2013). Residential combustion (41%), on-road transportation (37%) and industrial non-combustion (13%) are the major anthropogenic sources of VOCs in India (Li *et al.* 2014).

Large variability of VOCs in the atmosphere with spatially and temporally variable sources makes their studies challenging, and require state-of-the art instrumentation over a network of stations. Limited studies found strong contrasts in the variations of VOCs in different environments of India (Sahu *et al.* 2016, Swamy *et al.* 2012 etc). Modeling studies, that could complement the understanding of VOC distributions and their chemistry-climate impacts are still very limited over the Indian Subcontinent. In this direction here we study some of the important VOCs over this region by combining the ground-based and satellite based measurements with a regional model WRF-Chem and reanalysis model fields during Jan 2011.

METHODOLOGY

Weather Research and Forecasting (WRF) model coupled with chemistry (WRF-Chem) version 3.9.1.1 (Grell *et al.* 2005) is used for the simulations of VOCs. The model domain is centred at 21°N and 82°E with grid extent of 274 in W-E and 352 in N-S direction respectively at 12 km horizontal resolution. The model consists of 50 vertical levels which extend from surface to 50 hPa. The initial and boundary conditions for meteorology and chemistry are used from the Era interim and MOZART (Model for Ozone and Related chemical Tracers) (Emmons *et al.* 2010) respectively. Regional Acid Deposition Model version 2 (RADM2) (Stockwell *et al.* 1990) with the Modal Aerosol Dynamics for Europe (MADE) (Ackermann *et al.* 1998) and the Secondary Organic Aerosol Model (SORGAM) (Schell *et al.* 2001) was used to simulate the chemistry. Anthropogenic emissions are based on EDGAR-HTAP inventory. The Fire INventory from NCAR (FINN) model provides high resolution, global emission estimates from open burning on daily basis at a horizontal resolution of ~1 km² and the model calculates the biogenic emissions online using MEGAN (Model of Emissions of Gases and Aerosols from Nature). The time step for the simulation was set at 72s, which is 6 times the grid resolution. The model simulation period is Jan 2011 and hourly output was stored for the analysis.

The model simulated non-methane VOCs are compared with observed data taken from different region over the country. Tropospheric column HCHO is compared with OMI (Ozone Monitoring Instrument) and GOME-2 (Global Ozone Monitoring Experiment) satellite retrieval data as well as from Monitoring Atmospheric Composition and Climate (MACC) reanalysis data during the study period.

RESULTS AND DISCUSSIONS

SIMULATION OF VOCS OVER INDIAN SUBCONTINENT

Table 1 shows monthly mean values of VOCs obtained from WRF-Chem during Jan, 2011. Due to its topographic heterogeneity and the variability of land use and land cover the Indian subcontinent has been divided into five broad sub regions for our work, viz., Indo Gangetic Plain (IGP)(22°N-30°N,76°E-88°E), North East India (NEI) (22°N-30°N, 88°E-98°E), Central India (CI) (22°N-25°N,76°E-84°E), West India (WI) (19°N-30°N,68°E-76°E) and South Peninsula (SI) (8°N-19°N,72°E-84°E). Maximum concentration of ethane is found to be higher over IGP (6.4 ppbv) followed by NEI (5.4 ppbv), WI (5.2 ppbv), CI (4.1 ppbv) and SI (2.9 ppbv). As the major sources of VOCs include natural gas, petrochemical industries, automobile exhaust, gasoline, industrial processes; so being an Industrial hub and mostly populous region and also being a region which is highly influenced by the anthropogenic emissions, maximum concentration of major VOCs are found over IGP. In NEI, apart from small scale industries and vehicular emission, during the winter season, commencement of brick kilns, agricultural waste burning and forest fires contribute to VOC loading. On the other hand, compared to other part of the region agricultural and industrial activities are rather less which contribute less VOCs in CI. In WI, mostly by large local emissions contribute to the VOC loading. As NEI is mostly forest covered (~66%) isoprene concentration is found to be higher over NEI (0.5 ppbv) compared to other part of the country.

Table1: Model simulated monthly averaged values of some major VOCs over Indian subcontinent during Jan, 2011

VOCs (ppbv)	IGP	NEI	CI	WI	SI
Ethane	6.4	5.3	4.1	5.2	2.9
Ehtene	7.4	4.4	4.1	4.2	2.0
Propane	14.5	9.1	8.9	9.1	4.6
Propene	1.3	1.0	0.9	0.7	0.5
Pentane	4.5	5.3	2.2	2.8	1.3
Acetaldehyde	5.0	4.0	3.8	3.4	2.4
Acetone	4.1	3.4	3.2	3.3	2.5
Toluene	2.8	1.8	1.4	1.7	0.7

VOC COMPARISON WITH OBSERVED DATA OVER INDIAN SUBCONTINENT

Table2: Comparison of WRF-Chem model simulated VOCs (ppbv) with observed data taken from various studies over Indian region during winter

VOCs (ppbv)	Ahmedabad (23°N,72.6°E, 49m amsl)		Mt Abu (24.6°N, 72.7°E, 1680 m amsl)		Kathmandu (27.68°N, 85.39°E, 1344 m amsl)		Nainital (29.4°N, 79.5°E, 195 8m amsl)		Hyderabad (17.47°N, 78.58°N, 536 m amsl)		Mumbai (19.1°N, 72.5°E, 14m amsl)		Hissar (25.5°E, 74.46°N, 215 m amsl)		Kanpur (26.43°E, 80.33°N, 126m amsl)	
	Obs	Mod	Obs	Mod	Obs	Mod	Obs	Mod	Obs	Mod	Obs	Mod	Obs	Mod	obs	Mod
Ethane	7.1	7.9	2.1	4.2	3.5	4.2	2.2	3.3	28.3	3.4	5.2	6.1	8.6	5.1	9.5	10.7
Ethene	4.4	8.0	.5	3.3	2.8	5.0	.9	4.8	3.1	3.1	4.3	3.7	9.3	.4.7	8.8	13.6
Propane	7.0	19.2	.6	6.9	4.4	8.3	.8	7.9	3.5	6.6	7.8	11.7	4.7	9	3.9	24.9
Propene	1.7	1.7	.3	.6	1.1	1.1	1	1.1	x	.60	6.8	.6	2.8	.8	2.2	2.4
Pentane	X	9.5	x	1.9	.9	1.4	.8	2.5	7.7	2.09	28.2	4.2	x	2.4	2.0	7.9

Some of the major alkanes and alkenes are compared with observed data at some stations over Indian subcontinent (Table 2). Simulated monthly averaged ethane mixing ratios (7.1 ppbv) agree relatively well with observed ethane value (7.9 ppbv) at Ahmedabad, a tropical urban site in West India. On the other hand,

at Mt Abu, a hill station in West India, and at Mumbai the simulated ethane mixing ratios are slightly overestimated. In central Himalaya's stations like Kathmandu and Nainital, observed mixing ratios are slightly smaller than that of simulated values. At Kanpur, the simulated ethane mixing ratios (10.7 ppbv) are slightly higher than that of observed values (9.5 ppbv), whereas modeled values (5.1 ppbv) are slightly under predicted the observed value (8.6 ppbv) at Hissar. In contrast to them, at Hyderabad, a station in South India the simulated values (3.4 ppbv) are highly underestimated the observed value by a factor of 7. Significant overestimation of model simulated propane mixing ratios at all the stations over Indian subcontinent are clearly noticed from the table. Simulated mixing ratios of ethene are over predicted at two stations in west India (by a factor ~ 2 in Ahmedabad and ~6 in Mt Abu), whereas its value slightly over predicted in Mumbai. Modeled ethene values are also over predicted in central Himalayan stations. On the other hand, WRF-Chem model well simulated the observed ethene mixing ratios (7.1 ppbv) at Hyderabad. All these modeled VOCs are comparable with the VOCs measurements carried out at different parts of the country to an extent. The observed differences may be due to uncertainties in emissions and in the computed meteorological variables.

HCHO DISTRIBUTION OVER INDIAN SUBCONTINENT: COMPARISON WITH REANALYSIS AND SATELLITE DATA

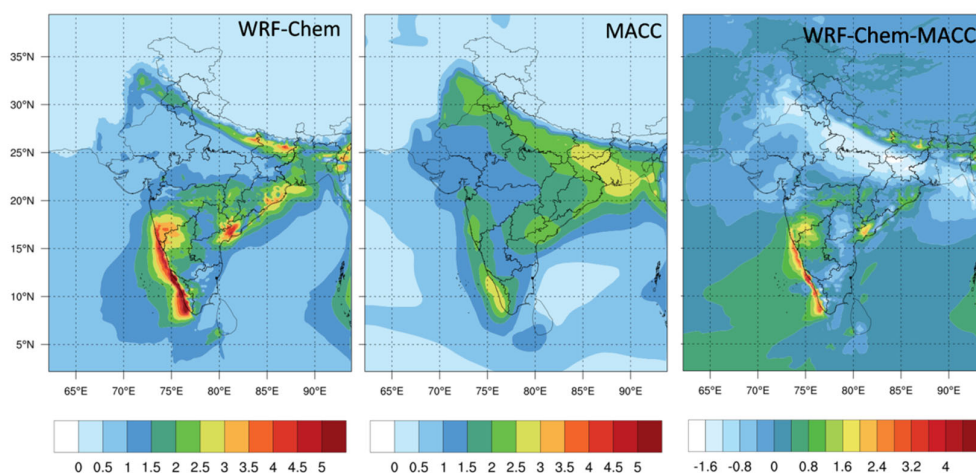


Fig 1: Spatial distribution of model simulated HCHO along with MACC reanalysis and their biases (ppbv) during January 2011

Fig 1 shows the spatial distribution of model simulated HCHO along with MACC reanalysis during January 2011. Model simulated average HCHO mixing ratios are found to be 2-7 ppbv over Indian subcontinent. Simulated mixing ratios of HCHO are found to be lower than those from MACC reanalysis over the IGP belt with a bias of about -1.6 ppbv. Increasing urbanization anthropogenic emissions of VOCs from biomass burning, industries, power plants and vehicles are present throughout the year over IGP which contribute to formaldehyde loading. HCHO levels are higher over CI as well as SI and much higher (above 5 ppbv for WRF-Chem, ~3 ppbv for MACC) over the coastal Arabian Sea downwind the Western Ghats during winter. Simulated and reanalysis ozone mixing ratios are also found to be higher over coastal Arabian Sea (not shown here), which further contributes to methane oxidation in both the cases. On the other hand, SI and NEI are mostly covered by vegetation contributes to the formation of comparatively high HCHO. In contrast, in WI, HCHO levels are lower as compared to other part of India in both WRF-Chem and reanalysis.

Fig 2 shows the comparison of model simulated tropospheric column HCHO with MACC reanalysis, OMI and GOME-2 over Indian Subcontinent. WRF-Chem overestimates the MACC column formaldehyde over the entire region except in NEI where it is slightly underestimated with a bias of -1.2×10^{15} molecules cm^{-2} .

In SI, modeled HCHO highly overestimated the MACC column data (with a bias of $\sim 2.5 \times 10^{15}$ molecules cm^{-2}). Model comparison with OMI shows underestimation of HCHO column all over India. In contrast, there is good agreement between the modeled and GOME HCHO column during the study period over IGP, NEI, CI and WI. The largest difference is over SI where WRF-Chem overestimated the GOME data by at least 1.7×10^{15} molecules cm^{-2} . Besides this, spatial distribution plots show the largest HCHO columns in the regions of higher biogenic VOC emissions and biomass burning.

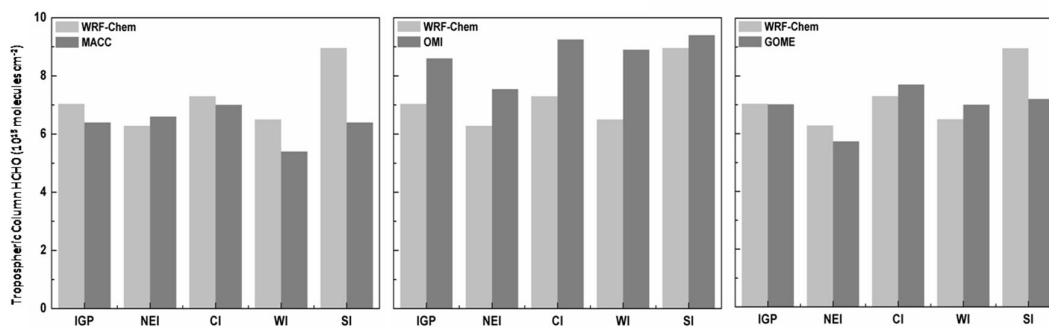


Fig 2: Comparison of WRF-Chem simulated tropospheric column formaldehyde with MACC reanalysis, OMI and GOME

CONCLUSION

- We investigate the distribution of some of the major VOCs using observations and model data over India during winter.
- The study highlights the spatial heterogeneity in the distribution with higher levels over the IGP and NEI, as well as the model ability to reproduce general features of VOCs seen in observational and reanalysis datasets.
- Modeled VOCs are comparable with the VOC measurements carried out at different parts of the country. Model biases are further revealed pointing towards uncertainties in input emissions and modeled meteorology / dynamics.
- As the concentrations of VOCs are higher over IGP and NEI, it is suggested that these could significantly affect tropospheric chemistry of these regions including the formation of secondary organic aerosols. More observations and yearlong model simulations would be needed to further understand the seasonal changes in VOC over this region.

ACKNOWLEDGEMENT

Authors are thankful to the ECMWF, TEMIS, OMI, GOME, MACC reanalysis for the data used in the study. Usage of the WRF-Chem model, Era-interim data, MOZART fields, Fire emissions from NCAR FINN, EDGAR-HTAP inventory etc are acknowledged. WRF-Chem simulations were performed on the Vikram-HPC at the PRL, Ahmedabad.

REFERENCES

- Ackermann, I. J., H. Hass, M. Memmesheimer, A. Ebel, F.S. Binkowski and U. Shankar (1998). Modal aerosol dynamics model for Europe: Development and first applications, *Atmos. Environ* **32**, 2981–2999.
- Emmons *et al.* (2010). Description and evaluation of the Model for Ozone and Related chemical Tracers, version 4 (MOZART-4), *Geosci. Model Dev* **3**, 43–67, doi:10.5194/gmd-3-43-2010.
- Grell *et al.* (2005). Fully coupled ‘online’ chemistry within the WRF model, *Atmos. Environ* **39**, 6957–75.

Kurokawa *et al.*(2013). missions of air pollutants and greenhouse gases over Asian regions during 2000–2008: Regional Emission inventory in ASia (REAS) version 2, *Atmos. Chem. Phys***13**, 11019-11058.

Li *et al.*(2014).Mapping Asian anthropogenic emissions of non-methane volatile organic compounds to multiple chemical mechanisms, *Atmos. Chem. Phys***14**, 5617–5638.

Sahu, L. K., R. Yadav, and D. Pal (2016). Source identification of VOCs at an urban site of western India: Effect of marathon events and anthropogenic emissions, *J. Geophys. Res. Atmos***121**, 2416–2433, doi:10.1002/2015JD024454

Swamy *et al.*(2012). Impact of Nitrogen Oxides, Volatile Organic Compounds and Black Carbon on Atmospheric Ozone Levels at a Semi Arid Urban Site in Hyderabad, *Aerosol and Air Quality Research***12**, 662–671

OCCURRENCE OF SINGLE AND MULTIPLE AEROSOL LAYERS OVER THE SUBHIMALAYAN REGION OF INDIA

P.DAHUTIA^{1,2}, B. PATHAK^{1,2} AND P.K. BHUYAN²

¹Department of Physics, Dibrugarh University, Dibrugarh-786004, Assam, India.

²Centre for Atmospheric Studies, Dibrugarh University, Dibrugarh-786004, Assam, India

KEYWORDS: Aerosol Vertical Distribution, Particulate Depolarization Ratio, Color Ratio, Aerosol Layers.

INTRODUCTION

Aerosol study helps in understanding their roles and interaction and thereby reducing the uncertainties in estimating the Earth's radiation budget (IPCC, 2013). The aerosol vertical distribution as a function of altitude is an important study to understanding the aerosol warming on the thermal structure as well as the stability of atmosphere (Satheesh *et al.*, 2009). Spatio-temporal variability in aerosols needs the characterization of regional and global which helps in improving the quantification of the aerosols on climate. Aerosol possesses large spatial and temporal variation in terms of their density, physical and chemical properties as well as complex mechanism of their interactions with radiation and clouds (Ramanathan *et al.*, 2001). Recent advancement in the remote sensing of aerosols and clouds viz., Cloud-Aerosol Lidar Infrared Orthogonal Polarization (CALIOP) on board Cloud-Aerosol Lidar Infrared Pathfinder Satellite Observation (CALIPSO) satellite (Winker *et al.*, 2010) provides a good opportunity to study the aerosol vertical distribution over a region as well as globally.

The North-Eastern region of India (NER) and adjoining South Asia including Bangladesh, Bhutan and Myanmar are geographically and topographically unique residing at the foothills of Himalayan range. The vertical distribution of aerosols including their microphysical studies is still limited over this region. The surface and columnar aerosol properties of aerosols are different in presence of distinct aerosol layer aloft (Ramanathan *et al.*, 2001) resulting a large error (as much as factor two) (Satheesh *et al.*, 2002) in translating the surface to column aerosol properties based on vertical profile of aerosols (Satheesh *et al.*, 2009). The climatological study of these aerosols layers height provides valuable information to minimize the errors over the study region. In this perspective, the present study is focused on the seasonal variability of the aerosol layer height statistics over the study region. Also, an attempt has been made to study the microphysical properties of these layer aerosols by studying the particulate depolarization ratio and color ratio. This study provides qualitative information about the seasonal variability of aerosol size as well as their shape.

METHODS

To study the aerosol layer height statistics and microphysical properties over NER and three adjoining South Asian countries Bangladesh, Bhutan and Myanmar stretching between 22-30°N and 88-98°E, we have selected eleven locations with varying altitude. These locations are: Dhaka (23.4°N, 90.2°E, 4 m above mean sea level (AMSL)), Agartala (23.9°N, 91.2°E, 14.9 m AMSL), Dhubri (26°N, 90°E, 28 m AMSL), Guwahati (26.2°N, 91.7°E, 55 m AMSL), Dibrugarh (27.3°N, 94.6°E, 111m AMSL), Banmawk (24.24°N, 95.51°E, 279 m AMSL), Imphal (24.75°N, 93.92°E, 765 m AMSL), Aizawl (23.7°N, 92.8°E, 1001 m AMSL), Shillong (25.6°N, 91.9°E, 1496 m AMSL), Tawang (27.6°N, 91.9°E, 2668 m AMSL) and Thimphu (27.5°N, 89.6°E, 2737 m AMSL). The study region belongs to a transition zone of tropics and extra-tropics possessing contrasting synoptic meteorology with prevailing calm northeasterly winds during winter (December-February), calm westerly during pre-monsoon (March-May) and moderate/strong westerly during monsoon (June-September) and calm northeasterly winds during post monsoon (October-November).

In this study we have used the Cloud Aerosol Lidar Infrared Orthogonal Polarization (CALIOP) on board Cloud Aerosol Lidar Infrared Pathfinder Satellite Observation (CALIPSO) Version 4.10 Level 2 aerosol-cloud merged layer (CAL_LID_L2_05kmMLay-Standard-V4-10) product for eleven years (June, 2006-May, 2017) and the quality of the data is controlled by following Winker *et al.* (2013). The seasonal variability of single-layer and multiple layer aerosols based on CALIPSO observations collected from a given grid ($1^\circ \times 1^\circ$) during the study period. Also, the microphysical parameter, viz., integrated attenuated color ratio (χ') defined as the ratio of the layer mean attenuated backscatter at 1064 nm to the layer mean attenuated backscatter at 532 nm. χ' is a common measurement size of the particle where the larger χ' indicates larger size particle (Liu *et al.*, 2017). The integrated particulate depolarization ratio (δ_p) at 532 is a post extinction quantity calculated from ratio of the layer integrated perpendicular and parallel polarization components of particulate backscatter coefficient within the layer. The value of δ_p is low for the spherical particle while it is large for non-spherical particles.

RESULTS AND DISCUSSIONS

The study of aerosol vertical distribution over the NER and adjoining region of south Asian countries shows the presence of multiple aerosol layers plausibly contributed by complex aerosol properties and weather condition that prevails over this region. The analysis of microphysical properties of single and multiple aerosol layers over this region shows the seasonal variation as indicated by the variability in the scatter plot of color ratio and particulate depolarization ratio (Figure 1). The average value of χ' and δ_p for single aerosol layers are found at 0.73 ± 0.37 and 0.21 ± 0.18 in winter; 0.95 ± 0.28 and 0.32 ± 0.17 in pre-monsoon; 0.98 ± 0.25 and 0.31 ± 0.17 in monsoon; and 0.78 ± 0.39 and 0.21 ± 0.17 in post monsoon respectively. Also, the average value of χ' and δ_p for multiple aerosol layers are found at 0.55 ± 0.33 and 0.17 ± 0.15 in winter; 0.68 ± 0.34 , 0.24 ± 0.16 in pre-monsoon; 0.84 ± 0.32 , 0.32 ± 0.19 in monsoon; and 0.67 ± 0.38 and 0.18 ± 0.16 in post monsoon respectively. The high χ' and δ_p during monsoon indicates the presence of large non-spherical particles in the single aerosol layer while the multiple layer consists of smaller aerosol with more non-spherical. Notably, the dependency of χ' and δ_p are less (0.24: single layer, 0.06: multiple layer) during monsoon while it is more during winter (0.54) and post monsoon (0.47). Therefore, the vertical distribution of aerosol properties for single aerosol layer different from the multiple aerosol layers over this study region.

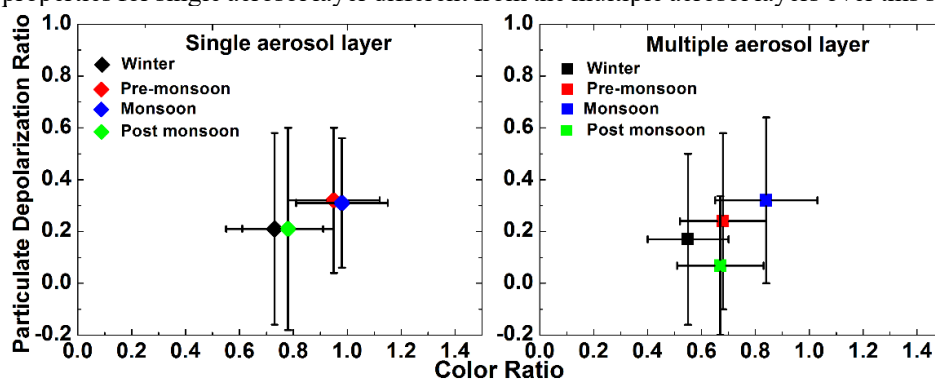


Figure 1. Scatter plot of seasonal variation of color ratio (χ') and particulate depolarization ratio (δ_p) for single (left panel) and multiple (right panel) aerosol layers. The vertical and the horizontal lines (error bar) represent the standard deviation from the mean value.

The statistical analysis of single and multiple aerosols layers also shows the variability in their characteristics and abundance. Over the region the occurrence of multiple aerosol layers is frequent in comparison to the single aerosol layers. Maximum occurrence of single layer is observed in post monsoon season (41.77%) and minimum in pre-monsoon season (29.04%) (Table 1). On the other hand, maximum occurrence of multiple aerosol layers is observed in pre-monsoon (70.96%) and minimum in post monsoon (58.23%). The variability in the contribution of single and multiple aerosol layers can be explained by the contribution of surface aerosols to the columnar aerosols. Notwithstanding the role of near surface aerosol

is primarily important as most of the aerosols are located on the Earth's surface. In general the surface aerosols within the atmospheric boundary layer (ABL) are well mixed chemically and physically due the presence of strong convective turbulence present in this tropical region. The strong convective activities also help in uplifting of aerosol to the elevated layers result in the formation of elevated aerosols layers (EALs). Also, the synoptic meteorological condition helps in the advection of aerosols from the distant sources leading the formation of aerosols layers in the free troposphere by these long-range transported aerosols. The uplifting of aerosols to the elevated levels by convective turbulence as well as long-range transported aerosols leads by synoptic meteorological condition causes the formation of these single and multiple layers. Therefore the presence of high convective activities associated with long range transported aerosols results in the lower occurrence of single aerosol layers thereby increases the higher occurrence of multiple aerosol layers over this region during pre-monsoon season. On the other hand, low convective activities and locally transported aerosols due to calm wind resulting higher contribution of single layers and lower contribution of multiple aerosol layers during post monsoon season.

Season	%							
	contribution		Lower		Middle		Upper	
	Sing le	Multip le	Single (ATA/AB A)	Multiple (ATA/AB A)	Single (ATA/AB A)	Multiple (ATA/AB A)	Single (ATA/AB A)	Multiple (ATA/AB A)
Winter	39.0	60.94	32.98/52.	22.86/48.	26.18/18.	41.55/22.	40.83/52.	35.59/29.
Pre- monsoon	29.0	70.96	3.84/18.6	1.95/16.6	15.54/14.	24.40/26.	80.62/66.	73.65/57.
Monsoon	34.5	65.45	9.97/14.5	32.98/52.	9.10/9.72	32.98/52.	32.98/52.	80.92/75.
Post monsoon	41.7	58.23	31.82/45.	19.45/38.	19.37/16.	33.03/21.	48.81/38.	47.52/40.

Table 1. Percentage contribution of seasonal single and multiple aerosol layers and their contributions according to lower, middle and upper layers. ATA and ABA stands for Aerosol Top Altitude and Aerosol base Altitude respectively.

For the detail analysis of aerosol layers we have vertically classifying this layer into upper, middle and lower layers with altitudes of 4.5 to 16.5 km, 2.5 to 4.5 km, and less than 2.5 km respectively (Zhang *et al.*, 2012) to investigate the contribution of this layers to the vertical distribution of aerosols. Notably, we consider the upper level height up to 16.5 km in the present study to the aerosol characteristics throughout the tropospheric column. The aerosols layers at the lower and middle layer are mainly originated from both the local sources like convective activities added by other meteorological conditions and long-range transported aerosols. During pre-monsoon season, the contribution of aerosol at the aerosol top layer at lower 3.5% and middle 15.54% layers are lowest resulting maximum 80.62% contribution by upper layer of aerosol top altitude. The strong convective turbulence due to large diurnal heating coupled with moderate precipitation increases the uplifting of aerosols over this region (Gogoi *et al.*, 2011). Apart from this long-range transported aerosols (Gogoi *et al.*, 2009) from distant source region together with biomass-burning activities resulting peak aerosol loading in this region. Also, the elevated aerosols layers (EALs) over this region is prominent (Sharma *et al.*, 2009; Pathak *et al.*, 2016) throughout the years. Post monsoon season possesses with 31.82% (lower) and 19.37% (middle) of aerosol top layers while 32.98% (lower) and 26.16% (middle) during winter season attributed by minimal convective activities and contribution of local aerosol sources. The contribution of local aerosol sources is higher in post monsoon in comparison to winter season as obtained from the study of air mass trajectory analysis which might be one of the possible reasons of more contribution of single layers during post monsoon than winter. Though the presence of EALs during post monsoon, the probability of building up of aerosol at the elevated levels are less due to the scavenging effect of aerosols by monsoon season (Pathak *et al.*, 2016). The aerosol transportation from the distant aerosol source region to the present study region during winter plausibly causes larger contribution of low and middle level aerosols during winter than post monsoon season.

CONCLUSIONS

The long-term (June,2006-May,2017) study of aerosol single and multiple layers and their characteristics from the color ratio and particulate depolarization ratio have been studied by the aerosol-cloud merged layer product of CALIOP on board CALIPSO satellite over the North-Eastern region (NER) of India and adjoining south Asia.

1. The single and multiple aerosol layer possesses different aerosol environment as obtained from the scatter plot of color ratio and particulate depolarization ratio. The aerosols for single layers are larger and non-spherical in comparison to the multiple aerosol layers which is more prominent during monsoon season.
2. The contribution of multiple aerosol layers is higher than single layers over this region. The occurrence of single layer is comparatively high during the period of low convective activities season post monsoon followed by winter. On the other hand, occurrence of single layer is minimum during the seasons of strong convective activities pre-monsoon followed by monsoon.
3. The vertical study of aerosol single layers shows higher occurrence of surface aerosols in winter followed by post monsoon and minimum in pre-monsoon. These aerosols impact on the reduction of solar radiance through extinction at the surface which in turn effect on the Earth's radiation budget. Also, the seasonal variability in aerosol layer height indicate the variability in atmospheric thermal structure and thereby the atmospheric stability over this region.

ACKNOWLEDGEMENTS

Authors are thankful to CALIPSO (<https://www-calipso.larc.nasa.gov>) science team for the data support. PD is grateful to ISRO-GBP-ARFI for providing her with an assistantship. BP is a Junior Associate in the Abdus Salam International Centre for Theoretical Physics, Italy.

REFERENCES

- Gogoi, M.M., B. Pathak, K.K. Moorthy, P.K. Bhuyan, S.S. Babu, K. Bhuyan, G. Kalita. (2011). Multi-year investigations of near surface and columnar aerosols over Dibrugarh, north-eastern location of India: heterogeneity in source impacts. *Atmos. Environ.***45**, 1714-1724.
- Gogoi, M.M., K.K. Moorthy, S.S. Babu, P.K. Bhuyan. (2009). Climatology of columnar aerosol properties and the influence of synoptic conditions: First-time results from the northeastern region of India, *J. Geophys. Res.***114**, D08202.
- Intergovernmental Panel on Climate Change (IPCC). (2013). The Physical Science Basis: Working Group I Contribution to the Fifth Assessment Report of the IPCC, Climate Change 2013. Cambridge University Press, Cambridge, United Kingdom and New York, NY, USA, 2013.
- Liu, B., Y. Ma, W. Gong, M. Zhang. 2017. Observations of aerosol color ratio and depolarization ratio over Wuhan. *Atmos. Poll. Res.* **8**, 1113-1122
- Pathak, B., T. Subba, P. Dahutia, P.K. Bhuyan, *et al.* (2016). Aerosol characteristics in north-east India using ARFINET spectral optical depth measurements. *Atmos. Environ.*, **125**, 461-473.
- Ramanathan, V., P.J. Crutzen, J. Lelieveld *et al.* (2001) Indian Ocean Experiment: An integrated analysis of the climate forcing and effects of the great Indo-Asian haze, *J. Geophys. Res.*,**106** (D22), 28371-28398.
- Satheesh, S. K. (2002). Radiative forcing by aerosols over Bay of Bengal region, *Geophys. Res. Lett.*,**29**(22), 2083.

Satheesh, S.K., V. Vinoj, S.S. Babu *et al* (2009). Vertical distribution of aerosols over the east coast of India inferred from airborne LIDAR measurements, *Ann. Geophys.* **27**, 4157-4169.

Sharma, A.A., S.K. Kharol, K.V.S. Bardarinath. (2009). Satellite observation of unusual dust event over north-east India and its relation with meteorological conditions. *J. Atmos. Sol. Terres. Phys.*, **71**, 2023-2039.

Winker, D.M., J. Pelon, Jr. Coakley, J.A. Ackerman, *et al.* (2010). The CALIPSO Mission: A Global 3D View of Aerosols and Clouds, *Bull. Amer. Meteor. Soc.* **91**, 1211-1229.

Winker, D.M., J.L. Tackett, B.J. Getzewich, *et al* (2013). The global 3-D distribution of tropospheric aerosols as characterized by CALIOP. *Atmos. Chem. Phys.* **13**, 3345-3361.

Zhang, J.Q., C.Tang, Y.Han. (2012). Aerosol structure and vertical distribution in a multi-source dust region. *J. Environ. Sci.* **24**(8) 1466-1475.

CHARACTERIZATION OF BIOAEROSOLS IN POST-MONSOON SEASON AT VARIOUS LOCATIONS OF AN EDUCATIONAL INSTITUTE IN NORTHEAST INDIA

ANKITA KHATANAR^{1,2}, BINITA PATHAK², P. K. BHUYAN², A. K. BURAGOHAIN³, AND DEBAJIT BORAH¹

¹Centre for Biotechnology and Bioinformatics, Dibrugarh University-786004

²Centre for Atmospheric Studies and Department of Physics, Dibrugarh University-786004

³Department of Molecular Biology and Biotechnology, Tezpur University-784028

KEYWORDS: Bioaerosols; Microbial diversity, Inhalable particulate matter; ambient air quality.

INTRODUCTION

Aerosols can be defined as the colloidal suspension of fine solid particles or liquid droplets in the atmosphere. Bioaerosols are a major part of atmospheric aerosols. They are particulate matters usually associated with compounds of biological origin. Study of aerosols, and in particular, bioaerosols, is necessary to understand the impact of aerosols in various areas such as climate change and human health (Dave *et al.*, 2017). The monitoring of particulate matter (PM) concentrations PM₁, PM_{2.5} and PM₁₀ (particulate matter of sizes <1µm, <2.5 µm and <10 µm) is considered important, as bioaerosols ranging in size from 1.0 to 5.0 µm usually remain airborne whereas larger particles tend to deposit on surfaces after a short period of time. Three principle sampling methods are widely used *viz.*, filtration, impaction and liquid impingement and these techniques have also been incorporated in sampling devices. However, there are no standard techniques for the same (Yao, 2018). In this study, characterization of ambient air quality in terms of overall particulate matter concentration, mass values of inhalable, thoracic and alveolar particulate matter and microbial diversity was carried out during post-monsoon season at different locations of Dibrugarh University which is the eastern most university in India located in Assam by using a laser detection based portable aerosol spectrometer with a built-in impactor system (Grimm and Eatough, 2009).

METHODS

Air samples were collected using GRIMM Portable Laser Aerosol Spectrometer-11.A (GRIMM Aerosol Technik Ainring GmbH & Co.KG., Germany) capable of continuous monitoring of airborne particles as well as for measuring the particle count distribution. A greased glass slide acts as an impactor in the instrument which collects the aerosols in the form of a spot on its surface. It principally involves the detection of particles on the basis of the angle created due to the laser light scattering by single particles passes through the air passage. This enables the instrument to detect very fine particles as small as 0.25-0.3 µm. The data collected was retrieved using the Grimm Windows Software-V2.5TM. After sampling the glass slides were cultured for the isolation of possible microbes on bacterial media agar plates by overlay method followed by incubation at 37°C for 24 hrs. Preliminary identification of the bacterial isolates was done by performing colony characterization, Gram Staining, microscopic study and biochemical tests (according to Bergey's Manual of Systemic Bacteriology).

RESULTS & DISCUSSIONS

The study shows that the locations with the highest anthropogenic activities show high particle counts with corresponding higher Inhalable particulate matter. Microbial analysis of the samples reveals the presence of 85 and 15% of culturable Gram +ve and -ve bacterial strains respectively. Out of these, 45% were predicted as *Corynebacterium* sp., followed by 25% of *Bacillus* sp., 15% of *Streptococcus* sp., 10% of *Escherichia coli* whereas 5% of Gram negative cocci could not be identified. Microscopic analysis shows the presence of large number dust particles in the aerosol samples of the market complex and highest numbers of pollens in the aerosols of institutional botanical garden.

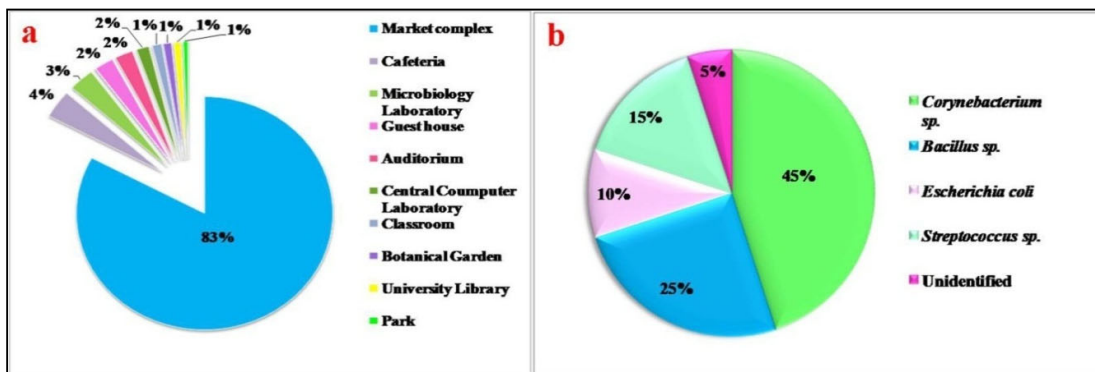


Fig 1: a-Percentage contribution of total PM counts of bioaerosol samples collected in different location; b-Percentage distribution of predicted microbes in total bioaerosols sample

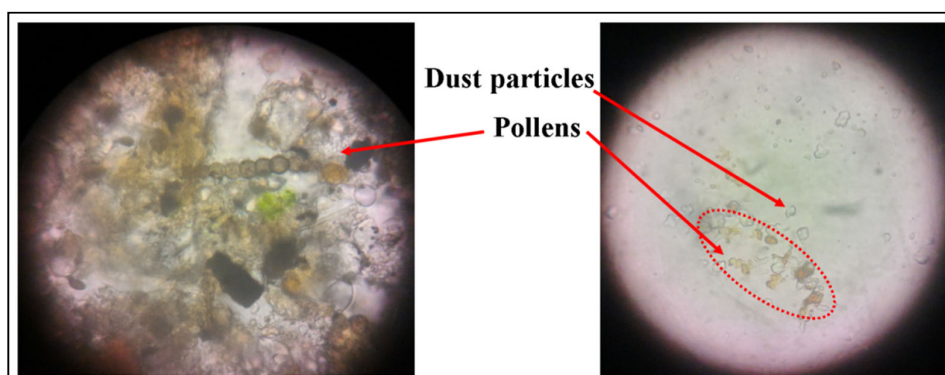


Fig2: Microscopic photographs of large numbers of pollens present in the bioaerosols of Botanical garden (on left) and large numbers of dust particles but with negligible numbers of pollens in the bioaerosols sample collected from the market complex (on right)

CONCLUSIONS

The study shows highest count of particulate matter (counts of PM₁, PM_{2.5} and PM₁₀) with corresponding high IAQ values in the university’s market complex with higher anthropogenic activities but all other locations show significantly less PM count, indicating comparatively healthier environment with good ambient air quality. On the other hand, microbial analysis shows highest percentage of *Corynebacterium* sp. followed by *Bacillus* sp. which are responsible mostly for common skin disease.

ACKNOWLEDGEMENTS

This work was funded by Science and Engineering Research Board (DST-SERB) under grant No. ECR/2016/001321.

REFERENCES

- Dave, P., Bhushan, M., & Venkataraman, C. (2017). Aerosols cause intraseasonal short-term suppression of Indian monsoon rainfall. *Scientific Reports*, 7(1). doi: 10.1038/s41598-017-17599-1
- Grimm, H., & Eatough, D. (2009). Aerosol Measurement: The Use of Optical Light Scattering for the Determination of Particulate Size Distribution, and Particulate Mass, Including the Semi-Volatile Fraction. *Journal Of The Air & Waste Management Association*, 59(1), 101-107. doi: 10.3155/1047-3289.59.1.101

Yao, M. (2018). Reprint of bioaerosol: A bridge and opportunity for many scientific research fields. *Journal Of Aerosol Science*, 119, 91-96. doi: 10.1016/j.jaerosci.2018.01.009

AEROSOL NUMBER CONCENTRATION AND INHALED PARTICLE NUMBER IN AN EDUCATIONAL INSTITUTION LOCATED IN THE LOWER HIMALAYAS, INDIA

VIGNESH PRABHU*, ASHISH SONI, VIJAY SHRIDHAR

Environmental pollution assessment laboratory, School of Environmental and Natural Resources, Doon University, Dehradun-248006, Uttarakhand

KEYWORDS: Hindu Kush Himalaya, Particle Number, Indoor Air Quality, Inhaled Particle Number.

INTRODUCTION

One of the criteria pollutant is the atmospheric particulate matter (PM), that includes a broad class of substances existing as discrete particles over a wide range of sizes, viz Respirable particulate matter (PM₁₀) are those particles that have an aerodynamic diameter ≤ 10 microns, fine particles (PM_{2.5}) are those that have an aerodynamic diameter ≤ 2.5 microns and ultrafine particles (PM_{1.0}) have aerodynamic diameter ≤ 1 microns. Numerous epidemiological studies have found an association between outdoor atmospheric pollution and adverse human health issues (Fromme *et al.* 2007). However, Indoor air quality (IAQ) in the workplace have recently caught the attention of researchers and policy makers, because of the increase in health issues from the public (Niu *et al.* 2015). IAQ has vital implications on health of students/teachers and workers, on considering the significant amount of time spent indoors. Few studies regarding IAQ at different working environments are popular in developed countries, but scarce in the developing countries like India. Taking this into account, the present study was conducted at three indoor locations in Doon University, situated in Doon Valley, during the post-monsoon season of 2017.

METHODS

We estimated the particulate matter (PM) concentration and particle number count (PNC) in the range of 10 nm to 35 μm using the portable wide range aerosol spectrometer MINI-WRAS (Model No 1371, Grimm, Germany). Sampling was carried out in class room (180m³), library (1440m³) and canteen (210m³) of the Doon University. Sampling was carried out in the canteen during preparation of food, while during teaching hours in class room, and working time in the library. In every location, the sampler was run for one hour for consecutively three weeks. The instrument was cleaned with an air pump after every sampling to avoid any bias. In all the locations, the sampler was placed at the height of about 120 cm from ground level. Indoor temperature ($^{\circ}\text{C}$) and relative humidity (%) was monitored using a portable meter. The average number of people were 8, 25 and 20 in the canteen, classroom and library during sampling. The sampler location in the classroom, canteen and library is represented by a green color triangle; and the mean particle count in classroom, canteen, and library is also shown in Figure. 1.

RESULTS & DISCUSSIONS

The trend of PM_{1.0}, PM_{2.5} and PM₁₀ were observed to be canteen > classroom > library. The higher concentration of PM in canteen can be attributed to the process of roti making and other activities in food preparation. Though the cooking system is gas based, the higher PM in the canteen can cause of health issues among workers. In the classroom, one hour average value of PM₁₀, PM_{2.5} and PM_{1.0} was observed to 96.2 \pm 18.2 $\mu\text{g}/\text{m}^3$, 42.78 \pm 4.29 and 29.71 \pm 3.87 $\mu\text{g}/\text{m}^3$. Wide range in the standard deviation value of PM₁₀ can be attributed to the frequent movement of people inside the classroom. Low value of PM in the library can be attributed to the dry and wet washing of the floor every morning, which leads to a decrease in the PM from the floor surface. Further, the alveoli ($\leq 4\mu\text{m}$), thoracic ($\leq 10\mu\text{m}$) and inhalable fraction ($\leq 100\mu\text{m}$) were 91.44, 108.66, 164.34; 70.37, 87.04, 125.61; and 88.95, 103.73, 131.30 $\mu\text{g}/\text{m}^3$, respectively at canteen, classroom, and library. During the study period, a bimodal distribution was observed for the particles in the size range 10 nm to 35 μm . The ratio of fine to ultrafine is higher in classroom followed by canteen and library.

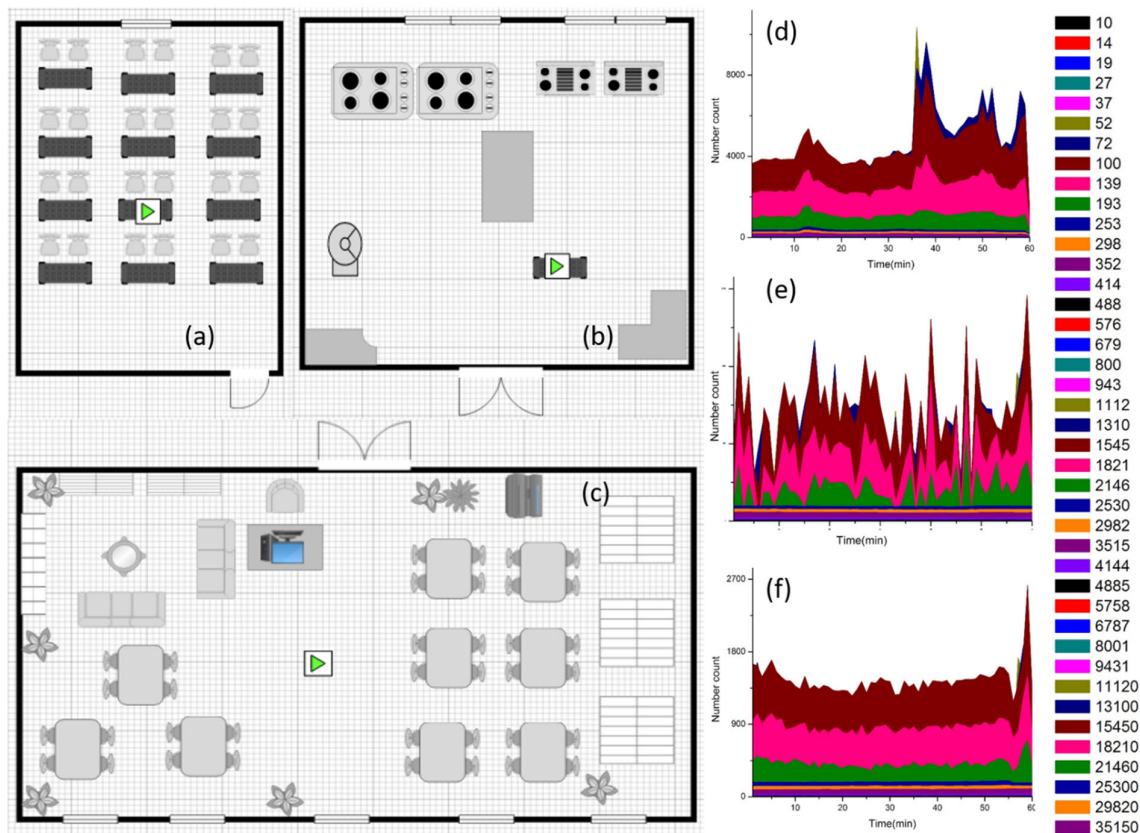


Figure. 1 Sampler location shown by green triangle in classroom (a), canteen (b), and library (c); And, the particle count by size (nm) in canteen (d), classroom (e), and library (f).

The total particle count from 10nm to 35 μm in the classroom, library and canteen was observed to be 6537, 6642, 23702. The mean of particle count in the inhalable ($>11 \mu\text{m}$), thoracic (11-3.5 μm) and respirable fraction ($<3.5 \mu\text{m}$) are mentioned in the Table. 1. Higher particle count in the canteen can be due to the food particles that get suspended during the process of roti making. In the canteen, the range of PNC was observed to be from 16810 to 48940, in the classroom, the range of PNC was observed to be from 2407-12230 and in the library, the range of PNC was observed to be from 5953 to 8281. Interestingly, there were no particles above 25000 nm size range in classroom and library. Similar kind of observations were reported in London (Jones *et al.* 2000), and Helsinki, Barcelona (Paatero *et al.* 2005).

	Inhalable fraction ($>11\mu\text{m}$)	Thoracic fraction (3.5-11 μm)	Respirable fraction ($<3.5\mu\text{m}$)	IR	IPN		
					IF	TF	RF
Classroom	0.001	0.305	6537	9.3	0.0093	2.8365	60794
Library	0.001	0.073	6642	9.3	0.0093	0.6789	61770
Canteen	0.002	0.099	23702	12	0.024	1.188	284424

Table. 1 The Particle Number Count, Inhalation Rate and Inhaled Particle Number at each site
Determining the inhaled particle number per minute (IPN) is very important in understanding the negative impact of the atmospheric particles on human health. The following equation is used to calculate the exposure of students to the particulate matter.

$$\text{IPN (N/min)} = \text{PNC (N/cm}^3\text{)} \times \text{IR (L/min)}$$

The inhalation rate (IR) for sitting adult (age 21-30) is about 9.3L/min, during light intensity activity is 12L/min. In the classroom and library, the sitting IR is used, whereas for the canteen, light intensity activity IR was used. The PNC from 10nm to 11,120 nm was used for calculating the IPN. The particles below 10 µm are usually considered as respirable fraction (Kim *et al.* 2017), however, in this study, 11µm was used, due to the limitation in the instrument design. In all the sites, more than 99% of particles inhaled were in the respirable fraction of the PM, that can penetrate deep into the alveoli of the human respiratory system.

CONCLUSIONS

The particle mass concentration and number distribution were examined in three different indoor environments in Doon university. PM concentration was found to be high in the canteen followed by classroom and library. High PM in the canteen can be attributed to the activities involved in the process of food preparation. In other sites, higher PM in the indoor environment can be attributed to the continuous suspension and re-suspension of PM in the floors. Exposure assessment showed that the people working in the canteen get exposed to higher PM when compared to the people in the classroom and library. More than 99 % of particles inhaled were in the respirable fraction of the PM in all the sites. Few recommendation like vacuum based cleaning system and screening of the windows can be implemented to decrease the indoor particles.

ACKNOWLEDGEMENTS

We are thankful for School of Environment and natural resources department of Doon University for the valuable support.

REFERENCES

- Fromme, H., Twardella, D., Dietrich, S., Heitmann, D., Schierl, R., Liebl, B., and Rden, H (2007). Particulate matter in the indoor air of classrooms-exploratory results from Munich and surrounding area. *Atmospheric Environment*, **41(4)**, 854–866.
- Jones, N. C., Thornton, C. A., Mark, D., and Harrison, R. M (2000). Indoor/outdoor relationships of particulate matter in domestic homes with roadside, urban and rural locations. *Atmospheric Environment*, **34(16)**, 2603–2612.
- Kim, M., Park, S., Namgung, H., and Kwon, S (2017). Estimation of inhaled airborne particle number concentration by subway users in Seoul, Korea. *Environmental pollution*, **231**, 663–670.
- Niu, X., Guinot, B., Cao, J., Xu, H., and Sun, J (2015). Particle size distribution and air pollution patterns in three urban environments in Xi'an, China. *Environmental Geochemistry and Health*, **37(5)**, 801–812.
- Paatero, P., Aalto, P., Picciotto, S., Bellander, T., Castao, G., Cattani, G., et al (2005). Estimating time series of aerosol particle number concentrations in the five HEAPSS cities on the basis of measured air pollution and meteorological variables. *Atmospheric Environment*, **39(12)**, 2261–2273.

CONCENTRATION AND SIZE SEGREGATED DISTRIBUTION OF FUNGAL BIOAEROSOLS IN AN OPEN LANDFILL SITE IN DEHRADUN, INDIA

M. SANDEEP¹, S. VIJAY¹

¹Environmental Pollution Assessment Laboratory, School of Environment and Natural Resources, Doon University, Dehradun- 248001, India

KEYWORDS: Bioaerosol Monitoring, Correlation, Fungal Bioaerosols, Size Segregated Distribution

INTRODUCTION

Dehradun, the capital city of North Indian state - Uttarakhand, is witnessing a rapid growth in its population since Uttarakhand became the 27th state of India on November 2000. The management of solid waste in Dehradun is under the responsibility of Dehradun Municipal Corporation (DMC). Spread across an area of 5.36 hectares of land, Sahastradhara landfill site was the sole trenching ground in the city before it was shut for use on November 2017. The practice of open and unscientific waste dumping rendered the surrounding residential area reasonably uninhabitable due to obnoxious odor and chances of contamination by waste generated pathogenic microorganisms (bioaerosols) (Yang *et al.*, 2008). Bioaerosols, chiefly in the respirable size fractions (<5 µm), are of prime importance due to their ability to infiltrate and infect the deeper parts of respiratory (Breza-Boruta, 2012). The bioaerosol dispersion and transport in the atmosphere is determined by a number of factors, including meteorological conditions, the time of the year, climatic conditions, type of source (Jones and Harrison, 2004) etc. The objectives of the study was to study the size differentiated fungal bioaerosols in an open landfill site in terms of temporal variation and relationship with prevailing meteorological conditions.

METHODS

A six-stage Anderson cascade impactor (Tisch Environmental, flow rate 28.3 liters/ min) was used to collect culturable fungal particles in the aerodynamic size ranges, ≥ 7.1 µm, 7.0–4.7 µm, 4.7–3.3 µm, 3.3–2.1 µm, 2.1–1.1 µm and 1.1–0.65 µm. The sampler was kept at a breathing height of 1.5 m in an open residential area located approximately 40 meters away from the periphery of the landfill site. Sampling was conducted for 15 minutes three times a day, three days a month for a period of one year (from September 2016 – August 2017). Samples were collected in Trypticase soy agar, incubated at 25°C for 3–7 days and enumerated in laboratory after positive-hole statistical correction as colony forming units. The bioaerosol concentration was expressed in terms of colony-forming units (CFU) per unit volume of air (CFU/m³). The on-site meteorological measurements for temperature, relative humidity and wind speed was done by a hand held Hygro - Thermo Anemometer (Extech 45160 3-IN-1). Global Data assimilation system (GDAS: <ftp://arlftp.arl.hq.noaa.gov/pub/archives/gdas0p5>), available for every 3 h was used to obtain the on-site wind direction data while rainfall data was retrieved from the online web portal of Indian Meteorological Department (<aws.imd.gov.in>). The collected data was analyzed using SPSS Version 16 for one way analysis of variance (ANOVA). The correlation coefficient was determined to identify the relationship between different variables.

RESULTS & DISCUSSIONS

The overall range and the mean total concentration of the collected fungal aerosols were obtained as 157.83 – 1666.85 CFU/m³ and 821.488 CFU/m³, respectively.

Temporal Distribution of Fungal Bioaerosols

Significant seasonal differences in mean fungal concentrations were observed between all the seasons ($p < 0.05$) except between summer and winter; and summer and monsoon (Fig.1). These decreased in

following order: monsoon (1314.18 ± 188.45 CFU/m³), autumn (890.41 ± 139.61 CFU/m³), summer (642.56 ± 259.30 CFU/m³) and winter (438.80 ± 184.67 CFU/m³). In terms of monthly variations, the monsoonal months from June to August exhibited significantly higher fungal concentrations with almost all of the other months ($p < 0.05$). The highest concentration was recorded in August (1486.29 ± 171.25 CFU/m³) and lowest in January (331.72 ± 83.65 CFU/m³). Similar results with maximum and minimum values observed in monsoon and winter respectively were also reported by Patil and Kakde, 2017.

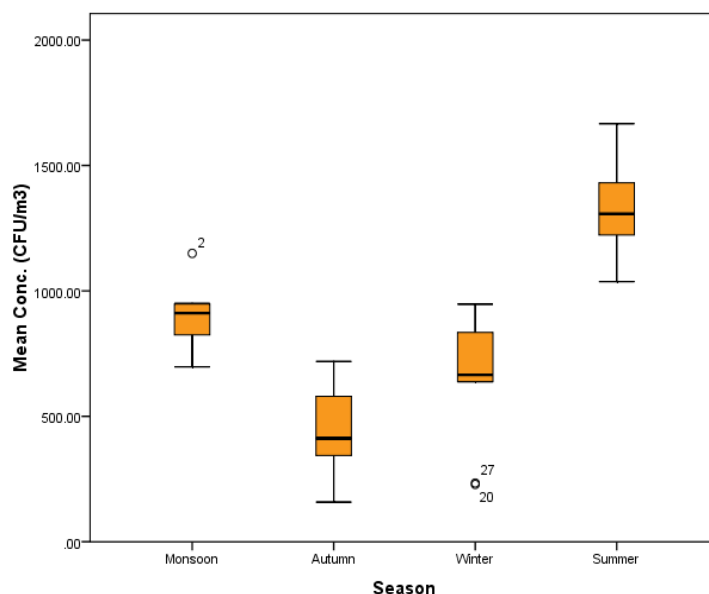


Fig. 1. Seasonal Variation pattern of total fungal concentrations at Landfill site

Particle Size distribution of airborne Fungi

The size segregated average fungal concentration for the sampling year is shown in Fig. 2. The highest concentration of fungal isolates was obtained from the size fraction with aerodynamic diameter $4.7 - 3.3 \mu\text{m}$ (196.19 ± 142.32 CFU/m³) and the lowest from $1.1 - 0.65 \mu\text{m}$ (32.31 ± 27.70 CFU/m³). Interestingly, the size fractions between $4.7 - 2.1 \mu\text{m}$ exhibited significantly higher fungal values in comparison to the fine size fractions ($< 2.1 \mu\text{m}$) ($p < 0.05$). The high fungal concentrations at the size fraction with aerodynamic diameters belonging to stage 3 and stage 4 have also been reported in the studies conducted by Li *et al.*, 2011; Raisi *et al.*, 2013.

Statistical Analysis

The relationship of fungal concentrations with meteorological parameters showed a significantly high correlation only with relative humidity ($r = 0.76$, $p < 0.01$). This may be attributed to the fact that relative humidity facilitates the mycelial growth in fungus (Jones and Harrison, 2004; Ponce-Caballero *et al.*, 2013). Thus the elevated levels of relative humidity in monsoon (60% - 80%) compared to other three seasons (20% - 57%) can be assigned to its highest fungal concentration during the rainy season. Moreover, no significance was observed between fungal concentration and other meteorological parameters (wind speed, temperature and rainfall).

The correlation between all of the size fractions is represented in Table 1. The concentration of the size fraction $4.7-3.3 \mu\text{m}$ displayed strongly positive correlation with $3.3 - 2.1 \mu\text{m}$ ($r = 0.935$, $p < 0.05$) indicating that these can be related to same sources. Significant correlations were also observed for the size fractions, $> 7.0 \mu\text{m}$ with $7.0 - 4.7 \mu\text{m}$ ($r = 0.68$, $p < 0.05$) and $1.1-0.65 \mu\text{m}$ ($r = 0.50$, $p < 0.05$); and between $1.1-0.65 \mu\text{m}$ and $2.1 - 1.1 \mu\text{m}$ ($r = 0.58$, $p < 0.05$).

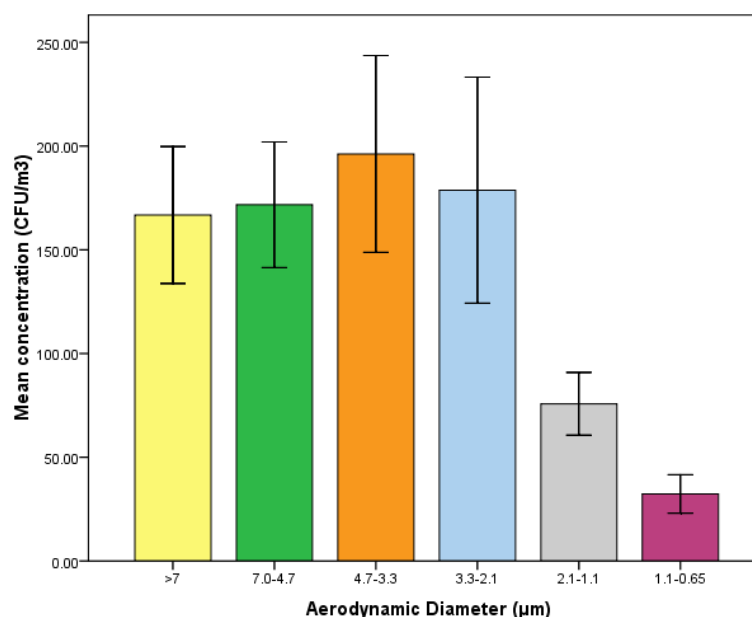


Fig.2. Size distribution of airborne fungal bioaerosols at Landfill site

Size Fractions	>7.0 µm	7.0-4.7 µm	4.7-3.3 µm	3.3-2.1 µm	2.1-1.1 µm	1.1-0.65 µm
>7.0 µm	1					
7.0-4.7 µm	0.680	1				
4.7-3.3 µm	-0.094	0.307	1			
3.3-2.1 µm	-0.209	0.193	0.935	1		
2.1-1.1 µm	0.012	0.154	0.332	0.271	1	
1.1-0.65 µm	0.500	0.585	0.097	0.077	0.227	1

Table 1. Correlation coefficients (r) of different size fractions

CONCLUSION

In the present study, the size segregated cultivable, fungal bioaerosol monitoring was conducted in the ambient air of a landfill site in Dehradun between September 2016 to August 2017. The mean concentration values varied significantly across the measurement period with monsoonal rains associated high relative humidity attributing to their highest fungal levels. The size segregated fungal mean concentrations showed nearly equal distribution in the coarse size fractions with the two maxima observed in the size fractions, 4.7 – 3.3 µm and 3.3 – 2.1 µm. This indicates the prevalence of the fungal propagules with the ability to infect tracheal and bronchial regions of the respiratory system. No significant association between majorities of size fractions shows the uniqueness of their respective sources. This is the only reported study of size segregated fungal distribution from the Sahastradhara landfill site while it was fully functional. However, the waste is still uncovered and as per DMC, 10 lakh tonne of waste is accumulated in the site. Additional studies are required to establish the limits of exposure and understand the health detrimental effects of fungal bioaerosols released from such landfill sites in India.

REFERENCES

Jones, A. M., & Harrison, R. M. (2004). The effects of meteorological factors on atmospheric bioaerosol concentrations - A review. *Science of the Total Environment*, 326(1–3), 151–180.

Li, M., Qi, J., Zhang, H., Huang, S., Li, L., & Gao, D. (2011). Concentration and size distribution of bioaerosols in an outdoor environment in the Qingdao coastal region. *Science of the Total Environment*, 409(19), 3812–3819.

Patil, N. S., & Kakde, U. B. (2017). Assessment of fungal bioaerosol emission in the vicinity of a landfill site in Mumbai, India. *International Journal of Environment and Waste Management*, 20(1), 75.

Ponce-Caballero, C., Gamboa-Marrufo, M., Lopez-Pacheco, M., Ceron-Palma, I., Quintal-Franco, C., Giacomani-Vallejos, G. and Loria-Arcilam, J.H. (2013). Seasonal variation of airborne fungal propagules indoor and outdoor of domestic environments in Mérida, Mexico. *Atmosfera*, 26(3), 369–377.

Raisi, L., Aleksandropoulou, V., Lazaridis, M., & Katsivela, E. (2013). Size distribution of viable, cultivable, airborne microbes and their relationship to particulate matter concentrations and meteorological conditions in a Mediterranean site. *Aerobiologia*, 29(2), 233–248.

Yang, K., Zhou, X. N., Yan, W. A., Hang, D. R., & Steinmann, P. (2008). Landfills in Jiangsu province, China, and potential threats for public health: Leachate appraisal and spatial analysis using geographic information system and remote sensing. *Waste Management*, 28(12), 2750–2757.

Zagro, P. I., & Zdrowotnego, E. (2012). Bioaerosols of the Municipal Waste Landfill Site As a Source of Microbiological Air Pollution and Health Hazard, 19(08), 851–862.

AEROSOL DYNAMICS IN THE INDIAN SECTOR OF SOUTHERN OCEAN AND COASTAL ANTARCTIC REGION DURING AUSTRAL SUMMER- ITS IMPLICATION ON LOCAL CLIMATE.

A. A. SHAIKH¹, H. B. MENON¹ AND S. NEHA SHAIKH¹

¹Department of Marine Sciences, Goa University, University P.O, Goa 403206, India.

KEYWORDS: Aerosol Characterization, Direct Aerosol Radiative Forcing, Indian Sector Of Southern Ocean And Antarctic Coast

INTRODUCTION:

Over the last few decades, earth faces the potential of rapid climatological changes. Global warming, polar ice melting, ozone depletion, changes in ocean circulation, changes in cloud radiative effects and increase in anthropogenic aerosols are among some of the issues that have grabbed attention in recent past (B. A. Wielicki et al, 1995). A lot of factors affect the climate, from which aerosols are the most diverse and challenging to understand due to their flux and distribution with respect to space and time. To have a better understanding of tackling the global climate change issues an insight on aerosols dynamics and atmospheric processes is necessary.

Aerosols are particles suspended in the Earth's atmosphere. They can be liquid or solid, and their diameters range from 0.01 μ m to 100 μ m (Boucher et al, 2013). They can be natural or anthropogenic in nature. Out of most of the natural aerosol systems, marine aerosols strongly influence the local and regional climate. As for the anthropogenic, black carbon is an absorbing type of aerosol which has the potential to alter the radiation budget, precipitation pattern and cloud life (Jacobson, 2001; Menon et al, 2002). Overall to understand the role of aerosols in climate change, it is important to know the source of aerosols, related removal processes and local meteorological parameters that affect the aerosol dynamics.

METHODS

The study was carried out on-board S.A Agulhas during 9th Southern Ocean Expedition that begin from 8th January 2017 till 25th February 2017. The data presented is of January 2017 (onward leg of the Expedition). The study area (28°S to 69°S) is divided in two zones, Indian sector of Southern Ocean (28°S to 60°S) and coastal Antarctic region (60°S to 69°S). The various observations carried onboard included Black carbon (BC) mass concentration by a seven channel Aethalometer (AE-42). The BC mass concentration is estimated from absorbance at 880 nm (Hansen et al., 1984). Quartz Crystal Microbalance (QCM) was used to measure aerosol particle size distribution, particle size ranged from 0.05 to 25 microns. Aerosol optical depth (AOD) measurements were carried out using MICROTOPS II sunphotometer at 380, 440, 500, 675 and 1020 nm under cloud free condition. Planetary Boundary Layer (PBL) height was estimated from lapse rate method obtained from Pisharoty radiosondes (B-3) launched at predefined stations. All the data was further used for the estimation of Direct Aerosol Radiative Forcing (DARF) using SBDART model and heating rate.

RESULTS & DISCUSSIONS

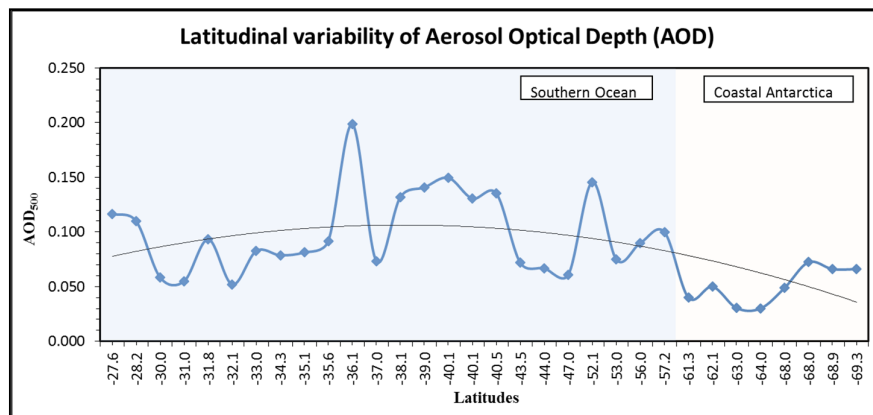


Figure 1. Latitudinal Variability of Aerosol Optical Depth (AOD_{500})

Latitudinal variation in AOD_{500} is studied for onward leg from 28.00°S to 69.23°S as represented in figure 1. Non-uniform variation in AOD_{500} is observed along the latitudes. Overall a decreasing trend is seen from mid-latitudes towards the higher latitudes. The average values (0.099) for Southern ocean (SO) is higher as compared to that of Antarctic coast (0.050), this is because there is long range transport of aerosols and more turbulent winds in the SO region as compared to the Antarctic coast where most of the aerosols are in-situ produced. An unexpected increase was observed in AOD_{500} , between 35.00°S and 45.00°S . The HYSPLIT back trajectory for this region revealed long range transport of aerosols from South American continent. Moreover, it is the Sub Tropical Frontal zone, hence complexity in the in-situ produced aerosols are expected. A slight increase in AOD_{500} is seen towards the Antarctic Coast, this is due to the advection of aerosols from the Antarctic land and highly productive coastal waters.

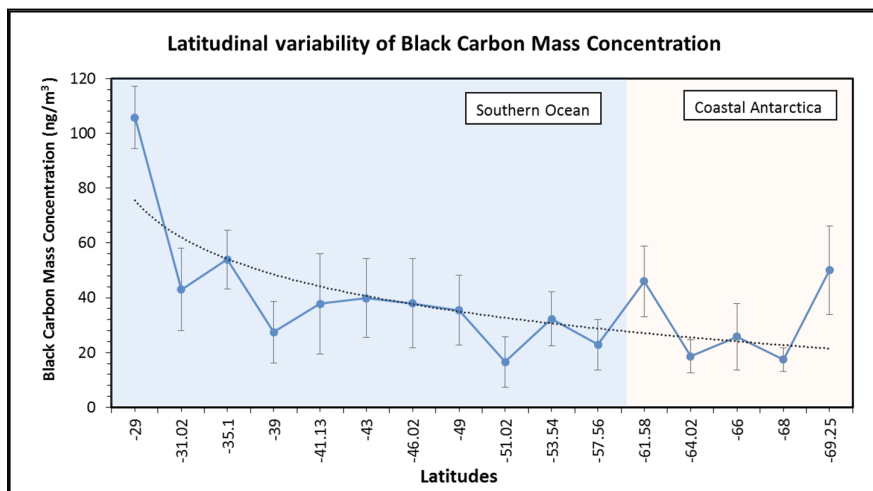


Figure 2: Latitudinal variability of Black Carbon Mass Concentration.

Figure 2 revealed a gradual decrease in Black Carbon mass concentration (BC) with irregular distribution as we move towards higher latitudes and is ranging between 16 to 150 ng m^{-3} . The values near the continent (29.00°S) are almost three times ($105.81 \pm 11.37 \text{ ng m}^{-3}$) higher than the open ocean, due to proximity to continents. In the Southern Ocean the average value of BC mass concentration was $33.59 \pm \text{ng m}^{-3}$ which is higher than coastal Antarctic region where the average value was $31.57 \pm 10.28 \text{ ng m}^{-3}$, reason being the long range transport and in-situ produced BC.

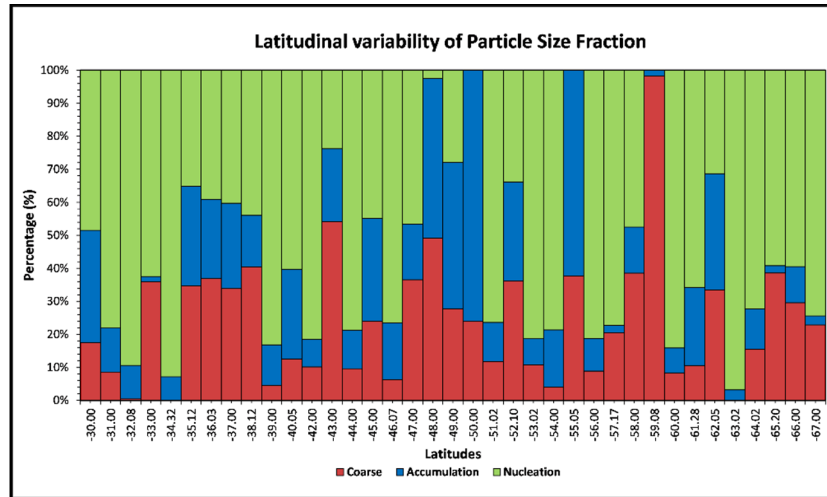


Figure 3: Latitudinal variability of Particle Size fraction.

QCM data revealed a clear dominance of fine mode (Nucleation and Accumulation) particles (73.92%) over coarse mode particles in January, this is because phytoplankton produced dimethylsulphate (DMS) derived sulphate aerosols and BC in the region; except for 59.08°S where coarse mode is 98.29% reason being the high wind speed (28 knots) leading to a turbulent conditions favorable for suspension of sea salt in atmosphere. Also, HYSPLIT back trajectory of 240hrs confirms that the winds were from over the oceanic region at 59.08°S.

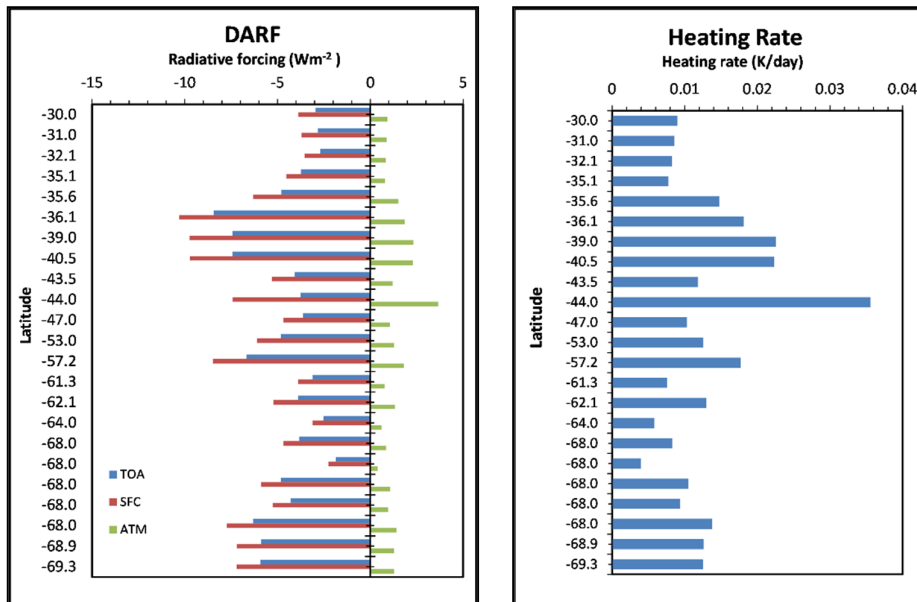


FIGURE 4: Latitudinal variability of Direct Aerosol Radiative Forcing and Heating rate

The Top of Atmosphere (TOA) forcing in the SO region during the study period ranged from -8.45 to -2.69 Wm⁻² corresponding surface forcing (SFC) ranged from -10.3 to -3.54 Wm⁻². However, in the Antarctic region TOA forcing ranged from -6.31 to -1.85 Wm⁻² and STC forcing ranged from -7.73 to -2.25 Wm⁻². The atmospheric forcing in both the regions ranged from 0.79 to 3.65 Wm⁻² and 0.4 to 1.41 Wm⁻² respectively, which is a result of the amount and type of aerosols present in the respective areas. The associated heating rates were in the range 0.007 to 0.035 K/day for SO and 0.0039 to 0.013 K/day for Antarctic coast.

CONCLUSIONS

A decreasing trend from the mid latitudes towards the high latitudes in AOD₅₀₀ and BC values, due to dominance of continental advected aerosols in mid-latitudinal area. An unexpected increase in AOD₅₀₀ and BC values were seen from 35.00°S to 45.00°S, being Sub Tropical front (SFT) region where there is in-situ input of sulphate aerosols and high wind speeds. Also, there is long range transport of aerosols from the South African continent.

A clear dominance of fine mode particles (73.92%) was seen over the coarse mode particles (26.08%). Highest percentage of aerosols are seen in the nucleation mode, which may be due to BC and gas to particle conversion (DMS).

Higher atmospheric forcing is a resultant of, difference between high SFC forcing and low TOA forcing. Since the TOA and SFC forcing more or less remained the same, no much difference was seen in the atmospheric forcing trends along the latitudes. Except for the 35.00°S to 45.00°S and at 68° S, where high forcing is a resultant of increase in composite aerosols.

The heating rate followed the exact trend of atmospheric forcing, as it is proportional to it. The positive atmospheric forcing and heating rate showed the influence of absorbing type of aerosols.

ACKNOWLEDGEMENTS

The authors wish to extend their gratitude to Space Physics Laboratory (SPL) of Indian Space Research Organization (ISRO) for the R&D project under Aerosol Radiative Forcing over India (ARFI) programme. We also thank Director, National Centre for Antarctic and Ocean Research (NCAOR) for permitting us to participate in the 9th Southern Ocean Expedition and the Vice Chancellor, Goa University for extending access to the facilities.

REFERENCES

- Boucher, O., D. Randall, P. Artaxo, C. Bretherton, G. Feingold, P. Forster, V. M. Kerminen, Y. Kondo, H. Liao, U. Lohmann, P. Rasch, S.K. Satheesh, S. Sherwood, B. Stevens and X.Y. Zhang (2013). Clouds and Aerosols. In *Climate Change 2013: The Physical Science Basis. Contribution of Working Group I to the Fifth Assessment Report of the Intergovernmental Panel on Climate Change*. (Cambridge University Press, Cambridge, U.K), 571 – 657.
- Hansen, A.D.A., H. Rosen and T. Novakov (1984). The Aethalometer: an instrument for the real time measurements of optical absorption by aerosol particles. *J. Sci. Total Environ* **36**,191–196.
- Jacobson, M.Z. (2001). Strong radiative heating due to mixing rate on black carbon in the atmospheric aerosols, *J. Nature* **409**, 695-697.
- Menon, S., J. Hansen, L. Nazarenko and Y. Luo (2002). Climate effects of black carbon aerosols in China and India. *J. Science* **80**, 2250 -2253.
- Wielicki, B.A., R.D. Cess, M.D. King, D.A. Randall and E.F. Harrison (1995). Mission to Planet Earth: role of clouds and radiation in climate, *J. Bulletin of American Meteorological Society* **76**, 11.

IMPACT OF SURFACE LAYER ENERGY AND FLUX EXCHANGES ON THE NEAR SURFACE BLACK CARBON AEROSOLS OVER A TROPICAL COASTAL REGION GOA

S. NEHA SALIM¹, H. B. MENON¹, N. V. P. KIRAN KUMAR², A. A. A. SHAIKH¹

¹Department of Marine Sciences, Goa University, Taleigao, Goa-403206, India.

²Space Physics Laboratory, Vikram Sarabhai Space Centre, Thiruvananthapuram, Kerala-695022, India.

KEYWORDS: Atmospheric Boundary Layer, Micrometeorology, Fluxes, Turbulent Kinetic Energy, Turbulence Statistics, Trajectories, Aerosols.

INTRODUCTION

The land and atmosphere exchange energy, momentum and moisture through several thermal and mechanical processes within the surface layer both vertically and horizontally which result in the surface layer forcing (Mahrt, 2012). Previous studies have reported large diurnal and seasonal variations in the atmospheric conditions, convective and wind driven mechanisms; all of these characteristics varied based on the surface features of a location (Asnani, 1993). Therefore, in order to have an accurate description of local weather and land-atmosphere energy transfer, it is essential to parametrize the surface layer characteristics existing over the study area. Thus, the paper explains the results for the preliminary studies carried out on the surface layer meteorological conditions and the energy flux exchanges at a tropical coastal station Goa (15° 27'N, 73° 50'E) along the west coast of India. This has been carried out for the time series observations obtained for the period of summer-monsoon (SMS) and post-monsoon (PMS) seasons of the year 2015 in order to understand the accumulation and removal mechanism of the black carbon (BC) (i.e., absorbing type of aerosols) vis a vis the effect of turbulence on the atmospheric boundary layer (ABL).

SITE, INSTRUMENTATION AND METHOD

The experiment conducted at the Goa University Campus, Goa (15° 27' N, 73° 50'E, 50m AMSL) (Figure. 1) was to understand the characteristic exchanges of energy and fluxes within the surface layer and its role in governing the mesoscale processes and regional meteorology with its direct effect on the black carbon concentration. This site has been one of the experimental stations under two multi-institutional projects, Network of Observatories for Boundary Layer Experiments (NOBLE) and Aerosol Radiative Radiative Forcing Over India (ARFI) of the (ISRO-GPB) Geosphere, Biosphere Programme by the Space Physics Laboratories of Indian Space Research Organization.



Figure 1. Geographical representation of the study area along with the instrumentation setup.

To carry out the study, a 32m tall meteorological tower has been installed. Background meteorological observations such as air temperature (AT), relative humidity (RH), wind speed (WS), wind direction (WD), atmospheric pressure (P) and rainfall (R) were obtained from low frequency sensors mounted on the tower at 18m level above the ground. To estimate the turbulent fluxes and to analyse stability the orthogonal components of wind and virtual temperature observations were obtained from high frequency sensor mounted at 20m level of tower. The measurements for black carbon mass concentration were obtained using AE31 Aethalometer having seven wavelengths (370, 470, 520, 590, 660, 880 and 950 nm). BC mass concentration were estimated from the absorbance values at 880 nm. High frequency data were used for analysing surface layer turbulence characteristics through estimation of sensible heat flux (H), momentum flux (τ), turbulent kinetic energy (e) and stability parameter (z/L) using eddy correlation method (Kaimal and Finnigan 1994) and Monin-Obukhov similarity theory. The magnitude of mechanical turbulence is quantified using turbulent kinetic energy/mass (e) while vertical exchange of momentum and energy fluxes are quantified through momentum flux (τ) and sensible heat flux (H). Along with this stability parameter (z/L) is also estimated. These parameters were computed using the following equations,

$$e = \frac{1}{2} * [\overline{u'^2} + \overline{v'^2} + \overline{w'^2}] \quad \text{———— (1)} \quad \tau = \rho * \sqrt{(\overline{u'w'})^2 + (\overline{v'w'})^2} \quad \text{———— (2)}$$

$$H = \rho * C_p (\overline{w'\theta'_v}) \quad \text{———— (3)} \quad L = - \frac{u_*^2 \overline{\theta'_v}}{(\kappa g \overline{w'\theta'_v})} \quad \text{———— (4)}$$

Where, u' , v' and w' are the fluctuations of the orthogonal wind components, ρ is air density, C_p is the specific heat of air at constant pressure, $\overline{\theta'_v}$ is the averaged fluctuation in virtual temperature, z is the reference height of observation (here 20m) and L is the Obukhov length. Turbulence characteristics is quantified using M-O similarity theory through non-dimensionalized standard deviation of wind components and virtual temperature (u , v , w and t) normalized using frictional velocity (u_*) and scaling temperature (T_*) with its variation studied against z/L (Foken and Wichura, 1996). Aerosol optical depth due to black carbon AOD(BC) have been estimated using equation, (Hess et al., 1998)

$$AOD(BC) = (ABL \text{ height in kms}) * \frac{x}{0.000059} * (6.385 * 10^{-7}) \quad \text{———— (5)}$$

where, x is the BC mass concentration in ngm^{-3} . ABL height was evaluated using HYSPLIT MODEL; wherein mixed layer depth (MLD) was retrieved on the diurnal scale for the study period. HYSPLIT back trajectory analysis was used to compute trajectories of air parcel to investigate their provenance.

RESULTS AND DISCUSSIONS

Seasonal mean diurnal variability of parameters along with the respective standard deviations obtained from low and high frequency sensors mounted at 18m and 20m levels above ground (representative height for observation) are shown in Figure 2. The vertical lines indicate standard deviation. On most of the clear days, due to enhanced solar insolation, an increase in thermal inversion was noticed. The inversion peaks around 12:00LT then gradually decreases after sunset around 17:00LT. The mean difference in the day-time and the night-time air temperature during SMS is $\sim 3^{\circ}\text{C}$ while it is 5°C during PMS. Seasonal mean RH was high during SMS $\sim 88.08 \pm 4.96\%$ while it was low during PMS, $\sim 83.36 \pm 10.55\%$. The atmospheric pressure over the site exhibits semi-diurnal oscillations with two prominent maxima and minima. Maxima occurred around 10:00LT and 22:00LT respectively while minima occurred around 04:00LT and 17:00LT during both the seasons. Diurnal variation of surface winds exhibits a peak in the noon hours and minimum during the mid-night and early morning hours (Figure 2(c).) During SMS, seasonal mean wind speed was $\sim 5.01 \pm 1.10 \text{ms}^{-1}$ while during PMS it was $\sim 3.51 \pm 0.78 \text{ms}^{-1}$; which indicates an increased wind speed during SMS due to the strong south-west monsoonal winds. Figure 1(d). distinctly shows the presence of local land-sea breeze phenomenon during PMS; wind direction indicates the onset of day-time sea breeze from $\sim 08:00\text{LT}$ throughout the day while the onset of night-time land-breeze is marked by shift in direction of wind at $\sim 19:00\text{LT}$. This diurnal flow of land-sea breeze is significantly reduced during SMS due to south-west monsoonal winds. Sensible heat flux (H) varies in-phase with the solar insolation attaining peak value of $\sim 146.76 \pm 39.73 \text{Wm}^{-2}$ during SMS and $\sim 232.79 \pm 52.21 \text{Wm}^{-2}$ during PMS at 13:00LT. The day-time mean sensible heat flux is positive indicating heat flux transport from the surface to the atmosphere while night-time heat flux is negative indicating transport directed towards the surface. Average turbulent kinetic energy observed during SMS is higher than during PMS reaching peak value $\sim 1.90 \pm 0.70 \text{m}^2 \text{s}^{-2}$ (15:30LT) during SMS while it is $\sim 1.50 \pm 0.75 \text{m}^2 \text{s}^{-2}$ (12:30LT) during PMS which is

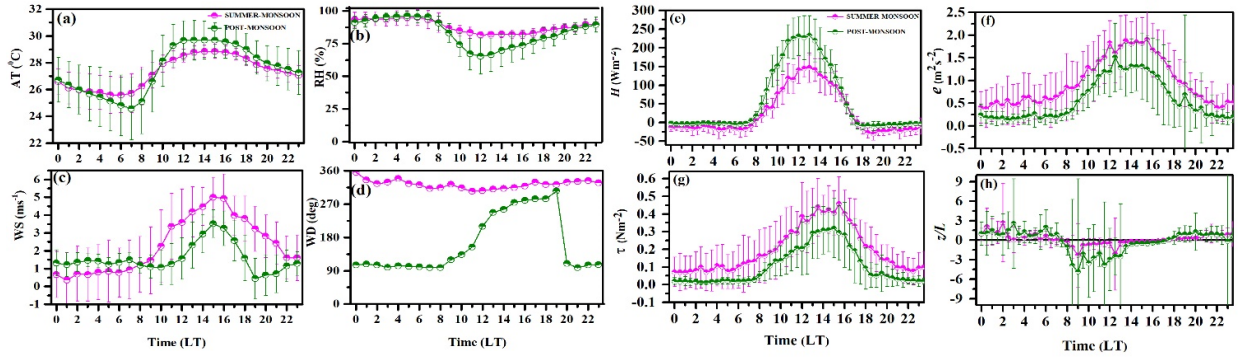


Figure 2. diurnal mean seasonal fluctuations of (a) Air temperature, (b) Relative humidity, (c) Wind speed, (d) Wind direction, (e) Sensible heat flux (H), (f) Turbulent kinetic energy (e), (g) Momentum flux (τ), (h) Stability parameter (z/L).

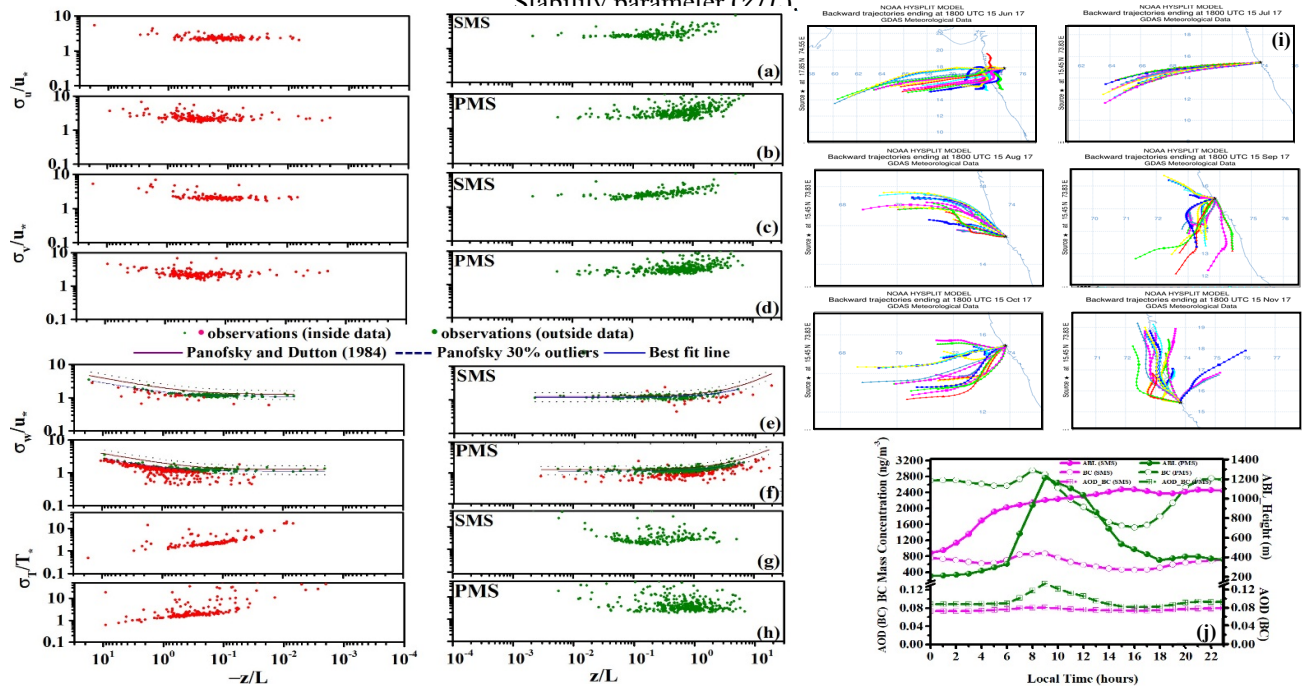


Figure 3. Fluctuations in the normalized standard deviation of (a)-(b) zonal wind component(u), (c)-(d) meridional wind component(v), (e)-(f) vertical wind component(w), (g)-(h) virtual temperature (T) against (z/L), (i) HYSPLIT derived monthly back trajectories, (j) seasonal diurnal variations in ABL height, black carbon (BC) mass concentration and aerosol optical depth due to black carbon.

attributed to the high magnitude of wind speeds accounted during SMS. During the night-time, horizontal components of wind are high which resulted in night-time increase in turbulent kinetic energy. Momentum flux (τ) varies in-phase with e in all seasons reaching average peak value $\sim 0.46 \pm 0.15 \text{ Nm}^{-2}$ (15:30LT) during SMS while it is $\sim 0.32 \pm 0.17 \text{ Nm}^{-2}$ (15:00LT) during PMS. During the day-time (08:00-17:00LT), z/L values were negative indicating instability, while it was positive during the remaining hours of the day exhibiting near-neutral conditions. To understand turbulence characteristics, normalized standard deviation of orthogonal wind component and virtual temperature were studied against z/L as depicted in (Figure 3(a-h)). In Figure 3(a-d), the values of σ_u/u_* and σ_v/u_* increases strongly with increase in z/L under strongly stable regions which can be due to damping of the motion of turbulent eddies due to the stabilizing effects. The variation in σ_w/u_* with z/L agrees with $1/3$ power law during free convection under unstable regions and followed similarity relationship under stable atmospheric conditions. The stability range between -0.1

to 0.1 reveals less scatter in σ_w/u_* values which indicates that σ_w/u_* is independent of z/L in this region. In addition, an increase in σ_w/u_* values were observed with increase in instability. As z/L approaches near-neutral condition, σ_w/u_* decreases attributing to the suppression in the magnitude of vertical wind due to negative buoyancy. Figure 3(i). shows the monthly HYSPLIT back trajectories of air parcel during the period of study. Trajectories shows seasonal reversal in wind pattern. Figure 3(j). shows the seasonal mean diurnal variation of ABL height along with BC mass concentrations and the respective aerosol optical depth. Their coupled variation shows strong seasonally varying cycle with high values accounted during PMS and low during SMS. Mass concentration of BC and AOD(BC) exhibit distant diurnal variation controlled by ABL height. Diurnal variability reveals high values of BC concentration as well as AOD(BC) between 06:00LT to 10:00LT which reaches a minimum around 16:00LT. It further increases from 17:00LT attaining next peak at 22:00LT until midnight. The observed seasonal mean BC concentration and AOD(BC) during SMS was $648.7 \pm 209.4 \mu\text{gm}^{-3}$ and 0.018 while during PMS it was $2358.6 \pm 542.4 \mu\text{gm}^{-3}$ and 0.046 respectively.

CONCLUSIONS

Present study has been carried out to understand surface layer characteristics at a coastal station and its implication on the dispersion of black carbon (BC) aerosols. The highlights of the study are given below:

1. SMS was marked by an increase in precipitation, high wind speeds and reduced solar insolation while during PMS an increase in solar insolation and low wind speeds were observed.
2. The magnitude of thermally induced turbulence measured from sensible heat flux (H) was found to be the lowest during SMS with its seasonal mean $\sim 24.62 \pm 59.09$ (13:00LT) Wm^{-2} while high during PMS $\sim 54.80 \pm 87.34 \text{ Wm}^{-2}$. The magnitude of mechanically induced turbulence measured from turbulent kinetic energy (e) and momentum flux (τ) was observed to be large during SMS while low values were observed during PMS. Thus, during SMS, instability within the surface layer was induced greatly by mechanical forcing with less contribution from thermal forcing while during PMS, instability was as a result of both thermal and mechanically induced forcing.
3. Irrespective of any season, the fluctuations of vertical wind with stability parameter agrees with 1/3 power law for free convection under unstable conditions while under stable conditions it is independent of z/L due to the influence of negative buoyancy on the vertical motion of eddies. The fluctuations of the horizontal velocities against z/L shows large scatter which is attributed to motion of the large convective eddies controlling their variances.
4. These diurnal and seasonal variabilities greatly influence the concentration of black carbon aerosols. Observed concentration of black carbon (BC) aerosols were lower during SMS as a result of its removal by precipitation and dispersion by high wind speeds, however stable calm conditions with low wind speeds prevailing in PMS resulted in less dispersion and increased trapping of black carbon aerosols.

ACKNOWLEDGEMENTS

This study has been conducted as a part of ISRO-GBP(NOBLE) and ISRO-GPB(ARFI) Project. We gratefully acknowledge ISRO for funding the project. We are thankful to the V.C. of Goa University for the facilities rendered. Timely support extended from Dr. K. Rajeev, SPL is greatly acknowledged.

REFERENCES

- Asnanai G.C. (1993). Tropical Meteorology. Vol 1 Indian Institute of Tropical Meteorology India. 603 pp.
- Foken, T., & Wichura, B. (1996). Tools for quality assessment of surface-based flux measurements. *Agricultural and forest meteorology*, 78(1-2), 83-105.
- Hess, M., Koepke, P., & Schult, I. (1998). Optical properties of aerosols and clouds: The software package OPAC. *Bulletin of the American meteorological society*, 79(5), 831-844.

Kaimal, J. C., & Finnigan, J. J. (1994). *Atmospheric boundary layer flows: their structure and measurement*. Oxford university press.

Mahrt, L. (2010). Variability and maintenance of turbulence in the very stable boundary layer. *Boundary-layer meteorology*, 135(1), 1-18.

AEROSOL CHARACTERIZATION IN THE SUBTROPICAL HUMID REGION OF NORTHERN INDIA

PRAYAGRAJ SINGH¹, ADITYA VAISHYA², SHANTANU RASTOGI¹

¹Department of Physics, Deen Dayal Upadhyaya Gorakhpur University, Gorakhpur - 273 009, India.

²Space Physics Laboratory, Vikram Sarabhai Space Centre, ISRO, Thiruvananthapuram - 695 022, India.

KEYWORDS: Central Igp, Bc, Ångström Exponent, Aod.

INTRODUCTION

The Indo-Gangetic plain (IGP) in South Asia is especially unique region in terms of aerosols loading and diversity that varies seasonally, which is influenced by various natural and anthropological aerosols due to its large-scale urbanization and high pollution emissions (Lawrence and Lelieveld, 2010). Thus, it is essential to discriminate atmospheric aerosols into different types because of differences in sources, meteorology, and regional dynamics of the region. Aerosols have a different climatic effect due to their size, composition and absorptive nature. Most of the aerosols are highly reflecting in nature that exerts a negative radiative forcing on the atmosphere. While some of the other aerosols such as mineral dust and black carbon (BC), absorb the shortwave radiation, leading to positive forcing within the atmosphere and negative forcing at the surface. The IGP is well recognized to be one of the most dominant sources of absorbing aerosols Such as mineral dust and BC. In recent years, the study of BC aerosols over the IGP region has gained considerable attention by the research community due to its adverse effects on air quality and changes in the surface temperatures, in addition to influencing visibility, human health, crop yields and terrestrial ecosystems. Apart from its direct effect on the atmosphere, BC has also influence cloud droplet number concentrations and related alterations of cloud properties (Kaufman et al., 2002).

Hence, the long-term measurement of BC is important as it is one of the major anthropogenic components of an aerosol system for the evaluation of emission control measures and to assess impacts on health and climate (Ramanathan and Carmichael, 2008). Along with, examining aerosol optical depth (AOD) and Ångström exponent (α) are the essential parameters for understanding the aerosol size distribution and their source strength. The present study comprises the radiative characteristics of BC mass concentration and AOD measurements at Gorakhpur, in the central IGP. The results are analyzed to identify the relative contribution of both anthropogenic and natural sources during different seasons to the aerosol loading over the study region.

MEASUREMENT SITE AND METHODOLOGY

Ground-based aerosol measurements were carried out on the second floor of the Physics Department building at DDU Gorakhpur University campus (26.75°N; 83.38°E; 85 m amsl). The measurement site typically experiences a subtropical humid climate and geographically located in the Terai belt of eastern Uttar Pradesh, at the foothills of Shivalik Himalaya i.e. central IGP. The measurement site is adjacent to the state and national highways that carry heavy traffic load, with no direct effect of industrial activities exists. The major sources of aerosols are from vehicular emissions, domestic heating, biomass burning activities as well as local and long-range transport of dust. Climatic conditions over this region are experiences very hot and dry during Pre monsoon (Pre M), hot and humid during monsoon (M) and Post monsoon (Post M), and dry during Winter (W) season. Western disturbances in W season bring occasional rains and formation of dense fog over this part of the IGP. Depressions and moderate low-pressure systems, over the northern Bay of Bengal, formed during M season bring moderate to heavy rainfall over this region.

Near real-time measurements of spectral optical attenuation made by using multi-wavelength Aethalometer (AE 33) at seven wavelengths (370, 470, 520, 590, 660, 880 and 950 nm) is used in the calculation of BC mass concentration. From the spectral attenuation measurements, spectral values of absorption coefficient

as well as absorbing Ångström exponent (α_{abs}) were estimated. The instrument is operated at a flow rate of 2 LPM and the data is logged with a time resolution of 1 minute. The other details related to instruments, data collection, analysis, correction and procedures are discussed in several earlier publications (Drinovec et al., 2015; Vaishya et al., 2017). Spectral AOD measurements were obtained by using a passive ground-based Multi-Wavelength Radiometer (MWR) at ten narrow wavelength bands centered at 380, 400, 450, 500, 600, 650, 750, 850, 935 and 1025 nm. The working principle of MWR is based on filter wheel radiometer technique and radiation passes through a field limiting optics with a field of view is $<2^\circ$ (Moorthy et al., 1988). The instrument operates in a fully automatic mode employing a passive equatorial mount and the measurements collected at regular intervals of 2 minute over the entire wavelength range. Spectral AODs were estimated from the MWR following Langley plot technique at each of the wavelengths on all clear and partly clear days. The details about the instrument, its measurement protocol and cloud screening of the raw data are discussed by several investigators (Gogoi et al., 2009; Moorthy et al., 1999). In the present study, we report four years data (March 2014- February 2018) of BC and AOD measurements over the Gorakhpur region.

RESULTS AND DISCUSSIONS

The slope of the absorption coefficient and wavelength dependency represents a constant called as α_{abs} which is a useful parameter in the identification of the sources of BC. The absorption coefficient of BC shows strong wavelength dependence for emission sources like biomass burning while weaker wavelength dependence for fossil fuel combustion (Kirchstetter et al., 2004). In the present study, in order to ascertain source characteristics of BC over Gorakhpur, daily values of α_{abs} and BC are used. Figure 1 shows the variation of α_{abs} with respect to BC mass concentration during different season. It is seen that α_{abs} value remains high ranging from 1.0 to 2.1 and 0.8 to 2.0, with $\sim 55\%$ and $\sim 60\%$ values of α_{abs} was observed in the range of 1.2-1.5 indicating biomass burning as major source of BC during Post M and W season. It also shows the higher BC values, often exceeding $20 \mu\text{g m}^{-3}$ during the months of Post M and W season. During M season, relatively low values of α_{abs} and BC was observed in the range of 0.4-1.5 and $0.5- 13.5 \mu\text{g m}^{-3}$ indicates dominant contribution of fossil fuel emission. It may be due to rainfall occurred during this season resulting in to washout of BC. Whereas, during Pre M season, $\sim 85\%$ of α_{abs} are observed in the range of 1-1.6 suggests the mix contribution to BC from biomass burning and fossil fuel emissions.

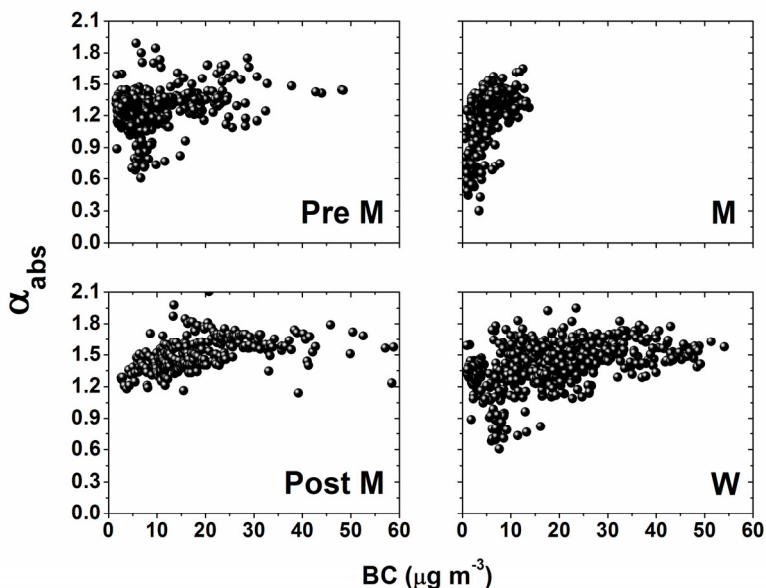


Figure 1. Correlation plot of absorbing Ångström exponent with BC mass concentration.

For the present study, the characterization of dominant aerosol types over the study region is performed by using measurements of AOD₅₀₀ and Ångström exponent at 380-850 nm ($\alpha_{380-850}$) due to their strong dependence on wavelength. In this method, the correlation of AOD₅₀₀ and $\alpha_{380-850}$ can be used to determine the physically interpretable cluster region of different types of aerosol sources in higher aerosol loading region. Figure 2 (a) shows the correlation plot between AOD₅₀₀ and $\alpha_{380-850}$ by using MWR measurements to characterize the types of aerosols over the GKP region. We have observed four major aerosol types viz., desert dust (DD), Urban/industrial and biomass burning (UB), continental average (CA) and mixed type (MT) aerosols represented by dark grey, purple, red and blue colored filled circles respectively. The threshold values of AOD₅₀₀ and $\alpha_{380-850}$ for DD aerosols attributes presence of coarse mode particles transported from arid/semi-arid regions is >0.5 and <0.6, While for UB aerosols which includes fine mode particles originated by anthropogenic activities is >0.4 and >1. The threshold value for CA aerosols, also delineate as background aerosol type is <0.2 and <1. The remaining values of AOD₅₀₀ and $\alpha_{380-850}$ are falls in the range of 0.23 to 1.57 and 0.16 to 2.35 respectively remains considered as MT aerosols.

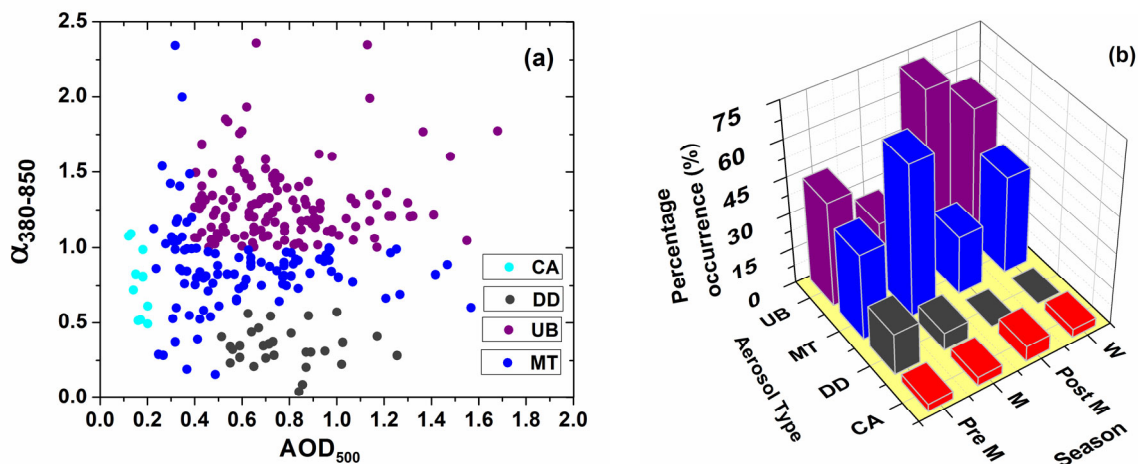


Figure 2. (a) Correlation plot of Aerosol optical depth at 500 nm (AOD₅₀₀) with Ångström exponent at 380-850 nm ($\alpha_{380-850}$) for the identification of dominant aerosol types over the study region, and (b) Percentage contribution of identified aerosol types for different season over the study region. Here, CA, DD, UB, and MT represents Continental average, Desert dust, Urban/industrial and biomass burning, and Mixed type aerosols, respectively.

The percentage contribution of each aerosol types for different season over the study region is presented in Figure 2 (b). The study revealed that the UB and MT type aerosols are mostly dominant throughout the study period. During Post M and W season, the UB type aerosols have maximum contribution (71.4% and 56.2% respectively) suggesting dominance of fine mode aerosols due to biomass burning and anthropogenic activities. The MT aerosols are observed more than 25% throughout the study period while maximum contribution was observed during M (63%) followed by W (40.4%) and Pre M (36%) season. The MT aerosols are formed due to coagulation and hygroscopic growth of different sizes of aerosol particles belonging to different emission sources under high RH conditions. During the study period, the percentage contribution of DD is highest during Pre M (17.3%) followed by M (7.4%) season and found to be completely negligible during Post M and W season. The contribution of CA type aerosols is found to be 6.4% during Post M season and relatively insignificant (~2%) in the rest of the season.

CONCLUSIONS

Higher values of α_{abs} (>1) during Post M and W season indicates biomass burning as major source of BC. On the contrary, the lower values of α_{abs} was observed during M season suggests the dominant contribution of fossil fuel emission While Pre M season shows the mix contribution to BC from biomass burning and fossil fuel emissions.

UB and MT type of aerosols are found to be most dominant. UB type of aerosols have maximum contribution during Post M (71.4%) and W (56.2%) season. MT aerosols are observed more than 25% throughout the study period while maximum contribution was observed during M (63%) season. While the DD type of aerosol are more frequently occurred in Pre M season.

ACKNOWLEDGEMENTS

This work is carried out under the Aerosol Radiative Forcing over India (ARFI) project of ISRO-GBP.

REFERENCES

Drinovec, L. *et al.*, The " dual-spot" Aethalometer: an improved measurement of aerosol black carbon with real-time loading compensation, *Atmospheric Measurement Techniques* **8**(2015), pp. 1965-1979.

Gogoi, M.M., Krishna Moorthy, K., Babu, S.S., Bhuyan, P.K., Climatology of columnar aerosol properties and the influence of synoptic conditions: First-time results from the northeastern region of India, *Journal of Geophysical Research: Atmospheres* **114**(2009).

Kaufman, Y.J., Tanré, D., Boucher, O., A satellite view of aerosols in the climate system, *Nature* **419**(2002), p. 215.

Kirchstetter, T.W., Novakov, T., Hobbs, P.V., Evidence that the spectral dependence of light absorption by aerosols is affected by organic carbon, *Journal of Geophysical Research: Atmospheres* **109**(2004).

Lawrence, M., Lelieveld, J., Atmospheric pollutant outflow from southern Asia: a review, *Atmospheric Chemistry and Physics* **10**(2010), p. 11017.

Moorthy, K.K., Nair, P.B., Murthy, B., A study on aerosol optical depth at a coastal station, Trivandrum, *IJRSP* **17**(1988), pp. 16-22.

Moorthy, K.K., Niranjana, K., Narasimhamurthy, B., Agashe, V., Murthy, B., *Aerosol climatology over India: 1-ISRO GBP MWR network and database, ISRO-GBP-SR-03-99*. Indian Space Res. , Bangalore (1999) 69 pp.

Ramanathan, V., Carmichael, G., Global and regional climate changes due to black carbon, *Nature geoscience* **1**(2008), p. 221.

Vaishya, A., Singh, P., Rastogi, S., Babu, S.S., Aerosol black carbon quantification in the central Indo-Gangetic Plain: Seasonal heterogeneity and source apportionment, *Atmospheric Research* **185**(2017), pp. 13-21.

STUDIES ON SEASONAL VARIATION OF INDOOR RADON, THORON AND PROGENY CONCENTRATIONS AROUND HEMAVATHI RIVER BASIN, KARNATAKA, INDIA

R.S.NIRANJAN¹ AND C.NINGAPPA²

¹Department of Physics, Government First Grade College For Women, Holenarasipura Taluk, India.

²Department of Physics, Vidya Vikas Institute of Engineering and Technology, Mysuru-570028,India.

(*Correspondence at ningappacvviet@gmail.com)

KEYWORDS : Season, Radon, Ssntd, Dose

ABSTRACT

The seasonal variation of radon, thoron and their progeny concentration in indoor dwellings was measured around Hemavathi river basin, Karnataka state, India. Pinhole dosimeter based on Solid State Nuclear Track Detectors (SSNTDs) have been used for the measurement during 2017-18. The annual effective dose due to radon, thoron and their progeny in the study area ranges from 1.99 to 4.74 mSv.y⁻¹.

INTRODUCTION

The primordial radionuclides present on the earth crust are responsible for the terrestrial background radiation. Radioactive nuclides are present in different amounts in soils, building materials, water, rocks and atmosphere. Radionuclides ⁴⁰K, ²³⁸U, ²³²Th, ²²²Rn, ²²⁰Rn and their progeny were present in indoor are transferred to human beings through ingestion and inhalation (Bodansky D et al., 1989). Exposure to high concentrations of radon and its short-lived progeny for a long period leads to the occurrence of lung cancer (Axelson O et al., 2002). Granite is one of the most important rocks used for the flooring in dwellings. Granite has high concentration of radionuclides than compared to other type of rocks (Sannappa J. et al., 2003; Ningappa C et al., 2008). The radiation emitted from granites contributes higher exposure dose to the human beings living in granite floor dwellings. Inhalation dose received by human beings is also depends on the type of dwellings. In view of this, studies on environmental radiation levels are very important. The aim of the present study was to measure the concentrations of radon, thoron and their progenies and the estimation of total annual effective dose due to radon, thoron and their progeny concentrations.

STUDY AREA

The area of the study is Hemavathi river basin (12°32' -13°08' N and 75°24'- 76°26' E), South Karnataka, India (Shown in Fig-1). This river originates from the Western Ghats at an elevation of about 1,219 m near Ballalarayana durga in Chikmagalur District, Karnataka State and flows through Chikamagalur, Kodagu, Hassan and Mandya districts before joining the river Kaveri at Krishna Raja Sagar (KRS). The common types of rocks are Charnokite, gneisses, unclassified crystallines, slates, phyllites & schists, Dharwars, Granite, peninsular gneiss, major type of rock found is peninsular gneiss (MICHI 2017).

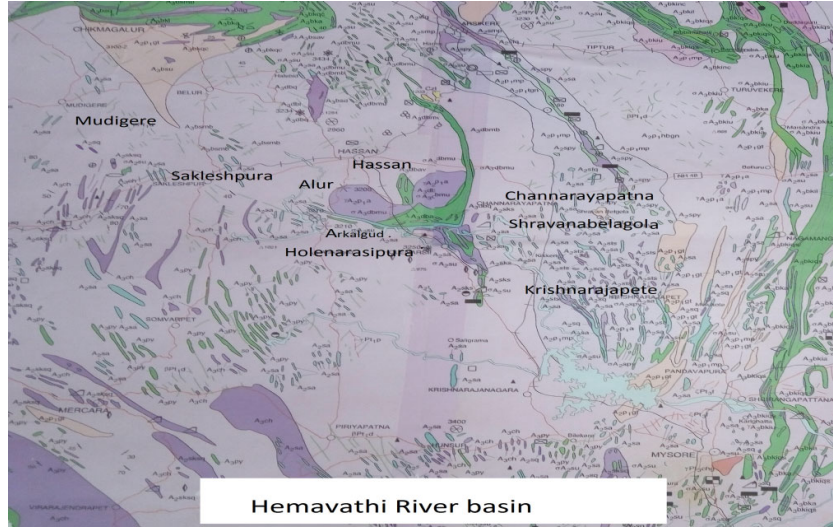


Figure 1. Hemavathi river basin.

MATERIALS AND METHODS

Indoor radon, thoron and their progeny were measured using pin hole dosimeter cup based on Solid State Nuclear Track Detectors (SSNTDs). Pinhole dosimeters were suspended from the mid-point of the house at a height of 2 m from ground level. At the end of the stipulated period of exposure, the dosimeters were retrieved and are etched with 2.5N NaOH solution for 1 h at a bath temperature of 60°C. The track density of alphas in the film was determined using a spark counter. The concentration of radon (CR) and thoron (CT) were calculated using following equations (Oufnia, L D et al.,2005).

$$C_R(Bqm^{-3}) = \frac{T_1 - B}{txK_r} \quad (1)$$

$$C_T(Bqm^{-3}) = \frac{T_2 - T_1}{txK_t} \quad (2)$$

where, T1 and T2 are the track density (tracks cm⁻²) of the film in the radon and radon + thoron chamber, B is the background track density in unexposed LR-115 detector, measured as 6 tracks cm⁻², t is the period of exposure (days) and Kr (0.017±0.002 tracks cm⁻² d⁻¹ Bq⁻¹ m⁻³) and Kt (0.010±0.001 tracks cm⁻² d⁻¹ Bq⁻¹ m⁻³) are the calibration factors of radon and radon + thoron chambers, respectively. Equilibrium equivalent thoron concentrations (EETC) were calculated using equation (Oufnia, L D et al., 2005).

$$EETC(Bqm^{-3}) = \frac{T_T - B}{txS_T} \quad (3)$$

Where, T_T is the track density in Direct Thoron Progeny sensor (DTPS), and S_T is the sensitivity factor for thoron progeny (0.94 ± 0.027 tracks cm⁻² d⁻¹ Bq⁻¹ m⁻³). The tracks obtained from DTPS were eliminated from Direct Radon Progeny Sensor (DRPS) as mentioned in equation 4 (Oufnia, L D et al., 2005).

$$T_{Rn} = T_{DRPS} - \left[\frac{\eta_{RT}}{\eta_{TT}} \right] T_{DTPS} \quad (4)$$

Where, T_{Rn} are tracks only due to radon progeny, T_{DRPS} are total tracks in DRPS, T_{DTPS} are total tracks in DTPS, η_{RT} is the track registration efficiency (0.01 ± 0.0004) for radon progeny in DRPS and η_{TT} is the track registration efficiency (0.083 ± 0.004) for thoron progeny in DTPS. The equilibrium equivalent radon progeny concentrations (EERC) is calculated using equation 5 (Oufnia, L et al., 2005).

$$EERC(Bqm^{-3}) = \frac{T_{Rn} - B}{txS_R} \quad (5)$$

where, S_R is the sensitivity factor for radon progeny (0.09 ± 0.0036 tracks cm⁻² d⁻¹ Bq⁻¹ m⁻³). The total annual effective dose received by the individuals in indoor environment is the sum of the annual effective dose from radon (AEDR) and from thoron (AEDT) (Oufnia, L D et al., Surinder Singha D et al., 2005).

$$AEDR = [(C_R \times 0.17) + (EERC \times 9)] \times 8760 \text{h} \times 0.8 \times 10^{-6} \quad (6)$$

$$AEDT = [(C_T \times 0.11) + (EETC \times 40)] \times 8760 \text{h} \times 0.8 \times 10^{-6} \quad (7)$$

RESULTS AND DISCUSSION

The ^{222}Rn and ^{220}Rn gas concentrations were measured in two types of dwellings for four seasons and the results are summarized in Table 1 to Table 4. It can be observed from the Tables that the indoor radon concentration (C_R) varied from 21.57 to 171.24 Bq.m⁻³. The thoron concentration (C_T) varied from 17.78 to 164.74 Bqm⁻³. The variation in the values of C_R and C_T might be due to the difference in topography in different geographic location of each village, ventilation conditions and building materials used in the construction of the houses used for investigation. Maximum annual effective dose has been observed during winter and minimum during summer. Maximum total annual effective doses of radon, thoron and their progeny were observed in concrete roofing and granite floor dwellings of Sharavanabelagola of Channarayapatna taluk dwellings in winter season as compared to other dwellings of the study area. Granites have higher activity of radionuclides such as ^{226}Ra , ^{232}Th and ^{40}K . Low annual effective dose is observed in mangalore tile(R) cement (F) dwellings at Sakleshpura taluk during summer, because of good ventilation. The total annual effective dose obtained in the study area is within the safe range from 3 to 10mSv.y⁻¹ (ICRP 2011) and also below the recommended reference level of 10 mSv.y⁻¹ (WHO 2009).

CONCLUSION

Granite floor and concrete roof dwellings have high annual effective dose, compared to mangalore tile (R) cement (F) dwellings. Annual effective dose is maximum in winter season and minimum in summer season. The total annual effective dose obtained in the study area is within the safe range recommended by ICRP and WHO.

REFERENCES

- Axelsson O., Fredrikson M., Akerblom G., Hardell L (2002). Leukemia in childhood and adolescence and exposure to ionizing radiation in homes built from uranium containing alum shale concrete. *Epidemiology* 13, 11146–11150.
- Bodansky D., David Bodansky, Maurie A., Roskin., David, R.S. (Eds.) (1989). Overview of the Indoor Radon and its Hazards. (University of Washington Press, Seattle and London) pp. 3–15.
- ICRP (International Commission on Radiological Protection) (2011). Lung cancer risk from radon and progeny and statement on radon. ICRP Publication-115. Pergamon Press, Oxford.
- Mining Information Clearing house of India(MICHI), Ministry of Mines, Government of India (2017).
- Ningappa, C., Sannappa., J., Chandrashekara, M. S., and Paramesh, L., (2008). Concentrations of radon and its daughter Products in and around bangalore city. *Radiation Protection Dosimetry* (2008), Vol. 130, No. 4, pp. 459–465.
- Oufnia, L., Misdaqb, M.A., Amraneb, M. (2005) Radon level and radon effective dose rate determination in Moroccan dwellings using SSNTDs. *Radiation Measurements*. 40(1), 118–123.
- Sannappa, J., Chandrashekara, M. S., Sathish.L A., Paramesh, L., Venkataramaiah, P., (2003) Study of background radiation dose in Mysore city, Karnataka State, India. *Radiation Measurements* 37, 55 – 65.
- Surinder Singha., Rohit Mehrab., Kulwant Singhaa., (2005) Seasonal variation of indoor radon in dwellings of Malwa region, Punjab. *Atmospheric Environment*. 39(40), 761–7767.
- WHO (World Health Organization) (2009). Hand book on indoor radon: a public health perspective. WHO Press, Geneva.

Table 1. Indoor ^{222}Rn , ^{220}Rn and their progeny concentrations and total annual effective dose during summer (March – May)

Sr.No	Location name	Type of house	Number of houses	Concentration. (Bq.m ⁻³)		Eq..Ev..Prog. Conc. (Bq.m ⁻³)		Total Annual eff. dose (mSv.y ⁻¹)
				^{222}Rn	^{220}Rn	EERC	EETC	
1	Mudigere	Mangalore Tile(R) Cement(F)	5	27.45	20.00	26.19	1.35	2.08
2	Sakleshpura	Mangalore Tile(R) Cement(F)	6	21.57	17.78	27.14	1.13	2.07
3	Alur	Mangalore Tile(R) Cement(F)	4	22.88	18.89	25.31	1.25	1.99
4	Hassan	Concentrate (R) Granite (F)	6	67.97	38.89	32.15	1.86	2.66
5	Arkalgud	Mangalore Tile(R) Cement(F)	5	54.25	20.00	28.68	1.44	2.29
6	Holenarasipura	Concentrate (R) Granite (F)	6	73.86	61.11	34.53	1.38	2.70
7	Shravanabelagola	Concentrate (R) Granite (F)	4	81.05	135.56	39.89	1.62	3.17
8	Krishnarajanagara	Mangalore Tile(R) Cement(F)	6	32.03	62.22	33.44	1.13	2.51

Table 2. Indoor ^{222}Rn , ^{220}Rn and their progeny concentrations and total annual effective dose during spring (June- August)

Sr.No	Location name	Type of house	Number of houses	Concentration. (Bq.m ⁻³)		Eq..Ev..Prog. Conc. (Bq.m ⁻³)		Total Annual eff. dose (mSv.y ⁻¹)
				^{222}Rn	^{220}Rn	EERC	EETC	
1	Mudigere	Mangalore Tile(R) Cement(F)	5	31.37	34.44	1.51	28.08	2.26
2	Sakleshpura	Mangalore Tile(R) Cement(F)	6	25.49	11.11	1.32	28.78	2.23
3	Alur	Mangalore Tile(R) Cement(F)	4	22.22	13.33	1.34	28.72	2.22
4	Hassan	Concentrate (R) Granite (F)	6	67.97	63.33	1.90	29.82	2.54
5	Arkalgud	Mangalore Tile(R) Cement(F)	5	32.03	14.44	1.50	30.24	2.38
6	Holenarasipura	C Concentrate (R) Granite (F)	6	80.39	72.22	1.61	41.92	3.25
7	Shravanabelagola	Concentrate (R) Granite (F)	6	92.81	83.33	1.88	43.15	3.42
8	Krishnarajanagara	Concentrate (R) Granite (F)	4	40.52	53.33	1.81	37.45	2.96

Table 3. Indoor ^{222}Rn , ^{220}Rn and their progeny concentrations and total annual effective dose during Autumn (September- November)

Sr.No	Location name	Type of house	Number of houses	Concentration. (Bq.m ⁻³)		Eq..Ev..Prog.. Conc. (Bq.m ⁻³)		Total Annual eff. dose (mSv.y ⁻¹)
				^{222}Rn	^{220}Rn	EERC	EETC	
1	Mudigere	Mangalore Tile(R) Cement(F	5	32.68	30.00	26.95	1.44	2.17
2	Sakleshpura	Mangalore Tile(R) Cement(F	6	27.45	15.56	28.03	1.28	2.17
3	Alur	Mangalore Tile(R) Cement(F	4	24.18	17.78	25.73	1.49	2.08
4	Hassan	Concentrate (R) Granite (F)	6	67.32	51.11	26.64	2.09	2.39
5	Arkalgud	Mangalore Tile(R) Cement(F	5	56.21	13.33	28.20	1.49	2.27
6	Holenarasipura	C Concentrate (R) Granite (F)	6	81.05	75.56	40.36	1.52	3.13
7	Shravanabelagola	Concentrate (R) Granite (F)	6	85.62	151.11	43.89	1.56	3.42
8	Krishnarajanagara	Concentrate (R) Granite (F)	4	48.37	94.44	36.67	1.25	2.79

Table 4. Indoor ^{222}Rn , ^{220}Rn and their progeny concentrations and total annual effective dose during winter (December- February).

Sr.No	Location name	Type of house	Number of houses	Concentration. (Bq.m ⁻³)		Eq..Ev..Prog.. Conc. (Bq.m ⁻³)		Total Annual eff. dose (mSv.y ⁻¹)
				^{222}Rn	^{220}Rn	EERC	EETC	
1	Mudigere	Mangalore Tile(R) Cement(F	5	47.06	47.78	32.97	1.91	2.71
2	Sakleshpura	Mangalore Tile(R) Cement(F)	6	38.56	26.67	30.22	1.75	2.46
3	Alur	Mangalore Tile(R) Cement(F)	4	33.99	28.89	28.25	1.77	2.34
4	Hassan	Concentrate (R) Granite (F)	6	83.66	96.67	47.48	2.29	3.81
5	Arkalgud	Mangalore Tile(R) Cement(F	5	52.29	27.78	42.95	1.80	3.30
6	Holenarasipura	C Concentrate (R) Granite (F)	6	146.41	82.22	52.95	2.14	4.18
7	Shravanabelagola	Concentrate (R) Granite (F)	6	171.24	164.44	56.74	2.96	4.74
8	Krishnarajanagara	Concentrate (R) Granite (F)	4	51.63	98.89	36.65	2.43	3.13

IDENTIFICATION OF SOURCE REGIONS AND TYPE OF AEROSOLS DURING HIGH AEROSOLS EVENTS OVER GUJARAT

NISHA VAGHMARIA AND M.E. JAMES

Department of Physics, Electronics & Space Sciences,
Gujarat University, Ahmedabad, India.

KEYWORDS: Aerosol Optical Depth, High Aerosol Events, Aerosol Source Regions, Aerosol Subtypes, Duststorm, Stubble Burning.

INTRODUCTION

Atmospheric aerosols play an important role in the land-atmosphere-ocean system through the radiative forcing. The impact of aerosols on the earth's system depends on its characteristics such as type, size, concentration etc.. Even though these characteristics may change during the transport, they are initially determined by the source regions from where particles are entered into the atmosphere. The Gujarat State which is bounded by Arabian Sea in the west experiences seasonal changes in the predominant winds. The major part of State falls under arid or semi-arid type of climate. The State experiences episodes of high aerosol content in the atmosphere on certain occasions. In this paper, an attempt has made to identify source regions and sub-types of aerosols during such events of high aerosol content over Gujarat State during 2012. Remote sensing is an established method for the detection and mapping of high aerosol events, and has been also used to identify the aerosol types and the source regions.

METHODS

The AOD data from MODIS onboard the Aqua and Terra satellites have been used to detect incidences of high aerosol events over Gujarat during the year 2012. Seasonal distribution of area averaged monthly AOD values over Gujarat and surrounding region for the year 2012 has been analysed. For spatial analysis, five different geographical regions of $1^{\circ} \times 1^{\circ}$ grid namely Kutch region, Saurashtra region, N.Gujarat region, S.Gujarat region and Arabian Sea region have been selected. Temporal variations of AOD for all 5 regions separately and for the State and the surrounding area have been analyzed. The HYSPLIT back trajectories at different levels using high resolution GDAS data during the high impact events have been used to track and identify the source regions (Alam et al., 2011). Data from CALIPSO have been used to identify the sub-types of the aerosols and to assess the vertical profile of atmospheric aerosols (Omar et al., 2009). The NCEP reanalysis data have been used to better understand synoptic situations related to the high aerosol episodes.

Seasonal distribution of area averaged monthly AOD values over Gujarat and surrounding region for the year 2012 has shown high values of more than 0.6 during the four monsoon months and about 0.3 during the non-monsoon months. Since, the data availability during monsoon months is very limited, further analysis has been carried out for only non-monsoon months. Any day which satisfies at least one of the following criteria has been considered as a high aerosol event (i) area averaged AOD for the State and the surrounding area > 0.5 (ii) at least two regions $AOD > 0.6$ (iii) at least two consecutive days at any region $AOD > 0.6$.

RESULTS & DISCUSSIONS

The area averaged AOD over Gujarat and surrounding area during non-monsoon months exceeded 0.60 on three occasions; 1.24 on 20th March, 0.76 on 27th May and 0.63 on 6th Nov. 31 days during the non-monsoon months are found to be high aerosol events; 11 days in pre-monsoon months, 15 days in post monsoon months and 5 days in winter months. Conditions for these 31 days have been analyzed for its source region and its sub-types. Details of the results are discussed in the paper.

CONCLUSIONS

Most of the high aerosol episodes over Gujarat are found to be linked to the intrusion of dust particles from Middle East and Arabian countries (Alam et al., 2014; Mitra et al., 2013), stubble burning in Punjab and Haryana (Venkataraman et al., 2006; Mishra and Shibata, 2012) or foggy (hazy) conditions over northeastern part of the country. The AOD values were found to be high over source regions a few days before the high aerosol episodes over Gujarat, depending on pathways. Presence of typical aerosols types in the atmosphere evidenced by CALIPSO confirms the results of source regions inferred from back trajectory analysis.

REFERENCES

- Alam, K., Qureshi, S., & Blaschke, T. (2011). Monitoring spatio-temporal aerosol patterns over Pakistan based on MODIS, TOMS and MISR satellite data and a HYSPLIT model. *Atmospheric Environment*, 45(27), 4641–4651. doi:10.1016/j.atmosenv.2011.05.055
- Alam, K., Trautmann, T., Blaschke, T., & Subhan, F. (2014). Changes in aerosol optical properties due to dust storms in the Middle East and Southwest Asia. *Remote Sensing of Environment*, 143, 216–227. doi:10.1016/j.rse.2013.12.021
- Mishra, A. K., & Shibata, T. (2012). Synergistic analyses of optical and microphysical properties of agricultural crop residue burning aerosols over the Indo-Gangetic Basin (IGB). *Atmospheric Environment*, 57, 205–218. doi:10.1016/j.atmosenv.2012.04.025
- Mitra, A. K., Sharma, A. K., Soni, V. K., & Kundu, P. K. (2013). Characteristics of recent dust storms over the Indian region using real time multi-satellite observations from the direct broadcast receiving system at IMD. *Advances in Space Research*, 51(7), 1195–1203. doi:10.1016/j.asr.2012.11.017
- Omar, A. H., Winker, D. M., Vaughan, M. A., Hu, Y., Trepte, C. R., Ferrare, R. A., Rogers, R. R., Lee, Kuehn, R. E., Liu, Z., Hostetler, C. A. (2009). The CALIPSO Automated Aerosol Classification and Lidar Ratio Selection Algorithm. *Journal of Atmospheric and Oceanic Technology*, 26(10), 1994–2014. doi:10.1175/2009jtecha1231.1
- Venkataraman, C., Habib, G., Kadamba, D., Shrivastava, M., Leon, J.-F., Crouzille, B., Boucher, O., Streets, D. G. (2006). Emissions from open biomass burning in India: Integrating the inventory approach with high-resolution Moderate Resolution Imaging Spectroradiometer (MODIS) active-fire and land cover data. *Global Biogeochemical Cycles*, 20(2), n/a–n/a. doi:10.1029/2005gb002547

LEVELS OF BTEX DURING TRANSITIONAL PERIOD OF SUMMER AND WINTER ALONG A ROADSIDE AREA OF EAST DELHI

A.GARG¹ AND N.C. GUPTA¹

¹University School of Environment Management, Guru Gobind Singh Indraprastha University, Sector- 16 C, Dwarka, New Delhi – 110078, India

KEYWORDS: Urban Air, Roadside Area, Health Effects, Btex.

INTRODUCTION

The urban air quality of Delhi is deteriorating at an alarming level due to urbanisation, industrialization, the growth of motor vehicles and consumption of more products (Guttikunda, 2012). The volatile organic compounds (VOCs) such as benzene, toluene, ethylbenzene, and xylene (BTEX) have been considered as hazardous air pollutants (HAPs) by United States Environmental Protection Agency (USEPA) (Presto et al., 2016). These compounds have carcinogenic and mutagenic properties and possess various short and long-term effects on human health (Majumdar et al., 2011). The short-term adverse effects include nose and throat discomfort, sleeplessness, impaired short-term memory, tremors, headache, skin problems, fatigue, and dizziness. While the long-term exposure to benzene can lead to more adverse effects like genotoxicity, haematotoxicity, reproductive effects with various cancer, loss of coordination, lung cancer, anemia, leukemia, and damage to the liver, kidney and central nervous system (Zhang et al., 2012; Kerbachi et al., 2008). The motor vehicles run on gasoline are considered as major emission sources of these compounds. Therefore, this study has been designed to find out the levels of these compounds in ambient air of roadside location of East Delhi.

METHODS

A roadside location (28.6988°N and 77.2926°E) of Shahdara, a suburban region in the East Delhi, India, which is situated near the banks of Yamuna River has been selected for the study. The location is surrounded by two main roads- 100 feet road and Shahdara-Loni-Saharanpur Marg road. The monitoring area is also surrounded by an old, large temple "Shree Durga Mandir" and also by Makki mosque. The area is a mixed type with residential and many commercial activities including timber market. The area is high traffic congested in nature due to more commuters from Delhi NCR. The sampling was carried out during transitional period i.e. March month (12/03/2018-18/03/2018) of ending on winter season and starting of summer season. The Benzene Handy Sampler (BHS) was used for the sampling and situated at height of two meters above the ground level at the sampling site. The charcoal tubes (ORBO™32) were used as an absorbing media. The ambient air was sucked through the tube using a portable low flow (BHS) sampler with a flow rate of about 30-35 ml/min and sampling duration 120 minutes) in a way that first of all, the air flow saved the sampling layers. This process results in an enrichment of the embedded relevant substances in the activated charcoal. As the sampling time completed, the sampling charcoal tubes were removed off from sampling train. The tubes were wrapped with aluminum foil and placed in an opaque, clean and airtight container which can immediately be sent to the laboratory and placed in a refrigerator (< 4°C). Samples collected through active sampling technique (activated charcoal tube method) were desorbed using Carbon disulphide (CS₂) in an ultrasonic bath for 30 minutes. CS₂ desorbed samples were subjected to further analysis using gas chromatography (GC) fitted with a capillary column and flame ionization detector (FID).

RESULTS & DISCUSSIONS

The levels of B, T, E, and X were observed as 2.56 - 7.32, 6.0 - 21.51, 1.69 - 7.17 and 3.63 - 11.72 µg/m³ respectively (Figure 1). The levels of Benzene during weekdays observed were higher than the standard level (i.e. 5 µg/m³) as prescribed by National ambient air quality standards (NAAQS) (CPCB, 2009). While during weekend, the levels were under the NAAQS of benzene. During weekdays, the motor vehicles run on diesel, petrol and gasoline are the major sources for such higher concentration on the roadside areas.

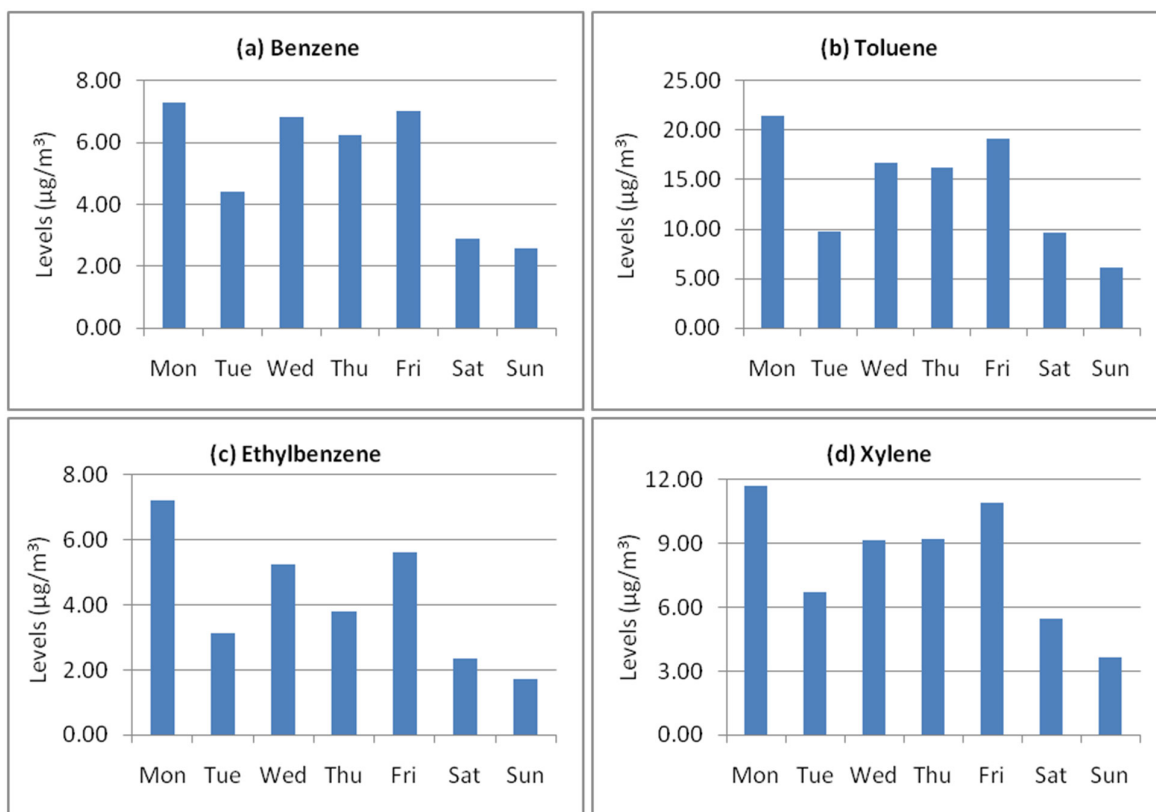


Figure 1. Levels of BTEX within a week (a) Benzene, (b) Toulene, (c) Ethylbenzene and (d) Xylene

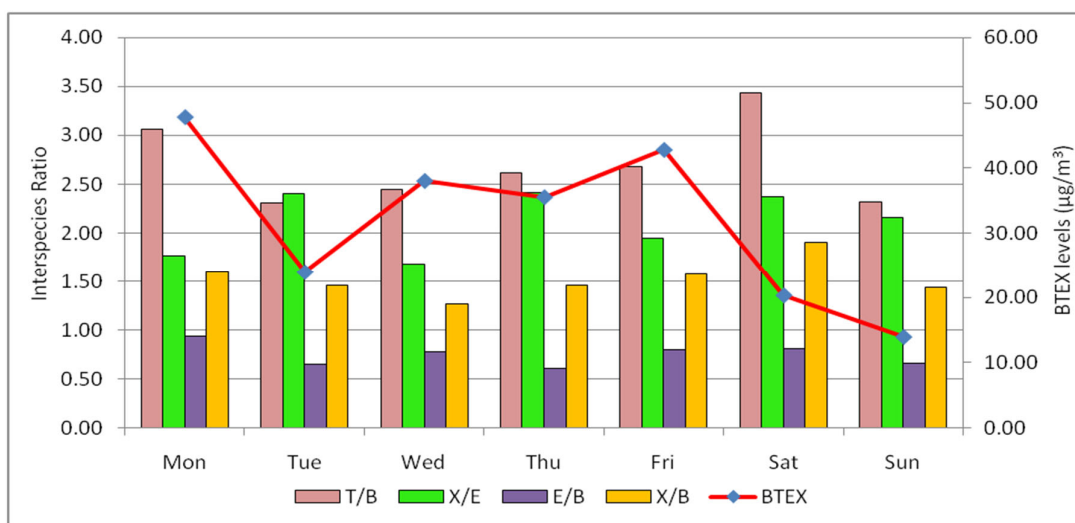


Figure 2. Levels of interspecies ratios and BTEX levels within a week

Also, the concentrations of total BTEX ranged from 13.92 to 47.71 $\mu\text{g}/\text{m}^3$ (Figure 2). The total BTEX concentrations were observed almost double during weekdays as compared to the weekend. The total BTEX levels ranked maximum to minimum as Monday > Friday > Wednesday > Thursday > Tuesday > Saturday > Sunday. The interspecies ratio of BTEX has been considered as a potential indicator to find out the emission sources by some researchers. The ratios of toluene/benzene (T/B), xylene/ethylbenzene (X/E), Ethylbenzene/Benzene (E/B), and xylene/benzene (X/B) are illustrated in Figure 2. Generally, the high T/B ratio is an important indicator of the traffic emissions. A T/B ratio of 2.30- 3.44 can reveal the same traffic-originated emission sources and it has been interpreted that Benzene and toluene are the components of gasoline and may be released into the atmosphere through automobile exhausts.

CONCLUSIONS

This study aimed to assess the levels of BTEX compounds in the ambient air of the roadside location of East Delhi. The concentrations of BTEX were almost twice during the weekdays in compare with the weekend suggesting the effect of motor vehicles on BTEX level. From this study, we can conclude that high traffic density and the number of vehicles on the city streets and roads may be the major reason behind deteriorating the air quality and affecting the human health.

ACKNOWLEDGEMENTS

One of the authors Ms. Anchal Garg gratefully acknowledges the scholarship provided by GGSIP University, New Delhi vide letter no: GGSIPU/DRC/Ph.D/Adm./IPRF/2017/178 dated 08/03/17.

REFERENCES

CPCB (Central Pollution Control Board), *Revised National Ambient Air Quality Standards*, (NAAQS Notification dated 18th November, 2009).

Guttikunda, S. K. (2012). Air pollution in Delhi, *Economic and Political Weekly*, **47**, 24-27.

Kerbach, R., Boughedaoui, M., Bounoua, L. and Keddad, M. (2006). Ambient air pollution by aromatic hydrocarbons in Algiers. *Atmospheric Environment*, **40(21)**, 3995-4003.

Majumdar, D., Mukherjee, A. K., & Sen, S. (2011). BTEX in ambient air of a Metropolitan City. *Journal of Environmental Protection*, **2(01)**, 11.

Presto, A.A., Dallmann, T.R., Gu, P., Rao, U., 2016. BTEX exposures in an area impacted by industrial and mobile sources: source attribution and impact of averaging time, *Journal of the Air & Waste Management Association*, **66**, 387-401.

Zhang, Y., Mu, Y., Liu, J., & Mellouki, A. (2012). Levels, sources and health risks of carbonyls and BTEX in the ambient air of Beijing, China, *Journal of Environmental Sciences*, **24(1)**, 124-130.

GENERATION OF NANOAEROSOLS THROUGH AUTOMOBILES AND ESTIMATION OF THEIR EFFECTS ON HUMAN HEALTH: AN INVESTIGATORY CASE STUDY IN DELHI / NCR

SWATI JOSHI¹, ASHISH K KACHHAWA²

¹University School of Environment Management, Guru Gobind Singh Indraprastha University
New Delhi – 110078, India.

² Research & Development Centre, Indian Oil Corporation Limited
Sector – 13, Faridabad (HR) – 121 007

KEYWORDS: Aerosol from exhaust, Nanoparticles in ambient air, Health effects of ultrafine particulates

ABSTRACT

The study was carried out to measure number & size distribution of ultrafine particulates emitted from different category of vehicles (Diesel, Gasoline, CNG, & LPG with open loop arrangement) with the help of chassis dynamometer assisted tests. The present work elaborates the investigations primarily made for quantification of nanoparticles which are mainly generated through mobile sources i.e., large no. of vehicles in Delhi /NCR. Recent studies worldwide suggest that number concentration could be a much better predictor and indicator of health effects of aerosols than mass concentration and in this direction India is also leapfrogging to BS VI regime which will incorporate particulate matter (PM) mass emission and the introduction of particle number (PN) limits for light and heavy duty vehicles (LDV & HDV).

This paper precisely elaborates the generation of nanoaerosol from transport sector and thereon adoption of methodologies which can be suitable to assess the level of nanoparticle pollution in ambient air to eventually come out with concrete control strategies. During the experiments a Portable Engine Exhaust Particle Sizer Spectrometer (TSI-Model-3090) was utilized to measure the particle numbers & size distribution of nanoparticles. The results clearly show that emissions of ultrafine particulate matter level are significantly influenced by driving conditions & type of fuel used. The present work is concluded by depicting the results in terms of number & size distribution of nanoparticles which are generated through different category of vehicles. The conclusion also elaborates about the various methodologies which can be adopted by researchers / policy makers for the quantification of nanoparticles in ambient air directly causing the severe health hazards.

INTRODUCTION

Atmospheric aerosol particles, also known as atmospheric particulate matter (PM) are microscopic solid or liquid matter suspended in atmosphere. These aerosols are derived from a wide range of natural and anthropogenic sources on earth and within the atmosphere. PM is broadly classified as coarse particles (aerodynamic diameter >2.5 µm), fine particles (aerodynamic diameter between 0.1 and 2.5 µm) and ultra-fine particles (UFP, aerodynamic diameter <0.1 µm) (Pope and Dockery, 2006). These small sized particles are highly variable in composition however knowledge on their composition is far more comprehensive.

Vehicle emission is one of the major sources of nanoparticles in urban areas (Shi and Harrison 1999; Shi, J. et al. 2001) Therefore, a clear understanding on nanoparticle formation and emission from vehicle is critically important for the quantitative assessment of nanoparticle exposure levels to public health. The nanoparticles in vehicle exhaust is known to be a complex mixture of different volatile and non-volatile species often showing a bimodal particle size distribution with a nucleation mode smaller than 50 nm and a larger accumulation mode that mainly contains aggregates of primary particles (Kittelson 1998). The contribution of road traffic to Particulate Matter pollution is larger (60%) due to the high number of nuclei particles formed from the unburnt fuel and lubricant or secondary formation, reaching 90% in cases of busy roads.

Atmospheric nanoaerosol represent an area of growing health concern as particulates in nano range has been shown to have adverse impact on the human health. Epidemiological studies (e.g., Pope, 2000) and

toxicological studies (e.g., Oberdörster, 2000) have associated nanoparticle pollution with respiratory and cardio-vascular disorders. Nanoparticles of a diameter below 0.1 μm are considered more harmful than larger particles because they have higher surface area to mass ratio which allows greater contact for adsorbed compounds to interact with biological surfaces. Particles greater than 2.5 μm are trapped into the nostrils of humans and are removed by natural defence mechanism (i.e. sneezing & coughing) whereas, inhaled nanoparticles (< 100 nm) can penetrate deep into the alveolar membrane of lungs and through the blood they can be transported to other organs where they can directly exert a toxic effect (Oberdörster et al., 2004).

METHODS

The measurement of nanoparticles from vehicular exhaust was done through simulated tests on different type of vehicles with the help of real time nanoparticle analyzer. The vehicles operating on different fuels were tested on 120 kW chassis dynamometer with duty cycle MIDC (Modified Indian Driving Cycle) at varying speeds for a definite time period i.e., 1180 seconds representing the mix of city & urban driving. The emissions are taken from the exhaust by a tailpipe sample probe which is connected to sampling inlet of EEPS (Engine Exhaust Particle Sizer) and EEPC (Engine Exhaust Condensation Particle Counter) system. Data acquisition is done by utilizing EEPS software connected with the EEPS system which is capable of measuring the real time size distribution and number of particles when vehicle is driven.

RESULTS & DISCUSSIONS

The results clearly show that there is generation of nanoparticles in ultrafine range. Diesel-fuelled vehicles, though less in numbers than gasoline powered vehicles, are the greatest contributors to total number concentrations. However, emissions from Gasoline-fuelled vehicles are more uncertain as they are depending on driving conditions. Nanoparticles from liquefied petroleum gas (LPG) vehicles were showing the highest counts with the open loop arrangement type of fuel induction and needed immediate attention as majority of commercial vehicles in cities are plying on LPG fuel with open loop arrangement. The generation of nanoparticles in lower size ranges were seen with compressed natural gas (CNG) powered vehicles and for comparison between sequential and carburetion type of CNG Fuel induction system are to be studied further.

CONCLUSIONS

The present study majorly focuses on generation of nano range particulate matter which are being emitted in ambient air by vehicular exhaust. The majority of vehicle population in city of Delhi is covered by passenger cars running on conventional fuel i.e., CNG, LPG, gasoline & diesel. Fuel type and vehicle driving conditions significantly affect the particle size distribution and the number concentrations of the nucleation mode. Nanoparticles are of greater concern as they have adverse effect on human health.

REFERENCES

- Harris, S.J. & Maricq, M.M. (2001). Signature size distributions for diesel and gasoline engine exhaust particulate matter. *Journal of Aerosol Science*, Vol. 32, No. 6, (June 2001), pp. 749–764, ISSN 0021-8502
- Harrison, R., Jones, M. & Collins, G. (1999). Measurements of the physical properties of particles in the urban atmosphere. *Atmospheric Environment*, Vol. 33, No. 2, (January 1999), pp. 309–321, ISSN 1352-2310
- Kittelson, B.D. (1998). Engines and nanoparticles: a review. *Journal of Aerosol Science*, Vol. 29, No. 5-6, (June 1998), pp. 575–588, ISSN 0021-8502
- Kittelson, D., Watts, W. & Johnson, J. (2006). On-road and laboratory evaluation of combustion aerosols – Part1: summary of diesel engine results. *Journal of Aerosol Science*, Vol. 37, No. 8, (August 2006), pp. 913–930, ISSN 0021-8502

- Kittelson, D.B., Watts, W.F. & Johnson, J.P. (2004). Nanoparticle emissions on Minnesota highways. *Atmospheric Environment*, Vol. 38, No. 1, (January 2004), pp. 9–19, ISSN 1352-2310
- Kulmala, M., Vehkamäki, H., Petäjä, T., Dal Maso, M., Lauri, A., Kerminen, V.-M., Birmili, W. & McMurry, P.H. (2004). Formation and growth rates of ultrafine atmospheric particles: a review of observations. *Journal of Aerosol Science*, Vol. 35, No. 2.
- Oberdörster, G., Oberdörster, E. & Oberdörster, J. (2005). Nanotoxicology: an emerging discipline evolving from studies of ultrafine particles. *Environmental Health Perspectives*, Vol. 113, No. 7, (July 2005), pp. 823–839, ISSN 0091-6765
- Oberdörster, G., Sharp, Z., Atudorei, V., Elder, A., Gelein, R., Kreyling, W. & Cox, C. (2004). Translocation of inhaled ultrafine particles to the brain. *Inhalation Toxicology*, Vol. 16, No. 6-7, (June 2004), pp. 437-445, ISSN 0895-8378
- C.A. Pope & D.W. Dockery (2006). Health Effects of Fine Particulate Air Pollution: Lines that Connect. ISSN 1047-3289 *J. Air & Waste Manage. Assoc.* 56:709–742
- Shi, J. & Harrison, R.M. (1999). Investigation of ultrafine particle formation during diesel exhausts dilution. *Environmental Science and Technology*, Vol. 33, No. 21, (September 1999), pp. 3730–3736, ISSN 0013-936X
- Shi, J., Evans, D., Khan, A., Harrison, R. (2001). Sources and concentration of nanoparticles (<10 nm diameter) in the urban atmosphere. *Atmospheric Environment*, Vol. 35, No. 7, (July 2001), pp. 1193–1202, ISSN 1352-2310

INDOOR PHTHALATES AND POTENTIAL HEALTH RISKS: A CRITICAL REVIEW

R. KAUR, G. SHARMA, A. KUMARI, R. SHARMA, R. KAUR AND S. RAJPUT

Department of Botanical and Environmental Sciences, Guru Nanak Dev University, Amritsar-143005, Punjab, India

KEYWORDS: Phthalates, Emerging environmental pollutants, Indoor air, Health consequences

INTRODUCTION

Phthalates are the emerging environmental pollutants and have been used extensively as plasticizers in various consumer products. These are endocrine disrupting compounds which directly affect the actions of normal intrinsic hormones. Their widespread use in PVC, polishes, cosmetics, glues, toys etc. results in their ubiquitous presence in indoor and outdoor environment. The concentration of phthalate esters in indoor air is several orders of magnitude higher than outdoor.

METHODS

Literature was surveyed for the presence of phthalates in the indoor environment and its qualitative and quantitative analysis. Most of the researchers have taken samples from multi-location indoor environments such as day care centers, children bedrooms, workplaces, houses etc. Air sampling was performed by drawing commercially available SPE (solid-phase extraction) cartridges, Sep-Pak PS Air cartridge (Water, USA) or pumping air through Tenex adsorbant tubes etc. samples were extracted using solvents like acetone, dichloromethane, n hexane with 6% diethyl ether etc. The extracted samples were analyzed through gas chromatography mass spectrometry (GC/MS), gas chromatography-tandem mass spectrometry with electron ionization (GC-EI/MS/MS), liquid chromatography mass spectrometry (LC-MS/MS) etc.

RESULTS AND DISCUSSION

In most of the studies, air samples collected from different sites have reported the presence of diethyl phthalate (DEP), di(2-ethylhexyl) phthalate (DEHP), di-n-butyl phthalate (DBP), benzyl-butyl phthalate (BBP), dimethyl phthalate (DMP), dihexyl phthalate (DHP) etc. Tran and Kannam (2015) determined nine phthalate esters from 60 indoor air samples from homes, offices, laboratories, schools, salons and public places and found median concentration of total phthalate in indoor air ranged from 143-2600 ng/m³. In another study, Bu et al. (2016) reported high levels of DMP and DEHP in air samples of residential apartments. Tuomainen et al. (2004) reported symptoms of asthma among employees working in an office building having PVC floor covering. Langer et al. (2010) reported 5 phthalate esters viz. DEP, DBP, DEHP, BBP and di (isobutyl phthalate) (DiBP) from Danish homes (500 bedrooms) and 151 day care centers. Bamai et al. (2018) has reported effect of indoor phthalates on childhood eczema and wheeze in children with and without filaggrin gene mutations.

CONCLUSIONS

The presence of high concentrations of phthalate esters in indoor environment can pose serious threats to human health. Therefore, quality and safety of building materials and other products should not be compromised that have potential health risks.

ACKNOWLEDGEMENTS

The authors are highly thankful to Department of Botanical and Environmental Sciences, Guru Nanak Dev University, Amritsar for providing necessary facilities to carry out the present work.

REFERENCES

- Bamai, Y.A., Araki, A., Nomura, T., Kawai, T., Tsuboi, T., Kobayashi, S., Miyashita, C., Takeda, M., Shimizu, H. and Kishi, R. (2018). Association of filaggrin gene mutations and childhood eczema and wheeze with phthalates and phosphorus flame retardants in house dust: The Hokkaido study on Environment and Children's Health. *Environ Int* **121**, 102-110.
- Kubwabo, C., Rasmussen, P.E., Fan, X., Kosarac, I., Wu, F., Zidek, A. and Kuchta, S.L. (2013). Analysis of selected phthalates in Canadian indoor dust collected using household vacuum and standardized sampling techniques. *Indoor Air*, **23**(6), 506-514.
- Langer, S., Weschler, C.J., Fischer, A., Bekö, G., Toftum, J., and Clausen, G. (2010). Phthalate and PAH concentrations in dust collected from Danish homes and daycare centers. *Atmosph Environ*, **44**(19), 2294-2301.
- Tran, T. M., and Kannan, K. (2015). Occurrence of phthalate diesters in particulate and vapor phases in indoor air and implications for human exposure in Albany, New York, USA. *Arch Environ Contam Toxicol*, **68**(3), 489-499.
- Tuomainen, A., Seuri, M., Sieppi, A. (2004). Indoor air quality and health problems associated with damp floor coverings. *Int Arch Occup Environ Health*, **77**(3), 222-226.

SHORT-CHAIN SATURATED DICARBOXYLICACIDS (C₂-C₄) IN AEROSOLS COLLECTED AT BELLARY STATION IN SOUTH INDIA

S. K. R. BOREDDY¹, DIVYAVANI¹, K. KAWAMURA^{1, #}, K. NARASIMHULU², SHALINI V^{2,3},
K. RAMAGOPAL³

¹Institute of Low Temperature Science, Hokkaido University, Sapporo-060-0819, Japan

²Department of Physics, SSA Government First Grade College (Autonomous), Bellary-583101,
Karnataka, India

³Department of Physics, Sri Krishnadevaraya University, Ananthapur-515003, Andhrapradesh, India

[#]Now at Chubu Institute for Advanced Studies, Chubu University, Kasugai 487-8501, Japan

KEYWORDS: Dicarboxylic acids, secondary formation, particulate matter, Bellary.

INTRODUCTION

Low molecular weight dicarboxylic acids (diacids) are important constituents of organic aerosols and ubiquitous in the atmosphere (Kawamura and Bikkina, 2016). Due to the low vapor pressures, these compounds are almost exclusively partitioned into a particulate phase and significantly contribute to the water-soluble fraction of organic aerosols. Thus, particles enriched with diacids can aid in act as cloud condensation nuclei and have an impact on the earth's radiative forcing.

METHODS

To better understand the sources and formation processes of organic aerosols in southern peninsular India, Daily TSP (total suspended particulate) samples were collected on pre-combusted quartz fiber filters using a high volume sampler at Bellary site in south India during the period from 25 January to 15 February, 2016. The aerosol samples were analyzed for diacids and inorganic species using a gas chromatography with a flame ionization detector (GC/FID) and IC, respectively (Boreddy *et al.*, 2017).

RESULTS & DISCUSSIONS

The average molecular distribution of dicarboxylic acids was characterized by a predominance of oxalic (C₂) acid followed by succinic (C₄) and malonic (C₃) acids during the sampling period at Bellary station. Significant strong positive correlations ($R^2 > 0.80$; $p < 0.01$) among C₂, C₃, and C₄ diacids suggesting that these acids could have the similar sources; either emitted primarily or secondarily formed via photochemical oxidation of various VOCs in the atmosphere.

Regression analyses among mass concentrations of diacids and chemical tracers revealed that concentration of C₂ showed strong positive correlations ($R^2=0.71$ and 0.65 ; $p < 0.01$) with sulfate (SO₄²⁻, a tracer for anthropogenic sources) and aerosol liquid water content (ALWC), respectively. These results suggest that the formation of diacids at Bellary site may be associated with aqueous phase photooxidation of organic precursors which are majorly produced from anthropogenic sources. However, we should not ignore biomass and biogenic sources for diacids formation over the sampling site. These results also suggest that the primary emission of diacids from fossil fuel combustion sources are not significant at Bellary site in southern India as confirmed by the poor correlation ($R^2=0.03$; $p > 0.05$) between C₂ and elemental carbon (EC), since EC is primarily emitted from fossil fuel combustion sources.

The C₄ can be degraded to C₃ and C₂ due to the decarboxylation reactions (Kawamura and Ikushima, 1993). Therefore, the ratios of C₂/C₄ and C₃/C₄ were used in many previous studies to evaluate photochemical aging and track the possible sources of diacids. In this study, the mean ratio of C₃/C₄ at Bellary was 0.91 ± 0.16 and is higher than those reported for fresh aerosols emitted from fossil fuel combustion (ave. 0.35) and biomass burning (0.51–0.66) emissions and relatively close to aged aerosols. These results imply that aerosols at Bellary site were significantly processed under aqueous-phase medium during the sampling period.

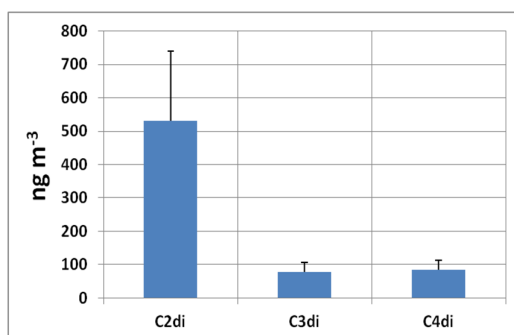


Figure 1. Mean molecular distribution of short-chain saturated diacids in aerosols from Bellary site, south India.

R ²	C ₂	C ₃	C ₄	SO ₄ ²⁻	EC	ALWC
C ₂	1					
C ₃	0.88	1				
C ₄	0.80	0.81	1			
SO ₄ ²⁻	0.71	0.60	0.56	1		
EC	0.03	0.09	0.18	0.06	1	
ALWC	0.65	0.45	0.55	0.84	0.06	1

Table 1. Regression analyses among diacids and chemical markers at Bellary, south India

CONCLUSIONS

Short-chain saturated diacids in Bellary aerosols are mainly associated with secondary formation of aqueous-phase photochemical oxidations of anthropogenic VOCs. The results obtained in this study may have significant implication related to aerosol indirect radiative forcing.

ACKNOWLEDGEMENTS

This study was in part supported by the Japan Society for the Promotion of Science (JSPS) through grant-in-aid No. 24221001 and UGC (SWRO).

REFERENCES

- Kawamura, K. and S. Bikkina (2016). A review of dicarboxylic acids and related compounds in atmospheric aerosols: molecular distributions, sources and transformation, *Atmos. Res.* **170**, 140–160.
- Boreddy, S. K. R., K. Kawamura, and E. Tachibana (2017). Long-term (2001–2013) observations of water-soluble dicarboxylic acids and related compounds over the western North Pacific: trends, seasonality and source apportionment, *Sci. Rep.* **7**, 8518. Doi:10.1038/s41598-017-08745-w
- Kawamura, K. and K. Ikushima (1993). Seasonal changes in the distribution of dicarboxylic acids in the urban atmosphere. *Environ. Sci. Technol.* **27**, 2227–2235

STUDY OF SIZE-SEGREGATED ATMOSPHERIC AEROSOL OVER RAIPUR, CHHATTISGARH, INDIA

J. NIRMALKAR¹, M. MAHILANG² AND M.K. DEB^{2*}

¹Indian Institute of Science Education and Research, Bhopal, Madhya Pradesh, 462066, India

²School of Studies in Chemistry, Pt. Ravishankar Shukla University, Raipur, Chhattisgarh, 492010, India

Keywords: Seasonal variation, Particulate matters, Ambient aerosols, Raipur city.

INTRODUCTION

Particulate matters (PMs) are solid particles and liquid droplets in air. PMs have some physical, optical and chemical properties on which their toxicity to the environment as well as human health is dependent. Atmospheric aerosol contains mixture of organic and inorganic chemical components. In recent years, atmospheric aerosols have become an emerging issue due to their specific role in atmospheric properties, including its number, concentration, optical properties, size and chemical compositions. Besides all these properties, size and mass of the aerosols are most important because the size and mass of the aerosol give information about emission source and relates with human health (Schwartz and Dockery, 1992; Hall and Wynder, 1984), and reflects their aesthetic and climate effects via their light scattering properties (Schwartz et al., 2006). Recent studies suggest that aerosols emitted from anthropogenic activities like biomass burning are responsible for climate forcing effect and global warming (Cavazos-Guerra et al., 2016). The process responsible for production, transportation, physical and chemical evolution and the removal of PMs are strongly related to the size distribution of the atmospheric PMs (US EPA 2009). This study over a Raipur in Central India reports the concentration of airborne size-segregated PMs and their variability during study period.

METHODS

Ambient aerosol samples were collected from Raipur (21.2469° N and 81.5974° E) on 80 mm quartz microfiber filters during October 2012 to February 2013, for 24 hr using non-viable Anderson sampler (Model TE 20-800, USA, 28.3±0.3 L min⁻¹). Field blanks were also collected during the study period. Before the filter was used for sample collection, it was pre-baked at 450 °C for 6 h to remove the absorb impurities. Sampling apparatus (i.e. Andersen sampler) was installed on the rooftop of a two-storied building (approximately, 15 m above the ground). All filters were weighed before and after sampling on an analytical balance (Sartorius CP225D; precision of 10 µg) after conditioning in a clean room at controlled temperature (20±5°C) and relative humidity (40±2%) for 24 hrs.

RESULTS & DISCUSSIONS

Size-segregated aerosol

Mass concentrations of aerosols in coarse and fine size fraction are listed in Table 1. High mass loading of coarse particles observed during winter (139.6 µg/m³) followed by Pre-monsoon (109.4 µg/m³), Post-Monsoon (100.8µg/m³) and Monsoon (74.28µg/m³). Whereas high loading in fine size fraction were highest in Monsoon (121.18µg/m³) followed by Winter (116.7 µg/m³), Pre-monsoon (103 µg/m³) and Post-monsoon (81.51 µg/m³). Higher mass loading during study period was mainly due to the biomass burning and soil dust resuspension over study locations. Coarse particles during Monsoon was significantly low compared to other seasons due to wash out effect of rainfall.

Table 1. Statistical summary of atmospheric aerosols in different seasons

Seasons	Coarse particles				Fine Particles			
	Avg ^a	SD ^b	Min ^c	Max ^d	Avg ^a	SD ^b	Min ^c	Max ^d
Winter	139.6	16.87	120.9	171.9	116.7	14.84	99.81	137.5
Pre-Monsoon	109.4	19.58	80.30	142.9	103.4	28.94	75.95	161.8
Monsoon	74.28	20.35	39.01	112.6	121.1	42.67	68.10	215.3
Post monsoon	100.8	52.97	35.12	193.7	81.51	45.58	20.43	145.7

a = average, *b*=Standard deviation, *c*=Minimum, *d*=Maximum

The results showed that the 24 hours mean concentrations of PM₁₀ and PM_{2.5} were considerably higher than the NAAQS (CPCB, 2009) of India. Therefore, it is recommended that some effective control measures should be implemented to reduce the local anthropogenic pollution in Raipur.

Correlation between Particles

Correlation between aerosols in different season is Shown in Figure 2. We have found good correlation between coarse and fine particles ($R^2 > 0.60$) during almost all seasons during study period. This might be due to significant mass concentration of fine and coarse particle over the study location.

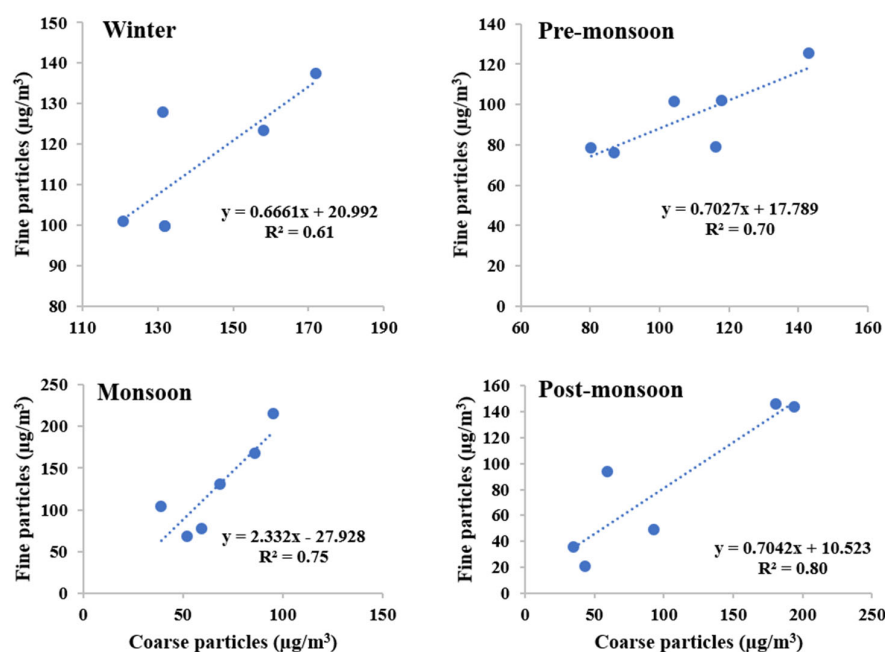


Figure 2. Correlation between atmospheric aerosols in different seasons

CONCLUSIONS

High mass loading of coarse particles observed during winter (139.6 µg/m³) followed by Pre-monsoon (109.4 µg/m³), Post-monsoon (100.8µg/m³) and Monsoon (74.28µg/m³). Whereas high loading in fine size fraction were highest in monsoon (121.18µg/m³) followed by winter (116.7 µg/m³), summer (103 µg/m³) and post monsoon (81.51 µg/m³). We have found strong correlation between coarse and fine particles ($R^2=0.80$) during Post Monsoon season because of biomass burning.

ACKNOWLEDGEMENTS

Authors are thankful to the School of Studies in Chemistry, Pt. Ravishankar Shukla University Raipur, India for providing laboratory supports. The authors also would like thank to National Postdoctoral Fellowship Science Fellowship, Science and Engineering Research Board, Govt. of India, DST-FIST (LEVEL-I) and UGC-SAP (DRS-II), New Delhi for financial provision.

REFERENCES

Schwartz, J., Dockery, D.W. (1992). Increased mortality in Philadelphia associated with daily air pollution concentration. *Am. Rev. Resp. Dis.* 145, 600-604.

Tisch Environmental, Inc. Manufacturer of air pollution monitoring equipment, instruction manual, 8 Stage Non-Viable Cascade Impactor Tisch Environment, Inc. 145 South Miami Ave 2006.

CPCB, 2009. Central pollution Control Board, India. National Ambient Air Quality Standards (NAAQS). Gazette notification, New Delhi, India.

Schwartz, J., Dockery, D.W. (1992). Increased mortality in Philadelphia associated with daily air pollution concentration. *Am. Rev. Resp. Dis.* 145, 600-604.

Cavazos-Guerra, C., Lauer, A., Herber, A., Butler, T. M., Rinke, A. and Dethloff, K. (2016). Implications on atmospheric dynamics and the effect on black carbon transport into the Eurasian Arctic based on the choice of land surface model schemes and reanalysis data in model simulations with WRF. *Atmos. Chem. and Phy.*, doi: 10.5194/acp-2016-942.

Deshmukh, D.K., Deb, M.K., Verma, D. and Nirmalkar, J. (2013). Seasonal air quality profile of size-segregated aerosols in the ambient air of a central Indian region. *Bulletin of Environmental Contamination and Toxicology*, 91, 1098-704.

SUMMERTIME BLACK AND BROWN CARBON (BC AND BrC) IN THE EASTERN INDO-GANGETIC PLAIN

A. RANA¹ AND S. SARKAR^{1,2}

¹Department of Earth Sciences, Indian Institute of Science Education and Research (IISER) – Kolkata, Mohanpur – 741246, West Bengal, India.

²Centre for Climate and Environmental Studies, Indian Institute of Science Education and Research (IISER) – Kolkata, Mohanpur – 741246, West Bengal, India.

KEYWORDS: Carbonaceous aerosols, Optical properties, Angstrom exponent, Concentration-weighted trajectory (CWT).

INTRODUCTION

Among aerosol chemical constituents, black carbon (BC) is the most potent climate forcing agent (radiative forcing estimate: $+1.1 \text{ W m}^{-2}$; Bond *et al.*, 2013) with pronounced effects on atmospheric stability, large scale circulation, monsoon patterns and snow albedo (Tiwari *et al.*, 2013 and references therein). In India, large internal heterogeneities exist for BC emission inventories, which translate into uncertainties in model-predicted atmospheric BC concentrations and corresponding climate effects on regional scales. Field-based measurements of BC aerosol concentrations, diurnal and seasonal variations, sources, and optical properties are therefore vital to constrain regional model predictions. Another fraction of carbonaceous aerosols, termed brown carbon (BrC), has emerged recently as a possibly significant contributor to aerosol climate forcing. BrC refers to the light-absorbing fraction of atmospheric organic carbon (OC), and is associated with both primary (biomass/bio-fuel combustion) and secondary (atmospheric photooxidation) sources, with effects on the surface UV budget and tropospheric chemistry (Mok *et al.*, 2016). However, field studies on BrC optical properties and sources are highly scattered globally and are rare in India, which demands concerted efforts in this direction.

The Indo-Gangetic Plain (IGP) is considered to be the predominant area source of BC in India and recent estimates show that West Bengal, located in the eastern IGP, is the second largest BC emitter nationally (Paliwal *et al.*, 2016). Increased emission from this region is attributed to very high population densities, outflow from megacities (e.g., Kolkata), presence of numerous brick-kilns and thermal power plants, use of biomass fuels and kerosene lamps for domestic energy production, and open crop residue burning (Paliwal *et al.*, 2016). Despite such high emissions, field-based studies investigating BC distribution, sources and optical properties in this region are rare while those on BrC are non-existent. This limits our understanding of the impact of regionally transported (and photochemically aged) emissions on aerosol optical properties in the eastern IGP. This lack of surface measurement data also signifies that regional model estimates of BC cannot be validated for this region. In view of the above, we present here the first measurements of summertime BC and BrC, corresponding light absorption parameters, and potential source sectors at a rural site affected by regional emissions in the eastern IGP.

METHODS

STUDY AREA: The study was carried out at Mohanpur (22°96'N, 88°56'E), a rural area in Nadia district, West Bengal, characterized by agricultural fields and village settlements, with reduced vehicular traffic. The nearest town is Kalyani (population: 0.1 million) around 10 km to the W and the megacity Kolkata (population: 4.9 million) lies ~50 km to the S-SW. A cluster of small- and medium-scale industrial units are located ~10 km to the W, and the 450 MW Bandel coal-fired power station is situated ~15 km to the NW of the site. On a regional scale, clusters of large thermal power plants and steel industrial complexes in West Bengal, Odisha, Bihar, Jharkhand and Chhattisgarh are located within 500 km of the study area.

SAMPLING AND ANALYSIS:

TIME-RESOLVED MEASUREMENTS OF AEROSOL BC AND BrC: a 7-wavelength (370-950 nm) Aethalometer (AE-33, Magee Scientific) was employed during late summer (May-July) 2018 to collect BC

concentration and aerosol light absorption data at a time resolution of 1min. Aerosol light absorption coefficients (b_{abs}) were determined from wavelength-dependent BC mass absorption efficiencies (MAE) and BC mass density data. Assuming a BC Angstrom exponent (AE) of 1, a power law equation was used to estimate BC absorption across the entire wavelength range, followed by the determination of residual absorption by BrC ($b_{\text{abs(BrC)}}$). Subsequently, the wavelength dependence of BrC light absorption (AE_{BrC}) was calculated from a fit of $b_{\text{abs(BrC)}}$ vs wavelength. Diurnal variations of BC, b_{abs} , $b_{\text{abs(BrC)}}$ and AE_{BrC} were also studied. Finally, a two-component mixing model was employed for a preliminary assessment of fossil fuel vs biomass burning sources of BC.

TIME-INTEGRATED OPTICAL MEASUREMENTS OF AEROSOL AQUEOUS AND ORGANIC EXTRACTS: a low-volume $PM_{2.5}$ sampler (APM550 MFC, Envirotech) was deployed to collect 24 h $PM_{2.5}$ during April-July 2018 ($n=29$) using pre-combusted 47 mm quartz filters (QMA, Whatman). $PM_{2.5}$ loads were determined using a microbalance (Mettler-Toldeo, sensitivity: 0.01 mg) after conditioning in a constant temperature and RH chamber. A fraction of these samples ($n=5$) were extracted separately with 20 ml ultrapure water and 10 ml methanol for 30 min in an ultrasonicator to get water- and organic-extractable fractions of $PM_{2.5}$, respectively. The extracts were filtered through 0.22 μm PVDF syringe filters (Rankem), and were analyzed for optical characteristics of organic aerosol chromophores using UV-Vis (Evolution 201, Thermo-Fisher) and fluorescence (FluoroMax-3, Horiba) spectrometers. Corresponding b_{abs} were calculated and were used to estimate AE values of water- and organic-extractable fractions (Hecobian *et al.*, 2010), and to comment on potential BrC sources.

AIR MASS TRAJECTORY CLUSTERS AND CONCENTRATION WEIGHTED TRAJECTORIES (CWTS): To identify aerosol transport pathways and potential source sectors over this region, we calculated daily wind backward trajectories using GDAS meteorological data and the HYSPLIT transport and dispersion model (<https://www.ready.noaa.gov/HYSPLIT.php>). HYSPLIT was run for 96 hours backward at a starting height of 100 m to calculate daily trajectories followed by clustering based on standard protocol. Subsequently, BC, b_{abs} , $b_{\text{abs(BrC)}}$ and AE_{BrC} values were apportioned to each cluster. Directional gradients of source contributions were established by calculating concentration weighted trajectories (CWTs) for BC, b_{abs} , $b_{\text{abs(BrC)}}$ and AE_{BrC} (TrajStat; <http://www.meteothinker.com/>).

RESULTS & DISCUSSIONS

DIURNAL VARIATIONS OF BC, AND RELATIVE CONTRIBUTIONS OF FOSSIL FUEL vs BIOMASS BURNING

Daily averaged BC concentration for the study period varied from 0.9-7.5 $\mu\text{g m}^{-3}$, with an overall mean of $3.6 \pm 2.0 \mu\text{g m}^{-3}$. BC levels were significantly higher ($p < 0.01$) during nighttime (mean: $4.1 \pm 1.9 \mu\text{g m}^{-3}$) compared to daytime (mean: $3.1 \pm 1.3 \mu\text{g m}^{-3}$), possibly due to increased residential fuel use emissions, and accumulation resulting from lower nocturnal mixing depths. The diurnal profile of BC (Fig. 1a) shows an increasing trend after 1700 h lasting till 0200 h, and a secondary peak at 0700-0800 h. Based on results of the two-component mixing model, fossil fuel use is responsible for the overwhelming majority (83%) of the observed BC levels, and this component (BC-FF) tracks the total BC profile very well. It therefore appears that the secondary BC peak at 0700-0800h is related to morning traffic even though the site is well away from major roads. The post-evening increasing trend of BC is also reproduced by the BC-FF component, possible due to increased nighttime movement of diesel trucks on the National Highway around 1.5 km away. The biomass burning component (BC-BB), on the other hand, contributes 17% to total BC, and shows a distinctly different diurnal profile. There appears to be a notable rise in BC-BB during 0600-0800 h, possible from morning cooking activities, and a much larger peak at 2100 h followed by a decline, suggesting enhanced residential fuel use during the evening.

TIME-RESOLVED BrC LIGHT ABSORPTION CHARACTERISTICS

The overall aerosol b_{abs} shows a similar wavelength dependence ($AE = 1.2$, Fig. 1b) as pure BC ($AE = 1$). Extrapolating b_{abs} for BC to lower wavelengths gives an estimate of BrC absorption in the UV-Vis region. The $b_{\text{abs(BrC)}}$ at 370 nm is used as a proxy of total BrC absorption, and its diurnal variation is shown in Fig. 1a. It is clear that $b_{\text{abs(BrC)}}$ follows a similar hourly profile as BC-BB, suggesting co-emission. The high

overall mean AE_{BrC} (4.4, Fig. 1b) with notable peaks ($AE_{BrC} = 4-6.5$) during 0600 and 2100 h (Fig. 1c) also strongly support a biomass burning source (Hecobian *et al.*, 2010). This might indicate that smoldering combustion of biofuels in the residential sector produce substantial amounts of BrC chromophores along with BC. Interestingly, the hourly $b_{abs}(BrC)$ profile shows a slowly increasing trend during afternoon hours, which is mirrored by a AE_{BrC} peak of ~ 7.5 at 1100-1200 h. This possibly suggests secondary BrC formation from atmospheric processes in the afternoon as a consequence of increased emissions of biogenic volatile organic compounds in response to heat stress followed by photochemical oxidation in the presence of oxidants (OH, O₃, etc.). Overall, the relative contributions of BrC to total and BC-associated light absorption were considerable (15% and 18%, respectively, at 370 nm), which establishes that BrC is a significant component of light absorbing aerosol in the eastern IGP.

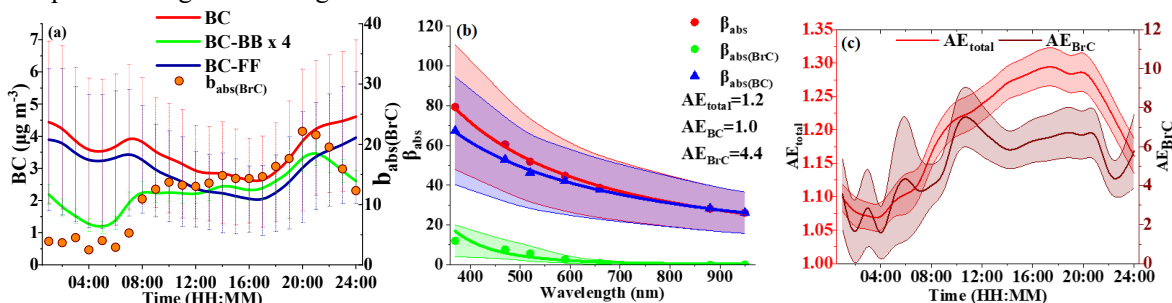


Figure 1. Diurnal variation of total BC, fossil-fuel and biomass burning (x 4) BC, and $b_{abs}(BrC)$ (a); wavelength dependence of total, BC and BrC absorption (b); and total and BrC AE (AE_{total} , AE_{BrC}) (c).

OPTICAL PROPERTIES OF AEROSOL EXTRACTS

UV-Vis absorption for water and organic extracts were converted to corresponding b_{abs} , and were used to estimate corresponding AE (Fig. 2a). The averaged AE for the water extracts was 7.2, which confirms the presence of water soluble BrC chromophores. Previous studies have reported AE values of ~ 7 for aqueous extracts of water-soluble humic like substances (HULIS) from biomass burning plumes and fresh secondary organic aerosol (SOA) (Hecobian *et al.*, 2010 and references therein). In comparison, methanol extracts showed an averaged AE of 6.2. Fluorescence spectra for the aqueous extracts (Fig. 2b) showed a strong peak at ~ 420 nm, similar to that observed for aqueous extracts of HULIS with polyconjugated structures (Varga *et al.*, 2001). For organic extracts (Fig. 2c), the fluorescence intensity was elevated, the peak at ~ 420 nm was broader, and a strong peak appeared at ~ 320 nm suggesting that a substantial fraction of aerosol chromophores are water-insoluble. Overall, this chemical-optical characterization of aerosol liquid extracts confirm a substantial presence of organic chromophores, and supports the conclusions from *in situ* optical measurements presented in the previous section.

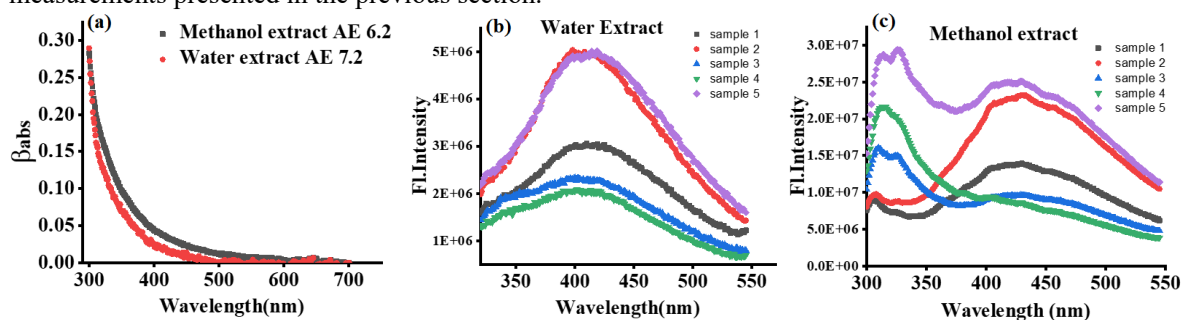


Figure 2. Optical characteristics of aqueous and organic extracts of PM_{2.5}: a) relationship between b_{abs} and λ for UV-Vis spectra; b) fluorescence spectra of water extract; c) fluorescence spectra of methanol extract.

POTENTIAL SOURCE SECTORS

The majority of air masses arrived from the SW, and two trajectory clusters were identified: i) originating over Bay of Bengal; ii) originating over the Arabian Sea and travelling over central and peninsular India. A CWT plot of BC concentration (Fig. 3a) shows that moderate amounts of BC were transported across central

India and eastern coast to the study site, with scattered high values potentially associated with power plant clusters in Odisha and Chhattisgarh, industrial centers in peninsular India, and ship tracks over Bay of Bengal. On the other hand, $b_{\text{abs(BrC)}}$ showed relatively higher values associated with air mass transport over central India compared to other pathways. Summertime forest fires over central India (especially, Chhattisgarh and coastal Odisha) could potentially be responsible for the high $b_{\text{abs(BrC)}}$ (along with BC) observed here (Venkataraman *et al.*, 2006).

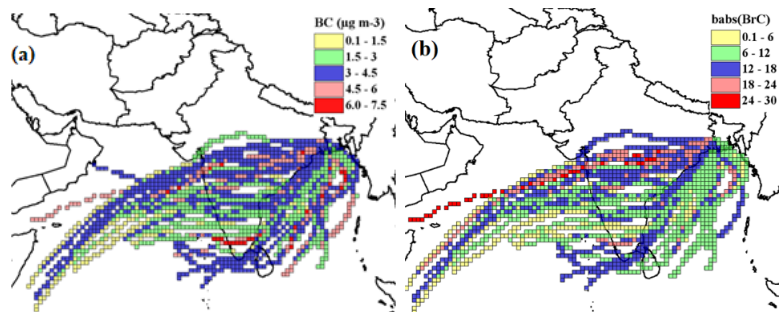


Figure 3. CWT plots of BC (a) and $b_{\text{abs(BrC)}}$ (b) for the study period.

CONCLUSIONS

This pilot study on summertime aerosol optical characteristics in the eastern IGP found that BC in this region has a strong fossil-fuel derived signature mixed with a residential fuel use derived component. Aerosol BrC, predominantly sources from smoldering biofuel combustion and secondary processes, makes a non-trivial contribution to total aerosol light extinction. Aqueous and organic aerosol extracts show a strong wavelength dependence of UV-Vis absorption, consistent with the presence of polyconjugated HULIS chromophores, in addition to broad fluorescence signatures. There also appears to be considerable contribution from regional/long-range atmospheric transport to aerosol BC and BrC in the eastern IGP.

ACKNOWLEDGEMENTS

AR and SS acknowledge IISER-Kolkata for provision of Integrated Ph.D. fellowship and Start-up Grant, respectively, for the duration of this work.

REFERENCES

- Bond, T.C., S.J. Doherty, D.W. Fahey, P.M. Forster, T. Berntsen *et al.*, (2013). Bounding the role of black carbon in the climate system: A scientific assessment, *J. Geophys. Res. Atmos.* **118**, 5380.
- Hecobian, A., X. Zhang, M. Zheng, N. Frank, E.S. Edgerton and R.J. Weber (2010). Water-soluble organic aerosol material and the light-absorption characteristics of aqueous extracts measured over the Southeastern United States, *Atmos. Chem. Phys.* **10**, 5965.
- Mok, J., N.A. Krotkov, A. Arola, O. Torres, H. Jethva *et al.*, (2016). Impacts of brown carbon from biomass burning on surface UV and ozone photochemistry in the Amazon Basin, *Sci. Rep.* **6**, 36940.
- Paliwal, U., M. Sharma and J.F. Burkhart (2016). Monthly and spatially resolved black carbon emission inventory of India: uncertainty analysis, *Atmos. Chem. Phys.* **16**, 12457.
- Tiwari, S., A.K. Srivastava, D. Bisht, P. Parmita, M.K. Srivastava and S.D. Attri (2013). Diurnal and seasonal variations of black carbon and PM_{2.5} over New Delhi, India: Influence of meteorology, *Atmos. Res.* **125-126**, 50.
- Varga, B., G. Kiss, I. Ganszky, A. Gelencser and Z. Krivacsy (2001). Isolation of water-soluble organic matter from atmospheric aerosol, *Talanta* **55**, 561-572.

Venkataraman, C., G. Habib, D. Kadamba, M. Shrivastava, J.F. Leon et al., (2006). Emissions from open biomass burning in India: Integrating the inventory approach with high-resolution Moderate Resolution Imaging Spectroradiometer (MODIS) active-fire and land cover data, *Global Biogeochem. Cycles***20**, GB2013.

REGIONAL SULFATE DRIVES LONG-TERM RISE IN AOD OVER MEGACITY KOLKATA, INDIA

P. RAWAT¹ AND S. SARKAR^{1,2}

¹Department of Earth Sciences, Indian Institute of Science Education and Research (IISER) – Kolkata, Mohanpur 741246, Nadia, India.

²Centre for Climate and Environmental Studies, Indian Institute of Science Education and Research (IISER) – Kolkata, Mohanpur 741246, Nadia, India.

KEYWORDS: Aerosol optical depth (AOD); Sulfate; Black carbon (BC); Organic carbon (OC); Concentration weighted trajectory (CWT).

INTRODUCTION

Kolkata (22°32'N, 88°20'E; metropolitan population: 14.1 million), the capital of West Bengal, is currently considered to be the second-most polluted metropolis in India (WHO, 2018). The averaged PM_{2.5} in Kolkata was 74 µg m⁻³ during 2016, which is around 7.5 times the WHO standard (WHO, 2018). An early attempt at PM_{2.5} source apportionment in Kolkata (ADB, 2005) ascribed the observed levels to emissions from diesel buses and trucks (37%), industries and power plants (17%), road dust (15%), and gasoline passenger cars and two-wheelers (12%). As a consequence of these emissions, it has been estimated that ~70% of the city population suffers from air quality induced respiratory disorders (Mukhopadhyay, 2009), and that there are ~6500 yearly cases of excess mortality (Gurjar and Nagpure, 2015).

In view of this, long-term monitoring of PM_{2.5} and associated chemical fractions is urgently needed for the Kolkata region to better constrain health impact estimates and to inform policy. However, there is a severe lack of sustained monitoring of airborne pollutants in the city. In the absence of ground-based measurements, satellite-derived products such as aerosol optical depth (AOD; interchangeably referred to as aerosol optical thickness, AOT) fractionated into chemical components can provide vital insights into long-term evolution of overall aerosol loads over Kolkata as well as the relative importance of major chemical fractions and sources. Previous studies from Kolkata have reported AOD values ranging from 0.4-0.7, indicating substantial aerosol loads; however, these studies are constrained both by the small time scale investigated (typically, 2-9 y; e.g., Jethva *et al.*, 2005; Ramachandran, 2007; Ramachandran and Cherian, 2008, 2012; Kumar *et al.*, 2018) and by a lack of knowledge regarding the relative contributions of aerosol chemical components to total aerosol light extinction.

To address this issue, we present here the first long-term (2001-2017) record of AOD fractionated into chemical components (dust, sea-salt, sulfate, black carbon (BC), and organic carbon (OC)) over the Kolkata area. For this purpose, we combine daily gridded moderate resolution imaging spectroradiometer (MODIS; Aqua and Terra) data for AOD with modeled AOT values associated with individual aerosol chemical components using the modern-era retrospective analysis for research applications v.2 (MERRA-2) platform for this region. Consequently, we evaluate corresponding long-term trends and seasonality, and use a concentration weighted trajectory (CWT)-based approach to identify aerosol transport pathways over Kolkata and delineate the impacts of regional vs long-range emissions.

METHODS

MODIS datasets – AOD and Angstrom exponent (AE)

For this study, we retrieved daily MODIS Deep Blue AOD at 550 nm (collection 06, level 2, 10 km spatial resolution, radiance level 1B with QA_≥ 2, 3) during 2001-2017. Data were mainly obtained from Terra, and supplemented by that from Aqua in some cases to make up for blind spots. AOD values above 1.0 were filtered out in order to remove biases due to possible cloud contamination. Similarly, daily AE values were also extracted from MODIS Deep Blue C6 L2 data to study, in conjunction with AOD, aerosol sizes and potential sources.

MERRA-2 dataset of aerosol chemical component AOTs

To investigate optical properties of aerosol chemical components, we used MERRA-2 Aero hourly AOT data for the same time period as MODIS AOD. MERRA-2 is a reanalysis system using the Goddard Earth Observing System Model v5 (GEOS-5), which contains an atmospheric particulate matter module based on the Goddard Chemistry, Aerosol, Radiation and Transport (GOCART) model. GOCART treats the sources, sinks and chemistry of major aerosol chemical components (BC, OC, sulfate, dust and sea-salt) while MERRA-2 computes the modeled extinction AOT values for each of these components.

Clustered air masses and concentration weighted trajectories

To identify aerosol transport pathways and potential source sectors over the Kolkata region, we calculated daily wind backward trajectories using NCEP/NCAR Reanalysis data (<https://www.esrl.noaa.gov/>) and the HYSPLIT transport and dispersion model (<https://www.ready.noaa.gov/HYSPLIT.php>). HYSPLIT was run for 96 hours backward at a starting height of 100 m to calculate daily trajectories. This was followed by clustering of trajectories based on standard HYSPLIT cluster analysis protocol. Subsequently, AOD, AE and AOT values were apportioned to each cluster. Directional gradients of source contributions were established by calculating concentration weighted trajectories (CWTs) for AOD, AE and chemical component AOTs (TrajStat; <http://www.meteothinker.com/>).

RESULTS & DISCUSSIONS

Figure 1a shows yearly averaged AOD and AE for the past 17 y (2001-2017) over Kolkata, while the inset shows the trend of monthly AOD for the same period. The overall averaged AOD for the study period is 0.68 ± 0.18 , which is ~ 5 times the global land mean AOD (0.13 ± 0.05) (Mao *et al.*, 2014), indicating substantial aerosol loads over this region. A Mann-Kendall test coupled with Thiel-Sen slope estimation reveals that AOD has been increasing significantly ($p < 0.001$) over Kolkata in the past 17 y at a rate of 0.010 y^{-1} . This translates to an overall increase of 32% over the study period, roughly at the rate of $2\% \text{ y}^{-1}$. On the other hand, AE values, which represent the wavelength dependence of AOD, have not changed significantly (Mann-Kendall test, $p > 0.05$) over the past 17 y (Fig. 1a) suggesting that despite increasing urbanization and associated emissions, source composition and emission profiles have probably remained unchanged for this region. The averaged AE for 2001-2017 (1.49 ± 0.6) strongly shows an overall dominance of combustion-related accumulation-mode aerosol over Kolkata. Averaged AOD over Kolkata for winter (DJF), summer (MAM), monsoon (JJA) and post-monsoon (SON) seasons (Fig. 1b) are 0.68 ± 0.17 , 0.72 ± 0.16 , 0.64 ± 0.20 , and 0.66 ± 0.18 , respectively, with a significant overall seasonality (ANOVA, $p < 0.05$), and the averaged summer AOD being significantly higher (Bonferroni post-hoc test, $p < 0.05$) than winter, monsoon and post-monsoon.

Figure 2a shows yearly averaged AOT apportioned into major aerosol chemical components – sulfate, BC, OC, dust and sea-salt. Sulfate dominates aerosol light extinction with a mean contribution of $\sim 50\%$, followed by OC (18%), dust (16%), BC (8%) and sea-salt (8%). Moreover, sulfate AOT shows a strong positive trend of 0.007 y^{-1} ($p < 0.001$) and a rise of $\sim 70\%$ between 2001 and 2017. Aerosol OC and BC AOT, on the other hand, show significantly increasing trends of 0.002 y^{-1} ($p < 0.01$) and 0.0004 y^{-1} ($p < 0.01$), respectively, with overall enrichments of $\sim 40\%$ and $\sim 20\%$, respectively, during 2001-2017. In comparison, sea-salt AOT shows an insignificant ($p > 0.05$) positive trend of 0.0001 y^{-1} while dust AOT exhibits a similarly insignificant ($p > 0.05$) negative trend of -0.0008 y^{-1} . This potentially reflects stable emission strengths and transport efficiencies of dust and sea-salt for this region on a timescale of decades. Overall, it is clear from the discussion above that the steady rise in AOD for the past 17 y over Kolkata is driven primarily by aerosol sulfate. This is consistent with the analysis of de Meij *et al.*, (2012) who observed, using emission inventories (EMEP, REAS, IPCC) and AOD data (MODIS, MISR, AERONET), that AOD trends over Asia are mostly constrained by anthropogenic SO_2 emissions.

The monthly distribution of chemically speciated AOT values (Fig. 2b) brings out the distinct seasonalities of anthropogenic and natural aerosol components. Dust and sea-salt exhibit similar seasonal profiles, with more pronounced extinction during summer and monsoon (ANOVA with post-hoc test, $p < 0.05$) as compared to other months. This is a direct consequence of – i) increased loading of coarse aerosol during the summer due to dry conditions and persistent strong winds; and ii) influx of sea spray aerosol

transported by SW monsoon winds travelling over the northern Indian Ocean and the Bay of Bengal. Extinction associated with anthropogenic components, i.e., sulfate, BC and OC, are significantly higher (ANOVA with post-hoc test, $p < 0.05$) in winter and post-monsoon as compared to summer. For sulfate AOT, the observed seasonality implies that increased emissions of SO_2 from domestic fuel use and open biomass burning during winter and post-monsoon outweigh enhanced photochemical formation of sulfate during summer. Combustion activities during these periods are also responsible for increased primary emissions of carbonaceous aerosol (BC and OC).

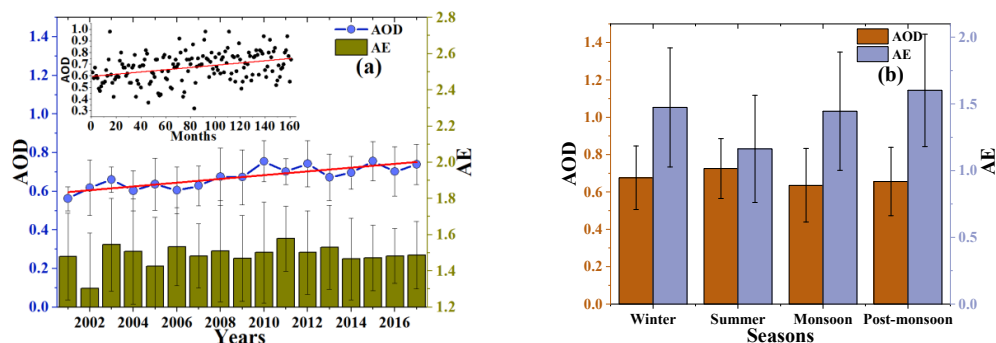


Figure 1. MODIS-derived yearly averaged trends (2001-2017) (a), and seasonal distribution (b) of AOD and AE over Kolkata. The inset in (a) shows the trend of monthly averaged AOD values for the study period.

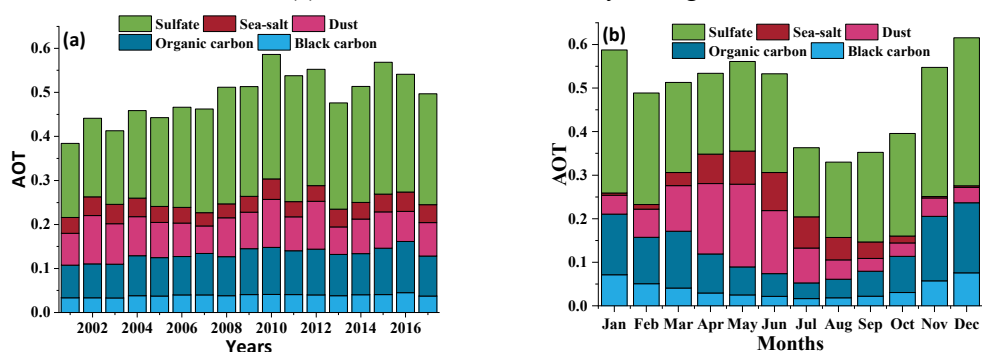


Figure 2. MERRA-2 derived yearly averaged trends (2001-2017) (a) and monthly distribution (b) of AOT associated with aerosol chemical components (sulfate, sea salt, dust, organic carbon and black carbon) over Kolkata.

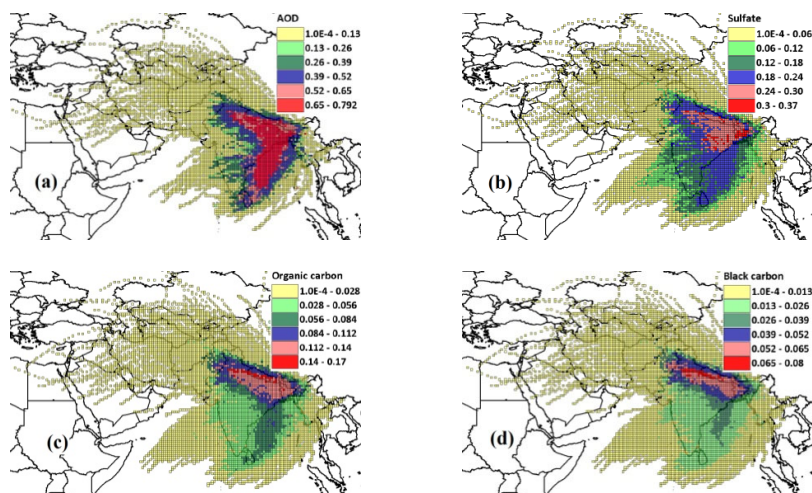


Figure 3. Yearly averaged CWT plots of AOD (a), AOT associated with sulfate (b), AOT associated with OC (c) and AOT associated with BC (d) over Kolkata.

Annual averaged CWTs for AOD, sulfate, OC and BC are presented in Fig. 3a-d, respectively, which clearly indicate substantial transport of aerosol from the central IGP and Bay of Bengal to Kolkata. Among

chemical components, CWT for sulfate AOT (Fig. 3b) shows highest values mostly in clusters in the regional vicinity (~250 km, to the E, W and NW) of the study area. As with AOD, sulfate AOT source sectors over the IGP are limited to western Uttar Pradesh and do not extend as far as the northwestern states. There is a strong indication that a substantial fraction of the sulfate AOT is associated with thermal units in Jharkhand, Odisha and Chhattisgarh. In addition, high sulfate AOT is also associated with the fertile Ganges Brahmaputra Plains of Bangladesh, where intense agricultural activities and associated biomass burning are practiced. In fact, around 90% of SO₂ emissions in Bangladesh are estimated to be from biomass combustion (Arndt *et al.*, 1997). Annual averaged CWTs for OC and BC AOTs are very similar to each other (Fig. 3c and 3d), and distinctly different from that of sulfate. Both BC and OC AOTs show a strong long-range component with the highest sectors associated with emissions in the northwestern and central IGP. Especially, BC and OC AOT during post-monsoon (data not shown) have a non-trivial long-range component with source sectors stretching as far back as the northwestern IGP, to areas over Punjab that practice post-harvest agricultural residue burning during this season. Therefore, BC and OC from long-range sources compete with regional emissions and contribute significantly to aerosol light extinction over Kolkata.

CONCLUSIONS

Using daily MODIS outputs, we have shown here that AOD over the megacity Kolkata has increased consistently during the period 2001-2017, and that this increase is predominantly driven by regional sulfate, followed by long-range OC. So far, air quality management policy for Indian megacities have only targeted within-the-city emissions from vehicular traffic, industries, power plants, etc. This study shows the need to bring regional and long-range emissions under the purview of these policies as well.

ACKNOWLEDGEMENTS

PR acknowledges INSPIRE fellowship provided by the Department of Science and Technology, Government of India during the course of this work. SS acknowledges Start-up Grant provided by IISER-Kolkata for the duration of this study.

REFERENCES

- ADB, 2005. Strengthening environmental management at the state level (cluster) component E – strengthening environmental management at West Bengal Pollution Control Board. Asian Development Bank, TA No. 3423 – IND, New Delhi, 107 pp.
- Arndt, R., Carmichael, G.R., Streets, D.G., Bhatti, N., 1997. Sulfur dioxide emissions and sectorial contributions to sulfur deposition in Asia. *Atmos. Environ.* 31, 1553-1572.
- Gurjar, B.R. and Nagpure, A.S., 2015. Indian megacities as localities of environmental vulnerability from air quality perspective. *J. Smart Cities.* 1, 15-30.
- Jethva, H., Satheesh, S.K., Srinivasan, J., 2005. Seasonal variability of aerosols over the Indo-Gangetic basin. *J. Geophys. Res.* 110, D21204.
- Kumar, M., Parmar, K.S., Kumar, D.B., Mhawish, A., Broday, D.M., Mall, R.K., Banerjee, T., 2018. Long-term aerosol climatology over Indo-Gangetic Plain: Trend, prediction and potential source fields. *Atmos. Environ.* 180, 37-50.
- Mao, K.B., Ma, Y., Xia, L., Chen, W.Y., Shen, X.Y., He, T.J., Xu, T.R., 2014. Global aerosol change in the last decade: An analysis based on MODIS data. *Atmos. Environ.* 94, 680-686.
- Meji, A.D., Pozzer, A., Lelieveld, J., 2012. Trend analysis in aerosol optical depths and pollutant emission estimates between 2000 and 2009. *Atmos. Environ.* 51, 75-85.
- Mukhopadhyay, K., 2009. *Air Pollution in India and its impact on the health of different income groups.* Nova Science Publishers, Inc., New York. 186 pp.

Ramachandran, S., 2007. Aerosol optical depth and fine mode fraction variations deduced from Moderate Resolution Imaging Spectroradiometer (MODIS) over four urban areas in India. *J. Geophys. Res.* 112, D16207.

Ramachandran, S., Cherian, R., 2008. Regional and seasonal variations in aerosol optical characteristics and their frequency distributions over India during 2001–2005. *J. Geophys. Res.* 113, D08207.

WHO, 2018. WHO global ambient air quality database (update 2018). World Health Organization, Geneva. Available online at <http://www.who.int/airpollution/data/cities/en/>

GRAVIMETRIC AND REAL TIME MEASUREMENT OF INDOOR PM_{2.5}, BC AND PN CONCENTRATION DURING COOKING IN BIOMASS COOKSTOVES

D. SARIKA¹, C. VENKATARAMAN^{1,3}, H.C. PHULERIA^{1,2}

¹ Interdisciplinary Programme in Climate Studies, IIT Bombay, Mumbai, 400076, India

² Centre for Environmental Science and Engineering, IIT Bombay, Mumbai, 400076, India

³ Department of Chemical Engineering, IIT Bombay, Mumbai, 400076, India

KEYWORDS: Cookstove measurement, PM_{2.5}, Black carbon, Particle number concentration, biomass fuel

INTRODUCTION

Around the world, more than 3 billion people are depended upon solid fuels such as biomass (Wood, dung cake and agricultural residue) and coal, for the purpose of cooking, heating and boiling water (WHO 2006). In India, about 770 million population lives are dependent on solid fuel for cooking purpose alone. Because of the easy availability and affordable price of these solid fuels, makes it a boon for the vulnerable section to meet their daily needs (Venkataraman et al. 2010). A large section of the society, especially the one residing in the rural areas are quite reluctant to adopt the costlier cleaner fuel such as LPG. As per the year 2005 data, among these households, 90% of the biomass fuel is being used by rural population and 27% by the urban population (Venkataraman et al. 2010). Gaseous and particulate matter emitted during biomass fuel burning in traditional cookstoves is associated with climate change and various health effects due to indoor air pollution in rural households of India.

METHODS

To capture particulate emissions during actual cooking conditions in the field using various fuel types, real-time as well as gravimetric PM measurements were conducted. Measurements were done during 23-27th March 2017 in Bamhane Village in Dhule district of Maharashtra. Total 8 measurements were captured in 8 different kitchens with four each during lunch and dinner. The cooking time varied between 35-55 minutes during dinner and 60-75 minutes during lunch. Mixed fuels (neem and cotton) were used during dinner whereas crop residue (cotton, mirchi and tur) was used during lunch. Almost in every households, some scrap papers or kerosene are commonly used as ignitors. The cooking fuels and ignitors used, types of food prepared and sampling conditions are described in table 1.

Particulate matter (PM_{2.5}), black carbon (BC) and particle number concentration (PNC) using DustTrak (Model: 8530), microAeth (Model: AE-51) and Pegasor AQTM respectively were measured during real world cooking traditional biomass chulhas. For gravimetric measurements, a multi-stream sampler was used having a flow rate 20.2 LPM for PM_{2.5} and mass was collected on 2 teflon membrane filters (47 mm, 2-mm pore size, Whatmann Corp., PA, USA) and 2 Tissue Quartz (Grade QM-A, 47 mm, 2.2 um pore size, Whatmann Corp., PA, USA) at flow rates of 6.3, 4.5, 5.0 and 4.4 LPM maintained by critical orifices. The filters were pre- and post-conditioned in controlled environment (temperature 30-35°C and RH 45-50%) for 12 h and were stored at -4°C in cold storage after field sampling. The particle mass was determined as a difference of post-weight and pre-weight of the filter measured with Sartorius microbalance (detection limit 1 µg; Sartorius, Goettingen, Germany).

Prior to start of every cooking activity, the background levels of particulates were measured for 10-20 minutes in the kitchen.

HID	Fuel used	Ignitors used	Cooking time (mins)	Items cooked	Inlet heights (m)				
					GS	DT	MA	PG	
Meal cooked: Dinner									
1	Neem	Paper	40	Chapati, papad, vegetables	1.5	0.7	0.7	0	
3	Neem/ Cotton	Kerosene, dung cake	54	Khichdi	1.8	1.0	1.0	0.5	
5	Neem/ Cotton	Kerosene, cotton, paper	35	Khichdi, papad	1.2	1.2	1.2	0.6	
7	Cotton/ Saagon	Paper, onion peels, plastic	54	Khichdi, papad	1.0	1.0	1.0	0.5	
Meal cooked: Lunch									
2	Tur	Cotton sticks, paper	76	Chapati, bhakri, 2 vegetables, papad	2	2	2	1.7	
4	Cotton	Kerosene	76	Chapati, kadhi, 2 vegetables	1.8	1.8	1.8	1.2	
6	Mirchi	Kerosene, onion peels, paper	61	Kadhi, bhakri, vegetable	1.5	1.5	1.5	0.4	
8	Cotton	Plastic paper	61	Chapati, vegetable, papad	1.2	1.2	1.2	1.0	
GS=Gravimetric sampler, DT=DustTrak, MA=MicroAeth, PG=Pegasor									

Table 1: Cooking and fuel use characteristics and measurements settings in 8 households

RESULTS AND DISCUSSIONS

Average gravimetric and real time PM_{2.5} concentration during dinner (MF and FW) was 788±261 µg/m³ and 568±408 µg/m³ and during lunch (CR) was 3467±1747 µg/m³ and 5562±3184 µg/m³ respectively. Real time BC and PN concentration during dinner was 86±61 µg/m³ and 68±61 (*10³)/cm³ and during lunch 150±102 µg/m³ and 295±265 (*10³)/cm³ respectively. Average background PM_{2.5}, BC and PN concentration in the kitchen before cooking were 88.6±42 µg/m³, 8.6±6 µg/m³ and 9.2±5 (*10³)/cm³ respectively. Real time cooking emission levels on comparison with background for PM_{2.5} were 6.4 times for mixed fuel and 63 times for crop residue, for BC, it is 10 times for mixed fuel and 17 times for crop residue and for particle number concentration, it is 7.4 times for mixed fuel and 32 times for crop residue

Mean pollutant concentration for PM_{2.5} from biomass (logs, sticks, twigs, corn stalks, hay and straw) burning during steady state condition in traditional cookstoves is about 9835 µg/m³ (Leavey et al. 2015). Our study shows PM_{2.5} concentration as 3618 ± 8922 µg/m³ for all fuels (firewood and crop residue) used.

Black carbon concentration of 91.7 ± 52.9 µg/m³ was measured from traditional stoves in Udaipur field study (Patange et al. 2015). Rehman et al., 2011 reported 54 ± 73 µg/m³ of BC during morning cooking hours in indoor environment and 62 ± 61 µg/m³ which is 2-3 times higher than our findings. Similarly the

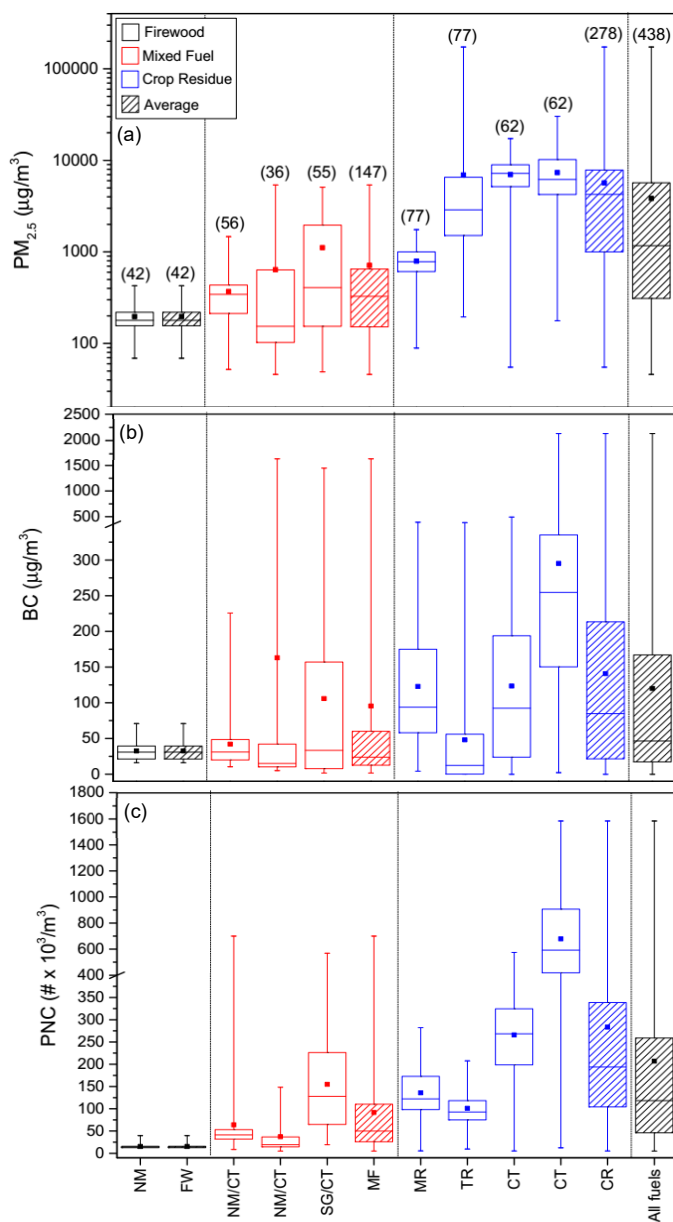


Figure 1: Box plot showing (a) $PM_{2.5}$, (b) Black Carbon and (c) Particle Number concentration from different fuel type (Firewood, mixed fuel and crop residue). The boxes represent the 25th and 75th percentiles, while middle line is 50th percentile, and square point shows the mean value. The outer lines shows minimum and maximum values. (NM-Neem, FW-firewood, CT-Cotton, SG-Saagon, MF-Mixed fuel, MR-Mirchi, TR-Tur, CR-Crop residue)

outdoor BC concentration was found to be around $25 \mu\text{g}/\text{m}^3$ which is 4 times higher than our BC concentration prior cooking inside kitchen. The high outdoor BC value is observed due to contribution from vehicular emissions which is absence in our case as there was no source present.

In our study, the $PM_{2.5}$, BC and PNC emissions from ignitors are observed to be (min-max) mean \pm SD (69-10200) $1702 \pm 2366 \mu\text{g}/\text{m}^3$, (4-2121) $336 \pm 539 \mu\text{g}/\text{m}^3$, (5-733) $125 \pm 189 (*10^3)/\text{cm}^3$. Fedak et al., (2018) have measured emission factor for ignitors used such as kerosene, kindling, plastic bags, and papers and observed their $PM_{2.5}$ emissions (mg) as 496, 355, 2 and 127 per start up event respectively. It can be seen that short term burning of ignitors materials can lead to significance increase in emission levels.

In fig 1(a), the PM_{2.5} emissions from crop residue specifically cotton as cooking fuel was observed to be the highest, followed by mixed fuel which also has cotton in it. The levels are significantly higher when compared to firewood fuel which is neem. Similar trend is observed for BC and PNC in fig 1(b) and 1 (c).

SUMMARY

Our first result suggests that the PM_{2.5}, BC and PN concentration was observed more for crop residue than mixed fuel and firewood used during dinner. On comparison of different cooking fuel type cotton is observed to be the most polluting fuel. The emissions generated during cooking have implications on health of women and children in rural areas and also the emissions tend to impact climate health.

ACKNOWLEDGEMENT

A part of this work is supported by IRCC internship grant 2016-17, IIT Bombay and from DST-Coe. The families of Bamhane village in Dhule district for allowing us to conduct measurement in their kitchen and my colleagues and project staff Mr. Rohan Rane, Ms. Pradnya Vernekar and Mr. Nirav Lakinwala for their help in the field work.

REFERENCES

- Fedak, K. M., Good, N., Dahlke J., Hecobian A., Sullivan A., Zhou Y., Peel J.L., and Volckens J.,2018. "Chemical Composition and Emissions Factors for Cookstove Startup (Ignition) Materials", *Environmental Science & Technology*, 52, 9505–9513.
- Leavey A., Londeree J., Priyadarshini P., Puppala J., Schechtman K.B., Yadama G., and Biswas P., 2015. "Real-Time Particulate and CO Concentrations from Cookstoves in Rural Households in Udaipur, India." *Environmental Science & Technology*, 49, 7423–743.
- Patange, O. S., Ramanathan N., Rehman H., Tripathi S.N., Misra A., Kar A., Graham E., Singh L., Bahadur R., and Ramanathan V., 2015. "Reductions in Indoor Black Carbon Concentrations from Improved Biomass Stoves in Rural India." *Environmental Science & Technology*, 150304142330004. doi:10.1021/es506208x.
- Rehman, I. H., Ahmed, T., Praveen, P. S., Kar, A., & Ramanathan, V. (2011). Black carbon emissions from biomass and fossil fuels in rural India. *Atmospheric Chemistry and Physics*, 11(14), 7289–7299.
- Venkataraman, C., A.D. Sagar, G. Habib, N. Lam, and K.R. Smith. 2010. "The Indian National Initiative for Advanced Biomass Cookstoves: The Benefits of Clean Combustion." *Energy for Sustainable Development* 14 (2). Elsevier B.V.: 63–72. doi:10.1016/j.esd.2010.04.005.
- WHO. 2006. "Household Energy and Health Household Energy and Health." *Energy*.

ABSORPTION PROPERTIES OF BROWN CARBON IN FRESHLY EMITTED AND AGED AMBIENT AEROSOL OVER AN URBAN SITE IN MUMBAI

C. SARKAR¹, S. YADAV¹, H. PHULERIA², C. VENKATARAMAN^{1,3}

¹Interdisciplinary Program in Climate Studies, Indian Institute of Technology, Bombay, Powai, Mumbai-400076, India.

²Centre for Environmental Science and Engineering, Indian Institute of Technology, Bombay, Powai, Mumbai-400076, India.

³Department of Chemical Engineering, Indian Institute of Technology, Bombay, Powai, Mumbai-400076, India.

KEY WORDS: Brown Carbon, Aerosol Monitoring, Absorption Coefficient, Carbonaceous Aerosols

INTRODUCTION:

Atmospheric particulate matter (PM), a large part (10% to 90%) of which is constituted of organic aerosols (OA), has profound effects on air quality, atmospheric chemistry, and climate forcing. While major parts of OA efficiently scatter visible (vis 400 – 700 nm) radiation, some constituents can absorb IR and UV radiation. Recent studies showed that a significant and highly variable fraction of carbonaceous organic aerosols absorb radiation in the near-UV (300–400 nm) and visible ranges (Satheesh and Moorthy, 2005, Bond and Bergstrom, 2006, Bond et al., 2013). These absorbing OA termed as “brown carbon” (BrC), has emerged in recent scientific literature (Bond and Bergstrom, 2006, Ramanathan et al., 2007, Andreae and Gelencsér, 2006). The molecular composition of OC and its evolution during various processes of atmospheric aging have been the subject of extensive research over the past decade (Ervens et al., 2011, Hallquist et al., 2009, Herckes et al., 2013). Recently, brown carbon has been identified as a significant constituent of ambient particulate matter in India, as arising in source emissions from agricultural residue burning (Chakraborty et al., 2016)

A number of field studies on BrC optical properties and composition conducted over eastern and southern Asia indicate that biomass burning is not the only source of BrC in the region. Aerosols optical and chemical analysis showed that a major fraction of BrC were high-MW secondary products likely produced through fossil fuel combustion. The authors also proposed that the strongly absorbing BrC might be related to photochemically aged SOA produced from anthropogenic emissions of VOC with fossil carbon (Du et al., 2014, Cheng et al., 2011).

The present study is focussed on an understanding of the absorption properties of BrC in ambient aerosols emitted freshly versus photochemically aged aerosol. A case study was also done to identify the BrC contribution emitted during biomass burning events.

METHODOLOGY:

For the present study PM₁₀ samples were collected in the campus of IIT-Bombay during the month of Feb-March, 2018 at morning (7am-11am) and afternoon (12pm-4pm) basis. The morning samples were considered as freshly emitted aerosol whereas afternoon samples were considered as a mixture of freshly emitted and photochemically aged aerosol samples. PM₁₀ samples were collected using Envirotech high volume sampler (flow rate of 1m³min⁻¹ using pre-backed (850°C for 1hr) Quartz and GFA filter papers from 28th February 2018 to 25th March 2018. A total of 33 samples were collected during the whole sampling period. In addition to the high volume samples PM₁₀ samples were also collected by low volume samplers using PTFE filter papers for gravimetric analysis and BC measurement. A portion of high volume PM₁₀ samples were subjected to serial extraction using ultrapure Milli-Q water followed by methanol extraction. The absorption of the water and methanol extracts were measured using UV-Vis spectrometer (200-800nm scan). WSOC concentration were measured using a TOC analyser. BC concentrations were measured by a dual wavelength (880-370nm) OT-21 (Magee Scientific) instrument using optical attenuation method. Meteorological data is collected from the nearest met station located at Bandra. Absorption coefficient ($b_{\text{abs}}(\lambda)$) mass absorption coefficient (MAC_{λ}) and Absorption angstrom exponent (AAE) of the solvent extracts were defined by the following equations.

$$b_{\text{abs}}(\lambda) = (A_{\lambda} - A_{700}) \times (V_{\text{ext}} \times \ln(10)) / (V_{\text{aero}} \times L) \dots\dots\dots[1]$$

$$\text{MAC}_{\lambda} = b_{\text{abs}}(\lambda) / C \dots\dots\dots[2]$$

$$b_{\text{abs}}(\lambda) = k \times \lambda^{-\text{AAE}} \dots\dots\dots[3]$$

RESULTS AND DISCUSSION:

The average PM10 concentration ($184.8 \pm 80.9 \mu\text{g m}^{-3}$) for the whole measurement period was much higher than national air quality standards of India (24 hr average $100 \mu\text{g m}^{-3}$). BC concentration ($8.4 \pm 3 \mu\text{g m}^{-3}$) was comparable with the previous studies made over Mumbai (Chowdhury et al 2007) other metropolitan cities in India like Delhi (Singh et al., 2010) and Kanpur (Nair et al., 2007) located over Indo-Gangetic-Plane. The WSOC concentration ($12.7 \pm 7.4 \mu\text{g m}^{-3}$) was also comparable with the IGP location (Rastogi et al., 2015).

Morning and afternoon variability of aerosol components and its absorption properties are shown in Figure 1. Lower PM10 and BC concentration (Figure 1a,b) during afternoon compared to the morning period could be attributed to the dilution effect due to elevated mixing layer height during afternoon period. There was no significant difference in WSOC concentration between morning and afternoon and WSOC/PM10 ratio was also similar (Figure 1a and 1f).

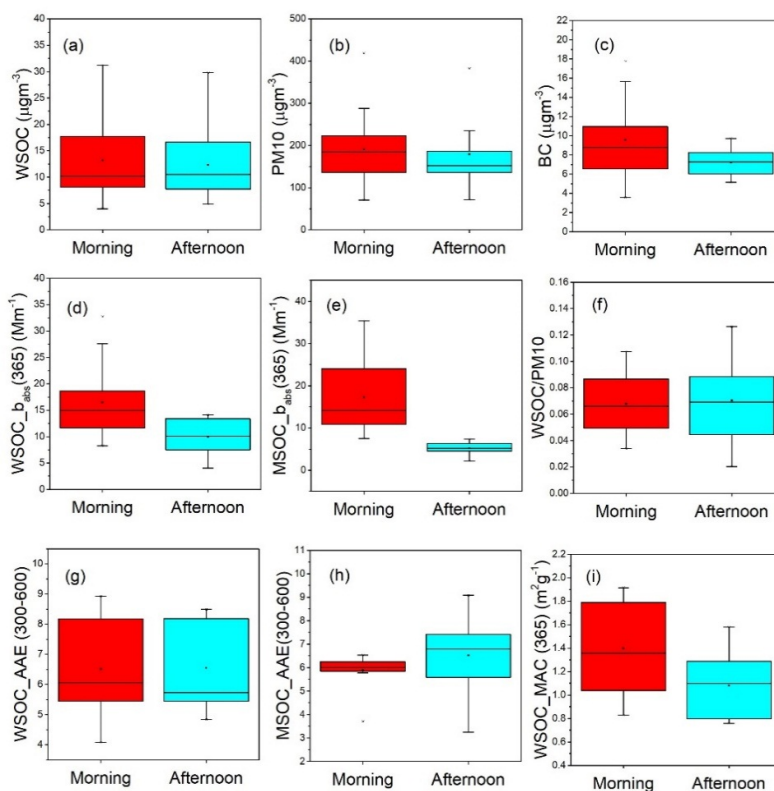


Figure 1: Morning and afternoon variability of aerosol components and absorption parameters of solvent extracts.

For the present study absorption coefficient at 365 nm ($b_{\text{abs}}(365)$) of solvent extracts are considered as the surrogate of BrC concentration. Figure 1d and 1e show higher $b_{\text{abs}}(365)$ (water and methanol extracts) and higher MAC_{365} of WSOC (figure 1i) during morning period. No significant difference in mean AAE of WSOC (6.5 ± 1.5) was observed for freshly emitted and aged WSOC (Figure 1g) but AAE for water soluble BrC varied a wide range (8.9-4.1). AAE for MSOC did not varied much (mean 5.9 ± 0.7) in the morning freshly emitted BrC but varied a wide range (3.2 – 9.1) in the afternoon (Figure 1h) indicate the aged BrC compounds formed in the afternoon has wide range of absorption bands compared to the freshly emitted MSOC.

Good correlation coefficient (R^2 : 0.59) between BC and WSOC concentration (Figure 2a) for the morning samples suggest they may both arise from primary anthropogenic emission like vehicular activity or any burning activity. Weak or no correlation (R^2 : 0.02) in the afternoon period, indicates additional sources of WSOC other than primary anthropogenic emission. Further study of photochemical activity is needed to examine possible secondary photochemical formation of WSOC during the afternoon period (figure 2b).

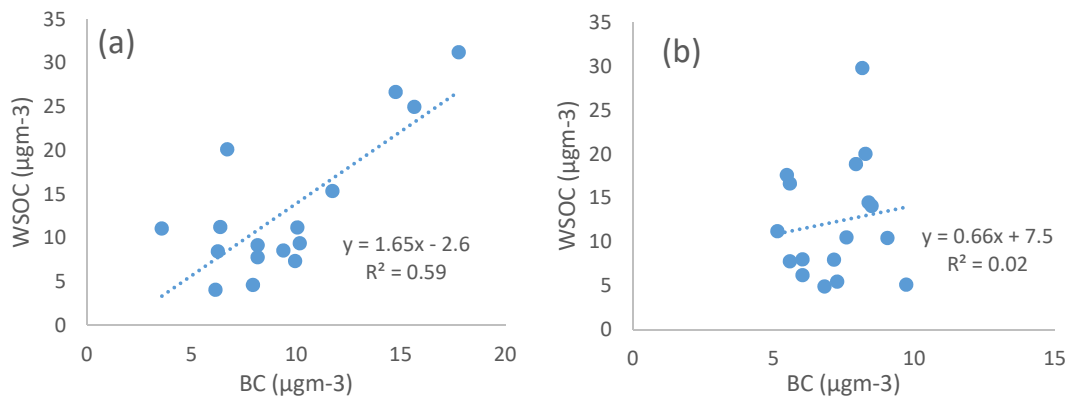


Figure 2: Correlation between BC and WSOC concentration measured during morning and afternoon period.

Daily average time series of aerosol components and their absorption properties are shown in figure 3a and 3b. High PM₁₀, WSOC, BC mass concentration was observed during three occasions on 1st, 13th and 25th of March. $b_{\text{abs}}(\lambda)$ _WSOC and $b_{\text{abs}}(\lambda)$ _MSOC was also higher in those days compared to other days. To investigate further we have calculated 3-day back trajectory analysis for each sampling day (500m above ground level) and collected MODIS V6 active fire count data in central and western India. Figure 4a and 4b show that during high aerosol mass concentration and high absorption coefficient event (13th and 25th March) the air trajectories are associated with land air mass coming from central and western Indian regions passing over the fire spot areas. On the other hand, during 9th and 10th March aerosol components and absorption coefficients were at lower level associated to trajectories coming from marine regions (figure 4).

CONCLUSIONS

Water soluble and methyl only soluble BrC compounds have significant absorption in the lower wavelength region. Freshly emitted primary BrC compounds were found to be more absorbing than photochemically aged BrC. Regional air mass transport from regions of active fires was linked to enhanced BrC contribution over the atmosphere in Mumbai.

ACKNOWLEDGMENTS

Authors like to acknowledge IIT-Bombay and NCAP-COELESCE project for providing financial support for this study.

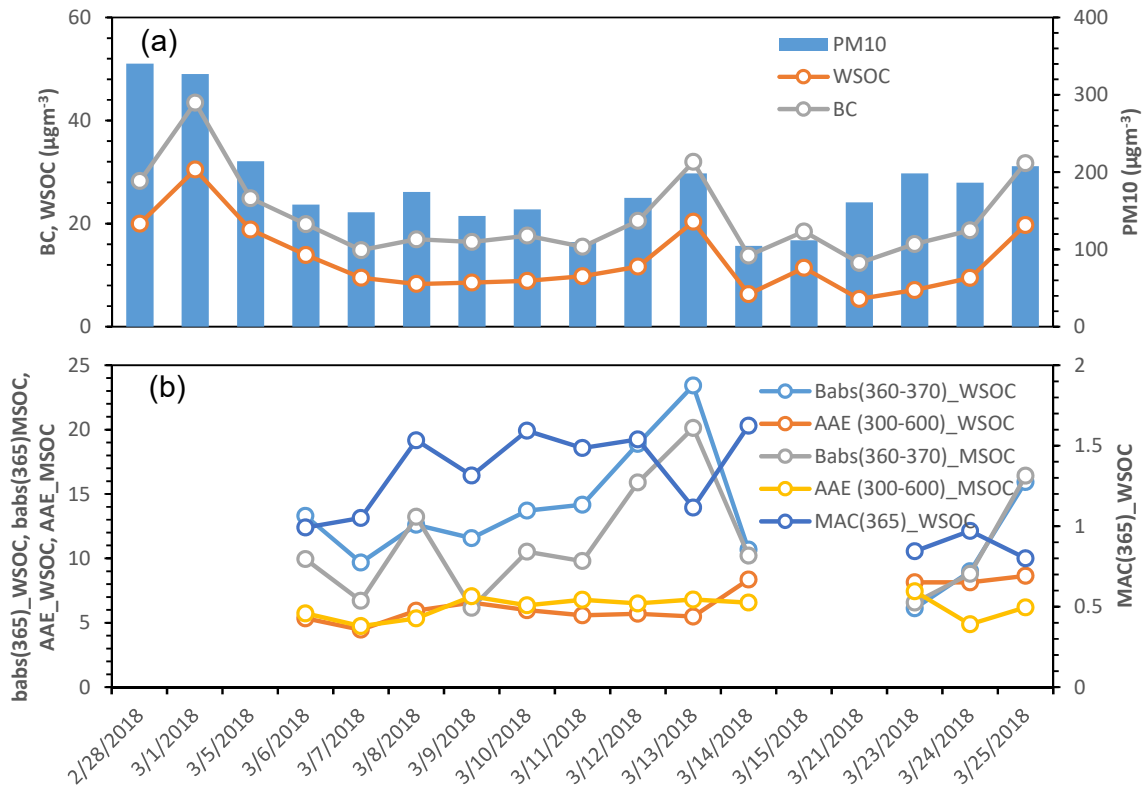


Figure 3: Day to day variation of aerosol components and absorption parameters.

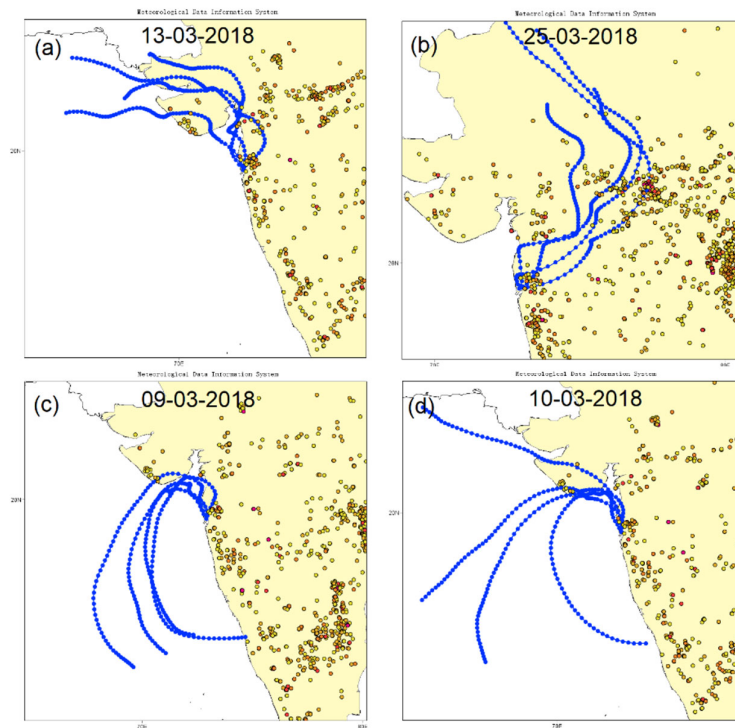


Figure 4: (a,b) Biomass burning episode associated to land mass trajectories with high aerosol components and higher absorption parameters (c,d) trajectories associated to marine air mass having lower aerosol concentration and absorption parameters.

REFERENCES

- Andreae, M.O. and Gelencsér, A., 2006. Black carbon or brown carbon? The nature of light-absorbing carbonaceous aerosols. *Atmospheric Chemistry and Physics*, 6(10), pp.3131-3148
- Bond, T. and Bergstrom, R.: Light Absorption by Carbonaceous Particles: An Investigative Review, *Aerosol Sci. Technol.*, 40, 27–67, 2006.
- Bond, T.C., Doherty, S.J., Fahey, D.W., Forster, P.M., Berntsen, T., DeAngelo, B.J., Flanner, M.G., Ghan, S., Kärcher, B., Koch, D. and Kinne, S., 2013. Bounding the role of black carbon in the climate system: A scientific assessment. *Journal of Geophysical Research: Atmospheres*, 118(11), pp.5380-5552.
- Chakraborty, A., Gupta, T. and Tripathi, S.N., 2016. Chemical composition and characteristics of ambient aerosols and rainwater residues during Indian summer monsoon: Insight from aerosol mass spectrometry. *Atmospheric Environment*, 136, pp.144-155.
- Cheng, Y., He, K.B., Zheng, M., Duan, F.K., Du, Z.Y., Ma, Y.L., Tan, J.H., Yang, F.M., Liu, J.M., Zhang, X.L. and Weber, R.J., 2011. Mass absorption efficiency of elemental carbon and water-soluble organic carbon in Beijing, China. *Atmospheric Chemistry and Physics*, 11(22), pp.11497-11510.
- Chowdhury, Z., Zheng, M., Schauer, J.J., Sheesley, R.J., Salmon, L.G., Cass, G.R. and Russell, A.G., 2007. Speciation of ambient fine organic carbon particles and source apportionment of PM_{2.5} in Indian cities. *Journal of Geophysical Research: Atmospheres*, 112(D15).
- Du, Z., He, K., Cheng, Y., Duan, F., Ma, Y., Liu, J., Zhang, X., Zheng, M. and Weber, R., 2014a. A yearlong study of water-soluble organic carbon in Beijing I: Sources and its primary vs. secondary nature. *Atmospheric Environment*, 92, pp.514-521.
- Ervens, B., Turpin, B.J. and Weber, R.J., 2011. Secondary organic aerosol formation in cloud droplets and aqueous particles (aqSOA): a review of laboratory, field and model studies. *Atmospheric Chemistry and Physics*, 11(21), pp.11069-11102.
- Hallquist, M., Wenger, J.C., Baltensperger, U., Rudich, Y., Simpson, D., Claeys, M., Dommen, J., Donahue, N.M., George, C., Goldstein, A.H. and Hamilton, J.F., 2009. The formation, properties and impact of secondary organic aerosol: current and emerging issues. *Atmospheric Chemistry and Physics*, 9(14), pp.5155-5236.
- Herckes, P., Valsaraj, K.T. and Collett, J.L., 2013. A review of observations of organic matter in fogs and clouds: Origin, processing and fate. *Atmospheric Research*, 132, pp.434-449.
- Nair, V.S., Moorthy, K.K., Alappattu, D.P., Kunhikrishnan, P.K., George, S., Nair, P.R., Babu, S.S., Abish, B., Sathesh, S.K., Tripathi, S.N. and Niranjana, K., 2007. Wintertime aerosol characteristics over the Indo-Gangetic Plain (IGP): Impacts of local boundary layer processes and long-range transport. *Journal of Geophysical Research: Atmospheres*, 112(D13).
- Ramanathan, V., Li, F., Ramana, M.V., Praveen, P.S., Kim, D., Corrigan, C.E., Nguyen, H., Stone, E.A., Schauer, J.J., Carmichael, G.R. and Adhikary, B., 2007. Atmospheric brown clouds: Hemispherical and regional variations in long-range transport, absorption, and radiative forcing. *Journal of Geophysical Research: Atmospheres*, 112(D22).
- Rastogi, N., Patel, A., Singh, A. and Singh, D., 2015. Diurnal variability in secondary organic aerosol formation over the Indo-Gangetic plain during winter using online measurement of water-soluble organic carbon. *Aerosol Air Qual. Res.*, 15(6), pp.2225-2231.
- Sathesh, S.K. and Moorthy, K.K., 2005. Radiative effects of natural aerosols: A review. *Atmospheric Environment*, 39(11), pp.2089-2110

Satish, R., Shamjad, P., Thamban, N., Tripathi, S. and Rastogi, N., 2017. Temporal characteristics of brown carbon over the central Indo-Gangetic Plain. *Environmental Science & Technology*, 51(12), pp.6765-6772.

Singh, S., Soni, K., Bano, T., Tanwar, R.S., Nath, S. and Arya, B.C., 2010. Clear-sky direct aerosol radiative forcing variations over mega-city Delhi. In *Annales Geophysicae* (Vol. 28, No. 5, pp. 1157-1166). European Geosciences Union.

HEALTH RISKS OF PM-BOUND TRACE METALS IN MUMBAI SLUMS

ABHAY ANAND¹, SUMAN YADAV² AND HARISH C. PHULERIA^{1,2}

¹Centre for Environmental Science and Engineering, IIT Bombay, Mumbai, 4000076, India.

²Interdisciplinary Programme in Climate Studies, IIT Bombay, Mumbai, 400076.

KEYWORDS: Pm_{2.5}, Trace Elements, Bio-Availability, Urban Slums

INTRODUCTION

Many studies have reported that the bioavailable (water-soluble) fraction of PM-bound trace metals are more strongly associated with air pollution related health effects compared to the total concentrations. This study hence was conducted to assess the bioavailable concentration of airborne trace metals and investigate their associated cancer risk in slums of Mumbai; a critical subpopulation of Mumbai city both in terms of the magnitude of the population and also air pollution risks.

METHODS

24 hour averaged gravimetric PM_{2.5} monitoring was conducted at a fixed background outdoor site each in a near-highway slum (n=21 days) and urban background slum (n=17 days) in Mumbai. The water soluble-trace metals were extracted from the PM_{2.5} filter samples by ultra-sonicating at room temperature for 1-hour duration and then analyzed using ICP-AES.

RESULTS & DISCUSSIONS

Cd, Cu, Zn and Pb were the major anthropogenic source marker elements detected in both slums. The moderate to high correlations between Cu, Zn and Cd indicates traffic emissions in both slums whereas the moderate correlations between Cu and Ba indicates contributions from brake wear. The concentrations of Cd and Cu were 4-times and 2-times higher in the near-highway slum compared to urban-background slum, indicating the increased contribution from local traffic emissions ($p < 0.05$). The influence of traffic sources could be also responsible for the higher weekday Cd and Zn concentrations compared to weekends ($p < 0.20$). The other elements detected were Al, Fe, Ca, Mg and Mn which are mainly crustal in origin, suggested by their high inter-correlations. Risk calculations show that the cancer risks of bioavailable fraction of Cd is significantly higher in near-highway slum (13.4×10^{-6}) compared to background slum (3.4×10^{-6}).

CONCLUSIONS

The results suggest that the health risks due to PM-bound toxic metals could be higher in those slums located nearer to major traffic highways.

REFERENCES

Pant, P., Shukla, A., Kohl, S.D., Chow, J.C., Watson, J.G. and Harrison, R.M. (1986). Characterisation of ambient PM_{2.5} at a pollution hotspot in New Delhi, India and inference of sources, Atmospheric Environment 105, 178-189.

CHARACTERIZATION OF WATER SOLUBLE ORGANIC CARBON AND RELATED FUNCTIONAL GROUPS BY ^1H NMR AT SUBURBAN MUMBAI

YADAV S.¹, SALVE N.V.² AND PHULERIA H.C.*^{1,2}

¹IDP in Climate Studies, Indian Institute of Technology Bombay, Powai, Mumbai - 400076, India

²Centre for Environmental Science and Engineering, Indian Institute of Technology Bombay, Powai, Mumbai - 400076, India

KEYWORDS: Water Soluble Organic Carbon; Nuclear Magnetic Resonance; Photochemical activity.

INTRODUCTION

Organic aerosols are of concern due to their roles in several atmospheric processes comprising heterogeneous reactions, radiative forcing, and regional visibility degradation, as well as their adverse impact on human health (Gupta et al., 2004; Lopes et al., 2015). Organic compounds that are emitted directly in particulate form from sources like agricultural-waste burning, biomass burning, construction, road traffic, re-suspension of mineral dust, industrial activities and power plants contribute to primary organic aerosols (POA); whereas, those formed in the atmosphere through different physico-chemical transformation processes result into secondary organic aerosols (SOA) (Kaul et al., 2011; Singh and Gupta, 2016). Inadequate understanding on SOA formation on spatial and temporal scale leads to measurement-modeling mismatch (Rastogi et al., 2015; Heald et al., 2011), and among chief causes of large uncertainty in the assessment of aerosol effects on air quality and climate. The present study aims to determine the WSOC concentration and its characteristics from atmospheric particulate matter during a photochemically active period and morning peak traffic hours at an urban background location.

METHODS

The study was conducted in Mumbai (19.0760° N, 72.8777° E), which is the commercial capital located on the West coast of India. Particulate matter sampling was done on the rooftop (18 m) of the Centre for Environmental Science and Engineering (CESE) building in the IIT Bombay campus. The campus is surrounded by a national park, pond and a link road which are within 2 km distance. Morning (7-11 am) and afternoon (12-4 pm) pairs of PM₁₀ samples were collected on tissue quartz filters using a high volume air sampler (at ~1 m³/min flow rate) and on PTFE filter substrates using a low volume sampler (flow rate = 5 L/min). A total of 17 morning/afternoon paired samples (total 32) were collected during February- March, 2018. The average temperature during morning and afternoon period were as 30.7±1.2 °C and 33.4±2.6 °C respectively whereas the relative humidity observed was as 51.0±10.7% and 48.4±12.6% respectively. The PM₁₀ mass was determined gravimetrically using the PTFE filters. The quartz filters were packed and stored in deep freezer (4°C) until analysis. Quartz filters were extracted in 25 ml Milli Q water and water-soluble organic carbon (WSOC) was measured using a TOC analyzer (URL-7). The Nuclear Magnetic Resonance (NMR) spectrum was obtained using a Bruker 750 MHz NMR instrument with a probe of 5mm Triple resonance H/C/N nuclei with 2H lock and 50 G/cm gradient along Z axis. Data was acquired 1024 times. The sweep width was 12019.23 Hz. The remaining aliquots of the water extracts were dried under vacuum and re-dissolved in deuterium oxide (D₂O) for functional group characterization by proton nuclear magnetic resonance (^1H -NMR) spectroscopy (Decesari et al., 2000). Sodium 3-trimethylsilyl-(2,2,3,3-d₄) propionate (TSP-d₄) was used as the referred internal standard.

RESULTS & DISCUSSIONS

PM₁₀ mass concentration

Average PM₁₀ was 174.5±61 µg m⁻³ (range: 82.5 to 288 µg m⁻³) and 151.0±66.4 (range: 71.6 to 382.5) in the morning and afternoon periods, respectively (Figure 1(a)). The higher mass concentration in the morning can be attributed to the and local sources and vehicular traffic emissions as it is mostly office going period

and JVLR road is ~500 m away from the sampling site. Similar trend of high concentration in morning rush hours was observed by Bathmanabhan et al., (2010) and Rastogi et al., (2015).

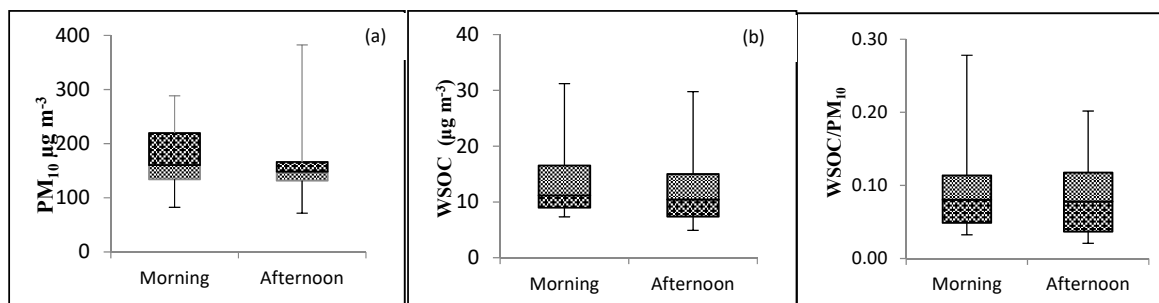


Figure 1: (a) PM_{10} and (b) WSOC and (c) WSOC/ PM_{10} concentration for morning (7-11 am) and afternoon (12-4 pm) period

Water soluble organic carbon concentration

The measured WSOC concentrations reveal a large day-to-day variability. It ranged from 7.3 to 31.2 $\mu\text{g m}^{-3}$ (median: 11.1, average: 14.4, sd: 7.4) during morning hours and 6.7 to 29.7 $\mu\text{g m}^{-3}$ (median: 10.4, average: 12.2, sd: 6.7) during afternoon periods. Although the average WSOC concentration was slightly higher in afternoon but no significant difference in WSOC concentration was observed between morning and afternoon periods (Figure 1(b)) and the WSOC/ PM_{10} (Figure 1(c)) concentration also followed the same trend with no significant difference. Rastogi et al., (2015) observed higher WSOC concentration in morning and lower in afternoon in Patiala. Whereas Zhang et al., (2012) reported higher WSOC concentration in afternoon at Los Angeles while at Atlanta (which was ~400 m away from heavily travelled highway) higher WSOC concentration was reported during morning hours. The temporal variability of WSOC in the atmosphere is expected to be driven by emission sources, physico-chemical transformations, transport and deposition processes (Sullivan et al., 2004; Zhang et al., 2012; Rastogi et al., 2015). The decrease in WSOC concentration during afternoon hours may be attributed to several factors such as increase in the mixing layer height and/or, there may be a volatile loss of semi-volatile WSOC as ambient air temperature increases to its maximum during afternoon hours. The higher WSOC concentration in morning corresponds to the time when vehicular emissions etc. are used at their maximum, suggesting them as major sources of the precursors of observed WSOC.

^1H NMR characterization

Although the characterization of specific individual organic species becomes difficult, the extracted WSOC showed NMR peaks in four main categories of functional groups carrying C-H bonds: (i) unfunctionalized alkyls (H-C), (ii) aliphatic carbons bound to an unsaturated carbon atom (H-C=C=), (iii) aliphatic alcohols, ethers, and esters (H-C-O), (iv) aromatic rings (H-Ar). For a further understanding of the ^1H NMR data, a quantitative integration of each spectral region was performed in order to assess the abundance of each functionality in WSOC samples (Figure 2). The relative abundance of each type of proton is calculated as a percent ratio between the integral of protons in a particular region and the integral of total protons. It can be seen that there is a decrease in the abundance of aromatic protons in the afternoon. The loss of aromatic protons was compensated by the increase in either of the remaining three types of protons. The relative abundance of protons for summer obtained by Decesari et al. (2011) were 55% for H-C, 45% for H-C=C=, 5% for H-C-O and 2% for Ar-H. The abundance of aliphatic and aromatic protons in the present study was comparable with the study conducted by Decesari et al., (2011). Looking at the average abundance of each type of proton, it can be seen that the loss in aromatic protons has been mainly compensated by the increase in the protons in the alkane region. This region mainly contains the aliphatic groups in alpha position to carboxyls or other unsaturated carbon atoms and terminal methylene groups which are away from the functional groups attached to an aliphatic chain (Decesari et al., 2011). The spectrum of the present study features all of the peaks obtained by Decesari et al. (2011), but less sharp. If we consider that the aromatic groups have a long chain substitution, loss in the H-C=C= protons can be explained (Decesari et al., 2007) considering the photochemical transformation that leads to the ring opening. Slight higher loss of H-C=C= protons is observed in the afternoon.

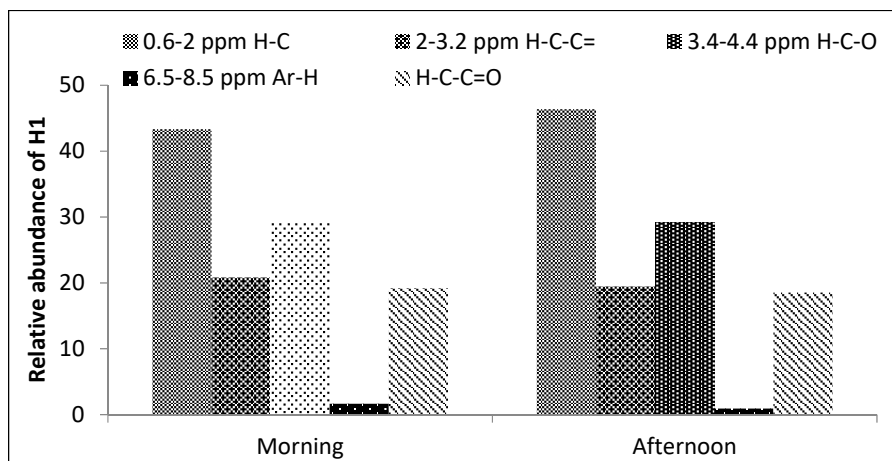


Figure 2: Relative abundance of each functionality in PM₁₀ WSOC samples collected during morning and afternoon periods

CONCLUSIONS

The difference between the morning and afternoon was observed as marginal in WSOC and higher in mass concentration of particulate matter at the sampling site which indicates the presence of local sources and vehicular emissions. The NMR characterization shows the effect of photochemical oxidation in terms of decrease in the abundance of aromatic protons; although the difference is very low. This study highlights the need for studies on WSOC characterization to understand the nature of organic compounds so to better understand their role in air quality and climate impacts of the aerosols.

REFERENCES

- Bathmanabhan S., Nagendra S. and Madanayak S. (2010), Analysis and interpretation of particulate matter – PM₁₀, PM_{2.5} and PM₁ emissions from the heterogeneous traffic near an urban roadway. *Atmospheric Pollution Research*, 1 (3): 184-194.
- Decesari S., Facchini M. C., Fuzzi S. and Tagliavini E. (2000), Characterization of water-soluble organic compounds in atmospheric aerosol: A new approach. *Journal of Geophysical Research*, 105(D1): 1481-1489.
- Decesari S., Mircea M., Cavalli F., Fuzzi S., Moretti F., Tagliavini E., and Facchini M. C. (2007), Source Attribution of water-soluble organic aerosol by nuclear magnetic resonance spectroscopy. *Environmental Science & Technology*, 41: 2479-2484.
- Decesari S., Finessi E., Rinaldi M., Paglione M., Fuzzi S., Stephanou E. G., Tziaras T., Spyros A., Ceburnis D., O'Dowd C., Dall'Osto M., Harrison R. M., Allan J., Coe H. and Facchini M. C. (2011), Primary and secondary marine organic aerosols over the North Atlantic Ocean during the MAP experiment. *Journal of Geophysical Research*, 116: D22210- D22231.
- Gupta, T., P. Demokritou and P. Koutrakis (2004), Development and performance evaluation of a highvolume ultrafine particle concentrator for inhalation toxicological studies, *Inhal. Toxicol.*, **16**,851.
- Heald, C.L., Coe, H., Jimenez, J.L., Weber, R.J., Bahreini, R., Middlebrook, A.M., Russell, L.M., Jolleys, M., Fu, T.M., Allan, J.D., Bower, K.N., Capes, G., Crosier, J., Morgan, W.T., Robinson, N.H., Williams, P.I., Cubison, M.J., DeCarlo, P.F. and Dunlea, E.J. (2011). Exploring the Vertical Profile of Atmospheric Organic Aerosol: Comparing 17 Aircraft Field Campaigns with a Global Model. *Atmos. Chem. Phys.* 11: 12673–12696.

Kaul, D.S., T. Gupta, S. N. Tripathi, V. Tare and J. L. Collett (2011), Secondary organic aerosol: A comparison between foggy and non-foggy days, *Environ. Sci. Technol.*, **45**, 7307.

Lopes, S.P., Matos, J.T.V., Silva, A.M.S., Duarte, A.C., Duarte, R.M.B.O., (2015). ¹H NMR studies of water- and alkaline-soluble organic matter from fine urban atmospheric aerosols. *Atmos. Environ.* 119, 374-380.

Singh, D.K. and T. Gupta (2016), Role of transition metals with water soluble organic carbon in the formation of secondary organic aerosol and metallo-organics in PM₁ sampled during post monsoon and pre-winter time, *J. Aerosol Sci.*, **94**, 56.

Sullivan, A.P., Weber, R.J., Clements, A.L., Turner, J.R., Bae, M.S. and Schauer, J.J. (2004). A Method for Online Measurement of Water-soluble Organic Carbon in Ambient Aerosol Particles: Results from an Urban Site. *Geophys. Res. Lett.* 31: L13105.

Zhang, X., Liu, Z., Hecobian, A., Zheng, M., Frank, N.H., Edgerton, E.S. and Weber, R.J. (2012). Spatial and Seasonal Variations of Fine Particle Water-soluble Organic Carbon (WSOC) over the Southeastern United States: Implications for Secondary Organic Aerosol Formation. *Atmos. Chem. Phys.* 12: 6593–6607, doi: 10.5194/acp-12-6593-2012.

INFLUENCE OF AEROSOL RADIATIVE EFFECTS ON ATMOSPHERIC THERMAL STRUCTURE AND DYNAMICAL RESPONSE OVER INDIA IN THE ECHAM6-HAM2 GCM

KAUSHIK MUDUCHURU¹ AND CHANDRA VENKATARAMAN^{1,2}

¹Interdisciplinary Program in climate studies, Indian Institute of Technology Bombay, Powai, Mumbai, India.

²Department of chemical engineering, Indian Institute of Technology Bombay, Powai, Mumbai, India

KEYWORDS: aerosol and climate change, aerosols in gcms, carbonaceous aerosols, dynamical response

INTRODUCTION

Absorbing aerosols attenuate incoming solar radiation through both scattering and absorption. On synoptic and global scales, aerosols have been implicated in a weakening of the South Asian monsoon, through increasing regional planetary albedo and weakening the overturning circulation (Bollasina et al. 2011; Krishnan et al. 2015), with additional drying over the peninsula from countering of the westerly monsoonal flow (Patil et al. 2018). Aerosol absorption heats the atmosphere differentially, thereby changing the mesoscale thermal structure of the atmosphere. Scattering and absorbing aerosols contribute towards cooling the surface, with absorbing aerosols additionally heats atmospheric layers in which they reside. This could lead to heating aloft, with surface cooling, thus stabilizing the atmosphere and suppressing convection (Wang 2013, Ramanathan et al., 2005), with related reductions in rainfall. Atmospheric stabilization of lower troposphere has been shown to also act through decreases in cloud fraction and cloud liquid water path (Johnson et al., 2004; Persad et al., 2012).

Here we study differences in alteration of stratiform and convective precipitation by absorbing aerosols over India, using GCM simulations, and examining modulation of the thermal structure of the lower troposphere and thermodynamic response.

METHODS

Experiments using ECHAM6-HAM2 (6th Generation coupled chemistry GCM from MPI-Meteorology) were performed with transient simulations of three ensemble members for a period of 40 years to simulate climate responses to both aerosols and SST forcings. The three ensemble members were generated by slightly perturbing model parameters, by about 0.01%, related to coefficients for horizontal diffusion for divergence, vorticity, and temperature. The aerosol module HAM is represented as seven overlapping lognormal modes with each mode described by three moments aerosol number, number median radius and standard deviation, where the standard deviation in HAM is fixed and set to 1.59 for the nucleation, Aitken and accumulation models and to 2.00 for the coarse modes. The aging of insoluble to soluble models is assumed to occur with a e-folding time of one day. Each of the modes have varying median diameters and the modes are externally mixed with internally mixed aerosol species.

The HA experiment with aerosol emissions fixed at 2010 was contrasted with LA experiment with aerosol emissions fixed at 1971 levels. Differencing the HA and LA experiments will help understand the role of increased aerosol emissions on the precipitation response. The peak monsoon months of July-August for 40 years (1971-2010) are considered for calculating the climatology as it represents the maximum rainfall period for the core monsoon region.

RESULTS & DISCUSSION

Here we contrast spatial heterogeneity in aerosol effects on rainfall, through analysis in two regions, north-India (23-30 N, 75-90 E; NI) and south India (10-18 N, 73-81 E; SI). The HA and LA simulation with other forcing kept same is differenced to extract the fast-atmospheric response to aerosol changes. Figure 1 represents the 1971-2010 peak monsoon (July-August) climatological mean rainfall (mm day⁻¹) differences between HA and LA simulations. The total precipitation (Figure 1a) response to aerosol changes shows an increase over the NI and decreases over SI. The NI region shows a large increase in stratiform rainfall (Figure 1c) with decreases in convective rainfall (Figure 1b). The drying over SI region is due to decreases in both stratiform and convective precipitation. The simulated changes in stratiform precipitation (Figure

1c) show an increase of 0.6 mm day⁻¹ over the Indo-Gangetic plains and increases of a lesser magnitude over the north Indian regions. Stratiform rainfall over the peninsular region showed a decrease of 0.4 mm day⁻¹ for stratiform rainfall with less decreases for the convective rainfall. To explain the opposing changes in total precipitation between the NI and SI regions, the convective and stratiform precipitation changes are examined in terms of aerosol effects on local dynamics and thermodynamics.

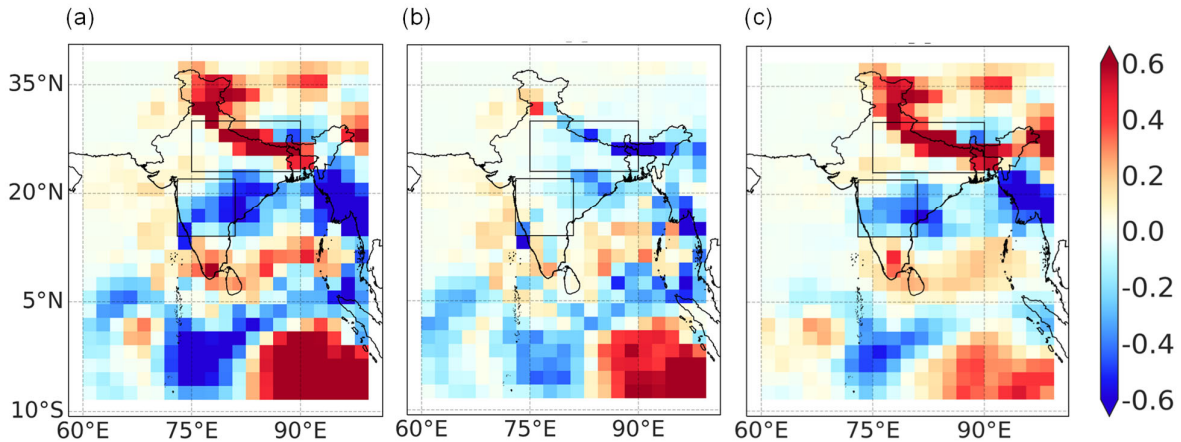


Figure 3: Difference between HA and LA in (a) total precipitation (mm day⁻¹) (b) convective component (mm day⁻¹) and, (c) stratiform component (mm day⁻¹) of the total precipitation during peak summer monsoon months of July-August for the years 1971–2010.

The aerosol effects on modulating the thermodynamic and local dynamics are shown in Figure 2. Absorbing aerosols act to heat the layers where they exist and differentially cool the layers below, causing a reduction in the local lapse rate which is shown to trap moisture in the boundary layer. The simulated increases in column water vapor content (Figure 2a) over NI region leads to larger increases in cloud water content (Figure 2c) compared to SI region. The lower tropospheric stability (Figure 2b) calculated as the temperature difference between 700 hPa and surface, serve as proxy for local convective activity. The strong response of cloud water in the lower troposphere is suggested to be linked to increased stability of the lower troposphere. The increased cloud water response could lead to the simulated wetting over the northern India region, which suggests a significant role of absorbing aerosols in modulating stratiform rainfall.

CONCLUSIONS

The simulated response of stratiform precipitation to increases aerosols shows strong heterogeneity over the Indian land regions with increases over the northern regions with decreases over the southern region. The overall stratiform rainfall pattern agrees with total rainfall but convective precipitation changes also contribute to the net change in total precipitation. The results suggest that the increased absorbing aerosols changed the thermodynamic structure of the lower troposphere by heating the layers above the surface thereby stabilizing the atmosphere. The stabilization of the lower troposphere reduces the convective strength locally and traps the boundary layer moisture. The simulated increases in stratiform rainfall suggests close connection to increases in moisture over the northern regions and the decrease over southern India is associated with decreases in moisture. The increased stabilization over northern India corresponds to decreases in convective precipitation with decreases of lesser intensity over south India. This work will attempt to describe the responses of both stratiform and convective rainfall in a coupled GCM with online chemistry. The reasonable estimation of the stratiform to convective precipitation ratio along with opposing effects of aerosols on stratiform and convective precipitation warrant for more study to understand the effects of aerosols on simulated precipitation changes over India.

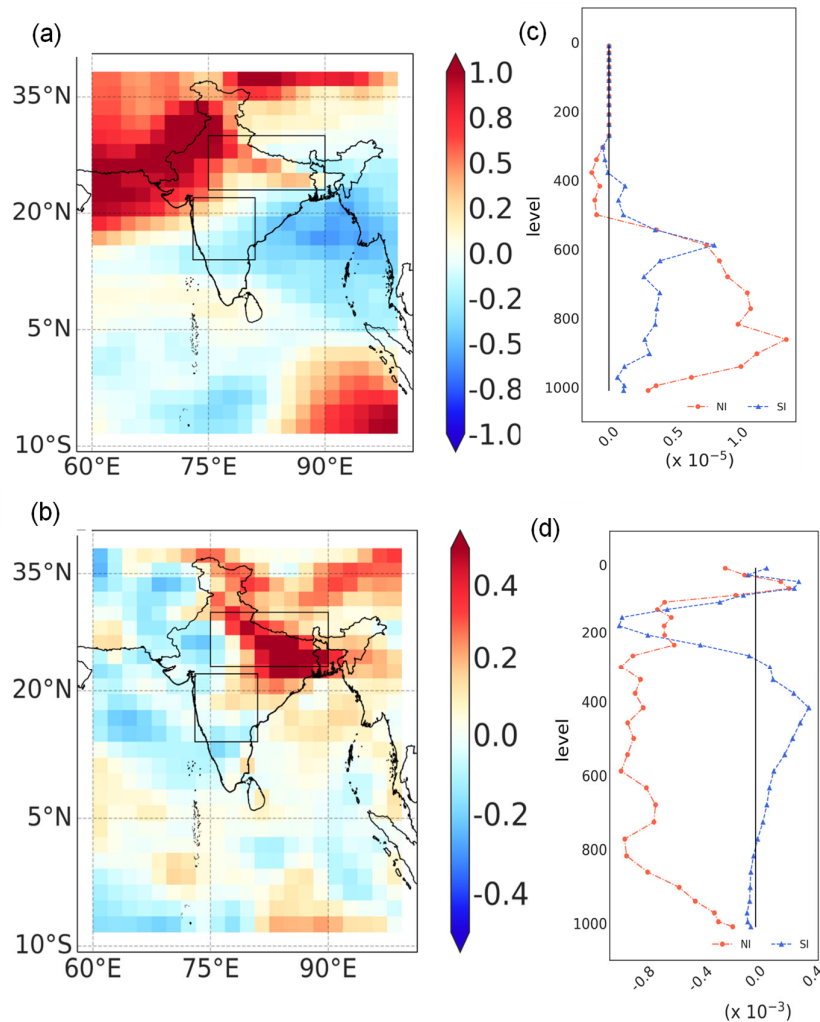


Figure 4: Difference between HA and LA in (a) column integrated water vapor mixing ratio (kg m^{-2}), (b) lower tropospheric stability (K), (c) vertical profile of vertical velocity (m s^{-1}), and (d) Cloud Water (kg kg^{-1}) during peak summer monsoon months of July-August for the years 1971–2010. The lower tropospheric stability is defined as the potential temperature difference between 700 hPa and surface given in kelvin.

REFERENCES

- Guo L, Turner AG, Highwood EJ (2016) Local and remote impacts of aerosol species on Indian summer monsoon rainfall in a GCM. *Journal of Climate* 29(19):6937-6955
- Wang, Chien (2013) Impact of anthropogenic absorbing aerosols on clouds and precipitation: A review of recent progresses. *Atmospheric research* 122: 237-249.
- Persad, G.G., Ming, Y. and Ramaswamy, V., 2012. Tropical tropospheric-only responses to absorbing aerosols. *Journal of Climate*, 25(7), pp.2471-2480.
- Meehl GA, Arblaster JM, Collins WD (2008) Effects of black carbon aerosols on the Indian monsoon. *Journal of Climate* 21(12):2869-2882
- Lau K, Kim M, Kim K (2006) Asian summer monsoon anomalies induced by aerosol direct forcing: the role of the Tibetan plateau. *Climate dynamics* 26(7-8):855-864

Ramanathan V, Chung C, Kim D, Bettge T, Buja L, Kiehl J, Washington W, Fu Q, Sikka D, Wild M (2005) Atmospheric brown clouds: Impacts on south Asian climate and hydrological cycle. *Proceedings of the National Academy of Sciences of the United States of America* 102(15):5326-5333

INFLUENCE OF RECENT CHANGES IN AEROSOL ABUNDANCE ON TEMPERATURE RESPONSE AND SNOW COVER FRACTION OVER THE HIMALAYAN REGION

A. SHARMA¹ AND C. VENKATARAMAN^{1,2}

¹Interdisciplinary Program in Climate Studies, Indian Institute of Technology Bombay, Powai, Mumbai, India.

²Department of Chemical Engineering, Indian Institute of Technology Bombay, Powai, Mumbai, India.

KEYWORDS: Aerosols In Gcms, Carbonaceous Aerosols, Aerosol And Climate Change, Himalayas

INTRODUCTION

Recent studies have shown long term increase in surface-air temperature (Bhutiya et al, 2009; IPCC 2007; Du et al. 2004) and decrease in snow cover fraction (Immerzeel et al. 2009, Gurung et al. 2011) over Hindu-kush himalayas (HKH). Ramanathan et al., 2007 showed that the greenhouse warming in the atmosphere is doubled due to the presence of Asian brown clouds (ABCs) over South Asia, and may lead to significant loss of snow and glacier mass in the Himalayas. The heat energy present in the atmosphere due to the presence of the absorbing aerosols is transferred from the atmosphere to the land to enhance land surface temperatures and resulting in acceleration of snow melt (Lau et al., 2010). The studies have shown that the transportation and deposition of absorbing aerosols like black carbon on the snow and ice surface can darken the surface, enhance the absorption of radiation and accelerate snow/ice melting (Quinn et al., 2011). In this study we use long-term general circulation model simulations driven by evolving aerosols to understand recent changes in aerosol abundance and its effects on temperature and snow cover over HKH region.

METHODS

For this study, simulations are made with fully coupled aerosol-climate general circulation model, ECHAM6-HAM2 at T63 resolution for 40 years from 1971-2010. The model simulations which represent the present day are performed with prescribed evolving observed sea surface temperature (SST) and sea ice concentration (SIC) using the monthly varying Atmospheric Model Intercomparison Project (AMIP) data sets. The AEROCOM emission inventory is used for evolving aerosol emissions from 1971 to 2010 (Dentener et al., 2006).

RESULTS & DISCUSSION

In order to understand the effects of recent increases in aerosol emissions over India on temperature response, the difference between two climatological periods are considered: present decade i.e. 2001-2010 and past decade i.e. 1971-1980. The difference between present and past decades showed average increase in 2m temperature by 1.2 °C and decrease in snow cover fraction by 0.04 over HKH (Figure 1). Also the western Himalayas is less warm by 0.8 °C than central and eastern Himalayas by 1.7 °C and 1.4 °C respectively. The snow cover fraction result shows more decrease in central and eastern Himalayas by 0.045 and 0.037 respectively when compared to western Himalayas by 0.026. The decadal difference in columnar aerosol optical depth (AOD) is an increase of 0.16, with simultaneous increases in black carbon (BC) and dust AOD, suggest increase in absorbing aerosol abundance in the region (Figure 2). Studies like Bonasoni et al. (2010) showed high levels of pollutants during pre-monsoon can affect the southern Himalayas and valley circulation may result into arrival of chemicals emitted by anthropogenic sources up to the Tibetan plateau. The distribution of BC AOD is more in the central Himalayas, possibly from higher anthropogenic emissions in Indo-Gangetic plains, which needs further evaluation of transport pathways. Dust AOD is also enhanced in central Himalayas over other regions. The dissimilarity in the aerosol composition in all the three regions is likely to a factor in differences in temperature response and snow cover changes among the three regions. Such large contributions of absorbing aerosols to AOD in the HKH are important to consider, because of aerosol radiative forcing effects on the surface energy balance.

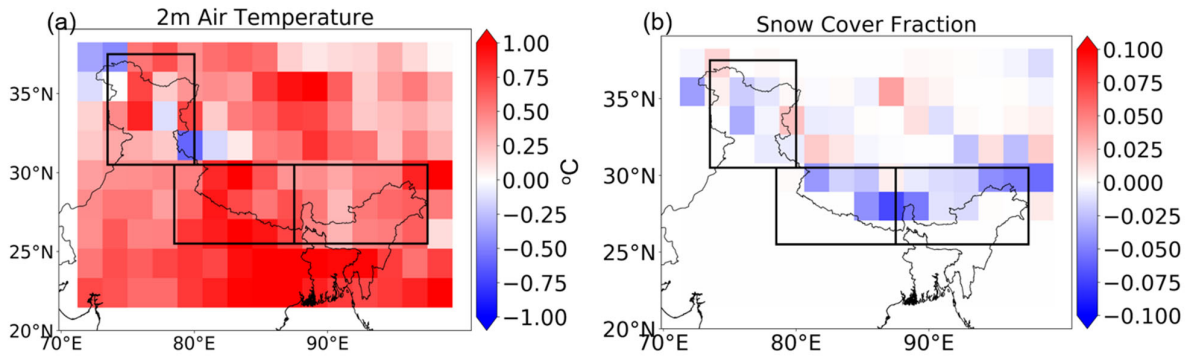


Figure 1. Difference between recent decade (2001-2010) and historical decade (1971-1980) during MAM in (a) 2m temperature and (b) Snow cover fraction.

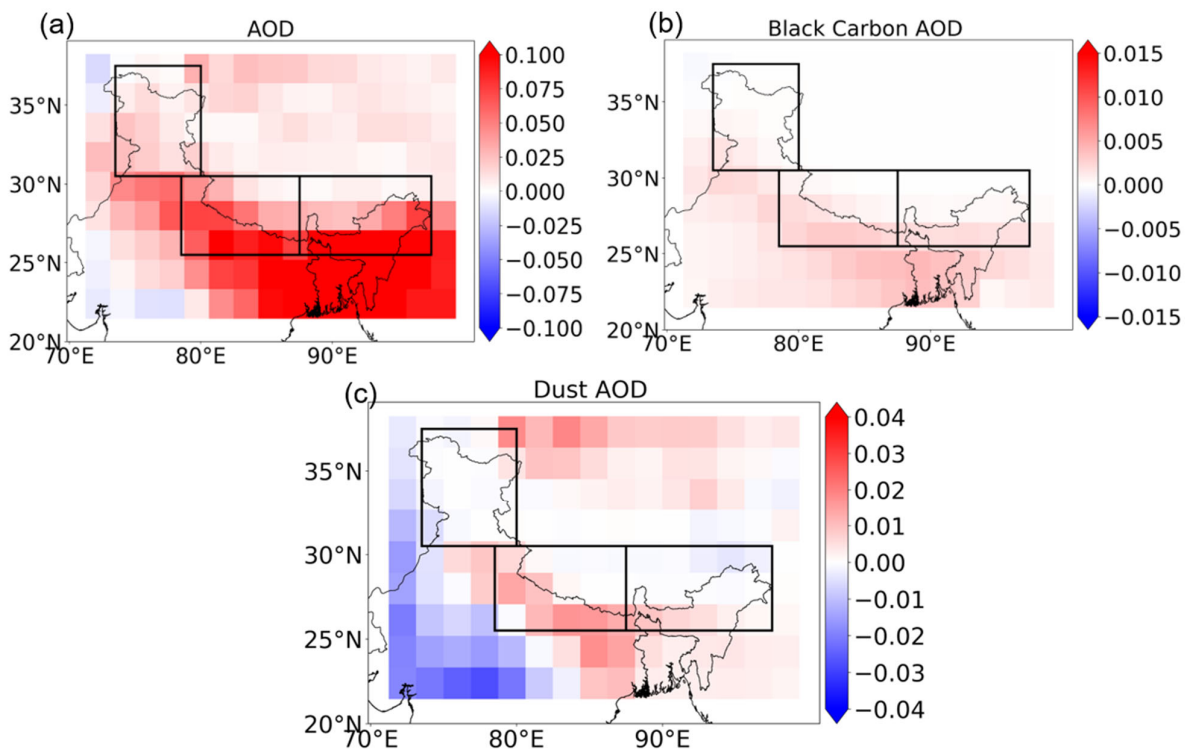


Figure 2. Difference between recent decade (2001-2010) and historical decade (1971-1980) during MAM in (a) Columnar AOD (b) Black carbon AOD and (c) Dust AOD.

CONCLUSIONS

The decadal differences showed an average increase in 2m temperature by 1.2 °C and decrease in snow cover fraction by 0.04 which can be due to the contribution of absorbing aerosols like BC and dust to total AOD in summer months over HKH. The future work would investigate decadal changes in aerosol radiative forcing and heating rates, during 1971-2010, to assess aerosol effects on climate change in the HKH.

ACKNOWLEDGMENTS

The authors would like to thank the NCAP-COALESCE project funded by the Ministry of Environment Forests and Climate Change.

REFERENCES

- Bhutiyani, MR; Kale, VS; Pawarc, NJ (2009) 'Climate change and the precipitation variations in the northwestern Himalaya: 1866–2006.' *International Journal of Climatology* 30(4): 535–548
- Bonasoni, P., Cristofanelli, P., Marinoni, A., Pradhan, B.B., Fuzzi, S., Gobbi, G.P., Vuillermoz, E. and Laj, P., 2010. High concentration of black carbon observed in the high himalayyas. *UNEP Black Carbon E-bulletin*, 2(2), p.15273.
- Dentener, F., et al. (2006), Emissions of primary aerosol and precursor gases in the years 2000 and 1750 prescribed data-sets for AeroCom, *Atmos. Chem. Phys.*, 6, 4321-4344.
- Du, MY; Kawashima, S; Yonemura, S; Zhang, XZ; Chen, SB (2004) 'Mutual influence between human activities and climate change in the Tibetan Plateau during recent years.' *Global and Planetary Change* 41(3–4): 241–249
- Gurung, DR; Kulkarni AV; Giriraj A; Aung KS; Shrestha B; Srinivasan J (2011b) 'Change in seasonal snow cover in Hindu Kush– Himalayan Region.' *The Cryosphere Discuss* 5(2): 755–777
- Immerzeel, WW; Droogers, P; de Jong, SM; Bierkens, MFP (2009) 'Large-scale monitoring of snow cover and runoff simulation in Himalayan river basins using remote sensing.' *Remote Sensing of Environment* 113: 40–49
- IPCC (2007) *The fourth assessment report: Climate change 2007, Synthesis Report*. Cambridge, UK: Cambridge University Press
- Lau, W.K., Kim, M.K., Kim, K.M. and Lee, W.S., 2010. Enhanced surface warming and accelerated snow melt in the Himalayas and Tibetan Plateau induced by absorbing aerosols. *Environmental Research Letters*, 5(2), p.025204.
- Quinn, P.K., Stohl, A., Arneth, A., et al., 2011. *The Impact of Black Carbon on Arctic Climate*. Arctic Monitoring and Assessment Programme (AMAP), Oslo
- Ramanathan, V., Li, F., Ramana, M.V., Praveen, P.S., Kim, D., Corrigan, C.E., Nguyen, H., Stone, E.A., Schauer, J.J., Carmichael, G.R. and Adhikary, B., 2007. Atmospheric brown clouds: Hemispherical and regional variations in long-range transport, absorption, and radiative forcing. *Journal of Geophysical Research: Atmospheres*, 112(D22).

MITIGATION OF ABSORBING AEROSOLS AND THEIR CLIMATE IMPACTS OVER INDIA: INFLUENCE OF SECTORAL INTERVENTIONS.

K. Tibrewal¹ AND C. Venkataraman^{1,2}

¹Interdisciplinary program in Climate Studies, Indian Institute of Technology Bombay, Powai, Mumbai – 400 076, India.

²Department of Chemical Engineering, Indian Institute of Technology Bombay, Powai, Mumbai – 400 076, India.

KEYWORDS: Aerosol And Climate Change, Carbonaceous Aerosols, Aerosol Sources, Mitigating Interventions

INTRODUCTION

While, carbon dioxide (CO₂) has been recognised as the primary catalyst for global climate change (Stocker et al. 2013), other forcing elements, like short-lived climate pollutants (SLCPs) (UNEP 2017), also cause significant climate impacts. They include aerosols and precursor gases such as methane, carbon monoxide, nitrous oxide, volatile organic compounds and sulphur dioxide (CCAC 2014). Based on their interaction with the solar radiation, aerosols can be broadly classified as absorbing and scattering. Absorbing aerosols, as the name suggests, absorb large part of the radiation incident on them. This leads to increases in net-downward radiation thus causing warming, while the latter scatter most of the radiation, decreasing the net-downward radiation and thus causing cooling (CCAC 2014). Absorbing aerosols mostly comprise of black carbon (BC) and dust. BC is a form of particulate matter released as a by-product of incomplete and inefficient combustion. Latest assessment estimates a radiative forcing of about 1.1 W m⁻², with a warming effect of nearly 50% of that of CO₂ making it the second largest contributor to global warming (Bond et al. 2013). Thus, there is a growing consensus on the potential of mitigation strategies targeting absorbing aerosols to alleviate near term climate change with a potential to reduce warming due to their rapid temperature response (Wallack and Ramanathan 2009; UNEP/WMO 2011; Shindell et al. 2012).

Mitigation of any pollutant require understanding of emitting sectors and interventions proposed to control emissions. For India, actions that address GHG emissions will not automatically cut SLCP emissions as these are emitted from unrelated sectors. Moreover, implementing polices to improve air quality primarily results in reducing NO_x and SO₂ emissions, which are cooling in nature, thus leading to unmasking of GHG warming. Thus, the objective of this study is to assess the influence of sectoral interventions on their potential to reduce emissions of absorbing aerosols – black carbon. It is followed by estimating the benefit in climate impacts in terms of CO₂-eq to emphasize on the significance of controlling BC to alleviate near term climate warming, complimenting CO₂ reductions.

METHODS

Assessment of mitigation follows evaluation of future emissions scenarios for 2030 and 2050 assuming different levels of energy efficiency and deployment of low-emissions technologies. The scenarios comprise of a reference (REF) with no change in current (2015) regulations, corresponding to very slow uptake of new technology scenario and two alternate scenarios (S2 and S3). S2 assumes adoption of promulgated and proposed regulations, corresponding to effective achievement of targets with implementation barriers while, S3 includes adoption of ambitious regulations, corresponding to those well beyond promulgated regulations. The detailed assumptions in future evolution of (i) sectoral demand, (ii) technology mix, (iii) energy consumption, and (iv) technology-linked emission factors are described in our previous study (Venkataraman et al. 2018). Mitigation of absorbing aerosols is expressed in terms of “emissions reduction potential (ERP)” of BC which is estimated as percentage reduction in emissions in an alternate scenario with respect to the reference scenario. Analysis is carried out to study the influence of different sectors to the total ERP of BC. Finally, the emissions are converted into CO₂-eq using global warming potentials (GWP-20) (Myhre et al. 2013) to represent climate impacts.

RESULTS & DISCUSSIONS

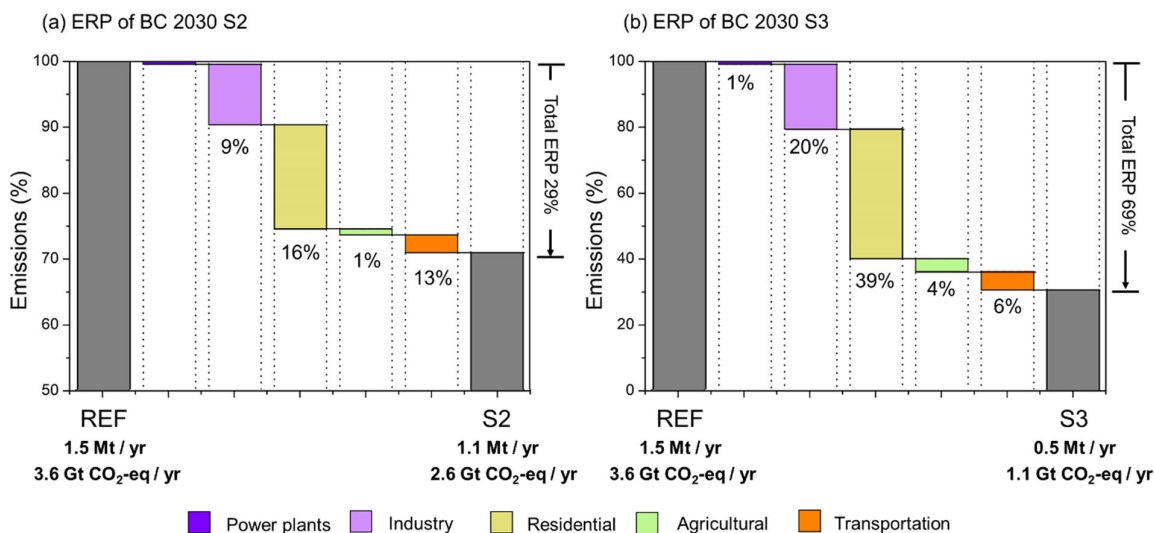


Figure 1. Emissions reduction potential (ERP) of black carbon (BC) in 2030 under (a) S2 and (b) S3 scenario.

In 2030, under REF scenario, emissions of BC increase by a factor of 1.2 from present day (Venkataraman et al. 2018). Implementation of several sectoral mitigation strategies at different levels of control as assumed in the alternate scenarios, resulted in an overall emissions reduction potential of 29% for BC in S2 (Fig. 1a) and 69% in S3 (Fig. 1b). The highest contribution is estimated from residential sector with a reduction potential of nearly 16% in S2 and 39% in S3. It is followed by controls assumed in industries with a reduction potential of 9% in S2 and 20% in S3 and transport with 13% in S2 and 6% in S3. No major controls were assumed in agricultural sector in S2. However, as ambitious controls are assumed in agricultural sector, a 4% reduction potential is estimated in S3. Power plants are estimated to have meagre reduction potential of less than 1% in both scenarios.

Mitigation of BC resulted in reducing SLCP warming (in terms of CO₂-eq) by nearly 21% (in S2) and 50% (in S3) in 2030. In S2 scenario, reduction in BC warming is found as a result of interventions such as PAT scheme in industries and shifts to electricity and solar energy in residential with further reductions coming from improving energy efficiencies of existing traditional technologies in all sectors, retrofitting Bull's trench kilns to zig-zag kilns and shifts to cleaner fuels like LPG for cooking and gasifiers for informal industries. In S3, interventions mentioned earlier along with greater shifts to zig-zag kilns, manufacturing of resource efficient and non-fired bricks and total phase out of open burning of agricultural residue. Under both scenarios, sectors dominating the control in BC warming include residential (contributed nearly 44-50%) followed by industries (with ~40% contribution) and agricultural sector (2-12%) with minor contributions from power plants and transportation.

CONCLUSIONS

Mitigation of BC emissions primarily came from residential sector followed by controls in industry and agricultural sector, which involved shifts to cleaner fuels for cooking and cleaner practices in brick manufacturing. This mitigation of BC emissions resulted in significant reductions in SLCP warming emphasizing the significance of BC targeted interventions to obtain near-term reductions in warming as complimentary to reductions in GHGs.

ACKNOWLEDGEMENT

This study was supported by National Carbonaceous Aerosols Programme – Carbonaceous aerosol emissions, source apportionment & climate impacts (NCAP-COALESCE) project.

REFERENCES

- Bond TC, Doherty SJ, Fahey DW, et al (2013) Bounding the role of black carbon in the climate system: A scientific assessment. *J Geophys Res Atmos* 118:5380–5552. doi: 10.1002/jgrd.50171
- CCAC (2014) Climate and Clean Air Coalition - Annual report. Climate and Clean Air Coalition (CCAC), Paris
- Myhre G, Shindell D, Bréon F-M, et al (2013) Anthropogenic and natural radiative forcing. In: Stocker TF, Qin D, Plattner GK, et al. (eds) *Climate Change 2013: The Physical Science Basis. Contribution of Working Group I to the Fifth Assessment Report of the Intergovernmental Panel on Climate Change*. Cambridge University Press, Cambridge, United Kingdom and New York, NY, USA, pp 658–740
- Shindell D, Kuylentierna JCI, Vignati E, et al (2012) Simultaneously Mitigating Near-Term Climate Change and Improving Human Health and Food Security. *Science* (80-) 335:183–189. doi: 10.1126/science.1210026
- Stocker TF, Qin D, Plattner GK, et al (2013) IPCC, 2013: *Climate Change 2013: The Physical Science Basis. Contribution of Working Group I to the Fifth Assessment Report of the Intergovernmental Panel on Climate Change*, 1535 pp
- UNEP (2017) *The Emissions Gap Report 2017*. United Nations Environment Programme (UNEP), Nairobi
- UNEP/WMO (2011) *Integrated Assessment of Black Carbon and Tropospheric Ozone*
- Venkataraman C, Brauer M, Tibrewal K, et al (2018) Source influence on emission pathways and ambient PM_{2.5} pollution over India (2015–2050). *Atmos Chem Phys* 18:8017–8039. doi: 10.5194/acp-18-8017-2018
- Wallack JS, Ramanathan V (2009) The other climate changers: Why black carbon and ozone also matter. *Foreign Aff* 105–113

AN OBSERVATIONAL ANALYSIS OF AEROSOL CLOUD INTERACTION OVER INDIA

MAINAK DAS¹, CHANDRA VENKATARAMAN^{1,2} AND ARPITA MONDAL^{1,3}

¹Interdisciplinary Program in Climate Studies, Indian Institute of Technology Bombay, Powai, Mumbai 400 076, India.

²Department of Chemical Engineering, Indian Institute of Technology Bombay, Powai, Mumbai 400 076, India.

³Department of Civil Engineering, Indian Institute of Technology Bombay, Powai, Mumbai 400 076, India.

KEYWORDS: Aerosol Cloud Interaction, Aerosol Indirect Effect, Modis Aqua.

INTRODUCTION

Aerosols can interfere with thermal radiation & precipitation through clouds, by acting as the nuclei of cloud droplets. This is known as aerosol indirect effect. Theoretically, an increase in aerosol amount results in smaller droplets in constant liquid water path, which shows more scattering by the droplets & more albedo (Twomey, 1974). These small droplets can further reduce precipitation efficiency and enhance cloudiness & albedo (Albrecht, 1989). The indirect effect of aerosols is quantified as the relative change in any of the cloud microphysical variables [cloud optical depth (COD), cloud droplet effective radius (CDER) or cloud droplet number concentration (N_d)] to change in aerosol amount; which is termed as ‘Aerosol-cloud interaction (ACI)’ (McComiskey et al., 2009). ACI can be often influenced by aerosol chemical composition & size distribution, dynamics & thermodynamics of atmosphere, meteorology etc. Previous findings on the effect of atmospheric moisture on ACI were contradictory & inconclusive. Kaufman & Fraser (1997) reported a dependence of ACI on water vapour, whereas Feingold et al. (2001) denied the hypothesis. Yuan et al. (2008) & Ten Hoeve et al. (2011) showed systematic change in ACI for variable water vapour. Liu et al. (2017) reported no significant change in ACI except for droplet size increase under increasing water vapour. No such study on ACI’s moisture dependence has been done on Indian landmass. A few studies reported a contrasting behaviour of ACI in abundant & deficient monsoon years (Panicker et al., 2010; Patil et al., 2017), which can be characterized as seasons with high & low water vapour respectively. In this study, we analyse ACI for warm clouds of the Indian region for different levels of water vapour present in the atmosphere using satellite observations.

DATA & METHODOLOGY

We choose COD & CDER as the representative variables of cloud microphysics (McComiskey & Feingold, 2012). Aerosol optical depth (AOD) is considered as the proxy variable for aerosol abundance. The daily observational gridded data (Level 3, $1^\circ \times 1^\circ$) for cloud variables [cloud top pressure-CTP, cloud top temperature-CTT, COD, CDER], aerosol [AOD (550 nm)] & available moisture [total precipitable water-TPW] are collected from MODIS Aqua collection 6 (Platnick et al., 2003; Seemann et al., 2003; Remer et al., 2005) dataset, for the year 2002-2015. We restrict our analysis within the landmass of India (70° – 90° E, 10° – 28° N)(Krishnan et al., 2016) (Fig. 1a.).

To reduce the data retrieval uncertainty, pixels having COD greater than 5.0 & AOD less than 1.0, are selected (Nakajima & King, 1990; Sarangi et al., 2017). The process of formation and the properties of ice particles are different from liquid water droplets. Also, warm clouds & precipitation are more frequent in India and contributes majorly to the hydrology. The clouds with ice at top are rejected by applying CTT greater than 273K. To separate the warm clouds from lower tropospheric dense fog, tall anvil or deep convective clouds, the study is limited to CTP between 450 hPa & 850 hPa (Gryspeerd & Stier, 2012). We remove pixels having water vapour level less than 1.5 cm & greater than 6cm ($\sim 5^{\text{th}}$ & $\sim 95^{\text{th}}$ percentile of the whole TPW dataset after previous screenings) to get rid of the extreme cases.

All the data available after previous screenings are stratified as i) high (TPW>3.2cm) & low (TPW<3.2 cm) moisture & ii) JJAS (data of JJAS) & nonJJAS (data of the months other than JJAS) clouds. For high and low moisture scenarios, the data are further divided into 3 smaller bins with equal binwidths of 0.6 cm

& 0.9 cm respectively. So, low moisture has sub-scenario of 1.5-2.1cm, 2.1-2.6cm & 2.6-3.2cm. Similarly, high moisture has sub-scenario of 3.2-4.1cm, 4.1-5.1cm & 5.1-6cm.

The AOD-COD and AOD-CDER relationships are calculated for each TPW bins in each scenario. The AOD range is divided into 6 bins having equal number of data points (i.e. ~17 percentile of total data points) in each bin. For each AOD bin, the COD & CDER are averaged & represented along with their standard error (Fig. 1b.-e.). Similar analysis is also done for JJAS & nonJJAS clouds. Results are presented in Fig. 2 a. & b.

RESULTS & DISCUSSIONS

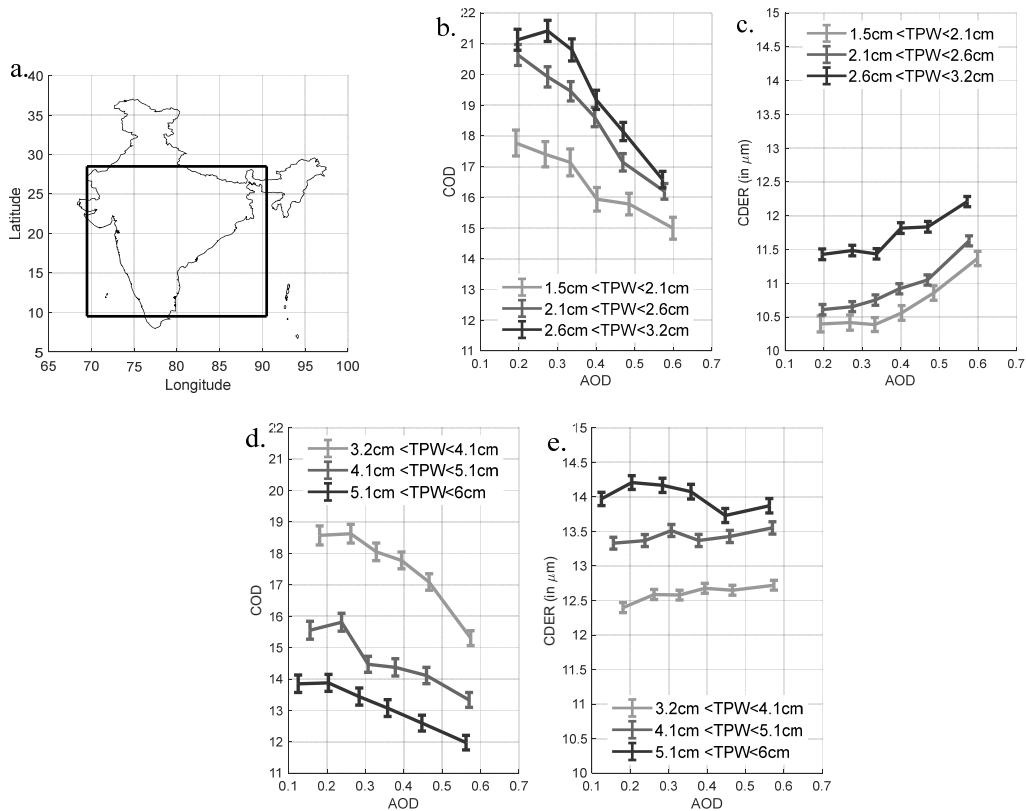


Figure 1. a. Location of the study region, b. AOD-COD relationship for low water vapour condition, c. AOD-CDER relationship for low water vapour condition, d. AOD-COD relationship for high water vapour condition, e. AOD-CDER relationship for high water vapour condition

The aerosol indirect effects in high & low moisture scenario are presented in Fig. 1b,c & Fig. 1 d,e respectively. It can be seen that CDER increases & COD decreases as AOD increases. The pattern indicates a total reduction in cloud droplet number concentration. The rate of droplet activation is reducing with increased amount of aerosol in the atmosphere. Similar findings were reported by Yuan et al. (2008) & Liu et al. (2017) for southeastern US & Eastern China respectively. The explanations hypothesized by them are - i) presence of synoptic front ii) abundance of giant CCN iii) presence of low soluble aerosol iv) semi-direct effect of aerosol etc. Grypsperdt & Stier (2012) found a similar reduction in droplet number concentration sensitivity towards AOD & attributed it to satellite retrieval error over land surface for low cloudiness.

Also, clouds of lower moisture scenario are found to have smaller droplet size & higher cloud optical depth than the clouds formed in higher moisture condition. There is a systematic increase in the droplet radius as the water vapour increases, in both the scenarios. After the activation of a cloud droplet, the

growth extent of the droplet is dependent on the ambient supersaturation. This is reflected as the increase in droplet effective radius with TPW. However, the behaviour of COD to water vapour is opposite in high & low water vapour condition.

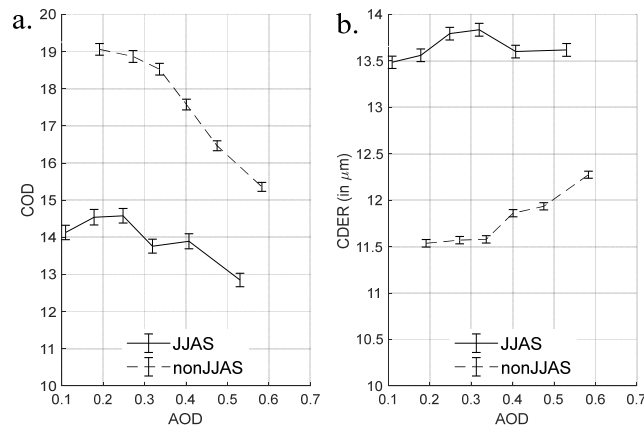


Figure 2.a. AOD-COD relationship for monsoon & non-monsoon clouds, b. AOD-CDER relationship for monsoon & non-monsoon clouds.

There is a steady increase in ACI from lower value of moisture to higher. In high moisture scenario, droplet effective size is hardly influenced by aerosol. The aerosol effect on COD is also getting diminished as the water vapour increases. However, in low water vapour scenario the responses are quite steeper. Similar pattern can also be seen between the clouds of monsoon & non-monsoon, which are characterized by high moisture & low moisture respectively (Fig. 2). The process behind such behaviour may involve the competition between particles for water vapour. For similar aerosol amount in the column, the competition for water vapour is more in low moisture scenario. As water vapour amount increases, the inter particle dependency of activation and growth reduces. Hence a reduction in ACI is evident. Also, most of the tall clouds are formed in high water vapour scenario. Satellite can only measure cloud microphysics at the top of the cloud which might not have any dependence on coincident aerosol interaction happening at the cloud base. So, the weak dependence found in high moisture condition might be a reflection of this indifference in tall clouds.

CONCLUSIONS

The study describes the dependency of aerosol cloud interaction on atmospheric water vapour for warm clouds in the Indian landmass. From low to high water vapour condition the droplet size steadily increases. However, the optical depth might increase or decrease depending on the amount of moisture present. The aerosol cloud interaction is found to be dependent on moisture availability & it gets saturated in presence of high water vapour, which can be either due to reduction in inter particle competition for water vapour or satellite retrieval limitation. Aerosol-cloud interaction is a microscale process & further investigations in finer spatio-temporal resolution are needed to find the process level explanations for the phenomenon.

REFERENCES

- Albrecht, B. A. (1989). Aerosols, Cloud Microphysics, and Fractional Cloudiness. *Science*, 245(4923), 1227–1230.
- Feingold, G., Remer, L. A., Ramaprasad, J., & Kaufman, Y. J. (2001). Analysis of smoke impact on clouds in Brazilian biomass burning regions: An extension of Twomey's approach. *Journal of Geophysical Research: Atmospheres*, 106(D19), 23907–23922.
- Gryspeerd, E., & Stier, P. (2012). Regime-based analysis of aerosol-cloud interactions. *Geophysical Research Letters*, 39(21), 1–5.

- Kaufman, Y. J., & Fraser, R. S. (1997). Confirmation of the smoke particles effect on clouds and climate. *Science*, 277(5332), 1636–1639.
- Krishnan, R., Sabin, T. P., Vellore, R., Mujumdar, M., Sanjay, J., Goswami, B. N., ... Terray, P. (2016). Deciphering the desiccation trend of the South Asian monsoon hydroclimate in a warming world. *Climate Dynamics*, 47(3–4), 1007–1027.
- Liu, Y., De Leeuw, G., Kerminen, V. M., Zhang, J., Zhou, P., Nie, W., ... Petäjä, T. (2017). Analysis of aerosol effects on warm clouds over the Yangtze River Delta from multi-sensor satellite observations. *Atmospheric Chemistry and Physics*, 17(9), 5623–5641.
- McComiskey, A., & Feingold, G. (2012). The scale problem in quantifying aerosol indirect effects. *Atmospheric Chemistry and Physics*, 12(2), 1031–1049.
- McComiskey, A., Feingold, G., Frisch, A. S., Turner, D. D., Miller, M. A., Chiu, J. C., ... Ogren, J. A. (2009). An assessment of aerosol-cloud interactions in marine stratus clouds based on surface remote sensing. *Journal of Geophysical Research Atmospheres*, 114(9), 1–15.
- Nakajima, T., & King, M. D. (1990). Determination of the Optical Thickness and Effective Particle Radius of Clouds from Reflected Solar Radiation Measurements. Part I: Theory. *Journal of the Atmospheric Sciences*.
- Panicker, A. S., Pandithurai, G., & Dipu, S. (2010). Aerosol indirect effect during successive contrasting monsoon seasons over Indian subcontinent using MODIS data. *Atmospheric Environment*, 44(15), 1937–1943.
- Patil, N., Dave, P., & Venkataraman, C. (2017). Contrasting influences of aerosols on cloud properties during deficient and abundant monsoon years. *Scientific Reports*, 7.
- Platnick, S., King, M. D., Ackerman, S. A., Menzel, W. P., Baum, B. A., Riédi, J. C., & Frey, R. A. (2003). The MODIS cloud products: Algorithms and examples from terra. *IEEE Transactions on Geoscience and Remote Sensing*, 41(2 PART 1), 459–472.
- Remer, L. A., Kaufman, Y. J., Tanré, D., Mattoo, S., Chu, D. A., Martins, J. V., ... Holben, B. N. (2005). The MODIS Aerosol Algorithm, Products, and Validation. *Journal of the Atmospheric Sciences*, 62(4), 947–973.
- Sarangi, C., Tripathi, S. N., Kanawade, V. P., Koren, I., & Sivanand Pai, D. (2017). Investigation of the aerosol-cloud-rainfall association over the Indian summer monsoon region. *Atmospheric Chemistry and Physics*, 17(8), 5185–5204.
- Seemann, S. W., Li, J., Menzel, W. P., & Gumley, L. E. (2003). Operational Retrieval of Atmospheric Temperature, Moisture, and Ozone from MODIS Infrared Radiances. *Journal of Applied Meteorology*, 42, 1072–1091.
- Ten Hoeve, J. E., Remer, L. A., & Jacobson, M. Z. (2011). Microphysical and radiative effects of aerosols on warm clouds during the Amazon biomass burning season as observed by MODIS: Impacts of water vapor and land cover. *Atmospheric Chemistry and Physics*, 11(7), 3021–3036.
- Twomey, S. (1974). Pollution and the planetary albedo. *Atmospheric Environment*, 8(12), 1251–1256.
- Yuan, T., Li, Z., Zhang, R., & Fan, J. (2008). Increase of cloud droplet size with aerosol optical depth: An observation and modeling study. *Journal of Geophysical Research*, 113(D4), D04201.

DIFFERENT METRICS USED IN SITE SELECTION FOR AIR QUALITY MONITORING

N. L. LEKINWALA¹, M. BHUSHAN^{1,2} and C. VENKATARAMAN^{1,2}

¹Department of Chemical Engineering, Indian Institute of Technology Bombay,
Powai, Mumbai – 400 076, India.

²Interdisciplinary Program in Climate Studies, Indian Institute of Technology Bombay,
Powai, Mumbai – 400 076, India.

KEYWORDS: Coefficient Of Divergence, Mutual Information, Correlation Coefficient, Site Selection, Aerosol Measurement And Air Quality Monitoring

INTRODUCTION

Air Quality Monitoring (AQM) is a systematic measurement of certain pollutants level over a long time in the ambient surroundings. For effective air quality management, ambient air monitoring can be used to obtain data which provide information about the extent of pollution, the trends in the air quality, implement the standard and evaluate air quality models. Monitoring can be of two types, urban, which is often used to keep a check on the levels while background pollution levels are used to understand the transport of air pollutants both local and long-range transport. Choice of sites for monitoring is essential as it governs the study related to the data and the decisions made compared to the standards. Area of representativeness of a monitoring site helps us identify how well does the site represent the region around it well. Such an activity aims to optimize the process, i.e., obtain most information by a minimum number of sites which in turn reduces the cost of operation. A top-down approach using satellite data can be for this purpose.

Aerosol Optical Depth (AOD) is one of the several satellite-derived data products. AOD is a columnar property and is the measure of extinction of the sunlight as it reaches the ground, it compares the radiation on the top of the atmosphere and at the ground. The data used for this result is a high-resolution data obtained from NASA's Aqua and Terra Satellite which has Moderate Resolution Imaging Spectroradiometer (MODIS) sensor and MAIAC Algorithm. MAIAC is a new advanced algorithm which uses time series (TMS) analysis and a combination of pixel- and image-based processing to improve the accuracy of cloud detection, aerosol retrievals, and atmospheric correction. The satellite data for the Indian region at 1 km x 1 km is available at <https://modis-land.gsfc.nasa.gov/MAIAC.html>

The coefficient of Divergence (COD) and Correlation coefficient (r) are some of the metrics that are widely used in the studies for comparing ground-based measurements in nearby monitoring stations (Wongphatarakul *et al.* 1998, Kim *et al.* 2005, Wilson *et al.* 2005, Xie *et al.* 2012). The use of satellite data was proposed in Bharadwaj *et al.* 2018. In this study, we propose the use of Mutual Information as an additional metric which can be used to get a better insight about the site. Both the COD and r is briefly explained in the methods section.

METHODS

The correlation coefficient is a mathematical metric used for comparing two vectors of data and checking the linear relationship between them. In our case, the site where the monitoring station is to be set up is our reference site which lies in a cell in the data while all the other cells are used for comparison sequentially and write it on to a data matrix.

$$r_{A,E} = \frac{\frac{1}{n} \sum_{t=1}^n (x_{A,t} - \bar{x}_A) (x_{E,t} - \bar{x}_E)}{\sqrt{\frac{1}{n} \sum_{t=1}^n (x_{A,t} - \bar{x}_A)^2} \sqrt{\frac{1}{n} \sum_{t=1}^n (x_{E,t} - \bar{x}_E)^2}}$$

where,

$x_{A,t}$ is the value of AOD at the A Site at the t^{th} time instant and similarly for the site B

The COD is one another metrics which compare the data point-wise. The COD values in one cell averaged over the time are used to compare the spatial difference in the values of AOD. If the values are close or similar, the COD value will be close to zero as compared to values which are entirely different, the value of COD will be unity.

$$\text{COD}_{A,E} = \sqrt{\frac{1}{n} \sum_{t=1}^n \left(\frac{x_{A,t} - x_{E,t}}{x_{A,t} + x_{E,t}} \right)^2}$$

While both the metrics mentioned looks at the linear relationship in the data but it may not be the case always. AOD data, which is proxy for the aerosols, may not be related linearly but may show some non-linear or functional relationship due to transport and other atmospheric processes. Mutual information (MI) is one such way of determining non-linearity in the data. While MI has not been used in air quality measurement applications, it is dominantly used in decision making in flood management, i.e., hydrological management systems (Alfonso *et al.* 2010). Generally used on analysis of discrete, its use is extended to continuous random variables with a simple modification. The expression gives the mutual information of two continuous random variables x and y ,

$$I(x, y) = \int_X \int_Y f(x, y) \log \left(\frac{f(x, y)}{f(x)f(y)} \right) dx dy$$

where,

$f(x, y)$ is the two-dimensional density estimate of x and y and,
 $f(x)$ and $f(y)$ are the marginal of x and y obtained from $f(x, y)$

The method includes computing a joint probability distribution function (using a kernel density estimate in python) of the two variables which is then used to compute marginal probability distribution function for each variable. This method involves integration and is computationally expensive, and a trade-off with the accuracy can be made if the number of discrete points in the integration is reduced.

RESULTS & DISCUSSIONS

High Altitude Cloud Physics Laboratory is one of the many sites in the National Carbonaceous Aerosols Programme - COALESCE project. Both COD and r plots (figure.1) shows that the High Altitude Cloud Physics Laboratory at Mahabaleshwar shown by the red marker in both the plots. The desired value of COD is less than 0.2 which is evident by the white color in the plot (Wongphatarakul *et al.* 1998). Similarly, high r -value is observed around the site. These metrics can be used to conclude that the site is regionally representative and can be used for monitoring. Figure 2 shows the HACPL site by red diamond, has high mutual information almost all over Maharashtra but to the south of the site. This reduction in the mutual information may be attributed to the Western Ghats. Thus, it can be concluded that AOD has an excellent non-linear relationship and can be considered as a site which is regionally representative.

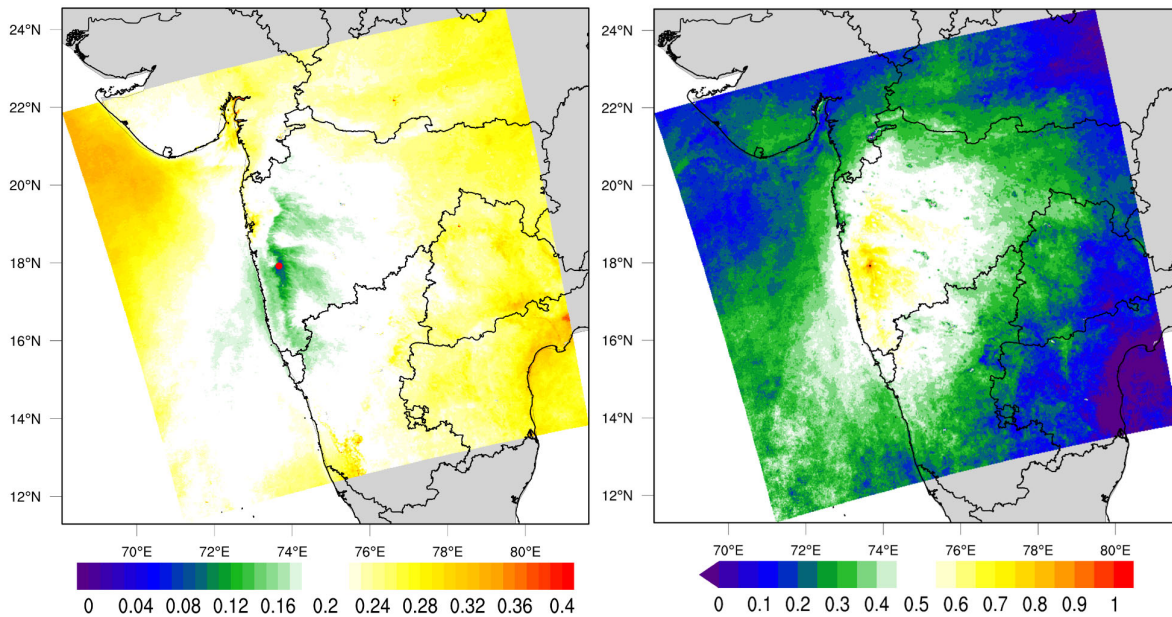


Figure 1. COD Plot (left) and Correlation Coefficient Plot (right) for the HACPL site at Mahabaleshwar for the Winter season (J,F) for the years 2004-2011

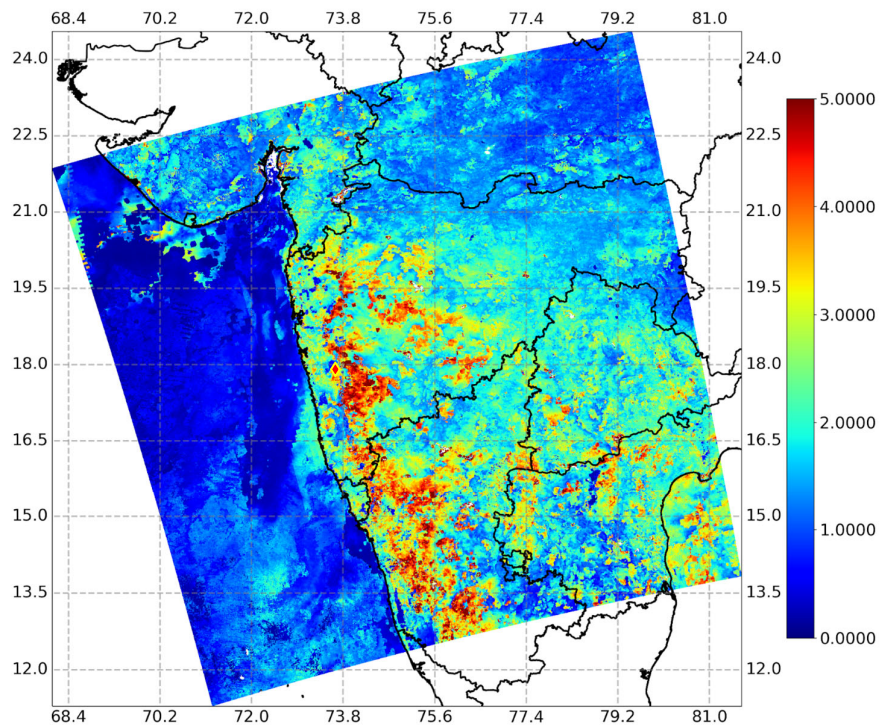


Figure 2. Mutual Information calculated around the HACPL Lab, Mahabaleshwar.

CONCLUSIONS

Mutual Information of the AOD and other satellite-derived data can be used for checking the eligibility of a site as regionally representative. Currently, this method under development and following are the issues that are yet to be tackled

1. Theoretically, mutual information can have values ranging from 0 to ∞ which makes it hard to interpret and set some bounds. A proper normalization scheme is yet to be developed.
2. Mutual information for sample realized from a 2-dimensional normal distribution can be determined analytically; the current algorithm estimates the values with a positive bias which can be attributed to,
 - a. Numerical Integration: Numerical integration with less number of the discrete points give results that are not accurate and increasing the number of discrete points increases the computational burden significantly.
 - b. Kernel Density Estimation: Kernel Density Estimation depends on number of parameters and the effects of these parameters like bandwidth are yet to be studied.

ACKNOWLEDGEMENTS

This work was supported by the Ministry of Environment, Forests and Climate Change, Government of India. The COD and Correlation Coefficient codes were developed by Ankur Bhardwaj (IISER Bhopal), Kunal Bali (IITD) and Prof. Ramya Sunder Raman (IISER Bhopal); the codes were used with the appropriate modifications and are applied to the data in a different way as used by them.

REFERENCES

- Alfonso, L., Lobbrecht, A. and Price, R., 2010. Information theory-based approach for location of monitoring water level gauges in polders. *Water Resources Research*, 46(3).
- Bharadwaj A. Raman. S. R, Bali K. (Personal Communication on May, 2018)
- Kim, E., Hopke, P.K., Pinto, J.P. and Wilson, W.E., 2005. Spatial variability of fine particle mass, components, and source contributions during the regional air pollution study in St. Louis. *Environmental science & technology*, 39(11), pp. 4172-4179.
- Wilson, J.G., Kingham, S., Pearce, J. and Sturman, A.P., 2005. A review of intraurban variations in particulate air pollution: Implications for epidemiological research. *Atmospheric Environment*, 39(34), pp. 6444-6462.
- Wongphatarakul, V., Friedlander, S.K. and Pinto, J.P., 1998. A comparative study of PM_{2.5} ambient aerosol chemical databases. *Environmental Science & Technology*, 32(24), pp. 3926-3934.
- Xie, M., Coons, T.L., Dutton, S.J., Milford, J.B., Miller, S.L., Peel, J.L., Vedal, S. and Hannigan, M.P., 2012. Intra-urban spatial variability of PM_{2.5}-bound carbonaceous components. *Atmospheric environment*, 60, pp.486-494.

EMISSIONS FROM OPEN-FIELD BURNING OF AGRICULTURAL RESIDUE IN VADODARA, GUJARAT

T.S. KAPOOR¹, VERNEKAR P.¹, C. VENKATARAMAN^{1,2} AND H. C. PHULERIA^{1,3}

¹ Interdisciplinary Program in Climate Studies, Indian Institute of Technology-Bombay, Mumbai – 400 076, India.

² Department of Chemical Engineering, Indian Institute of Technology-Bombay, Mumbai – 400 076, India.

³ Centre for Environmental Science and Engineering, Indian Institute of Technology-Bombay, Mumbai – 400 076, India.

KEYWORDS: Biomass Open Burning, Agricultural Residue, Carbonaceous Emissions

INTRODUCTION

With the green revolution and an increasing food demand, the agricultural produce in India increased steadily from the 1980s (Burney & Ramanathan, 2014). This increase in produce also increases the amount of residue left behind after harvest which can be used for purposes like thatching, fodder and as fuel for residential households and in industries. However the left over portion is often burned off on the field and sometimes is the more economical and time saving process (Gupta, 2014). These emissions can contribute to about 7% of the total BC emissions of our country (Paliwal et al., 2016; Pandey et al. 2014). Emission estimations employing the bottom-up inventory approach use parameters from the literature which are either driven by opinions or by outdated measurements that are not necessarily representative of the specific regions. These factors render the estimated emissions inaccurate and uncertain.

The NCAP-COALESCE project aims to prepare an emission inventory for the agriculture residue burning sector to tackle the shortcomings of previous methods. A pilot survey conducted in Vadodara, Gujarat to understand the feasibility of the prepared survey questionnaire and overall methodology. This study talks about the methodology and some results, in the form of activity and emissions from the district.

METHODS

Nation-wide surveys will be conducted by 14 institutes to estimate the activity, or the amount of field burning of crop residues. The surveys include crop residue weight measurements during the two common harvest seasons (rabi and kharif). A survey questionnaire has been prepared so as to estimate: a) the uses of crop residue b) fraction of crop residue subjected to field burning c) weight of crop residue per unit weight of crop produce, through weight measurements d) weight of residue per unit area of farmland (used in top down approach). These are important parameters for estimating emissions. As part of the NCAP-COALESCE project, a pilot survey was conducted in five villages in Vadodara district of Gujarat during from 30th March to 5th April, 2018.

For estimating emissions from burning of crop residue, the bottom up approach has been used which employs equation 1, where the subscripts ‘c’ represents a crop and the ‘p’ represents a pollutant. EM_p is the emission of a pollutant from burning of crop residue, P is the crop production, RCR is the residue to crop ratio, DMF is the dry matter fraction in the crop residue, FB is the fraction of crop residue actually subjected to on-field burning, FAO is the fraction of crop residue actually oxidised when subjected to field burning and EF is the emission factor or the weight of emissions per unit mass of residue burned.

$$EM_p = \sum_c P_c \times RCR_c \times DMF_c \times FB_c \times FAO_c \times EF_{c,p} \quad \dots (1)$$

The crop production data was obtained from the Open Government data platform (data.gov.in) and averaged over the years 2010-12. RCR was obtained from the survey for a few of the crops and the rest for from literature (Jain et al., 2014). FB values which are in most urgent need for validation (Streets et al., 2003) were estimated from field survey as opposed to empirical methods or expert opinions followed by previous

studies. The values of fraction actually oxidized (*FAO*), dry matter fraction(DMF) and emission factor (*EF*) were taken from literature (Andreae & Merlet, 2001; IPCC, 2006; Turn et al., 1997).

RESULTS & DISCUSSIONS

A total of 59 surveys were conducted, 11 from one of the villages and 12 each from the other four. 21 crops (with banana and wheat being the most dominant ones) were found during the survey. Majority of the turdal stalk (70%) and around 40% of the residue from cotton and castor stalk are used for residential cooking. A very small amount of the crop residue is used for thatching. Significant amounts of banana and castor leaves residue are used for other purposes which primarily include incorporation of the residue back into the field as an organic fertilizer and also the use of residue as flooring in residential households.

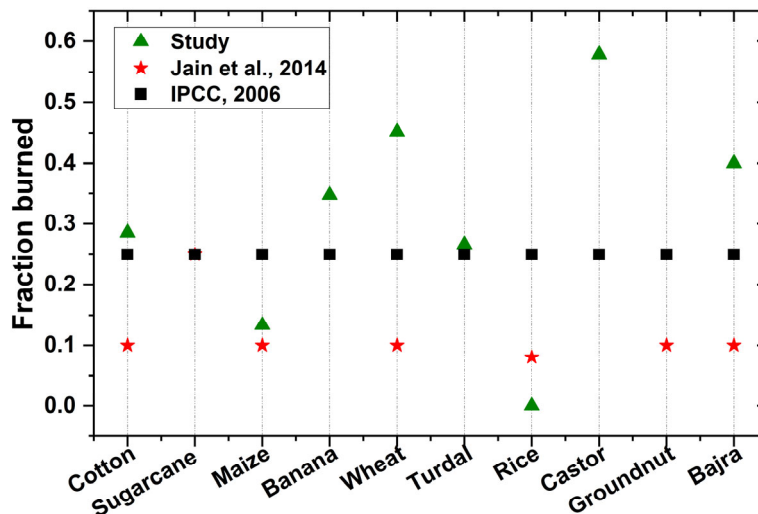


Figure 5: Fraction of crop residue burned, comparison with literature

Previous studies have used arbitrary values of FB which are based mostly on expert opinion or the IPCC prescribed value of 0.25 for developing countries (IPCC, 2006). A few studies (Pandey et al., 2014; Venkataraman et al., 2006) have also estimated FB by first estimating the quantity used for other purposes and attributing the rest as being burned on field. Figure 1 shows field based mean FB values obtained from our survey, their comparison with the IPCC good practice guidelines (IPCC, 2006) and from latest literature (Jain et al., 2014). The obtained activity by using these parameter values has been shown in Figure 2. For comparison purposes, the variation in production, FB and RCR has also been shown. There is very little variation in *DMF*(0.8-0.88) and *FAO*(0.9). We see that cotton, by far, has the highest activity because of its high production and the variation activity of other crops depends mainly on FB and RCR. Both of these parameters are being determined as a part of the survey.

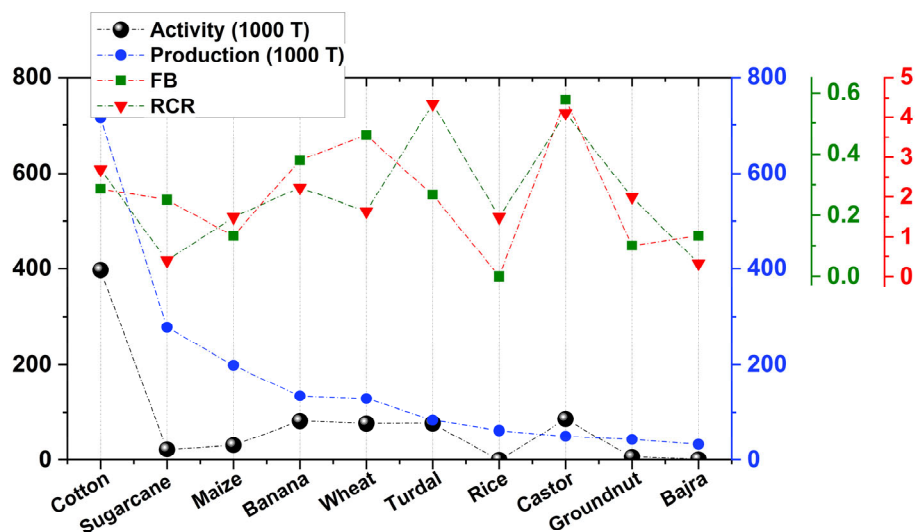


Figure 6: Crop-wise activity and factors used to estimate it.

The obtained activity were then multiplied with crop and pollutant specific emission factors from literature (Andreae & Merlet, 2001; IPCC, 2006; Turn et al., 1997) to obtain total emissions (Figure 3). Burning of cotton contributes to about half of the emissions for all species. Figure 2 shows the % contributions with the numbers in brackets showing emissions in Gg. While banana, turdal, castor and wheat contribute around 10% each. The current inventory estimates for emissions in India completely neglect emissions from residue burning from banana and castor. This may lead to an underestimation in emissions for this region. Further surveys will be needed to ascertain whether these crops have a significant contribution to a national scale inventory.

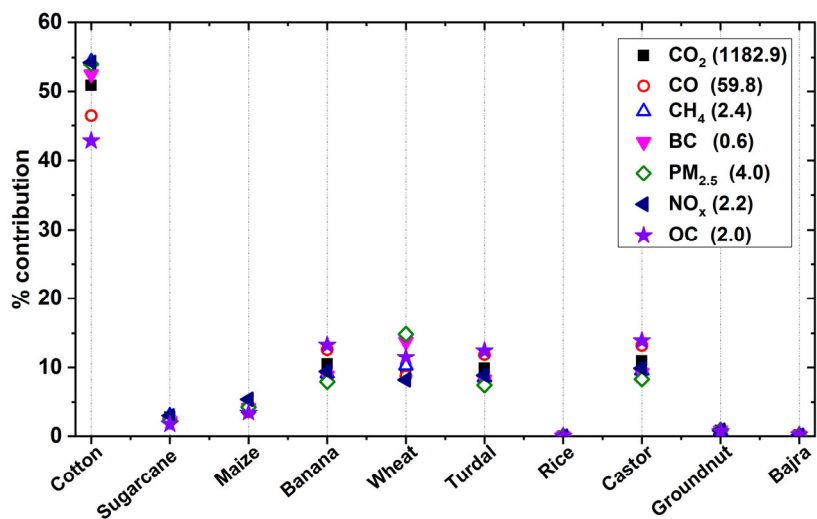


Figure 7: Percentage contribution of emissions by crops. Magnitude of emissions (Gg/year) are shown in brackets in the legend.

CONCLUSIONS

Emissions from the on-field burning of crop residue were quantified by employing the bottom up approach and using updated, regionally relevant parameters to estimate activity. Crop wise variation in activity showed that the variation is driven not only by the amount of production but also by the residue to crop ratio and the fraction of crop residue burned on field. This necessitates employing accurate values in emission estimates by using survey based parameters. When looking at the estimates of emissions using literature based emission factors, cotton contributes to a large amount of emissions and other crops such as banana

and castor which have thus far been neglected in inventories also contribute significant amounts (~10 % of total each). This may be leading to an underestimation in emissions by previous studies.

ACKNOWLEDGEMENTS

This work was supported by the Ministry of Environment Forests and Climate Change.

REFERENCES

- Andreae, M. O., & Merlet, P. (2001). Emissions of trace gases and aerosols from biomass burning. *Global Biogeochemical Cycles*, *15*(4), 955–966. <https://doi.org/10.1029/2000GB001382>
- Burney, J., & Ramanathan, V. (2014). Recent climate and air pollution impacts on Indian agriculture. *Proceedings of the National Academy of Sciences*, *111*(46), 16319–16324. <https://doi.org/10.1073/pnas.1317275111>
- Gupta, R. (2014). Low-hanging fruit in Black Carbon mitigation: crop residue burning in south asia. *Climate Change Economics*, *05*(04), 1450012. <https://doi.org/10.1142/S2010007814500122>
- IPCC. (2006). 2006 IPCC Guidelines for National Greenhouse Gas Inventories Volume 4 Agriculture, Forestry and Other Land Use. *2006 IPCC Guidelines for National Greenhouse Gas Inventories Volume 4 Agriculture, Forestry and Other Land Use*, 94.
- Jain, N., Bhatia, A., & Pathak, H. (2014). Emission of air pollutants from crop residue burning in India. *Aerosol and Air Quality Research*, *14*(1), 422–430. <https://doi.org/10.4209/aaqr.2013.01.0031>
- Paliwal, U., Sharma, M., & Burkhardt, J. F. (2016). Monthly and spatially resolved black carbon emission inventory of India: Uncertainty analysis. *Atmospheric Chemistry and Physics*, *16*(19), 12457–12476. <https://doi.org/10.5194/acp-16-12457-2016>
- Pandey, A., Sadavarte, P., Rao, A. V., & Venkataraman, C. (2014). A technology-linked multi-pollutant inventory of Indian energy-use emissions: II. Residential, agricultural and informal industry sectors. *Atmospheric Environment*, *99*, 341–352. <https://doi.org/10.1016/j.atmosenv.2014.09.080>
- Streets, D. G., Bond, T. C., Carmichael, G. R., Fernandes, S. D., Fu, Q., He, D., ... Yarber, K. F. (2003). An inventory of gaseous and primary aerosol emissions in Asia in the year 2000. *Journal of Geophysical Research: Atmospheres*, *108*(D21). <https://doi.org/10.1029/2002JD003093>
- Turn, S. Q., Jenkins, B. M., Chow, J. C., Pritchett, L. C., Campbell, D., Cahill, T., & Whalen, S. A. (1997). Elemental characterization of particulate matter emitted from biomass burning: Wind tunnel derived source profiles for herbaceous and wood fuels. *Journal of Geophysical Research*, *102*, 3683–3699.
- Venkataraman, C., Habib, G., Kadamba, D., Shrivastava, M., Leon, J. F., Crouzille, B., ... Streets, D. G. (2006). Emissions from open biomass burning in India: Integrating the inventory approach with high-resolution Moderate Resolution Imaging Spectroradiometer (MODIS) active-fire and land cover data. *Global Biogeochemical Cycles*, *20*(2), 1–12. <https://doi.org/10.1029/2005GB002547>

RE-ESTIMATING ON-ROAD VEHICLES AND TRAVEL CHARACTERISTICS OF DELHI CITY: A VEHICLE SURVEY APPROACH

MOHD SHAHZAR KHAN, ASIF ANSARI, MAHAK BANSAL, YAWAR HASAN, IMAM HUSSAIN, UMAR NAHVI, JAI PRAKASH AND GAZALA HABIB*

Aerosol Research and Characterization Laboratory, Indian Institute of Technology, Delhi, New Delhi-110016, India.

KEYWORDS: Survival fraction, fuel consumption, PM_{2.5}, trace gases

INTRODUCTION

The rapidly growing economic conditions serve as the major catalyst in making on-road transport as one of the fastest growing sectors in the capital city, Delhi. The city is amongst the highest vehicle ownership regions in India with around 10 million total registered vehicles among all categories in the year 2016 (MoRTH yearbook, 2016) using diesel, gasoline and CNG as the major fuel sources. This large number of vehicles is responsible for the increase in emissions of the extensive amount of trace gases [CO₂, CO and NO_x] and particulate pollutants, which have a considerable direct impact on the climate change.

In the present scenario, where an extensive research is being undertaken on climate change assessment, it has become essential to quantify with greater accuracy the total emissions of pollutants. However, the main problem in estimating the emissions is the efficacy of the approach used to calculate the on-road vehicle count. The conventional method of using data from the regional transport office has proved to give overestimated values (Mohan et al. 2009).

So, this research followed a survey-based approach to estimate the on-road vehicles in different categories. The survey data was used as an input in estimating the survival fraction by optimizing the difference in survey data and registration/sale data. This allowed us to determine the parameters related to vehicle retirement lifetime (L_{50}), and the shape of the survival curve (α). The mileage and annual average distance values from the survey data were used to estimate the fuel consumption, and the emission factors from previous work (Jaiprakash and Habib, 2018 a,b) for each pollutant were incorporated to finally compute the total emission for those pollutants for Delhi city.

METHODS

On-Road survey for vehicular data

The questionnaire for vehicular survey consisted of the following ten parts: (1) Type of vehicle (2) Type of fuel (3) Make/Model/Year (4) Engine Capacity (CC) (5) Mileage (km/litre) (5) Average/Range of speed (km/hr) (6) Odometer Reading (km) (7) Daily Distance travel (km) (8) Fuel consumption/day/week/month (L) (9) Maintenance frequency or servicing (per year or /km) (10) Vehicle lifetime/Retirement period (y). The survey was done under National Carbonaceous Aerosol Program-COALESCE (NCAP-COALESCE).

The survey area was divided into 5 parts- North, South, East, West and Central Delhi to have an overall average estimate of the entire Delhi region. The survey locations were selected near the fuel stations and toll plazas to have the maximum frequency of vehicles that helped in generating considerable sample data sets. The fuel stations helped in generating data for 2-wheelers, cars and LMVs whereas, the toll plazas provided an interaction with heavy-duty vehicle (HDVs) drivers. The data collection was done via a personal interaction with the driver or vehicle owner.

Estimation of survival fraction, on-road vehicles and Total emissions

After conducting the vehicular survey on different vehicle category (2Ws, Cars, LMVs, HDVs and Buses) in Delhi city, the fraction of each category vehicles for each age are calculated, then the fraction of vehicles in 5 years age-bins (0-5y, 6-10y, 11-15y, >16y) with each year fraction for each vehicle category. A total number of in-use and on-road vehicles are estimated by using the Vehicle registration data and survival

fraction (Survival fraction of a particular vehicle type of particular age is the fraction of that vehicle registered data which is present in the base year after surviving) for each vehicle category. For determining the survival fraction, the Log-logistic survival function (which is used by Pandey et al., 2014) is used. The optimum value of survival fraction parameters shape factor (α) and vehicle retirement lifetime (L_{50}) is estimated by applying the Root Mean Square Error (RMSE) method on the %share of vehicles in 5y age-bins by survey data and % share of the vehicle in 5y age-bins by survival function model. After finding the optimum value of α and L_{50} , the number of the on-road vehicles of each age for each vehicle category is determined by using these optimum parameters and registration data. Then the total number of in-use and on-road vehicles present in the base year is determined for each vehicle category. The fuel consumption (in Kg) for different vehicles is estimated by using the total on-road vehicle, Annual average distance travel, mileage and fuel density. Then the total emission of pollutants from different vehicles is determined by using the fuel consumption and emission factors for different pollutants which are to be taken from the previous study done by Jaiprakash and Habib (2018). This whole methodology for survival fraction and total emission is shown in a Flowchart in Figure 1.

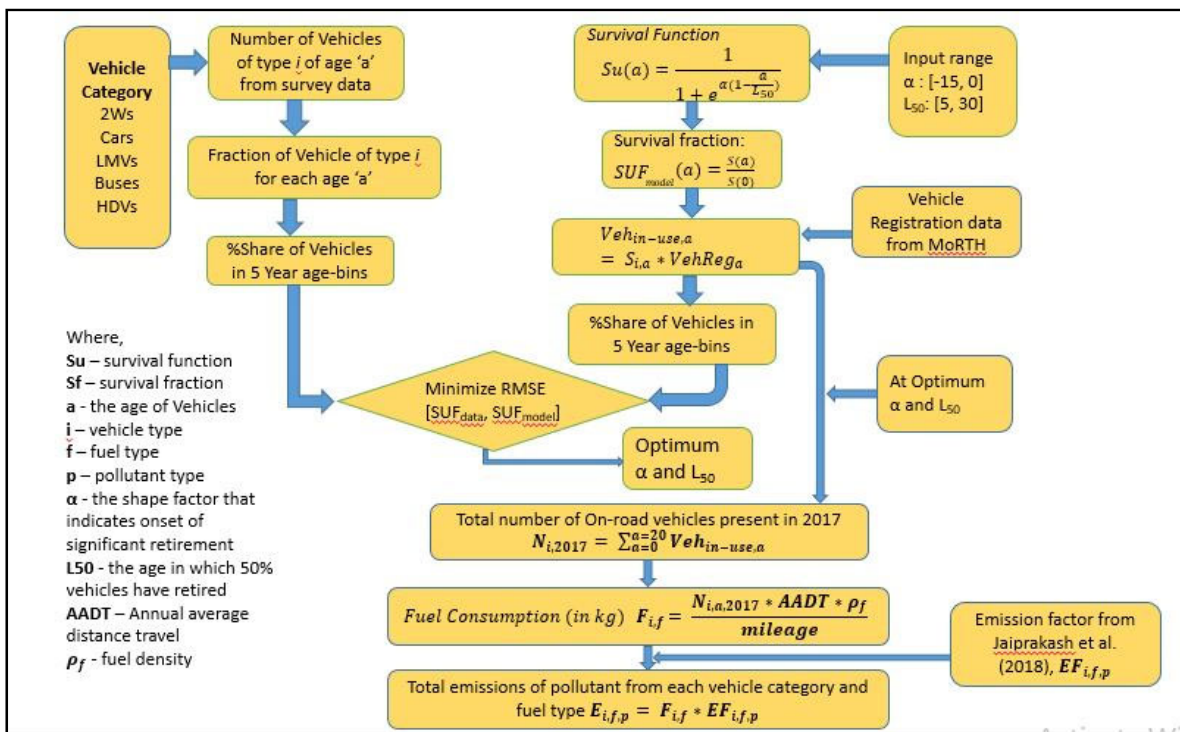


Figure 1: Optimisation of survival fraction parameters using survey data, Estimation of on-road vehicles and total pollutant emissions

RESULTS & DISCUSSIONS

The survival rate with respect to the age of different categories of vehicles is shown in Figure 2. The survival fraction curve for LMVs and buses is followed the same shape. For LMV (Goods) the survival fraction parameters-shape factor and vehicle retirement lifetime which are shown in the figure are close to values reported previously by Pandey et al. (2014). For two-wheelers, the survey based shape factor was different than previous study Pandey et al. (2014), but the retirement age (L_{50}) was close to previous work. In the case of cars, the value of shape factor is nearly the same, but the retirement age from the present study is nearly half when compared with the Pandey et al. (2014).

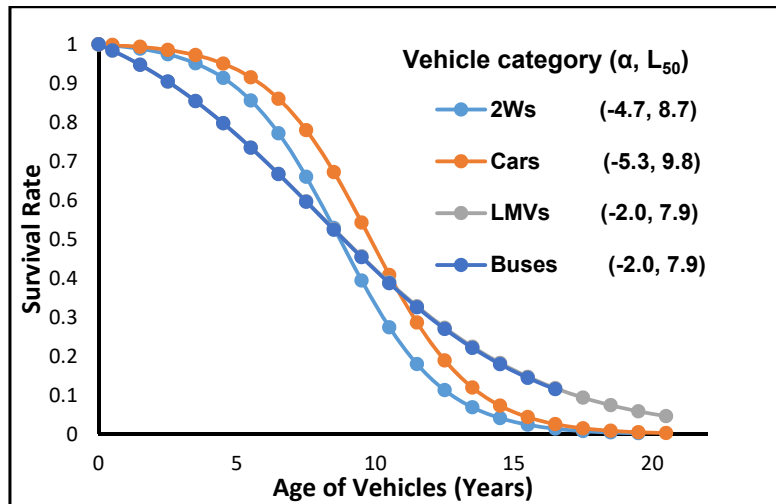


Figure 2: Survival Fraction vs Age of Vehicles for different category

The total number of on-road vehicles of different categories in Delhi city for the base 2017 are shown in Figure 3. The number of on-road two-wheelers and cars are higher than LMVs goods and buses. On-road traffic volumes for different vehicle categories in Delhi were close to the previous study by Jaiprakash and Habib et al. (2018).

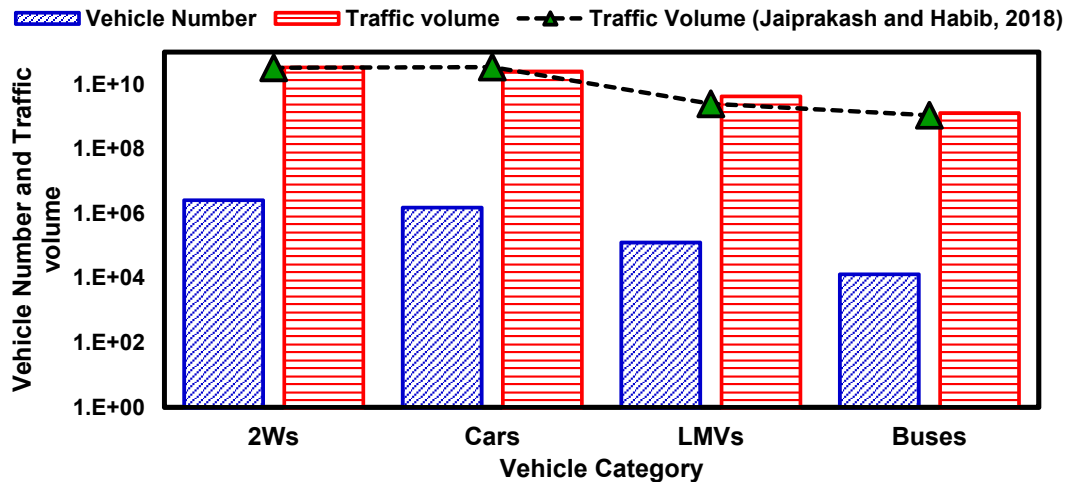


Figure 3: Number of on-road vehicles and traffic volume

The fuel consumption by different vehicle categories will be estimated using the on-road vehicles number, mileage, annual average distance travel from survey data and fuel density. The total emissions of pollutants will also be estimated using fuel consumption and emission factors. The fuel consumption and emissions will be discussed to understand how effective survey data is in lessening the uncertainty in emissions.

ACKNOWLEDGEMENTS

This work was supported by the Ministry of Environment, Forest and Climate Change under the National Carbonaceous Aerosol Program (NCAP). We greatly appreciate all the drivers and vehicle owners who willfully spent their time and helped in survey data collection. We are also thankful to all the students and staff members of Deptt. of Civil Engineering, IIT Delhi who have supported in the survey and on-road measurements during the research.

REFERENCES

- Goel, R., Guttikunda, S. K., Mohan, D., & Tiwari, G. (2015). Benchmarking vehicle and passenger travel characteristics in Delhi for on-road emissions analysis. *Travel Behaviour and Society*, 2(2), 88–101. <https://doi.org/10.1016/j.tbs.2014.10.001>
- Mohan, D., Tsimhoni, O., Sivak, M., Flannagan, M.J., 2009. *Road Safety in India: Challenges and Opportunities* Transportation Research Institute. The University of Michigan, Ann Arbor, USA.
- MORTH. (2018). *Road Transport Year Book (2015-2016)*, Ministry of Road Transport and Highways, (February). <https://doi.org/June 2012>
- Pandey, A., & Venkataraman, C. (2014). Estimating emissions from the Indian transport sector with on-road fleet composition and traffic volume. *Atmospheric Environment*, 98, 123–133. <https://doi.org/10.1016/j.atmosenv.2014.08.039>
- Prakash, J., & Habib, G. (2018). A technology-based mass emission factors of gases and aerosol precursor and spatial distribution of emissions from on-road transport sector in India. *Atmospheric Environment*, 180(August 2017), 192–205. <https://doi.org/10.1016/j.atmosenv.2018.02.053>
- Baidya, S., Borken-Kleefeld, J., 2009. Atmospheric emissions from road transportation in India. *Energy Pol.* 37 (10), 3812–3822. <http://dx.doi.org/10.1016/j.enpol.2009.07. 010>.

COMPLEXITY OF SHORT-LIVED CLIMATE FORCERS (SLCFS) IN RURAL INDIA: VARIABILITY AND CHEMISTRY OF BLACK AND BROWN CARBON AND OZONE INTERPLAY AT A UNIQUE BIOMASS-BURNING HOTSPOT OF GLOBAL SIGNIFICANCE IN THE INDO GANGETIC PLAINS (IGP)

JAI PRAKASH^{1,2}, HARSH RAJ MISHRA², BHILOK CHAND², MATTIAS HALLQUIST^{2,3}, GAZALA HABIB¹, GEETAM TIWARI¹, KALYAN MITRA³, VERONICA GERETTI³, JAN B. C. PETTERSSON^{2,3}, JOHAN BOMAN^{2,3}, HÅKAN PLEIJEL^{2,4}, RAVI KANT PATHAK^{2,3*}

¹Department of Civil Engineering, Indian Institute of Technology Delhi, New Delhi-110016 India

²Indo Gangetic Plains –Center for Air Research and Education, Hamirpur, U.P., India,

³Atmospheric Science Department of Chemistry and Molecular Biology, University of Gothenburg, Sweden,

⁴Department of Biology and Environmental Science, University of Gothenburg, Sweden

(*Corresponding at ravikant@chem.gu.se)

KEYWORDS: Ozone, BC, BrC, trace gases, IGP-CARE, Rural India.

INTRODUCTION

Short-lived climate forcers (SLCFs) are thought to impact the global climate and human health (UNEP, 2011; IPCC 2013, Bond et al., 2013). Indo Gangetic Plains (IGP) region, burning biomass for cooking and agricultural practices, by 750 million people, is an important source of air pollutants both regionally and globally. The key SLCFs includes atmospheric aerosol -black carbon (BC), light absorbing organic aerosol (OA): referred as brown carbon (BrC), atmospheric brown clouds (ABC), sulfate and nitrate aerosol, tropospheric ozone (O₃), carbon monoxide (CO), and nitrogen oxides (NO_x). The photochemical processing of these emissions yields high levels of O₃ and SOA that interact with BC, altering its health and climate effects. In addition to adverse health effects and ability to alter the regional climate, O₃ (especially) affects vegetation, notably reducing crop yields, in the vulnerable environment thereby reducing food supplies for the IGP-region in India.

This study aims to understand the variability of the SLCFs –black carbon (BC), Brown carbon (BrC) and ozone (O₃), by long term measurements combined with intensive campaigns and laboratory experiments to elucidate the relevant processes involved in rural India. In this study, we measured high resolution concentrations of BC, BrC, O₃, CO, and NO_x at a rural site in IGP region called as “Indo-Gangetic Plains Centre for Air Research and Education (IGP-CARE) to unravel the key atmospheric processes and chemistry involved in transformations of gases, BC and BrC mostly originating from the burning of biomass. The real time long-term measurement of SLCFs at IGP-CARE are being carried out since January 2017. Here the dataset is presented from January 2017 to December 2017.

METHODS

Site description

In the present study, the real time long-term measurement of SLCFS (BC, BrC, O₃, CO, and NO_x) are being carried out since January 2017 at new monitoring station at the rural site in IGP-region called “Indo-Gangetic Plains Centre for Air Research and Education (IGP-CARE). Here the dataset is presented from January 2017 to December 2017. The IGP-CARE is situated in agricultural fields adjacent to a forest by the River Burma (a tributary of the River Betwa) surrounded by six villages in the Hamirpur district, Uttar Pradesh [25° 48' 55.5" N; 79° 55' 07.5" E, India: Figure 1). The power facility was equipped with a solar power generation system to avoid any local emission biases.

Real time measuring instruments

Real time O₃ measurement was carried out using Serinus 10 O₃ analyzer (E020010, Ecotech ACOEM Group, Australia) which works on ultraviolet (UV) absorption method and combination scrubber (MnO₂) technology. The scrubber is used as catalytic in ambient air and remove the effect of interference of O₃ and determine the final O₃. The minimum detection limit (MDL) of Ozone analyzer was found to be 0.5 ppb with precision $\pm 0.2\%$ at a flow rate of 0.5 L min⁻¹. Real-time NO_x (NO+NO₂) was measured using Serinus 40 NO_x analyzer (Model No. E020040, Ecotech ACOEM Group, Australia) and followed the luminescence method. The MDL value of NO_x analyzer was 0.4 ppb with precision $\pm 0.5\%$ at a flow rate



Figure 1 Satellite view of the rural site of IGP-Region in India called as “IGP-CARE.”

of 0.3 L min⁻¹

CO was determined using Serinus 30 CO analyzer (Model No. E020030, Ecotech ACOEM Group, Australia), which is based on Non-Dispersive Infrared (NDIR) principle. The minimum MDL of CO analyzer was 40 ppb with precision $\pm 0.1\%$ at a flow rate of 1.0 L min⁻¹. BC and UVPM were measured by Black Carbon Monitors (BC 1050 series, Met One Instruments, Inc.) on quartz filter tape at two wavelengths (375 and 880 nm). BC is the single absorbent of light at 880 nm, while UVPM is measured at 375. The instrument MDL value was $< 8 \text{ ng m}^{-3}$ (with 1 min resolution). K (ATN) correction factor was applied for BC and UVPM correction. The following method was adopted from Jimenez et al. (2007). Calibration of all instruments was done regularly by an ozone generator and zero air generator. The height of the sample in-let from the ground surface is 20 m. On-site meteorological parameters such as temperature, pressure, relative humidity, precipitation, wind speed, and wind direction were also collected using Automatic Weather Station (AWS) [Davis Vantage Pro 2, Davis Instruments Corporation, USA] during the sampling period.

All instruments were operated continuously every day for 00:00 h Indian Standard Time (IST). Ozone O₃, trace gases (CO and NO_x), BC, and UVPM data were monitored at each 1 s interval, while meteorological parameters were recorded at 5 min interval. Therefore, all data was fixed for all the parameters on 1 h average basis to perform statistical analysis. However, raw data files were extracted and separated into individual time series for SLCPS. In the present work, data of NO_x and CO missing from July-September, 2017 due to power interruptions, equipment malfunctions, system failures. Therefore, in this study, we intend to limit discussion for this missing data.

RESULTS & DISCUSSIONS

very large concentration range of BrC [50-150 $\mu\text{g m}^{-3}$], and daily mean: 3.4 ± 3.8 (0.2-7.9) $\mu\text{g m}^{-3}$ in the form of episodic peaks were observed in winter, and a few peaks were also observed during summer [daily mean: 1.7 ± 2.1 (0.6-4.8) $\mu\text{g m}^{-3}$] and autumn [daily mean: 3.0 ± 1.5 (2.2-5.9) $\mu\text{g m}^{-3}$] [Figure 2, Panel A]. A similar pattern was observed in BC concentration and BrC/BC ratio [Figure 2, Panel B and C]. Interestingly, a sharp increase in BC and BrC concentrations were found in the evening (after 06:00 PM). The high concentrations of BrC and BC in January were possibly due to biomass burning for cooking and heating.

A while in summer and autumn, high concentrations can be attributed to biomass burning in the indigenous brick firing processes and open biomass burning in north IGP. Very interesting diurnal variations of BrC/BC ratio was shown, and it sharply decreased during day hours (08:00-17:00 IST), and slowly increased in the night (18:00-23:00 IST) [Figure 3] especially in winter and autumn season, which indicates bleaching of BrC which we thought to be affected by temperature, ozone/radical chemistry. The filter tape collected from black carbon monitor will be analysed using chemical Ionization Mass Spectrometer (CIMS) for molecular speciation of BrC, and diurnal molecular profile will be characterized. Further, for the investigation and contribution of local or regional sources, conditional bivariate probability function (CBPF) and air mass back-trajectories will also be analysed during the sampling period.

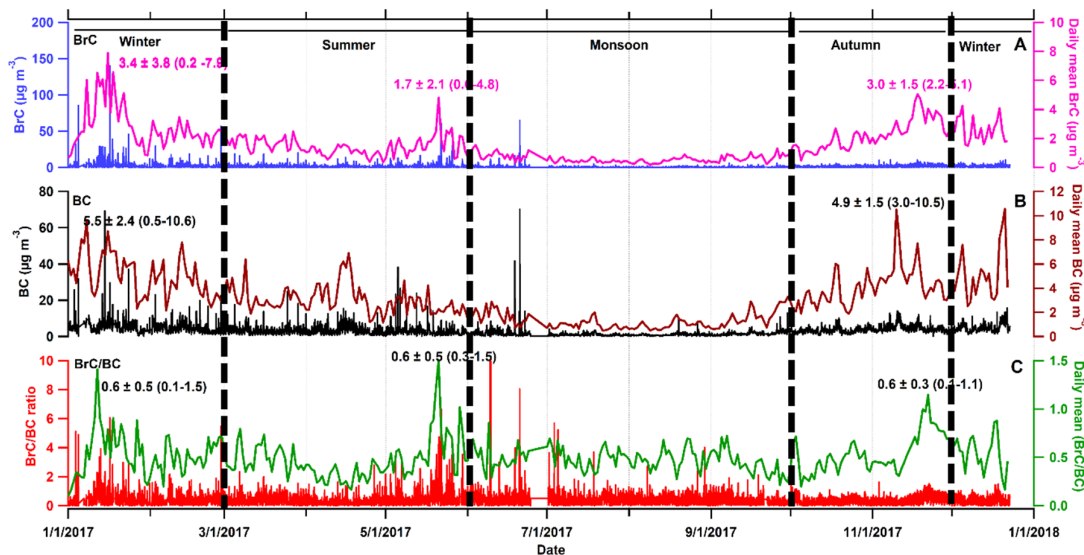


Figure 2 Time series plots of BrC, BC, BrC/BC ratio during the year 2017 over the IGP-CAR

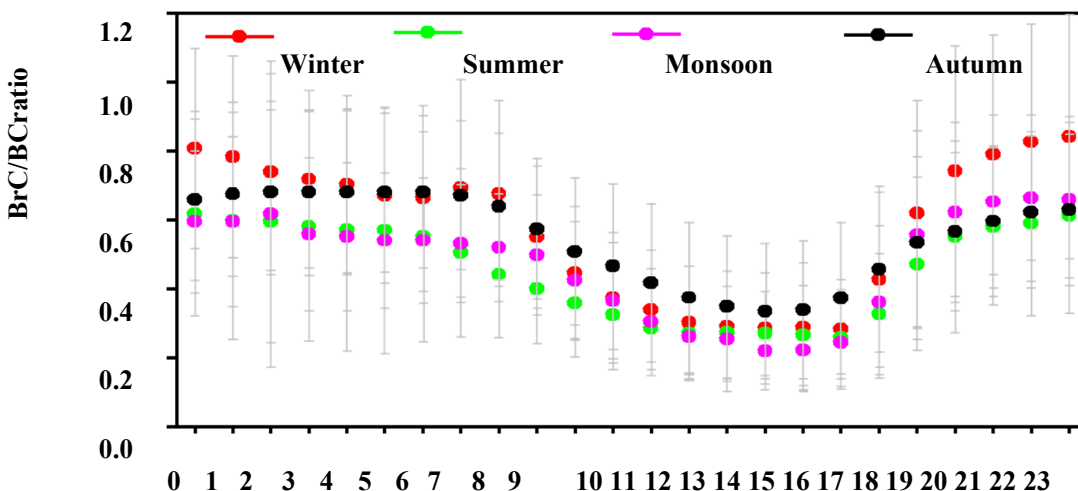


Figure 3 Seasonal, diurnal variation of BrC/BC ratio during the sampling period at IGP-CARE. Indian Standard time (IST)

ACKNOWLEDGEMENT

This project is funded by The Swedish Research Council, Vetenskapsrådet (VR) under the U-Forsk Grant (dr No. 348-2014-3496). We are grateful to The Swedish Research Council, Vetenskapsrådet (VR), Sweden.

REFERENCES

UNEP, WMO. "Integrated assessment of black carbon and tropospheric ozone: Summary for Decision Makers." Nairobi: United Nations Environment Programme (2011).

IPCC, The Physical Science Basis, Cambridge University Press, UK. (2013)

Bond, Tami C., et al. "Bounding the role of black carbon in the climate system: A scientific assessment."

Journal of Geophysical Research: Atmospheres 118.11 (2013): 5380-5552.

Sinha et al. "Chemical composition of pre-monsoon air in the Indo-Gangetic Plain measured using a new air quality facility and PTR-MS: high surface ozone and strong influence of biomass burning." Atmospheric Chemistry and Physics 14, (2014): 5921-5941.

ACKNOWLEDGEMENT

+

EMISSIONS OF PARTICLE-BOUND ELEMENTS FROM ON-ROAD VEHICLE EMISSION: AN ASSESSMENT OF POTENTIAL HEALTH RISK

JAI PRAKASH* AND GAZALA HABIB

Aerosol Research and Characterization Laboratory, Indian Institute of Technology, Delhi, New Delhi-
110016, India.

KEYWORDS: On-road vehicle, PM_{2.5}, Particle-bound elements, Carcinogenic risk.

INTRODUCTION

In the present time, the on-road transport is one of the fastest growing sectors in India due to economic growth. This sector has been identified as a significant emitter of climate and health-related pollutants (Reynolds et al., 2011). Briefly, diesel, gasoline, and compressed natural gas (CNG) fuel is used for on-road transport throughout the world, and emitted substantial quantities of pollutants such as trace gases [Carbon di-oxide (CO), Hydrocarbon (HC), Nitrogen oxides (NOX), Volatile organic carbons (VOCs)] and aerosol especially fine aerosol such as PM_{2.5} (particulate matter with aerodynamic diameter 2.5 µm or less). Fine aerosol contains carbonaceous constituents [black carbon (BC), organic carbon (OC)], inorganic acidic species (sulphate and nitrate), organic compounds and trace metals. The heavy metals such as Cr, Co, Ni, As, Cd, Pb and others have attracted great attention due to their potential health effects (Betha et al., 2013). Several epidemiological studies have shown association of PM pollution from vehicles with health problems, morbidity and mortality (Isley et al., 2018). In order to characterize the particle-bound metals compositions and relative toxicity of PM_{2.5} emissions from vehicle, PM_{2.5} masses were collected during on-road operation of diesel, gasoline, and CNG powered vehicles. A portable dilution system (PDS) was used to achieve rapid and homogenous mixing and cooling of exhaust gas with clean dilution air to simulate the process happens in the atmosphere. This system provides a complete gas-to-particle partitioning at near atmospheric condition. The relative non-cancer risk and cancer risk of PM-bound heavy metals for diesel, gasoline, and CNG powered vehicles were estimated. To the best of our knowledge, there is limited studies, which aimed at source-specific emission risk of fine aerosol.

METHODS

On-Road Experimental Set-up

On-road vehicle experiments with diesel, gasoline, and CNG powered cars were carried out using an Aerosol Emission Measurement System (AEMS) (Fig. 1) mounted on a trolley. The trolley was towed behind the passenger car during each experiment. The AEMS consists of five main components including portable dilution sampler (PDS), heated duct, and heated particle sampling probe, dilution air assembly, and a power supply unit. The details of the AEMS and description of various instruments are published in Jaiprakash et al. (2016) and Jaiprakash and Habib (2017). A fraction of sample exhaust was drawn with the help of a heated particle sampling probe and introduced inside the PDS. The particle sampling probe line was heated approximately 10–20°C above the exhaust temperature to avoid thermophoresis losses. The vehicles were selected from various age groups (BS-II/post-2000; BS-III/post-2005, and BS-IV/post-2010) and fuel type (diesel, gasoline and CNG). The vehicles characteristics i.e model age, engine capacity, after-treatment device, and odometer reading are tabulated in Table 1.

During experiments the vehicles were driven by their owner on a fixed route of 10 km consisted of heavy traffic ring road, road with lean traffic inside the institutional area, and six traffic signals (Jaiprakash and Habib, 2017). As the MIDC cycle consists of 10 km distance travel in 20 min, therefore, the route length of

10 km was selected in present work which was covered in 40 ± 5 min due to traffic congestion. For each vehicle the experiments were performed at least 3 times and total 49 experiments were conducted. The vehicles were hired on hourly payment basis, therefore, the limited number of vehicles were assessed and 3 repeated experiments were done for each vehicle. Before each test vehicle's engine was allowed to cool down for half an hour. However, no soaking was performed, therefore, the emission measured in the present work must be considered as emissions from hot start operation. The vehicle speed was recorded with pocket global positioning monitor (Garmin Model 60 CSx). The emissions from three 2-wheelers and two 3-wheelers (auto-rickshaw) of various BS categories were measured by placing the vehicles on jacks and operating them according to MIDC under no load condition. The MIDC cycle of 108 s was repeated 20 times therefore, total run time was 36 mins. The wheels were suspended during measurement, therefore, the emissions from two wheelers and three wheelers did not include the effect of drag due to wind or the effect of resistance due to road friction, hence, the emissions might be lower than values reported from chassis dynamometer.

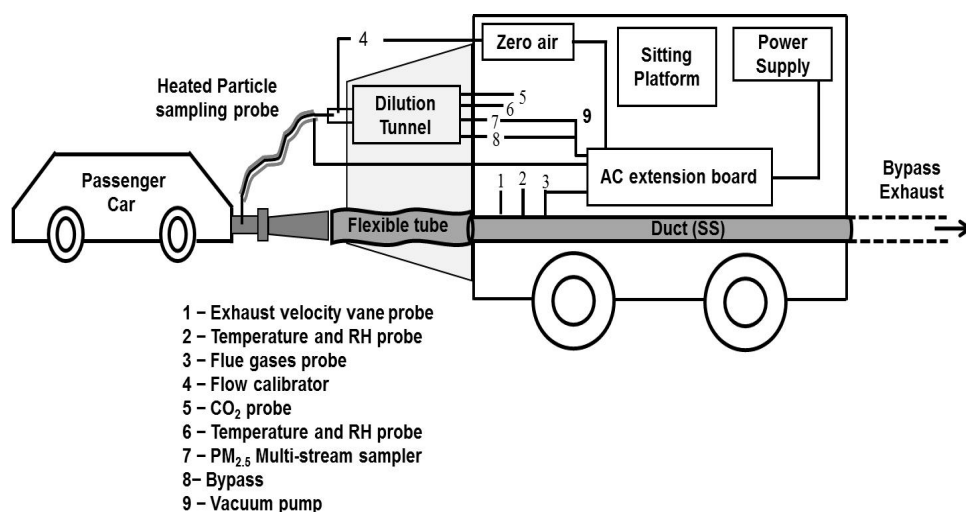


Figure 1 Mobile sampling system for on-road operation of vehicle emission measurement

PM_{2.5} and its Chemical Characterization

For gravimetric analysis, PM_{2.5} were collected using a multi-stream aerosol sampler discussed in previous work (Habib et al., 2008). PM_{2.5} mass was collected on 2 Tissue Quartz (Pall flex 2500 QAT-UP; Pallflex Corp., NY, USA) and 2 Teflon membrane filters (47 mm, 2-mm pore size, Whatmann Corp., PA, USA) at flow rates of 6.3, 4.5, 5.0 and 4.4 LPM maintained by critical orifices. The filter conditioning, baking, and weighing were discussed in earlier work (Jaiprakash et al., 2016). The particle mass were calculated using gravimetrically collected mass, sampling volume, dilution ratio. The field and dynamic blanks were also analysed gravimetrically following same procedure. The average PM_{2.5} mass on field and dynamic blanks was approximately $6.5 \pm 1.8 \mu\text{g}$ which was $<1\%$ of sampled mass in each experiment.

For trace metals, a half portion of Teflon filter was divided into small fragments and selected trace metals were extracted using nitric acid (HNO₃) following a standard procedure (Gupta et al. 2011; Herlekar et al. 2012). All the extracts were further diluted with ultrapure water to the desired volume and 15 trace elements were determined using Inductively Coupled Plasma–Mass Spectrometer (ICP-MS, Agilent, 7900) which is installed in the Department of Biochemical Engineering and Biotechnology at IIT Delhi. The concentration of trace elements in the extract was converted in mass concentration (ng m^{-3}) using volume sampled. The quality control/quality assurance of chemical analysis of collected PM_{2.5} samples, and blank filter were demonstrated in our previous work (Jaiprakash and Habib 2017)

Human Health Risk Assessment Human health risk was assessed on the basis of observed mean concentrations of particulate-bound trace metals and its exposure route i.e inhalation only. Exposure dose in terms of life time average daily dose, non-carcinogenic risk and carcinogenic risk can be expressed as (ADD_{inh} in mg kg⁻¹ day⁻¹), Hazard Quotient [HQ], and ECR and calculated by following equation (1), (2), and (3).

$$\begin{aligned}
 \text{ADD}_{\text{inh}} &= \frac{C \times \text{IR} \times \text{CF} \times \text{EF} \times \text{ED}}{\text{BW} \times \text{AT}} \\
 \text{(1), HQ} &= \frac{\text{ADD}_i}{\text{RfD}_i} \\
 \text{(2), ECR} &= \frac{\text{ADD}_i}{\text{IUR}_i} \\
 \text{(3)} &
 \end{aligned}$$

where C is the concentration of the particle-bound PM ($\mu\text{g m}^{-3}$); IR is inhalation rate of air; CF is a unit correction factor as 0.001, EF is exposure frequency; ED is exposure duration; BW is the average body weight; and AT is the average time, HQ is the non-cancer risk of the via inhalation; RfD_{inh} is the reference dose (mg kg⁻¹day⁻¹) of the ith heavy metals, and IUR is the Inhalation Unit Risk ($\mu\text{g m}^{-3}$)⁻¹ of the particle bound metals, obtained from the USEPA database.

Table 1 Characteristics of selected vehicles for on-road emission measurement

Vehicle Model	Bharat Stage Norms	Year	Engine Technology	After-treatment devices	Engine Capacity (Liter)	Odometer Reading (km)	Exhaust Temp. (°C)	Temp. (°C) at end of dilution tunnel	Residence time (sec.)
4W-Diesel									
Innova (N=3)	BS-II	2004	CRDI	EGR ^a	2.4	185032	80± 4	39 ± 3	6.5 ± 1.1
Indica (N=4)	BS-III	2007	CI	EGR	1.4	86384	79± 10	36 ± 7	7.0 ± 0.9
Swift Dzire (N=3)	BS-IV	2012	CRDI	EGR+DOC	1.2	128454	80± 3	32 ± 6	6.5 ± 0.8
Ertiga (N=6)	BS-IV	2014	CRDI	EGR+DOC	1.3	33127	77± 4	36 ± 2	6.4 ± 0.9
4W-Gasoline									
Zen (N=3)	BS-II	2001	SI	TWC+EGR	1.0	127294	80± 3	36 ± 3	5.8 ± 0.3
Swift Dzire (N=3)	BS-III	2008	MPFI	TWC+EGR ^b	1.2	85454	79± 5	42 ± 2	4.9 ± 0.1
i10 (N=3)	BS-IV	2010	MPFI	TWC+EGR ^c	1.2	46550	79± 12	39 ± 7	4.8 ± 0.1
4W-CNG									
Optra (N=3)	BS-III	2006	SI	TWC+EGR	1.2	114944	82± 10	42 ± 3	5.5 ± 0.1
i10 (N=3)	BS-IV	2010	MPFI	TWC+EGR ^c	1.2	46956	70± 10	31 ± 1	5.2 ± 0.1
3W-CNG									
Bajaj (N=3)	BS-II	2008	SI	Carburetor+TWC	0.8	48543	65± 3	34 ± 1	7.5 ± 0.8
Bajaj (N=3)	BS-III	2015	MPFI	Carburetor+TWC	0.8	14817	61± 2	31 ± 1	7.1 ± 0.6
2W-Gasoline									
Caliber (N=3)	BS-I	2001	SI	Carburetor	0.12	47709	66± 6	33 ± 2	5.8 ± 0.3
Activa (N=3)	BS-II	2009	SI	Carburetor+TWC	0.12	28543	69± 4	31 ± 1	7.3 ± 0.1
Activa (N=3)	BS-III	2014	SI	Carburetor+TWC	0.12	2973	67± 5	34 ± 2	7.6 ± 0.2

Note: N= Set of experiment; CNG=Compressed Natural Gas; BS=Bharat Stage; EGR=Exhaust Gas Recirculation; TC = Turbocharger; DOC = Diesel Oxidation catalyst; TWC = Three way catalytic convertor, ^aEGR with cooler for diesel vehicle ^bTWC+EGR with oxygen sensor heating capabilities for cold-start operation ^cTWC+EGR with coupler catalyst

RESULTS & DISCUSSIONS

In this study, 16 trace metals (Al, Ti, V, Cr, Mn, Fe, Co, Ni, Cu, Zn, As, Se, Sr, Ag, Cd, Ba, and Pb) were characterized by ICP-MS (Agilent, 7900, UK). Selenium (Se) was found below detection limit in all the samples, while the Al was found below detection limit in 28 samples out of 46. Among trace elements, the emission factors were highest from 4W-diesel ($11.3 \pm 7.9 \text{ mg km}^{-1}$) followed by 4W-gasoline ($4.8 \pm 2.7 \text{ mg km}^{-1}$), 4W-CNG ($4.0 \pm 0.01 \text{ mg km}^{-1}$), 3W-CNG ($2.8 \pm 1.7 \text{ mg km}^{-1}$), and were lowest from 2W-gasoline ($1.6 \pm 1.1 \text{ mg km}^{-1}$). The Pearson correlation analysis was also done, which indicates that the elements (Al, Fe, Zn, Pb, and Cu) emitted from after-treatment devices, additives in lube oil, and wearing of engine components and they were contributed 2–14%, 3–8% and 11–12% of total PM_{2.5} for 4-Wheelers of diesel, gasoline, and CNG respectively. Further, In order to assess the associated potential carcinogenic and non-carcinogenic health risk from the exposure to these trace elements will also be discussed in this work.

ACKNOWLEDGEMENTS

This work was supported by Department of Science and Technology, India under fast-track scheme (SR/FTP/ES-183/2010). We are grateful to taxi services near IIT campus for participation by providing their vehicles for measurement. We also thanks to students, staff and colleagues of Civil Engineering Department, IIT Delhi for their support in on-road measurement study.

REFERENCES

- Betha, R., Balasubramanian, R., 2013. Emissions of particulate-bound elements from biodiesel and ultra-low sulfur diesel : Size distribution and risk assessment 90, 1005–1015.
- Gupta, T., Jaiprakash, Dubey, S., 2011. Field performance evaluation of a newly developed PM_{2.5} sampler at IIT Kanpur. *Sci. Total Environ.* 409, 3500–3507. <https://doi.org/10.1016/j.scitotenv.2011.05.020>
- Habib, G., Venkataraman, C., Bond, T.C., Schauer, J.J., 2008. Chemical, Microphysical and Optical Properties of Primary Particles from the Combustion of Biomass Fuels. *Environ. Sci. Technol.* 42, 8829–8834. <https://doi.org/10.1021/es800943f>
- Herlekar, M., Joseph, A.E., Kumar, R., Gupta, I., 2012. Chemical speciation and source assignment of particulate (PM₁₀) phase molecular markers in Mumbai. *Aerosol Air Qual. Res.* 12, 1247–1260. <https://doi.org/10.4209/aaqr.2011.07.0091>
- Isley, C.F., Nelson, P.F., Taylor, M.P., Stelcer, E., Atanacio, A.J., Cohen, D.D., Mani, F.S., Maata, M., 2018. Reducing mortality risk by targeting specific air pollution sources: Suva, Fiji. *Sci. Total Environ.* 612, 450–461. <https://doi.org/10.1016/j.scitotenv.2017.08.225>
- Jaiprakash; Gazala Habib; Samresh Kumar, Habib, G., Kumar, S., Kumar, S., 2016. Evaluation of portable dilution system for aerosol measurement from stationary and mobile combustion sources. *Aerosol Sci. Technol.* 50, 717–731. <https://doi.org/10.1080/02786826.2016.1178502>
- Jaiprakash, Habib, G., 2017. Chemical and optical properties of PM_{2.5} from on-road operation of light duty vehicles in Delhi city. *Sci. Total Environ.* 586, 900–916. <https://doi.org/10.1016/j.scitotenv.2017.02.070>
- Reynolds, C.C.O., Grieshop, A.P., Kandlikar, M., 2011. Climate and health relevant emissions from in-use indian three-wheelers fueled by natural gas and gasoline. *Environ. Sci. Technol.* 45, 2406–2412. <https://doi.org/10.1021/es102430p>

Venkataraman, C., 2005. Residential Biofuels in South Asia: Carbonaceous Aerosol Emissions and Climate Impacts. *Science* (80). 307, 1454–1456. <https://doi.org/10.1126/science.1104359>

CHEMICAL CHARACTERIZATION OF AMBIENT PM_{2.5} AT GHAZIABAD, MOST POLLUTED INDUSTRIAL CITY IN INDIA.

LOVLEEN GUPTA¹, RAMYA SUNDER RAMAN² AND GAZALA HABIB¹

¹Department of Civil Engineering, Indian Institute of Technology, Delhi – 110016, India.

²Department of Earth and Environmental Sciences, Indian Institute of Science Education and Research, Bhopal – 462066, India.

KEYWORDS: PM_{2.5}, Ambient Aerosols, Ghaziabad, Chemical Characterization

INTRODUCTION

Ghaziabad is an industrial and semi-urban city sharing border on one side with New Delhi, Indian national capital. Several articles in the Indian and International press have termed Ghaziabad as the most polluted city in India. The 24 hour average PM_{2.5} concentrations reported¹ in Ghaziabad during April 2017²- Dec 2017 were 145.35±132.9 µg/m³. During this period, PM_{2.5} maxima was as high as 752.19 µg/m³. These PM concentrations are way above the Indian National Ambient Air Quality Standard (NAAQS) which is 60 µg/m³ for PM_{2.5} (24 hour average). Further, daily average PM concentrations were always above the standards except during the monsoon period (June – August).

A number of chemical characterization studies have been carried out in India so far. However, a large number of them focuses on Total Suspended Particulate (TSP) matter and PM₁₀, while lately, a few of studies have included PM_{2.5}. Most of those studies included ions and trace elements, few also determined OC-EC and Elements. However, there are very few (Jain et al., 2017; Nagar et al., 2017; Pant et al., 2015b; S K Sharma et al., 2016; Sharma et al., 2014; S K Sharma and Mandal, 2017) which have included ions, elements and OC-EC. Moreover, all of these studies have focused on Delhi, the national capital except Nagar et al., 2017 which has done sampling in Ghaziabad but only for five days (from 19-23 Jan 2015). Such short dataset is not enough in order to open the discussion on remedial measures to be taken to prevent further deterioration of local air quality and health of residents of the city. Thus, it is of utmost importance to carry out complete chemical characterization of ambient air in Ghaziabad to protect the health of the city residents.

This study aims to understand the complete chemical composition of PM_{2.5} in Ghaziabad. The study presents preliminary results on the ambient concentrations of Organic and Elemental Carbon (OC and EC), water soluble ions and trace elements for the three month period from (June – August 2018).

METHODS

Site Selection:

Based upon the historical meteorological data and 5 day back trajectories from HYSPLIT (Hybrid Single Particle Lagrangian Integrated Trajectory) Model, two sites – one upwind and other downwind in the prominent wind direction have been selected in Ghaziabad to collect PM_{2.5} samples. Site location is shown in Figure 1. The two sites, henceforth called “Site A” and “Site B” are at an aerial distance of 9 km from each other and “Site A” (site closer to Delhi) is at an aerial distance of about 4 km from Delhi boundary.

The key criteria followed during site selection is:

- No continuous sources of pollution within 1 km in the dominant wind direction;
- No ground or air traffic within 100 m;
- No surface storage of agricultural products, fuels, etc. within 100 m; and

¹ <http://www.cpcb.gov.in/CAAQM/frmReportdisplay.aspx>, <http://www.cpcb.gov.in/CAAQM/mapPage/frmindiamap.aspx>

² Data is not available prior to April 2017

- Unrestricted air flow in all directions around the sampler.

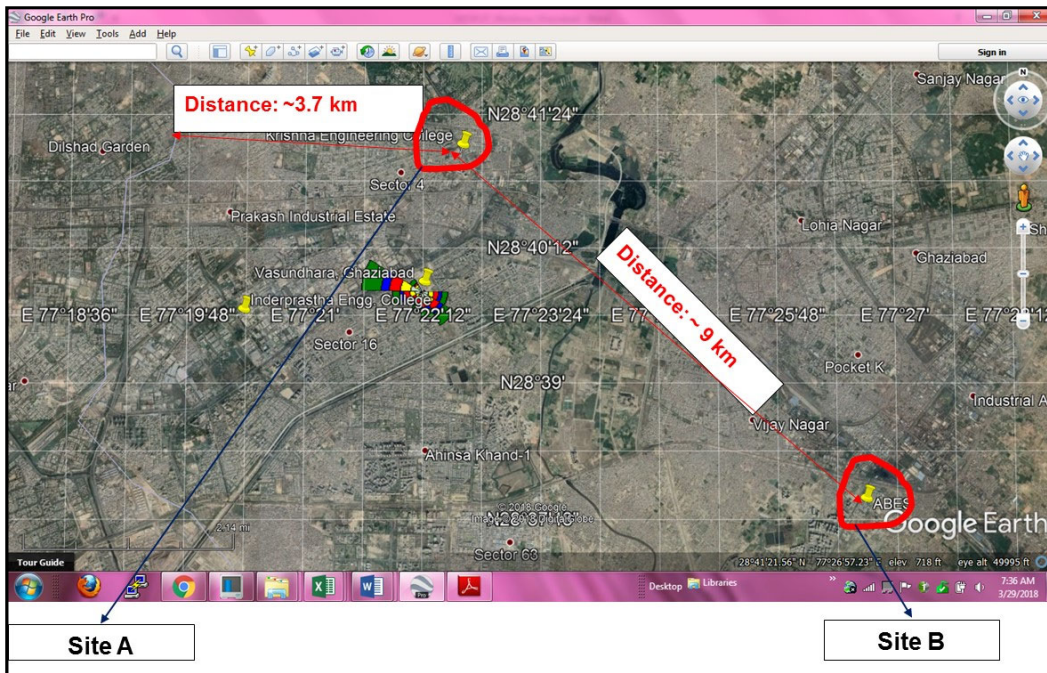


Figure 8: Site locations in Ghaziabad



Figure 9: Site pictures showing Sampler and Weather Station

SAMPLE COLLECTION

Following equipments have been installed at both the sites:

1. URG 3000 ABC sampler having dual stage filter holders and flow rate of 8.25 lpm (litres per minute) in each stream for sample collection; and
2. Automatic weather station (Spectrum Watchdog 2000 Series) to record in situ meteorological parameters.

The actual site pictures are shown in Figure 2.

24 hour integrated samples (9:00 AM to 9:00 AM) collected every third day on multiple substrates, viz:

- Nylon for Ion analysis using Ion Chromatograph (IC);
- Quartz for OC/EC analysis using IMPROVE A protocol; and
- Teflon for Elemental analysis using ED-XRF

Additionally, Field Blanks are being collected twice in a month and 10% of the filters are being collected as Lab Blanks. Back up quartz are being collected for artefact correction in OC-EC.

RESULTS & DISCUSSIONS³

The statistics including minimum, mean, maximum and number of values for PM_{2.5} concentration, Elemental concentrations and OC-EC for both the sites is presented in Table 1 and Table 2. The analysis is on-going. Preliminary results are being presented here. Results from ion analysis and from few more samples will be included in the conference talk.

Species	Arithmetic Mean ($\mu\text{g}/\text{m}^3$)	Geometric Mean ($\mu\text{g}/\text{m}^3$)	Minimum ($\mu\text{g}/\text{m}^3$)	Maximum ($\mu\text{g}/\text{m}^3$)	No. of Values
PM _{2.5}	82.31	76.79	46.94	229.66	28
Si	10.55	7.88	1.51	46.74	16
S	5.65	5.42	3.30	9.86	16
Cl	5.52	4.35	0.99	14.82	16
Al	3.72	2.85	0.74	17.10	16
K	3.23	2.95	1.47	6.27	16
Fe	3.16	2.52	0.94	14.34	16
Ca	3.08	2.07	0.50	18.27	16
Zn	1.09	0.99	0.18	1.77	16
Pb	0.70	0.56	0.05	1.60	16
Ti	0.27	0.20	0.05	1.25	16
Mn	0.15	0.12	0.05	0.48	16
Cu	0.11	0.06	0.01	0.45	16
Cr	0.03	0.03	0.01	0.08	16
Cd	0.03	0.02	0.01	0.08	16
Sr	0.03	0.02	0.00	0.17	16
As	0.03	0.02	0.01	0.06	16
Ni	0.01	0.01	0.01	0.03	16
Rb	0.01	0.01	0.00	0.03	16
V	0.01	0.01	0.00	0.03	16
OC	14.29	14.12	9.54	16.64	8
EC	9.62	9.25	6.28	16.48	8

Table 3: Site A - Descriptive summary of PM_{2.5} concentration and its chemical constituents

Species	Arithmetic Mean ($\mu\text{g}/\text{m}^3$)	Geometric Mean ($\mu\text{g}/\text{m}^3$)	Minimum ($\mu\text{g}/\text{m}^3$)	Maximum ($\mu\text{g}/\text{m}^3$)	No. of Values
---------	---	--	---	---	---------------

³ The analysis is ongoing. Preliminary results are being presented here. However, complete analysis will be presented in the conference.

PM _{2.5}	82.33	74.96	31.87	222.88	28
Si	7.17	5.82	1.68	14.88	16
S	5.24	4.98	2.79	10.10	16
Cl	2.98	2.02	0.44	9.39	16
K	2.94	2.72	1.26	5.74	16
Al	2.69	2.21	0.51	5.31	16
Fe	2.30	1.96	0.61	3.97	16
Ca	1.92	1.48	0.29	4.32	16
Zn	1.55	1.18	0.22	4.39	16
Pb	1.37	1.03	0.18	2.94	16
Ti	0.17	0.15	0.04	0.31	16
Mn	0.11	0.08	0.02	0.38	16
Cu	0.06	0.02	0.00	0.43	16
As	0.04	0.03	0.01	0.10	16
Cr	0.02	0.01	0.00	0.07	16
V	0.01	0.01	0.00	0.04	16
OC	19.49	16.48	7.72	82.43	17
EC	9.45	8.36	2.94	18.84	17

Table 4: Site B - Descriptive summary of PM_{2.5} concentration and its chemical constituents

CONCLUSIONS

In response to the revised NAAQS and the need to better understand the nature of fine PM over Ghaziabad, two monitoring sites were set up to measure PM_{2.5} mass and its chemical constituents. Samples are being collected every third day starting 24th May 2018. Chemical analysis is on-going. The key findings from the results so far are:

1. The average PM_{2.5} concentrations at Site A and Site B are $82.31 \pm 36.79 \mu\text{g}/\text{m}^3$ and $82.33 \pm 40.75 \mu\text{g}/\text{m}^3$ respectively which is higher than NAAQS despite it being the monsoon season.
2. Reconstructed soil mass indicates soil as a significant component of PM_{2.5} mass. It is 45.2% soil in PM_{2.5} for Site A and 40.8% of soil in PM_{2.5} for Site B.
3. An examination of air parcel trajectory ensembles suggests that for soil, potential regional source locations are likely to be located along Middle East and Africa.
4. Potassium is co-varying well with the other soil components. Thus, indicating that Potassium is likely to be from a crustal source. Once, the ion analysis results are ready, it can be more concretely concluded.

ACKNOWLEDGEMENTS

The authors are thankful to Uttar Pradesh Pollution Control Board (UPPCB) for funding this research.

REFERENCES

Jain, S., Sharma, S.K., Choudhary, N., Masiwal, R., Saxena, M., Sharma, A., Mandal, T.K., Gupta, A., Gupta, N.C., Sharma, C., 2017. Chemical characteristics and source apportionment of PM_{2.5} using PCA/APCS, UNMIX, and PMF at an urban site of Delhi, India. *Environ. Sci. Pollut. Res.* 24, 14637–14656. doi:10.1007/s11356-017-8925-5

Nagar, P.K., Singh, D., Sharma, M., Kumar, A., Aneja, V.P., George, M.P., Agarwal, N., Shukla, S.P., 2017. Characterization of PM_{2.5} in Delhi: role and impact of secondary aerosol, burning of biomass, and municipal solid waste and crustal matter. *Environ. Sci. Pollut. Res.* 24, 25179–25189. doi:10.1007/s11356-017-0171-3

Pant, P., Shukla, A., Kohl, S.D., Chow, J.C., Watson, J.G., Harrison, R.M., 2015b. Characterization of ambient PM_{2.5} at a pollution hotspot in New Delhi, India and inference of sources. *Atmos. Environ.* 109, 178–189. doi:10.1016/j.atmosenv.2015.02.074

Sharma, S.K., K Mandal, B.T., Srishti Jain, B., Saraswati, B., Sharma, B.A., Saxena, M., 2016. Source Apportionment of PM 2.5 in Delhi, India Using PMF Model. *Bull. Environ. Contam. Toxicol.* 97, 286–293. doi:10.1007/s00128-016-1836-1

Sharma, S.K., Mandal, T.K., 2017. Chemical composition of fine mode particulate matter (PM 2.5) in an urban area of Delhi, India and its source apportionment. *Urban Clim.* doi:10.1016/j.uclim.2017.05.009

AIR QUALITY SIMULATIONS OVER DELHI USING WRF-CHEM: INFLUENCES OF LOCAL EMISSIONS AND DYNAMICS

SHUKLA. K¹, OJHA. N² AND KHARE. M³

^{1,3} Indian Institute of Technology Delhi, Department of Civil Engineering, Delhi India.

²Physical Research Laboratory, Space and Atmospheric Sciences division, Ahmedabad, Gujarat, India.

KEYWORDS: Surface Ozone, aerosols, air quality modeling, Urban pollution, WRF-Chem, Air quality forecasting

ABSTRACT

Air quality degradation is a major concern over rapidly developing Indian region, especially densely populated National capital Delhi. Delhi experiences periods of elevated O₃ mixing ratios during pre-monsoon / spring while particulate pollution is highest during late autumn and winter, frequently exceeding national and international criteria. Here we investigate the effects of local and regional emissions and the meteorology / dynamics on ozone and particulate matter in Delhi using the Weather Research and Forecasting model coupled with chemistry (WRF/Chem). Anthropogenic emissions are included from the Emissions Database for Global Atmospheric Research – Hemispheric Transport of Air Pollution (EDGAR-HTAP) inventory, while Biogenic and fire emissions are based on the MEGAN and FINN databases respectively. Sensitivity of O₃ chemistry to various factors primary emissions, local meteorology are investigated using high resolution nested simulations with outer domain covering entire north India (12 Km x 12 km resolution) and a nested domain (4 km x 4 km resolution) centred at Delhi. Model simulations successfully reproduce the spatial distribution of O₃ with enhanced mixing ratios, over most of the Indo-Gangetic Basin (IGB), especially over the north-western part (~100 ppbv) during pre-monsoon. Interestingly, mean ozone concentration of Delhi is slightly lower (~70 ppbv) than IGB, attributed to stronger titration through anthropogenic NO_x emissions and photolysis influenced by aerosol loading here. Mean nitrogen dioxide (NO₂) of Delhi are simulated to be up to 16-18 ppbv, while much lower values can be seen at other parts of the IGB (8 ppbv or less). Similar to NO₂, mean carbon monoxide (CO) at Delhi is also significantly higher (~ 1 ppmv) as compared to other parts of the northern India. The initial simulations for aerosols (PM_{2.5} and PM₁₀) underestimate the concentration of particulate matter (~75-100 ug/m³ PM_{2.5} and 105-165 ug/m³ PM₁₀) in comparison to ground-based observations. The effects of solar radiation, relative humidity, temperature, pressure, water vapor content and wind speed has also been studied at mentioned resolutions. It is interesting to show that improved meteorology and local dynamics significantly helps reducing the biases in air quality simulations, complementing earlier studies suggesting the needs to improve anthropogenic emissions in this region. Possible impacts of stronger Delhi emissions and role of aerosol on the chemistry downwind are being studied using sensitivity simulations.

ACKNOWLEDGEMENTS

This work was supported by University Grant Commission -Junior Research Fellowship, Physical Research Laboratory, and Department of Civil Engineering, IIT Delhi. Usage of WRF-Chem, Era interim, EDGAR-HTAP inventory, FINN, MOZART chemical fields and observational data of Delhi from CPCB is acknowledged.

ULTRAFINE AND FINE AEROSOL EXPOSURE AND EFFECT ON HEART RATE OF HEALTHY ADULTS: A CASE STUDY AT IIT DELHI

NISAR ALI BAIG^{*1}, KASHISH JAIN¹, SANDEEP SINGH², SIDDHARTHAN DEEPTI², GAZALA HABIB¹

¹Department of Civil Engineering, Indian Institute of Technology Delhi, India

²Department of Cardiology, All India Institute of Medical Sciences Delhi, India

KEYWORDS: Heart rate variability, cardiovascular disease, mixed effect model, fine particulate matter

INTRODUCTION

Air pollution has been emerging as one of the most prevalent issues globally as well as in India. The outdoor air pollution alone accounts for the fifth largest burden in India causing loss of life expectancy as per the Global Burden of Disease (GBD) report, 2010. The heavy air pollution concentrations are further confirmed by the recent studies (Jaiprakash et al. 2017; Pant et al. 2017) where an extremely high particulate matter [PM_{10} (aerodynamic matter less than 10 μm)] concentration during post-monsoon and winter have been reported for Delhi. The increasing risk on health has attracted many researchers to work in the areas of air pollution and its effect on health. Numerous research initiatives have been undertaken to establish a relationship between ambient aerosol and respiratory illnesses globally. The cardiovascular health deterioration has also been highly linked to this increasing burden (Pope et al. 2004) and the smaller coronary arteries (Makaryus et al. 2010; Pant et al. 2017) among Indian individuals become a compounding factor making them more vulnerable to Cardiovascular diseases (CVDs) such as arrhythmia and other heart diseases. This incites the need to establish a link between the ambient and personal concentration of ultrafine and fine aerosol (UFP, $PM_{1.0}$, and $PM_{2.5}$) and CVD for Indian region, the study area yet to be explored. The present study thus focussed on finding a correlation between the exposure of particulate matter and heart rate variability (HRV) parameters of healthy individuals exposed to vehicle and re-suspended road dust.

METHODS

The study involved selecting a cohort of healthy individuals to be monitored and checked for heart rate variability against the exposure from fine particulate matter PM_{10} and $PM_{2.5}$.

SITE SELECTION

The main gate of IIT Delhi campus was selected for conducting the study which is near the main ring road and caters heavy traffic volumes during morning and evening hours making vehicular emissions and re-suspended dust as the primary sources of pollution. The site also characterized easy installation of equipment and sufficiently significant data on PM mass concentration. There was no major source of pollution identified from within the institutional area apart from vehicular movement and diesel generators.

COHORT SELECTION

The security guards were selected as the subjects for the study because of their direct exposure to the pollutants. A questionnaire survey was conducted to determine the healthy individuals amongst them based on their health data and diet details. Those with any medical history or into the use of alcohol or smoking did not form a part of the cohort. In total, 100 volunteers were finally selected. The subjects were provided with an activity chart to make a record of any sudden activity such as running, brisk walking or emotional distress etc. that may ultimately lead to artifacts in the ECG data. The aerosol and health monitoring were done from January to December 2017.

PARTICULATE MATTER MONITORING

The mass concentration values for particulate matter are widely used in standards and by regulatory bodies. So the real-time data was collected for mass concentrations recorded at 1 min interval using Mini-WRAS (Wide Range Aerosol Spectrometer GRIMM Model 1.371). The personal monitoring was done using cascade impactor loaded with quartz filter which was clipped to the subject's collar for the collection of fine aerosol mass (aerodynamic diameter $\leq 2.5 \mu m$).

HEALTH MONITORING

The health monitoring was done to determine the heart rate variability using 6-lead ECG Holter systems (RMS Ltd. Model I and Schiller Technology, Switzerland) at the 1-minute interval for a period of 6-8 hours to determine the occupational exposure. Each day monitoring data comprised of a preliminary health investigation using a blood pressure meter, SpO_2 i.e. Saturation of Peripheral Oxygen and pulse rate using a pulse oximeter. Any discrepancy in the data leads to cancellation of

health monitoring of that individual for that particular day. The data was processed using ECG software for noise removal and getting the HRV parameters.

STATISTICAL ANALYSIS

A linear mixed-effects model was used to determine the correlation between HRV measures and particle mass and number concentration (separately for the ultrafine particle, PM_{1.0} and PM_{2.5}) and the percent change in HRV parameters associated with IQR increase of each pollutant was determined.

RESULTS & DISCUSSIONS

The results from the linear mixed effect model will be presented. The relation between ultrafine and fine aerosol number and mass concentration and HRV parameter will be discussed.

ACKNOWLEDGEMENTS

We greatly acknowledge the support of security guards for voluntarily becoming a part of the cohort. The study was funded by Science Education Research Board (SERB), Department of Science and Technology Government of India (grant number SB/S3/CEE/061/2013).

REFERENCES

- Jaiprakash, Singhai A, Habib G, et al (2017) Chemical characterization of PM_{1.0} aerosol in Delhi and source apportionment using positive matrix factorization. *Environ Sci Pollut Res* 24:445–462. doi: 10.1007/s11356-016-7708-8
- Pant P, Habib G, Marshall JD, Peltier RE (2017) PM_{2.5} exposure in highly polluted cities: A case study from New Delhi, India. *Environ Res* 156:167–174. doi: 10.1016/j.envres.2017.03.024
- Makaryus AN, Dhama B, Raince J, et al (2010) Coronary Artery Diameter as a Risk Factor for Acute Coronary Syndromes in Asian-Indians. 5–7. doi: 10.1016/j.amjcard.2005.05.018
- Pope C, Young B (2006) Health effects of fine particulate air pollution: lines that connect. *J Air Waste Manag Assoc* 56:709–742
- Nunan, D., Sandercock, G. R. H., & Brodie, D. A. (2010). A Quantitative Systematic Review of Normal Values for Short-Term Heart Rate Variability in Healthy Adults. *Pacing and Clinical Electrophysiology*, 33(11), 1407–1417. <https://doi.org/10.1111/j.1540-8159.2010.02841.x>
- Adar SD, Gold DR, Coull BA, et al (2007) Focused exposures to airborne traffic particles and heart rate variability in the elderly. *Epidemiology* 18:95–103. doi: 10.1097/01.ede.0000249409.81050.46
- Wu S, Deng F, Niu J, et al (2010) Association of heart rate variability in taxi drivers with marked changes in particulate air pollution in Beijing in 2008. *Environ Health Perspect* 118:87–91. doi: 10.1289/ehp.0900818
- Weichenthal S, Kulka R, Dubeau A, et al (2011) Traffic-related air pollution and acute changes in heart rate variability and respiratory function in urban cyclists. *Environ Health Perspect* 119:1373–1378. doi: 10.1289/ehp.1003321

HEALTH EFFECTS OF OUTDOOR PM_{2.5} IN LUCKNOW IN THE HIGH RISK MONTHS OF OCTOBER- JANUARY

SHUBHANSHU TRIPATHI,VIKRAM CHOUDHARY,PRASHANT RAJPUT, TARUN GUPTA

Department of Civil Engineering ,IIT Kanpur, Kanpur- 208016

KEYWORDS: PM_{2.5}, Health effects, Lucknow

INTRODUCTION

Global Burden of Disease comparative risk assessment for year 2015 reported submicron particulate mass (PM_{2.5}) to be third leading factor for premature deaths among various other environmental factors in India. This study reported that exposure of air pollution led to at least 1 million deaths and 49 million Disability Adjusted Life Years (DALYs) in 2015 (Special Report 21 HFI et al 2017). India is home to 10 of the top 20 cities with the highest annual average levels of PM_{2.5} as per the WHO Urban Ambient Air Quality Database (2016). Lucknow is among the most polluted cities in the world with Air Quality Index reaching hazardous and very unhealthy multiple times in the winter months. PM_{2.5} is linked to many adverse health effects like acute and chronic respiratory symptoms (such as asthma and cough and wheeze), and increased risk of mortality from non-communicable diseases such as chronic obstructive pulmonary (lung) disease, heart disease, stroke, and lung cancer(C. Arden et.al), and from lower-respiratory infections(Jonathan et.al 2012).Thus, in this study we try to monitor the number of patients who reported respiratory and cardiology diseases at Lohia Hospital, Lucknow. In this study, we have analyzed number of patients with the change in levels of PM_{2.5} in the Lucknow region from October 2017 to January 2018.

METHDOLOGY

PM_{2.5} data was collected from CPCB automatic monitoring station at Lalbagh, Lucknow(26.845948 N, 80.941466 E). Lalbagh is situated in the center of the city. Thus, PM_{2.5} concentration at Lalbagh have been used as average concentration for whole city. In this context, daily maximum PM 2.5 concentration have been retrieved from October 2017 – January 2018 and monthly average was estimated .

Furthermore, the patient data of Lucknow region was collected from Ram Manohar Lohia Hospital, Gomti Nagar Lucknow.(26 52' 8.09" N ,81 00' 16.93"). This hospital caters to patient coming from all over state but we are interested only in patients who were from Lucknow. Patients who registered at OPD for respiratory related diseases and cardiology related diseases from October 2017 – January 2018. Now, linear correlation analysis has been performed between PM_{2.5} concentration and the number of patients on monthly basis. We also looked at the sex ratio of the patients trying to know who is more susceptible to pollution.

RESULTS AND DISCUSSION

The number of respiratory patients gave a strong correlation of 0.7586 with the monthly average concentration of PM_{2.5}. Though, the correlation with the number of cardiology patients was low coming out to be 0.04. Figure 1 gives the trend of patients with PM_{2.5} concentration on monthly basis. The ratio of number of monthly chest and cardio patients also gave a good correlation with the concentration. We performed t test for monthly average concentration of PM_{2.5} for subsequent months. The t-value obtained is given in Table 1

Months	t-value
Oct- Nov	3.6094
Nov-Dec	0.5376
Dec- Jan	0.7702

Table 1. t-value obtained from the monthly average concentration of PM_{2.5} between subsequent months

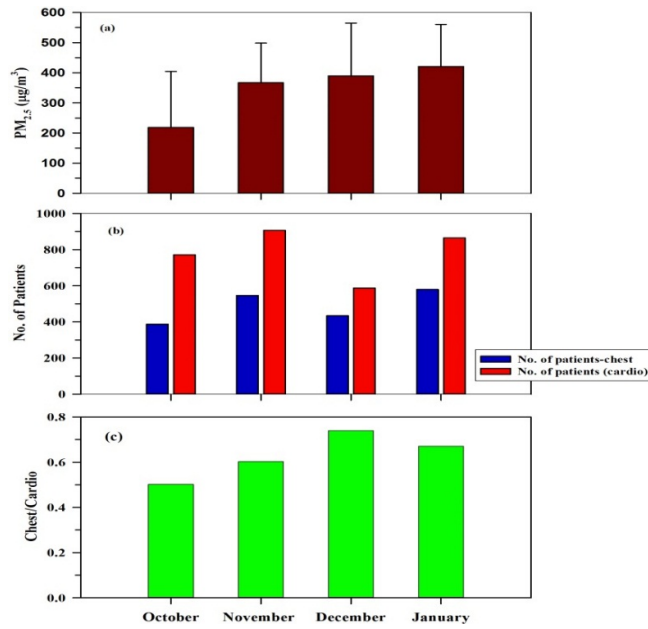


Figure1. Monthly data of (a) Concentration of PM_{2.5}(µg/m³) (b) Number of Patients (Chest and Cardiology) (c) Ratio of number of Chest and Cardio Patients

We calculated the susceptibility of males and females individually to the rise in concentration of PM_{2.5}. Among the respiratory patients, female patients showed a better correlation of 0.7969 as compared male patients who gave a correlation of 0.680. In the cardio patients, female patients gave a moderate correlation of 0.228 while the male patients had negative correlation. The ratio of male to female patients suggests that number of male patients with chest problem increases with outdoor concentration of PM_{2.5} as they go out more often compared to females and are more prone to exposure in the outdoor conditions. The ratio of cardio male and female patients suggests that female cardio patients are more prone to increasing PM_{2.5} concentration. Figure 2 gives monthly male and female patient variation of respiratory and cardio patients.

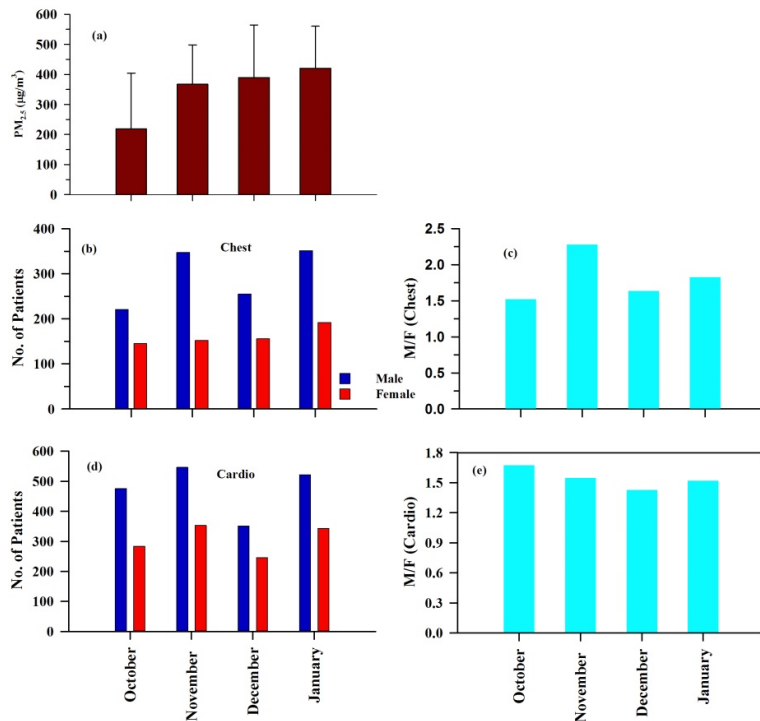


Figure 2. Monthly variation of (a) Concentration of PM_{2.5}(µg/m³) (b) Number of Respiratory Male and female patients (c) Ratio of number of male and female chest patients (d) Number of Cardio Male and Female patients (e) Ratio of number of male and female Cardio patients

CONCLUSIONS

Important outcomes from the study are listed below :

- (a) Respiratory patients have a high dependence on PM_{2.5} concentration of the city while cardio patients are not related to it.
- (b) Females are more susceptible to high pollution levels than males. Female cardio patients have some dependence on the high pollution levels.

ACKNOWLEDGEMENT

This study was carried out by the support of CMO of Ram Manohar Lohia Hospital who helped in availing the patient data.

REFERENCES

Jonathan O Anderson, Josef G Thundiyil, Andrew Stolbach (2012) . *Clearing the Air: A Review of the Effects of Particulate Matter Air Pollution on Human Health* (Journal of Medical Toxicology)

Global Burden of Disease Working Group(2017) *Special Report 21: Burden of Disease Attributable to Major Air Pollution Sources in India*

C. Arden Pope III, PhD; Richard T. Burnett, PhD; Michael J. Thun, MD(2002) *Lung Cancer, Cardiopulmonary Mortality, and Long-term Exposure to Fine Particulate Air Pollution* (Journal of American Medical Association)

GIS-BASED EMISSION INVENTORY OF AIR POLLUTANTS AND GREEN HOUSE GASES IN THREE CITIES OF UTTAR PRADESH AND DEVELOPMENT OF WEB-BASED TOOL FOR AIR QUALITY MANAGEMENT

ASHUTOSH K. PATHAK¹, PAVAN K. NAGAR¹, DHIRENDRA SINGH¹, MUKESH SHARMA¹ AND RITIKA SAXENA¹

¹Department of Civil Engineering, Centre for Environmental Science and Engineering, Indian Institute of Technology Kanpur, Kanpur – 208016, India

KEYWORDS: Emission Inventory, Pm, Ghgs, Web-Based Tool

INTRODUCTION

The emission of greenhouse gases (GHGs) and particulate matter (PM) is a matter of concern for global warming, climate change and public health (Houghton and Callander, 1992; Meinshausen *et al.*, 2009). Preparation of emission inventory (EI), which is a structured collection of information about emissions of pollutants, is the first step for developing air quality action plan. A quality EI should be able to provide a reliable estimate of total emissions of different pollutants, their spatial and temporal distribution, identification and characterization of all possible sources and tracking progress towards air pollution control. Three cities Kanpur, Lucknow, and Varanasi in the state of Uttar Pradesh (UP) were selected for this study as these are the large and fast-growing cities. Policy-makers and researchers face challenges in forming effective air quality management strategies in absence of structured EI. The primary objective of this study is to provide a qualitative region-specific EI for air pollutants and GHGs and develop a web-based decision-making tool for air quality management.

METHODS

The bottom-up approach was used for the development of EI for the base year 2014. The land-use maps were digitalized for Kanpur, Lucknow and Varanasi using the GIS tool, ArcMap (ESRI, 2006) consisting of various layers such as settlements, forests, agriculture, road network, water bodies, industries etc. The activity data were collected from field surveys and regional offices of UP Pollution Control Board, Lucknow. The emission factors developed by USEPA (2000) and CPCB (2011), New Delhi were used.

Various human activities generate GHG emissions (e.g. energy production and use, manufacturing and agricultural processes, land use changes, and waste disposal) and on the other side, some of the activities act as sinks where GHGs emissions are captured and stored (e.g. forests). The EI of GHGs was developed as per the Tier-2 methodology of IPCC (IPCC, 2006).

The EI is prepared for 2×2 km grids for each city. A tool is designed as a web-based application so that all information can be seen, retrieved and analysed remotely from any location. This tool has two modules: (1) Front End: web interface developed on HTML using PHP and javascript and (2) Back End: Mysql Database which controls the front end.

RESULTS AND DISCUSSION

Based on the primary data, the source activities for air pollutants in three cities were classified as: transport (motor vehicles), commerce, industry, domestic cooking in households, institutes, offices and other non-point sources. The contributions of PM_{2.5} emissions from various sources are shown in Figure 1. The highest contributing source was road dust followed by vehicles, municipal solid waste (MSW) burning and domestic. The total emissions from the sources for PM₁₀, PM_{2.5}, NO_x, SO₂ and CO emission load for three cities presented in Table 1. The emissions of air pollutants are highest in Kanpur followed by Lucknow and Varanasi.

Table 1. Total Emissions (in tonnes/day) from all Sources in three Cities

City	PM ₁₀	PM _{2.5}	NO _x	SO ₂	CO
Lucknow	139	68	74	3	162
Kanpur	150	74	98	28	200
Varanasi	59	28	14	1	92

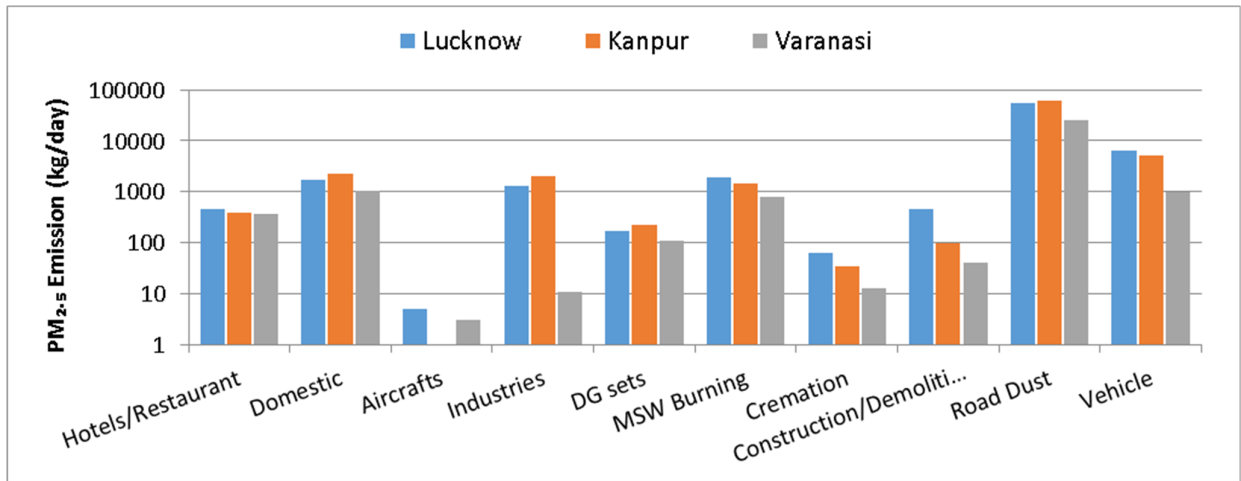


Figure 1. PM_{2.5} emission load for three cities from different sources

The main sources for GHGs are energy, industries, land use (deforestation, afforestation, soil disturbances, other biomass burning), agriculture, animal wastes, wetlands, transportation and landfills. The top three contributors to tCO₂e (equivalent CO₂ emission) are livestock (63%), agriculture (14%) and croplands (11%) in Lucknow district; livestock (58%), croplands (16%) and landfill (8%) in Kanpur district; livestock (67%), agriculture (14%) and croplands (12%) in Varanasi district. The tCO₂e emission load in the Lucknow, Kanpur and Varanasi districts are 141.65×10^4 , 167.32×10^4 and 124.72×10^4 tonnes/day respectively.

A web-based tool for retrieval of emission data and decision making for air quality management in urban areas of three selected cities was developed (Figure 2). This tool will help the policy and decision makers to identify the emission related hotspots with detailed source specific information on pollutants (PM₁₀, PM_{2.5}, SO₂, NO_x and CO) in multiple grids of 2x2 km.

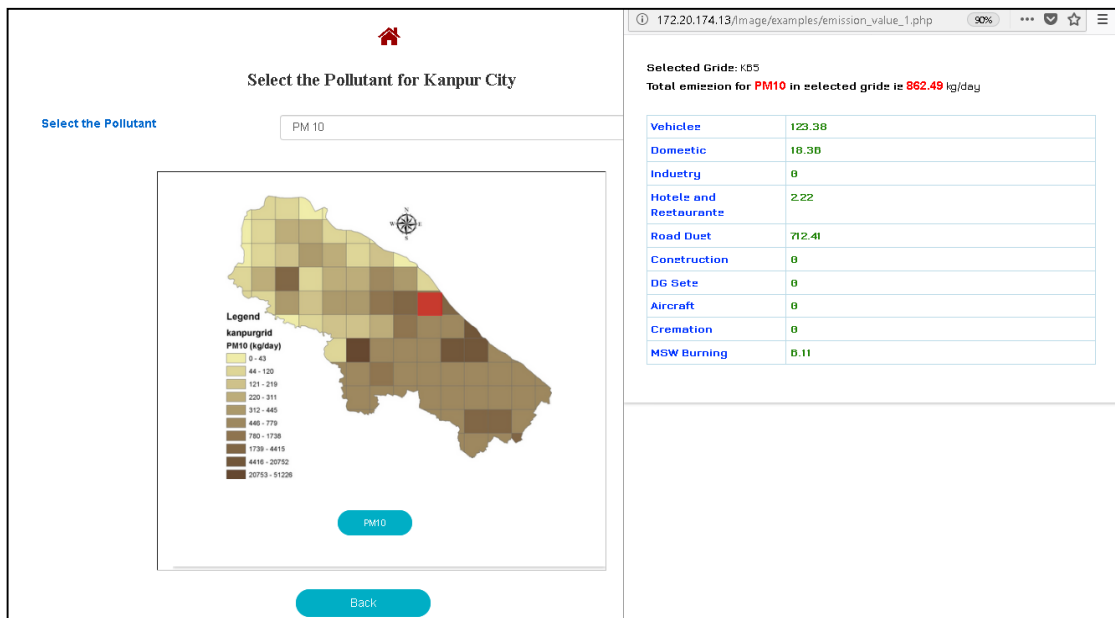


Figure 2. Web-based application tool for EI (e.g. PM₁₀ emission in selected grid in Kanpur City)

CONCLUSIONS

The road dust is the major contributing source for PM₁₀ and PM_{2.5}. Vehicles are the major source for NO_x and CO. The highest contributor to tCO₂e is livestock in all three districts. The GIS-based digital EI can be used for developing effective action plan. The developed web-based tool will help the policy and decision makers to identify the emission related hotspots with detailed source specific information on pollutants.

REFERENCES

CPCB (2011). *Air quality monitoring, emission inventory and source apportionment study for Indian cities*. National Summary Report, Central Pollution Control Board, Government of India, New Delhi, India

ESRI (2006). *ArcGIS Desktop: Release 9.2* [Computer Software].

Houghton, J.T. and Callander, B.A. (1992). *Climate Change 1992, the Supplementary Report to the IPCC Scientific Assessment*, CAMBRIDGE UNIVERSITY PRESS.

IPCC (2006). *IPCC Guidelines for National Greenhouse Gas Inventories*. Intergovernmental Panel of Climate Change (IPCC).

Meinshausen, M., Meinshausen, N., Hare, W., Raper, S.C.B., Frieler, K., Knutti, R., Frame, D.J. and Allen, M.R. (2009). *Greenhouse-gas emission targets for limiting global warming to 2°C*. *Nature* 458, 1158–1162. doi:10.1038/nature08017.

USEPA (2000). *AP 42, Fifth Edition, Compilation of Air Pollutant Emission Factors*. <http://www3.epa.gov/ttnchie1/ap42/>

TRANSFORMATION AND EVOLUTION OF ORGANIC AEROSOL (OA) DURING FOG PROCESSING

A. K. MANDARIYA¹, T. GUPTA^{1,2}, S.N. TRIPATHI^{1,2}

¹Department of Civil Engineering, Indian Institute of Technology, Kanpur, UP-208016
India.

²Center for Environmental Science and Engineering, Indian Institute of Technology, Kanpur, UP-208016
India.

Correspondence to: Prof. Tarun Gupta, tarun@iitk.ac.in and Prf. S.N. Tripathi, snt@iitk.ac.in

Keywords: SOA, Aqueous-phase Processing, OOA, ALWC

INTRODUCTION

Atmospheric aerosols especially PM₁ (aerodynamic diameter $\leq 1\mu\text{m}$) contain a significant fraction of organic and ionic species. Among all organic aerosol (OA) is a dominant component in PM₁. Worldwide field observations indicate that secondary OA (SOA, processed in the atmosphere) dominates over primary OA (Hallquist et al. 2009; Crippa et al. 2014). Our understanding towards the effects of aqueous-phase processing on the formation mechanism as well as evolutionary processes of SOA is incomplete, especially in a highly polluted complex environment like Kanpur, situated at IGP India. Also, a Worldwide number of experimental as well as modeling studies indicate towards the aqueous-phase pathway is an essential missing pathway of SOA formation (McNeill 2015). SOA formation affected by various meteorological factors like ambient temperature (T), relative humidity (RH) (Donahue et al. 2006; Seinfeld and Pandis 2006), as well as aerosol loading (Chakraborty et al. 2016). The recent studies showed that high-resolution time of flight mass spectrometer (HR-ToF-AMS, called AMS) is an excellent instrument to study the real-time OA. Recent studies in Kanpur based on AMS have shown that oxygenated OA (OOA) derived from positive matrix factorization (PMF) analysis of AMS based OA mass spectra, is a good approximation of SOA (Zhang et al. 2005, 2011; Chakraborty et al. 2018). The recent studies by Chakraborty et al. indicate towards the possibility of different aging mechanism and evaluation pathway in pre-fog, fog, and post fog environment (Chakraborty et al. 2015, 2016). However, these studies not highlighted the effect of aqueous-phase processing on OA. These conclusions motivate the current study.

Kanpur is situated at the center of IGP which faces several fog episodes in cold and high humid winter every year. To fill the gap in between field and laboratory-based measurement of SOA in the heavily polluted environment, a detailed insight of effect of aqueous-phase processing on SOA formation mechanism as well as its evaluation pathway is necessary to investigate in fog processing in Kanpur. Kanpur' atmosphere is very sophisticated and heavily polluted. Also, to formulate an effective mitigation strategy for fog episodes in IGP region, a holistic picture of SOA formation mechanism and its evaluation pathways are desired.

METHODS

Real-time measurements were carried out in the city of Kanpur (26.5°N, 80.3°E, and 142 m above mean sea level), located in the center of Indo-Gangetic Plain (IGP) in winter 2016. It is a large urban environment (population of ≈ 4.5 million (Government of India, 2011)) affected by numerous PM₁ sources during wintertime include mostly biomass burning, industrial emission, crustal dust, coal combustion, secondary aerosol, vehicular emission, domestic fuel combustion, leather tanning industries, and brick kilns (Chakraborty and Gupta 2010; Gupta and Mandariya 2013; Rai et al. 2016; Rajput et al. 2016b, a). The beginning and end of Fog were characterized by having a liquid water content (LWC) $\geq 80 \text{ mg/m}^3$ and $< 80 \text{ mg/m}^3$ respectively for more ≥ 5 min (Gilardoni et al. 2014; Chakraborty et al. 2015).

An HR-ToF-AMS (AMS) (DeCarlo et al. 2006) was deployed to measure the real-time chemical composition of non-refractory particles of aerodynamic diameter less than $1 \mu\text{m}$ (NR-PM₁) in 2 min time resolution. The Ambient wet aerosol was pre-conditioned at RH $<15\%$ by a diffusion silica-gel dryer before entering into the AMS. A cloud combination probe (CCP, Droplet Measurement Technologies) was also deployed at the rooftop of the laboratory building (at the height of 10 m above ground level) to measure the real-time liquid water content of fog droplets. A collocated temperature and RH sensor (Vaisala, Inc. Humicap, HMT337 accuracy of $\pm 1\%$ for RH $< 90\%$) were installed to measure ambient T and RH respectively.

RESULTS AND DISCUSSIONS

The overall NR-PM₁ loading varied from 16.83 to 477.08 µg/m³ (mean±1 standard deviation: 166.59±76.49). However, nighttime loading (176.17±27.27 µg/m³) was significantly higher than to daytime (156.06±39.87 µg/m³). Among all PM₁ species, OA was observed highest mass fraction (averaged 53.90%) followed by NO₃⁻ (averaged 16.04%), SO₄²⁻ (averaged 14.25%), NH₄⁺ (averaged 11.34%), and Cl⁻ (averaged 4.47%). The good correlation (r²=0.71, p<0.01) of NR-PM₁ mass loading with aerosol liquid water content (ALWC) indicates towards its aqueous-phase production pathway. Oxygenated OA (OOA-1 and OOA-2), oxidized biomass burning OA (O-BBOA), and BBOA were also showed good correlation with ALWC. This result indicates towards the role of aqueous-phase production pathway of these OA factors. Different Vankrevelen slopes indicate its different evaluation pathway during fog processing periods.

CONCLUSIONS

This study describes the role of aqueous-phase production pathway in the enhancement of NR-PM₁, OA, and its components during winter fog processing. Our results also indicate the importance of BBOA in the formation of O-BBOA and OOA-1 through aqueous-phase pathway. Our findings also might be useful to understand the formation of reactive oxygen species and brown carbon from biomass burning emission through the aqueous-phase pathway. Also, might be useful to minimize the uncertainty in the modeled SOA.

ACKNOWLEDGMENT

We also acknowledge the support of IIT Kanpur for providing us with HR-ToF-AMS for PG research and teaching.

REFERENCES

- Chakraborty A, Bhattu D, Gupta T, et al (2015) Journal of Geophysical Research : Atmospheres. 9006–9019. doi: 10.1002/2015JD023419.
- Chakraborty A, Gupta T (2010) Chemical characterization and source apportionment of submicron (PM₁) aerosol in Kanpur Region, India. Aerosol Air Qual Res 10:433–445. doi: 10.4209/aaqr.2009.11.0071
- Chakraborty A, Gupta T, Tripathi SN (2016) Combined effects of organic aerosol loading and fog processing on organic aerosols oxidation, composition, and evolution. Sci Total Environ 573:690–698. doi: 10.1016/j.scitotenv.2016.08.156
- Chakraborty A, Mandariya AK, Chakraborti R, et al (2018) Realtime chemical characterization of post monsoon organic aerosols in a polluted urban city: Sources, composition, and comparison with other seasons. Environ Pollut 232:310–321. doi: 10.1016/j.envpol.2017.09.079
- Crippa M, Canonaco F, Lanz VA, et al (2014) Organic aerosol components derived from 25 AMS data sets across Europe using a consistent ME-2 based source apportionment approach. Atmos Chem Phys 14:6159–6176. doi: 10.5194/acp-14-6159-2014
- DeCarlo PF, Kimmel JR, Trimborn A, et al (2006) Field-deployable, high-resolution, time-of-flight aerosol mass spectrometer. Anal Chem 78:8281–8289. doi: 10.1021/ac061249n
- Donahue NM, Robinson AL, Stanier CO, Pandis SN (2006) Coupled partitioning, dilution, and chemical aging of semivolatile organics. Environ Sci Technol 40:2635–2643. doi: 10.1021/es052297c
- Gao S, Ng NG a L (2004) Particle Phase Acidity and Oligomer Formation in Secondary Organic Aerosol. Environ Sci Technol 38:6582–6589
- Gilardoni S, Massoli P, Giulianelli L, et al (2014) Fog scavenging of organic and inorganic aerosol in the po valley. Atmos Chem Phys 14:6967–6981. doi: 10.5194/acp-14-6967-2014
- Gupta T, Mandariya A (2013) Sources of submicron aerosol during fog-dominated wintertime at Kanpur. Environ Sci Pollut Res 20:5615–5629. doi: 10.1007/s11356-013-1580-6

Hallquist M, Wenger JC, Baltensperger U, et al (2009) and Physics The formation , properties and impact of secondary organic aerosol : current and emerging issues. 5155–5236

McNeill VF (2015) Aqueous organic chemistry in the atmosphere: Sources and chemical processing of organic aerosols. *Environ Sci Technol* 49:1237–1244. doi: 10.1021/es5043707

Rai P, Chakraborty A, Mandariya AK, Gupta T (2016) Composition and source apportionment of PM₁ at urban site Kanpur in India using PMF coupled with CBPF. *Atmos Res* 178–179:506–520. doi: 10.1016/j.atmosres.2016.04.015

Rajput P, Gupta T, Kumar A (2016a) The diurnal variability of sulfate and nitrate aerosols during wintertime in the Indo-Gangetic Plain: implications for heterogeneous phase chemistry. *RSC Adv* 6:89879–89887. doi: 10.1039/C6RA19595D

Rajput P, Mandaria A, Kachawa L, et al (2016b) Chemical characterisation and source apportionment of PM₁ during massive loading at an urban location in Indo-Gangetic Plain: Impact of local sources and long-range transport. *Tellus, Ser B Chem Phys Meteorol* 68:. doi: 10.3402/tellusb.v68.30659

Seinfeld JH, Pandis SN (2006) *ATMOSPHERIC From Air Pollution to Climate Change SECOND EDITION*

Zhang Q, Alfarra MR, Worsnop DR, et al (2005) Deconvolution and Quantification of Hydrocarbon-like and Oxygenated Organic Aerosols Based on Aerosol Mass Spectrometry Deconvolution and Quantification of Hydrocarbon-like and Oxygenated Organic Aerosols Based on Aerosol Mass Spectrometry. *Environ Sci Technol* 39:4938–4952. doi: 10.1021/es048568l

Zhang Q, Jimenez JL, Canagaratna MR, et al (2011) Understanding atmospheric organic aerosols via factor analysis of aerosol mass spectrometry: A review. *Anal Bioanal Chem* 401:3045–3067. doi: 10.1007/s00216-011-5355-y

DEVELOPMENT AND EXPERIMENTAL VALIDATION OF COUPLED FLOW-AEROSOL DYNAMICS MODEL FOR A GLOWING WIRE

K.GHOSH^A, S.N. TRIPATHI^{A,B}, MANISH JOSHI^C, Y.S. MAYYA^D, ARSHAD KHAN^C, B.K. SAPRA^C

^a Department of Civil Engineering, IIT, Kanpur 208 016, India

^b Centre for Environmental Science and Engineering, IIT, Kanpur 208 016, India

^c Radiological Physics and Advisory Division, Bhabha Atomic Research Centre, Mumbai 400 085, India

^d Department of Chemical Engineering, IIT Bombay, Mumbai 400 076, India

KEYWORDS: Nanoparticles, K-Epsilon model, Buoyancy, CFD, Hot wire generator, Aerosol modelling

INTRODUCTION

The understanding of nanoparticles (including systems) is crucial in the context of ongoing technological developments. Applications of nanoparticle aerosols span diverse areas [1]. We have developed a CFD coupled aerosol microphysics model [2] in context of aerosol generation from a glowing wire. The governing equations can be solved implicitly for mass, momentum, energy transfer along with aerosol dynamics. The computationally efficient framework can simulate temporal behavior of total number concentration and number size distribution. This formulation uniquely couples standard K-Epsilon scheme with boundary layer model with detailed aerosol dynamics through residence time. This model uses measured temperatures (wire surface and axial/radial surroundings) and wire compositional data apart from other usual inputs for simulations. The model predictions show that bulk fluid motion and local heat distribution can significantly affect the aerosol behavior when buoyancy effect in momentum transfer is considered. Buoyancy generated turbulence was found to be affecting parameters related to aerosol dynamics and transport as well.

The model was validated by comparing simulated predictions with results obtained from six controlled experiments performed with a laboratory made hot wire nanoparticle generator. Condensation particle counter (CPC) and scanning mobility particle sizer (SMPS) were used for measurement of total number concentration and number size distribution at the outlet of reactor cell during these experiments. Our model-predicted results were found to be in reasonable agreement with observed values.

The developed model is fast (fully implicit) and numerically stable. It can be used specifically for applications in context of behavior of aerosol particles generated from glowing wire technique and in general for other similar large scale domains. Incorporation of CFD in aerosol microphysics framework provides a realistic platform to study natural convection driven systems/ applications. Aerosol dynamics sub-modules (nucleation, coagulation, wall deposition) have been coupled with Navier Stokes equations modified to include buoyancy coupled K-Epsilon turbulence model. Coupled flow-aerosol dynamics equation was solved numerically and in implicit scheme. Wire composition and temperature (wire surface and cell domain) were obtained/measured, to be used as input for the model simulations. Model simulations showed significant effect of fluid properties on the dynamics of aerosol particles. The role of buoyancy was highlighted by observation and interpretation of nucleation zones in the planes above the wire axis. The model was validated against measured temporal evolution, total number concentration and size distribution at the outlet of hot wire generator cell. Experimentally averaged and simulated total number concentrations were found to match closely, barring values at initial times. Steady state number size distribution matched very well for sub 10 nm particle diameters while reasonable differences were noticed for higher size ranges. Although tuned specifically for the present context (i.e. aerosol generation from hot wire generator), the model can also be used for diverse applications e.g. emission of particles from hot zones (chimneys, exhaust), fires and atmospheric cloud dynamics.

METHODS

Model setup & Numerical scheme

In order to reduce complexity and to save computational cost, numerical simulations were performed for 2D geometry. This simplification is justified for the present case as the main flow direction was driven by natural convection (i.e. the direction of gravity). Approximating the case to 2D fluid flow, fluid properties were estimated in X-Y planes and subsequently convoluted with aerosol dynamical equation at designated nodes [3]. The physical problem considered in this work is a two-dimensional projection of a cylindrical chamber, made of stainless steel with length and diameter are of 12 cm and 6 cm, respectively, which are of the same geometrical configuration as the one used in

experiments (see Figure 1). Nichrome coil (0.1 mm diameter, 20 turns) used as vapour source was projected as a rectangular box (3 cm x 1 cm) source of heat for simulations. The chamber has been divided into small grids of dimension 1 x 1 cm for computation of heat, mass, fluid and particle characteristics. To avoid complications in computation, fixed grid sizing scheme has been employed for simulations, which is also less expensive. Experimental condition of fluid flow (no guided flow except natural convection) was maintained by performing simulations in absence of external flow. The chamber has been maintained particle free before each experiment. 25 logarithm size bins (1) are used in aerosol dynamics model, ranging from 1 nm to 300 nm. Enhanced wall function [4] was used for getting accurate solution near the boundary layer. Radiation coefficient (specifying radiation loss of wire in glowing condition) was taken as 0.28 - 0.3 [5] for the simulations.

Experimental Setup

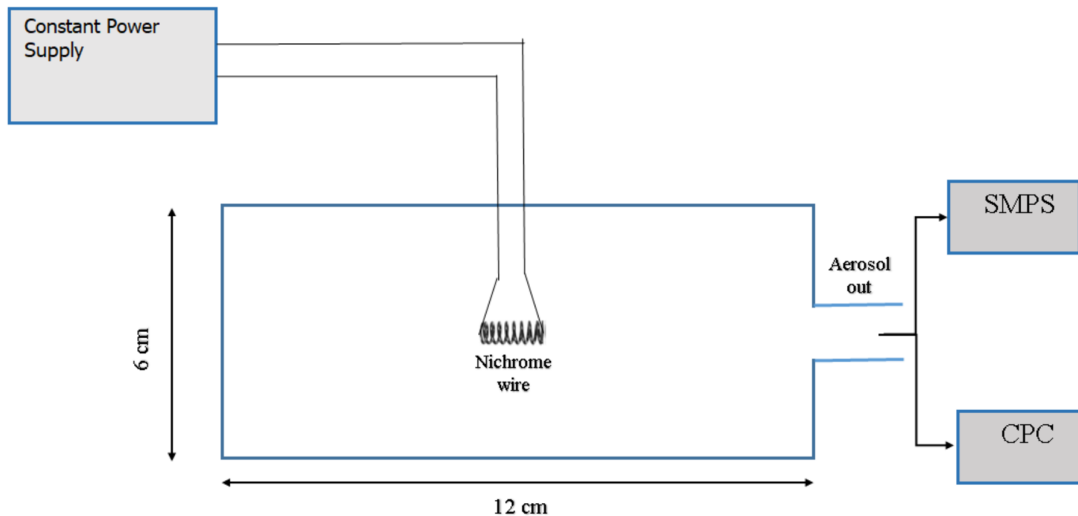


Figure 10: Experimental Setup

Six experiments were performed in controlled conditions in HWG chamber under ambient chamber conditions. Figure 1 shows the schematic diagram of power supply set-up and instrumentation employed for aerosol particle measurements. Constant power supply was used to maintain the power (20 Watt) given to glowing wire. Temperature sensor (K-type Thermocouple) was used for measuring temperature of wire surface as well as other parts of the chamber throughout all experiments. For comparison with model simulated results, GRIMM 5.403 CPC (measuring aerosols having diameter larger than 4.5 nm) was used to measure integral aerosol number concentration, while GRIMM Scanning mobility particle sizer (SMPS) (5-350 nm in 45 size channels) was employed for measuring number size distribution measurements. In addition, X-ray dispersion (XRD) techniques were utilized for determining the chemical characteristics of the wire, both before (unburnt) and after (burned) the experiment. One end of the generator was connected to CPC and SMPS for aerosol measurements and all other ports are connected with hepa filters. No external flow has been used during experiments except the sampling flow (0.3 lpm) of the instruments.

RESULTS & DISCUSSIONS

The model developed under this work has been used to calculate the essential characteristics of the fluid flow namely velocity, temperature, density and viscosity. Accurate prediction of spatial temperature profile is crucial as it is directly linked to the aerosol microphysical model, specifically for estimating nucleation rate profile in the chamber [6]. For the case of aerosol formation through electrically heated wire surface, temperature of the surface as well as nearby space is at significantly higher temperature than the other regions of the enclosing chamber. Such a scenario is expected to result in creating nucleation zones where conversion of vapor to particle is more probable. Further the spatial temperature profile is also dependent on the temperature generated buoyancy forces for which Navier Stokes (N-S) equation was modified in the K-Epsilon turbulent scheme used in the model. As a first step, model simulated steady state temperature profile in the hot wire cell/chamber was compared with the actual temperature measurements during the experiments. Figure 2 compares the average spatial temperature profile generated from six such experiments with simulations performed for experimental conditions (electrical power supplied to the wire = 20 Watt).

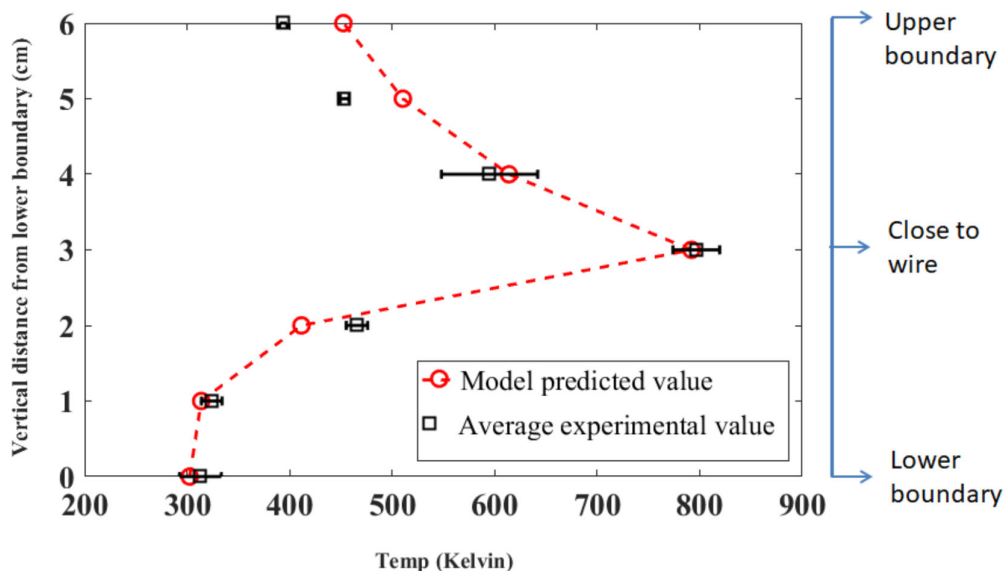


Figure 11: Steady state spatial temperature profile: Experiments and simulation

The experimental results for number concentration and number size distribution were obtained at the outlet of the hot wire chamber (see Figure 1). Therefore simulated results of only the outlet grid (1 x 1 cm) were used for this comparison. The time series of total number concentration of aerosol particles (greater than 4:5 nm to 300 nm size bins) is shown in Figure 3. Red line in the above figure is drawn for model predicted results while black circles (with error bars) are averaged number concentration measured during six experiments. As can be seen, model could predict the total number concentration reasonably well. The difference noticed for the initial times is due to warm-up time taken by the wire before becoming red hot. The experimental profile however followed the model predicted trend at later times. The steady state concentration after about 500 seconds is due to inter balance of formation and depletion terms.

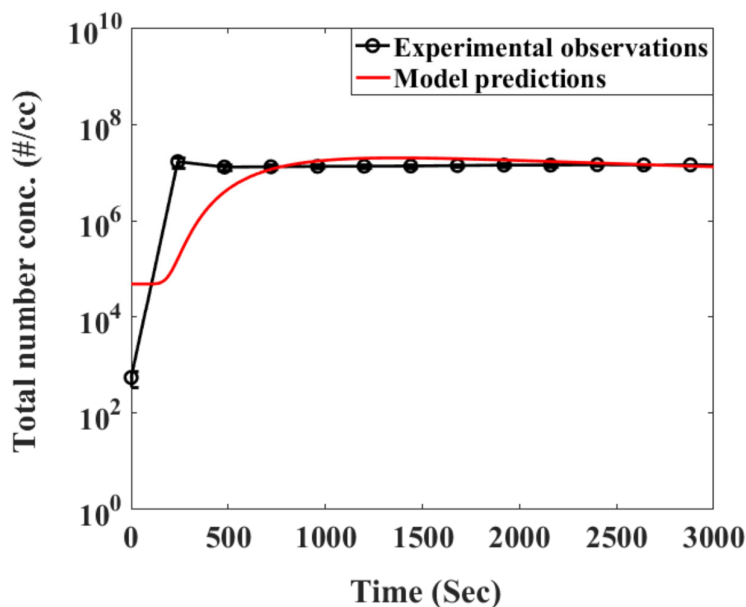


Figure 12: Time series of total number concentration: Theory and Experiment

CONCLUSIONS

This work discusses the development of a model which can successfully be used for studying evolution of number concentration and size distribution of nanoparticles generated from glowing wire conditions. The developed model has been tested against results obtained from experiments performed using hot wire generator. Incorporation of CFD in aerosol

microphysics framework provides a realistic platform to study natural convection driven systems/ applications. Aerosol dynamics sub-modules (nucleation, coagulation, wall deposition) have been coupled with Navier Stokes equations modified to include buoyancy coupled K-Epsilon turbulence model. Coupled flow aerosol dynamics equation was solved numerically and in implicit scheme. Wire composition and temperature (wire surface and cell domain) were obtained/measured to be used as input for the model simulations. Model simulations showed significant effect of fluid properties on the dynamics of aerosol particles. The role of buoyancy was highlighted by observation and interpretation of nucleation zones in the planes above the wire axis. The model was validated against measured temporal evolution, total number concentration and size distribution at the outlet of hot wire generator cell. Experimentally averaged and simulated total number concentrations were found to be closely matching, barring values at initial times. Steady state number size distribution matched very well for sub 10 nm particle diameters while reasonable differences were noticed for higher size ranges. Although tuned specifically for the present context (i.e. aerosol generation from hot wire generator), the model can also be used for diverse applications e.g. emission of particles from hot zones (chimneys, exhaust), flares and atmospheric cloud dynamics.

ACKNOWLEDGEMENTS

The present study was supported in part by Health, Safety and Environmental group, Bhabha Atomic Research Centre, Government of India. Authors are thankful to Pallavi Khandare and Amruta Nakhwa for providing help during experiments. They are also indebted to Professor Pratim Biswas for his support in the correction of the manuscript. The authors gratefully acknowledge the financial support provided by Board of Research in Nuclear Science (BRNS), Department of Atomic Energy (DAE), Government of India to conduct this research under project no. 36(2,4)/15/01/2015-BRNS.

REFERENCES

- Z. Zhang, "Comparison of micro-and nano-size particle depositions in a human upper airway model", *Journal of Aerosol Science*, vol. 36, pp. 211-233, 2005.
- K. Ghosh, "Modeling studies on coagulation of charged particles and comparison with experiments," *Journal of Aerosol Science*, vol. 105, pp. 35-47, 2017.
- W. Lu, "Modelling and measurement of air aerosol particle distribution in a ventilated two-zone chamber," *Building and Environment*, vol. 31, pp. 417-423, 1996.
- A. Rincon-Casado, "New natural convection heat transfer correlations in enclosures for building performance simulation," *Engineering Applications of Computational Fluid Mechanics*, vol. 11, pp. 340-356, 2017.
- T. Makino, "Study of the radiative properties of heat resisting metals and alloys:(1st report, optical constants and emissivities of nickel, cobalt and chromium)," *Bulletin of JSME*, vol. 25, pp. 804-811, 1982.
- L. Laakso, "Model studies on ion-induced nucleation in the atmosphere," *Journal of Geophysical Research: Atmospheres*, vol. 107, p. D20, 2002.

SEASONAL VARIATION OF CARBONACEOUS AND WATER-SOLUBLE INORGANIC CONSTITUENTS OF PM_{2.5} AEROSOLS OVER A MEGACITY, NEW DELHI

H. S. BHOWMIK¹, S. NARESH¹, D.BHATTU², N.RASTOGI³, A. S. H. PREVOT² and S. N. TRIPATHI¹

¹ Department of Civil Engineering and Centre for Environmental Science and Engineering, Indian Institute of Technology Kanpur, Kanpur, Uttar Pradesh – 208016, India

²Laboratory of Atmospheric Chemistry, Paul Scherrer Institut, Villigen PSI, 5232, Switzerland

³ Geosciences Division, Physical Research Laboratory, Ahmedabad 380009, India

KEYWORDS: Carbonaceous Aerosol, Elemental Carbon (EC), Organic Carbon (OC), Water Soluble Organic Carbon (WSOC)

INTRODUCTION

The mammoth increase in the atmospheric concentrations of carbonaceous species (EC and OC) is led by the emissions from sources like biomass and waste burning, coal combusted power plants and vehicular emission, etc. Since Delhi is a heavily populated megacity with all the above mentioned anthropogenic activities, it is essentially important to study the aerosol bulk composition, especially their carbonaceous fraction and inorganic constituents. During winter (November-February), a large part of NCR region faces severe air pollution conditions like degradation of air quality, visibility problems, and even smog formation and associated health issues. This study focuses on the measurement of both carbonaceous species and water-soluble inorganic constituents in PM_{2.5} aerosols collected at a site in New Delhi. Here, we recapitulate the measurement of OC, EC, WSOC and several cations and anions carried out on the filters collected for half a year.

METHODS

SAMPLING

In order to study the carbonaceous constituents and inorganic species in the urban aerosols, influenced by anthropogenic activities in the NCR region, Indian Institute of Technology Delhi site was chosen. High volume PM_{2.5} samples were collected on prebaked 8 x 12 inches quartz Whatman filter papers for 12 hrs and 24 hrs during Jan-mid Mar and mid Mar-May 2018, respectively. After collecting the samples, filters were stored at -20°C in the deep freezer prior to analysis.

ELEMENTAL CARBON (EC) AND ORGANIC CARBON (OC) ANALYSIS:

The EC-OC analysis was carried out on the collected filters for EC and OC mass concentration using EC-OC Carbon Analyser (Sunset laboratory, USA) at CESE, IIT Kanpur. Total carbon (TC) and Total Carbonaceous Aerosol (TCA) can be calculated as,

$$\begin{aligned} \text{TC} &= \text{OC} + \text{EC} \\ \text{TCA} &= \text{OC} \times 1.6 + \text{EC} \end{aligned}$$

The operating parameters of the EC-OC analyzer can vary with the thermal protocol used for analysis. The most commonly used protocols are NIOSH870, IMPROVE_A and EUSAAR_2. All protocols are comparable for TC but OC and especially EC concentration can vary significantly. IMPROVE_A and EUSAAR_2 protocols with relatively low peak temperature in inert mode and classify more carbon as EC compared to NIOSH protocol. In this study, the analysis was done with EUSAAR_2 protocol as it separates EC better from OC compared to IMPROVE_A. The EC-OC analysis was done using Thermo Optical Transmittance (TOT) protocol and the contribution of EC and OC from the blank filters (<0.2 µg/cm²) was removed from the sampled filters.

WATER SOLUBLE ORGANIC CARBON (WSOC) AND INORGANIC CONSTITUENTS ANALYSIS:

9 cm² punch area of each collected filter was taken in a borosilicate test tube and extracted in 30 ml of ultrapure de-ionised water (resistivity~18.2MΩ.cm). The filters were soaked overnight to ensure complete solubilization of the ions followed by 50 mins of sonication and filtration using 0.2 µm quartz filter paper. The water-soluble inorganic ions and WSOC analysis were carried out on the filtrate using an Ion-Chromatograph (Metrohm 883 Basic IC Plus for cations and 882

Compact IC plus for anions) and TOC-L analyser (SHIMADZU -TOC-L-CPN). One blank with every set of 10 samples was analysed to get their inherent concentrations on the filter.

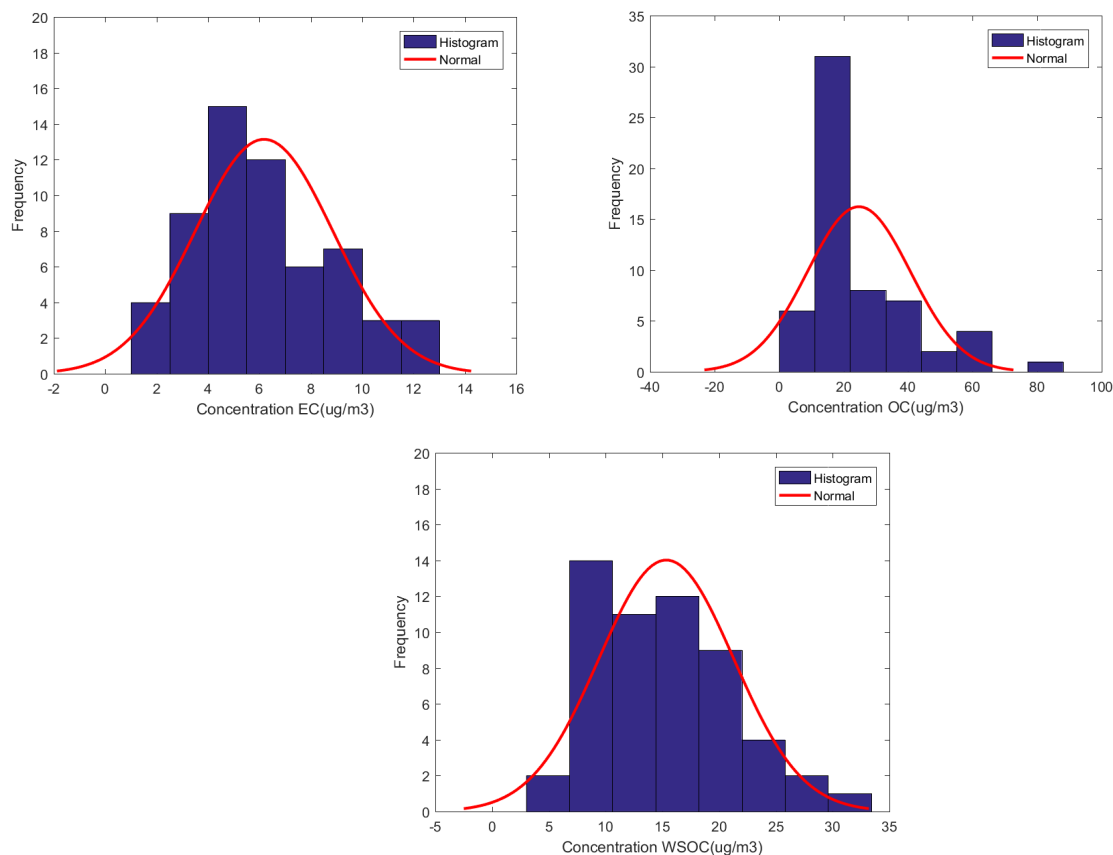


Figure 1. Probability Density Function for the mass concentration of EC, OC and WSOC in PM_{2.5} from a megacity New Delhi during the sampling period of Jan 2018 to May 2018.

RESULTS & DISCUSSIONS

CONCENTRATION OF OC AND EC

The temporal variation of the carbonaceous species (EC, OC and WSOC) in PM_{2.5} aerosols is presented in fig.1. The mass concentration is high in January-February (avg for EC, OC and WSOC: 6.51±2.92, 31.33±15.83 and 20.1±4.95 μg m⁻³, respectively) and gradually decreases in April-May (avg for EC, OC and WSOC: 5.39±2.32, 14.69±8.04 and 10.87±3.42 μg m⁻³, respectively) and this decrease could be due to the meteorological conditions (increased boundary layer height due to high temperature and high wind speed leading to better dispersion) or varying source strength of emissions. Again, the day-night variability in EC, OC and WSOC showed higher values during night time (avg for EC, OC and WSOC: 7.454±2.180, 35.77±19.026 and 18.81±5.12 μg m⁻³ respectively) compared to day time (avg for EC, OC and WSOC: 5.22±2.89, 21.52±9.56 and 15.97±5.40 μg m⁻³ respectively) and can be attributed to primary emissions. To infer the emission sources of carbonaceous aerosols, OC/EC and K⁺/OC ratios can be used. In this study, K⁺/OC ratios (avg~0.068±0.028) in January-February, are similar to the ones reported for agricultural waste burning emission. The OC/EC ratios (avg~5.09±1.65) during January-February are also high enough indicating the dominance of biomass burning emissions compared to the lower OC/EC ratios from vehicular exhausts or rather fossil fuel emissions. Saarikoski et al. (2008) found an OC/EC ratio of 0.71 and 6.6 representing vehicular and biomass burning sources, respectively. A low correlation (R²=0.34) was observed between OC and EC indicating their emission from different sources of origin.

WSOC/OC RATIO

The avg value of WSOC/OC ratios during January-February is 0.72. Again, the WSOC/OC ratios are found similar during day (avg~0.66±0.47) and night time (avg~0.59±0.26). We observed lower WSOC/OC ratios (avg~0.72±0.2) during Jan-Feb compared to Mar-May (avg~0.75±0.16). A value of 0.32±0.14 has been reported during December,2004 in Hisar (Rengarajan et al., 2007). Higher WSOC/OC ratios (0.5-0.8) were found during peak of biomass burning season in the Indo Gangetic-Plain region (Ram and Sarin, 2010).

MAJOR ANIONS IN AEROSOL CHEMICAL COMPOSITION

Among the inorganic species, the mass concentration and fraction of SO_4^{2-} is greater followed by that of NO_3^- . During the day time the SO_4^{2-} concentration is more due to the photochemical oxidation of SO_2 whereas during night the NO_3^- concentration is more due to N_2O_5 hydrolysis reaction. The calculated aerosol neutralization factor of NH_4^+ is also higher during winter (ANF=0.29). The diurnal variation shows a higher value of ANF during night time (avg~0.33±0.24) compared to day time (avg~0.25±0.2).

$$\text{ANF} = \text{NH}_4^+ / (\text{SO}_4^{2-} + \text{NO}_3^-)$$

Where ANF is Aerosol neutralization factor of Ammonia; defined as the ratios of equivalent concentrations of NH_4^+ to the sum of SO_4^{2-} and NO_3^- .

This suggests that the fine mode aerosols are acidic during winter time.

CONCLUSIONS

The current study shows that about 43% and 21% of the measured species (mainly including OC, EC, NH_4^+ , SO_4^{2-} , NO_3^- and K^+) in the $\text{PM}_{2.5}$ mass is carbonaceous and inorganic aerosol respectively during January-February,2018 where as their contribution is 22% and 16% respectively during March-April,2018. Carbonaceous aerosols are dominated by organic carbon (~80%) with higher water soluble fraction (~51%) during January-February, 2018 and gradual decrease in their concentration in April-May (~68% OC and 42% WSOC). WSOC/OC contribution in Delhi was found to be very high (around 0.72) indicating significant contributions from Secondary Organic Aerosols (SOA). Higher OC/EC ratio and K^+ /OC ratio suggests that the emissions are dominated by biomass burning during winter months.

ACKNOWLEDGEMENTS

The authors are thankful to R.V Satish Kumar and Pawan Kumar for the sampling and collection of the filters in IITD site and Madhav Patel for his support and help. We also wish to acknowledge the professor-in-charge of the Environmental Engineering Laboratory, IIT Kanpur for providing the instrumental support for analysis. This work is financially supported by the Department of Biotechnology, Government of India (Grant No. BT/IN/UK/APHH/41/KB/2016-17).

REFERENCES

- Singh, R. P.; Dey, S.; Tripathi, S. N.; Tare, V.; Holben, B. N. Variability of aerosol parameters over Kanpur, northern India. *J. Geophys. Res.* 2004, 109, D23206 DOI: 10.1029/2004JD004966.
- Andreae, M. O. Soot carbon and excess fine potassium: Longrange transport of combustion-derived aerosols. *Science* 1983, 220 (4602), 1148–1151.
- Saarikoski, S.; Timonen, H.; Saarnio, K.; Aurela, M.; Jarvi, L.; Keronen, P.; Kerminen, V.-M.; Hillamo, R. Sources of organic carbon in fine particulate matter in northern European urban air. *Atmos. Chem. Phys.* 2008, 8, 6281–6295.
- Cao JJ, Wu F, Chow JC et al (2005) Characterization and source apportionment of atmospheric organic and elemental carbon during fall and winter of 2003 in Xi'an, China. *Atmos Chem Phys* 5:3127–3137. doi:10.5194/acp-5-3127-2005
- Kirpa Ram, M.M. Sarin and S.N. Tripathi, Temporal trends in atmospheric $\text{PM}_{2.5}$, PM_{10} , elemental carbon, organic carbon, water-soluble organic carbon, and optical properties: Impact of biomass burning emissions in the Indo-Gangetic plain, *Environmental Science & Technology*, 46, 686-695, 2012.

Saarikoski, S.; Timonen, H.; Saarnio, K.; Aurela, M.; Jarvi, L.;Keronen, P.; Kerminen, V.-M.; Hillamo, R. Sources of organic carbon in fine particulate matter in northern European urban air. *Atmos. Chem.Phys.* 2008, 8, 6281–6295.

Kirpa Ram, M.M. Sarin, and S.N. Tripathi, A 1 year record of carbonaceous aerosols from an urban site in the Indo-Gangetic plain: Characterization, sources and temporal variability, *Journal of Geophysical Research* R2010JD014188, 2010.

AEROSOL PARTICLE NUMBER SIZE DISTRIBUTION STUDY IN DELHI NCR

SUNEETI MISHRA¹, PURURSHOTTAM KUMAR¹, VIPUL LALCHANDANI¹, NAVANEETH M. THAMBAN¹,
SHASHI TIWARI², DEEPIKA BHATTU³, S.N.TRIPATHI¹

¹Department of Civil Engineering, Indian Institute of Technology, Kanpur – 208016, India.

²Department of Civil Engineering, Manavrachna University, Faridabad-121004, India.

³Paul Scherrer Institute, Villigen, Switzerland

KEYWORDS: Aerosol, Ultrafine, Number Size Distribution, Particulate Matter.

INTRODUCTION

New Delhi, the capital of India, is one of the pollution hotspots of the world. The city is surrounded by various small, medium and large-scale industries situated in and around the city. It also suffers from the intense pressure of urbanization, industrialization and densely populated regions. The city also has one of the largest vehicular density in the country (Guttikunda & Calori, 2013). All these potential factors lead to numerous environmental problems in the city and its vicinity, and sequential degradation of ambient air quality. It has been estimated to cause ~12000 premature deaths per year due this degradation in air quality. In last five years (2010-2015), a rapid increase (10 g m^{-3}) in the per capita $\text{PM}_{2.5}$ mean concentration over India has been observed and attributed as high mortality risk factor. Despite of many recent efforts (1996-2010), such as, cutting down the sulfur content of diesel and petrol, and transition (2002) to compressed natural gas (CNG), and shutdown of the “hazardous” industries and “odd-even traffic intervention, 2016” policy, the annual average $\text{PM}_{2.5}$ levels persisted at alarming levels ($110\text{-}120 \mu\text{g m}^{-3}$) during 2011-2015 (Cohen et al.,2017, Barber et al.,2017, Narain et al., 2007). The size of particulate matter play a crucial role in impacting the climate forcing, adverse health effects and also influences the cloud condensation nuclei (CCN).

The particulate matter are divided into three categories depending on their size: ultrafine particles ($<100\text{nm}$), fine ($<2.5 \mu\text{m}$): and coarse ($>2.5 \mu\text{m}$). High ultrafine particles concentration in ambient aerosol increases human health risk as they are potent enough to penetrate through the lungs and causes several health problems (COPD, ischaemic heart disease, and lung cancer) (Cohen et al.,2017). The fine particles are also of respirable size range, known as accumulation size range, and are generally associated with anthropogenic emissions. These are responsible for health effects as well as light scattering and visibility reduction. The coarse particles generally have natural sources and have very low residence time (sea salt aerosols, crustal aerosols etc.). The size distribution of aerosols has been studied in different parts of the world as well as some regions in India (Vu et al.,2014, Asmi et al., 2016, Kanwade et al.,2014, Bonn et al.,2002, Maso et al., 2005).

Methodology

The sampling site, Faridabad (77.2837°E , 28.45036°N) is situated in the southern part of Delhi NCR. Over this region, high number of smog episodes are frequently reported during the winters due to various sources contributing to the air quality (Gadi et al.,2018). The site experienced dense vehicular traffic on the adjoining main road just 200 m away from the site during the days (weekdays). In the immediate vicinity of the site there is slight vegetation cover and very less residential area.

The number concentration was measured at the site by Scanning Mobility Particle Sizer (SMPS, MODEL 3938). It consists of a long Differential Mobility Analyzer (DMA, TSI MODEL 3081) and a butanol-based Condensation Particle Counter for counting the particle number concentration (TSI, MODEL 3772).The inlet impactor with nozzle diameter of 0.071cm was used to remove the bigger particles from the whole system. The sheath flow was 3.0 lpm and the flow rate was 0.3 lpm. Particle number concentration was measured at 5 minute time resolution. The size-dependent diffusion loss correction and multiple charge correction was applied to all the data points. The particles were measured from 13.6 nm to 736 nm, with SMPS measuring 64 channels per decade. The data used for analysis here is from sampling date 1st March 2018-15th March 2018 with number of samples being 4137 (N=4137).

RESULTS AND DISCUSSION

Temporal and diurnal variation of aerosol number size distribution was measured and large variation in the data has been observed. The average number concentration during the entire period varies from ~1100 to 30000 (#/cc). The frequency distribution of the sum of particle number concentration is shown in Fig.1.

Number size distribution

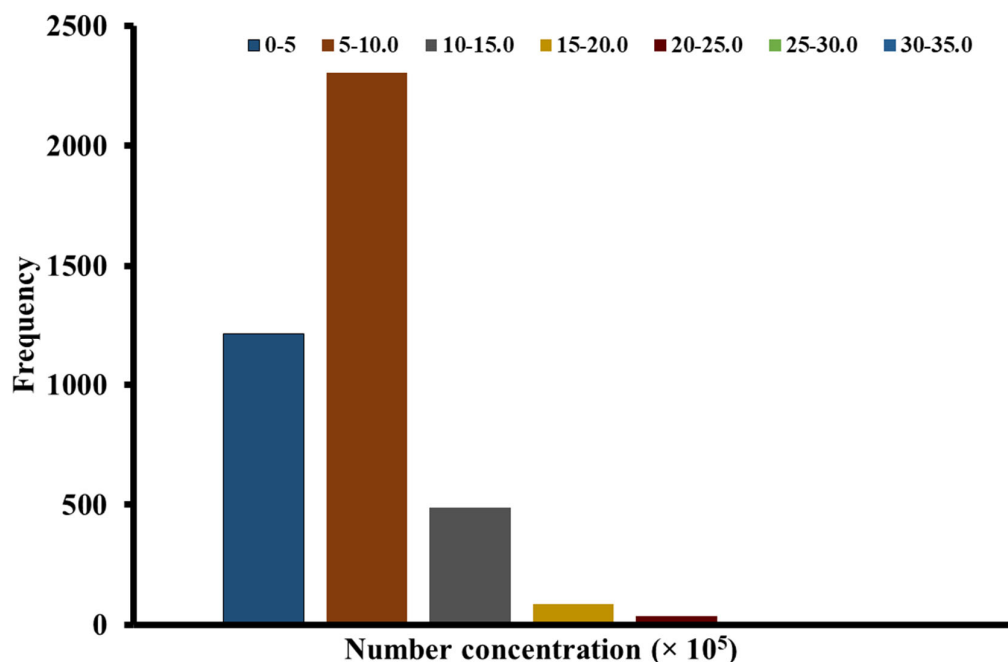


Figure 1. Frequency for different range of number concentration of aerosols measured at the site.

The particle number concentration curve showed unimodal, bimodal and at times, trimodal at different events during the entire study period. Their temporal and spatial variation along with the diurnal properties was closely studied to understand the particle formation and the time of the day to find their source. During the afternoon & evening session modes increased in the nucleation & accumulation range as compared to morning. Strong nucleation & accumulation modes observed at specific time interval suggest different sources contributing to the particulate matter concentration.

High aerosol concentration was observed at the site during the day and evening. The number concentration peaks during traffic hours.

REFERENCES

- Gadi, R., Saxena, M., Sharma, S. K., & Mandal, T. K. (2018). Short-term degradation of air quality during major firework events in Delhi, India. *Meteorology and Atmospheric Physics*, 1-12.
- Nel, A. (2005). Air pollution-related illness: effects of particles. *Science*, 308(5723), 804-806.
- Harrison, R. M., & Yin, J. (2000). Particulate matter in the atmosphere: which particle properties are important for its effects on health?. *Science of the total environment*, 249(1-3), 85-101.
- Barber, R. M., Fullman, N., Sorensen, R. J., Bollyky, T., McKee, M., Nolte, E., ... & Abd-Allah, F. (2017). Healthcare Access and Quality Index based on mortality from causes amenable to personal health care in 195 countries and territories, 1990–2015: a novel analysis from the Global Burden of Disease Study 2015. *The Lancet*, 390(10091), 231-266.
- Kanawade, V. P., Tripathi, S. N., Siingh, D., Gautam, A. S., Srivastava, A. K., Kamra, A. K., ... & Sethi, V. (2014). Observations of new particle formation at two distinct Indian subcontinental urban locations. *Atmospheric environment*, 96, 370-379.
- Cohen, A. J., Brauer, M., Burnett, R., Anderson, H. R., Frostad, J., Estep, K., ... & Feigin, V. (2017). Estimates and 25-year trends of the global burden of disease attributable to ambient air pollution: an analysis of data from the Global Burden of Diseases Study 2015. *The Lancet*, 389(10082), 1907-1918.

- Narain, U., & Krupnick, A. (2007). The Impact of Delhi's CNG Program on Air Quality.
- Kanawade, V. P., Shika, S., Pöhlker, C., Rose, D., Suman, M. N. S., Gadhavi, H., ... & Sahu, L. K. (2014). Infrequent occurrence of new particle formation at a semi-rural location, Gadanki, in tropical Southern India. *Atmospheric environment*, 94, 264-273.
- Vu, T. V., Delgado-Saborit, J. M., & Harrison, R. M. (2015). Particle number size distributions from seven major sources and implications for source apportionment studies. *Atmospheric Environment*, 122, 114-132.
- Asmi, E., Kondratyev, V., Brus, D., Laurila, T., Lihavainen, H., Backman, J., ... & Uttal, T. (2016). Aerosol size distribution seasonal characteristics measured in Tiksi, Russian Arctic. *Atmospheric Chemistry and Physics*, 16(3), 1271-1287.
- Bonn, B., & Moorgat, G. K. (2002). New particle formation during a- and b-pinene oxidation by O₃, OH and NO₃, and the influence of water vapour: particle size distribution studies. *Atmospheric Chemistry and Physics*, 2(3), 183-196.
- Dal Maso, M., Kulmala, M., Riipinen, I., Wagner, R., Hussein, T., Aalto, P. P., & Lehtinen, K. E. (2005). Formation and growth of fresh atmospheric aerosols: eight years of aerosol size distribution data from SMEAR II, Hyytiälä, Finland. *Boreal Environment Research*, 10(5), 323.
- Guttikunda, S. K., & Calori, G. (2013). A GIS based emissions inventory at 1 km× 1 km spatial resolution for air pollution analysis in Delhi, India. *Atmospheric Environment*, 67, 101-111.

BIOAEROSOL LOAD INVENTORY AT CENTRAL IGP REGION, IIT KANPUR

AMAN D. GUPTA, VIVEK SRIVASTAVA, PRASHANT RAJPUT AND TARUN GUPTA

Department of Civil Engineering, Indian Institute of Technology Kanpur, Kanpur-208016, India

KEYWORDS: Bioaerosol, GPB, GNB, Fungi

INTRODUCTION

Bio-aerosols are airborne particles that are biological in origin. Bioaerosols can be formed from nearly any process that involves biological materials. Inhalation of bioaerosol may result in various health hazards like allergies, respiratory infections, initiating oxidative stress inside our body or even cancer (mycotoxins). According to (WHO, 1999) fifty percent deaths in developing world are caused from infectious diseases like respiratory infections, measles, tuberculosis, etc., and are linked to bioaerosols (Lacey and Dutkiewicz 1994; Schweigert et al. 2000; Ghosh et al. 2013). They also play important role in atmospheric processes like cloud formation. They contribute to organic carbon content of aerosols and cloud nuclei thus imparting hygroscopic properties to it (Urbano et al. 2011). The bioaerosol study done at IIT Kanpur (central IGP Region) tries to understand the factors regulating its ambient abundance. There is basically scarcity of data set on bioaerosols from the Indian region which results in lack of understanding about their abundance and impact on health and climate.

METHODS

The current study deals with the baseline study on bioaerosol concentrations measured at various sampling sites inside IIT Kanpur campus, and subsequently to identify and characterize them through morphological and phenotype studies. The bioaerosol sampling was carried out by employing an in-house designed and tested Bioaerosol Sampler (Chauhan and Gupta, 2017). The sampler works on the principle of impaction in which bioaerosols ($>1 \mu\text{m}$ aerodynamic diameter) from air are captured in the petri dish (used as impaction substrate) containing agar media (Kumar and Gupta 2015). The sampler was run for 3 minutes at a flow rate of 12 litres per minute for each agar media. Samples were collected in different seasons at regular microenvironments with the IIT Kanpur academic campus.

Three types of Agar media were used for categorising three different types of bioaerosols namely: Gram Positive bacteria (GPB) -Mannitol Salt Agar Base, Gram Negative bacteria (GNB)-MacConkey Agar and Fungi-Sabouraud Chloramphenicol Agar. Various types of staining namely: Simple Stain, Gram Stain, Acid Fast Stain, Spore Stain and Negative Stain, were employed to complete the morphological and phenotype studies (Cappuccino and Sherman, 2004; Johnson and Case, 2007).

RESULTS AND DISCUSSION

The concentration of sum of viable bioaerosols (= GPB + GNB + Fungi) colonies measured herein averaged at $\sim 500 \text{ CFU/m}^3$ in post-monsoon, 350 CFU/m^3 in winter, 400 CFU/m^3 in pre-monsoon and at 310 CFU/m^3 in monsoon season (Figure 1; CFU: Colony-forming unit). In other words, the average concentration of total viable bioaerosols colonies varied from about 300 to 500 CFU/m^3 at Kanpur location in the IGP. Gravimetric determination of PM_{10} showed variability from ~ 20 – $400 \mu\text{g m}^{-3}$ during the course of this study.

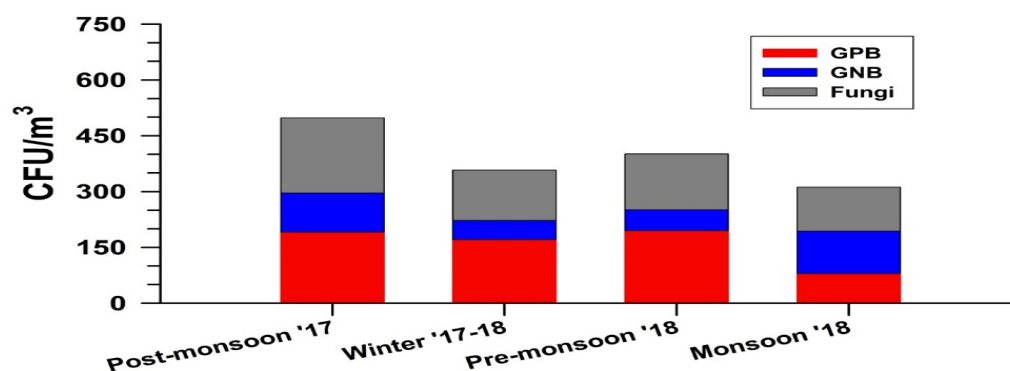


Figure 1. Bioaerosol loading in central IGP at Kanpur.

	<i>GPB</i>	<i>GNB</i>	<i>FUNGI</i>	<i>PM10</i>	<i>Temp</i>	<i>Humidity</i>
<i>GPB</i>	1					
<i>GNB</i>	0.04	1				
<i>FUNGI</i>	0.15	0.28	1			
<i>PM10</i>	0.02	-0.09	-0.03	1		
<i>Temp</i>	0.31	-0.02	0.11	-0.07	1	
<i>Humidity</i>	-0.41	-0.24	-0.02	0.22	-0.31	1

Figure 2. Correlation Matrix Of Bioaerosol load with Temperature and Humidity.

The statistical analysis conducted to find relationship between bioaerosol concentration in all the three categories (GPB, GNB, Fungi) and meteorological parameters (Temperature, Humidity and PM concentration) showed poor correlation among them. The qualitative analysis of bioaerosol samples showed various genera of Bacillus and Coccus bacteria under both GPB and GNB category. Among fungi, Aspergillus spp. was most abundant fungi present in ambient air. Penicillium, Clostridium, Fusarium, Rhizopus, Mucor, were some other fungi found in the sampled microenvironments. Overall highest monthly average concentration for both GPB and GNB were obtained in the month of April (pre monsoon). But, highest fungal concentration was obtained in month of November (post monsoon).

REFERENCES

- Cappuccino, J.G., Sherman, N., 2004. Microbiology: A Laboratory Manual, Sixth. ed. Pearson Benjamin Cummings Publications.
- Ghosh B., Lal H., Kushwaha R., et al (2013) Estimation of bioaerosol in indoor environment in the university library of Delhi. Sustain. Environ. Res. 23:199–207
- Johnson, T.R., Case, C.L., 2007. Laboratory Experiments in Microbiology, Eighth. ed. Pearson Benjamin Cummings Publications.
- Kumar A, Gupta T (2015) Development and Laboratory Performance Evaluation of a Variable Configuration PM1/PM2.5 Impaction-Based Sampler. Aerosol Air Qual Res 2015:768–775. doi: 10.4209/aaqr.2014.11.0307
- Lacey J, Dutkiewicz J (1994) Bioaerosols and occupational lung disease. J Aerosol Sci 25:1371–1404. doi: 10.1016/0021-8502(94)90215-1
- Schweigert MK, Mackenzie DP, Sarlo K (2000) Occupational asthma and allergy associated with the use of enzymes in the detergent industry - A review of the epidemiology, toxicology and methods of prevention. Clin Exp Allergy 30:1511–1518. doi: 10.1046/j.1365-2222.2000.00893.x
- Urbano R, Palenik B, Gaston CJ, Prather KA (2011) Detection and phylogenetic analysis of coastal bioaerosols using culture dependent and independent techniques. Biogeosciences 8:301–309. doi: 10.5194/bg-8-301-2011

EXPERIMENTAL AND ANALYTICAL STUDY ON AEROSOL BEHAVIOR IN PIPING ASSEMBLY UNDER VARYING FLOW CONDITIONS

A.K DWIVEDI¹, ARSHAD KHAN³, S.N. TRIPATHI¹, MANISH JOSHI³, GAURAV MISHRA² DINESH NATH¹,
NAVEEN TIWARI⁴, B.K. SAPRA³

¹ Department of Civil Engineering, IIT, Kanpur 208 016, India

² Nuclear Engineering and Technology Programme, Department of Mechanical Engineering, IIT, Kanpur 208 016, India

³ Radiological Physics and Advisory Division, Bhabha Atomic Research Centre, Mumbai 400 085, India

⁴ Department of Chemical Engineering, IIT, Kanpur 208 016, India

KEYWORDS: Aerosol, Deposition, Coagulation, Modelling, CFD, Population Balance Model

INTRODUCTION

In a nuclear reactor accident scenario, a large number of fission products may release to the piping system of the primary heat transport. The released fission products, mostly in the form of the aerosol, get deposited on the inner surface of the piping system mainly due to gravitational settling and thermophoretic deposition. The removal processes in the complex piping system are controlled to a large extent by the thermal-hydraulic conditions like temperature, pressure and flow rates. These parameters generally vary with time and therefore must be carefully monitored to predict the aerosol behavior in the piping system. Aerosol concentrations in a reactor accidents situation can typically be as high as 100 g/m^3 , and the corresponding number density can exceed $10^{13}/\text{m}^3$ (Sher et al., 1994). The removal process of aerosol depends on the size of particles that determines how many particles get deposit or travel across the bends and reach to the other end of the piping system. The released aerosol particles typically have a range of sizes varying from $0.1 \mu\text{m}$ to $10 \mu\text{m}$ Williams (1990). In a quasi-steady state environment with no continuous source of aerosol, an aerosol subjected to particle growth by coagulation and gravitational deposition onto surface develops a size distribution that is well approximated by a log-normal distribution. Whereas, when there is a continuous source of aerosol or when there are complex processes involving engineered safety features much more complicated size distributions develop. The released aerosol gets deposited onto the inner surface of the piping system by various mechanisms like gravitational settling, Brownian diffusion, thermophoretic deposition, and by other deposition mechanisms (Modi et al., 2014). To quantify the correct estimate of deposition, the identification and understanding of the aforementioned deposition mechanisms are of great importance. These mechanisms are significantly affected by different flow and thermodynamic conditions. Thermophoresis also plays a significant role in particle deposition. Shimada et al. (1994), and Stratmann and Fissan (1989) performed experimental studies with particle sizes (380 nm down to below 20 nm) and found good agreement of experimental data with theoretical models using a thermophoretic coefficient expression of Talbot et al. (1980). Maruyama et al. (1999b) have performed a series of aerosol deposition experiments to investigate the deposition of fission product vapor and aerosols onto the inner surface of the reactor coolant piping system during a reactor accident. The aerosol deposition experiments in the piping assembly to investigate the dry deposition of metal aerosols were studied by (Modi et al., 2014). The experimental results were then compared with SOPHAEROS model of computer code ASTEC (Accident Source Term Evaluation Code) and found to be within 8% of those estimated by the code. In their study, they have also found that the thermophoresis was major deposition mechanism in the regions of the high-temperature gradient. While gravitational settling was dominant in the sections having a low thermal gradient.

The modeling of aerosol transport processes needs a coupling of the aerosol dynamic and thermal hydraulic models. In the STORM experiment, the pipe is steamred by tin oxide (SnO_2) aerosol with nitrogen and steam as a carrier gas. In this experiment, the deposit was formed mainly by thermophoresis, which resulted in a much denser and stronger particle layer. Longest and Xi (2007) simulated the transport and deposition of fine aerosol particles in a duct with an elbow using the commercial CFD software FLUENT. They found that a direct Lagrangian transport model with appropriate user-defined routine provides an effective approach for predicting the deposition of nanoparticles.

In the present study, a series of experiments were performed in the piping system of the National Aerosol Test Facility (NATF), BARC using metal aerosols (zinc) in dry environments to study the spatial distribution of particles mass and number concentration, and their depletion due to various removal mechanisms in the piping system. The experiments were performed at two different carrier gas flow rates. For gravitational deposition, we have used Crump and Seinfeld (1981) model and fan model Shimada et al. (1989). The commercial CFD software FLUENT is used to determine the distribution of temperature, velocity, pressure, and turbulence quantities in the piping system. In addition to the in-built models for turbulence, heat transfer and flow in the commercial CFD code (FLUENT), a new sub-model PBM (population balance

model) is used to describe the coagulation process and to compute the number concentration along with the size distribution at different sections of the piping. In the sub-model coagulation kernels are incorporated through user-defined function (UDF). The experimental results are compared with the CFD modeled results.

EXPERIMENTAL SETUP

The experiments are performed in the National Aerosol Test Facility (NATF) facility which is a medium-scale facility for carrying out aerosol behavior experiments under simulated nuclear accident conditions. The experimental setup is mainly comprised of a Plasma Torch Aerosol Generator, aerosol delivery piping system, compressed air delivery system, a powder feeder, and a plenum chamber. The plenum chamber is a doubled walled water-cooled stainless steel chamber of volume 0.04 m^3 (length 0.6 m, and diameter 0.3 m). The experiment setup is schematically shown in Fig. 1. The total length of the piping system is 3 m consisting of six straight sections, and three 90° angle bends all having an inner diameter of 124 mm. For the measurement of the carrier gas and wall temperature, 16 numbers of factory-calibrated K-type thermocouples at different points in the piping assembly are used, and the data is recorded online through data logger.

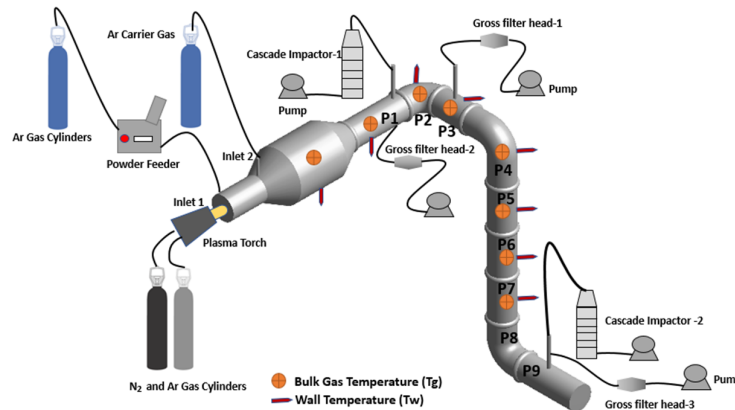


Figure 1: Experimental setup

EXPERIMENTAL PROCEDURE

The experiments were performed at two different carrier gas flow. The ZnO aerosol was generated by vaporizing Zn Powder using the plasma torch. The evaporated material was then transported through inlet 1 to the plenum chamber where it nucleates and forms aerosol particles. The metal powder was injected into the flame at different feed rates 1-3 g/min in various sets of experiments. During the experiment, aerosol sampling was carried out at regular intervals using the gross filter paper sampler for the estimation of the total mass concentration. The sampling was done through the ports provided in pipe section 1, 3 and 9. The experiments were performed with carrier gas flow rates 100 lpm (EXP-I) and 150 lpm (EXP-II) and each set of experiments were performed with two powder feeding rates, 1 g/min (EXP-Ia) and 3 g/min (EXP-Ib). Once the system cools down the test sections were disassembled, and the deposited aerosols on the inside surface of the piping section were scraped carefully using the brush. The collected powder samples were then analyzed using Scanning electron microscopy (SEM) and X-ray diffraction analysis (XRD) for particle morphology and composition.

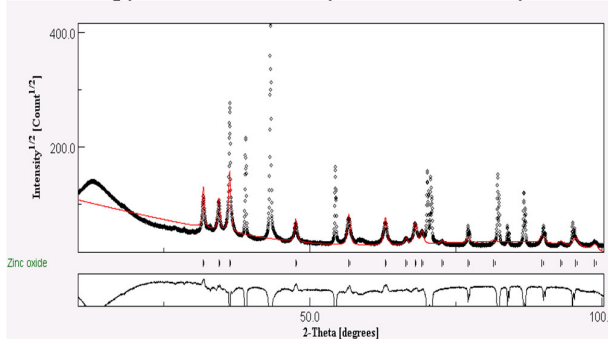


Figure 2: XRD images

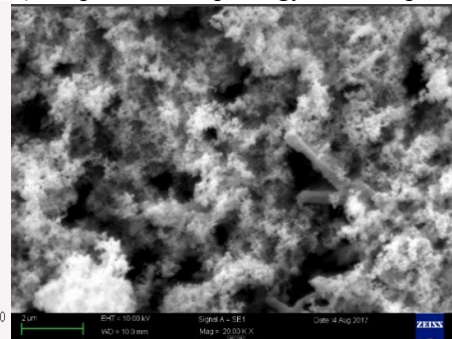


Figure 3: SEM image

The results of the XRD and SEM examination showed that most particles are in nanometer size range and consist of zinc oxide Fig. 2. The SEM micro graph of the deposited particles, Fig. 3, reveal that most of the particles are highly agglomerated, which is expected for the plasma torch-generated aerosols.

RESULTS AND DISCUSSION

The geometry of the 3D physical model is created in ANSYS design modular (ANSYS Inc., U.S.A) and meshing are done using ANSYS meshing tool. The CFD-PBM coupled model is then solved using FLUENT 16.0. Simulations were performed for 15 minutes flow time. The PBE (population balance equation) is solved by the discrete method. The particles size is discretized into 11 bins with size range (0.01 - 8 μm). The following boundary conditions are shown in Table 1. As the nucleation process is not modeled in the present study, a constant nanoparticle (10 nm) source term is included in the modeling.

Table 1 shows the operating thermohydraulic conditions for modelling

Parameters	Velocity(m/s)	Species	T(K)	Volume fraction
Inlet 1	3.8	(Ar, Zn particles)	2300	Ar = 1 Zn particles = 10^{-5} Size=0.01 μm
Inlet 2	31.0	Ar	293	Ar = 1 Zn particles = 0
Walls	No-slip	-	Heat loss	-

Table 2: Parameters used for Zn metal aerosol deposition experiment

Boundary	Exp-I(a)	Exp-I(b)	Exp-II
Power of Torch (KW)	15	15	15
Run Time (min)	20	26	10
Total weight of power aerosolized (g)	22.2	71.9	11
Total flow rate of carrier gas (lpm)	100	100	150

DEPOSITION OF ZINC OXIDE AEROSOL

The quantity of Zinc oxide deposited on the inner surface of individual sections of the plenum chamber and piping sections are shown in Table 3 and Table 4, respectively. It can be seen a huge amount of ZnO deposition is observed near the inlet of the plenum chamber (where the plasma torch is fitted). Since the plenum chamber has 3 sections (diverging, horizontal, converging) of different lengths, so the mass deposited in different sections is normalized with their respective lengths. It can be calculated from the table that in 100 lpm experiment (Exp-Ia), out of 35.38 % of total percent mass deposited in the piping system, 31.18 % deposits in the plenum chamber itself and remaining 4.2 % deposits in the pipe sections. Similarly, in Exp-II experiment, total percent mass deposited in the piping system is 43.4 %, out of which 41.6 % deposits in plenum chamber, and 1.84 % in piping sections. The deposition of ZnO along the piping sections decreases as we move along the length as can be seen in Table 4

Table 3: Total amount of Zinc oxide deposited (in g) on the inner sections of the plenum chamber. The quantity in parenthesis are the mass deposited per unit length (in g/cm)

Exp.	Near Plasma	Diverging	Horizontal	Converging
Exp-I(a)	4.2722 (0.28)	1.062 (0.06)	1.696 (0.05)	0.725 (0.04)
Exp-I(b)	8.9474 (0.59)	3.5872 (0.21)	7.2971 (0.24)	2.6048 (0.15)
Exp-II	2.7981 (0.18)	0.5118 (0.03)	0.9174 (0.03)	0.3652 (0.02)

Table 4: Total amount of Zinc oxide deposited (in grams) on the inner sections of the piping sections

Exp.	P-1	P-2	P-3	P-4	P-5	P-6	P-7	P-8	P-9
Exp-I(a)	0.2676	0.0543	-	-	-	-	-	-	-
Exp-I(b)	1.0786	0.5169	0.4089	0.234	0.222	0.1165	0.0942	0.1821	0.2017
Exp-II	0.1732	0.0201	0.007	-	-	-	-	-	-

To see the effect of bend air samples are drawn before and after the bend using a gross filter sampler. The mass concentration of ZnO before and after the bend for 100 and 150 lpm experiments are measured and shown in Table 5. It can be seen that the relative loss in mass concentration is more in case of high flow rate.

Table 5: showing the mass conc. Before and after bend

Experiment	Mass conc. (g/m ³) (before bend)	Mass conc. (g/m ³) (after bend)	Relative % difference
Exp-I(a)	0.68	0.55	19.11
Exp-I(b)	0.58	0.48	17.24
Exp-II	1.145	0.91	23.5

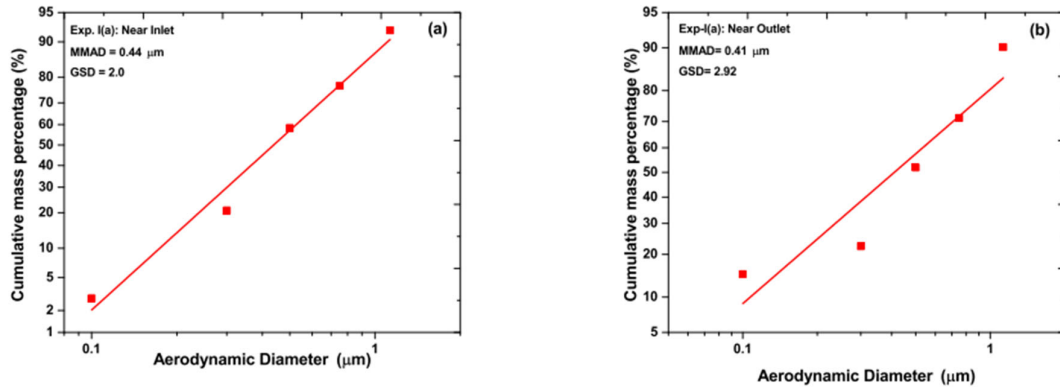


Figure 4: Aerosol Mass size distribution for 100 lpm (a,b)

To obtain the aerosol mass size distribution, the aerosol-laden air was sampled by a PASS 11-stage cascade impactor Fig.4. The values of MMAD at inlet and outlet for 100 lpm are 0:44 μm and 0:41 μm with the geometric standard deviation (GSD), 2 and 2.92, respectively. The mass mean aerodynamic diameter (MMAD) decreased along the length of the test assembly which can be attributed to the loss of large size particles due to impaction on the piping wall

TEMPERATURE PROFILES

Temperature gradients are measured in all the pipe sections and plenum chamber using the thermocouples. High radial temperature gradient is observed in the plenum chamber owing to its water-cooled walls, and hence maximum thermophoretic deposition is found in the diverging section of the plenum chamber as compared to other sections. The temperature gradient decreases towards the outlet monotonically as can be seen in Figs. 5 (a,b).

COMBINED EFFECT OF THERMOPHORESIS AND GRAVITATION ON PSD AND MASS DEPOSITION

Aerosol removal processes (i.e. dry deposition and thermophoresis) modify the number concentration and particle size distribution (PSD). The PSD is plotted for with-and-without considering the deposition phenomena (dry deposition and thermophoresis) Fig. 6. It can be seen that the distribution changes significantly due to the thermophoresis and depositional effects for the small and larger sizes as compared to the intermediate particles size.

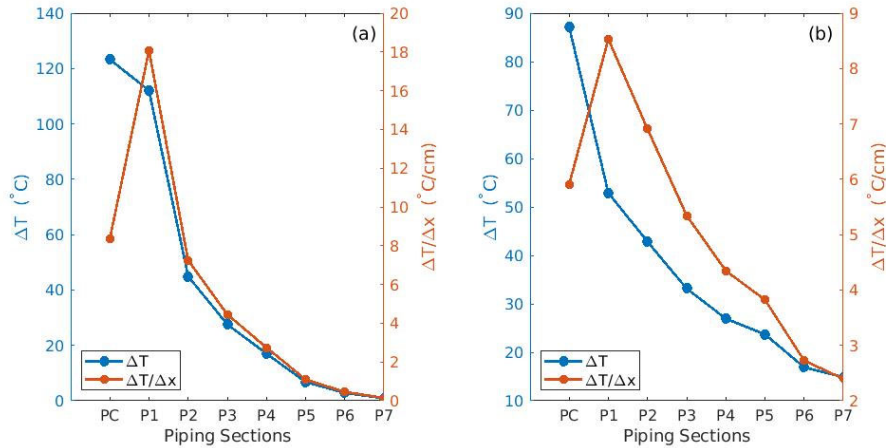


Figure 5: Temperature gradients at different sections of the piping system: (a) 100 lpm (b) 150 lpm

This net result of these effects will reflect in the total mass and number concentrations. The red curve shows the size distribution without any depositional losses.

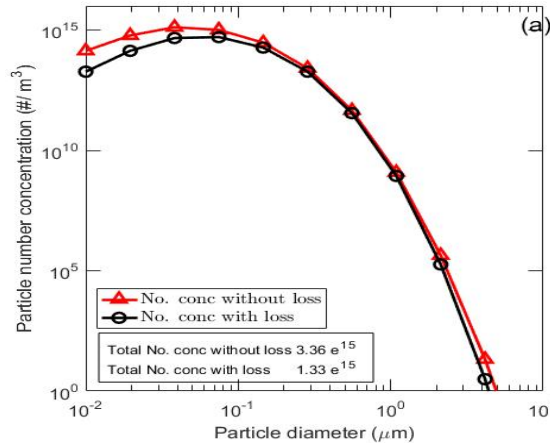


Figure 6 : (a) The effect of deposition and thermophoresis on particle size distribution,

In the table below the mass concentrations by experiment and simulation are compared for P-1 and P-9. It can be seen that after including the depositional and thermophoretic effects the results are in good agreement.

Table 6: showing the mass concentrations by experiment and simulation

	P-1	P-9
Measured Mass Conc. (g/m3)	1.1	0.91
Simulated Mass Conc. (g/m3) (without deposition)	1.66	1.76
Simulated Mass Conc. (g/m3) (Thermophoresis +deposition)	1.00	0.93

SUMMARY AND CONCLUSION

In the present work, experiments are conducted in the piping system of the National Aerosol Test Facility (NATF) with metal aerosols in dry environments with two different carrier gas flow rates. The computational fluid dynamics modeling approach is used to predict the aerosol behavior in the piping system. It is found that most of the Zn particles (more than 35 %) deposit near the inlet of the plenum chamber and a low deposition is obtained in piping sections. The MMAD decreases along the length of the test assembly which shows that large particles get deposited or removed in the course of flow and only fine particles travel to the end of the piping system. The simulation results using ANSYS Fluent match well with the experimental results of bulk gas temperature and mass concentration. The effect of a bend is also observed, and it is found that the relative loss in mass concentration at bends is more in case of high flow rate. The simulation results show that the

thermophoresis and depositional effects are more dominating for the small and larger sizes as compared to the intermediate particles size. Both SEM and XRD analysis on the collected samples show the samples are highly agglomerated non-spherical and composed mainly of ZnO.

ACKNOWLEDGMENT

The present study was supported in part by Health, Safety and Environmental group, Bhabha Atomic Research Centre, Government of India. The authors also gratefully acknowledge the financial support provided by Board of Research in Nuclear Science (BRNS), Department of Atomic Energy (DAE), Government of India to conduct this research under project no. 36(2,4)/15/01/2015-BRNS.

BIBLIOGRAPHY REFERENCES

Crump, J. G. and Seinfeld, J. H. (1981). Turbulent deposition and gravitational sedimentation of an aerosol in a vessel of arbitrary shape. *Journal of Aerosol Science*, 12(5):405-415.

Gelbard, F. and Seinfeld, J. H. (1979). The general dynamic equation for aerosols. theory and application to aerosol formation and growth. *Journal of Colloid and Interface Science*, 68(2):363-382.

Ghosh, K., Tripathi, S., Joshi, M., Mayya, Y., Khan, A., and Sapra, B. (2017). Modeling studies on coagulation of charged particles and comparison with experiments. *Journal of Aerosol Science*, 105:35-47.

Longest, P. W. and Xi, J. (2007). Effectiveness of direct lagrangian tracking models for simulating nanoparticle deposition in the upper airways. *Aerosol Science and Technology*, 41(4):380-397.

Maruyama, Y., Shibasaki, H., Igarashi, M., MAEDA, A., HARADA, Y., HIDAKA, A., SUGIMOTO, J., HASHIMOTO, K., and Nakamura, N. (1999a). Vapor condensation and thermophoretic aerosol deposition of cesium iodide in horizontal thermal gradient pipes. *Journal of nuclear science and technology*, 36(5):433-442.

Modi, R., Khan, A., Joshi, M., Ganju, S., Singh, A., Srivastava, A., Sapra, B., and Mayya, Y. (2014). Metal oxide aerosol dry deposition in laminar pipe flow at high thermal gradients and comparison with sophraeros module of astec reactor accident analysis code. *Annals of Nuclear Energy*, 64:107 - 113.

Parker, S., Foat, T., and Preston, S. (2008). Towards quantitative prediction of aerosol deposition from turbulent flows. *Journal of Aerosol Science*, 39(2):99-112.

Sapra, B., Mayya, Y., Khan, A., Sunny, F., Ganju, S., and Kushwaha, H. (2008). Aerosol studies in a nuclear aerosol test facility under different turbulence conditions. *Nuclear Technology*, 163(2):228-244.

Seinfeld, H. J. and Pandis, N. S. (1998). *Atmospheric Chemistry and Physics, from air pollution to climate change*. John Wiley, New York.

Sher, R., Hoover, M., Newton, G., and Rahn, F. (1994). Aerosol behavior in nuclear facilities. *Transactions of the American Nuclear Society*, 70(CONF-940602).

Shimada, M., Okuyama, K., and Kousaka, Y. (1989). Influence of particle inertia on aerosol deposition in a stirred turbulent flow field. *Journal of Aerosol Science*, 20(4):419-429.

Shimada, M., Seto, T., and Okuyama, K. (1994). Wall deposition of ultrafine aerosol particles by thermophoresis in nonisothermal laminar pipe flow of different carrier gas. *Japanese journal of applied physics*, 33(2R):1174.

Singh, S., Khan, A., Das, T., Sapra, B., Pushparaja, and Mayya, Y. (2005). Indigenous development 465 of an aerodynamic size separator for aerosol size distribution studies. *Current Science*, pages 1426-1433.

Stratmann, F. and Fissan, H. (1989). Experimental and theoretical study of submicron particle transport in cooled laminar tube flow due to combined convection, diffusion, and thermophoresis. *Journal of Aerosol Science*, 20(8):899- 902.

Talbot, L., Cheng, R., Schefer, R., and Willis, D. (1980). Thermophoresis of particles in a heated boundary layer. *Journal of fluid mechanics*, 101(4):737-758.

Vohra, K., Ghosh, K., Tripathi, S., Thangamani, I., Goyal, P., Dutta, A., and Verma, V. (2017). Submicron particle dynamics for different surfaces under quiescent and turbulent conditions. *Atmospheric Environment*, 152:330-344.

Waldmann, L. and Schmitt, K. (1966). Thermophoresis and diffusiophoresis of aerosols. *Aerosol science*, pages 137-162.

Williams, M. (1990). Nuclear aerosol behavior during reactor accidents

A STUDY ON HYGROSCOPIC GROWTH OF CSI AND CSOH PARTICLES

GAURAV MISHRA¹, ANIL KUMAR MANDARIYA², S.N. TRIPATHI², MARIAM³,
MANISH JOSHI³, ARSHAD KHAN³, B.K. SAPRA³

¹ Nuclear Engineering and Technology Programme, Department of Mechanical Engineering, IIT, Kanpur 208 016, India

² Department of Civil Engineering, IIT, Kanpur 208 016, India

³ Radiological Physics and Advisory Division, Bhabha Atomic Research Centre, Mumbai 400 085, India

KEYWORDS: Fission product aerosols, CsI, CsOH, Hygroscopic growth, HTDMA

INTRODUCTION

The behavioural studies of fission product aerosols are extremely important in the context of probable environmental hazard in the event of a severe nuclear reactor accident. Fission Product aerosols are generated in such a case are expected to travel from primary heat transport system to the containment and may get released to the environment. Presence of steam also affect their dynamic behaviour and fate. Interaction of aerosol particles with water vapour in subsaturation domain affects their physical as well as chemical characteristics. Cesium exits naturally in the environment mainly from terrestrial erosion. It is also released into the atmosphere through mining and milling of ores. In the ambient air, cesium attached to particles approximately according to their available aerosol surface area. Radioactive compounds of cesium (CsI and CsOH) forms major part of fission product aerosols, which may be released into the air in huge amounts by nuclear power plants during nuclear accidents and also at the time of nuclear weapons testing [1]. Severe nuclear reactor accidents that involve considerable core melting generate large source terms of fission product aerosols to the environment. High amounts of radioactivity were released in atmosphere by the reactor accident at the Fukushima Daiichi Nuclear Power Plant triggered by the massive earthquake and tsunami on March 11, 2011, and radioactive plume spread over the northern Hemisphere [2], [3]. The majority of materials, such as control materials, structural materials, fission products, will have released and condensed into or onto aerosols. A chemical equilibrium estimate of materials vaporization and condensation onto aerosols in a severe accident indicates that in a specific nuclear reactor, the aerosol produced amount to about 1.4 % of the total core mass and is made up of structural materials(3 %), control materials (73%) and fission products (24 %) [4]. Hence the total aerosol mass generated is roughly four times that of the mass of fission product aerosols. Generally FeO, MnO, Ni, SnO₂ and ZrO₂ are the aerosols produced from the structural materials while Ag, B₂O₃ and Cd aerosols are produced from control material. The fission product aerosols are mainly consists of BaO, CdI₂, Ce₂O₃, CsBO₂, CsI, CsOH, La₂O₃, MoO₂ and SnTe [5]. Cesium, with a half-life of 30 years is highly reactive and combines readily with other elements, especially oxygen, other gases and nonmetals. Cesium is treated as a hazardous material because it reacts violently with water. Cesium also reacts violently with sulfur, phosphorous, acids, and halogens (fluorine, chlorine, bromine, iodine and astatine). The lifetime, along with its reactive nature makes it a concern for human health. Radioactive isotopes of cesium are produced in nuclear power plants by the fission of uranium in fuel rods and also by the explosion of nuclear weapons. In this study, the hygroscopic properties at different relative humidity of laboratory generated single salt CsI (Cesium Iodide) and CsOH (cesium hydroxide) aerosols were investigated. These salts are common constituents of fission product aerosols. Cesium salt is one of the major fraction of the total nuclear aerosols formed inside the containment of a nuclear reactor. Regulatory guide 1.183 [6] assumes that 95% of the iodine released, in reactor accident is in the form of CsI. Growth curves in humid air and the deliquescence relative humidity (DRH) of 100 nm particles were measured at room temperature (298K). In this study a comparison of experimental data with theoretical values is done for 100 nm dry diameter particles for both the salts.

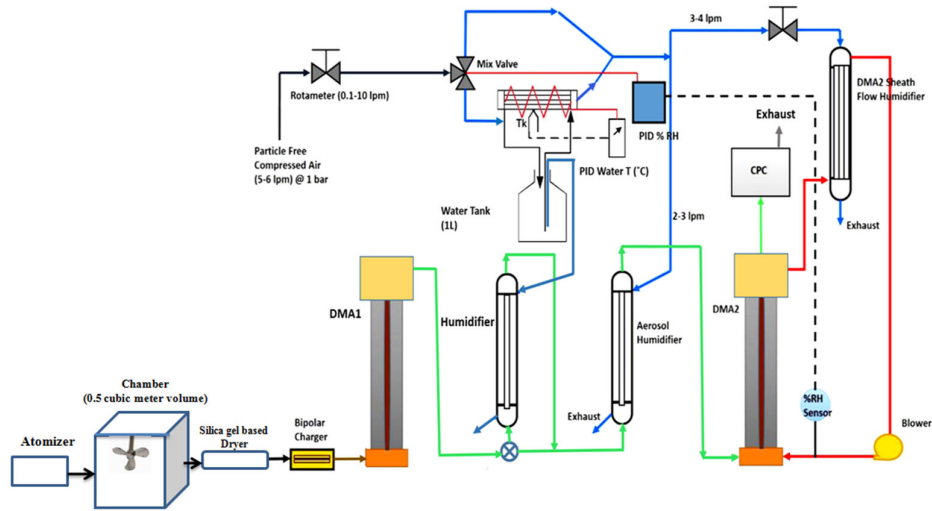


Figure 1: Experimental Setup

METHODS

The HTDMA system was used to determine the hygroscopic growth of CsI and CsOH particles. This system has been employed and discussed in detail in available literature [7], [8], [9], [10]. Hygroscopic growth of particles with diameter 100 nm has been measured in the humidity range of 20% to 94% RH with an accuracy of $\pm 1\%$ RH employing above discussed experimental setup. The growth factor measurement accuracy depends on the uncertainty in controlling and measuring RH [11]. Necessary protocols, due calibration procedures including offset calibration are followed during these experiments. All the data collected with this experimental setup is then corrected with TDMAinv toolkit developed by Gysel et al. 2009 [11]. This inversion algorithm uses a full TDMA kernel function and it also approximates the inverted growth factor probability density function (GF-PDF) as a piecewise linear function [12], [11]. The relative humidity inside the second DMA varies little around the fixed target value which causes a simultaneous variability in measured growth factors. So the measurements within a range of $\pm 2\%$ of target RH were considered for that particular RH and growth factors were recalculated according to the approach suggested by Gysel et al., 2009 [11].

THEORETICAL APPROACH

In the theoretical growth model of Brechtel and Kreidenweis 2000 [13], modified Kohler equation is developed in terms of parameters to be determined from HTDMA studies. The advantage of using this model is the parameterization of osmotic coefficient data itself. This model assumes the surface tension of solution droplet same as that of pure water.

$$RH = 100a_w \exp\left(\frac{4\sigma_{drop}\bar{v}_l}{RTD_{drop}}\right) \quad (1)$$

where RH is in percentage, \bar{v}_l is partial molar volume of the solution, σ_{drop} is surface tension of droplet, R is universal gas constant, T and D_{drop} are temperature and diameter of droplet respectively. a_w is the water activity and for aqueous solutions of ionic compounds, it can be defined as [14] :

$$a_w = \exp\left(\frac{-M_w v \phi m}{1000}\right) \quad (2)$$

where M_w is the molecular weight of pure water, v is total number of ions of salt present in solution, ϕ is osmotic coefficient of solution and m is molality of the solution. Due to the unavailability of purely theoretical model, a semi empirical model is considered for calculating the osmotic coefficient [15], [16].

$$\phi = 1 - |Z_1 Z_2| \left(\frac{A_\phi I^{0.5}}{1 + b_{\phi I} I^{0.5}} \right) + \frac{2v_1 v_2}{v} \{ \beta_0 + \beta_1 \exp(-\alpha I^{0.5}) \} m + 2(v_1 v_2)^{1.5} C_\phi m^2 / v \quad (3)$$

where the value of α and b_{pit} are 2 and 1.2 at 298K, respectively, Z_1 and Z_2 are charges on the ions respectively, v_1 and v_2 are the number of different molecules of ions produced by dissociation of a single molecule of solute, v is sum of total ions $v = v_1 + v_2$, I is solution's ionic strength and m is the molality of the solution. The coefficients β_0 , β_1 and C_ϕ are dependent on the chemical composition of solute. The values of these coefficients are tabulated by Pitzer and Mayorga, 1973 ([17]) for various salts. The ionic strength of the solution can be calculated using the relation:

$I = 0.5 \sum m_i Z_i^2$ where m_i is molality of species i and Z_i is charge on the ion of that species. The value of Debye-Huckel coefficient for the osmotic function A_ϕ is 0.392 for water at 25^oC [13].

With the help of above model, theoretical growth factor curve with respect to relative humidity for CsI and CsOH have been generated as a part of this study. The theory of Brechtel and Kreidenweis, 2000 is the most relevant for predicting the theoretical growth factors of examined salts as it uses the actual solution properties such as osmotic coefficient and density.

RESULTS & DISCUSSIONS

Growth factor is the ratio of wet diameter and initial dry diameter (D_0) of the particle. Growth factors measured for CsI and CsOH at different dry diameters were used for interpreting the growth factor curve. Reproducibility and repeatability of the data was ascertained by performing 25 - 30 measurement runs for each RH value performed under room temperature (typically 23 to 27 ^oC). The results are as follows:

Cesium Iodide (CsI)

Fig.2 shows the measured hygroscopic growth factors for cesium iodide particles with a dry diameter of 100 nm. The increasing and decreasing pattern of the growth factor with RH can be easily distinguished for CsI aerosols. The equilibrium size of CsI particle at a particular RH shows a dependency on its RH history. This dependency can be explained by hysteresis effect between its increasing RH and decreasing RH growth factors. Growth factor curves obtained for increasing and decreasing RH conditions were used for estimating DRH and ERH values for the test particles.

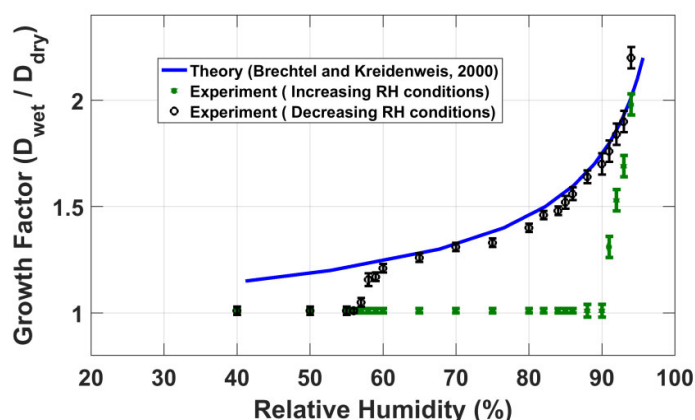


Figure 2: Experimental and theoretical hygroscopic growth factors of 100 nm dry CsI particle

When starts from low RH, the dry CsI particles do not change their size until they reach the DRH, where a solution droplet is formed. The small growth of particles just below the DRH point is caused by water adsorption on defected sites of the lattice as described by Gysel et al.,2002 [16]. After the DRH, further increase in relative humidity leads to particle growth by condensation and this growth is responsible for high dilution of the solution droplet which is well explained by Kohler theory. Starting from high RH, the size of droplets decreases by evaporation of water. These droplets can also exist below the DRH in metastable equilibrium state as a supersaturated solution. Continuous decrement in relative humidity leads to crystallization of the solution droplets and lowest data point in decreasing growth factor trend provided ERH for CsI particles. The crystallization may occur above the actual ERH of the salt due to the presence of some insoluble impurities [16].

In addition to the experimental values, theoretical growth factor curve is also plotted in Fig.2. The agreement between the experimental values and theoretical model of Brechtel and Kreidenweis,

2000 is very good within the experimental errors. The deliquescence transition point was measured at $91 \pm 1\%$ RH and is in good agreement with literature data of CRC handbook of chemistry and physics [18]. The experimental efflorescence relative humidity for CsI was measured at $59 \pm 1\%$ RH.

CESIUM HYDROXIDE (CSOH)

In Fig. 3, the measured hygroscopic growth factors for cesium hydroxide particles with a dry diameter of 100 nm are shown. The growth factor pattern with increasing and decreasing RH cannot be easily distinguished for CsOH aerosols. Measurements show that the equilibrium size of CsOH particles at a particular RH is independent from its RH history.

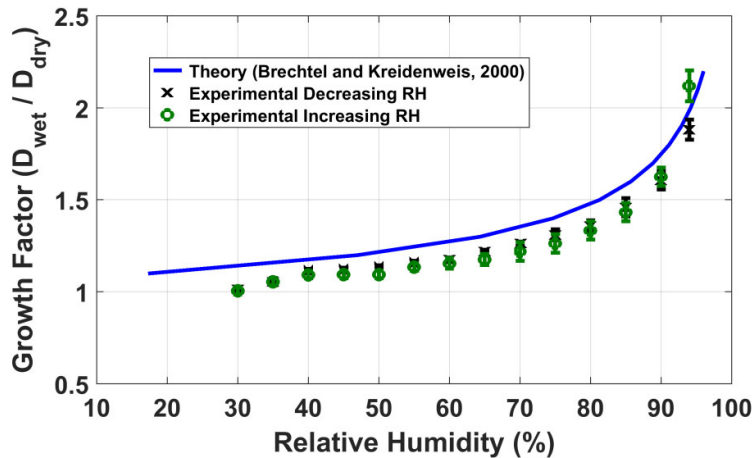


Figure 3: Experimental and theoretical hygroscopic growth factors of 100 nm dry CsOH particle

As shown in Fig.3, CsOH exhibits continuous water uptake with increasing RH and no phase transition or deliquescence transition is observed. Such hygroscopic behavior indicates that CsOH particles are in liquid state and retain some water even at very low relative humidity. Due to missing crystallization, an approximately constant growth factor of 1.02 was observed in the low RH range for CsOH particles. This type of hygroscopic behavior is also observed for some other atmospheric particles of interest such as Sodium Nitrate, Citric acid and Phthalic acid [16], [19]. Theoretical growth factor curve is also plotted in addition to the experimentally measured growth factors in Fig. 3. The assumption taken are same as that of taken for theoretical predictions of CsI particles in this study. The experimental growth factors are slightly smaller than the theoretical values over the whole RH range. Theoretical model of Brechtel and Kreidenweis, 2000 is over predicting the growth factors within the whole RH range but the trend of curve is similar to experimental growth factors. This is because of the assumptions taken for calculation of the osmotic coefficient on account of unavailability of values of few coefficients used in the equation. As the hysteresis effect is missing in the growth factor measurements of CsOH particles, there is no significant difference between the measured growth factors of increasing and decreasing RH.

CONCLUSION

In this study, the hygroscopic growth of laboratory generated CsI and CsOH aerosols were investigated utilizing a HTDMA system. Kohler equation based theoretical model is used for predicting the hygroscopic growth curves of both type of aerosols. The DRH and ERH of CsI salt were found to be $91 \pm 1\%$ and $59 \pm 1\%$ respectively. CsOH exhibits continuous water uptake and no phase transition was found with increasing RH, so no DRH was observed for this salt. The minimum relative humidity obtained within the experimental limitations in decreasing RH measurements was not low enough for the crystallization of CsOH particles with no apparent ERH. Theoretical growth factor curves were also justifying the measured growth factors for both the examined salts. In the case of nuclear reactor accidents, there may be a chance of release of these water soluble compounds (i.e. CsI, CsOH) into the containment and the environment. The growth factors obtained during this study could be used as an important data in getting realistic source term or deposition rate predictions in various containment codes such as ASTEC, MELCOR or RELAP6. The experimental results presented in this study fills the gap on our knowledge of hygroscopic fission product aerosol behaviour and these results can also be used for aerosol model validation in containment codes.

ACKNOWLEDGEMENTS

The present work was supported by Health, Safety and Environmental group, Bhabha Atomic Research Centre, Government of India. The authors gratefully acknowledge the financial support from the Board of Research in Nuclear Science (BRNS), Department of Atomic Energy (DAE), Government of India to conduct this research under project no. 36(2,4)/15/01/2015-BRNS. The authors also thankful to Dr. Martin Gysel, Aerosol Physics Group, Paul Scherrer Institute, Switzerland, for providing TDMA_{inv} toolkit for HTDMA data correction.

REFERENCES

- E. Buckle, Nucleation and growth of caesium iodide aerosols, *Journal of Aerosol Science* 22 (2)(1991) 135 – 147.
- J. D. Leon, D. Jaffe, J. Kaspar, A. Knecht, M. Miller, R. Robertson, A. Schubert, Arrival time and magnitude of airborne fission products from the fukushima, japan, reactor incident as measured in seattle, wa, usa, *Journal of Environmental Radioactivity* 102 (11) (2011) 1032 – 1038.
- Z. Y. I. Y. Adachi Kouji, Kajino Mizuo, Emission of spherical cesium-bearing particles from an early stage of the fukushima nuclear accident, *Scientific Reports* 3 (2013) 2554.
- R. P. Wichner, R. D. Spence, A chemical equilibrium estimate of the aerosols produced in an overheated light water reactor core, *Nuclear Technology* 70 (3) (1985) 376–393.
- R. Sher, R. & Hobbins, *Transport and Removal of Aerosols in Nuclear Power Plants Following Severe Accidents* American Nuclear Society, 2011.
- U. N. R. Commission., Regulatory guide 1.183 (draft was issued as DG-1081) [microform] : alternative radiological source terms for evaluating design basis accidents at nuclear power reactors / U.S. Nuclear Regulatory Commission, Office of Nuclear Regulatory Research, U.S. Nuclear Regulatory Commission, Office of Nuclear Regulatory Research [Washington, DC], 2000.
- E. Weingartner, M. Gysel, U. Baltensperger, Hygroscopicity of aerosol particles at low temperatures. 1. new low-temperature h-tdma instrument: setup and first applications, *Environmental Science & Technology* 36 (1) (2002) 55–62,
- M. Gysel, E. Weingartner, S. Nyeki, D. Paulsen, U. Baltensperger, I. Galambos, G. Kiss, Hygroscopic properties of water-soluble matter and humic-like organics in atmospheric fine aerosol, *Atmospheric Chemistry and Physics* 4 (1) (2004) 35–50.
- J. Duplissy, M. Gysel, M. R. Alfarra, J. Dommen, A. Metzger, A. S. H. Prevot, E. Weingartner, A. Laaksonen, T. Raatikainen, N. Good, S. F. Turner, G. McFiggans, U. Baltensperger, Cloud forming potential of secondary organic aerosol under near atmospheric conditions, *Geophysical Research Letters* 35 (3) (2008)
- P. Villani, D. Picard, V. Michaud, P. Laj, A. Wiedensohler, Design and validation of a volatility hygroscopic tandem differential mobility analyzer (vh-tdma) to characterize the relationships between the thermal and hygroscopic properties of atmospheric aerosol particles, *Aerosol Science and Technology* 42 (9) (2008) 729–741.
- M. Gysel, G. McFiggans, H. Coe, Inversion of tandem differential mobility analyser (tdma) measurements, *Journal of Aerosol Science* 40 (2) (2009) 134 – 151.
- J. Duplissy, M. Gysel, S. Sjogren, N. Meyer, N. Good, L. Kammermann, V. Michaud, R. Weigel, S. Martins dos Santos, C. Gruening, P. Villani, P. Laj, K. Sellegri, A. Metzger, G. B. McFiggans, G. Wehrle, R. Richter, J. Dommen, Z. Ristovski, U. Baltensperger, E. Weingartner, Intercomparison study of six htdmas: results and recommendations, *Atmospheric Measurement Techniques* 2 (2) (2009) 363–378.

F. J. Brechtel, S. M. Kreidenweis, Predicting particle critical supersaturation from hygroscopic growth measurements in the humidified tdma. part i: Theory and sensitivity studies, *Journal of the Atmospheric Sciences* 57 (12) (2000) 1854–1871.

R. Robinson, R. & Stokes, *Electrolyte Solutions: Second Revised Edition*, 2012.

K. S. Pitzer, Thermodynamics of electrolytes. i. theoretical basis and general equations, *The Journal of Physical Chemistry* 77 (2) (1973) 268–277.

M. Gysel, E. Weingartner, U. Baltensperger, Hygroscopicity of aerosol particles at low temperatures. 2. theoretical and experimental hygroscopic properties of laboratory generated aerosols, *Environmental Science & Technology* 36 (1) (2002) 63–68,

K. S. Pitzer, G. Mayorga, Thermodynamics of electrolytes. ii. activity and osmotic coefficients for strong electrolytes with one or both ions univalent, *The Journal of Physical Chemistry* 77 (19) (1973) 2300–2308.

W. Haynes, *CRC Handbook of Chemistry and Physics*, 97th Edition, CRC Press, 2016.

C. Peng, M. N. Chan, C. K. Chan, The hygroscopic properties of dicarboxylic and multifunctional acids: measurements and unifac predictions, *Environmental Science & Technology* 35 (22) (2001) 4495–4501

DESIGN OF A NOVEL ECCENTRIC IMPACTOR PM SAMPLER: AN APPROACH TO REDUCE PARTICLE BOUNCE OFF IN SINGLE STAGE INERTIAL IMPACTOR

KANISKA BISWAS¹, TARUN GUPTA¹

¹ Indian Institute of Technology, Kanpur, 208016 India

KEYWORDS: Aerosol Instrumentation, Single stage Inertial Impactor, Particulate Matter, Particle Bounce- Off, Eccentric Nozzle.

INTRODUCTION

Air sampling is executed to collect air suspended particulate matters for air quality monitoring, asserting pollutants source, instigating control, protecting human health and global well-being, control and mitigation is the best way to save humanity and the world from the adversity of air pollution. Government bodies, air pollution control boards, and air pollution researchers are interested in measuring air pollution for source identification and quantification of air pollutants to decide on the control and mitigation action. Air is a large matrix of suspended particulate matters called aerosols. Interesting, only small particles below a particular size, can enter into the human lungs. Air pollution researchers are keenly interested in analyzing that particle size range to estimate the true health risk. Accordingly, they need to size specifically collect that particular size range through air sampling. The target size range particles are captured on a filter paper, and later it is analyzed through multiple instruments for detailed chemical compositions. Inertial impactors are based on impaction theory and useful due to their design simplicity and fairly good collection efficiency (Marple and Willeke, 1976; McFarland et al., 1978). Several impactors have been developed by researchers and are widely used for size-segregated aerosol collection (Marple et al., 1991; Furuuchi et al., 2010). Inertial impactors have an innate problem of particle bounce off which perturbed the inlet flow and incurs errors in the estimation. The theoretical calculation of particle collection efficiency does not hold good in actual in the presence of particle bounce off. Due to overloading and inefficient collection of larger particles at the impaction surface, newer larger particles start getting bounced off from the impaction surface and reenters into the flow. It happens when particle loading is high, or sampling is prolonged for a long duration (Turner and Hering, 1987). In this present research, we would like to present the design of an eccentric impactor which has less particle bounce-off in its group.

METHODS

The design depicts a simple way out to solve the problem of particle bounce-off in the inertial impactor. The cause of particle bounces off is found to have similarity with the problem associated with total load deposition in a single point. Providing new impaction location after has been decided and the possible way of better utilization of the impaction surface is explored. The impaction nozzle is made little eccentric and keeping other boundary conditions unaffected, the off centric nozzle is rotated with the help of spur gear mechanism while keeping the impaction plate fixed. Due to eccentricity, the nozzle finds a new location on the impaction plate when rotated. This is a simple mean in which the total non-target particle loading at one single center points for a longer duration, is instead distributed to 4 distinct off centric points around the center. With a 90-degree rotation of the nozzle plate, it forms four deposits on the impaction plate. In this research a PM_{2.5} impactor developed and tested in our laboratory before (Gupta et al., 2011) is considered for dimensions and the modification with eccentric impactor is improvised. The solution thus provided is generic and can be applied to other pm impactors of the similar kind.

RESULTS & DISCUSSIONS

The new PM sampler with eccentric nozzle (Fig. 1) comprises of the following parts: I) Air inlet cap and rain protection, II) Upper casing, III) Impaction nozzle, IV) Teflon bush, V) Impaction plate, VI) Impaction plate holder, VII) Wire mesh, VIII) Filter paper holder, IX) Base holder.

The new eccentric nozzle impaction sampler and a conventional impaction sampler were run in colocation for 4 hours. The flow rate for both the cases was set to be 15 LPM with the rotameter. After sampling the impactor plates of the two samplers were observed (Fig. 2). For the conventional sampler, a larger impaction spot was formed compared to the smaller four spots of the eccentric design. This qualifies a lesser particle bounce-off.

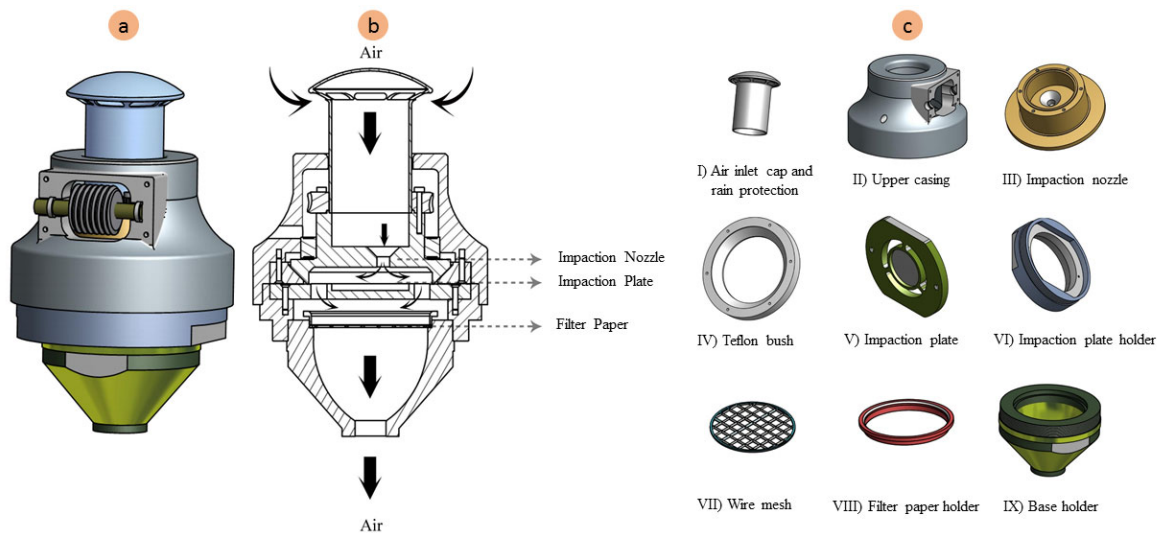


Figure 1: a) Eccentric Impactor PM sampler, b) Cross section of Eccentric Impactor PM sampler, c) Individual components of Eccentric Impactor PM sampler

After 4 hours of air sampling



Figure 2: Comparison of impaction surfaces of the conventional impactor and eccentric impactor after 4 hours of collocated sampling at 15 LPM.

CONCLUSIONS

Particle bounce off is a problem is a crucial problem in inertial impactors and promotes errors in particle collection. It can be understood that this problem was not in the impaction theory but the design of the impactor. In this novel eccentric impactor design, just by distributing the total load into four different points, particle bounce off is reduced. From the visual observation of the four smaller spots from the new impactor indicates less particle bounce-off. The solution is generic and can be applied to any single stage inertial impactor of the similar kind. The total number of impaction points and the time interval can also be altered as per contextual requirements.

ACKNOWLEDGMENTS

We are thankful to SIDBI, IIT Kanpur for filing an Indian patent application 201611022179 dated June 28, 2016, on this work.

REFERENCES

- Marple V. A. and Willeke K. (1976). Impactor design, *Atmospheric Environment* 10, 891-896.
- McFarland A. R., Ortiz CA., and Bertsch RWJ. (1978). Particle collection characteristics of a single-stage dichotomous sampler, *Environmental Science and Technology* 12, 679-682.
- Marple V.A., Rubow K. L., and Behm S. (1991). A micro orifice uniform deposit impactor (MOUDI): description, calibration and use, *Aerosol Science Technology* 14, 434-446
- Furuuchi M., Choosong. T, Hata M., Otani Y., Tekasakul P. and Takizawa M. (2010). Development of a personal sampler for evaluating exposure to ultrafine particles, *Aerosol and Air Quality Research*, 10(1), 30–37.
- Turner J. R., and Hering S. V. (1987). Greased and oiled substrates as bounce-free impaction surfaces, *Journal of Aerosol Science* 18(2), 215–224.
- Gupta T., Jaiprakash, and Dubey S., (2011). Field performance evaluation of a newly developed PM2.5 sampler at IIT Kanpur, *Science of the Total Environment*, 409(18), 3500–3507.

CARBONACEOUS AND MINERALOGICAL COMPOSITION OF AEROSOL DURING EL-NIÑO INFLUENCED INDIAN SUMMER MONSOON

PRADHI RAJEEV, PRASHANT RAJPUT AND TARUN GUPTA

¹Department of Civil Engineering, Indian Institute of Technology, Kanpur – 208016, India.

KEYWORDS: Indo-Gangetic Plain; Aerosol Composition, Sw-Monsoon, Mineral Dust.

INTRODUCTION

High particulate and organic matter concentration has been reported in Indo-Gangetic plain (IGP) especially during post-monsoon and wintertime (Dey et al., 2012). During SW-monsoon, generally significantly low particle concentration in troposphere has been reported due to high convective mixing and wet deposition due to rainfall. But in 2015, south-west monsoon was expected to be influenced by El Niño (Zhang et al., 1997) that leads to weaken the Indian summer monsoon (Krishnamurthy and Krishnamurthy, 2014). Thus, due to low moisture content in top soil and high wind speed, higher upliftment of mineral dust (coarse- and fine-mode) will occur (Dey and Tripathi, 2007). This enhancement of mineral aerosols in ambient levels will lead to multiple surface interactions of ambient pollutants. In this regard, we have assessed aerosol chemical characteristics in the IGP during SW-monsoon (July–September 2015).

METHODS

Kanpur (26.30 °N; 80.14 °E) is situated in central part of IGP was sampling site. Annual wet-precipitation was recorded to be ~375 mm (45% occurred during SW-monsoon) in year 2015 over the study region. Temperature and RH during sampling varied from 22.1–37.4 °C and 53–97%, respectively. PM_{2.5} samples onto quartz filters using a high volume air-sampler (flow-rate: 0.97 m³/min) (Kumar and Gupta, 2015). PM_{2.5} mass concentrations have been ascertained gravimetrically after equilibrating quartz filters at about 25 °C temperature and 40% RH. Water-soluble inorganic species (WSIS) have been measured using a dual channel ion-chromatograph (Metrohm) (Rajeev et al., 2016; Chakraborty and Gupta, 2010; Gupta and Mandaria, 2013). The measurement of HCO₃⁻ has been performed in all samples by titration with a 5 mM HCl solution using Methyl orange solution as pH indicator. Organic carbon (OC), elemental carbon (EC) and water-soluble organic carbon (WSOC) concentrations were determined using Sunset Lab EC-OC analyzer (NIOSH protocol) and TOC analyzer, respectively (Rajeev et al., 2018). Metal concentration of aerosol samples was measured using ICP-OES (Rajeev et al., 2018).

RESULTS AND DISCUSSION

CHEMICAL COMPOSITION OF PM_{2.5}

Large variation in PM_{2.5} concentration has been observed with average value of 42.2 (± 22.4) µg/m³. The total aerosol composition consist of 36.8% mineral dust (MD), 34.7% water soluble inorganic species (WSIS), 21.8% total carbonaceous aerosols (TCA) and 6.7% unidentified matter (UM). Figure1 shows the temporal variability of PM_{2.5} concentration and its constituent fractions. Total carbonaceous aerosol (TCA) and mineral dust (MD) has been estimated using TCA = OM + EC, where OM = 1.6*OC and Al as a proxy (Al = 8% of upper continental mineral dust), respectively (Turpin and Lim, 2001; McLennan, 2001). Mineral dust temporal variability is quite similar to that of PM_{2.5} and MD has highest contribution ~37% to aerosol loading due to high wind speed and less rainfall (influence of El-Niño) during this period. To differentiate aerosol composition of different air-masses, air mass back trajectories analysis for 7 days during aerosol sampling (500 m amsl) has been done. Air mass back trajectories (Stein et al., 2015) during this period shows long-range transport from Indian Ocean and traversing through Arabian Sea (marine) (Type 1), through Bay of Bengal (Type 2) and some terrestrial air masses (Type 3) arrives at the receptor site. Majority of air masses (Type 1) through west direction is associated with significantly large amount of mineral dust.

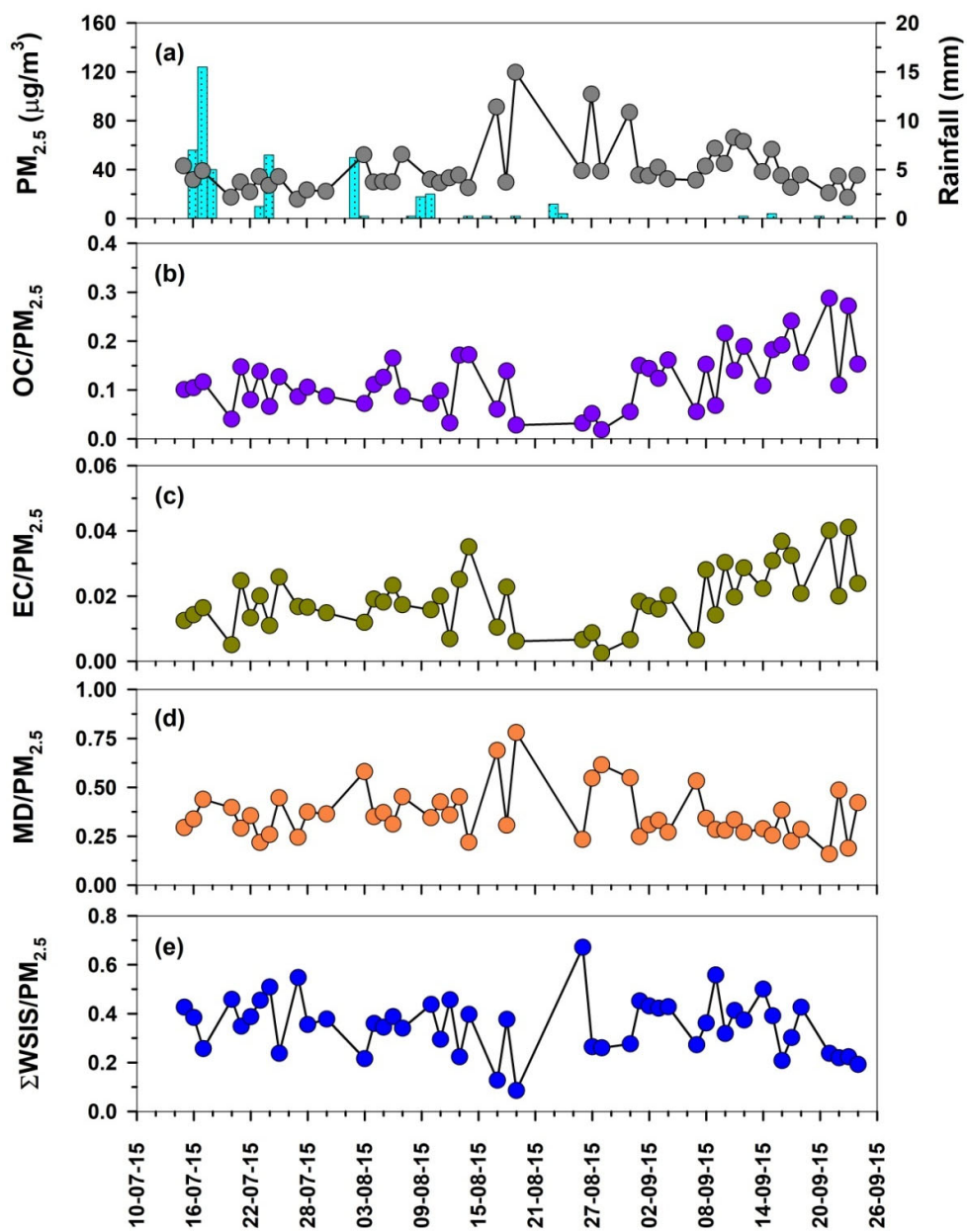


Figure 1. Mass closure and temporal variability of $PM_{2.5}$ and various fractions of $PM_{2.5}$ in the IGP (Kanpur) during monsoon period. *Blue vertical bar in (a) shows rainfall amount in mm during the entire period.

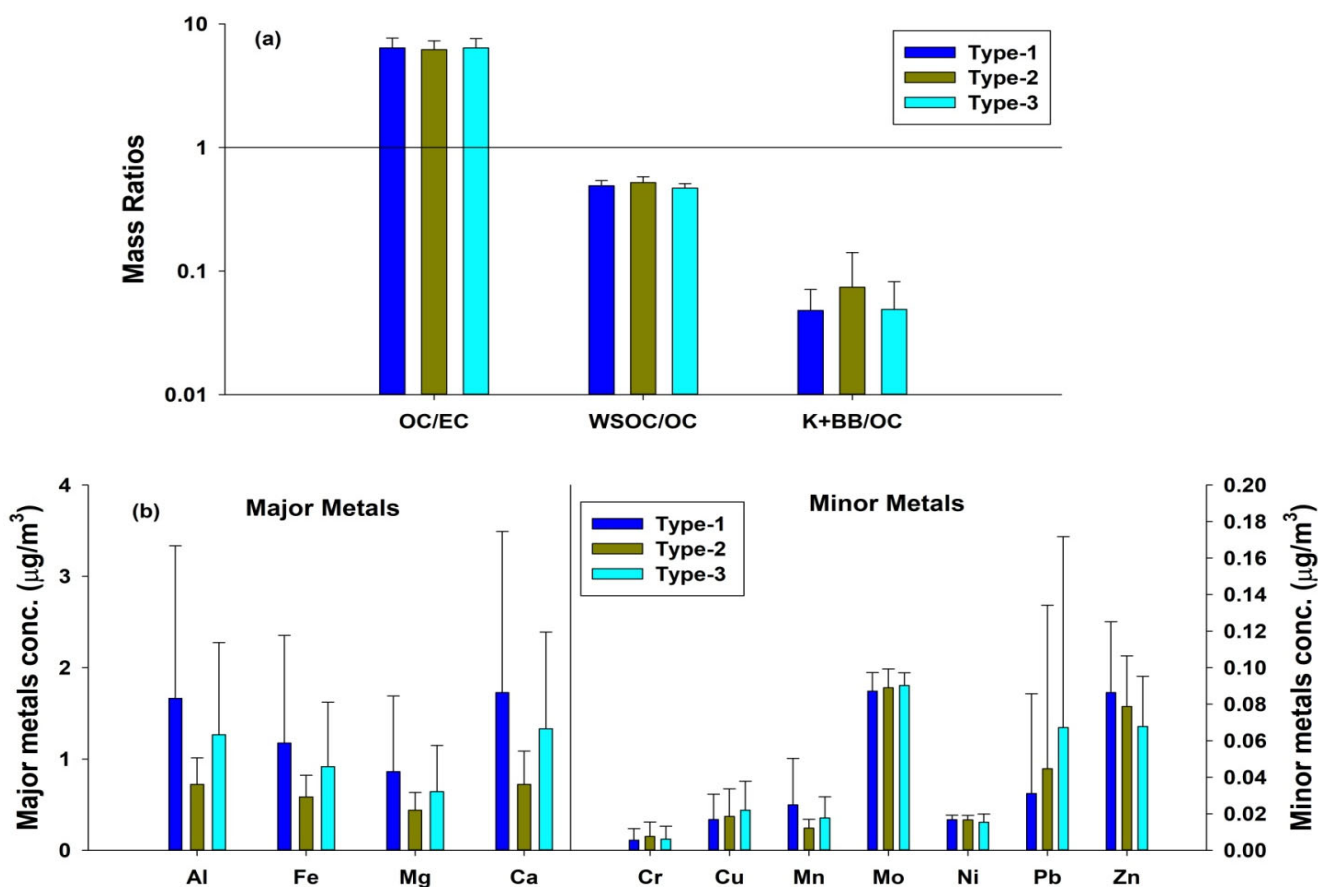


Figure 2. (a) Characteristic mass ratios – OC/EC, WSOC/OC and $\text{K}^+_{\text{BB}}/\text{OC}$ (b) concentration of major and minor metals present in aerosols in different air-masses arriving at the receptor site during SW-monsoon.

CHARACTERISTICS OF CARBONACEOUS AEROSOLS

Figure 2a shows the characteristic ratios OC/EC, WSOC/OC and $\text{K}^+_{\text{BB}}/\text{OC}$ of aerosol for three air-masses. There is no significant difference in mass ratios of OC/EC, WSOC/OC (exception being difference in Type-2 versus Type-3 air-mass) and $\text{K}^+_{\text{BB}}/\text{OC}$ of all three types of air-masses. Comparing these ratios with biomass burning and fossil fuel combustion characteristic ratios suggests well-mixed sources with dominance of biomass burning emissions at the site. Around 49% of the total OC is water-soluble (WSOC/OC ratio = 0.49 ± 0.05) suggesting significant emission from biomass burning emission or SOA formation. There is a significant difference in WSOC/OC ratio for Type-2 and Type-3 air-masses.

MINERALOGICAL COMPOSITION

Major (Al, Fe, Ca, Mg) and minor (Cr, Co, Mn, Mo, Ni, Pb, Zn) metal concentration in aerosols of different air-masses arriving at the receptor site during SW-monsoon has been shown in figure 2b. Since mineral aerosol constitutes about 37% of total aerosol loading, it is essential to understand the mineralogical composition of aerosol. Elemental ratios of crustal metals - Fe/Al, Ca/Al and Mg/Al are $0.73 (\pm 0.08)$, $1.02 (\pm 0.08)$ and $0.54 (\pm 0.10)$, respectively. In literature, these Fe/Al, Ca/Al and Mg/Al ratios have been reported as 0.44, 0.37 and 0.17, respectively for upper continental crust (McLennan, 2001) and for soil re-suspension (~ 0.9) (Engelbrecht et al., 2016). Thus it is evident that these metals are dominantly due to the upliftment of mineral dust. These ratios show significant difference in type-1 air mass as compared to other air-masses. Significant difference in mineral dust fraction of $\text{PM}_{2.5}$ in Type-1 and Type-2 air-masses and in their characteristic Fe/Al ratio has been observed. These indicate transport of mineral dust from Thar Desert.

CONCLUSIONS

We have assessed the aerosol composition during an El-Niño influenced Indian summer monsoon. Water-soluble inorganic species, organic carbon, elemental carbon, water-soluble organic carbon and metals has been studied in aerosols. Higher

contribution of mineral dust in $PM_{2.5}$ has been observed which is attributed to the El-Niño impact on Indian summer monsoon. Carbonaceous and mineral dust characteristics have been assessed utilizing characteristic and elemental ratios of aerosol.

ACKNOWLEDGEMENTS

This study has been carried out by utilizing internal funds from IIT Kanpur.

REFERENCES

- Dey, S., L. D. Girolamo, A. V. Donkelaar, S.N. Tripathi, T. Gupta and M. Mohan (2012), Variability of outdoor fine particulate ($PM_{2.5}$) concentration in the Indian Subcontinent: A remote sensing approach. *Remote Sensing of Environment*, 127, 153–161.
- Zhang, Y., J.M. Wallace and D.S. Battisti, (1997), ENSO-like Inter decadal Variability: 1900-93, *Journal of Climate*, 10, 1004-1020.
- Krishnamurthy, L. and V. Krishnamurthy, (2014), Influence of PDO on South Asian summer monsoon and monsoon-ENSO relation, *Clim. Dyn.*, 42, 2397-2410.
- Dey, S. and S.N. Tripathi, (2007), Estimation of aerosol optical properties and radiative effects in the Ganga basin, northern India, during the wintertime, *J. Geophys. Res.* 112, D03203.
- Kumar, A. and T. Gupta, (2015), Development and laboratory performance evaluation of a variable configuration $PM_1/PM_{2.5}$ impaction-based sampler, *Aerosol and Air Quality Research* 15, 768-75.
- Chakraborty, A. and T. Gupta, (2010), Chemical Characterization and Source Apportionment of Submicron (PM_1) Aerosol in Kanpur Region, *Aerosol and Air Quality Research* 10, 433-445.
- Gupta, T. and A. Mandaria, (2013), Sources of Submicron Aerosol during Fog Dominated Wintertime at Kanpur, *Environmental Science and Pollution Research* DOI: 10.1007/s11356-11013-11580-11356.
- Rajeev, P., Rajput, P., Gupta, T., 2016. Chemical characteristics of aerosol and rain water during an El-Niño and PDO influenced Indian summer monsoon. *Atm. Environ.*, 145, 192-200.
- Rajeev, P., Rajput, P., Singh, A.K., Gupta, T., 2018. Study of temporal variability and mass closure of $PM_{2.5}$ and its chemical constituents during weak south-west monsoon. *Atm. Poll. Res.*, 9, 864-870.
- Turpin, B.J., Lim, H.J., 2001. Species contributions to $PM_{2.5}$ mass concentrations: revisiting common assumptions for estimating organic mass. *Aerosol. Sci. Technol.* 35, 602–610.
- McLennan, S.M., 2001. Relationships between the trace element composition of sedimentary rocks and upper continental crust. *G-cubed* 2.
- Stein, A.F., Draxler, R.R., Rolph, G.D., Stunder, B.J.B., Cohen, M.D., Ngan, F., 2015. NOAA's HYSPLIT atmospheric transport and dispersion modeling system. *Bull. Am. Meteorol. Soc.* 96 (12), 2059–2077.
- Engelbrecht, J.P., Moosmüller, H., Pincock, S., Jayanty, R.K.M., Lersch, T., Casuccio, G., 2016. Technical note: mineralogical, chemical, morphological, and optical interrelationships of mineral dust re-suspensions. *Atmos. Chem. Phys.* 16 (17), 10809–10830.

INFLUENCE OF COOKING FUEL ON PM_{2.5} BOUND PAHs EMISSION AND ASSOCIATED HEALTH RISK

DEEPSHIKHA OLA¹, SAURABH KUMAR¹, ANUBHA GOEL^{1,2}, DIVYAM GARG¹

¹Department of Civil Engineering, Indian Institute of Technology, Kanpur – 208016, India.

²APTL, Centre for Environmental Science and Engineering CESE, IIT Kanpur, Kanpur – 208016 (UP), India

KEYWORDS: PPAHs, Biomass, LPG, Carcinogenic, B[a]P, ILCR.

INTRODUCTION

Use of solid fuels, biomass, and coal, for cooking purposes and heating homes, is practiced by around 3 billion people, primarily by people in developing countries with low and medium resources. Fang et al., (1999) reported that 2.7% of the global burden of disease is attributable to indoor air pollution. Poorly ventilated homes can have concentrations of respirable particles, from indoor smoke, 100 times the acceptable levels (Hetland et al., 2000) causing extremely high levels of exposure for mostly women and young children. Particle-bound Polycyclic Aromatic Hydrocarbons (PPAHs) found in indoor air are one of the significant health concerns for the public due to their carcinogenic nature (Xue and Warshawsky, 2005). Benzo(a)pyrene (BaP) has been classified by IARC as the most carcinogenic and positively genotoxic PAH due to its toxic effects on various cells and tissues, and other body systems of animals (Food Safety Authority of Ireland, 2009). The total concentrations of PAHs recorded in the residential air in Hangzhou, China (Zhu et al., 2009) ranged from 425 to 36,200 ng m⁻³, with the highest concentrations noted in the kitchens.

The objective of this study is to determine the difference in the levels of PM_{2.5} bound total and carcinogenic PAHs from cooking practice using biomass and LPG as fuel. Finally estimating the cancer risk attributable to the inhalation of PPAHs along with seasonal variation for the four cases (LPG- Winter and Autumn; Biomass- Winter and Summer) has been attempted.

METHODS

Data Collection: An extensive literature review was carried out to ascertain the air quality data availability for two different domestic fuel used for cooking. The concentration profiles of PAHs bound to PM_{2.5} from the literature was extracted from China for different seasons.

Description of studies from China for different fuel type:

Biomass burning: A traditional rural biomass cook stove in the kitchen (Ding et al., 2012) was used for cooking and a chimney was used for ventilation. 24 hr sampling was conducted using PM_{2.5} sampler for four days in winter (W, Jan 2010) and three days in summer (S, Jun 2010). A meal was cooked three times a day, and no one smoked in the household.

LPG: The house selected was one story consisting of a kitchen and living area where ventilation in the kitchens was generally based on the natural draft (Wu et al., 2015). A low volume stationary PM_{2.5} sampler was used for sampling for nine consecutive days during autumn (A, Sep to Oct 2012) and winter (W, Jan 2013).

Selected Analytes

The 16 PAHs focused in this study are listed in the priority list of list of pollutants by US-EPA including carcinogenic (B[a]P, B[b]F, B[k]F, Chr, IP, D[ah]A and B[a]A) and non-carcinogenic PAHs (Nap, AcPy, Ant, B[ghi]P, Flu, FL, PA, Acp, and Pyr).

Health Risk Assessment

B[a]P equivalent concentration (B[a]P-TEQ)

BaP-TEQ is calculated by multiplying the concentrations of each PAH compound with its TEF or PEF for cancer potency relative to B[a]P (Nisbet and LaGoy, 1992). B[a]P_{eq} levels for respective cooking fuel type were calculated as follows:

$$B[a]P_{eq} = \sum Conci \times TEQi \quad (1)$$

Where, $Conc_i$ is the concentration and TEF_i toxic equivalency factor for the 16 priority PAHs.

Incremental Lifetime Cancer Risk (ILCR)

Linear dose carcinogenic risk equation was used to calculate the risk through inhalation as the exposure route for a person of an age group from 20 to 60 years.

$$ILCR = LADD \times CSF \quad (2)$$

$$LADD = (C \times IR \times RT \times VF \times ED \times cf) \div (BW \times AT_c) \quad (3)$$

Where, LADD is the lifetime average daily intake dose ($mg\ kg^{-1}\ d^{-1}$), and CSF is the cancer slope factor ($mg\ kg^{-1}\ d^{-1}$)⁻¹ for exposure due to inhalation route, cf is the conversion factor, AT_c is the averaging time for carcinogens (d), RT is the residence time, VF is visiting frequency, ED is exposure duration (y) and IR and BW are inhalation rate and body for respective age group.

RESULTS & DISCUSSIONS

Concentration profile of PPAHs from two domestic fuels

The seasonal variation of 16 US-EPA listed priority PAHs bounded to PM_{2.5} was quite significant in the case of biomass burning. The daily mean concentration of PPAHs was greater from biomass emission than LPG emission and higher values were seen in winter in both studies. Similarly, non-carcinogenic PAHs were found to occur in higher concentration in case of biomass for the four cases (2 from each study). The same trend in concentration was not observed for carcinogenic PAHs. The carcinogenic concentration was observed to be less than 50% of the total PAHs from biomass emission while it was more than 60% of the total PAHs emission from LPG burning.

HUMAN HEALTH RISK ASSESSMENT

Carcinogenic Toxic Equivalent (B[a]P-TEQ)

Both, total and carcinogenic, concentrations were exceptionally high in winter from biomass emission, and so was the equivalent carcinogenic concentration (Figure 1 & Figure 2). B[a]P and D[ah]A together contributed the highest in B[a]P_{eq} concentration for LPG emission in both the seasons; 78% in winter and 83% in autumn, respectively. In the case of emission from biomass burning B[a]P alone contributed more than 65% in the two seasons.

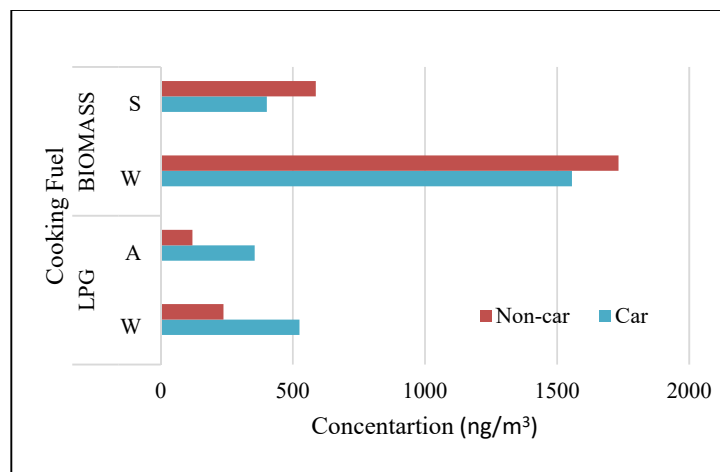


Figure 1. PM_{2.5} bound carcinogenic and non-carcinogenic PAHs emission from two types of cooking fuel

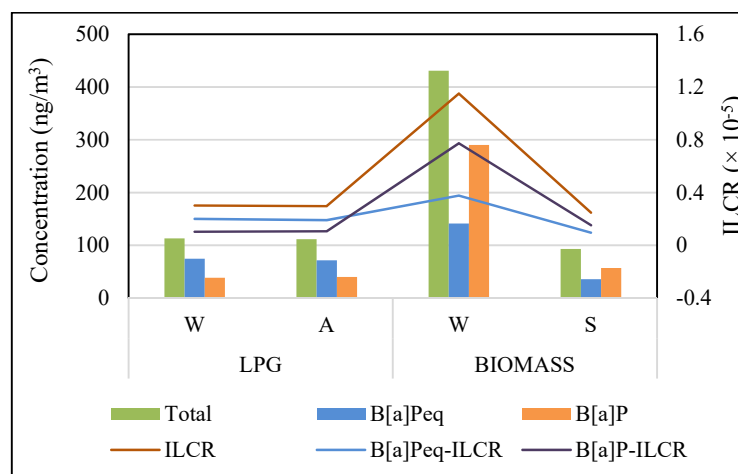


Figure 2. B[a]P_{eq} concentration and corresponding cancer risk

Incremental lifetime cancer risk

The lifetime cancer risk was calculated for a person exposed to the PAHs from the two type of domestic fuel in different seasons. The 50th & 90th percentile LADD for B[a]P_{eq} was in the order of 10⁻⁶ & 10⁻⁷ from inhalation as the exposure route (Table 2). Figure 2 provides with the particular relation between the carcinogenic- and non-carcinogenic- B[a]P_{eq} concentration and the corresponding cancer risk. Except for the risk associated with biomass in winter season, the risk is above 10⁻⁶ which is above the US EPA acceptable limit of 10⁻⁶ for the inhalation as the sole mode of exposure route. The risk associated with inhalation is above 10⁻⁵ for biomass emissions in winter indicating the health risk is significant.

Domestic fuel	Lifetime average daily dose through inhalation (mg kg ⁻¹ day ⁻¹)	
	50 th percentile	95 th percentile
LPG		
Winter	1.00 × 10 ⁻⁰⁶	1.436 × 10 ⁻⁰⁶
Autumn	9.354 × 10 ⁻⁰⁷	1.267 × 10 ⁻⁰⁶
Biomass		
Winter	3.398 × 10 ⁻⁰⁶	4.254 × 10 ⁻⁰⁶
Summer	7.779 × 10 ⁻⁰⁷	1.051 × 10 ⁻⁰⁶

Table 1. Lifetime average daily inhalation intake from Biomass and LPG emission

CONCLUSIONS

The contribution of carcinogenic PAHs to the total PM_{2.5} bound PAHs is significant outlining the health risks due to exposure. Contribution of carcinogens was > 50% for emission from LPG reaching up to 75% in the autumn season while it was 47% in the winter season. The incremental lifetime cancer risk due to exposure to LPG emission in winter and autumn seasons, ~3.0 × 10⁻⁶, is higher than the risk estimated, in summer season due to emissions from biomass burning (2.476 × 10⁻⁶). Recently, cleaner fuel like LPG and electricity are becoming more popular for cooking as well as heating purposes. High levels of carcinogenic PAHs in LPG leading to higher cancer risks confirms that we cannot make an obvious remark that LPG, which is known as a cleaner fuel, is less harmful.

The parameters considered for risk calculation are kept the same for both the fuel type thus B[a]Peq is what plays an important and crucial role in determining the cancer risk. The cancer risk estimated here is an understatement as the risk is because of inhalation only. If other exposure routes like dermal and ingestion were to be considered, the cancer risk is likely to be higher.

REFERENCES

- Ding J., Zhong J., Yang Y., Li B., Shen G., Su Y., Wang C., Li W., Shen H., Wang B., Wang R., Huang Y., Zhang Y., Cao H., Zhu Y., Simonich L.M. S., Tao S. (2012). *Environmental Pollution*. 169, 160-166.
- Fang L., Wargocki P., and Witterseh T. (1999). 8th International Conference on Indoor Air Quality and Climate - Indoor Air'99 (Edinburgh), Vol. 2, 107.
- Food Safety Authority of Ireland (2009). Toxicology factsheet series.
- Hetland, R.B., Refsnes, M., Myran, T., Johansen, B.V., Uthus, N., and Schwarze, P.E. (2000). *J. of Toxicology and Environmental Health-Part A* 60, 47-65.
- Nisbet, I.C.T. and LaGoy, P.K., 1992. *Regulatory Toxicological Pharmacology*. 16, 290–300.
- Wu F., Wang W.,; Man Y. B., Chan C.Y., Liu W., Tao S., Wong M.H. (2015). *Science of Total Environment*. 512-513, 194.
- Xue, W. and Warshawsky D. S. (2005). *Toxicology and applied pharmacology* 206 (1), 73.
- Zhu, L.Z., Lu, H., Chen, S.G., and Amagai, T. (2009). *J. Hazardous Material*, 162, 1165–1170.

CHARACTERIZATION OF AMBIENT AEROSOLS AND THEIR SOURCES THROUGH CARBON STABLE ISOTOPE MEASUREMENTS

GYANESH KUMAR SINGH¹, PRASHANT RAJPUT¹, DEBAJYOTI PAUL² AND TARUN GUPTA¹

¹Department of Civil Engineering and APTL at Center for Environmental Science and Engineering (CESE), IIT Kanpur, Kanpur- 208 016, India

²Department of Earth Sciences, IIT Kanpur, Kanpur- 208 016, India

KEYWORDS: Particulate Matter, Stable Isotope, Wsoc, Pollutants.

INTRODUCTION

A wide variety of natural as well as anthropogenic sources contribute to atmospheric aerosol loading (Putaud et al., 2010). An adverse impact on human health is caused due to high concentration of fine particles (Dockery et al., 1993). Major anthropogenic sources of aerosols include biomass burning, industrial emissions and fossil-fuel combustion. Coarser particles have lesser residence time as compared to fine aerosols. A dominant fraction of atmospheric fine-particles is constituted by organic matter (OM) and elemental carbon (EC). Atmospheric transformation creates complexity in characterization of emission sources of carbonaceous aerosols (Garbaras et al., 2008). For characterization of the sources of pollutants, determining their proportional inputs and understanding processes in an ecosystem stable isotope are utilized (Singh et al., 2018). Aerosol particulate matter are characterized by high precision stable isotope ratio measurements. Both compound specific as well as bulk analysis of stable isotope have been found useful in this regard (Hoefs, 1997; Flanagan, 2005). Processes related to aerosol ageing can also be understood using stable isotope ratio measurements such as carbon and nitrogen (Rudolf, 2007; Wang and Kawamura, 2006). Chemical composition in conjunction with isotope analysis can provide significant information to chemical transformation and characterization of carbonaceous aerosols.

METHODS

Aerosol (PM_{2.5}) samples were collected on pre-combusted 47 mm diameter quartz-fiber filters at the roof top of CESE building, IIT Kanpur. Samples were collected by an air-sampler working at a flow-rate of 15 L/min. The samples were stored at -19 °C until chemical and isotopic analysis. Sampling was conducted during winter season in the month of December. For stable isotope determination, appropriate filter size based on mass to signal ratio was taken, placed into pre-cleaned tin cup and closed, then inserted into an elemental analyzer (Flash EA 2000, Thermo Scientific) using an auto sampler. Continuous flow isotope ratio mass spectrometer (EA-IRMS) has been utilized for stable isotopic measurements in aerosol samples. Stable isotope ratio mass spectrometer (Thermo Scientific Delta V Plus) is coupled with elemental analyzer and conflo IV universal interface for measurements. This facility is located in the Advanced Centre for Material Science (ACMS) lab, IIT Kanpur. For the determination of water-soluble organic carbon (WSOC), total organic carbon analyzer (TOC Shimadzu) using a non-dispersive infrared detection (NDIR) technique was used.

RESULTS & DISCUSSIONS

Temporal variability of $\delta^{13}\text{C}$ values in atmospheric aerosols has been shown in Figure 1. $\delta^{13}\text{C}$ of the TC varied between ~ -26.2 to -24.5% in aerosol samples. Due to mixed sources such as coal combustion (-24.9 to -21%) (Widory 2006; Gleason and Kyser 1984), C3 plants (-20 to -32%) (Smith and Epstein 1971) and C4 plants (-6 to -19%) (Deines 1980), vehicle exhaust (-28 to -26%) (Widory 2006), and biomass/bio-fuel combustion emissions (-29.4 to -25.9%) (Agnihotri et al. 2011) the $\delta^{13}\text{C}$ values of ambient aerosols can be variable. The carbon isotope ratio variations obtained on different sampling events signifies the dominance of diverse sources. As for example, when coal combustion was dominant the values tended to be more on the enriched side (i.e. nearer to -24%). As, Kanpur in the IGP is located far away from the ocean consequently the prominent sources of carbonaceous aerosols can be biomass and fossil-fuel combustion, secondary formation and/or biogenic emissions. Enrichment in the ^{13}C of the TC was observed with increment in the carbon content. WSOC which is enriched in ^{13}C influences the $\delta^{13}\text{C}$ of TC as seen in the previous study (Fisseha et al. 2009). An increase in $\delta^{13}\text{C}$ can be caused due to higher fraction of WSOC and vice-versa but further studies would be required to confirm the same. Impact of secondary organic aerosol formation and aging during long range transport of aerosols can be dominant factor for the observed variability of $\delta^{13}\text{C}$ in PM_{2.5}. Also, $\delta^{13}\text{C}$ of the black carbon (BC) does not change significantly from source on transport of aerosols.

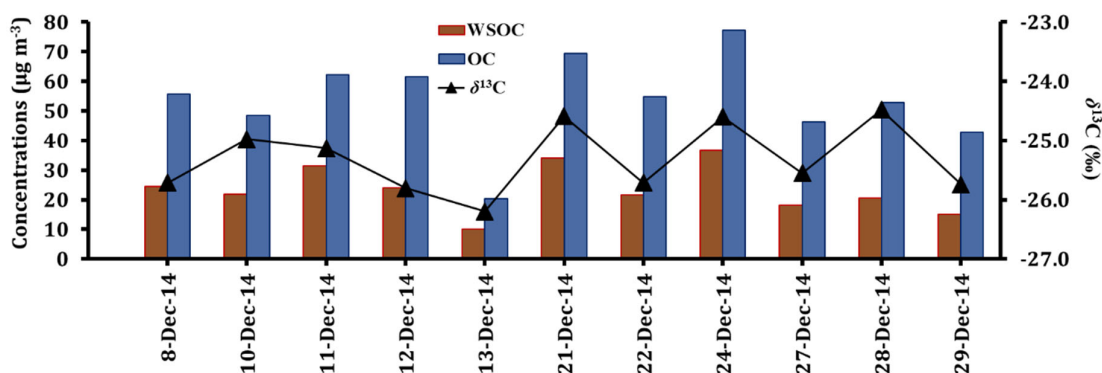


Figure 1. Temporal variation of $\delta^{13}\text{C}$, WSOC and OC.

The $\delta^{13}\text{C}$ of various sources assessed in this study are given in table 1. The $\delta^{13}\text{C}$ of coal from a power plant (at Panki), showed average value of $-23.1 \pm 0.9\text{‰}$ ($n = 11$). $\delta^{13}\text{C}$ of gasoline (petrol), diesel and bio-diesel exhaust PM samples (at 100% load) showed values of $-26.1 \pm 0.01\text{‰}$ ($n = 6$), $-26.3 \pm 0.2\text{‰}$ ($n = 3$) and $-26.5 \pm 0.1\text{‰}$ ($n=4$) respectively. The $\delta^{13}\text{C}$ of paddy ranged was found to be $-29.9 \pm 0.1\text{‰}$ ($n=3$) which is a major source of carbonaceous aerosols in IGP. These source-specific $\delta^{13}\text{C}$ values for local emissions has been done first time for this region.

Fuels	$\delta^{13}\text{C}$ (vs V-PDB)
Petrol (Gasoline)	$-26.1 \pm 0.01\text{‰}$ ($n=6$)
Bio-Diesel	$-26.5 \pm 0.1\text{‰}$ ($n=4$)
Diesel	$-26.3 \pm 0.2\text{‰}$ ($n=3$)
Coal	$-23.1 \pm 0.9\text{‰}$ ($n=11$)
Paddy	$-29.9 \pm 0.1\text{‰}$ ($n=3$)

Table 1. Characterization of fuels.

CONCLUSIONS

This study presents temporal variability of $\delta^{13}\text{C}$ values of $\text{PM}_{2.5}$ aerosols along with WSOC and OC for Kanpur city which is located in central IGP. An increase in $\delta^{13}\text{C}$ with increase in WSOC was observed in this study suggests the dominance of secondary aerosol formation and/or aging along with other sources of ambient PM. The $\delta^{13}\text{C}$ value of various source samples have also been recognized in this study which assists in characterization of fuels as well as aerosols.

ACKNOWLEDGEMENTS

This work was supported by the financial support from Indian Institute of Technology Kanpur (India).

REFERENCES

- Agnihotri R, Mandal TK, Karapurkar SG, Naja M, Gadi R, Ahammed YN, Kumar A, Saud T and Saxena M (2011) Stable carbon and nitrogen isotopic composition of bulk aerosols over India and northern Indian Ocean. *Atmospheric Environment* **45(17)**: 2828-2835
- Deines, P. (1980). "The isotopic composition of reduced organic carbon." *Handbook of environmental isotope geochemistry*: 329-406.
- Dockery, D. W., C. A. Pope, X. Xu, J. D. Spengler, J. H. Ware, M. E. Fay, B. G. J. Ferris and F. E. Speizer (1993). "An Association between Air Pollution and Mortality in Six U.S. Cities." *New England Journal of Medicine* **329(24)**: 1753-1759

- Fisseha R, Saurer M, Jäggi M, Siegwolf RT, Dommen J, Szidat S, Samburova V and Baltensperger U (2009) Determination of primary and secondary sources of organic acids and carbonaceous aerosols using stable carbon isotopes. *Atmospheric Environment* **43(2)**: 431-437
- Flanagan, L. B. (2005). 1 - Introduction: Stable Isotopes and Earth System Science. *Stable Isotopes and Biosphere Atmosphere Interactions*. San Diego, Academic Press: 1-5.
- Garbaras, A. (2008). "Tracing of atmospheric aerosol sources using stable carbon isotopes." *Lithuanian Journal of Physics and Technical Sciences* **48**: 259-264.
- Gleason JD and Kyser TK, (1984) Stable isotope compositions of gases and vegetation near naturally burning coal. *Nature*, **307(5948)**, pp 254-257
- Hoefs, J. and J. Hoefs (1997). *Stable isotope geochemistry*, Springer.
- Putaud, J.-P., R. Van Dingenen, A. Alastuey, H. Bauer, W. Birmili, J. Cyrys, H. Flentje, S. Fuzzi, R. Gehrig and H.-C. Hansson (2010). "A European aerosol phenomenology–3: Physical and chemical characteristics of particulate matter from 60 rural, urban, and kerbside sites across Europe." *Atmospheric Environment* **44(10)**: 1308-1320.
- Rudolph, J. (2007). Gas Chromatography–Isotope Ratio Mass Spectrometry. *Volatile Organic Compounds in the Atmosphere*, Blackwell Publishing Ltd: 388-466.
- Singh, D. K. and T. Gupta (2016). "Role of transition metals with water soluble organic carbon in the formation of secondary organic aerosol and metallo-organics in PM1 sampled during post monsoon and pre-winter time." *Journal of Aerosol Science* **94**: 56-69.
- Singh, G.K., Paul, D., Rajput, P. and Gupta, T., 2018. Stable Carbon Isotope and Bulk Composition of Wintertime Aerosols from Kanpur. In *Environmental Contaminants* (pp. **209-220**). Springer, Singapore.
- Smith BN and Epstein S (1971) Two categories of $^{13}\text{C}/^{12}\text{C}$ ratios for higher plants. *Plant physiology* **47(3)**: 380-384
- Wang, H. and K. Kawamura (2006). "Stable carbon isotopic composition of low-molecular-weight dicarboxylic acids and ketoacids in remote marine aerosols." *Journal of Geophysical Research: Atmospheres* **111(D7)**.
- Widory D (2006) Combustibles, fuels and their combustion products: A view through carbon isotopes. *Combustion Theory and Modelling* **10(5)**: 831-841

COMPARISON OF INDOOR AND OUTDOOR BIOAEROSOL CONCENTRATION AND COMPOSITION AT INDO GANGETIC PLAINS AND THEIR EFFECT ON HUMAN HEALTH VIVEK SRIVASTAVA

VIVEK SRIVASTAVA¹, AMAN D. GUPTA² DR. TARUN GUPTA³

^{1,2,3}Environmental Engineering, Department of Civil Engineering, Indian Institute of Technology Kanpur, Kalyanpur, Kanpur – 208016, India.

KEYWORDS: Morphological study, bacterial composition, health consequences of bioaerosol, Biochemical tests for species identification and differentiation.

INTRODUCTION

Bioaerosol constitutes a small fraction of the total aerosol contents of atmosphere which mainly comprises of bacteria, fungal spores, virus, yeast and bacterial debris but its health effects are not in correspondence with their fraction in ambient air and its ability to acts as potential hazard for human health can't be ignored. (Miyakawa et al., 2015; Pöschl et al., 2010; Prussin et al., 2015). Constituents of bioaerosol serve as a good substrate for ice nucleation as well as cloud condensation nucleation. (Fröhlich-Nowoisky et al., 2016; Hawkes et al., 2011). Around 30% of the total aerosol load in ambient air is from bioaerosol (particles whose size < 0.2 µm) which can constitute bacteria (gram positive, gram negative, actinomycetes), virus, fungi and similar products (Faridi et al., 2015, DMU-FOLU et al. 2004). Humans usually remain exposed to them and can easily get infected through dermal contact, ingestion and inhalation and can cause many other detrimental health effects. (Abdel Hameed et al. 2009; Nasir et al. 2012) The most concerned are the particles which are capable of affecting the human health are bacteria and fungi. (Faridi et al., 2015, Mentese et al. 2009, 2012b; Pastuszka et al. 2000) Ambient air pollution has taken a toll of around 3 million lives in 2012 and major fraction of these were from low to middle income group countries (LMIGC) which carries in themselves more than 80% of the global population. (Ambient Air Pollution: a global assessment of exposure and burden of disease, WHO,

2016)

METHODS

Meteorological parameters like temperature and relative humidity (measured with HTC-1 Hygrometer and Temperature Scale), rainfall (Weather-risk.com) etc. are proved to play a significant role in exaggerating or downgrading the concentration as well as predominance of certain bacterial presence in PM10 which is monitored and recorded through PALAS WELAS 2000 Series, an online monitoring instrument for ambient air quality determination and an Indigenous Single Stage Impact Air Sampler (PM10) was used to collect distinctly the Gram Positive, Gram Negative and Fungal Spores on 35mm sterilized disposable Petri dishes containing different agar that can act as selective as well as differential Meteorological parameters like temperature and relative humidity (measured with HTC-1 Hygrometer and Temperature medium for identification purpose. The ambient air was made to impact on the agar containing Petri dish for 3 minutes at the flow rate of 12 LPM (Rajput, Anjum & Gupta, 2017). The typical colonies formed after incubation at 37±0.5°C and 10% CO₂ were used to form pure culture using sterilized Platinum or Nickel loops and their colony morphology was studied and then they were first subjected to six differential staining viz. Simple, Negative, Gram, Acid fast, Capsule, Endospore formation and wet mount. (Rajput, 2017) (Eduarda & Heederik, 1998) The stained smears were observed under bright field microscope (Nikon Eclipse 2000) with 1000X zoom to get an approximate precursor required for presumptions of the bacterial genera. Then the required biochemicals such as Catalase; Oxidase; lactose; sucrose or glucose fermenting; aerobic, anaerobic, aero-tolerant or facultative; comparison of the colonies formed on selective and differential agar medium like Brain Heart Infusion Agar, Triple Sugar Iron Agar, XLD agar, Pseudomonas agar, Salmonella and Shigella agar, Simon's Citrate Agar, EMB agar, SIM medium test, MR-VP test, Mannitol Salt Agar, MacConkey Agar etc. were used to get our bacterial genera assured and then some further test were done to narrow down the investigation to the species level

RESULTS & DISCUSSIONS

The number concentration during intermediate warm months of March, April and May and then again showed a hike during monsoon season (Jun-Jul-Aug) particularly its affect lasts for the upcoming first fortnight after the fall. The Post-Monsoon data collection and sampling is under progress. The higher figures during the winters can be attributed to the higher mean relative humidity during winters that leads to denser aerosol which also corresponds positively with the number of patients with asthmatic attack reported during that duration to the nearest medical facilities. The bacteriological count had also diminished as compared to that reported in the winters as the temperature in the summers ($42 \pm 4^{\circ}\text{C}$) was quite high as compared to the $22\text{-}35^{\circ}\text{C}$ being taken as the range of optimum growth for the bacteria. Cladosporium was found to be the most abundant mould constituting 47% of the total viable colonies with aspergillus at the second with 21%, Penicillium with 18% and the other important genera like Rhizopus, Helminthosporum and Mucor at CESE Courtyard and WL Backyard where plenty and variety of vegetation is available.

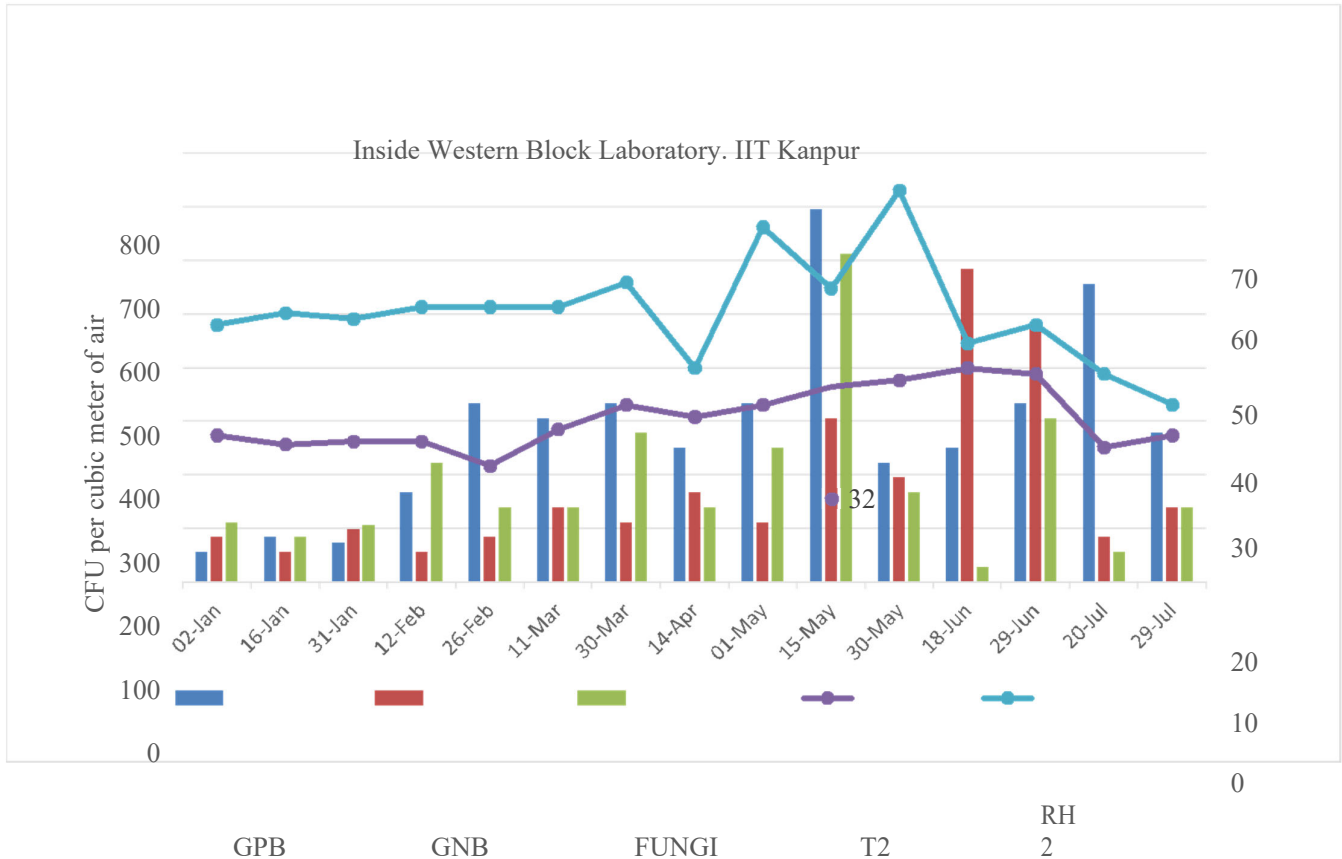


Figure 2. Shows the variation in viable bioaerosol count on Mannitol Salt Agar (MSA), MacConkey Agar (MAC) and Sabouraud Chloramphenicol Agar (SCA) in CFU/m³ as per the changes in relative humidity: Rh (in %) and temperature: T (in °C) inside Atmospheric Particles Technology Laboratory (APTL in), inside Western Block Laboratories and inside residential house at city side.

Medical data was collected from Health Centre, IIT Kanpur, the central medical facility provided to all the IIT residents and also from Sub-Divisional Railway Hospital, LOCO Colony, Kanpur, a Government Public hospital at the Central Kanpur, nearest to our sampling site at city side where >96% of the resident dwelling within 1km radius reported for any kind of medical issues.

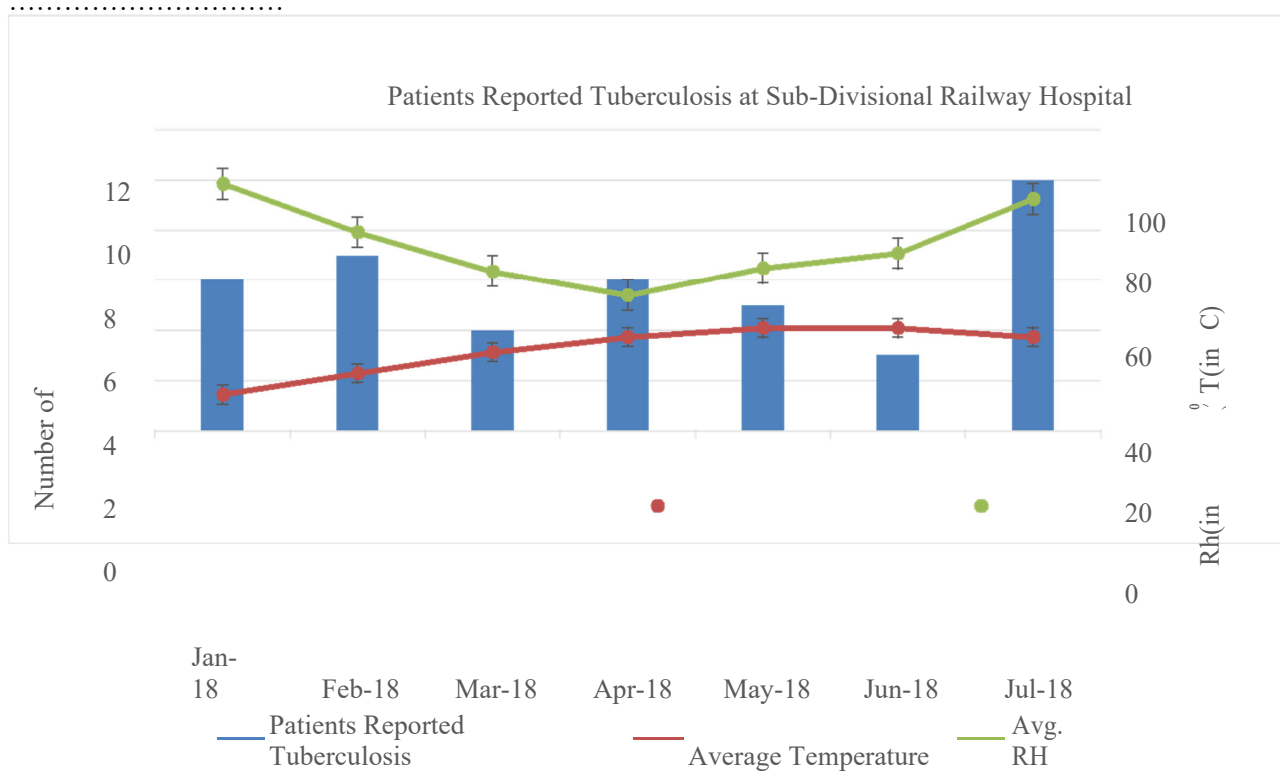


Figure 3. (a) Shows the number of patients reported at Sub-Divisional Railway hospital during various months of study. (b) shows the number of patients reported chest or respiratory disease as a fraction of the total number of patients reported in various months.

CONCLUSIONS

The pollution level in terms of Bioaerosol concentration constituting GPB,GNB and Fungal spores at city side is much greater than that at the IITK situated at the outskirts of the city when outdoor ambient environment is taken into account but enumeration of fungal spores were almost same when indoor micro environ were considered although the GPB and GNB concentration were higher at city side through entire period of our study with the difference being exaggerated during the monsoonal fall owing to the good sanitation at Institute, absence of stray animal and thus the faecal waste generated by them was minimal, no stagnant water body is there in the ~1045 acres campus of IIT Kanpur also lessen the potential sources of fungal spores generation and dwelling. The lesser fraction of bacteria confirmed on the cell cultures were pathogenic as *Escherichia coli*, *Staphylococcus epidermidis*, *Staphylococcus pyogenes*, *Proteus mirabilis* etc. as compared to that found at city side *Staphylococcus aerogenes*, *Staphylococcus aureus*, *Bacillus subtilis*, *Klebsiella Pneumoniae* *Mycobacterium tuberculosis* and *Sarcina spp.* other than those found at institute owing to the mismanaged dumping of waste by the residents, spreading of organic waste like faecal waste, domestic garbage and dead bodies of stray animals leads to increased accumulation of the SPM in the ambient air. The mold concentration present indoor was found quite different and varying than that of outdoor. The main fungal genera found during the study both indoor and outdoor were *Aspergillus*, *Alternaria*, *Cladosporium* and *Fusarium* which constitutes ~70% of the total CFU enumerated round the study.

	Avg. T	Avg. RH	GPB IN	GNB IN	FUNGAL SPORES IN	GPB OUT	GNB OUT	FUNGAL SPORES OUT	Patients Reported Tuberculosis	Patients Reported to Hospital	Patients with Chest Problems	Patients with Asthma
Avg. T	1											
Avg. RH	-0.84	1										
GPB IN	0.83	-0.82	1									
GNB IN	0.68	-0.23	0.53	1								
FUNGAL SPORES IN	0.60	-0.31	0.54	0.91	1							
GPB OUT	0.40	-0.73	0.77	0.03	0.28	1						
GNB OUT	0.68	-0.67	0.28	0.10	-0.02	0.00	1					
FUNGAL SPORES OUT	0.23	0.11	0.15	0.44	0.31	0.48	0.27	1				
Patients Reported Tuberculosis	-0.59	0.30	0.21	0.53	-0.37	0.23	0.58	-0.90	1			
Patients Reported to Hospital	-0.09	0.62	0.30	0.54	0.29	0.73	0.27	0.54	-0.33	1		
Patients with Chest Problems	-0.23	0.69	0.22	0.49	0.30	0.54	0.57	0.30	-0.06	0.93	1	
Patients reported Asthma	-0.45	0.02	0.47	0.77	-0.57	0.02	0.13	-0.49	0.53	-0.62	-0.65	1

Table 2. Shows the correlation between the major constituents of bioaerosol and their interdependence with the parameters liable to be affecting them.

REFERENCES

- Miyakawa, T., Kanaya, Y., Taketani, F., Tabaru, M., Sugimoto, N., Ozawa, Y., Takegawa, N., 2015. Ground-based measurement of fluorescent aerosol particles in Tokyo in the spring of 2013: potential impacts of nonbiological materials on autofluorescence measurements of airborne particles. *J. Geophys. Res.*
- Faridi, S., Hassanvand, M. S., Naddafi, K., Yunesian, M., Nabizadeh, R., Sowlat, M. H., ... Alimohammadi, M. (2015). Indoor/outdoor relationships of bioaerosol concentrations in a retirement home and a school dormitory. *Environmental Science and Pollution Research*, 22(11), 8190–8200. <https://doi.org/10.1007/s11356-014-3944-y>
- Herrero, A. D., Ruiz, S. S., Bustillo, M. G., & Morales, P. C. (2006). Study of airborne fungal spores in Madrid, Spain. *Aerobiologia*, 22(2), 135–142. <https://doi.org/10.1007/s10453-006-9025-z>

WHO. (2016). Ambient Air pollution: a global assessment of exposure and burden of disease. *WHO*. Retrieved from <http://www.who.int>

Eduarda, W., & Heederik, D. (1998). Methods for Quantitative Assessment of Airborne Levels of Noninfectious Microorganisms in Highly Contaminated Work Environments. *Aihaj*, 59(2), 113–127. [https://doi.org/10.1202/0002-8894\(1998\)059<0113:MFQAOA>2.0.CO;2](https://doi.org/10.1202/0002-8894(1998)059<0113:MFQAOA>2.0.CO;2)

Faridi, S., Hassanvand, M. S., Naddafi, K., Yunesian, M., Nabizadeh, R., Sowlat, M. H., ... Alimohammadi, M. (2015). Indoor/outdoor relationships of bioaerosol concentrations in a retirement home and a school dormitory. *Environmental Science and Pollution Research*, 22(11), 8190–8200. <https://doi.org/10.1007/s11356-014-3944-y>

Johnson, T. R., & L.case, C. (2007). *Laboratory Experiments in Microbiology*. PEARSON.

Rajput, P. (2017). Supplementary file of One year record of bioaerosols and particles concentration in Indo-Gangetic Plain : Implications of biomass burning emissions to high-level of endotoxin exposu ...

Supplementary Material (Environmental Pollution 2017) One year record of bioaerosols and particles concentration in Indo- Gangetic Plain : Implications of biomass burning emissions to high-level of endotoxin exposure Prashant Rajput , Manzar Hussain Anjum and Tarun Gupta, (March).

Rajput, P., Anjum, M. H., & Gupta, T. (2017). One year record of bioaerosols and particles concentration in Indo-Gangetic Plain: Implications of biomass burning emissions to high-level of endotoxin exposure.

Environmental Pollution, 224(January2018), 98–106. <https://doi.org/10.1016/j.envpol.2017.01.045>

DEPOSITION MODELING OF AMBIENT AEROSOLS IN HUMAN RESPIRATORY SYSTEM: A 1-Y LONG RECORD FROM KANPUR IN INDO-GANGETIC PLAIN

PRASHANT RAJPUT, SAIFI IZHAR AND TARUN GUPTA

Department of Civil Engineering, Indian Institute of Technology Kanpur, Kanpur - 208 016, India.

Keywords: Impact of Aerosols on Human Health, Aerosol Monitoring and Characterization.

INTRODUCTION

Global Burden of Disease (GBD) research program reveals that currently in India about 1 million people (including male and female) are losing their life every year due to malnutrition, unhygienic condition and respiratory diseases (GBD, 2015). In order to estimate particles deposition in human respiratory system we have conducted a 1 Y long study from central IGP (at Kanpur) assessing size distribution of ambient particles and regional (extrathoracic: HEAD, tracheobronchial: TBL and pulmonary region: PUL) deposition of fine and coarse particles in human respiratory tract utilizing MPPD (Multiple Path Particle Dosimetry) (Rajput et al., 2018). Lung deposition modeling is widely considered to estimate deposition mass by taking into account for exposed concentration, health status of the exposed population and standard breathing parameters (Anjilvel and Asgharian, 1995; Izhar et al., 2018; Rajput et al., 2018). Indo-Gangetic Plain (IGP) has a large stretch from north-west to north-east region in India and it is the shelter for nearly 50% of the Indian population. Our study location is strategically situated in central part of the IGP. It is worthwhile mentioning that besides the primary emission the secondary aerosol formation enhances PM loading significantly in lower atmosphere (Rajput et al., 2016; Sorathia et al., 2018).

METHODS

Ambient particles number concentrations (PNC) have been measured on 130 days (spread over a 1 Y period; June 2015–May 2016) utilizing aerosol spectrometer (PALAS; welas[®] 2000, Germany) at Indian Institute of Technology Kanpur (26.30 °N; 80.14 °E) (Rajput et al., 2018). Aerosol spectrometer was housed in Atmospheric Particle Technology Lab (APTL; in Centre for Environmental Sciences and Engineering building). The spectrometer was operated for 1 hour (12:30 h–13:30 h, local time; data resolution: 1 minute time interval) on each sampling day. Quantification of size-segregated aerosols deposition into different regions of human respiratory tract has been determined by a computational model [Multiple Path Particle Dosimetry: MPPD], developed by the Chemical Industry Institute of Toxicology (CIIT, USA, currently The Hamner Institutes for Health Sciences) and the Dutch National Institute for Public Health and the Environment. This model takes into account for diffusion, sedimentation and impaction of particles within the airway bifurcations of human lung and calculates the deposition fraction (DF).

RESULTS & DISCUSSION

Variability of PM concentration

During the entire study period, the PM₁, PM_{2.5} and PM₁₀ showed significantly large variability: varied from ~ 10–290, 15–310 and 20–400 $\mu\text{g m}^{-3}$, respectively. The highest concentration of PM_{2.5} (fine particles) has been observed during post-monsoon (October–November), whereas the lowest concentration is observed during June and July months (in SW-monsoon). In a sharp contrast, mass concentration of coarser particles (PM_{10-2.5}) is relatively high during summer (March–May) and in SW-monsoon (June–September). The annual average mass concentrations of PM_{2.5} and PM₁₀ is higher by about a factor of 2 as compared to the threshold limit (PM_{2.5}: 40 $\mu\text{g m}^{-3}$ and PM₁₀: 60 $\mu\text{g m}^{-3}$) provided by NAAQS (National Ambient Air Quality Status India 2009) (NAAQS, 2009). Moreover, the annual mean PM_{2.5} concentration (~ 90 $\mu\text{g m}^{-3}$) is higher

by a factor of 9 as compared to the value reported in safety guidelines by the World Health Organisation (WHO, 2006) (WHO recommended annual mean $PM_{2.5}$: $10 \mu\text{g m}^{-3}$).

PM mass size distribution

Seasonal variability of aerosol mass size distribution (covering $0.3\text{--}10.3 \mu\text{m}$; aerodynamic diameter) is presented in figure 1 (Figure 1a, b, c, d). The ambient aerosols at Kanpur showed tri-modal peak distributions during monsoon (June–Sept) and winter (Dec–Feb), whereas tetra-modal peak distributions is observed during post monsoon (October–November) and summer (March–May).

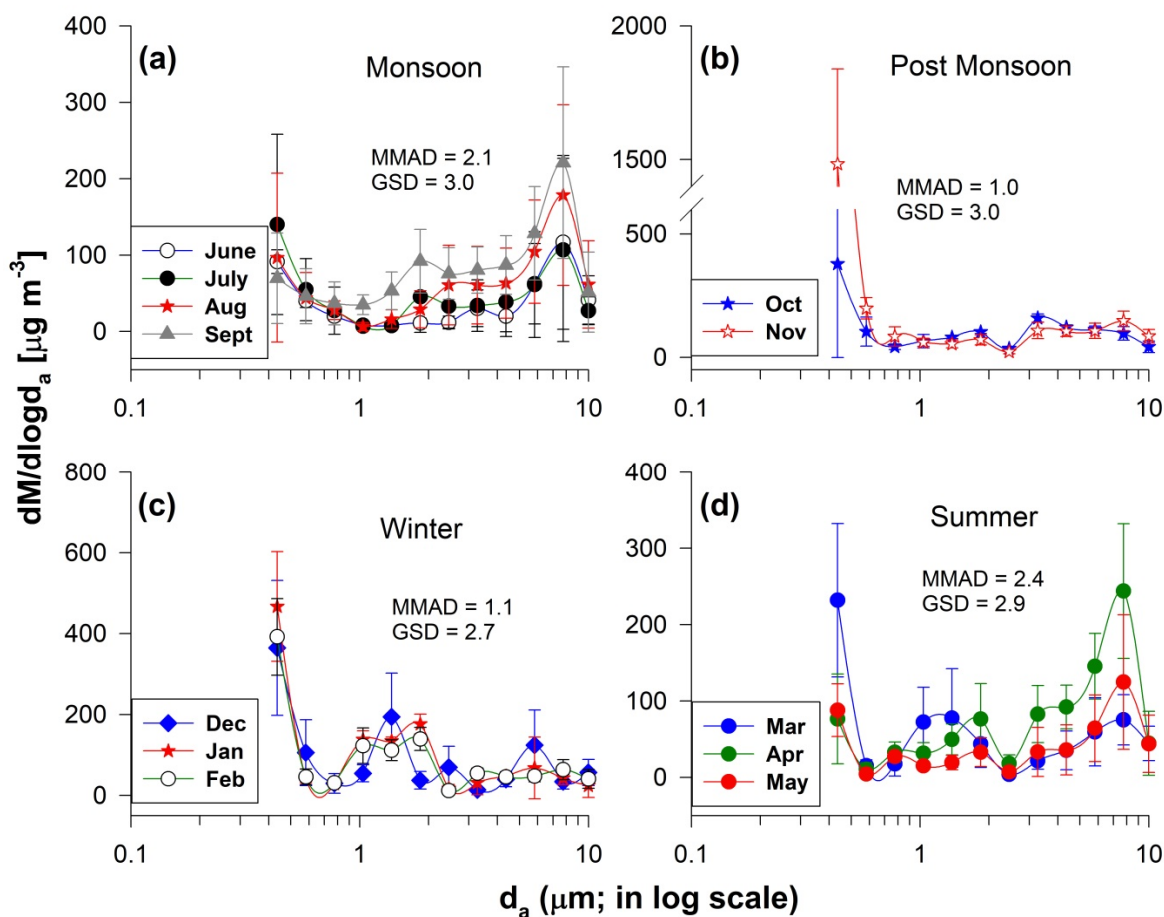


Figure 1. Aerosol mass size distribution at Kanpur in IGP. Here, d_a : aerodynamic diameter, MMAD: mass median aerodynamic diameter and GSD: geometric standard deviation.

The two peaks (in fine fraction; below $2.5 \mu\text{m}$) centring at $< 0.5 \mu\text{m}$ and $1.4\text{--}1.8 \mu\text{m}$ were common in all seasons. The other peak/s mode in monsoon was at $7.8 \mu\text{m}$, in post monsoon was at 3.2 and $7.8 \mu\text{m}$, in winter was at $5.8 \mu\text{m}$ and in summer was at 3.2 and $7.8 \mu\text{m}$. The MMAD (\pm GSD) were found to be $2.1 \mu\text{m}$ (± 3.0), $1.0 \mu\text{m}$ (± 3.0), $1.1 \mu\text{m}$ (± 2.7) and $2.4 \mu\text{m}$ (± 2.9) during monsoon, post monsoon, winter and summer season, respectively. The modal peak (and its intensity) at $7.8 \mu\text{m}$ in conjunction with higher MMAD of $2.1\text{--}2.4 \mu\text{m}$ suggest that coarse fraction particles are relatively high during summer and monsoon. However, modal peak characteristics at $< 0.5 \mu\text{m}$, $1.4\text{--}1.8 \mu\text{m}$, $3.2 \mu\text{m}$ and $5.8 \mu\text{m}$ in conjunction with low MMAD ($\sim 1.0 \mu\text{m}$) suggest the high mass abundance of fine particles during post monsoon and wintertime in IGP. During the post-monsoon, PM concentration in the size-range ($0.3\text{--}0.4 \mu\text{m}$) is ~ 2 times higher than that in winter season (Figure 1b, c). This is mainly attributable to large-scale post-harvest paddy-

residue burning emission in upwind IGP during post monsoon season (Rajput et al., 2011). Atmospheric variability of PM levels in winter season over the IGP is mainly attributed to bio-fuels (twigs, wooden-blocks and cow-dung cake) burning, fossil-fuel combustion, secondary aerosols formation and shallower boundary layer height (Rajput et al., 2016).

Mass deposition fraction (DF) as a function of particle size

The variability in regional (in HEAD, TB and PUL) mass deposition fraction of fine ($PM_{2.5}$) and coarse particles ($PM_{10-2.5}$) is shown in figure 2. The total PM mass average deposition is $\sim 34, 65, 41$ and $34 \mu g$ in monsoon, post monsoon, winter and in summer, respectively. Fine and coarse particles mass DF showed large variability in different seasons. However, the pattern of PM mass deposition remained quite similar during all the seasons: HEAD (maximum PM deposition) > PUL > TB (minimum PM deposition).

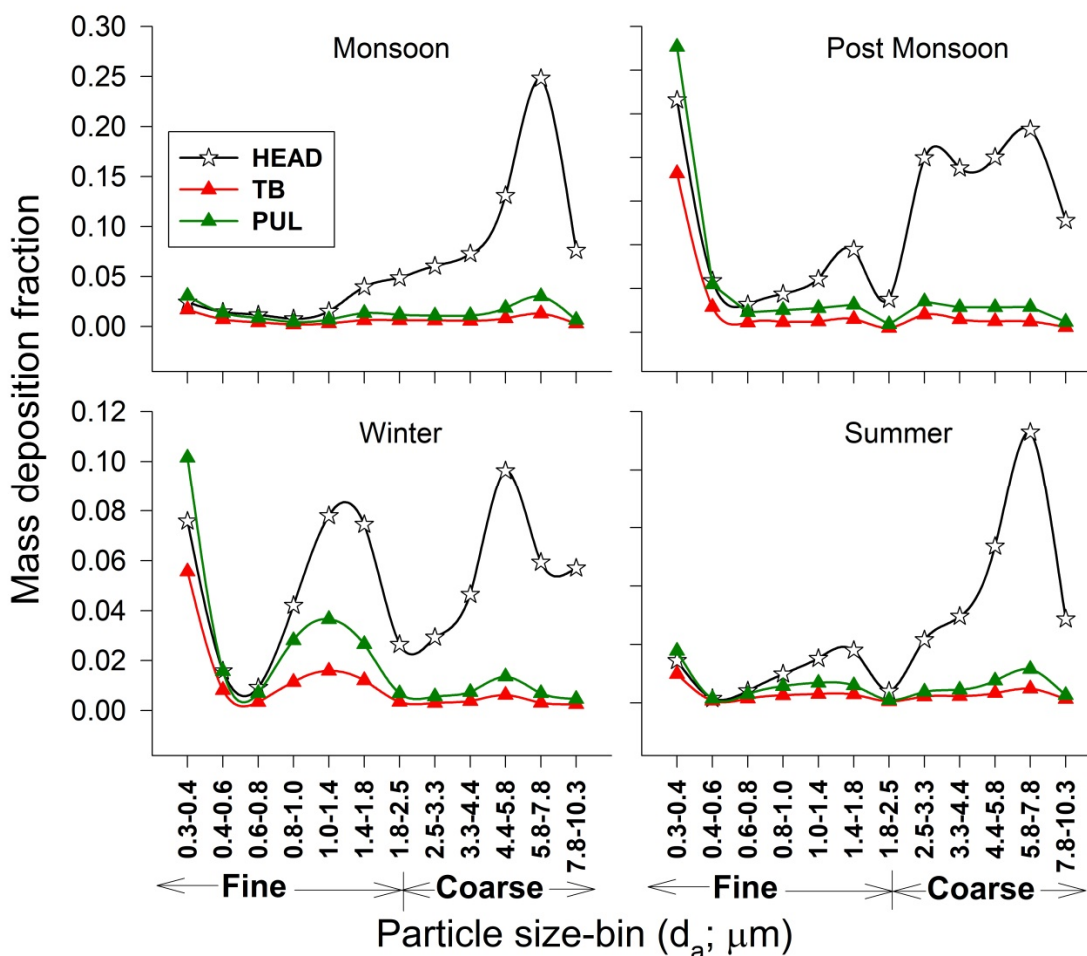


Figure 2. Aerosol mass deposition fraction varying as a function of particle size. $PM_{2.5}$ and $PM_{10-2.5}$ represent fine and coarse particles, respectively.

On an average, most of the exposed coarse particles ($\sim 83\%$) deposited in HEAD region, attributable to both sedimentation and inertial impaction of PM. In a sharp contrast, the mass DF of fine particles at TB and PUL region are relatively high as compared to the coarser ones. Fine particles are found to penetrate deeper and deposit quite significantly ($\sim 33\%$) in the PUL region. It is important to mention here that we have considered normal breathing parameters (sitting position; model test subject: male) in this study for the estimation of DF. A recent study carried out at Hungary has shown that DF varies significantly under

different breathing condition e.g. PM deposition fraction in HEAD was reported to decrease monotonically from 26% (while sleeping) to 9.4% (under heavy exercise condition) with a parallel increase from 14.7% (while sleeping) to 34% (under heavy exercise condition) in the PUL region (Salma et al., 2015).

CONCLUSIONS

A 1 Y long monitoring of ambient aerosols has been carried out from central IGP (Kanpur). Average concentrations of PM_{2.5} (fine), PM_{10-2.5} (coarse) and PM₁₀ (total) varied from ~ 40–150, 30–70 and from 90–220 µg m⁻³, respectively during the entire study. PM mass size distribution analysis (covering 0.3–10.3 µm) revealed multi-modal peak distributions in monsoon (tri-modal: < 0.5; 1.4–1.8; 7.8 µm), post monsoon (tetra-modal: < 0.5; 1.4–1.8; 3.2; 7.8 µm), winter (tri-modal: < 0.5; 1.4–1.8; 5.8 µm) and in summer (tetra-modal: < 0.5; 1.4–1.8; 3.2; 7.8 µm). The MMAD (± GSD) were found to be 2.1 µm (± 3.0), 1.0 µm (± 3.0), 1.1 µm (± 2.7) and 2.4 µm (± 2.9) during monsoon, post monsoon, winter and summer season, respectively. MPPD analysis was performed to assess deposition of PM (for 1h exposure) into different regions of human airways: HEAD, TB and PUL. Accordingly, the total PM mass average deposition is ~ 34, 65, 41 and 34 µg during monsoon, post monsoon, winter and summer, respectively. The fine and coarse particles mass DF show large variability during different seasons while the pattern of PM mass deposition remained quite similar: HEAD (maximum PM deposition) > PUL > TB (minimum PM deposition). This study, documenting PM mass deposition in different regions of human respiratory tract, calls for immediate measures to improve regional air quality and, serves as baseline information to reduce personal exposure in IGP.

ACKNOWLEDGEMENT

This study has been carried out utilizing internal funds from IIT Kanpur. PR is thankful to the Council of Scientific & Industrial Research, India for granting CSIR-SRA fellowship (Pool Scientist # 8934-A/2017).

REFERENCES

- Anjilvel, S. and B. Asgharian (1995), A multiple-path model of particle deposition in the rat lung, *Fundamental and Applied Toxicology*, **28**, 41-50.
- GBD (2015), Institute for health metrics and evaluation (IHME), GBD compare, Seattle, WA: IHME, University of Washington, (accessed [30-09-2016]).
- Izhar, S., P. Rajput and T. Gupta (2018), Variation of particle number and mass concentration and associated mass deposition during diwali festival, *Urban Climate*, **24**, 1027-1036.
- NAAQS (2009), National ambient air quality standards, Central Pollution Control Board, India. Gazette notification, New Delhi.
- Rajput, P., S. Izhar and T. Gupta (2018), Deposition modeling of ambient aerosols in human respiratory system: Health implication of fine particles penetration into pulmonary region, *Atmospheric Pollution Research*, <https://doi.org/10.1016/j.apr.2018.08.013>.
- Rajput, P., et al. (2016), Chemical characterisation and source apportionment of PM₁ during massive loading at an urban location in Indo-Gangetic Plain: Impact of local sources and long-range transport, *Tellus B*, **68**, 30659.
- Rajput, P., M.M. Sarin, R. Rengarajan and D. Singh (2011), Atmospheric polycyclic aromatic hydrocarbons (PAHs) from post-harvest biomass burning emissions in the Indo-Gangetic Plain: Isomer ratios and temporal trends, *Atmospheric Environment*, **45**, 6732-6740.

Salma, I., et al. (2015), Lung burden and deposition distribution of inhaled atmospheric urban ultrafine particles as the first step in their health risk assessment, *Atmospheric Environment*, **104**, 39-49.

Sorathia, F., P. Rajput and T. Gupta (2018), Dicarboxylic acids and levoglucosan in aerosols from Indo-Gangetic Plain: Inferences from day night variability during wintertime, *Science of the Total Environment*, **624**, 451-460.

WHO (2006), World health organization, 2006. Air quality guidelines for particulate matter, ozone, nitrogen dioxide and sulfur dioxide. Global Update 2005. In: Summary of Risk Assessment, WHO/SDE/PHE/OEH/06.02.

A FIELD SURVEY BASED CASE STUDY ASSESSING THE IMPACTS OF RURAL COOKING PRACTICES AND VENTILATION CONDITIONS ON HUMAN HEALTH

SHUBHANSHI SINGH¹, RUCHIN TEJAWAT¹, ANUBHA GOEL^{1,2}, RADHIKA MUNDRA¹

¹Department of Civil Engineering, Indian Institute of Technology, Kanpur – 208016

²Center for Environmental Science and Engineering CESE, IIT Kanpur – 208016

INTRODUCTION

The World Health Organization (WHO) reports approximately 4.3 million people, mainly in developing countries, die from household air pollution emitted by rudimentary biomass and coal cookstoves. More than 70% of the rural population in India is to date dependant on the conventional unprocessed bio-fuels including fuelwood, crop residue, and dung cakes, for daily cooking purpose. These fuels have a very low efficiency in terms of energy and the smoke released on burning them has a number of pollutants including particles, organic carbon (OC & VOCs) and elemental carbon (EC), sulfur and nitrogen oxides, and certain carcinogenic compounds^[2]. The easy availability and the low cost of these fuels are the major reasons for the practice being continued.

The objective of this case study is to examine the health impacts of the rural cooking practices by first-hand field visit data collection. Data collected from the questionnaire survey in homes was statistically analysed for correlations among the factors affecting indoor air quality in cooking areas. The motivation for this study came from a health camp which was conducted in March 2018 at a small village Bansathi, 10 km away from IIT Kanpur. Here people were examined for various health problems related to eyes, skin, breathing, and throat infection. Data on type of fuel used for cooking and quality of water used was also collected. It was observed that cow dung cakes were the major fuel and most people were suffering from breathing and throat related problems.

METHODOLOGY

Data collection through on Field Survey using Questionnaire (May – July 2018)

Relevant information for this research was collected by conducting field visit i.e., first-hand questionnaire survey by visiting a few houses. The questionnaire for the survey was prepared with the view to identify possible parameters impacting air quality in cooking areas which in turn that would help in rightly suggesting alternatives to mitigate health impacts. Some sections in the survey form were filled by visual inspection of the houses, like the location of the kitchen, structure of a house, type of stove, type of fuel, duration of cooking per meal, time of cooking the meals and other biomass burning dependent activities. The last part of the form asked about the health problems (eye, skin, throat, breathing, cough) faced by the residents (focusing on the person in charge of cooking activity in the house). Lung capacity of residents was estimated by measuring the Peak Expiratory Flow (PEF) by using the Peak Flow Meter (unit: liter/min (L/min)). It was measured for 52 people of the village. Other than the surveys at houses, we also contacted the local hospitals (both government and private with general physicians) to collect relevant health data.

Selection of Houses for survey

The survey was conducted in the village of Bansathi (around 26°30'00 N 80°09'00 E) located roughly 10 km from IIT Kanpur. The village is divided into 5 *poorbas* (*Beharampur, Chintapurwa, Jogindera, main Bansathi, Krishna Nagar*). The survey included 5 visits to the village, randomly selecting around 10-15 houses from each *poorba*. A total of 61 houses were covered in the survey.

Assessment of ventilation conditions

The ‘openness percentage’ of cooking area was estimated and calculations performed for *Probable indoor air speed (PIAS)*.

Openness percentage

The openness percentage of each house was calculated by measuring the height, width, and length of the kitchen area and calculating the percentage of the area open. The values of openness percentage are not exact as the houses are not constructed in a very planned manner. Then the analysis was dependent on two categories of openness percentage:

- Openness percentage $\leq 20\%$;
- Openness percentage $> 20\%$

This demarcation was made based on standards by ASHRAE (American Society of Heating, Refrigeration and Air-conditioning Engineers).

Probable indoor air speed (PIAS)

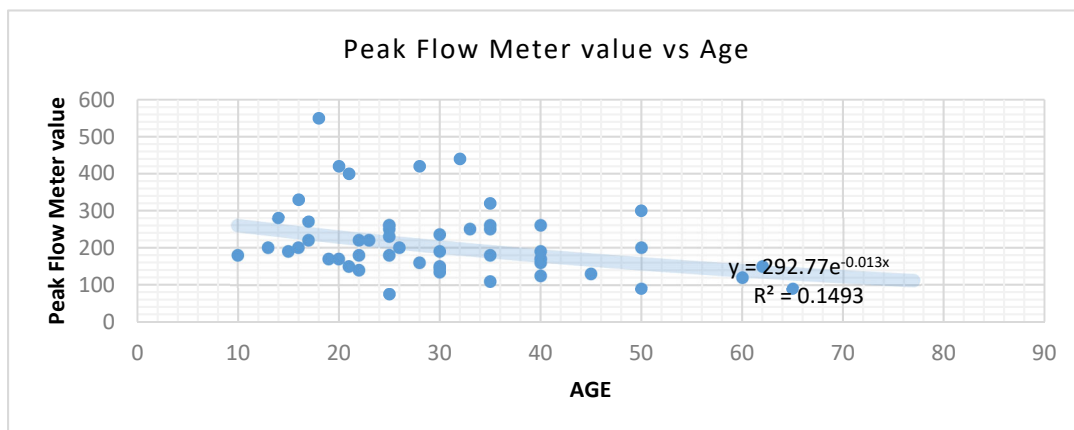
The probable indoor airspeed was calculated as per the IS 3362:1977^[1] and the ambient weather data of Kalyanpur, Kanpur was used as of Wednesday, May 23, 2018 (source: weather.com). The code specifies steps that can be used to give the value of PIAS in terms of the outdoor airspeed. These speeds are dependent on the temperature and the relative humidity. The outdoor weather data was considered for 0800-0900 hours as that was the most probable time of cooking in the village.

RESULTS & DISCUSSIONS

Observations on health of people in the village

Respiratory health indicator: Lung Capacity

The graph below suggests an indirect relation between peak expiratory flow (PEF) measure using a peak flow meter. The results are in accordance with the fact that with an increase in age, the health or capacity of lungs decreases. The average age of people is between 20-50 yrs. It was observed that PEF for males was in general higher than that for females.



PEFs for a maximum number of people (especially the females) lie below 300L/min which, as per the standards, is much lower value than that for a healthy person.

Visits to **local hospitals and government hospitals** where doctors are mainly general physicians, revealed that the most prevalent problems are Asthma, Diarrhoea, Cold / Cough, Malaria, Heat Stroke, Cardiac Arrest. Out of these, asthmatic problems and cold/ a cough are most frequent. On an average 150 people visit the doctor in a month. Most of them are females (nearly 60%).

Ventilation conditions

These were found to be quite poor and the summary of observations is listed below.

1. Openness percentage <20% (for All houses surveyed)
2. The PIAS are obtained for 30 houses and the results as per the standards are:

Number of houses with desirable wind speed for thermal comfort = 0/30

Number of houses with minimum wind speed for just acceptable warm conditions = 17/30.

Factors impacting the indoor air quality of cooking areas

Results from the survey were compiled and responses for different questions compared on a percentage basis. The results reveal that,

1. *Chulha* is the primary stove (Stove 1) with dung cakes as the primary fuel.
2. Exposure occurs mainly during cooking: total duration about 3 hours/ day for 3 meals a day
3. Most people use biomass burning for room heating.
4. Exposure through smoking (either active or passive) is also significant

Chemical composition of emissions from cow dung cakes as reported by previous studies

An examination of research articles reveals that emissions from conventional fuels release many harmful substances that are likely to impact the health of exposed population adversely. Various components measured from cowdung smoke include PM, OC, EC, SO₂, NO, NO₂, Cl⁻, PO₄³⁻, NO₃⁻, Na⁺, K⁺, NH₄⁺^[4]. It is clearly seen that exposure to smoke from burning cow dung cakes poses a significant health risk and is a likely factor impacting peoples' health in the village.

Influence of factors affecting air quality on Human health

Using statistical methods^[3] like chi-square test and odds ratio, major factors likely to impact indoor air quality (i.e. Stove type, smoking exposure, openness percentage, biomass burning for room heating, cooking time) were correlated with health problems observed (i.e. eye, cough, skin, breathing, throat). The results obtained suggest the following trend in terms of descending severity of health issues: Eye > Cough > Skin > Breath > Throat.

CONCLUSION

The results from this study suggest that health of the people is severely impacted by cooking practices. It can be inferred that

- Respiratory health of the residents, as noted through Lung Capacity results, is in general poor. Use of chulha as a primary stove (in 75% houses) and dung cakes as fuel (for cooking, heating, etc.) is a major reason and likely accounts for women showing greater health problems. Further research on composition of emissions from chulhas used in this region and providing an alternative to this cooking mechanism is strongly recommended.

- The indoor environment is far below thermal comfort standards as noted from PIAS results. Poor ventilation conditions result in greater exposure to cooking fumes. Contrary to expectations, openness \propto Health Problems; strongly suggesting that some pollutant in the ambient air might be impacting air quality and health. Monitoring of ambient air quality with focus on impact of agricultural activities needs to be conducted.

ACKNOWLEDGEMENTS

We are grateful to Dr. Shivam Tripathi and Mr. Surya for constantly providing support during the project planning and helping us out in all possible ways. We thankfully acknowledge the support provided by Mr. Supreme, Ms. Saraswati, Mr. Yogesh and Mr. Manoj that made visits to Bansathi village and data collection convenient.

REFERENCES

IS 3362:1977 Code of practice for natural ventilation of residential buildings.

Larry D. Claxton (2014). The history, genotoxicity, and carcinogenicity of carbon-based fuels and their emissions.

Agresti, A. An Introduction to Categorical Data Analysis-Wiley (1996).

Sen, Avirup, Mandal, T. K., Sharma, S. K., Saxena, M., Gupta, N. C., Gautam, R., ... Gadi, R. (2014). Chemical properties of emission from biomass fuels used in the rural sector of the western region of India.

Satsangi, P. Gursumeeran, Yadav, S., Pipal, A. S., & Kumbhar, N. (2014). Characteristics of trace metals in fine (PM_{2.5}) and inhalable (PM₁₀) particles and its health risk assessment along with in-silico approach in the indoor environment of India.

Kandpal, J. B., Maheshwari, R. C., & Kandpal, T. C. (1995). Indoor air pollution from combustion of wood and dung cake and their processed fuels in domestic cookstoves.

Deka, Pratibha, & Hoque, R. R. (2015). Chemical characterization of biomass fuel smoke particles in rural kitchens of South Asia.

IMPACTS OF AIR MASSES ON FOG WATER CHEMICAL COMPOSITION AND CONTRIBUTION IN THE INDO GANGETIC PLAIN

SAIFI IZHAR¹, TARUN GUPTA¹, AND ARNICO K. PANDAY²

¹Department of Civil Engineering, Indian Institute of Technology, Kanpur – 208016, India.

²International Centre for Integrated Mountain Development (ICIMOD), Khumaltar, Lalitpur, Nepal

KEYWORDS: Indo Gangetic Plain; Fog Water; Aqueous Processing; Cluster Analysis

INTRODUCTION

The Indo-Gangetic Plain (IGP) is regarded as one of the hotspots in world for the occurrence of fog during winter time. The availability of moisture with high relative humidity and low temperature coupled with significant aerosol loading aid towards formation of night time fog in this region (Chakraborty et al., 2016; Ghude et al., 2017). These radiation fogs is the mixture of gaseous species, liquid droplets, wet aerosol and dry particulate matter which results in the complex interactions among these phases exists causing in the enrichment of organics and inorganics pollutants concentration within the fog droplets (Seinfeld and Pandis, 1998). Investigations into fog physicochemical parameters have received very much attention as organic and inorganic contaminants from fog water is indirect indicator towards regional aerosol characteristics. There are limited studies on the fog water characteristics reported in the IGP which are mainly focused on urban areas (Ambade, 2014; Chakraborty et al., 2016; Ghude et al., 2017), but not a single study has been reported for the rural areas of the IGP. It is important to look insight the differences in fog water composition spatially based on the land cover characteristics. Thus in this present work the main objectives included fog water physical and chemical characterization and their concentrations and contribution at rural site located in the northern edge of IGP at Southern Nepal.

METHODS

Sampling site at Lumbini (27.49°N, 83.28°E, 150 m, above sea level) is situated in northern edge of IGP at Southern Nepal. The sampling measurements were carried out from 7th Dec 2017 to 22nd Jan 2018, out of which 28 fog water samples were collected, one sample per night. The night time RH and temperature during the foggy night sampling averaged around $99.9 \pm 0.08\%$ and $9.7 \pm 1.7\text{ }^{\circ}\text{C}$ respectively, with average visibility was consistently lower than 150 m. Passive string collectors as described by Skarżyńska et al., 2006 was used for the collection of the fog water samples which was stored in pre-cleaned high density polyethylene (HDPE) bottle. The pH and electrical conductivity have been measured using Orion Star TM A329 pH and conductivity meter. The cations and anions have been measured using a dual channel ion-chromatograph (Metrohm). The DOC concentration was measured using total organic carbon analyser (TOC-V CPN; Shimadzu Corporation model). The impacts of air masses on the fog water composition and concentration were determined by performing the back trajectory analysis using the TrajStat software (Wang et al., 2009). 72 hours back trajectories starting at 500 m above the ground level, for every sampling day were computed. Then the trajectories were clustered on the basis of their similarities in terms of spatial distribution using the clustering tool. The optimum number of clusters were based on the change in total variance.

RESULTS AND DISCUSSION

Chemical composition of fog water:

The statistical values for the physical and chemical constituents of fog water during the entire sampling is presented in Table 1. SO_4^{2-} and NO_3^- were found to be major anions with concentration varying from 13 to

50 mg/l and 47 to 240 mg/l respectively, whereas NH_4^+ and Ca^{2+} were found to be major cations with concentration varying from 11 to 44 mg/l and 11 to 43 mg/l respectively in the fog water samples collected at our site. These four dominant ions concentrations contributed about 86 % of total inorganic ions in the fog water (NO_3^- (27.1 %), NH_4^+ (23.7 %), Ca^{2+} (22.5), SO_4^{2-} (12.1 %)). Inorganic ions followed this decreasing trend in their equivalent concentration, $\text{NO}_3^- > \text{NH}_4^+ > \text{Ca}^{2+} > \text{SO}_4^{2-} > \text{Mg}^{2+} > \text{Cl}^- > \text{Na}^+ > \text{K}^+$. The average ratio of total cations to total anions equivalent concentration was around 1.27, which suggested the presence of organic anionic species including acetate, formate, tartarate etc., (Gilardoni et al., 2014; Giulianelli et al., 2014). This can also be confirmed by the significant DOC concentration in the collected fog water samples. However, the SO_4^{2-} contribution is significantly less compared to NO_3^- due to the limited number of industries which uses sulfur-rich fossil fuel and besides this region is a largely agricultural dependent area. The $\text{NO}_3^-/\text{SO}_4^{2-}$ mass ratio was found to be 2.9 ± 1 . This ratio has been used as a site remoteness indicator (Weathers et al., 1988); but this high ratio indicated that being rural location, it is highly impacted by pollution sources. The positive correlation between SO_4^{2-} and NO_3^- ($r=0.61$, $p<0.05$) showed the secondary formation inside fog water through aqueous processing mechanism (Ervens et al., 2011; Guo et al., 2012). The pH value showed alkaline nature of fog water which was affected by fog scavenging of anthropogenic emission and crustal sources. The anthropogenic and secondary emission had the excess of acidifying anions (NO_3^- , SO_4^{2-} and Cl^-) whereas the crustal and biogenic sources had dominant alkaline cations (NH_4^+ , Ca^{2+} and Mg^{2+}). The Neutralization Factor was found to be highest for NH_4^+ (0.64) followed by Ca^{2+} (0.59) and Mg^{2+} (0.14). This showed that ammonium and calcium mainly contributed towards neutralizing the fog water samples. Compared to the fog water composition reported for urban areas including Delhi and Kanpur, it was found to be that our sampling site had excess of nitrate whereas all other inorganic species found to be greater in urban areas. Thus the differences in composition concentration of fog water within IGP showed that it is influenced by the land cover characteristics. In terms of solute concentration in the fog water, the differences between TIC (188 ± 62 mg/l) and DOC (200 ± 80 mg/l) concentration were very marginal. This further showed that organic composition in fog water is similar in percentage to the TIC concentration, but DOC values are significantly higher than nitrate, sulfate or ammonium ion concentration.

Parameters	MIN	25th percentile	AVERAGE	75th percentile	MAX
Cl^- (mg/l)	1.8	4.8	6.1	7.5	11
NO_3^- (mg/l $\times 10$)	4.7	6.8	9.1	10	24
SO_4^{2-} (mg/l)	13	25	32	38	50
Na^+ (mg/l)	0.01	1.4	3.4	4.7	11
NH_4^+ (mg/l)	11	17	22	26	44
K^+ (mg/l)	2.9	4.3	5.7	7.2	9.2
Ca^{2+} (mg/l)	11	18	24	28	43
Mg^{2+} (mg/l)	1.4	2.1	3.7	5.1	11
TIC (mg/l $\times 10$)	9.3	15	19	24	39
DOC (mg C/l $\times 10$)	9.6	13	20	27	36
pH	6.3	6.7	6.7	6.8	7.1
EC ($\mu\text{S}/\text{cm} \times 10$)	15	22	27	31	50

Table 1: Statistical values for the physical and chemical constituents of fog water during the entire sampling

Influence of air masses on fog water chemical composition:

Four different types of clusters namely Cluster1 (C1) to Cluster4 (C4) were obtained and shown in Figure 1. C1, C2 and C3 were originated from North West direction but their path length varied significantly. C1 was locally driven, C2 originated from upwind cities of Indo Gangetic Plain and path length was greater than C1 and C3 seems to be long range transport originating from countries Iran and Turkmenistan. C4 was

locally driven but originated from South-East direction. The contribution of each species to total solute concentration is shown in Figure 2.

The variation in concentration of chemical species were largely observed for nitrate (70.6 to 126.3 mg/l), sulfate (17.8 to 42.4 mg/l), calcium (16.7 to 30.1 mg/l) and DOC (148.8 to 207.3 mg/l). The major differences observed among the four clusters is the contribution of DOC to the total solute concentration. 60.9 % for C4, 53 % for C1, 51.3 % for C2 and 37.7 % for C3. A very interesting trend emerged which shows that the locally driven air masses have higher percentage contribution and as the backward trajectory path length increased the percentage contribution for DOC decreased significantly. This outcomes may indicate that some fraction of DOC is not related with long range transport of anthropogenic air masses, but with rural source that are perhaps biogenic and agricultural origin. On the other side the nitrate percentage contribution followed opposite trend. 32 % for C3, 23.3 % for C2, 21.5 % for C1 and 20.7 % for C4. This trend showed that long range transported air masses had enriched nitrate concentration compared to locally driven air masses. Similarly sulfate showed decrement in their contribution to the total solute concentration from long range transported to locally driven air masses (5.2 % for C4 to 10.8 % for C3). It is also important to note that regardless of cluster types, the sulfate concentration remained significantly lesser than nitrate concentration. However the ammonium concentration and contribution remained similar in all cluster types. There is no significant differences observed in the concentration and contribution of all chemical species between cluster 1 and 2. The major reason for that is the air mass origination upwind to the sampling site which fall within IGP. Thus these chemical changes in the fog water associated with the air masses are of importance for the chemical rates and dissolution of the different chemical species.

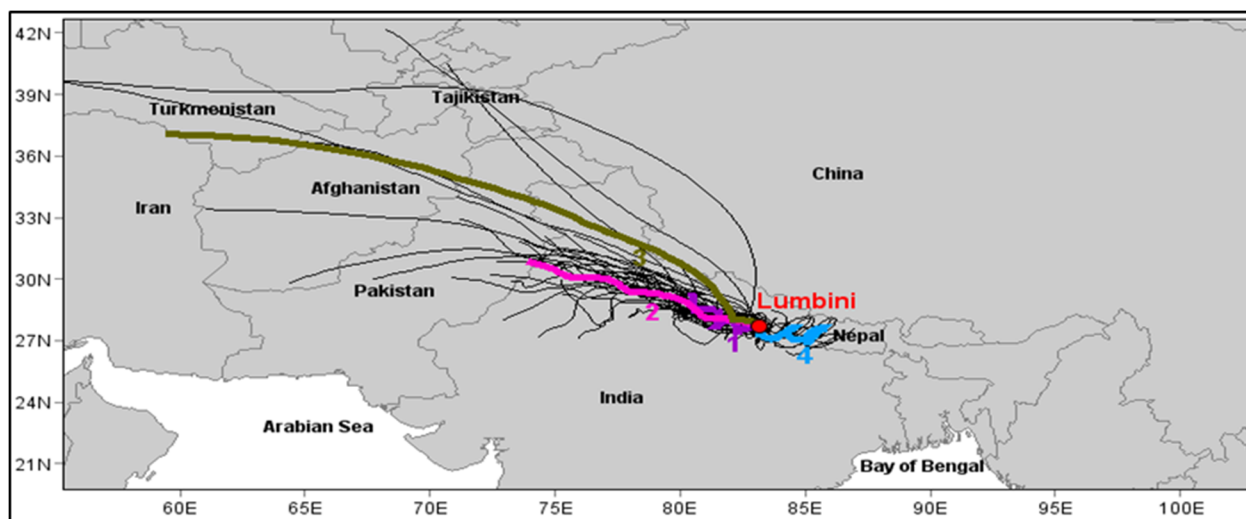


Figure 1. Backward air trajectory for 72 hours for the entire sampling duration at height of 500m above ground level. Black lines denotes trajectory for a particular day and violet, pink, dark yellow and cyan colour represents the four cluster types Cluster1 to Cluster4 respectively. The red dot points the sampling site, Lumbini.

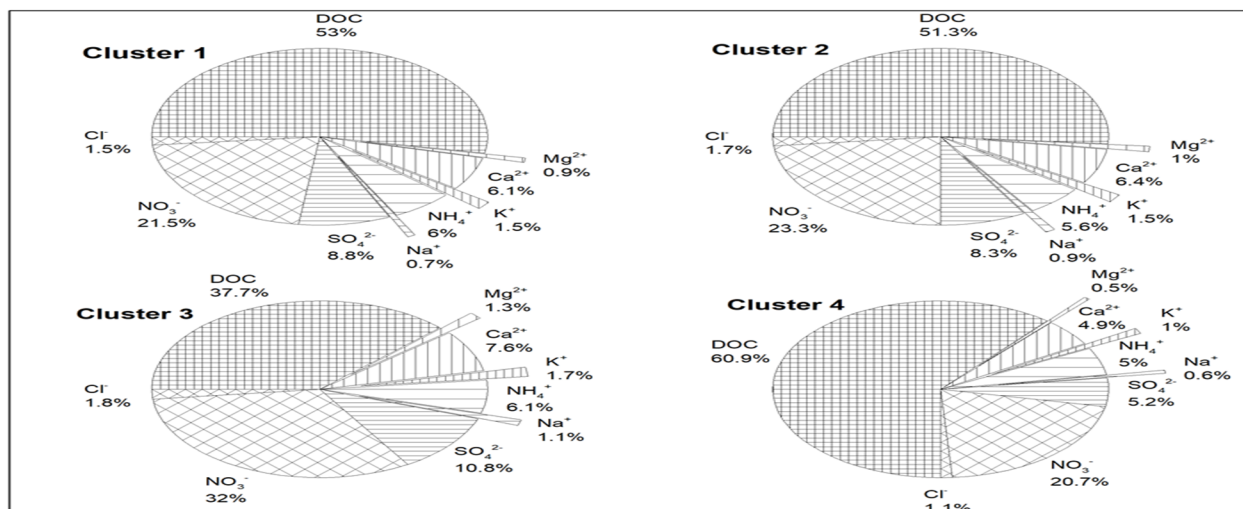


Figure 2: Fog water percentage contribution of chemical species for the four different types of cluster

CONCLUSIONS

We document chemical characteristics of fog water samples during winter time in the rural part of Indo-Gangetic Plain. The major anionic species were NO_3^- (27.1 %) and SO_4^{2-} (12.1 %), whereas major cationic species were NH_4^+ (23.7 %) and Ca^{2+} (22.5). The pH was found to be alkaline which corroborated well with the trend in inorganic concentration of the fog water. Cluster analysis results for backward air mass trajectory showed that the contribution of inorganic species including nitrate and sulfate was significantly higher for long range associated air masses whereas regional air masses had significant DOC contribution.

ACKNOWLEDGEMENTS

This study was partially supported by core funds of ICIMOD contributed by the governments of Afghanistan, Australia, Austria, Bangladesh, Bhutan, China, India, Myanmar, Nepal, Norway, Pakistan, Sweden, and Switzerland. The lab analysis was done in IIT Kanpur.

REFERENCES

- Ambade, B., 2014. Characterization and source of fog water contaminants in central India. *Nat. Hazards* 70, 1535–1552. <https://doi.org/10.1007/s11069-013-0892-7>
- Chakraborty, A., Ervens, B., Gupta, T., Tripathi, S.N., 2016. Characterization of organic residues of size-resolved fog droplets and their atmospheric implications. *J. Geophys. Res. Atmos.* 121, 4317–4332. <https://doi.org/10.1002/2015JD024508>
- Ervens, B., Turpin, B.J., Weber, R.J., 2011. Secondary organic aerosol formation in cloud droplets and aqueous particles (aqSOA): a review of laboratory, field and model studies. *Atmos. Chem. Phys.* 11, 11069–11102. <https://doi.org/10.5194/acp-11-11069-2011>
- Ghude, S.D., Bhat, G.S., Prabhakaran, T., Jenamani, R.K., Chate, D.M., Safai, P.D., Karipot, A.K., Konwar, M., Pithani, P., Sinha, V., Rao, P.S.P., Dixit, S.A., Tiwari, S., Todekar, K., Varpe, S., Srivastava, A.K., Bisht, D.S., Murugavel, P., Ali, K., Mina, U., Dharua, M., Rao, J., Padmakumari, B., Hazra, A., Nigam, N., Shende, U., Lal, D.M., Chandra, B.P., Mishra, A.K., Kumar, A., Hakkim, H., Pawar, H., Acharja, P., Kulkarni, R., Subharthi, C., Balaji, B., Varghese, M., Bera, S., Rajeevan, M., 2017. Winter Fog Experiment Over the Indo-Gangetic Plains of India. *Curr. Sci.* 112, 767.

<https://doi.org/10.18520/cs/v112/i04/767-784>

Gilardoni, S., Massoli, P., Giulianelli, L., Rinaldi, M., Paglione, M., Pollini, F., Lanconelli, C., Poluzzi, V., Carbone, S., Hillamo, R., Russell, L.M., Facchini, M.C., Fuzzi, S., 2014. Fog scavenging of nitrate and organic aerosol Fog scavenging of organic and inorganic aerosol in the Po Valley Fog scavenging of nitrate and organic aerosol Fog scavenging of nitrate and organic aerosol. *ACPD Atmos. Chem. Phys. Discuss* 14, 4787–4826. <https://doi.org/10.5194/acpd-14-4787-2014>

Giulianelli, L., Gilardoni, S., Tarozzi, L., Rinaldi, M., Decesari, S., Carbone, C., Facchini, M.C., Fuzzi, S., 2014. Fog occurrence and chemical composition in the Po valley over the last twenty years. *Atmos. Environ.* 98, 394–401. <https://doi.org/10.1016/J.ATMOSENV.2014.08.080>

Guo, J., Wang, Y., Shen, X., Wang, Z., Lee, T., Wang, X., Li, P., Sun, M., Collett, J.L., Wang, W., Wang, T., 2012. Characterization of cloud water chemistry at Mount Tai, China: Seasonal variation, anthropogenic impact, and cloud processing. *Atmos. Environ.* 60, 467–476. <https://doi.org/10.1016/j.atmosenv.2012.07.016>

Seinfeld, J.H., Pandis, S.N., 1998. *Atmospheric chemistry and physics : from air pollution to climate change*.

Skarżyńska, K., Polkowska, Ż., Namieśnik, J., 2006. Sample Handling and Determination of Physico-Chemical Parameters in Rime, Hoarfrost, Dew, Fog and Cloud Water Samples -a Review. *Polish J. Environ. Stud* 15, 185–209.

Wang, Y.Q., Zhang, X.Y., Draxler, R.R., 2009. TrajStat: GIS-based software that uses various trajectory statistical analysis methods to identify potential sources from long-term air pollution measurement data. *Environ. Model. Softw.* 24, 938–939. <https://doi.org/10.1016/J.ENVSOFT.2009.01.004>

Weathers, K.C., Likens, G.E., Bormann, F.H., Eaton, J.S., Kimball, K.D., Galloway, J.N., Siccama, T.G., Smiley, D., 1988. Chemical Concentrations in Cloud Water from Four Sites in the Eastern United States, in: *Acid Deposition at High Elevation Sites*. Springer Netherlands, Dordrecht, pp. 345–357. https://doi.org/10.1007/978-94-009-3079-7_18

RELATIONSHIP BETWEEN AIR POLLUTANTS AND METEOROLOGICAL PARAMETERS AND EXAMINATION OF POSSIBLE INTER-DEPENDENCE OF POLLUTANT LEVELS IN TWO MAJOR INDIAN CITIES WITH VARYING CLIMATIC CONDITIONS

SHUBHAM RATHI¹, ANUBHA GOEL^{1,2}, SUPREME JAIN¹

¹Department of Civil Engineering, IIT Kanpur, Kanpur – 208016 (UP), India

²Centre for Environmental Science and Engineering CESE, IIT Kanpur, Kanpur – 208016 (UP), India

KEYWORDS: Urban air pollution, Particulate matter, CO, NO_x, ozone, temperature, Statistical analysis

INTRODUCTION

Recently it has been reported that 14 of the world's 15 most polluted cities are in India (World Health Organisation, 2018). An exponential increase in demand for motorised vehicles is a natural follow up to economic growth and an increase in population and size of Indian cities. The number of registered vehicles are estimated to more than double by 2019 over numbers recorded in 2011 (Government of India (GOI), 2016).

Anthropogenic emission from industries, automobiles and residential sectors are the major sources of urban air pollution. The air pollutants emitted by automobiles and other sources are detrimental to human health. At elevated concentration, they cause adverse impacts on vegetation, animal life, buildings and monuments, weather and climate, and on the aesthetic quality of the environment, directly or indirectly (Bhaskar & Mehta, 2010). Meteorological conditions can weaken or improve air quality. Pollutants can rapidly be transported hundreds of kilometres by strong winds, whereas during weak wind circumstances, pollutants can accumulate around the source of their release. Through the process of wet scavenging, rain that cleans the atmosphere can pollute the environment. This study examines air quality data from two Indian cities with the aim to examine the temporal relationship between air pollutants and meteorological parameters. It investigates how air pollutant levels vary with changing meteorological conditions. The possibility of the ties among various air pollutants has been studied.

DATA COLLECTION AND ANALYSIS TECHNIQUES

Data collection: Data for levels of air pollutants namely **PM_{2.5}, CO, NO₂, and O₃** and meteorological parameters namely **temperature, relative humidity and precipitation** for two Indian metropolitan cities' (Delhi and Mumbai) are collected from Central Pollution Control Board (CPCB) website. These two cities are selected as they both have different climatic conditions due to their geographical location, i.e. one is inland while another one is coastal. Air pollutants concentration for the last three years period (2015-2017) while a longer-term dataset for metrological parameters (2007-2017) to minimise climatic variability, were utilised.

Statistical Data analysis: Data for pollutant levels and meteorological parameters has been plotted on both normal and lognormal scale using MATLAB R2016a software to obtain i) Correlation between air pollutants and meteorological parameters, and ii) correlation among different air pollutants. Based on the collected data an annual trend 5th order polynomial regression curve for both cities was plotted for each air pollutant and meteorological parameters.

RESULTS AND DISCUSSIONS

In Delhi, most of the time, concentrations of air pollutants including PM_{2.5}, CO, NO₂, and O₃ exceed the National Ambient Air Quality Standards (NAAQS) while in Mumbai it exceeds only in rare occasions. In Mumbai daily average PM_{2.5} concentration lies in good and satisfactory Air Quality Index (AQI) categories

($25 \mu\text{g}/\text{m}^3$ - $90 \mu\text{g}/\text{m}^3$) for all data collected while in Delhi daily average $\text{PM}_{2.5}$ concentration lies in the poor and very poor categories of AQI ($125 \mu\text{g}/\text{m}^3$ - $300 \mu\text{g}/\text{m}^3$) for most of the data collected. Exceptions are some summer months where it reaches the satisfactory range in AQI ($60 \mu\text{g}/\text{m}^3$).

Correlation with meteorological parameters: In most cases the correlation between meteorological parameters and pollutant levels measured is negative. High negative correlation (-0.20 to -0.71) of all air pollutants concentrations with precipitation was found for both cities in keeping with washout through wet scavenging. Relative humidity also shows a negative correlation (-0.23 to -0.89) with all air pollutants for both cities except CO which shows very low positive correlation (0.15). Correlation with temperature is also negative (-0.34 to -0.66) for Delhi most likely due to higher rates of diffusion in summer lead to faster transport resulting in lower concentrations except ozone. The production of ozone is increased in abundance of sunlight which leads to a positive correlation (0.73). In Mumbai temperature doesn't correlate well with any air pollutants most likely due to moderate climate in the city. Moderate climate in Mumbai is owing to its location by the coast where average temperature varies merely 7°C (from 27°C to 33°C) for a whole collected, likely doesn't change turbulence and boundary conditions significantly.

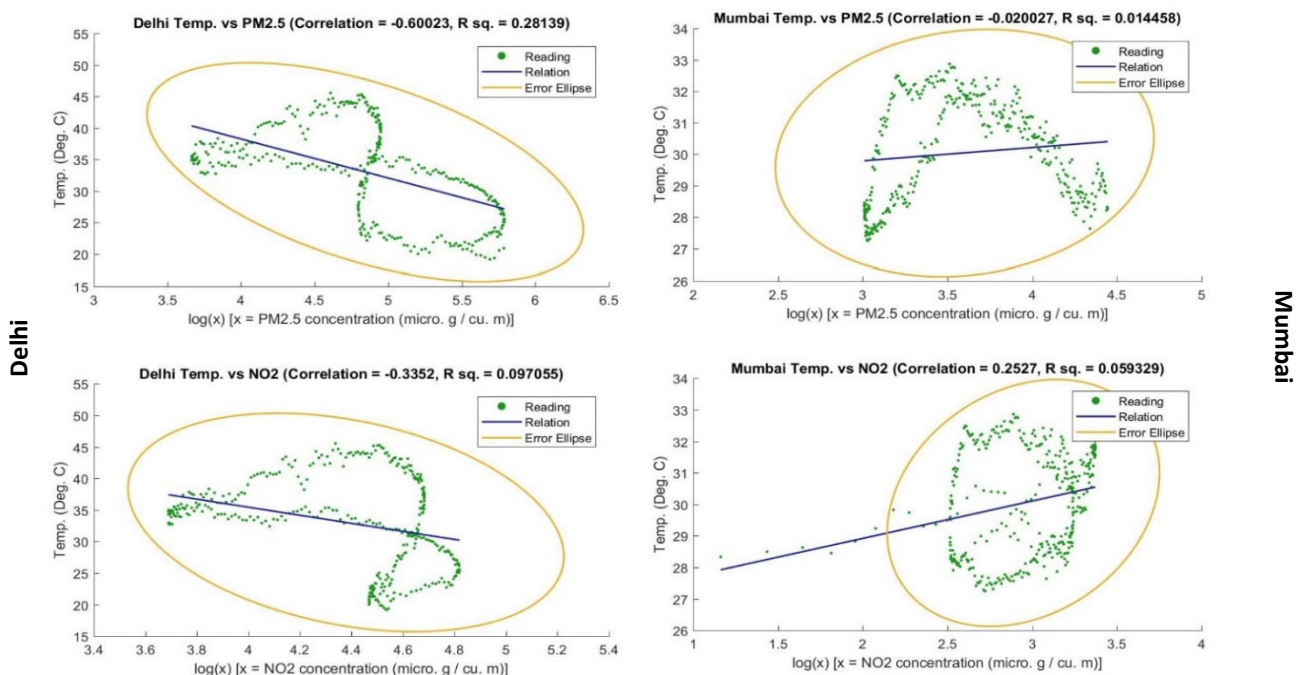


Figure 1: Correlation of various air pollutants with temperature on a lognormal scale in both cities

Correlation of $\text{PM}_{2.5}$ and NO_2 with temperature for both cities is presented in Figure 1*. Negative correlation for both parameters with temperature is observed for Delhi, with Pearson's coefficient value of -0.60 and -0.34 for $\text{PM}_{2.5}$ and NO_2 respectively. High variation in temperature observed over a year, where higher temperature causes greater mixing and increase of boundary layer, is a likely factor towards decreasing pollutant concentration with temperature. Contrary to Delhi, in Mumbai $\text{PM}_{2.5}$ shows almost no correlation or precisely speaking very little negative correlation (-0.02) with temperature while NO_2 shows small positive correlation (0.25) with temperature.

Correlation among pollutants: Photolysis of NO_2 forms troposphere O_3 and hence the two gases are expected to show a highly positive correlation. Although, the correlation is seen in a few cases in both the cities, the relation doesn't seem to be very strong (Figure 2*). This might be due to several other factors like meteorological parameters and trace gases that might be hindering the process of photolysis leading to the formation of ozone. CO is a precursor to the formation of NO_2 in the troposphere (Seinfeld & Pandis, 2006) and accounts for a slightly significant positive correlation (0.47) for NO_2 with CO in Delhi (Figure

2*). As in the case of other parameters, in Mumbai, it shows almost no correlation with CO maybe due to the intrusion of sea salt aerosols from

Delhi

ampers the photolysis process of NO_2 .

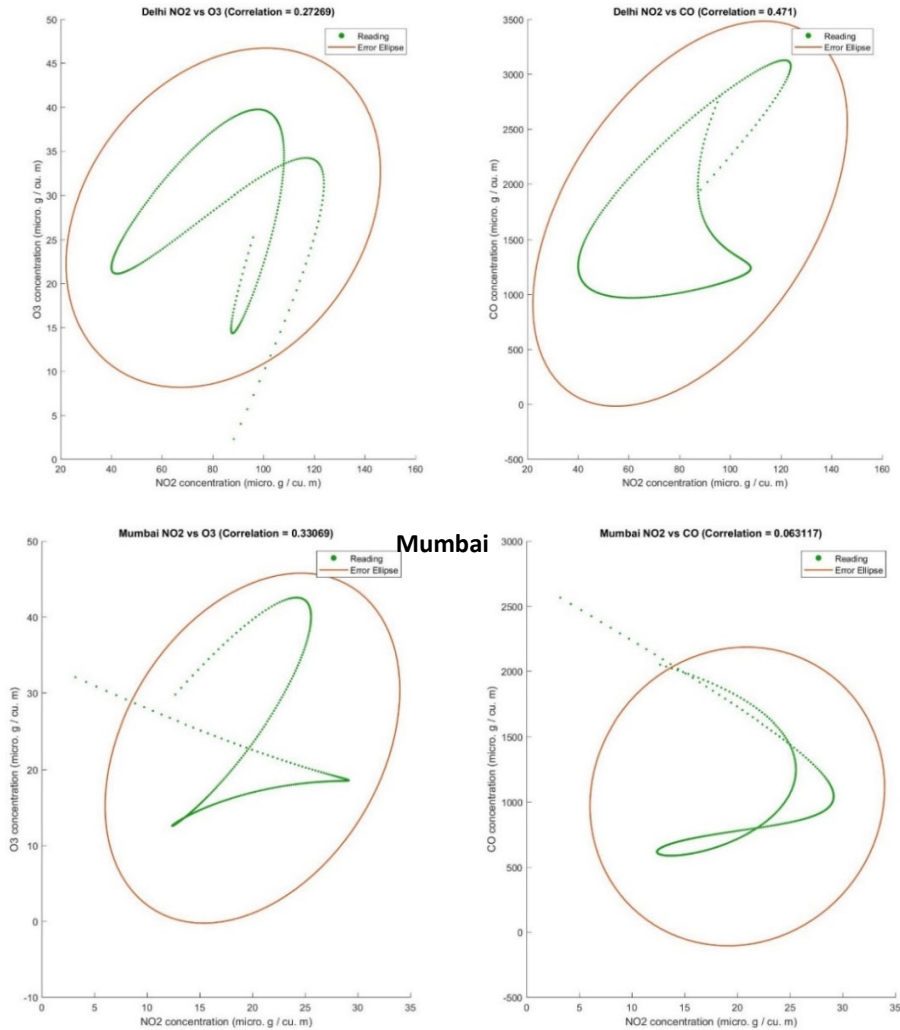


Figure 2: Correlation of NO_2 with O_3 and CO in both cities

*To keep abstract within page limits, all the figures and comparisons provided here are for only some of the pollutant and meteorological parameters.

CONCLUSIONS

Variation in geographical location of the two cities seems to have an impact on pollutant levels and relationship with meteorological conditions. Delhi has higher air pollutants concentration as compared to Mumbai and relationship with meteorological parameters is stronger. In Delhi, the concentration of all pollutants except ozone increases in winter season due to lower inversion layer condition and decreases in summer season due to turbulence which causes dispersion of pollution. Location of Mumbai by the seaside along with limited variation in temperature over a year, seems to be primary factors affecting pollutant levels. Only a small data set of three-year data for air pollutants could be analysed in this study and results clearly show that inter-relationship among pollutant levels needs further examination. Addition of data from oncoming years will add confidence in the correlations and help analyze more clearly the dependency of various parameters with each other.

ACKNOWLEDGEMENT

We want to thank Prateek Roy, Vinay Duli, Suresh Kuthadi and Ajeet Kumar who worked in undergraduate project course to help in data collection and preliminary analysis.

REFERENCES

Bhaskar, B. V., & Mehta, V. M. (2010). Atmospheric particulate pollutants and their relationship with meteorology in Ahmedabad. *Aerosol and Air Quality Research*, 10(4), 301–315. <https://doi.org/10.4209/aaqr.2009.10.0069>

Government of India (GOI). (2016). Open Government Data (OGD) Platform India. Retrieved August 21, 2018, from <https://data.gov.in/catalog/total-number-registered-motor-vehicles-india>

Seinfeld, J. H., & Pandis, S. N. (2006). *Atmospheric Chemistry and Physics: From Air Pollution to Climate Change*. *Atmospheric Chemistry and Physics*. <https://doi.org/10.1063/1.882420>

World Health Organisation. (2018). WHO Global Ambient Air Quality Database (update 2018). Retrieved August 21, 2018, from <http://www.who.int/airpollution/data/cities/en/>

PRELIMINARY APPROACH OF MONITORING POSSIBLE LINKAGE BETWEEN HEALTH EFFECTS AND OUTDOOR PM_{2.5} FROM A POLLUTED URBAN ENVIRONMENT

SHUBHANSHU TRIPATHI, VIKRAM CHOUDHARY, PRASHANT RAJPUT, TARUN GUPTA

Department of Civil Engineering, IIT Kanpur, Kanpur - 208 016, India

KEYWORDS: Impact of Aerosols on Human Health.

INTRODUCTION

The relationship between increasing levels of air pollution and morbidity and mortality rates (due to respiratory diseases) is known for a quite long time (Dockery et al., 1993). Recent research on exposure assessment of particulate matter has revealed severe implications to human health due to inhalation (GBD, 2015; Rajput and Gupta, 2016; Rajput et al., 2018). Assessment on morbidity and mortality due to major diseases, injuries and risk factors is being continuously carried out through Global Burden of Disease (GBD) research program (GBD, 2015). The GBD risk assessment report for year 2015 reveals high particulate matter (PM_{2.5}: particles having aerodynamic diameter $\leq 2.5 \mu\text{m}$) concentration to be one of the leading factors for causing premature deaths in India. Furthermore, the report explores that in India the exposure to air pollutants has led to at least 1 million deaths and 49 million people experiencing Disability Adjusted Life Years (DALYs) in 2015 (Special Report 21 HFI et al. 2017). India is home to 10 of the top 20 cities among the highest annual average levels of PM_{2.5} as per the WHO Urban Ambient Air Quality Database (2016). Lucknow, located in northern India, is among the most polluted cities in the world with Air Quality Index reaching hazardous and very unhealthy multiple times in the post-monsoon and winter months. PM_{2.5} has been linked previously to many adverse health effects like acute and chronic respiratory diseases (such as asthma and cough) and increased risk of mortality from non-communicable diseases such as chronic obstructive pulmonary (lung) disease, heart disease, stroke, lung cancer (Pope III et al., 2002) and from infections in lower-respiratory tract (Anderson et al., 2012). In this study, we have made attempts to collect the number of patients with reported respiratory and cardiology diseases from a major hospital and monitored its co-variability with ambient levels of PM_{2.5} in the Lucknow region from October 2017 to January 2018.

METHODOLOGY

PM_{2.5} data was collected from CPCB (Central Pollution Control Board, India) automatic monitoring station at Lalbagh, Lucknow (26.8 N, 80.9 E). Lalbagh is situated in the city center. The daily PM_{2.5} concentration was retrieved from October 2017–January 2018 and then monthly average has been estimated. Furthermore, the disease specific patient data from Lucknow region was collected from Ram Manohar Lohia Hospital, Gomti Nagar Lucknow (26.0 N, 81.9 E). This hospital caters to patient coming from all over state (U.P.), however, we collected data for disease specific patients only approaching from Lucknow region in order to assess and link up with PM_{2.5} variability observed from aforementioned site in the city center. Briefly, the patients data was recorded who got registered at OPD (Out Patient Department, in Lohia Hospital) for respiratory and cardiology related diseases from October 2017–January 2018. Linear correlation analysis has been performed between PM_{2.5} concentration and the number of patients on a monthly basis. We also looked at the sex (male-to-female) ratio of the patients trying to know who is more susceptible to air pollution.

RESULTS & DISCUSSION

Figure 1 gives the variability in number of patients (respiratory or chest and cardio) along with PM_{2.5} concentration on monthly basis. Basically, the number of respiratory patients exhibited a strong correlation ($R^2 = 0.75$, $p < 0.05$) with the monthly average concentration of PM_{2.5}. However, the correlation of PM_{2.5}

with the number of cardiology patients was found to be insignificantly low ($R^2 = 0.04$). The ratio of number of chest-to-cardio patients (on a monthly basis) also shows a quite significant variability (~ 0.5 – 0.7).

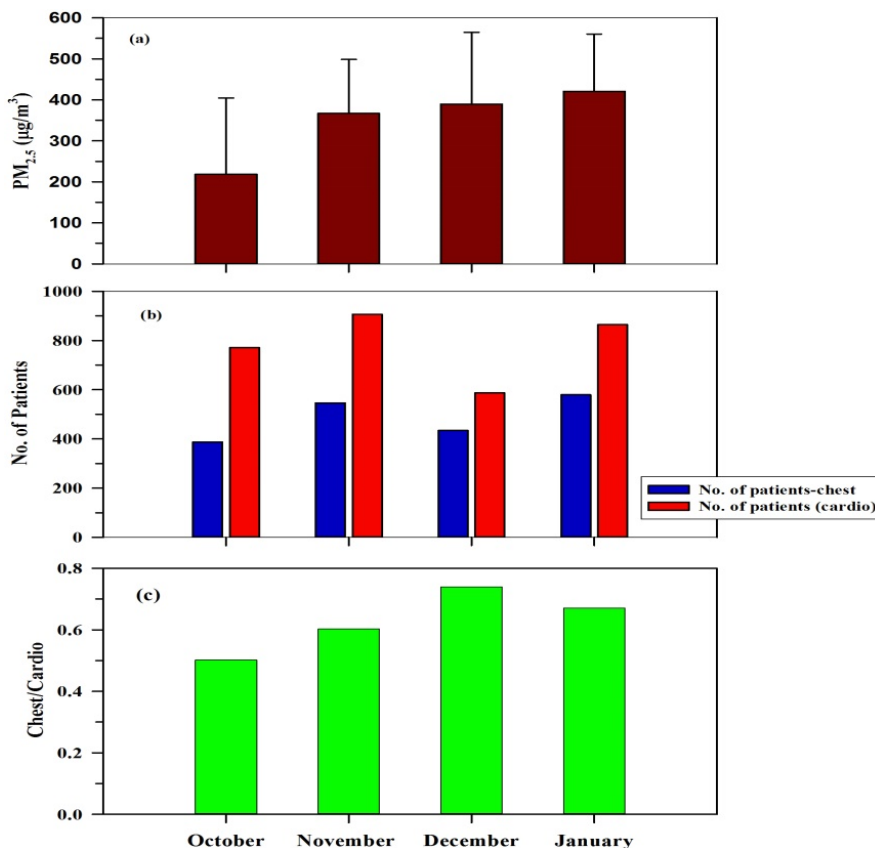


Figure 1. Monthly data of (a) Concentration of $PM_{2.5}$ ($\mu g/m^3$) (b) Number of Patients (Chest and Cardiology) (c) Ratio of number of chest and cardio patients.

We calculated the susceptibility of males and females individually with the varying concentration of $PM_{2.5}$. Figure 2 shows monthly male and female patients variation due to respiratory and cardio diseases. Among the respiratory patients, the female patients showed a better correlation of 0.79 as compared to the male patients for whom correlation of 0.68 was found ($p < 0.05$). In a sharp contrast, in the cardio disease subjects, the female patients gave a low correlation of 0.2 while the male patients had insignificant correlation. For respiratory and cardio male-to-female patients ratio > 1 suggests that the health of male subjects are more affected by outdoor $PM_{2.5}$ compared to the females as they spend relatively more time in outdoor air compared to the females. This observation revisits our previous finding of outdoor air pollution impact on human health of $PM_{2.5}$ (Rajput et al., 2018). More data set on disease specific patients would be required to better understand the impact of air pollution on human health.

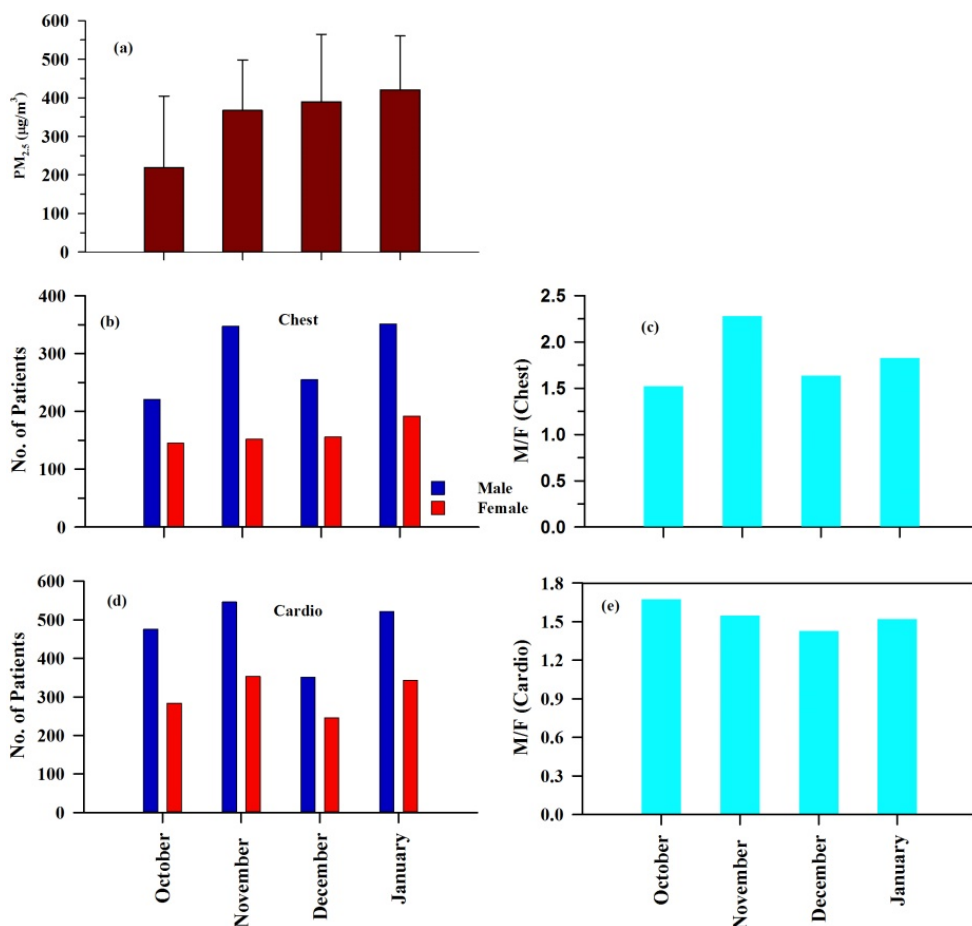


Figure 2. Monthly variation of: (a) concentration of PM_{2.5} (µg/m³), (b) Number of respiratory male and female patients, (c) ratio of number of male-to-female chest patients, (d) number of cardio Male and female patients and (e) ratio of number of male-to-female cardio patients.

CONCLUSIONS

Important outcomes based on preliminary study are:

- It appears that respiratory patients have a high direct linkage with PM_{2.5} concentration while cardio patients have little less direct affect by PM concentration.
- Males are more susceptible to outdoor air pollution levels than females.
- More study is required to better understand the linkage between air pollution and human health.

ACKNOWLEDGEMENT

This study has been carried out utilizing internal funds from IIT Kanpur. We thank the CMO of Ram Manohar Lohia Hospital who helped in availing the patient data. PR is thankful to the Council of Scientific & Industrial Research, India for granting CSIR-SRA fellowship (Pool Scientist # 8934-A/2017).

REFERENCES

Dockery, D.W., et al. (1993), An association between air pollution and mortality in six U.S. Cities, *New England Journal of Medicine* **329**, 1753-1759.

GBD, 2015. Institute for health metrics and evaluation (IHME), GBD compare, Seattle, WA: IHME, University of Washington, 2015 (accessed [30-09-2016]).

Global Burden of Disease Working Group (2017), Special Report 21: Burden of Disease Attributable to Major Air Pollution Sources in India.

Jonathan O Anderson, Josef G Thundiyil, Andrew Stolbach (2012), Clearing the Air: A Review of the Effects of Particulate Matter Air Pollution on Human Health, *Journal of Medical Toxicology*.

Pope III, C. A., Burnett, R. T., Thun, M. J. (2002), Lung Cancer, Cardiopulmonary Mortality, and Long-term Exposure to Fine Particulate Air Pollution, *Journal of American Medical Association*.

Rajput, P., Gupta, T. (2016), A facile digestion protocol for metal analysis in ambient aerosols: Implications to mineral dust characteristics and human health impact, *Journal of Energy and Environmental Sustainability* **2**, 24-29.

Rajput, P., Izhar, S., Gupta, T. (2018), Deposition modeling of ambient aerosols in human respiratory system: Health implication of fine particles penetration into pulmonary region, *Atmospheric Pollution Research* <https://doi.org/10.1016/j.apr.2018.08.013>.

IMPACT OF FOG PROCESSING ON LIGHT ABSORPTION PROPERTIES OF BROWN CARBON AEROSOLS IN INDO-GANGETIC PLAIN

VIKRAM CHOUDHARY, PRASHANT RAJPUT AND TARUN GUPTA

Department of Civil Engineering and APTL at Center for Environmental Science and Engineering (CESE), IIT Kanpur, Kanpur- 208 016

KEYWORDS: Carbonaceous aerosols, Aerosol monitoring and characterization

INTRODUCTION

Anthropogenic aerosols are predominantly derived from biomass burning emission and secondary transformations in the Indo-Gangetic Plain (IGP) (Rajput et al., 2018; Sorathia et al., 2018). Some of the aerosol species have been known to cause radiative imbalance in the Earth's atmosphere through scattering and absorption of solar radiation. The potential light absorbing carbonaceous aerosol species include elemental carbon (EC) and brown carbon (BrC). The EC absorbs solar radiation strongly in UV-Vis-NIR region, whereas BrC aerosols show strong solar absorption in UV or near blue region (300–400 nm) and moderate in visible region (Chen and Bond, 2010; Hecobian et al., 2010). The IGP experience dense foggy episodes during winter season (December–February). Previous studies (Kaul et al., 2011; 2012) have reported that fog/aqueous processing leads to enhanced secondary organic aerosol formation and evolution. Moreover, recent studies (Lee et al., 2014; Choudhary et al., 2017b; Satish et al., 2017) have suggested that photo-oxidation and aqueous processing leads to varying absorption properties and chemical composition of atmospheric BrC. Thus, it is important to assess spatial-temporal variability records in properties of BrC. Towards this, we have studied influence of fog processing on various absorption properties viz. absorption coefficient (b_{abs}), mass absorption efficiency (MAE), spectral dependence of absorbing component of refractive index (k_{abs}) spectra and direct radiative forcing of BrC relative to EC ($\text{DRF}_{\text{BrC}}/\text{DRF}_{\text{EC}}$).

METHODOLOGY

Sampling site (Kanpur: 26.30 °N, 80.14 °E) is located in central part of the IGP. Besides local sources, long-range transport of pollutants impacts the atmospheric composition and chemistry over central IGP. PM_{10} (particulates with aerodynamic diameter $\leq 10 \mu\text{m}$) samples have been collected during foggy ($n = 17$) and non-foggy nights ($n = 19$) onto preconditioned quartz filters using a low-volume air-sampler (Kumar and Gupta., 2015) on roof-top of Centre for Environment Science and Engineering (CESE) building inside the premises of Indian Institute of Technology Kanpur (India) during November 2014–February 2015 from 23:00 h–7:00 h. The identification of foggy and non-foggy episodes has been made based on physical observations and assessment of meteorological parameters viz. relative humidity (RH), ambient temperature (T) and visibility index. The foggy episodes are generally associated with high RH ($> 90\%$) and low visibility ($\leq 1\text{km}$) (Vautard et al., 2009). The extraction (sonication) of aerosol samples has been carried out by taking a portion of filter (3.14 cm^2) in 25 ml of Milli-Q (resistivity: $18.2 \text{ M}\Omega \text{ cm}$). Blank filters ($n = 4$) were also extracted and processed in the same way to aerosol samples. Soon after the sonication, each aqueous extract was filtered through a $0.22 \mu\text{m}$ filter in amber colored glass vial. Furthermore, the filtered aqueous extracts were subjected to determination of WSOC on a TOC analyzer and absorbance signal was measured on a dual-channel UV-VIS spectrophotometer (Choudhary et al., 2017a; Choudhary et al., 2017b). The concentrations of EC, OC and attenuation of EC (at 660 nm) have been measured by thermal-optical transmittance method using NIOSH protocol on a Sunset Lab EC-OC analyzer (Birch and Cary., 1996). The reported concentration and absorbance signal represent blank corrected values.

RESULTS AND DISCUSSION

Mass absorption efficiency

As discussed earlier, this study assesses influence of fog processing on absorption properties viz. b_{abs} , MAE, k_{abs} of BrC and EC. It is noteworthy that, absorption properties of BrC and EC have been assessed at 365 nm and 660 nm, respectively. The mathematical formulation to estimate b_{abs} and k_{abs} of BrC and of EC have been discussed in previous literatures (Choudhary et al., 2017a; Choudhary et al., 2017b). The linear regression analysis have been carried out between b_{abs} and concentration of BrC and EC as shown in figures 1a and 1b, respectively. The slope of linear regression represents MAE.

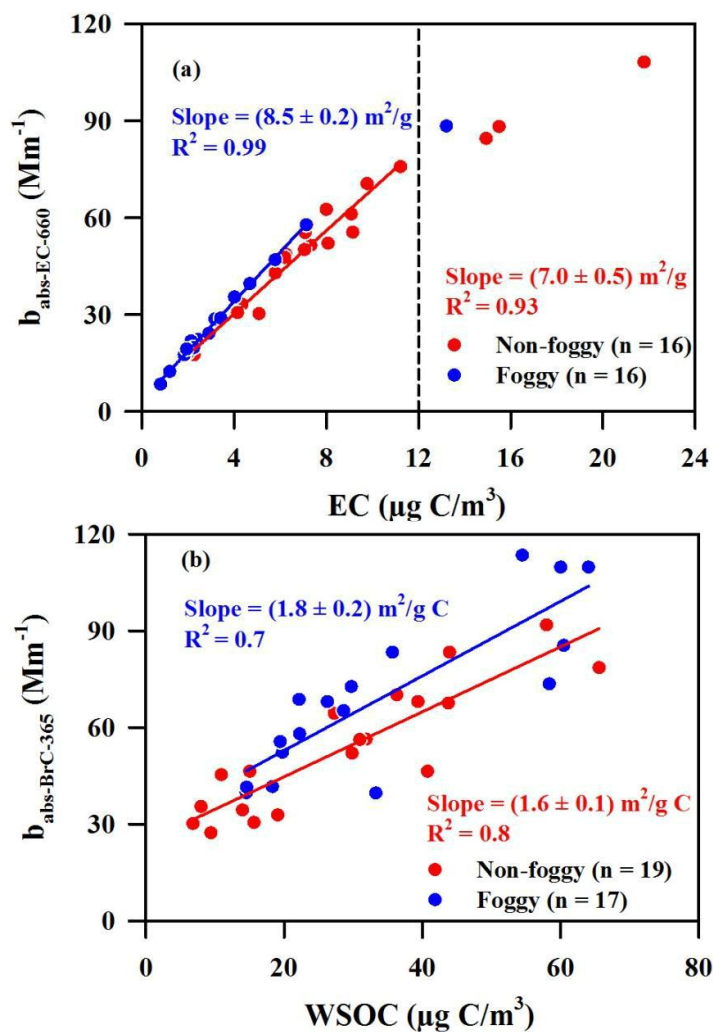


Figure 1. Linear regression analysis of: (a) $b_{\text{abs-EC-660}}$ of EC with its mass concentration and, (b) $b_{\text{abs-BrC-365}}$ of water-extractable BrC with WSOC in PM_{10} during foggy and non-foggy episodes at Kanpur.

As mentioned above, the slope of linear regression plot between $b_{\text{abs-EC-660}}$ (Mm^{-1}) and EC ($\mu\text{g C/m}^3$) represents $\text{MAE}_{\text{EC-660}}$. The $\text{MAE}_{\text{EC-660}}$ during foggy episodes (8.5 ± 0.2) $\text{m}^2/\text{g C}$ is relatively higher ($t = 1.11$; $p < 0.05$) as compared to that during non-foggy episodes (7.0 ± 0.5) $\text{m}^2/\text{g C}$ (Figure 1a). The enhancement ($\sim 20\%$) in $\text{MAE}_{\text{EC-660}}$ could be due to change in mixing state and lensing effect through coating formation on EC surface. It is worthwhile mentioning here that quite similar EC/ PM_{10} ($= 0.03$) during non-foggy and foggy episodes overrules the plausibility of change in $\text{MAE}_{\text{EC-660}}$ due to its source variability.

2.

The WSOC concentrations were found to be almost similar ($t = 0.9$; insignificant difference) during foggy and non-foggy events. However, $b_{\text{abs-BrC-365}}$ during foggy episodes was significantly higher ($t = 2.2$, significant difference) than that during the non-foggy episodes. This observation is also reflected

in higher $MAE_{BrC-365}$ during foggy episodes (1.8 ± 0.2) m^2/g C ($t = 3.8$; $p < 0.05$) as compared to that during the non-foggy episodes (1.6 ± 0.1) m^2/g C (Figure 1b). The enhancement of $\sim 20\%$ in MAE_{EC-660} (arising due to lensing effect through coating formation on EC surface) and of $\sim 15\%$ in $MAE_{BrC-365}$ has been attributed to fog-processing of carbonaceous aerosols. The influence of fog-processing in altering chemical composition of submicron aerosols has also been noted e.g. WSOC/OC and OC/EC ratios showed higher values during foggy periods.

Spectral dependence and direct radiative forcing

Spectral dependence of k_{abs} has also been assessed herein during foggy and non-foggy episodes (Figure 2a). Thus, it can be observed from figure 2a that spectral dependence of solar absorption behavior of BrC (k_{abs} spectra) during foggy and non-foggy periods look quite similar. Thus, it is inferred that spectral dependence of k_{abs} spectra has insignificant impact of the fog/aqueous processing.

Direct radiative forcing of BrC relative to that of EC has also been assessed across the solar spectrum ranging from 300–2500 nm and estimated using solar emission flux values and light absorption attenuation due to BrC in normalization with that of EC. Solar emission flux or spectral irradiance ($W/m^2/nm$), corresponding to clear sky condition, has been retrieved from Air Mass 1 Global Horizontal (AM1GH) spectral Irradiance model. The mathematical formulations to calculate direct radiative forcing of BrC relative to that of EC have been discussed in recent literatures (Choudhary et al., 2017a; Choudhary et al., 2017b). In the model, reference wavelengths (λ_0) have been taken as 365 and 660 nm for BrC and EC, respectively.

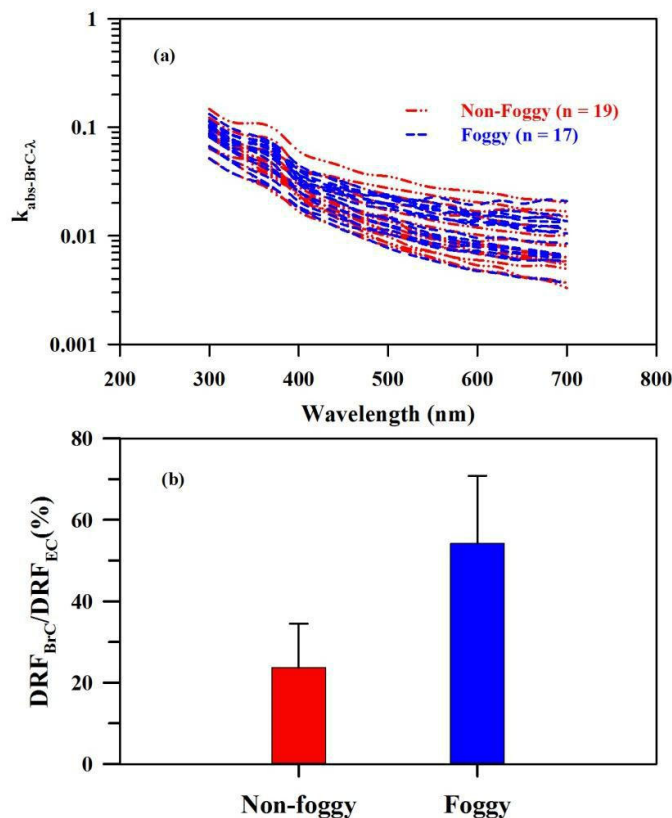


Figure 2. Figure showing: (a) Spectral dependence of k_{abs} of BrC and, (b) direct radiative forcing (DRF) of BrC relative to that of EC over Kanpur.

Figure 2b shows atmospheric direct radiative forcing of BrC relative to that of EC (DRF_{BrC}/DRF_{EC}) during foggy and non-foggy episodes in the IGP. In this study, average DRF_{BrC}/DRF_{EC} during non-foggy episode was found to be 24 (± 10)%, whereas relatively higher value of 54 (± 16.5)% has been estimated during the foggy episode. A large variability in relative DRF of BrC urges to monitoring absorption properties and radiative forcing of BrC from different geographical locations.

CONCLUSIONS

Important outcomes from our study are summarized below:

- (i) MAE of BrC and EC exhibited ~ 15 and $\sim 20\%$ enhancement due to fog-processing, respectively.
- (ii) Fog processing has insignificant influence on k_{abs} spectral dependence of BrC.
- (ii) DRF_{BrC}/DRF_{EC} during foggy episodes is relatively higher (by a factor of 2) as compared to that during non-foggy episodes.

ACKNOWLEDGEMENT

This study has been carried out with aid of internal funds from IIT Kanpur and partial funds were provided by Indian National Science Academy to Prof. Tarun Gupta to complete this study. PR is thankful to the Council of Scientific & Industrial Research, India for granting CSIR-SRA fellowship (Pool Scientist # 8934-A/2017).

REFERENCES

- Birch, M.E. Cary, R.A. (1996), Elemental carbon-based method for occupational monitoring of particulate diesel exhaust: methodology and exposure issues, *Analyst*, **121**, 1183-1190.
- Chen, Y., and T. C. Bond (2010), Light absorption by organic carbon from wood combustion, *Atmos. Chem. Phys.*, **10**, 1773.
- Choudhary, V. et al. (2017), Synergistic effect in absorption properties of brown carbon and elemental carbon over IGP during weak south-west monsoon, *Aerosol Science and Engineering*, **1**, 138-149.
- Choudhary, V. et al., 2018, Light absorption characteristics of brown carbon during foggy and non-foggy episodes over the Indo-Gangetic Plain, *Atmospheric Pollution Research*, <https://doi.org/10.1016/j.apr.2017.11.012>.
- Hecobian, A. et al. (2010), Water-Soluble Organic Aerosol material and the light-absorption characteristics of aqueous extracts measured over the Southeastern United States, *Atmos. Chem. Phys.*, **10**, 5965.
- Kaul, D.S., Gupta, T. Tripathi, S.N. (2012), Chemical and microphysical properties of the aerosol during foggy and nonfoggy episodes: a relationship between organic and inorganic content of the aerosol, *Atmos. Chem. Phys. Discuss.*, 2012, 14483-14524.
- Kaul, D.S. et al. (2011), Secondary Organic Aerosol: A Comparison between Foggy and Nonfoggy Days, *Environmental Science & Technology*, **45**, 7307-7313
- Kumar, A., and T. Gupta (2015), Development and laboratory performance evaluation of a variable configuration $PM_1/PM_{2.5}$ impaction-based sampler, *Aerosol Air Qual. Res.*, **15**, 768.

Lee, H.J. et al. (2014), Effect of Solar Radiation on the Optical Properties and Molecular Composition of Laboratory Proxies of Atmospheric Brown Carbon, *Environ. Sci. Technol.*, **48**, 10217.

Rajput, P., Singh, D.K., Singh, A.K., Gupta, T. (2018), Chemical composition and source-apportionment of sub-micron particles during wintertime over Northern India: New insights on influence of fog-processing, *Environmental Pollution*, **233**, 81-91.

Satish, R. et al. (2017), Temporal Characteristics of Brown Carbon over the Central Indo-Gangetic Plain, *Environmental Science & Technology*, **51**, 6765-6772.

Sorathia, F., P. Rajput and T. Gupta (2018), Dicarboxylic acids and levoglucosan in aerosols from Indo-Gangetic Plain: Inferences from day night variability during wintertime, *Science of the Total Environment*, **624**, 451-460.

Vautard, R., Yiou, P., van Oldenborgh, G.J., 2009. Decline of fog, mist and haze in Europe over the past 30 years. *Nature Geoscience* 2, 115.

ASSESSMENT OF FINE PARTICLE PROFILE IN SURFACE MINE USING AN ARTIFICIAL NEURAL NETWORK MODEL

M DHULIYA¹, S. GAUTAM^{1,3*}, S. MAJUMDAR², A.K. PATRA³, A. GUPTA¹

¹Department of Environmental Science & Engineering, Marwadi University, Rajkot, Gujarat – 360 003, India

²Department of Electronics & Communication Engineering, NIT Meghalaya – 793 003, India

³Department of Mining Engineering, Indian Institute of Technology, Kharagpur, Kharagpur – 721 302, India

KEYWORDS: Opencast Mine, Particulate Matter, Artificial Neural Networks.

INTRODUCTION

Generation of huge quantity of PM during mining activities is of concern for the environment as well as human health [Gautam et. al 2012]. Earlier studies show that PM from different kind of mining operations contribute to significant adverse effect on human health in the form of black lung, asthma, cardiovascular diseases and lung cancer [Hendryx & Ahern 2008]. However, only a few studies have provided information about generation, estimation and contribution of PM during mining operations in opencast mines [Zhang et. al 2013]. The study for dispersion of PM is therefore important because it will determine the level and duration of exposure of PM on mines workers. The PM travels and distributed in all benches from source [Gautam et. al 2014]. Thus, the concentration of PM contributes to the enhanced concentration for all benches of mine. With opencast mines going deeper day by day due to higher production, the study of dispersion and movement of PM in the mine needs attention.

Several empirical models have been developed to estimate the concentration of PM in a workplace environment. Statistical approaches sometimes under-perform the PM concentration from different sources [Onder & Yigit 2009]. Recently, Artificial Neural Network (ANN) model is being used for predicting concentration from the source then the evaluation is done by the experimental data. It shows fast processing with several input and output variables. Earlier studies reported that ANN based air quality models give better results than the other statistical model with good accuracy [Kumar & Goyal 2013]. ANN models have been very accurate in many environmental application areas, especially indoor environment. Hence, the advantages of ANN over statistical model can be concluded as (i) It do not require detailed physical models; (ii) It is more compact than large experiment data; (iii) It requires few training points to accurately model the standards; (iv) It can be trained on only a few experiments data; (v) It can be much more accurate than statistical models, when limited experimental data are available. As ANN models are shown so advantageous some drawbacks are also there. For example (i) In order to create training sets to obtain ANN models valid for a large range; intensive measurements have to be done; (ii) These models are very poor outside the range of the training set. These drawbacks can be overcome by implementing prior information into the design of neural networks.

However, very few studies have shown the usefulness of ANN model in order to, investigate the concentration inside opencast mine and validation of experimental data set to predict PM concentration profile with meteorological input variable inside opencast mine. In this work, ANN models were developed and tested to predict PM concentrations profile at Malanjkhand Copper Project (MCP). The results indicated that the ANN network was able to predict concentrations and shows significant agreement between the experimental results and the ANN model.

METHODS

Study site

The study was conducted in Malanjkhand Copper Project (MCP) of Hindustan Copper Limited (HCL) of India. The detail description of study area is described in our previous published research article [Gautam & Patra 2014].

ANN model

ANN model is implemented through the data collected from the experimental results. The data are divided into three parts they are as follows: Training: These are presented to the network during training of the model, and the network is adjusted according to its error; Validation: These are used to measure network generalization and to halt training when generalization stops improving; (Gautam et. al 2012) Testing: These have no effect on training and so provide an independent measure of network performance during and after training. Steps include data collection and assessment of PM and Meteorological parameters. The methodology of data collection of the study area for PM and meteorological parameters are mentioned in previous published article [Gautam & Patra 2014].

RESULTS & DISCUSSIONS

PM forecasting

The ANN model architecture of Fig. 1 is employed in this study to provide particle concentration in MCP mines. The monitored seven types of particle concentration at MCP mine have been utilized to train seven networks with each network corresponding to one particle concentration. All seven networks successfully achieved the target $R \approx 85\%$. However, evaluation for the ANN model performance has been developed utilizing different input patterns ranging between inputs like wind speed, humidity, temperature and depth.

In the context of this study, the authors used these performance indices to make sure that the proposed model could provide consistent levels of accuracy during all periods. The advantages of utilizing these two statistical indices as a performance indicator of the proposed model are first, to make sure that the highest error while evaluating the performance is within the acceptable error for such a forecasting model. This is done while utilizing the RMSE to ensure that the summation of the error distribution within the validation period is not high. Consequently, by using both indices it guarantees the consistent level of errors by providing a great potential for having the same level error while examining the model for unseen data in the testing period. The trial and error procedure for selecting the best parameter set of certain ANN architecture was performed, and the results (Fig.2) is explicating showing that the adopted procedure is the right way. Hence, once the network weights and biases are initialized during the training process, the weights and biases of the network are iteratively adjusted to minimize the network performance function mean square error (MSE) – the average squared error between the network outputs and the target outputs. In order to overcome and improve the proposed model performance, there is a great importance of input variables. The importance of input variables is described below.

Prediction of PM concentrations

The neural network developed and tested for this study was able to forecast the particle concentrations at a site. Comparative results obtained from an independent set of particle concentrations from a site and a relative error between the ANN model and the datasets (Figs. 2 and 3). The correlation coefficients (R) between real and forecasted data were very high in all the cases,

being 0.8, 0.85, 0.8, 0.89, 0.69, 0.67 and 0.78 for one site only; and the various other details are shown in the Table. 1.

Figure 2 shows the experimental results got from the MCP mines and adjacently the absolute error, between the ANN model and experimental results. The value R indicates the relation between outputs and targets (i.e. the experimental dataset found from the MCP mines). If R=1, this indicates the exact linear relationship between outputs and the target. If R is close to zero then there is no relationship between outputs and the target. The comparison of the results has been shown in Figure 3, which is nearly the same as the output derived from the ANN and the experimental dataset.

CONCLUSIONS

A supervised neural network (e.g., multilayer feed-forward networks) is generally used for prediction of fine PM concentration profile inside copper mine in the Madhya Pradesh state. This type of network is developed from a set of known variables and the end goal of the model is to match the predicted output values with the observed via ‘supervision’ of the training process by the analyst. ANN models were developed and tested to predict $PM_{0.23-0.3}$, $PM_{0.3-0.4}$, $PM_{0.4-0.5}$, $PM_{0.5-0.65}$, $PM_{0.65-0.8}$, $PM_{0.8-1}$, $PM_{1-1.6}$ concentrations profile inside opencast copper mine. The result shows that the ANN predictions given similar values as compared to experimental values. The results from the total measurement in mine indicated best performance on the test data by using ANN model with experimental results (PM concentration and meteorological data), where the concentration of PM decreased with increase in the distance (vertical) from the source. The R values of relationship between the real and the forecasted data of PM is varied from 0.67 to 0.85. The results of different size of PM are also indicated that wind speed, temperature and relative humidity play important role to transport PM from the source to different place inside the mine. Thus, it can be stated that the neural network models are able to predict the PM concentration profile inside opencast mine with good accuracy measure, so as to simplify implementation of acceptable control actions efficiently in advance. All the locations/ levels inside the opencast mines and its air quality are a serious concern for health of mine worker.

REFERENCES

- Gautam, S., Patra, A.K., & Prusty, B.K. (2012). Opencast mines: a subject to major concern for human health. *International Research Journal of Geology and Mining* **2**(2), 25–31.
- Hendryx, M., & Ahern, M.M. (2008). Relations between health indicators and residential proximity to coal mining in West Virginia. *American Journal of Public Health* **98** (4), 669-671.
- Zhang, X., Chen, W., Ma, C., & Zhan, S., (2013). Modeling particulate matter emissions during mineral loading process under weak wind simulation. *Science of the Total Environment* **449**, 168-173.
- Gautam, S., Kumar, P., & Patra, A.K. (2014). Occupational exposure to particulate matter in three Indian opencast mines. *Air Quality, Atmosphere and Health* doi: 10.1007/s11869-014-0311-6.
- Onder, M., & Yigit, E., (2009) Assessment of respirable dust exposures in an opencast coal mine. *Environmental Monitoring and Assessment* **152**, 393–401.
- Kumar, A., & Goyal, P. (2013). Forecasting of air quality index in Delhi using neural network based on principal component analysis. *Pure and Applied Geophysics* **170**, 711–722.

Gautam, S., & Patra, A.K. (2014). Dispersion of particulate matter generated at higher depths in opencast mines. *Environmental Technology and Innovation* doi: 10.1016/j.eti.2014.

Net. name	Training performance	Test performance	Training error	Test error	Training algorithm / epoch numbers	Error function	Hidden activation	Output activation	Output
MLP 4-35-1	0.82	0.67	0.0032	0.0043	TRAINLM/67	SOS	Tanh	Identity	PM _{0.23-0.3}
MLP 4-25-1	0.71	0.65	0.0023	0.003	TRAINLM/45	SOS	Tanh	Identity	PM _{0.3-0.4}
MLP 4-55-1	0.79	0.63	0.0025	0.0031	TRAINLM/17	SOS	Tanh	Identity	PM _{0.4-0.5}
MLP 4-35-1	0.75	0.69	0.0035	0.0035	TRAINLM/19	SOS	Tanh	Identity	PM _{0.5-0.65}
MLP 4-35-1	0.8	0.71	0.0022	0.0023	TRAINLM/23	SOS	Tanh	Identity	PM _{0.65-0.8}
MLP 4-29-1	0.85	0.6	0.009	0.006	TRAINLM/35	SOS	Tanh	Identity	PM _{0.8-1}
MLP4-60-1	0.56	0.67	0.01	0.009	TRAINLM/32	SOS	Tanh	Identity	PM _{1-1.6}

Table 1. Best network architectures for each particle dataset

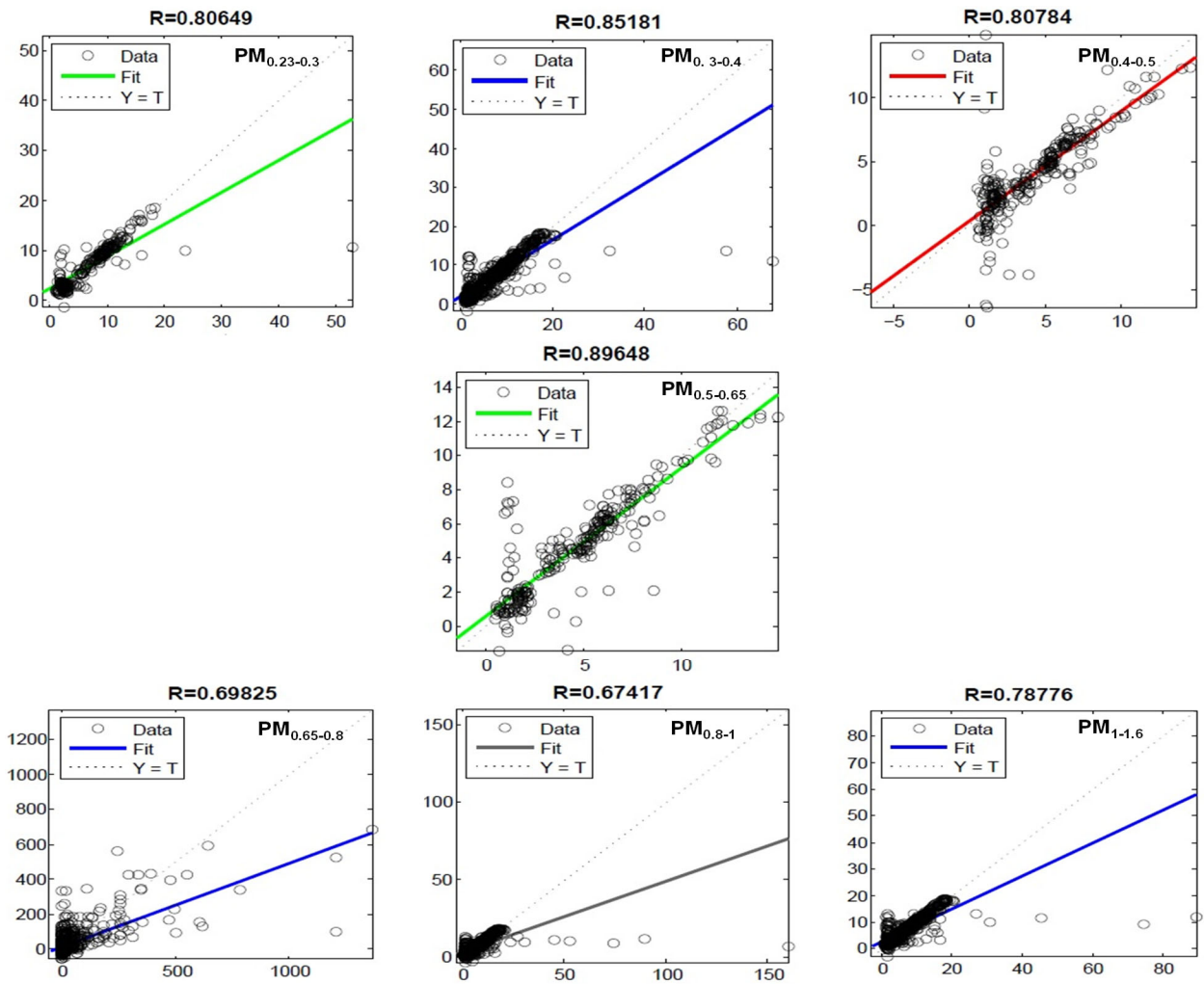


Figure 3. Performance of developed ANN model validation with experimental concentrations of PM at MC

EVALUATING THE ESTIMATED CONCENTRATION AND OPTICAL PROPERTIES OF AEROSOL COMPONENT FROM THE AERO-OPT (MATLAB PACKAGE)

SHIKHA VERMA¹, PRATIK TAGWALE¹, MUKUL KUMAR¹ AND SHUBHA VERMA¹

¹Department of Civil Engineering, Indian Institute of Technology

Kharagpur-721302, India.

KEYWORDS: Aero-Opt, Trust Region Optimisation Method.

INTRODUCTION

Aerosol plays an important role in energy budget of the Earth, both directly by the scattering and absorption of solar radiation and indirectly by modifying cloud properties. It is required to know the adequate aerosol optical and chemical properties of particulate atmospheric species that affects regional radiation forcing, the radiation balance, and thus climate. Since atmospheric aerosol concentrations peak close to major source regions thus giving rise to regional hot-spots, aerosol-induced radiative impact could be more significant on a local to regional scale than the global, which in turn can have strong implications for the regional hydrological cycle. It is difficult to quantify such impacts at a finer resolution of the urban scale using large-scale chemistry-climate models due to their coarser resolution and inefficiency to simulate fine scale aerosol properties. The properties of aerosol particles are highly variable, both in time and space due to variety of sources for different species, their short residence time, large influence of prevailing meteorological conditions and the various complex aerosol dynamic processes. This is valid for the number density (amount of particles per volume), microphysical properties like size distribution, refractive index and shape, and for the vertical distribution. There is still a lack of understanding of aerosols impact on the regional climate system. The spatio-temporal variability in aerosol properties thus poses a challenge to the scientific community in terms of modeling of aerosol physical, chemical and optical properties needed for an accurate assessment of their interactions with climate on a regional to global scale.

Moreover, it is not feasible to measure the concentration of all species of aerosol in the atmosphere due to various constraints including the lack of proper experimental setup or facilities. Ground based observational data (e.g. aerosol optical depth, angstrom exponent, black carbon concentration, total aerosol mass concentration) is available but are limited in content. On the other hand, Satellite based observations provide continuous retrievals of aerosol data and their quantification globally, but are coarsely-resolved. Aerosol species contributing to the aerosol budget at a fine grid resolution is required to be established.

In this present study, a software tool, AeroOpt (a Matlab package) is developed that can help integrating the available observations to adequately obtain the aerosol mass and aerosol optical depth closure. Tool leads to estimate aerosol species mass concentration and their optical properties for the particular location and spatial distribution for the entire region by optimising a constrained nonlinear multivariable objective function. The included aerosol species consists of water soluble, water insoluble, soot, sea-salt (accumulation mode), sea-salt (coarse mode), mineral (nuclei mode), mineral (accumulation mode), mineral (coarse mode), mineral (transported) and sulfate respectively. The tool is user-friendly, computationally efficient, and can be handled to modify the grid-resolution, change observational aerosol parameters as per their availability.

METHODS

AeroOpt is an indigenously developed matlab package that estimates the concentration and optical properties of aerosol components. It is of two types. The first type is to be used in order to estimate the aerosol concentrations of a point station by giving the input parameters of only that particular station. The second type is useful in case the user wants to calculate the aerosol concentration of a region or spatial distribution at a chosen grid resolution. It allows the calculation of the optical properties of aerosols for eight different relative humidity and 61 wavelengths. It calculates optical properties that include extinction

coefficient, scattering coefficient, absorption coefficient, single scattering albedo, asymmetric factor, aerosol optical depth, normalized extinction coefficient, lidar ratio, mass extinction cross section, mass absorption cross section, special turbidity, phase function and visibility.

The optical properties of aerosol species is calculated, allowing external mixing of components (i), using the formula

$$\theta = \sum_i \theta_i^1 N_i \quad (1)$$

where θ is the optical parameter under consideration and θ^1 is the optical parameter normalised to 1 particle cm^{-3} .

To implement the trust region optimisation approach (Byrd, 2000), an objective function is constructed which will take a set of variables or a vector as an input i.e. $f(x)$ (where x is a vector) and give a scalar as output. The objective function is minimised by given algorithm untill convergence is met.

We can find mass concentration of ten aerosol species by minimising the objective function given as:

Objective function:

$$\begin{aligned} &= f(x_1, x_2, x_3, x_4, x_5, x_6, x_7, x_8, x_9, x_{10}) \\ &= (\text{aod_model}(x_1, x_2, x_3, x_4, x_5, x_6, x_7, x_8, x_9, x_{10}) - \text{aod_measured})^2 \\ &\quad + (\text{ae_model}(x_1, x_2, x_3, x_4, x_5, x_6, x_7, x_8, x_9, x_{10}) - \text{ae_measured})^2 \\ &\quad + ((x_1 + x_2 + x_3 + x_4 + x_5 + x_6 + x_7 + x_8 + x_9 + x_{10}) - \text{tmass_measured})^2 \end{aligned}$$

Subject to constraints

$$\begin{pmatrix} 0 & 0 & 1 & 0 & 0 & 1 & 1 & 1 & 1 & 1 & 1 & 0 & 0 & 0 & 0 & 1 & 1 & 1 & 1 & 1 \end{pmatrix} (x_1 \ x_2 \ x_3 \ x_4 \ x_5 \ x_6 \ x_7 \ x_8 \ x_9 \ x_{10}) = \begin{pmatrix} \text{bcmass_measured} & \text{tmass_measured} \end{pmatrix} \quad (2)$$

Here $x_1, x_2, x_3, x_4, x_5, x_6, x_7, x_8, x_9, x_{10}$ represent the mass concentration of the ten aerosol species, and bcmass_measured , tmass_measured , aod_measured , ae_measured represent mass of black carbon, the total aerosol mass, aerosol optical depth (AOD) and angstrom exponent (AE) respectively., aod_model and ae_model are created functions which take the mass concentrations as input and give corresponding values of the aerosol optical depth and angstrom exponent are calculated by model.

The Mie equations for AOD (τ), extinction coefficient (σ_e), Angstrom exponent (AE or α) were used in the model as given below:

$$\tau = \sum_j \sigma_{e_j}^1 N_j(0) \int_{H_{j,\min}}^{H_{j,\max}} e^{-\frac{h}{Z_j}} dh = \sum_j \sigma_{e_j}^* \frac{x_j * \text{tmass}}{\text{mass}_i} \int_{H_{j,\min}}^{H_{j,\max}} e^{-\frac{h}{Z_j}} dh \quad (3)$$

$$\sigma_e(\lambda) = \beta \lambda^{-\alpha} \quad \text{where,} \quad \alpha = \frac{\log[\sigma_e(\lambda_2)] - \log[\sigma_e(\lambda_1)]}{\log(\lambda_1) - \log(\lambda_2)} \quad (4)$$

The flowsheet and input interface of AeroOpt is presented in Figures 1(a) and 1(b) respectively.

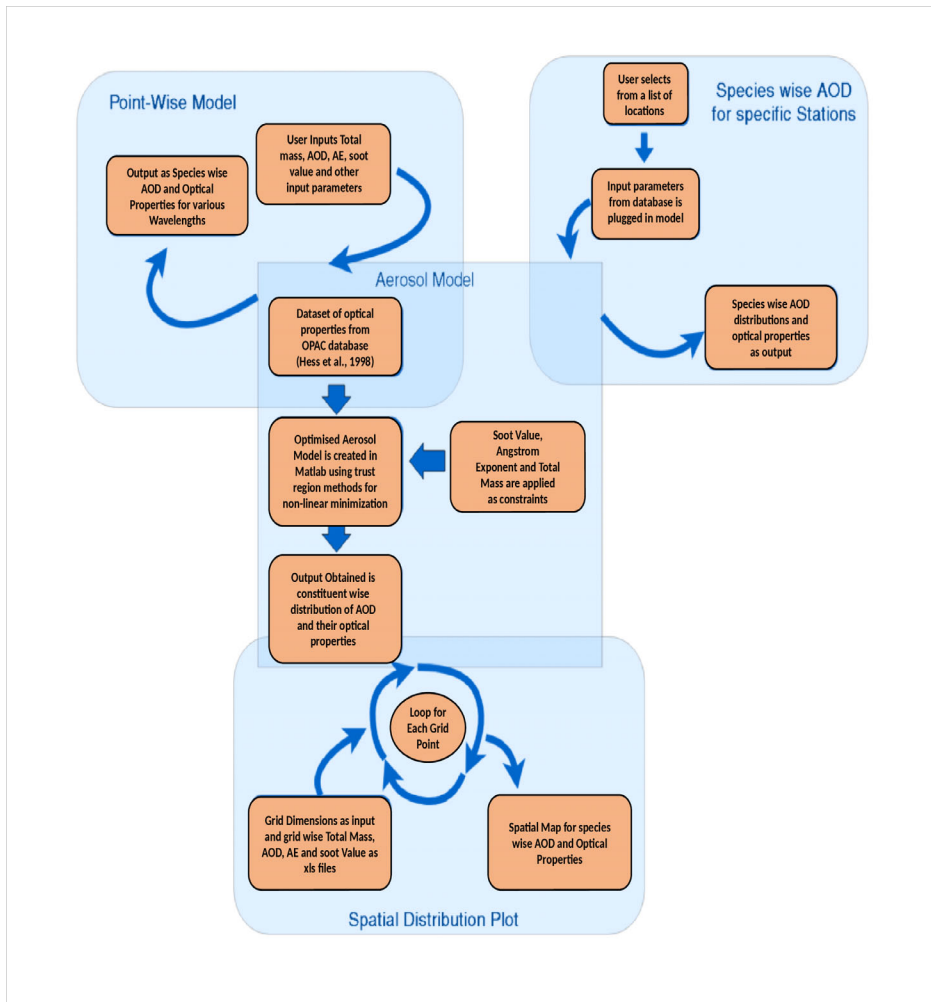


Figure 1. a) Flowsheet of AeroOpt model

Mass of Soot(ug/m3)	<input type="text" value="Edit Text"/>			Properties to be calculated		
TotalMass(ug/m3)	<input type="text" value="Edit Text"/>			<input type="radio"/> Extinction Coefficient	<input type="radio"/> Scattering Coefficient	
Relative Humidity	<input type="text" value="Edit Text"/>			<input type="radio"/> Absorption Coefficient	<input type="radio"/> Single Scattering Albedo	
AOD	<input type="text" value="Edit Text"/>	<input type="text" value="Edit Text"/>	Wave length(in um) at which AOD is measured			
Angstrom Coeffit	<input type="text" value="Edit Text"/>	<input type="text" value="Edit Text"/>	<input type="text" value="Edit Text"/>	Wave length(in um) at which Angstrom coeffit is measured		
Mixing Layer Height	<input type="text" value="Edit Text"/>			<input type="radio"/> Norm. ext. Coefficient	<input type="radio"/> Lidar Ratio	
Mineral Transported Height	<input type="text" value="Edit Text"/>			<input type="radio"/> mass ext. cross section	<input type="radio"/> mass abs. cross section	
Height Profile			Wavelengths to be calculated			
	Hmin	Hmax	Z	<input type="radio"/> 0.25 um <input type="radio"/> 0.75 um <input type="radio"/> 3.20 um <input type="radio"/> 6.5 um <input type="radio"/> 10.0 um <input type="radio"/> 17.2 um <input type="radio"/> 0.30 um <input type="radio"/> 0.80 um <input type="radio"/> 3.39 um <input type="radio"/> 7.20 um <input type="radio"/> 10.6 um <input type="radio"/> 18.0 um <input type="radio"/> 0.35 um <input type="radio"/> 0.90 um <input type="radio"/> 3.50 um <input type="radio"/> 7.90 um <input type="radio"/> 11.0 um <input type="radio"/> 18.5 um <input type="radio"/> 0.40 um <input type="radio"/> 1.00 um <input type="radio"/> 3.75 um <input type="radio"/> 8.20 um <input type="radio"/> 11.5 um <input type="radio"/> 20.0 um <input type="radio"/> 0.45 um <input type="radio"/> 1.25 um <input type="radio"/> 4.00 um <input type="radio"/> 8.50 um <input type="radio"/> 12.5 um <input type="radio"/> 21.3 um <input type="radio"/> 40.0 um <input type="radio"/> 0.50 um <input type="radio"/> 1.50 um <input type="radio"/> 4.50 um <input type="radio"/> 8.70 um <input type="radio"/> 13.0 um <input type="radio"/> 22.5 um <input type="radio"/> 0.55 um <input type="radio"/> 1.75 um <input type="radio"/> 5.00 um <input type="radio"/> 9.00 um <input type="radio"/> 14.0 um <input type="radio"/> 25.0 um <input type="radio"/> 0.60 um <input type="radio"/> 2.00 um <input type="radio"/> 5.50 um <input type="radio"/> 9.20 um <input type="radio"/> 14.8 um <input type="radio"/> 27.9 um <input type="radio"/> 0.65 um <input type="radio"/> 2.50 um <input type="radio"/> 6.00 um <input type="radio"/> 9.50 um <input type="radio"/> 15.0 um <input type="radio"/> 30.0 um <input type="radio"/> 0.70 um <input type="radio"/> 3.00 um <input type="radio"/> 6.20 um <input type="radio"/> 9.80 um <input type="radio"/> 16.4 um <input type="radio"/> 35.0 um		
Mixing Layer Height	<input type="text" value="Edit Text"/>	<input type="text" value="Edit Text"/>	<input type="text" value="Edit Text"/>	<div style="text-align: center;">Calculate</div> <input type="button" value="Spatial Plot"/> <input type="button" value="Specific Location Simulation"/>		
Mineral Transported Height	<input type="text" value="Edit Text"/>	<input type="text" value="Edit Text"/>	<input type="text" value="Edit Text"/>			
Mixing Layer Height	<input type="text" value="Edit Text"/>	<input type="text" value="Edit Text"/>	<input type="text" value="Edit Text"/>			
Mixing Layer Height	<input type="text" value="Edit Text"/>	<input type="text" value="Edit Text"/>	<input type="text" value="Edit Text"/>			

Figure 1. b) Input Interface for AeroOpt model

RESULTS AND DISCUSSIONS

The comparison of Aerosol optical depth (AOD) and Angstrom Exponent (AE) from AeroOpt with observations at 10 cities (Remote area (Anantpur), North India (Delhi, Patiala, Agra and Kanpur), South India (Hyderabad and Trivandrum), East India (Bhubaneswar and Kolkata)) is presented in Figures 2(a) and 2 (b).

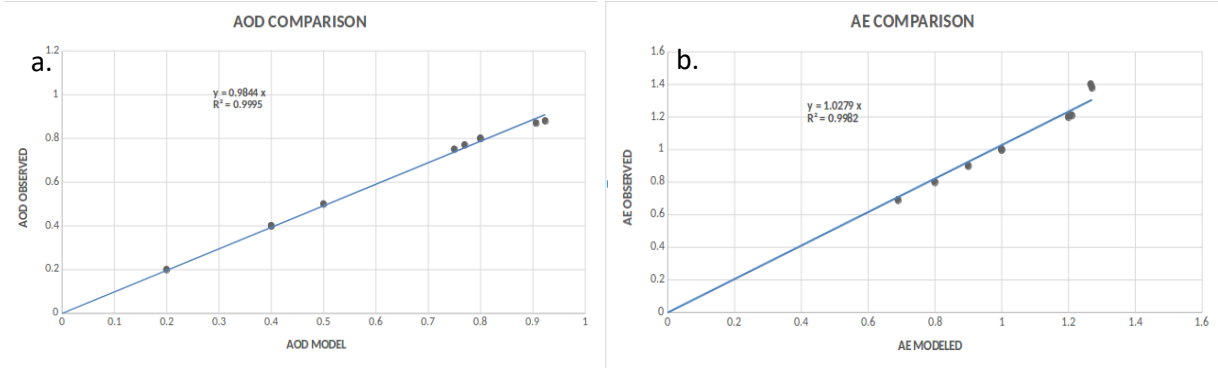


Figure 2. Comparison between Observed and Modeled for a) AOD, b) AE

Observed and modeled values of AOD and AE are found to be well correlated with each other ($R^2 = 0.99$). Further, the comparison of AOD and AE estimated for AeroOpt with observations at three locations namely Delhi, Kanpur and Ahmedabad is presented in Table 1.

S.no.	Stations	Time Period	AOD		Bias%	AE		Bias%	SSA		Bias%
			Observed	Modeled		Observed	Modeled		Observed	Modeled	
1.	Delhi	December	0.91	0.910	0.004	1.27	1.27	0.008	0.68	0.7	2.94
2.	Kanpur	December-February	0.619	0.65	5.02	1.267	1.216	4.05	0.90	0.85	5.56
3.	Ahmedabad	December-March	0.309	0.317	2.87	1.04	1.035	0.469	0.73	0.78	6.85

Table 1. Validation of tool with measured values of aerosol single scattering albedo (SSA)

The efficacy of AeroOpt tool is tested through validating optical properties of aerosols including SSA obtained from tool with the measured values for the three stations of mainland India. The relative bias between model and observations for the estimated AOD and AE is within 5% and that for the SSA is within 7% .

CONCLUSION

AeroOpt is intended to serve as a tool to users who need to describe the optical properties of aerosol composition in the atmosphere. Using limited information such as the Aerosol Optical depth, AE, total particulate matter and soot mass, the tool is able to estimate the optical properties of different aerosol species at different wavelengths and relative humidity. It can further be used by introducing more constraints in the objective function to get more accurate results as per availability of measured data.

REFERENCES

Hess, M., Koepke, P., & Schult, I. (1998). Optical properties of aerosols and clouds: The software package OPAC. *Bulletin of the American meteorological society*, 79(5), 831-844.

Byrd, R.H. (2000). A trust region method based on interior point techniques. *Mathematical Programming*, 149-185.

SOURCES AND IMPLICATION OF BLACK CARBON (BC) AEROSOLS SIMULATED OVER HINDUKUSH-HIMALAYAN (HKH) REGION ON GLACIER SNOWMELT RUNOFF

SAUVIK SANTRA¹, SHUBHA VERMA¹, KOJI FUJITA², INDRAJIT CHAKRABORTY¹, OLIVIER BOUCHER³, TOSHIHIKO TAKEMURA⁴, JOHN F. BURKHART⁵, FELIX MATT⁵ AND MUKESH SHARMA⁶

¹Department of Civil Engineering, Indian Institute of Technology Kharagpur, India

²Graduate School of Environmental Studies, Nagoya University, Nagoya, Japan

³Institut Pierre-Simon Laplace, Centre National de la Recherche Scientifique/Sorbonne Université, 75252 Paris Cedex 05, France

⁴Research Institute for Applied Mechanics, Kyushu University, Fukuoka, Japan

⁵Department of Geosciences, University of Oslo, Norway

⁶Department of Civil Engineering, Indian Institute of Technology Kanpur, India

KEYWORDS: Aerosol and Climate Change, Black Carbon in glacial snowpack, Snow albedo reduction, Annual glacier runoff increase.

INTRODUCTION

Emissions of black carbon (BC) aerosols arise from the combustion of fuel for residential cooking, industrial and transportation usage, and from open biomass burning. Black carbon impacts the climate through a direct effect by absorbing sunlight and an indirect effect through cloud alterations in precipitation efficiency. Another impact due to absorbing aerosols such as BC exists on the cryosphere by altering the ablation rate of ice. Deposited black carbon over snow enhances absorption of solar radiation, darkens the upper mixing layers of the snowpack thereby reducing the snow albedo and leading to accelerated melting of snow (Flanner et al., 2007). Available observational studies over the Hindukush-Himalayan (HKH) region suggests the region being exposed to considerable particulate pollution and deposition of BC. Further, the impact of BC aerosols on the snowpack, surface radiation, and temperature changes over the HKH region based on simulations in global climate models suggest a significant effect of anthropogenic forcing over the HKH region as compared to that over the Tibetan Plateau. However, the ability of coarse-gridded models to simulate adequately the snow depth and thereby the BC concentration in snow and atmospheric BC radiative forcing is limited.

The influence of the albedo change on the glacial mass balance due to an excess and preponed snow melting and thereby the glacier runoff is expected to affect the downstream hydrology. This impact is specifically of concern for the HKH region as the Himalayan glaciers are the source of major rivers in South Asia namely Ganges, Indus, Yamuna, and Brahmaputra (also known as Tsangpo). The inaccessible terrain and severe weather conditions in the higher Himalayan region hinder the measurement of atmospheric BC concentration and BC concentration in the snow at regular spatial as well as temporal intervals. The measured data may thus serve as a location and time specific primary data and not a representative sample of the regional distribution.

The simulated BC concentration, using atmospheric chemical transport models (CTMs), which is validated by measurements, can be utilized to predict the spatial mapping of BC distribution over the HKH region. In order to spatially map as adequately as possible the estimates of atmospheric BC concentration and BC concentration in snow (BC_C) including the corresponding snow albedo reduction (SAR) over the HKH region, an integrated approach merging the relevant information from observations with a relatively consistent atmospheric chemical transport model estimates is applied in the present study. Numerical simulations of annual glacier runoff height and snow-albedo are carried out using glacial mass balance model to evaluate the impact of BC-induced SAR on increase in annual snowmelt runoff from glaciers. To find out the sources of BC aerosols over the HKH region, BC simulation in atmospheric General Circulation Model (GCM) is analysed.

METHODS

In the present study, we evaluate BC concentration estimated from three free running aerosol simulations (*freesimu*) using Laboratoire de Météorologie Dynamique atmospheric General Circulation Model (LMD-ZT GCM) (Verma et al., 2011) and Spectral Radiation Transport Model for Aerosol Species (SPRINTARS) over the HKH region. This evaluation includes comparison of simulated BC concentration with available observations for winter (monthly average of December, January, and February) and pre-monsoon (monthly average of March, April, and May) season, at locations, classified as low-altitude (LA) stations (e.g. Nainital, Kullu, and Dehradun), which are in close proximity to emission sources; and high-altitude (HA) stations (e.g. Hanle, NCO-P, and Satopanth), which are relatively remotely located and mostly influenced by transport of aerosols. Constrained aerosol simulation (*constrsimu*) is also formulated (Kumar et al., 2018) and estimates are evaluated over the LA stations.

The two *freesimu* with the LMD-ZT GCM comprises of (i) LMD-ZT GCM - with India emissions (GCM-indemiss), (ii) LMD-ZT GCM coupled to the Interactions between Aerosols and Chemistry (INCA) model (LMDORINCA) with global emissions, or namely GCM-INCA. Aerosol simulations in GCM are also referred to as free running aerosol simulations (*freesimu*) since simulated aerosol fields are not constrained by observations, unlike constrained simulations.

The constrained simulation (*constrsimu*) approach takes into account the influence of a possible discrepancy in base emissions, the localized effect of high emission flux (from the plains near LA), and the combined effect of inter-annual variability in meteorological effects (Kumar et al., 2018). This is used to establish an alternate approach for estimating the atmospheric BC concentration by surpassing the error induced specifically due to emissions in source regions which prevail in case of the free running aerosol simulations. In constrained simulations, GCM-indemiss AOD is constrained by the observed AOD. An inversion algorithm is formulated to obtain the surface concentration of BC from constrained AOD of aerosol constituents. It may be notable that constrained simulations are considered only for the LA stations. The HA stations which are far away from the source of emissions, the impact of regional emission bias is postulated to be minor and aerosol pollutants are primarily governed by the atmospheric transport processes (simulated atmospheric residence time) from the surrounding regions. Our postulate is supported by the fact that BC from *freesimu* of GCM-indemiss that are underestimated by a large factor at LA stations match consistently well with available observations at HA stations. Hence, in the present study, simulated BC from GCM-indemiss is considered a suitable choice (based on analysis of the performance of the model with measurements) for evaluation of BC-induced SAR and its impact on annual snowmelt runoff from the glaciers under study.

BC concentration in the snow ($\mu\text{g kg}^{-1}$) during pre-monsoon and winter is calculated using atmospheric BC concentration from GCM-indemiss and dry deposition velocity, taking into account the interseasonal and spatial variation of snow density over the study region. Percentage SAR corresponding to the calculated BC_C is estimated using an empirical model as well as using an online radiative model (Snow, Ice, and Aerosol Radiation (SNICAR) (Flanner et al., 2007)). Values estimated using both the models compare well. To quantify the impact of BC-induced SAR on annual snowmelt runoff for the glacier, we calculated the mass balance and runoff from nine selected glaciers with an energy and mass balance model (Fujita and Ageta, 2000). The selected glaciers are widely distributed over the HKH region and located near the zone of high BC_C values. The estimated impact of BC-induced SAR on annual glacier runoff is affected not only by the amount of BC_C but also by glacier hypsometry and climatic setting. To quantify these effects, we further calculated the sensitivity of annual glacier runoff to albedo change with two different configurations, (1) with a single glacier hypsometry at different ERA-Interim grids, and (2) with different glacier hypsometries at a single ERA-Interim grid. The configuration (1) demonstrates how different climatic settings affect the annual runoff sensitivity while configuration (2) shows how different altitudinal profiles affect the results.

In order to examine the source of BC aerosols over the HKH region due to emissions from different types combustion sectors and that from near-by or far-off regions, source and region-tagged BC simulation in LMD-ZT GCM is evaluated.

RESULTS & DISCUSSIONS

Model estimates (free running simulations and constrained simulations) are compared to measurements. The predictions of the models, especially of GCM-indemiss at the high altitudes are in more sanguinity with the measured than rest other models. It may be noted that HA stations are accompanied with relatively lower values of measured BC concentration compared to LA stations.

At LA stations, estimated values of BC concentration from *freesimu* of GCM-INCA and GCM-indemiss are underestimated by a large factor. At LA stations, we also evaluate the estimates from *constrsimu* with measurements. Estimates of BC concentration from the *constrsimu* exhibit a better concurrence than that from *freesimu* with the measured concentration at all the three LA stations.

As *freesimu* of GCM-indemiss has the highest conformity with the measurements at HA stations, hence we utilize BC concentration simulated in GCM-indemiss to estimate BC_C and BC-induced SAR and their impact over the HKH region. The estimated value of BC_C from the present study compares well with that obtained from previous work and has a variation of 10% to 27% from the earlier studies. These estimates compare relatively well at Hanle and NCOP, however, at Satopanth during winter they are overestimated compared to the respective measured value.

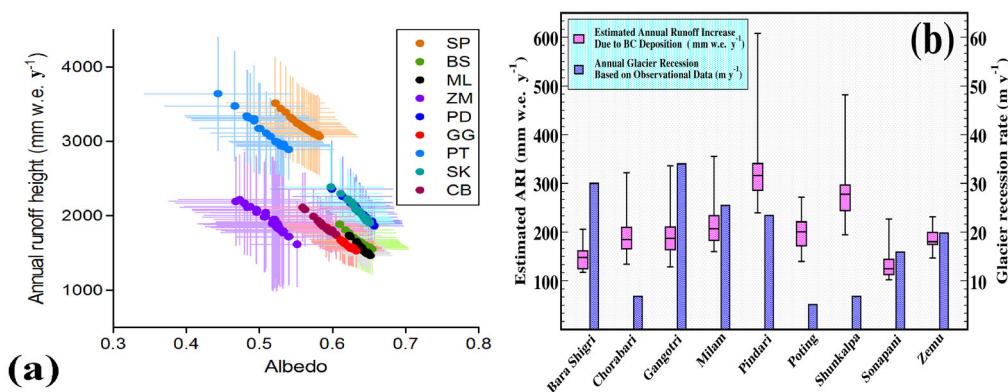


Figure 1: (a) Simulated impact of albedo reduction on annual glacier runoff (mm w.e. y^{-1}) from the Sonapani (SP), Bara Shigri (BS), Milam (ML), Zemu (ZM), Pindari (PD), Gangotri (GG), Poting (PT), Shunkalpa (SK) and Chorabari (CB) glaciers, (b) Estimated increase in annual glacier runoff (mm w.e. y^{-1}) and average yearly recession ($m y^{-1}$) for the nine glaciers.

The simulated impact of albedo reduction on annual snowmelt runoff (mm of water equivalents per year, mm w.e. y^{-1}) from glaciers using a glacial mass balance model (Fujita and Ageta, 2000) is presented in Figure:1a. The Sensitivity of annual glacier runoff to albedo change was found to be more negative than that for the cold Tibetan glaciers. Figure:1b presents the estimated annual runoff increase (ARI) in mm w.e. y^{-1} along with glacier wise average annual recession in meters (as obtained from available observational studies) for the nine glaciers under study. The calculated values of ARI have the highest value for the Pindari glacier followed by that for the Shunkalpa glacier. Although the ARI for Milam glacier found to be lower than the Pindari, this glacier witnesses the highest percentage increase of ARI w.r.t. the control run (with the null value of BC_C), followed by Pindari. From Figure:1b, it can also be seen that the Gangotri glacier is the most rapidly shrinking one among the HKH glaciers under study, having a maximum yearly recession of as high as 34 meters, followed by Bara Shigri, Milam, and Pindari.

The relative distribution of BC surface concentration and BC-AOD due to BC emissions originating from the near-by region, IGP (BC concentration or BC-AOD due to emissions from the IGP to the total BC concentration or BC-AOD) and far-off region, Africa-west Asia (AFWA) during winter and pre-monsoon seasons over the HKH region is estimated. It is observed that while BC concentration and BC-AOD due to

emissions from the IGP has a slightly higher value during pre-monsoon than winter, it is vice-versa for that due to emissions from AFWA. This feature is inferred likely due to emissions of biomass burning (crop-waste and forest fires) which is more prominent during pre-monsoon over the IGP but that during winter over AFWA as obtained from the information of fire counts data from satellite-based measurements. It is observed that, while BC surface concentration during winter and pre-monsoon are influenced mostly due to biofuel emissions over part of the HKH region south to 30°N (where there is a relatively higher contribution from emissions over the IGP), these are due to biomass burning over north to 30°N, thus corroborating the above inference.

CONCLUSIONS

BC concentration estimated from *freesimu* performed better over higher altitude (HA) HKH stations than that over lower altitude (LA) stations. The estimates from *constrsimu* mirrored well the measurements when implemented for LA stations. Estimates of BC concentration in snow (BC_C) was consistent with that obtained from the available study, and its spatial mapping led to identify the hot-spot zone over the HKH region. Analysis of BC_C over the identified glaciers located in the vicinity of the hot-spot zone over the HKH region showed specifically high BC_C and BC-induced SAR over glaciers near to the Manora peak, over the northern Himalayan region, with their highest being that for Pindari and Poting. Using long-term BC simulations from SPRINTARS, the relative (%) rate of increase of BC_C for the present years (with respect to 1961) is estimated being the highest for the glacier (Zemmu) near eastern Himalayan region. Sensitivity analysis of annual glacier runoff to BC-induced albedo change indicated that HKH glaciers are more sensitive than cold Tibetan glaciers. The source-specific contribution to atmospheric BC aerosols by emission sources led to identifying the potential emission source being primarily from the biofuel combustion in the Indo-Gangetic plain for areas south to 30°N, and from open burning from a more remote region for areas north to 30°N.

ACKNOWLEDGEMENTS

This work was supported through a grant received from the Department of Science and Technology (INT/NOR/RCN/P05/2013) and from the Ministry of Environment, Forest, and Climate Change (14/10/2014-CC (Vo.II)), Govt. of India.

REFERENCES

- Flanner, M. G., Zender, C. S., Randerson, J. T., and Rasch, P. J.: Present-day climate forcing and response from black carbon in snow, *J Geophys. Res.*, 112, D11202, 2007.
- Fujita, K. and Ageta, Y.: Effect of summer accumulation on glacier mass balance on the Tibetan Plateau revealed by mass-balance model, *Journal of Glaciology*, 46, 244–252, 2000.
- Kumar, D. B., Verma, S., Boucher, O., and Wang, R.: Constrained simulation of aerosol species and sources during pre-monsoon season over the Indian subcontinent, *Atmospheric Research*, 214, 91–108, 2018.
- Verma, S., Venkataraman, C., and Boucher, O.: Attribution of aerosol radiative forcing over India during the winter monsoon to emissions from source categories and geographical regions, *Atmos. Environ.*, 45, 4398–4407, <https://doi.org/10.1016/j.atmosenv.2011.05.048>, 2011

CHEMICAL SIGNATURES OF URBAN, OPEN BURNING AND DUST TRANSPORTATION IN A TROPICAL URBAN ENVIRONMENT OVER EASTERN INDIAN REGION

B. PRIYADHARSHINI¹, S. VERMA¹, A. CHATTERJEE², S. K. SHARMA³, T. K. MANDAL³ AND K. DUBEY¹

¹Department of Civil Engineering, Indian Institute of Technology Kharagpur, Kharagpur -721302, India.

²Bose Institute, Environmental Sciences Section, P1/12, C.I.T. Scheme VII-M, Kolkata- 700 054, India.³CSIR-National Physical Laboratory, Dr K. S. Krishnan Road, New Delhi 110012, India.

KEYWORDS: Aerosol Chemical Characterization, Water-Soluble Inorganic Ions, Carbonaceous Aerosols.

INTRODUCTION

Knowledge of aerosol chemical composition provides essential information about sources and processes that can affect the aerosol concentration at a particular place (Zhang et al., 2017). The chemical composition of aerosols has an important role in determining their relative efficiency to absorb and scatter the solar radiation. Also, the amount of water-soluble aerosol species in the atmosphere would impact the development of cloud condensation nuclei and thereby contribute to the quantity, lifetime, and brightness of clouds (Rosenfeld et al., 2008). Though the atmospheric abundance of aerosol constituents is known in general, the chemical composition would exhibit temporal and spatial heterogeneity owing to the short residence time of aerosol species, influence from the source- and region-specific emission sources and meteorological effects. This heterogeneity thereby leads to uncertainty in the prediction of aerosols-induced climatic impacts, and therefore, necessitates examining temporal features of aerosol chemical species on a regional to local scale, and that distinctly for fine and coarse aerosols.

In the present study, we examined the fine aerosol (aerodynamic diameter $\leq 1.6 \mu\text{m}$) chemical constituents of water-soluble inorganic ions (WSII) and carbonaceous aerosols (CA, organic carbon (OC) and elemental carbon (EC)) over a tropical urban atmosphere in the lower Indo-Gangetic plain (IGP), at Kolkata, in eastern India, during the daytime hours (10 00- 16 00 IST). Sampling is done using a devised submicron aerosol sampler (SAS) with the two- stage staged filter units (SFU) for the simultaneous but discrete sampling of WSII and CA. Discrete sampling using separate substrates is done for a better characterization of WSII and CA. The chemical sampling is carried out during daytime hours (10 00-16 00 IST) to evaluate the relative abundance of daytime fine aerosol chemical composition in the urban atmosphere. The daytime mean aerosol concentration exhibits a low hourly variability and corresponds to the well-mixed layer of atmosphere. The daytime analysis of aerosol chemical characteristics thus aids in linking, the change in the temporal feature (e.g., the trend of monthly mean values) of the measured tracer aerosol species concentration in the atmosphere, primarily to the impact of emission sources. Also, this analysis leads to account for aerosol species which would be interacting with the incoming solar radiation and influencing the aerosol optical depth in the eastern India urban atmosphere.

The primary focus of the present study is on the fine aerosol-chemistry through the investigation of the temporal variation of the water-soluble inorganic species, organic and elemental carbonaceous species, along with the partitioning of the aerosols into natural and anthropogenic aerosols. This study also intends to determine the probable sources of aerosol and their monthly variation over a tropical megacity, Kolkata, where air pollution is already a severe concern. This urban atmosphere in eastern India is also typical as it evinces a strong outflow of aerosol pollutants from the IGP (Kumar and Verma, 2016).

METHODS

Sampling of ambient fine aerosol particles was carried out over a tropical eastern India urban atmosphere in the lower IGP, at Kolkata. Measurements were carried out at the Indian Institute of Technology (IIT), Kharagpur, Extension Centre (22.57°N, 88.42°E) situated at the outskirts of Kolkata city, on the rooftop of a building 12 m above the ground level from September 2010 to August 2011. A SAS with two SFU's was

indigenously designed and fabricated at the workshop of IIT Kharagpur using the considerations of Norwegian Institute for Air Research (NILU) protocol (Mayol-Bracero et al., 2002; Gabriel et al., 2002). The framework of SAS consisted of two SFU's in parallel with a common inlet of 20 mm connected to a pick-off tube of 1.8 cm and a suction pump. The air sucked using a suction pump passes via the common inlet, bifurcates to parallel conduit consisting of four perforated stainless steel filter holders each sandwiched between two polyethylene rings of diameter 34 mm. Nuclepore filter paper (47 mm, 8.0 μm) was placed on the first stage of both the SFU to collect the coarser fraction ($\geq 1.6 \mu\text{m}$, calculated based of the filter face velocity). While a Quartz filter (Pallflex Tissuquartz 2500 QAT-UP) was placed on the one side, a PTFE membrane filter of pore size 2.0 μm was placed on the other side of the SFU's second stage. The Quartz filter and PTFE filters were used for the collection of respectively the carbonaceous and WSII species. Discrete sampling using separate substrates is helpful for a better characterization of WSII and CA; e.g., PTFE for WSII and Quartz for CA through thermal carbon analysis.

The SAS was designed to maintain a flow rate of 25 L min^{-1} to achieve a face velocity of 47 cm s^{-1} . At the calculated face velocity of 47 cm s^{-1} corresponding to the designed flow rate of 25 L min^{-1} of the devised SAS, the nuclepore filter would entrap particles of cut-off diameter 1.3 μm . However, during the study period over the tropical urban environment, the average face velocity obtained was 28 cm sec^{-1} . Also, the devised SAS is designed to transmit particle with 50% efficiency, or "cut-size," of 6.8-9.6 μm and that with 90% efficiency of 2.6-3.7 μm . Hence, the coarse fraction collected on nuclepore filter would consist of particles larger than 1.6 μm (cutoff-size) (calculated for an average face velocity of 28 cm sec^{-1}) and smaller than 10 μm (50% cutoff-size of the sampler transmission) aerodynamic diameter. Based on the above, the cut-off size for particle collected on PTFE which is chemically characterized in the present study is 1.6 μm . The analysis of WSII species and CA were carried using Metrohm 761 Compact Ion chromatography (IC) and OC/EC (Model: DRI 2001A, USA) analyzer using Interagency Monitoring of PROtected Visual Environments (IMPROVE-A) protocol. The handling of filters (both PTFE and Quartz) and their quality assurance were maintained following the considerations of NILU protocol.

RESULTS & DISCUSSIONS

The monthly mean concentrations of the total WSII (T_{WSII} : sum of analyzed WSII species) are shown in Figure. 1a. The monthly mean of T_{WSII} is estimated as 45-86 $\mu\text{g m}^{-3}$ with an annual mean of $65 \pm 13 \mu\text{g m}^{-3}$. It is seen that species such as Ca^{2+} , Cl^- , Mg^{2+} , NO_3^- , Na^+ and SO_4^{2-} contributes relatively higher to T_{WSII} than NH_4^+ , K^+ , PO_4^{3-} and F^- at the study site. Annual mean concentrations of WSII showed a relative predominance of cations (anions) consisting of Ca^{2+} , Mg^{2+} , and Na^+ (Cl^- , NO_3^- and SO_4^{2-}), with secondary aerosols (NH_4^+ , NO_3^- , and SO_4^{2-}) and Ca^{2+} each constituting 25% and 30% respectively, of the T_{WSII} . The highest monthly mean concentration of SO_4^{2-} and NO_3^- are observed during February and March and May, respectively. Pronounced peak in monthly mean of non-sea salt- K^+ (nss- K^+) concentration is noticed during October and April months implying the strong influence of biomass burning emissions. Enhanced concentration of nss- K^+ reported in the present study is also consistent with the peak in fire counts obtained from ATSR World Fire Atlas (WFA) over Indian region. The mass ratio of NO_3^- to SO_4^{2-} greater or lesser than one has been used to identify the relative predominating influence of respectively mobile or stationary sources to atmospheric aerosols. The monthly mean ratio of NO_3^- to SO_4^{2-} is between 0.56 and 4.72 with an annual mean value of 1.6 ± 1.2 . This ratio is ≥ 1 during the during the entire study period except that during September and February, when it is ≤ 1 . The pattern of this ratio at the study site thus indicates a relatively predominant influence of mobile sources compared to the stationary sources to atmospheric aerosol throughout the study period except during September and February. Among the sea salt (SS), anthropogenic (AN) and dust (DT) sources of the T_{WSII} , a relatively predominant contribution of DT in August and of AN in November, April and May is inferred (Figure. 1b).

Monthly mean concentration of OC and EC during the period of study are 19-34 $\mu\text{g m}^{-3}$ and 4-11 $\mu\text{g m}^{-3}$ with the annual mean of OC ($24 \pm 5 \mu\text{g m}^{-3}$) being three times the EC ($7 \pm 2 \mu\text{g m}^{-3}$). The estimated monthly mean of secondary organic carbon-SOC (primary organic carbon-POC) values using EC tracer method is about 23-61% (39-77%) of the respective monthly mean of total OC. The annual mean concentration of OC is three times higher than EC with 43% of it being secondary OC. Total estimated aerosol mass (Figure 1c) analyzed in the present study is calculated by summing the individual species measured (i.e., EC,

particulate organic matter (POM) ($OC \times 1.6$), and the water-soluble ions) and does not include insoluble inorganic components (fly ash and mineral dust). The fractional contribution of the monthly mean (September to July) of WSII, POM and EC is respectively 45-69%, 27-45%, and 4-10% of that of the total estimated aerosol mass concentration (sum of WSII, POM, and EC). The calculated monthly mean of OC to EC ratio during the study period is 2-5 with an annual mean value of 3. Peak in OC to EC ratio is observed during the months of October-November and then during the months of March to July. The trend of the monthly mean of $nss-K^+$ indicates the highest peak during October and April with moderate peak during November-January-May-September. The peak in the values of OC-EC ratio is concordant to $nss-K^+$ during most of the period, thereby indicating a predominant influence of biomass combustion sources to OC measured in eastern India urban atmosphere. Based on analysis of the OC-EC thermograms the major sources of OC are inferred to be the paved dust, coal combustion, and biomass burning, these of EC are industrial/motor-vehicle emissions, coal combustion, and motor vehicle exhaust.

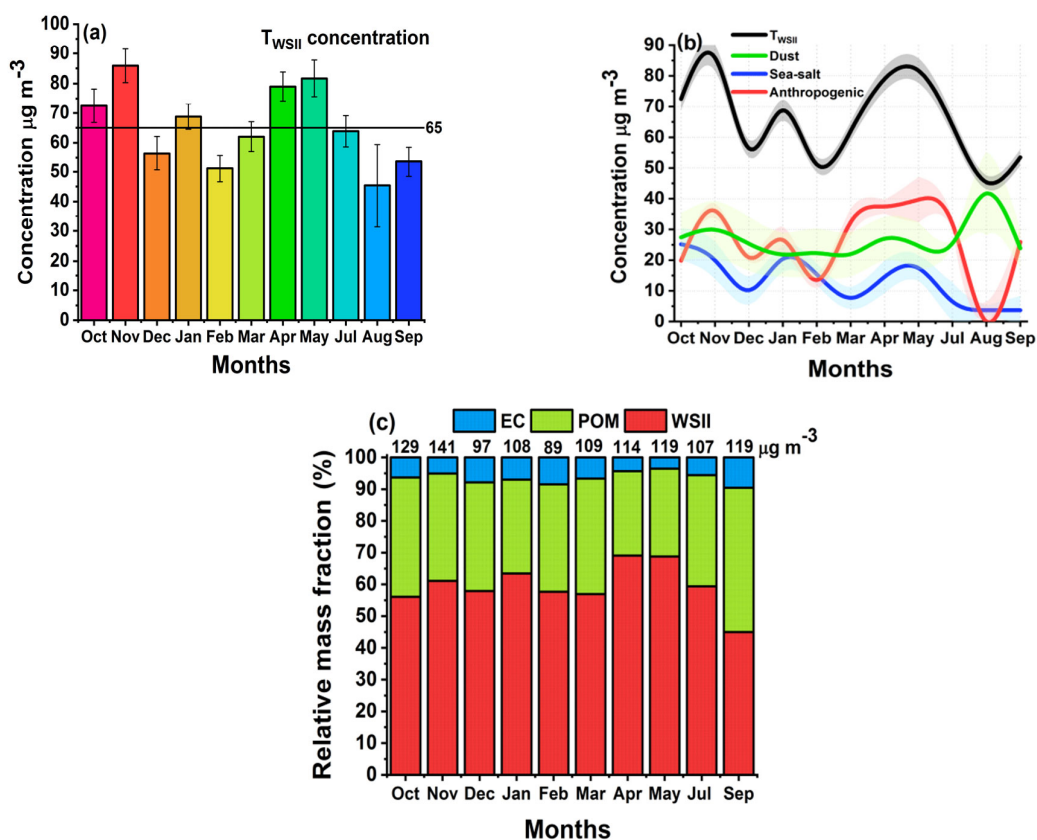


Figure 1. (a) Total monthly mean concentration of water-soluble inorganic ions. The T_{WSII} annual mean concentration is marked as a solid black line, (b) Temporal trend of monthly mean concentration of SS, AN and DT aerosols along with T_{WSII} at Kolkata. Shaded regions along with line plot indicate the standard deviation, (c) The relative fractional distribution of monthly mean of WSII, POM and EC. The monthly mean of total estimated concentration is also shown at the top of each bar.

CONCLUSIONS

In the present study, the daytime sampled fine aerosol particles (cut-off size of $1.6 \mu m$) were chemically characterized to evaluate the relative abundance of ambient aerosol species, their temporal variation, and probable sources at urban atmosphere Kolkata.

The most abundant WSII species throughout the period of study were Ca^{2+} , Mg^{2+} and Na^+ among the cations, these were Cl^- , NO_3^- and SO_4^{2-} among the anions. The mean of the secondary WSII aerosols (NH_4^+ , NO_3^- and SO_4^{2-}) over the entire period of study was estimated constituting 25% of that of T_{WSII} , which was nearly equivalent to that of Ca^{2+} (30%).

While the peak in the monthly mean concentration of SO_4^{2-} was observed during the winter month (February), this of NO_3^- was during the summer months (March and May). The trend of the monthly mean of nss-K^+ exhibited pronounced peaks in months of October and April, implying the predominant influence of biomass burning emissions at the study site in these months.

The monthly mean OC concentration exhibited a larger variability than EC, with the annual mean concentration of OC being three times that of EC, and that 43% of it comprised of the secondary OC. The monthly mean of OC to EC ratio exhibited temporal peaks in concurrence with that of nss-K^+ .

The chemical characterization of fine aerosol particles suggested the signatures of mixed influence of urban, open burning, and dust impacting atmospheric aerosols over eastern Indian urban atmosphere.

ACKNOWLEDGEMENTS

Computing resources and experimental work at the Indian Institute of Technology Kharagpur were supported through a grant received from the Department of Science and Technology, Govt. of India (SR/FTP/ES-54/2007). The financial support from the Indian Ministry for Human Resource Development is also acknowledged.

REFERENCES

- Gabriel, R., Mayol-Bracero, O. L., and Andreae, M. O. (2002). Chemical characterisation of submicron aerosol particles collected over the Indian Ocean. *J. Geophys. Res. Atmos.* 107.
- Kumar, D. B., and Verma, S. (2016). Potential emission flux to aerosol pollutants over Bengal Gangetic plain through combined trajectory clustering and aerosol source fields analysis. *Atmos. Res.* 178: 415-425.
- Mayol-Bracero, O. L., Gabriel, R., Andreae, M. O., Kirchstetter, T., Novakov, T., Ogren, J., Sheridan, P., and Streets, D. (2002). Carbonaceous aerosols over the Indian Ocean during INDOEX: Chemical characterisation, optical properties and probable sources. *J. Geophys. Res. Atmos.* 107.
- Rosenfeld, D., Lohmann, U., Raga, G.B., O' Dowd, C.D., Kulmala, M., Fuzzi, S., Reissell, A. and Andreae, M.O. 2008. Flood or drought: how do aerosols affect precipitation? *Science.* 321: 1309-1313.
- Zhang, Y., Tang, L., Croteau, P. L., Favez, O., Sun, Y., Canagaratna, M. R., Wang, Z., Couvidat, F., Albinet, A., Zhang, H. and Sciare, J. (2017). Field characterization of the $\text{PM}_{2.5}$ aerosol chemical speciation monitor: insights into the composition, sources, and processes of fine particles in eastern China. *Atmospheric Chem. Phys.* 17: 14501-14517.

SEASONAL VARIATION IN BLACK CARBON BURDEN SIMULATED WITH WRF-CHIMERE MODEL OVER INDIAN SUBCONTINENT

S. GHOSH¹, S. VERMA², R. RAY² AND K. DUBEY²

¹ Advanced Technology Development Centre Indian Institute of Technology Kharagpur, West Bengal - 721 302, India.

² Department of Civil Engineering Indian Institute of Technology Kharagpur, West Bengal -721 302, India.

KEYWORDS: Black Carbon, Chimere, Seasonal Variability, Uncertainty.

INTRODUCTION

The abundance of absorbing aerosols during the pre-monsoon season over the Indian subcontinent, consisting of locally emitted black carbon (BC) and of dust transported from near-by and far-off region have been suggested leading to elevated atmospheric heating effect. Role of BC aerosols in influencing the regional hydrological cycle is evidenced through studies with aerosol-chemistry-climate models (Fadnavis et al., 2017). Increase in BC emissions from combustion of fossil fuels (coal and oil) for energy and transportation, industrial and agricultural activities, biomass burning and deforestation are the major concerns in this context. Unlike greenhouse gases which are long-lived and uniformly distributed over the globe, aerosols exhibit a large temporal and spatial variation due to their various sources of emission, sinks and short residence time in the atmosphere. The spatial distribution and magnitude of BC radiative forcing could thus be different over the tropical and non-tropical world regions during different seasons, causing climate responses due to aerosol related air pollution which differs regionally and globally.

Over south Asia, BC emissions are inferred being mostly arising from residential biofuel usage (Venkataraman et al., 2005). In addition, season- and region-specific anthropogenic activity (e.g. open biomass burning from agricultural crop-waste and forest biomass) lead to high rise BC emissions being injected in the upper layers of the atmosphere. Besides the season-specific anthropogenic influence, the inter-seasonal atmospheric processes attributed to meteorological effects would lead to seasonal variability in the atmospheric BC distribution and its mixing with the atmospheric aerosol constituents. Seasonal variability is inferred being exhibited in observed BC concentration over the Indian region with the highest value reported generally between November and February at stations over the Indo-Gangetic plain. It is necessary to understand the prevalent factors that control the seasonal cycle of atmospheric BC burden. There are a few available studies on the seasonal cycle of BC simulated with the regional or global model (e.g. Kumar et al., 2015). While the model BC concentration was found reproducing the observed seasonality relatively well, it deviated by a large value with-respect-to the observed BC magnitude. The possible reasons for the discrepancy between model and measurements as inferred in available studies included inadequate BC emissions, the discrepancy in meteorology, aerosol processes and representation of mixing state of aerosols, and too coarse resolution in the model.

In the present study, we evaluate the seasonal cycle of BC concentration over the Indian subcontinent, driven by seasonal changes in emission flux (Smog-India, Pandey et al., 2014) and meteorological conditions. This is done simulating the BC concentration ($0.25^\circ \times 0.25^\circ$ spatial resolution) for a period of one year over the Indian region in a Chemistry Transport Model (CTM) CHIMERE. Station wise simulated BC mass concentration values were compared with observed data of each station for all the seasons in order to find the variation in uncertainty in model evaluated values. Hence, the specific objective of this study is to analyze the influence of BC emission and meteorological conditions in the seasonal variability of simulated BC surface concentration using CTM over the Indian subcontinent and to find the season to season alteration of uncertainty in model evaluated BC mass.

METHODS

Weather Research and Forecasting Model (WRF) coupled with CHIMERE was configured to simulate the surface concentration of BC for the present study. The initial meteorological conditions and lateral boundary conditions incorporated in CHIMERE were obtained from WRF simulation using Modern-Era Retrospective analysis for Research and Applications, Version 2 (MERRA 2) dataset. The chemical boundary conditions and land uses were obtained from a global aerosol model, LMDz4-INCA (Laboratoire de Météorologie Dynamique General Circulation Model coupled with INCA: Interaction with Chemistry and Aerosols) and GLCF (Global Land Cover Facility). Second order Van Leer scheme was applied for horizontal transport phenomena in CHIMERE. BC simulations were carried out over the domain of Indian subcontinent extending from 6° N to 38° N and 68° E to 99° E for all the twelve months (January to December), 2015. Monthly emission datasets extracted from Smog-India (2015) emission inventory (Pandey et al., 2014) with $0.25^\circ \times 0.25^\circ$ horizontal resolution were used for simulation of BC burden. The total annual emission calculated for the Smog-India bottom-up inventory over India is 1325 Gg y^{-1} . Hourly simulation of BC was carried out for each day of all the months for the year 2015 using Smog-India emission dataset. Measurements data in the present study are classified in terms of six seasonal periods, i.e. (i) Winter (Win): November and December, (ii) Winter monsoon (Wmon): January and February, (iii) Transition summer (Tsumm): March, (iv) Summer (Summ): April and May, (v) Southwest Monsoon (SWmon): June, July, August and September, (vi) Transition winter (Twin): October. Transition months are characterizing transition periods from the southwest monsoon (high RH, high temperature, wet season) to the winter season (low RH, low temperature, dry season) and that from the winter to the summer season (high RH, high temperature, dry season) respectively. Station wise simulated BC mass obtained from model for all the seasons were compared with station wise observed data as obtained from available literatures to find the season with highest or least uncertainty factors.

RESULTS AND DISCUSSIONS

The spatial distribution of emission flux over India during Wmon and SWmon is presented in Figure 1 (a) and (b), respectively. BC emission strength during Wmon is higher by 20% than that during SWmon. To understand the meteorological processes influencing the seasonal variability we analyzed inter-seasonal fluctuations of WRF simulated meteorological data provided in Table 1. The study indicates lower mean surface temperature (19.5°C) and means relative humidity (RH) (55%) and weak North-easterly wind (mean speed 1.3 m s^{-1}) for most of the regions over India during Wmon. Wind speed and direction at 997 hPa during Wmon and SWmon are presented in Figure 1 (c) and (d), respectively. Highest wind speed is found during SWmon with a mean of 4 m s^{-1} . Temperature is higher during Summ and SWmon ranging between 25° and 35°C . Maximum RH up to 95% is observed during SWmon.

Simulated BC burden shows a seasonal pattern in mass alteration providing the highest mass concentration during Wmon followed by Win and Tsumm and relatively lower mass value during SWmon and Summ (refer to Figure 1 (e) and (f), respectively). A patch of high BC mass value is visible over Indo-Gangetic plain (IGP) for all the seasons. Seasonal variation is observed due to changes in prevailing meteorological condition in each season as well as due to varying local emissions and long range atmospheric transport. During Win and Wmon low ventilation coefficients due to weak wind speed (1.3 m s^{-1}) and shallow mixing layer height cause less dispersion of particles giving rise to high BC surface concentration varying mostly from 4 to $10 \mu\text{g m}^{-3}$. A lower concentration of BC mass (less than $4 \mu\text{g m}^{-3}$) is found over most of the part of the Indian subcontinent during SWmon due to higher level of RH (mean 85%) and strong wind field (4 m s^{-1}) resulting dispersion and wet removal of aerosol particles from the atmosphere. Model estimated BC mass concentrations for stations over India were further compared with observed data to evaluate the uncertainty in model simulation for all the season in order to find the season with best and least compatibilities between simulated and measured values.

Parameters	Inter-seasonal influence*					
	Win	Wmon	Tsumm	Summ	SWmon	Twin
Temp (°C)	20	19.5	24.5	29	29.5	26
RH (%)	60	55	69	65	85	70
Wind speed (m s ⁻¹)	1.4	1.3	2.2	2.5	4	2.1

*All the values are seasonal mean of parameters

Table 1. Inter-seasonal variation in meteorological parameters

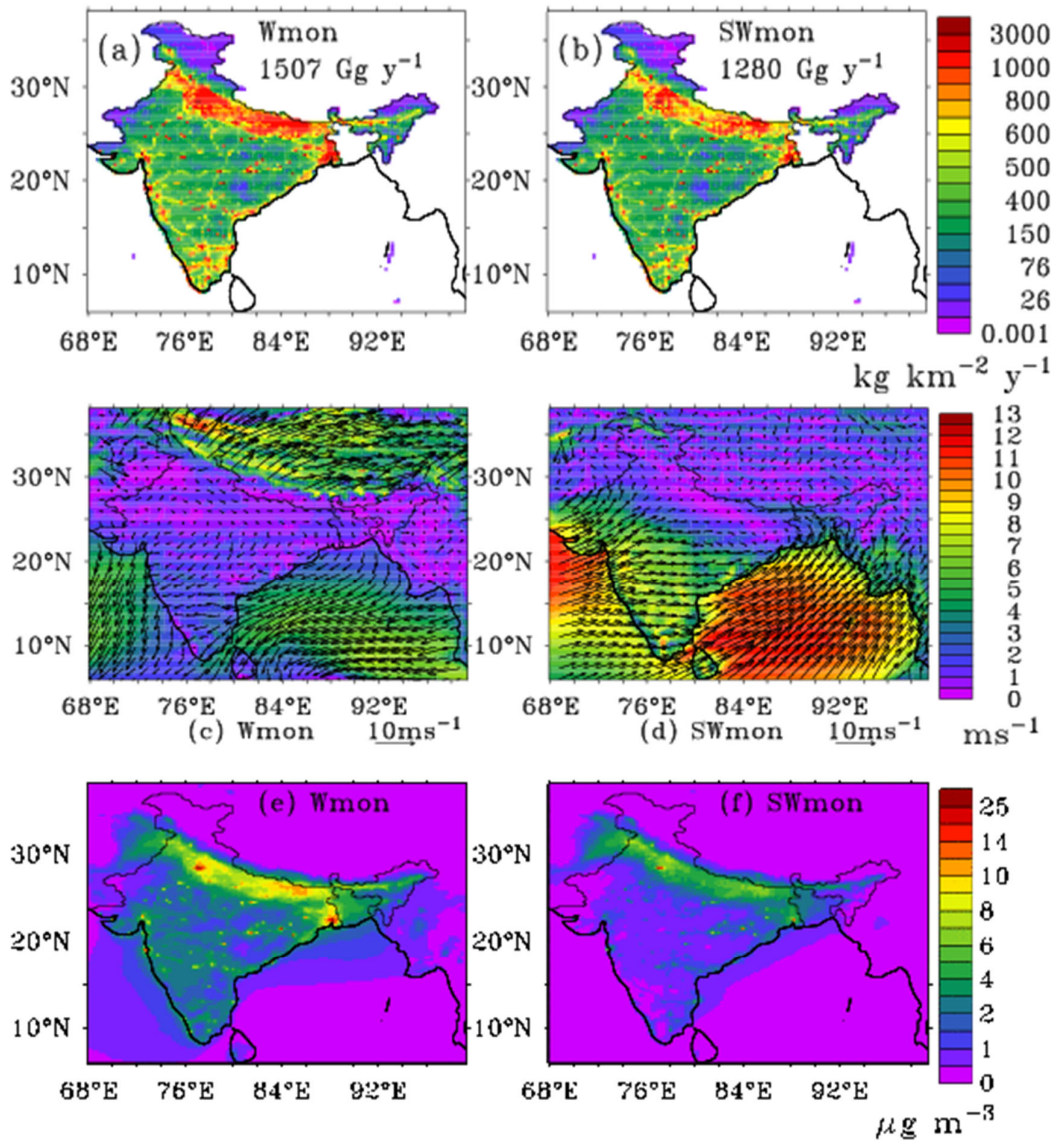


Figure 1. Spatial distribution of (a-b) emission flux during Wmon and SWmon, (c-d) wind speed during Wmon and SWmon, (e-f) BC surface concentration during Wmon and SWmon over Indian subcontinent

ACKNOWLEDGEMENTS

Computing resources and experimental work at Indian Institute of Technology, Kharagpur were supported through grants received from Ministry of Environment, Forest and Climate Change (Reference No: 14/10/2014-CC (Vol. II)).

REFERENCES

- Fadnavis, S., Kalita, G., Kumar, K. R., Gasparini, B., Li, J. L. F., (2017), Potential impact of carbonaceous aerosol on the upper troposphere and lower stratosphere (UTLS) and precipitation during Asian summer monsoon in a global model simulation, *Atmos. Chem. Phys.*, **17**, 11637–11654.
- Kumar, R., Barth, M. C., Pfister, G. G., Nair, V. S., Ghude, S. D., Ojha, N., (2015). What controls the seasonal cycle of black carbon aerosols in India? *J. Geophys. Res. Atmos.* **120**, 7788–7812.
- Pandey, A., Sadavarte, P., Rao, A. B., Venkataraman, C., (2014), Trends in multi-pollutant emissions from a technology-linked inventory for India: II. Residential, agricultural and informal industry sectors, *Atmos. Env.*, **99**, 341-352.
- Venkataraman, C., Habib, G., Eiguren-Fernandez, A., Miguel, A.H., Friedlander, S.K., (2005). Residential biofuels in South Asia: carbonaceous aerosol emissions and climate impacts. *Science*, **307**, 1454– 1456.

POTENTIAL OF SIMULATED ATMOSPHERIC BLACK CARBON (BC) BURDEN AND ITS RADIATIVE RESPONSE TO THE EMISSION STRENGTH EFFICACY OVER THE INDIAN REGION IN A CHEMICAL TRANSPORT MODEL (CHIMERE)

S. GHOSH¹, S. VERMA² AND R. RAY²

¹Advanced Technology Development Centre
Indian Institute of Technology Kharagpur, West Bengal -721 302, India.

²Department of Civil Engineering
Indian Institute of Technology Kharagpur, West Bengal -721 302, India.

KEYWORDS: Black Carbon Simulation, Bc Emission Strength, Chimere, Model Validation, Sensitivity.

INTRODUCTION

Black carbon (BC) is released into the atmosphere from various combustion processes of carbon-based fuels (Bond et al., 2013). It is one of the constituents of concern among the atmospheric aerosol pollutants because of its complex role towards climatic impacts, degradation of air quality including adverse impacts on human health. Among aerosol constituents, BC aerosols are considered as the strongest contributor towards intensifying the warming of the troposphere (Ramanathan and Carmichael, 2008). Since atmospheric BC concentrations peak close to major source regions thus giving rise to regional hot-spots, the impact of BC-induced radiative effect could be more significant on a regional scale to local scale than on the global; which in turn can have strong implications on the regional hydrological cycle.

The estimated atmospheric BC burden indicate a large uncertainty specifically over the regions where the atmosphere is observed to be laden with a large pollutant level of BC concentration. For example, recent evaluation of BC concentration from global aerosol multi-models using global BC emissions showed BC estimated in global model simulation were only about 8% to 46% of observed BC concentrations over Indian region during the winter season (December-January-February) (Pan et al., 2015). The simulated BC concentration in a regional chemical transport model over India was found to be better correlated with measured surface BC concentration during pre-monsoon than during winter, but was still underestimated by a factor of 2 to 4 times during the pre-monsoon season and 4 to 9 times during winter based on measurements over the Indo-Gangetic plain (IGP) and Himalayan stations. Due to the inclusion of various complex physical-chemical atmospheric and aerosol processes in these models, in conjunction with inherent uncertainty in inputs to the model, e.g., aerosol emissions and their properties, a systematic approach is required to improve the prediction of aerosols. The atmospheric BC burden is related with the BC emission strength and atmospheric residence time of BC. While the atmospheric residence time of BC aerosols is independent of the emission strength, it is an indication of simulated aerosol processes and properties affecting the burden.

In the present study, we evaluate the impact of BC emissions source strength on simulated atmospheric BC burden over the Indian region for the winter month of December. This is done by carrying out model experiments comprising of high-resolution BC transport simulations in a chemical transport model, CHIMERE, extracting BC emission strengths over Indian region available from five BC inventory database. This study also examines the efficacy of available BC emissions to simulate BC concentration with respect to observations over India during the winter month. The winter month is chosen as the Indian subcontinent is specifically laden with the highest surface concentration of anthropogenic pollutants as obtained from observational studies and a high discrepancy is envisaged between model and observations. The specific objectives of the present study are as follows: (i) evaluation of the impact of BC emission strength effect on BC burden simulated for December month in CHIMERE, (ii) statistical analysis of the compatibility between observed and modeled data, (iii) assessment of the sensitivity of the model output towards the variability in emission strength.

METHODS

Present study was carried out in a Chemical Transport Model (CTM) CHIMERE coupled with Weather Research and Forecasting (WRF). Meteorology obtained from WRF model was incorporated with CHIMERE. The meteorological initial conditions and lateral boundary conditions for the model were obtained from the National Centers for Environmental Prediction (NCEP) meteorological fields. The chemical boundary conditions and land uses were obtained from a global aerosol model, LMDz4-INCA (Laboratoire de M'eteorologie Dynamique General Circulation Model coupled with INCA: Interaction with Chemistry and Aerosols) and GLCF (Global Land Cover Facility). Horizontal transport is solved with the second-order Van Leer scheme. Sub-grid scale convective fluxes and representation of turbulent mixing are considered. BC transport simulations were carried out at a horizontal resolution of $0.1^\circ \times 0.1^\circ$ over the IGP region extending from 20° N to 30.8° N and 75° E to 89.9° E for the winter month of December. The five sets of emission database with emission strength in the range of 388 to 2534 Gg y^{-1} over India (refer to Table 1 for details), were implemented in CHIMERE. Bottom up BC emissions over India were collected from Smog-India for the year 2015 (Pandey et al., 2014). BC emissions over India for 2000 with spatial resolution $0.25^\circ \times 0.25^\circ$ is referred to as "Base emission". Global BC emission inventories (EDGAR, PKU) were re-gridded to the horizontal resolution of emission inventories over India, i.e., Base, Smog-India ($0.25^\circ \times 0.25^\circ$). Constrained BC emission ($0.25^\circ \times 0.25^\circ$) are as per estimated by Verma et al., 2017. Hourly simulation of BC was carried out for each day of the month of December using each of the five inventory dataset. Simulated BC mass for seventeen stations obtained from model were compared with station wise observed data as obtained from available studies to find underestimation factors. Statistical analysis (Pearson's correlation, Mean Bias (MB), Normalized Mean Bias (NMB), Normalized Mean Error (NME) and Root Mean Square Error (RMSE)) were carried out to show the compatibility between the modeled and the observed value. Grid wise mean and variance in BC emissions implemented over India were estimated. The correlation analysis was performed between the variances of emission and BC mass concentration to indicate the sensitivity of the model output to the changes in input.

Description of aerosol module in CHIMERE			
Aerosol dynamics	Absorption, nucleation, coagulation, aging BC POM		
Mixing, scheme	Internal, bin		
Deposition	In cloud or below cloud wet deposition, dry deposition for all aerosol species except coarse (sea salt and dust through sedimentation)		
Sulfate chemistry (Prescribed oxidants)	OH, CH_3O_2 , Fe^{2+} , Mn^{2+}		

Setup for simulation experiment			
Serial No.	BC emission database	Types of emission database (Resolution)	Annual BC emission strength over India (Gg y^{-1})
1	Base emission (Reddy and Venkataraman, 2002a,b)	India ($0.25^\circ \times 0.25^\circ$)	388
2	Smog-India (Pandey et al., 2014)	India ($0.25^\circ \times 0.25^\circ$)	1325
3	EDGAR	Global ($1^\circ \times 1^\circ$)	1079
4	Peking University BC Inventory (PKU)	Global ($0.1^\circ \times 0.1^\circ$)	744
5	Constrained (Verma et al., 2017)	India ($0.25^\circ \times 0.25^\circ$)	2534

Table 1. Simulation experiments of Black Carbon aerosols in CHIMERE

SUMMARY AND CONCLUSIONS

The spatial distribution of the mean of surface BC concentration estimated over the IGP from BC transport simulations in CHIMERE for the winter month of December is shown in Figure 1. These estimates are shown from simulation experiments using three sets of BC emission strength as input in the model, i.e. Base

(Figure 1a), Smog-India (Figure 1b) and Constrained (Figure 1c). The hourly mean of simulated surface BC concentration exhibited a 2 to 5 times lower value during daytime hours than that during the late evening and early morning hours associated with meteorology. In contrast to the diurnal feature over plains, the peaked BC concentration was estimated during late afternoon hours (14 h LT – 17 h LT) over high altitude location (Nainital), which was consistent with the observational data.

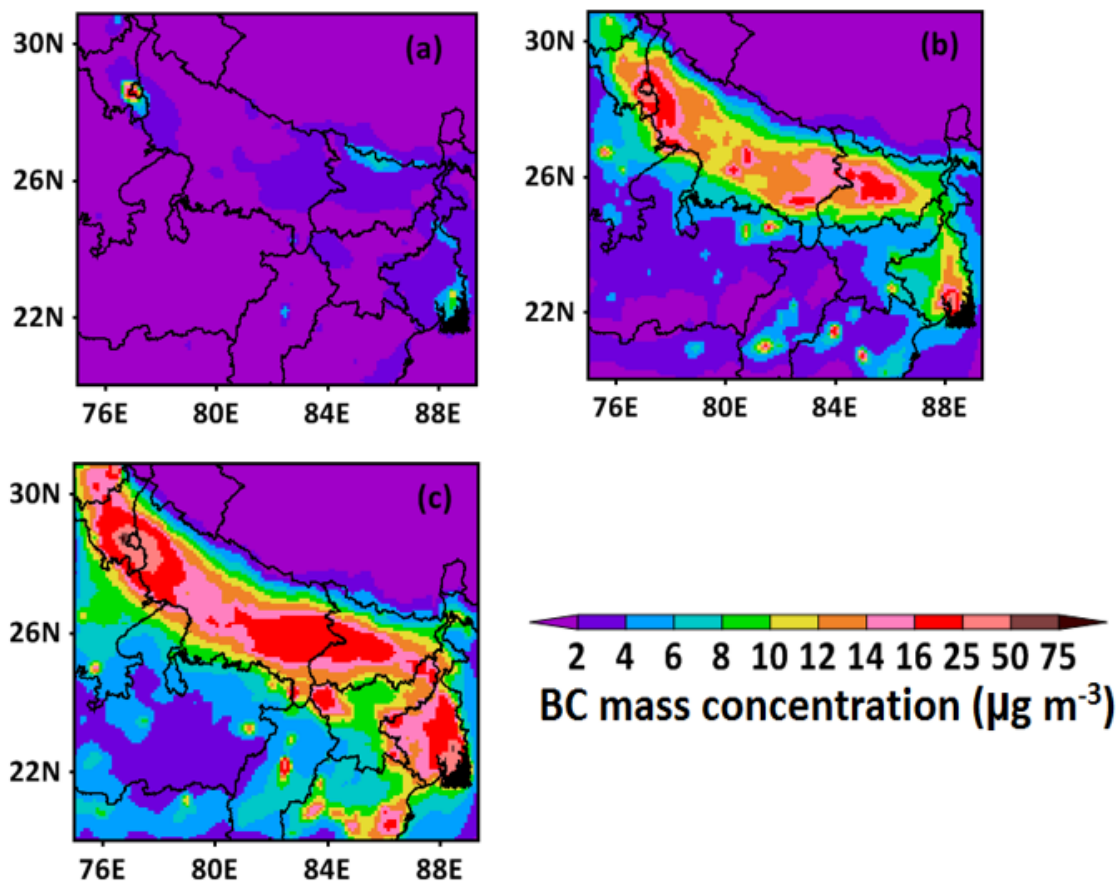


Figure 1. Spatial distribution of simulated monthly mean BC mass concentration over IGP due to BC emission strength from (a) Base, (b) Smog-India, (c) Constrained BC emissions.

The simulation experiments indicate a significant improvement in simulated BC concentration over the IGP using Smog-India and Constrained BC emissions compared to the base BC emissions based on the comparison of simulated BC concentration with observed counterparts at about seventeen number of stations. This comparison showed that while simulated BC concentration was underestimated by a factor of greater than two-times (as high as twenty three times) the observed counterparts at stations using the base BC emission, it was found concurring relatively well the observation (ratio of measured to modeled BC concentration within a factor of one) for about 65% and 88% respectively of the total numbers of observed data analyzed using Smog-India and Constrained BC emission.

The features of spatial distribution (Figure 1) also indicated the presence of BC hot-spot zones of high values of BC surface concentration, specifically at three locations, eastern India zone, Bihar-eastern Uttar-Pradesh zone, northern-India zone. These hot-spot zones are noted being found in all five simulation experiments with different BC emission strengths. Also, the correlation analysis between spatial variance in BC emission strength (using five datasets of BC emission strength) and the corresponding simulated BC concentration was strong (coefficient of correlation is greater than 0.7) over the IGP compared to that being moderate to

weak over central India. This analysis thereby indicated the sensitivity of BC emission strength in improving the prediction of BC concentration over the IGP, unlike that over central India. Estimated BC concentration is further used to evaluate the impact on atmospheric solar radiation extinction due to BC aerosols and the BC-induced radiative forcing.

ACKNOWLEDGEMENTS

This work was supported through a grant received from the Ministry of Environment, Forest, and Climate Change (14/10/2014-CC (Vo.II)), Govt. of India at the Indian Institute of Technology, Kharagpur.

REFERENCES

- Bond, T. C., Doherty, S. J., Fahey, D. W., Forster, P. M., Berntsen, T., DeAngelo, B. J., Flanner, M. G., Ghan, S., Karcher, B., Koch, D., Kinne, S., Kondo, Y., Quinn, P. K., Sarofim, M. C., Schultz, M. G., Schulz, M., Venkataraman, C., Zhang, H., Zhang, S., Bellouin, N., Guttikunda, S. K., Hopke, P. K., Jacobson, M. Z., Kaiser, J. W., Klimont, Z., Lohmann, U., Schwarz, J. P., Shindell, D., Storelvmo, T., Warren, S. G., Zender, C. S., (2013). Bounding the role of black carbon in the climate system: A scientific assesment. *J. Geophys. Res.* **118**, 1–173.
- Pan, X., Chin, M., Gautam, R., Bian, H., Kim, D., Colarco, P. R., Diehl, T. L., Takemura, T., Pozzoli, L., Tsigaridis, K., Bauer, S., Bellouin, N., (2015). A multi-model evaluation of aerosols over South Asia: common problems and possible causes. *Atmos. Chem. Phys.* **15**, 5903–5928.
- Pandey, A., Sadavarte, P., Rao, A. B., Venkataraman, C. (2014), Trends in multi-pollutant emissions from a technology-linked inventory for India: II. Residential, agricultural and informal industry sectors, *Atmos. Env.*, **99**, 341-352.
- Ramanathan, V., and Carmichael, G. (2008). Global and regional climate changes due to black carbon. *Nature Geoscience*, **1**, 221–227.
- Reddy, M. S., and Venkataraman, C. (2002a). Inventory of aerosol and sulphur dioxide emissions from India: I - Fossil fuels combustion. *Atmos. Environ.*, **36**, 677–697.
- Reddy, M. S., and Venkataraman, C. (2002b). Inventory of aerosol and sulphur dioxide emissions from India: II - Biomass combustion. *Atmos. Environ.*, **36**, 699–712.
- Verma, S., Reddy, D. M., Ghosh, S., Kumar, D. B., Chowdhury, A. K., (2017). Estimates of spatially and temporally resolved constrained black carbon emission over the Indian region using a strategic integrated modelling approach. *Atmos. Res.*, **195**, 9–19.

SPATIO-TEMPORAL VARIATIONS OF PM_{2.5} MASS OVER INDIA USING REGIONAL CLIMATE MODEL

ROHIT SRIVASTAVA¹ AND SHERIN H. BRAN²

¹Indian Centre for Climate and Societal Impacts Research (ICCSIR), Mandvi, Kachchh, Gujarat, India.

²National Astronomical Research Institute of Thailand, Chiang Mai, Thailand.

KEYWORDS: Pm_{2.5}, Wrf-Chem, India.

INTRODUCTION

Atmospheric particulate matters (PM) are solid, liquid or mixture of solid particles and liquid droplets suspended in air. PM are generally categorized based on their sources, structures, chemical and physical processes, which are PM_{2.5} (diameter < 2.5 μm, fine mode) and PM₁₀ (diameter < 10 μm, coarse mode). These are the current largest threats to climate change, biodiversity and health effects. On a small (regional) scale, they can give rise to pollution toxicity while on the global scale, they can have significant impact on climate. Particulate matter also has crucial impact on human health, especially on respiratory and cardiovascular diseases. The fine mode particles can penetrate deep into the lungs easily when compared to coarse mode particles, which enhance the pulmonary, respiratory and mutagenic diseases. The economic loss due to premature mortalities in India associated with PM_{2.5} and other pollutants was reported to be about 640 billion USD in 2011 (Ghude et al., 2016). Particulate matters (aerosols) have a significant role in climate change by modifying cloud, optical properties and radiative forcing.

In Asia, India is one of the hot spots which experiences large amounts of PM which can have adverse impacts on health and climate. The sources of particulate matters are mainly from natural and anthropogenic, likely sea spray, suspension of soil particles, biomass burnings (Indoor and outdoor), incomplete combustion of fossil fuels and biofuels. The major sources of fine particles over the Indian sub-continent are mainly from anthropogenic activities such as burning of agricultural residues, fossil fuels, biomass burning (Ramanathan and Carmichael, 2008). An increasing trend of fine mode aerosol loading over South Asia was found in the past years (Srivastava, 2017). In the present study, the spatio-temporal variations of PM_{2.5} mass are investigated over the Indian sub-continent and adjoining oceanic regions using a regional climate model (Weather Research and Forecasting model coupled with Chemistry (WRF-Chem)).

METHODS

The study has utilized WRF-Chem version 3.6.1, which can simulate meteorological as well as chemical fields (Grell et al., 2005). Model simulations are performed over the Indian sub-continent and adjoining oceanic regions with a latitudinal range of 6°N to 36°N and a longitudinal range from 66°E to 96°E. Horizontal resolution of simulations is 20 km and the vertical profile has 51 layers limiting the maximum height of 35 km from the surface, in that 38 layers are within 10 km range, as aerosols are mainly confined within 10 km.

The utilized chemical mechanism in the study is Model for Ozone and Related chemical Tracers (MOZART4) linked with Goddard Chemistry Aerosol Radiation and Transport (GOCART) bulk aerosol scheme (MOZCART). Initial and lateral boundary conditions for the chemical field were obtained from the output of MOZART4 (Emmons et al., 2010) with 6 h resolution. Anthropogenic emissions of particulate matters were obtained from the Emission Database for Global Atmospheric Research collaboratively with Task Force Hemispheric Transport of Air Pollution (EDGAR-HTAP) at a global horizontal grid resolution of 0.1° x 0.1°. National Centre for Environmental Prediction, Final Analysis (NCEP/FNL) meteorological data at a temporal resolution of 6 h and spatial resolution of 1° x 1° were used for initial and lateral boundary conditions. The biogenic emissions of trace species were calculated online using the Model of Emissions of Gases and Aerosols from Nature (MEGAN) and the biomass burning emissions were obtained from the Fire Inventory from NCAR version 1 (FINNV1).

RESULTS & DISCUSSIONS

Spatial variation of PM_{2.5} mass concentration and wind at 1000 hPa simulated from WRF-Chem during winter season of 2008 are shown in Figure 1. High spatial variability in PM_{2.5} mass concentration was found over Indo-Gangetic Basin (IGB) in all the seasons, which vary from 60 – 200 $\mu\text{g m}^{-3}$. IGB is one of the densely populated region in the world, therefore the production of fine mode (PM_{2.5}) particles was found high by local emission including household, vehicular, mining and urbanization. Higher mass concentrations ($> 50 \mu\text{g m}^{-3}$) were found during winter (December-February), while lower in monsoon season (June-September) (Bran and Srivastava, 2017). Less amount of solar radiation during winter, lowers the surface wind speed, give rise to weak vertical dispersion and diffusion of aerosols (PM_{2.5}). In monsoon, high rainfall causes wet scavenging and leads to decrease in surface PM_{2.5} mass. PM_{2.5} mass was found to be high over the Bay of Bengal (BOB), when compared to that over the Arabian Sea (AS) through the seasons. During winter, PM_{2.5} mass exhibit maximum (10 - 30 $\mu\text{g m}^{-3}$) in BOB and AS (Bran and Srivastava, 2017). This higher mass is attributed to transport of anthropogenic aerosols from IGB by wind.

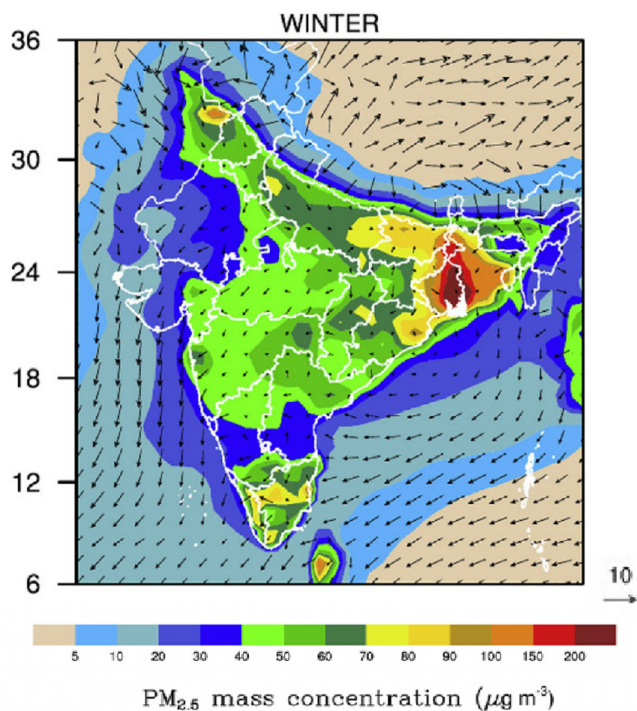


Figure 1. Spatial variations of surface PM_{2.5} mass concentration over Indian subcontinent and adjoining oceanic regions during winter (December – February) 2008. The wind vectors at surface are also shown.

CONCLUSIONS

The emission of PM_{2.5} over the Indian subcontinent has increased in the recent years. The frequency of human health related problems such as lung diseases, morbidity and mortality issues are also increased.

High amounts of PM_{2.5} (60 - 200 $\mu\text{g m}^{-3}$) were found over IGB. Calm wind and the lower boundary layer help to increase the mass concentration during winter, while wet scavenging due to high rainfall results decrease in PM_{2.5} mass in monsoon season. Simulated PM_{2.5} was comparable with observations across the distinct locations in India. Annual mean of PM_{2.5} over the Indian subcontinent was estimated to be 35

9 $\mu\text{g m}^{-3}$. Highest annual mean of PM_{2.5} mass was found over West Bengal ($82 \pm 33 \mu\text{g m}^{-3}$) while the lowest mass was estimated over Jammu & Kashmir ($14 \pm 11 \mu\text{g m}^{-3}$). The simulated PM_{2.5} mass concentration was found to be high over the states, where the observed respiratory disorders were also high. The detailed results on spatio-temporal variations on PM_{2.5} over Indian regions will be presented and discussed.

ACKNOWLEDGEMENTS

This work was supported by Science and Engineering Research Board (SERB), Department of Science and Technology (DST), Govt. of India.

REFERENCES

- Emmons, L., S. Walters, P. Hess, J.-F. Lamarque, G. Pfister, D. Fillmore, C. Granier, A. Guenther, et al. (2010). Description and evaluation of the model for ozone and related chemical tracers, version 4 (mozart-4), *Geosci. Model Dev.* **3**, 43 – 67.
- Ghude, S.D., D. Chate, C. Jena, G. Beig, R. Kumar, M. Barth, G. Pfister, S. Fadnavis, P. Pithani (2016). Premature mortality in India due to PM_{2.5} and ozone exposure, *Geophys. Res. Lett.* **43**, 4650–4658.
- Grell, G.A., S. E. Peckham, R. Schmitz, S. A. McKeen, G. Frost, W. C. Skamarock, B. Eder (2005). Fully coupled online chemistry within the WRF model. *Atmos. Environ.* **39**, 6957 – 6975.
- Ramanathan, V., G. Carmichael (2008). Global and regional climate changes due to black carbon. *Nat. Geosci.* **1**, 221 – 227.
- Srivastava, R. (2017). Trends in aerosol optical properties over south Asia, *Int. J. Climatol.* **37**, 371 – 380.
- Bran S. H., R. Srivastava (2017). Investigation of PM_{2.5} mass concentration over India using a regional climate model, *Env. Pollut.* **224**, 484 – 493.

IDENTIFICATION OF SOURCE REGION OF SECONDARY AEROSOL DURING FOG EVOLUTION IN THE URBAN ATMOSPHERE "DELHI" INDIA DURING 2016-17

S. TIWARI¹, P. SATEESH², A.K. SHRIVASTAVA¹, D.S. BISHT¹, V.K. SONI³, S. DEVARAJ⁴, G. P. SHIVSHANKARA⁵

¹Indian Institute Meteorological Department, New Delhi Branch, 110060, India

²Centre for Ocean-Atmospheric Science and Technology, Amity University Rajasthan, Jaipur, India

³India Meteorological Department, New Delhi, 110060, India

⁴Department of Civil Engineering, Dayananda Sagar College of Engineering, Bangalore- 560078, India

⁵Department of Civil Engineering, P.E.S. College of Engineering, Mandya- 571401, India

KEYWORDS: Aerosol optical depths, Western Disturbance, chemicals species, Cluster analysis

INTRODUCTION

India is currently suffering from serious atmospheric pollution due to urbanization and fast development of the economy. Extremely severe pollutions level during the post-monsoon and winter periods was observed in most parts of the northern part of India and got attention all over the world. During the foggy/hazy period in above mentioned both periods, it was characterized by lower visibility, higher atmospheric particle loadings (in respect of aerosol optical depths or particulate matter) which have significant impacts on the regional air quality. During the winter period, a system called Western Disturbance (WD) generate which brings enough moisture subsequently widespread rain occurred that support the fog formation in the entire northern part of India. The fog formation is the common meteorological feature that leads to a massive number of cancellations/ delayed the flights, disrupted train schedules, economic loss, impacts on human health etc. The WD affects the hills (Jammu and Kashmir states) region also that leads to suddenly reversal of wind pattern from dry and cool northwesterly flows to humid Easterlies or Southeasterlies and causes widespread fog in the plains areas over Northern India. Due to calm wind conditions, the fog could not disperse and lead to longer durations of fog (Ali, et al., 2004; Tiwari et al., 2011).

In view of the above importance, during the winter foggy period of 2016-2017 were selected to study the aerosol characterizes and its source region over Delhi. Off-line data of chemicals species (F^- , Cl^- , SO_4^{2-} , NO_2^{2-} , NO_3^- , Na^+ , K^+ , NH_4^+ , Ca^{2+} , and Mg^{2+}) through particle in a liquid sampler in $PM_{2.5}$ were collected during the winter foggy period of 2016-2017 to understand the pollution level over megacity. The source region of pollutants in the particle in liquid (PIL) was also studied by concentrated weighted trajectory analysis during the study period.

METHODS

During the study period, the Particle Into Liquid Sampler (PILS: Applikon analytical Model no-ADI2081) in which ambient particles (through $PM_{2.5}$ cyclone) was mixed with saturated water vapor to produce droplets was used to collect liquid samples. It was developed for rapid automated online and continuous measurement of the ambient aerosol bulk composition. Collected liquid samples were analyzed for both anions and cations with Metrohm 850 professional Ion Chromatography (IC) and with help of Metrohm 838 autosampler with anion column-Metrosep A Supp 5-150/4.0\cation column-Metrosep C 4 - 150/4.0. The accuracy of measured ions were (in

ppb)- F⁻ (5) Cl⁻ (5), NO₂⁻ (10), NO₃⁻ (5), SO₄²⁻ (10), Na⁺ (5), NH₄⁺ (10), K⁺ (5), Ca²⁺ (20) and Mg²⁺ (10).

RESULTS & DISCUSSIONS

Chemical Characteristics of liquid samples over Delhi

Mean mass concentrations of measured ions in particles in the liquid samples during the winter season of 2016-17 over IGI airport are depicted in Fig.1. The highest concentrations were calcium (22%) followed by sulfate (19%), chloride, ammonium and nitrate (Fig. 1). The higher sulfate and nitrate indicate the enhancement of secondary aerosols formation during the foggy period. For source identification of secondary aerosol was studied and is given below.

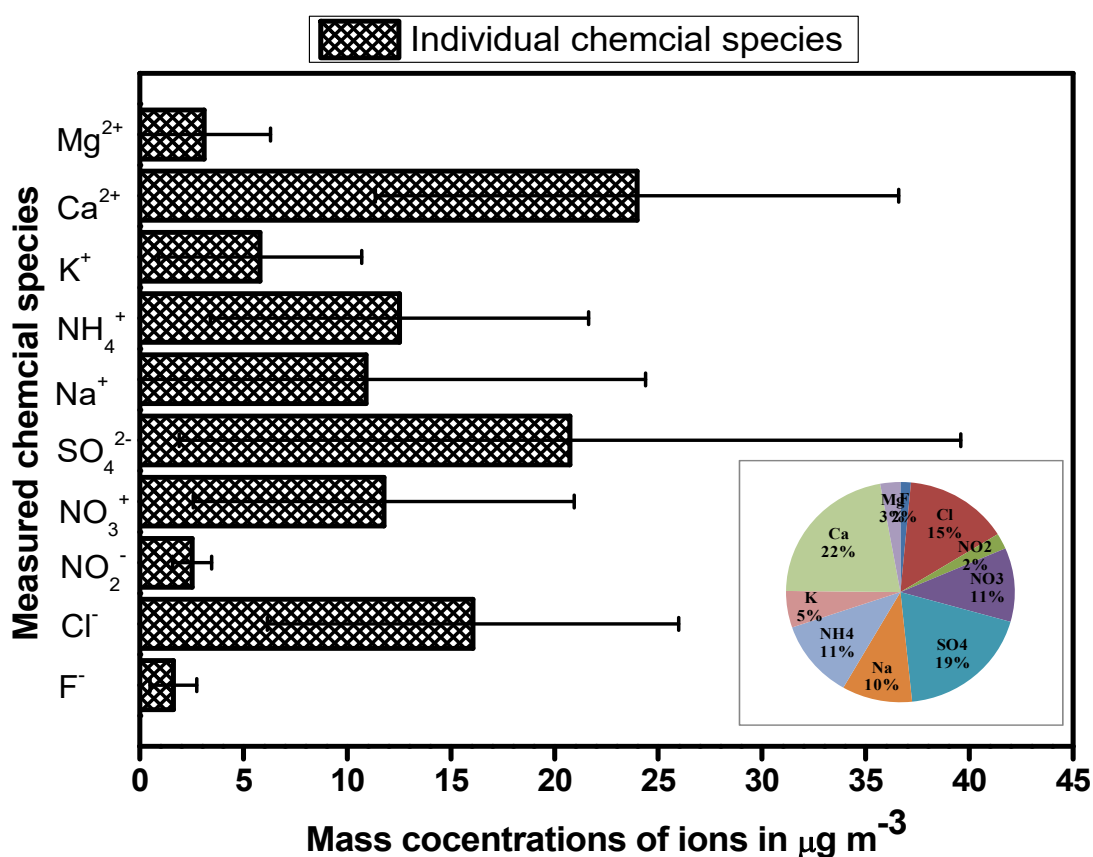


Figure 1: Mean mass concentrations of measured ions in particles in the liquid samples during the winter season of 2016-17 over IGI airport Delhi

Source region identification

The back air-mass trajectory analysis was performed for air parcels (500 m above ground level) arriving at the receptor site at Indira Gandhi International airport (IGI) Delhi using the NOAA HYSPLIT (Hybrid Single-Particle Lagrangian Integrated Trajectory) model (Draxler and Rolph, 2003) (NOAA ARL website <http://www.arl.noaa.gov/ready.html>) in order to assess potential source regions on the observed atmospheric pollutants over receptor site. In this analysis, The

National Weather Service's National Centers for Environmental Prediction (NCEP) GDAS (Global Data Assimilation System) global reanalysis data was used as input to the model for determining the 5-day air-mass back trajectory. Trajectories were calculated every hour, coinciding with the time of sampling. Trajectory length was chosen to be five days, which is motivated by the comparably short residence time of water-soluble inorganic species in the lower atmosphere.

In the present study, we have adopted air-mass clustering techniques in order to identify characteristic transport patterns associated with the aerosol liquid chemical sampling for particles $<2.5 \mu\text{m}$ during years 2016-17. Clustering techniques have been widely adopted in literature to study the relation between characteristic transport patterns and the measured concentration of various tracers. In the current study, air-mass trajectories were clustered based on their latitude-longitude pairs for each hourly endpoint belonging to the trajectories, and prior clustering the trajectories were recalculated on an equidistant grid. The clustering algorithm used was kmeans clustering in Matlab. A various number of the cluster were tried, but 6 clusters provided a reasonable balance between inter-cluster variability and number of clusters. The result is shown in Figure 2, as cluster centroids. All clusters centroids initially exhibit more or less similar transport history, i.e. arriving from NW, although cluster 6 on average shows somewhat higher variability in the air flow around and close to Delhi. Cluster 4 and five are classified as fast traveling air masses, based on the large distance traversed during the five days of transport. Cluster 3 and 6, on the contrary, are short, and thus indicative of slower wind speeds. Cluster 1 and 3 are the most common ones, followed by cluster 2 and cluster 6. Both clusters 4 and 5 only have a small number of members. The corresponding average observed chemical speciation associated with each cluster is shown in the figure. In addition to this, cluster-wise individual chemical species mass concentrations ($\mu\text{g m}^{-3}$) were also separated and presented in Table 1. The table also presents the number of members in each cluster.

Out of six clusters (Fig.2), only one cluster (no.6) passes from the Indian subcontinent in the northwest direction (mostly from South Haryana State covering with industrial zone Faridabad and Okhla in Delhi) which is $\sim 19\%$ of the total air masses. However, rest of the five clusters show transport patterns of air masses originating outside India which suggest potential influence from source regions outside of India. The concentrations of secondary acidic species (sulphate: 18 and nitrate: $28.9 \mu\text{g m}^{-3}$) in cluster (no. 6) were higher more than a factor of two than the mean values of rest of the clusters (7.4 and $12.4 \mu\text{g m}^{-3}$) respectively of secondary acidic species when the air masses pass within the Indian subcontinent. In addition to this, it was observed that the sum of measured ions was also much higher ($128.2 \mu\text{g m}^{-3}$) than the mean values of all other one to five cluster ($85.3 \mu\text{g m}^{-3}$) which is clearly indicated that this region is the source region of secondary acidic species that are affecting downwind direction region. Slow transport over heavily polluted source areas allows for the build-up of the large concentration of anthropogenic pollutants.

The most abundant transport type (cluster 3, $\sim 30\%$) originates from northern Pakistan (Lahore) including Punjab and Haryana in India and the sum of the measured chemical species ($68.6 \mu\text{g m}^{-3}$) in cluster three was similar to cluster one to five.. Cluster 1 (29%) The second largest cluster (Cluster 1; 29%) including transport from north Afghanistan and Pakistan. Cluster no. 2 (22%) includes transport from Iran, North Pakistan, and southern Afghanistan, and cluster 6 (18%) is associated with transport from the north of Rajasthan, South Haryana including two major industrial environments as Faridabad in Haryana and Okhla in Delhi. During the studied period, the average sum of measured ionic species were 88.9 and $72.1 \mu\text{g m}^{-3}$ respectively. This lower concentrations of species in all three clusters (from 1 to 3) may be due to the wet deposition process of the measured species. Cluster no. 4 and 5 have an almost negligible number of members, only two days, Cluster 5 includes fast transport from central via Poland, Ukraine, Russia, and Turkmenistan. Cluster 4 includes rapid transport over northern Africa via north Iran, middle

Afghanistan and north Pakistan including north-west part of India Soil oriented species especially were highest in cluster 4, and ammonium ion was highest in cluster 5 as compared to other all clusters.

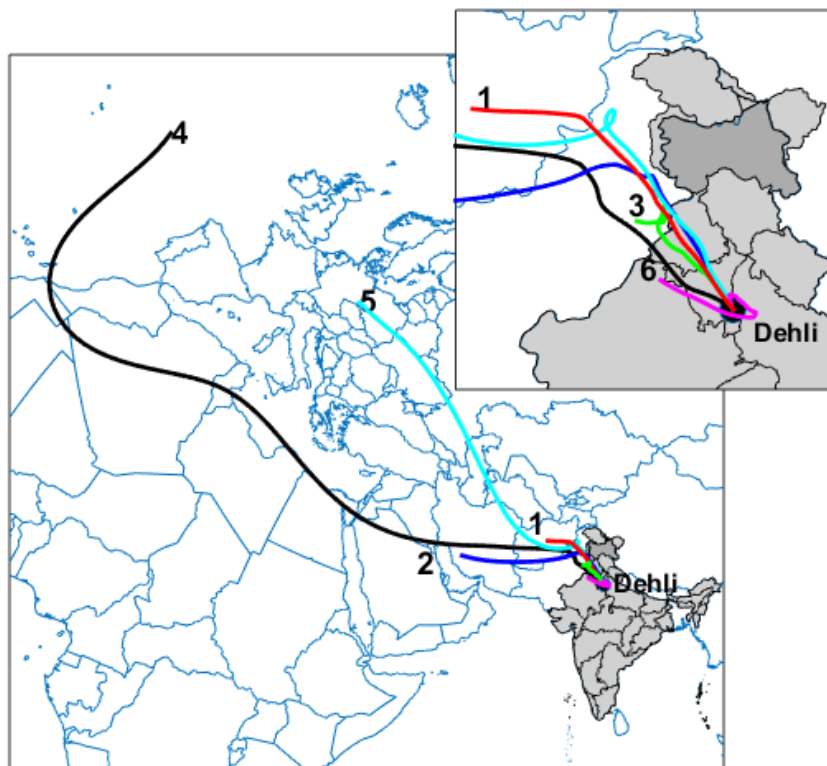


Figure 2: Total cluster trajectories over the receptor site "Delhi" in winter of 2016-17

	No.	F ⁻	Cl ⁻	NO ₂ ²⁻	NO ₃ ⁻	SO ₄ ²⁻	Na ⁺	NH ₄ ⁺	K ⁺	Ca ²⁺	Mg ²⁺	No. of trajectories
Cluster number	1	0.9	18.4	2.3	6.5	11.5	5.5	16.0	4.1	22.5	1.2	109
	2	0.2	12.2	2.5	6.0	11.0	3.4	13.3	3.1	19.6	0.8	83
	3	0.8	10.9	3.2	7.7	9.8	3.8	10.8	3.0	17.2	1.4	115
	4	3.0	11.2	2.2	5.7	13.1	9.5	5.3	6.0	32.9	4.4	2
	5	0.0	23.9	2.7	11.1	16.7	2.4	20.3	4.9	21.3	0.5	2
	6	1.2	15.3	1.8	18.0	28.9	10.5	15.0	5.1	29.2	3.2	70
												381

Table 1: Concentrations of chemical species ($\mu\text{g m}^{-3}$) in each cluster of trajectories in particles in liquid samples along with No. of trajectories over IGI airport Delhi in winter of 2016-17

REFERENCES

Ali, K., Momin, G.A., Tiwari, S., Safai, P.D., Chate, D.M., Rao, P.S.P., 2004. Fog and precipitation chemistry at Delhi, North India. *Atmospheric Environment*, 38, 25, August 2004, 4215–4222.

Draxler, R. R. and Rolph, G. D., 2003: HYSPLIT (HYbrid Single-Particle Lagrangian Integrated Trajectory) Model access via NOAA ARL READY website (<http://www.arl.noaa.gov/ready/hysplit4.html>), NOAA Air Resources Laboratory, Silver Spring, MD.

Tiwari, S., Payra, S., Mohan, M., 2011. Visibility degradation during foggy period due to anthropogenic urban aerosol at Delhi, India. Atmospheric Pollution Research, doi: 10.5094/APR.2011.014,pp,116-120.

EVALUATION OF THE SKYNET CALIBRATION METHODOLOGIES FOR DIRECT AND DIFFUSE SOLAR IRRADIANCE

SHANTIKUMAR S. NINGOMBAM¹, VICTOR ESTELLÉS², M. CAMPANELLI³, DORJE ANGCHUK⁴, COLWELL STEVE⁵, AND JON SHANKLIN⁶

¹Indian Institute of Astrophysics, Bangalore, India,

²Dept. Física de la Terra i Termodinàmica, Universitat de València C/Dr Moliner, Valencia, Spain,

³Consiglio Nazionale delle Ricerche, Istituto Scienze dell'Atmosfera e del Clima, via Fosso del Cavaliere, Roma, Italy,

⁴Indian Astronomical Observatory, (IAO), Hanle, Ladakh, India,

⁵British Antarctic Survey, High Cross, Madingley Road, Cambridge, U.K.

(*Correspondence at: shanti@iiap.res.in)

ABSTRACT

The present work was performed to examine the stability and consistency of calibration coefficients of five Sky radiometers (Prede, POM-01) operated under a network (SKYNET/ESR) from Hanle and Merak stations in Ladakh (India), Halley and Rothera stations in Antarctica, and Valencia (Spain) during May, 2007-December, 2014. The instrument observes direct and diffuse sky irradiance at seven discrete wavelengths in UV-VIS-NIR region and data were processed using Skyrad.Pack (version 4.2) to retrieve the aerosol optical and physical parameters. The software has different modules and each module has own rejection criteria to remove the outliers due to various factors while processing. The calibration coefficients examined in the present work are solid view angle (SVA(λ)) and calibration coefficients (FOI(λ)) for each filters and these parameters are updated periodically (monthly) in the instrument parameter files using the fresh in-situ data. The study observed that drift of FOI(λ) and SVA(λ) are 2.1% - 4.9% and 0.74% - 3.05% per year, respectively, at 500 nm even at low aerosol aged-background sites. The ratio between normal Langley (NL) and improved Langley (IL) at Hanle and Merak stations were ~ 1 due to its low aerosol optical depth (AOD). Further, the retrieved AOD using inversion method is in fairly agreement with the measured AOD using the FOI(λ), with $R^2 \sim 1.0$ at all the wavelengths over Hanle and Merak. Obtaining such good correlation are the indication of proper calibration coefficients used in the observation. The present study also noticed that frequent calibration of the instrument is needed preferably once in a month as $\sim 5\%$ variation of FOI(λ) may causes improper AOD values or significant loss of data (i.e., rejected while processing) due to the improper calibration coefficients.

KEY WORDS: Sky radiometers; Skyrad.Pack; calibration coefficients; solid view angle; improved Langley

INTRODUCTION

Many instruments and techniques have been developed during the last few decades for studying the optical and microphysical features of atmospheric aerosols over the globe. In this regards, different international or regional networks have been emerged, such as AERONET (Holben et al., 2001), SKYNET (Nakajima et al., 1996); Takamura and Nakajima, 2004), or Aerosol Radiative Forcing over India network (ARFINET) (Moorthy et al., 2013) since the last few decades. Further, depending on satellite data have many unresolved issues as reported by several authors (Remer et al., 2005; Kahn et al., 2007) in the case of low aged-background sites in addition to the limitations

of spatial and temporal coverage. Besides, the retrieval errors of the satellite data are much higher than the observed AOD over the aged-background sites. Therefore, ground based data have many advantages. However, regular maintenance and periodic calibration of such ground based instruments are very important to obtain good accuracy of the estimated parameters. Generally, high-altitude mountainous and remote oceanic regions are considered as an ideal place to calibrate such Sky radiometers as these regions are far from any sources of dust-anthropogenic origin.

Further, it is not possible for shipping of instruments regularly for calibration purpose, and in this case Sky radiometer (Prede, POM-01) has many advantages due to its in-situ calibration facilities. Two calibration constants are calculated on monthly basis, namely: the solar calibration constants $F_{0I}(\lambda)$, which is the amount of solar radiation incident at the top of the atmosphere; and the solid view angle (SVA(λ)) or the solid opening angle of each filter. The first calibration constant ($F_{0I}(\lambda)$) is calculated by using improved ($F_{0I}(\lambda)$) or normal Langley methods ($F_{0N}(\lambda)$). The second calibration constant (SVA(λ)) is calculated by applying the solar disk scanning method using the in-situ data on regular basis, preferably once in a month.

The aim of the present work is to examine the stability and consistency of calibration coefficients from five stations which have different geographical locations of low aerosol aged-background, namely: Halley (75.58°S; 26.65°W; 30 m amsl) and Rothera (67.57°S; 68.13°W; 30 m, amsl) in Antarctica; Hanle (32.78°N; 78.97°E; 4500 m amsl) and Merak (33.78°N; 78.62°E; 4310 m amsl) on high mountain in Ladakh, India; and Valencia (39.51°N; 0.42° W; 60 m amsl), an urban site in Spain. The data used in the present work are taken during May, 2007 to December, 2014.

METHODOLOGY

The instrument measures direct and diffuse sky irradiance at seven discrete wavelengths (315, 400, 500, 675, 870, 940, and 1020 nm). However, for aerosol studies, we excluded 315 nm and 940 nm. The mathematical equation of the incoming monochromatic direct solar irradiance arriving at the ground, $F(\lambda)$ in $\text{Wm}^{-2}\mu\text{m}^{-1}$ is given by:

$$F = F_0 \exp(-m_o \tau) \quad (1)$$

$$R(\Theta) = \frac{E(\Theta)}{F \Delta \Omega m_o}$$

where $F_0(\lambda)$ is the extraterrestrial irradiance (used as instrument's calibration) or the direct solar irradiance at the upper limit of the atmosphere, m_o is the optical air mass that can be approximated as the inverse of the cosine of the solar zenith angle, and τ is the total optical depth which includes the aerosol, molecular and Rayleigh scattering contributions. In turn, the monochromatic diffuse sky irradiance $E(\Theta)$ ($\text{Wm}^{-2}\mu\text{m}^{-1}$) at a scattering angle Θ , can be expressed as the normalized irradiance $R(\Theta)$. Finally, the solid value angle (SVA(λ)) represented by $\Delta \Omega$, is expressed in the following Equation 2.

$$\Delta \Omega = \iint_{\Delta A} \frac{E(x, y)}{E(0, 0)} dx dy = \iint_{\Delta A} f(x, y) dx dy \quad (2)$$

where x and y are polar coordinates that determine the position of the optical axis with respect to the position of the sun (expressed in radians) and $f(x,y)$ is the response function of the filter corresponding to the normalized irradiance field. The irradiance field is measured at a grid of 21 X 21 points in zenithal and azimuthal planes about the solar disk with an angular resolution of 0.1 degree and a domain ΔA of $2^0 \times 2^0$. The disk scan is performed for all the available wavelengths.

Figure 1(a) shows the measurements taken at Valencia site during a clear sky condition with a very low aerosol burden (AOD=0.06 at 500 nm). Corresponding images of an all-sky observation system are taken from a Sieltec SONA all-sky camera. The software has its own rejection criteria and Figure 1(c) shows the rejected case of disk scan data with the corresponding cloudy sky condition with an irregular spatial distribution of the solar irradiance as shown in Figure 1(d).

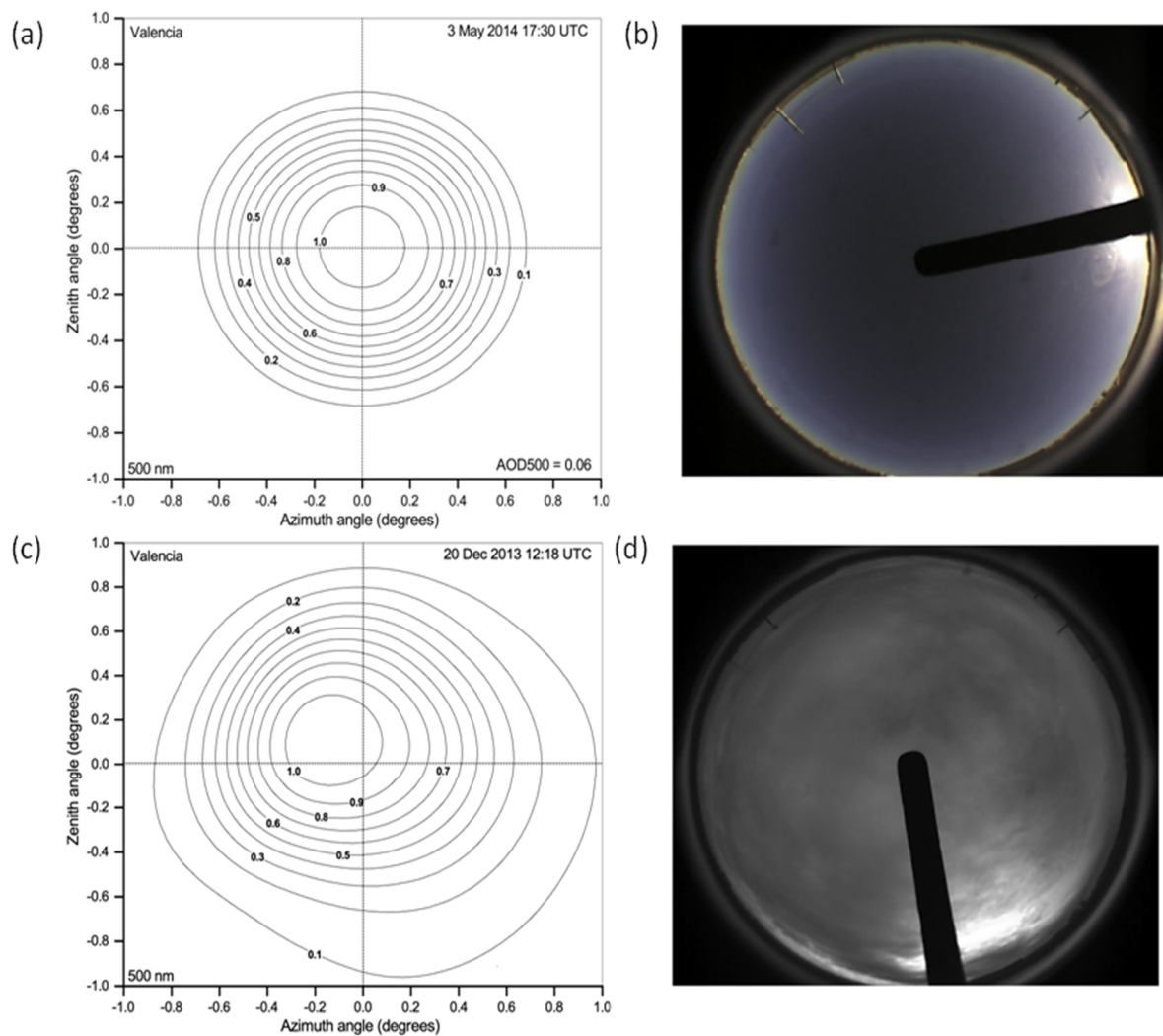


Figure 1:(a, c) Isoline representation of the irradiance in a $2^0 \times 2^0$ square around the sun, used for the estimation of the solid view angle, and corresponding images of the sky obtained with a SONA all-sky camera: (b) accepted case, retrieved on 3 May, 2014 at 17:28 UTC; (d) rejected case, retrieved on 20 December, 2013 at 12:18 UTC.

RESULTS AND DISCUSSION

In the present work, we examined series of SVA (λ) and F0I (λ) obtained from four instruments operated at various environmental conditions during 2007 to 2014. Table 1 shows SVA deviation (absolute) at Hanle and Merak with 0.74% and 0.59% from 33 and 161 observations during 2009-2010, and 2011-2014, respectively at 500 nm. The deviation is slightly poorer over Antarctic sites with 3.05% and 2.5% from 102 and 28 observations during 2007-2014 and 2012-2013 from Rothera and Halley stations, respectively. Further, the deviation over Valencia is 0.91% from 118 observations during 2008-2014. The temporal drifting of SVA (λ) indicates the instability of the instrument and the present study suggests a frequent (once in a month) calibration of SVA (λ) is recommended.

Figure 2 shows the fair correlation between measured (using F0I(λ)) and retrieved (inversion method) AOD at 5 wavelengths during January - December 2014. The high correlation coefficients ($R^2 \sim 1.0$) observed are the indication of proper calibration coefficients used in the observation. The deviation of F0I (%) at the five SKYNET sites varied from 4.9% to 2.1 % per year at 500 nm which indicates that a frequent calibration of instrument is essential to obtain high accuracy of retrieved parameters. The accuracy of AOD observed at Hanle and Merak sites are ~ 0.01 at 500 nm (Ningombam et al., 2014). Further, AOD data used from the SKYNET (version 4.2) are also quality controlled data products.

Table 1: Yearly deviation (absolute) of SVA(λ) and F0I (λ) at five Skynet sites during 2007-2014 at 500 nm.

Stations	No. Obs	SVA (dev.%)	F0I dev (%)
Hanle	33	0.74	4.9
Merak	161	0.59	3.9
Valencia	118	0.91	2.4
Rothera	103	3.05	2.1
Halley	28	2.50	3.2

The temporal drift of F0I(λ) varied from 4.9% and 3.9% over Hanle and Merak sites from 33 and 161 observations during 2009-2010 and 2011-2014, respectively. The temporal drifts are moderate over Rothera and Valencia with 2.1% and 2.4% from 103 and 118 observations during 2007-2014, and 2008-2014, respectively as seen in Table 1. However, the deviation is 3.2% for Halle from 28 observations during 2012-2013. Such high temporal drift of F0I (λ) over the aged background site in Antarctica suggested that a frequent calibration of instrument is very necessary to obtain high accuracy of retrieved parameters.

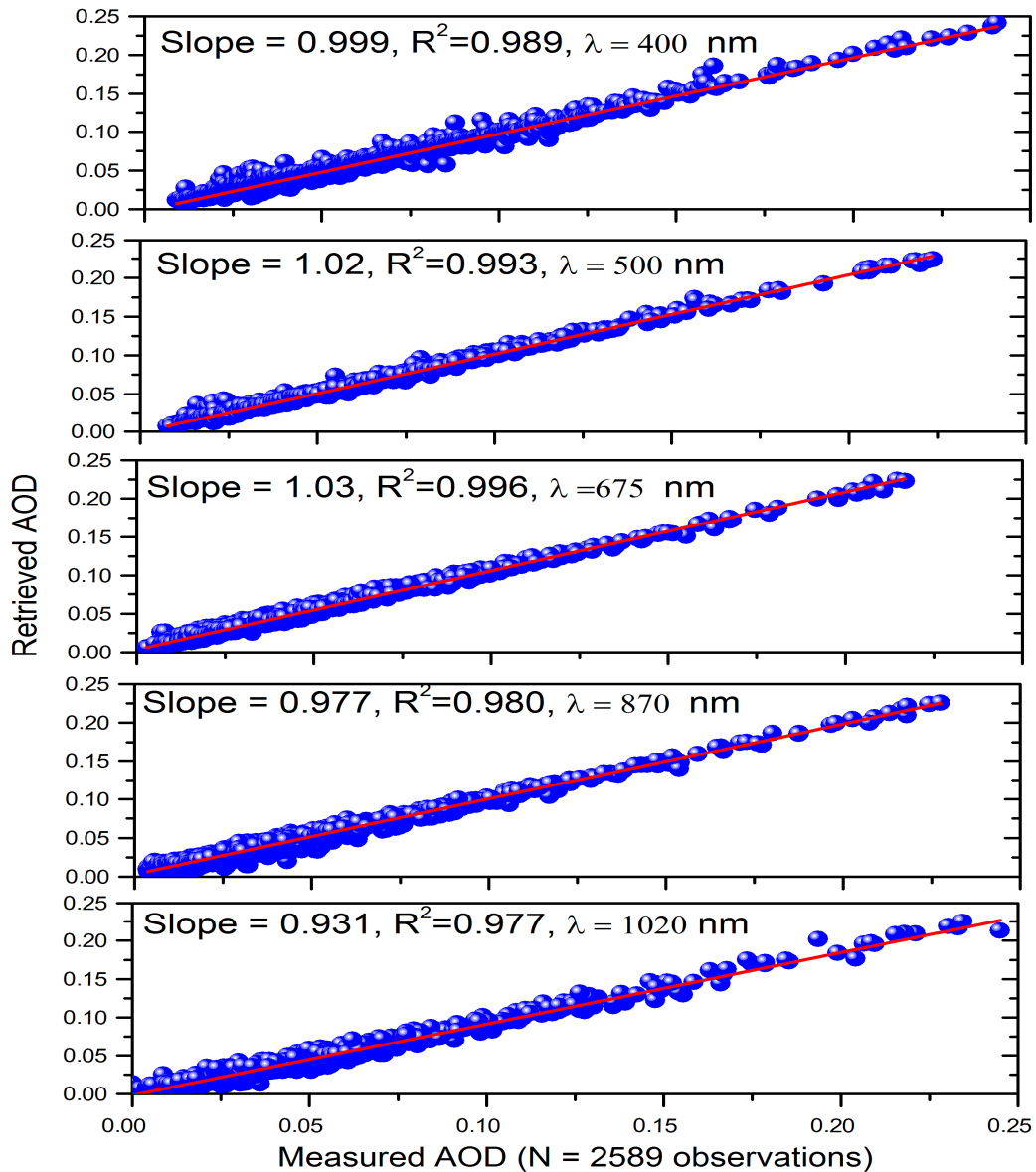


Figure 2. Measured (using estimated $F0I(\lambda)$) and retrieved (inversion method) AOD at five wavelengths over IAO-Hanle during January - December 2014.

CONCLUSION

Based on the collection of calibration data obtained from various stations during 2007-2014, the following main conclusions may be made:

The correlation between the measured (using estimated $F0I(\lambda)$) and retrieved (inversion method) AOD at five wavelengths during January, 2016 to December, 2016 is ~ 1.0 which indicates the calibration coefficients used in the observation are appropriate.

It is found that SVA (λ) deviation (absolute) at Hanle and Merak are 0.74% and 0.59% from 33 and 160 observations during 2009-2010 and 2011-2014 respectively, at 500 nm. The deviation is slightly poorer over Antarctic sites with 3.05% and 2.5% from 102 and 28 observations during 2007-2014 and 2012-2013 from Rothera and Halley stations, respectively. Further, the deviation over Valencia is 0.91% from 118 observations during 2008-2014. The study noticed that SVA(λ) is independent of the site characteristics. However, the stability of FOI (λ) depends on the characteristics of the site.

Temporal drift of FOI (λ) at the five SKYNET sites varied from 4.9% to 2.1 % per year which indicates that a frequent calibration of instrument is essential to obtain high accuracy of retrieved parameters. Further, 5% variation of FOI(λ) may causes improper AOD values or significant loss of data (i.e., rejected while processing) due to the improper calibration coefficients.

REFERENCES

- Takamura, T., and Nakajima, T.,2004. Overview of SKYNET and its activities, *Opt. Pura Apl.*, 37, 3303-3308.
- Moorthy, K. K., et al., 1.,2013. Buildup of aerosols over the Indian Region. *Geophys. Res. Lett.*, 40,1011-1014, doi:10.1029/2012GL054876.
- Remer, L. A., et al., 2005. The MODIS algorithm, products and validation. *J. Atmos. Sc.*, 62, 947-973.
- Kahn, R. A., et al., 2007. Satellite-derived aerosol optical depth over dark water from MISR and MODIS: Comparisons with AERONET and implications for climatological studies. *J. Geophys. Res.*, 112, D18205, doi:10.1029/2006JD008175.
- Ningombam, S.S., et al., 2014. Calibration of a Sky radiometer (Prede) using observations obtained from Hanle and Merak high-altitude stations in Ladakh. *Atmos. Res.*, 143, 118-128.

MOBILITY ANALYSIS AS A TOOL FOR CHARACTERIZATION OF NON-SPHERICAL NANOPARTICLES

T. THAJUDEEN¹, S. WAWRA², J. WALTER², C. LÜBBERT² AND W. PEUKERT²

¹School of Mechanical Sciences, Indian Institute of Technology Goa, GEC Campus, Farmagudi, Ponda, Goa-403401, India.

²Institute of Particle Technology, Friedrich Alexander University Erlangen-Nuremberg, Erlangen, 91058, Germany.

KEYWORDS: Hydrodynamic diameter, mobility measurement, multidimensional characterization.

INTRODUCTION

Multidimensional characterization of nanoparticles is quite relevant and important as in addition to size, particle shape and structure also plays a huge role in determining the functionality. Non-spherical nanoparticles are quite ubiquitous, and shape plays a major role in the excellent product properties of these nanoparticles. Scanning mobility particle sizer (SMPS), one of the most commonly used characterization techniques, classifies and measures particles based on their electrical mobility (Knutson and Whitby, 1975). There have been recent advances made in accurately relating the electrical mobility of non-spherical nanoparticles to their geometrical parameters. Recent experimental and computational studies have shown that precise mobility calculations can be made with the knowledge of two geometrical parameters, namely the hydrodynamic diameter (d_h) and the orientationally averaged projected area (PA). (Thajudeen et al. 2015)

Analytical Ultra Centrifugation (AUC) is considered among the most accurate means of determining the size of colloidal nanoparticles (Carney et al. 2011). Sedimentation coefficient distribution obtained from AUC measurements is related to the particle mass and hydrodynamic diameter, for non-spherical nanoparticles. Combination of AUC and SMPS measurement has been used to predict the average length and diameter of ZnO and Gold nanorods in a sample (Thajudeen et al. 2017). The nanorods were transferred from the colloidal system to be dispersed in air using electrospray ionization (ES). The combination of ES-SMPS and AUC has proved to be a powerful combination for multidimensional characterization of nanoparticles. In this study, it is proposed to use this combination for determination the length and diameter distributions of nanorods and to study the prospects of using SMPS as a tool for characterizing non-spherical nanoparticles.

THEORY

Owing to the linear relationship between the drag force and the scalar friction factor, the friction factor plays a prominent role in the motion of aerosol particles. The typical sizes of aerosol particles in the range of the background gas mean free path makes the momentum transfer a non-continuum process. The friction factor is then a function of the momentum transfer Knudsen number and for non-spherical nanoparticles depend on the d_h and PA of the particle, with the appropriate slip correction factor. The friction factor for a non-spherical particle is given by:

$$f = \frac{3\pi\mu d_H}{1 + Kn(1.257 + 0.4\exp(-1.1/Kn))}$$

where μ is the viscosity of the gas and the Knudsen number based on the geometric parameters and gas mean free path λ is given by:

$$Kn = \frac{\lambda}{2PA/\pi d_h}$$

The mobility of particles, which is related to the inverse of the friction factor is measured in SMPS and have implicit information of d_h and PA for non-spherical nano aerosol particles. AUC can be used as an additional measurement technique, where the measurement provides supplementary information to the available mobility data. Particles in an AUC cell move under the influence of centrifugal force caused by rotation, which causes spatial variation in the particle concentration. The change in particle concentration is measured and can be related to the sedimentation coefficient of the particles. The sedimentation coefficient, s of a colloidal particle is given as:

$$s = \frac{m(1 - \frac{\rho_s}{\rho_p})}{3\pi\mu d_h}$$

where ρ_s is the density of the solvent, ρ_p is the density of the particle and m is the mass of the particle. It has been shown that with the combination of the mobility distribution of the particles from SMPS and the sedimentation coefficient distribution of the particles. In this study, we propose to use the sedimentation coefficient and mobility distributions to predict the length and diameter distributions of the nanorods in a sample, independently.

RESULTS & DISCUSSION

A combination of SMPS and AUC was used to successfully measure the average length and diameter of ZnO and Gold nanorods (Thajudeen et al. 2017). This was done by comparing the representative values of both the distributions to calculate the average values of length and diameter of the nanorods in the sample. For obtaining the length and diameter distributions of the nanorods in the sample, the cumulative distributions of mobility and sedimentation coefficient are utilized. Various data points from the respective distributions are used to predict the corresponding length and diameter values. These are then used to obtain the two-dimensional distributions.

Table 1. Comparison of the length and diameter values obtained using the sedimentation coefficient and mobility data.

	Length (actual, nm)	Diameter (actual, nm)	Length (retrieved, nm)	Diameter (retrieved, nm)
x10	86.8	17.4	92.5	17.8
x25	92.8	18.6	96.4	18.9
x35	95.7	19.1	97	19.4
x50	99.6	19.9	100	20.1
x65	103.4	20.7	100.3	20.8
x75	106.3	21.3	103.9	21.3
x90	112.4	22.5	105.3	22.3

Shown in table 1 is the data obtained for gold nanorods based on numerical simulations. The dimensions of nanorods are determined from a known distribution and the sedimentation

coefficient distribution and the mobility distribution for the ensemble is calculated accordingly. The values from the respective cumulative distributions are used to calculate the corresponding length and diameter of the nanorods in the sample. An important aspect is the effect of the different weightage of the particle concentration on the measurements in AUC and SMPS. The results suggest that the method can reliably get information on the diameter distribution, but the error is larger in the case of length distribution. More simulations are being done to study this better. Experimental results will also depend on the noise in the measurements and this will also need to be studied carefully.

CONCLUSIONS

In the recent past, a combination of SMPS and AUC has been successfully used to determine the average length and diameter of nanorods in a sample. In this study the method is extended to predict the length and diameter distributions of the nanorods, independently. Simulation results show that the diameter distribution can be ascertained accurately, while the error is larger in the case of length distribution. More systematic studies are required to look at the feasibility of using the orthogonal techniques for the retrieval of two-dimensional distribution. SMPS proves as a promising technique for the multidimensional characterization of nanoparticles, as the mobility distribution inherently contains information on two distinct length parameters, namely the hydrodynamic diameter and the orientationally average projected area. This gives the unique opportunity of combining it with other techniques for characterizing non-spherical nanoparticles.

ACKNOWLEDGEMENTS

TT acknowledges funding from Alexander von Humboldt foundation. The authors acknowledge the funding from Deutsche Forschungsgemeinschaft (DFG) through the center of excellence 'Engineering for advanced materials'.

REFERENCES

- Knutson E.O and Whitby K.T. (1975). Aerosol classification by electric mobility: apparatus, theory, and applications. *Journal of Aerosol Science*. 6(6).443-451.
- Thajudeen T., Jeon S., Hogan C.J (2015) The mobility of flame synthesized aggregates/agglomerates in the transition regime. *Journal of Aerosol Science*. 80: pp. 45-57.
- Carney R.P, Kim J.Y, Qian H, Jin R, Mehenni H, Stellacci F, Bakr O.M. (2011) Determination of nanoparticle size distribution together with density or molecular weight by 2D analytical ultracentrifugation. *Nature Communications*. 7:335.
- Thajudeen T., Walter J., Srikantharajah R., Luebbert C., Peukert W. (2017) Determination of the length and diameter of nanorods by a combination of analytical ultracentrifugation and scanning mobility particle sizer. *Nanoscale Horizons*. 2, pp 253-260.

PHYSICAL AND CHEMICAL PROPERTIES OF ATMOSPHERIC AEROSOL AT ALAKNANDA VALLEY (SRINAGAR) IN THE CENTRAL HIMALAYA REGION

D.S. BISHT^{1,*}, A.S. GAUTAM², R.S. NEGI³, M. JOSHI², A.K. SRIVASTAVA¹, S. TIWARI¹

¹Indian Institute of Tropical Meteorology (Delhi Branch), New Delhi

²Department of Physics, HNB Garhwal University, Srinagar, Uttarakhand

³Department of Rural Technology, HNB Garhwal University, Srinagar, Uttarakhand

KEYWORDS: Particulate Matter; Carbonaceous Aerosol; Chemical Species; Trajectory Analyses

INTRODUCTION

The atmospheric aerosol is linked to air quality, adverse health effects and heat balance of the Earth directly through absorbing/scattering the solar radiation, indirectly by influencing cloud microphysics and possibly by changing the heterogeneous chemistry of reactive greenhouse gases (IPCC, 2007). The enhanced pollutant emissions associated with the fast-growing economies of Southeastern Asian countries have led to the progressive increase of aerosol concentrations above the natural background (Ram et al., 2010; Chatterjee et al. 2010). Aerosol-enriched boundary layer air can be transported to the higher altitudes by valley-breeze processes on the Himalayan slopes, which is a matter of concern as glaciers are noted to retreat over the Himalayan sites (Ashish et al. 2006; Gautam et al. 2013). The direct and indirect effects of aerosols depend on size distribution and chemical composition of atmospheric aerosols (Jung et al., 2018). Apart from the size of aerosols, assessment of their chemical composition as a function of time is of crucial importance to understand atmospheric processes such as radiative transfer, cloud droplet nucleating ability, acidification, precipitation chemistry and dry deposition. The rapid growth of industries, vehicles, population, and anthropogenic activities resulted in higher concentrations of fine mode particles in the megacities of most of the rapidly developing countries in Asia (Akimoto, 2003; Bisht et al. 2015a). Many studies have indicated that particulates in the accumulation mode ($d < 2.5 \mu\text{m}$) particle are the most critical to human health, visibility degradation etc (Pope et al. 1995; Dholakia et al. 2014; Bisht et al. 2015a). There is no studies were made for fine particulates ($\text{PM}_{2.5}$: particles less than 2.5 microns) and inhalable particle (PM_{10} : ≤ 10 microns) over the Alaknanda basin, located in the state of Uttarakhand. The present study is the first attempt to take the observations of particulate matters (PMs) and its water-soluble chemical constituents over Alaknanda basin to understand their loading over high altitude region. The very limited studies were conducted over the other parts of Himalayas (Ram et al. 2010; Chatterjee et al. 2010). Due to the above-mentioned importance and lack of physical and chemical data of atmospheric aerosols over Himalayan environment, a year-long measurements of PMs ($\text{PM}_{2.5}$ and PM_{10}) and its chemical constituents were made over Srinagar, Garhwal, Uttarakhand along with meteorological parameters (MPs). The impact of meteorological parameters on PMs and its chemical constituents were also studied to quantify the accumulation or dispersion of the measured secondary aerosols in the study region because the basin region has a tendency to accumulate the pollutants by the circulation of air masses. Further, we have tried to study the transportation of measured atmospheric aerosols over the study region using air mass back-trajectory analyses.

INSTRUMENTATIONS AND METHODOLOGY

PM_{2.5} and PM₁₀ aerosol sampling were conducted on the campus of the Hemvati Nandan Bahuguna Garhwal University (HNBGU) at Srinagar Garhwal, Chauras Campus, from During Dec 2015 to Dec 2016 on the rooftop of the building (~ 1.5 m above the ground level). Sampling on PMs were carried out using single stage PM_{2.5} and PM₁₀ samplers, which provides information about aerosol mass concentrations of sizes up to 2.5 and 10 µm respectively. Both PMs Samples were collected once in a week using APM 550 and APM-460 samplers (M/s Envirotech Pvt. Ltd., India) for PM_{2.5} and PM₁₀ respectively. The sampling cycles were 24 hr and 8 hr with a flow rate of one cubic meter per hour for collecting sufficient mass of PMs. The particle concentrations were determined gravimetrically by the difference in their weights before and after the sampling. One-fourth of sample filters were extracted with ultrapure water (50 ml) via ultra-sonication for 60 min. thereafter, the liquid samples were filtered through a prewashed Whatman filter No. 41 into pre-cleaned polypropylene bottles. All filtered samples were preserved at 4°C in a refrigerator. The major anions (F⁻, Cl⁻, NO₂⁻, NO₃⁻ and SO₄²⁻) and cations (Na⁺, K⁺, NH₄⁺, Ca²⁺ and Mg²⁺) were quantitatively determined by Ion Chromatograph (DIONEX-2000, (USA). The analytical column Ion Pac-AS 15 with micro-membrane suppressor ASRS ultra II 2 mm, 38 mm Potassium Hydroxide and the IonPac-CS17 column with micro-membrane suppressor CSRS ultra II 2 mm, 6 mm methyl sulfonic acid as eluents and de-ionized water as regenerator were used for anions and cations respectively. The cation and anion standards were procured from Dionex for calibration. The detection limit for ion chromatographic analysis was around 0.02 ppm for measured ions. Field blanks were also collected during sampling period and analyzed as samples the concentrations of field blank were found within the detection limits (Bisht et al., 2015b)

RESULTS & DISCUSSIONS

The figure 1 shows monthly averages of PM_{2.5} and PM₁₀ concentrations along with their Indian National Ambient Air Quality Standards (NAAQS). The PM₁₀ concentration was varied between 79.6 µgm⁻³ (August) and 154.1 µgm⁻³ (December) with an annual mean 111.8 (±23.4) µgm⁻³ which is about more than two times higher than the standard set by NAAQS (60 µgm⁻³ for PM₁₀) indicated (Fig. 1) by a box with solid lines. The higher PM₁₀ levels may be due to windblown dust during the summer or pre-monsoon months, from the adjoining together with the thermodynamic conditions in the planetary boundary layer, which influence the pollutant dispersion. During the study period, annual mean PM_{2.5} concentration was 78.7 (±25.1) µgm⁻³ which is about more than two times higher the annual standard set by NAAQS (40 µgm⁻³ for PM_{2.5}). PM_{2.5} concentrations varied between 39.4 µg m⁻³ (August) and 125.3 µgm⁻³ (December), it is due to meteorological effect as higher winds and mixing layer depth that improve the dispersion of particles in the atmosphere during the summer season, however, the frequent thermal inversions, conditions and stable atmospheric boundary layer during the winter causes stagnation of particulates in the lower atmosphere (Tripathi et al. 2006). Tripathi et al. (2006) reported ~75% contribution of tiny particles to the total mass of aerosols at Kanpur (Indo-Gangetic Basin site) and significant association with the prevailing foggy conditions in the winter season. Many recent studies have indicated that particulates in the accumulation mode (d < 2.5 µm) particle are the most critical to human health, visibility degradation etc (Pope et al. 1995).

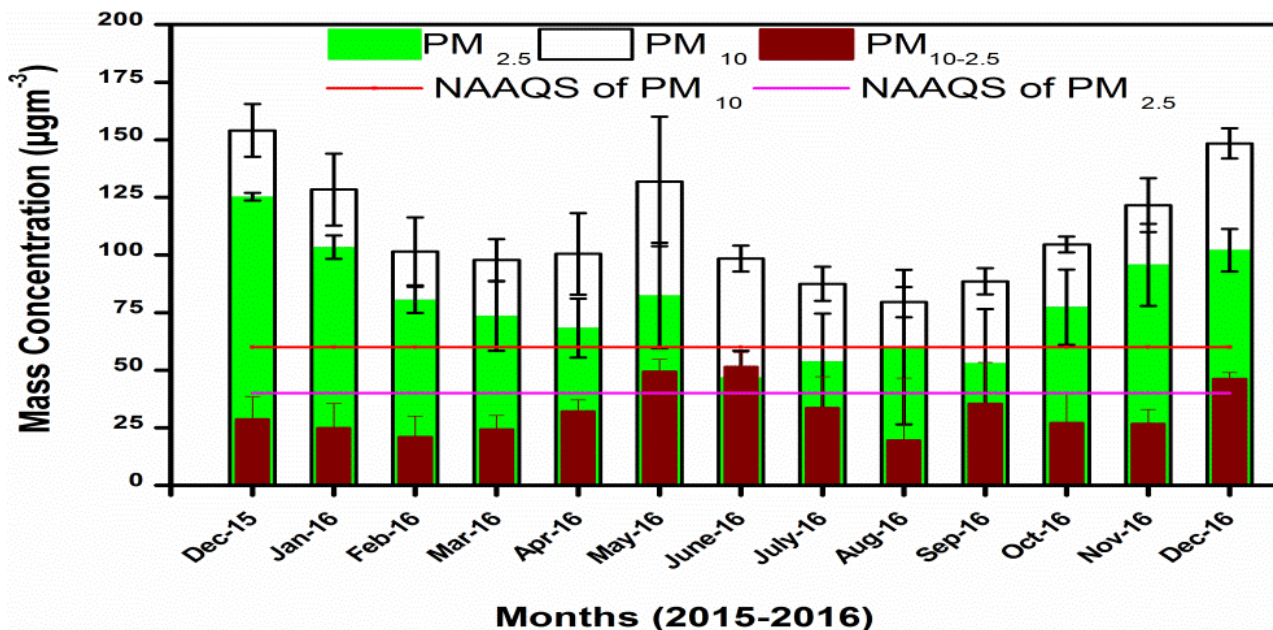


Figure 1: Monthly variations of PM_{2.5}, PM₁₀ and PM_{10-2.5} mass concentrations.

However, coarse mode particles ($d > 2.5 \mu\text{m}$) are mainly produced by natural processes. These include sea-salt aerosols produced by direct dispersal of ocean water and crustal aerosols originating from the solid surface of the Earth. At this point, it is worthy to note that although PM₁₀ is a better indicator of total suspended particulate (TSP), it may not necessarily represent a true picture of more hazardous fine particulate. This situation is particularly important in the Indian context, where a significant proportion of PM₁₀ may be due to locally generated wind-driven dust in the coarse fractions (i.e. PM₁₀) and which may not be as harmful as PM_{2.5} (Sharma and Maloo 2005).

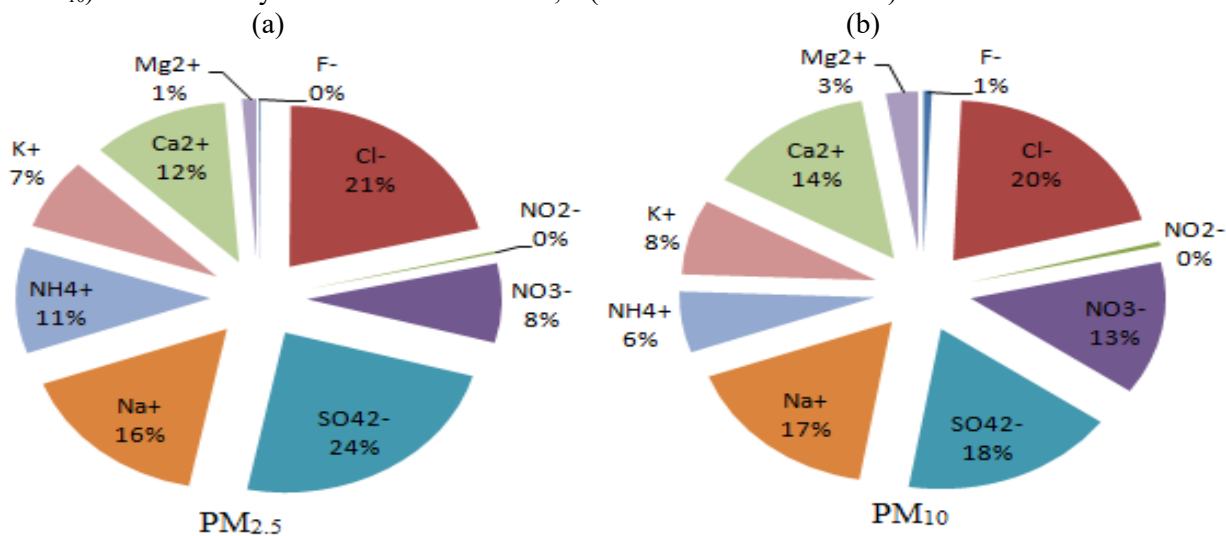


Figure 2: Percentage contribution of different chemical species in PM_{2.5} and PM₁₀

The difference between the concentrations of PM₁₀ and those in PM_{2.5} is the contribution of the coarse fraction (PM_{10-2.5}). The mass concentrations of PM_{10-2.5} varied corresponding to the variations in PM_{2.5} and PM₁₀, as shown in Fig. 1. The monthly mean variation in PM_{10-2.5}

concentrations provides the clear picture of the fraction of coarser aerosol particles at the observation site, which shows significantly higher fractions during summer months and lower fractions during winter months. To understand the contributions of PM_{2.5} in PM₁₀, the ratio of PM_{2.5}/PM₁₀ is found to be $\sim 0.69 \pm 0.1$, varying from 0.49 (August) to 0.82 (December) shows that the ratio is much smaller during the monsoon and summer months, indicating that the lesser fine particle fraction in PM₁₀, suggesting the dominance of coarser particles due to mineral dust transported from the adjacent desert region. However, the ratio is much higher during the winter months indicating that the larger fine particle fractions in PM₁₀ at this location. These high fractions of fine mode particles attributed to low-level inversion and favorable meteorological conditions for accumulation of pollutants in lower atmosphere, which are emitted from the various anthropogenic sources such as biomass burning in open fields, domestic fuel in rural settings, emissions from thermal power plants, brick kilns, fossil fuel burning and vehicular exhausts (Venkataraman et al. 2005; Tripathi et al. 2006). The percentage contribution of water-soluble ionic species (F⁻, Cl⁻, SO₄²⁻, NO₃⁻, Na⁺, K⁺, Mg²⁺, and Ca²⁺) in PM_{2.5} and PM₁₀ are given in figure 2. Among all the chemical species in PM₁₀, the mean concentration of chloride was highest (12.99 $\mu\text{g m}^{-3}$) followed by SO₄²⁻ (mean: 11.5 $\mu\text{g m}^{-3}$) which is the second highest concentration varied from 3.1 to 17.8 $\mu\text{g m}^{-3}$. However, SO₄²⁻ concentrations (8.0 \pm 4.8) $\mu\text{g m}^{-3}$ in PM_{2.5} varied between 0.6 $\mu\text{g m}^{-3}$ to 17.7 $\mu\text{g m}^{-3}$. In PM₁₀, the concentration of fluoride (F⁻) ion was 0.4 $\mu\text{g m}^{-3}$; however, in PM_{2.5}, it was low concentration (0.03 $\mu\text{g m}^{-3}$). The ionic abundance, showed in the order of SO₄²⁻ > Cl⁻ > Na⁺ > Ca²⁺ > NH₄⁺ > NO₃⁻ > K⁺ > Mg²⁺ in PM_{2.5} and Cl⁻ > SO₄²⁻ > NO₃⁻ > Na⁺ > Ca²⁺ > K⁺ > NH₄⁺ > Mg²⁺ in PM₁₀.

The percentage contributions of each chemical species in both PMs sample are shown in Fig. 2. The measured total water-soluble ionic fraction contributed approximately 43% of the total PM_{2.5}, of which anions and cations account for about 32 and 11% respectively (Fig. 2a). On the other hand, it was about 57% of the total PM₁₀ with 30 and 27% for anions and cations, respectively (Fig. 2b). The major unanalyzed portion in PM₁₀ (43%) and PM_{2.5} (56%) samples were due to carbonaceous aerosols such as black carbon and organic carbons, and other insoluble hard metals. However, in PM₁₀, the analyzed ionic species consists of secondary inorganic aerosols (SO₄²⁻ and NO₃⁻) which contribute approximately 18% of the PM₁₀ mass (19.12 $\mu\text{g m}^{-3}$) followed by, salt aerosols (Na⁺ and Cl⁻: 20% (23.31 $\mu\text{g m}^{-3}$), and mineral dust (K⁺, Mg²⁺ and Ca²⁺), around 13% (14.97 $\mu\text{g m}^{-3}$). However, in PM_{2.5}, the secondary inorganic aerosols (SO₄²⁻ and NO₃⁻) were approximately 14.9% (12 $\mu\text{g m}^{-3}$), 16% salt aerosols, (12.97 $\mu\text{g m}^{-3}$) and 9% mineral dust (7 $\mu\text{g m}^{-3}$). However, the difference in PM₁₀ could be due to soil-derived.

CONCLUSIONS

Mass concentrations of particulate matters (PM_{2.5} and PM₁₀), their chemical characteristics along with organic and elemental carbon mass concentration and their sources have been studied at a rural location in the Alaknanda basin (in Himalayan region) in Northern India for Srinagar Garhwal site. The concentrations of PM₁₀ and PM_{2.5} were $111.8 \pm 20.9 \mu\text{g m}^{-3}$ and $78.7 (\pm 25.1)$ during the study period. The measured chemical species were found a large variability in the different season due to the impact of emissions and meteorological parameters. The mean PM_{2.5}/PM₁₀ ratio was found to be 0.69 (± 0.1) to be which varied from 0.61 in June due to the coarse mode of mineral dust to 0.82 in December due to the dominance of fine mode anthropogenic particles. The measured water-soluble (WS) chemical species of PM₁₀ and PM_{2.5} were 57% (54 $\mu\text{g m}^{-3}$) and 43% (34 $\mu\text{g m}^{-3}$) during the study period. Large fractions of the unanalyzed portion in PMs were carbonaceous aerosols and/ or secondary aerosols. Higher concentrations WS species were during the winter season followed by summer, post-monsoon and monsoon seasons. Neutralization of acidic species due to cations was estimated and found that NH₄⁺ play a crucial role in neutralization in the winter season, however, the contrary feature was observed in the summer season where Ca²⁺ was

responsible for the neutralization of acidic components in the PMs samples which were transported from the inland region during summer. Cluster analysis was performed for the source region and it was observed that the continental landmasses of Southern Afghanistan (summer season) and Western region of Pakistan (summer and winter season) and adjoining states of Uttarakhand and could be the cause of higher PM_{2.5} and PM₁₀ over the study region.

REFERENCES

- Akimoto, H. (2003). Global air quality and pollution. *Science* 302, 1716–1719.
- Ashish, A., V. Joshi, A. Sharma and S. Anthwal (2006). Retreat of Himalayan glaciers indicator of climate change, *Nature and Science* 4, 53-60.
- Bisht, D.S., U.C. Dumka, D.G. Kaskaoutis, A.S. Pipal, A.K. Srivastava, V.K. Soni, S.D. Attri, M. Sateesh and S. Tiwari (2015a). Carbonaceous aerosols and pollutants over Delhi urban environment: temporal evolution, source apportionment and radiative forcing. *Sci Total Environ* 521-522, 431-445.
- Bisht DS, Srivastava AK, Pipal AS, Srivastava MK, Pandey AK, Tiwari S and G. Pandithurai (2015b). Aerosol characteristics at a rural station in southern peninsular India during CAIPEEX-IGOC: physical and chemical properties, *Environ Sci Pollut Res* 22, 5293-5304.
- Chatterjee, A., A. Adak, A.K. Singh, M.K. Srivastava, S.K. Ghosh, S. Tiwari et al. (2010) Aerosol Chemistry over a High Altitude Station at Northeastern Himalayas, India. *PLoS ONE* 5(6), e11122.
- Dholakia, H.H., D. Bhadra and A. Garg (2014). Short term association between ambient air pollution and mortality and modification by temperature in five Indian cities, *Atmos Environ* 99, 168-174.
- Gautam, R., N.C. Hsu, W.K.M. Lau and T.J. Yasunari (2013). Satellite observations of desert dust-induced Himalayan snow darkening, *Geophys Res Lett*, 40(5), 988-993.
- IPCC (2007). Intergovernmental Panel on Climate Change. Fourth Assessment Report, Cambridge University Press, Cambridge, Section 2.2. 37 p.
- Jung, C.H., J.Y. Lee, J. Um, S.S. Lee and Y.P. Kim (2018). Chemical composition based aerosol optical properties according to size distribution and mixture types during smog and Asian dust events in Seoul Korea, *Asia Pac J Atmos Sci* 54(1),19-32.
- Pope, C.A., M. Thun, J. Namboodira, D.W. Dockery, J.S. Evans, F.W. Speizer and C.W. Heath Jr (1995). Particulate air pollution as a predictor of mortality in a prospective study of US adults, *Am. J. Respir Crit Care Med* 151, 669-674.
- Ram, K., M.M. Sarin and P. Hegde (2010). Long-term record of aerosol optical properties and chemical composition from a high-altitude site (Manora Peak) in Central Himalaya, *Atmos Chem Phys* 10(23), 11791-11803.
- Sharma, M. and S. Maloo (2005). Assessment of ambient air PM₁₀ and PM_{2.5} and characteristics of PM₁₀ in the city of Kanpur, India, *Atmos. Environ.* 39, 6015-6026.

Tripathi, S.N, et al. (2006). Measurements of atmospheric parameters during Indian Space Research Organization Geosphere Biosphere Programme Land Campaign II at a typical location in the Ganga basin: 1. Physical and optical properties, J Geophys Res 111(D23209), 1-14.

Venkataraman, C., G. Habib, A. Figure-Fernandez, A.H. Miguel and S.K Friedlander (2005). Residential bio-fuels in south Asia: carbonaceous aerosol emissions and climate impacts, Science 307, 1454-1456.

LONG-TERM ASSESSMENT OF NEAR-SURFACE AIR POLLUTANTS AT AN URBAN STATION IN INDO-GANGETIC BASIN

A.K. SRIVASTAVA^{1*}, N. KISHORE^{1,2}, H. NANDAN², S. AGRAWAL³, D. S. BISHT¹, S. TIWARI¹ AND MANOJ K. SRIVASTAVA⁴

¹Indian Institute of Tropical Meteorology (Branch), Prof Ramnath Vij Marg, New Delhi, India

²Department of Physics, Gurukula Kangri University, Haridwar, India

³Central Pollution Control Board, New Delhi, India

⁴Department of Geophysics, Banaras Hindu University, Varanasi, India

(*Correspondence at: A. K. Srivastava atul@tropmet.res.in)

KEYWORDS: Air Quality; Particulate Matter; NAAQS; Indo-Gangetic Basin; Back trajectory.

INTRODUCTION

Many Indian cities, especially those over the Indo-Gangetic Basin (IGB), are amongst the most polluted cities in the world. This conglomeration of polluted cities in the IGB makes it one of the world's most populated and polluted river basin (Dey and Di Girolamo, 2010). New Delhi, one of the urban mega-cities situated in the north-western part of IGB in northern India, suffers from the intense pressure of urbanization, industrialization and dense population, which causes severe air quality. The severely degraded air quality of New Delhi has received much attention in recent years as it poses potential health hazards (Maji *et al.*, 2015 and references therein). Recent studies showed that the emission loads over New Delhi and its surroundings are still increasing rapidly (Sahu *et al.*, 2011, 2015; Mishra and Goyal, 2015). Additionally, high pollutants also lead to urban and regional haze, deleterious impacts on regional ecosystem, crop yield and climate change. Thus, the precautionary measures are needed to chase the mitigation policy and manage current emissions of air pollutants.

METHODS

Data presented in this work is collected by Central Pollution Control Board (CPCB) at Mayapuri site in Western New Delhi from 2005 to 2012. Several criteria pollutants are being monitored at this site, including sulphur dioxide (SO₂), nitrogen dioxide (NO₂), respirable suspended particulate matter (RSPM) and suspended particulate matter (SPM). Measurements of these criteria pollutants are not available for later half the year 2006, for SO₂ during the year 2010 and for SPM for the year 2012 due to instrument malfunctioning. A total of 556 days of dataset was obtained over the entire study period.

RESULTS & DISCUSSIONS

Daily (with dots) and monthly (with solid line) mean time series of the measured near-surface criteria pollutants at New Delhi are shown in Figure 1. The daily mass concentration of NO₂ was found to vary from 13.5 to 142.1 $\mu\text{g m}^{-3}$, with a mean value of $62.0 \pm 27.6 \mu\text{g m}^{-3}$ over the entire time period. For about 27% of data samples of NO₂ was found to exceed the corresponding National Ambient Air Quality Standard (NAAQS) level (80 $\mu\text{g m}^{-3}$). It is found that the NO₂ levels crossing the safe standard (i.e. NAAQS), particularly in the post-monsoon and winter periods. This could be attributed to the industrial (largely from power plants) along with the vehicular sources (George *et al.*, 2013). Further, the daily mass concentration of SO₂ was found to vary from 2 and 48.7 $\mu\text{g m}^{-3}$, with a mean value of $12.4 \pm 8.2 \mu\text{g m}^{-3}$. Surprisingly, the daily mass concentration of

SO₂ was found to be about six times below to its 24-hour NAAQS value (80 μg m⁻³). This could be attributed to the use of low sulphur content fossil-fuel, use of fuel gas de-sulfurization for industrial processes and/or implementation of CNG vehicles. On the other hand, daily mean PM₁₀ mass concentration varied between 10.7 and 843 μg m⁻³, with a mean of 253.7±134 μg m⁻³ over the entire time period. It was found to be substantially higher than its 24-hour NAAQS value (100 μg m⁻³) for about 87% of the days of total observation days. SPM was found to vary from 64 to 1104 μg m⁻³ with a mean of 529.2±213.1 μg m⁻³, which was higher than its prescribed 24-hour NAAQS value (200 μg m⁻³) for about 99% of days of the total observation days.

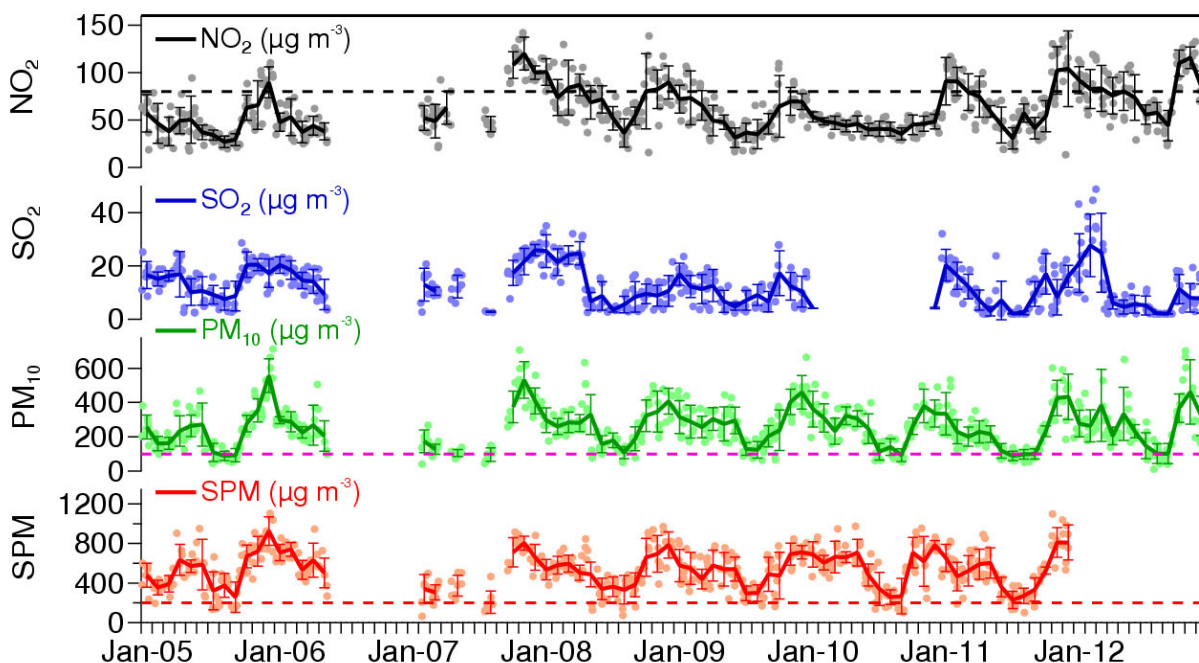


Figure 1. Daily (dots) and monthly (solid line) time series of mass concentrations of NO₂, SO₂, PM₁₀ and SPM at Delhi during the entire study period. The dotted line indicates 24-hour averaged NAAQS level for NO₂ (80 μgm⁻³), SO₂ (80 μgm⁻³), PM₁₀ (100 μgm⁻³) and SPM (200 μgm⁻³).

Despite of the past efforts, such as cutting down the sulfur content in diesel/petrol, use of clean fuels (CNG/LPG), and shutdown the hazardous industries, the annual average levels of NO₂, PM₁₀ and SPM at New Delhi were found to be persisted at their alarming levels during the study period. However, the annual average level of SO₂ has been controlled significantly, which could be attributed due to the above efforts. These air pollutants were found to be highest during the winter/post-monsoon period, which are of major concern for both climate and health.

To understand the potential source sectors of these criteria pollutants, 5-day air mass backward trajectories were analyzed over the station at 1000 m above ground level using HYSPLIT model (Draxler and Rolph 2010). Four different air mass trajectory clusters were identified over the entire time period only for those days when measurements are available; namely ‘North-Northwest (N-NW)’, ‘West-Southwest (W-SW)’, ‘Southeast (SE)’ and ‘local slow moving (LSM)’ air trajectories. Table 1 shows percentage occurrence of clustered air mass back trajectory along with the corresponding mean mass concentrations of measured air pollutants at New Delhi. Results show that station received maximum air masses from N-NW direction (~42%). However, air mass trajectory cluster was contributed to be lower (~10%) over the station for LSM. For each of these

clusters, we have further calculated mean mass concentrations for air pollutants (Table 1). The higher mass concentrations for all pollutants were associated with the trajectories from N-NW region. It is not surprising as the wind direction is mostly N-NW during the winter/post-monsoon season over the station. However, the lowest mean mass concentrations of air pollutants were observed to be associated with the SE trajectory cluster, which could be due to wet scavenging of air pollutants during the monsoon season.

Table 1. Mean mass concentrations of measured air pollutants for observed trajectory clusters at Delhi.

	trajectory occurrence (%)	NO ₂ (µg m ⁻³)	SO ₂ (µg m ⁻³)	PM ₁₀ (µg m ⁻³)	SPM (µg m ⁻³)
N-NW	41.7	71.9±29.6	15.4±8.6	314.2±122	608.8±190.2
W-SW	16.1	25.1±27.5	3.6±5.5	102.4±130.8	209.2±257.3
SE	17.0	23.3±26.6	2.92±5.1	69.1±92.6	141.4±200.1
LSM	9.5	56.9±40.8	9.8±8.1	241.8±188.8	438.2±336.1
M	15.7	50.5±31.2	10.7±8.8	198.2±128.5	408.0±268.2

N-NW: North-northwest; W-SW: West-southwest; SE: Southeast; LSM: Local slow moving; M: Mixed

CONCLUSIONS

- The mean mass concentrations of NO₂, SO₂, PM₁₀ and SPM at New Delhi were observed to be about 62±28, 12±8, 254±134 and 529±213 µg m⁻³, respectively with significant intra- and inter-annual variability over the entire study period.
- Mean mass concentrations of NO₂, PM₁₀ and SPM were found to exceed by ~27%, 87% and 99%, respectively, compared to their prescribed NAAQS levels. However, the mass concentration of SO₂ was never exceeded its NAAQS.
- Air mass cluster analyses suggested that the maximum air mass contribution (~42%) was from N-NW direction, which was associated with higher loading of all air pollutants. However, lower mean mass concentrations of air pollutants were associated with SE trajectory cluster.

ACKNOWLEDGEMENTS

Authors are thankful to the CPCB for providing air quality data and India Meteorological Department for surface meteorological data of New Delhi, which have been used in this study. We are also thankful to NOAA Air Resources Laboratory (ARL) for providing HYSPLIT PC-version model via <http://www.arl.noaa.gov/ready.php>.

REFERENCES

Dey S, Di Girolamo L, (2010) A climatology of aerosol optical and microphysical properties over the Indian subcontinent from 9 years (2000–2008) of Multiangle Imaging Spectroradiometer (MISR) data, *J. Geophys. Res.* 115 D15204. doi:10.1029/2009JD013395.

Draxler R R, Rolph G D, (2010) HYSPLIT (HYbrid Single-Particle Lagrangian Integrated Trajectory) Model access via NOAA ARL READY Website (<http://ready.arl.noaa.gov/HYSPLIT.php>); *NOAA Air Resources Laboratory*, Silver Spring, MD.

George M P, Kaur B J, Sharma A, Mishra S, (2013) Delhi smog 2012: Cause and concerns, *J. Pollut. Eff. Cont.* 1(1) 103 doi: 10.4172/jpe.1000103.

Maji S, Ahmed S, Siddiqui W A, (2015) Air quality assessment and its relation to potential health impacts in Delhi, India, *Curr. Sci.* 109(5) 902-909.

Mishra D, Goyal P, (2015) Quantitative Assessment of the emitted criteria pollutant in Delhi urban area, *Aerosol Air. Qual. Res.* 15 1601-1612.

Sahu S K, Beig G, Parkhi N, (2011) Anthropogenic emission of PM_{2.5} and PM₁₀ for air quality forecasting during Commonwealth Games 2010 Delhi, *Atmos. Environ.* 45 6180-6190.

Sahu S K, Beig G, Parkhi N, (2015) High resolution emission inventory of NO_x and CO for mega city Delhi, India, *Aerosol Air. Qual. Res.* 15 1137-1144.

LONG TERM VARIABILITY AND TREND ANALYSIS OF BLACK CARBON OVER NY-ÅLESUND, ARCTIC

SUNIL M. SONBAWNE¹, ROHINI BHAWAR², SHWETA MUKIM², and SANJOY K. SAHA¹

¹ Indian Institute of Tropical Meteorology, Pashan Road, Pune-411008, INDIA

² Department of Atmospheric and Space Sciences, Savitribai Phule Pune University, Pune

(*Correspondence at sunil@tropmet.res.in)

KEYWORDS: Black Carbon, Airmass transport, Ny-Ålesund

INTRODUCTION

When fossil fuels, wildfires, industrial combustion, and other organic material burn, they release smoky soot into the atmosphere. Even Gas flaring may currently be a significant source as well, with a significant share occurring at high latitudes [Quinn *et al.*, 2011; Stohl *et al.*, 2013]. A major component of soot is black carbon, which consists of pure carbon particles that absorb solar radiation and promote global warming. The black carbon emission sources in the Arctic has been found to result from long range transport from the Soviet Union, Europe, N. America and East Asia [Sharma *et al.*, 2013].

In this present study, we present and discuss the concentration, sources and temporal variations of aerosol black carbon observed during summer Arctic 2011-2013, at Indian Arctic Station, HIMADRI, Ny-Ålesund, (79°N, 12°E, 8 a.m.s.l). Here we discuss BC measurement is of particular interest of peak summer month (JULY) of each year. We find an unusual increase in BC concentration in 2011 as compare in 2012 and 2013. This study will provide valuable BC observations at the settlement site as regards the limited data available in the Arctic.

METHODS

High resolution long term ground-based observation of BC were made during summer Arctic from 2010-2015 at Indian Arctic station, HIMADRI, Ny-Ålesund, (79°N, 12°E, 8 a.m.s.l) using seven wavelength aethalometer model AE42. During the observation period the aethalometer were operated under 50% maximum attenuation to keep the loading at a low level. The device measures the attenuation of light transmitted through particles accumulate on a quartz filter and thus this change in optical attenuation which convert particle light absorption to BC concentrations, which rely on some assumptions [Sharma *et al.* 2004]. The specific mass absorption coefficient $\alpha_{ap} = 15.9 \text{ m}^2 \text{ g}^{-1}$ was used to calculated BC mass concentrations, In this study, only 880nm data at 10min temporal resolution of the measuring period during peak summer arctic month of July are reported here. The scattering correction wasn't employed in this study since aerosols in these remote areas were well-aged, requiring little or no correction [Hansen *et. al.* 2007]. Meteorological parameters were also collected simultaneously with temporal resolution of 30 min. Variability of BC for the month of July for years 2010-2015 have been analyzed and the results are presented and discussed in the paper.

RESULTS AND DISCUSSION

Besides day to day variation Fig 1, BC concentration exhibited a pronounced mean hourly variation of BC mass concentration is shown in Fig. 2. This diurnal variation in BC might be due to the variation in emission form local sources, such as ship emission, power plant and vehicular movement, and also from the long-range transport from the neighboring countries. This variation

is also attributed to variation in surface temperature as 24 hrs day light present over this location. During the month of July 2011 and 2012 Fig.2 BC concentration showed a gradual increasing in trend from 0600 LT (local time hrs) and peak around at 1300 LT ($40 \pm 00\text{ng/m}^3$) which went on decreasing till 1800 LT, minimum BC of $10 \pm 00\text{ng/m}^3$

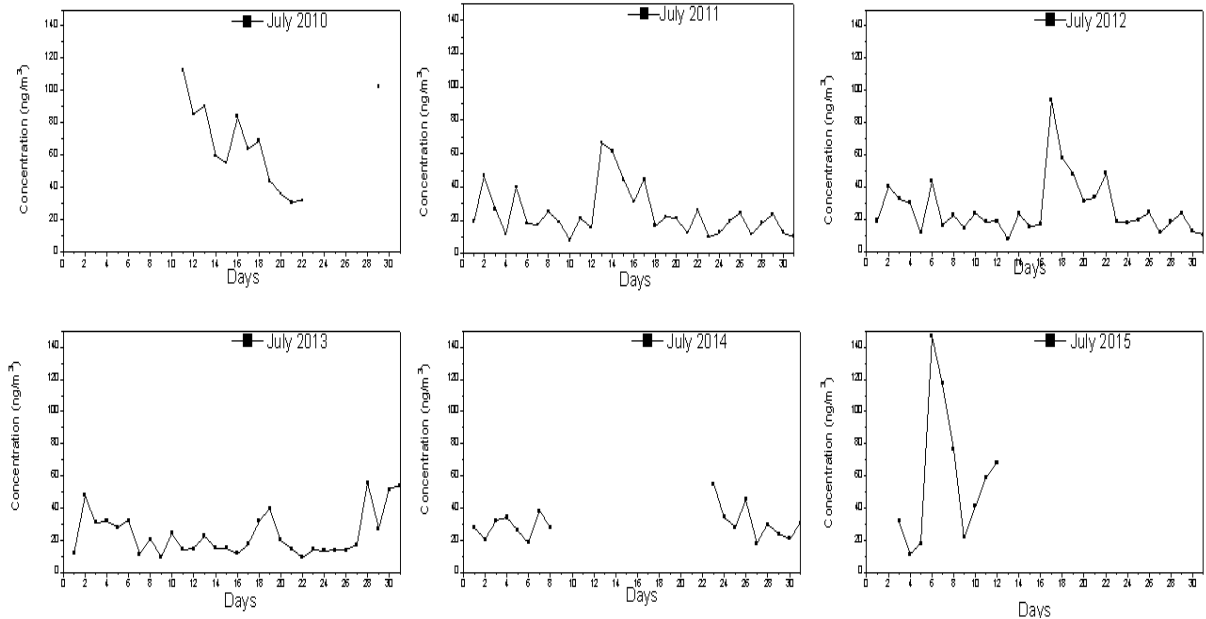


Figure 1: Day to day variability in BC in month of July for years, 2010, 2011, 2012, 2013, 2014 and 2015

Same diurnal pattern is observed in 2010 and 2015, with higher values of BC, but the days which went into averaging are very less. In 2013, Fig.2 shows that the BC concentration is much low of $36 \pm 00\text{ng/m}^3$ as compare to previous years with the same variation trend. Monthly mean BC mass concentration during 2011-13 in July month was found to be maximum during second week of July in 2011 and third week of July in 2012. It was observed that the maximum BC loading in the atmosphere at Observation station site was during 0800-1600 LT in July month of all the years.

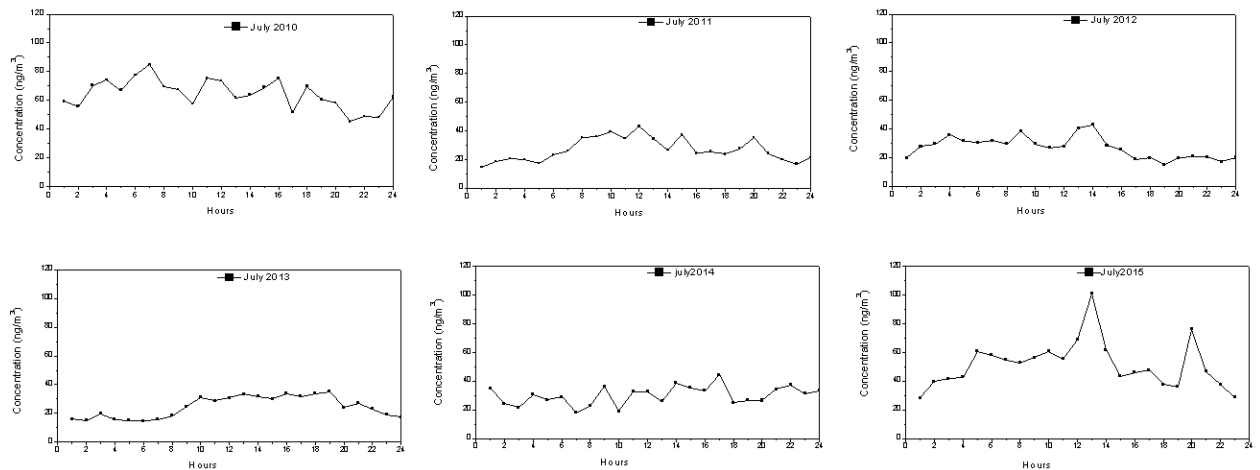


Figure 2: Averaged diurnal variation of BC for month of July during years 2010- 2015

Fig 1 depicts the variation of mean daily BC concentration at HIMADRI during 1st July to 31st July of every year are plotted. It can be seen that daily mean BC value varied from 10 to > 50 ng/m³ for all years. Seven day air mass back trajectory for two days are plotted (Fig. 3) for 18 July 2012 (high BC concentration) and 20 July 2013 (low BC concentration) were There is an indication of long range transport of air mass traveling from Russia, Greenland and sometimes from region near Northern Europe, at an altitude of 0.5 to 1 km emerging at the observational station. Specifically, during high BC values at the station we observe the air mass is coming from higher altitudes than when the BC concentration is low. This will be further supported with more evidences.

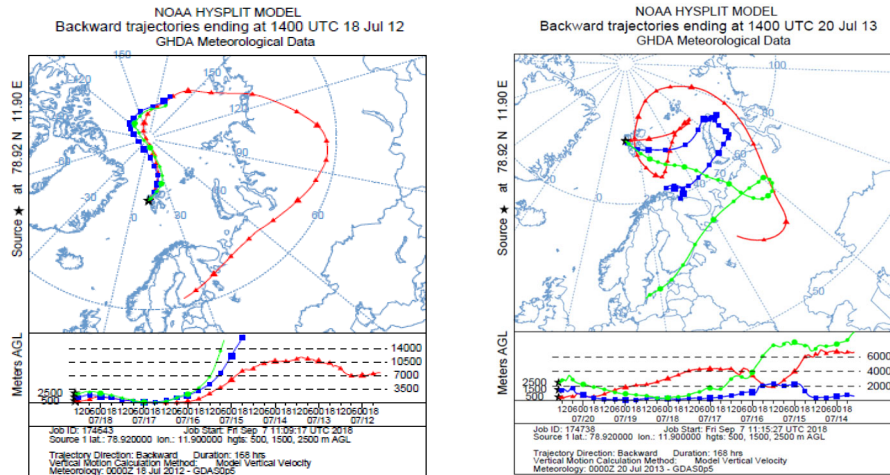


Figure 3: Seven day back trajectory analysis for two days in July month.

CONCLUSION

Observations were undertaken at the Indian Arctic Station, Himadri in the Arctic Summer of 2010-15 to study the temporal variations in mass concentrations of surface black carbon aerosols and their sources. Preliminary results indicate: The mass concentration of BC at Himadri was observed to be second and third week on July 2011 and 2012. Emissions from local human activities as well long range transport from distant source regions are attributed to contribute for the observed BC over Himadri.

The mean diurnal variation of BC showed high variation during 0800 to 1600 hrs local time whereas the rest of the period showed more or less stable BC mass concentration.

However, these results are based on the observations that were confined to a short period of about 30 days of July 2011, 2012 and 2013. Therefore, more observations and analysis for a longer period of time are required for further reaffirmation. We will be analyzing more datasets for different months to find out the seasonal variability and trend of BC concentration over Arctic.

ACKNOWLEDGEMENTS

The authors are thankful to the Director, IITM for encouragement and support. Thanks to National Centre for Antarctic and Ocean Research, Ministry of Earth Sciences for providing financial, logistic support and infrastructure facility during the observational period at Arctic, NY-Alesund.

REFERENCES

QUINN, P.K., A. STOHL, A. ARNETH, T. BERNTSEN, J. F. BURKHART, J. CHRISTENSEN, M. FLANNER, K. KUPIAINEN, H. LIHAVAINEN, M. SHEPHERD, V. SHEVCHENKO, H. SKOV, AND V. VESTRENG (2011), The Impact of Black Carbon on Arctic Climate, *Arctic Monitoring and Assessment Programme (AMAP), Oslo*, 72 pp., ISBN-978-82-7971-069-1.

SHARMA, S., M. ISHIZAWA, D. CHAN, D. LAVOUÉ, E. ANDREWS, K. ELEFThERiADIS, AND S.MAKSYUTOV (2013), 16-year simulation of Arctic black carbon: transport, source contribution, and sensitivity analysis on deposition, *J. Geophys. Res.*, **118**, 1-22.
doi:10.1029/2012JD017774.

A.STOHL, Z. KLIMONT, S. ECKHARDT, K. KUPIAINEN, V. P. SHEVCHENKO, V. M.KOPEIKIN, AND A. N. NOViGATSKY (2013), Black carbon in the Arctic: the underestimated role of gas flaring and residential combustion emissions, *Atmos. Chem. Phys.*, **13**, 8833-8855, 2013, <https://doi.org/10.5194/acp-13-8833-2013>

CHEMICAL CHARACTERIZATION OF FINE PARTICULATE DURING FOG AND NON-FOG PERIOD OF THE WINTER SEASON OF 2017-18 AT DELHI

PRODIP ACHARJA AND KAUSHAR ALI

Indian Institute of Tropical Meteorology Dr. Homi Bhabha Road, Pashan
Pune-411008

KEYWORDS: Fine Particulate, Chemical Composition, Trace Gases, Winter

INTRODUCTION

Indo-Gangetic Plain (IGP) receives episodes of fog, occasionally extending to days, during winter season and thus it is an ideal region to investigate role of chemical nature of the fine particles in the boundary layer in tandem with meteorology in the development and dispersal of fog over the region. During the winter months, temperature reaches to very low level and the frequency of Western Disturbances (WD), the only weather phenomenon causing rainfall over that region during the colder months, is increased (Ali et al., 2004). This weather system supplies moisture over the region which is essential for the fog formation.

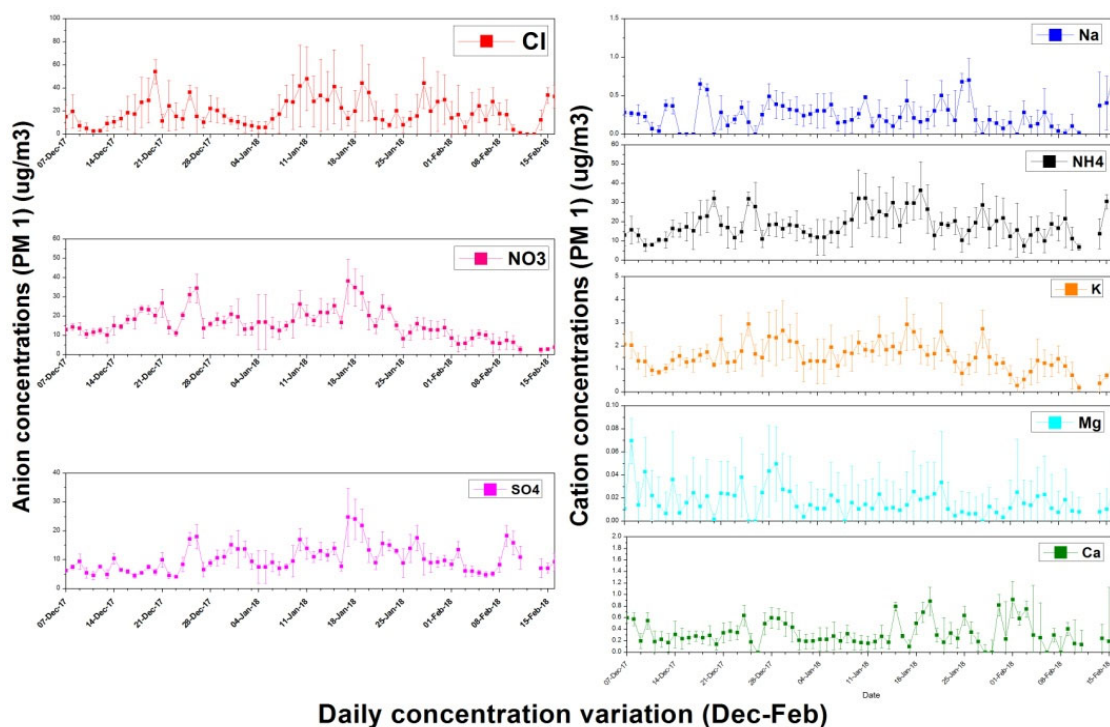
Physical characterization of inorganic water-soluble components of fine particles and precursor trace gases are important to understand the role of chemical species in the development and dispersal of fog over a region. As such, the present work aims at investigating chemical composition of fine particles and their variability on different time scales at Indira Gandhi International Airport, New Delhi.

METHODS

Field campaign under Winter Fog Experiment (WIFEX) program of the Ministry of Earth Sciences (MoES) was conducted by the Indian Institute of Tropical Meteorology (IITM), Pune at Indira Gandhi International Airport (IGIA) Delhi (28.56° N, 77.09° E, 237m asl), during a period from 01 December 2017 to 15 February 2018. Concentration of trace gases and inorganic chemical composition of fine particulates (PM₁ and PM_{2.5}) was monitored simultaneously for the first time in India in hourly resolution using Monitor for AeRosols and Gases in ambient Air (MARGA) (Metrohm Applikon B.V. Schiedam, NL). MARGA provides concentrations of NO₃⁻, Cl⁻, SO₄²⁻, Na⁺, NH₄⁺, K⁺, Mg²⁺ and Ca²⁺ ions in the fine particulate along with NH₃, HNO₃, HNO₂, HCl, SO₂ gases (Rumsey et al., 2014), based on trace gas collection via Wet Rotating Denuders (WRD) and aerosol collection via steam-jet aerosol collector (SJAC; Khlystov et al., 1995).

RESULTS & DISCUSSIONS

Figure 1 shows daily variation of the concentration of water soluble chemical species of PM₁. On an average, the chloride and nitrate dominated the total anion inorganic-PM₁ aerosol with a significant contribution of >75%. The mean mass concentration of chloride, nitrate and sulfate was 19.72 ± 13.26 , 15.95 ± 4.30 and $10.30 \pm 3.31 \mu\text{g m}^{-3}$ respectively. The ammonium dominated the total cation inorganic-PM₁ aerosol with a significant contribution of >80%. The mean mass concentration of ammonium was $18.69 \pm 7.46 \mu\text{g m}^{-3}$.



Daily concentration variation (Dec-Feb)

Figure 1. Daily variation of the concentration of water soluble chemical species of PM₁ in unit of $\mu\text{g}/\text{m}^3$ during Dec 2017 to Feb 2018

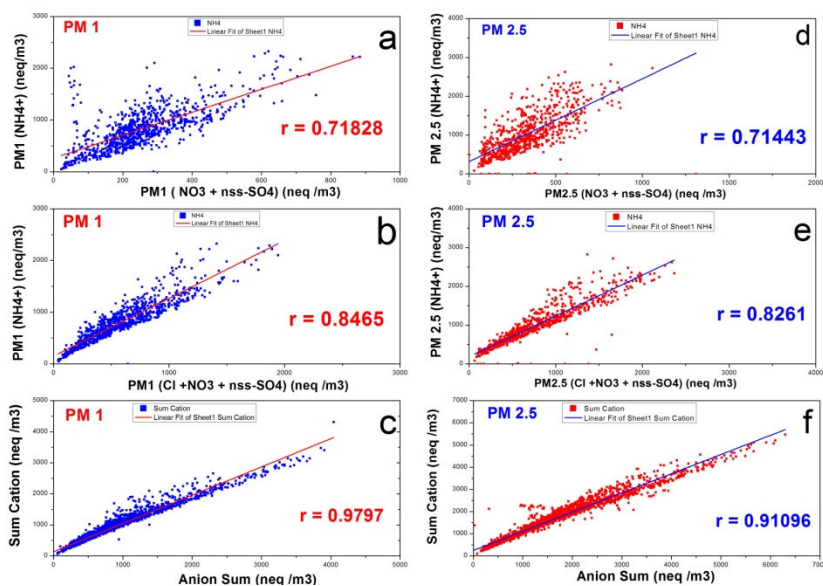


Figure 2. Measured ion balance for the month Dec 2017 to Feb 2018 in nano-equivalents per cubic metre. **(a)** Neutralization of PM₁ NH₄⁺ by PM₁ nss-SO₄²⁻ and PM₁ NO₃⁻, **(b)** Neutralization of PM₁ NH₄⁺ by PM₁ anions (Cl⁻, NO₃⁻ and SO₄²⁻) **(c)** ion balance of measured PM₁ anions (Cl⁻,

NO_3^- and SO_4^{2-}) and measured PM_{10} cations (NH_4^+ , Na^+ , K^+ , Ca^{2+} and Mg^{2+}), (d) neutralization of $\text{PM}_{2.5}$ NH_4^+ by $\text{PM}_{2.5}$ nss-SO_4^{2-} and $\text{PM}_{2.5}$ NO_3^- , (e) Neutralization of $\text{PM}_{2.5}$ NH_4^+ by $\text{PM}_{2.5}$ anions (Cl^- , NO_3^- and SO_4^{2-}) (f) ion balance of measured $\text{PM}_{2.5}$ anions (Cl^- , NO_3^- and SO_4^{2-}) and measured $\text{PM}_{2.5}$ cations (NH_4^+ , Na^+ , K^+ , Ca^{2+} and Mg^{2+})

The extent of neutralization process could be affected by the particle size and the deliquescent and hygroscopic properties of aerosol products. Figure 2a and d shows the neutralization of NH_4^+ presented in ambient air by NO_3^- and nssSO_4^{2-} in PM_{10} and $\text{PM}_{2.5}$ size range respectively. The correlation between these cations and anions is 0.72 and 0.71 (highly significant) respectively. After including Cl^- in the anion sum, the neutralization of NH_4^+ by the anions is improved. After including total measured anion mass and cation mass, the ion balance becomes more perfect. The correlation coefficient between cations and anions of PM_{10} and $\text{PM}_{2.5}$ equal to 0.97 and 0.91 respectively indicating thereby that neutralization is very good.

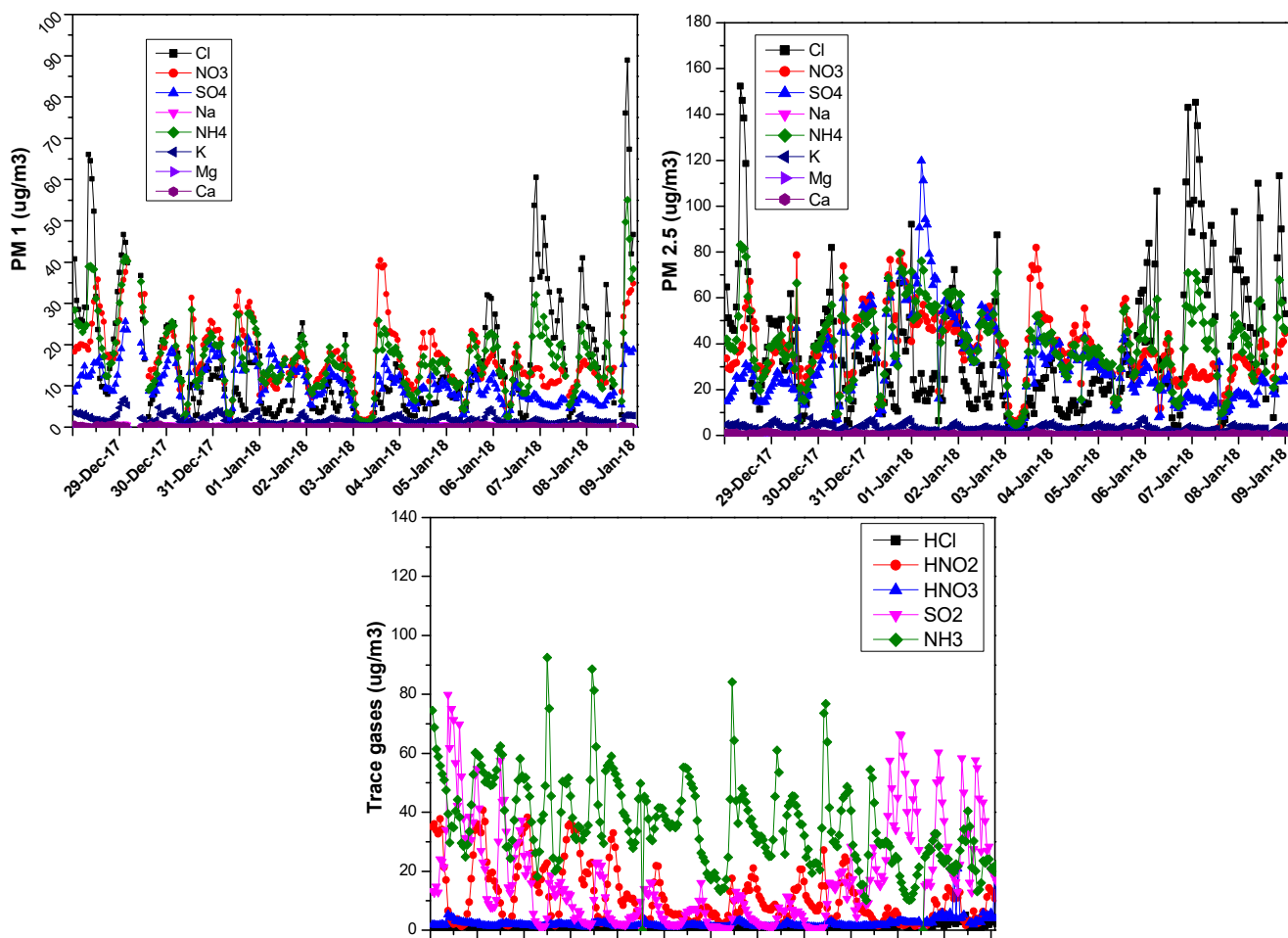


Figure 3: Daily variation of the concentration of water soluble chemical species of PM_{10} and trace gases in unit of $\mu\text{g}/\text{m}^3$ during first fog episode (29 Dec 2017 to 09 Jan 2018)

A specific local event of fog is picked out from the data record which is shown in Figure 3. It shows very high concentrations of chloride and ammonium from first week of Dec 2017 till 29/12/2017. On 30 Dec 2017, there was sudden decrease in chloride concentration and increase in sulfate and nitrate concentration. The concentration of NH_4^+ remained high for the whole period. SO_4^{2-} , NO_3^- and NH_4^+ concentrations were very high for the period (30/12/2017 to 07/01/2018).

Then Cl^- concentration started increasing and dominated sulfate and nitrate concentration from 07/01/2018 onwards. Maximum Cl^- concentration of $69.13 \mu\text{g m}^{-3}$ occurred on 08 January 2018 at the time of dissipation of fog which dominated other anions in balancing the cations. Basically, local sources are important in the development of the fog. When fog episode is over, major chemical species observed in the fine particulate are transported from distant regions to the north west of Delhi; as revealed by the backward trajectory analysis.

CONCLUSIONS

Online real-time simultaneous measurements of precursor trace gases and fine particulate (PM_{10} and $\text{PM}_{2.5}$) compositions provided new insights into the temporal evolution of life span of fog from the pre-fog state, through the whole fog life cycle, to the post-fog period.

Long range transport of fine particles from regions to the north west of Delhi continuously reached at the measurement site. However, dense to very dense fog occurred over the measurement area when calm local winds (south-easterly through south-westerly) brought fine mode hygroscopic particulates [e.g., $(\text{NH}_4)_2\text{SO}_4$ / NH_4HSO_4 and NH_4NO_3] in abundance and modulated the prevailing aerosol composition over the area.

The inorganic aerosol composition showed abundance of ammonium sulfate and ammonium nitrate during the foggy periods and higher ammonium chloride during the non foggy periods. The neutralization state of the inorganic components was biased towards cations, NH_4^+ appeared to be dominant neutralizer of the acidic components PM_{10} and $\text{PM}_{2.5}$ followed by Ca^{2+} , H^+ and Mg^{2+} .

ACKNOWLEDGEMENTS

We thank the Director, Indian Institute of Tropical Meteorology (IITM), Pune for encouragement and support throughout the study period.

REFERENCES

- Ali, K., Momin, G.A., Tiwari, S., Safai, P.D., Chate, D.M. and Rao, P.S.P., 2004. Fog and precipitation chemistry at Delhi, North India. *Atmospheric Environment*, 38(25), pp.4215- 4222.
- Rumsey, I.C., Cowen, K.A., Walker, J.T., Kelly, T.J., Hanft, E.A., Mishoe, K., Rogers, C., Proost, R., Beachley, G.M., Lear, G. and Frelink, T., 2014. An assessment of the performance of the Monitor for AeRosols and GAses in ambient air (MARGA): a semi-continuous method for soluble compounds. *Atmospheric Chemistry and Physics*, 14(11), pp.5639-5658.
- Khlystov, A., Wyers, G.P. and Slanina, J., 1995. The steam-jet aerosol collector. *Atmospheric Environment*.

ROLE OF WINDS ON SINK MECHANISM OF FINE MODE AEROSOLS

L.YANG¹, PANDITHURAI G^{1*}.

¹Indian Institute of Tropical Meteorology, Pune, India.

(Correspondence at: pandit@tropmet.res.in^{1*} / yang.lian@tropmet.res.in¹)

KEYWORDS: Scavenging, Sink Mechanism, Monsoon Winds, Aerosols

ABSTRACT

Over the past century, sources of fine mode aerosols had increased and monsoon rainfall remains as one of the most efficient sink process via wet scavenging. However, monsoon is a coupled phenomenon with strong south westerly winds. Wind actions are projected as predominant mechanism in advection of these fine mode aerosols during rainfall events. In this study, we try to reveal the role of wind action over the sink mechanism of fine mode aerosols at a high altitude observatory, Mahabaleshwar. Our analysis shows that during active phase, rainfall preceding wind action are robust in ventilating in-situ fine mode aerosols. Thus, slower wind velocity rainfall conditions favours better scavenging of fine mode aerosols as relative to faster wind velocity. Moreover, we show that local and long range transport as well impact these removal processes by means of change in regime shift of natural to anthropogenic sources during initial phase to final phase transitions.

INTRODUCTION

Past studies suggest particles of aerodynamic diameter between 50nm to 2 μ m fall under Greenfield gap and are less efficient in removal through wet deposition. But other study had shown that scavenging processes are size dependent, suggesting coarser particles wash-out are faster as relative to fine mode. While, other studies have shown the role of meteorological factors in recharge and discharge of pollutants in below cloud wet scavenging. However such study was limited due to poor temporal resolution datasets. Moreover, satellite in-situ based microphysical sink mechanisms could not be explained such small variations due to poor temporal resolution. Therefore, in-situ observations at very high temporal resolution located at HACPL (High Altitude Cloud Physics Laboratory), Mahabaleshwar (N°17.926402, E°73.660314) at 1,353 amsl on windward side of Western Ghats gives us a new opportunity to understand such microphysical processes. Here, we explore the role of wind actions over sink of fine mode particles using multiple in-situ instruments.

DATA AND METHODOLOGY

Below cloud scavenging are majorly estimated through two approaches. Scavenging efficiency (Chate et al., 2007; Seinfeld & Pandis, 1998),(Ohata et al., 2016) is a measure of estimating washed out concentration empirically taking different microphysical processes into consideration such as Brownian diffusion, directional interception, inertial impaction, thermo-diffusion-phoresis and electro-scavenging. On the other hand, scavenging ratio is a more simplistic approach computed as the ratio of aerosol concentration in rainwater to concentration in the air at same the vicinity of precipitation as first order approximation. But, here we use simple yet robust technique to account scavenging particle by using below mentioned equation to quantify removal of particles based on mass and number concentration from ambient atmosphere during rainfall event.

$$PSC\% = \frac{\sum_{t_1=1}^{t_2=N} Q \cdot (N_{K(n-1)} - N_{K(n+10)})}{\sum_{t_1=1}^{t_2=N} Q} \times \frac{1}{\frac{1}{N} \sum_{t_1=1}^{t_2=N} N_{K(n-1)}} \dots\dots\dots (1)$$

Positive scavenging percentage (PSC%) is the number of aerosol particles denoted by $N_{k(n-1)}$ before and after $N_{k(n+10)}$ rain event in the equation positively scavenging out after a rain event divided by number of particles before being washed out.

RESULTS AND DISCUSSION

The 24hrs collected rainwater concentration showed clear differential source chemical composition during initial and final phases of monsoon rainfall. Backward trajectory during initial (Fig1.a) monsoon rain showed arrival height of air masses at downwind from cross sub Saharan region descending from 2500 to 1500m. With clear Saharan and local crustal signatures with elevated Ca~59%, Mg~18% (Fig2.a) were found to be enhanced in rainwater composition. Nonetheless Mg can also be contributed from sea salt NSS and SS analysis showed major fraction of Mg is seasalt generated to be about 15% of total contribution. On the other hand, during monsoon departure (Fig1.b) phases, anthropogenic source enhancement was observed in rainwater with high amount of continental air mass laden with SO_4 ~63% and Ca~25%, was found in the rainwater. The Ca% in rainwater concentration was found to be lower by a factor of 2 and increase in SO_4 by a factor of 3. The source and conceived air mass for scavenging showed pathway dependence of scavenged aerosol concentration for in-situ. Primarily these transitions from natural to anthropogenic regime shift were well observed in the rainwater composition during monsoon rain.

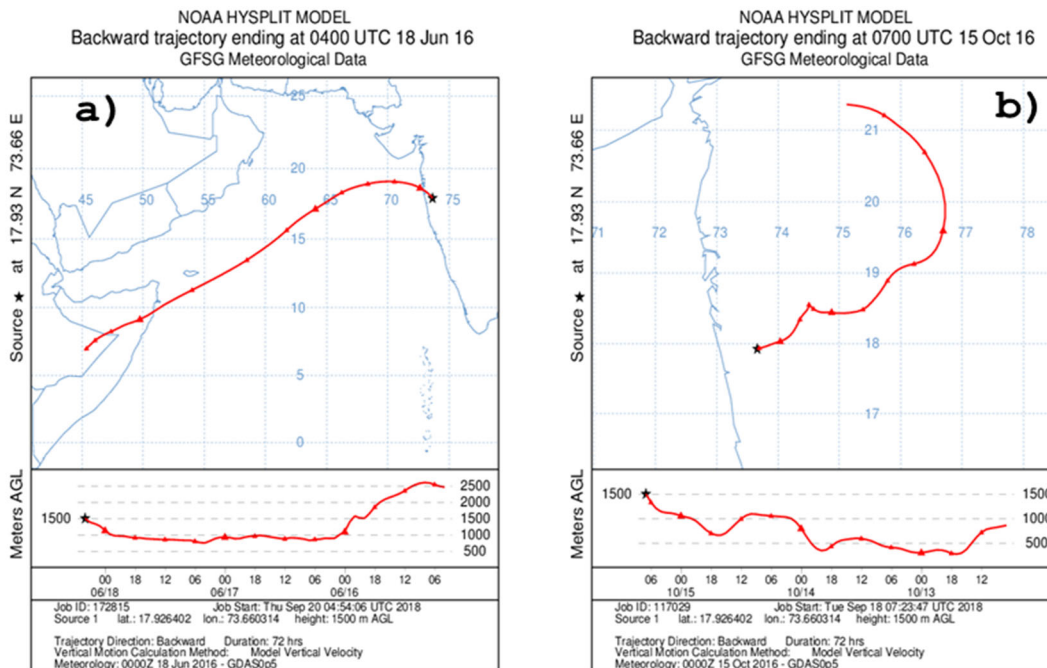


Figure1. Hysplit backward trajectory at 1500AGL for 72hrs for initial (a) and final (b) monsoon phases rainfall event at Mahabaleshwar.

The number concentration distribution during initial and departure phases of rainfall event showed uni and bimodal distribution respectively (Fig2.). Before rain event, stagnation of fine mode aerosols showed clear dominance of PM1 size aerosols and with increased aerosol number concentrations upto $\sim 360 \text{ cm}^{-3}$. However, during initial monsoon phases very low aerosol number concentration $\sim 150 \text{ cm}^{-3}$ were observed. Similar factor of highest modes of number concentration of about 2 was also observed in rainwater concentrations. This suggests that gradual increase in number concentration in final phase of monsoon is correlated well with increased SO_4 in rainwater concentration.

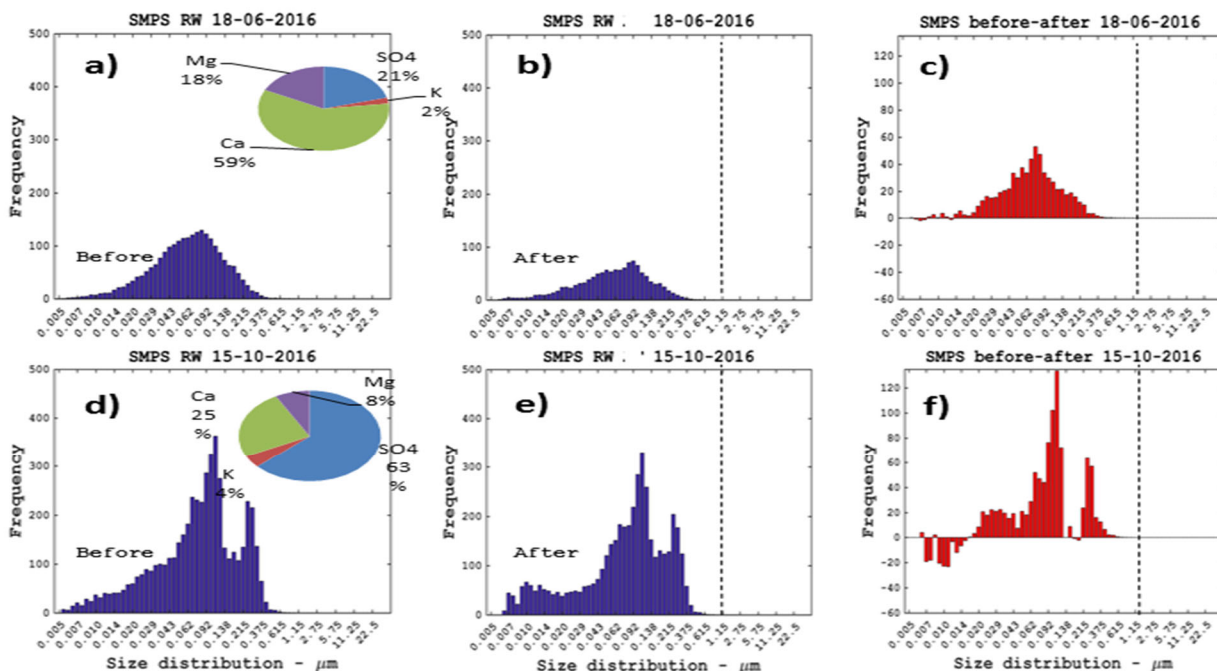


Figure2. Before (a,d) and after (b,e) rainfall number concentration during monsoon rainfall 2016 (HACPL-Mahableshwar). Pie chart depicts rainwater concentration of chemical species collected 24hrs. And before-after (c-f) number concentration after rain. Dotted line is PM1 μm size cut-off bin.

The number size distribution from SMPS (Scanning Mobility Particle Sizer Spectrometer) discrete size bins evaluation also showed fine mode aerosol pre-dominance ($< 1 \mu\text{m}$ aerodynamic diameter). The rain wash out were found to be maximum during final monsoon rain fall upto $\sim 130 \text{ cm}^{-3}$ (Fig2.f) as relative to initial phase $\sim 50 \text{ cm}^{-3}$ (Fig2.e). The slow wind speed conditions were found to be favourable for stagnation of higher aerosols and increased scavenging mechanisms. The wind speed and directions were found to be of very prominence with respect to recharge and discharge of below cloud particles.

CONCLUSION

The results substantiate peculiarity during initial (Fast wind speed regime) and final (slow wind speed regime) phase of monsoon rainfall period during 2016. Before minus after rainfall event reveals final phase of monsoon removal activities were highly efficient with greater source stagnation due to slower wind condition and higher rainwater sulphate concentration.

ACKNOWLEDGEMENT

We would like to acknowledge Director, IITM and NCAP (National Carbonaceous Aerosol Programme) project for providing all support. HACPL (High Altitude Cloud Physics Laboratory) Mahabaleshwar is fully funded by Ministry of Earth Sciences. We also thank HACPL and HYSPLIT NOAA team for all the datasets of in-situ instruments, and lightning network datasets.

REFERENCES

- Barrie, L. a. (1985). Scavenging ratios, wet deposition, and in-cloud oxidation: An application to the oxides of sulphur and nitrogen. *Journal of Geophysical Research*, *90*, 5789–5799. <https://doi.org/10.1029/JD090iD03p05789>
- Chate, D. M., Ali, K., Momin, G. A., Rao, P. S. P., Praveen, P. S., Safai, P. D., & Devara, P. C. S. (2007). Scavenging of sea-salt aerosols by rain events over Arabian Sea during ARMEX. *Atmospheric Environment*, *41*(32), 6739–6744. <https://doi.org/10.1016/j.atmosenv.2007.04.051>
- Ohata, S., Moteki, N., Mori, T., Koike, M., & Kondo, Y. (2016). A key process controlling the wet removal of aerosols: New observational evidence. *Scientific Reports*, *6*, 1–9. <https://doi.org/10.1038/srep34113>
- Seinfeld, J. H., & Pandis, S. N. (1998). Chemistry of the atmospheric aqueous phase. *Atmospheric Chemistry and Physics: From Air Pollution to Climate Change*, 337407.

NEW PARTICLE FORMATION: INFLUENCE OF PLANETARY BOUNDARY LAYER AND AIR MASS

VYOMA. SINGLA, SUBRATA MUKHERJEE AND G. PANDITHURAI

Indian Institute of Tropical Meteorology, Pune - 411 008, India.

KEYWORDS: NPF, Cluster analysis, NR-PM₁, PBL.

INTRODUCTION

New particle formation (NPF) has become a topic of great interest in atmospheric and environmental sciences. Although the nucleation phenomenon has been intensively studied in the past, there still exist large uncertainties related to dominant mechanisms of NPF and the controlling parameters. The formation of new particles significantly impacts atmospheric aerosol population. The newly formed particles are the source of approximately half of the atmosphere's cloud condensation nuclei (CCN), thus modifying cloud properties and affecting climate indirectly (Kerminen et al., 2012). However, what fraction of CCN is attributable to NPF is still highly uncertain (Merikanto et al., 2009).

The formation of new particles in free troposphere is believed to contribute to a large amount of the aerosol population of the whole atmospheric column (Merikanto et al., 2009). Few studies of NPF events in the free troposphere have been made by using ground-based measurements at high altitude stations of Izana (3,200 m above sea level (asl), Canary Islands; Rodriguez et al., 2009), Jungfraujoch (3,580 m asl, Switzerland; Tröstl et al., 2016), Storm Peak Laboratory (3,210 m asl, northwestern Colorado; Yu and Hallar, 2014), Nepal Climate Observatory at Pyramid (NCO-P) site (5,079 m asl, Nepal; Venzac et al., 2008) and Chacaltaya (5,240 m asl, Bolivia; Rose et al., 2017). Although rare, these studies provided an indication that new particle formation is not limited to surface layer but extends through entire atmospheric column. Recently, measurements have shown indications that NPF can take place with a high frequency at high altitudes (Venzac et al., 2008). In the present study we have tried to address the effect of boundary layer and air mass origin on the new particle formation recorded at High Altitude Cloud Physics Laboratory (HACPL) (1,378 m asl, Mahabaleshwar). To address this, the particle number size distribution (PNSD) data during 4-months time period (November 2016 to February 2017) was utilized.

Although nucleation phenomena have been intensively studied in the past, there still exist large uncertainties concerning the dominant mechanisms of new particle formation (NPF) in the atmosphere and the controlling parameters.

METHODS

The measurements were made at HACPL (17.92° N, 73.65° E) located in the Western Ghats mountain range in south-west India. The measurement site is situated in a rural town, Mahabaleshwar and surrounded by the dense forest all around. During the study period, HACPL is strongly influenced by anthropogenic pollution, both local and long range transport (Mukherjee et al., 2018). The aerosol chemical composition, particle number concentration (PNC) and cloud condensation nuclei (CCN) number concentration were measured by using Time of Flight - Aerosol Chemical Speciation Monitor (ToF-ACSM, Aerodyne), Wide Range Aerosol Spectrometer (WRAS, GRIMM) and CCN counter (DMT CCNC-100) respectively. The meteorological

conditions (Solar radiation (SR), surface temperature (T), relative humidity (RH), wind speed (WS) and wind direction (WD)) were also recorded using an Automatic Weather Station (AWS).

The characteristic parameters of NPF events - growth rate (GR), formation rate (FR), condensation sink (CS) and coagulation loss (Coag) were calculated following the methodology of Dal Maso et al., 2005. The FR of 5nm particles was calculated at the beginning of each event. The GR was obtained by fitting a first-order polynomial to the geometric mean diameters (GMD) of the nucleation mode particles. The condensation sink was calculated based on the assumption that the properties of condensable vapors were similar to sulfuric acid, an important condensable gas for the condensational growth of nucleated particles. Coag represents the scavenging of particles due to coagulation of freshly nucleated particles. The number concentration of aerosol particles in the size range of 5-25 nm was used to estimate the FR and GR. The CS and Coag were calculated using the entire PSND (~5-900 nm). The units of FR, GR, CS and Coag are $\text{cm}^{-3}\text{s}^{-1}$, nm h^{-1} , s^{-1} and $\text{cm}^{-3}\text{s}^{-1}$ respectively.

RESULTS & DISCUSSIONS

NPF events were observed on ~40% of the measurement days (47 days out of 115 days). These NPF events comprised of 13 strong events (nucleation mode (N_{nuc}) particle number concentration $> 6.0 \times 10^3 \text{ cm}^{-3}$) and 34 weak events. In this study, one strong NPF event - 17th February 2017 and one non NPF event - 10th February 2017 was selected for assessing the role of planetary boundary layer, meteorology and air mass on the nucleation phenomenon. Figure 1 gives the colorplot of size distribution of aerosol particles on 17th and 10th February 2017. On 17th February, sudden enhancement in nucleation mode number concentration was observed at 13:00h (N_{nuc} concentration $\sim 1.4 \times 10^4 \text{ cm}^{-3}$). At this hour, a considerable decrease in WS and RH was observed, whereas SR, T and WD reflected a stable pattern. The FR of particles (J_5) was calculated as $2.4 \text{ cm}^{-3}\text{s}^{-1}$. The CS and Coag were calculated as 2.1 s^{-1} and $1.8 \text{ cm}^{-3}\text{s}^{-1}$ respectively. These newly formed particles later grew at a rate of 3.0 nm h^{-1} till the early morning of 18th February and shifted the particle size distribution from nucleation to an Aitken (N_{ait}) and/or accumulation (N_{acc}) regime. On the other hand, the non-NPF day (10th February) did not reflect any increase in N_{nuc} concentration during the daytime. The meteorology and calculated CS on this day was similar to that observed on NPF day.

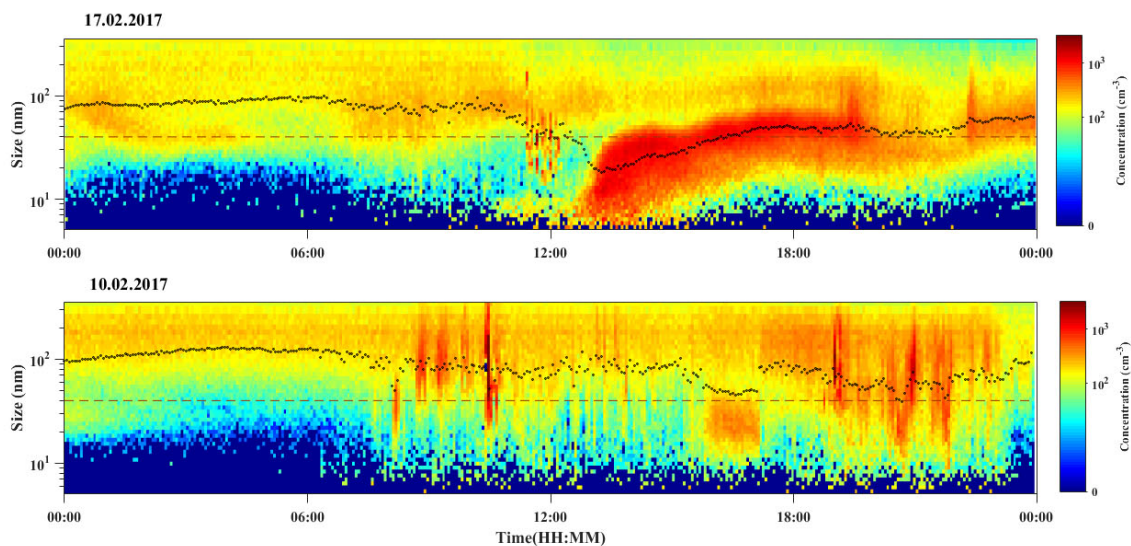


Figure 1: The spectrum of the particle number size distribution on a strong NPF day - 17th February 2017 (upper panel) and a non-NPF day - 10th February 2017 (lower panel). The horizontal dashed

line in both the panels represents the diameter of particles at 40 nm and black dotted line represents the Geometric Mean Diameter of particles.

Effect of planetary boundary layer: Following the methodology of Rose et al., 2017, the hourly averaged value of the standard deviation of the horizontal wind direction (σ_θ) was calculated to evaluate whether the site was under the influence of free troposphere (FT) or the planetary boundary layer (PBL). The magnitude of $\sigma_\theta \geq 12.5$ indicates the unstable atmospheric conditions and hence under the influence of PBL. While $\sigma_\theta < 12.5$ reflects the stable atmospheric conditions and is equivalent of being in FT. The parameter - σ_θ was calculated for both NPF and non-NPF day (Figure 2). It was observed that the sampling site was influenced by FT all through the day whereas on non-NPF day, the sampling site experienced transition from FT to PBL around 10:00h and vice-versa at 18:00h. The sampling site is thus believed to get influence local emissions. This phenomenon has possibly led to the inhibition of NPF event on that day.

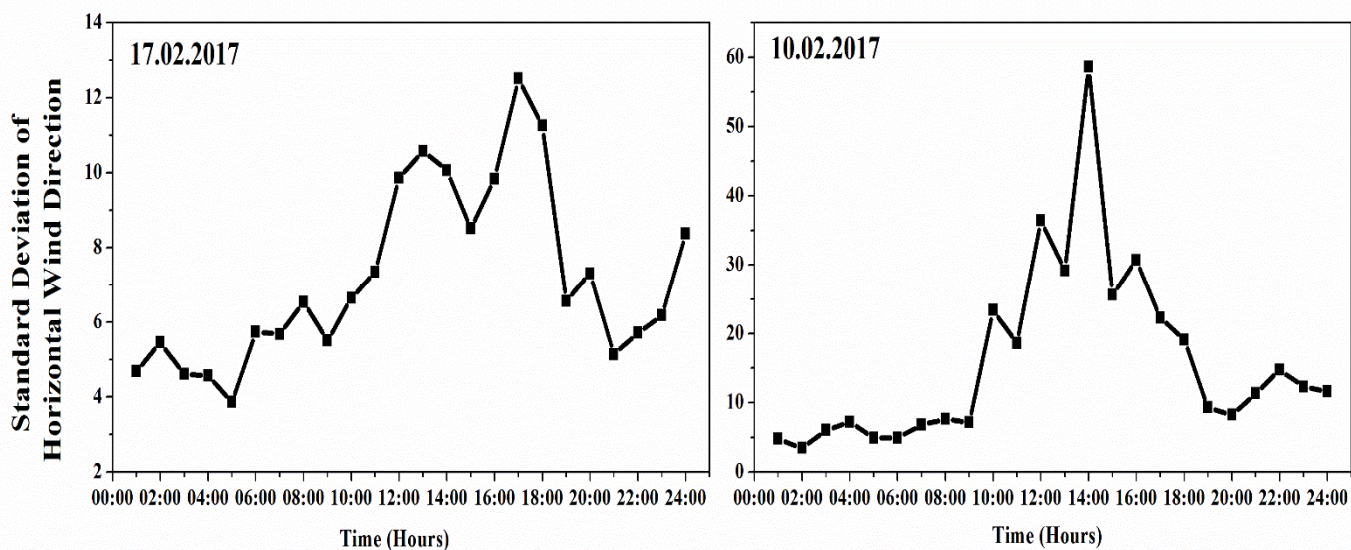


Figure 2: Diurnal variation of hourly averaged value of the standard deviation of the horizontal wind direction on NPF day (17.02.17) and non-NPF day (10.02.17).

EFFECT OF AIR MASS: Since the site is impacted by different sources, the cluster analysis was performed by using Zefir (Petit *et al.*, 2017) to investigate if NPF events are influenced by specific air mass type. Air mass back trajectories were simulated by using the Hybrid Single-Particle Lagrangian Integrated Trajectory (HYSPLIT) transport and dispersion model (Draxler and Rolph, 2003). The 120 hour backward trajectories were calculated for every hour terminating at a height of 100 m above the ground level with a total of 2760 trajectories. The transport pathways of the observed air masses were grouped into five clusters on the basis of total spatial variance (TSV). Each cluster congregated into different geographical origin (s). The PNSD of each cluster was constructed by averaging the particle number size distribution for each time step belonging to that particular cluster. It was observed that the clusters associated with continental air mass favoured NPF events at the sampling site. The fire hotspots derived from MODIS (Moderate Resolution Imaging Spectro-radiometer) indicated that the continental clusters were influenced by biomass burning affected areas. The chemical composition of each cluster evaluated and presented in Table 1. The mass concentration of sulfate, ammonium, biomass burning organic aerosol (BBOA) and oxygenated OA (OOA) was higher for the

continental clusters 1-3 as compared to the foreign clusters 4-5. The chemical information on BBOA and OOA was extracted through Positive Matrix Factorization. With a reported lifetime of 3.8 ± 0.8 days (Edwards *et al.*, 2006), biomass burning plumes are often transported for thousands of kilometers (Andreae *et al.*, 1988). Therefore, it was assumed that the formation of new particles took place under the influence of biomass burning affected anthropogenic pollution. The chamber study by Henningan *et al.*, 2012 has shown that exposing the biomass burning plume to UV light initiates photo-oxidation thereby creating a strong nucleation burst. The field studies have also reported the nucleation activity in fresh (Hobbs *et al.*, 2003) and aged fire plumes (Andreae *et al.*, 2001).

Cluster	Sulfate	Ammonium	BBOA	OOA
C1	3.5 ± 3.1	1.5 ± 1.2	2.1 ± 2.4	4.0 ± 2.7
C2	2.9 ± 1.7	1.0 ± 0.8	1.6 ± 2.2	3.1 ± 2.1
C3	3.4 ± 3.0	1.5 ± 1.2	1.5 ± 2.2	3.5 ± 2.6
C4	1.2 ± 0.9	0.6 ± 0.4	1.3 ± 1.8	1.7 ± 1.1
C5	1.4 ± 1.7	1.1 ± 0.8	1.3 ± 1.3	2.0 ± 1.4

Table 1: Summary of secondary aerosol components, both organics and inorganics. The mass concentration is represented as mean \pm standard deviation ($\mu\text{g m}^{-3}$) for the five clusters.

CONCLUSIONS

The simultaneous measurements of particle number size distribution, aerosol chemical composition and meteorology were performed at Mahabaleshwar from November 2016 to February 2017 for identifying the nucleation events. Ample NPF events were observed with a frequency of $\sim 40\%$. All the NPF events began around 10:00-11:00 hours. Ten of the strongest NPF events observed had an average growth rate, formation rate, condensation sink and coagulation of $2.6 \pm 0.4 \text{ nm h}^{-1}$, $2.8 \pm 1.4 \text{ cm}^{-3} \text{ s}^{-1}$, $2.2 \pm 2.9 \times 10^{-2} \text{ s}^{-1}$ and $1.6 \pm 1.0 \text{ cm}^{-3} \text{ s}^{-1}$ respectively. The calculated standard deviation of horizontal wind direction revealed that the stable atmospheric conditions in the FT favoured NPF events. The cluster analysis of backward trajectories further suggested that the continental air masses influenced by biomass burning favoured the nucleation events at HACPL.

ACKNOWLEDGEMENTS

The data used in this study are from the data repository of HACPL, part of IITM, Pune. HACPL is fully funded by Ministry of Earth Sciences (MoES), Government of India, New Delhi. Vyoma Singla extends special thanks to DST, SERB for NPDF fellowship (Fellowship number: PDF/2017/002428) and Director, IITM for providing all the facilities.

REFERENCES

Andreae, M. O., Artaxo, P., Fischer, H., Freitas, S. R., Grégoire, J. M., Hansel, A., Hoor, P., Kormann, R., Krejci, R., Lange, L., Lelieveld, J., Lindinger, W., Longo, K., Peters, W., De Reus, M., Scheeren, B., Silva Dias, M. A. F., Ström, J., Van Velthoven, P. F. J. and Williams, J (2001). Transport of biomass burning smoke to the upper troposphere by deep convection in the equatorial region, *Geophys. Res. Lett.* **28(6)**, 951–954.

- Andreae, M.O., Browell, E.V., Garstang, M., Gregory, G.L., Harriss, R.C., Hill, G.F., Jacob, D.J., Pereira, M.C., Sachse, G.W., Setzer, A.W. and Dias, P.L (1988). Biomass burning emissions and associated haze layers over Amazonia, *J. Geophys. Res. Atmos.* **93(D2)**, 1509-1527.
- Dal Maso, M (2005). Formation and Growth of Fresh Atmospheric Aerosols Eight Years of Aerosol Size Distribution Data From SMEAR, *Boreal Environ. Res.* **10**, 323–336.
- Draxler, R.R. and Rolph, G.D (2003). HYSPLIT (HYbrid single-particle Lagrangian integrated trajectory) model access via NOAA ARL READY. NOAA Air Resources Laboratory, Silver Spring, MD. Dostupnna: <http://ready.arl.noaa.gov/HYSPLIT.php> (06. 06. 2010.).
- Edwards, D. P., Emmons, L. K., Gille, J. C., Chu, A., Attié, J. L., Giglio, L., Wood, S. W., Haywood, J., Deeter, M. N., Massie, S. T., Ziskin, D. C. and Drummond, J. R (2006). Satellite-observed pollution from Southern Hemisphere biomass burning, *J. Geophys. Res. Atmos.* **111(14)**, 1–17.
- Hobbs, P. V., Sinha, P., Yokelson, R. J., Christian, T. J., Blake, D. R., Gao, S., Kirchstetter, T. W., Novakov, T. and Pilewskie, P (2003). Evolution of gases and particles from a savanna fire in South Africa, *J. Geophys. Res. Atmos.* **108(D13)**, 8485.
- Kerminen, V. M., Paramonov, M., Anttila, T., Riipinen, I., Fountoukis, C., Korhonen, H., Asmi, E., Laakso, L., Lihavainen, H., Swietlicki, E., Svenningsson, B., Asmi, A., Pandis, S. N., Kulmala, M. and Petäjä, T (2012). Cloud condensation nuclei production associated with atmospheric nucleation: A synthesis based on existing literature and new results, *Atmos. Chem. Phys.* **12(24)**, 12037–12059.
- Merikanto, J., Spracklen, D. V., Mann, G. W., Pickering, S. J. and Carslaw, K. S (2009). Impact of nucleation on global CCN, *Atmos. Chem. Phys.* **9**, 8601–8616.
- Mukherjee, S., Singla, V., Pandithurai, G., Safai, P. D., Meena, G. S., Dani, K. K. and Anil Kumar, V. (2018). Seasonal variability in chemical composition and source apportionment of submicron aerosol over a high altitude site in Western Ghats, India, *Atmos. Environ.* **180**, 79–92.
- Petit, J. E., Favez, O., Albinet, A. and Canonaco, F (2017). A user-friendly tool for comprehensive evaluation of the geographical origins of atmospheric pollution: Wind and trajectory analyses, *Environ. Model. Softw.*, **88**, 183–187.
- Rose, C., Sellegri, K., Moreno, I., Velarde, F., Ramonet, M., Weinhold, K., ... & Laj, P (2017). CCN production by new particle formation in the free troposphere. *Atmos. Chem. Phys.* **17(2)**, 1529-1541.
- Tröstl, J., Herrmann, E., Frege, C., Bianchi, F., Molteni, U., Bukowiecki, N., ... & Gysel, M. (2016). Contribution of new particle formation to the total aerosol concentration at the high-altitude site Jungfraujoch (3580 m asl, Switzerland), *J. Geophys. Res. Atmos.* **121(19)**, 11692-11711.
- Venzac, H., Sellegri, K., Laj, P., Villani, P., Bonasoni, P., Marinoni, A., ... & Facchini, M. C (2008). High frequency new particle formation in the Himalayas. *Proceedings of the National Academy of Sciences*, **105(41)**, 15666-15671.

Yu, F., & Hallar, A. G (2014). Difference in particle formation at a mountaintop location during spring and summer: Implications for the role of sulfuric acid and organics in nucleation, *J. Geophys. Res. Atmos.* **119(21)**, 12246-12255.

THE BLACK CARBON OSCILLATION (BCO) MODE DETECTED IN THE CAIPEEX MEASUREMENTS

RAHUL P R C¹, ROHINI L BHAWAR², P.D.SAFAI¹, THARA PRABHAKARAN¹ and AVINASH PARDE²

¹ Indian Institute of Tropical Meteorology, Pashan Road, Pune-411008, INDIA

² Department of Atmospheric and Space Sciences, Savitribai Phule Pune University, Pune

(*Correspondence at: rcreddy@tropmet.res.in)

KEYWORDS: Black Carbon, CAIPEEX, Tropical Station

INTRODUCTION

Black carbon (BC) aerosols strongly absorb solar radiation, which warms climate. However, accurate estimation of BC's climate effect is limited by the uncertainties of its spatiotemporal distribution, especially along the vertical stratifications in the atmosphere. Similar studies [Rahul et al, 2014] from The Cloud Aerosol Interaction and precipitation Enhancement Experiment (CAIPEEX) black carbon aircraft measurements over the Indo-Gangetic plains revealed for the first time the presence of two layers of black carbon, which resulted in the escalating/doubling the heating rates over the glaciers. In the present study, the CAIPEEX measurements of black carbon during 2010 and 2011 reveal an intriguing pattern of variability of the black carbon loading over Hyderabad, a global tropical station. For the first time it is observed that there exists an inter-annual oscillatory (sinusoidal) pattern, of the black carbon loading. This pattern is not *only* identified at the ground level but is *also* observed in the BC loading along the latitudes, up-until 5-6KM into the atmosphere.

METHODS

CAIPEEX was undertaken by the Indian Institute of Tropical Meteorology, Pune and was aimed to study and understand the interactions between aerosols and clouds that influence the precipitation mechanism.

A twin engine Piper Cheyenne N361 JC pressurized aircraft from Southern Ogallala Aquifer Rainfall (SOAR) Program, TX, USA was employed for observations. The aircraft speed while sampling varied between 90 and 100 m/s. Each flight lasted for about 2 to 3 h duration during the period 12.00 to 16.00 LT when the boundary layer is generally fully evolved leading to the establishment of strong convective motions prior to the initiation of sampling. The aircraft made several ascents and descents to penetrate the clouds during the course of each flight, as the chief objective of the mission was to study the cloud microphysics and aerosol–cloud interactions.

Vertical variability of black carbon concentrations derived from these CAIPEEX experiments used for the analysis in this study, the aircraft measurements were collected in-situ during the CAIPEEX campaign over Hyderabad (17.47° N, 78.43° E) during Oct 2010, Oct 2011 and Nov 2011.

RESULTS AND DISCUSSION

Figure 1, represents the vertical mean profiles obtained during October 2010, October 2011 and during November 2011.

From the plots it can be observed that at the ground level 0 – 500 meters the BC value is 3500 ng/m^3 during Oct 2010, while during Oct 2011 the BC value is 2500 ng/m^3 (and nearly 1000 ng/m^3 during November 2011); likewise, if carefully analyze the BC values along the altitudes we tend to see an oscillatory mode between 2 consecutive years. What is often expected is that the preceding year's BC measurements will be lesser than following years; but here this is not the case, is vice a versa. Such pattern of variability was never caught especially along the vertical profiles and this was possible only due to the CAPEEX measurements. Such oscillations are more distinctly seen between 4 – 7km. A detailed examination of day-to-day variability will be presented in the complete paper. The plots presented here are only the mean plots so to as give an idea into the observed results. We found a concrete proof (figure 2) of our proposed result in a previous paper published in 2014, though this paper had other objective results we use the results to consolidate our findings with the CAPEEX data.

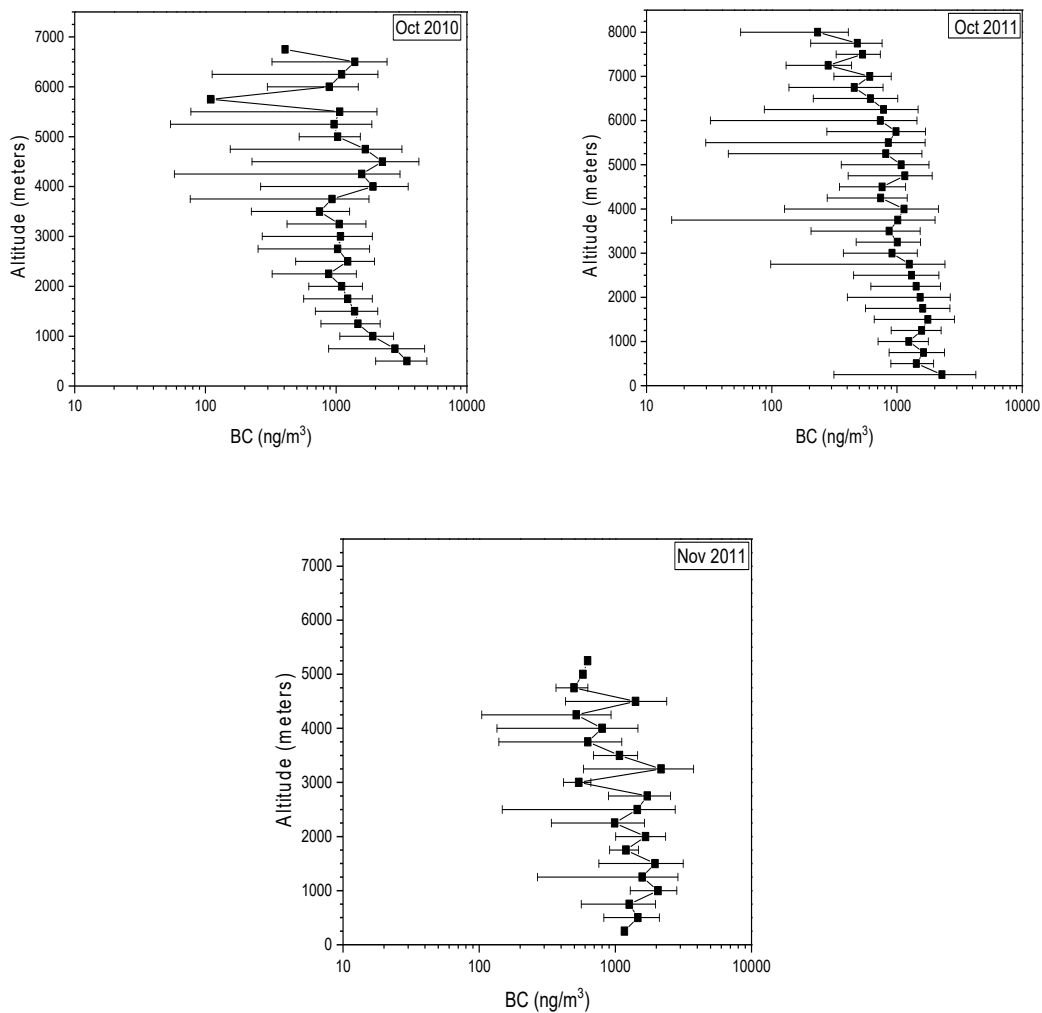


Figure 1: Mean black carbon profiles over Hyderabad obtained during CAIPEEX

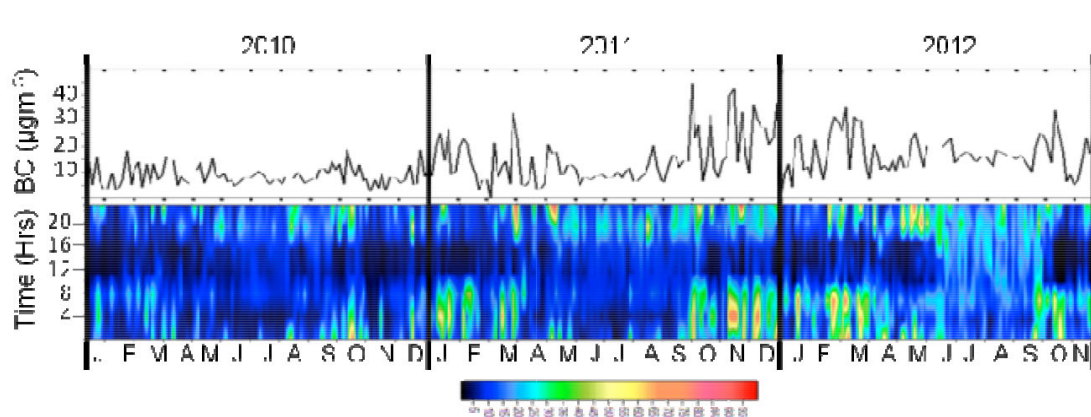


Figure 2 : Daily (top panel) and hourly (bottom panel) Aethalometer AE31 (Magee scientific) derived BC variations during 2010-2012 [Subin and Biswadip, 2014]

The above figure 2 can be considered as a concrete proof of our proposed result presented in Figure 1, the aethalometer measurements concurrently show the inter-annual mode of oscillation in the BC loading at the surface. Clearly seen are the variability's of BC loadings in an inversion mode compared with the previous years, for example in 2010, the months in which the BC loading show a peak are followed by the next immediate year (2011) with the same months showing dips in BC loadings for the same months and what's more interesting is that during the 3rd year (2012) the peaks again go up in unison to the peaks observed during 2010. This pattern of variability is noticed during almost in all the months on the year.

CONCLUSION

Inter-annual variability's of meteorological parameters turn out to be crucial/critical when they exhibit in specific modularity of pattern like El Nino or QBO. It is interesting to identify such pattern in the loadings of black carbon. Though this study is brief, the objective is to highlight the persistence of such a pattern of variability in the BC loading over the global tropical station of Hyderabad. CAIPPEX results reveal a sinusoidal inter-annual variability of the BC values, from surface level to 5-6Kms into the atmosphere. Detailed work incorporating as to why these oscillations are caused is being investigated. Further the implications of such variability on the radiative forcing will also be investigated.

ACKNOWLEDGEMENTS:

The authors are thankful to the Director, IITM for encouragement and support.

REFERENCES

Rahul, P.R.C, R. L. Bhawar, D. C. Ayantika, A. S. Panicker, P. D. Safai, V. Tharaprabhakaran, B. Padmakumari & M. P. Raju, Double blanket effect caused by two layers of black carbon aerosols escalates warming in the Brahmaputra River, Nature Scientific Reports 4 : 3670 | DOI: 10.1038/srep03670

Subin Jose and Biswadip Gharai, Study on black carbon and its characterization at an urban location, Hyderabad during 2010 to 2012, International Journal of Environmental Monitoring and Analysis 2014; 2(2): 100-105

ESTIMATION OF NITRATE IN ORGANIC AND INORGANIC FORM AT A HIGH ALTITUDE SITE IN WESTERN GHATS

SUBRATA MUKHERJEE, VYOMA SINGLA, G. PANDITHURAI AND P. D. SAFAI

Indian Institute of Tropical Meteorology, Pune – 411 008, India.

KEYWORDS: Nr- PM_{10} , Acsm, Pmf, Organo-Nitrate.

INTRODUCTION

Recent studies have shown that organic aerosols (OA) contribute a substantial fraction (~30-70%) of the total aerosol mass. These organic aerosols are believed to originate from both natural (wildfires) and anthropogenic sources (fossil fuel combustion and biomass burning). Further, a large fraction of OA is contributed by secondary organic aerosol (SOA). These SOA's are formed either by the gas-phase oxidation of volatile organic compounds or aqueous-phase oxidation (Hallquist et al., 2009). Of the known SOA precursors, isoprene and monoterpenes contribute significantly to the global SOA budget, owing to their large global emission rates (Guenther et al., 1995) and high reactivity with atmospheric oxidants - hydroxyl radical (OH), ozone (O_3), and nitrate radical (NO_3).

Organonitrates (ON) have been recently identified as one of the important SOA species (Lim et al., 2016, Ng et al., 2007). ON are formed in the atmosphere either by photochemical (OH-initiated) or nocturnal (NO_3 -initiated) oxidation of biogenic and anthropogenic VOCs in the presence of NO_x (Hallquist et al., 1999). ON is an important component of NO_y in the gas phase and influences the nitrogen cycle and ozone production (Rosen et al., 2004). Ng et al., 2007 has identified the oxidation of isoprene and monoterpene with NO_3 as a significant source for ON. In the present study, an attempt has been made to identify the presence of organo nitrate and its quantification by using Positive matrix factorization (PMF). The NR- PM_{10} data was acquired by Time of Flight - Aerosol Chemical Speciation Monitor (ToF-ACSM) at High Altitude Cloud Physics Laboratory (HACPL), Mahabaleshwar during winter season was used in this study. Mahabaleshwar is a rural town in the Western Ghats of India, where ~80% of the land is covered with forest. Therefore HACPL is influenced by both fresh anthropogenic emissions (vehicular, fossil fuel combustion, etc.) and biogenic emissions. This study intends to strengthen our knowledge about the sources, processes and associated chemical characteristics of ON in the ambient air.

METHODS

The study was carried out at High Altitude Cloud Physics Laboratory (HACPL), Mahabaleshwar (17.92° N, 73.65° E), situated at a height of 1378 m AMSL during winter (December, January and February) season of 2016-2017. The Non-refractory (NR) PM_{10} aerosol chemical composition was acquired with Time of Flight - Aerosol Chemical Speciation Monitor (Fröhlich et al., 2013). PMF method was used in this study to apportion the measured total nitrates. PMF technique was applied to organic spectrum at first and then it was applied to Organic+ NO_x mass spectrum. This method could unequivocally determine the relative contributions of organic and inorganic nitrates (Xu et al., 2015). The PMF analysis of merged (NO_3^{+org}) mass spectra deconvolved a nitrate inorganic aerosol (NIA) factor along with other organic aerosol factors. The optimal solution for PMF analysis on the organic mass spectra and the merged mass spectra were selected on the basis of minimum change in Q/Q_{exp} and covariability with the external tracer (EC data). The selected factors were further validated by comparing the mass spectrum reported in literature. The total nitrate functionality was apportioned into organic and inorganic signals with the following set of equations (Xu et al., 2015),

$$[\text{NO}_{\text{org}}^+] = \sum ([\text{OA factor}]_i \times f_{\text{NO}_i}) \quad \dots \text{i)}$$

$$[\text{NO}_2^+_{\text{org}}] = \sum ([\text{OA factor}]_i \times f_{\text{NO}_2_i}) \quad \dots \text{ii)}$$

$$\text{NO}_3_{\text{org}} = \frac{([\text{NO}_{\text{org}}^+] + [\text{NO}_2^+_{\text{org}}])}{0.95} \quad \dots \text{iii)}$$

where $[\text{OA factor}]_i$ is the mass concentration of i th OA factor and f_{NO_i} and $f_{\text{NO}_2_i}$ are the mass fraction of NO^+ and NO_2^+ respectively in the i th OA factor. Since the mass spectrum of nitrate (measured by ACSM) was dominated with signals of NO_x ions and the sum of which accounts for 95% to total nitrate mass, a factor of 0.95 was applied in equation iii). Finally the nitrate functionality from inorganic nitrate was calculated by subtracting NO_3_{org} from the total nitrate, measured by ACSM.

RESULTS AND DISCUSSION

PMF analysis on OA mass spectra has deconvoluted into 4 factors –hydrocarbon like organic aerosol (HOA), biomass burning organic aerosol (BBOA), semi volatile oxygenated organic aerosol (SVOOA) and low volatile oxygenated organic aerosol (LVOOA). Both the OOA showed afternoon build up and evening high indicating importance of photochemical oxidation and its subsequent partitioning under low planetary boundary layer (PBL) conditions. Diurnal variation of LVOOA showed high background throughout the day which is an indicative of contribution from long range transport. The f_{44} of LVOOA was found to be ~ 0.4 (high degree of oxygenation) which in turn supports its nonlocal origin. Whereas, SVOOA was freshly formed in the atmosphere. On the other hand both the HOA and BBOA showed higher concentration during morning and evening hours depicting the influence of local emissions around the observation sites.

The PMF analysis on $\text{OA}+\text{NO}_x$ resulted an additional factor - nitrate inorganic aerosol (NIA) in addition to the 4 PMF factors - HOA, BBOA, SVOOA and LVOOA (figure 1a). The mass spectra and diurnal variation of PMF factors through OA and $\text{OA}+\text{NO}_x$ were compared and presented in Table 1. A good correlation ($r = 0.89$ to 0.98) among different factors validated the individual PMF methodology. In terms of percentage contribution, BBOA (25%) contributed maximum to the total aerosol mass followed by LVOOA (24%), SVOOA (23%), HOA (19%) and NIA (9%). The NIA factor was characterized by the signals of NO^+ and NO_2^+ at m/z 30 and 46 respectively. In terms of mass, these two ions contributed $\sim 78\%$ of this factor, with remaining species from organic fragments. The ratio of $\text{NO}^+/\text{NO}_2^+$ for NIA factor was observed as 1.7, which is close to 1.11 - a value for NH_4NO_3 determined while calibration of ACSM. Moreover, the mass concentration of NIA factor correlated strongly ($r = 0.95$; p -value = 0.005) with the mass concentration of nitrate (as measured with ACSM), thus referring this factor as NH_4NO_3 factor. Based on different physicochemical properties of organic and inorganic components of nitrate, NO_x ions tend to form association with other organic factors as well. Consequently, 70% of NO_x -ions were apportioned to NIA factor, 21% to LVOOA, 6% to SVOOA, with minor contributions to BBOA (0.5%) and HOA (2.5%). Based on this distribution of NO_x ions with organic and inorganic factors, an estimation of nitrate in organic and inorganic form was made, referred to as organic nitrate and inorganic nitrate respectively. Considering only the OA factors, approximately 90% of the organic nitrate was found to be associated with OOA factors.

	PMF _{OA}	PMF _{OA+NOx}	p-value
Mass	HOA	0.98	0.005
Spectrum	BBOA	0.97	0.005
	SVOOA	0.97	0.005
	LVOOA	0.91	0.004
	HOA	0.95	0.004
Time Series	BBOA	0.97	0.004
	SVOOA	0.87	0.005
	LVOOA	0.89	0.004
	HOA	0.95	0.004

Table1: Inter comparison of Mass spectrum and time series of factors derived from PMF analysis on OA and OA+ NOx data

Figure (1b) depicts the diurnal variation of organic nitrate (ON) and inorganic nitrate (ION). The mean mass concentration of ON and ION was found to be $0.32 \pm 0.2 \mu\text{gm}^{-3}$ and $0.67 \pm 0.6 \mu\text{gm}^{-3}$ respectively. The two forms contributed 32% (organic) and 68% (inorganic) to the total nitrate mass. The diurnal variation of ION closely resembled the variation of nitrate aerosol with higher mass concentration than ON throughout the day. Lower ION concentration observed during the daytime with significant enhancement in the early morning and evening. This phenomenon was observed due to gas-particle partitioning of HNO₃ under high relative humidity and low temperature conditions. This feature was evident from Figure 1b as well where production of ION follows synchronous variation with K_p, an equilibrium constant of partitioning of ammonium nitrate. K_p was calculated using equation:

$$k(T) = k(298) \exp \left\{ a \left(\frac{298}{T} - 1 \right) + b \left[1 + \ln \left(\frac{298}{T} \right) - \frac{298}{T} \right] \right\}$$

Where, T is the ambient temperature in Kelvin. $K(298) = 3.35 \times 10^{16} \text{ (atm}^{-2}\text{)}$, $a = 75.11$ and $b = -13.5$.

Further ON aerosol observed a relatively flat pattern with higher concentration during daytime (14:00 to 16:00 h) and evening hours (20:00 to 22:00 h). Since formation of ON did not follow the K_p path, it is believed that the daytime high was due to photochemical production of ON from the oxidation of biogenic VOCs in the presence of NO_x, while nocturnal oxidation of VOCs by nitrate radical led to night-time concentration of ON. The NO⁺/NO₂⁺ ratio for nitrate associated with LVOOA was observed as ~ 8.75 , much higher than ratio of NH₄NO₃. On an average, organic nitrate makes up to 3% of the total NR-PM₁ aerosol with dominance of inorganic nitrate over organic nitrate. The results are indicative of the presence of organonitrate in the ambient air. However, while dealing with UMR data of ACSM, some interference ($\sim 4\%$) by organic components was observed at m/z 30 in this study. Therefore this may lead to uncertainty in the quantification of organic nitrate and thus the mass concentrations of organic nitrate may be read as an upper limit. Since these aerosol components are the product of atmospheric processing (gas to particle conversion through subsequent adsorption), are believed to be highly oxidized and aged in nature. These species are hence expected to act as cloud condensation nuclei after attaining optimum size under favourable meteorological conditions.

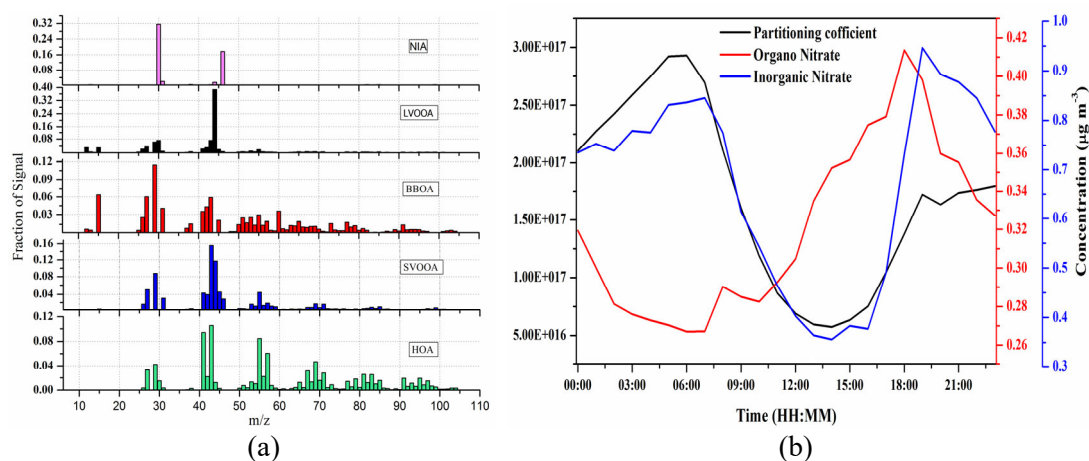


Figure 1: a) PMF results for OA+NO_x spectrum, b) Diurnal variation of organic (ON) and inorganic (ION) form of nitrate along with partitioning coefficient (K_p).

CONCLUSIONS

ToF-ACSM was used to measure NR-PM₁ aerosol at Mahabaleshwar during the winter of 2016-17. The PMF analysis of organic with NO_x mass spectra provided intrinsic information on interactions between organic and inorganic components of aerosol. The PMF on OA+NO_x analysis enabled the quantification of organic nitrate aerosol. The total nitrate functionality was contributed with ~32% by organic form and ~68% by inorganic form. The photochemical oxidation of VOCs by hydroxyl and nocturnal oxidation by nitrate radical were recognized as the major sources of organic nitrate during the daytime and late evening hours respectively. The results suggested the relative importance of both biogenic and anthropogenic emissions as the probable precursors for organonitrate formation at this site during the study period.

ACKNOWLEDGEMENTS

The authors are grateful to the Director, IITM, Pune, India, for the support and encouragement given to undertake this work. HACPL is fully funded by Ministry of Earth Sciences, Govt of India. VyomaSingla extends special thanks to DST, SERB for N-PDF fellowship (Fellowship number: PDF/2017/002428)

REFERENCES

- Fröhlich, R., Cubison, M.J., Slowik, J.G., Bukowiecki, N., Prévôt, A.S.H., Baltensperger, U., Schneider, J., Kimmel, J.R., Gonin, M., Rohner, U., Worsnop, D.R., Jayne, J.T. (2013). The ToF-ACSM: a portable aerosol chemical speciation monitor with TOFMS detection. *Atmos. Meas. Tech* 6, 3225–3241. doi:10.5194/amt-6-3225-2013
- Guenther, A., Hewitt, C.N., Erickson, D., Fall, R., Geron, C., Graedel, T., Harley, P., Klinger, L., Lerdau, M., McKay, W.A., Pierce, T., Scholes, B., Steinbrecher, R., Tallamraju, R., Taylor, J., Zimmerman, P. (1995). A global model of natural volatile organic compound emissions. *J. Geophys. Res.* 100, 8873.

Hallquist, M., Wangberg, I., Ljungstrom, E., Barnes, I., and Becker, K. H. (1999). Aerosol and product yields from NO₃ radical-initiated oxidation of selected monoterpenes, *Env. Sci. & tech.* 33, 553–559.

Hallquist, M., Wenger, J.C., Baltensperger, U., Rudich, Y., Simpson, D., Claeys, M., Dommen, J. (2009). The formation, properties and impact of secondary organic aerosol: current and emerging issues. *Atmos. Chem. Phys.* 9, 5155–5236.

Lim, Y. Bin, Kim, H., Kim, J.Y., Turpin, B.J. (2016). Photochemical organonitrate formation in wet aerosols. *Atmos. Chem. Phys.* 16, 12631–12647.

Ng, N.L., Chhabra, P.S., Chan, a. W.H., Surratt, J.D., Kroll, J.H., Kwan, a. J., McCabe, D.C., Wennberg, P.O., Sorooshian, A., Murphy, S.M., Dalleska, N.F., Flagan, R.C., Seinfeld, J.H. (2007). Effect of NO_x level on secondary organic aerosol (SOA) formation from the photooxidation of terpenes. *Atmos. Chem. Phys.* 7, 5159–5174.

Rosen, R.S. (2004). Observations of total alkyl nitrates during Texas Air Quality Study 2000: Implications for O₃ and alkyl nitrate photochemistry. *J. Geophys. Res.* 109, D07303.

Xu, L., Suresh, S., Guo, H., Weber, R.J., Ng, N.L. (2015a). Aerosol characterization over the southeastern United States using high-resolution aerosol mass spectrometry: Spatial and seasonal variation of aerosol composition and sources with a focus on organic nitrates. *Atmos. Chem. Phys.* 15, 7307–7336.

ON THE MEASUREMENT OF ICE NUCLEI CHARACTERISTICS OVER A HIGH ALTITUDE STATION IN THE INDIAN REGION

V. ANIL KUMAR¹, G. PANDITHURAI¹, GOURIHAR R. KULKARNI², ANUPAM HAZRA¹, ROHIT D. PATIL¹, SACHIN S. PATIL¹, SHRIKANT D. DUDHAMBE¹, P.P. LEENA¹, K. NIRANJAN³

¹Indian Institute of Tropical Meteorology, Pashan, Pune, India

²Pacific Northwest National Laboratory, Richland, WA, USA

³Andhra University, Vishakapatnam

KEYWORDS: Ice nuclei, Heterogeneous nucleation, Aerosol, Spectrometer for ice nuclei (SPIN).

ABSTRACT

First in-situ measurement of ice nuclei (IN) concentration over Indian region were obtained from a high altitude station in the Western Ghats region of India. In this study, SPectrometer for Ice Nuclei (SPIN), a continuous flow diffusion chamber (CFDC) is used to measure IN concentration in the ambient air. Data observed during Feb to July 2018 is used in this study. We measured IN concentration at water sub-saturated condition ($RH_w < 100\%$) and water supersaturated condition ($RH_w > 100\%$) to study ice formation under different conditions. Experiments are conducted to measure ice nuclei at different temperature and supersaturations with respect to ice. In this study, temperature was varying from -23.7 to -35.7 °C and ice supersaturation in the range 13.1 to 48.8 %. At heterogeneous ice formation temperature, the ice particle concentration was varying from 0.095 to 47.75 L⁻¹. Comparison of our observation is in agreement with old observations from this region. Comparison with aerosol properties shows a strong positive correlation with aerosol mean diameter.

INTRODUCTION

Prediction of ice nuclei in cloud models is still a difficult process. The main reason is lack of understanding as it difficult to take observations of ice particle using current technologies. More observations of natural ice nuclei at different environmental conditions are required to utilize laboratory results to parameterization for models (*Hoose and Mohler 2012*). Observation of ice particles started several hundred years back, the Field and experimental studies of Ice nuclei started since several years. Several techniques have developed since last fifty years for their measurement. Simple and early method was to use a cloud chamber where sample air is cooled by sudden expansion to create super saturation (*Bigg 1957*). In another technique, aerosol samples were collected on membrane filters. These filters are exposed to freezing temperatures and super saturation inside diffusion chamber to identify IN. Continuous flow diffusion chamber (CFDC) is widely used for IN measurements. which is used for online measurements of IN in an air sample (e.g., *Rogers, 1988; DeMott et al., 2003a*). The SPectrometer for Ice Nuclei (SPIN) is a CFDC commercially available ice nuclei counter manufactured by Droplet Measurement Technologies (DMT) in Boulder, CO.

A review of results from several laboratory experiments to study heterogeneous ice nucleation was compiled by *Hoose and Mohler (2012)*, they observed that due to differences in methodology and non standardized reports, the onset condition for heterogeneous conditions spread over large range of temperature and ice supersaturation. So one of the important recommendations was the need of coordinated experiments with different instruments to resolve instrument dependent difference.

De Mott et al., 2010, compared IN data from nine different studies from different locations, they observed a variation of 3 orders of magnitude in IN concentration at any given temperature. This shows the high variability of IN concentration in the atmosphere. The main factors influencing the IN concentration at a particular location are the physiochemical properties of aerosol particles and their transport processes. Other factors, like aerosol particle surface area, time for which the particles are exposed to supersaturation, aerosol chemical composition, contact angle between particles and water, crystallographic structure of particles, and the mineralogy of aerosols, may also affect the ice nucleation activity (Kanji et al., 2008; Kulkarni et al., 2009; Welti et al., 2009; Kulkarni and Dobbie, 2010).

Ice nuclei measurement over India are very sparse (e.g., Prabhakar and Ramana Murty, 1962; Paul, 2000, Patade et al., 2014, Wagh et al., 2017). All the early studies used offline methods for measuring IN for several days (no continuous measurements available) and from few locations. More and continuous IN measurement is required to develop a better parameterization to improve regional climate prediction.

In this study, we measured ice nuclei concentration over the high-altitude station Mahabaleshwar, located in the Western Ghats region of India. Properties of ambient aerosol particle is also analysed to understand its impact on ice activation.

METHODS

Observations were carried out during the period Feb to July 2018, from the High Altitude Cloud Physics Laboratory at Mahabaleshwar (17.92° N, 73.66°E) which is at an altitude of 1348 m above mean sea level. Concentration of ice nuclei was measured with Spectrometer for Ice nuclei (SPIN). Aerosol physical properties are simultaneously measured using a SMPS. IN measurements are carried out at water subsaturation and supersaturation conditions at different heterogeneous ice nucleation temperatures ranging -24 to -36°C.

RESULTS & DISCUSSIONS

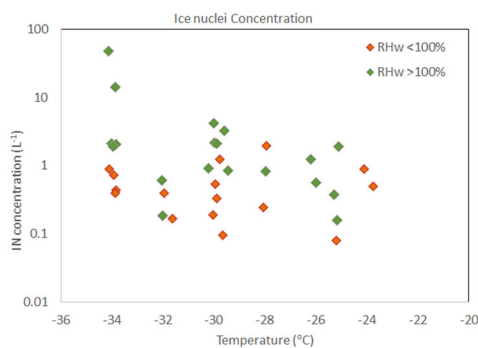


Figure 1. Ice nuclei concentration at different temperature at water sub-saturated and supersaturated conditions

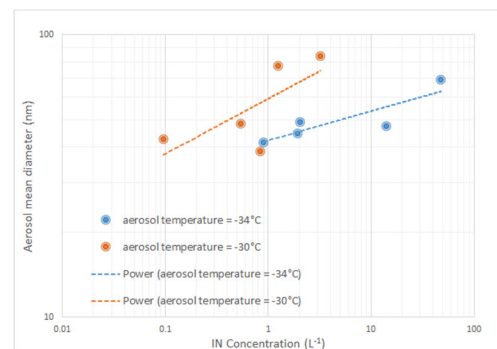


Figure 2. Ice nuclei concentration versus aerosol mean diameter at aerosol temperatures -30°C & -34°C.

Fig. 1 shows the ice nuclei concentration at sub-saturated and supersaturated conditions with respect to water at different heterogeneous temperatures. In this study, the aerosol temperature was varied from -23.7 to -35.7 °C and ice supersaturation in the range 13.1 to 48.8 %. The measured the IN concentration was varying from 0.095 to 47.75 L⁻¹ and increases with decreasing temperature. At same aerosol temperature, a large variation of IN concentration is observed. The observations are comparable with other studies conducted in India using offline techniques (Patade et al., 2014, Wagh et al., 2017).

Fig. 2 compares the concentration of IN with aerosol mean diameter at two different aerosol temperatures -30°C and -34°C. The ice concentration seems to increase with mean aerosol diameter. This shows the sensitivity of aerosol size to produce Ice nucleation. The variation of IN with aerosol size at two temperatures shows that, at a particular aerosol size lower temperature can produce more ice particles than at higher temperature.

CONCLUSIONS

- 1) This is the first study in India, measuring IN online using a CFDC.
- 2) The concentration of IN was found to increase with decreasing temperature.
- 3) A strong positive correlation observed between concentration of IN and ambient aerosol size.
- 4) Large variation of IN concentration is observed at any given temperature.
- 5) The concentration of IN can be related to concentration of larger aerosol particles and temperature.

ACKNOWLEDGEMENTS

Authors are thankful to director, IITM for encouragement. IITM and HACPL are fully funded by Ministry of Earth Sciences, Govt of India.

REFERENCES

- Bigg, E.K. (1957). A new technique for counting ice-forming in aerosols. *Tellus* 9, 394-400.
- DeMott, P. J., Prenni, A. J., Liu, X., Kreidenweis, S. M., Petters, M. D., Twohy, C. H., Richardson, M. S., Eidhammer, T., and Rogers, D. C. (2010). Predicting global atmospheric ice nuclei distributions and their impacts on climate, *P. Natl. Acad. Sci. USA*, 107, 11217–11222,.
- Hoose, C. and O. Mohler (2012). Heterogeneous ice nucleation on atmospheric aerosols: a review of results from laboratory experiments. *Atmos. Chem. Phys.* 12, 9817–9854.
- Kanji, Z. A., O. Florea, and J. P. D. Abbatt (2008). Ice formation via deposition nucleation on mineral dust and organics: Dependence of onset relative humidity on total particulate surface area. *Environmental Research Letters*, 3(2), 025004, doi: 10.1088/1748-9326/3/2/025004.
- Kulkarni, G., S. Dobbie, and J. B. McQuaid (2009). A new thermal gradient ice nucleation diffusion chamber instrument: Design, development and first results using Saharan mineral dust. *Atmospheric Measurement Techniques*, 2(1), 221–229, doi: 10.5194/amt-2-221-2009.

Kulkarni, G., and S. Dobbie, (2010). Ice nucleation properties of mineral dust particles: Determination of onset RHi, IN active fraction, nucleation time-lag, and the effect of active sites on contact angles. *Atmospheric Chemistry and Physics*, 10(1), 95–105, doi: 10.5194/acp-10-95-2010.

Paul, S. K. (2000). A study of chloride aerosol, total aerosol and ice nuclei in the Indian regions. *Pure Appl. Geophys*, 157(9), 1541–1556, doi: 10.1007/PL00001132.

Patade, S., B. Nagare, S. Wagh, R. S. Mahes Kumar, T. V. Prabha, and P. P. Kumar, (2014). Deposition ice nuclei observations over the Indian region during CAIPEEX. *Atmospheric Research*, 149, 300–314, doi: 10.1016/j.atmosres.2014.07.001.

Prabhakar, K., and B. E. V. Ramana Murty, (1962). Some preliminary studies on freezing nuclei concentration in air at Delhi. *J. Met. Geophys.*, 13, 3–6.

Wagh S.D., Nagare B., More S.D., Pradeep Kumar P. (2017). Multiyear observations of deposition-Mode Ice Nucleating particles at two high-altitude stations in India. *Advances in Atmospheric Sciences*, 34, December 2017, 1437-1446.

Welti, A., F. Luond, O. Stetzer, and U. Lohmann, (2009). Influence of particle size on the ice nucleating ability of mineral dusts. *Atmospheric Chemistry and Physics*, 9(18), 6705–6715, doi:10.5194/acp-9-6705-2009.

EVALUATION OF SIMULATED PM CONCENTRATIONS USING WRF-CHEM OVER INDIA DURING A PRE-MONSOON MONTH

S. MAJI AND G. BEIG

Indian Institute of Tropical Meteorology, Dr. Homi Bhabha Road, Pashan, Pune-411008

KEYWORDS: Aerosols, Air Quality Forecasting, PM_{2.5}, PM₁₀.

INTRODUCTION

Aerosols play a major role in modulating climate. Aerosol especially particulate matters have adverse effect on health. Simulation of particulate matter over India is very less. Recent studies have focused on simulation particulate matter using regional models. In this study we have conducted a study on particulate matter over India during May 2017 (1st May -30th t May 2017) using regional climate model WRF-Chem at 12 km resolution. Our results shows model under predicts both PM_{2.5} and PM most of the places.

METHODS

Regional model WRF with chemistry (WRF-Chem-3.9.1) was used for simulating gas and aerosols using the following configuration:

Model domain: 264 x260x35 grids

Model top 50 hPa

Model horizontal resolution 12 Km

Meteorological input used: NCEP Final reanalysis data (ds083.2)

Chemical boundary condition used: MOZART4-GEO5 global model output from NCAR.

Chemical mechanism used: MOZCART (MOZART chemistry with GOCART dust option)

Emission input: EDGAR-HTAPv2. Mission input is only at first level.

Biogenic emission used: MEGAN

No fire emissions were used in this study.

WRF_chem domain

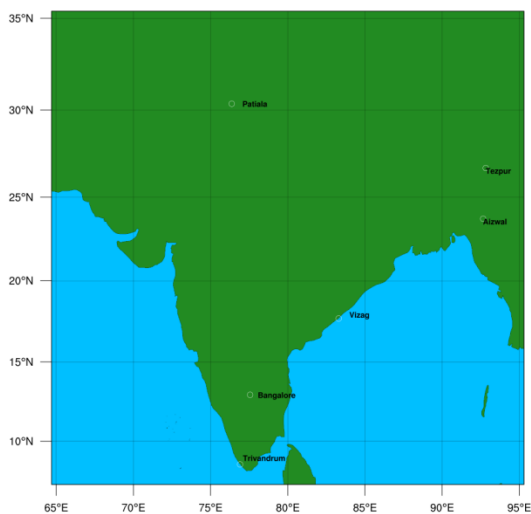


Figure 1 showing the model domain used for this study.

PM2.5 and PM10 observation data used for model evaluation were obtained from 6 stations under MAPAN (Modeling Air Pollution and Networking) project. Location of these stations is provided in the following table:

Station	Latitude	Longitude	Height	Type
Aizwal	23.73	92.66	2754 ft	Urban
Bangalore	12.94	77.56	3033 ft	Urban metropolitan
Patiala	30.35	76.37	853 ft	urban
Tezpur	26.70	92.83	239 ft	urban
Vizag	17.7	83.3	16 ft	Coastal urban
Trivandrum	8.52	76.90	74 ft	Coastal urban

RESULTS & DISCUSSIONS

Model performance was evaluated using the hourly PM2.5 and PM10 observations at 6 sites: Aizwal, Bangalore, Patiala, Tezpur, Trivandrum and Vizag. Bangalore is a typical urban metropolitan with traffic and industrial emission. Patiala is an urban area present in Indo-Gangetic Plain in north-western part of India. Trivandrum and Vizag both are coastal city. During pre-monsoon Patiala will be impacted by biomass burning and fire activities and other typical urban activities like traffic, industry and residential emissions etc.

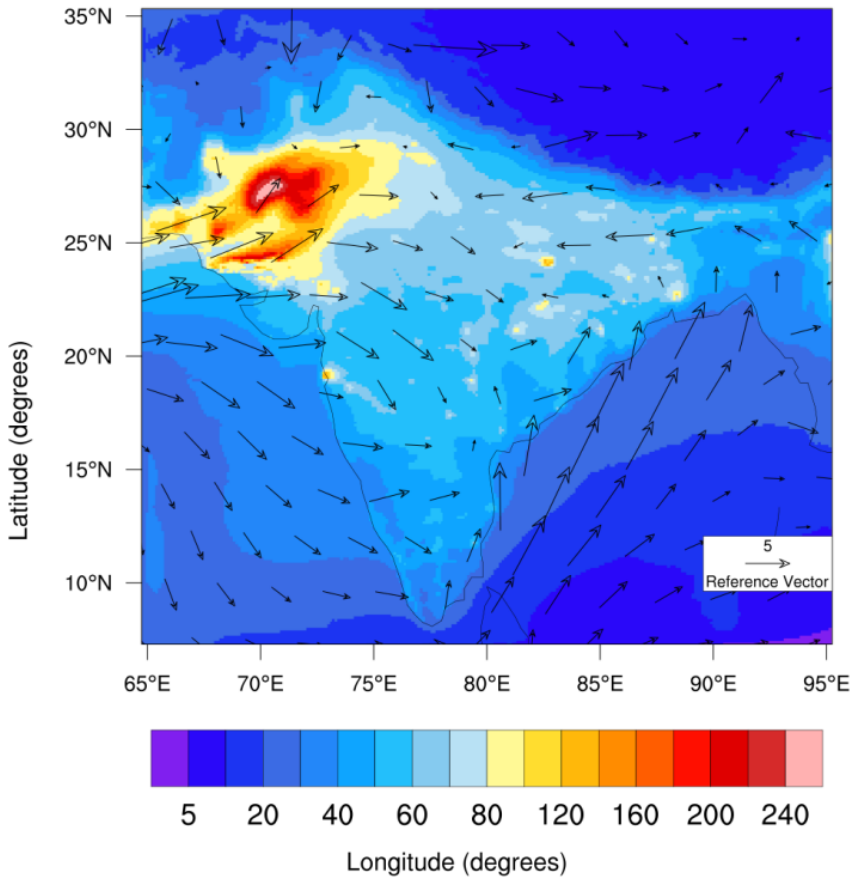


Figure2: WRF-Chem simulated PM 2.5 concentrations ($\mu\text{g}/\text{m}^3$) for the study period (1st May 2017-23rd May 2017).

Figure 2 shows the special distribution of simulated PM 2.5 concentrations (in $\mu\text{g}/\text{m}^3$) over the modelling domain. Very high PM 2.5 concentration was observed over Thar desert region of India and Pakistan. This is associated with high wind speed. PM 2.5 values in the range 70-80 $\mu\text{g}/\text{m}^3$ is simulated over Indo-Gangetic Plain region. This is due to contribution from transported dust and local pollution. High values of PM2.5 over the Arabian Sea region are due to outflow from the land areas of Middle East. Sea Salt have contributed to the high values of PM2.5 (40-60 $\mu\text{g}/\text{m}^3$) in western coast of India. High PM 2.5 values are also simulated over scattered industrial and city areas over IGP region.

EVALUATION OF PM2.5 AND PM10

Table 2 shows model performance for PM2.5 and PM10 over 6 MAPAN stations. The model is over predicting PM2.5 and PM10 concentrations over all stations except Patiala where model is under predicting PM2.5 values. The table show Mean Bias (MB), Gross Error (GE), Mean Normalised Error (MNE), Mean Fractional Bias (MFB) and correlation coefficient.

All these metrics were calculated using hourly data. Definitions of these metrics were taken from Sánchez-Ccoyllo *et al.*, 2018. As mentioned in Kumar *et al.*, 2016 MFB of 60% for daily averaged data is used as a criterion for good prediction of PM10. It is seen that model performs good for predicting PM2.5 concentrations in different sites whereas PM10 concentration is well predicted in Vizag.

Stations	Aizwal		Bangalore		Patiala		Tezpur		Trivandrum		Vizag	
	PM2.5	PM10	PM2.5	PM10	PM2.5	PM10	PM2.5	PM10	PM2.5	PM10	PM2.5	PM10
Model (ug/m3)	38.40	81.88	51.11	107.87	56.84	128.42	48.86	80.74	35.71	75.16	49.44	104.34
Observation (ug/m3)	25.17	46.34	32.43	68.30	83.97	127.37	18.46	32.33	20.52	33.50	25.46	67.31
Man Bias (ug/m3)	13.22	35.53	16.88	39.57	-27.13	1.04	30.40	48.40	15.19	33.54	23.97	37.03
Gross Error (ug/m3)	20.34	43.33	20.22	51.76	38.14	62.62	30.60	48.50	16.52	41.67	24.91	41.60
MNE	1.64	1.66	0.80	1.09	0.40	0.52	2.14	1.80	1.12	1.37	1.58	0.77
MFB (%)	-41.6	-55.54	-44.71	-44.92	38.53	-0.81	-90.32	-85.61	-54.03	-76.7	-64.01	-43.15
Pearson's correlation	0.14	0.17	0.30	-0.30	0.29	0.19	0.27	0.12	0.03	0.25	0.53	0.52

Table2: comparison of simulated hourly PM2.5 and PM10 using observations.

EVALUATION OF METEROLOGY

Different statistical metrics were calculated using hourly simulated and observed meteorological data for the study period. Table 3 summarises the evaluation of meteorology.

		Aizwal	Bangalore	Patiala	Tezpur	Trivandrum	Vizag
Temp	observed	26.17	27.97	31.61	26.58	27.90	31.83
	predicted	24.33	27.04	33.94	27.62	28.08	28.86
	mb	-1.84	-0.93	2.33	1.03	0.17	-2.97
	rmse	3.47	2.56	3.78	2.61	2.80	4.14
ws	observed	2.72	1.52	2.83	2.75	2.21	2.32
	predicted	2.86	3.72	4.42	4.57	3.52	4.45
	mb	0.13	2.20	1.58	1.82	1.30	2.13
	rmse	1.98	2.54	3.06	2.95	2.04	2.51
wd	observed	137.90	226.23	158.2	161.60	211.82	224.82
	predicted	187.23	234.08	164.15	95.11	257.87	269.24
	mb	49.33	7.84	5.94	-66.5	51.93	44.42
	rmse	98.45	90.96	117.85	99.03	110.68	103.80
rh	observed	81.76	55.36	47.90	82.98	80.99	81.82
	predicted	81.62	63.30	32.34	67.56	84.36	85.50
	mb	-0.14	7.94	-15.56	-15.42	3.53	3.69
	rmse	15.13	18.00	20.66	19.81	6.39	6.68

Table3. Comparison of predicted and measured meteorological parameters (hourly data) during the study period.

It can be seen that bias for most of the sites wind speed is over-predicted. This is associated with low resolution topography which cannot resolve wind properly. Most of the values does not correspond to the The report for the MM5 Meteorological Model over the continental U.S. prepared for the U.S. EPA (Tesche and Tremback, 2002).

TIME SERIES OF PM2.5 AND PM10:

Figure 3 and Figure 4 shows the time series of PM 2.5 and PM10 concentrations. At every site model is predicting the daily variation well. Model is overproducing PM2.5 and PM 10 at every site except at Patiala. Overall in the time series high and low episodes were well caught by the model. Higher wind speed may have eroded more dust which may have contributed to high PM10.

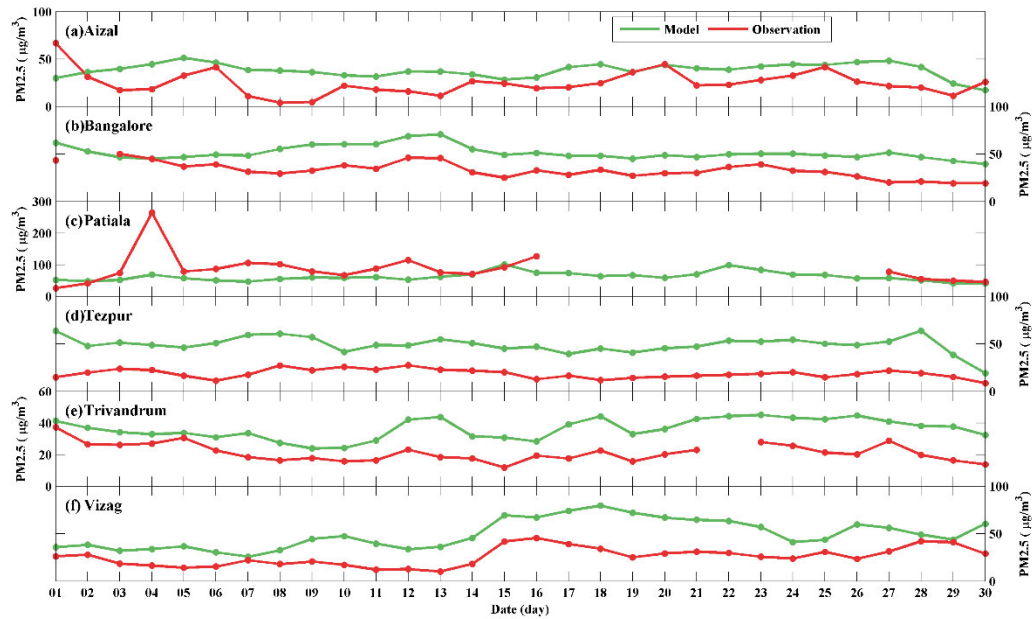


Figure 3. Time series of daily PM_{2.5} concentrations ($\mu\text{g}/\text{m}^3$) for the observation period (1st to 30th May 2017). X axis represents day of March 2017 while Y-axis represents PM 2.5 concentrations (in $\mu\text{g}/\text{m}^3$).

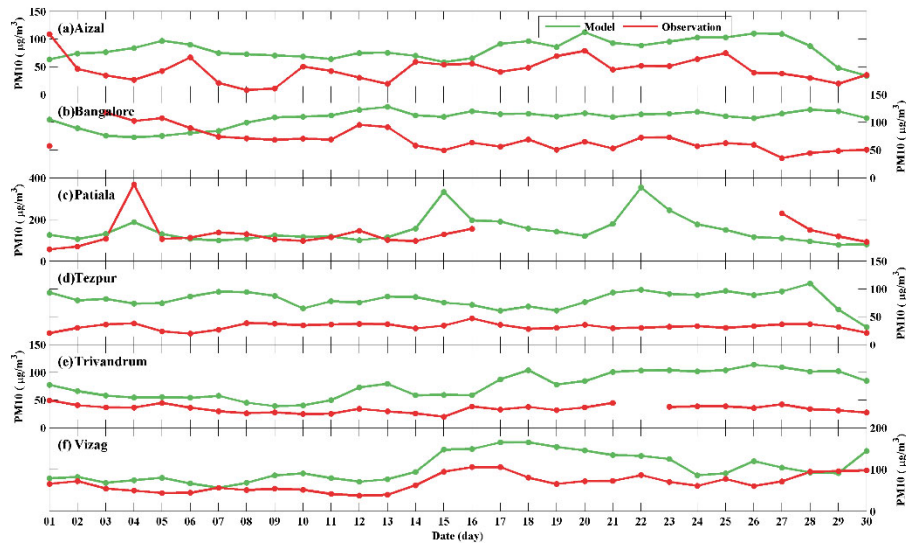


Figure 4. Time series of daily PM₁₀ concentrations (microgram/m³) for the observation period (1st to 30th May 2017). X axis represents day of March 2017 while Y-axis represents PM 10 concentrations (in $\mu\text{g}/\text{m}^3$).

Proper prediction of PM_{2.5} is associated with prediction of biogenic and anthropogenic components. Biogenic component will depend on proper prediction of temperature. Dry

deposition is another factor. Higher wind speed may have led to less dry deposition which may have contributed to high PM_{2.5}.

Proper prediction of PM₁₀ is associated with proper prediction of PM_{2.5} and dust. Higher wind speed may have impacted dust emission from erodible surfaces which associated with low dry deposition may have led to high PM₁₀. Rainfall is also under predicted (not shown here) which is another factor contributing to higher PM at all sites.

Occasional high levels of PM values were not well caught by model. These may be due to improper boundary condition used and no-inclusion of fire emissions. Although the wind is not properly predicted, model is still able to catch the day to day variation of particulate matter. This may be associated with chemical boundary condition used, emissions used.

CONCLUSIONS

WRF-Chem model was evaluated using PM_{2.5} and PM₁₀ hourly data at 6 stations from different urban areas in India. In all stations PM_{2.5} and PM₁₀ were overpredicted except Patiala.

Although day to day variation is captured well by model, model overestimated both PM_{2.5} and PM₁₀. This is associated with simulated high wind speed and low rainfall.

Not only the meteorological conditions but chemical boundary conditions and anthropogenic emissions were important in prediction of day to day variation.

So, we need more resolved model (high resolution) with more detailed emission e.g fire and diurnal anthropogenic emissions for proper prediction of PM in our current set-up.

ACKNOWLEDGEMENTS

This work was supported by SAFAR IITM Pune.

REFERENCES

Kumar et al., Application of WRF-Chem Model to Simulate PM₁₀ Concentration over Bogota, *Aerosol and Air Quality Research*, 16: 1206–1221, 2016

Sánchez-Ccoyllo et al., 2018. Modeling Study of the Particulate Matter in Lima with the WRF-Chem Model: Case Study of April 2016, *International Journal of Applied Engineering Research* ISSN 0973-4562 Volume 13, Number 11 (2018) pp. 10129-10141

Tesche, T.W. and Tremback, C. (2002). Operational Evaluation of the MM5 Meteorological Model over the Continental United States: Protocol for Annual and Episodic Evaluation, Draft Protocol prepared under Task Order 4TCG-68027015 for the Office of Air Quality Planning and Standards. U.S. Environmental Protection Agency.

CHARACTERISTIC FEATURES OF ORGANIC AND ELEMENTAL CARBON: ESTIMATION OF SOURCES OVER A HIGH ALTITUDE STATION

M.P.RAJU*, P.D.SAFAI, G.PANDITHURAI AND K.K.DANI

High Altitude Cloud Physics Laboratory, Mahabaleshwar
Indian Institute of Tropical Meteorology, Pune – 411 008, India.

(*Correspondence at: mpraju@tropmet.res.in)

KEYWORDS: OC, EC, POC, SOC, High Altitude station, Temporal and Diurnal variations.

INTRODUCTION

Particulate matter in the atmosphere is known to cause adverse health effects, reduce visibility, and affect global climate via radiative forcing. Carbonaceous aerosols are broken down into three categories: Organic Carbon (OC), Elemental Carbon (EC) and Carbonate Carbon (CC). CC is negligible in fine particles for most regions except those under the influence of mineral dust (Cao et al., 2005). EC aerosols are produced exclusively from incomplete combustion and a large percentage of this production is attributed to human activities (Bond and Bergstrom, 2006, Arhami et al., 2006). OC aerosol formation is attributed to both natural and human sources (Bond and Bergstrom, 2006). OC may be released directly into the atmosphere or formed when gas-phase materials released into the air are photolyzed to form secondary organic aerosols. OC also affects visibility and climate and, along with EC, is believed to cause adverse health effects in humans (Andreae and Gelencser, 2006). The secondary organic carbon (SOC) is formed by oxidation of volatile organic reactive species in the atmosphere (Safai et al., 2014). Both, OC and EC have different optical and chemical properties and thereby show different impacts on the atmosphere.

METHODS AND EXPERIMENTAL SITE

The Sunset OCEC analyser (Model 4G) uses a modified NIOSH5040 thermal-optical protocol (Birch and Cary, 1996). The analysis was performed in two stages: an aliquot of sample filter (1.5 cm²) was stepwise heated in a furnace up to 820°C in a non-oxidizing atmosphere, then it is cooled to 550°C and then again the filter was heated up to 870°C in an oxidizing atmosphere. During each step carbon is oxidized to CO₂ and then reduced to methane detected by a Non-Dispersive Infrared detector (NDIR). A calibration was performed at the end of each analysis. A diode photo detector continuously monitored the transmittance of light from a laser diode through the sample filter during the volatilization and combustion process. The carbon evolved before this line is quantified as OC and that evolved after this line but before methane calibration peak is quantified as EC. One hour cycle was used in which the instrument sampled for 45 min and analysed the sample collected on the quartz filter for 15 min.

Measurements of OC and EC were continuously monitored at High Altitude Cloud Physics Laboratory (HACPL), Indian Institute of Tropical Meteorology, Mahabaleshwar (17°55'N, 73°40'E 1400m AMSL). Mahabaleshwar is a hill station in India's forested Western Ghats range, southwest of Pune. Located about 120 km southwest of Pune, Mahabaleshwar is a vast plateau measuring 150 km², bound by valleys on all sides. Climate of this area is suitable for cultivation of Strawberries, The average annual temperature is 20.4 °C and the average annual rainfall is > 5000 mm. As of 2011 India census, Mahabaleshwar had a population of 12,737. Thus, the observational

site can be considered as a non-urban least polluted site. Observations on OC and EC were carried out during summer season of 2017 (March to May).

RESULTS & DISCUSSIONS

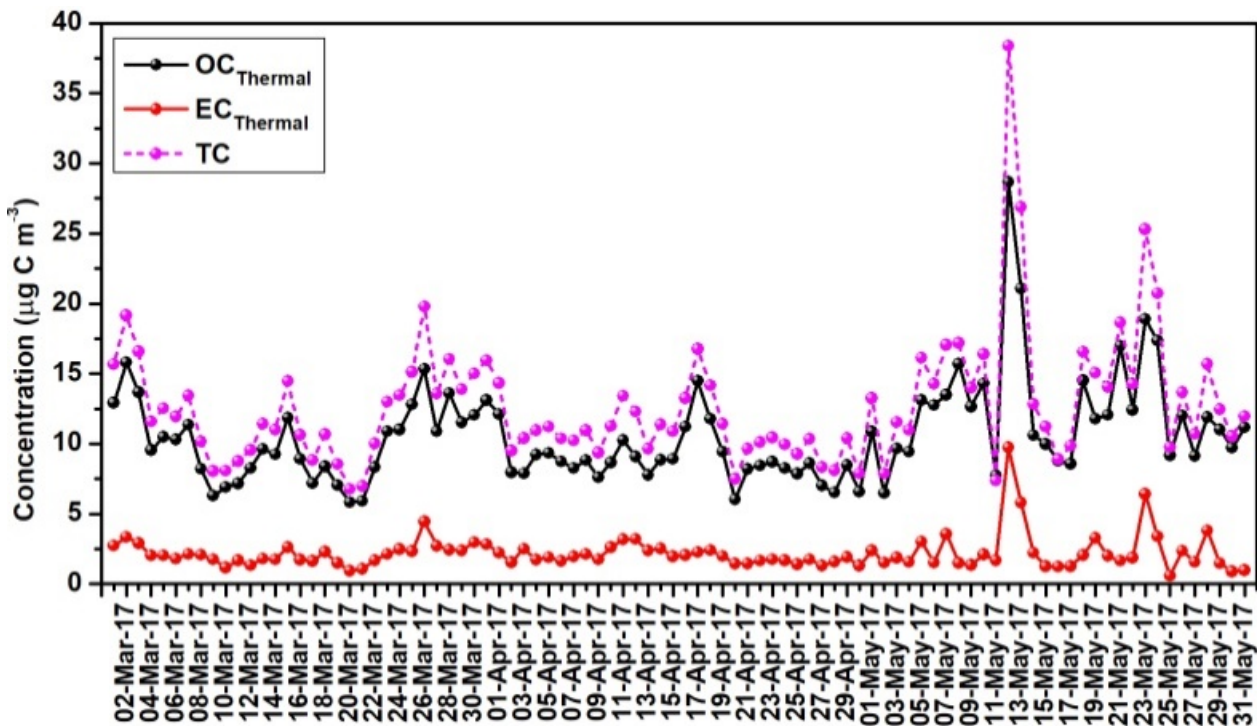


Figure 1 Time series of OC EC and TC during summer 2017 over Mahabaleshwar.

Figure 1 depicts the time series of thermal OC, thermal EC and TC for the 92 days (2208 samples) of data collected in this study. Thermal OC has a mass loading range of 5.8–28.7 $\mu\text{gC}/\text{m}^3$, whereas thermal EC has a much lower mass loading range of 0.6–9.7 $\mu\text{gC}/\text{m}^3$. EC measurements were often near or below the limit of detection (LOD), whereas OC measurements rarely approached the LOD. The monthly mean values of thermal OC, thermal EC and TC shows high during May (12.64 ± 4.37 , 2.45 ± 1.88 , 14.96 ± 6.13) followed by March (10.14 ± 2.74 , 2.15 ± 0.72 , 12.28 ± 3.4) then April (8.83 ± 1.75 , 1.97 ± 0.49 , 10.79 ± 2.03). OC is more hydrophilic than EC and thereby its scavenging is faster compared to EC whereas EC is hydrophobic when freshly emitted but becomes hydrophilic as it ages out and when it comes into contact with sulphate or sea salt and then gets scavenged.

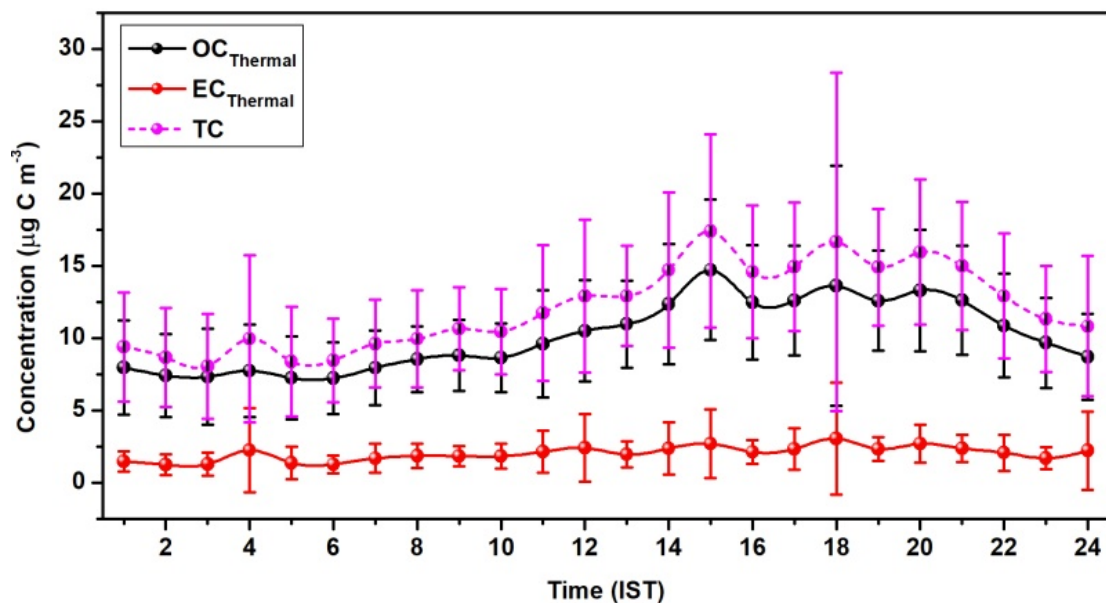


Figure 2 Diurnal variation of OC, EC and TC over Mahabaleshwar.

Hourly variation of OC, EC and TC are shown in figure 2, the vertical bar represents the standard deviation. OC contributed about 83% to the total organic carbon for this period whereas only 17% is from EC. It is clear from the figure 2 that the diurnal variation of EC throughout the study period is almost remain same; whereas OC started increases from 06:00 hours and attain maximum at 15:00 hours ($14.71 \mu\text{gC}/\text{m}^3$) then slowly it decreased and reached minimum at 24:00 hours ($8.7 \mu\text{gC}/\text{m}^3$). The error bar for OC is higher compared to EC representing more variation than that in EC concentration.

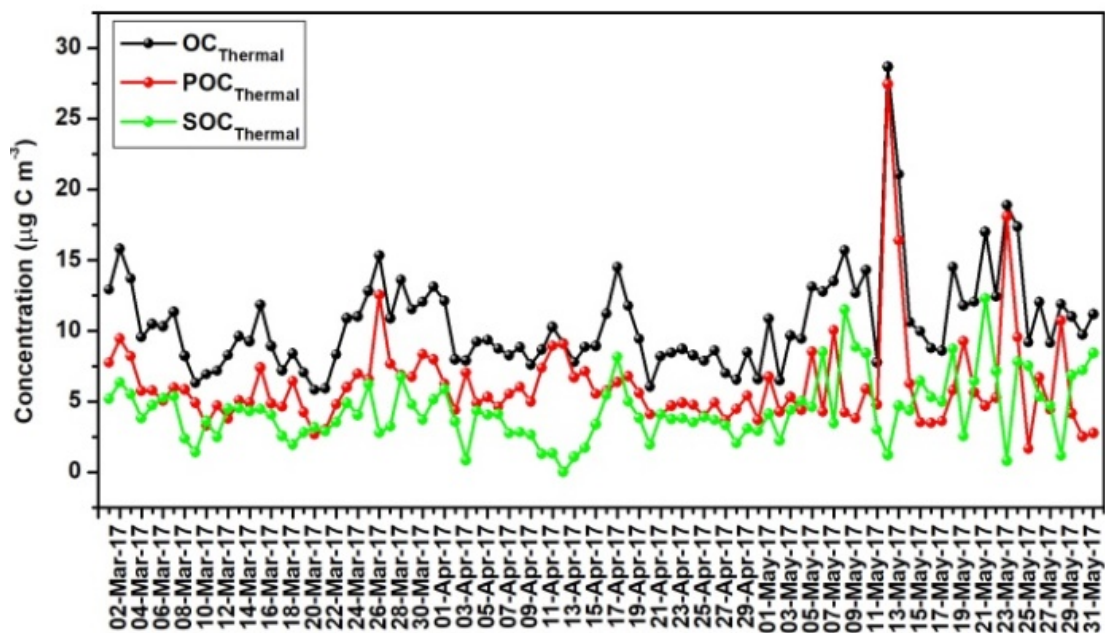


Figure 3 Day-to day variations of OC, POC and SOC during summer 2017 over Mahabaleshwar.

It is very difficult to quantify POC and SOC from OC as there is no simple direct analytical technique for this. Some indirect methodologies are generally applied for the evaluation of SOC in ambient aerosols. However, there are certain assumptions made to compute SOC and POC in EC tracer method (Cabada et al., 2004). POC is following a similar trend and showed a strong correlation ($r=0.78$) with OC, whereas with SOC the correlation was weak ($r=0.38$). POC correlated well with EC ($r=0.99$) indicating similar role of incomplete combustion sources viz, wood burning activity/biomass burning. The monthly mean of Primary OC, Secondary OC and OC showed high during May followed by March and April months.

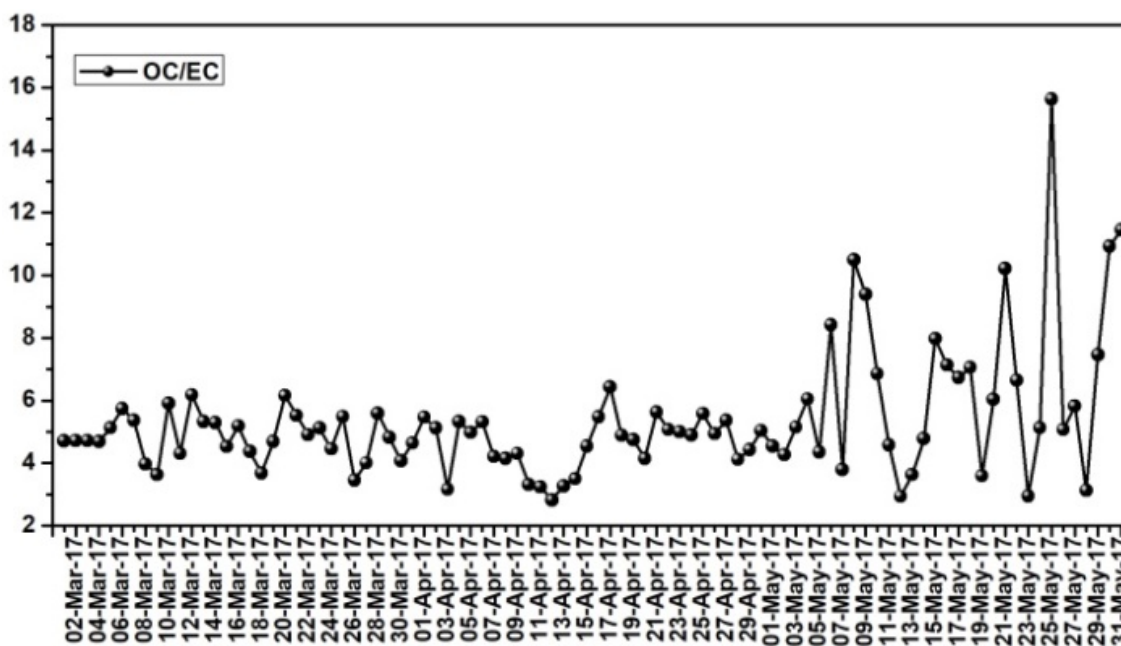


Figure 4 OC/EC ratio and characterization of combustion sources

OC/EC ratio is used to assess the possible contribution of emission sources which may include fossil fuels, biomass burning/wood burning (Figure 4). These ratios are generally used to indicate the presence of primary as well as secondary organic aerosols (Chow et al., 1996). OC/EC ratio < 2 indicating fossil fuel source and > 4 indicating biomass burning. Mean OC/EC ratio for the entire study period was 5.34. OC/EC ratio observed to be maximum during 25 May 2017 (15.63) and minimum 12 April 2017 (2.82), which could be interpreted by stronger biomass burning

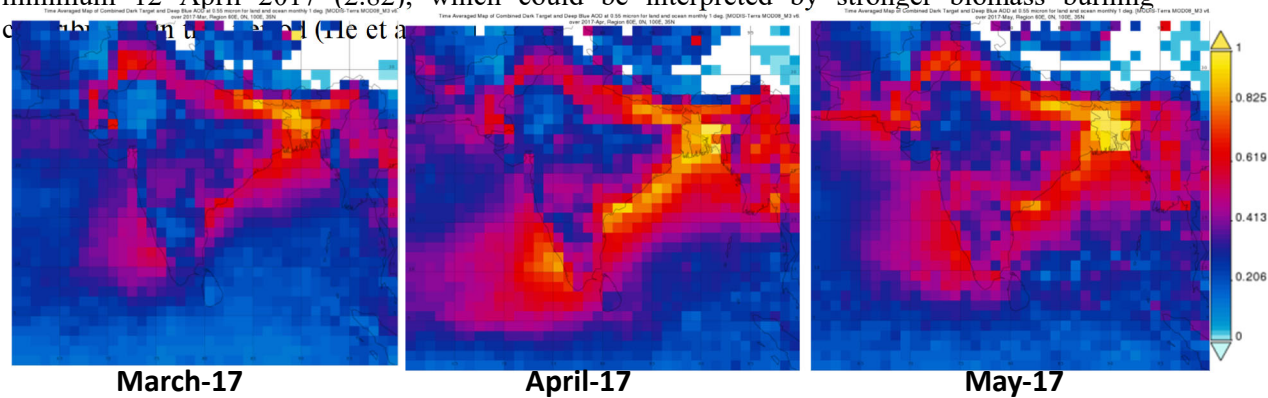


Figure 5 Monthly mean AOD over India.

Aerosol optical depth (AOD) has been obtained using Level-3 MODIS gridded atmosphere monthly global product 'MODIS-Aqua MYD08_M3 v6.1'. Monthly average MYD08_M3 v6.1 product files are available in Hierarchical Data Format (HDF-EOS) at spatial resolution of 1 degree by 1 degree. Figure 5 shows an example of a typical AOD 0.55 micron scene monitored by AQUA during MAM-2017 period over India confining to Mahabaleshwar region, It can be found that high concentrations of monthly mean AOD were observed during May (~0.4) followed by April (~0.3) and March (~0.3) months. AOD over Mahabaleshwar shows similar trend and the results are well compared with thermal EC obtained from OCEC analyser.

CONCLUSIONS

The results of the characteristic study of OCEC using OCEC analyser over high altitude station Mahabaleshwar during Mar-May 2017 indicated:

1. The monthly mean values of thermal OC, thermal EC and TC were high during May (12.64 ± 4.37 , 2.45 ± 1.88 , 14.96 ± 6.13) followed by March (10.14 ± 2.74 , 2.15 ± 0.72 , 12.28 ± 3.4) then April (8.83 ± 1.75 , 1.97 ± 0.49 , 10.79 ± 2.03) respectively.
2. OC contributed about 83% to the total organic carbon for this period whereas only 17% is from EC. OC was about 5 times more than EC.
3. POC followed a similar trend and showed a strong correlation ($r=0.78$) with OC, whereas with SOC the correlation was weak ($r=0.38$). POC correlated well with EC ($r=0.99$) indicating similar role of incomplete combustion sources.
4. OC/EC ratio for the entire study period was 5.34 indicating biomass burning is the prominent source at Mahabaleshwar.

ACKNOWLEDGEMENTS

Authors are thankful to Prof. Ravi Shankar Nanjundiah, Director, IITM for providing the facilities and encouragement during the course of the study. Authors are thankful to the scientific staff of HACPL, Mahabaleshwar for their constant support during this work.

REFERENCES

- Andreae, M. O and Gelencser, A (2006). Black carbon or brown carbon? The nature of light-absorbing carbonaceous aerosols. *Atmospheric Chemistry and Physics* **6**:3131–3148.
- Arhami, M., Kuhn, T., Fine, P.M., Delfino, R.J and Sioutas, C (2006). Effects of sampling artifacts and operating parameters on the performance of a semi-continuous particulate elemental carbon/organic carbon monitor. *Environmental Science and Technology* **40**, 945-954.
- Birch, M.E., Cary, R.A (1996). Elemental carbon-based method for monitoring occupational exposures to particulate diesel exhaust. *Aerosol Science and Technology* **25**, 221-241.
- Bond, T.C and Bergstrom, R.W (2006). Light absorption by carbonaceous particles: an investigative review. *Aerosol Science and Technology* **40**, 27-67.
- Cabada, J.C., Pandis, S.N., Subramanian, R., Robinson, A.L., Polidori, A and Turpin, B (2004). Estimating the secondary organic aerosol contribution to PM_{2.5} using the EC tracer method. *Aerosol Science and Technology* **38**, 140-155.

Cao, J. J., Lee, S. C., Zhang, X. Y., Chow, J. C., An, Z. S and Ho, K. F (2005). Characterization of airborne carbonate over a site near Asian dust source regions during spring 2002 and its climatic and environmental significance. *Journal of Geophysical Research* **110**:D03203.

He, M., Zheng, J.Y., Yin, S.S., Zhang, Y.Y (2011). Trends, temporal and spatial characteristics, and uncertainties in biomass burning emissions in the Pearl River Delta, China. *Atmospheric Environment* **45**, 4051–4059.

Safai, P.D., Raju, M.P., Rao, P.S.P and Pandithurai, G (2014). Characterization of carbonaceous aerosols over the urban tropical location and a new approach to evaluate their climatic importance. *Atmospheric Environment* **92** 493-500.

SODIUM AEROSOL CHARGING AND CONCENTRATION DECAY UNDER UNIPOLAR ION FIELD IN CLOSED CHAMBER

USHA PUJALA, AMIT KUMAR, P.N SUJATHA, V.SUBRAMANIAN, C.V. SRINIVAS AND R.BASKARAN

Radiological Safety Division, HBNI, Indira Gandhi Centre for Atomic research, Kalpakkam – 603102, India.

KEYWORDS: Corona Ioniser, Coagulation, Concentration Reduction Factor (Crf), Average Charge.

INTRODUCTION

The technique of unipolar charging is widely used worldwide for faster reduction of air-borne contaminations in indoor-environments (Mayya et. al., 2004). In this context the present study is carried out to understand the behaviour of micrometer sized sodium aerosols with and without the unipolar negative ion field. As the sodium combustion aerosols are predominantly in micrometer size range, it is expected that they become highly charged and enhance the decay process due to electrostatic dispersion and deposition. Measurements of number concentration decays and size distributions of sodium aerosol with and without charging are carried out with Optical Particle Counter (OPC). Also, the average number of charges obtained by sodium aerosols due to diffusion and field charging mechanisms are calculated and compared with that of charge measurements carried out by Electrical Low Pressure Impactor (ELPI). All the results are presented in this paper.

MATERIAL AND METHODS

Sodium combustion aerosol is generated in 1 m³ cylindrical chamber (diameter -150 cm, height-60 cm) made of stainless steel which is grounded. The efficiency of sodium aerosol removal by Negative Ion Generators (NIG) in the closed chamber is studied. Two numbers of NIG's are fixed at a height of 20 cm from the floor at two different positions inside the chamber. The ion concentration is in the range of 1E06 to 9E06 /cm³ without shadow (zero ion conc.) regions at the backside of ioniser. Experiments are carried out in 4 different conditions of ioniser i.e. i) no charge condition, ii) continuous exposure to negative ions with 2 ionisers are on; iii) 1 min exposure with 1 ioniser on; iv) 2 min exposure with 2 ionisers on. In each experiment corona ioniser is made on at 5th min after generation of aerosol.

Sodium aerosols are charged to negative ions in the closed chambers predominantly by diffusion charging. The average number of charges, n_d , obtained by the diffusion charging in a time period, t , by a particle diameter d_p , can be found from the following equation [Hinds, 1982].

$$n_d = \frac{d_p k T}{2 K_E e^2} \ln \left[1 + \frac{\pi K_E d_p \bar{C}_i e^2 N_i t}{2 k T} \right] \dots (1)$$

Here $K_E = 1/4\pi\epsilon_0 = 9E09$, C_i is the mean thermal speed of the ions (240 m/s), k is the Boltzmann's constant (1.38E-23 J/K), T is the operating temperature of the system (293 K), e is the elementary electrical charge (1.6E-19 coulomb), N_i is the number concentration of unipolar ions. Eq-1 shows that the charge acquired by particle by diffusion charging is proportional to diameter of particle.

The unipolar ions generated from the needles of ionisers are traversed along the electric field lines between the needle (-5 kV) and chamber surface and lost to the walls. While traversing, the ions will deposit over the particles and the aerosols get charged by field charging process. Hence Field charging is also considered in this study although it is lesser in extent than diffusion charging process.

In the absence of diffusion charging, the number of charges, n_f , acquired by particle during a time 't' in an electric field 'E' with ion number concentration N_i can be found from the following equation [Hinds, 1982].

$$n_f = \left(\frac{3\varepsilon}{\varepsilon + 2} \right) \left(\frac{Ed_p^2}{4e} \right) \left(\frac{\Pi e Z_i N_i t}{1 + \Pi e Z_i N_i t} \right) \dots (2)$$

Here ε is the dielectric constant of aerosol (57 for NaOH), Z_i is the mobility of ions (1.5E-04 m²/V.s) and E is the electric field inside the chamber (assumed to be uniform) i.e. 6100 v/m.

Number concentration of aerosol is measured at various periods of time with OPC (Model No.1.108, M/s Grimm, Germany) through dilutor (Model No.1.177, M/s Grimm, Germany). Dilution factors are measured in each experiment to derive the actual concentrations. ELPI (Classic -R, Dekati) is used to measure the number and charge-size distribution of aerosol at various time periods. For ELPI and OPC, sampling flow rates are 10 lpm and 1.2 lpm respectively. Ambient air is supplied to maintain atmospheric pressure inside the chamber throughout the experiment (30 min) which may acts as homogenisation of ion concentration. To measure number and charge size distributions, the internal charger of ELPI is switched ON and OFF alternatively (Subramanian et.al. 2012). During charger ON condition, the number concentration (N) of particles in each size (d_p) is calculated from the corresponding measured currents (I) using the characteristic charger response function ($E_{ch}(d_p)$) i.e. given below (Matthewset.al. 2011).

$$N = \frac{I}{E_{ch}(dp)} = \frac{I}{Pn_c e Q} \dots (3)$$

Here n_c is the number of elementary charges obtained by particle due to internal charger which is provided by manufacturer and P is penetration through the charger which is assumed to be 1 for both charger ON and OFF conditions. Combined together, Pn_c is the characteristic parameter of each stage during ON condition. Q is the sample flow rate of ELPI i.e. 10 lpm. During charger OFF condition, number concentrations obtained during ON conditions are used to determine the unknown charges (n) possessed by the actual aerosol from the corresponding measured currents.

RESULTS AND DISCUSSIONS

The measured initial number concentrations of sodium aerosols are nearly same around 7E05 /cm³ during all the experiments. Number concentration decay of sodium aerosol measured by OPC for the said conditions is shown in Fig 1. The concentration reduction factor (CRF), which is the ratio of the initial to the final concentration (C_0/C_∞) is used to represent the efficiency of aerosol removal under the field of negative ions (Mayya et. al., 2004). This study shows that under no charge conditions, CRF is 2.5 in 30 minute. Under continuous exposure of ions, CRF is enhanced predominantly by the order of 10⁴. This is due to continuous charging of aerosols to higher charge levels, which results in electrostatic dispersion and deposition over chamber surfaces. This study also shows that partial exposure is also effective for enhancing the CRF by more than one order (i.e. 10 to 20 times). In this case, aerosols are charged to the particular charge levels up to ioniser ON condition and concentration decay is effective till that time and then decay follows almost similar trend to that of uncharged condition. The difference in two curves is due to 'ON' conditions of NIG.

The size distributions of sodium aerosols at various time periods, the corresponding Count Median Diameters (CMD) and Geometric Standard Deviation (GSD) measured by OPC are given in the Table 2. It is observed that under uncharged condition both CMD and GSD is increasing as expected due to coagulation and decay processes. Under the continuous charged condition, CMD is not much varied but GSD found to be reduced i.e. distribution become narrowed. Nearly the same CMD shows that the coagulation is not effective under unipolar charged condition while reduction in GSD could be attributed to reduction in concentration with progress of time.

The charge-size distributions obtained by sodium combustion aerosol in 3 different charging conditions are shown in Fig.2. It is observed that continuous charging makes the particles to highly charged level compared to that of partial charging conditions. The number of charges found to be increased when the particle size is increased. The count median aerodynamic diameter (CMAD) of the size distribution of sodium aerosol measured by ELPI is $1.05 \mu\text{m}$ and corresponding geometric diameter is $0.817 \mu\text{m}$. The average number of charges measured during 1 min, 2 min and continuous exposure conditions at the time periods mentioned in the Fig.2 corresponding to $0.817 \mu\text{m}$ stage are -50, -75 and -155 respectively. The calculated values of total average number of elementary charges for $0.817 \mu\text{m}$ particles by diffusion and field charging mechanisms for the time period using Eq-1 & 2 are -61, -79 and -85 respectively. This shows that measured charges are comparable with calculated values during the short duration exposure conditions and disagreement is predominant as charge levels are more during continuous charging. Similarly, the number concentrations of aerosols measured by ELPI are found to be smaller than that of OPC by one order during this condition. The difference in average number of charge determined by ELPI under continuous charged condition for $0.817 \mu\text{m}$ may be due to measurement uncertainty in ELPI for measuring particle number concentration in the case of pre-existing higher number of opposite charges possessed by particles.

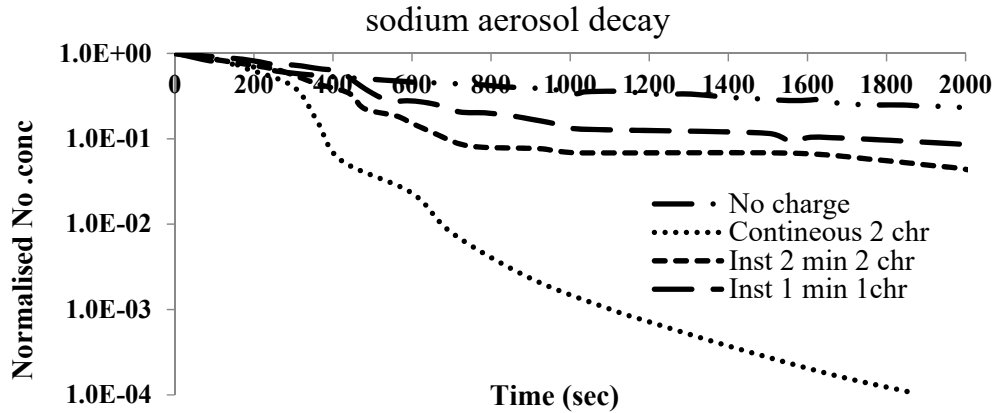


Figure 1. Decay of sodium aerosols concentration under uncharged and unipolar charged conditions.

Table 1. Variation of size with time measures by OPC

Time (min)	CMD (μm)&(σ)			
	No charge	Continuous exposure	1 min exposure	2 min exposure
2	0.42 (1.77)	0.38 (1.97)	0.42 (1.78)	0.43 (1.95)
6	0.46 (1.72)	0.46 (1.9)	0.48 (1.75)	0.5 (1.92)
14	0.53 (1.8)	0.45 (1.82)	0.47 (1.5)	0.45 (1.51)
24	0.58 (2.3)	0.43 (1.4)	0.44 (1.46)	0.45 (1.48)
30	0.61 (2.1)	0.42 (1.4)	0.42 (1.44)	0.43 (1.44)

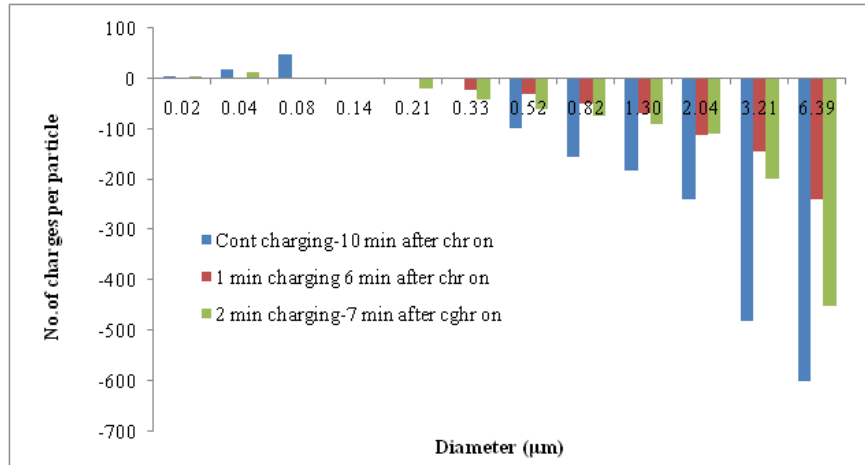


Figure 2. Measured charge-size distribution by ELPI in 3 different charging conditions.

SUMMARY

The study shows that concentration reduction factor is enhanced by the order of $1E04$ during the continuous exposures of unipolar ion field than the un-charged conditions (i.e CRF of 2.5) of sodium aerosols. Short duration of exposures is also found to be useful to enhance the decay process of aerosol concentration. The aerosol size distribution is narrowed down under continuously charged condition and could be due to electrostatic dispersion. Mismatch is observed between OPC and ELPI measured number concentrations during continuous exposure as well as the average number of charges measured and calculated.

ACKNOWLEDGEMENTS

Authors are thankful to Shri Arshad Khan and Dr. B.K. Sapra, EBS, RPAD, BARC for their suggestions to initiate the studies on unipolar charging mechanisms of aerosols.

REFERENCES

Mayya, Y.S., Sapra, B.K., Arshad Khan and Faby Sunny (2004). Aerosol removal by unipolar ionization in indoor environments, *J. Aerosol Science*, 35, 923–941.

W. C. Hinds, (1982), *Aerosol Technology*, John Wiley & Sons.

Matthews, J.C., Wright, M.D., Biddiscombe, M.F., Usmani, O.S. and Hensshaw, D.L (2011). Aerosol charge state characterisation using an ELPI. *J. Physics, Conference series*, 301, 012026.

Subramanian, V., Amit Kumar, Baskaran, R., Misra, J., and Venkatraman, B. (2012). An experimental study on the charging of non-radioactive aerosols with and without the presence of gamma radiation, *J. Aerosol Science*, 52, 98–108.

DETERMINATION OF DEPOSITION VELOCITY OF MIXED AEROSOLS BY CHEMICAL TECHNIQUES

USHA PUJALA¹, AMIT KUMAR¹, P.N. SUJATHA¹, S. VIJAYALAKSHMI², R. ANANTHARAYANAN³, V. SUBRAMANIAN¹, C.V. SRINIVAS¹, AND R. BASKARAN¹

¹Radiological and environmental safety division,

²Materials chemistry division,

³Real time systems division, Indira Gandhi Centre for Atomic Research, Kalpakkam – 603 102, India.

KEYWORDS: Mixed Aerosol, Deposition Velocity, Deposition Flux, Turn Table, Elemental Analysis.

INTRODUCTION

The environmental source term during the Core Disruptive Accident (CDA) conditions in Sodium cooled fast Reactors (SFR's) depends on the suspended number concentration decay of aerosols contains of radioactivity inside the containment. During the accidental conditions, the containment will be bottled up with mixed aerosols of multiple species in terms of size, chemical speciation, shape, mixing state and this diversity complicates the agglomeration and concentration decay process. Among the mixed aerosols, sodium combustion aerosols in micrometer size range are dominant in terms of size and mass concentration (4 g/m³) than sub micrometer sized aerosols of fission product, fuel and structural materiel aerosols (~ 200 mg/m³). Though the aerosol processes are dominated by that of sodium aerosols, it is important to understand the mixed aerosols behaviour for realistic estimation of the suspended concentrations. This paper addresses the issues of counting techniques in dealing with the mixed aerosols and the details of proposed method of aerosol sampling and analysis by chemical techniques such as Flame AES and ICP-MS for the quantitative assessment of mixed aerosol parameters to determine the deposition velocity. In this context experiments are carried out initially with 2-component systems i.e. sodium and fission product SrO₂ aerosols to determine the deposition velocity and it is compared with that of single component sodium aerosols that was found in previous studies.

METHODS

Experimental approaches available in literature for determining deposition velocity are based on the mass transfer of a substance on to the surfaces irrespective of the deposition mechanism in a confined environment which is directly proportional to the suspended concentration. There are two different experimental approaches used in literature to measure deposition velocity. First approach is indirect method by monitoring the particle concentrations (mass or number) with time under defined conditions (Jamriska et al., 2003). For a particular initial concentration, the deposition velocity can be obtained from the slope of a linear least-squares regression line fitted to the normalised concentration decay [$\ln(C(t)/C(0))$] verses time. Second one is direct assessment by measuring the deposition flux and suspended concentrations (mass or number) of particles (Tencer et al., 2008).

$$V_d = -\frac{J}{C} \quad \dots (1)$$

Here 'J' is deposition flux and 'C' is airborne concentration

It is to be noted that the deposition velocity obtained from these two methods gives average physical velocity of set of particles arriving at the surface. In the present study, 2nd method is adopted as it can be applicable for mixed aerosols of multi component systems with large size range and chemical composition.

Experiments are carried out at Aerosols Test Facility (ATF) (Baskaran et.al. 2009). It consists of 1 m³ aerosol chamber of diameter 150 cm and height 60 cm. Sodium combustion cell is used for the production of sodium aerosols and a 25 kW thermal plasma torch is used for the production of non-radioactive SrO₂ aerosols. After the generation, the aerosols are hovered inside the aerosol chamber. Set of experiments are carried out at 50% RH by generating the sodium aerosols of initial mass concentration 3.07 g/m³ and mixed aerosols of mass concentration 3.12 g/m³ (i.e. SrO₂ aerosol is 50 mg/m³). The initial mass concentrations are measured by filter paper sampling (10 lpm, 1min on to 47 mm GF/A filter paper) followed by gravimetric analysis.

SAMPLE COLLECTION AND ANALYSIS

Turn table (Baskaran et al., 2009; Misra et.al, 2013) equipped with glass plates is used to collect the depositing aerosol sample at the bottom of the chamber at regular intervals of time to obtain the transient deposited mass flux. The collection plate of turntable shown in Fig.1 is provided with 16 cups each of 25 mm diameter, on to which glass plates are mounted. For one rotation with 16 cups, total time taken is 17.15 min in case of 60 s exposure time. The suspended mass concentration samples corresponding to the mass fluxes at various time periods are collected by filter paper sampling each with flow rate of 10 lpm for 1 min on to 47 mm GF/A filter papers.

It is to be noted that, the application of counting particle techniques such as OPC or PC for measuring suspended concentrations is limited from the point of view of size range and hence not feasible in mixed aerosol conditions. Also, the gravimetric technique is limited from the point of view of sensitivity in accurately determining the contribution of small fractions of masses contributed by sub micrometer particles and also quantities of the glass plate deposit samples collected are small. Hence the chemical techniques are used in this study for analysing the mass concentrations and deposition fluxes to determine the deposition velocity.

The aerosols sampled over filter papers and glass plates are transferred to 0.1 N HNO₃ solution and the collected masses are quantified using elemental analysis techniques such as Flame Atomic Emission Spectroscopy AES and Inductively coupled plasma Mass Spectrometry ICP-MS respectively for sodium and strontium. ICP-MS technique is used to detect strontium element in mixed aerosol and this technique can detect strontium up to 1 ppb level. Sodium element is analyzed by Flame AES technique which detects the sodium up to 100 ppb level. From the concentrations of sodium and strontium in the solutions, mass flux (F) deposited over different time periods and corresponding and the suspended mass concentrations (M) are determined using the formulae given below.

$$M \left(\frac{g}{m^3} \right) = \frac{\text{Conc. of element in sol.} \left(\frac{g}{l} \right) * \text{Vol. of HNO}_3 \text{ (l)} * \text{Molar mass of compound}}{\text{Atomic weight of element} * \text{vol. of chamber air sampled over FP (m}^3\text{)}} \\ F \left(\frac{g}{m^2 - s} \right) \\ = \frac{\text{Conc. of element in sol.} \left(\frac{g}{l} \right) * \text{vol. of HNO}_3 \text{ (l)} * \text{Molar mass of compound}}{\text{Atomic weight of element} * \text{area of the glass plate (m}^2\text{)} * \text{Exposure time (s)}}$$

The chemical species of sodium aerosols after suspending in the chamber will be the combination of NaOH and Na₂CO₃. Even though both NaOH and Na₂CO₃ are equally distributed in the aerosol for first 13 minutes immediately after sodium fire at 50% RH, it is assumed that all the particles are converted to NaHCO₃ before transferring to 0.1 NHNO₃ solutions during the delay period between sampling and analysis. Molar mass and atomic weights of N₂CO₃ and Na are 106 & 23; whereas for SrO₂ and Sr are 119 & 87.62 respectively

RESULTS AND DISCUSSIONS

The variation of mixed aerosol mass concentration and deposition velocity with time is plotted in Fig.2. Initial mass concentration of mixed aerosols measured within 0–30 s by chemical analysis is 2.53 g/m³ and this value is smaller by 19% from that of measured value by gravimetric analysis of filter paper (3.12 g/m³). The error associated with gravimetric analysis due to sampling flow rate and time period is around 10%. Where as in case of chemical techniques usage, the additional error associated could be due to the transfer of aerosol on filter paper to the standard 50 ml HNO₃ solution. In case of mass flux measurement, the error associated could be due to the transfer of aerosol from glass plates to standard HNO₃ solutions, dilution of sample further for analysing SrO₂ with ICP-MS etc. The mass concentrations corresponding to mass fluxes at various time periods within the experimental period are measured by chemical techniques and observed that at the end of 930 s, it is decreased from 2.53 g/m³ to 1.73 g/m³. The mass flux is observed to be increasing from 3.5E-03 g/m²-sec to 6.3E-03 g/m²-sec. The initial deposition velocity of mixed aerosols is found to be 0.14 cm/s. The deposition velocity ranges between 0.14 cm/s to 0.36 cm/s within the experimental period. The average deposition velocity of sodium aerosols measured within the study period is 0.23 cm/s with uncertainty around 20%. This is observed to be more compared to that of sodium aerosols velocity around 0.12 cm/s (Misra et.al, 2013). It is to be noted that the exponential decay of mass concentration is not reached to steady state within 17 mins as the coagulation and gravitational settling are competing with each other and the equilibrium is not yet reached. Therefore, the study is needed to be extended for more time at least up to 1 hour and the efforts are under progress.

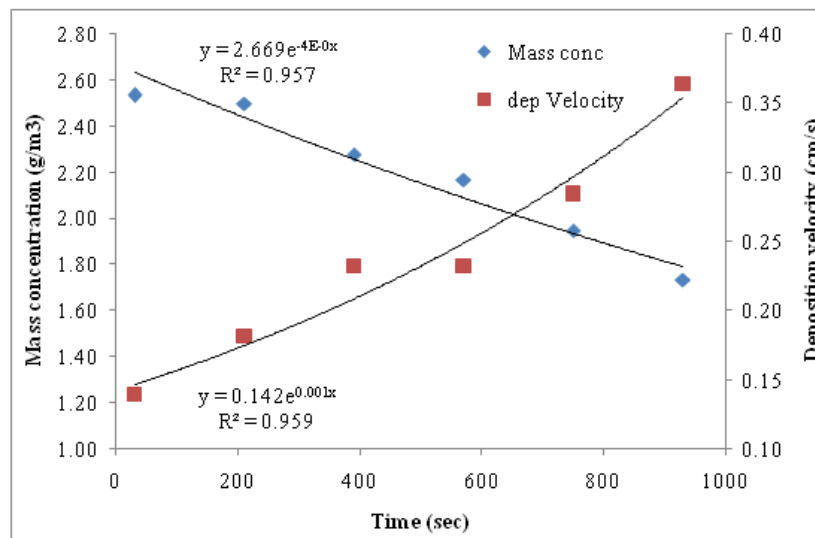


Fig.2. Variation of mass concentration and deposition velocity of mixed aerosol with time

CONCLUSIONS

This study shows that, the method adopted here is useful for quantifying both the individual and mixed aerosols to arrive at the mass deposition velocities. This provides better comparisons of the behaviour of mixed aerosol systems compared to the individuals of various size ranges and chemical species using same technique. The deposition velocity of mixed aerosols of sodium and SrO₂ observed in this study is 0.23 cm/s. Hence the mixed aerosol deposition velocity is more than that of sodium aerosol within the error associated with experimental and analytical methods. It is to be noted that, though the concentration of SrO₂ aerosols present in mixed aerosols is much smaller than sodium aerosols, the mixed aerosols deposition velocity is shown to be significantly higher than sodium aerosols. The uncertainties during sampling to chemical analysis are found to be up to 20% and the insufficient experimental time 17.15 min as the aerosol processes to reach equilibrium is need to be corrected.

REFERENCES

- M. Jamriska & L. Morawska, (2003). Quantitative Assessment of the effect of surface deposition and coagulation on the dynamics of surface deposition and coagulation on the dynamics of sub-micrometer particles indoors, *J. Aerosol Science and Technology*, 37, 425-436.
- Tencer, M. (2008). Deposition of Aerosol (“Hygroscopic Dust”) on Electronics – Mechanism and Risk, *J. Microelectronics and Reliability*, 48, 584–593.
- R. Baskaran, V. Subramanian, J. Misra, R. Indira, P. Chellapandi and Baldev Raj, (2009). Aerosol Characterization and Measurement Techniques Towards SFR Safety Studies, *IEEE Proceedings of ANIMMA International Conference Held*. ISBN No. 978-1-4244-5208-8, IEEE Catalogue No. CFP09241-CDR.
- J. Misra, V. Subramanian, Amit Kumar, R. Baskaran and B. Venkatraman, , (2013) Investigation of Aerosol Mass and Number Deposition Velocity in a Closed Chamber, *J. Aerosol and Air Quality Researc.*, 13, 680–688.

SODIUM AEROSOL LEAKAGE THROUGH CONCRETE SPECIMENS

SUJATHA P. N.^{1,2}, AMIT KUMAR¹, KALPANA KUMARI³, USHA PUJALA^{1,2},
SUBRAMANIAN V.¹, VENKATA SRINIVAS C.^{1,2}, PREETHA R.³ AND BASKARAN R.^{1,2}

¹Radiological Safety Division, Health Safety and Environment Group, IGCAR, Kalpakkam
603102, India.

²Homi Bhabha National Institute, Indira Gandhi Centre for Atomic Research, Kalpakkam
603102, India.

³Civil Engineering Group, IGCAR, Kalpakkam, Tamil Nadu –603102, India.

KEYWORDS: sodium aerosol, leak rates, concrete cracks.

INTRODUCTION

During Core Disruptive Accident (CDA) in Sodium cooled Fast Reactors (SFR), Reactor Containment Building (RCB) is bottled up with sodium, fission product, fuel aerosols and radioactive gases. Due to pressure raise in RCB, these aerosols may leak through various leak paths such as cracks, pores and failed seals and contribute to environmental source term. The leak rate of sodium aerosol and gases plays crucial role in estimating the environmental source term, which is essential for reactor safety analysis. There is also a possibility that these aerosols plug the leak paths due to deposition of aerosols in the paths and may reduce the radioactive gas leak (PFBR-PSAR, 2004). This helps in the reduction of the environmental source term and hence the radiological dose exposure to the public around the reactor vicinity.

To understand the aerosol leakage, experimental studies on aerosol leakage through various types of leak paths have been carried out in Aerosol Test Facility (ATF), RSD. Initial experiments were conducted with straight stainless steel capillaries of various dimensions. A parametric study (both experimental and theoretical) on the effect of the differential pressure across the capillary, mass concentration of aerosols, dimensions of the capillaries and relative humidity inside the aerosol chamber on the aerosol leakage behavior were carried out (Sujatha et al., 2016 and 2017). The above study provided good understanding of the plugging mechanism and aerosol leakage behavior for the given conditions. The transport of aerosol and gas through concrete crack may be different from the capillary due to difference in morphology (size, length, geometry etc) of both leak paths. In this regard, the study of sodium aerosol penetration through concrete cracks in concrete walls of RCB is needed for better understanding of the aerosol and gas leakage behavior under CDA condition. Towards this assessment of aerosol leakage rates, a simple (straight) concrete leak path and for various aerosol mass concentrations was studied. In the current paper, the details of concrete specimen preparation, experimental methodology, results and analysis are described.

MATERIAL AND METHODS

To conduct sodium aerosol leakage experiments through concrete cracks, concrete cylinders were cast with through leak paths of varying diameters simulating nearly straight cracks at concrete laboratory, Civil Engineering Group. The detailed description of concrete specimen with leak paths casting is explained below:

Fabrication of concrete specimens with leak paths

Cylindrical concrete specimens of grade M30 were prepared using ordinary portland cement (43 grade) conforming to IS 8112. The concrete mix was prepared with given specification in a drum mixer in the laboratory. The prepared concrete mix was cast in 4 cylindrical moulds (cut out from a PVC pipe) of size 9 cm internal diameter and 5 cm height in accordance with IS 516. Before setting of concrete, each specimen was fixed with a sampling tube (blue color) of 5 cm length and 0.5 cm diameter. The metal wires with diameters 640 μm , 740 μm and 820 μm were inserted into the specimen through sampling tube. The sampling tube and metal wires were positioned at the center of each of the specimens. The photograph of concrete specimens cast in cylindrical moulds is shown in Fig. 1(a) and (b). These specimens were kept in humidity chamber (90% RH) for 24 hours. Thereafter, they were cured for 28 days in the laboratory curing tank filled with water at a temperature of $28 \pm 1^\circ \text{C}$ to attain the required strength. The water temperature was maintained constant throughout the curing period. During the curing period, the metal wire inserted in each specimen was moved in and out on alternate days to ensure that a hole is formed and wire is not embedded during hydration process. Total four numbers of specimens were prepared - three concrete specimens with three metal wires of diameters, namely 640 μm , 740 μm and 820 μm and the fourth cement specimen (as standby) with 820 μm metal wire. After curing the cylindrical specimens were removed from water and dried for 2 weeks under sun. The metal wires were taken out from the specimens so that the straight holes (leak paths) in the concrete specimens were formed.



Fig. 1. Concrete specimens along with sampling tube and wire (a) Top view (b) Vertical view

Sodium aerosol leakage studies through concrete leak path

The sodium aerosol leakage experiments were conducted in ATF. The detailed description of ATF was explained elsewhere (Baskaran et al., 2004). The schematic diagram of present experimental setup is shown in Fig. 2. To begin with, concrete specimen with leak path of diameter 640 μm is attached to one of the ports of the aerosol chamber by sealing around specimen using rubber gasket around the PVC pipe, which ensures the leak tightness tested at 15 kPa pressure of aerosol chamber. A plastic pipe of length 35.5 cm and 0.5 cm diameter is connected to the sampling tube fixed in the specimen and the other end of the plastic pipe is placed in 200 ml de-ionized water contained in gas washing bottle. The conductivity of the water is continuously monitored by conductivity meter (Hanna make, Edge EC Hi2003-02).

The initial suspended mass concentration of aerosols is measured by filter paper sampling technique using 47mm filter holder and gravimetric analysis. Microbalance (Sartorius make, Secura 26 Model and Design 1) is used for weight measurements.

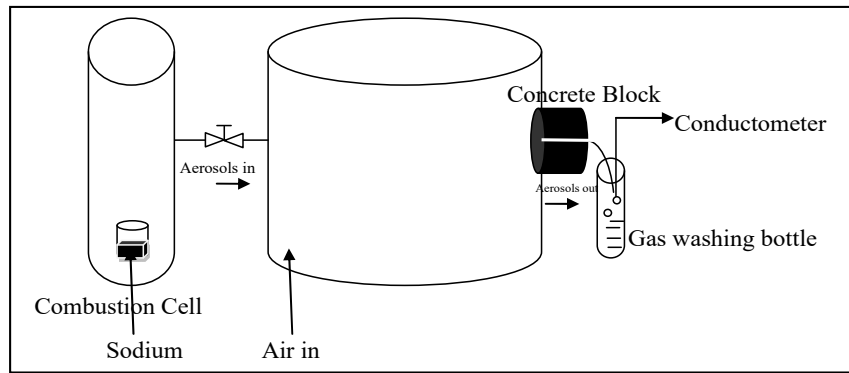


Fig. 2. Schematic diagram of aerosol leakage experiment

Air is purged in to the aerosol chamber to raise the pressure of the aerosol chamber to 10 kPa. Aerosols leak out through the leak path in the concrete specimen and pass to the gas washing bottle containing water through plastic pipe. The conductivity is correlated to sodium mass by using pre-established calibration graph. A set of experiments were performed for three specimens of different leak sizes by varying aerosol mass concentration in the range 0.5-3.5 g/m³. After the plugging of the leak path (with no change in the conductivity), the specimen was removed from the chamber. The plugged mass in the specimen was measured by washing the leak path with water and thus measuring the conductivity. To repeat the experiment with the same specimen, the specimen was dried under sun for 2-3 days. The total cumulative error in measuring aerosol mass concentration in aerosol chamber is 5-7% and the mass of the aerosols deposited in the plastic pipe is also taken into account.

RESULTS AND DISCUSSIONS

It was observed from all the experiments that as the time progresses, the cumulative aerosol mass collected in the gas washing bottle increase and becomes saturated. The time over which the cumulative aerosol mass becomes saturated is called as the plugging time. The plugging time, aerosol leaked mass and plugged mass in the leak path of concrete specimen are given in Table 1.

S.No	Leak path Diameter (μm)	Initial Mass concentration of aerosols (g/m ³)	Leaked aerosol mass (mg)	Plugged aerosol mass(mg)	Plugging time (min)
1	640	0.62	0.36	3.55	15
2	640	3.47	0.35	8.96	9
3	740	1.07	0.42	3.42	14
4	740	1.57	0.41	4.25	6
5	820	1.44	0.69	16.89	12
6	820	2.11	0.57	27.75	6

Table 1: Leaked mass and plugged mass of aerosols in the specimens.

The following inferences are drawn from the results:

- a. For fixed pressure of aerosol chamber, the leaked mass increases with the increase of leak path diameter.

- b. Plugged aerosol mass is more when compared to leaked aerosol mass for a constant leak path dimension for all initial concentration. This is due to the roughness of the concrete surface in the crack. In case of leakage studies through stainless steel capillaries (smooth), it was observed that the leaked mass is more than the plugged mass.
- c. The plugged mass of aerosol increases with the increase of leak path diameter. Larger the leak path diameter, more particles will be deposited in the crack.
- d. The plugged mass increases with increase of aerosol mass concentration for a particular leak path diameter.
- e. The plugging time decreases with increase of aerosol mass concentration for a particular leak path dimension. This may be attributed to the fact that if the concentration is high, more is the particles available for deposition and hence the leak path gets plugged faster.
- f. The initial size distribution (Mass Median Diameter-MMD) of sodium aerosols is 1.4 μm for relative humidity of 75% (Subramanian and Baskaran, 2007). Further, the size of aerosols increases in aerosol chamber with progress of time due to coagulation and hygroscopic nature of aerosols (Amit et al., 2015). This would result in the faster plugging of leak path.

Summary

The concrete specimens with three different leak path diameters namely 640 μm , 740 μm and 820 μm were cast at Concrete laboratory and the specimens were used for aerosol leakage experiments. The preparation of concrete specimens was standardized and would be used for future experiments. The effect of dimension of the leak path and the mass concentration of aerosols on the plugged mass, leaked mass and plugging time was studied. The results showed that for fixed pressure of aerosol chamber, the leaked mass and plugged mass increases with the increase of leak path diameter. The plugged aerosol mass in the leak path is more compared to leaked aerosol mass for a constant leak path dimension. This gives an understanding of aerosol leakage through concrete cracks under accidental conditions.

REFERENCES

- Amit Kumar, Subramanian, V., Baskaran, R. and Venkatraman, B. (2015). Size Evolution of Sodium Combustion Aerosol with Various RH%, *Aerosol and Air Quality Research*, 15: 2270–2276.
- Baskaran R., Selvakumaran T. S., and Subramanian V. (2004). Aerosol Test Facility for Fast Reactor Safety Studies, *Indian J. Pure Appl. Phys.*, 42, 873-878.
- PFBR Preliminary safety analysis report, PFBR-PSAR (2004). Chapter 15 Engineered safety features to mitigate accidents.
- Subramanian, V., Baskaran, R. (2007). Initial Size Distribution of Sodium Combustion Aerosols, *Nucl. Technol.*, 160, 308.
- Sujatha P.N., Amit Kumar, Usha Pujala, Subramanian V., and Baskaran R, Effect of pressure on sodium aerosol leakage through capillaries, *IASTA-2016*, PRL, Ahmedabad, pp. 523-526.
- Sujatha P.N., Amit Kumar, Usha Pujala, R.AnanthaNarayan, Subramanian V., Baskaran R.,

Venkatraman,B. (2017). Parametric studies on aerosol leakage through capillaries,
IGC/HSEG/RSD/
RIAS/92614/FR/3036/REV – A.

STUDIES ON CHEMICAL BEHAVIOR OF SODIUM FIRE AEROSOL IN CLOSED AND OPEN ENVIRONMENT

V. SUBRAMANIAN, AMIT KUMAR AND R. BASKARAN

Radiological Safety Division, Indira Gandhi Centre for Atomic Research, HBNI, Kalpakkam-603102, India.

KEYWORDS: Sodium Fire Aerosol, Sodium Carbonation, Chemical Speciation

INTRODUCTION

Sodium cooled Fast Reactors (SFR's) and any research facility warrant safety with respect to sodium fire aerosols and its chemical hazard particularly the toxicological impact on environment, occupational workers and to the public. The sodium fire aerosols are mainly composed of sodium oxide (Na_2O) or higher oxides of sodium (Na_2O_2 and NaO_2) depending upon the ratio of sodium to oxygen available during the onset of sodium fire (Sophy et al., 1982). Sodium aerosol carbonation is the process in which, sodium combustion aerosols (sodium oxide) is getting converted into hydroxide, carbonate and finally to bicarbonate upon reaction with atmospheric air moisture and CO_2 (Clough and Garland, 1971). The conversion of sodium oxide to hydroxide aerosol take less than millisecond (Cooper, 1980) while hydroxide to carbonate and finally to bicarbonate takes few tens of second to few tens of minute depending upon the experimental conditions such as aerosols concentration, particle characteristics (size, density and porosity), Relative Humidity (RH) and CO_2 concentration available at reaction time. The chemical hazard due to sodium fire aerosol involves quantification of many parameters such as spatio-temporal and physo-chemical behavior of aerosols.

In this context, many experiments on carbonation of sodium fire aerosol were carried out in different condition (sodium amount, pool, spray fire, inside closed volume and open atmosphere) across the world. At higher RH (more than 40%) and wind velocity 2 m/s, the sodium fire aerosols are bicarbonate form at more than 120 m distance from the release point (Bunz et al., 1979, and Hofmann et al., 1979). The conversion of NaOH to Na_2CO_3 takes second for 0.1 μm size and taken several minutes for 10 μm (Ramsdale S. A., 1989). The NaOH aerosols convert to Na_2CO_3 in free atmosphere and the chemical conversion from NaOH to Na_2CO_3 is 5 times faster at 50% relative humidity when compared to 5% and the small aerosol have higher carbonate than large particle (Chardon and Jordon, 1989). In recent time, experimental studies on chemical behavior of sodium fire aerosol is carried out at Aerosol Test Facility (ATF) (Subramanian et al., 2009) and theoretical study by Gilardi and co-worker (Gilardi et al., 2013). The chemical kinetic model based on "reactive absorption CO_2 in the core of NaOH " was developed by Gilardi et al., and validation of model carried out by ATF experimental data (Plantamp et al., 2016 and Subramanian et al., 2014). The studies on real time chemical species of aerosol generated in sodium fire with variation of relative humidity and CO_2 concentration carried out by Ananthanarayan et al., and found that higher humidity promotes carbonation process faster. The ratio of NaOH to Na_2CO_3 is more when CO_2 concentration is less (Ananthanarayan et al., 2015). The NaHCO_3 is not found 30 - 60 minute from the initial ejection of aerosol in closed environment (ATF).

In the open atmosphere dispersion of sodium fire aerosol showed that, the aerosols are found in the form of bicarbonate (NaHCO_3) for wind speed 5-8 m/s, relative humidity 50-80% and sodium aerosol release rate of 5-8 g/s (Baskaran et al., 2016). Srinivas et al., incorporated chemical

conversion factor into the dispersion model and found that for the aerosol release rate 8.2g/s with the size of aerosol (MMD) - 4.0 μm and density of aerosol as NaOH (2.23 g/m^3), nearly complete conversion of NaOH aerosol to Na_2CO_3 occurs after 300 m distance (Srinivas et. al., 2018).

It is interesting to note here that there exists progressive conversion of sodium hydroxide into carbonate (Na_2CO_3) when the experiments are conducted in closed environment (ATF), while in the open environment the experiment showed that species is bicarbonate (NaHCO_3) even at shorter distance and less than 100 s. The conversion of bicarbonate in the open atmosphere is due to unlimited availability of moisture and CO_2 , when the aerosols are dispersed in the open atmosphere and become converted while travelling in the downwind distance. Hence it is customary to show that depletion of concentration of CO_2 and moisture under closed environment with progress of time when carbonation is in progress under closed environment. Experiments are carried out for evaluation of CO_2 content, Relative Humidity and chemical nature of sodium aerosol in closed environment with progress of time during sodium aerosol carbonation process and the results are presented in this paper.

MATERIAL AND METHODS

Sodium aerosols are generated under controlled atmosphere and bottled-up in a closed environment at ATF. The detailed description of ATF, aerosol generation system, Data Acquisition System (DAS), aerosol diagnostics equipments and various sensors (temperature, humidity, pressure etc.) are explained elsewhere (Amit Kumar, Ph.D, 2017 and Baskaran et al., 2004). The environment is kept at a desired RH% and CO_2 content for the conduction of the experiment. The RH% is adjusted by using a humidifier (bubbling through water column or passing through silica gel column). Dehumidification of the chamber below 40% is achieved by blowing hot air inside the chamber while discharging the chamber air through exhaust. Thus RH% can be adjusted from 20% to 90% inside the chamber. The RH% is continuously monitored on-line by using Humidity monitor (capacitance type) (Make: Rotronics, INC, USA – HC2 series) inserted into the chamber. The Relative humidity data continuously recorded in DAS and display to computer monitor. The CO_2 content is kept at the ambient atmospheric content ($\sim 380\text{ppm}$) or purged with nitrogen in order to reduce the content by 100ppm. The CO_2 content is measured on line by using CO_2 analyzer (M/s Prism Gas Detection Pvt. Ltd., Mumbai and Model No., GA-150).The aerosols from the chamber are made to bubble through a water column filled in the gas washing bottle. The water column removes the sodium aerosols and the air is passed into the gas analyzer.

The parameters like quantity of sodium and duration of combustion is adjusted to get the initial mass concentration of 3 to 3.5 g/m^3 for the experiments. The initial aerosol mass concentration is measured using filter paper sampling arrangement and gravimetric analysis. The chemical nature of sodium combustion aerosol is analyzed by conductometric titration methods, the details of the techniques is explained in our earlier work (Subramanian et al., 2009 and Ananthanarayan et. al., 2015).

RESULTS AND DISCUSSION

The experiments were conducted by keeping the aerosol chamber at three different relative humidity conditions viz 90%, 50% and 20% and maintaining CO_2 content inside the aerosol chamber at 380 ppm. Fig. 1 shows the depletion trend of NaOH content with progress of time during carbonation of sodium aerosols inside the aerosol chamber. It is observed from Fig. 1 that, in the case 90% RH, the initial formation of NaOH is 80%, while it is 53 and 58% in the case of 50% RH and 20% RH respectively. The NaOH content formed at 90% RH condition is due to presence of higher moisture content in the atmosphere, whereas, formed content of NaOH in 50%

and 20% is almost same, since there is no enhanced content of moisture and the considerable part of oxide is converted into carbonate upon gas phase reaction with CO_2 . In 90% RH case, since NaOH fraction is more, and the particle is of solution of NaOH, which enhances the diffusion of CO_2 on to the particle, resulting the quantity of CO_2 consumed is also large. The reduction of CO_2 content inside the aerosol chamber is shown in Fig.2. The CO_2 content in the aerosol chamber reduces to 70 ppm in 10 minutes (Fig. 2). In the case of 50% and 20% RH conditions, the progress of carbonation is almost equal upto the sample collected between 20-21 minute and gets completed in 60-61 minute with slight difference in the sample collected in 30-31 minute. The marginal difference in the curves in Fig.1, for 50% and 20% RH conditions is attributed to the variation in diffusion of CO_2 on to the particle due to particle porosity and density (the curve for 50%RH condition is below that of 20% RH condition). In all the cases, at the end of carbonation, the CO_2 content in the chamber reduced between 30-60 ppm. The variation of RH% inside the aerosol chamber with progress of time is shown in Fig.3. It is observed in Fig.3, that, in all the cases the RH% content begins to fall in the initial period of time and then begin to rise slowly. In case of 90% RH condition, the RH content reduces to 75% in about 40 minutes and slowly begin to rise. In case of 50% RH condition, the RH content reduces to 37% in 20 minutes and slowly begin to rise.

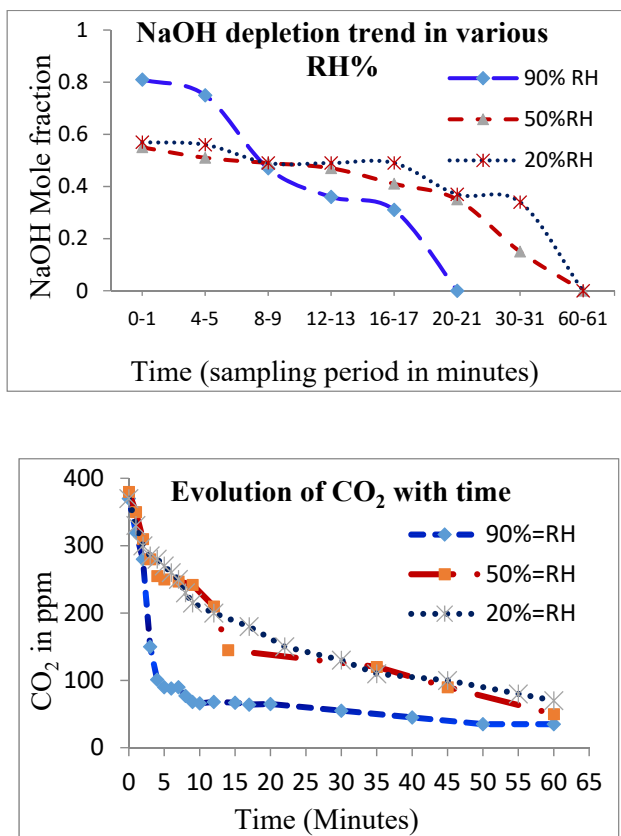


Fig.1 Depletion of NaOH in carbonation of aerosols, Fig.2 Evolution of CO_2 content in aerosol chamber.

Similarly, in case of 20% RH condition, the RH content reduces to 12% in 5 minutes and then slowly begins to rise. The reduction in the initial period of time shows (i) the initial formation of NaOH aerosols by reaction of oxygen and air released from the combustion cell, (ii) chemical reaction to form carbonate by absorption of CO_2 and (iii) finally bi-carbonate by absorption of CO_2 and moisture. All above chemical reactions are exothermic which rise the temperature of the

surrounding gas. Apart from chemical reaction, the sodium aerosols are hygroscopic in nature which having tendency to absorb the moisture (Amit et al., 2015). The rise in RH content in the latter period may be attributed to condensation of moisture inside the chamber due to cooling from outside.

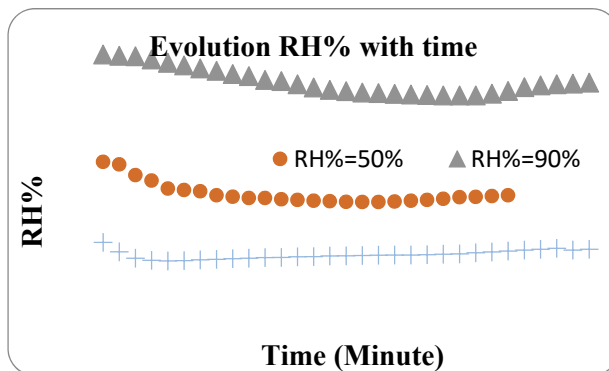


Fig.3 Evolution of RH% in aerosol chamber.

In the case of closed environments, it is clear from the above study the relative humidity, CO₂ and aerosol concentration depleted over a period of time. But in open atmospheric condition, the relative humidity and CO₂ concentration is almost constant. The progress of carbonation is faster since the availability of reactive species viz. moisture and CO₂ are unlimited in open environments and the concentration of the aerosols are very low due to dilution and dispersion of sodium plume. While in closed environments the aerosol concentration is high and moisture and CO₂ also getting reduced due to carbonation process. The carbonation of sodium aerosol is slower in closed environment when comparison to open environment experiments.

SUMMARY

It is concluded from experiment that carbonation of sodium aerosol is completed with available atmospheric CO₂. Carbonation is faster in high humid condition, which reduce the chemical toxicity due to the reduction of hydroxide. The evolution of CO₂ content with progress of time during carbonation of sodium aerosols shows agreement with the experimental observation of carbonation trend and with observed mole fractions of hydroxide and carbonate species. The RH% in the chamber reduces during the initial period of time as soon as the aerosols are fed inside and shows marginal rise afterwards. The rise in RH% content is due to condensation effect. The work is very useful to understand the availability of relative concentration of the reactive species and final product. The quantification of species is useful in developing a revised model taking into account of reacting environment.

FUTURE WORK

The experiment will be carried out to simulate the open atmospheric condition in ATF and validate our experimental result for atmospheric condition.

REFERENCES

Amit Kumar (2016), "Sodium metal aerosol characterization in cover gas region", Ph.D thesis, HBNI.

- Amit Kumar, Subramanian V., Baskaran R, and Venkatraman B. (2015), "Size Evolution of sodium combustion aerosol with various RH%", *Aerosol and Air Quality Research*, 15, 2270 - 2276 (2015).
- Ananthanarayanan R., Subramanian V., Sahoo P., Misra J., Kumar A., Baskaran R., Venkatraman B., and Murali N. (2015), "Experimental Investigations on Carbonation of Sodium Aerosol Generated from Sodium Fire in the Context of Fast Reactor Safety", *Annals of Nuclear Energy*, 80, 188–194.
- Baskaran R., Selvakumaran T. S. and Subramanian V. (2004), "Aerosol Test Facility for Fast Reactor Safety Studies", *Indian J. Pure Appl. Phys.*, 42, 873-878.
- Bunz H., Jordan S. and Lindner W. (1979), "The behavior of sodium fire aerosols, "International Working Group on Fast Reactors, Vienna (Austria); 25, 9 p-71-75.
- Chardon W. and Jordon S. (1989), "Aerosol release from sodium fires and their consequences for reactor components", *Specialists' meeting on sodium fires, Physics and Power Engineering Institute, Obninsk (USSR)*, 342, p. 43-56.
- Clough W.S. and Garland J.A. (1971), "The behavior in the atmosphere of the aerosol from a sodium fire", *Journal Nuclear Energy*, 25, 425-435, 1971.
- Cooper D.W. (1980), " Prediction of the rates of chemical transformation of sodium fire aerosols", *Proceedings of the CSNI specialists meeting on nuclear aerosols in reactor safety*, 181-195.
- Gilardi, T., Chassery, A., Baskaran, R., Subramanian, V., Latge, C. and Perrais, C. (2013), "Modelling of the Chemical Behavior of Sodium Fire Aerosols during Atmospheric Dispersion", *Proceedings of the International Conference on Fast Reactors and Related Fuels, IAEA, March, Paris. 4-7 Mar 2013.*
- Hofmann Ch., Jordon S. and Lindner W. (1979), "Chemical reaction of sodium fire aerosol in the free atmosphere", *Journal of aerosol science*, 10, 191-192.
- Plantamp A., Gilardi A., Muhr H. and Perrais C. (2016), "Modeling of the chemical behavior of sodium fire aerosols during atmospheric dispersion", *Aerosol Science and Technology*, 50, 705–716.
- Ramsdale S.A. (1989), "The chemical conversion and dispersion of toxic sodium fire aerosol in the atmosphere", *Journal of Aerosol Science*, 20, 1401-1404.
- Sophy Y., Loubriat, Bentz, A., Gerosa, A., Freslon and Piatti, U. (1982), "The ESMEALDA project for studying extensive sodium fire", *International topical meeting on LMFBR safety, Lyon (France); 19-23 Jul 1982.*

Srinivas C. V., Subramanian V., Amit Kumar, Usha P., Sujatha P.N., Baskaran R. and Venkatraman B. (2018). Modelling on Atmospheric dispersion of sodium aerosol for consequence analysis during accident leaks.IARP- 2018.

Subramanian V., Sahoo P., Malathi N., Ananthanarayanan R., Baskaran R., and Saha B. (2009), "Studies on Chemical Speciation of Sodium Aerosols Produced in Sodium Fire", Nuclear Technology, 165, 257–269.

Subramanian V., Kumar A., Ananthanarayanan R., Sahoo P., Baskaran R. and Venkatraman B. (2014), "Sodium aerosol carbonation – experimental results and phenomenological modeling", Proceeding of Indian Aerosol Science and Technology Association, 154-156.

Baskaran R., Subramanian V., Amit Kumar, Gopalakrishnan V., Srinivas C.V., Bhagavat Singh, Usha Pujala, Sujatha N., Krishnakumar S., Chandramouli S., Ashok Kumar A., Anathanarayanan R., Nashine B.K. and Venkatraman B. (2016), "Sodium aerosol dispersion experiments in open environment for Environmental Impact Assessment Studies", IGC - 342.

COMPARISON OF SODIUM METAL AEROSOL CHARACTERISTICS IN INERT GAS

AMIT KUMAR, SUJATHA P.N., USHA PUJALA, SUBRAMANIAN V., SRINIVAS C.V.
AND BASKARAN R.

Radiological Safety Division, Indira Gandhi Centre for Atomic Research, HBNI, Kalpakkam-
603102 INDIA.

KEYWORDS: Sodium metal aerosol, cover gas, sodium cooled fast reactor

INTRODUCTION

In Sodium cooled Fast Breeder Reactor (SFR) Argon gas is used as cover gas between sodium pool surface and top shield. The Argon gas is replaced with helium gas in cover gas region by more than 70 to 80% when Fast Breeder Test Reactor (FBTR) is in operating condition. The temperature of top shield is maintained at 120°C and sodium pool temperature varies from 200°C to 550°C depending upon whether the reactor is in operation or shutdown condition. The pressure of argon cover gas is kept at 0.35 kPa above atmosphere and temperature of argon gas depends on sodium pool temperature. The evaporation of sodium from the pool surface and subsequent condensation in the cover gas region produce sodium aerosols. The characteristics of sodium aerosols in cover gas region has been studied in our earlier work and reported (Amit et al., 2015 and 2016)

In SFR, the main vessel is covered by safety vessel to withhold sodium in the event of leakage from the main vessel and to ensure safe sodium level in the main vessel. Nitrogen gas is used between main and safety vessels to prevent sodium fire and resultant generation of radioactive aerosols in case of sodium leaks from main to safety vessel. The total volume of nitrogen filled in the space between main and safety vessel is 276m³ (Revathy et al., 2017). The expected temperature of leaked sodium from main vessel to safety vessel ranges from 180°C - 400°C depending on the state of reactor (normal operation or shutdown). The temperature of nitrogen gas during various reactor operating conditions varies from 100°C to 380°C. The pressure inside the nitrogen gas space is 104±0.5kPa and 100.5±0.3kPa during normal operation and fuel handling (Revathy et al., 2017). In the event of leakage of sodium, it forms sodium pool depending upon leaked quantity at the lowest part of the space. The sodium evaporates from the pool surface and starts condensing to form sodium metal aerosol in the nitrogen gas space which is to be detected for safety purposes. In this regard, apart from other method (gamma radiation detector), the utilization of Sodium Ions Detection (SID) is one of the important options to detect the presence of sodium metal aerosols. The feasibility of SID in detecting the sodium aerosols will be qualified by estimating the sodium metal aerosol characteristics in the nitrogen gas space for various sodium pool temperatures. In this context, a series of experiments were carried out in TP-1 of SILVERINA loop with various sodium pool temperatures in argon and nitrogen cover gas region and results were analyzed for sodium metal aerosol characteristics for various sodium pool temperature. In this paper, the details of experiments carried out in argon and nitrogen gas space, experimental set-up for aerosol sampling, results and analysis, the comparison of sodium aerosol in argon, nitrogen and helium, conclusion and future work are presented in detail.

MATERIAL AND METHODS

The experiments are conducted in Test Pot-1 of SILVERINA loop at FRTG for both gas argon and nitrogen. The details of TP-1 and SILVERINA loop is explained elsewhere (Amit et. al., 2015). The TP-1 vessel is filled with liquid sodium before start of the experiment. The sodium level in the test post is maintained at the required level by using discrete type of level sensor. The pressure of cover gas region and height of the cover gas space is 0.35 bar above atmosphere and 800 mm respectively which are maintained in all the experiments. The diameter of the sodium pool is 762 mm. The sodium aerosol sample is drawn from near the top flange (200 mm from the top flange) through sampling line. The sampling flow rate is fixed for all experimental runs at 2 lpm and the sampling time is varied according to sodium pool temperature. The cover gas along with suspended sodium metal aerosol sampled through sodium metal aerosol sampling system and characterization is carried out at Aerosol Test Facility (ATF). The details of sampling and characterization techniques of sodium metal aerosol in argon gas region are explained in our earlier work (Amit et. al., 2014). The sodium metal aerosol characteristics in argon gas space for pool temperatures in the range 250°C to 550°C are explained in our earlier work (Amit et. al., 2015) and used for comparison. The experiments for sodium aerosol characterization in nitrogen gas are carried out for sodium pool temperatures 150°C to 400°C. The results of experiments and analysis of sodium aerosol characteristics in nitrogen gas are discussed and compared with that of argon and helium gas.

RESULTS AND ANALYSIS

The measured sodium metal aerosol characteristics (mass concentration and size distribution) in argon and nitrogen cover gas of TP-1 in SILVERINA loop is given in table 1 and 2 respectively. The sodium metal aerosol mass concentration and size (MMD) in cover gas region increases with increase of sodium pool temperature for both gas. The difference of aerosol mass concentration in argon and nitrogen gas increases with increase of sodium pool temperature. In case 150 and 200°C sodium pool temperature, the aerosol size is not observed, it may be due to low aerosol concentration in the sample. The sodium aerosol size distribution for both argon and nitrogen cover gas region for sodium pool temperature 300 and 400°C is shown in Fig.1. The distribution is found to be similar pattern. The mode of size - distribution is shifted to the larger size range and size-distribution has become wider for nitrogen gas when compared to the argon gas case. The MMD of sodium aerosol presence in nitrogen gas is large when compared to the argon gas for sodium pool temperature 300 and 400 °C (see table 1 and 2). The

standard deviation of the MMD progressively increased when the sodium pool temperature increases from 300 to 400°C for both the cover gases (argon and nitrogen).

Tp (°C)	MMD (μm)	C (g/m ³)	Tp (°C)	MMD (μm)	C (g/m ³)
250	1.52	0.04	150	--	0.01
300	2.92	0.28	200	--	0.03
350	3.95	1.32	300	5.71	0.13
400	5.10	4.29	400	7.11	1.92
450	5.92	10.52			
500	8.07	14.66			
550	9.62	26.83			

Table 2 Sodium aerosol characteristics in nitrogen gas.

Table 1. Sodium aerosol characteristics in argon gas.

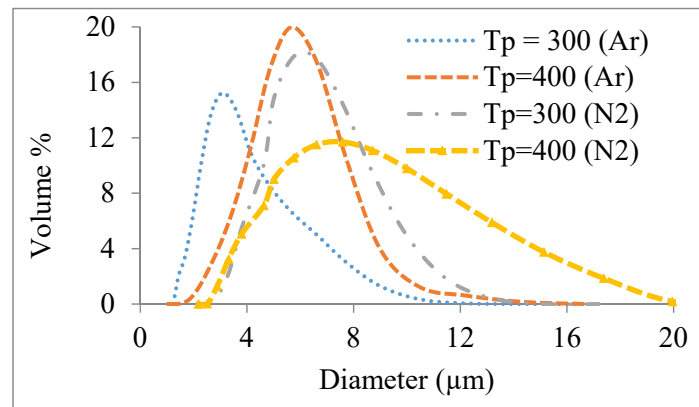


Fig. 1 Comparison of volume - size distribution of sodium aerosol in argon and nitrogen gas.

It is well known from the experience of French Rapsodie reactor that aerosol formation is reduced if helium is used as cover gas. Similar studies on sodium aerosol characteristics in cover gas of argon and helium were carried out by Minges in 1993. He reported that, the aerosol mass concentration is more in argon gas as compared to the helium gas for fixed sodium pool temperature and cover gas height. He has explained that, the difference in aerosol formation in argon and helium is due to temperature gradient between sodium pool surface and cover gas (or top shield). The temperature gradient between

sodium pool surface and top shield is more for argon as compared to nitrogen and then to helium due to the thermal conductivity of Helium > Nitrogen > Argon. The aerosol is formed in the cover gas region during convection when super saturation occurs. The mixture of argon gas and sodium vapor has specific weight lower than that of the argon alone, which enhances the convection. The opposite happens in the case of helium gas, the convection will be suppressed. The convection is the main sodium transport mechanism in argon but diffusion is more important in some situation with helium (Hotchkiss et al., 1997). Similarly, in the case of nitrogen, the convection is less than that of argon but more than that of helium because specific weight of (nitrogen + sodium) is less than (argon + sodium) and greater than (helium + sodium). The major difference between argon and helium cover gas is the dependence of density of the sodium saturated gas on the respective gas medium and its temperature at that place. The higher temperature gradient in the case of argon favors the super saturation of sodium vapors thereby resulting in higher aerosol concentration.

CONCLUSION

The characteristics of sodium metal aerosols are studied in TP-1 of SILVERINA loop for argon and nitrogen as cover gas. The comparison of sodium aerosol characteristics in argon and nitrogen gas is carried out. The sodium aerosol mass concentration and size (MMD) increases with the increase of sodium pool temperature for argon and nitrogen gases. The aerosol mass concentration is more for argon gas when compared to nitrogen for a particular sodium pool temperature. The aerosol size (MMD) is large in nitrogen gas compared to argon gas. A comparison of aerosol characteristics is carried out for Argon, nitrogen and Helium (based on available literature). The aerosol mass concentration is more in argon due to enhanced natural convection of argon in the presence of aerosol when compared to nitrogen and helium in presence of aerosols.

ACKNOWLEDGMENT

The authors wish to acknowledge the S. Chandramouli, S. Krishnakumar and FRTG control room staffs of SILVERINA loop for their help in conducting the experiments.

REFERENCES

Amit Kumar, Subramanian V., Baskaran R., Krishnakumar S., Chandramouli S. and Venkatraman B., "Development and validation of methodology for characterization of sodium aerosols in cover gas

region”, *Aerosol and Air Quality Research*, Vol. 14, No. 5, pp.1534-1541, 2014.

Amit Kumar, Subramanian V., Krishnakumar S., Baskaran R., Chandramouli S. and Venkatraman B., “Characterization of sodium aerosol in cover gas T. region of SILVERINA loop”, *Aerosol and Air Quality Research*, Vol. 15, U. No. 5, pp. 1813 - 1822, 2015.

Amit Kumar, Subramanian V., Krishnakumar S., Baskaran R., Chandramouli S. and Venkatraman B., “Studies on Geometrical effect on sodium aerosol T. characteristics in cover gas region”, *Aerosol and Air Quality U. Research*, Vol.16, No. 8, pp.1832-1840, 2016.

Amit Kumar, Subramanian V., Baskaran R., and Venkatraman B., “Effect of Gamma radiation on sodium aerosol characteristics in cover gas region”, Proceedings of the 32nd International Conference on Radiological Safety in Workplace, Nuclear facilities and Environment (IARPIC-2016), February 22-25, 2016, Convection Centre, DAE Township Anupuram, 603127, Tamilnadu, India.

Amit Kumar, Subramanian V., Ajay Rawat, Srinivas C. V., Baskaran R. and Venkatraman B. “Theoretical estimation of radiation induced charging Of sodium metal aerosol in argon cover gas environment”, Proceedings of National Symposium (NSRP-21), March 5-7, 2018, Raja Ramanna Centre for Advance Technology (RRCAT), Indore - 452013, India.

Hotchkiss, R. C., and Roberts, R. A, "Sodium deposition from fast reactor gas blankets - factors influencing the choice of argon or helium cover gas optimization of sodium-cooled fast reactors", Proceedings of the international conference organized by the British Nuclear Energy Society in London, 28 November - 1 December 1977.

Minges J. and Schutz W., "NACOWA experiments on LMFBR cover gas aerosols, heat transfer and fission product enrichment", Report No.: KfK 5250, December 1993.

Revathy S., Anbuchelian M., Krishnakumar S., Amit Kumar, Subramanian V., Chandramouli S., Sylvia J.I., Babu B., Baskaran R., Nashine B.K., Venkatraman B. and Selvaraj P., "Testing of sodium aerosol detector in nitrogen environment", IGC/FRTG/SFG/DD&RSD /RIS/99130/EX/3038/REV-A.

ANALYSIS OF MIXED NaK AEROSOLS BY ION CHROMATOGRAPHY

R. ANANTHANARAYANAN¹, AMIT KUMAR², V.SUBRAMANIAN²,
M.SIVARAMAKRISHNA¹, R.BASKARAN² AND B.K.PANIGRAHI¹

¹Innovative Sensors Section, IGCAR, Kalpakkam – 603102, India.

²Radiological Safety Division, IGCAR, Kalpakkam – 603102, India.

KEYWORDS: Mixed Aerosol, Ion Chromatograph, Sodium-Potassium Aerosol, Liquid metal combustion.

INTRODUCTION

Qualitative and quantitative information on sodium aerosols is very important from fast reactor safety point of view (Subramanian et al., 2008). For a proper hazard evaluation chemical technique employed to assay these aerosols should be highly reliable. In particular, in case of mixed aerosol species quantification should be precise and accurate and preferably rapid. In one of the mixed aerosol condition like NaK, the use of Ion chromatography (IC) is explored and it is a versatile technique having many salient features such as (i) simultaneous assay of multiple ions, (ii) trace assay of most ions down to few $\mu\text{g/L}$, (iii) short analysis times (usually <20 minutes) and (iv) applicable to variety of sample matrices.

NaK is a sodium potassium alloy formed by mixing 78% potassium and 28% Na. Many desirable properties of NaK such as high boiling point (785°C), low vapour pressure, ability to remain in liquid state at room temperature, compatibility with structural materials makes it a suitable coolant in fast reactors such as Dounreay fast reactor (Chan, 1993). It is used in cold trap of Fast Breeder Test Reactor at Kalpakkam, India. NaK is hazardous due to its high chemical reactivity and care is required for its safe disposal. At IGCAR 50 Liters of NaK was disposed by pool combustion method (Subramanian, 2016). Aerosols were collected at different locations from the release point and were quantified for their speciation using IC.

IC used for analysis was completely developed in house. Conductivity detector, which constitutes an important component of IC, is based on pulsating sensor (Ananthanarayanan et al., 2012). Pulsating sensors are of four types, namely, conductivity based, dielectric based, inductance based and emf based (Sahoo et al., 2010). Unlike commercially available sensors the first electronic response is in digital domain in the form of rectangular pulses of 5V magnitude and hence these sensors greatly simplify the instrumentation. In this paper the detailed description of simultaneous

quantification of sodium and potassium ions in NaK compound aerosols using IC is presented.

METHODS

An in-house developed IC was used to quantify sodium and potassium ions in aerosol samples collected from the combustion of NaK alloy. The IC consists of (i) an eluent reservoir, (ii) Rheodyne valve with 100 μL loop (iii) high pressure pump, (iv) 4 mm x 300 mm (internal diameter (ID) x length) separator column, (v) 6 x 150 mm suppressor column filled with Dowex 1x8 resin in hydroxide form, (vi) a pulsating type conductivity detector and (vii) a Graphical User Interface (GUI) to record the chromatograms.

50 liters of NaK was burnt at Fast Reactor Test Group disposal yard. Burning of NaK produced large amount of sodium and potassium compound aerosols. Aerosol samples were collected at various distances from the source point in downward wind direction, on filter papers using large volume air samplers. Aerosols deposited on the filter papers were carefully transferred to de-ionized water by crushing the filter paper in water. Water enriched with aerosols was transferred to a volumetric flask. The process was repeated several times using small quantities of water till the background conductivity reached conductivity of crushed blank filter paper which is $< 10 \mu\text{Scm}^{-1}$. The final solution was made up to 25 mL for all the samples.

RESULTS & DISCUSSIONS

A low capacity pellicular cation exchange resin was used in the separator column. The resin was synthesized in-house and its capacity was experimentally determined to be $35\mu\text{eq/g}$. Based on initial studies, the optimized conditions for complete baseline separation was determined. For all analysis a sample loop of 100 μL and 10mM methane sulphonic acid at a flow rate of 1mL/min was used. Figure 1 shows a typical chromatogram generated for one of the aerosol samples.

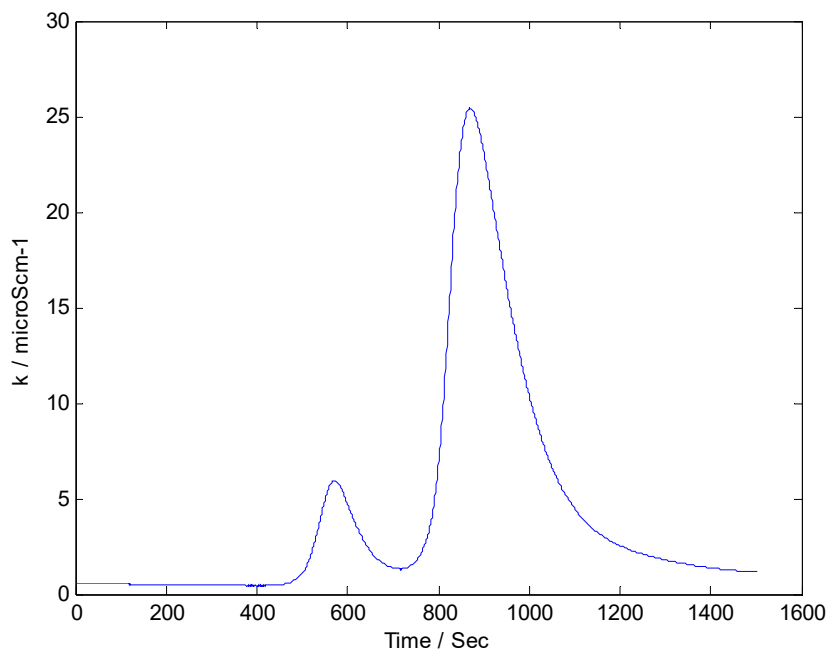


Figure 1. Typical chromatogram of an aerosol sample showing the separation of sodium and potassium ions. First and second peaks are due to Na^+ and K^+ ions respectively.

From the figure it is seen that complete baseline separation of the two ions, namely, sodium and potassium, is achieved. The smaller peak is due to sodium ions while the larger peak is due to potassium ions. The individual peak positions were identified by injecting the ions separately. In order to quantify the two cations calibration curves were generated by injecting standards containing sodium and potassium. Peak area under the curve as a function of concentration for sodium and potassium ions are shown in figure 2(a) and figure 2(b) respectively. Anion analysis was carried out by pulsating conductometric titration technique (Ananthanarayanan et al., 2015) which gives accurate quantification of various species present on the filter paper. The results of the experimental campaign is presented in table 1. Aerosol samples were collected at a distance of about 10m from the burning location for three different durations. It is observed from the table that chemical analysis of NaK aerosols shows the presence of sodium carbonate, sodium bicarbonate, potassium carbonate and potassium bicarbonate. In sample A, 6.84 mg of bicarbonate is divided between 82% K and 18% of Na. In sample B, the mass of both K (92%) and Na (8%) existed in carbonate and bicarbonate forms. In sample C both K (94%) and Na (6%) existed in

carbonate and bicarbonate forms. The presence of higher content of bicarbonate is due to the progressive conversion of carbonate species in the filter paper reacting with moisture content in the air which is pulled by the sampler. It is to be noted that sampler is pulling not only the aerosols but also the air surrounding the sampler.

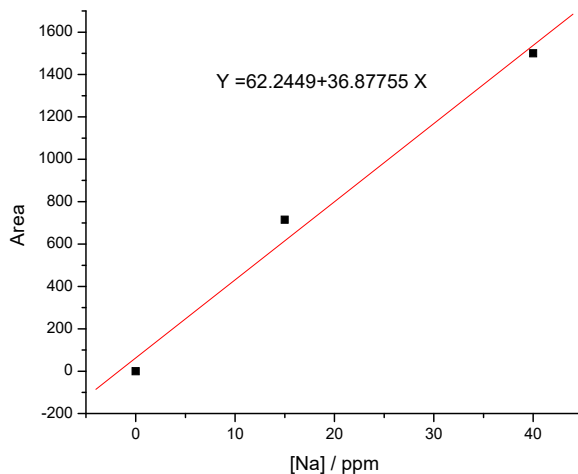


Figure 2. Calibration curve generated for (a) sodium ion and (b) potassium ion

Sl.no	Sample designation	Conc Na / mg	Conc K /mg	Conc CO ₃ ²⁻ /mg	Conc HCO ₃ ⁻¹ / mg
1.	Sample A (2 minutes sampling time)	0.733	3.3418	-	6.84
2.	Sample B (10 minutes sampling time)	5.63	70.93	36.0	65.73
3.	Sample C(40 minutes sampling time)	7.08	112.32	54.72	112.24

Table 1. Quantification of various species present in the aerosol samples. Anions were analyzed by conductometric titration technique.

CONCLUSIONS

Simultaneous determination of sodium and potassium aerosols is achieved with in-house developed IC. Use of 10mM methane sulphonic acid at a flow rate of 1mL/min gave complete base line separation. It takes about 25 minutes for each analysis. The anionic species present in the aerosols were quantified by conductometric titration technique.

ACKNOWLEDGEMENTS

The authors acknowledge Dr. B. Venkatraman, Director Health and Safety Engineering Group and Shri. Prabakar Rao, Head, Security and Innovative Sensors Division for their constant encouragement and support. Authors acknowledge the help of Shri Chandramouli for ensuring safe handling of NaK alloy and Shri M.Manogaran's for his help in chemical analysis.

REFERENCES

Ananthanarayanan. R, Sahoo. P, Murali. N (2012). Digital conductometry for determination of boron in light water and heavy water at trace levels, *Indian J. Chem. Technol.* 19, 278.

Ananthanarayanan. R, Subramanian. V, Sahoo. P, Misra. J, Amit Patel, Murali. N, Venkatraman. B (2015) Experimental investigations on carbonation of sodium aerosols generated from sodium fire in the context of fast reactor safety, *Ann. Nucl. Energy* 80, 188.

Chan, S.H.(1993). Multiphase turbulent liquid metal fuel combustion, *Prog. Energy Combust. Sci.* 19, 105.

Sahoo. P, Ananthanarayanan. R, Malathi. N, Rajiniganth. M.P, Murali.N, Swaminathan.P. (2010) Pulsating potentiometric titration technique for assay of dissolved oxygen in water at trace level, *Anal. Chim. Acta* 669, 17.

Subramanian. V (2016). Aerosol characterization in sodium-potassium alloy disposal in open atmosphere, IASTA-2016, Ahmedabad.

Subramanian. V, Sahoo. P, Malathi. N, Ananthanarayanan. R, Baskaran. R, Saha. B (2008). Studies on chemical speciation of sodium aerosols produced in sodium fire, *Nucl. Technol.* 65, 257.

PHYSICAL AND CHEMICAL CHARACTERIZATION OF SODIUM COMBUSTION AEROSOLS

ARJUN PRADEEP¹, K. E. JEBAKUMAR, G. VENKAT REDDY, G. PUNITHA and D. PONRAJU

¹Safety Engineering Division, Indira Gandhi Centre for Atomic Research, Kalpakkam, Kancheepuram, Tamil Nadu – 603102, India.

KEYWORDS: sodium combustion aerosols, sodium fire, containment.

INTRODUCTION

The waste generated from sodium fire experimental facilities has to be disposed by sodium-mist water reaction in contained air atmosphere. Keeping this as objective, the Sodium Disposal Facility (SDF) is developed at Safety Engineering Division, IGCAR to dispose laboratory scale sodium in batch mode. The SDF consists of a mist chamber, where sodium-water mist reaction takes place intermittently. In case of accidental sodium fire inside mist chamber during disposal process, sodium compound aerosols are generated, which have to be disposed in a safe and environment friendly manner to the atmosphere. Combustion aerosols generated during sodium fire in containments consists of primary reaction products, such as sodium oxide (Na_2O) and sodium peroxide (Na_2O_2) and secondary reaction products such as sodium hydroxide (NaOH) and sodium carbonate (Na_2CO_3) depending upon the Relative Humidity (RH) and CO_2 present in the enclosed air. Inhalation of sodium combustion aerosol damages mucous membrane and upper respiratory tract. Symptoms include nose and throat irritation with labored breathing and can result in lung edema (Ballif *et al.*, 1979). Due to the harmful nature of sodium combustion aerosols, they have to be characterized both physically and chemically for better understanding and designing suitable air cleaning systems before venting.

Sodium combustion aerosols form a polydisperse colloidal system which exhibits a range of particle sizes unlike a monodisperse system in which particles are of uniform size. Physical characterization involves evaluation of aerosol mass concentration and Particle Size Distribution (PSD). The PSD is typically represented in the form of a cumulative (undersize) distribution curve. The most commonly used function for PSD is the log normal distribution which can be completely defined by two quantities: the Mass Median Aerodynamic Diameter (MMAD - that is, the diameter such that half the airborne mass, of sodium presumably, occurs on particles of a smaller aerodynamic diameter) and the Geometric Standard Deviation (GSD – which describes how spread out the values are in the distribution). Experimental results from various experimental facilities show that the initial MMAD in

typical pool fire is of the order of $1\ \mu\text{m}$ with GSD of 2 (Baskaran *et al.*, 2004). The chemical characterization involves the evaluation of conversion rate of sodium combustion aerosols to less harmful sodium carbonate.

This paper reports results of physical and chemical characterization of sodium combustion aerosols inside the mist chamber, which is essential for enhancing the safety features of SDF for disposal operations. The study also presents the use of filter paper, Para Particle Aerosol Size Separator (PPASS)-01 (Singh *et al.*, 2005) and wash bottle sampling for physical and chemical characterization of aerosols respectively. The filter paper sampler and particle size separator measures mass concentration and PSD of sodium combustion aerosols respectively, generated from in-house experiment. The measurements are useful to understand the settling behavior of aerosols in containments and design of suitable air cleaning systems, which is necessary for safe access of personals in Sodium-cooled Fast Reactor (SFR) containments after a sodium fire accident. Finally the description of aerosol samplers, experimental setup details and post-experiment data analysis is highlighted in this paper.

DESCRIPTION OF AEROSOL EQUIPMENTS

The measurement approach used for physical characterization of aerosol is passive sampling. The filtration technique and particle size analyzer are used for the passive aerosol sampling. In the filtration technique a closed face type filter holder is used, that can hold 47 mm diameter circular disk. Whatman glass microfiber filters of 0.45 micron pore size are used for the determination of mass concentration. A Millipore vacuum, pressure pump with a capacity of 38 *lpm* coupled with rotameter is used for maintaining a constant volumetric flow of 15 *lpm* through the filter. The cumulative experimental errors associated with measurement in time, flow rate and mass is nearly $\pm 10\%$. An electronic analytical balance (M/s SHIMADZU Corporation, Japan, Model No. AUX220) with accuracy and precision of 0.0001 g is used for the gravimetric analysis. The particle size analyzer used is a seven stage Para Particle Aerodynamic Size Separator Model PPASS-01 (size range 0.53-8.95 μm). This sampler operates at a volumetric flow rate of 45 *lpm*, with an accuracy of $\pm 5\ \text{lpm}$, which is achieved by a flow meter with air flow control. The chemical sampling is carried out using 250 ml capacity gas wash bottles containing 200 ml of distilled water. A Millipore vacuum, pressure pump with a capacity of 38 *lpm* coupled with rotameter is used for maintaining a constant volumetric flow of 10 *lpm* through the wash bottle. The quantities of hydroxide and carbonate were obtained by titration method.

EXPERIMENT

The experimental setup consists of chamber and associated sampling systems as shown in Fig. 1. The sodium pool fire is generated by heating 50 g sodium (laboratory scale (Marimuthu *et al.*, 1984)) inside a rectangular chamber of volume 1.125 m³ and made of stainless steel. The chamber is provided with an inspection glass window and filled with normal atmosphere initially. The Barnstead|Thermolyne Cimarec hot plate is used for heating the stainless steel tray kept inside the experimental chamber to 224 °C. Sodium is placed on the hot tray and further heated till it catches fire. Duration of sodium fire was 3 minutes. The aerosol diagnostic equipments are used to sample the gas stream from the top of the experimental chamber to get representative sodium combustion aerosol characteristics.



Figure 1. Photo of experimental setup with sampling system



Figure 2. Stages of 50 g sodium (a) before burning (b) burning

The typical stages of sodium pool fire inside the experimental chamber are shown in Fig. 2. During sodium burning aerosols are generated, which are measured using the aerosol diagnostic equipments to measure the aerosol characteristics.

RESULTS & DISCUSSION

Lab scale sodium pool fire test (50 g) was carried out in the contained experimental chamber as discussed. Non-isokinetic aerosol sampling is done using filter paper sampler and PPASS-01 from the air stream contained in the chamber for physical characterization. The initial mass concentration and size distribution parameters of sodium combustion aerosols, measured are as follows.

Initial aerosol concentration = 1.2 g/m^3

Initial MMAD = $1.6 \mu\text{m}$

Initial GSD = 2.2

The mass size distribution represented by the cumulative percentage of mass collected in the various stages of the size separator is shown in Table 1. The log normal size distribution is obtained by plotting cumulative distribution of the masses content with respect to aerodynamic diameters on a log-probability graph. The straight line fit is used to estimate the size distribution parameters such as MMAD and the GSD. The initial PSD for sodium combustion aerosol generated in experiment is given in the Fig. 3 (a). The MMAD $d_{50\%}$ is the particle size that corresponds to 50% cumulative mass. The GSD is found as the ratio $d_{84\%}/d_{50\%}$ where $d_{84\%}$ is the diameter corresponding to 84% cumulative mass.

Table 1. Mass size distribution from PPASS-01

Stage	Size range (micron)	ECD (micron)	initial mass of filter paper (mg)	final mass of filter paper (mg)	Net mass (mg)	% in size range	Cumulative % less than size range
1	>8.95	8.95	293.9	295.1	1.2	2.25	97.75
2	7.91-8.95	7.91	295.4	296	0.6	1.12	96.63
3	6.09-7.91	6.09	296.4	296.6	0.2	0.37	96.25
4	4.15-6.09	4.15	295.9	297.6	1.7	3.18	93.07
5	2.94-4.15	2.94	294.5	299.4	4.9	9.18	83.90
6	1.03-2.94	1.03	301.5	329.4	27.9	52.25	31.65
7	0.53-1.03	0.53	294.7	308.5	13.8	25.84	5.81
Filter total	<0.53	0	417.3	420.4	3.1	5.81	0
					53.4	100	

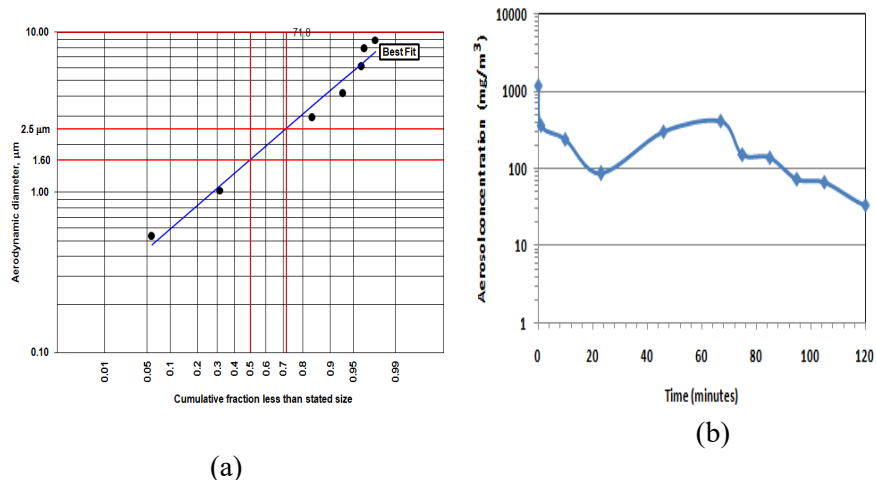


Figure 3. Sodium combustion aerosol (a) Log-normal plot for initial PSD (b) mass concentration

The sampling time for filtration and PPASS-01 is 1 min. The mass concentration of sodium aerosols inside the experimental chamber is measured for about 120 minutes using filter paper samplers. The aerosol mass concentration behavior in experimental chamber is shown in Fig. 3 (b). From Fig. 3 (b), the mass concentration of sodium aerosols inside the chamber is observed to be initially 1.2 g/m^3 and further decreases to 33 mg/m^3 in 120 minutes due to aerosol depletion phenomena (settling, thermophoresis and diffusiophoresis). The sampling time for wash bottle is 3 min. The chemical composition of aerosol with respect to time is shown in Fig. 4. Reported NaOH includes unreacted sodium oxides and no differentiation has been made between unreacted sodium oxides and sodium hydroxide inside chamber during analysis.

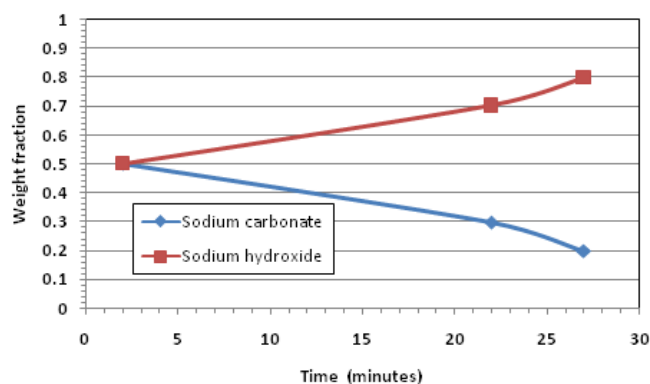


Figure 4. Temporal variation of sodium compound aerosol composition in chamber

After 2 minutes of sodium fire ~50% of aerosols becomes carbonate as observed in literature (Jordan *et al.*, 1988). After 30 minutes of sodium fire 80% of aerosols becomes carbonate. The study also shows that the maximum fraction of sodium released from the 50 g sodium pool fire as smoke is 0.027. The study thus benchmarks the facility for sodium fire aerosol measurements and design suitable safety measures to handle sodium compound aerosols in case of accidental sodium fire during disposal studies.

CONCLUSIONS

In-house lab scale sodium fire experiment (50 g) was carried out in a contained 1.125 m³ experimental chamber of Sodium Disposal Facility (SDF), IGCAR for sodium combustion aerosol characterization. Filtration technique and particle size separator are used to evaluate the aerosol mass concentration and size distribution respectively. The MMAD for 50 g pool fire case was measured to be 1.6 micron and GSD as 2.2 for an initial mass concentration of 1.2 g/m³. The measurement results indicate that the sodium combustion aerosols are polydisperse in nature as observed in literature. The aerosol concentration reduces to 33 mg/m³ in 120 minutes due to aerosol depletion phenomena. The conversion of 80% of sodium combustion aerosol to less harmful carbonate within 30 minutes showed that chemically the aerosols are safe for personal access much before the reduction in physical concentration due to settling. This study is useful for benchmarking the facility for future sodium disposal studies and fundamental understanding of behavior of sodium combustion aerosols in contained atmospheres of Sodium-cooled Fast Reactors.

ACKNOWLEDGEMENTS

Ms. S. Hymakumari is acknowledged for providing necessary assistance in conducting the experiments. The authors are grateful to Dr. A. K. Badhuri, Director, IGCAR for providing constant encouragement.

REFERENCES

Ballif J. L., B. Ford and U. I. Davies (1979) *Liquid metals fire control engineering handbook*, (No. HEDL-TME-79-17).

Baskaran, R., T. S. Selvakumaran and V. Subramanian (2004). Aerosol test facility for fast reactor safety studies, *Indian Journal of Pure & Applied Physics*42, 873.

Singh, S., A. Khan, T. Das, B. K. Sapra, Pushparaja and Y. S. Mayya (2005). Indigenous development of an aerodynamic size separator for aerosol size distribution studies, *Current Science*, pp.1426-1433.

Marimuthu, K., D. S. Mitragotri, and A. R. Sundararajan (1984). Sodium Fires and Aerosols: Behavior of Radioiodine, *Journal of Nuclear Science and Technology*21, no. 9, 686-693.

Jorden, S., W. Cherdron, J. C. Malet, R. Rzekiecki and Y. Himeno (1988). Sodium Aerosol Behavior in Liquid Metal Fast Reactor Containments, *Nucl. Technol.*81, 183.

HEAVY METAL ENRICHMENT ON INDOOR FINE PARTICULATE MATTER IN DIFFERENT SOCIO-ECONOMIC ZONES OF DELHI

A. GARG¹ AND C. GHOSH²

¹Department of Environmental Studies, Indraprastha College for Women, University of Delhi, Delhi – 110 054, India

²Environmental Pollution Laboratory, Department of Environmental Studies, University of Delhi, Delhi – 110 007, India

KEYWORDS: PM_{2.5}, Heavy Metal, Indoor, Socio-Economic Zone etc.

INTRODUCTION

Indoor air pollution simply means the level of pollution inside house or office where people spend maximum quality time and it is now considered as a serious threat to human health. The fine particulate matter which is considered as a major pollutant of outdoor environment is also a potentially harmful pollutant present within Indoor environment. Fine particulate matter (PM_{2.5}) gets generated from various sources such as building material and equipment, cleaning products, furniture, insect repellent, cooking and heating facilities or from tobacco smoke and also through infiltration of outdoor air (Viegi *et al.*, 2004; Azuma *et al.*, 2008; Billionnet *et al.*, 2011). The level of toxicity is further aggravated by the enrichment of heavy metals on the indoor fine particulate matter. Most of the individual spend 80–90 % of their time in public and private indoor environments which makes them vulnerable to toxic effect of such metallic indoor particulate pollution. Thus, the undertaken study evaluates the concentration of fine particulate matter and heavy metals enriched on them in indoor environment and understand their source distribution; indoor sources or infiltration from outdoor polluted air in indoor environment.

METHODOLOGY

Study site

There is a vast diversification in the residential pattern (type-design-area) of Delhi leading to zoning or clustering of homes of similar socioeconomic rank in an area. For the present study three Socio-Economic Zones were selected which were distinct in their economic status and lifestyle, i.e. EZ I (High income class), EZII (Middle income class) and EZIII (low income class).

Particulate matter and Heavy metal analyses

The PM_{2.5} sampling was carried out simultaneously for indoor and outdoor environment using Envirotech APM 550 EL. During sampling instrument was run consecutively for eight hours (NAAQS, 2011) - 8:00 to 16:00 hours. For monitoring PTFE filter paper was used and filters were vacuum desiccated prior and after air sampling for 24 hours to remove any moisture held in the filter paper.

Concentration of nine heavy metals – Cadmium (Cd), Lead (Pb), Zinc (Zn), Copper (Cu), Manganese (Mn), Chromium (Cr), Cobalt (Co), Iron (Fe) and Nickel (Ni) were assessed by acid digestion of filter paper (AOAC, 1990 and NAAQS, 2011).

Indoor or Outdoor source of heavy metal enriched fine particulate matter

Indoor/Outdoor (I/O) ratios were quantified using the methodology followed by Diapouli et al. (2008) and Koponen et al. (2001) for PM_{2.5} and selected nine heavy metals to quantify the infiltration of toxic air pollutants from outdoor environment.

RESULT AND DISCUSSION

The observed result (Figure 1), indicates that outdoor air of Low Socio-Economic Zone (EZ III) was the most polluted site reporting maximum average concentration of outdoor PM_{2.5} (294.23 µg/m³) followed by Middle Socio-Economic Zone (EZ II) (280.75 µg/m³) and High Socio-Economic Zone (EZ I) (PM_{2.5}, 256.56 µg/m³). The result is well justified by the fact that EZ III is near to hub of pollution emitting sources like petroleum refueling station (adjacent to the colony, within 10 meters), factories (opposite to the slum area, nearest fabrication factory was 20 meters away), traffic intersection (25 meters away) and close proximity to waste dumping site (20 meters) and open sewer drain (10 meters).

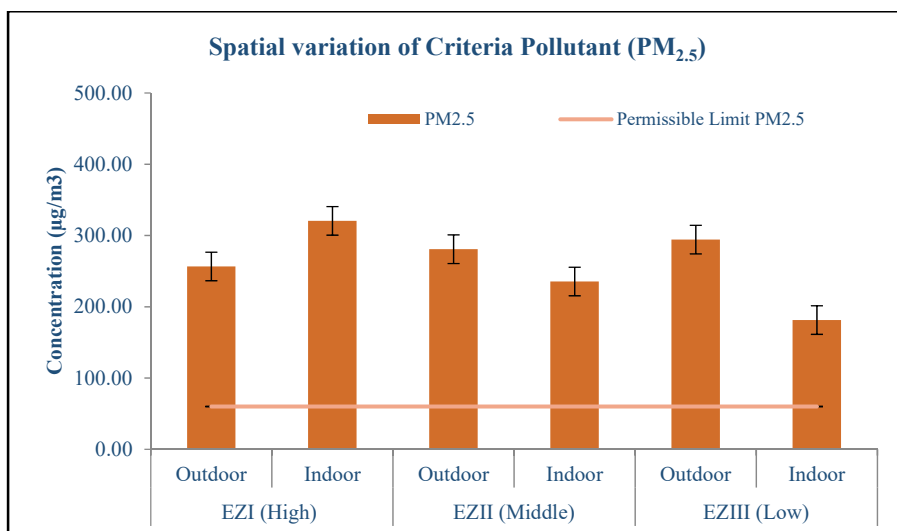


Figure 1: Spatial Variation in PM_{2.5} at Various Socio-Economic Zones, EZI (High), EZII (Middle) and EZIII (Low)

The Levels of indoor PM_{2.5} concentration peaked in High Socio-Economic Zone (EZ I) followed by EZ II and EZ III (Figure1). Under day-to-day lifestyle practices, EZI keep their windows, balconies close or covered either for keeping the home clean/dust free and also to prevent leakage of air-conditioned air, creating insulation or for privacy/security reasons. These practices hinder the mixing of ambient air which generally acts as diluents in reducing the higher concentration of pollutants raised indoors as an outcome of various emission sources and life style activities.

The analyses of heavy metal enrichment on particulate matter showed EZIII (Low Socio-Economic Zone) to be the most metal polluted site for both indoor and outdoor, followed by EZII (Middle Socio-Economic Zone) and EZI (High Socio-Economic Zone) (Figure 2). The trend at each site showed that outdoor and indoor environment is highly polluted with metals like Zn and Fe. Various studies have already reported high concentration of Fe and Zn in Delhi's air (Shridhar *et al.*, 2010; Khillare and Sarkar, 2012; Sharma *et al.*, 2015). Where, the major source of Zn is from vehicular emission, lubricating oil and abrasion of tires (Begum *et al.*, 2004) and that of Fe is from re-suspended dust or crustal dust (Srivastava and Jain, 2007; Srivastava *et al.*, 2009; Chelani *et al.*, 2010).

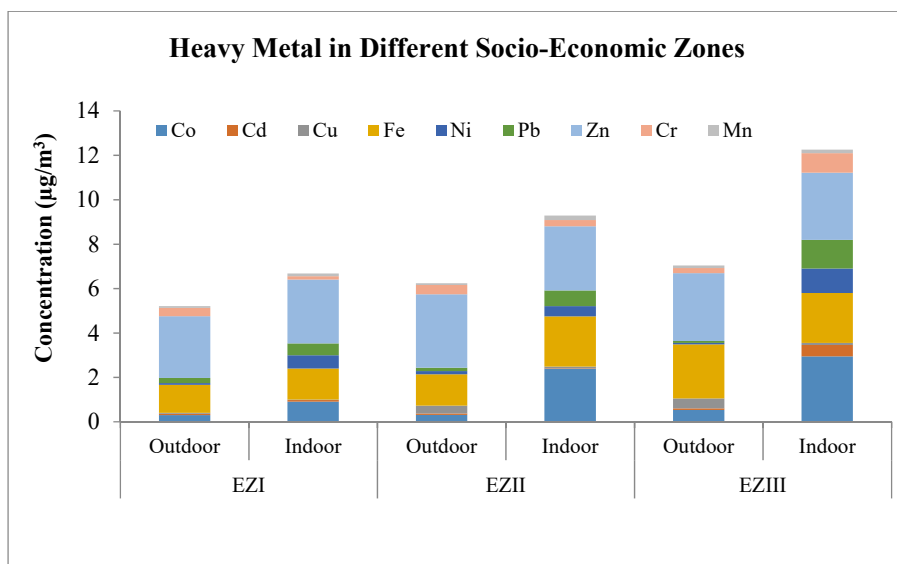


Figure 2: Heavy Metal Enrichment on $\text{PM}_{2.5}$

Indoor Outdoor Ratios

As shown in Table 1, the I/O ratios were depicted that at EZI and EZII Ni and Pb are the only metals with indoor sources and at EZIII Cd, Pb and Cr are the metals released from indoor sources, rest all metals have been infiltrated from outdoor air.

Table 1: I/O ratios of heavy metals enriched on of $\text{PM}_{2.5}$

Socio-Economic Zone	Co	Cd	Cu	Fe	Ni	Pb	Zn	Cr	Mn
EZI	0.32 7	0.11 5	0.92 2	0.85 4	1.65 2	1.63 2	0.68 1	0.54 8	0.78 9
EZII	0.97 0	0.39 6	0.77 8	0.61 0	1.03 9	1.05 9	0.85 9	0.84 9	0.98 5
EZIII	0.73 5	1.03 4	0.33 2	0.70 6	0.74 2	1.10 6	0.69 4	1.11 0	0.62 2

Dust from walls or any renovation activities can increase these metals within indoor environment. Also, higher concentration of Pb, Ni and Cr in EZIII (Low income group) could be because of the use of inferior quality fuel

(Kulshrestha *et al.*, 2014); solid waste burning is also a cause of higher Cr contamination in the environment (Borai *et al.*, 2002). Higher concentration of Cd in EZIII could be attributed to the use of kerosene in this economic zone. It has been also reported that use of mosquito coil can result in generation of metals like Cd, Pb and Cr in indoor environment (Roy *et al.*, 2009; Kasumba *et al.*, 2016).

CONCLUSION

The study concludes that socio economic status greatly influences the concentration of PM_{2.5} in indoor environment. The habit of high income residential setup to keep their windows and balconies closed piled up the concentration of pollutant inside their houses and thus High Income group (EZI) showed highest indoor concentration of PM_{2.5}. However, indoor metallic particle concentration was more at EZIII (Low income group) owing to their close proximity to traffic intersection and industrial area. Finally I/O ratios showed that metals like Pb, Ni, Cr and Cd can come from various indoor sources like paints, use of inferior quality fuel and burning mosquito coil. Thus, in an urban area the indoor air quality of a residential setup depends on its economic status and lifestyle activities of the inhabitants.

ACKNOWLEDGEMENTS

Author acknowledges Rajiv Gandhi National Fellowship (RGNFD) and MoES for providing financial support.

REFERENCES

- Azuma, K., Uchiyama, I., Uchiyama, S., & Kunugita, N. (2016). Assessment of inhalation exposure to indoor air pollutants: screening for health risks of multiple pollutants in Japanese dwellings. *Environmental research*, 145, 39-49.
- Begum, B. A., Kim, E., Biswas, S. K., & Hopke, P. K. (2004). Investigation of sources of atmospheric aerosol at urban and semi-urban areas in Bangladesh. *Atmospheric Environment*, 38(19), 3025-3038.
- Billionnet, C., Gay, E., Kirchner, S., Leynaert, B., & Annesi-Maesano, I. (2011). Quantitative assessments of indoor air pollution and respiratory health in a population-based sample of French dwellings. *Environmental research*, 111(3), 425-434.

Borai, E. H., El-Sofany, E. A., Abdel-Halim, A. S., & Soliman, A. A. (2002). Speciation of hexavalent chromium in atmospheric particulate samples by selective extraction and ion chromatographic determination. *TrAC Trends in Analytical Chemistry*, 21(11), 741-745.

Chelani, A. B., Gajghate, D. G., ChalapatiRao, C. V., & Devotta, S. (2010). Particle size distribution in ambient air of Delhi and its statistical analysis. *Bulletin of environmental contamination and toxicology*, 85(1), 22-27.

Diapouli, E., Chaloulakou, A., & Spyrellis, N. (2008). Indoor and outdoor PM concentrations at a residential environment, in the Athens area. *Global NEST Journal*, 10(2), 201-208.

Kasumba, J., Hettick, B., French, A., Wickliffe, J. K., Lichtveld, M. Y., Hawkins, W. B. & Klein, D. (2016). Analysis of Pesticides and Toxic Heavy Metals Contained in Mosquito Coils. *Bulletin of environmental contamination and toxicology*, 97(5), 614-618.

Khillare, P. S., & Sarkar, S. (2012). Airborne inhalable metals in residential areas of Delhi, India: distribution, source apportionment and health risks. *Atmospheric pollution research*, 3(1), 46-54.

Koponen, I. K., Asmi, A., Keronen, P., Puhto, K., & Kulmala, M. (2001). Indoor air measurement campaign in Helsinki, Finland 1999—the effect of outdoor air pollution on indoor air. *Atmospheric Environment*, 35(8), 1465-1477.

Kulshrestha, A., Massey, D. D., Masih, J., & Taneja, A. (2014). Source characterization of trace elements in indoor environments at urban, rural and roadside sites in a semi arid region of India. *Aerosol Air Qual. Res*, 14, 1738-1751.

NAAQS Monitoring and Analysis Guidelines. Guidelines for the Measurement of Ambient Air Pollutants, (2011) vol I. CPCB, India

Roy, A. A., Baxla, S. P., Gupta, T., Bandyopadhyaya, R., & Tripathi, S. N. (2009). Particles emitted from indoor combustion sources: size distribution measurement and chemical analysis. *Inhalation toxicology*, 21(10), 837-848.

Sharma, P., Kumar, S., Garg, A., & Ghosh, C. (2015). Analyzing the effect of atmospheric trace elements on selected plant species. *Environmental Earth Sciences*, 74(12), 7793-7800.

Shridhar, V., Khillare, P. S., Agarwal, T., & Ray, S. (2010). Metallic species in ambient particulate matter at rural and urban location of Delhi. *Journal of Hazardous Materials*, 175(1-3), 600-607.

Srivastava, A., & Jain, V. K. (2007). Size distribution and source identification of total suspended particulate matter and associated heavy metals in the urban atmosphere of Delhi. *Chemosphere*, 68(3), 579-589.

Srivastava, A., Gupta, S., & Jain, V. K. (2009). Winter-time size distribution and source apportionment of total suspended particulate matter and associated metals in Delhi. *Atmospheric Research*, 92(1), 88-99.

Viegi, G., Simoni, M., Scognamiglio, A., Baldacci, S., Pistelli, F., Carrozzi, L., & Annesi-Maesano, I. (2004). Indoor air pollution and airway disease [State of the Art]. *The International Journal of Tuberculosis and Lung Disease*, 8(12), 1401-1415.

DUST STORM OVER THE ARABIAN SEA DURING THE SUMMER SEASON-THE JULY 2016 CASE

D. G. KASKAOUTIS¹, A. RASHKI², A. MOFIDI³, U. C. DUMKA⁴

¹Institute for Environmental Research and Sustainable Development,
National Observatory of Athens, 11810 Athens, Greece

²Natural Resources and Environment College, Ferdowsi
University of Mashhad, Mashhad - 91735, Iran

³Department of Geography, Ferdowsi University of Mashhad,
Mashhad - 91735, Iran

⁴Aryabhata Research Institute of Observational Sciences, Nainital, 263 001,
India

KEYWORDS: dust, monsoon, shamal, levar, Arabian sea

INTRODUCTION

In this study, we examine the atmospheric circulation patterns, which are associated with contrasting wind regimes (southwest monsoon, Shamal and Levar winds), desert dust outflows and accumulation of dust over the Arabian Sea during the summer season. Several dust plumes of various intensity and from different sources, such as Arabian Peninsula, Somalia, Iran, and transport pathways affected the Arabian Sea. The present study emphasizes on the period 11th to 16th July 2016, using meteorological data from ECMWF ERA-Interim reanalysis along with satellite (MODIS, MISR, and CALIPSO) and model (MERRA-2) simulations over the Middle East, Arabian Peninsula and southwest Asia. The results shed light on the characteristics and driving forces of the contrasting wind regimes that are responsible for dust outbreaks that are finally accumulated over the Arabian Sea and on the specific role of the Inter-Tropical Discontinuity.

DATASETS

The meteorological data were obtained from the ECMWF ERA-Interim atmospheric reanalysis. We used the mean sea level pressure (MSLP) and the geopotential height at 700 hPa (Z700) ($0.5^\circ \times 0.5^\circ$), as well as the vector wind from 1000 hPa to 400 hPa, over the South west Asia at 6-hr intervals. Further, we have used the MODIS and MISR derived AOD along with vertical profiles of total attenuated backscatter from CALIPSO, also supported by MERRA-2 dust simulations.

RESULTS & DISCUSSIONS

During the study period (11 – 16 July 2016) contrasting dust plumes of various intensity, originated from the deserts in the Arabian Peninsula, Somalia and Sistan (Iran), impacted the Arabian Sea resulting in high (MODIS/MISR AODs > 1.5 - 2) dust accumulation over a “hot-spot” aerosol-laden area (Fig. 1). The Indian/Pakistan thermal low-pressure system, extended over south Iran, north Arabian Sea and the Arabian Peninsula with secondary lows, dominated at sea level, while high-pressure systems existed over the Caspian Sea, east Mediterranean and east tropical Africa (Kaskaoutis et al., 2016). At 700 hPa, an extent ridge of southwest-to-northeast axis dominated from east Sudan and the southwest Arabian Peninsula to Iran, also connected with the high-pressure system over the Caspian Sea, while the Indian sub-continent was affected by the summer monsoon trough. These atmospheric circulation systems initiated contrasting wind regimes, namely the southwest monsoon flow, the Shamal and Levar winds dominated with varying intensity over the Middle East and SW Asia. The strong (>20 - 25 ms^{-1} at 950 hPa) southwest monsoon winds off the Horn of Africa, were able to emit dust from the deserts in Somalia and south-eastern Arabian Peninsula and to carry them over the central and north parts of the Arabian Sea. These dust plumes were merged with those coming from Iran (Sistan dust storm) triggered by the strong ($\sim 20 \text{ms}^{-1}$ at 850 hPa) Levar wind, as well as those originated from Iraq and the deserts in the east Arabian Peninsula, which were transported by the northwest Shamal ($\sim 10\text{-}14 \text{m s}^{-1}$ at 950 hPa) wind (Bou Karam et al., 2017). The end result was the large dust-aerosol loading over the central/north Arabian Sea ($\sim 15^\circ - 24^\circ \text{N}$, $60^\circ - 67^\circ \text{E}$). This area is characterized by weak winds ($< 5 \text{ms}^{-1}$) and by convergence of the southerly monsoon flow with the northerlies Shamal and Levar, defining the position of the ITD, which seems to play an important role in dust accumulation over the Arabian Sea. The CALIPSO vertical profiles revealed presence of multiple aerosol layers along the position of the ITD over the north Arabian Sea, with the lower plumes ($\sim 500 \text{m}$) to be originated from Somalia and southeast Arabian Peninsula, while the upper ones ($\sim 4000 \text{m}$) from the South West Asia.

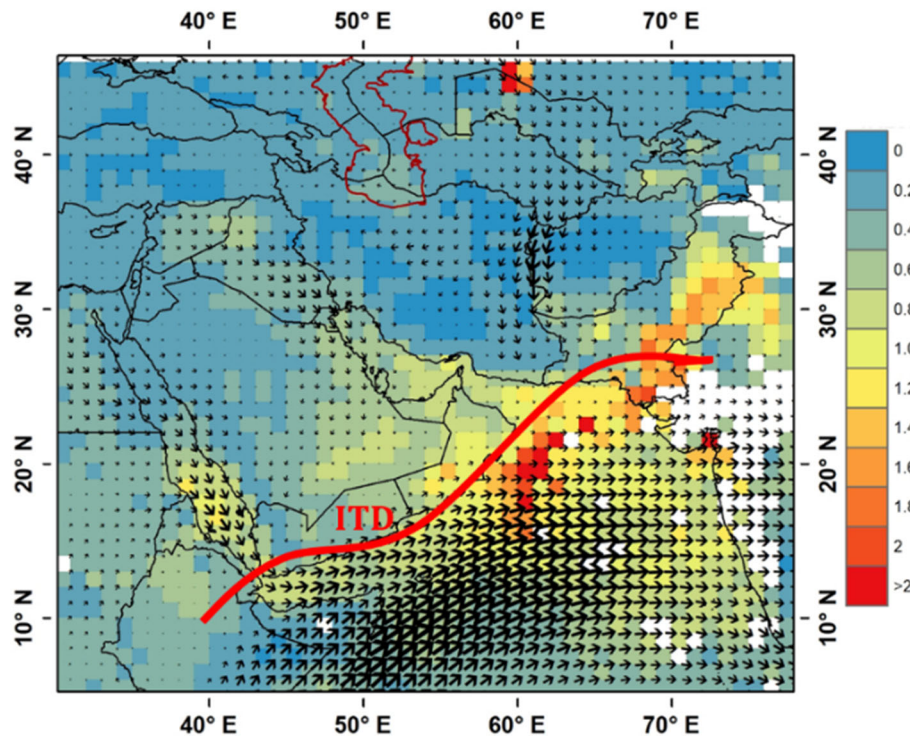


Figure 1: Terra-MODIS AOD₅₅₀ spatial distribution, superimposed with the vector wind at 850 hPa averaged for the period 10 – 19 July 2016.

CONCLUSIONS

The main findings from this study can be summarized in the following:

1. High dust accumulation over the north/central Arabian Sea due to merge of contrasting dust plumes
2. The “hot-spot” dust-laden area is characterized by weak wind conditions
3. Inter-Tropical Discontinuity (ITD) plays a major role in dust accumulation and relative influence of each wind regime
4. Presence of multiple dust layers in the vertical from different origins along the position of ITD

ACKNOWLEDGEMENTS

ERA-Interim reanalysis, MODIS, MISR and MERRA-2 mission scientist and associated NASA personnel for providing the required datasets are gratefully acknowledged.

REFERENCES

Bou Karam, F.D., Flamant, C., Chaboureau, J.P., Banks, J., Cuesta, J., Brindley, H., Oolman, L., 2017. Dust emission and transport over Iraq associated with the summer Shamal winds. *Aeol. Res.* 24, 15–31.

Kaskaoutis, D.G., Houssos, E.E., Rashki, A., Francois, P., Legrand, M., Goto, D., et al., 2016. The Caspian Sea – Hindu Kush Index (CasHKI): a regulatory factor for dust activity over southwest Asia. *Glob. Planet. Change* 137, 10–23.

LONG-TERM (2007-2017) MEASUREMENTS OF AEROSOL CHARACTERISTICS AT URBAN STATIONS DELHI AND LUCKNOW

SUNIL KUMAR^{1,2*}, A. K. SRIVASTAVA² and V. PATHAK¹

¹Department of Civil Engineering, Institute of Engineering and Technology,
Lucknow, India

²Indian Institute of Tropical Meteorology (Branch), Prof. Ramnath Vij
Marg, New Delhi, India

(*Correspondence at Sunil Kumar (sunilcs0101@gmail.com))

KEYWORDS: Indo-Gangetic Basin, Aerosol Optical Depth, Aerosol Single Scattering Albedo, UV-Aerosol Index.

INTRODUCTION

Atmospheric aerosols play important role to change in climate system. Atmospheric aerosols are known to disturb the radiative balance of the overall earth system through the directly or indirectly. (IPCC; 2001, 2007). Aerosol possess direct radiative forcing because they scatter and absorb solar radiation in the atmosphere. Aerosol also disturb the rainfall and formation ability ice, water and mixed phase clouds that caused an indirect radiative forcing accomplice with these adjustments in the cloud properties (Rosenfeld *et al.*, 2008; Sathesh and Moorthy, 2005; Breon *et al.*, 2002 Ramanathan *et al.*, 2001; Russell *et al.*, 1999). Last two decades observed the physical, chemical and optical properties of aerosols and their temporal variabilities has been essentially improved our understanding and estimation of direct and indirect radiative effects. (Lodhi *et al.*, 2013). However, the uncertainties on their effect on the atmosphere and climate are still high and the understanding level is less than that of the greenhouse gases (IPCC, 2007). An essential factor which adding to this uncertainty is large to heterogeneity in optical and microphysical properties of aerosol over spatial and temporal scales (Lodhi *et al.*, 2013).

In this study, we present the climatology of atmospheric aerosol characteristics using long term measurements of columnar aerosol properties from different satellites during January 2007 to December 2017 (11 years' period) over the highly polluted Indo-Gangetic Basin (IGB) region. The study was carried out at two different urban stations: Delhi (28.7° N, 77.3° E) in the western IGB and Lucknow (26.85° N, 80.95° E) in the central IGB regions to characterize spatial heterogeneity in aerosol characteristics such as Aerosol

Optical Depth at 550 nm (AOD_{550}), Ångstrom Exponent at 412/470 nm ($\text{ÅE}_{412/470}$), Aerosol Single Scattering Albedo at 500 nm (SSA_{500}) and UV-Aerosol Index (AI). Our study shows steadily high aerosol loading at both the stations during the period of measurements, with relative dominance at Delhi.

METHODS

Measurements of columnar aerosol optical properties were retrieved from Moderate Resolution Imaging Spectroradiometer (MODIS) and Ozone Monitoring Instrument (OMI) satellite. MODIS-derived level 3 daily QA weighted data (MYD08_D3_06) on a spatial resolution of $1^\circ \times 1^\circ$ and Ozone Monitoring Instrument (OMI) satellite used to construct the daily mean aerosol products in the present study. Since aerosols over India are composed of both natural and anthropogenic components during different seasons, respective trends in fine and coarse mode particles were also analyzed by examining the variability in Ångström exponent (AE) at 412/470 nm obtained from MODIS and Aerosol Single Scattering Albedo at 500 nm (SSA_{500}) and UV-Aerosol Index (AI) obtained from OMI. The magnitude of AE provides qualitative approximation about the dominant size of particles, with higher magnitude implies dominance of fine mode aerosols while lower magnitude implies dominance of coarse mode aerosols (Eck *et al.*, 1999; Srivastava *et al.*, 2008). The changes in the size of fine mode particles are possible due to coagulation which increases with increasing aerosol loading under suitable atmospheric condition (Li *et al.*, 2007) thereby resulting in an increase of coarse mode concentration. Potential temperature change artery has been identified and discussed using concentration weighted trajectory analysis of 5-days air mass back trajectories from the Air Resources Laboratory (ARL), National Oceanic and Atmospheric Administration (NOAA).

RESULTS & DISCUSSIONS

Our study shows steadily high aerosol loading at both the stations during the period of measurements, with relative dominance at Delhi. Daily variation of AOD, AE, SSA and AI 0.6 to 3.4 (0.05 to 3.5), 0 to 1.8 (0 to 1.8), 0.8 to 1.0 (0.8 to 1.0) and -1.1 to 5.1 (-1.3 to 3.4) at Delhi (Lucknow) stations.

Month	Delhi (AOD_{550nm})	Lucknow (AOD_{550nm})
January	0.9±0.3	0.9±0.2
February	0.6±0.1	0.5±0.1
March	0.4±0.1	0.4±0.06
April	0.5±0.05	0.5±0.1
May	0.6±0.1	0.6±0.1

June	0.8±0.1	0.7±0.1
July	0.9±0.2	0.6±0.4
August	0.6±0.1	0.4±0.2
September	0.4±0.1	0.4±0.1
October	0.8±0.1	0.6±0.1
November	1.0±0.1	0.9±0.1
December	0.8±0.1	0.9±0.2

Table 1. Monthly average of AOD (550 nm) at Delhi and Lucknow station during study duration (2007-2017).

Seasonal variation (Figure 1.) of AOD, AE, SSA and AI shows higher values in Post-Monsoon/Winter at Delhi and Lucknow station. AOD dominate higher values in winter/Post-Monsoons show higher dense haze, fog and smog which are largely due to growth of population and increasing urbanization/industrialization.

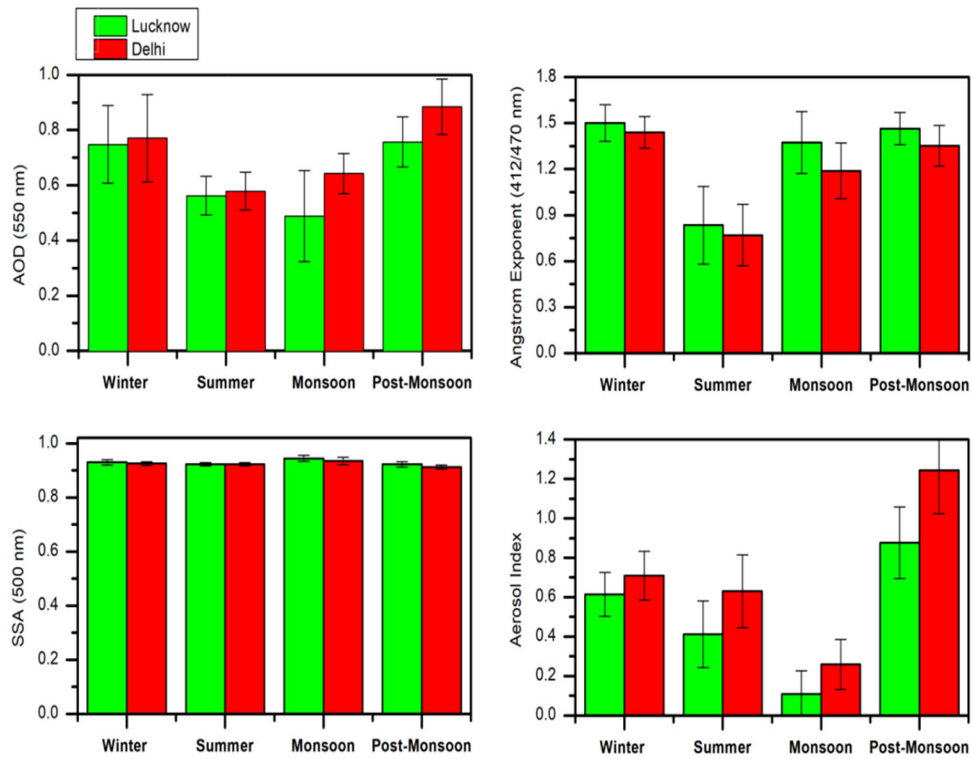


Figure 1. Seasonal mean of AOD, AE, SSA and AI at Delhi and Lucknow stations during study period (2007-2017).

Annual mean (Figure 2.) variation of AOD, AE, SSA and AI 0.60 ± 0.15 to 0.76 ± 0.30 (0.54 ± 0.25 to 0.76 ± 0.33), 1.00 ± 0.45 to 1.28 ± 0.28 (1.05 ± 0.36 to 1.45 ± 0.28), 0.91 ± 0.01 to 0.93 ± 0.01 (0.92 ± 0.01 to 0.93 to 0.01) and 0.55 ± 0.41 to 0.77 ± 0.48 (0.35 ± 0.35 to 0.55 to 0.44) at Delhi (Lucknow) stations. AODs values higher in Delhi comparison to Lucknow suggests Delhi is highly polluted compared to Lucknow. Study further reveals that the coarse-mode aerosols dominate during summer (Mar-Jun) and monsoon (Jul-Sep) seasons, whereas fine mode particles enhanced during post-monsoon (Oct-Nov) and winter (Dec-Feb) seasons. Potential temperature change artery has been identified and discussed using concentration weighted trajectory analysis of 5-days air mass back trajectories from the Air Resources Laboratory (ARL), National Oceanic and Atmospheric and Administration (NOAA).

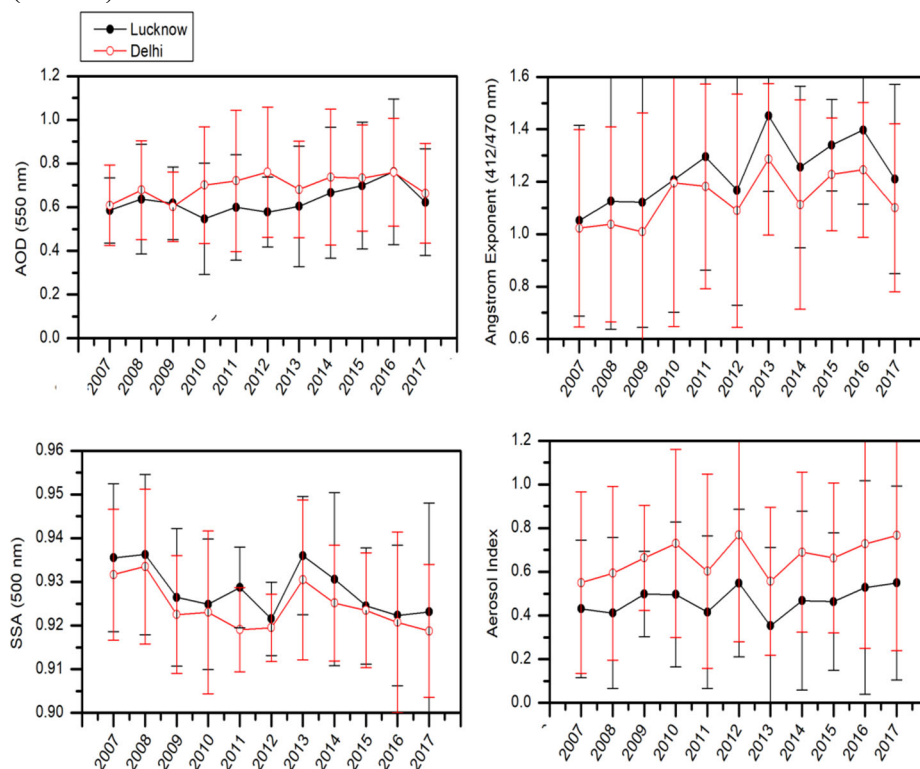


Figure 1. Annual variations of AOD, AE, SSA and AI at Delhi and Lucknow stations during study period (2007-2017)

CONCLUSIONS

MODIS and OMI derived product AOD, AE, SSA and AI were carried urban stations, Delhi and Lucknow in Indo-Gangetic Basin (IGB) during the period from January 2007 to December 2017. The major findings of the present study are as follows:

1. Annul mean variation of AOD, AE, SSA and AI 0.60 ± 0.15 to 0.76 ± 0.30 (0.54 ± 0.25 to 0.76 ± 0.33), 1.00 ± 0.45 to 1.28 ± 0.28 (1.05 ± 0.36 to 1.45 ± 0.28), 0.91 ± 0.01 to 0.93 ± 0.01 (0.92 ± 0.01 to 0.93 to 0.01) and 0.55 ± 0.41 to 0.77 ± 0.48 (0.35 ± 0.35 to 0.55 to 0.44) at Delhi (Lucknow) stations.
2. Daily variation of AOD, AE, SSA and AI 0.6 to 3.4 (0.05 to 3.5), 0 to 1.8 (0 to 1.8), 0.8 to 1.0 (0.8 to 1.0) and -1.1 to 5.1 (-1.3 to 3.4) at Delhi (Lucknow) stations.
3. AOD dominate higher values in Winter/Post-Monsoons show higher dense haze, fog and smog which are largely due to growth of population and increasing urbanization/industrialization.

ACKNOWLEDGEMENTS

Authors express their sincere gratitude to the Director, IITM, Pune for support and encouragement throughout the study. We sincerely acknowledge MODIS and OMI satellite for the use of aerosol products and imageries in this study. SK expresses his gracious thank to Director, IITM for providing the necessary infrastructure facilities to carry out his research work at IITM (Delhi Branch).

REFERENCES

Bréon, F. M., D. Tanré, and S. Generoso (2002), Aerosol effect on cloud droplet size monitored from satellite, *Science*, 295(5556), 834–838, doi:10.1126/science.1066434.

Eck, T.F., Holben, B.N., Reid, J.S., Dubovik., Smirnov, A., O'Neill, N.T., Slutsker, I., Kinne, S., (1999). The wavelength dependence of the optical depth of biomass burning, urban and desert dust aerosols. *J. Geophys. Res.* 104: 31333–31350

Intergovernmental Panel on Climate Change (IPCC) (2001), In The Scientific Basis: Climate Change (2001), edited by J. T. Houghton, Y. Ding, D. J. Griggs, M. Noguer, V. D. Linden, and D. Xiaosu, Cambridge Univ., Press, New York, USA.

Intergovernmental Panel on Climate Change (IPCC) (2007), in *Climate Change (2007): The Physical Science Basis. Contribution of Working Group I to the Fourth Assessment Report of the Intergovernmental Panel on Climate Change*, edited by S. Solomon, D. Qin, M. Minning, Z. Chen, M. Marquis, K. B. Averyt, M. M. B. Tignor, and H. L. Miller, pp. 1–18, Cambridge Univ., Press, New York, USA.

Li, Z., Xia, Z., Cribb, M., Mi, W., Holben, B., Wang, P., Chen, H., Tsay, S., Eck, T.F., Zhao, F., Dutton, E.G., Dickerson, R.E., (2007). Aerosol optical properties and their radiative effects in northern China; *J. Geophys. Res.* *112*, D22S07.

Lodhi, N. K., Beegum, S. N., Singh, S., & Kumar, K. (2013). Aerosol climatology at Delhi in the western Indo-Gangetic Plain: Microphysics, long-term trends, and source strengths. *Journal of Geophysical Research: Atmospheres*, *118*(3), 1361-1375.

Ramanathan, V., P. J. Crutzen, J. T. Kiehl, and D. Rosenfeld (2001), Aerosols, climate, and the hydrological cycle, *Science*, *7*, 294(5549), 2119–2124.

Rousseau, D.-D., D. Duzer, J. L. Etienne, G. Cambon, D. Jolly, J. Ferrier, and P. Schevin (2004), Pollen record of rapidly changing air trajectories to the North Pole, *J. Geophys. Res.*, *109*, D06116, doi:10.1029/2003JD003985.

Russell, P. B., P. V. Hobbs, and L. L. Stowe (1999), Aerosol properties and radiative effects in the United States East Coast haze plume: An overview of the Tropospheric Aerosol Radiative Forcing Observational Experiment (TARFOX), *J. Geophys. Res.*, *104*(D2), 2213–2222, doi:10.1029/1998JD200028.

Satheesh, S. K., J. Srinivasan, and K. K. Moorthy (2006b), Spatial and temporal heterogeneity in aerosol properties and radiative forcing over Bay of Bengal: Sources and role of aerosol transport, *J. Geophys. Res.*, *111*, D08202, doi:10.1029/2005JD006374.

Srivastava, A.K., Devara, P.C.S., Rao, Y.J., Bhavanikumar, Y., Rao, D.N., (2008). Aerosol optical depth, ozone and water vapor measurements over Gadanki, a tropical station in peninsular India. *Aerosol and Air Quality Research*, *8*(4), 459-476.

WINTER AEROSOL CHARACTERIZATION AT AN URBAN COASTAL SITE (BHUBANESWAR) LOCATED IN THE DOWNWIND OF INDO-GANGETIC PLAINS

SUBHASHMITA PANDA, R. BOOPATHY, TRUPTI DAS

Department of Environment and Sustainability, Institute of Minerals & Materials Technology (CSIR), Bhubaneswar, India

KEYWORDS: Water soluble ion, trace metal, morphology

INTRODUCTION

Atmospheric particulate matter (PM) is directly emitted into the air (primary PM) or generated in the atmosphere from precursor gases (secondary PM). The PM composition is highly variable in space, time and meteorological parameters (Rastogi and Sarin, 2005). It plays an important role in various physicochemical processes occurring in the troposphere by scattering and absorbing solar radiation, provides active sites for the uptake of several chemical species and trace gases; thereby understanding phase changes and hence modifying the atmospheric radiative properties (Ramanathan et al., 2001a). In addition, aerosol particles are closely coupled with atmospheric chemistry as several chemical reactions occurring in the atmosphere are often mediated via their surface properties. The chemical reactions could further lead to change in the physical and optical properties through changes in their size distribution (from fine to coarse mode due to interaction of acidic species with mineral dust) and from hydrophilic to hydrophobic character (Dentener et al. 1996; Rastogi and Sarin 2006). Exposure to PM may lead to number of negative health effects such as increasing respiratory systems, reduction of lung function, asthma, cough, throat cardiac arrhythmias and so on (Kunzli et al., 2000).

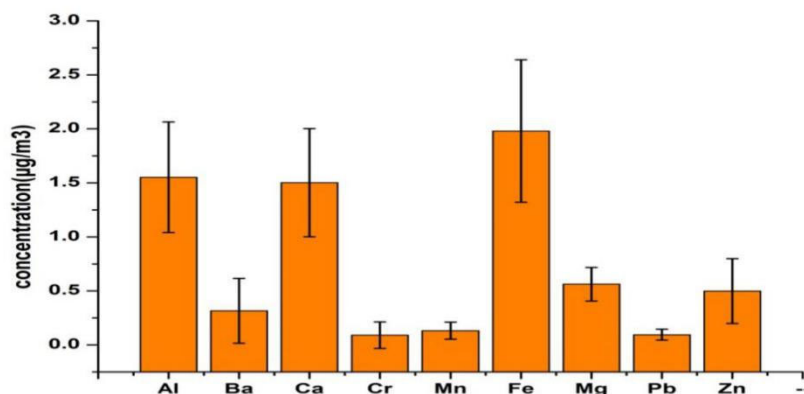
Present study reports the chemical composition of PM₁₀ during winter (Dec 2016-Feb 2017) at Bhubaneswar (BBR, 20.30°N, 85.83°E), one of a rapidly growing urban coastal site in the eastern belt of India. BBR being situated in the downwind of Indo-Gangetic Plain (IGP) and is a strategic location for outflow of pollutant from IGP to Bay of Bengal (BoB). Mahapatra et al., 2014a, Panda et al. 2015 claimed high Black carbon (BC), PM, elemental carbon (EC), organic carbon (OC) concentration over BBR in winter compared to other season. Therefore an attempt has been made to study the chemical composition of PM for its water soluble ions and metals concentration and micro-structural property of PM over the study site. The

composition and evaluation may be helpful to access the possible sources of emission which are responsible for the air quality local and regional emission.

METHODS

High volume sampler (HVS) was placed on the roof top of CSIR-IMMT, Bhubaneswar at a height of about 20 m above the ground level. The site is situated at a distance of 1.5km from National Highway-5 and is surrounded by plantation inside the institute premises. PM₁₀ samples were collected using pre-baked (550°C for 30 min in muffle furnace) quartz microfiber filter paper. Samples were collected thrice a week for 24 hour with an average flow rate of 1m³/min. Before sampling, the papers were numbered and kept in the desiccators for 24 hour and weighed using weighing balance (least count: 0.00001 g). After exposure, the papers were also preserved and desiccated for 24 hour before weighing.

One fourth of the sample filters were soaked in 40 ml of aqua regia solution (HNO: HCl in 3:1) and kept on hot plate at 150°C for digestion until to have a clear solution. After complete digestion the solution were filtered and up to required volume for analyses of trace elements using using Inductively Coupled Plasma Optical Emission Spectroscopy (ICP-OES) (Make:Perkin Elmer).The other one fourth of portion of the filter paper were treated with deionised water for extraction of water soluble ions and tested using Ion chromatography (IC) (Dionex ICS 1000 model). The microstructural analysis



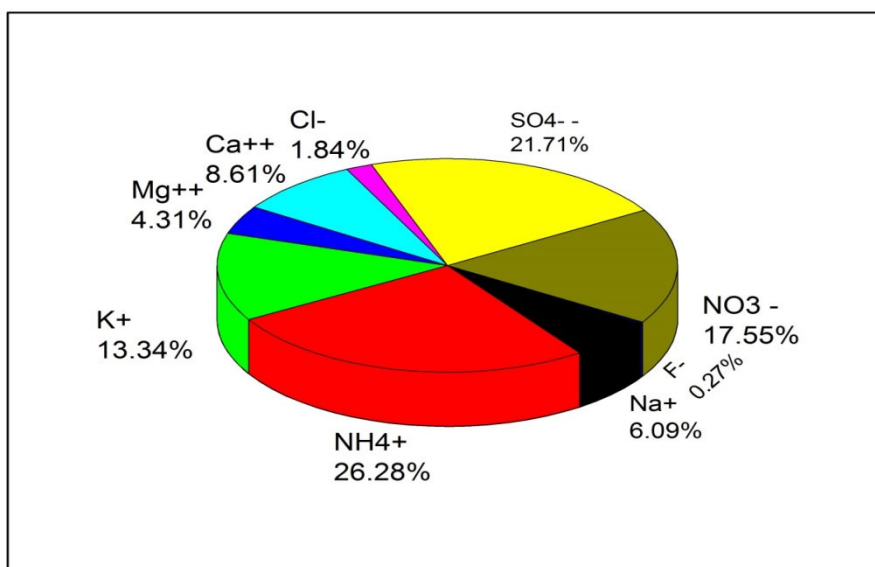
of samples were also done using Scanning electron microscopy coupled with energy dispersive spectrometer (SEM-EDS).

Fig. 1 Heavy metal concentration over BBR during winter

RESULTS & DISCUSSIONS

The average PM_{10} mass loading was found to be $109.58 \pm 32.58 \mu\text{g}/\text{m}^3$ during the study period from December 2016 to February 2017. This is observed to be higher than the standard permissible mass concentration as per WHO. Further the chemical speciation analysis confirmed the presence of many trace metals in the PM_{10} samples. Among the studied major metals, Fe was found to be the highest mass concentration followed by Ca, Al, Mg, Zn. The highest concentration of Fe may be due to dominance of lateritic soil in BBR (fig.1) (P.S. Mahapatra et al, 2012). Airborne soil and dust is the major constituent for the presence of Ca, Al, Fe, Mg (Lough et al.2005). There are reports for the possible sources of Zn, Mn, Pb, Ba, Fe are attributed to vehicular emission (Querol et al. 2008). The study location BBR is also one of the rapidly growing city in the eastern part of India, hence increase in vehicular emission are also one of the major sources of PM_{10} .

The estimated water soluble ion constitute contributed to nearly 47% of PM_{10} and the observed increase in the trend is $\text{NH}_4^+ > \text{SO}_4^{2-} > \text{NO}_3^- > \text{K}^+ > \text{Ca}^{2+} > \text{Na}^+ > \text{Mg}^{2+} > \text{F}^- > \text{Cl}^-$ respectively. Secondary inorganic aerosols (ammonium, sulphate and nitrate) found to be dominant over the site being originate from anthropogenic sources as well as natural source from ocean and volcanic activities. NH_4^+ is the basic component which will neutralise the acidic component (HCl , H_2SO_4 , HNO_3) in the ambient air. The other possible emission through long range transport, like biomass burning, wood



burning and vegetative crop residue burning are also responsible for K^+ and anthropogenic SO_4^{2-} ion from IGP belt during winter (Panda et al.2015).

Fig.2 Water soluble inorganic ion concentration over BBR during winter

Fig.3a shows the SEM micrographs for the PM sample BBR and Fig 3b shows the spectral analysis for identification of possible elemental composition of particle. The irregular, spherical, spheroidal and cluster like shapes of particles confirmed the freshly emitted soot or carbonaceous particles-with carbon and oxygen. The aggregate of particles indicate the growth and formation of secondary particles due to age and meteorological factors. The elemental composition of particles shows that oxygen and carbon are dominant over other elements this could be due to all the trace elements are always present in the form of oxides. The concentration trend of elements is $O > C > Si > S > Al > Fe > K > Ca$ (Fig. 3c). This indicates the presence of soot and tarballs particles. This type of particle are originated from gasoline and diesel exhausts as well as from biomass burning (Parth et al.,2012).

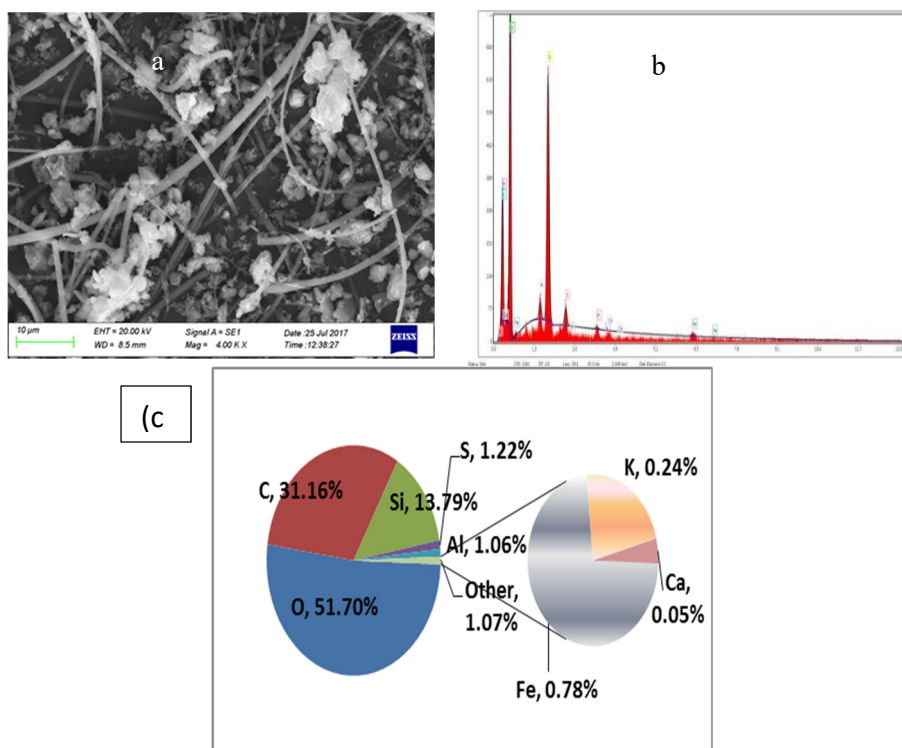


Fig.3 (a) SEM images of PM₁₀ (b) EDX spectrum of PM10 (c) Percentage distribution chart Element observed in EDX for PM

CONCLUSION

In the present study, the concentration of WSI and metal in PM₁₀ were estimated during winter (dec2016-feb2017) at BBR site. The average concentration of PM₁₀ was found to be $109.58 \pm 32.58 \mu\text{g}/\text{m}^3$ and metals contribute nearly 6%(w/w) and WSI contributes to 47% (w/w) of the total mass of PM₁₀. The possible sources for Soot and tar particles are vehicular emission over the site. The positive linear correlation of SO_4^{2-} and NO_3^- with NH_4^+ indicates formation of secondary organic aerosols at the study site. Further, the ratio of $\text{SO}_4^{2-}/\text{NO}_3^-$ concentration was observed to be >1 which signifies the atmospheric acidity during winter season. The back trajectory indicates the large air masses coming from eastern IGP to the study site are the major contribution of aerosol mass during winter season.

ACKNOWLEDGMENT

The authors are thankful to the ISRO-GBP for the financial support through ARFI network project. Also thank the Director CSIR-IMMT and Head of the Department for the extend to use internal facility in CSIR-IMMT, Bhubaneswar.

REFERENCES

- Dentener, F.J., Carmichael, G.R., Zhang, Y., Lelieveld, J. and Crutzen, P.J. (1996). Role of mineral aerosol as a reactive surface in the global troposphere. *Journal of Geophysical Research* 101: doi: 10.1029/96JD01818. issn: 0148-0227.
- Kunzli, N., et al. (2000) Public-Health Impact of Outdoor and Traffic-Related Air Pollution: A European Assessment. *The Lancet*, 356, 795-801.
- Lough, G.C., Schauer, J.J., Park, J.S., Shafer, M.M., DeMinter, J.T., Weinstein, J.P., 2005. Emissions of metals associated with motor vehicle roadways. *Environ. Sci. Technol.* 39, 826e836.
- Mahapatra PS, Panda S, Das N et al (2014a) Variation in black carbon mass concentration over an urban site in the eastern coastal plains of the Indian sub-continent. *Theor Appl Climatol* 117:133–147. doi:10.1007/s00704-013-0984-z

Mahapatra PS et al.(2012) Urban air-quality assessment and source appointment studies for Bhubaneswar, Odisha. *Theor Appl Climatol* doi:10.1007/s00704-012-07329

Panda et al. (2016) Organic and elemental carbon variation in PM_{2.5} over megacity Delhi and Bhubaneswar, a semi-urban coastal site in India. *Nat Hazards* (2016) 80:1709–1728. Doi: 10.1007/s11069-015-2049-3

Querol, X., Alastuey, A., Moreno, T., Viana, M.M., Castillo, S., Pey, J., Rodriguez, S., Artinano, B., Salvador, P., Sanchez, M., Garcia Dos Santos, S., HerceGarraleta, M.D., Fernandez-Patier, R., Moreno-Grau, S., Negral, L., Minguillon, M.C., Monfort, E., Sanz, M.J., Palomo-Marin, R., Pinilla-Gil, E., Cuevas, E., de la Rosa, J., Sanchez de la Campa, A., 2008. Spatial and temporal variations in airborne particulate matter (PM₁₀ and PM_{2.5}) across Spain 1999e2005. *Atmos. Environ.* 42, 3964e3979

Ramanathan, V., Crutzen, P.J., Kiehl, T.T., Rosenfeld, D., 2001a. Aerosols, climate and hydrological cycle. *Science* 294,2119-2124.

Rastogi, N., Sarin, M.M., 2005. Long term characterisation of ionic species in aerosols from urban and high altitude sites in western India; role of mineral dust and anthropogenic sources. *Atmospheric Environment* 43,6159-6167.

Rastogi, N., Sarin, M.M., 2006. Chemistry of aerosols over a semi-arid region: Evidence for acid neutralisation by mineral dust.

THE SUB-DAILY VARIABILITY IN AEROSOLS AND ITS RADIATIVE EFFECT INFERRED FROM GROUND AND SATELLITE MEASUREMENTS

T.MUKHERJEE^{1,2,3}, V.VINOJ²

¹International Centre for Integrated Mountain Development, Nepal

²School of Earth, Ocean and Climate Science, Indian Institute of Technology, Bhubaneswar, Odisha, India.

³Department of Atmospheric Science, University of Calcutta, West Bengal, India

KEYWORDS: Aerosol optical depth, AERONET, diurnal variability, Indo-Gangetic Plains, MODIS

INTRODUCTION

The importance of atmospheric aerosols and their influence on climate and human health are well known. Atmospheric aerosols can influence climate directly by scattering or absorbing solar radiation (Atwater, 1970; Ensor et al., 1971) and indirectly by affecting cloud droplet concentrations (Dipu et al., 2013; Gu et al., 2012; Lohmann and Feichter, 2004; Menon et al., 2002; Ning et al., 2015; Panicker et al., 2010; Rotstajn and Lohmann, 2002; Takemura et al., 2005). Several studies have reported the rapid increase of aerosol loading over Indian region (Babu et al., 2013; Kaskaoutis et al., 2012; Kiran Kumar et al., 2013; Krishna Moorthy et al., 2013; Ramachandran et al., 2012; Sarkar et al., 2006; Sreekanth, 2016). Recently, it was also shown that dust aerosols over the Indian region has decreased by about 20% since the start of the 21st century (Pandey et al., 2017).

In addition to the long term variation, aerosols also exhibit diurnal variation. Large diurnal variability of aerosol optical properties (AOP) have been observed throughout the world (Mazzola et al., 2010; Smirnov, 2002; Zhang et al., 2012). Fine mode aerosols like BC has a typical diurnal variation, depending on the boundary layer conditions (Babu and Moorthy, 2002; Baxla et al., 2009; Dey and Tripathi, 2008; Pant et al., 2006; Vinoj et al., 2010). These diurnal variations could alter the direct aerosol radiative forcing by significant amount (Kassianov et al., 2013; Kuang et al., 2015; Wang et al., 2015; Xu et al., 2016) thereby introducing large bias in the estimation of direct radiative forcing on regional scales (Arola et al., 2013). Understanding these requires satellite based measurements for their distinct advantage of making measurements on large spatial scales. Most satellites providing high quality measurements on a regular basis are polar orbiting in nature. Their

limitation lies in its ability to provide only snapshots at a given time (absence of sub daily data points). Therefore, study of diurnal or sub daily variability requires station based measurements capable of providing high temporal resolution datasets or geostationary satellites capable of providing accurate aerosol retrievals. It may also be mentioned that aerosol impact assessments on regional and global scales uses satellite observations (mostly polar orbiting) to constrain model simulations. In this context, the objective of this study is to understand sub daily variability in aerosols over the Indian region using multiple ground and multiple satellite based measurements. In addition, we also investigate the effect of this on aerosol radiative forcing estimates.

METHODS

The aerosol optical depth (AOD) at 500 nm were retrieved from Aerosol Robotic NETwork (AERONET) version 2 level 1.5 all points for seven stations (Jaipur, Gual Pahari, Nainital, New Delhi, Kanpur, Gandhi College and Bhola) across the Indo-Gangetic Plains for the period since 2001 depending on their availability. The AOD at 500 nm were also obtained from two satellites platforms (Terra and Aqua) that retrieve aerosols using similar sensors (MODIS) but at two different timings depending on their overpass. Thus, level 3 AOD values with a spatial resolution of 1 degree from two different satellite having different overpass time (MODIS Terra at 10:30 IST (5 UTC) and MODIS Aqua at 13:30 IST (8 UTC)) were utilized. The AOD differences between Terra (10:30 IST) and Aqua (13:30 IST) overpass time were then estimated for ground based AERONET observations data and is termed as AOD Difference Range (ADR). Similarly, the AOD difference between Terra and Aqua satellite AOD's were termed as Satellite AOD Difference Range (SDR).

$$\text{ADR} = \text{AERONET AOD}_{500} (10:30 \text{ IST}) - \text{AERONET AOD}_{500} (13:30 \text{ IST})$$

(1)

$$\text{SDR} = \text{Terra AOD}_{550} - \text{Aqua AOD}_{550}$$

(2)

We have calculated the change in aerosol radiative forcing due to this diurnal variation of aerosol. To calculate the forcing difference, Aerosol Radiative Forcing Efficiency (ARFE) was retrieved from AERONET. The ARFE along with ADR (ΔAOD from Observations) and SDR (ΔAOD from satellites) is used to calculate the radiative forcing due to sub-daily variability of aerosols. Thereafter, annual and seasonal variability of ARFE over the stations have been calculated from AERONET data and is multiplied with ADR to generate ARF difference over the stations. To generate the spatial ARF difference over Indian region, lowest minimum ARFE value (by magnitude) among all the stations has been taken and multiplied with SDR. This is done to obtain the

lowest radiative forcing estimate possible for the whole region. In addition, the SDR does not cover the whole day's observation. Therefore, the estimates given here provides the lowest estimate possible due to sub-daily variability.

$$\text{ARF Diff}_{\text{stn}} = \text{ARFE} * |\text{ADR}| \quad (3)$$

$$\text{ARF Diff}_{\text{spa}} = \text{ARFE} * |\text{SDR}| \quad (4)$$

To validate our results we attempted to calculate ARF difference by creating ARFE map over Indian region using CERES short wave flux.

RESULTS & DISCUSSIONS

It is observed that the AOD over Jaipur (to the west of IGP) has negligible diurnal variability, whereas Bhola to the eastern part has a large variability thereby showing a clear gradient/spatial variability in sub daily AOD's. In terms of percentages, Jaipur depicts ~20% change diurnally while Gandhi College shows ~49% change. It is also evident that the morning time AOD become higher from west to east. This signifies the presence of aerosol diurnal variation throughout the Indian region along with high aerosol loading in the morning. Both SDR and ADR show a clear gradient from west to east. The, spatial variability of SDR is explored over Indian region reiterates the observations made using surface measurements regarding the West-East gradient in sub-daily variability. Though the signs are not comparable, the gradient is clear.

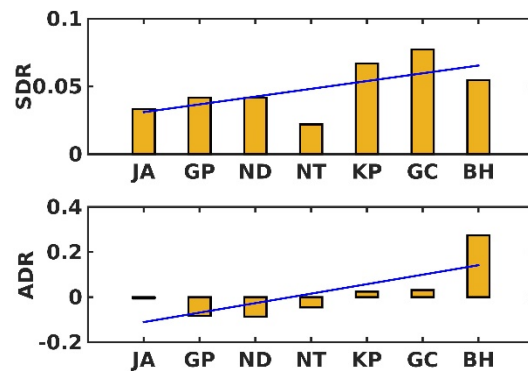


Figure 1. Variation of SDR and ADR over different AERONET stations

The annual change in SDR lies between ~5% to the west increasing to ~20% in the East. It is evident that the difference between two satellites is significant throughout the study region. SDR during winter (DJF) builds a clear gradient from west to east. The gradient is well pronounced over Indo-Gangetic Plain (IGP). It is surprising to witness that two different satellite with only three hours of difference between their overpass times can experience ~20% of change in the AOD value over the eastern Indian region.

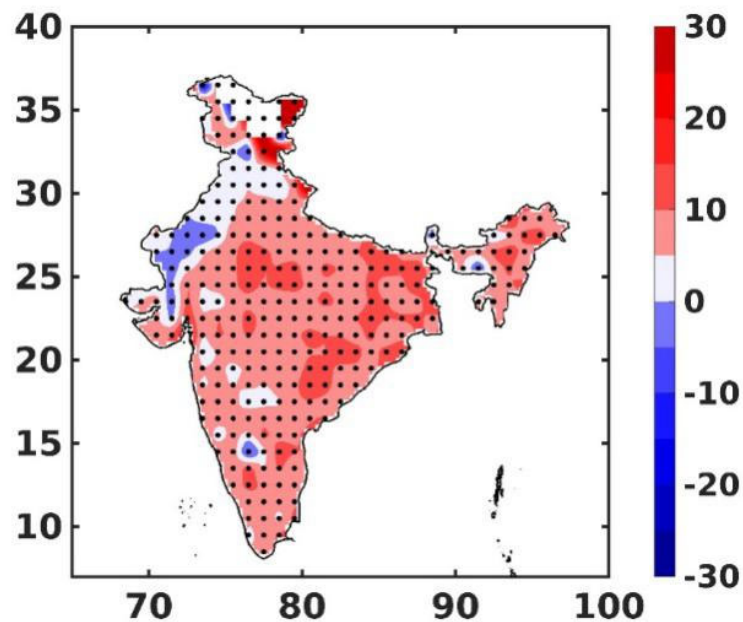


Figure 2. Annual variation of SDR over Indian region. Black Dots denotes 95% significance level using both MODIS Terra and Aqua retrievals.

Further we have explored whether the model derived AOD can capture the diurnal variation. To investigate that, SDR is calculated from extinction coefficient generated by MERRA output. It appears that MERRA is unable to capture the diurnal change over Indian region. Our study indicates that daytime variation of relative humidity may cause the diurnal variation of AOD. In addition, changes to emissions may also create these variabilities. Model emission files are mostly updated every month and hence, diurnal variability in emissions are not captured by them. Also, diurnal variation induced by meteorology requires models to be able to simulate meteorological parameters such as planetary boundary layer height, relative

humidity, winds etc. These may be the limitations that makes models to be unable to capture these sub-daily variabilities.

The ARF difference (BOA) has been calculated for AEONET stations and in spatial scale using equations (3) and (4). Annually the ARF difference because of diurnal variation of AOD over Jaipur is $\sim 1 \text{ W m}^{-2}$ while Gandhi College it increases to $\sim 5 \text{ W m}^{-2}$. Both the annual and seasonal data shows minimum ARF difference at the western part while maximum at the east. The ARF difference at the Western part is $\sim 6 \text{ W m}^{-2}$ while it increases to $\sim 20 \text{ W m}^{-2}$ gradually towards the East. The gradient of ARF difference is more pronounced over IGP. It is surprising to witness that even at the top of the atmosphere the ARF difference reaches more than 4 W m^{-2} during winter. The ARF difference map generated from CERES data also shows that even in TOA the gradient of forcing difference exists, though the values are not higher. All these evidences demonstrates the importance of diurnal variation of AOD on aerosol radiative forcing. It is important that models are able to capture such diurnal variability, if aerosol induced impact assessment studies are to be undertaken.

CONCLUSIONS

1. The study reveals large sub-daily variability in AOD over the Indian region.
2. These variabilities have a clear spatial gradient from West to East over the IGP with maximum changes observed to be as high as $\sim 49\%$ over Eastern IGP.
3. The same spatial variability from satellites were smaller ($\sim 20\%$).
4. The aerosol forcing differences due to these sub-daily variability could be $\sim 15 \text{ W m}^{-2}$ at the bottom of the atmosphere while more than 1.5 W m^{-2} at the top of the atmosphere.
5. MERRA is unable to capture these sub-daily variability and this aspect need to be explored further if impact assessments are to be carried out.

ACKNOWLEDGEMENTS

This study was partially supported by core funds of ICIMOD contributed by the governments of Afghanistan, Australia, Austria, Bangladesh, Bhutan, China, India, Myanmar, Nepal, Norway, Pakistan, Sweden, and Switzerland. The authors also want to express their gratitude to Indian Institute of Technology, Bhubaneswar, India and the Aerosol Radiative Forcing over India (ARFI) project of Indian Space Research Organisation for their support.

The authors also acknowledge Dr. Bhupesh Adhikary, ICIMOD, for his valuable review about the study.

REFERENCES

- Arola, A., Eck, T.F., Huttunen, J., Lehtinen, K.E.J., Lindfors, A. V., Myhre, G., Smirnov, A., Tripathi, S.N., Yu, H., 2013. Influence of observed diurnal cycles of aerosol optical depth on aerosol direct radiative effect. *Atmos. Chem. Phys.* 13, 7895–7901. <https://doi.org/10.5194/acp-13-7895-2013>
- Atwater, M.A., 1970. Planetary albedo changes due to aerosols. *Science* 170, 64–6. <https://doi.org/10.1126/science.170.3953.64>
- Babu, S.S., Manoj, M.R., Moorthy, K.K., Gogoi, M.M., Nair, V.S., Kompalli, S.K., Satheesh, S.K., Niranjana, K., Ramagopal, K., Bhuyan, P.K., Singh, D., 2013. Trends in aerosol optical depth over Indian region: Potential causes and impact indicators. *J. Geophys. Res. Atmos.* 118. <https://doi.org/10.1002/2013JD020507>
- Babu, S.S., Moorthy, K.K., 2002. Aerosol black carbon over a tropical coastal station in India. *Geophys. Res. Lett.* 29, 13-1-13-4. <https://doi.org/10.1029/2002GL015662>
- Baxla, S.P., Roy, A.A., Gupta, T., Tripathi, S.N., Bandyopadhyaya, R., 2009. Analysis of diurnal and seasonal variation of submicron outdoor aerosol mass and size distribution in a northern Indian city and its correlation to black carbon. *Aerosol Air Qual. Res.* 9, 458–469. <https://doi.org/10.4209/aaqr.2009.03.0017>
- Dey, S., Tripathi, S.N., 2008. Aerosol direct radiative effects over Kanpur in the Indo-Gangetic basin, northern India: Long-term (2001-2005) observations and implications to regional climate. *J. Geophys. Res. Atmos.* 113, 1–20. <https://doi.org/10.1029/2007JD009029>
- Dipu, S., Prabha, T. V., Pandithurai, G., Dudhia, J., Pfister, G., Rajesh, K., Goswami, B.N., 2013. Impact of elevated aerosol layer on the cloud macrophysical properties prior to monsoon onset. *Atmos. Environ.* 70, 454–467. <https://doi.org/10.1016/J.ATMOSENV.2012.12.036>
- Ensor, D.S., Porch, W.M., Pilat, M.J., Charlson, R.J., Ensor, D.S., Porch, W.M., Pilat, M.J., Charlson, R.J., 1971. Influence of the Atmospheric Aerosol on Albedo. *J. Appl. Meteorol.* 10, 1303–1306. [https://doi.org/10.1175/1520-0450\(1971\)010<1303:IOTAAO>2.0.CO;2](https://doi.org/10.1175/1520-0450(1971)010<1303:IOTAAO>2.0.CO;2)

Gu, Y., Liou, K.N., Jiang, J.H., Su, H., Liu, X., 2012. Dust aerosol impact on North Africa climate: a GCM investigation of aerosol-cloud-radiation interactions using A-Train satellite data. *Atmos. Chem. Phys.* 12, 1667–1679. <https://doi.org/10.5194/acp-12-1667-2012>

Kaskaoutis, D.G., Singh, R.P., Gautam, R., Sharma, M., Kosmopoulos, P.G., Tripathi, S.N., 2012. Variability and trends of aerosol properties over Kanpur, northern India using AERONET data (2001–10). *Environ. Res. Lett.* 7, 024003. <https://doi.org/10.1088/1748-9326/7/2/024003>

Kassianov, E., Barnard, J., Pekour, M., Berg, L.K., Michalsky, J., Lantz, K., Hodges, G., 2013. Do diurnal aerosol changes affect daily average radiative forcing? *Geophys. Res. Lett.* 40, 3265–3269. <https://doi.org/10.1002/grl.50567>

Kiran Kumar, T., Gadhavi, H., Jayaraman, A., Sai Suman, M.N., Vijaya Bhaskara Rao, S., 2013. Temporal and spatial variability of aerosol optical depth over South India as inferred from MODIS. *J. Atmos. Solar-Terrestrial Phys.* 94, 71–80. <https://doi.org/10.1016/j.jastp.2012.12.010>

Krishna Moorthy, K., Suresh Babu, S., Manoj, M.R., Satheesh, S.K., 2013. Buildup of aerosols over the Indian Region. *Geophys. Res. Lett.* 40. <https://doi.org/10.1002/grl.50165>

Kuang, Y., Zhao, C.S., Tao, J.C., Ma, N., 2015. Diurnal variations of aerosol optical properties in the North China Plain and their influences on the estimates of direct aerosol radiative effect. *Atmos. Chem. Phys.* 15, 5761–5772. <https://doi.org/10.5194/acp-15-5761-2015>

Lohmann, U., Feichter, J., 2004. Global indirect aerosol effects: a review. *Atmos. Chem. Phys. Discuss.* 4, 7561–7614. <https://doi.org/10.5194/acpd-4-7561-2004>

Mazzola, M., Lanconelli, C., Lupi, A., Busetto, M., Vitale, V., Tomasi, C., 2010. Columnar aerosol optical properties in the Po Valley, Italy, from MFRSR data. *J. Geophys. Res. Atmos.* 115, 1–17. <https://doi.org/10.1029/2009JD013310>

Menon, S., Genio, A.D. Del, Koch, D., Tselioudis, G., 2002. GCM Simulations of the Aerosol Indirect Effect: Sensitivity to Cloud Parameterization and Aerosol Burden. *J. Atmos. Sci.* 59, 692–713. [https://doi.org/10.1175/1520-0469\(2002\)059<0692:GSOTAI>2.0.CO;2](https://doi.org/10.1175/1520-0469(2002)059<0692:GSOTAI>2.0.CO;2)

Ning, H., Li-juan, L., Bin, W., 2015. The Role of the Aerosol Indirect Effect in the Northern Indian Ocean Warming Simulated by CMIP5 Models. *Atmos. Ocean. Sci. Lett.* 2834, 411–416. <https://doi.org/10.3878/j.issn.1674-2834.14.0032>

Panicker, A.S., Pandithurai, G., Dipu, S., 2010. Aerosol indirect effect during successive contrasting monsoon seasons over Indian subcontinent using MODIS data. *Atmos. Environ.* 44, 1937–1943. <https://doi.org/10.1016/J.ATMOSENV.2010.02.015>

Pant, P., Hegde, P., Dumka, U.C., Sagar, R., Satheesh, S.K., Moorthy, K.K., Saha, A., Srivastava, M.K., 2006. Aerosol characteristics at a high-altitude location in central Himalayas: Optical properties and radiative forcing. *J. Geophys. Res. Atmos.* 111, 1–9. <https://doi.org/10.1029/2005JD006768>

Ramachandran, S., Kedia, S., Srivastava, R., 2012. Aerosol optical depth trends over different regions of India. *Atmos. Environ.* 49, 338–347. <https://doi.org/10.1016/j.atmosenv.2011.11.017>

Rotstayn, L.D., Lohmann, U., 2002. Tropical rainfall trends and the indirect aerosol effect. *J. Clim.* 15, 2103–2116. [https://doi.org/10.1175/1520-0442\(2002\)015<2103:TRTATI>2.0.CO;2](https://doi.org/10.1175/1520-0442(2002)015<2103:TRTATI>2.0.CO;2)

Sarkar, S., Chokngamwong, R., Cervone, G., Singh, R.P., Kafatos, M., 2006. Variability of aerosol optical depth and aerosol forcing over India. *Adv. Sp. Res.* 37, 2153–2159. <https://doi.org/10.1016/j.asr.2005.09.043>

Smirnov, a., 2002. Diurnal variability of aerosol optical depth observed at AERONET (Aerosol Robotic Network) sites. *Geophys. Res. Lett.* 29, 28–31. <https://doi.org/10.1029/2002GL016305>

Sreekanth, V., 2016. Discussion on linear long-term trends in aerosol and cloud properties over India and its surrounding waters. *Adv. Sp. Res.* 57, 2104–2114. <https://doi.org/10.1016/j.asr.2016.02.015>

Takemura, T., Nozawa, T., Emori, S., Nakajima, T.Y., Nakajima, T., 2005. Simulation of climate response to aerosol direct and indirect effects with aerosol transport-radiation model. *J. Geophys. Res. D Atmos.* 110, 1–16. <https://doi.org/10.1029/2004JD005029>

Vinoj, V., Satheesh, S.K., Moorthy, K.K., 2010. Optical, radiative, and source characteristics of aerosols at Minicoy, a remote island in the southern Arabian Sea. *J. Geophys. Res. Atmos.* 115, 1–19.

<https://doi.org/10.1029/2009JD011810>

Wang, Z., Liu, D., Wang, Y., Wang, Z., Shi, G., 2015. Diurnal aerosol variations do affect daily averaged radiative forcing under heavy aerosol loading observed in Hefei, China. *Atmos. Meas. Tech.* 8, 2901–2907. <https://doi.org/10.5194/amt-8-2901-2015>

Xu, H., Guo, J., Ceamanos, X., Roujean, J.L., Min, M., Carrer, D., 2016. On the influence of the diurnal variations of aerosol content to estimate direct aerosol radiative forcing using MODIS data. *Atmos. Environ.* 141, 186–196. <https://doi.org/10.1016/j.atmosenv.2016.06.067>

Zhang, Y., Yu, H., Eck, T.F., Smirnov, A., Chin, M., Remer, L.A., Bian, H., Tan, Q., Levy, R., Holben, B.N., Piazzolla, S., 2012. Aerosol daytime variations over North and South America derived from multiyear AERONET measurements. *J. Geophys. Res. Atmos.* 117, 1–13. <https://doi.org/10.1029/2011JD017242>

LONG TERM TREND IN PM10 ASSOCIATED METAL CONCENTRATION IN AN INSTITUTIONAL AREA OF DELHI

AMIT KUMAR YADAV, VICTOR VILUWA KENGA, P S KHILLARE

School of Environmental Science, Jawaharlal Nehru University, New Delhi

(*Correspondence at psk@mail.jnu.ac.in, amityadavecc@gmail.com)

KEYWORDS: PM10, Metals, Health risk, Delhi

INTRODUCTION

Atmospheric particulate matter is a major cause of concern in Delhi, particularly in winter season. Previous studies by various researchers have shown strong association between exposure to ambient respirable particles (inhalable thoracic particles, PM10 and fine particles PM2.5) and deleterious health effects. Further various researchers have established that it is not particulate mass concentration but its chemical composition that has greater influence on human health. Ambient particulate matters are important carriers of metals; a number of them are known to induce formation of reactive oxygen species (ROS) and hydroxyl radicals ($^{\circ}\text{OH}$) in biological tissues, while other can cause neurological disorder, various forms of cancers, heart disease and other ailments. Metals are emitted from different sources like biomass burning, fossil fuel (coal and petroleum) combustion etc. Source identification and a comprehensive assessment of risk to human health in urban environment is essential. With these objectives the present study reports characterization of the inhalable ambient particulate matters (PM10; aerodynamic diameter $\leq 10\mu\text{m}$) with respect to 8 major and trace elements (Fe, Mn, Cu, Cd, Cr, Co, Pb and Ni) collected during the months of winter (November to February) of two consecutive years and compared with data reported from same location and season earlier.

MATERIALS AND METHODS

Jawaharlal Nehru University (JNU) campus, site of the present study, with urban background is situated in Qutub Institutional (cum residential) area in south Delhi. The campus is covered with good vegetation and spread in 4 Km^2 area on the ridge of Aravali Hills. Sampling was carried out at the height of 13m from the ground on roof top of School of Environmental Sciences building. PM10, samples were collected during two consecutive seasons (Nov 2016- Feb 2017 and Nov 2017- Feb 2018) on whatman glass microfiber filter GF/A (8"x10") (pre- baked at 450 $^{\circ}\text{C}$ for 12 hours) once a week for 24-

h, using high- volume sampler (RDS, BioAnalytical Pvt. Ltd). Filters were conditioned in a desiccator over self indicating silica- gel for 48 hours before and after the sampling and mass of PM10 was determined gravimetrically using microbalance (Model AE 163, Mettler, sensitivity 0.0001g). Metals were extracted using Microwave digestion system (Speedwave MWS-3⁺, Berghof, Germany). Circular portion of 8cm diameter cut from each samples were digested with a mixture of acids (10ml HNO₃ + 3ml HF). Extracts were filtered with whatman no. 42 and volume made-up to 25ml with deionized MilliQ water. Metals analysis was carried out by Atomic absorption spectrometer system (Solaar M Series, Thermo Scientific).

RESULT AND DISCUSSION

Fig.1 shows the trend of PM10 level and distribution of associated metal concentration in winter season at JNU, Delhi. The level of PM10 is 2-3 times higher than the annual NAAQS value (60 $\mu\text{g m}^{-3}$). Concentration of Ni (10 ng m^{-3} and 4 ng m^{-3} in 2016-17 and 2017-18 respectively) was lower than the national standard (NAAQS for Ni: 20 ng m^{-3}) (MoEF 2009). Mean winter concentration of Pb (0.53 $\mu\text{g m}^{-3}$ in 2017-18) is slightly higher while considerably lower (0.32 $\mu\text{g m}^{-3}$ in 2016-17) than the stipulated NAAQS (Pb: 0.5 $\mu\text{g m}^{-3}$) while that for Cd (5 ng m^{-3} in 2017-18) was equal to European Union target (5 ng m^{-3} , EU Directive 2004/107/CE).

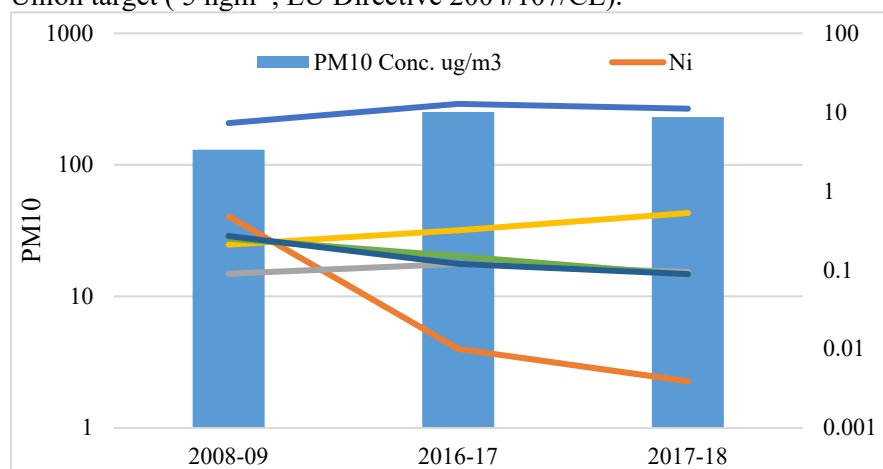


Figure 1. Mean concentration of PM10 and metals (both in $\mu\text{g m}^{-3}$) at JNU, New Delhi during winter season (November- December)

Location Co	Year Cd	PM10 Reference	Fe	Mn	Cu	Ni	Pb	Cr
JNU, Delhi 0.005	2017-18 0.005	230.8 Present study	11.1	0.09	0.09	0.004	0.53	0.09
JNU, Delhi 0.0008	2016-17 NR	252.1 Present study	12.8	0.12	0.15	0.01	0.32	0.12
JNU, Delhi 0.53	2011-12 0.01	246.5 Kumar et al., (2018)	10.0	0.18	0.17	NR	0.74	0.08
JNU, Delhi NR	2008-09 0.008	130.1 Sarkar et al., (2011)	7.3	0.27	0.25	0.48	0.21	0.09
*JNU, Delhi NR	1997-98 0.003	285.6 Khillare et al., (2002)	NA	NR	NR	0.077	0.28	0.05
*Delhi, India NR	2003-04 0.01	512.9 Shridhar et al., (2010)	16.4	0.74	3.7	0.15	0.44	0.35

Table1: Comparison of PM10 and elemental concentration (μgm^{-3}) observed at same location and season and in India.

*annual average

ENRICHMENT FACTOR (EF) AND INHALATION CANCER RISK (ICR)

EFs were calculated to understand the concentration of anthropogenic sources to atmospheric metals as $EF = (X_{\text{aerosol}}/Ref_{\text{aerosol}})/(X_{\text{ucc}}/Ref_{\text{ucc}})$ where X is the element under consideration in aerosol and upper continental crust (UCC) and Ref is element having typical crustal source. Fe was used as the reference element. Mn, Ni, Co and Cr were non- enriched in aerosol while Cu and Pb are moderately- enriched elements. Remaining element i.e. Cd was highly enriched with EF 149.3 in 2017-18.

Enrichment Factor (EF)			Inhalation Cancer Risk (ICR)	
Element	2016-17 2017-18	2017-18	Element	2016-17
Mn	0.57 9.3×10^{-6}	0.46	Ni	2.4×10^{-7}

Cu	24.7	17	Cd	-
9.8×10^{-6}				
Ni	1.37	0.58	Cr (VI)	
2.0×10^{-4}	1.6×10^{-4}			
Co	0.18	1.2		
Cr	8.6	7.5		
Cd	-	149.3		
Pb	45.5	86.6		

Table 2. Enrichment Factor (EF) and Inhalation Cancer Risk (ICR) of analyzed metal species in PM10 at JNU

Inhalation cancer risk was calculated for Cd, Cr (VI) and Ni by using equation $ICR = \sum (EC_i \times IUR_i)$ where EC_i is the ambient concentration of chemical i ($\mu\text{g m}^{-3}$) and IUR_i is the inhalation unit risk ($\mu\text{g m}^{-3}$). ICRs values found 2.0×10^{-4} and 2.4×10^{-6} for Cr (VI) and Ni in 2016-17 while it was 9.8×10^{-6} , 1.6×10^{-4} , and 9.3×10^{-7} for Cd, Cr (VI) and Ni respectively in 2017-18. ICR between 10^{-6} to 10^{-4} represent potential risk where as ICR greater than 10^{-4} indicate high potential health risk. Societal ICR was calculated by multiplying individual ICRs by Delhi population (i.e.17 million) and it was found up to 3501 excess cancer cases (3497 for Cr (VI) and 4 for Ni) in 2016-17 and 2936 (167 for Cd, 2752 for Cr (VI) and 16 for Ni) in 2017-18 may occur in Delhi due to life time inhalation exposure to these metals at their respective concentrations observed in this study.

CONCLUSION

Delhi, one of the most polluted city of the world experiences severe ambient air pollution all over the year and particularly in winter. This study shows PM10 level is always found 3-4 times higher than the national standard (NAAQS, PM10: $60 \mu\text{g m}^{-3}$) and an increasing trend seen in PM10 level since last 10 years in Delhi. Metals can cause serious health consequences and some of them are well known for their carcinogenic potential. High EF values for Pb and Cd indicating about the anthropogenic sources of metals. Further, the ICR values of Cd, Cr (VI) and Ni established potential health risk. Health risk due to metals estimated with a total 3501 and 2752 in 2016-17 and 2017-18 respectively excess cancer cases being likely in Delhi for lifetime inhalation exposure to these metallic species at their current concentrations. Uncontrolled construction work, rapid increase in automobiles and resuspension of road dust seems to be a potent source of suspended particulate matter in the atmosphere of Delhi. Policy makers should take note that the efforts are not sufficient to mitigate the high level of particulate load in ambient atmosphere of Delhi.

REFERENCES

Kumar et al., Chemical Characteristics of Fine and Coarse Particles during Winter over Two Urban Cities in North India, *Aerosol and Air Quality Research*, x: 1-18, xxxx.

Sarkar et al., Association of Polycyclic Aromatic Hydrocarbons (PAHs) and Metallic Species in a Tropical Urban Atmosphere- Delhi, India, *J Atmos Chem* (2011) 68:107-126.

Khillare et al., Spatial and Temporal Variation of Heavy Metals in Atmospheric Aerosol of Delhi, *Environmental Monitoring and Assessment* 90: 1-21, 2004.

Shridhar et al., Metallic Species in Ambient Particulate Matter at Rural and Urban Location of Delhi, *Journal of Hazardous Materials* 175 (2010) 600-607.

VARIATION OF NH₃ CONCENTRATION FROM AGRICULTURAL ACTIVITIES IN RELATION WITH METEOROLOGICAL PARAMETERS

SUDESH¹ AND U.C.KULSHRESTHA²

¹School of Environmental Sciences, Atmospheric Chemistry and Climate Change Group,
Jawaharlal Nehru University, New Delhi – 110067, India

KEYWORDS: Air quality, aerosol, fertilizer application, livestock

INTRODUCTION

India is mainly an agricultural country with about 65% of its population depending on agriculture. Until the middle of the 20th century Indian agriculture predominantly relied on the application of organic manure. After green revolution the consumption of inorganic fertilizers is increased substantially with the introduction high yielding varieties and development of irrigation facilities. Greater food requirements and increasing productivity to meet nutritional requirements of a growing population contribute in atmospheric NH₃. Due to increase in fertilizer usage and livestock numbers NH₃ emissions have increased substantially (Sutton et al., 1993). Atmospheric NH₃ is the most abundant basic gas which plays a significant role in the neutralization of aerosols and rain water. NH₃ gas acts as a precursor for secondary aerosol formation by combining with atmospheric acids viz. H₂SO₄, HNO₃, HCl due to its basic nature. This results in formation of secondary particulates such as ammonium sulphate (NH₄)₂SO₄, ammonium nitrate NH₄NO₃, ammonium chloride NH₄Cl, thereby, reducing air quality. NH₃ has a residence time of few days to few weeks whereas ammonium ion as an aerosol may have residence time of 1-15 days in atmosphere. Hence, ammonium (NH₄⁺) is a significant component of atmospheric aerosol. Ammonia and ammonium deposition causes eutrophication of aquatic ecosystems (Walker et al., 2000), soil and water acidification, forest damage (Bouwman et al., 1997).

METHODS

This study was carried out at a rural agricultural site in Chhuchhakwas village of Jhajjar district of Haryana state from July to October 2017. Gaseous ammonia samples were collected using a low volume pump set at a flow rate of LPM. Ammonia gas was absorbed in 25 mM H₂SO₄ in a standard impinger for 6h. The aerosol samples were collected on the PTFE filters (diameter 47

mm and pore size 0.2 μ m) placed upstream to the impingers. Collected gaseous NH₃ samples in absorbing solution (25 mM H₂SO₄) were prepared with the Indo-phenol blue method for further analysis using spectrophotometer. Wind roses were plotted using WR plot software.

RESULTS & DISCUSSIONS

On an average, NH₃ concentrations during day and night time were 93.04 & 168.29 μ g/m³ respectively. Figure.1 shows the variation of average day and night time concentration of NH₃ over the sampling months. Higher concentrations of NH₃ noticed during night time may be due to stable atmospheric conditions resulting in reduced atmospheric dispersion of gaseous NH₃. Similar observations have also been reported by Burkhardt et al. (1998), Singh and Kulshrestha (2012).

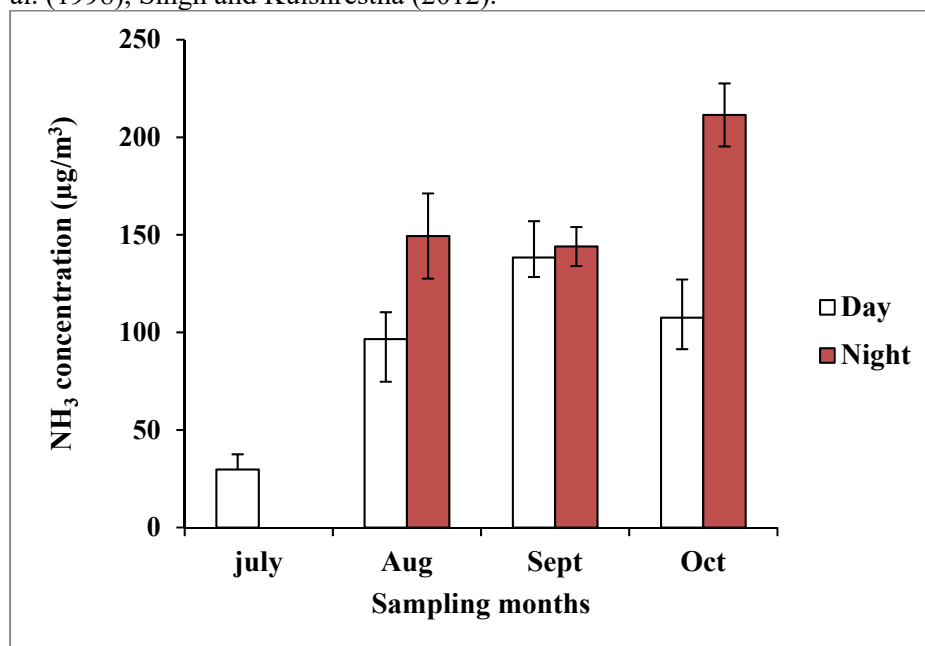


Figure 1. Average day- night time variation of NH₃ over the sampling months

CONCLUSIONS

- Average NH₃ concentrations during day and night time were 93.04 & 168.29 μ g/m³ respectively.
- NH₃ concentrations were higher during night time as compared to the day time. Stable atmospheric conditions might be the reason for these high values.

- Wind rose plots suggested local source influence which indicates the nearby agricultural fields to be the main source of NH₃ emissions at the sampling site.
- In order to reduce the emissions of Nitrogen, we need to reduce fertilizer usage, biomass burning, open dumping of animal waste.

ACKNOWLEDGEMENTS

We acknowledge the financial assistance from DST-Purse, UGC-DSA and UGC-JRF (Sudesh) which helped completion of this work.

REFERENCES

Bouwman, A.F. and Van Der Hoek K.W. (1997). Scenarios of animal waste production and fertilizer use and associated ammonia emission for the developing countries. *Atmos Environ*31, 4095–102

Burkhardt, J., Sutton, M. A., Milford, C., Storeton-West, R. L., and Fowler, D. (1998). Ammonia concentrations at a site in Southern Scotland from 2 years of continuous measurements, *Atmos. Environ*32, 325–331.

Singh, S. and Kulshrestha, U.C. (2012). Abundance and distribution of gaseous ammonia and particulate ammonium at Delhi, *India Biogeosciences* 9,5023–9.

Sutton, M. A., Flower, D. and Moncriefe, J. B. (1993). The exchange of atmospheric ammonia with vegetated surfaces. I: Unfertilized vegetation. *Quarterly Journal of the Royal Meteorological Society* 119(513), 1023-1045.

Walker, J.T., Aneja, V.P., Dickey, D.A. (2000). Atmospheric transport and wet deposition of ammonium in North Carolina. *Atmos Environ*34, 3407–18

PERSONAL EXPOSURE TO FINE AND COARSE MODE PARTICLE IN VARIOUS TRANSPORT MODES IN DELHI

AKASH KUMAR SINGH AND ARUN SRIVASTAVA*

School of Environmental Sciences, Jawaharlal Nehru University, Delhi-110067, India.

(*Correspondence at akashever01@gmail.com and srivastava02@hotmail.com)

KEYWORDS: commuting mode, exposure, particle number, size distribution.

INTRODUCTION

Rapid urbanization and unsustainable resource use has degraded every component of earth and adversely impacted the quality of life in especially in urban area. Traffic is an important source of particulate matter exposure to the commuter and associated adverse health impact (Apte et al., 2011; Both et al., 2013). Exhaust emission, application of the brake system, wear & tear of the tire are the main source of high particulates matter along roadside. Emission from the traffic constitutes aerosol particle mostly in the fine and ultrafine range that dominates the particles number concentration (Weijers et al., 2004). Recently, several studies of exposure of particle mass and numbers concentration inside and outside vehicles such as auto, buses, cars, motorcycle as well as for walking and cycling, have been conducted throughout the world. Latest studies have also suggested that particle number concentration is a better indicator of adverse health hazard rather than mass concentration. Because, fine and ultra-fine particles contribute to more than 90% of the particle number concentration, can reach and deposit in the deepest part of alveoli region of the lung (J. Kannosto, 2008; Jaques and Kim 2000). Although exposure to the mass concentration of particulate matter during travel has been widely studied, a very few studied have been conducted on the real-time personal exposure to particulate number concentration along a particular route in Delhi. So, the main objective of this study was to compare personal exposure of particle number concentration to various transport modes in Delhi.

METHODS

The study was carried out in National Capital Territory, New Delhi. Real-time particle number was measured along a fixed route from Jawaharlal Nehru University and Sagarpur and vice-versa. TSI AeroTrack Portable

Particle Counter, Model No.9310-01, USA was used to measure real-time particle number concentration. Measurement of aerosols was performed during rush-hours between morning and evening. Software provided with the particle counter was used to extract the data from the instrument to a personal computer. All the calculation was performed in Microsoft Excel Worksheet. On the basis of particles size range, the number of particles was then divided into fine (<2.5 μm) and coarse mode (>2.5 μm). Total suspended particulate matter, fine mode particle (FMP) and coarse mode particle (CMP) was calculated for the number size distribution and represented graphically. The particle size distribution was too presented in terms of fractional number ($F_n/\Delta\text{Logdp}$) size distribution.

RESULTS & DISCUSSIONS

The result of the study shows that the personal exposure to particle number concentration was influenced by different commuting modes during morning and evening rush hours. Exposure to the total number of particles in Car, Motorcycle and Auto in the morning was slightly higher than the evening rush hours in all the three commuting modes (Table 1). Highest exposure to the number of fine mode particles (FMP) was observed in Car followed by Motorcycle and Auto (Car > Motorcycle > Auto). Fine mode particles (FMP) concentration were several times higher than the coarser mode particles (CMP), which constituted approximately 97 to 99% of the total number of particles. While coarse mode particles were found to be approximately 1-3% of the total number of particles (Figure 1). Fractional number ($F_n/\Delta\text{Logdp}$) size distribution also shows that most of the particle number concentration falls in the fine mode range both in morning and evening rush hour (Figure 2).

Morning				Evening			
Transport	CAR	BIKE	AUTO	Transport	CAR	BIKE	AUTO
FM (%)	98.01	99.11	97.05	FM (%)	98.49	98.00	96.46
CM (%)	1.99	0.89	2.95	CM (%)	1.51	2.00	3.54

Table 1. Percentage of fine (FM) and coarse mode (CM) particle in various transport mode.

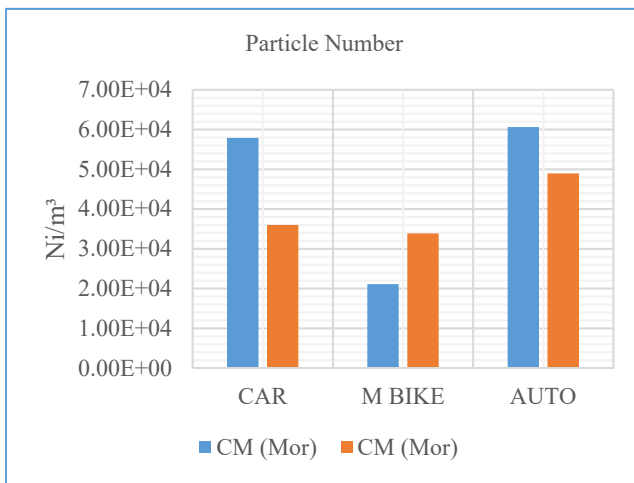
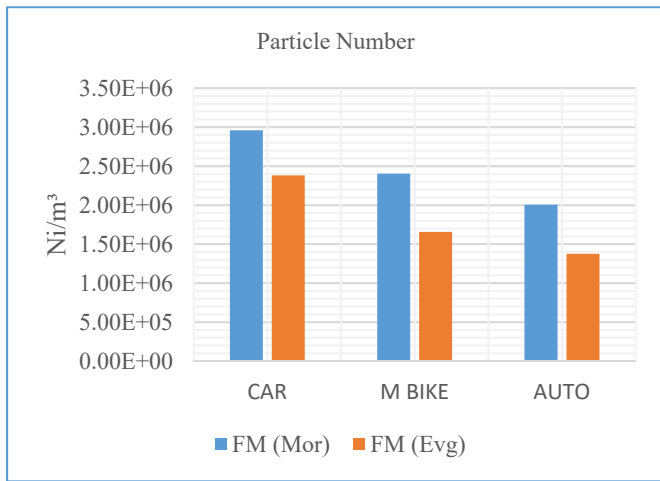


Figure 1. Number of fine and coarse particulate matter in different transport mode in morning and evening rush hour.

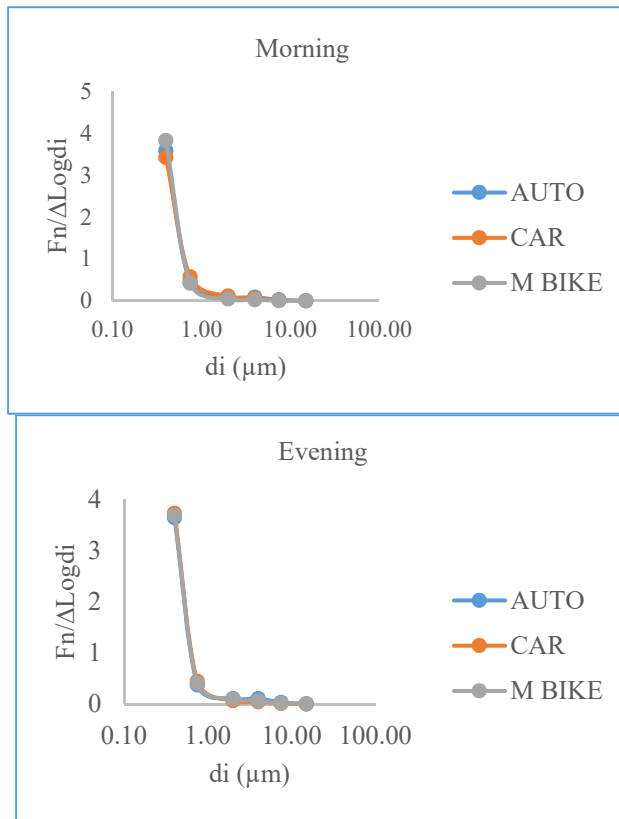


Figure 2. Fractional size distribution of particle number in an auto rickshaw, Car and Motorcycle. Each node in the figure represents the particle midpoint diameter (μm).

CONCLUSIONS

Exposure to the total number of particles in Car, Motorcycle and Auto in the morning was comparatively higher than the evening rush hours in all the three transportation modes. A clear variation in number, size distribution was seen. A slight shift in a peak in the number size distribution might be due to other factors on road such as wind speed, traffic congestion, constructional activities etc. Overall number dominates in the fine size range of particle size distribution. Peoples are regularly exposed to a higher number of aerosol particles in the respirable fine mode fraction that may be dangerous for the health in long-term. This study will help the commuter to choose suitable travel mode to reduce the personal exposure of particulate matter.

ACKNOWLEDGMENTS

Authors are highly thankful to University Grants Commission (UGC) for providing fellowship.

REFERENCES

Apte, J. S., Kirchstetter, T. W., Reich, A. H., Deshpande, S. J., Kaushik, G., Chel, A., & Nazaroff, W. W. (2011). Concentrations of fine, ultrafine, and black carbon particles in auto-rickshaws in New Delhi, India. *Atmospheric Environment*, 45(26), 4470-4480.

Both, A. F., Westerdahl, D., Fruin, S., Haryanto, B., & Marshall, J. D. (2013). Exposure to carbon monoxide, fine particle mass, and ultrafine particle number in Jakarta, Indonesia: Effect of commute mode. *Science of the Total Environment*, 443, 965-972.

Weijers, E. P., Khlystov, A. Y., Kos, G. P. A., & Erisman, J. W. (2004). Variability of particulate matter concentrations along roads and motorways determined by a moving measurement unit. *Atmospheric Environment*, 38(19), 2993-3002.

Kannosto, J., Lemmetty, M., Virtanen, A., Mäkelä, J. M., Keskinen, J., Junninen, H, & Kulmala, M. (2008). Mode resolved density of atmospheric aerosol particles. *Atmospheric Chemistry and Physics Discussions*, 8(2), 7263-7288.

Jaques, P. A., & Kim, C. S. (2000). Measurement of total lung deposition of inhaled ultrafine particles in healthy men and women. *Inhalation toxicology*, 12(8), 715-7.

SPATIAL VARIATION OF BTEX IN A SENSITIVE ENVIRONMENT OF THE DELHI

DUDUN MEHTA, RAJEEV KUMAR, ARUN SRIASTAVA

School of Environmental Sciences, Jawaharlal Nehru University, New Delhi
110067, India

(*Correspondence at mehtadudun@gmail.com, srivastava02@hotmail.com)

KEYWORDS: VOCs, BTEX, Delhi

INTRODUCTION

Volatile Organic Compounds (VOCs) comprise a series of compounds, out of which the BTEX are the ubiquitous pollutants and also one of the main concern hydrocarbons such as benzene, toluene, ethyl-benzene, 1, 2, 4-trimethylbenzene, xylenes isomers (m-xylene, p-xylene-o-xylene) etc.; all of which are known toxic air pollutants, and some of them are also responsible to cause carcinogen. Sources of these VOCs are reported to be emitted from vehicular exhaust (Latella et al., 2005) gasoline /gasoline powered vehicles (Hellen et al., 2003), and other biogenic sources (Guenther, 2006). Various activities governed by anthropogenic role such as fuel combustion, road-traffic, industrial processes and different solvents used, wood burning etc. play an important role for the emission of VOCs (Lanz et al., 2008; Demir et al., 2012). The exhaust of gasoline is four times contributor of VOCs as compared to diesel exhaust in most of the sub urban and urban areas but, the evaporated and liquid gasoline is the larger contributors in some areas also (Watson et al., 2001). Exposure to some BTEX (mainly benzene) can cause acute non-lymphocytic leukemia and a variety of other blood-related disorders in humans (Krewski et al., 2000). Benzene, which has been given priority to assess in urban environment, is considered as a genotoxic carcinogen (Hoque et al., 2008). Most of the VOCs in the ambient environment forms Tropospheric Ozone and Secondary Organic Aerosol (SOA), which harm all living creatures and pollute local air quality.

To our knowledge, limited study has been done of individual VOCs such as benzene, toluene ethylbenzene, m,p-xylene and o-xylene in any city of India. The uniqueness of the topography, land use pattern, meteorological condition and large number of vehicle in Delhi, the capital city of India, encouraged us to carry out this study. Therefore, the objective of the study is assessment of spatiotemporal variation of BTEX in the five zones, viz, petrol pump, CNG pump, heavy traffic density and institutional area.

METHODOLOGY

Delhi is a National Capital Territory of India. It is one of the largest cities in the northern part of India, which is situated at an altitude 216 m above the mean sea level and spread over an area of approximately 1,483 Km²; out of which the areas 700Km² is identified as urban and 783 Km² as rural respectively. By geographical distribution, Delhi is divided into three parts such as Delhi ridge (part of Aravali ridge), the Yamuna flood plain (rich in alluvial soil), and the Plains. In the present study, BTEX sample were collected during one month of summer season at 5 different sites in the year 2018. Location of the sampling site were from Delhi region was chosen viz. Petrol pump Munika, CNG Pump in Munirka, Jawaharlal Nehru University (JNU) campus, Kashmiri Gate and Connaught Place (CP) .

All the samples were collected in summer season (April to June) in 2018 by using the Standard Charcoal Tubes and investigated for BTEX loads by the prescribed protocols. The pump used in his study is “Gilian BDX-II Personal Air Sampling Pump. The sampling period for the BTEX was kept 4 hours with the flow rate of 100 ml/min. In the analytical steps, 2 ml amber colored glass vial was used for transferring the activated charcoal from the tube ORBOTM-32. After that, 1000µl of low benzene CS₂ (99% purity with < 0.001% benzene) was used as solvent for extraction, and it was put into an ultrasonicated bath for about half an hr. The analysis of BTEX was carried out on the basis of the previous studies: Masih et al., (2016, 2017). GC-FID (5700, Nucon Gas Chromatograph) was used for the determination of BTEX concentration.

RESULTS AND DISCUSSION

Maximum concentration of BTEX (47.33µg/m³) was found at site CNG pump Munirka while minimum at site JNU (25.73µg/m³). High level of VOCs at CNG pump could be attributing to very high automobile traffic density, slow movement of traffic and another petrol pump situated near the vicinity of CNG pump. Among BTEX benzene was found to be most abundant species followed by toluene, ethylbenzene, m,p-Xylene and o-xylene respectively. In the present study, BTEX concentrations are observed approximately in the similar variations as reported in different studies carried out in different parts of India (Srivastava et al., 2005; Srivastava et al., 2006), with higher concentration of benzene in comparisons to toluene. Again, it was also observed that concentration of toluene have been exceeded than benzene in some other parts of Delhi, where isomers of xylenes and ethylbenzene possessed comparatively lower amounts (Hoque et al., 2008; Singh et al., 2016; Kumar et al., 2017).

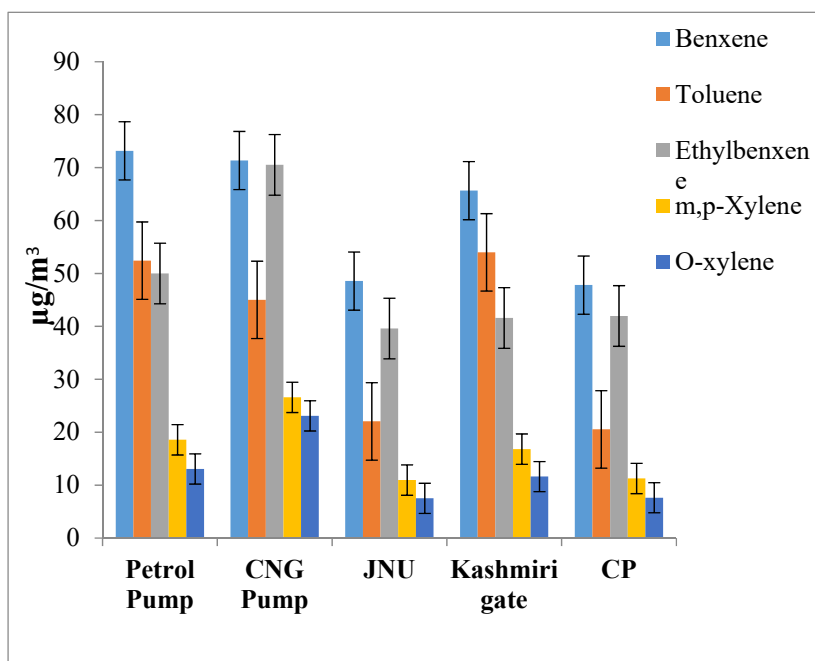


Figure 1: Mean concentration of BTEX at five different sites in Delhi

CONCLUSION

The concentration of BTEX was examined in the ambient air of five different sites of Delhi in summer season 2018. The average concentration of BTEX was observed to be highest at CNG pump Munirka ($47.303 \mu\text{g}/\text{m}^3$) followed by petrol pump Munirka ($41.43 \mu\text{g}/\text{m}^3$), Kashmiri gate ($37.92 \mu\text{g}/\text{m}^3$), CP ($25.83 \mu\text{g}/\text{m}^3$) and JNU ($25.73 \mu\text{g}/\text{m}^3$). Metrological condition, sources of emission and seasonal variability of OH radical play important role in the concentrations of BTEX in troposphere.

ACKNOWLEDGEMENTS

This work was supported by the CSIR.

REFERENCES

Hoque, R. R., Khillare, P. S., Agarwal, T., Shridhar, V., & Balachandran, S. (2008). Spatial and temporal variation of BTEX in the urban atmosphere of Delhi, India. *Science of the Total Environment*, 392(1), 30-40.

Dutta, C., Som, D., Chatterjee, A., Mukherjee, A. K., Jana, T. K., & Sen, S. (2009). Mixing ratios of carbonyls and BTEX in ambient air of Kolkata, India and their associated health risk. *Environmental Monitoring and Assessment*, 148(1-4), 97-107.

Kumar, P., & Yadav, S. (2013). Factors and sources influencing ionic composition of atmospheric condensate during winter season in lower troposphere over Delhi, India. *Environ. Monit. Assess* 185(3), 2795-2805.

Singh, D., Kumar, A., Singh, B. P., Anandam, K., Singh, M., Mina, U., & Jain, V. K. (2016). Spatial and temporal variability of VOCs and its source estimation during rush/non-rush hours in ambient air of Delhi, India. *Air Quality, Atmosphere & Health*, 9(5), 483-493.

Srivastava, A., Joseph, A. E., & Devotta, S. (2006). Volatile organic compounds in ambient air of Mumbai—India. *Atmospheric Environment*, 40(5), 892-903.

REACTIVE NITROGEN CHEMISTRY DURING WINTER SEASON ALONG THE URBAN TRANSECT OF NCR, DELHI

REEMA TIWARI AND U.C. KULSHRESTHA

School of Environmental Science, Atmospheric Chemistry and Climate
Change Group, Jawaharlal Nehru University, Delhi – 110067, India

KEYWORDS: N_r precursor gases, N_r particulates, diurnal ratios, gas – aerosol interactions

INTRODUCTION

As a key regulator of atmospheric oxidative capacity and secondary aerosol formations, the reactive nitrogen cycle has gained worldwide concern for their two to three times rise in the global N budgets over the last century (Fowler et al., 2013). This is evident from their altered chemical transformation pathways that has accelerated the atmospheric N depositions by ten folds with cascade of environmental problems resulting in air pollution, acidification and eutrophication of the ecosystem (Galloway et al., 2004; Reis et al., 2009). Their emission occurs primarily as NO_x ($NO + NO_2$) and NH_3 whose photochemical reactions and consequent residence time in the atmosphere has been detrimental to the spatio temporal evolution of N_r on a synoptic scale. Thus, the present study has been conducted for investigating various interactions during winter sason when low anticyclonic winds becomes favourable to the advections from west over the study region. For this purpose, diurnal samples of gaseous and particulate N_r species were collected simultaneously for understanding the photochemical control of their spatio temporal variability along the sampling transect. These were evaluated for their phase conversion processes where molar ratios of NO_x/NO_y and NH_3/NH_x were calculated for understanding transformation extent of such photochemical reactions.

METHODOLOGY

Measurements of N_r trace gases and particulates were made for three sampling sites near the urban agglomerates established along the km north west – south transect of the National Capital Region (NCR). Delhi was selected as a representative urban site where the source activities could be broadly classified as transport, fugitive, domestic fuel and garbage burning. Rohtak, which is located 70 km upwind to the major emission sources of the megacity Delhi, was selected as a sub urban or an urban background site. Third site i.e. Faridabad was selected 44.7 km downwind to Delhi near

Badarpur thermal power plant which was considered as a representative site for industrial emissions in NCR region.

Sampling was conducted for daytime (8.00 am to 5 pm) and night time (8.00 pm – 6.00 pm) separately during the period December 2016 to January 2017 using a low volume sampler assembly. Gaseous samples of NO₂, HNO₃ and NH₃ were collected in 20 ml absorbing solution of sodium hydroxide + sodium arsenite, deionized water and 2.5 mM H₂SO₄ respectively while aerosol samples were collected in 47 mm Teflon filter of 0.2 μm pore size kept upstream to the sampling train. The collection efficiency of the trace gases was found to be 75% for NO₂, 90% for HNO₃ and 85% for NH₃ with an insignificant overestimation in the ionic fraction of aerosols by ~2%.

Gaseous samples of NO₂ and NH₃ were analysed colorimetrically with UV – VIS spectrophotometer at 540 nm and 630 nm wavelengths respectively. Ion chromatography (Metrohm – 883 basic plus), on the other hand, was used in the analysis of gaseous HNO₃ samples for NO₃⁻ along with the water soluble fraction of aerosols for its major anions (F⁻, Cl⁻, NO₃⁻, SO₄²⁻) and cations (K⁺, NH₄⁺, Na⁺, Ca²⁺, Mg²⁺).

RESULTS AND DISCUSSIONS

Mean concentrations of NO_x-N, HNO₃- N and NH₃- N trace gases along with their ionic fractions in aerosol measurements have been given in Table 1. The results showed a spatial gradient of N_r precursor gases consistent with the site characteristic where the sum of their average values were observed to be highest at downwind Faridabad site (92.33 μg m⁻³) and lowest at upwind background Rohtak site (24.84 μg m⁻³). The corresponding particulate N_r (NH₄⁺ + NO₃⁻), on the other hand, showed ~ 2 times decline in their upwind concentration gradient accompanied by a ~ 4 times rise in their downwind concentration gradient from the urban representative site of Delhi.

Mode	Species	Rohtak (N = 25) (μgm ⁻³)	Delhi (N = 55) (μgm ⁻³)	Faridabad (N = 49) (μgm ⁻³)
Gaseous	NO _x	6.09 ± 0.93	15.84 ± 1.06	24.89 ± 4.18
	HNO ₃	4.18 ± 1.04	4.8 ± 1.01	28.27 ± 5.95
	NH ₃	14.57 ± 4.23	35.37 ± 3.22	39.17 ± 4.57
Aerosols	NH ₄ ⁺	0.97 ± 0.54	0.97 ± 0.4	0.22 ± 0.11
	NO ₃ ⁻	1.41 ± 0.88	0.43 ± 0.15	5.25 ± 2.48

Table 1. Average concentration of N_r precursor gases and their aerosols (μgm^{-3}) at three sites along the NCR transect.

Such observations were evaluated with one - way Anova test that confirmed the influence of local emission sources in generating inter site variability of N_r precursor gases ($p < 0.05$) unlike their particulate counterparts ($p > 0.05$) where high RSD values were observed for NH_4^+ (341 %) and NO_3^- (452%) which indicated a slow rate of nitrate aerosol forming reactions along the sampling transect. This was also evident from the ionic composition of particulates where presence of Ca^{2+} as the major base cation at all sites indicated stoichiometric preference of crustal aerosols over NH_4^+ in HNO_3 scavenging reactions.

The observed distribution patterns were further assessed for their diurnal behaviour in N_r photochemistry by calculating the average ratio of their day and night measurements (D/N) as shown in Fig 2. The results showed below unity ratio of NO_x at Delhi and Faridabad site which was found to be consistent with their photochemical conversions to NO_y species such as HNO_3 during daytime. But with the mean values of HNO_3 also showing below unity D/N ratios, the rapid daytime losses of oxidized N_r precursor gases cannot be ruled out at these downwind sites. Rohtak being the background site exhibited diel cycles with D/N >1 ratios for NO_x and NH_3 which is most likely to be the result of solar insolation triggering the breakdown of nocturnal boundary layer and the subsequent downward mixing of relatively undepleted polluted air masses that are present aloft (Zellweger et al., 2003).

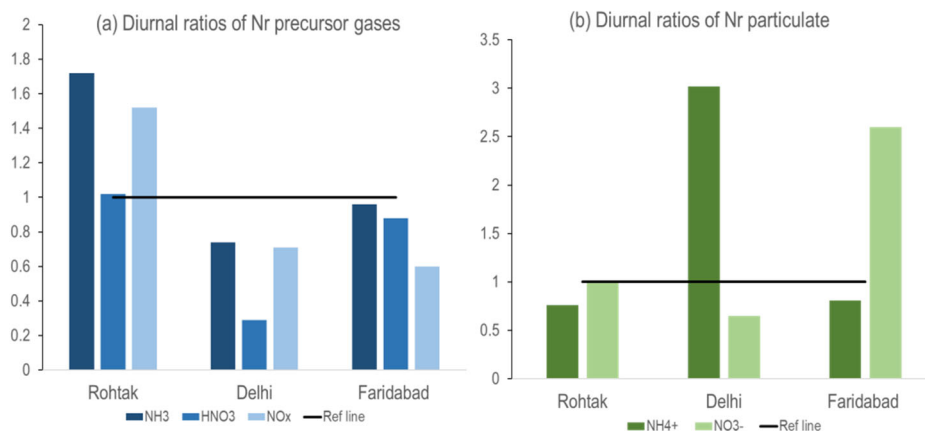


Fig 1. Mean diurnal ratios of (a) N_r precursor gases and (b) N_r particulates along the sampling transect

These diel cycles were elucidated with the molar ratios of NO_x/NO_y and NH_3/NH_x for evaluating the role of gas particle partitioning in N_r photochemistry and to provide an indicator of their chemical conversion efficiency and relative freshness of the N_r source emissions as well. NO_x being the principal component and primary photochemical precursor to NO_y ($\text{NO}_x + \text{HNO}_3 + \text{p NO}_3^-$) were defined for their fresh plumes with $\text{NO}_x/\text{NO}_y > 0.8$ (Neuman et al., 2006). Such ratios were observed throughout the diel cycle of site Delhi where NO_x measurements comprised 93% of the NO_y reservoir which is either indicative of local NO_x inputs or their reformation from NO_y in the absence of active photochemistry. The NO_x/NO_y ratios at upwind Rohtak (0.73) and downwind Faridabad (0.78) site were below the reference fresh plume ratio (0.8), thereby, suggesting their photochemical processing to a certain extent. Similarly, the transformation extent between NH_3 and NH_4^+ were also evaluated with the gaseous fraction of NH_x ($\text{NH}_3 + \text{p NH}_4^+$) where values greater than 0.5 signified local NH_3 sources dominating the NH_x deposition and transport (Meng et al., 2018). The results showed high daily average of NH_3/NH_x ratio at Faridabad site (0.99) with values ranging from 0.73 to 1 irrespective of their diurnal phases. Delhi exhibited slightly lower daily average (0.96) with their ratios at background Rohtak site (0.93) further confirming their diurnal cycles being dictated by the free availability of NH_3 but with a lesser dynamic NH_x system.

CONCLUSIONS

The study showed a spatial gradient of their N_r trace gases that were found to be consistent with land use pattern of the sites where a much pronounced inter - site variability of HNO_3 confirmed the influence of local emission sources in Noxidized distribution pattern. However, a limited photochemical transformation of these gaseous precursors to aerosols were evident from their respective day - night ratios (D/N) where daytime deposition losses of HNO_3 at Delhi and additional daytime NO_3^- inputs by the local industrial activities of Faridabad obscured the diurnal evolution of their oxidized N_r species along the sampling transect. These diurnal variations were characterized by the influence of boundary layer dynamics at the background Rohtak site. Such results were further corroborated with the molar ratios of NO_x/NO_y and NH_3/NH_x that confirmed their incomplete titrations of NO_x and NH_3 emissions irrespective of their diurnal phases.

ACKNOWLEDGEMENT

We sincerely thank the University Grants Commission of India for extending their financial support for conducting this research work.

REFERENCES

Fowler, D., Coyle, M., Skiba, U., Sutton, M.A., Cape, J.N., Reis, S., Sheppard, L.J., Jenkins, A., Grizzetti, B., Galloway, J.N. and Vitousek, P., (2013). The global nitrogen cycle in the twenty-first century. *Phil Trans R Soc B* 368: 20130164. <http://dx.doi.org/10.1098/rstb.2013.0164>.

Galloway, J.N., Dentener, F.J., Capone, D.G., Boyer, E.W., Howarth, R.W., Seitzinger, S.P., Asner, G.P., Cleveland, C.C., Green, P.A., Holland, E.A. and Karl, D.M., (2004). Nitrogen cycles: past, present, and future. *Biogeochemistry*, 70(2), pp.153-226.

Meng, Z., Xu, X., Lin, W., Ge, B., Xie, Y., Song, B., Jia, S., Zhang, R., Peng, W., Wang, Y. and Cheng, H., 2018. Role of ambient ammonia in particulate ammonium formation at a rural site in the North China Plain. *Atmospheric Chemistry and Physics*, 18 (1), pp. 167 – 184.

Neumann, J.A., Parrish, D.D., Trainer, M., Ryerson, T.B., Holloway, J.S., Nowak, J.B., Swanson, A., Flocke, F., Roberts, J.M., Brown, S.S. and Stark, H., (2006). Reactive nitrogen transport and photochemistry in urban plumes over the North Atlantic Ocean. *Journal of Geophysical Research: Atmospheres*, 111 (D23).

Reis, S., Pinder, R.W., Zhang, M., Lijie, G. and Sutton, M.A., (2009). Reactive nitrogen in atmospheric emission inventories. *Atmospheric Chemistry and Physics*, 9(19), pp. 7657 – 7677.

Zellweger, C., Forrer, J., Hofer, P., Nyeki, S., Schwarzenbach, B., Weingartner, E., Ammann, M. and Baltensperger, U., (2003). Partitioning of reactive nitrogen (NO_y) and dependence on meteorological conditions in the lower free troposphere. *Atmospheric Chemistry and Physics*, 3(3), pp. 779-796.

**WATER SOLUBLE ORGANIC CARBON AND ITS ASSOCIATION
WITH OTHER CARBONACEOUS AEROSOL SPECIES AT URBAN
AND RURAL SITES
IN INDO-GANGETIC PLAINS**

MANISHA MISHRA AND U.C. KULSHRESTHA

School of Environmental Sciences, Atmospheric Chemistry and Climate
Change Group, Jawaharlal Nehru University, New Delhi, 110067, India.

KEYWORDS: Fine aerosols, OC, EC, WSOC

INTRODUCTION

For the past few decades, seasonal appearance of a thick blanket of aerosol particles all over North India from Southern edge of the Himalayas to the Bay of Bengal has been attributed to various anthropogenic emissions. Studies have revealed that unique topography of North India and meteorological conditions during winters further lead to the accumulation of pollutants in the lower atmosphere. Indo-Gangetic Plain (IGP) is among one of the most densely populated regions around the world, where 70% population is still residing in the villages. Growing energy demands have led to the increased pollutant emission from industrial and transport sectors. Biomass such as woods, dung cake, dry leaves and crop residues used for traditional cooking and heating purposes and open field burning in rural areas have further added to the aerosol loadings in the atmosphere over the IGP.

METHODOLOGY

Indo-Gangetic plains are known for their very high population density and stationary sources of pollutant emission in the environment. Keeping in view the different land use patterns and its specific local sources, two sites have been selected for this study, one in Allahabad (as an urban site) and Madhupur, a village in Pratapgarh district of UP (as a rural site). Fine aerosols ($\leq 2.5\mu$) were collected on 47mm quartz filters using low volume custom based sampling unit operated at 15 LPM. Sampling was conducted during winter months from November 2016 to February 2017. TOC analyzer was used to measure the Water Soluble Organic Carbon (WSOC). For Organic Carbon (OC) and Elemental Carbon (EC), samples were analyzed on DRI thermal/optical analyzer (2001) using the IMPROVE_A protocol. Field blanks were also taken into account at each step to avoid over/under estimation in the calculations.

RESULTS AND DISCUSSIONS

The average concentration of OC, EC and WSOC in fine aerosols in ambient air is shown in Fig.1. The rural site has very high levels of OC, EC and WSOC as compared to the urban site. Average concentration OC and EC were found to be $35.9 \pm 2.5 \mu\text{g}/\text{m}^3$ and $25.6 \pm 1.9 \mu\text{g}/\text{m}^3$, respectively at the urban site and $71.8 \pm 7.4 \mu\text{g}/\text{m}^3$ and $48.4 \pm 5.0 \mu\text{g}/\text{m}^3$, respectively at the rural site. The abundance of carbonaceous aerosols in rural area can be attributed to the use of biofuel for cooking and heating purposes in winters (Singh et al., 2014). Higher correlation between OC and EC at the urban site ($r=0.84$) as compared to rural site ($r=0.51$), can be attributed to the gasoline and diesel combustion from vehicles (Ram and Sarin, 2010). Further, to investigate major sources, OC/EC ratios were also calculated. The OC/EC ratios at urban site ranged from 1.1 to 2.6 suggesting the dominant contribution from fossil fuel burning, whereas it ranged from 1.3 to 14.5 for 90% samples at the rural site owing to the biomass burning as a major source of pollution (Schauer et al., 2001; Zhang et al., 2007).

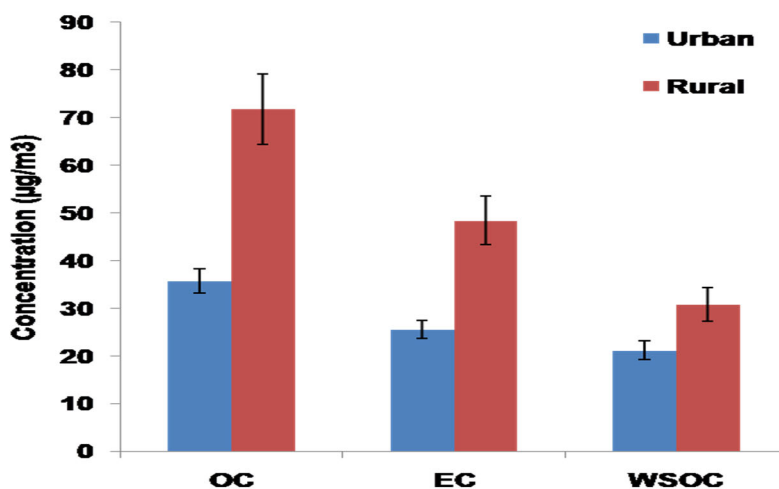


Fig.1 Mean concentration of OC, EC and WSOC at urban and rural sites.

WSOC is observed as one of the most important components in regulating various atmospheric processes (Kanakidou et al., 2005). Considering such high relevance, WSOC was calculated for each site. The mean concentration of WSOC was found to be $21.2 \mu\text{g}/\text{m}^3$ and $30.8 \mu\text{g}/\text{m}^3$ at urban and rural sites, respectively. This also suggests that about 60% of the OC is contributed by WSOC at the urban site and about 43% of at rural site.

WSOC/OC ratios are considered as an important indicator of the formation of Secondary Organic Aerosols (Xiang et al., 2016). Mean WSOC/OC ratio was found to be 0.61 at urban site and 0.48 at the rural site. The elevated ratio value at the urban site suggests the higher rate of formation of secondary organic aerosols (SOA). However, the lower WSOC/OC ratio and higher EC concentration at the rural site indicate the dominance of biomass burning as a primary source (Ram et al., 2012).

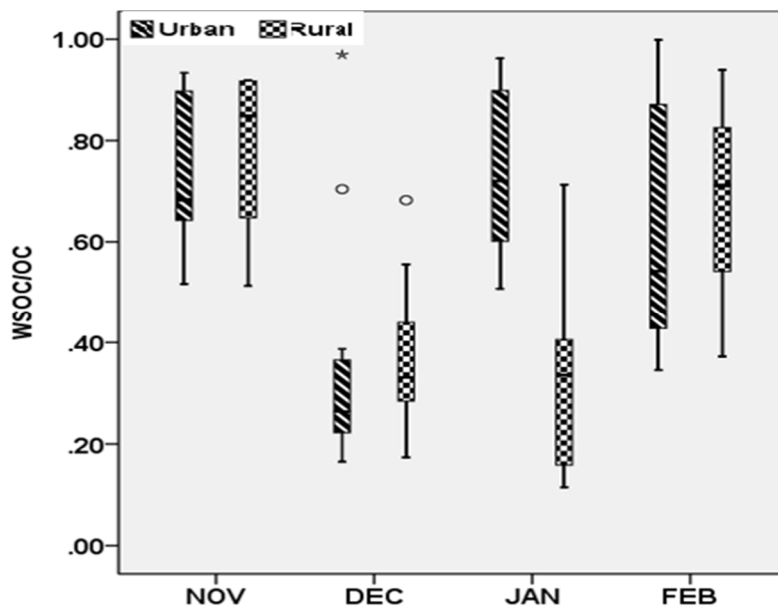


Fig.2 Variation of WSOC/OC in the winter months at urban and rural sites.

Monthly Variation in WSOC/OC ratio in winter months is shown in Fig.2. The December and January months show lower ratio as compared to the November and January months, which can be attributed to the increased biomass burning activities for winter time heating and cooking during the month of December and January. However, relatively lower ratio at rural site can be attributed to the open biomass burning for heating purposes and agriculture activities, though additional sources are also responsible (Singh et al., 2016).

CONCLUSIONS

On an average, the OC, EC and WSOC levels have been found to be higher at the rural site as compared to the urban site. Though the local sources varied at each site depending upon the local anthropogenic activities, biomass burning remained as a major source at rural site. December and January

months were recorded with higher emission from primary sources, particularly in rural area. The study suggests that the rural areas need a much more focused approach to curb air pollution, which, if not regulated, can negate all the efforts made to control pollution in the region.

ACKNOWLEDGMENT

We sincerely thank the financial support received from CSIR and Jawaharlal Nehru University, New Delhi, to conduct this research work. Analytical assistance provided by CIF, SES is gratefully acknowledged.

REFERENCES

Kanakidou, M., Seinfeld, J. H., Pandis, S. N., Barnes, I., Dentener, F. J., Facchini, M. C., ... & Swietlicki, E. (2005). Organic aerosol and global climate modelling: a review. *Atmospheric Chemistry and Physics*, 5(4), 1053-1123.

Ram, K., & Sarin, M. M. (2010). Spatio-temporal variability in atmospheric abundances of EC, OC and WSOC over Northern India. *Journal of Aerosol Science*, 41(1), 88-98.

Ram, K., Sarin, M. M., Sudheer, A. K., & Rengarajan, R. (2012). Carbonaceous and secondary inorganic aerosols during wintertime fog and haze over urban sites in the Indo-Gangetic Plain. *Aerosol Air Qual. Res*, 12(3), 359-370.

Schauer, J. J., Kleeman, M. J., Cass, G. R., & Simoneit, B. R. (1999). Measurement of emissions from air pollution sources. 2. C1 through C30 organic compounds from medium duty diesel trucks. *Environmental Science & Technology*, 33(10), 1578-1587.

Singh, S., Gupta, G. P., Kumar, B., & Kulshrestha, U. C. (2014). Comparative study of indoor air pollution using traditional and improved cooking stoves in rural households of Northern India. *Energy for sustainable development*, 19, 1-6.

Singh, R., Kulshrestha, M. J., Kumar, B., & Chandra, S. (2016). Impact of anthropogenic emissions and open biomass burning on carbonaceous aerosols in urban and rural environments of Indo-Gangetic Plain. *Air Quality, Atmosphere & Health*, 9(7), 809-822.

Xiang, P., Zhou, X., Duan, J., Tan, J., He, K., Yuan, C., ... & Zhang, Y. (2017). Chemical characteristics of water-soluble organic compounds (WSOC) in PM_{2.5} in Beijing, China: 2011–2012. *Atmospheric Research*, 183, 104-112.

Zhang, M., Han, Z., & Zhu, L. (2007). Simulation of atmospheric aerosols in East Asia using modeling system RAMS-CMAQ: Model evaluation. *China Particuology*, 5(5), 321-327.

IMPACT OF DIRECT RADIATIVE EFFECT OF ATMOSPHERIC BROWN CLOUDS ON ATMOSPHERIC STABILITY OVER INDIAN CORE MONSOON REGION

MANISH JANGID¹, SALONI SHARMA¹, AMIT K. MISHRA^{*1},
SACHCHIDANAND SINGH², KRISHAN KUMAR¹

¹School of Environmental Sciences, Jawaharlal Nehru University, New Delhi-67

²Environmental and Biomedical Metrology Division, CSIR-National Physical Laboratory, New Delhi-110012, India.

(*Correspondence at: amit.mishra.jnu@gmail.com,
amitmishra@mail.jnu.ac.in)

KEYWORDS: Aerosol, Atmospheric Brown Cloud, Direct Effect, Atmospheric Stability

INTRODUCTION

Atmospheric brown clouds (ABCs), a regional scale pollution layer containing aerosols from different sources (Ramanathan et al., 2007), could significantly modulate the radiation budget and regional climate (Ramanathan and Carmichael, 2008). The widespread cover of this regional haze over the Indian region is a matter of great concern (Burney & Ramanathan, 2014) due to its impact on human health, food security and weather conditions. Aerosols absorb and scatter the solar radiation thereby affecting the atmospheric temperature profiles and may results in perturbation in cloud processes and precipitation pattern (Lau and Kim, 2006; Nigam and Bollasina, 2010). Better understanding of changes in atmospheric structure under the influence of increasing atmospheric pollutants in form of ABCs is needed to reduce uncertainty in model simulations pertaining to Indian monsoon system.

DATA AND METHODS

12 years (2003-2014) Moderate Resolution Imaging Spectroradiometer (MODIS)-derived gridded daily averaged aerosol optical depth (AOD (τ) at 550 nm on $1^{\circ} \times 1^{\circ}$ spatial resolution) along with the Atmospheric Infra-Red Sounder (AIRS)-derived temperature ($1^{\circ} \times 1^{\circ}$ spatial resolution) at five pressure levels: 1000, 925, 850, 700, and 600 hPa are used to analyze the direct effect of aerosol on atmospheric stability over the Indian Core Monsoon Region (ICMR: 21° - 27° N; 80° - 90° E). The AIRS temperature data

are sorted according to AOD and divided into equally spaced bins of AOD. In addition, we have also used Cloud-Aerosol Lidar with Orthogonal Polarization (CALIOP) and Aerosol Robotic Network (AERONET) observations to characterize aerosol properties during pre-monsoon season (March, April and May) over the ICMR.

RESULTS AND DISCUSSION

Fig. 1 shows the association of atmospheric temperature profiles with aerosol loading over the ICMR during premonsoon season. It shows increase in AOD is associated with decrease in temperature below 700hPa, whereas no statistical significant changes are found at 700 and 600 hPa pressure levels. These observed cooling as a function of aerosol loading may explained as masking effect of aerosols (aerosol-radiation interaction). High aerosol loading enhances the lower tropospheric stability and thereby, can affect cloud formation and atmospheric ventilation over the region.

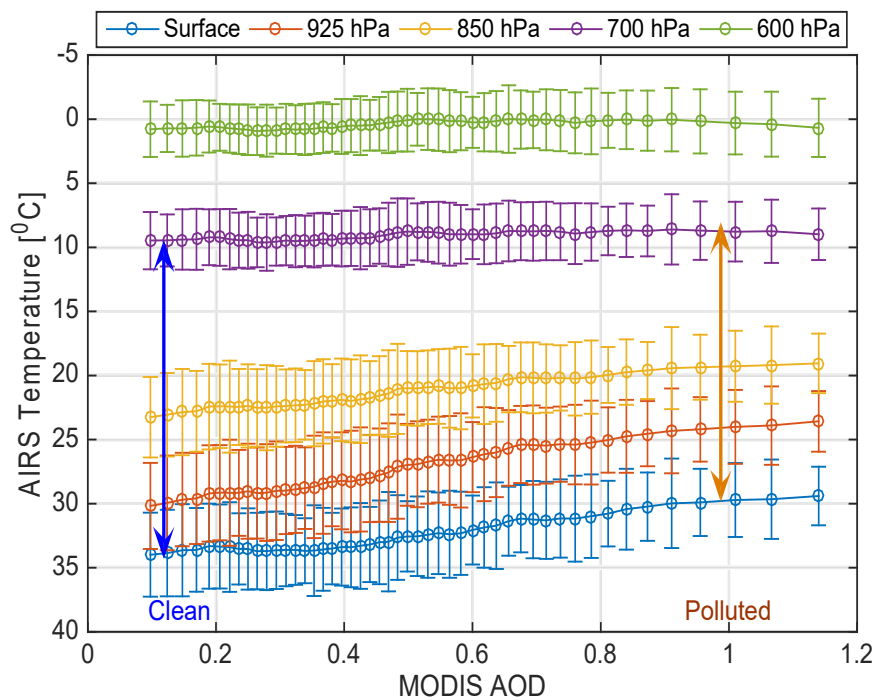


Fig. 1 Atmospheric Temperature profiles (at five pressure levels) as a function of AOD during the premonsoon season (MAM) of 2008 over the ICMR.

Fig. 2 (upper panel) shows tropospheric cooling per unit change in AOD ($dT/d\tau$) as a function of different cloud fractions (CF). It shows that $dT/d\tau$ first increases with CF (<0.4) and then decreases further with increase in CF (>0.4). This result could be understood as the competing radiative effect of clouds on ‘tropospheric cooling’ in SW and LW regime, e.g., in higher cloud cover cases, clouds may intercept more incoming solar radiation thereby increasing $dT/d\tau$, however, at the same time higher cloud cover cases would also be associated with more LW interception and thereby decreasing the cooling induced by aerosol alone (shown in Fig 3 lower panels).

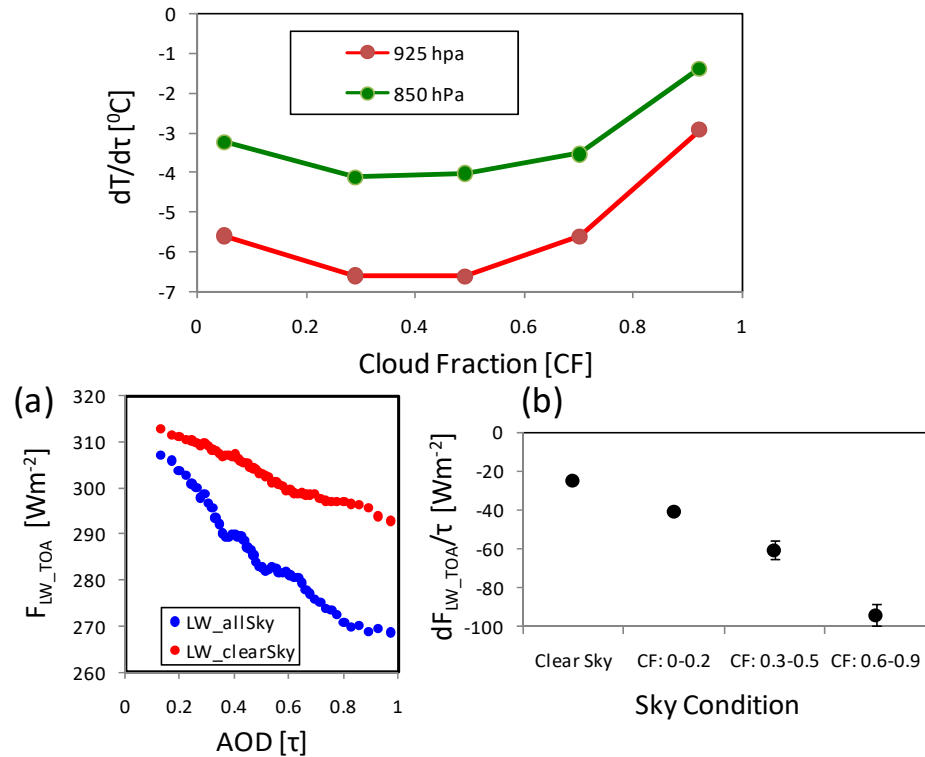


Fig. 2 $dT/d\tau$ as function of cloud cover (upper Panel) and outgoing LW radiation flux at TOA as a function of AOD in different sky conditions (lower panel).

Our analyses show increase in absorption aerosol optical depth (AAOD) and particle size with the increase of aerosol loading using AERONET data over the study region. CALIOP result shows dominance of larger (high CR values) and non-spherical (high PDR values) particles between 2-4 km altitude ranges. These results indicate the dominance of coarser and non-spherical

particles, which are absorbing in nature. The observed properties of aerosols in high aerosol loading indicate the dominance of dust particles during premonsoon season over the ICMR. Therefore, dust particles could be understood as major contributor for observed 'lower tropospheric cooling' over the region.

CONCLUSION

We have studied the direct radiative effect of aerosols on tropospheric vertical temperature profile over the Indian Core Monsoon Region (ICMR) using 12 years (2003-2014) multi-satellite and ground observations. We have observed aerosol induced 'lower tropospheric cooling' during the premonsoon season, which is consistent in last one decade. The effects of cloud cover on aerosol induced cooling are also studied and concluded that there is competing effect of clouds on dT/dt in SW and LW regime. The radiometer and lidar data analysis shows the dominance of dust particles, which are predominantly responsible for observed 'lower tropospheric cooling' during premonsoon season over the ICMR.

ACKNOWLEDGMENTS

AKM would like to acknowledge the Department of Science and Technology (DST) for providing research fund under DST Inspire Faculty scheme (DST/INSPIRE/04/2015/003253).

REFERENCES

- Ramanathan et al. (2007) *Nature*, Warming trends in Asia amplified by brown cloud solar absorption, 448(7153), 575-578.
- Ramanathan and Carmichael (2008) Global and regional climate changes due to black carbon, *Nature geoscience*, 1(4), 221-227.
- Burney and Ramanathan (2014) Recent climate and air pollution impacts on Indian agriculture, *PNAS*, 111(46), 16319-16324.
- Lau and Kim (2006) Observational relationships between aerosol and Asian monsoon rainfall, and circulation, *Geophys. Res. Lett.*, 33, L21810.
- Nigam and Bollasina (2010) "Elevated heat pump" hypothesis for the aerosol-monsoon hydroclimate link: "Grounded" in observations? *J. Geophys. Res.*, 115, D16201.

ATMOSPHERIC REACTIVE NITROGEN FLUXES AND SCAVENGING THROUGH WET AND DRY DEPOSITION IN WESTERN HIMALAYAS (INDIA)

ANSHU SHARMA¹ AND U.C.KULSHRESTHA²

School of Environmental Sciences, Atmospheric Chemistry and
Climate Change Group, Jawaharlal Nehru University, New Delhi-
110067, India.

INTRODUCTION

As the demand of food and energy security has been rising across the world, problem of accumulation of the reactive nitrogen species (Nr) as NO_3^- and NH_4^+ in the atmosphere is also noticed. Sources such as industries, transport, and increased agricultural activities have been termed as the major accelerators of the N cycle (Penuelas et al., 2012; Galloway et al. 2004). The consequences of such rise of Nr species are linked with climate change, human health, vegetation health, soil acidification, air quality, eutrophication, and ecosystems (Ianniello et al., 2011; Sun et al., 2004).

Though, the Nr has its direct emission pathways, but most of the Nr is dispersed by heterogeneous reaction as NO_x and NH_3 into the atmosphere. Once the Nr is released into the atmosphere, its fate is decided by several processes such as transformation, transport, and deposition depends on the species. Their deposition takes place through dry and wet removal processes (Singh et al., 2017) and affecting different ecosystems, mountains, water bodies etc.

In spite of the high importance of atmospheric Nr, their deposition wet and dry removal process is not extensively reported in the Himalayan region of India. Hence, the present study was carried out to understand the rain and dust chemistry with special emphasis on the estimation of wet deposition fluxes of NH_4^+ and NO_3^- in the Himalayan region.

METHODS

The site of this study Nirmand village is located in Kullu district of Himachal Pradesh of India (31.43°N and 77.65°E). This place is often called as Kashi of Himalayas. This Place is on the border of the Kullu District and Shimla District. It is located 87 km towards South from District headquarters Kullu and about 150 km North from Shimla.

Collection of samples

The study includes, the collection of rain water and dust fall. Rain water samples were collected during 2016 on event basis and dust samples were

collected from May, 2016-Dec, 2016. Rain water samples were collected using a manual set up of polypropylene funnel with a 14cm diameter and bottle of 1l capacity and dust samples were collected on Petri plates of 140-mm dimension every 8 days of ambient exposure at a 15m height from the ground. The assembly was prewashed before the collection of sample. Rain assembly was withdrawn after each event and the amount of rain water collected in the bottle was determined by using measuring cylinder before storing the sample in 125ml polypropylene bottles with thymol. Samples were later processed for analysis of pH, Electrical Conductivity (EC) and major ions.

RESULTS & DISCUSSIONS

pH of samples

The mean pH of rainwater was recorded as 6.77 ± 0.55 ranging from 5.95 to 8.03(Fig.1). This pH range is similar to the typical range found in this region (Kulshrestha, 2013). Many studies in northern parts of India (Delhi), has been explained based on the influence of crustal component (Ca^{2+}) which buffer the acidity generated by acidic gases such as SO_2 by Kulshrestha et al(2003c). They have also suggested that the instead of forming sulphuric acid, SO_2 on reaction with calcium form calcium sulphates in India region (Jain et al., 2000). The pH of aqueous extract of dustfall was found to be in the range of 6.98 - 7.59, with average 7.31 ± 0.18 (Fig.1), clearly observing the alkaline influence of dust.

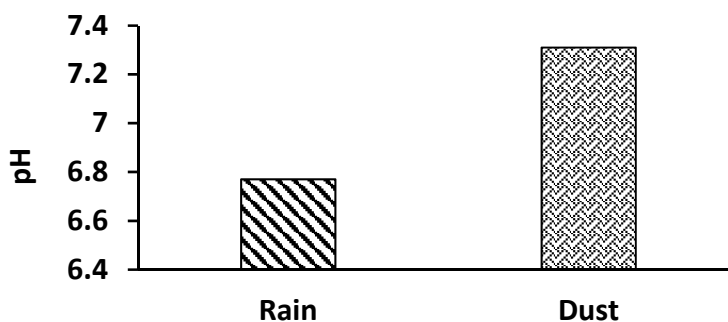


Fig. 1 Mean pH of rainwater and aqueous extract of dustfall

Ionic composition of samples

The percentage contribution of individual cations and anions in rainwater and dustfall samples were calculated, which has been depicted in Fig. 2. In the rain water Ca^{2+} was dominating followed by Mg^{2+} , K^+ , Na^+ and NH_4^+ , and among the anion HCO_3^- was dominating followed by SO_4^{2-} , NO_3^- and Cl^- . Whereas, in the dust among cations Ca^{2+} was the dominating ion followed by Mg^{2+} , Na^+ , K^+ , NH_4^+ and among anions SO_4^{2-} was dominating ion followed

by Cl^- , and NO_3^- . The dustfall flux of $0.18 \text{ mg/m}^2/\text{day}$ was observed at site, which was very lower as compared to dustfall flux reported in Delhi and other sites by other co-workers (Sharma et al., 2017; Tiwari et al., 2016).

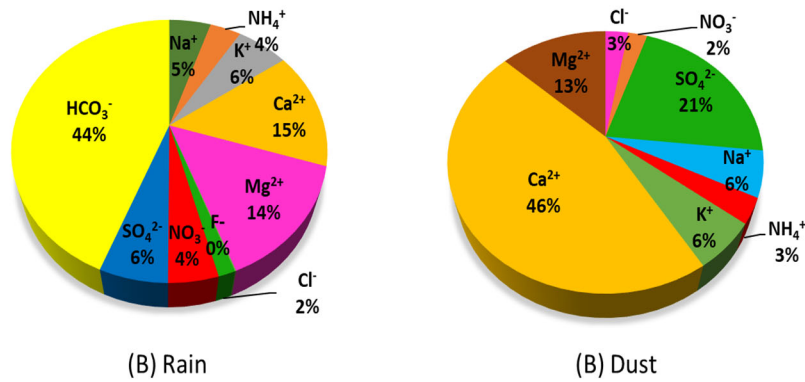


Fig. 2 Percentage contribution of ionic species in rain and dust

Deposition fluxes of Nr:

Wet deposition fluxes

Relative abundance of reduced (NH_4^+) and oxidized (NO_3^-) in rain water is shown in Figure 3 (a).

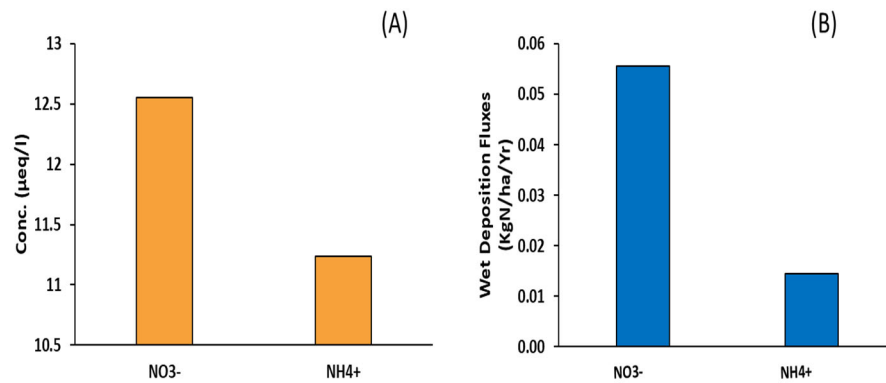


Figure 3. (a) The conc. of NH_4^+ and NO_3^- in rain water ($\mu\text{eq l}^{-1}$) and (b) Deposition fluxes ($\text{kgN ha}^{-1} \text{ y}^{-1}$) of NH_4^+ & NO_3^- at the site

The resulting wet deposition fluxes of Nr were calculated from their abundances in the rain water sample using the following formula (Du and

Liu, 2014).

$$R_i = \sum C_i \cdot P_i \cdot 0.01$$

Where R_i ($\text{kg ha}^{-1}\text{y}^{-1}$) is the annual wet deposition flux, C_i (mg/l) is the concentration of Nr for each precipitation event and P_i is the depth of precipitation (mm).

3.3.2 Scavenging pattern of Nr Species:

3.3.2a In wet precipitation

The Neutralization Factor (NF) values of Ca^{2+} , Mg^{2+} and NH_4^+ were estimated and found to be 1.52, 1.39 and 0.40, respectively. Results suggested that the Ca^{2+} is the most abundant crustal component participating in buffering of precipitation acidity. Similar results have been reported at various other stations in India, showing maximum neutralizing capacity for Ca^{2+} in the rainwater (Bisht et al., 2015; Kulshrestha et al, 2003c).

3.3.2b In dustfall deposition

Ca^{2+} (1.90) showed the highest neutralization ratios among all the base cations and the lowest neutralization ratio in the aqueous abstract of dustfall. The NF value indicated that the role of other neutrally agents such as NH_4^+ , Mg^{2+} and K^+ was very limited at this site.

CONCLUSION

The expanding industrial and agricultural sectors significantly contribute to the atmospheric Nr , which are eventually removed by rainfall and dustfall. This study revealed that the rainwater has pH value well above the acidic range. The order of measured ions in rain was as follows: $\text{HCO}_3^- > \text{Ca}^{2+} > \text{Mg}^{2+} > \text{K}^+ > \text{SO}_4^{2-} > \text{Na}^+ > \text{NO}_3^- > \text{NH}_4^+ > \text{Cl}^- > \text{F}^-$. Wet fluxes suggested highest contribution of NO_3^- over NH_4^+ , whereas dustfall fluxes suggested very similar ranges for NH_4^+ and NO_3^- . Neutralization factor suggested that the acidity in the rainwater is largely controlled by Ca^{2+} , whereas Mg^{2+} , K^+ and NH_4^+ played a minor role, which is true for dustfall extract too.

REFERENCES

Bisht, D. S. Tiwari, S. Srivastava, A. K. Singh, J. V. Singh, B. P. and Srivastava, M. K. (2015). High concentration of acidic species in rainwater at

Varanasi in the Indo-Gangetic Plains, India, *Natural Hazards*, 75(3), 2985-3003.

Du, E. and Liu, X. (2014). Chapter Nitrogen Deposition, Critical Loads and Biodiversity, pp. 49-56.

Galloway, J.N. Dentener, F.J. Capone, D.G. Boyer, E.W. Howarth, R. W. Seitzinger, P. Asner, G. P. Cleveland, C.C. Green, P.A. Holland, E.A. Kari,

D.M. Michaels, A.F. Porter, J.H. Townsend, A.R. and Voosmarty, C.J. (2004). Nitrogen cycles: past, present, and future, *Biogeochemistry* 70 (2), 153-226.

Ianniello, A. Spataro, F. Esposito, G. Allegrini, I. Hu, M. and Zhu, T (2011).

Chemical characteristics of inorganic ammonium salts in PM_{2.5} in the atmosphere of Beijing (China), *Atmos. Chem, Phys*, 11.

Jain, M. Kulshrestha, U. C. Sarkar, A. K. and Parashar, D. C. (2000). Influence of crustal aerosols on wet deposition at urban and rural sites in India, *Atmospheric Environment*, 34(29-30), 5129-5137.

Kulshrestha, U.C. Kulshrestha, M.J. Sekar, R. Sastry, G.S.R. and Vairamani, M. (2003c). Chemical characteristics of rainwater at an urban site of south-central India, *Atmos. Environ.* 37 (21), 3019-3026.

Kulshrestha U (2013). Acid rain in encyclopedia of environmental management ed S E Jorgensen I (New York: Taylor & Francis) pp 8-22

Penuelas, J. Sardans, J. Rivas-ubach, A. and Janssens, I.A. (2012). The human-induced imbalance between C, N and P in Earth's life system, *Glob. Change Biol*, 18, 3e6.

Sharma, A., Singh, S., & Kulshrestha, U. C. (2017). Determination of Urban Dust Signatures through Chemical and Mineralogical Characterization of Atmospheric Dustfall in East Delhi (India). *J. Ind. Geophys. Union* 21(2), 140-147.

Singh, S. Sharma, A. Kumar, B. and Kulshrestha, U. C. (2017). Wet deposition fluxes of atmospheric inorganic reactive nitrogen at an urban and rural site in the Indo-Gangetic Plain, *Atmospheric Pollution Research*, 8(4), 669-677.

Sun, Y. Zhuang, S. Wang, Y. Han, L. Guo, J. Dan, M. Zhang, W. Wang, Z. and Hao, Z. (2004). The air-borne particulate pollution in Beijing: concentration, composition, distribution and sources, *Atmos. Environ*, 38, 5991-6004

Tiwari, R., Gupta, G. P., & Kulshrestha, U. C. (2016). Summer Time Dustfall Fluxes of Reactive Nitrogen and Other Inorganic Species over the Tropical Megacity of Indo-Gangetic Plains. *Earth Interactions*, 20(23), 1-20.

BIOGENIC AND ANTHROPOGENIC ISOPRENE EMISSIONS IN THE AMBIENT AIR OF DELHI

PRABHAT KASHYAP¹, KRISHAN KUMAR^{1*}

¹School of Environmental Sciences, Jawaharlal Nehru University, Delhi-110067, India.

Tel No. +91-9311811585

(*Correspondence at kashyaprabhat@gmail.com¹, krishan_kumar@mail.jnu.ac.in^{1*})

KEYWORDS: Biogenic VOCs, Isoprene Emissions, Urban Vegetation.

INTRODUCTION

Terrestrial vegetation serves numerous functions to support the biosphere by regulating biogeochemical cycles and maintain the global energy balances. Along with this, they also emit various greenhouse gases such as carbon dioxide: CO₂; nitrous oxide: N₂O; methane: CH₄ (Menon et al., 2007) and plays a significant role in climatic system of the atmosphere. Apart from CH₄, they also emit significant amount of various biogenic volatile organic compounds (BVOCs) (Guenther, 2002). BVOCs (including isoprene, monoterpenes & sesquiterpenes) are the important class of volatile organic compounds (VOCs) that cause substantial impact on the atmospheric chemistry. Among all these BVOCs, isoprene (C₅H₈) quantitatively, the largest emitted compound on global scale with an annual global emission of 500 Tg C year⁻¹ (Guenther et al., 1995). The presence of carbon-carbon double bond in isoprene molecule makes it a very reactive compound that can readily attack the ozone (O₃), hydroxyl radical (OH) and nitrate (NO₃) species. The photo oxidation of isoprene with OH and indirectly with NO₃ radical leads to the formation of diverse secondary pollutants e.g., ozone, secondary organic aerosol (SOA), peroxyacetylnitrate (PAN), organic nitrates, carbon monoxide, carbonyls (Poisson et al., 2000), having the capability to cause a potential impact on regional and urban air quality.

The deciduous trees and certain shrubs are the key species for isoprene emission (Guenther et al., 2006) and its rate of emission is depends upon the intensity of solar radiation falls on the leaves surface and the ambient temperature (Guenther et al., 1991, 1993). Despite the biogenic sources, isoprene also emitted from anthropogenic sources as well (Borbon et al., 2001; Hellen et al., 2012; Wang et al., 2013). Major portion of anthropogenic isoprene comes directly into the ambient atmosphere from the vehicular exhaust (Borbon et al., 2001). This study quantify the ambient air isoprene in

2 different seasons from the major biogenic location as well as anthropogenic location of Delhi in order to understand the temporal and spatial characteristic of isoprene.

METHODS

The study was performed at two different locations of Delhi for two consecutive seasons (autumn and winter). To investigate the anthropogenic and biogenic emissions of isoprene, one site from traffic intersection i.e. Central Road Research Institute (CRRI) and another location from vegetative i.e. Yamuna Biodiversity Park (YBP) were selected. The vegetative site is located in the vicinity of isoprene emitting tree species (viz. *Ficus religiosa*, *Holoptelea integrifolia*, *Ficus virens*) (Varshney & Singh, 2003) in the central region of the park where the chance of anthropogenic emissions are very less. To examine the intraday variation of isoprene, samples were taken 3 times in a day (morning from 8 to 10 am, afternoon from 12 to 2 pm, and evening from 6 to 8 pm) in each seasons at both the sites. For the collection of samples, FLM Carbopack X thermal desorption tubes were used. Ambient air was passed through the tube at a flow rate of 100 ml/min with the help of portable VOC sampler. All samples were stored at less than 4°C until the final analysis and further the analysis was done with the help of Gas chromatography-mass spectrometry (GC-MS).

RESULTS & DISCUSSIONS

The results of the study suggested that the isoprene emissions during the autumn time at YBP vegetative location was far greater (9.88 ± 4.07 ppbv) than the concentration observed during winter season at the same site which was very less as 0.20 ± 0.11 ppbv (Figure 1). However, not much variation was observed at CRRI traffic site in the seasons. Even winter concentration of isoprene was slight higher (0.53 ± 0.10 ppbv) than the autumn concentration (0.50 ± 0.14 ppbv) at CRRI. This suggested that the biogenic isoprene is more prevalent than the anthropogenic and high temperature and solar intensity enhance the concentration. Figure 2 and figure 3 represent the intraday variation of isoprene concentration at both the sites in two different seasons. The average isoprene concentration at YBP is higher during afternoon time (13.95 ± 2.05 ppbv) with evening (9.89 ± 1.32 ppbv) and morning times (5.80 ± 2.52 ppbv) because of the high temperature and intense solar radiation during afternoon hours. High temperature during evening as compared to morning also contributes in the isoprene emissions. On the other hand, CRRI location were showing lesser concentration of isoprene during afternoon time (0.35 ± 0.20 ppbv) because of the presence of low vehicular load as compared to the peak hours during morning and evening time. During winter season, some surprising pattern was observed the average

concentration of isoprene were found to be higher during evening time (0.32 ± 0.51 ppbv at YBP; 0.62 ± 0.12 ppbv at CRRI) at both the locations. This might be because of the very low temperature during evening may decrease the mixing height and increase the persistency of pollutants. Winter results indicate that the biogenic isoprene emissions are very low during winter season.

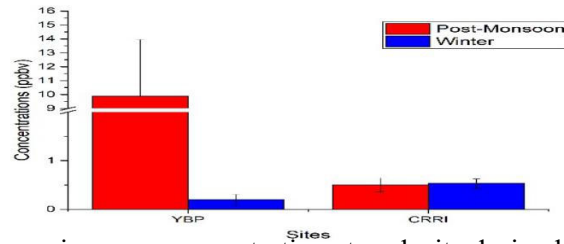


Figure 13. Average isoprene concentration at each site during both the season

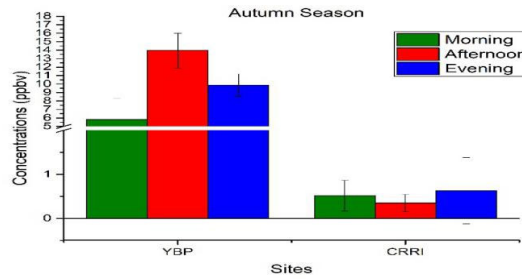


Figure 2. Intra-day variation of isoprene concentration during autumn season

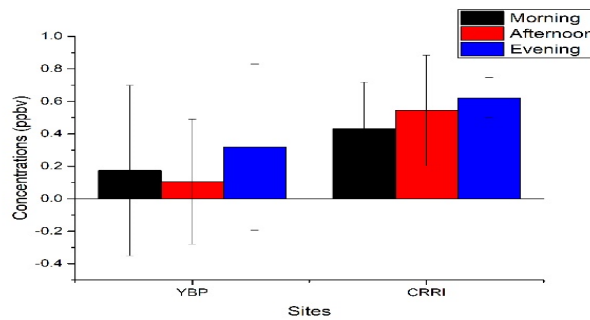


Figure 3. Intra-day variation of isoprene concentration during winter season

CONCLUSION

Atmospheric isoprene were measured at two different location of Delhi to understand its spatial and temporal variation. The result of the study suggested that the biogenic contribution of isoprene overwhelmed their anthropogenic counterpart during autumn season. The biogenic portion is always dominated during afternoon hours in autumn at YBP while lower at CRRRI location. High solar intensity and temperature influence the biogenic isoprene emission rate. However, vehicular load governs the anthropogenic emission rate. Further, not much variation was observed during winter season at both the sites this indicates that anthropogenic isoprene is abundant during the winter season.

ACKNOWLEDGEMENTS

The author is thankful to the University Grants Commission (UGC) for providing the financial support in the form of fellowship. We are also thankful to the Department of Science and Technology Government of India for providing the Promotion of University Research and Scientific Excellence Grant (DST-PURSE grant).

REFERENCES

- Borbon, A., Fontaine, H., Veillerot, M., Locoge, N., Galloo, J. C., & Guillermo, R. (2001). An investigation into the traffic-related fraction of isoprene at an urban location. *Atmospheric Environment*, 35(22), 3749-3760.
- Guenther, A. (2002). The contribution of reactive carbon emissions from vegetation to the carbon balance of terrestrial ecosystems. *Chemosphere*, 49(8), 837-844.
- Guenther, A. B., Monson, R. K., & Fall, R. (1991). Isoprene and monoterpene emission rate variability: observations with eucalyptus and emission rate algorithm development. *Journal of Geophysical Research: Atmospheres*, 96(D6), 10799-10808.
- Guenther, A. B., Zimmerman, P. R., Harley, P. C., Monson, R. K., & Fall, R. (1993). Isoprene and monoterpene emission rate variability: model evaluations and sensitivity analyses. *Journal of Geophysical Research: Atmospheres*, 98(D7), 12609-12617.
- Guenther, A., Hewitt, C. N., Erickson, D., Fall, R., Geron, C., Graedel, T., ... & Pierce, T. (1995). A global model of natural volatile organic compound emissions. *Journal of Geophysical Research: Atmospheres*, 100(D5), 8873-8892.

Guenther, A., Karl, T., Harley, P., Wiedinmyer, C., Palmer, P. I., & Geron, C. (2006). Estimates of global terrestrial isoprene emissions using MEGAN (Model of Emissions of Gases and Aerosols from Nature). *Atmospheric Chemistry and Physics*, 6(11), 3181-3210.

Hellén, H., Tykkä, T., & Hakola, H. (2012). Importance of monoterpenes and isoprene in urban air in northern Europe. *Atmospheric environment*, 59, 59-66.

Menon, S., Denman, K. L., Brasseur, G., Chidthaisong, A., Ciais, P., Cox, P. M., & Jacob, D. (2007). Couplings between changes in the climate system and biogeochemistry (No. LBNL-464E). Lawrence Berkeley National Lab. (LBNL), Berkeley, CA (United States).

Poisson, N., Kanakidou, M., & Crutzen, P. J. (2000). Impact of non-methane hydrocarbons on tropospheric chemistry and the oxidizing power of the global troposphere: 3-dimensional modelling results. *Journal of Atmospheric Chemistry*, 36(2), 157-230.

Varshney, C. K., & Singh, A. P. (2003). Isoprene emission from Indian trees. *Journal of Geophysical Research: Atmospheres*, 108(D24).

Wang, J. L., Chew, C., Chang, C. Y., Liao, W. C., Lung, S. C. C., Chen, W. N., ... & Chang, C. C. (2013). Biogenic isoprene in subtropical urban settings and implications for air quality. *Atmospheric environment*, 79, 369-379.

CONTROL OF EMISSIONS OF REACTIVE NITROGEN IN RURAL HOUSEHOLD THROUGH SOFT APPROACH

VERMA¹ AND U.C. KULSHRESTHA¹

¹School of Environmental Sciences, Jawaharlal Nehru University, New Delhi-110067, India

KEYWORDS: Ammonia, Biomass burning, LPG, Nitrogen Oxide.

INTRODUCTION

India is a developing country where a large proportion of population which is mainly rural, is dependent on Biomass Burning (BB) for cooking and heating. People from different regions use different types of biomass viz. cow dung cake (CDC), wood, crop residues, dried leaves and twigs, etc. to be burnt on their traditional cook stoves called *Chullah*. These handmade traditional cook stoves (*Chullah*) results into incomplete combustion of these inefficient sources of energy which then further result into the emissions of smoke (containing organic carbon and black carbon), CO, SO_x, NO_x, Particulate Matter (PM₁₀, PM_{2.5}), PAHs and other air pollutants (UNEP. 2002). Such emissions give birth to the potentially hazardous indoor air pollution which is significantly harmful for the residents of the house. Also, those people who are having LPG cylinders are not using it because of their rigid thought pattern that the food prepared on *Chullah* is healthier and tastier. This study has made an attempt to reduce the indoor air pollution by bringing about a shift in social behaviour of few rural household residents in Madhya Pradesh.

METHODS

The sampling was done in four households of Budhwada Village (Madhya Pradesh, MP). The samples were collected inside the house for cooking hours (morning and evening) and non-cooking hours (afternoon and night). The aerosol samples were collected on Quartz fibre filter and gaseous samples of NO_x and NH₃ in impingers with their respective absorbing reagents through vacuum suction pump at a flow rate of 1 litre per minute. The collected samples were then analysed for NO_x and NH₃ concentrations on UV-VIS Spectrophotometer. Also, the extract of the Quartz filter was analysed for major cations (Na⁺, NH₄⁺, K⁺) and anions (F⁻, Cl⁻, PO₄³⁻, SO₄²⁻) by Ion Chromatography (Metrohm 883 Basic IC Plus).

RESULTS & DISCUSSIONS

As is given in Table 1, during non-cooking times (NA), it was found that the concentration of the major cations (Na^+ , NH_4^+ , K^+) and major anions (F^- , Cl^- , SO_4^{2-}) were lower than when cooking is taking place. Highest emissions of NH_4^+ and K^+ were found when cooking is done using biomass burning (BB) as the fuel. This is so because in Budhwada village, people are using dung cake biomass as fuel (Singh & Kulshrestha, 2012). Then as a soft approach, the residents were advised to cook partial meal on Chullah and partial on LPG (BL), as a result of which the concentrations came down to some extent. Similar trend was found with the concentration of NO_x as in Figure 1. With BB, average NO_x concentration was $14.27\mu\text{g}/\text{m}^3$ whereas it was as low as $8.8\mu\text{g}/\text{m}^3$ with BL and $8.7\mu\text{g}/\text{m}^3$ with NA. In figure 2, the trend in average ammonia concentration is depicting that with BL there was a decrease of 59.5% in its concentration as compared with BB. But in NA time, the concentration of ammonia came out to be as high as $98.75\mu\text{g}/\text{m}^3$, which is because in these times the activities related to cattle was taking place in close proximity with the kitchen, where the sampling was being carried out.

	Na^+	NH_4^+	K^+	F^-	Cl^-	PO_4^{3-}	SO_4^{2-}
BB	6.83	13.97	6.70333 3	0.335	2.613 75	0.1566 67	1.3937 5
BL		9.295	1.18	0.315	1.155	0.175	0.46
NA	7.4233 33	6.644167	2.586	0.273	0.678	0.1566 67	0.708

Table 1: Concentration of major cations (Na^+ , NH_4^+ , K^+) and anions (F^- , Cl^- , PO_4^{3-} , SO_4^{2-}) in $\mu\text{g}/\text{m}^3$ with different fuels.

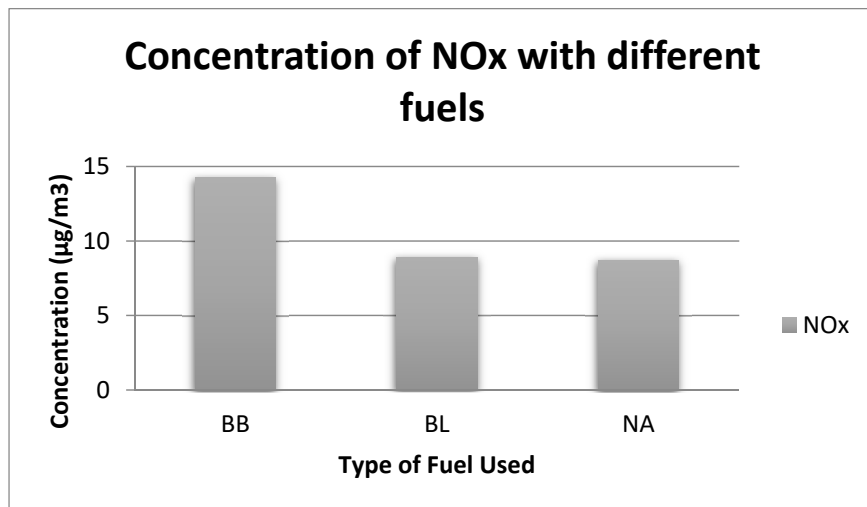


Figure 1: Concentration (in $\mu\text{g}/\text{m}^3$) of NO_x gas with different fuels.

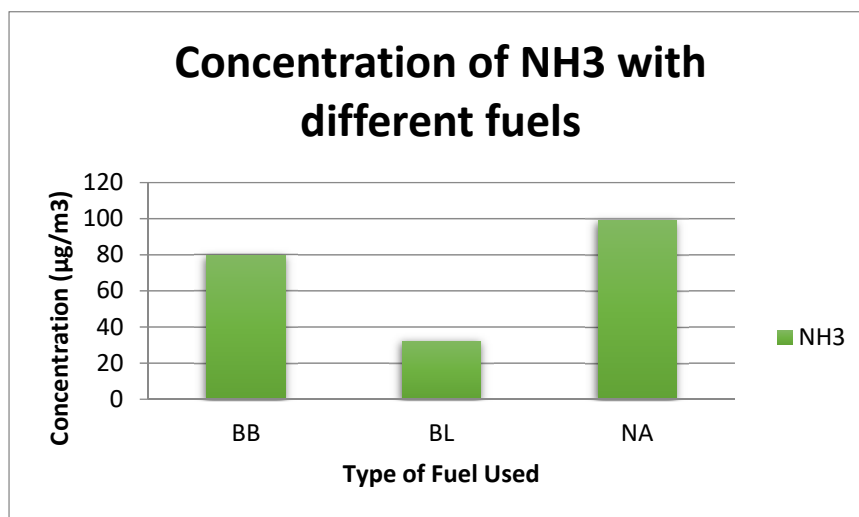


Figure 2: Concentration (in $\mu\text{g}/\text{m}^3$) of NH_3 gas with different fuels.

CONCLUSIONS

With the application of soft approaches in rural households which is by implementing nominal improvements in their traditional methods, a considerable reduction in indoor air pollution due to Chullah and biomass burning can be achieved.

ACKNOWLEDGEMENTS

This work was supported by CSIR-UGC Senior Research Fellowship and DST-Purse Grant.

REFERENCES

Singh, S. and Kulshrestha, U.C. (2012). *Abundance and distribution of gaseous ammonia and particulate ammonium at Delhi (India)*. Biogeosciences Discuss., 9, 191–207, 2012 doi:10.5194/bgd-9-191-2012.

Singh, S. and Kulshrestha, U.C. (2014). *Rural versus urban gaseous inorganic reactive nitrogen in the Indo-Gangetic plains (IGP) of India*. Environ. Res. Lett. 9 125004 (9pp).

UNEP (2002). [The Asian Brown Cloud: Climate and Other Environmental Impacts](#). United Nations Environmental Programme.

SOURCES AND CHARACTERISTICS OF AEROSOLS OVER A SMART CITY BHUBANESWAR IN SUMMER AND WINTER

DUDAM BHARATH KUMAR AND SASMITA SUSHREE

School of Civil Engineering Kalinga Institute of Industrial Technology,
Deemed to be University,
Bhubaneswar – 750124, India.

KEYWORDS: Sources, characteristics, summer, winter

INTRODUCTION

Growing increase in urbanization stresses the commuters in cities to use individual vehicles, which evolve massive amount of gaseous and aerosols emissions. Regional emissions from the urban local emissions while biomass burning emissions as long-range transport agents influence aerosol characteristics at urban landscapes. Aerosol characteristic over a station exhibits the behavior of pollutant over a period of time. Atmospheric pollution is influenced by the response of air pollutants to the changing meteorology at the station and emissions transported from the source regions (Stohl, 1998) In this study we discuss about the aerosol columnar characteristics obtained by the satellite based observations and possible influencing source emissions on transport of the aerosol towards the receptor (observation) station.

METHODS

Assessment of seasonal change in aerosol characteristics and their possible source fields those influencing the aerosol climatology are important to evaluate. In order to address the effect of local and long-range transport of aerosol emissions, we analyze the pollution episodes in summer (March) and winter (November) 2017 over a smart city Bhubaneswar. Time series data of aerosol optical depth (AOD) was obtained from Moderate Resolution Imaging Spectroradiometer (MODIS) satellite of combined Land and ocean product collection-6 Version 3.0 (C006 V3.0). Seven day Back-trajectories calculations at 10, 100, and 500m arrival heights were done through Hybrid Single Particle Lagrangian Integrated Trajectory (HYSPLIT). Trajectory statistics was performed based on K-means clustering and concentration weighted trajectory as suggested in previous studies (Wang et al., 2006).

RESULTS & DISCUSSIONS

Time series of day-wise aerosol optical depth (AOD) of March and November 2017 exhibit the same value 0.2-1.3, whereas the monthly mean AOD for the corresponding months do vary marginally (with difference 0.03) in terms of mean ($\pm 1\sigma$ standard deviation) as 0.53 ± 0.26 and 0.50 ± 0.21 . Transport of aerosol emissions from the regions of biomass burning (high rise fires) of central India and north-east India may be attributed to the variability of AOD in March; while those from open crop field burning regions of north-west India likely influence AOD variability in November. However, the AOD is observed to be highly consistent with the fire counts over the corresponding source regions for the respective months. It is also confirmed by the trajectory statistical analysis including trajectory clustering and concentration weighted trajectory (Figure 1).

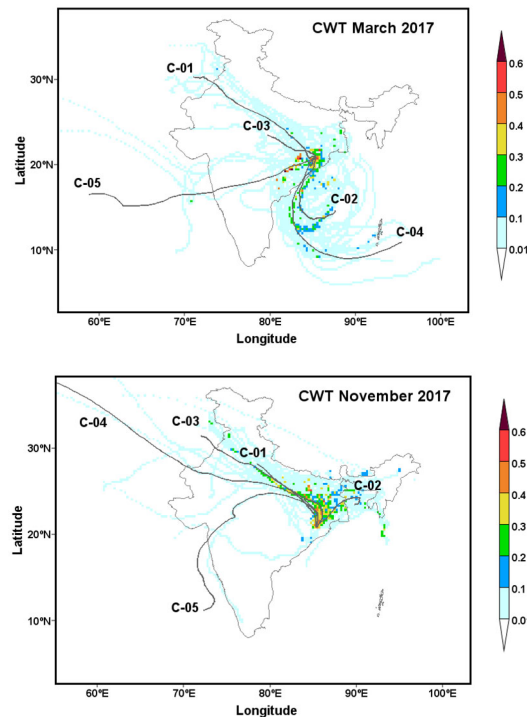


Figure 1. Schematic of concentration weighted trajectory and clusters (cluster with number: C-01, C-02,...C-05 those divided based on common paths and diversity) associated for the month of March (left panel) and November 2017 (right panel).

CONCLUSIONS

In summary, we observed aerosol optical depth from the satellite observations showing marginally difference between March and November. Trajectory statistical analysis showed high contribution of potential aerosols from regional level (eastern Indo-Gangetic region: November; Central eastern India: March) than that of long-range source regions, though most of the source fields fall over oceanic regions (particularly in March). Though influence of urban emissions, biomass burning events in terms of forest fires in March and those in terms of crop field burning activities in November are likely identified sources through our analysis. Setting-up of dispersion model coupled with wind fields may serve the purpose of studying the effects of potential source emissions towards aerosol parameters at the study stations.

ACKNOWLEDGEMENTS

This work was supported by the KIIT DU for its computational facility throughout the project work.

REFERENCES

- Stohl, A. (1998). Computation, accuracy and applications of trajectories - a review and bibliography, *Atmos. Environ.* **32**, 947-966.
- Wang Y. Q., X.Y. Zhang and R. Arimoto (2006). The contribution from distance dust sources to the atmospheric particulate matter loading in Xian, China during Spring, *Sci. Tot. Environ.*, **368**, 875-883.

**DISTINCT INFLUENCE OF LONG RANGE TRANSPORT ON THE
SEASONAL INHOMOGENETIES IN AEROSOL PROPERTIES
AND AIR POLLUTANTS
OVER UDAIPUR IN WESTERN INDIA**

B. M. VYAS¹ AND M. M. GOGOI²

¹Department of Physics, M.L. Sukhadia University, Udaipur-
313001, India

²Space Physics Laboratory, VSSC, Thiruvananthapuram-695022, India

KEYWORDS: atmospheric aerosols, aot, black carbon, PM_{2.5}, ozone.

INTRODUCTION

Day to day as well as seasonal variability in various air pollutants and aerosol loading over a particular region are distinctively governed by varieties of local source and sink mechanisms; such as, large number of anthropogenic emission activities, natural events, prevailing ground level meteorological conditions, boundary layer dynamic processes and wind dispersion phenomenon etc. In this regard, Udaipur (24.6°N, 74°E, 580 m a.s.l.), a semi-tropical arid and typical urban site located close to the south eastern end of the foothill of Arravali mountain range and near the Thar Desert, represents a unique site for understanding the role of distinct source processes and associated aerosols and air pollutant pathways. In addition, the characterization of air pollutants and aerosols from Udaipur is also important considering (i) primarily the scarcity of region specific long term data, (ii) its distinct nature of proximity to the tropical semiarid environment, which experiences a large change in seasonal pattern of surface aerosol loading due to both human made activities and natural mineral dust activity. Apart from the predominance nature of local emission sources, another most important regional contribution of aerosols and air pollutant burden over the site is related to synoptic scale of air mass flow and long range transports of atmospheric pollutants and aerosols from distant sources.

Realizing the need for identifying various originating source regions toward regional burden of air pollutants and aerosols over Udaipur, the present study investigates the air mass backward wind dispersion processes. For this, we have quantified the role of long range transport episodes on the daily recorded concentration levels of several air pollutant parameters, namely, surface ozone (O₃, ppbv), atmospheric black carbon aerosol mass concentration (M_{BC}, µg/m³), mass concentration of particulate matters of aerodynamic size less than 2.5µm (PM_{2.5}, µg/m³), aerosol optical thickness at wavelength

1020nm (AOT at 1020nm) and total water vapour column content (TWC, cm) over Udaipur.

DATABASE AND ANALYSIS

The present study is based on the synthesis of time series of computed daily values of O₃, M_{BC}, PM_{2.5}, AOT 1020 and TWC along with the computed air mass backward wind trajectories (BT) arriving at 500 m a.g.l. (region well within the atmospheric boundary layer) above the receptor site. BT have been estimated for 72 hour period based on Hybrid Single Particle Lagrangian Integrated Trajectory (HYSPLIT) model (Draxler & Rolph, 2003).

The round the clock observations of O₃, M_{BC} and PM_{2.5} were made by using Aethalometer (Model AE-31), Fine Size Particulate matters (Model-APM-550) and UV Photometric Ozone Analyser (Model 49-i), respectively. On the other hand, measurements of AOT at 1020 nm and TWC were made (on an hourly basis) during clear sky conditions by employing a hand held and microprocessor based Sun photometer (Model-542).

Air mass backward wind trajectories reaching at the observational site have been subjected to seasonal statistical analysis to evaluate the percentage contribution of various air mass pathways to distinct regions. In addition, the analysis also hints to the corresponding mean height (H, meter) of the transported pollutants across its travel path. Percentage occurrence of air mass flow across distinct sectors (e.g., N, NE, E, SE, S, SW, W and NW) with respect to the observational site is also estimated from the statistical analysis.

RESULTS & DISCUSSIONS

With respect to different seasons, the percentage contribution of trajectory clusters along with their average travel heights 'H' in the polar diagrams is investigated in the present study. Simultaneous seasonal mean values of O₃, M_{BC}, PM_{2.5}, AOT 1020 and TWC over each of the specified sectors are also presented for each season of winter (DJF), pre-monsoon (MAM), monsoon (JJAS) and post-monsoon (ON) based on the database collected during December, 2019 to November, 2013. During winter (Fig.1), maximum percentage occurrence (above 65%) of the air masses lies in the NE and NW sectors, having an average trajectory altitude of 558 m and 1398 m, respectively.

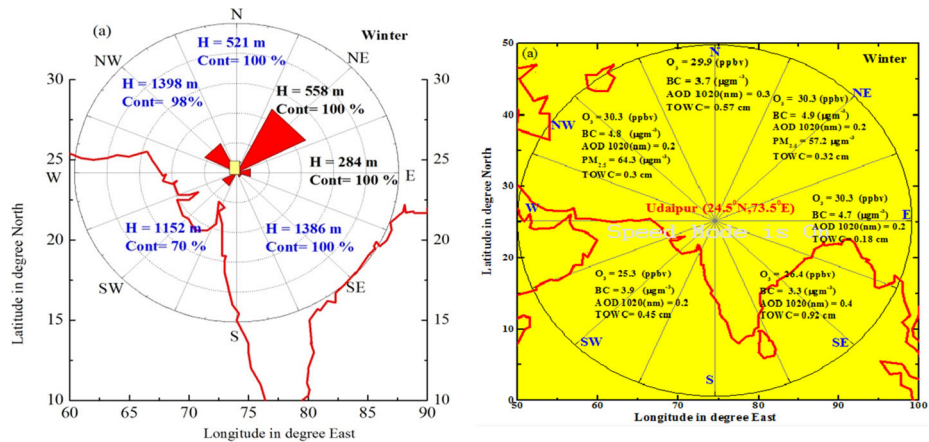


Figure-1

In the cold and dry condition, the air pollutants transported from NE and NW direction have the predominance of intense urban, industrial, and human made emission. Moreover, these source regions are densely populated urban and semi urban sites of North Western to Eastern Rajasthan including the central part of Indo Gangetic Plains (IGP). As a result, elevated levels of M_{BC} (~ 4.9 & $4.8 \mu\text{gm}^{-3}$), $PM_{2.5}$ (~ 57.2 & $64.3 \mu\text{gm}^{-3}$) and O_3 (~ 30.3 ppbv) are observed coinciding with the favorable circumstances. In contrast to this, the lower air pollutant burden of M_{BC} ($\sim 3.3 \mu\text{gm}^{-3}$ & $3.9 \mu\text{gm}^{-3}$) and O_3 (~ 26.4 & 25.3 ppbv) are noticed associated with the air mass conduits from SE and SW regimes, indicating the regions of lesser urban activity. Nevertheless, a slight enhancement in atmospheric column parameters such as AOT (~ 0.4 at 1020 nm) and TWC (~ 0.4 cm) is noticeable during the long range transport of aerosols from the SE sector relative to those observed during the transport of air masses from the NE and NW sectors (AOT ~ 0.2 at 1020 nm and TWC ~ 0.32 cm).

During pre-monsoon season (Fig.2), the maximum percentage (about 58%) of air mass is confined to SW sector, originating at the Arabian sea, and travelled through a small portion of the semi-arid land mass region located SW of the observational site. Thus, the dominant source during this season is of oceanic origin, traversing comparatively at lower altitude of 1082 m. However, the remaining ($\sim 37\%$) air mass is confined to the NW and W sectors, originating mainly over the semi-arid land mass as well as mineral dust active (Thar desert) regions of western India. The observed mean altitude of trajectory changes from 1114 m in the West sector to 1991 m in the NW sector, an increase by 90%. Moreover, mean trajectory altitude in NW and W sector (over the arid and semi-arid regions) increase by about 50% relative to air mass sectors originating in the marine region of Arabian sea. In line with

this, there is also a systematic reduction in the contribution of air parcels (~ 30%) from oceanic origin, compared to those in the NW sector (70%).

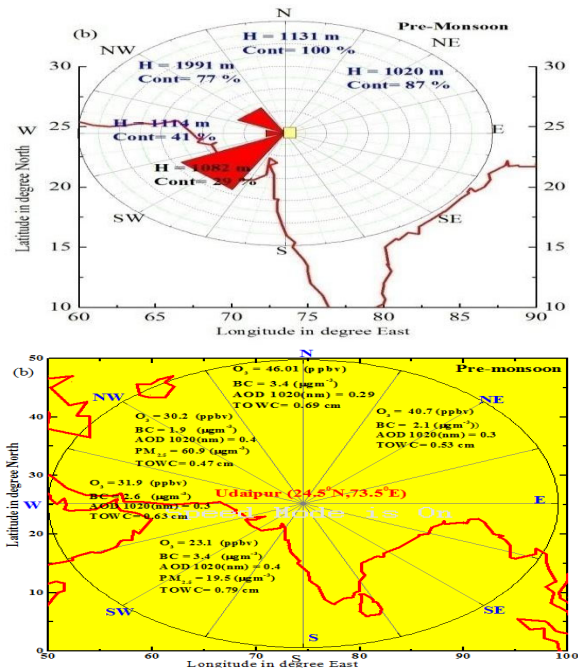


Figure-2

The plausible effect of the variation in air mass percent at different sectors is clearly noticeable from the decreasing levels of surface O_3 and $PM_{2.5}$ concentration from 30.3 ppbv (NW sector) to 23.1 ppbv (SW sector) and 60.9 (NW sector) to 19.5 $\mu g m^{-3}$ (SW sector), respectively. The contribution of continental origin for the higher levels of O_3 (40.7 & 46 ppbv) and M_{BC} (2.1 & 3.4 $\mu g m^{-3}$) is seen for the North and NE sectors, indicating the intense human activity and emissions over the urban and semi-urban land areas. However, there is a decreasing trend of TWC values from 0.79 cm (SW sector) to 0.47 cm (NW sector) associated with the change of air mass flow from Oceanic to continental (arid) origins.

During monsoon season, the majority of air mass (~ 85%) travels at lower heights (~ 286 m) in the SW sector (Arabian sea). Rest of air mass (less than 15%) in the W and NE sectors travels at relatively higher heights (~ 1038 m and 1379 m) over the continental source regions. Owing to dominant air mass from the Oceanic origin during this season, the concentration levels of various pollutants and aerosols parameters were also low, e.g., $PM_{2.5}$ ~ 14.9 $\mu g m^{-3}$, M_{BC} ~ 1.8 $\mu g m^{-3}$, O_3 ~ 11.3 ppbv. On the other hand, the values of each of the above parameters are higher (e.g., $PM_{2.5}$ ~ 15.5 & 19.9 $\mu g m^{-3}$, M_{BC} ~ 1.9

& $2.5 \mu\text{g m}^{-3}$, $\text{O}_3 \sim 15.5$ & 19.93 ppbv, respectively, for W and N sectors associated with the air mass originating at the Western and Northern regions of the observational site. However, values of TWC associated with the air mass of oceanic origin is higher (~ 2.5 cm) relative to those from the regions NE (~ 1.8 cm) of the observational site.

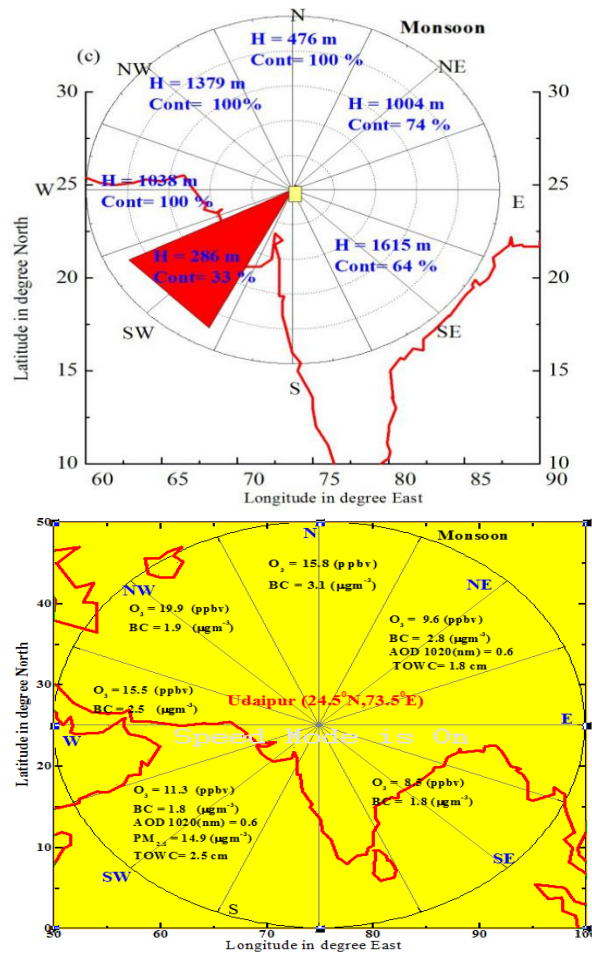


Figure-3

During post-monsoon season (Fig-4), the air mass shows mixed pattern, occurring more than 50% of trajectories in the SW (oceanic and semi-urban origin) and NE (industrial and urban origin) sectors, travel at an average height of 520 m. Associated with this, higher amount of O_3 (~ 35 ppbv), $\text{PM}_{2.5}$ ($\sim 61.7 \mu\text{g m}^{-3}$), M_{BC} ($\sim 3.5 \mu\text{g m}^{-3}$) and O_3 (~ 11.3 ppbv) concentrations are observed for the air mass in the NE sector compared to lower values of $\text{PM}_{2.5}$ ($\sim 34.3 \mu\text{g m}^{-3}$), M_{BC} ($\sim 3.2 \mu\text{g m}^{-3}$), O_3 (~ 17.8 ppbv) at different other sectors.

In case of AOT and TWC, there is insignificant variation in AOT, which remains nearly uniform (~ 0.6) for all the air mass sectors. But, there is slight enhancement in TWC (1.8 and 2.5cm) for the air mass trajectories originating at the IGP and NE Rajasthan.

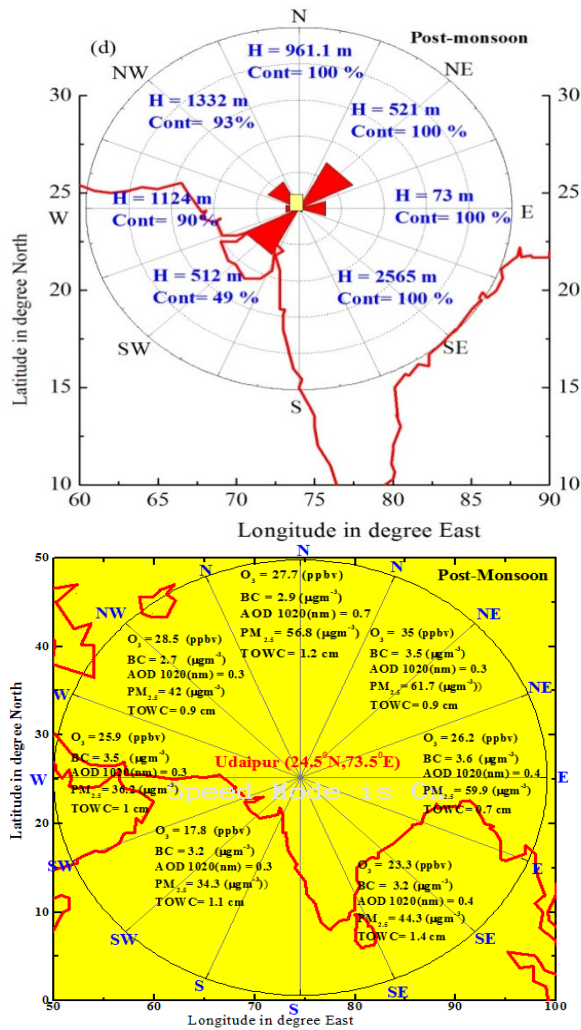


Figure-4

CONCLUSIONS

1. The day to day variation in percentage share of air mass flow over a particular sector as well as their averaged height of flow at different

seasons indicate that the surface level values of O₃, PM_{2.5} and M_{BC} is highest in winter (25.3 to 30.3 ppbv, 57.2 to 64.3 μg m⁻³, 3.3 to 4.9 μg m⁻³), followed by the values in the post monsoon (17.8 to 35 ppbv, 34.3 to 61.7 μg m⁻³, 2.7 to 3.6 μg m⁻³), and pre-monsoon (23.1 to 46.01 ppbv, 19.5 to 60.9 μg m⁻³, 1.9 to 3.4 μg m⁻³) and monsoon (8.5 to 19.9 ppbv). Interestingly, maximum values of AOT (~ 0.6) and TWC (1.8 to 2.5 cm respectively) is noticed in rainy season.

2. The daily variability in air pollution and aerosol burden in different seasons also linked the corresponding variation of advection type and direction of the air mass parcel.

ACKNOWLEDGEMENTS

This work was carried out as part of the ARFI project of ISRO GBP. Authors also whole heartedly thank Dr. K. Krishna Moorthy and Dr. S. Suresh Babu for providing necessary support for operating the aerosol observatory at Udaipur.

REFERENCES

Draxler, R.R., Rolph, G.D., (2003). HYSPLIT (Hybrid Single-Particle Lagrangian Integrated Trajectory) Model access via NOAA ARL READY Website (<http://www.arl.noaa.gov/ready/hysplit4.html>). NOAA Air Resources Laboratory, Silver Spring, MD.

AEROSOL OPTICAL DEPTH AND CARBONACEOUS AEROSOL OVER A SEMI-ARID LOCATION IN SOUTHERN INDIA: TEMPORAL AND SOURCE CHARACTERISTICS

R. M. RAJESHKUMAR¹, B. VIJAY BHASKAR¹ AND TOSHIHIKO TAKEMURA²

¹Department of Bioenergy, Madurai Kamaraj University, Madurai – 625 021, India

²Research Institute for Applied Mechanics, Kyushu University, Kasuga, Fukuoka - 816-8580, Japan

KEYWORDS: Black carbon, SPRINTARS, Aerosol optical depth, Absorption Angstrom exponent

INTRODUCTION

A major source of uncertainty in predicting the state of climate is variability in spatio-temporal distribution and optical properties of aerosol (Gharibzadeh et al., 2017). Aerosol particles affect the troposphere directly by scattering and absorbing incoming solar radiation and indirectly by altering cloud microphysical properties, which can in turn affect the cloud albedo and their lifetime (Twomey, 1977). Black carbon (BC) aerosol formed from incomplete combustion of carbonaceous fuels, is of major research interest due to its abundance and light absorbing characteristics. In addition to real time measurement, satellite retrieval data are widely used for examining aerosol distributions from regional to global scales. Aerosol optical depth (AOD) is a quantitative measure of the extinction of solar radiation due to aerosols when the solar radiation passes through the atmosphere and reaches the Earth's surface (Rajesh et al., 2016). The AOD value depends on the concentration of aerosols in the atmosphere and aerosol size distribution. BC mass concentration collected from Spectral Radiation Transport model for Aerosol Species (SPRINTARS), Modern-Era Retrospective analysis for Research and Applications, Version 2 (MERRA-2) and a seven wavelength based Aethalometer AE-31 were compared for the study period (from May-2014 to May-2014) to comprehend the difference in real time and satellite data. In this study, aerosol concentration (black carbon, organic matter, sulfate, soil dust, and sea salt) from both natural and anthropogenic sources over a semi-urban site located in southern India collected using MERRA-2 and their contributions to AOD were analyzed.

METHODS

Madurai (9°91'N, 78°54'E) one of the major cities in South India, which is 100 m above the mean sea level, is the second largest and most densely populated city in the southern state of Tamil Nadu. It has a surface area of 52.8 km² with an estimated population of 3.2 million in 2011. The rapid urbanization, increased industrialization and improved trade and commerce have resulted in augmentation of mushrooming population. Madurai has the typical climate of the Deccan plateau and remains hot and humid during most of the year with very bright sunshine during summer season manifested by the temperature ranging from 27°C to 40°C. Therefore, the climate is quite hot during the summer season. Winter starts from December and lasts till February with the temperatures ranging between 20°C and 30°C and the climate remains pleasant during this time, as the temperature rarely falls below 20°C. The city receives the major share of rainfall between the months of October and November. The total amount of rainfall received over the entire study period is 2480 mm with ~48% rain during the post monsoon season and almost 0% rainfall during winter.

Continuous and near-real time measurement of aerosol spectral absorption started in Madurai from June, 2014, using a seven wavelength Aethalometer (Model AE-31, Magee Scientific, USA; <http://www.magescientific.com>) (Hansen et al., 1984). The Aethalometer measures the attenuation of light that passes through a quartz fiber filter media, on which aerosol particles are deposited, and hence quantifies (1) the magnitude of absorption, in terms of absorption coefficient b_{abs} (Mm⁻¹), and (2) amount of absorbing aerosols, in terms of black carbon (BC) mass concentration (μgm^{-3}), using a conversion factor. The Absorption Angstrom exponent (AAE) is calculated from the b_{abs} values, assuming a power law dependency (Angstrom, 1964) of b_{abs} on the wavelength λ as represented in Equation 1 where, β is a constant.

$$b_{\text{abs}}(\lambda) = \beta\lambda^{-\text{AAE}} \quad \rightarrow (1)$$

Spectral Radiation-Transport Model for Aerosol Species (SPRINTARS) is a numerical model which has been developed by Atmosphere and Ocean Research Institute, University of Tokyo, National Institute for Environmental Studies, and Japan Agency for Marine-Earth Science and Technology, for simulating effects on the climate system and condition of atmospheric pollution by atmospheric aerosols on the global scale (Takemura et al., 2005 and Takemura and Tomoe, 2011). SPRINTARS is based on an atmosphere-ocean general circulation model, MIROC, and it is also incorporated into a global cloud resolving model. SPRINTARS treats main tropospheric aerosols both from natural and anthropogenic sources (black carbon, organic matter, sulfate, soil dust, and sea salt). The model was simulated with the resolution of 1.125° (latitude) x 1.125° (longitude) at 56 pressure levels. Clear sky aerosol optical parameters and mass concentrations of BC were retrieved

using SPRINTARS during May 2014 to May 2016 at 550 nm over the study location.

Modern-Era Retrospective analysis for Research and Applications, Version 2 (MERRA-2) is a NASA reanalysis for the satellite era using the Goddard Earth Observing System Data Assimilation System Version 5 (GEOS-5.2.0) by the NASA GSFC Global Modeling and Assimilation Office (GMAO) (Rienecker et al., 2011). The model includes the finite-volume dynamical core of Putman and Lin (2007), which uses a cubed-sphere horizontal discretization at an approximate resolution of $0.5^\circ \times 0.625^\circ$ and 72 hybrid-eta levels from the surface to 0.01 hPa (Ronald Gelaro, et al., 2017). MERRA-2 averaged monthly data M2TMNXAER v5.12.4 is used in this study (from May 2014 to May 2016).

RESULT AND DISCUSSION

Observed BC mass concentration shows a decreasing trend from December-January-February to March-April-May and then increases (Figure 1). The high BC observed during December- January-February and June-July-August-September are due to the reduced boundary layer height and rainfall activities and increased wind flow the measurement site. Low BC concentration is observed during March-April-May as the atmospheric boundary layer height is higher because of higher surface temperature and stronger convection. October-November months with frequent rainfall activities reduces the BC concentration at those months. The monthly BC trend approximately matches for MERRA and SPRINTARS, but the magnitudes are very low for MERRA. The significant difference in the SPRINTARS and MERRA magnitude may be due to differences in the emission inventory and floating population data as the study site gets around 2 million visiting population during the June-July-August-September months. The species-wise AOD contributions were obtained from MERRA in order to provide an estimate of the chemical composition of aerosols over the study location (Figure 2). MERRA data reveals the dominance of Sulfate followed by dust, carbon and sea salt particles over the study site for the entire study period. AOD due to dust contributes to 50 %, whereas due to carbon (BC+OC) it contributes to 13 and 19 % at 550 nm from MERRA. MERRA shows the significant sea salt contribution (5 to 13%) throughout the year but with huge contribution during the summer and monsoon months. The AAE calculated from observed data also showed the dominance of aerosols from fossil fuel sources so does the SPRINTARS and MERRA but with slight difference in values.

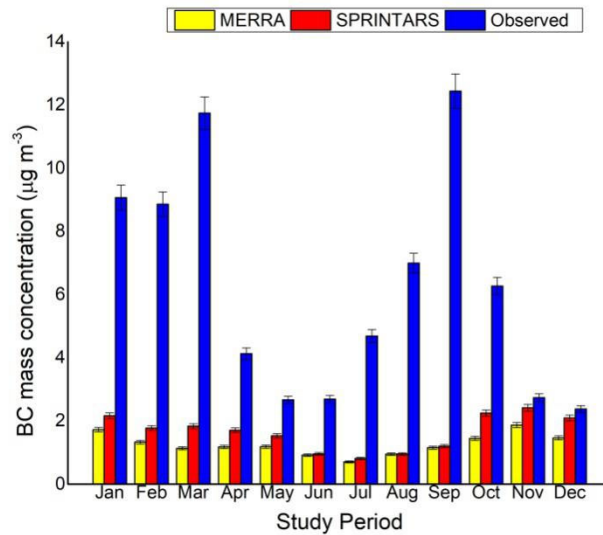


Figure 1. Monthly variations of black carbon aerosols over Madurai from an Aethalometer observation, a reanalysis product (MERRA) and an IPCC model (SPRINTARS). Vertical bars represent $\pm \sigma$ deviation from the mean.

CONCLUSION

BC mass concentration collected from Spectral Radiation Transport model for Aerosol Species (SPRINTARS), MERRA-2 and a seven wavelength based Aethalometer AE-31 were compared for the study period (from May-2014 to May-2014) to comprehend the difference in real time and satellite data. Variability in aerosol concentration (black carbon, organic matter, sulfate, soil dust, and sea salt) and their contributions to AOD were examined over an urban location (Madurai) in western India during May-2014 to May-2016 using MERRA data. The mean percentage species-wise AOD contribution from MERRA reveals the dominance of sulfate type aerosol over the study site at 550 nm.

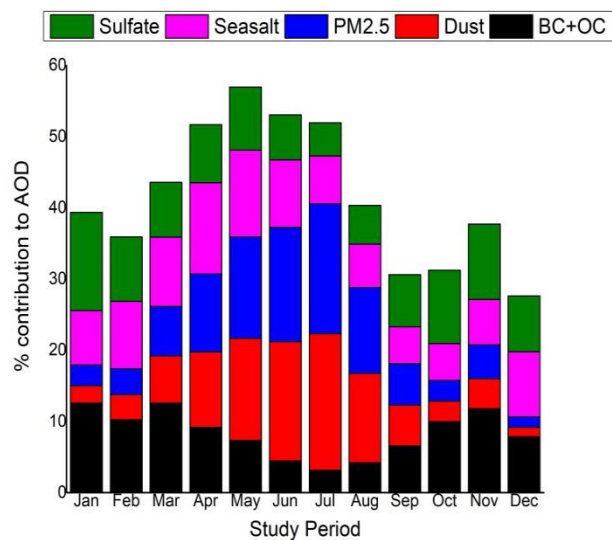


Figure 2. Percentage contribution of Sulfate, sea salt, PM_{2.5}, Dust and (BC+OC) to the total AOD at the study site.

ACKNOWLEDGEMENTS

The authors thank the DST-SERB funding agency and Department of Bioenergy, Madurai Kamaraj University, Madurai for providing fund and space for the research work.

REFERENCES

- Ångström, A., (1964). The parameters of atmospheric turbidity, *Tellus*. Vol. 16, pp. 64-75.
- Gharibzadeh, M., K. Alam, Y. Abedini, A.A. Bidokhti, A. Masoumi (2017). Monthly and seasonal variations of aerosol optical properties and direct radiative forcing over Zanzan, Iran, *Journal of Atmospheric and Solar-Terrestrial Physics*. doi: 10.1016/j.jastp.2017.09.006.
- Hansen, A.D.A., H. Rosen, T. Novakov (1984). The aethalometer: an instrument for the real time measurements of optical absorption by aerosol particles. *Sci Tot Environ.*, Vol. 36, pp. 191–196

Putman, W., and S.J. Lin (2007). Finite-volume transport on various cubed-sphere grids. *J. Comput. Phys.*, 227, 55–78, doi:<https://doi.org/10.1016/j.jcp.2007.07.022>.

Remer L. A., Y. J.Kaufman, D. Tanré, S. Mattoo, D.A. Chu, J.V. Martins, R.R. Li, C. Ichoku, R.C. Levy, R.G. Kleidman, T.F. Eck, E.Vermote, and B.N. Holbe (2005). The MODIS aerosol algorithm, products, and validation, *J. Atmos. Sci.*, 62, 947-973.

Remer, L. A., R. G. Kleidman, R. C. Levy, Y.J. Kaufman, D. Tanre, S. Mattoo, J. V. Martins, C. Ichoku, I. Koren, H. Yu, and B. N. Holben (2008). Global aerosol climatology from the MODIS satellite sensors, *J. Geophys. Res.*, 113, doi:10.1029/2007JD009661.

Rienecker, M.M., M.J. Suarez, R. Gelaro, R. Todling, J. Bacmeister, E. Liu, M.G. Bosilovich, S.D. Schubert, L. Takacs, G.-K. Kim, S. Bloom, J. Chen, D. Collins, A. Conaty, A. da Silva, et al. (2011). MERRA: NASA's Modern-Era Retrospective Analysis for Research and Applications. *J. Climate*, 24, 3624-3648.

Ronald Gelaro, et al., (2017). **MERRA-2 Overview: The Modern-Era Retrospective Analysis for Research and Applications, Version 2 (MERRA-2)**, *J. Clim.*, doi: [10.1175/JCLI-D-16-0758.1](https://doi.org/10.1175/JCLI-D-16-0758.1)

Takemura, T., T. Nozawa, S. Emori, T. Y. Nakajima, and T. Nakajima (2005). Simulation of climate response to aerosol direct and indirect effects with aerosol transport-radiation model. *Journal of Geophysical Research*, 110, D02202, doi:10.1029/2004JD005029.

Twomey, S. A. (1977). The influence of pollution on the shortwave albedo of clouds, *J. Atmos.*, 34, 1149– 1152.

ASSESSMENT OF INDOOR AIR POLLUTION DURING CONSTRUCTION ACTIVITIES

DENIL VACHHANI¹, NIRMIT KAPADIYA¹, NISARG VAGADIYA¹,
ABHISHEK GUPTA¹, SNEHA GAUTAM¹

¹Department of Environmental Science & Engineering, Marwadi Education
Foundation Group of Institution, Rajkot – 360001, India.

KEYWORDS: indoor pollution, air quality index, construction activity

INTRODUCTION

Due to a rapid increase in the population of India, there is hyper increase in the demand of residential areas resulting in a large number of constructional activities. With a demand of smart city, need of constructional activity will be at more pace as of today (Esplugues et. al 2010). Constructional activity also leads to an increase in the indoor air pollution for fixed area or for a specific location. Construction activities that contribute to indoor air pollution include land clearing, operation of diesel engines, demolition, burning, and working with toxic materials. All construction sites generate high levels of air pollutions (typically from concrete, cement, wood, stone, silica) and this can carry for very far distances over a long period of time. Due use of this raw materials in construction work there is release of the pollutant such as PM_{2.5}, PM₁₀, Humidity, Temperature, CO₂, AQI, TOC which leads to the harmful health effect to the workers and near living society peoples. Among this all pollutants the major amount of the pollutant which is generated is PM₁₀, with the size of less than 10 micron in diameter which is invisible with naked eye. In major cities there is between 20-150 micrograms of particulates (PM₁₀ 10 micron) per cubic meter of air. The amount of the PM₁₀ over worldwide on the basis of year 2003-2010, as now there will big change in the countries as in the modern era (WHO 2000; WHO 2006).

According to the World Health Organization (WHO) it is today the single biggest environmental health risk with around 3.7 million premature deaths worldwide per year because of the ambient air pollutions (WHO, 2010). Among the most serious indoor air quality health issues is the potential exposure to construction/renovation-generated pollutants in the society areas. The constructions sites or renovation sites provides many potential exposure opportunities to pollutants (Zhao et. al, 2008). As the use of the raw materials for the construction activities such as cement, fine sand, red bricks, soils which lead to the PM_{2.5} and PM₁₀. The application of tile adhesive, roofing materials, paints, and other products used during construction work provide point sources of volatile organic compounds (VOCs). There is also

production of CO₂ by the use of the transport vehicles of supply of raw materials and used for the construction works like digging then filling the concrete trucks, and by the smoking of the workers working at the sites. Similar type of study was carried out by Mandarick et al, 2018 for a photocopying shop at different location within shop.

METHODS

For current study indoor air quality was monitored for construction site and reconstruction activity. Total 2 sites were selected in different areas of the Rajkot. Monitoring of the concentration of pollutant present in indoor environment such as Air quality index, PM_{2.5}, PM₁₀, Humidity, Temperature and CO₂ was carried out. Sampling was done on 12hr basis. Sampling was carried out for a month, twice a week with the help of sensor based instrument of Airveda.

RESULTS & DISCUSSIONS

Sampling was done at two constructional sites, where results shown the variation in AQI, PM_{2.5}, PM₁₀, CO₂, Humidity, Temperature along day time. The results at site 1 was average in the morning and it goes high as the work been started, the level of the PM₁₀ was high due to the ongoing work of application of the tiles at the site so by the use of adhesive chemicals the range of the PM₁₀ reached high, as the range of other parameters where in the average state (Good as per Indian AQI) (Fig 1).

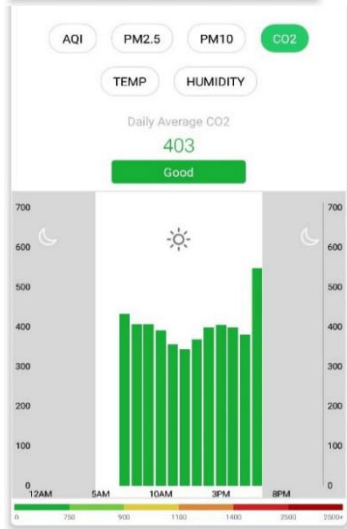
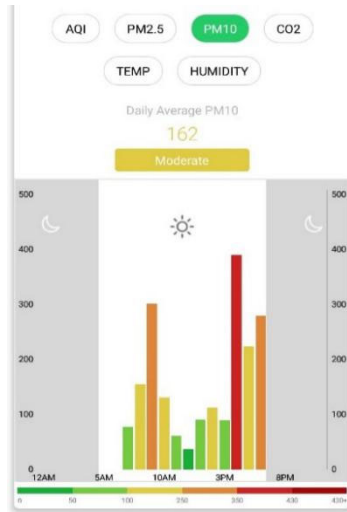
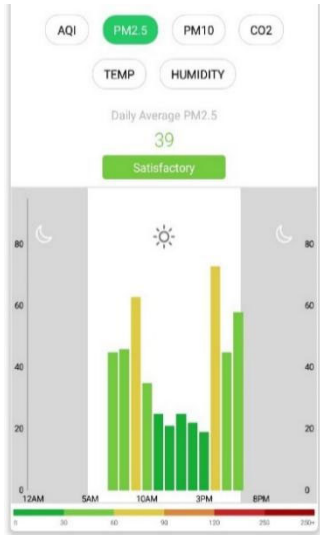
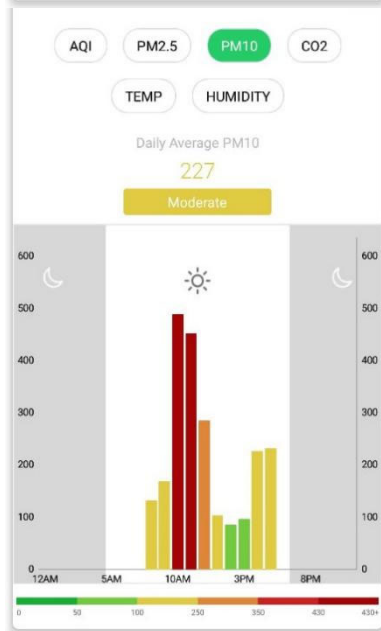
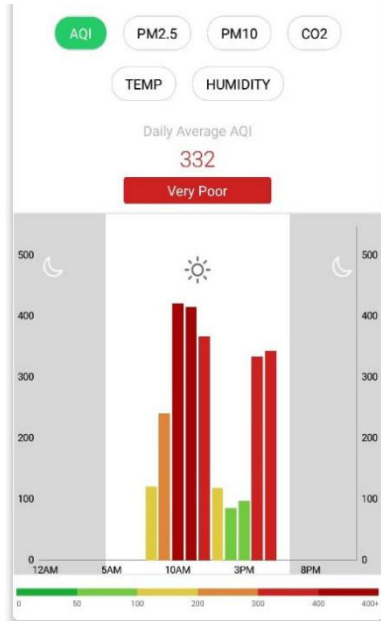




Figure 1: Variation in PM₁₀, PM_{2.5}, CO₂ concentration and variation in Humidity, temperature, AQI at reconstruction site.



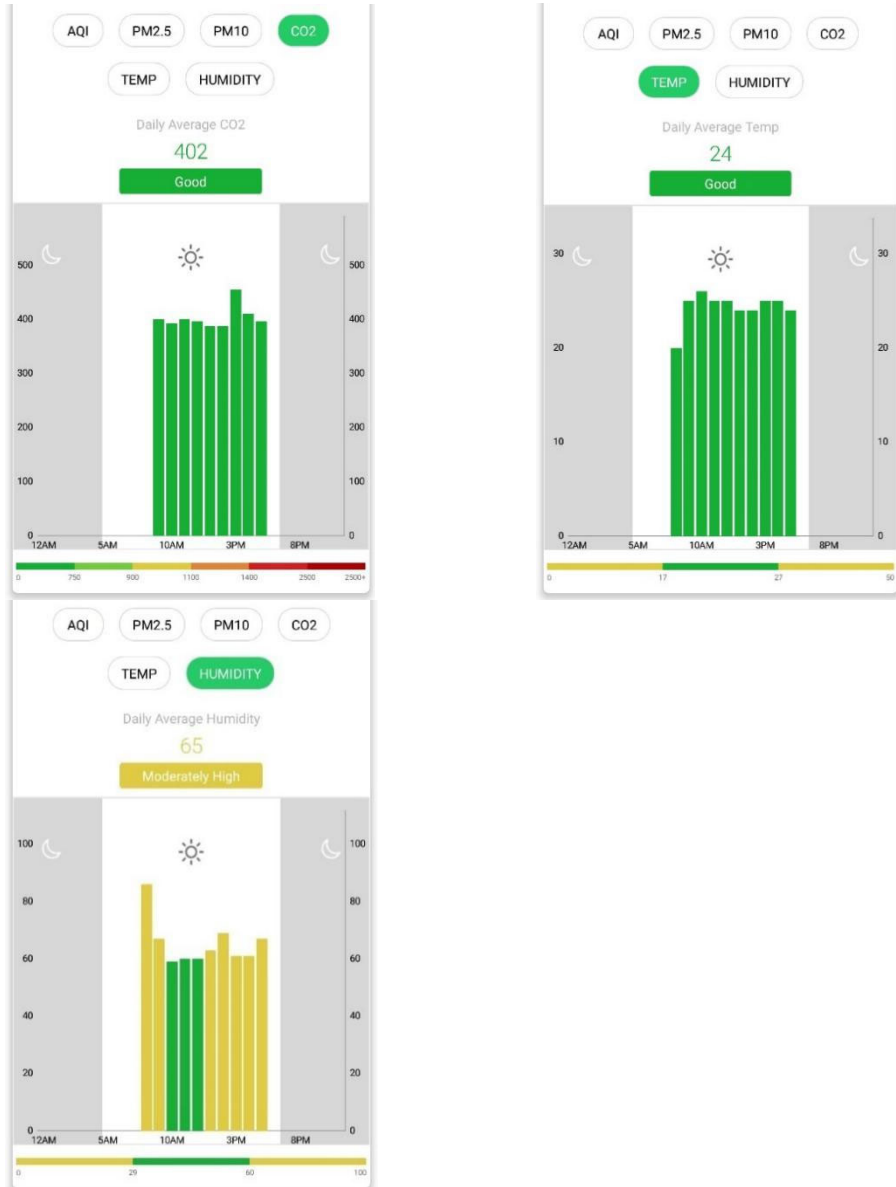


Figure 2: Variation in PM₁₀, PM_{2.5}, CO₂ concentration and variation in Humidity, temperature, AQI at construction site.

Result for site 2 i.e. constructional site where cement and concrete based work is going on, was found to be under very poor condition. AQI was very high i.e. 332 (Fig 4) which on higher level. Application of sand, cement, grit & concrete has also resulted in increased concentration of PM_{2.5} and PM₁₀.

A total of 10 sample at each site were collected, variation in PM₁₀, PM_{2.5} were done for day time as shown in Fig 5, Fig 6. In the renovations sites the range of the PM_{2.5} were in very good conditions but due to the flooring work there is peak values in the PM₁₀. It got high due to the use of the adhesive chemicals and other cement materials and grinding work done at the sites

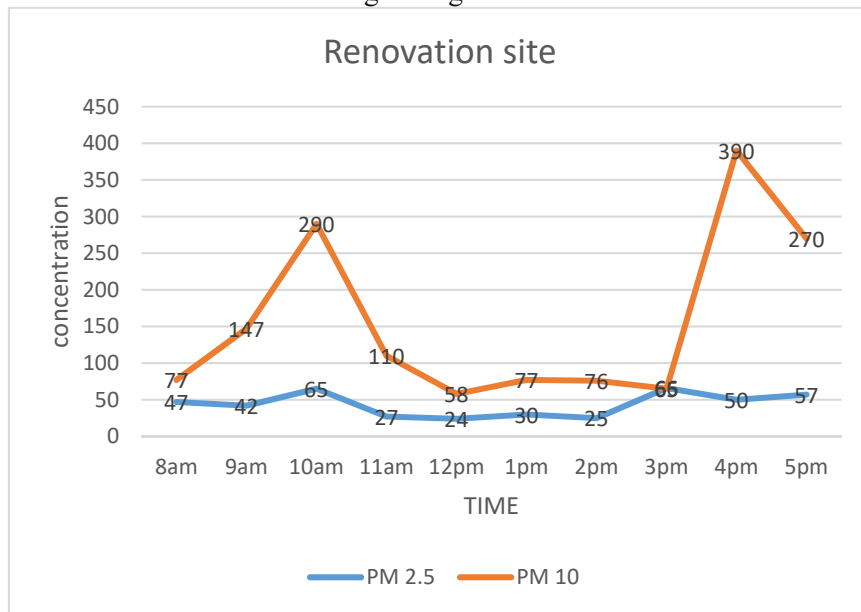


Figure 3: Average concentration of PM₁₀, PM_{2.5} at Site 1

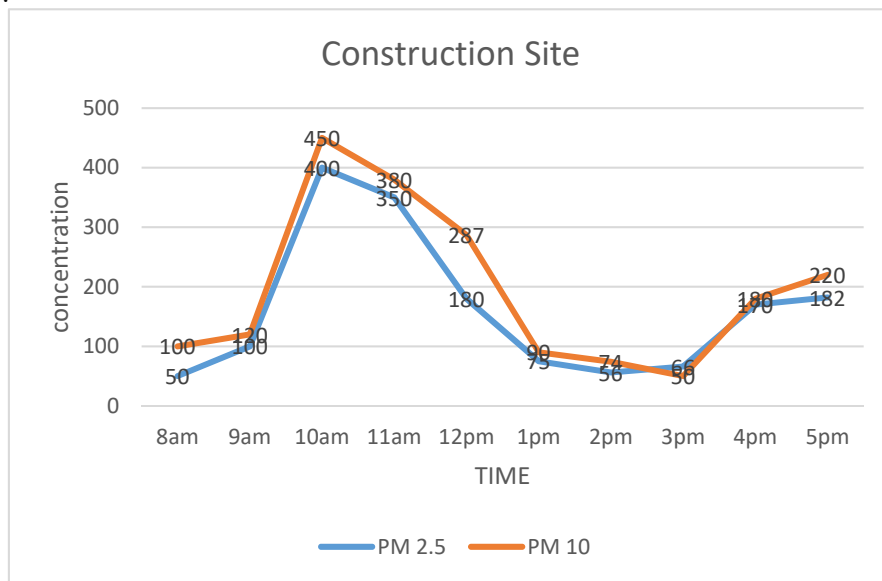


Figure 4: Average concentration of PM₁₀, PM_{2.5} at Site 2

EFFECT OF AIR POLLUTIONS AT CONSTRUCTION SITES

The effects due to the generation of pollutant at the construction sites are very dangerous to the health of the workers and if there is near by society area is there. The effects have two types :- 1) Acute and 2) Chronic; The acute effects are that which can show the result on the spot such as headache, cough, mold spores, itching, eye burning, runny noses which can be caused by the use of the chemicals at the sites for the different purposes. The chronic effects are the effects which are show after the duration of the period or which can be a permanent also. The effects caused are cancer, asthma, skin diseases, stress occurrence, discomfort of working due the unfresh atmosphere, Etc.

REFERENCES

Mandarić S., S. Aksentijević and J. Kiurski (2018). Statistical approach for characterization of photocopying indoor pollution, *Air Quality, Atmosphere & Health*. 11(7), 867-881.

Esplugues A, F. Ballester, M. Estarlich, S. Llop, V. Fuentes, E. Mantilla and C. Iñiguez (2010) Indoor and outdoor concentrations and determinants of NO₂ in a cohort of 1-year-old children in Valencia, Spain. *Indoor Air*, 20,213–223.

Zhao, Z., Z. Zhang, Z. Wang, M. Ferm, Y. Liang and D. Norbäck (2008). Asthmatic symptoms among pupils in relation to winter indoor and outdoor pollution in schools in Taiyuan, China. *Environ. Health Persp.* 116, 90–97.
WHO (2000). Air Quality Guidelines for Europe. Copenhagen, Denmark. World Health Organization Regional Office for Europe.

WHO (2006). Air Quality Guidelines Global Update 2005. Copenhagen, Denmark, World Health Organization Regional Office for Europe.

WHO (2010). Guidelines for Indoor Air Quality: Selected Pollutants. Copenhagen, Denmark: World Health Organization Regional Office for Europe.

LONG-TERM OBSERVATIONS OF BLACK CARBON AEROSOL OVER A RURAL LOCATION IN SOUTHERN PENINSULAR INDIA: ROLE OF DYNAMICS AND METEOROLOGY

V. RAVI KIRAN¹, S. TALUKDAR¹, M. VENKAT RATNAM¹ AND A. JAYARAMAN²

¹ National Atmospheric Research Laboratory (NARL), Gadanki – 517 112
²J1407, Brigade Metropolis, Bangalore, 560048, India

KEYWORDS: black carbon, seasonal trends, sources.

INTRODUCTION

Black Carbon (BC) is a primary anthropogenic aerosol originated from biomass burning and incomplete combustion of fossil fuel. BC formed out of pure graphitic carbon is an important component of carbonaceous aerosol. Climate effects of BC aerosol are multi fold. They do absorb the incoming solar radiation in short wavelengths leading to warming within the atmosphere and cooling at surface (Bond et al., 2013). The warming produced by the direct effect (absorption) of BC is found to be next to the carbon dioxide (Jacobson, 2001). Ten years (2008–2017) of Black Carbon (BC) observations obtained using Aethalometer (AE-37) are analyzed to investigate the seasonal trends and temporal variability over a tropical site Gadanki (13.5°N, 79.2°E) located in south-east India. The study is aimed to know the dominant source of BC over the observational location and their trends.

METHODS

Data from Aethalometer are subject to filter effects. The raw data has been corrected using methods suggested in (Weingartner et al., 2003). Aethalometer is sensitive to the temperature fluctuations inside the measurement chamber. In fact we have noticed negative values in the data set during numerous occasions. According to the manufacturers these negative values are not the wrong signals, however, corresponds either to very low concentrations of BC or to the fluctuations in the environmental conditions inside the measurement chamber. It has been noticed that, every negative value is followed by a high positive value in order to bring the instrument response back to the normal condition. Therefore, it is recommended to average out both the values to nullify the abnormal response of the instrument. In the present analysis entire five minute interval data set has been averaged out for every one hour to avoid unwanted negative values as well as

to make the data in to uniform time resolution throughout the observational period. On top of this, the quality of hourly means is assured by following three criteria of the data reduction. Only those hourly means are considered for final analysis where there are no further negative values at any wavelength, power law dependency is followed by the absorption coefficients at all seven wavelengths and finally hourly mean should be an average of at least six data points (50% of the data in an hour are ensured). These three conditions are strictly followed and hourly means are separated for the final analysis.

RESULTS & DISCUSSIONS

Diurnal variations of BC have two peak structures one in the morning (~08 IST) in all seasons and second in the evening (~20 IST) only during the pre-monsoon (March–May). Intra-annual variation in BC indicated February and March months as the bio-mass burning with highest BC mass concentration (3000–5000 ng/m³). It has been found that during pre-monsoon season 46% of air parcel pathways (back trajectories) passing across the in-land regions of southern peninsular India are reaching the source location contributing to the surface BC. The lowest BC (~1500 ng/m³) is noticed during the monsoon months (June–September). The average BC (2200 ng/m³) represents observational site as a typical rural site.

The inter-annual variability of BC did not show any significant trend. However, trends in the maximum (March) BC values show statistically significant decreasing trend (fig.1) suggesting reduction in bio-mass burning sources during March supported by the decrease in the MODIS fire counts. Diurnal variation in the absorption angstrom exponent indicates that the morning and evening peaks are contributed by the bio-mass combustion with values above threshold of 1. However, angstrom exponent values are found below 1 during noon time of monsoon season suggesting fossil fuel contribution. Strong coupling is found between aerosol concentration and tropospheric dynamics, meteorology in addition to the sources.

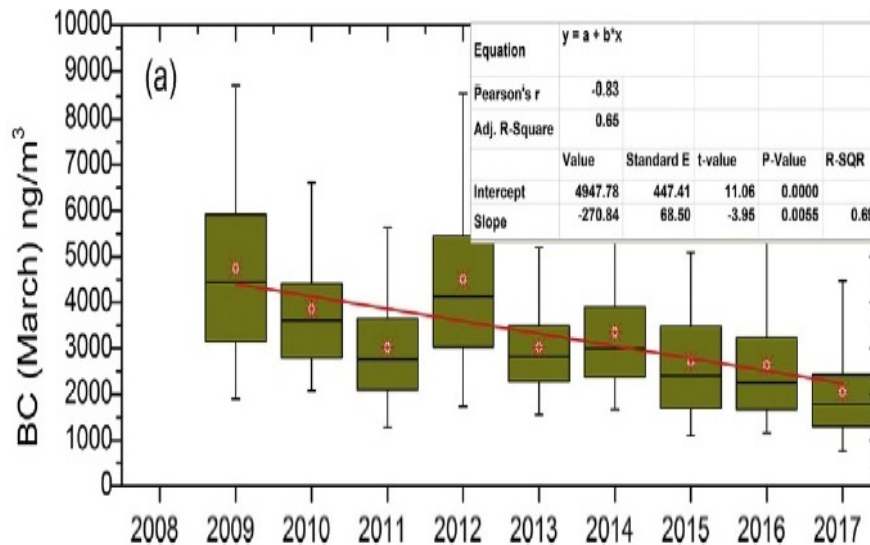


Figure 1. Seasonal decreasing trend in the BC observed over Gadanki

CONCLUSIONS

1. From long term Aethalometer observations (2008-2017) from Gadanki, intra-annual variability in BC indicates highest in the months of February and March (Ravi Kiran et al., 2018)
2. Statistically significant decreasing seasonal trend in maximum values (March) is attributed to the decreasing local sources of bio-mass burning.
3. The absorption angstrom exponent over Gadanki is observed within a narrow range of 1 and 1.2 suggesting mostly the BC is fossil fuel originated.
4. Source segregation based on absorption angstrom exponent is qualitative, acts as a first approximation for identification of sources; however, a dedicated methodology is required details of which will be the discussed in the conference.

ACKNOWLEDGEMENTS

We greatly acknowledge useful discussion made with Prof. B.V. Krishna Murthy.

REFERENCES

- Bond, T. C., Doherty, S. J., Fahey, D. W., Forster, P. M., Berntsen, T., Deangelo, B. J., ... Zender, C. S. (2013). Bounding the role of black carbon in the climate system: A scientific assessment. *Journal of Geophysical Research Atmospheres*, *118*(11), 5380–5552. <https://doi.org/10.1002/jgrd.50171>
- Jacobson, M. Z. (2001). Strong radiative heating due to the mixing state of black carbon in atmospheric aerosols. *Nature*, *409*(6821), 695–697. <https://doi.org/10.1038/35055518>
- Ravi Kiran, V., Talukdar, S., Venkat Ratnam, M., & Jayaraman, A. (2018). Long-term observations of black carbon aerosol over a rural location in southern peninsular India: Role of dynamics and meteorology. *Atmospheric Environment*. <https://doi.org/10.1016/j.atmosenv.2018.06.020>
- Weingartner, E., Saathoff, H., Schnaiter, M., Streit, N., Bitnar, B., & Baltensperger, U. (2003). Absorption of light by soot particles: Determination of the absorption coefficient by means of aethalometers. *Journal of Aerosol Science*, *34*(10), 1445–1463. [https://doi.org/10.1016/S0021-8502\(03\)00359-8](https://doi.org/10.1016/S0021-8502(03)00359-8)

CONTRIBUTION OF NON-EXHAUST PARTICULATE MATTER EMISSIONS FROM ROAD TRAFFIC IN DELHI

A.BISWAL¹, V. SINGH¹ & A.P. KESARKAR¹

¹National Atmospheric Research Laboratory, Gadanki – 517112, India

KEYWORDS: Urban air quality, Megacity Delhi, Particular matter, Non-Exhaust, Vehicular emissions

INTRODUCTION

Particulate matter emission from different sources into the atmosphere is very significant in terms of human health and air quality. The anthropogenic sources of particulate matter are emissions from various sources such as industries, power plants, vehicular traffic, biomass burning, etc. On road vehicular emissions are the main contributors to the total emissions from the transport sector especially near the roads (Singh et al., 2014). Particles are not only emitted from the engine exhaust but also from abrasion of tires, road and brake wear as well as from resuspension of the dust from the road surface. The emissions which are not due to the exhaust are called non-exhaust emissions, such as brake wear, tire wear, road wear and resuspension. The mass, sizes and chemical composition of non-exhaust particles depend on fleet composition, type of road, tire quality, vehicle weight and silt load on the road. Estimation of vehicular non-exhaust emission for a megacity like Delhi, one of the polluted cities, is very essential to compare the significance of non-exhaust emission with exhaust emission. While there is a technological reduction in the exhaust emission due to the implementation of the Bharat/Euro emission norm, the non-exhaust emission keeps on increasing due to the increase in vehicle kilometres travelled and amount of dust present on the road due to the human activities. Sahu et al., (2010) has estimated the dust resuspension as windblown dust for NCR Delhi, and concluded that wind-blown dust is approximately 4 times higher than exhaust PM emission. In this work, we have estimated the on road vehicular non-exhaust PM emission due brake wear, tire wear, road wear and resuspension at 100m x 100m grid over National Capital Territory of Delhi (NCTD). The relative contribution of non-exhaust emissions has also been estimated according to the road and vehicle type.

METHODOLOGY

The domain for this study includes the NCT of Delhi with an area of 1483 sq.km, situated in the north of India located at around 28°34'N and 77°12'E,

and has an elevation of 216m (709 ft) above mean sea level. The details about the road network, vehicle categories and traffic counts, and the methodology used for exhaust emission has been described in Singh et al., (2018). The emission factors for the brake/tire wear and road wear has been taken from the EMEP/EEA air pollutant emission inventory guidebook - 2009 (EMEP/EEA, 2009). The resuspension of dust has been calculated using the methodology described in the Emission Factor document (USEPA, 2011). The resuspension of the dust depends on the vehicle weight, speed and silt load on the road. Silt load is a measure of the amount of dust per unit area and expressed as g/m^2 . As silt load measurement are limited for Delhi, it has been estimated based on the literature survey (Amato et al., 2012; Pant et al., 2015; Zhang et al., 2017) and population activity.

RESULTS AND DISCUSSIONS

Vehicular non-exhaust particular matter emission has been calculated over NCT Delhi and then gridded at a very high resolution of 100 m^2 . The gridded emission has been shown in figure 1. The total annual PM emission has been estimated to be 17 Gg/year, out of which exhaust and non-exhaust have been estimated to be 4.5 Gg/year (26%) and 12.5 Gg/year (74%) respectively. Among non-exhaust emissions, brake/tire wear, road wear and resuspension have been estimated to be 1.09 Gg/year (9%), 0.49 Gg/year (4%) and 10.9 Gg/year (87%) respectively as shown in Figure 2. It shows resuspension of the dust as the dominant source which contributed 64% followed by exhaust emission contributing to 27% of the total PM emissions in Delhi.

Major roads have significant total emission because of higher vehicle counts and longer road length contributes both exhaust and non-exhaust emissions; however, the non-exhaust contribution of minor roads increased w.r.t. exhaust emission due to higher dust load.

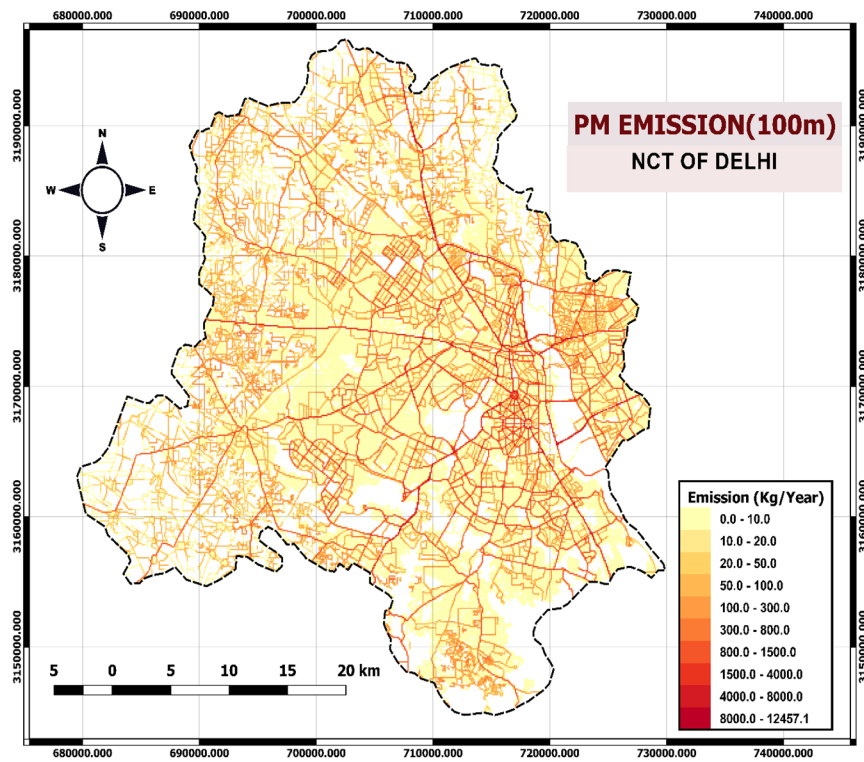


Figure 14. Gridded vehicular exhaust and non-exhaust PM emissions at 100 sq.m resolution.

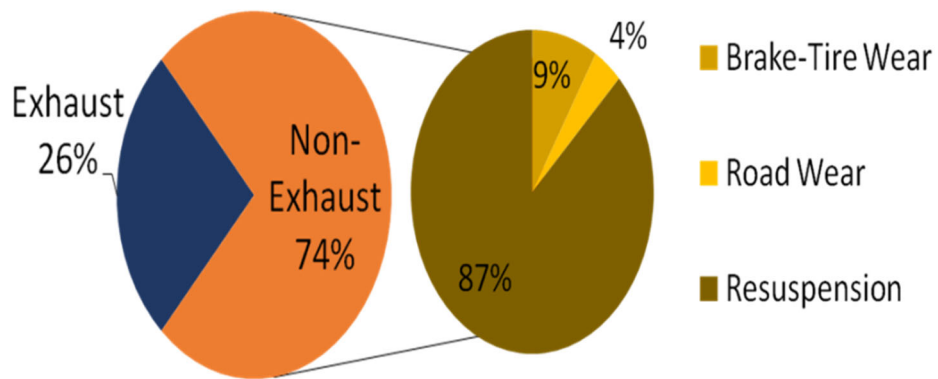


Figure 15. Percentage contribution of exhaust and non-exhaust emissions.

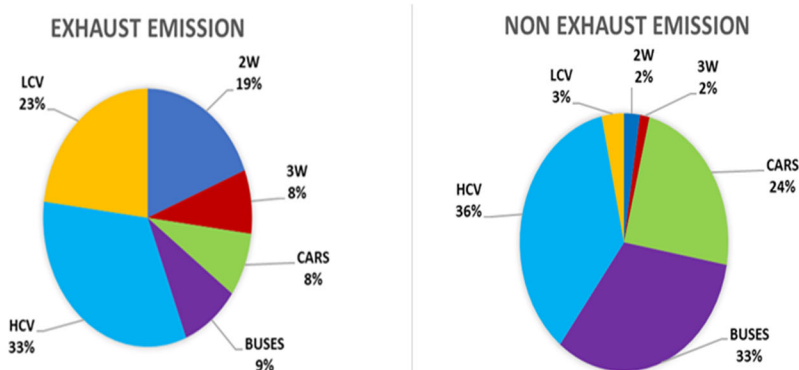


Figure 16. Percentage contribution among different vehicle types for exhaust and non-exhaust emissions

The contribution of each type of vehicle has also been estimated for both exhaust and non-exhaust emissions and shown in figure 3. The buses and cars which have only 9% and 8% contribution respectively in exhaust emission, however, show a significant contribution of 33% and 24% respectively in non-exhaust emissions. It clearly indicates that the use of cleaner fuel and new emission norms may not impact the non-exhaust component of vehicular emissions. Stricter measures are also required to control the non-exhaust emissions to improve the urban air quality.

CONCLUSIONS

Our estimation of PM emission includes both exhaust and non-exhaust vehicular activity from the road transport sector over a developing megacity NCT of Delhi for the year 2010. The non-exhaust emission includes brake/tire wear, road wear and particulate matter resuspension. The resuspension is directly related to the silt load on a given road, so the silt load has been estimated and assigned to every road links of NCT Delhi. The total annual PM emission has been estimated as 17 Gg/year, out of which exhaust and non-exhaust have been estimated as 4.5 Gg/year and 12.5 Gg/year respectively. The different types of non-exhaust emissions such as brake/tire wear, road wear and Particulate matter resuspension have been estimated as 1.09 Gg/year, 0.49 Gg/year and 10.9 Gg/year respectively. The non-exhaust PM emission contributes 74% to the total vehicular PM emission, out of which the major contributor is the Particulate matter resuspension which contributes to 87% of the total non-exhaust emissions.

ACKNOWLEDGEMENTS

Authors are thankful to the NARL and MoES India to support this work under the Indo-UK Joint programme on Atmospheric Pollution and Human Health in an Indian Megacity. The paper does not discuss policy issues and the conclusions drawn in the paper are based on the interpretation of results, and in no way reflect the viewpoint of the funding agency.

REFERENCES

Amato, Fulvio, Angeliki Karanasiou, Teresa Moreno, Andres Alastuey, J. A. G. Orza, J. Lumbreras, R. Borge, E. Boldo, C. Linares, and Xavier Querol. "Emission factors from road dust resuspension in a Mediterranean freeway." *Atmospheric environment* 61 (2012): 580-587.

EMEP/EEA Air Pollutant Emission Inventory Guidebook. No. Part B. Technical report, 2009.

Emission Factor Documentation for AP-42, Section 13.2.1, Paved Roads - January 2011, USEPA.

Pant, Pallavi, Stephen J. Baker, Anuradha Shukla, Caitlin Maikawa, Krystal J. Godri Pollitt, and Roy M. Harrison. "The PM10 fraction of road dust in the UK and India: Characterization, source profiles and oxidative potential." *Science of the Total Environment* 530 (2015): 445-452.

Sahu, Saroj Kumar, Gufran Beig, and Neha S. Parkhi. "Emissions inventory of anthropogenic PM2.5 and PM10 in Delhi during Commonwealth Games 2010." *Atmospheric Environment* 45, no. 34 (2011): 6180-6190.

Singh, Vikas, Ranjeet S. Sokhi, and Jaakko Kukkonen. "PM2.5 concentrations in London for 2008–A modeling analysis of contributions from road traffic." *Journal of the Air & Waste Management Association* 64, no. 5 (2014): 509-518.

Singh, Vikas, Saroj Kumar Sahu, Amit P. Kesarkar, and Akash Biswal. "Estimation of high resolution emissions from road transport sector in a megacity Delhi." *Urban Climate* 26 (2018): 109-120.

Zhang, Wei, Yaqin Ji, Shijian Zhang, Lei Zhang, and Shibao Wang. "Determination of Silt Loading Distribution Characteristics Using a Rapid Silt Loading Testing System in Tianjin, China." *Aerosol and Air Quality Research* 17, no. 9 (2017): 2129-2138.

CHEMICAL CHARACTERISATION OF PM 2.5 COLLECTED AT A TROPICAL RURAL SITE GADANKI

CHAITHANYA D. JAIN¹, B. SOORYAKALA² AND M. VENKAT RATNAM¹

¹National Atmospheric Research laboratory, Dept. of Space, Gadanki, India.

²Department of Physics, Andhra University, Visakhapatnam, India.

(*Correspondence at: chaithanya.jain@narl.gov.in)

KEYWORDS: Aerosols, Ion Chromatography, Fine Particulate Sampler, PM_{2.5}, Chemical Characterisation, Aerosol Chemistry.

INTRODUCTION

Atmospheric Particulate Matter (PM) or Atmospheric aerosols are microscopic solid or liquid matter suspended in the earth's atmosphere. PM is a complex mixture of both organic and inorganic particles, such as a dust, pollen soot, smoke and liquid droplets etc. (Boucher, 2015).

Aerosols play a significant role in the atmospheric science as they effect the radiation budget, they are involved in heterogeneous chemical transformations like acid rain formation, photochemical smog formation; they influence the cloud formation processes, air quality and visibility. These adverse effects eventually add up to the bigger problems such as regional and global climate change. Physico-chemical properties, such as size, chemical composition and concentrations decide the magnitudes of above said effects. Aerosols have a very complex and variable chemical composition (Calvo et al., 2013). They are generally composed of variable amounts of sulphate, nitrate, ammonium, sea salt, crustal elements and carbonaceous compounds (elemental and organic carbon) and other organic materials. Each particle has its own chemical composition owing to its source and chemical transformations. Typical chemical composition of aerosols can vary at different locations, times, weather conditions and particle size fractions. In the present study, the chemical characterization of the PM_{2.5} particles collected at atropical site Gadanki has been carried out with the objective to study the chemical composition and their potential sources in order to understand their influence on atmospheric radiation budget.

EXPERIMENTAL DETAILS

National Atmospheric Research Laboratory (NARL), where the PM_{2.5} samples were collected, is situated in a tropical village called Gadanki (13.5°N, 79.2°E) in the State of Andhra Pradesh. The elevation of NARL Gadanki about 375m above sea level and surrounded by Eastern Ghats. There are significant number of paddy fields and animal husbandry around Gadanki. There will be lot of Biomass burning activity around Gadanki similar to any other typical rural village in India. There is a National Highway (NH 206) connecting Chittoor and Tirupati passes through Gadanki and has moderate to heavy traffic. Considerable portion of the traffic is diesel fueled heavy-duty trucks making a significant vehicular emission source. Therefore, Gadanki ideally represents a typical rural site in tropical conditions.

APM 550 low volume sampler from Envirotech Instrument Pvt. Ltd. is used for sampling of aerosols on the glass micro fiber filters (1.2 µm pore size). APM 550 uses manual method for sampling fine particles (PM_{2.5} fraction). The sampler has a wins impactor standardized by USEPA for ambient air quality monitoring. Water-soluble chemical ions in the aerosol samples have been extracted to the sample solution using deionized water (obtained from Elga Purelab Option Q7) and chemical ion analysis has been carried out using Metrohm Eco-925 Ion Chromatography (IC) system. Eco-925 IC system Metrohm Eco-925 is capable of analyzing anions (F⁻, Cl⁻, Br⁻, NO₂⁻, NO₃⁻, SO₄²⁻, PO₄³⁻, ASO₄³⁻, ASO₃³⁻) on Metrosep A supp-5 250/4.0 column. Cations (Na⁺, K⁺, Ca⁺², Mg⁺², Li⁺, and NH₄⁺) and trace metal (Cd⁺², Ni⁺², Fe⁺², Co⁺², Ba⁺², Sr⁺², Mn⁺² and Zn⁺²) can be analyzed on Metrosep C6-15/4.0 column. Conductivity detector is used for the detection of different ions. Calibration was done using multiple ion standard solutions procured from sigma Aldrich.

RESULTS & DISCUSSIONS

About 14 different ions have been detected during the chemical ion analysis of the PM_{2.5} samples collected on different days. Fluoride, chloride, nitrate and sulphate ions have been present among the anions. Lithium, sodium, potassium, calcium, magnesium and ammonium ions have been detected among cations whereas in the trace metals nickel, zinc cobalt, cadmium have been present (Figure 1). Table 1 shows the average concentrations of the anions, cations and trace metals observed for the sampling days. Concentrations that were obtained in parts per million (ppm) from the ion chromatography analysis have been converted into µg/m³ using the following formula.

$$\text{Concentration of species (i) in } \mu\text{g/m}^3 = \frac{\text{Conc. of (i) in ppm} \times \text{Total vol. of extract in ml}}{\text{Total vol. of air in m}^3} \quad \text{----- 1}$$

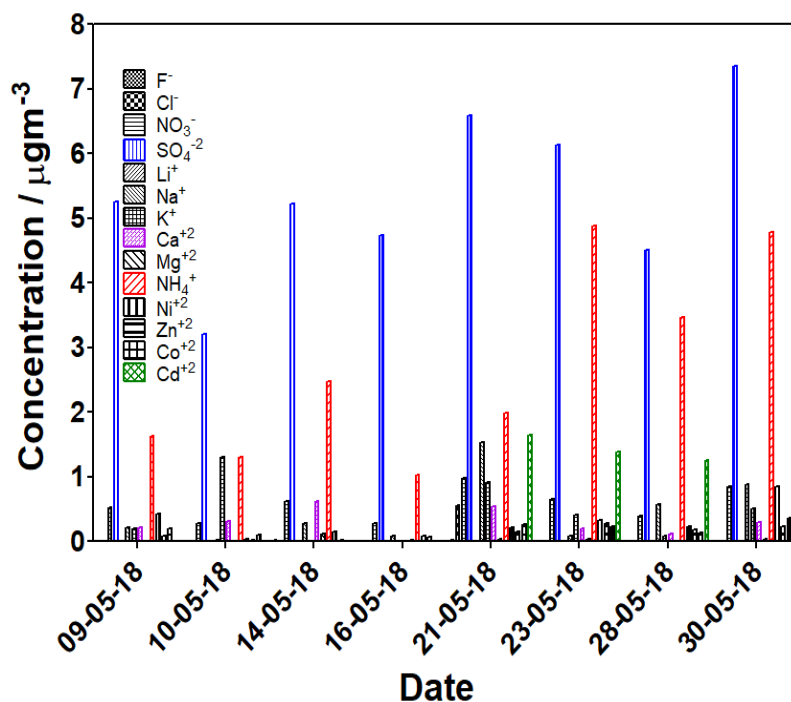


Figure 1: Total ions detected on different sample collection days.

Table 1: Mean concentrations of the anions, cations and trace metals observed in the PM_{2.5} samples during the collection days.

Category	Ions	Average concentration ($\mu\text{g/m}^3$)
Anions	F ⁻	0.0089
	Cl ⁻	0.5560
	NO ₃ ⁻	0.5732
	SO ₄ ⁻²	5.3759
Cations	Li ⁺	0.0067
	Na ⁺	0.4584
	K ⁺	0.5719
	Ca ⁺²	0.3301
	Mg ⁺²	0.0397

	NH ₄ ⁺	2.6930
Trace Metals	Ni ⁺²	0.2905
	Zn ⁺²	0.1294
	Co ⁺²	0.1821
	Cd ⁺²	1.2585

Among the anions, sulphate was dominant followed by nitrate and chloride. In the cations, ammonium was the dominant ion followed by potassium and sodium. Trace metals were dominated by cadmium followed by nickel and cobalt. Because there is a clear dominance of sulphate and ammonium in the chemical composition it can be hypothesized that the aerosols observed at Gadanki are of scattering type and have the negative radiative forcing effect which cools the surface (Wayne, 2000).

Sum of total concentrations of all the ions could make it up to 65% of the total mass loading on the filter papers indicating the missing ions, which were not detected. The ion balance method, which is a proxy method to estimate the acidity of the atmospheric aerosol samples (Hennigan et al., 2015) using the following formula,

$$[H^+] = \sum n_i [\text{anion}_i] - \sum n_i [\text{cation}_i]. \text{-----} 2$$

has given a positive value of 7.31 µg/m³ indicating the acidic nature of the PM_{2.5} samples obtained at Gadanki. This may have implications on air quality and the health of aquatic and terrestrial ecosystems. However, this value obtained for [H⁺] loading may be biased because of unmeasured ions such as organic acids. Therefore, it would be difficult to measure the acidity of the aerosol samples accurately owing to the analytical limitations with the ion chromatography system.

CONCLUSIONS

From the chemical characterisation studies, it is evident that there is a lot of anthropogenic influence on the PM_{2.5} collected at Gadanki. Sulphates and nitrates are the markers of anthropogenic origin (Rastogi, 2006) and they are dominating in the anion category. Similarly in the cation category ammonium and potassium ion dominance was observed which are thought to be emitted by the agricultural and biomass burning activity respectively (Kirchmann et al., 1998; Pachon et al., 2013).

This could support the expected results because NARL is situated near to a village household where agricultural and biomass-burning activities are predominant. More details of this study will be presented during the conference.

ACKNOWLEDGEMENTS

This work was supported by the Department of Space Atmospheric Science Program.

REFERENCES

Boucher, O., 2015. Atmospheric Aerosols: Properties and Climate Impacts. Springer Netherlands.

Calvo, A.I., Alves, C., Castro, A., Pont, V., Vicente, A.M., Fraile, R., 2013. Research on aerosol sources and chemical composition: Past, current and emerging issues. Atmospheric Research 120–121, 1–28. <https://doi.org/10.1016/j.atmosres.2012.09.021>

Hennigan, C.J., Izumi, J., Sullivan, A.P., Weber, R.J., Nenes, A., 2015. A critical evaluation of proxy methods used to estimate the acidity of atmospheric particles. Atmos. Chem. Phys. 15, 2775–2790. <https://doi.org/10.5194/acp-15-2775-2015>.

Kirchmann, H., Esala, M., Morken, J., Ferm, M., Bussink, W., Gustavsson, J., Jakobsson, C., 1998. Ammonia emissions from agriculture. Nutrient Cycling in Agroecosystems 51, 1–3. <https://doi.org/10.1023/A:1009738825468>.

Pachon, J.E., Weber, R.J., Zhang, X., Mulholland, J.A., Russell, A.G., 2013. Revising the use of potassium (K) in the source apportionment of PM_{2.5}. Atmospheric Pollution Research 4, 14–21. <https://doi.org/10.5094/APR.2013.002>.

Rastogi, N. and S., Manmohan, 2006. Atmospheric Abundances of Nitrogen Species in Rain and Aerosols over a Semi-Arid Region: Sources and Deposition Fluxes. *Aerosol and Air Quality Research* 6, 406–417. <https://doi.org/10.4209/aaqr.2006.07.0008>.

Wayne, R.P., 2000. *Chemistry of Atmospheres*. Oxford University Press.

ROLE OF DYNAMICS AND METEOROLOGY IN THE FORMATION AND MAINTENANCE OF ELEVATED AEROSOL LAYERS OVER INDIAN REGION

M. VENKAT RATNAM¹, P. PRASAD², M. ROJARAMAN¹, V. RAVIKIRAN¹, B.L. MADHAVAN¹, CHAITHANYA D JAIN¹, S. V. B. RAO² and A. JAYARAMAN³

¹National Atmospheric Research Laboratory, Dept. of Space, Gadanki, Tirupati – 517 502, India.

²Department of Physics, Sri Venkateswara University, Tirupati – 517 502, India.

³ J1407, Brigade Metropolis, Bangalore, India.

KEYWORDS: Aerosol Monitoring, Characterization, Aerosol vertical distribution, Dynamics

INTRODUCTION

Atmospheric aerosol and clouds play important role in our weather and climate. A recent discovery of high altitude (~ 16km) aerosol layer occurring during monsoon in the south Asian region using CALIPSO observations has started puzzling the atmospheric scientists. Very little is known on the composition and the formation mechanisms of this intense aerosol layer. This layer is of concern since it could play an important role on the climate and weather. One of the mechanisms for its formation is thought to be due to tropical deep convection through which boundary layer pollutants can reach UTLS region. To understand this enigmatic layer, balloon borne experiments along with ground based observations are being conducted under a ISRO-NASA collaborative program called as Balloon Borne measurement campaigns of Asian Tropopause Aerosol Layer (BATALL) (Vernier *et al.*, 2018). From Indian side, National Atmospheric Research Laboratory (NARL) has taken lead in conducting unique balloon borne observations to study the physical, chemical and radiative properties of this layer. In addition to these, NARL has made special effort to study this layer using its powerful MST radar and Lidar and other collocated experiments located at Gadanki. Several observational data have already been gathered since 2010. An overview on the formation and maintenance of elevated aerosol layers over Indian region is presented in this communication.

METHODS

MST radar is operated continuously during these campaigns and routinely during 2010-2017 to investigate the background mean vertical wind influence on the vertical transport. Long-term measurements of Mie lidar (1998-2017) and micro-pulse lidar (2010-2017) is used to investigate tropospheric and UTLS aerosols including cirrus clouds. Rainwater chemistry is also made to know the dominant chemical species present in the lower troposphere. WRF-Chem simulations are also performed at NARL to see the pathways for ATAL. Satellite measurements of aerosols and trace gases are also analyzed while interpreting the results. Batal campaigns mainly include several in situ measurements of aerosols and clouds including background meteorological parameters (T, RH, U and V) and trace gases (UTLS water vapor, Ozone).

RESULTS & DISCUSSIONS

Figure 1 shows schematic of the seasonal variation of the vertical distribution of aerosol over south-east Indian region. It is clear that elevated aerosol layer persists during monsoon season and restrict to boundary layer during other seasons. Back trajectory analysis revealed that Low Level Jet (LLJ) is responsible for this layer formation. Rain water chemical analysis also suggested the source as Arabian sea spray. MST radar from Gadanki revealed upward vertical velocities during ISM in the free troposphere (marked with arrows). Any long range transported aerosols reaching Gadanki can be transported to the upper troposphere due to the background upward vertical wind during monsoon season. Thus, deep (penetrating) convection may not be necessary to transport the aerosols in to UTLS. However, aerosols are likely to undergo rainout or washout during the monsoon season. Existence of strong shears in the horizontal wind during monsoon season can also restrict the vertical transport (Venkat Ratnam *et al.*, 2018). Nevertheless, long-term Mie lidar observations from Gadanki confirm the presence of aerosols in the UTLS region similar to CALIPSO. Long-range transport from north part of India through tropical easterly jet is observed as a main source for the observed UTLS region aerosols. Existence of Anti-cyclonic flow in the UTLS region makes confinement of aerosols and trace gases and redistribution to other regions through Brewer Dobson and Walker circulations. Significant influence of QBO and ENSO in the ATAL is also noticed using long-term measurements. Thus, dynamics play a major role in the formation and maintenance of the elevated aerosol layers. Gas to aerosol formation can be considered as a most possible source for the UTLS region aerosols other than dynamics. Radiative forcing due these aerosols and their effects on cirrus and water vapour needs to be estimated.

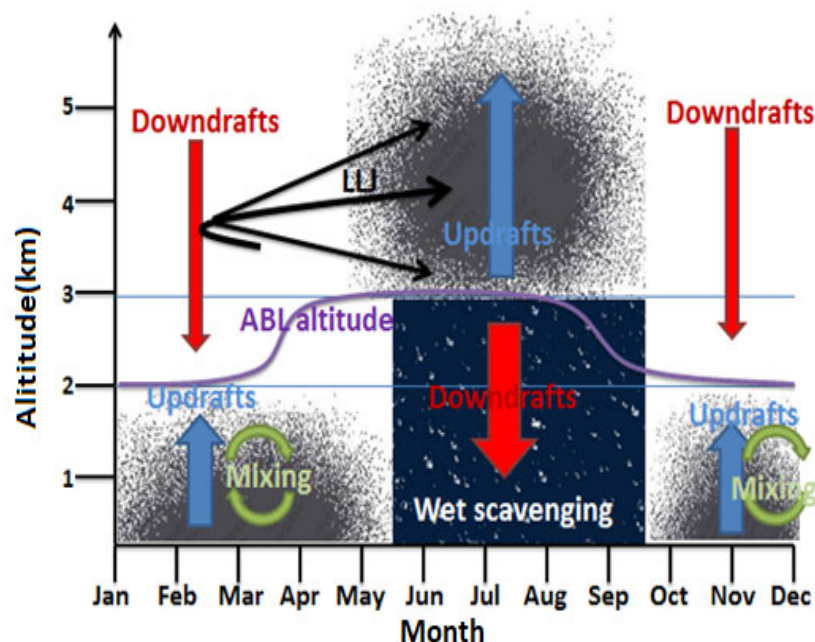


Figure 1. Schematic showing the seasonal variation of the vertical distribution of aerosol over south-east Indian region. Red (blue) arrows show the downdrafts (updrafts). Monthly mean variation of ABL altitude is shown in purple color line.

Based on the preliminary studies made using the in situ observations collected during Batal campaigns, it is now clear that ATAL is comprised of mostly small ($r < 0.25 \mu\text{m}$), liquid ($\sim 80\text{-}95\%$) aerosols with relatively low (< 1.2) scattering ratio at 532nm (Vernier *et al.*, 2018). Chemical analysis of particles collected near the tropopause indicates the dominance of nitrate aerosol with concentration of about 100 ng/m^3 , which is puzzling. Interestingly, no sulfate aerosol is noticed which was thought to be the major composition, thus opening new direction in future thinking on ATAL. This result is in contrast with the expectation of increasing influence of sulfur emissions in Asia over the past few decades on aerosol trends in the UTLS region. A regional chemical transport model WRF-Chem coupled with meteorology from NARL also show the presence of Nitrates within the Asian Summer Monsoon anticyclone region. Long-range transport from north part of India through tropical easterly jet is seen as a main source for the observed ATAL besides convection.

CONCLUSIONS

Existence of elevated aerosol layer (above ABL) during monsoon season in the troposphere is noticed. Long-range transport through LLJ is found as a source for the observed elevated aerosol layer. Rain water samples collected over Gadanki conforms the Arabian sea influence. Deep convection persisting overhead Bay of Bengal can influence the transport of troposphere pollutants to the UTLS. However, Aerosols are likely to undergo rainout or washout during the monsoon season and no major source exists. Existence of strong shears in the horizontal wind during monsoon season can also restrict the vertical transport. However, long-term Mie lidar observations confirm the presence of aerosols in the UTLS region similar to CALIPSO. Long-range transport from north part of India through TEJ as a main source for the observed UTLS region aerosols. Regional simulation of ATAL using coupled chemistry-meteorology model WRF-Chem also confirms this feature. Existence of Anti-cyclonic flow in the UTLS region makes confinement of aerosols and trace gases and re-distribution to other regions through BD and Walker circulations. Dynamics play a major role in the formation and maintenance of the elevated aerosol layers. Gas to aerosol formation can be considered as a most possible source for the UTLS region aerosols other than dynamics. At present it is not clear on the relative roles of convection verses long-range transport and natural verses anthropogenic sources on the formation of ATAL. In future, quantification of role of convection in transporting the boundary layer aerosols to UTLS region, relative roles of convection and long-range transport need to be investigated.

ACKNOWLEDGEMENTS

Authors thanks staff of NARL who has dedicatedly operated MST radar and lidar used in the present study. BATAL campaigns are jointly conducted by ISRO-NASA. We greatly acknowledge the TIFR-Balloon Facility, Hyderabad and Banaras Hindu University, Varanasi for conducting the campaigns.

REFERENCES

J.-P. Vernier, T. D. Fairlie, T. Deshler, M. Venkat Ratnam, H. Gadhavi, B. S. Kumar, M. Natarajan, A. K. Pandit, S. T. Akhil Raj, A. Hemanth Kumar, A. Jayaraman, A. K. Singh, N. Rastogi, P. R. Sinha, S. Kumar, S. Tiwari, T. Wegner, N. Baker, D. Vignelles, G. Stenchikov, I. Shevchenko, J. Smith, K. Bedka, A. Kesarkar, V. Singh, J. Bhate, V. Ravikiran, M. Durga Rao, S.

Ravindrababu, A. Patel, H. Vernier, F. G. Wienhold, H. Liu, T. N. Knepp, L. Thomason, J. Crawford, L. Ziemba, J. Moore, S. Crumeyrolle, M. Williamson, G. Berthet, F. Jégou, and J.-B. Renard, BATAL: The Balloon Measurement Campaigns of the Asian Tropopause Aerosol Layer, *Bulletin of the American Meteorological Society*, 955-973, 2018.

Venkat Ratnam, M., P. Prasad, M. Roja Raman, V. Ravikiran, S.V.B. Rao, B.V. Krishna Murthy, and A. Jayaraman, Role of dynamics on the formation and maintenance of the elevated aerosol layer during monsoon season over south-east peninsular India, *Atmospheric Environment* 188 (2018) 43–49.

MODELLING STUDY OF REGIONAL TRANSPORT ON PARTICULATE MATTER CONCENTRATION DURING A POLLUTION EPISODE IN DELHI

V.SINGH¹, A.P. KESARKAR¹ & J.N. BHATE¹

¹National Atmospheric Research Laboratory, Gadanki – 517112, India

KEYWORDS: WRF-Chem, Particular Matter, PM2.5, PM10, Delhi Pollution

INTRODUCTION

In recent years, deteriorating air quality has become a significant environmental concern due to the direct impact on the visibility, climate and human health. The problem is even worse in the megacity like Delhi which experiences severe air pollution episode during winter months (Chowdhury et al., 2017). Air pollution episodes are usually characterized by abnormally high concentrations of air pollutants during prolonged periods. It is known that that fine particulate matter (airborne particles with an aerodynamic diameter of less than 2.5 μm (PM2.5) is an important contributor to air pollution, especially in winter. The sources of PM2.5 include the directly emitted aerosols and the secondary aerosols formed from gaseous precursors such as NO_x, SO₂, and VOCs through chemical reactions. The winter pollution episodes are closely related to the meteorological conditions which lead to the stable atmosphere just after the pollutions have been transported regionally from the source region to the affected region. The enhanced regional contribution in addition to the local sources leads the elevated levels of pollution. The contribution of the regional transport and role of the meteorology in elevated levels of pollutions needs to be investigated to design intervention measures. In the recent years, air quality models have been used extensively to model the underlying mechanisms affecting the transport of pollutants. The use of Eulerian chemistry transport models driven by meteorological models has been an exciting development and has enabled complex air pollution problems involving multiple pollutants, non-linear chemistry and multiscale dynamical processes to be studied and understood to a greater extent. Compared with relatively low number measurements in the spatial domain and very few measurements vertically, chemical transport modelling systems can be advantageous for extensive 3D simulations and also for hypothetical emission scenarios analysis to study the source and transport of the pollution. One among such models is the 3D coupled meteorology and chemistry model Weather Research and Forecasting with Chemistry (WRF-Chem) (Grell et al., 2005) having appropriate

representation of the interactions among atmospheric physics, dynamics, and composition Baklanov et al. (2014). In this study, WRF-Chem model has been used to simulate and study the Delhi severe pollution episode of November 2016.

METHODS

A WRF-Chem modelling system (Grell et al., 2005) has been set up to simulate the Delhi pollution episode. The modelling system is set to run on South Asia domain having 27km grid resolution. Meteorological initial and boundary conditions are derived from the NCEP-GFS data available every six hours. Anthropogenic emissions have been obtained from HTAP-EDGAR (Janssens-Maenhout et al., 2015) that contains the annual anthropogenic emissions of greenhouse gases and air pollutants at 0.1x0.1 spatial resolution. The biogenic emissions have been processed using MEGAN (Guenther et al., 2006). FINN emission estimates are based on the framework described by Wiedinmyer et al. (2011). Simulations have been carried out with MOZCART chemical scheme. The MOZCART scheme uses the MOZART gas phase chemistry (Emmons et al., 2010) and GOCART aerosols (Chin, 2002). The MOZART mechanism includes 85 gas-phase species, 12 bulk aerosol compounds, 39 photolysis and 157 gas-phase reactions. The chemical mechanism consists of an updated isoprene oxidation scheme and a treatment of volatile organic compounds. The GOCART simulates major tropospheric aerosol components, including sulfate, dust, black carbon, organic carbon, and sea-salt aerosols. The chemical boundary conditions have been derived from MOZART. A number of hypothetical simulations have been carried out to see the impact of crop burning on Delhi air pollution. A detailed analysis has been carried out to study the role of emissions and meteorology leading to the severe pollution episode in and around Delhi.

RESULTS AND DISCUSSION

A severe pollution event was observed in Delhi during the first week of November in 2016 when the PM_{2.5} levels exceeded the NAAQS. The FINN fire counts analysis shows increased fire counts in the Northwest region which are associated with increased activity of the agricultural crop burning. Simulations have been carried out with and without FINN fire emissions to study the impact of crop burning emissions on Delhi pollution episode.

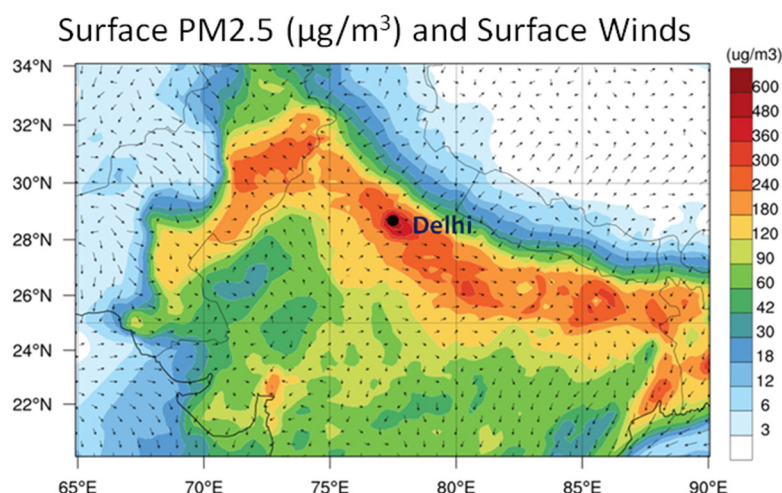


Figure 17. Simulated surface PM2.5 concentration with FINN fire emissions

The simulated spatial distribution of surface PM2.5 concentration with FINN Fire emission is shown in Figure 1. The simulated level of PM2.5 over Delhi shows the highest concentration in the range of 300-400 $\mu\text{g}/\text{m}^3$ over Delhi as compared to a simulation without FINN fire which simulates the concentration in the range 200-250 $\mu\text{g}/\text{m}^3$. It indicates that the emissions due to the residual crop burning have a significant impact on Delhi air quality. While the residual crop burning happens 300-500 km away from Delhi, the pollutants are transported due to the prevailing meteorological conditions. The horizontal wind at 850 hPa has been shown in Figure 2. The synoptic weather analysis suggests northwesterly dry ($\text{RH} < 30\%$) winds approaching towards Delhi. The dryness of the winds can be attributed to the dry mass emissions occurred due to residual crop burning in the the regions which are located in the northwest of Delhi. Generally, during the winter months, the boundary layer over the north Indian region is shallow especially due to prevailing of cold weather over this region. Thus the advection of dry mass from west/northwest directions towards Delhi and stable atmosphere prevailing over Delhi lead to high pollution episode over this region. The study emphasized that the regional and local contributions are very important to determine the air quality of Megha cities besides from global long-range transport.

Horizontal winds and RH as 850 hPa

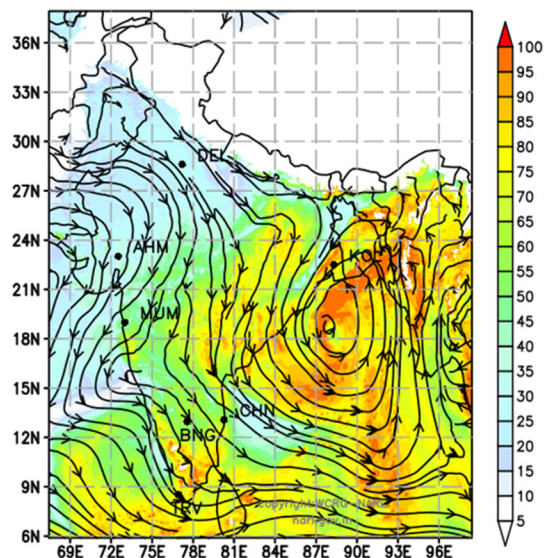


Figure 2: Horizontal winds and RH at 850 hPa at 12 UTC on 5th November 2016

CONCLUSIONS

A coupled chemistry-meteorology model WRF-Chem has been used to study the impact of crop burning emissions during a Delhi pollution episode. The synoptic weather analysis suggests northwesterly dry winds approaching towards Delhi transporting the emitted pollution from the source region towards Delhi increasing the level of PM_{2.5} by 100-200 $\mu\text{g}/\text{m}^3$. Thus the modelling simulations suggest that the severe pollution episode was associated with the advection of dry mass from west/northwest directions towards Delhi and stable atmosphere prevailing over Delhi lead to high pollution episode over this region. The study emphasized that the regional and local contributions are very important to determine the air quality of Megha cities besides from global long-range transport.

ACKNOWLEDGEMENTS

Authors are thankful to the NARL and MoES India to support this work under the Indo-UK Joint programme on Atmospheric Pollution and Human Health in an Indian Megacity. The paper does not discuss policy issues and

the conclusions drawn in the paper are based on the interpretation of results, and in no way reflect the viewpoint of the funding agency.

REFERENCES

- Baklanov, A., Schlünzen, K., Suppan, P., Baldasano, J., Brunner, D., Aksoyoglu, S., Carmichael, G., Douros, J., Flemming, J., Forkel, R. and Galmarini, S., 2014. Online coupled regional meteorology chemistry models in Europe: current status and prospects. *Atmospheric Chemistry and Physics*, 14(1), pp.317-398.
- Chin, M., P. Ginoux, S. Kinne, B. N. Holben, B. N. Duncan, R. V. Martin, J. A. Logan, A. Higurashi, and T. Nakajima, Tropospheric aerosol optical thickness from the GOCART model and comparisons with satellite and sunphotometer measurements, *J. Atmos. Sci.* 59, 461-483, 2002.
- Chowdhury, S., Dey, S., Tripathi, S.N., Beig, G., Mishra, A.K. and Sharma, S., 2017. "Traffic intervention" policy fails to mitigate air pollution in megacity Delhi. *Environmental Science & Policy*, 74, pp.8-13.
- Emmons, L. K., Walters, S., Hess, P. G., Lamarque, J.-F., Pfister, G. G., Fillmore, D., Granier, C., Guenther, A., Kinnison, D., Laepple, T., Orlando, J., Tie, X., Tyndall, G., Wiedinmyer, C., Baughcum, S. L., and Kloster, S., Description and evaluation of the Model for Ozone and Related chemical Tracers, version 4 (MOZART-4), *Geosci. Model Dev.*, 3, 43-67, 2010.
- Freitas, S. R., Longo, K. M., Alonso, M. F., Pirre, M., Marecal, V., Grell, G., Stockler, R., Mello, R. F., Sánchez Gácita, M., 2011a. PREP-CHEM-SRC 1.0: a preprocessor of trace gas and aerosol emission fields for regional and global atmospheric chemistry models. *Geosci. Model Dev.*, 4, 419-433.
- Grell GA, SE Peckham, R Schmitz, and SA McKeen, G Frost, WC Skamarock, and B Eder. 2005. Fully coupled 'online' chemistry in the WRF model. *Atmos. Environ.*, 39:6957-6976.
- Guenther, A., T. Karl, P. Harley, C. Wiedinmyer, P. I. Palmer, C. Geron (2006) Estimates of global terrestrial isoprene emissions using MEGAN (Model of Emissions of Gases and Aerosols from Nature), *Atmos. Chem. Phys.*, 6, 3181-3210.
- Janssens-Maenhout, G., Crippa, M., Guizzardi, D., Dentener, F., Muntean, M., Pouliot, G., ... & Denier van der Gon, H. (2015). HTAP_v2. 2: a mosaic of regional and global emission grid maps for 2008 and 2010 to study hemispheric transport of air pollution. *Atmospheric Chemistry and Physics*, 15(19), 11411-11432.

Wiedinmyer, C., S. K. Akagi, R. J. Yokelson, L. K. Emmons, J. A. Al-Saadi, J. J. Orlando, and A. J. Soja. "The Fire Inventory from Near (Finn): A High Resolution Global Model to Estimate the Emissions from Open Burning." *Geoscientific Model Development* 4, no. 3: 625-41, 2011.

TEMPORAL TRENDS IN RAIN WATER pH AND ION COMPOSITION OVER INDIA

SHWETA SINGH¹, VIKAS SINGH¹

National Atmospheric Research Laboratory, Gadanki, Tirupati, 517502

KEYWORDS: Rain water pH, below cloud scavenging, particles, sulfate, calcium

INTRODUCTION

Rain water studies for its chemical composition have been carried out in India since long time. As per the author's knowledge, oldest recorded study of rain water was carried out in 1938 in Bombay. As monsoon winds are responsible for most of the rainfall in Indian subcontinent, and rain being an important scavenger of atmospheric pollutants, several studies have covered the composition of rain water during monsoon. In other way, rain water is also a source of pollutants for all the receiving mediums on Earth, viz, soil, and water, thus, any change in the quality and quantity of the pollutants present in rain will affect the chemical composition of soil and water. Therefore, it is imperative to understand if there is some temporal variation in the chemical composition of rain. The pH of cloud water is considered to be 5.6 (Charlson and Rodhe, 1982), thus rain water pH values greater or less than 5.6 are considered to be alkaline or acidic respectively. In the continental regions, soil erosion, and anthropogenic activities are two main sources affecting the rain water quality (Kulshrestha, 2001). In most parts of India, soil pH is reported to be very high (up to 10.6), except south west coast, some parts of Odisha, and parts of North East states where pH of soil is acidic (Khemani, 1993). Owing to the higher concentration of Ca in most part of the Indian soil (Kulshrestha et al., 1995), reported acid rain events are very few, and that to be limited to industrial regions (Khemani, 1993). This study aims to review the rain water physical and chemical analysis related works carried out in India, and to analyze the reported results to visualize the trends. The analysed trends in physical and chemical composition of rain water will further be correlated to the possible sources.

METHODOLOGY

Rain water ion analysis related studies carried out in India were screened out using keywords like, "rain water", "ion analysis", "rain pH", "wet scavenging", etc. In total 62 papers, were found for the rain water chemical composition work. Out of these, cities for which highest number of papers

reported the results, were compiled to know the time variation in rain water pH. More number of works have been contributed in the 21st century, so those were compiled to know the spatial variation of rain water quality. Some of the long term studies like those carried out under Indian Meteorological Department's Background Air Pollution Monitoring Network (BAPMoN) stations, works were considered in a separate group to address rain water pH variation on a decadal basis. Here it is important to mention that, although chemical composition of rain water are also reported for non-monsoon seasons, in this work, we have compiled only those related to monsoon season.

More studies have been reported for rain water analysis in the 21st century. For these works, studies were categorized in a time slot of 5 years based on their year of work, and then, rain water pH distribution were studied. The observed trends in various categories were related to the observed ions, if reported.

RESULT AND DISCUSSION

The cities which were mostly reported for rain water chemical composition were Pune followed by Delhi. Therefore temporal trends of rain water pH was studied for these two cities. The yearly values of rain water pH for Pune and Delhi have been depicted in Figure 1.

As can be seen from the Figure 1, fluctuating trend of pH values have been found for rain water samples.

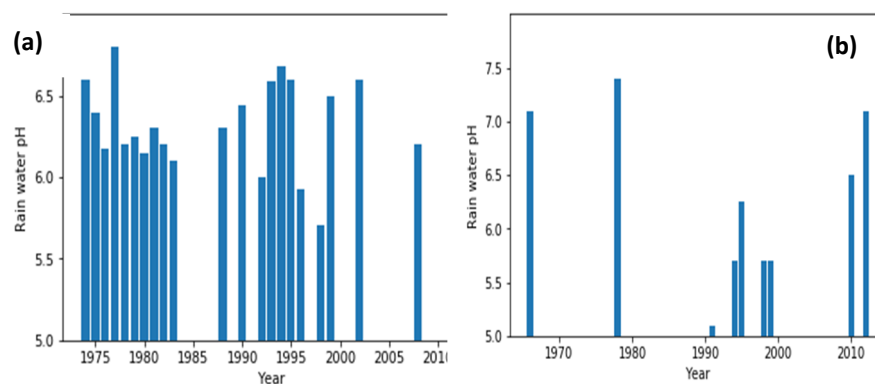


Figure 1. Yearly reported rain water pH values for (a) Pune, and (b) Delhi

For Pune, the rain water pH values are decreasing in the 1975-1985 decade whereas again rising values are shown for 1990-1995. This increase in rain water pH is again found to be decreasing in the fewer studies reported

after 2000. Overall, there is no significant trend analysed for rain water pH in Pune. In comparison to Pune, lesser number of studies have been carried out for the capital city Delhi. Similar to Pune, the rain water pH values for Delhi are also found to be fluctuating, with characteristic lower pH values in the decade 1990 to 2000. For the ten BAPMoN stations in India, the rain water pH was found to be decreasing across the three decades starting from 1974 to 2012.

Ions present in the rain water determine its pH value. Among the several ions reported for rain water samples collected in India, calcium and sulfate are considered to be the respective major alkaline and acidic species present in rain water. For studies which have reported the ionic concentration of rain, the pH values are correlated with the concentration of calcium and sulfate in rain water. Of the reported values of calcium and sulfate concentration in rain water, although most of the time concentration of calcium was higher than those of sulfate, the pH values are still reported to be alkaline. The anomalies in rain water pH that could not be addressed with the ionic content of rain water can be explained on the following basis:

- Role of ammonia gas in neutralizing the rain water acidity
- Role of organic acids towards rain water acidity
- Role of in-cloud scavenging
- Role of anthropogenic particles other than soil derived

Neutralization of acidity of rain water with ions like sodium and potassium are more restricted to coastal areas. In the inland regions, calcium is the major neutralizing species. In regions where agricultural activities are prevalent, ammonia also plays important role in buffering the rain water pH. Out of the four reasons mentioned above for explaining the anomalies in correlation of rain water pH and concentration of calcium and sulfate in rain water, the first three are addressed in many of the rain water works, yet, the importance of anthropogenic particles are seldom covered. Assuming the background soil and its alkaline content to be constant for a given time period, the nature of anthropogenic gases as well as particles decide the acidity or alkalinity of rain water. Thus, not only gases, but also particles originating from major anthropogenic activities are to be taken into account to define the quality of rain water at a given study region.

REFERENCES

- Charlson, R. J., & Rodhe, H. (1982). Factors controlling the acidity of natural rainwater. *Nature*, 295(5851), 683.
- Khemani, L. T. (1993). Air pollution and acid rain problems in the Indian region.

Kulshrestha, U. C., Sarkar, A. K., Srivastava, S. S., & Parashar, D. C. (1995). A study on short-time sampling of individual rain events at New Delhi during monsoon, 1994. *Water, Air, and Soil Pollution*, 85(4), 2143-2148.

Kulshrestha, U. C., Kulshrestha, M. J., Sekar, R., Vairamani, M., Sarkar, A. K., & Parashar, D. C. (2001). Investigation of alkaline nature of rain water in India. *Water, Air, and Soil Pollution*, 130(1-4), 1685-1690.

DESIGN AND CALIBRATION OF LED BASED BROADBAND INTEGRATING NEPHELOMETER

ARUN RAMACHANDRAN¹, P.K. ADHILSHA³, ARUN P THOMAS⁴,
NITHIN ALLWAYIN¹, SHREYA JOSHI⁵, SHEBIN JOHN¹, AISWARYA
SASEENDRAN¹, ANOOP PAKKATTIL¹, VISWANATH DEEPA²,
B.PONMANCHERY⁵, G.V. NAMBOOTHIRI⁵, RAVI VARMA*¹

¹Applied Optics and Instrumentation laboratory, Department of Physics,
National Institute of Technology Calicut, Calicut - 673601

²Department of Physics, VTM NSS, Dhanuvachapuram, Trivandrum

³Department of Physics, School of Natural Science, Jamia Millia Islamia,
New Delhi

⁴Department of Atmospheric Science, Cochin University of Science and
Technology, Cochin

⁵Optind Solutions Pvt. Ltd., Unit 9, Technology Business Incubator,
National Institute of Technology Calicut, Calicut – 673601

KEYWORDS: nephelometer, aerosol optical properties, rayleigh scattering.

INTRODUCTION

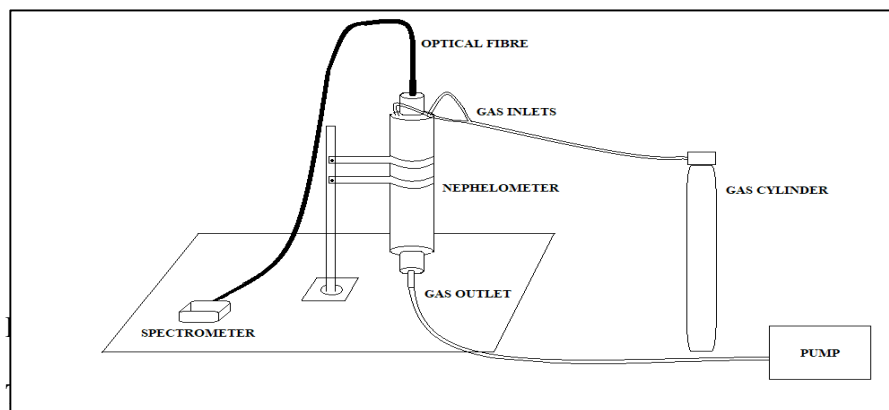
Aerosols interact with sunlight causing far reaching effect in earth atmosphere. Their scattering of sunlight can reduce visibility (haze) and they interact both directly and indirectly with the Earth's radiation budget and climate. The effect of the aerosols, however, will be opposite to the effect of the increasing atmospheric trace gases - cooling instead of warming the atmosphere. And this cooling effect of the pollution aerosols will be somewhat regionally dependent.

In this work an *LED based Broadband Integrating Nephelometer* was designed and a prototype was made to study the optical scattering properties of the atmospheric aerosols. Integrating nephelometers are instruments that directly measure the total light scattering coefficient of airborne particles (Heintzenberg J and Charlson R J, 1996). No assumptions about particle composition, size or shape are necessary, and this broadband integrating nephelometer has an added advantage of monitoring the aerosols in the broad spectral range.

METHODS

The purpose of this paper is to describe the design, fabrication and calibration of a broadband integrating nephelometer. It was designed using high bright

white LED light as the source. Combinations of 9 LEDs are used as the source of illumination, which covered a considerable range of scattering angles. A cylindrical geometry was employed whose interior walls were blackened in order to minimize the effect of wall scattering. This Nephelometer uses vertical sampling scheme in order to minimize the sampling losses and the sample was passed through the inlet at top end of the instrument. Steady and streamline flow of the gas is maintained at atmospheric pressure and a vacuum pump is employed at the exit. The light that gets scattered from the sample was measured using a CCD Spectrometer (Ocean Optics- QEPro 65) which shows the scattered photon count. Gas calibration was carried out using dry air and carbon dioxide. The schematic of the instrument is shown in figure 1 below.



Optics and Instrumentation laboratory, NIT Calicut. The initial testing for the sensitivity of the instrument was carried out by passing different laboratory standard gases like Nitrogen, Carbon dioxide, Dry air and Oxygen. The results were encouraging. The instrument responses at all wavelengths were distinctly observable. Figure 2 below shows the different scattering intensity levels for above mentioned gases at 485.514 nm.

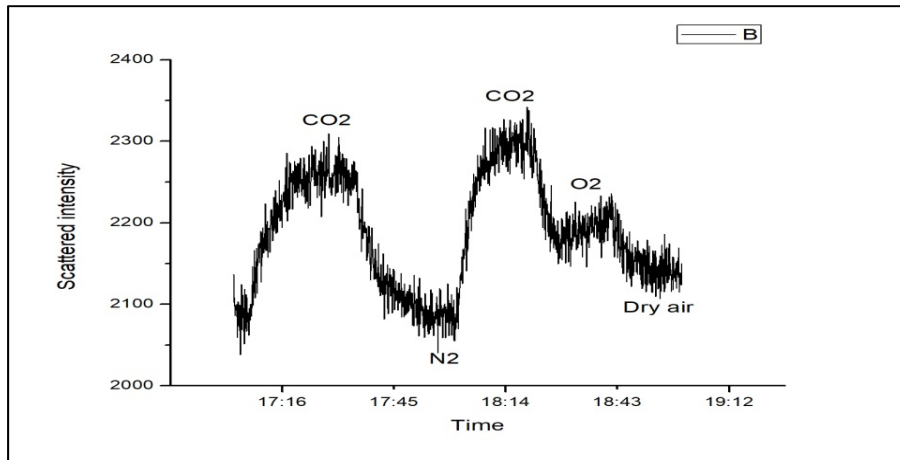


Figure 2. Scattering response of Carbon dioxide, Dry air, Nitrogen and Oxygen

Once the instrument was found to be sensitive for gases, the calibration of the same was done using Carbon dioxide and Dry air (Abu-Rahmah *et.al.*, 2006). The scattered intensity response, while passing these gases is shown in figure 3 below.

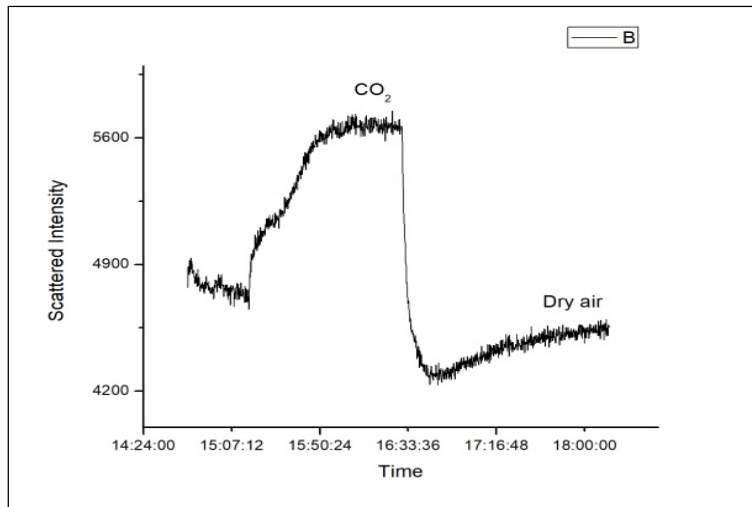


Figure 3. Scattered intensity levels while passing carbon dioxide and dry air

The calibration constant, C and wall scattering, WS was found from the response of the instrument for these two gases, at 485.514 nm. The equation for finding the calibration constants are as follows,

$$C = \frac{I(CO_2) - I(Dry\ air)}{(\alpha(CO_2) - \alpha(Dry\ air)) * d}$$

Where, $I(\text{CO}_2)$ and $I(\text{Dry air})$ are the scattered intensity while passing carbon dioxide and dry air respectively, $\alpha(\text{CO}_2)$ and $\alpha(\text{Dry air})$, the scattering coefficient of the gases and d is the optical path length through the instrument (Thalman R et.al., 2014; Snee M and Ubachs W, 2005; Shardanand, A D and Prasad Rao, 1977).

Also, the wall scattering (WS) was found by,

$$WS = \frac{I(\text{CO}_2)}{c} - \alpha(\text{CO}_2) * d$$

Table below shows the calibration constants obtained at 485.514 nm wavelength.

Wavelength (nm)	Calibration constant, C	Wall scattering constant, WS
485.514	$1.058 * 10^{-8}$	$3.85 * 10^{-5}$

Table 1. The calibration constant, C and wall scattering constant, WS of the instrument

The calibration constant C, and the wall scattering constant WS of the instrument was then used to find the scattering coefficient of another gas with unknown optical property. The instrument could be further coupled with another instrument which can measure the extinction coefficient of the species of interest (like, Cavity Enhanced Absorption spectrometer) and then the combined result could be used to study the Single Scattering Albedo (SSA) property of that species.

CONCLUSIONS

A broadband integrating nephelometer was designed and developed to measure the aerosol scattering coefficient directly. Being an LED based broadband instrument it could be used to monitor a variety atmospheric aerosols, in a broad spectral range in the visible region. The instrument was calibrated in the laboratory using dry air and CO_2 . The instrument could be

further modified to increase the sensitivity by carefully designing the geometry and the selection of the more stable LED light source.

ACKNOWLEDGEMENTS

The authors thankfully acknowledge the financial support from Kerala State Council for Science, Technology and Environment project – “003/SRSPS/2015/CSTE”. The authors also thank Optind Solutions Pvt. Ltd. for their timely support in the fabrication of the instrument.

REFERENCES

Heintzenberg J and Charlson R J (1996), Design and Applications of Integrating nephelometer –A Review, *Journal of Atmospheric and Oceanic Technology*, **13**, 987-1000

A Abu-Rahmah, W P Arnott and H Moosmuller (2006), Integrating nephelometer with a low truncation angle and an extended calibration scheme, *Measurement Science and Technology*, **17**, 1723-1732

Thalman R, Kyle J. Zarzana, M.A. Tolbert and R. Volkamer (2014), Rayleigh Scattering cross-section measurements of nitrogen, argon, oxygen and air, *J. Quantitative Spectroscopy and Radiative Transfer*, **147**,171-177.

Sneep M and Ubachs W (2005), Direct Measurement of the Rayleigh scattering cross section in various gases, *J. Quantitative Spectroscopy and Radiative Transfer*, **92**, 293-310

Shardanand, A D and Prasad Rao (March1977): Absolute Rayleigh scattering cross sections of gases and freons of stratospheric interest in the visible and ultraviolet regions, *NASA Technical Note*.

DISTRIBUTIONS, SOURCES, AND HEALTH RISKS OF ATMOSPHERIC PM_{2.5}- BOUND POLYCYCLIC AROMATIC HYDROCARBONS IN RURAL JAMSHEDPUR, INDIA

AMIT KUMAR¹, BALRAM AMBADE^{1*}, SUDHIR KUMAR SINGH²

¹Atmospheric Chemistry Laboratory, Department of Chemistry, National Institute of Technology Jamshedpur-831014, Jharkhand, India

²K. Banerjee Centre of Atmospheric & Ocean Studies, IIDS, Nehru Science Centre, University of Allahabad, Utter Pradesh, India

ABSTRACT

A study of 16 United States Environmental Protection Agency (USEPA) priority listed PAHs associated with particulate matter ≤ 2.5 (PM_{2.5}) was conducted in Rural Jamshedpur during the period January 2016 to December 2016. The PM_{2.5} mass was collected in polytetra- fluoroethylene filters with fine particulate sampler on seasonal basis. The concentrations of PAHs were extracted from PM_{2.5} determined through gas chromatography–mass spectrometry. The study revealed the PM_{2.5}, total PAHs, and BaPeq mass concentrations in the four seasons ranged from 3.57 to 37.54 ng m⁻³, 0.12 to 6.05 ng m⁻³, and 0.01 to 0.34 ng m⁻³ 0.01 to 0.28 ng m⁻³, respectively. The PM_{2.5}, total PAHs, and BaPeq mass concentrations were in the order winter > autumn > spring > summer and showed significant seasonal variations. The carcinogenic potency of PAHs in winter was about 4.12 times more than that in summer. Particle PAH emissions may be contributed from nearby industrial or domestic activities. Diagnostic correlation ratio analysis and principal component analysis (PCA) shows major sources to be coal burning (nearby the surrounding industrial activities mainly) in summer; and coal combustion and agricultural burning (by domestic activities mainly) in winter. In addition, coal combustion was a principal source in the rural zone and traffic emission also influences in the study.

KEYWORDS: USEPA, BaPeq, PCA, Coal Burning, Rural zone

INTRODUCTION

PAHs is the ubiquitous persistent organic pollutant fused with two or more aromatic fused rings. And have transport ability from one place to other place by association with the particulate matter under certain metrological condition. USEPA listed 16 PAHs on the basis of its toxicity. There are two

major common sources of PAHs in atmosphere are natural and anthropogenic sources. Natural sources includes forest fires, volcanic eruption etc.(Xu et al., 2006; Baek et al., 1991). Coal and petroleum combustion, Biomass burning, and coke and metal production are major anthropogenic sources. (Baek et al., 1991; Zhang and Tao, 2008). The concentration of PAHs are also depends on the size of airborne particle. High molecular weight molecules are found with the fine particulate matter (PM_{2.5}) in urban atmosphere (Harrison et al., 1996). PM_{2.5} is considered as aerodynamic particulate which can be easily inhaled and exposure of that responsible for the increased rate of mortality and morbidity due to cardiovascular and respiratory disease. Benzo (a) pyrene present in most PAHs sources and Classified as one of the major carcinogenic to humans. (IARC 2010).

The PAHs studies are getting attention due to their carcinogenic and mutagenic properties which threatening to the normal urban life. The current study focus on the concentration of BaP_{eq}, seasonal variation and sources of particle bound PAHs in atmosphere of Rural Jamshedpur, East Asia.

EXPERIMENTAL

Sampling site

The Study area named Rural Jamshedpur was chosen for collecting samples in the present study of Jamshedpur city (22° 48' " N and 86° 12' " E), East India (Figure 1)

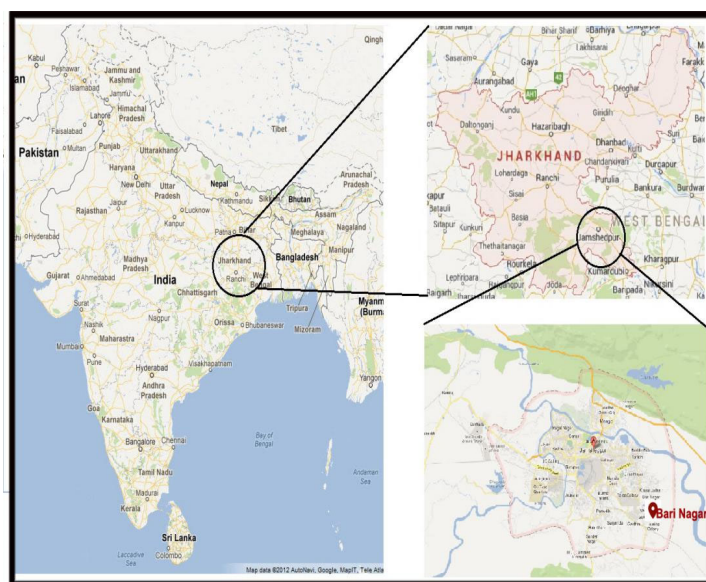


Fig 1: Sampling site in Jamshedpur Area.

MATERIALS AND METHOD

Sampling and analytical procedure

The particulate air samples were collected from pre-selected rural site of Jamshedpur, East Asia with high volume (HV) air sampler. PM was trapped on the polytetra- fluoroethylene filter aspirating air 3 L /min through XAD-2 resins by running sampler for 24 hour continuously. Sapling was done with the interval of one week. For simulating the human breathing zone the sampler was kept at the 5-6 feet above the ground. The XAD-2 resin tubes with teflon were prefiltered, extracted with dichloromethane and for 24 h and vacuum-dried in desiccator to calibrate the filters. After sampling the XAD-2 resins tubes with Teflon were extracted with dichloromethane (DCM) and the extracted was analysed by gas chromatography/mass spectroscopy (GC/MS).

RESULTS & DISCUSSIONS

Seasonal Concentration of of BaPeq:

The concentration of BaPeq in Rural Jamshedpur was determined between January 2016 to December 2016. To investigate the seasonal variation of PAHs and BaPeq concentration in atmosphere the year was divided into four periods viz Summer, Winter, Spring and Autumn season. The box plot shows the concentration of BaPeq in fig 2

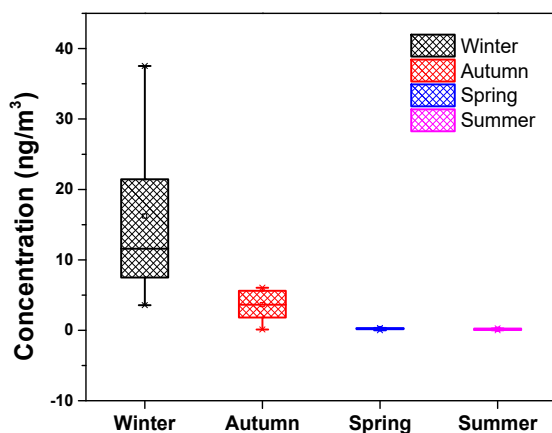


Fig 2: Concentration of BaPeq during winter, autumn, spring and summer

Source Apportionment

Principal Component Analysis (PCA) is a well-established tool for analysing assembly in multivariate data sets (Derwent *et al.*, 1995). Beginning with a huge number of correlated variables, it pursues to recognize a smaller number of independent factors (principal factors) that can be used to explain the variance in the data. The number of extracted principal components resembles to the integer and the nature of the variables encompassed. For the purpose of this study, the factors are the sources of combinations of PCA factor pattern and score plot of PCA depicted at table 2 and fig. 3.

Table 1: PCA factor pattern of BaPeq at Rural Jamshedpur

Observation	PC 1	PC 2	PC 3
Obser 1	-3.43	-0.78	-0.21
Obser 2	-1.94	-0.15	0.27
Obser 3	-0.98	0.03	1.09
Obser 4	0.51	1.19	-1.15
Obser 5	-0.47	0.84	0.05
Obser 6	0.54	-1.33	-1.01
Obser 7	-0.06	1.15	0.08
Obser 8	2.18	-0.56	0.04
Obser 9	2.97	-0.39	0.61
Obser 10	0.68	0.01	0.21
Eigen value	3.48	0.71	0.45
% of Variance	67.77%	14.07%	9.11%
Cumulative %	69.77%	83.85%	92.96%

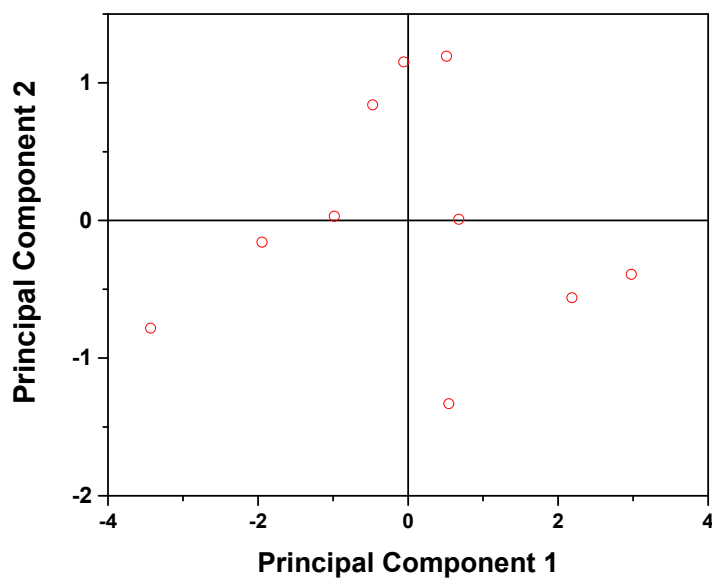


Fig 3: Score Plot of BaPeq

CONCLUSIONS

A PAHs concentration in Rural Jamshedpur air samples was collected between January 2016 to December 2016. There was a significant seasonal variations of PAHs concentration were observed with upper levels during winter seasons due to housing fuel burning for heating and other domestic purposes. The higher total BaPeq concentrations in Rural Jamshedpur were alarming signal for pollution risks.

ACKNOWLEDGEMENTS

This work was supported by the Science and Engineering Research Board (SERB) sponsored project file No. EEQ/2016/000504

REFERENCES

Baek, S.O., Field, R.A., Goldstone, M.E., Kirk, P.W., Lester, J.N., Perry, R., 1991. A review of atmospheric polycyclic aromatic hydrocarbons: sources, fate and behavior. *Water, Air, and Soil Pollution* 60, 79–300

IARC., 2010. Monographs on the Evaluation of the Carcinogenic Risks to Humans. In: Some Non-heterocyclic Polycyclic Aromatic Hydrocarbons and Some Related Exposures, vol. 92. World Health Organization, Switzerland, Lyon, France, p. 868.

Harrison, R.M., Smith, D.J.T., Luhana, L., 1996, Source apportionment of atmospheric polycyclic aromatic hydrocarbons collected from an urban location in Birmingham, U.K., Environ. Sci. Technol. 30: 825–832

Zhang, Y.X., Tao, S., 2008. Emission of polycyclic aromatic hydrocarbons (PAHs) from indoor straw burning and emission inventory updating in China. Annals of New York Academy of Sciences 1140, 218–22

Xu, S.S., Liu, W.X., Tao, S., 2006. Emission of polycyclic aromatic hydrocarbons in China. Environmental Science and Technology 40, 702–708

ASSESSMENT OF PARTICULATE MATTER VARIATION OVER WORLD HERITAGE SITE AND STEEL CITY OF INDIA

PRIYANJALI GOGIKAR¹ AND BHISHMA TYAGI¹

¹ Department of Earth and Atmospheric Sciences, National Institute of Technology Rourkela, Rourkela-769008, Odisha, India.

KEYWORDS: Aerosol, source apportionment, CPF, CBPF.

INTRODUCTION

The present scenario of air pollution in India constitutes ‘serious health emergency’ (Khilnani and Tiwari, 2018). More than one million premature deaths are noticed in India in the year 2015 and particulate matter (PM) were considered prime suspects in causing this devastating effect on living beings (Cohen et al., 2017). In spite of the mitigation measures promulgated by Central pollution control board (CPCB), PM concentrations are alarming and are causing deleterious effect on various living entities. Present study aims at assessment of air quality over two contrasting sites: (i) Agra, a world heritage site with no industries present in the city, and (ii) Rourkela, also referred to as Steel city of India, which is associated with India’s biggest steel plant, Steel Authority of India Ltd (SAIL) and many other industries. To assess the quality of air over these two sites, PM_{2.5} and PM₁₀ concentrations for a period of 2009-2013 for Rourkela and 2011 to 2015 for Agra are considered. Meteorological parameters (temperature, humidity, surface pressure, boundary layer height, wind speed and wind direction) are considered to understand the meteorological conditions prevailed over the study sites. As pollutants concentration is altered by seasonality and prevailing wind speed and wind directions, seasonal pollution roses are plotted to have an insight over the dominant wind directions that enhance the particulate matter load over the study sites. Moreover, long range transport of pollutants from various sources also contributes significantly in the enhancement of particulate matter load apart from the local source contribution (Gogikar and Tyagi, 2016). Therefore, source apportionment techniques like Conditional probability function (CPF) and conditional bi-variate probability function (CBPF) are employed in the present study to estimate both local and transboundary pollution. We have also calculated annual exceedance factor (AEF) for both the sites.

METHODS

Temporal variations of particulate matter along with the meteorology are considered over Agra and Rourkela. Seasonal pollution roses for PM_{2.5}, PM₁₀ and PM_{2.5}/PM₁₀ are plotted to understand the influence of wind speed and wind direction over the concentrations. The annual exceedance factor and percentage increase in PM_{2.5} and PM₁₀ concentrations are estimated to notice the exceedance over standard limit specified by CPCB and are mathematically calculated as follows (Kumar et al., 2014) (equation (1)):

$$\text{Annual Exceedance Factor} = \frac{\text{Observed annual average concentration of pollutant}}{\text{Critical annual average of pollutant}} \quad (1)$$

Source apportionment:

Identification of local and transboundary pollutants sources plays a vital role in the management of air quality over an area. Hence to identify plausible sources, receptor modelling techniques like CPF and CBPF are implemented in the present study.

Conditional probability function (CPF):

The CPF estimates the observed concentration probability which exceeds a predefined threshold level for a particular wind sector and is mathematically given as follows (Uria-Tellaetxe and Carslaw, 2014) (Equation (2)):

$$\text{CPF}_{\Delta v} = \frac{P_{\Delta v} / m \geq C}{Q_{\Delta v}} \quad (2)$$

where Δv indicates wind sector, $P_{\Delta v}$ indicates number of samples in the wind sector 'v' with concentration 'm' exceeding the critical percentile concentration C, $Q_{\Delta v}$ indicates total number of samples in the wind sector 'v'.

Conditional bivariate probability function (CBPF):

As an extension to CPF analysis CBPF analysis is performed by considering wind speed (Δs) as third variable in bivariate polar plot and is mathematically given as follows (Rai et al., 2016) (equation (3)):

$$\text{CBPF}_{\Delta v, \Delta s} = \frac{P_{\Delta v, \Delta s} / m \geq C}{Q_{\Delta v, \Delta s}} \quad (3)$$

RESULTS & DISCUSSIONS

The temporal variation of PM_{2.5} and PM₁₀ for both Agra and Rourkela depicted very high concentrations crossing the threshold values specified by CPCB. The annual average PM_{2.5}/PM₁₀ was found to be always >0.5 for Rourkela in all the seasons, whereas higher ratios were noticed in post-

monsoon (0.587) and winter (0.662) seasons for Agra. Higher ratios indicate that the dominant particles are $PM_{2.5}$ (Xu et al., 2017). The AEF values for both Agra and Rourkela are shown in Table I. AEF value of >1.5 (Khanum et al., 2017) is considered to be critically polluted condition for the study area.

Table I. Annual Exceedance Factor (AEF) for Agra (2011-2015) and Rourkela (2009-2013) (Critical value for $PM_{2.5}$ $40\mu g/m^3$ and for PM_{10} $60\mu g/m^3$ (CPCB Report, 2009)).

Winds play a vital role in transportation of pollutants (Guttikunda et al., 2012); therefore seasonal pollution roses for $PM_{2.5}$, PM_{10} , $PM_{2.5}/PM_{10}$ are plotted for both Agra and Rourkela (Figure I). For Agra (Figure I (a), (b), (c) and (d)), the dominant wind direction was found to be north-west in pre-monsoon, post-monsoon and winter seasons whereas south-south easterly and south-westerly and a component of north-west was noticed. Higher ratios were noticed in the north-west direction thereby indicating the transportation of fine PM from north-westerly. Similarly, for Rourkela (Figure I (e), (f), (g) and (h)), in pre-monsoon and monsoon seasons, the dominant wind direction was south-easterly and south-westerly with a minor component of wind in north-easterly where as in post-monsoon and winter seasons north-easterly. Except in monsoon season the fine particles were found to be dominating due

Period of study(Agra)	AEF($PM_{2.5}$)	AEF(PM_{10})	Period of study (Rourkela)	AEF($PM_{2.5}$)	AEF(PM_{10})
2011	5.16	6.07	2009	2.86	3.42
2012	4.38	5.43	2010	2.73	2.36
2013	3.74	4.55	2011	2.71	3.49
2014	3.77	4.58	2012	2.43	3.33
2015	3.76	4.53	2013	2.32	3.28

to north-easterly winds. To further explain the fine PM contribution from local and transboundary sources, receptor modelling techniques like CPF and CBPF analysis for $PM_{2.5}$, PM_{10} and $PM_{2.5}/PM_{10}$ is applied.

The CBPF analysis for $PM_{2.5}/PM_{10}$ is shown Figure II. For Agra (Figure II (a), (b), (c), (d)), during pre-monsoon, post-monsoon and winter seasons, north-westerly direction was found to responsible for the transportation of fine PM. In monsoon, north-easterly was found to be a dominant direction which transports fine PM whereas in winter along with north-west, south-east, north-east and south-west were found to be carrying the fine particulate load. The CPF results are not shown in the present paper, however, it was found that the results are of similar nature as of CBPF. The probability of winds associated with speeds greater than $5ms^{-1}$ indicate that fine particles are transboundary in nature whereas low speed winds indicate that sources are local in nature (Rai et al., 2016). The highly polluted regions like Delhi,

is situated in the north-west direction to Agra and might be responsible for transportation of fine PM to study site during all the seasons (Gogikar and Tyagi, 2016).

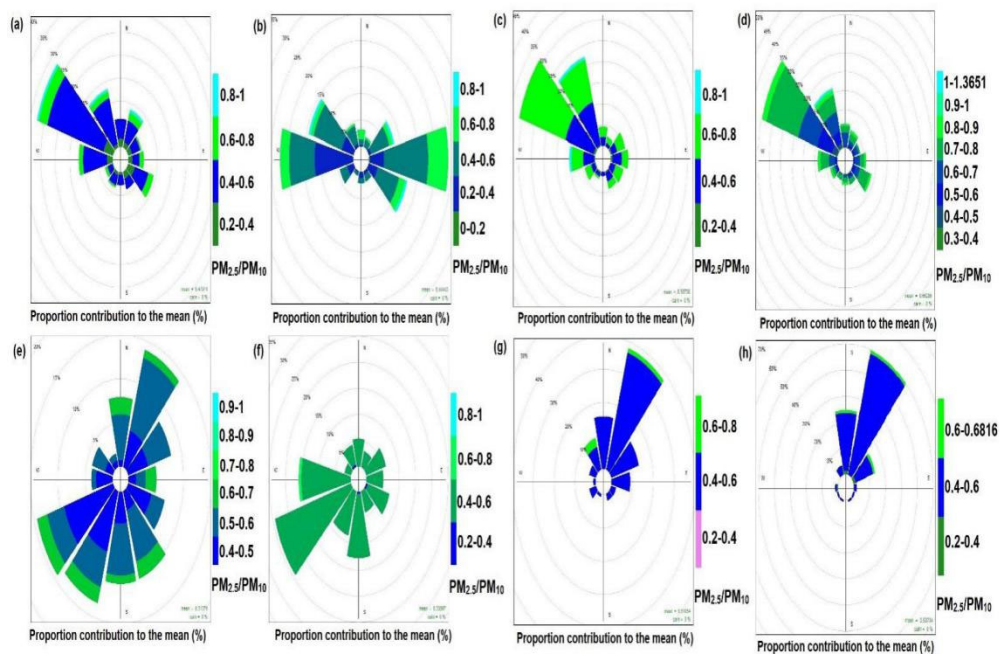


Figure I. Pollution rose plot of $PM_{2.5}/PM_{10}$ for Agra (a) Pre-monsoon, (b) Monsoon, (c) Post-monsoon, (d) Winter and for Rourkela (e) Pre-monsoon, (f) Monsoon, (g) Post-monsoon, (h) Winter.

CBPF analysis of $PM_{2.5}/PM_{10}$ for Rourkela (Figure II (e), (f), (g), (h)) reveals that winds associated with speeds $< 3\text{ms}^{-1}$ are responsible for high $PM_{2.5}$ load. Low wind speeds indicate that local sources like steel plant, vehicular exhaust, cement industry and many other medium and small scale industries situated in and around the city are responsible for high $PM_{2.5}$ in pre-monsoon, post-monsoon and winter seasons. During the monsoon season, winds with speed $> 6\text{ms}^{-1}$ were found to be loaded with $PM_{2.5}$ and reaching the study site. Talcher coal area which is considered to be Asia's largest coal field is situated in the south-easterly direction to Rourkela may be responsible for transportation of fine PM (<https://angul.nic.in/economy>).

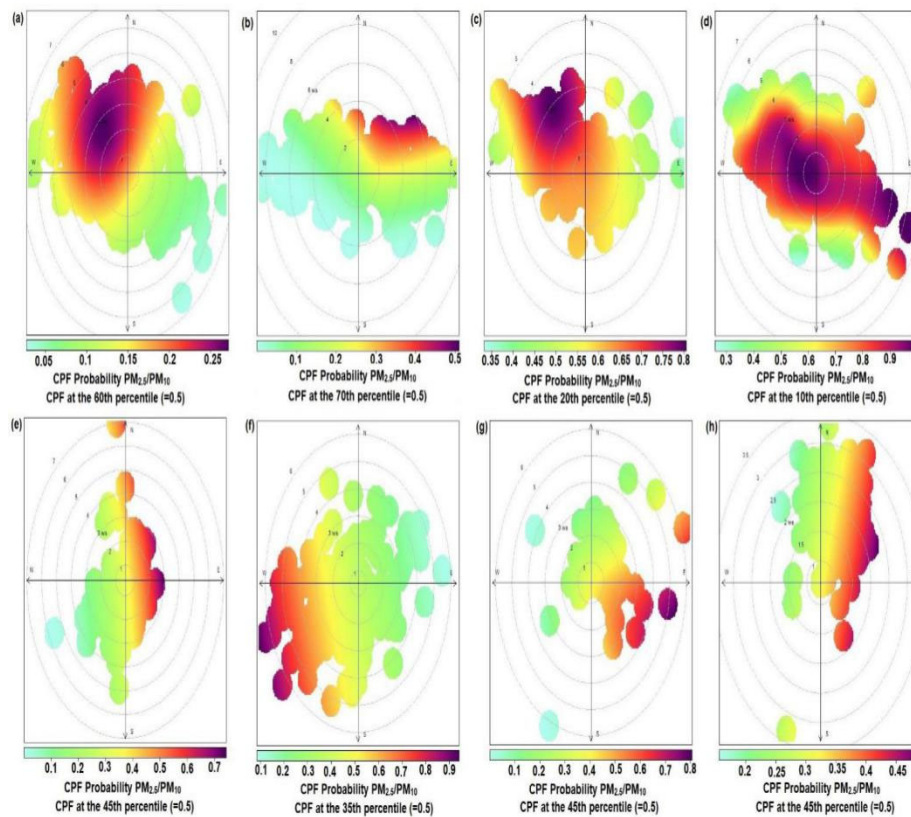


Figure II. CBPF analysis of $PM_{2.5}/PM_{10}$ for Agra (a) Pre-monsoon, (b) Monsoon, (c) Post-monsoon, (d) Winter and for Rourkela (e) Pre-monsoon, (f) Monsoon, (g) Post-monsoon, (h) Winter.

CONCLUSIONS

Identification of local and transboundary sources using receptor-modelling techniques is presented in the study for sites Agra and Rourkela. Some of the important conclusions drawn from the study are as follows:

- The PM concentrations at Agra and Rourkela are very high and annual exceedance factor reveals that both Agra and Rourkela are critically polluted regions.
- PM concentrations were found to be very high over Agra when compared to Rourkela, though Rourkela is highly industrialized.
- From CBPF analysis, it was noticed that Agra is getting exposed continuously to fine PM concentration from north-west direction.

- Highly polluted regions like Delhi present in north-west direction to Agra might be responsible for high PM load.
- For the industrial site Rourkela, local source emissions like (SAIL, vehicular exhaust etc.) were found to be dominating pre-monsoon, post-monsoon and winter seasons, whereas in monsoon season fine PM concentration is modulated by transboundary pollutants in south-easterly direction.

ACKNOWLEDGEMENTS

Ms. Priyanjali Gogikar would like to acknowledge National Institute of Technology Rourkela for providing fellowship for conducting research.

REFERENCES

Cohen, A. J., Brauer, M., Burnett, R. et al. (2017). Estimates and 25-year trends of the global burden of disease attributable to ambient air pollution: an analysis of data from the Global Burden of Diseases Study 2015. *The Lancet* 389(10082), 1907-1918.

CPCB Report (2009) National Ambient Air Quality Standards (NAAQS), Gazette Notification, New Delhi.

Gogikar, P. and Tyagi, B (2016). Assessment of particulate matter variation during 2011–2015 over a tropical station Agra, India. *Atmospheric Environment* 147, 11-21.

Guttikunda, S.K. and Gurjar, B.R. (2012). Role of meteorology in seasonality of air pollution in megacity Delhi, India. *Environmental Monitoring and Assessment* 184, 3199–3211.

Khanum, F., Chaudhry, M. N., and Kumar, P. (2017). Characterization of five-year observation data of fine particulate matter in the metropolitan area of Lahore. *Air Quality, Atmosphere & Health* 10(6), 725-736.

Khilnani, G. C. and Tiwari, P (2018). Air pollution in India and related adverse respiratory health effects: past, present, and future directions. *Current opinion in pulmonary medicine* 24(2), 108-116.

Kumar, S., Srinivas, N., Sunil, K.A (2014). Monitoring and assessment of air quality with reference to dust particles (PM₁₀ and PM_{2.5}) in urban

environment. *International Journal of Research in Engineering and Technology* 3, 2321-7308.

Rai, P., Chakraborty, A., Mandariya, A.K., Gupta, T (2016) Composition and source apportionment of PM₁ at urban site Kanpur in India using PMF couple with CBPF. *Atmospheric Research* 178(179),506-520.

Uria-Tellaetxe, I. and Carslaw, D.C (2014) Conditional bivariate probability function for source identification. *Environmental Modelling and software* 9, 1-9.

Xu, G., Jiao, L., Zhang, B., Zhao, S., Yuan, M., Gu, Y., and Tang, X. (2017). Spatial and temporal variability of the PM_{2.5}/PM₁₀ ratio in Wuhan, Central China. *Aerosol Air Quality and Research* 17(3), 741-751.

A SATELLITE OBSERVATION BASED STUDY ON AEROSOL-CLOUD-PRECIPITATION INTERACTION OVER TWO SMART CITIES OF ODISHA DURING PRE-MONSOON SEASON

SUNNY KANT and JAGABANDHU PANDA*

Department of Earth and Atmospheric Sciences, National Institute of Technology Rourkela, Odisha 769008, India

(*Correspondence at: pandaj@nitrkl.ac.in ; jagabandhu@gmail.com)

KEYWORDS: Aerosol, AOD, CER, COD and Rainfall

INTRODUCTION

The aerosol-cloud-precipitation (ACP) interaction is considered as an aerosol indirect effect (Koren *et al.*, 2012; Fan *et al.*, 2016; Kant *et al.*, 2018). However, this interaction is so far not well understood because changes in meteorological parameters are quite complex and uncertain (Fan *et al.*, 2016; Kant *et al.*, 2018). The impact of aerosols on size of cloud droplets is considered as first indirect effect whereas on cloud lifetime and vertical extent is considered as second indirect effect of aerosols. Increase in aerosol loading may decrease the cloud droplet's size and thereby, inhibiting the collision and coalescence process in warm clouds (Rosenfeld, 1999) resulting precipitation delay. Therefore, cloud droplets freeze at certain point and lead to the releasing of more latent heat, helping more energetic and persistent updrafts. Studies suggested that aerosols suppress rainfall in case of the warm (ice-free) clouds. The present study intends to focus on ACP interaction during pre-monsoon months over two cities i.e. Bhubaneswar and Rourkela, which are part of Govt. of India's smart city project. For this purpose, convectively driven rainfall cases are considered.

DATA AND METHODOLOGY

The initial study presented here is carried out over Bhubaneswar (20.29°N, 85.82°E; 33 m above the sea level). During pre-monsoon months, convective rainfall occurs due to convective activity. The present study uses 18 years of Moderate Resolution Imaging Spectroradiometer (MODIS)/Terra satellite retrieved level-2 (collection 6) datasets during 2000–2017 for the analysis of ACP interaction in the pre-monsoon months (March–May). The satellite parameters includes aerosol optical depth (AOD), cloud effective radius (CER) and cloud optical depth (COD). In this study, we have considered pre-monsoonal convective rainfall events and divided into five different categories from light to very heavy, viz., (i) < 0.5 mm/day (light), (ii) 0.5–2.5 mm/day (low), (iii) 2.5–5 mm/day (moderate), (iv) 5–10 mm/day (heavy), and (v) > 10 mm/day (very heavy) based on the magnitude of daily rainfall. The analyses would be extended to Rourkela (22.26°N, 84.85°E; 197.29m above the sea level) in the final version of the extended abstract by adopting similar methodology.

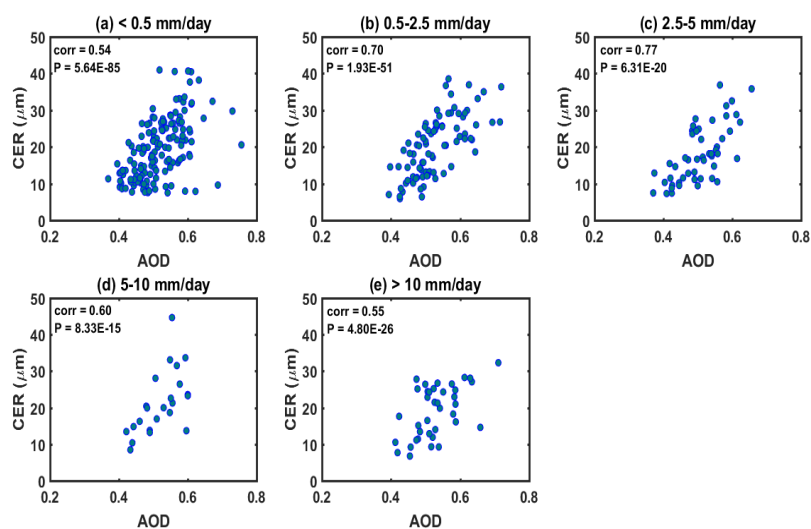


Figure 1: Scatter plot between AOD and CER. The data are sampled over the Bhubaneswar for pre-monsoon months during 2000 – 2017. Areas with daily rainfall (a) < 0.5, (b) between 0.5 and 2.5, (c) between 2.5 and 5.0, (d) between 5 and 10, and (e) > 10 mm/day. Here, ‘corr’ is the correlation coefficient and ‘P’ is the probability of observing t-statistic considered at 95% significance level in each plot.

RESULTS AND DISCUSSIONS

ACP interaction is analysed by considering several parameters like AOD, COD, CER and rainfall. During the day time, temperature is very high in the pre-monsoon months and atmosphere is quite unstable encouraging convection at the surface and may help in the formation of convective clouds too if sufficient moisture supply is there.

ACP interaction is studied in order to understand the effect of AOD on CER by considering MODIS derived level-2 data sets at 95% significance level. A positive correlation (0.54 to 0.77) between AOD and CER is evident over Bhubaneswar for all rainfall categories (Figure 1). CER gradually increases with AOD, up to 44.65 μm over Bhubaneswar due to locally produced anthropogenic aerosols. Significantly higher variability in CER ($5.89 \leq \text{CER} \leq 44.65\mu\text{m}$) is observed within AOD range 0.3–0.8. Significant positive relation between AOD and CER indicates more aerosol loading leads to larger CER during pre-monsoon months in all rainfall categories. Weak relationship between AOD and CER infers more aerosol loading leads to smaller CER.

Further, higher COD value (> 30) is observed when AOD is between 0.4 and 0.6 over Bhubaneswar with a variability $0.14 \leq \text{COD} \leq 51.92$ corresponding to the AOD range $0.47 \geq \text{AOD} \geq 0.38$. However, a

negative correlation was found in all rainfall regimes. It indicates that the cloud droplets vaporize making clouds too thin possibly due to the presence of absorbing aerosols (Alam *et al.*, 2014).

Over Bhubaneswar, AOD-rainfall relationship is found to be weakly positive for light rainfall regime but feebly negative for low and moderate regimes. Such a relationship can be attributed to the microphysical effect, which suppresses precipitation (Niu and Li, 2012). The relationship is noticeably positive (~0.3) in the heavy rainfall category and significantly positive (> 0.7) in the very heavy regime. This may be due to the invigoration effect that enhances convection.

CONCLUSIONS

The positive relationship between AOD and CER observed over Bhubaneswar city imply that other processes including dynamical (Kang *et al.*, 2015) and microphysical effects (Niu and Li, 2012) are responding to the indirect effect of aerosols on cloud droplets and also, indicate the presence of slightly soluble organic particles and CCN (Adesina *et al.*, 2016). A weak AOD-COD relationship indicates that AOD has less role to play in determining the radiative properties of clouds over Bhubaneswar. A strongly positive AOD-rainfall relationship during very heavy rainfall scenarios indicates a signature of encouraging heavy and very heavy rainfall instances. Relatively weaker relationship during light, low and moderate indicates negative feedback of aerosols during such scenarios even though moisture presence and intensity of convection may play a vital role.

The analyses for Rourkela is presently going on and would be incorporated in the final version of the extended abstract.

REFERENCES

- Adesina, A.J., K.R. Kumar and V. Sivakumar (2016). Aerosol-cloud-precipitation interactions over major cities in south Africa: Impact on regional environment and climate change. *Aerosol Air Qual Res* **16**(1), 195–211.
- Alam K., R. Khan, T. Blaschke and A. Mukhtiar (2014). Variability of aerosol optical depth and their impact on cloud properties in Pakistan. *J Atmospheric Sol-Terr Phys* **107**, 104–12.
- Fan, J., Y. Wang, D. Rosenfeld and X. Liu (2016). Review of aerosol–cloud interactions: Mechanisms, significance, and challenges. *J Atmos Sci* **73**(11), 4221–4252.
- Kang N., K. R. Kumar, Y. Yin, Y. Diao and X. Yu (2015). Correlation analysis between AOD and cloud parameters to study their relationship over China using MODIS data (2003–2013): impact on cloud formation and climate change. *Aerosol Air Qual. Res* **15**, 958–73.
- Kant, S., J. Panda, S.K. Pani and P.K. Wang (2018). Long-term study of aerosol–cloud–precipitation interaction over the eastern part of India using satellite observations during pre-monsoon season. *Theor Appl Climatol* 1–22. <https://doi.org/10.1007/s00704-018-2509-2>
- Koren, I., O. Altaratz, L.A. Remer, G. Feingold, J.V. Martins and R.H. Heiblum (2012). Aerosol-induced intensification of rain from the tropics to the mid-latitudes. *Nat Geosci* **5**, 118–122.
- Niu F. and Z. Li (2012). Systematic variations of cloud top temperature and precipitation rate with aerosols over the global tropics. *Atmos Chem Phys* **12**(18), 8491–8498.
- Rosenfeld, D. (1999). TRMM observed first direct evidence of smoke from forest fires inhibiting rainfall. *Geophys Res Lett* **26**, 3105–3108.

A SATELLITE BASED DECISION SUPPORT TOOL FOR MONITORING AND FORECASTING AIR QUALITY OVER INDIA

FALGUNI PATADIA¹, PRAVEEN NOOJIPADY¹

¹NexGen Earth Labs, Greenbelt, Maryland, USA

KEYWORDS: Air Quality , Aerosols, PM2.5, Monitoring, Forecasting, Satellite, Remote Sensing

INTRODUCTION

According to WHO's latest global ambient air quality database covering more than 4000 cities in 108 countries: "97% of cities in low and middle income countries, with more than 100000 inhabitants, do not meet the WHO air quality guidelines". Deteriorating in air quality increases the health risks (such as heart disease, lung cancer, chronic respiratory diseases) in the populations exposed to poor air quality. Many of the developing countries, including the Indian Subcontinent, African Continent and South American countries lack of real-time/long-term monitoring of air quality and there is a critical need for a decision support system to address this rising issue. We, at NexGen Earth Labs (NGEL), have developed a state-of-the-art air quality monitoring and forecasting system to help policy makers, multiple stakeholders and general public in making informed decisions related to air quality. This science-based research quality system is developed from integrating surface, satellite, and physical model inputs into a big-data analytics framework. Currently, the operational projects on NGEL's platform are : 1) global hourly PM2.5 air quality forecasts with real- time validation using surface measurements operated by government monitors 2) monthly mean PM2.5 extracted over 2000+ cities worldwide, facilitating a unique opportunity to analyze and monitor long-term data records and also serve as a guideline in places where surface measurements are limited or not available 3) tool for visualization and analysis of open source satellite estimated surface PM2.5 mass concentration and population exposure data available from Dalhousie University, Canada. We will introduce and demonstrate (with examples) the capabilities of our online tools for air quality monitoring, forecasting, analyzing historical data records and our low cost AQ monitoring system.

METHODS

NexGen Earth Labs (NGEL) currently has 3 monitoring and forecasting air quality tools :

3. global hourly PM2.5 air quality forecasts with real- time comparison with surface measurements operated by government monitors. Forecasting of PM2.5 at city level is performed using NASA's global model, real-time satellite observations and historical ground measurements into our big-data analytics system enabling global hourly forecasts for up to 10 days in advance
4. monthly mean PM2.5 extracted over 200 0+ cities worldwide, facilitating unique opportunity to analyze and monitor long-term data records and also serve as a guideline in places where surface measurements are limited or not available. Various "aerosol" components from "NASA's "MERRA)2" reanalysis" data "have" been "used" to "reconstruct" PM2.5 "mass" concentration "using" scientific "methods" outlined "in" scientific "literature" (e.g., "Malm" et "al.", "1994" "Chow" et "al.", "2015" "Turpin" and "Lim", "2001" "Provencal" et "al.", "2017");
5. Visualization and analysis of open source satellite estimated surface PM2.5 mass concentration and population exposure data available from Dalhousie University, Canada. Van Donkelaar et al. [2016], combined Aerosol Optical Depth (AOD) retrievals from the NASA MODIS, MISR, and SeaWiFS instruments with the GEOS-Chem chemical transport model, and subsequently calibrated to global ground-based observations of PM2.5 using Geographically Weighted Regression (GWR) to estimate the surface PM2.5 mass concentration. NGEL "is" only "providing" the "visualization" and "analysis" of "this" open "source" data, "with" no "modification" performed "on" the "data" set

RESULTS & DISCUSSIONS

In this section, we present an example of the utility of NGEL's current online tools. More examples will be presented at the meeting.

Air Quality Monitoring and Forecasting

At local level, over several ground monitors, NGEL is able to reasonably capture the spatial and temporal variations in PM_{2.5} concentrations. This builds reasonable confidence in NGEL's PM_{2.5} forecasts, which can be used with Figure 1: Hourly PM_{2.5} concentration over India. Map shows current values over ground stations. Line plots show data from ground monitors (green) and NGEL forecasts (blue) over Delhi, Chandrapur (Mah.) and Ahmedabad cities practical caveats in mind (e.g sudden rain showers)

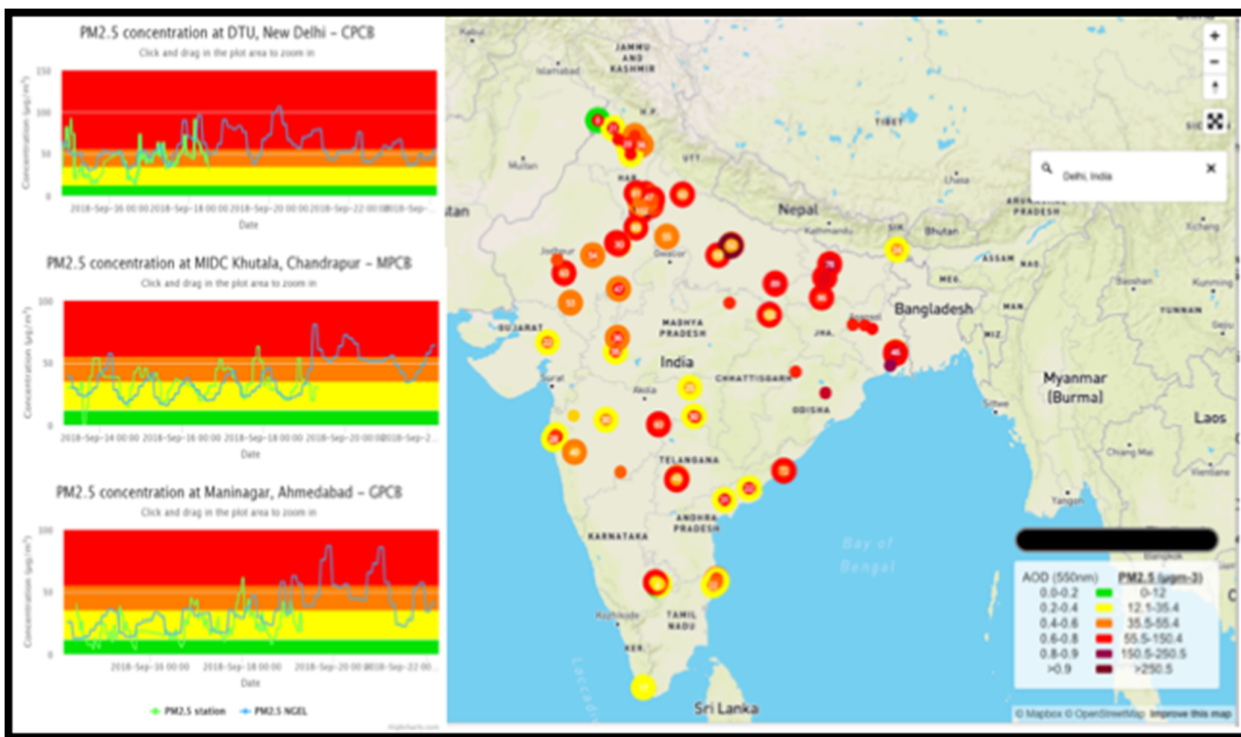


Figure 1: Hourly PM_{2.5} concentration over India. Map shows current values over ground stations. Line plots show data from ground monitors (green) and NGEL forecasts (blue) over Delhi, Chandrapur (Mah.) and Ahmedabad cities

Historical Data

While the seasonal variations over the 3 cities (Delhi, Chandrapur, Ahmedabad) remains similar through the past 17 years (2000 – 2017), Delhi has a much higher PM2.5 concentration compared to Chandrapur and Ahmedabad.

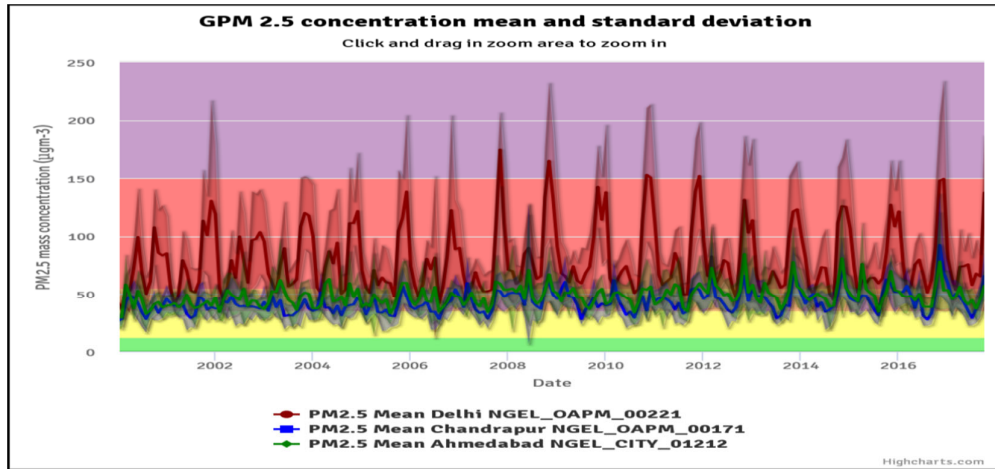


Figure 2: 17 year (2000-2017) record of monthly-mean ground PM2.5 concentration over Delhi (red), Chandrapur (Mah.)(blue) and Ahmedabad (green) cities

Population Exposure

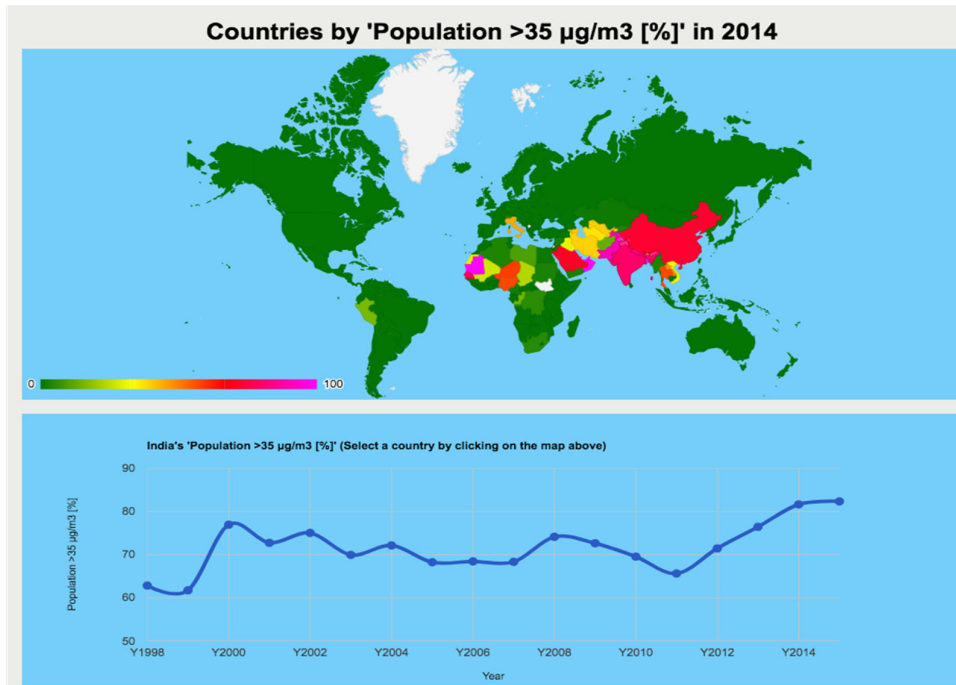


Figure 3: % of population exposed to > 35 µg/m3 annual mean PM2.5 concentration: (a) geographic mean values during 2014 (b) over India in the last 18 year

In the past 5 years (2011 – 2015), there is a rise in the % population being continually exposed to very poor air quality conditions.

CONCLUSIONS

The examples here demonstrate the utility of NGEL's current online tools. From the examples above, we see that the forecasting tool has reasonable skill to provide both spatial and temporal variation in PM2.5 concentrations at city level. Historical data facilitates building an understanding of the changes in PM2.5 over different cities. Concurrent supplementary information, such as the trend in annual mean PM2.5 concentration along with the trend exposure of population to air quality conditions, brings attention to the seriousness of the problem. Together, such reliable air quality datasets and analysis tools can aid policy making decisions

ACKNOWLEDGEMENTS

NGEL integrates NASA's model and satellites data into its data analysis system along with surface measurements of PM2.5 from OpenAQ (openaq.org). NGEL downloaded geographic mean annual average PM and exposure data from Dalhousie University, Canada."

RADIATION FORCING OF SPECIAL EVENTS OVER THE URBAN ENVIRONMENT OF AHMEDABAD CITY

DHWANILNATH GHAREKHAN¹, TEJAS TURAKHIA², RAJESH IYER², ABHA CHABRA³

1 –Civil Department, Institute of Technology, Nirma University, Ahmedabad-382 481, Gujarat (India)

2 – Department of Physics and Electronics, St Xavier's College, Ahmedabad-380 009, Gujarat (India)

3 – Space Application Centre, ISRO, Ahmedabad – 380 015, Gujarat (India)

(*Correspondence at: dhwanilnath@gmail.com, tejas.turakhia@sxca.edu.in)

KEYWORDS: radiation forcing, dust storm, diwali, aod, rtm;

INTRODUCTION

Radiative forcing (RF) is a way to quantify an energy imbalance imposed on the climatic system either externally (e.g., solar energy output or volcanic emissions) or by human activities e.g., deliberate land modification or emissions of greenhouse gases, aerosols, and their precursors. (IPCC, 1996). The aerosol effects on atmospheric radiation remain a major area of uncertainty in understanding the past and present climatic patterns and in predicting the future climatic trends. Recent scientific research planning documents [(Ramachandran, Srivastava, Kedia, & Rajesh, 2012), available at <http://www-NACIP/ucsd.edu>] emphasize the importance of absorbing aerosol components in directly impacting the earth-atmosphere radiation budget and in determining the aerosol-cloud interactions. Particles with no absorption have a negative (cooling) forcing while particles with substantial absorption can have a positive (warming) forcing. Simple calculations show that a small amount of strongly absorbing particles such as black carbon can change a negative aerosol forcing to a positive aerosol forcing. (Bergstrom, Pilewskie, Schmid, & Russell, 2003). The aerosol radiative forcing due to dust aerosols has been widely studied by many researchers using different approaches. However, no such scientific study on the impact over Ahmedabad using a modelling approach substantiated with field measurements and analysis of satellite images is available (Turakhia, Iyer, Chhabra, & Chauhan). Several studies have reported aerosol shortwave radiative forcing over the Indian sub-continent [(Jayaraman, et al., 1998), (Babu, Satheesh, & Moorthy, 1880); (Satheesh & Ramanathan, 2000)], which results in a net cooling at the earth's surface. In this paper, with the assistance of in situ measurements like sun photometer, we report the results of RF computed from a radiative transfer model (RTM) in the range of short wave radiation.

DESCRIPTION OF RESEARCH

St. Xavier's College (23.03° N, 72.48° E), Ahmedabad, was chosen as the study region because of its strategic location in the heart of the city's urban centre. Ahmedabad, commercial nerve-centre of Gujarat is predominantly a semi-arid region, has witnessed rapid urbanisation over the last two decades. The city is today an industrial hub with very heavy vehicular traffic and a lot of industries and thermal power plants in the suburban areas. The state of Gujarat is bound by Arabian Sea in the west and desert of Rajasthan in the northwest.

The study incorporates a pre and post phase to assess an overall impact.

1. The first one is a study of Aerosol RF (ARF) for a dust storm which originated near the Arabian region on the 3rd of April and travelled across India during 5-7th April, 2017. The AOD readings were taken from MODIS Aqua between the 3rd and the 10th April, 2017 and later calibrated for surface measurements based on the study undertaken by Harish Sen (Research analyst, Xavier's College, Ahmedabad). This AOD values are used as 24hour averaged input in the RF model.

2. We also studied the impact of Diwali festival on the radiation forcing over the Ahmedabad region. Extensive field measurements were carried out from pre-Diwali to post Diwali period i.e. 16th to 21st November, 2017. We measured PM concentration, Black Carbon concentration and AOD values during the above-mentioned period. In the Indian context, there are very few studies which focus on these elevated pollutant levels during Diwali. { (Barman, Sing, MPS, & Bhargava, 2008), (Chatterjee, et al., 2013), (Darga, Yogesh, & Mitra, 2006), (Devara, Vijayakumar, Safai, Raju, & Rao, 2015), (Simha, Devara, & Saha, 2013)}.

AOD readings were measured over a week to observe the effects on the presence of aerosol loading and its eventual effect on the earth’s radiation forcing due to the mentioned events under observation. The computations of both radiative forcing events were carried out using the Santa Barbara DISORT Atmospheric Radiative Transfer (SBDART) computer code. The Asymmetric Parameter (ASP) is an average of various components present in aerosols. RTM models provide instantaneous radiative forcing values, these values need to be averaged out over twenty-four hours to arrive at the figure of total radiative forcing. (McComiskey, et al., 2008) (Ganguly, Jayaraman, Rajesh, & Gadhavi, 2006). The change in temperature as indicated by the RF has been validated by temperature taken from time and date portal. (timeanddate.com, n.d.)

RESULTS & DISCUSSIONS

SBDART provides estimation of Downward Top of Atmosphere (TOA) radiation, Upward (TOA) radiation, Surface downward radiation and Surface reflected radiation. Radiative forcing has been calculated for – with and without aerosols. This leads to an estimation of the effect of aerosols on the atmosphere. The radiative forcing is estimated through the formula:

$$\Delta F_{S, TOA} = (f_a \downarrow - f_a \uparrow)_{S, TOA} - (f_o \downarrow - f_o \uparrow)_{S, TOA}$$

Where f_a and f_o respectively correspond to the fluxes with and without aerosols and the subscripts S and TOA refer to the Earth’s surface and top of the atmosphere. The arrows indicate the direction of the fluxes \downarrow = downward flux and \uparrow = upward flux. In the figures plotted ahead, the results are computed for the difference between “with” and “without aerosols”.

In both cases, the computations were done from visible to Short Wave Infra-Red (SWIR) i.e. from 0.25 to 4 μ m. The radiative forcing values have been averaged out to reflect for the 24hour day cycle. Results of both the events have been discussed below:

Dust Storm

Ahmedabad observed a dust storm event which started on 5th April and continued till 8th April with peak on 6th April. From the Up-Down ratio it can be observed there is a heavy dip on the 7th (figure 1) when the Dust Storm reached Gujarat.

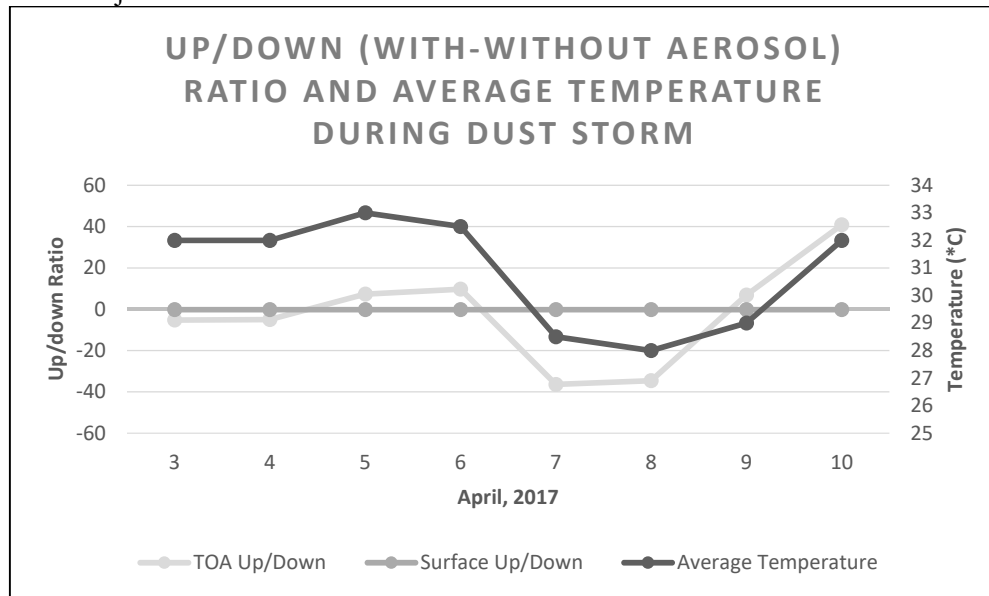


Figure 18 – Up/Down Ratio of radiations at surface and TOA during Dust Storm (3rd to 10th April, 2017)

The study reflects a loading of aerosols post 6th and the radiative forcing reduces drastically near the surface. This also reflects in the cooling effect of the surrounding as the radiative forcing significantly decreased during the time period (figure 1). This understanding is also validated through a temperature comparison extracted from time and date (timeanddate.com, n.d.). The temperature dropped by nearly by 2 degrees on the day of the Dust Storm. The wind speed from (timeanddate.com, n.d.), ranged from 9 to 13 Km/Hr from the 3rd to 5th while it peaked on the 6th. Between the 6th and the 8th the radiative forcing values hardly changed at TOA but altered by around 5% near the surface. Similar results have been reported by (Singh, Tiwari, Sharma, & Singh, 2016), (Prasad, et al., 2007) for the dust storms in the years 2012 and 2002.

Diwali

During Diwali festival, the bursting of firecrackers has considerable impact on the radiation forcing over the study region.

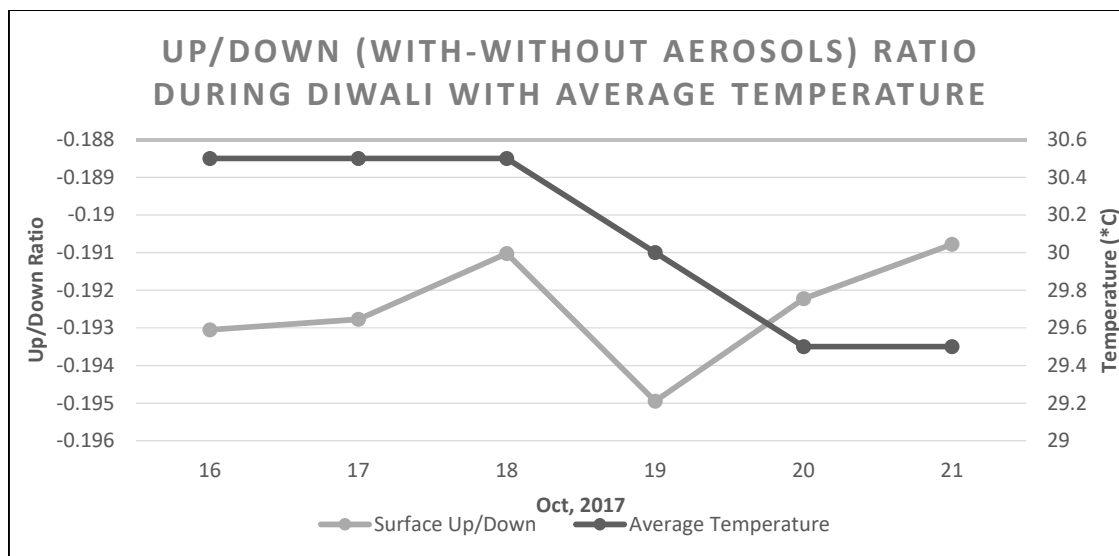


Figure 19 – Up/Down Ratios of Radiation at surface and TOA during Diwali (16th to 21st Oct, 2017)

We utilized the in-situ AOD measurements in the SBDART model. The results are showing a rise in the radiation forcing values on the 19th and post Diwali phase. These suggest a loading in the atmosphere, similar to the findings by (Vaghmaria, Mevada, & Maliakal, 2018). The averaged values depicted in the above graph validate the assumption that there will be a reduction in the radiative forcing (figure 2). The increase in carbon aerosols due to the bursting of firecrackers during Diwali, results in an increased absorption of radiation. The Up/Down ratio depicts a sudden drop since the day of Diwali. Also, during Diwali, the effect of aerosol loading wasn't significant at TOA, thus the difference of with and without aerosol came nil. This corresponds to a decrement of downward TOA radiation which results in increased loading, thus resulting in less radiation penetrating through the atmosphere to reach the surface. Diwali could be one of the factors leading to a temperature drop on the 19th and 20th after comparison from averaged temperature data acquired from Time and date portal. The computations reveal a rise in the radiative forcing on the 18th, which shows a decrement in aerosol loading. It once again drops from the 19th leading to an increase in the aerosol loading. A similar trend was observed during the dust storm event.

CONCLUSIONS

A comprehensive campaign to study the effects of special events in 2017 on radiative forcing was carried out. The study depicts an overall reduction of downward radiation at both altitudes compared with the surface. The additional aerosol caused due to the dust storm and Diwali festival has a considerable impact on the radiation forcing value, compared to the pre and the post events. Our study points out to the specific influence which natural and unnatural events have on the radiation forcing. Despite both events having different origins, they eventually resulted in aerosol loading in the atmosphere. There has been an observed reduction in the radiative forcing especially near the surface due to this aerosol loading resulting in drop of temperature. The results can be applied in the future investigations and understanding their impacts in the overall earth's radiation budget.

ACKNOWLEDGEMENTS

This study has been carried as a part of an ongoing research project titled: "Characterization of Aerosols, Black Carbon and Radiative Forcing over Urban Environment of Ahmedabad and Gandhinagar city, Gujarat, India" under the RESPOND Programme of DOS/ISRO under the guidance of scientists from Space Applications Centre, ISRO, Ahmedabad. Dr. Rajesh Iyer is thankful to DOS/ISRO for funding this research project.

The authors would also like to convey their regards to Dr. Harish Gadhvi, PRL for his valuable inputs in this study.

REFERENCES

- Babu, S. S., Satheesh, S. K., & Moorthy, K. K. (1880). Aerosol radiative forcing due to enhanced black carbon at an urban site in India. *Geophysical Research Letters* 29 (18).
- Barman, S., Sing, R., MPS, N., & Bhargava, S. (2008). Ambient Air quality of lucknow City (India) during use of firecrackers on Diwali festivale. *Environmental Monitoring Assessment* 137, 495 - 504.
- Bergstrom, R. W., Pilewskie, P., Schmid, B., & Russell, P. B. (2003). Estimates of the spectral aerosol single scattering albedo and aerosol radiative effects during SAFARI 2000. *Journal of Geophysical Research Vol 108*.
- Chatterjee, A., Sarkar, C., Adak, A., Mukherjee, U., Ghosh, S., & Raha, S. (2013). Ambient air quality during Diwali festival over Kolkatta mega-city in India. *Aerosol and Air Quality Research* 13(13), 1133 - 1144.
- Darga, S., Yogesh, K., & Mitra, D. (2006). Variability of aerosol optical depth and aerosol forcing over India. *Advance Space Research* 37 (12), 2153 - 2159.
- Devara, P., Vijayakumar, K., Safai, P., Raju, M., & Rao, P. (2015). Celebration-induced air quality over a tropical urban station, Pune. India. *Atmos Pollut Res* 6, 511 - 520.
- Ganguly, D., Jayaraman, A., Rajesh, T. A., & Gadhavi, H. (2006). Wintertime aerosol properties during foggy and nonfoggy days over urban center Delhi and their implications for shortwave radiative forcing. *Journal of Geophysical Research Vol 111*.
- IPCC. (1996). *Second Assessment Report*. Cambridge: Cambridge University Press.
- Jayaraman, A., Lubin, D., Ramachandran, S., Ramanathan, V., Woodbridge, E., Collins, W. D., & Zalpuri, K. S. (1998). Direct observations of aerosol radiative forcing over the tropical Indian Ocean during the January - February 1996 pre-INDOEX cruise. *Journal of Geophysical Research : Atmosphere Vol 103, Issue D12*.
- McComiskey, A., Schwartz, S. E., Schmid, B., Guan, H., Lewis, E. R., Ricchiazzi, P., & Ogren, J. A. (2008). Direct Aerosol Forcing: Calculation from Observable and sensitivities to inputs. *Journal of Geophysical Research, vol 113*.
- Prasad, A. K., Singh, S., Chauhan, S., Srivastava, M. K., Singh, R. P., & Singh, R. (2007). Aerosol radiative forcing over the Indo-Gangetic Plains during major dust storms. *Atmospheric Environment* 41, 6289 - 6301.
- Ramachandran, S., Srivastava, R., Kedia, S., & Rajesh, T. A. (2012). Contribution of natural and anthropogenic aerosols to optical properties and radiative effects over an urban location. *Environmental Research Letters* 7.
- Satheesh, S. K., & Ramanathan, V. (2000). Larger differences in the tropical aerosol forcing at the top of the atmosphere and Earth's Surface. *Nature* 405, 60 - 63.
- Simha, C., Devara, P., & Saha, S. (2013). Aerosol pollution and its impact on regional climate during Holi festival inferred from ground-based and satellite remote sensing observations. *Nat Hazards* 69, 889 - 903.
- Singh, A., Tiwari, S., Sharma, D., & Singh, D. (2016). Characterization and radiative impact of dust aerosols over northwestern part of India: a case study during a severe dust storm. *Archieves for meteorology geophysics and bioclimatology Series A*.

timeanddate.com. (n.d.). *historic Weather Ahmedabad*. Retrieved from Time and Date: <https://www.timeanddate.com/weather/india/ahmedabad/historic>

Turakhia, T., Iyer, R., Chhabra, A., & Chauhan, P. (n.d.). Radiative Forcing of Dust Aerosols in Urban Environment of Ahmedabad.

Vaghmaria, N., Mevada, N., & Maliakal, J. (2018). Impact of Diwali festival on aerosol optical properties over an urban city, Ahmedabad (City). *Aerosol and Air Quality Research*, 18, 522 - 532.

AIR POLLUTION AND HEALTH: INFLAMMATION AND REACTIVE OXYGEN SPECIES INDUCED BY PARTICULATE MATTER FROM HYDERABAD CITY

S. GANGAMMA¹, J. SARKAR¹, P. PRADHAN¹, VEEKSHEETHA¹, AND L. P. PRASANNA¹ National Institute of Technology Karnataka Surathkal, Mangalore, India

KEY WORDS: Innate immunity, Reactive oxygen species, inflammation, phagocytosis, air pollution

INTRODUCTION

Exposure to air pollution induce prolonged inflammation in the respiratory system and adversely affects the innate immune system. Epidemiological studies have suggested that airborne particulate matter (PM) exposure is correlated with inflammatory diseases in cardio-respiratory systems (Seaton et al., 1999; Brunekreef and Holgate, 2002; Brook et al., 2010). Therefore, PM induced inflammation in the lung is thought to mediate inflammatory diseases associated with PM exposure. However, very little is known about the biological pathways that lead to respiratory diseases. In the present study, we examined PM-induced reactive oxygen species and inflammatory cytokines from human innate immune cells. We also examined the influence of PM composition such as, trace metal elements, total protein concentration, bacterial concentration, endotoxin on PM induced inflammatory response.

METHODOLOGY

Air samples were collected from six ambient air quality monitoring sites distributed across the Hyderabad city. Particulate matter (PM-10) was collected using High volume samplers. A total of forty-nine 8 h average samples were collected on quartz de-pyrogenated fiber filter paper (Gangamma et al., 2011). Field blanks were also collected during sampling. PM on the filter was extracted into endotoxin free water. Endotoxin and protein levels in the PM samples were determined using a kinetic LAL assay and BCA methods. Total DNA and bacterial DNA were estimated using real time PCR. The DNA was extracted using a modified conventional method developed in our laboratory. The DNA was eluted into 20 μ l buffer and quantity of extracted DNA was measured with a Bio-spectrometer (Eppendorf, India). A 466-bp amplicon of bacterial 16S rDNA was amplified with a primer set (Liu et al., 2012). The PCR was performed with forward primer (5'-CCTACGGGDDGGCWGCA-3') and reverse primer (5'- GGACTACHVGGGTMTCTAATC -3'). These degenerative primers were synthesized from Sigma, India. The PCR products were confirmed using gel electrophoresis. Total bacterial concentrations (TBC) were calculated using standard graph generated using *Staphylococcus aureus* DNA. We have also measured reactive oxygen species (ROS). Monocytes were treated with 2',7'-Dichlorofluorescein diacetate (DCFDA) and subsequently with individual PM samples. Fluorescence was measured at 497nm excitation and 520nm emission wavelength and reactive oxygen species concentration was calculated. Cell viability was assessed using MTT assays. We have also carried out experiments to understand the effect of PM exposure on the phagocytic capacity of human monocytes, PBMC and U937 cells. Briefly, cells were stimulated with PM samples for different time intervals, washed and then incubated with bacteria for 30 min. Cells were lysed, lysate was serially diluted plated on TSA media and incubated at 37°C for 24 hr. Cell counts were used further to report effect of PM exposure on phagocytic properties human innate immune cells. Principal component analysis was carried out using R (version 3.4.3, R, 2013)). Other statistical methods and regression analysis were also carried out with R.

RESULTS & DISCUSSION

We have measured PM associated protein levels (n=49) using the BCA method. Total protein levels in Hyderabad city were ranged between 1.75 and 20 μ g/m³ with an average of 9 μ g/m³ and standard deviation of 5 μ g/m³. Large variation in protein concentration was observed across the sampling sites. High concentrations of protein were observed in Charminar sampling site. This sampling site is considered as commercial and traffic area. The concentrations of airborne protein in Hyderabad are comparatively high for an urban environmental setting (Menetrez et al., 2007; Chen and Hildemann, 2009). Endotoxin levels in the ambient PM samples were determined using the kinetic LAL assay. In the PM samples, concentrations of endotoxin varied over the range of 0.02- 10.4 EU/m³ with an average of 1.0 EU/m³ and standard deviation of 2.1 EU/m³. The concentration of endotoxin of field blanks was found to be below the detection limit of the assay. High concentrations of endotoxin were observed on Charminar sampling site. The concentration of airborne endotoxin significantly correlated with protein levels of PM samples (p<0.001).

We have also measured total bacterial DNA concentration of PM using real time PCR. Genomic DNA was extracted from PM samples collected from different sites in Hyderabad city. Total bacterial concentrations (TBC) were calculated using a standard graph generated through experiments. Total DNA levels were ranging between 83 and 595 ng/ μ L with an average of 275 ng/ μ L and standard deviation of 154 ng/ μ L. Total bacterial concentration was found to be correlated with endotoxin and protein ($p < 0.01$).

There is some similarity in the variation of protein concentration, PM mass and endotoxin across the sampling sites. High concentrations of protein and endotoxin were observed at Charminar sampling site. Similarly, high concentration of particulate matter was observed in Charminar sampling site. Moreover, there is a significant correlation between protein levels of samples and PM mass ($p < 0.001$). Charminar sampling site is dominated by commercial-traffic activities. There are very few studies that examine the non-exhaust traffic emissions. Also, there are very few studies that link airborne biological components to non-exhaust traffic emissions in urban area (Gangamma, 2018). However, emerging evidence indicate that these sources could be of importance (Amato et al., 2014).

PM samples were extracted for metal analysis using acid digestion. The extract was analyzed for trace elements with ICP-OES (Agilent Technologies). Ten dominant trace elements were retained after analysis. High concentration of Ca, Zn and Fe were found across the sampling sites. Highest concentration of Ca in PM was observed at Charminar sampling site. Principal component analysis has shown that biological components such as endotoxin and protein are likely associated with re-suspended dust and vehicular traffic sources. Reactive oxygen species induction in phagocytic cells was assessed using 2',7'-Dichlorofluorescein diacetate dye. Our experiments have shown that metals did not influence ROS production in monocytes. However, the total DNA level was found to be associated with ROS generation.

CONCLUSIONS

High levels of biological components such as protein, endotoxin and bacteria of PM were observed at Hyderabad sampling sites. Therefore, the present study calls for thorough characterization of biological components of the PM and their role in adverse health effects of PM exposure.

REFERENCES

- Amato, F., Cassee, F.R., van der Gon, H.A.D., Gehrig, R., Gustafsson, M., Hafner, W., Harrison, R.M., Jozwicka, M., Kelly, F.J., Moreno, T. and Prevot, A.S., 2014. Urban air quality: the challenge of traffic non-exhaust emissions. *Journal of Hazardous Materials*, 275, pp.31-36.
- Brook, R.D., Rajagopalan, S., Pope III, C.A., Brook, J.R., Bhatnagar, A., Diez-Roux, A.V., Holguin, F., Hong, Y., Luepker, R.V., Mittleman, M.A. and Peters, A., 2010. Particulate matter air pollution and cardiovascular disease: an update to the scientific statement from the American Heart Association. *Circulation*, 121(21), pp.2331-2378.
- Brunekreef, B. and Holgate, S.T., 2002. Air pollution and health. *The lancet*, 360(9341), pp.1233-1242.
- Chen, Q. and Hildemann, L.M., 2009. Size-resolved concentrations of particulate matter and bioaerosols inside versus outside of homes. *Aerosol Science and Technology*, 43(7), pp.699-713.
- Gangamma, S., 2018. Lancet Commission on pollution: action plans and human resource development in India. *The Lancet*, 391(10138), pp.2414-2415.
- Gangamma, S., Patil, R.S. and Mukherji, S., 2011. Characterization and proinflammatory response of airborne biological particles from wastewater treatment plants. *Environmental Science & Technology*, 45(8), pp.3282-3287.
- Liu, C.M., Aziz, M., Kachur, S., Hsueh, P.R., Huang, Y.T., Keim, P. and Price, L.B., 2012. Bact Quant: an enhanced broad-coverage bacterial quantitative real-time PCR assay. *BMC Microbiology*, 12(1), p.56.
- Menetrez, M.Y., Foarde, K.K., Dean, T.R., Betancourt, D.A. and Moore, S.A., 2007. An evaluation of the protein mass of particulate matter. *Atmospheric Environment*, 41(37), pp.8264-8274.
- R Core Team (2013). R: A language and environment for statistical computing. R Foundation for Statistical Computing, Vienna, Austria. URL <http://www.R-project.org/>.
- Seaton, A., Soutar, A., Crawford, V., Elton, R., McNerlan, S., Cherrie, J., Watt, M., Agius, R. and Stout, R., 1999. Particulate air pollution and the blood. *Thorax*, 54(11), pp.1027-1032.

AEROSOLS AND HEALTH: LUNG ADENOCARCINOMA TCGA GENE EXPRESSION ANALYSIS AMONG SMOKERS

S. GANGAMMA¹ AND P. PRADHAN¹

National Institute of Technology Karnataka Surathkal, Mangalore, India

KEY WORDS: Air pollution, Aerosols, Cigarette smoke, Lung cancer, Lung adenocarcinoma

INTRODUCTION

Air pollution exposure and smoking are major risk factors associated with lung cancer. While, lung squamous cell (LUSC) is found predominantly appear among smokers, incidence of lung adenocarcinoma (LUAD) is found associated with air pollution exposed, non-smoking and smoking populations. There is accumulation of evidence to support that distinct lung cancer subtypes may have derived from different 'cells of origin' in lung epithelium. Human lung epithelium is thought to comprise as many as 40 different cell types (Hogan et al., 2014; Tata and Rajagopal, 2017; Nikolić et al., 2018). Lung epithelial cell exhibit high plasticity, few of these cell types are considered as adult stem cells in the quiescent lung. Understanding the gene expression or genomic mutation pattern in these cells might be helpful to get insight into lung cancer biology. Compared with smoking, there is a paucity of studies on genomic mutations or gene expression associated with air pollution. Here, we analyzed gene expression data from The Cancer Genome Atlas (TCGA) with reference to smoking and lung cell types. We selected marker genes for few important lung cell types associated with lung maintenance, repair and cancer development for our analysis.

METHODOLOGY

The Cancer Genome Atlas (TCGA) RNASeq data was downloaded from Experiment Hub. The extracted files for LUAD (lung adenocarcinoma) and LUSC (lung squamous cell carcinoma) were contained 576 and 552 samples respectively. We used the TCGA barcode key to separate the control and malignant lung samples. There were 517 and 501 malignant samples in LUAD and LUSC data sets. Markers for lung cell such as type1 alveolar epithelial cells (AT1), type 2 alveolar epithelial cells (AT2), basal, neuroendocrine, club, and goblet cells were collected from the literature. These genes were mapped to the gene symbols in the TCGA data files. The data was also segregated into current smoker and lifelong non-smoker groups. Further, gene set analysis and differential gene expression analysis was carried out using the R packages limma (version 3.34.9) and DESeq2 (version 1.18.1). Gene Ontology (GO) analysis was carried out with GOdb (version 3.5.0) package in Bioconductor R. Other statistical methods and regression analysis were also carried out with R (version3.4.3, R, 2013).

RESULTS & DISCUSSION

Gene set analysis has shown that AT2 marker genes were down regulated and NE marker genes up regulated among LUAD smokers compared to LUAD non-smokers. The important AT2 genes were ABCA3, SFTP and NAPSA. Important marker genes for NE are ASCL1, NCAM and CGRP (CALCA). Differential gene expression analysis has shown that NE marker ASCL1 was up regulated in samples from current smokers. In lung expression of bHLH factor achaete-scute homolog 1 (ASCL1) activates NE differentiation (Rock and Hogan, 2011). High expression of ASCL1 is used as a marker for NE lung tumors such as small cell lung cancer (SCLC) and Large cell NE carcinoma.

Gene set analysis on LUAD and LUSC data sets has shown that basal cell markers are up regulated in LUSC samples. The origin of cell for LUSC is believed to be basal cells in the airway epithelium. Important markers for basal cells are KRT5, KRT14 and TP63. While, all the basal cells express cytoskeleton protein KRT5, only a subset of basal cells expresses KRT14. The weighted gene co-expression network analysis (WGCNA) on LUSC samples identified basal cell markers in a module. The cell of origin for LUAD is believed to be AT2 cells in the alveoli (Desai et al., 2014). However, cells of mixed origin such as club cells and BASCs are also reported along with AT2 (Sutherland, et al., 2014). Gene set analysis found that AT2, AT1 and club cells markers are up regulated in the LUAD samples. Secretory genes such as MUC5AC and MUC5B were also found in the LUAD samples.

CONCLUSIONS

There is accumulation of evidence to support that distinct lung cancer subtypes may have derived from different ‘cells of origin’. Understanding gene expression profiles of these cells might help to develop insight into the biology of the lung cancer and association between air pollution and lung cancer.

REFERENCES

- Desai, T.J., Brownfield, D.G. and Krasnow, M.A., 2014. Alveolar progenitor and stem cells in lung development, renewal and cancer. *Nature*, 507(7491), p.190.
- Hogan, B.L., Barkauskas, C.E., Chapman, H.A., Epstein, J.A., Jain, R., Hsia, C.C., Niklason, L., Calle, E., Le, A., Randell, S.H. and Rock, J., 2014. Repair and regeneration of the respiratory system: complexity, plasticity, and mechanisms of lung stem cell function. *Cell stem cell*, 15(2), pp.123-138.
- Love, M.I., Huber, W. and Anders, S., 2014. Moderated estimation of fold change and dispersion for RNA-seq data with DESeq2. *Genome biology*, 15(12), p.550.
- Nikolić, M.Z., Sun, D. and Rawlins, E.L., 2018. Human lung development: recent progress and new challenges. *Development*, 145(16), p.dev163485.
- R Core Team (2013). R: A language and environment for statistical computing. R Foundation for Statistical Computing, Vienna, Austria. URL <http://www.R-project.org/>.
- Semenova, E.A., Nagel, R. and Berns, A., 2015. Origins, genetic landscape, and emerging therapies of small cell lung cancer. *Genes and development*, 29(14), pp.1447-1462.
- Sutherland, K.D., Song, J.Y., Kwon, M.C., Proost, N., Zevenhoven, J. and Berns, A., 2014. Multiple cells-of-origin of mutant K-Ras-induced mouse lung adenocarcinoma. *Proceedings of the National Academy of Sciences*, p.201319963.
- Tata, P.R. and Rajagopal, J., 2017. Plasticity in the lung: making and breaking cell identity. *Development*, 144(5), pp.755-766.

ROLE OF OUTGOING LONGWAVE RADIATION ON CLOUD FRACTION OVER INDIA

RUCHITA SHAH^{1*} AND ROHIT SRIVASTAVA²

^{1,2}Department of Science, Pandit Deendayal Petroleum University, Raisan, Gandhinagar – 382421, India.

KEYWORDS: outgoing longwave radiation, cloud fraction, regional climate model, india.

ABSTRACT

Global warming may vary the amount of incoming shortwave radiation (SWR) as well as outgoing longwave radiation (OLR) and hence radiation budget of the earth. Trapped OLR by the atmosphere affects many atmospheric components such as aerosol concentration, cloud properties, cloud altitude and properties of greenhouse gases. Cloud condition and cloud-free condition also play a significant role in OLR of the earth. Present study focuses on effect of OLR on cloud macro physical property (here cloud fraction) over India and its adjoining oceans with the help of regional climate model 4.4 (RegCM 4.4) and satellite retrieval. India is monsoon dominated country and study of monsoon system for the normal rainfall year (i.e. 2010) may help to understand precipitation pattern. Two monsoonal months (June and September-start and end of monsoon season) are simulated by the model, retrieved by satellite and also get compared to validate the model. Patch of high range OLR (300-350 W/m²) is simulated with no cloud fraction over most of the regions of India during the month of June, 2010. Similarly, interpolation pattern of high range (250-400 W/m²) OLR is matching with low range (0-0.4) cloud fraction. This type of correlation between OLR and cloud fraction may help to know its direct (such as earth radiation budget) and indirect (such as absorption of OLR by greenhouse gases, concentration of water droplets, cloud formation processes and activation time to trigger for nucleation) effect, which may help to understand precipitation pattern.

INTRODUCTION

Along with OLR and SWR, clouds also play a significant role in earth's radiation budget. Any change in cloud properties may lead to vary cloud formation processes and hence precipitation pattern. Variation in any of these parameters may lead to change almost all components of earth-atmosphere system. Among all these parameters, present study focuses on OLR and its effect on cloud fraction during monsoon season of India. Such studies can be done using various types of models and also using satellite data. OLR can reemit back onto the earth's surface, can transmit through the atmospheric window, can absorb by the atmosphere and also can get emit by the atmosphere into the space. Presence as well as absence of cloud also lead to vary OLR budget. It also effects greenhouse gases present in the atmosphere, which in turn may vary cloud and rain formation processes. Present study use model simulation and satellite retrievals to demonstrate the monsoonal features (here July and September) of OLR and cloud fraction over India.

Earlier research study demonstrated that regional climate models (RegCM) are more reliable than global climate model to examine weather and climate conditions (*Kumar et al., 2011*). Such study is important for a country like India as it is monsoon dominated country and also gets highly influenced by south-west monsoon. Study of cloud processes with the help of cloud macro physical property such as cloud fraction may help to understand seasonal heterogeneity and regional climate variability over Indian subcontinent. To understand the role of OLR on cloud fraction, study here simulates the defined parameters, interpolates and also validate RegCM.

METHODS

For the present study, RegCM covers a region of 63°E-96°5'E to 5°N-33°5'N which includes Indian subcontinent and its adjoining oceanic regions. The model configured with a single domain of horizontal resolution of 60 km, 18 vertical levels and with model top at 50hPa. Initial atmospheric fields and time varying boundary conditions are derived from the National Centers for Environmental Prediction (NCEP) Reanalysis (NNRP1) with the grid of 2.5° x 2.5°. There are various convection schemes in RegCM, among them Grell convective scheme was implemented, as it has performed better than other convection schemes to simulate south west monsoon (Pattnayak et al., 2014 and Grell, 1993). Total cloud fraction and surface net upward longwave flux (W/m²) are simulated for a normal rainfall year (i.e. 2010) to understand the actual scenario of monsoon system on India.

AIRS (Atmospheric Infrared Sounder) is an imaging instrument onboard Aqua satellite in 2002. Similar parameters named total cloud fraction and net top of the atmosphere OLR (W/m^2) of daily resolution is deployed with $1^\circ \times 1^\circ$ spatial resolution for monsoon season of 2010. Both the satellite retrievals are linearly interpolated using matlab and are also used to validate the RegCM. Paper here will present features of two months – June (starting of monsoon) and September (end of monsoon) of 2010.

RESULTS & DISCUSSION

Simulation results of cloud fraction and OLR is shown below in figure 1. High cloud fraction (0.8) is captured over western coast of India, most part of Arabian Sea and small patch over north-western part, central India, mid of Bay of Bengal as well as western part of India (Figure 1a). Almost whole India is simulated with cloud free condition during the month of June. In case of OLR, high range of OLR (300-350 W/m^2) is captured over almost whole India, whereas low range (100-150 W/m^2) OLR is simulated with small patch over north-western part of India and near western coast of India. Current study aims to compare patches of cloud fraction with patches of OLR.

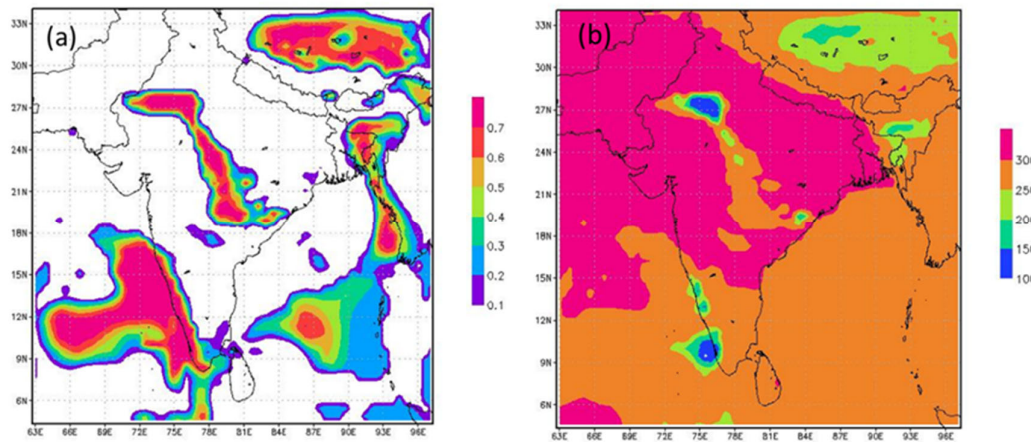


Figure 1. Simulation of (a) Cloud fraction and (b) OLR for the month of June, 2010.

It is clearly seen that patch of high OLR (350 W/m^2) is matching well with no cloud condition. It means that measured OLR at top of atmosphere in absence of cloud gets captured may be due to emission by the atmosphere and also transmission through the atmosphere. Emission as well as transmission process both help to emit outgoing infrared radiation into space.

Small patches of low (100-150 W/m^2) OLR is matching with high (0.7-0.8) cloud fraction over western coast and north-western region of India. Less OLR at top of atmosphere is may be due to presence of cloud which forces upcoming radiation to get reemit onto the earth's surface. This phenomenon may increase the temperature of lower atmosphere, which in turn may vary cloud formation processes and hence precipitation pattern.

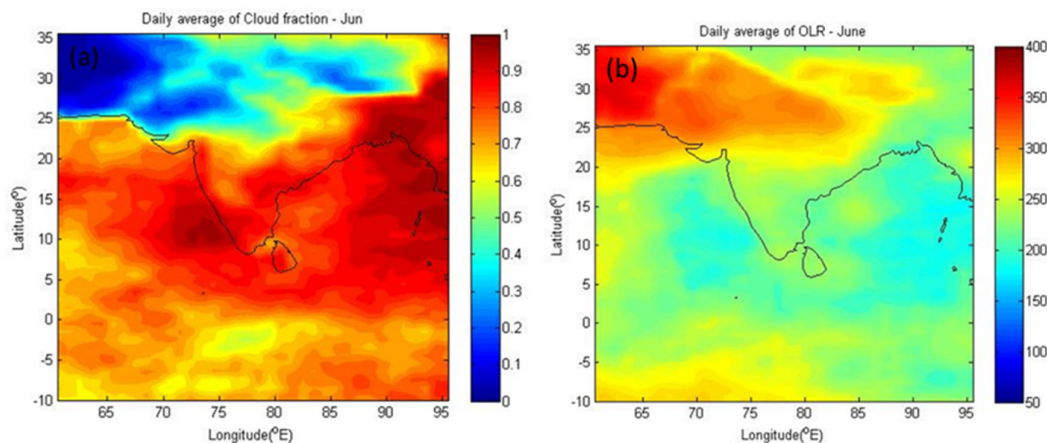


Figure 2. Satellite retrievals of (a) Cloud fraction and (b) OLR for the month of June, 2010.

Satellite retrievals of cloud fraction and OLR are interpolated using daily averaged data for the month of June (Figure 2). Interpolated patches of OLR and cloud fraction shows almost same results as that simulated by RegCM. Almost similar dependency of OLR and cloud fraction is observed for monsoon season (June-September) over India for normal rainfall year 2010. Hence, model simulated patches are almost matching with satellite retrieval patches which enhances the accuracy of the model. Also, it becomes important to validate the model before applying RegCM for future projection climate studies. These results show better performance of the model along with its validation. Further results for the month of September will be presented in the conference.

SUMMARY

Current study depict the effect of OLR on cloud macro physical property (here cloud fraction) for two monsoon months – June and September of normal rainfall year 2010 using model simulation and satellite data. Study of cloud properties, over monsoon dominated region, can become a significant tool to understand the effect of climate change and hence precipitation pattern. High range (300-350 W/m²) OLR over land regions of India is matching with cloud-free condition, which may signifies that OLR gets emitted by atmosphere as well as transmitted through atmosphere. Low range (100-150 W/m²) OLR gets captured with high range (0.7-0.8) cloud fraction, which depicts that infrared radiation gets trapped by the presence of clouds. This may increase the temperature of lower atmosphere and may vary atmospheric components. Almost similar features are observed with the help of satellite retrievals. Moreover, these simulated parameters are also get validated by interpolation patterns. Similar results are also obtained for four monsoon months (June-September) of India which also shows promising results. Though it requires long term data to clarify and strengthen these results. Thus, research carried out in this field may help to understand earth's radiation budget, effect of OLR on atmospheric components, seasonal heterogeneity as well as climate change.

ACKNOWLEDGEMENT

We would like to thank our university for providing computational facility.

REFERENCES

- Kumar, K.K., S. K. Patwardhan, A. Kulkarni, K. Kamala, K. K. Rao, and R. Jones (2011). Simulated projections for summer monsoon climate over India by a high-resolution regional climate model (PRECIS), *Current Science*, **101**.
- Pattnayak, K., S. K. Panda and S. K. Dash (2014). Annual cycles of circulation and precipitation over India simulated by a Regional Climate Model, *Vayumandal*, **38**, pp. 35 - 45.
- Grell, G. A. (1993). Prognostic evaluation of assumptions used by cumulus parameterization, *Mon. Wea. Rev.*, **121**, pp.764 - 787.

A LONG TERM SATELLITE BASED STUDY OF AEROSOL EFFECTS ON VISIBILITY OVER THE CAPITAL CITY OF ASSAM, GUWAHATI

J. BISWAS^{1*} and P. DAHUTIA²

¹Department of Physics, Pandu College, Guwahati-781012, Assam, India

²Department of Physics, Dibrugarh University, Dibrugarh-786004, Assam, India

KEYWORDS: AOD, Remote Sensing, Visibility, Air Quality

INTRODUCTION

Satellite remote sensing technique provides a primary tool to understand the role of atmospheric aerosol particles in Earth system science as well as climate (Reid *et al.*, 2013). Satellite data of pollutants in the atmosphere are becoming more extensively used in the decision-making as well as environmental management activities of public, private sector and non-profit organization (Duncan *et al.*, 2014). Remote sensing techniques are a very helpful tool for understanding Earth processes as well as evaluating performance of model predictions on weather and climate change. Instruments mounted on satellites can provide the spatial distribution of atmospheric aerosol; trace gases etc. on regional as well as global scale. In field experiments, data are usually available for some selected locations; hence satellite remote sensing fill the need for extensive data of atmospheric pollutants with greater temporal and spatial coverage than aircraft campaigns. The impact of pollutant on radiative balance, air quality and human health has led to significant attempt to measure atmospheric aerosols and trace gases by using ground based networks along with satellite observations. Proper evaluations of aerosols in addition to trace gases are necessary for the in progress global climate simulations because they play as vital components for Earth's climate change process.

Over recent years, a large number of long-term variation trends in atmospheric aerosol have been conducted by using Moderate Resolution Imaging Spectroradiometer (MODIS) data over different places in the world (Levy *et al.*, 2010, 2013; Guo *et al.*, 2011; Soni *et al.*, 2015; Dahutia *et al.*, 2017 etc.). Over vegetated land, MODIS retrieves Aerosol Optical Depth (AOD) at 3 visible channels with high accurateness, i.e., $\pm 0.05 \pm 0.2\tau$ (Remer *et al.*, 2005). The retrieved uncertainty of MODIS AOD at 550 nm is estimated to be $\pm (0.05 + 0.15 \text{ AOD}_{550})$ over land (Remer *et al.*, 2005, 2008; Levy *et al.*, 2013), but accuracy may be lower for some particular regions of the world depending on the assumptions on type of surface along with optical properties of aerosols. Visibility is a simply observable indicator of air quality over a region (Bäumer *et al.*, 2008): a high visibility generally means good air quality (Horvath, 1995). Clear sky visibility is reduced mainly by the presence of aerosols, whose types along with concentrations have an enormous impact on the amount of incoming solar radiation that reaches the surface of Earth (Wang *et al.*, 2009). A number of earlier studies on correlation of visibility or else visual range and aerosol properties were reported by Bäumer *et al.* (2008). According to Wang *et al.* (2009), visibility has decreased considerably since the mid-1980s over South and East Asia, South America, Australia, and Africa except Europe resulting in net global dimming over land.

The main goal of the present study is to assess the long term temporal distributions of atmospheric aerosols over Guwahati, North-East India for the period of January 2004 to December 2016. This study area is of importance with regard to air pollution due to the large population, unique topography and considerable sources of natural and anthropogenic emissions. Also, in this paper, we present the results of relationship between AOD and horizontal visibility to assess the atmospheric pollution of the study area.

DATA SOURCES

The moderate resolution imaging spectroradiometer (MODIS) sensor on board the NASA Earth Observing System (EOS) Terra and Aqua satellite based AOD data at 550 nm data are used for the period of January, 2004-December, 2016. The daily Level 3 data set of aerosol optical depth (AOD) at 550 nm and Ångström exponent (AE) with quality assured (QA) Collection 6 data has $1^\circ \times 1^\circ$ global resolutions (Levy *et al.*, 2013). For the present study, daily mean level-3 collection-6 MODIS AOD data sets (both Terra and Aqua) are obtained from the Giovanni web service (<http://disc.sci.gsfc.nasa.gov/giovanni>) on a $1^\circ \times 1^\circ$ spatial resolution, centred at the study location.

RESULTS & DISCUSSIONS

To examine the day-to-day variability of AOD over Guwahati, daily mean Aqua AOD at 550 nm for the 13-year period is plotted as shown in Fig. 1. The solid straight line in the figure corresponds to the linear best fit to the daily mean data of AOD. It is clearly seen from the figure that a significant long-term increasing trend of AOD exists over Guwahati which may be due to decreasing trend of monthly (mainly pre-monsoon and monsoon month) rainfall for the study period.

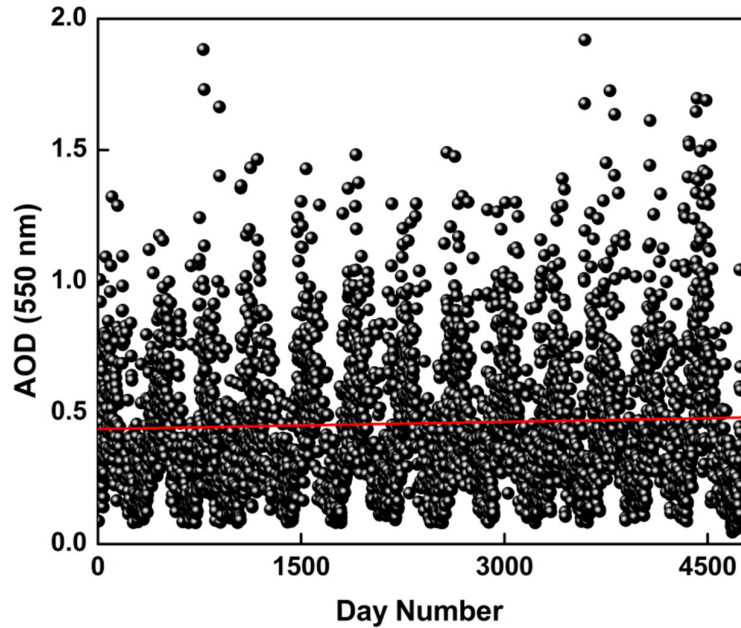


Figure 1. Day-to-day variability of daily mean Aqua AOD at 550 nm over Guwahati for the period of January 2004 to December 2016. The solid red straight line is the linear best fit to the daily mean data.

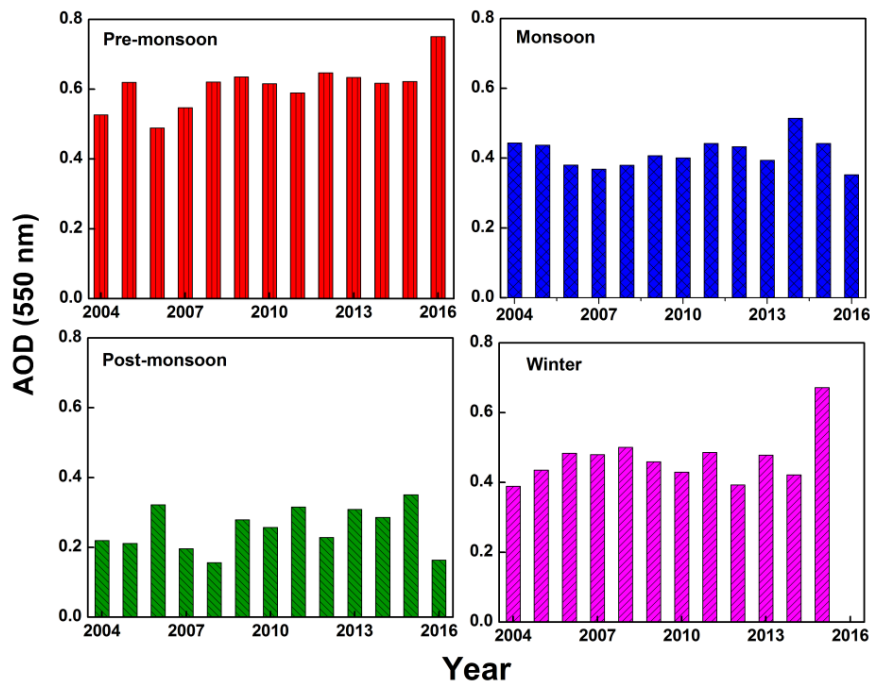


Figure 2. The seasonal variation of AOD at 550 nm over Guwahati for the period of January 2004 to December 2016.

The seasonal variation of AOD at 550 nm over Guwahati for the period 2004 to 2016 is shown in Fig.2. It shows highest value during pre-monsoon (March-May) season due to the intense biomass burning activities and lowest in post-monsoon (October-November) season mainly due to wash out of aerosols by rain in the preceding months without enough replacement. The seasonally averaged AOD reached its maximum in pre-monsoon (0.61 ± 0.06), followed by winter (December-February) (0.47 ± 0.07) and monsoon (June-September) (0.41 ± 0.04), with the minimum occurring in post-monsoon (0.25 ± 0.06) season. Strong seasonality in AOD was reported by Biswas *et al.* (2017) with a peak in pre-monsoon and dip in post-monsoon over nine different locations in North-East India and adjoining areas. Dahutia *et al.* (2017) also reported prominent longitudinal gradient in seasonal aerosol distribution over North-East India with higher AOD values in the western part (including Guwahati), which is mainly attributed to variability of source types and closeness to the western influences through transportation (Pathak *et al.*, 2014, 2016; Gogoi *et al.*, 2017).

The relative dominance of fine mode aerosols over the coarse mode can be determined from Ångström exponent. The value of the Ångström exponent is a qualitative indicator of size of aerosol particles (Ångström, 1929). Values of Ångström exponent ≤ 1 indicate size distributions dominated by coarse mode aerosols that are usually linked with dust and sea salt whereas values of Ångström exponent ≥ 2 indicate size distributions dominated by fine mode aerosols which are generally associated with urban pollution and biomass burning (Eck *et al.*, 1999). The monthly variation in Ångström exponent with Aqua AOD over Guwahati for the period January, 2004 to December, 2016 is shown in Fig.3. The monthly average AOD value varies from its highest value (0.63 ± 0.09) in the month of March to its lowest value (0.23 ± 0.05) in October for the study period over Guwahati. Ångström exponent value lying between 1 and 1.5 indicates major contributions from accumulation mode aerosols to the AOD (Beegum *et al.*, 2009). The observed Ångström exponent value varies from its minimum value (1.18 ± 0.05) in monsoon season to its maximum value (1.35 ± 0.09) in post-monsoon season. This in fact indicates size of aerosol particles in post-monsoon season is smaller than that in monsoon season.

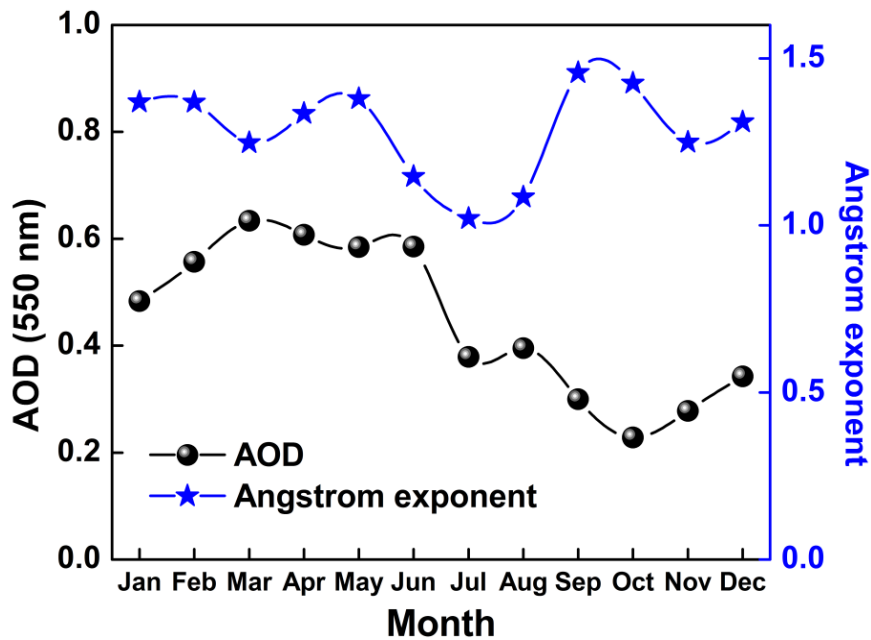


Figure 3. The monthly variation in Aqua AOD and Ångström exponent over Guwahati for the period of January, 2004 to December, 2016.

A relationship between visibility (V) and aerosol optical depth has been established by Vermote *et al.* (2002) to be used for *Visible Infrared Imaging Radiometer Suite (VIIRS)* data onboard the National Polar-orbiting Operational Environmental Satellite System:

$$V = 3.9449 / (AOD_{550} - 0.08498) \dots \dots \dots (1)$$

This equation is not valid for $AOD \leq 0.08498$.

The relationship between AOD and visibility is presented in Fig.4. The analysis showed that visibility is minimum during pre-monsoon months which are mainly due to higher values of AOD for the

season over the study region. A higher value of AOD represents higher column of aerosol loading in the atmosphere which scatter off light more effectively and hence resulting in lower visibility (Wang and Christopher, 2003). The monthly average visibility in Guwahati is highest (27.5 km) in October with a moderate reduction observed during the monsoon, reaching a minimum of 7.2 km in March. During winter month, local aerosol emissions are trapped within the boundary layer leading to higher surface concentrations and hence resulting lower visibility.

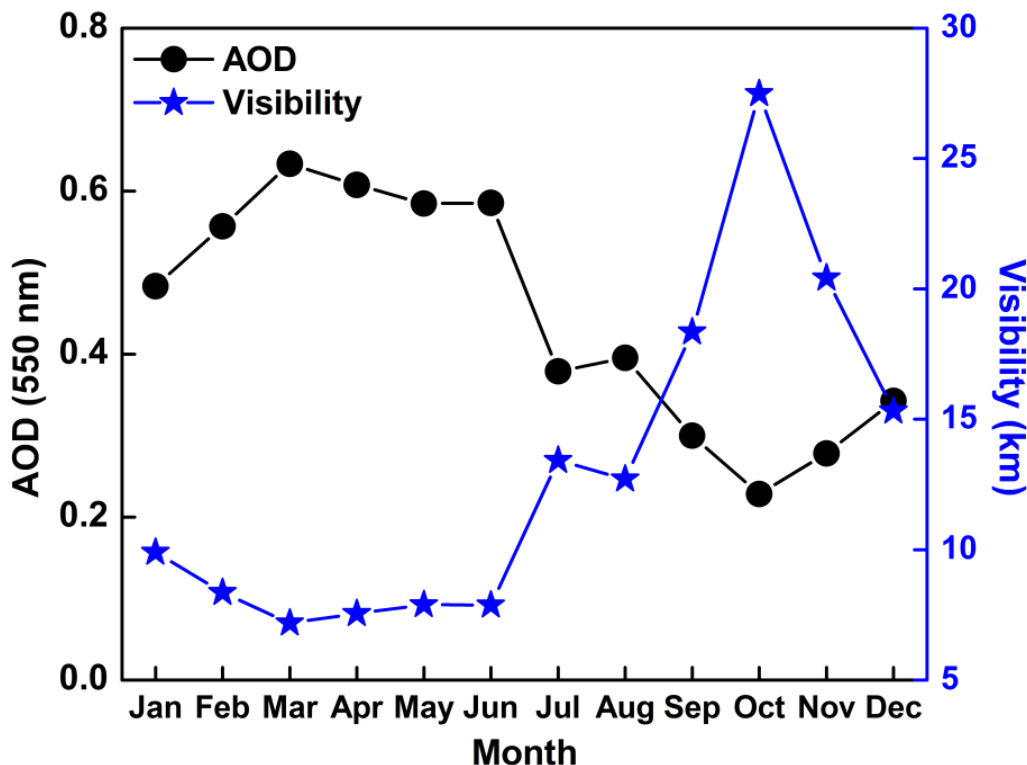


Figure 4. The monthly variation in Aqua AOD and visibility over Guwahati for the period of January, 2004 to December, 2016.

CONCLUSIONS

In this study long-term (January 2004-December 2016) variations of AOD and Ångström exponent have been studied by using satellite observations. For all the year of observations, the seasonal variation of AOD shows highest value during the pre-monsoon season and lowest in post-monsoon season over Guwahati. The seasonally averaged AOD reached its maximum in pre-monsoon (0.608 ± 0.06) season, followed by winter (0.469 ± 0.07) and monsoon (0.415 ± 0.04), with the minimum occurring in post-monsoon (0.253 ± 0.06) season. The observed Ångström exponent value varies from its minimum value (1.18 ± 0.05) in monsoon season to its maximum value (1.35 ± 0.09) in post-monsoon season which indicates size of aerosol particles in post-monsoon is smaller than that in monsoon season. The monthly average visibility in Guwahati is highest (27.5 km) in the month of October with a moderate reduction observed during the monsoon, reaching a minimum of 7.2 km in March. With increasing AOD values, horizontal visibility decreases over Guwahati.

ACKNOWLEDGEMENTS

Authors are thankful to Giovanni (<https://giovanni.sci.gsfc.nasa.gov/giovanni/>) science data team for the data used in this analysis.

REFERENCES

- Ångström, A. (1929). On the atmospheric transmission of Sun radiation and on dust in the air, *Geogr. Ann.* 11: 156-166.
- Bäumer, D., B. Vogel, S. Versick, R. Rinke, O. Möhler, and M. Schnaiter (2008). Relationship of visibility, aerosol optical thickness and aerosol size distribution in an ageing air mass over South-West Germany, *Atmos. Environ.* 42, 989-998.
- Beegum N., K. K. Moorthy and S. S. Babu (2009). Aerosol microphysics over a tropical coastal station inferred from the spectral dependence of Angstrom wavelength exponent and inversion of spectral aerosol optical depths, *J. Atm Solar-Terres. Phys.* 71: 1846–1857.
- Biswas, J., B. Pathak, F. Patadia, P.K. Bhuyan, M.M. Gogoi and S.S. Babu (2017). Satellite-retrieved direct radiative forcing of aerosols over North-East India and adjoining areas: climatology and impact assessment, *Int. J. Climatol.* 37 (Suppl.1): 298-317.
- Dahutia, P., B. Pathak and P. K. Bhuyan (2017). Aerosols characteristics, trends and their climatic implications over Northeast India and adjoining South Asia, *Int. J. Climatol.* doi: 10.1002/joc.5240.
- Duncan, B. N., A. I. Prados, L. N. Lamsal, Y. Liu, D. G. Streets et al (2014). Satellite data of atmospheric pollution for U.S. air quality applications: Examples of applications, summary of data end-user resources, answers to FAQs, and common mistakes to avoid, *Atmos. Environ.* 94: 647-662.
- Eck, T. F., B. N. Holben, J. S. Reid, O. Dubovik, A. Smirnov, N. T. O'Neill, I. Slutsker and S. Kinne (1999). Wavelength dependence of the optical depth of biomass burning, urban, and desert dust aerosols, *J. Geophys. Res.* 104(D24), 31,333-31,349.
- Gogoi, M. M., S. S. Babu, K. K. Moorthy, P. K. Bhuyan, B. Pathak, T. Subba, L. Chutia et al (2017). Radiative effects of absorbing aerosols over northeastern India: observations and model simulations, *J. Geophys. Res.* 122: 1132–1157.
- Guo, J.P., X.Y. Zhang, Y.R. Wu, Y. Zhaxi, H.Z. Che, B. La, W. Wang and X.W. Li (2011). Spatio-temporal variation trends of satellite-based aerosol optical depth in China during 1980-2008, *Atmos. Environ.* 4537: 6802–6811.
- Horvath, H. (1995). Estimation of the average visibility in central Europe, *Atmos. Environ.* 29: 241-246.
- Levy, R.C., S. Mattoo, L.A. Munchak, L. A. Remer, A.M. Sayer, F. Patadia and N.C. Hsu (2013). The collection 6 MODIS aerosol products over land and ocean, *Atmos. Meas. Tech.* 6: 989-3034.
- Pathak, B., A. Borgohain, P.K. Bhuyan, S. S. Kundu, S. Sudhakar, M. M. Gogoi and T. Takemura (2014). Spatial heterogeneity in near surface aerosol characteristics across the Brahmaputra valley, *J. Earth Syst. Sci.* 123: 651-663.
- Pathak, B., T. Subba, P. Dahutia, P.K. Bhuyan, K.K. Moorthy, M.M. Gogoi et al (2016). Aerosol characteristics in north-east India using ARFINET spectral optical depth measurements, *Atmos. Environ.* 125: 461–473.
- Reid, J. S., E. J. Hyer, R. S. Johnson, B. N. Holben, R. J. Yokelson, J. Zhang, et al (2013). Observing and understanding the Southeast Asian aerosol system by remote sensing: An initial review and analysis for the Seven Southeast Asian Studies (7SEAS) program, *Atmospheric Res.* 122: 403-468.
- Remer, L. A., Y. J. Kaufman, D. Tanre, S. Mattoo, D. A. Chu, J. V. Martins, R.-R. Li, et al (2005). The MODIS aerosol algorithm, products and validation, *J. Atmospheric Sci* 62: 947-973.
- Remer, L.A., R.G. Kleidman, R.C. Levy, Y.J. Kaufman, D. Tanre, S. Mattoo, J.V. Martins et al (2008). Global aerosol climatology from the MODIS satellite sensors, *J. Geophys. Res.* 113:D14S07.

Soni, K., K.S. Parmar and S. Kapoor (2015). Time series model prediction and trend variability of aerosol optical depth over coal mines in India, *Environ. Sci. Pollut. Res. Int.* 22: 3652-3671.

Vermote, E. F., S. Vibert, H. Kilcoyne, D. Hoyt and T. Zhao (2002). Suspended Matter Visible/Infrared Imager/Radiometer Suite algorithm theoretical basis document, SBRS Document # Y2390, Raytheon Systems Company, *Information Technology and Scientific Services*, Maryland, 2002.

Wang, J. and S.A. Christopher (2003). Intercomparison between satellite derived aerosol optical thickness and PM_{2.5} mass: Implications for air quality studies, *Geophys. Res. Lett.* 30 (21): 2095.

Wang, K., R. E. Dickinson and S. Liang (2009). Clear Sky Visibility Has Decreased over Land Globally from 1973 to 2007, *Science*, 323: 1468-1470.

EVOLUTION AND CHARACTERISTICS OF ORGANIC AEROSOL IN THE URBAN ATMOSPHERE THROUGH HIGHLY TIME RESOLVED MEASUREMENTS

ATINDERPAL SINGH, R.V. SATISH AND NEERAJ RASTOGI

Geosciences Division, Physical Research Laboratory
Ahmedabad – 380009, India.

KEYWORDS: Organic aerosol; Elemental ratios; Primary and secondary aerosol

INTRODUCTION

Submicron size particles are an integral part of Earth's atmosphere with significant impacts (direct and indirect) on human health, global climate, and visibility. An unprecedented increase in sub-micron particles concentrations over urban regions is a serious threat to both air quality and climate. Organic aerosol (OA), although reported to be a dominant fraction of submicron aerosol, are least understood component of fine aerosol due to their numerous sources, complex composition, tedious formation mechanism, and complicated atmospheric evolution (Hu *et al.*, 2013). OA can either be primary or of secondary origin. The primary OA (POA) are emitted directly in particulate form from the sources such as fossil fuel and biomass burning or mechanical processes, whereas, secondary OA (SOA) are produced from the oxidation of volatile organic compounds (VOCs) coming from different sources. Furthermore, the composition and properties of both POA and SOA may change dynamically throughout aerosol lifetime, because of intertwined processes including emission, oxidation, fragmentation and gas-to-particle partitioning. Until recent years, most of the studies have reported the properties of OA using filters based measurements (offline) which were unable to capture OA evolution in the atmosphere due to low time resolution of measurements. The present study investigates the evolution of OA in real-time using high-resolution time-of-flight aerosol mass spectrometer (HR-ToF-AMS) during the post-monsoon season (PoM; 19 September 2017 to 19 October 2017) over a big urban city (Ahmedabad) located in the semi-arid region of western India.

METHODS

Ahmedabad is a big urban city close to the southeast boundary of the great Thar Desert and northeast of the Arabian Sea. The detailed site description was reported elsewhere (Rastogi and Sarin, 2005). Real-time characteristics of non-refractory submicron aerosol (NR-PM₁), composed of organic aerosol (OA), SO₄²⁻, NO₃⁻, NH₄⁺ and Cl⁻, were studied using HR-ToF-AMS (Aerodyne Inc, USA) with one min time resolution in high sensitive V mode. Ambient air was sampled through a diffusion dryer prior to entering the HR-ToF-AMS. Ionization efficiency (IE), particle velocity and inlet flow calibrations were performed using established standard protocols (Canagaratna *et al.*, 2007). The m/z calibration and other threshold parameters of data acquisition board were checked daily and were very stable. Raw data of AMS were processed using the standard toolkit named SQUIRREL (v1.56) and PIKA (v1.15c) written in IGOR (Wavemetrics, Inc., Lake Oswego) to determine the mass concentrations of OA, SO₄²⁻, NO₃⁻, NH₄⁺ and Cl⁻.

RESULTS & DISCUSSIONS

A large variability has been observed in the mass concentration of OA (0.5–89 µg m⁻³), which is also found to be a dominant contributor to NR-PM₁ with the contribution of ~55% during the study period over Ahmedabad. These changes can be attributed to dynamical changes in emission sources and atmospheric processing of species, as well as changing meteorological conditions. Diurnal variation of OA showed a peak in the morning and late evening hours, which coincide with traffic rush hours. Lower concentrations of these species were observed during the middle of the day because of the combined effect of lesser anthropogenic activities, especially vehicular emission, and increase in the boundary layer height. Elemental ratio (O/C and H/C) of OA provide useful information in understanding their sources and atmospheric evolution (Canagaratna *et al.*, 2007). The elemental ratio had shown strong diurnal variation throughout the study period (Fig. 1).

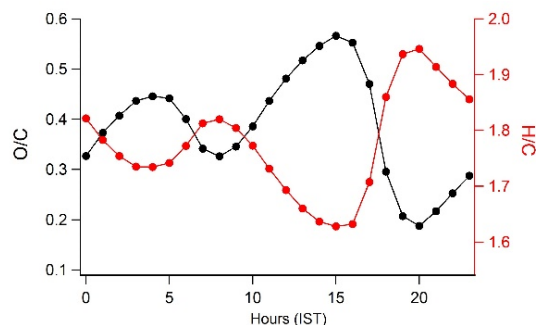


Figure 1. Diurnal trends in O/C and H/C

The O/C values peaked in late night and afternoon hours whereas H/C values showed exactly opposite trends during these hours. Both late night and afternoon peaks in O/C values suggest the photochemical formation of SOA (Xu *et al.*, 2018). The H/C peaked during rush hours, which indicate the dominance of primary OA from vehicular emissions. However, it is important to mention here that high H/C was also related to high OA but high O/C was related to low OA concentrations, suggesting measured OA was dominated by POA. Further, the OM/OC ratio followed the O/C trend, as expected. Its variation from 1.2 to 2.3, and a moderate peak during the early morning and a strong peak in the afternoon, is attributable to the increase in OM/OC ratio due to SOA formation. Significant variation in OM/OC values with strong diurnal trend suggests that a constant conversion factor used in OM estimation (from OC) can be a source of large uncertainty in their load assessment.

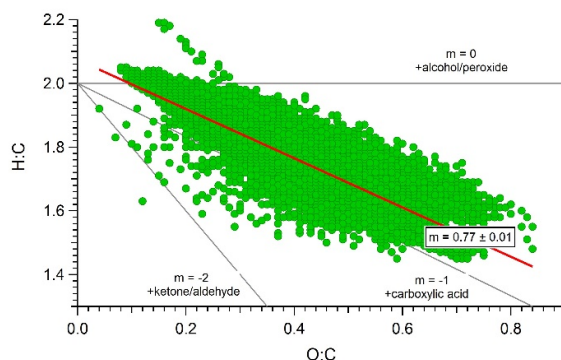


Figure 2. Representation of O/C and H/C in Van Krevelen (VK) diagram

The evolution of oxygenated OA (OOA) was studied using triangle plot between f44 (signal at m/z 44 to total organic signal) and f43 (signal at m/z 43 to total organic signal) (Ng *et al.*, 2010). The m/z 44 is mostly due to organic acids or their derivatives whereas m/z 43 is predominantly referred to non-acid oxygenates. The OOA in the right lower part of the triangle is less oxidized, non-acid OOA and expected to be consist of SV-OOA. Upper left part of the triangle represents aged OA which become more acidic, oxidized and consist of LV-OOA (Fig. not shown). Thus, OA becomes more acidic with evolution and their volatility decrease, and their ability to act as cloud nuclei increases (Cubison *et al.*, 2011 and references therein). Observations over the study region suggest that most of the OA are in the SV-OOA region (Ng *et al.*, 2010 and references therein). The slope of Van Krevelen (O/C vs H/C) diagram is often used to understand the bulk composition of OA (Heald *et al.*, 2010). In this study, the slope is found to be -0.77 ± 0.01 , which suggests that ambient OA is aging towards widely observed slope (-1) of OA i.e., carboxylation (Fig. 2). It also infers that the observed OA was a variable mixture of fresh and aged OA during the study period. Observed slope in the present study is found to be higher than that reported over Kanpur, India (-0.52 during winter, -0.65 during PoM, and -0.69 during monsoon, Chakraborty *et al.*, 2017).

CONCLUSIONS

Chemical composition and characteristics of NR-PM₁ were investigated during PoM season of 2017 using HR-ToF-AMS over Ahmedabad. The OA is found to be the major fraction (55%) of NR-PM₁. Diurnal trends of O/C and H/C during the study period revealed that SOA formation was dominant during late night and afternoon hours whereas primary OA was abundant during rush hours. Furthermore, our results indicate that

a substantial fraction of ambient oxygenated OA (OOA) was semi-volatile over study region. The slope of Van Krevelen (VK) diagram is found to be -0.77 ± 0.01 over study region, which suggests that ambient OA is aging towards widely observed slope (-1) of OA i.e., carboxylation. This study provides deeper insights of organic aerosol abundances and characteristics, hitherto lacking from this region.

REFERENCES

Canagaratna, M.R., et al. (2007). Chemical and microphysical characterization of ambient aerosols with the aerodyne aerosol mass spectrometer, *Mass Spectrom. Rev.* **26(2)**, 185–222.

Chakraborty, A., et al. (2017). Realtime chemical characterization of post monsoon organic aerosols in a polluted urban city: Sources, composition, and comparison with other seasons, *Environ. Pollut.* <https://doi.org/10.1016/j.envpol.2017.09.079>.

Cubison, M.J., et al. (2011). Effects of aging on organic aerosol from open biomass burning smoke in aircraft and laboratory studies, *Atmos. Chem. Phys.* **11**, 12049–12064.

Heald, C. L., et al. (2010). A simplified description of the evolution of organic aerosol composition in the atmosphere, *Geophys. Res. Lett.* **37**, L08803, <https://doi.org/10.1029/2010gl042737>, 2010.

Hu, W.W., et al. (2013). Insights on organic aerosol aging and the influence of coal combustion at a regional receptor site of central eastern China, *Atmos. Chem. Phys.* **13**, 10095–10112.

Ng, N.L., et al. (2010). Organic aerosol components observed in Northern Hemispheric datasets from Aerosol Mass Spectrometry, *Atmos. Chem. Phys.* **10**, 4625– 4641.

Rastogi, N. and Sarin, M.M. (2005). Long-term characterization of ionic species in aerosols from urban and high altitude sites in western India: Role of mineral dust and anthropogenic sources, *Atmos. Environ.* **39**, 5541–5554.

Xu, J., et al., (2018). Chemical characteristics of submicron particles at the central Tibetan Plateau: insights from aerosol mass spectrometry, *Atmos. Chem. Phys.* **18**, 427– 443.

REACTIVE OXYGEN SPECIES GENERATION CAPABILITY OF AMBIENT AEROSOL OVER THE ARABIAN SEA

ANIL PATEL AND NEERAJ RASTOGI

Geosciences Division, Physical Research Laboratory, Ahmedabad-380009, India

KEYWORDS: particulate matter, Reactive Oxygen Species (ROS), Marine Atmospheric Boundary Layer (MABL)

INTRODUCTION

In-situ generation of reactive oxygen species (ROS) through catalytic activity of ambient aerosol can affect the atmospheric oxidizing capability and secondary aerosol formation. They can also affect human health (on inhalation) and the marine micro-organisms (through dry or wet deposition) through in-situ ROS generation. The ROS are produced in the ocean biota through several pathways that includes photosynthesis in chloroplast and electron transport chain by the cell organelles such as mitochondria, endoplasmic reticulum and plasma membrane. Usually ROS formation in cells occurs through the reduction of molecular oxygen from biological reducing agents such as nicotinamide adenine dinucleotide (NADH) and nicotinamide adenine dinucleotide phosphate (NADPH). Electron transfer enzymes and active redox chemical species (e.g., redox active organics and transition metals in aerosol) assist these processes. The mechanism involves sequential univalent reduction of oxygen to form superoxide ($O_2^{\cdot-}$), hydrogen peroxide (H_2O_2), hydroxyl radical (OH^{\cdot}). Furthermore, other ROS sources in the marine environments include dry and wet atmospheric input of aerosol coming through long range transport which can rapidly increase surface water H_2O_2 concentration (Zika et al., 1982; Kieber et al., 2003). When the level of ROS concentrations are more than that can be handled by defense mechanism in living organisms, the situation is known as “oxidative stress”, which often leads to inflammation or even cell death by attacking on biomolecules such as lipids, proteins and DNA. A high level of $[H_2O_2]$ in seawater has been hypothesized to inhibit nitrification which is governed by Thaumarchaeotes (Ammonia Oxidizing Archaea (AOA), Tolar et al., 2016). The H_2O_2 production can induce oxidative damage to AOA and/or other organisms. The capability of ambient aerosol to generate ROS is known as their oxidative potential (OP). No studies, to best of our knowledge, are available on the OP of ambient aerosol over the marine environments and its consequences. The present work studies OP of aerosol over the marine atmospheric boundary layer of the Arabian Sea.

METHODS

PM_{10} (particulate matter with aerodynamic diameter less than or equal to 10 μm) samples were collected on tisuquartz filters using a high volume air sampler (flow rate: 1.13 $m^3 \text{ min}^{-1}$) during 15th April 2017 to 3rd May 2017 onboard Sagar Sampada (SS)-359 cruise over the Arabian Sea along the cruise track shown in Fig. 1. These samples were analyzed for their mass concentration by gravimetric analysis and chemical composition such as organic carbon (OC) and elemental carbon (EC), water-soluble organic carbon (WSOC), major ions (such as sulphate (SO_4^{2-}), nitrate (NO_3^-), chloride (Cl^-), sodium (Na^+), ammonium (NH_4^+), potassium (K^+), calcium (Ca^{2+}) and magnesium (Mg^{2+})) and water-soluble trace metals using standard techniques and established protocols reported elsewhere (Patel and Rastogi, 2018a).

Dithiothreitol (DTT) assay has been used to measure OP as per the procedure given in Patel and Rastogi (2018a), wherein DTT is being used as a surrogate of the biological reducing agents (NADH and NADPH) (Cho et al., 2005). Briefly in this assay, an aliquot of PM_{10} loaded filter was extracted in 1:1 mixture of methanol and Milli Q water (MeOH:MQ) using ultrasonication for 30 min (3 times, 10 min each). Subsequently, extracts were filtered through tisuquartz filters (25 mm, pore size 0.45 μm). Filtered extracts were incubated with 100 μM DTT made in 0.1 M (7.4 pH) phosphate buffer solution at 37 $^{\circ}C$ in an amber color glass vials. At various time intervals, a known amount of incubated mixture was taken out from the vial and added to 50 μl of 10 mM 5, 5'- dithiobis-2-nitrobenzoic acid (DTNB) to quench the reaction between DTT and soluble PM. The remaining DTT in incubated mixture immediately convert the DTNB to 2-nitro-5-thiobenzoic acid (TNB). Subsequently, the TNB was measured with UV-Visible spectrophotometer (UV-1800, Shimadzu) at 412 nm. The DTT consumption rate (μM DTT consumed per minute) is directly proportional to the concentration of redox active PM species present in the sample, and referred as OP.

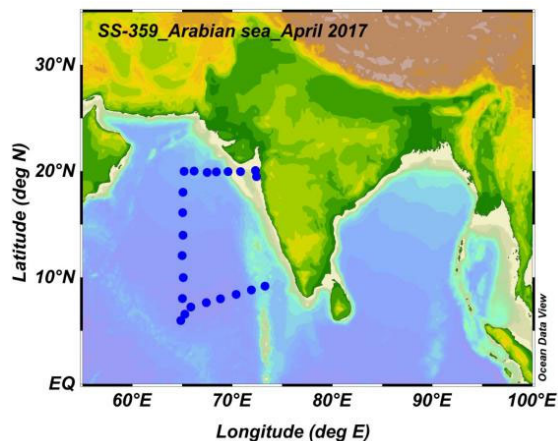


Figure 20. Map is showing the sampling locations over the Arabian Sea

RESULTS & DISCUSSIONS

Measured OP can be expressed in two different ways: one is volume normalized OP ($\text{nmol DTT min}^{-1} \text{m}^{-3}$ or OP m^{-3} or OP_V) and another is mass normalized OP ($\text{pmol DTT min}^{-1} \mu\text{g}^{-1}$ or $\text{OP } \mu\text{g}^{-1}$ or OP_M). The OP_V varied from 0.69 to 2.08 $\text{nmol DTT min}^{-1} \text{m}^{-3}$ (1.47 ± 0.37 ; average $\pm 1\text{SD}$) whereas OP_M varied from 6 to 26 $\text{pmol DTT min}^{-1} \mu\text{g}^{-1}$ (15 ± 6) during the study period. These values were lower than those observed over Patiala and comparable with those observed over Mt Abu (Patel and Rastogi, 2018a, b). Further, the EC is found to be positively correlated with mass normalized OP at high significance level ($p < 0.05$) with three different slopes for the samples corresponding to different air masses (Fig. 2). This observation suggests that different species emitted along with EC from different sources could be the cause of different slopes. While looking into their air masses back trajectories, three classes of air masses from different regions are observed. It is inferred that source(s) emitting EC associated with Indian continental air masses (A) also emit other species, which are 2 to 8 times more DTT active compared to those associated with open ocean (B) and/or the Arabian continental air masses (C) (Fig. 2). It is relevant to note that the slope (8) over the Arabian sea due to the Indian continental air masses (A) has been found to be similar to that documented over a high altitude site Mt. Abu (11, Patel and Rastogi, 2018b).

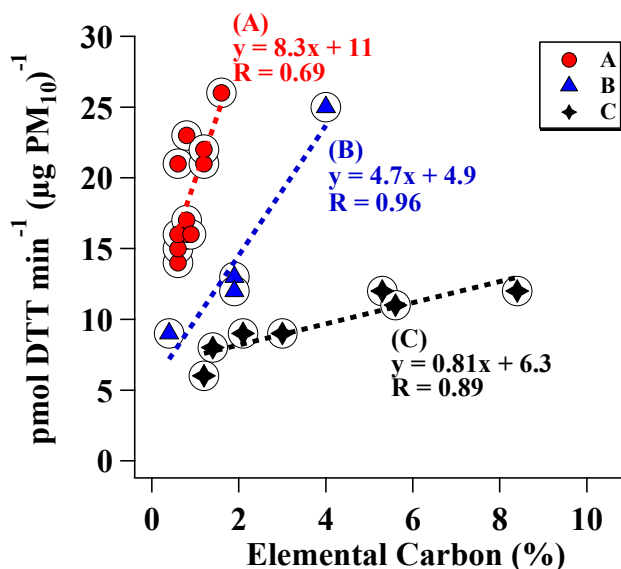


Figure 21. Scatter plot between mass normalized OP and % EC mass fraction.

Some water-soluble trace metals such as Ni, Cu, Mn, Zn, Sb and Pb have been found to be positively correlated with DTT activity at high significance level ($p < 0.05$), suggesting their capability to generate superoxide that may further converts to peroxide and ultimately to OH^\cdot radical. Atmospheric deposition of

these redox active species over ocean may lead to significant increase in ROS concentration in surface water, which may affect the ocean biogeochemical cycle by causing damage to marine organisms.

CONCLUSIONS

This work reports OP of aerosol collected during April-May, 2017 over the marine atmospheric boundary layer of the Arabian Sea. The OP exhibited significant variability with highest OP for the aerosol coming from Indian subcontinent. Further, species from the source (s) emitting EC over Indian subcontinent were found to be 2 to 8 times more DTT active compared to those associated EC from the Arabia. Water-soluble trace metals such as Ni, Cu, Mn, Zn, Sb and Pb have been found to be positively correlated with DTT activity at high significance level ($p < 0.05$).

Such studies have important implications. Atmospheric deposition of these redox active species over ocean may lead to significant increase in ROS concentration in surface water which may affect the marine biogeochemical cycle. Identification of these redox active chemical species and mechanism through which they can affect marine environments are important to understand to assess their effects.

ACKNOWLEDGEMENTS

We would like to thank Dr. Arvind Singh, the chief scientist, and all the other participants of the cruise SS-359 onboard ORV Sagar Sampada for their kind support during the aerosol sampling.

REFERENCES

- Cho, A. K., C. Sioutas, A. H. Miguel, Y. Kumagai, D. A. Schmitz, M. Singh, A. Eiguren-Fernandez and J. R. Froines (2005). Redox activity of airborne particulate matter at different sites in the Los Angeles Basin, *Env. Res.* **99**, 40–7.
- Zika, R.G., E. S. Saltzman, W. L. Chameides, and D. D. Davis (1982). H₂O₂ levels in rain water collected in South Florida and the Bahama Islands, *J. Geophys. Res.* **87**, 5015–5017.
- Kieber, D. J., B. M. Peake, and N. M. Scully (2003). “Reactive oxygen species in aquatic ecosystems,” in *UV effects in aquatic organisms and ecosystems*, eds E. W. Helbling and H. Zagarese, (Cambridge: The Royal Society of Chemistry), 251–290.
- Tolar, B. B., L. C. Powers, W. Miller, N. J. Wallsgrove, B. N. Popp, and J. T. Hollibaugh (2016). Ammonia oxidation in the ocean can be inhibited by nano molar concentrations of hydrogen peroxide, *Front. Mar. Sci.* **3**, 237.
- Patel, A., and N. Rastogi (2018a). Oxidative potential of ambient fine aerosol over a semi-urban site in the Indo-Gangetic Plain, *Atmos. Environ.* **175**, 127–134.
- Patel, A., and N. Rastogi (2018b). Seasonal variability in chemical composition and oxidative potential of ambient aerosol over a high altitude site in western India, **644**, 1268–1276.

NEUTRALIZATION OF AEROSOL ACIDITY BY AMBIENT AMMONIA: IMPLICATION TO AQUEOUS PHASE SO₂ OXIDATION

A. K. SUDHEER

Geosciences Division, Physical Research Laboratory,
Ahmedabad, Gujarat. – 380 009, India.

KEYWORDS: Aerosol Acidity, Gas-aerosol equilibrium, pH.

INTRODUCTION

Aerosol pH is a fundamental parameter of atmospheric particulates that influence its composition, growth, toxicity and nutrient availability upon deposition to various ecological systems. Sulphate is the strong regulator of aerosol acidity and ubiquitous inorganic component of fine particulate matter, produced by homogeneous and heterogeneous oxidation of SO₂. Though, NO₃⁻ also contribute to the acidic nature of fine particles, since HNO₃ and NH₄NO₃ are volatile/semi-volatile, it tends to partition more towards alkaline coarse particles. NH₃ is the most abundant alkaline gas in the Earth's atmosphere and is the dominant neutralizing trace gas for the acidic aerosol species. Recently it was hypothesized that gaseous ammonia plays a major role in near quantitative neutralization of aerosol acidity, caused by SO₄²⁻ and NO₃⁻ species, which significantly increase the aqueous phase SO₂ oxidation mediated via NO₂ (Wang et al., 2016).



This additional pathway of SO₂ oxidation is proposed to be the missing source for observed excess SO₄²⁻ in North China Plain that was not explained by chemical mechanisms in latest models like WRF-CMAQ (Cheng et al., 2016). This process can substantially contribute to the incorporation of gaseous NH₃ as well as NO₂ to particulate phase, thereby influence the net deposition fluxes of N-species, if the same is applicable globally. Hence, it is important to evaluate the possibility for such pathways in different environmental conditions with varying aerosol composition. The key parameters that control the NO₂ mediated aqueous phase oxidation of SO₂ is aerosol liquid water content and aerosol pH.

In this study, aerosol ionic composition and ambient NH₃ concentration data collected from Kochi, an urban location in west coast in southern India, is used to evaluate the aerosol pH by thermodynamic equilibrium (ISORROPIA-II) model and possible impact on NO₂ mediated heterogeneous oxidation of SO₂ is presented.

METHODS

Ionic composition of aerosol (PM_{2.5}) and associated trace gases, namely, NH₃, HCl and HNO₃ were measured at an urban coastal location in southern India (Kochi) using Ambient Ion monitor coupled to Ion Chromatography (AIM-IC) system. The AIM-IC system provides the data with hourly time resolution (Markovic et al., 2012; Sudheer et al., 2014). In AIM-IC, PM_{2.5} particles were extracted with deionized water using a steam jet collector and injected to two ion chromatographs for cation and anion analysis for aerosol composition. Prior to the steam jet collector, a parallel plate denuder is placed to remove the gaseous components in the sampled air, and the denuder solution was analyzed for cation and anion to obtain the ambient ammonia (NH₃), HCl and HNO₃ concentrations. The overall uncertainty in these measurements is between 10-15 %. This data is used for the estimation of H⁺ ion concentration and aerosol liquid water content with the thermodynamic inorganic equilibrium model ISORROPIA-II (Sudheer and Rengarajan, 2015; Fountoukis and Nenes, 2007). The model was run as a forward problem, using total NH⁺ as the sum of gas phase and particle phase ammonia. For NO₃⁻, and Cl⁻, particulate concentrations were taken as total since the gas phase concentrations were below detection limits. The model output of H⁺ ion concentration in air (H^+_{air}) and aerosol liquid water content is used for calculating aerosol pH.

RESULTS & DISCUSSIONS

Cation to anion ratio, NH₄⁺/SO₄²⁻ ratio or NH₄⁺/(SO₄²⁻+NO₃⁻) ratio are generally used as index for aerosol pH or aerosol acidity in the ambient atmosphere. Sometime H⁺ ion concentrations calculated from the pH of the deionized water extract of aerosol sample are used for the quantitative representation of aerosol pH. But, all these parameters do not consider the chemical equilibrium of these ionic constituents or modulated by large dilution compared to actual pH of deliquescent droplet particle in the air. Hence, we explored the

possibility of elevated pH due to high concentrations of ambient NH_3 as suggested by Wang et al. (2016), using thermodynamic equilibrium model ISORROPIA II.

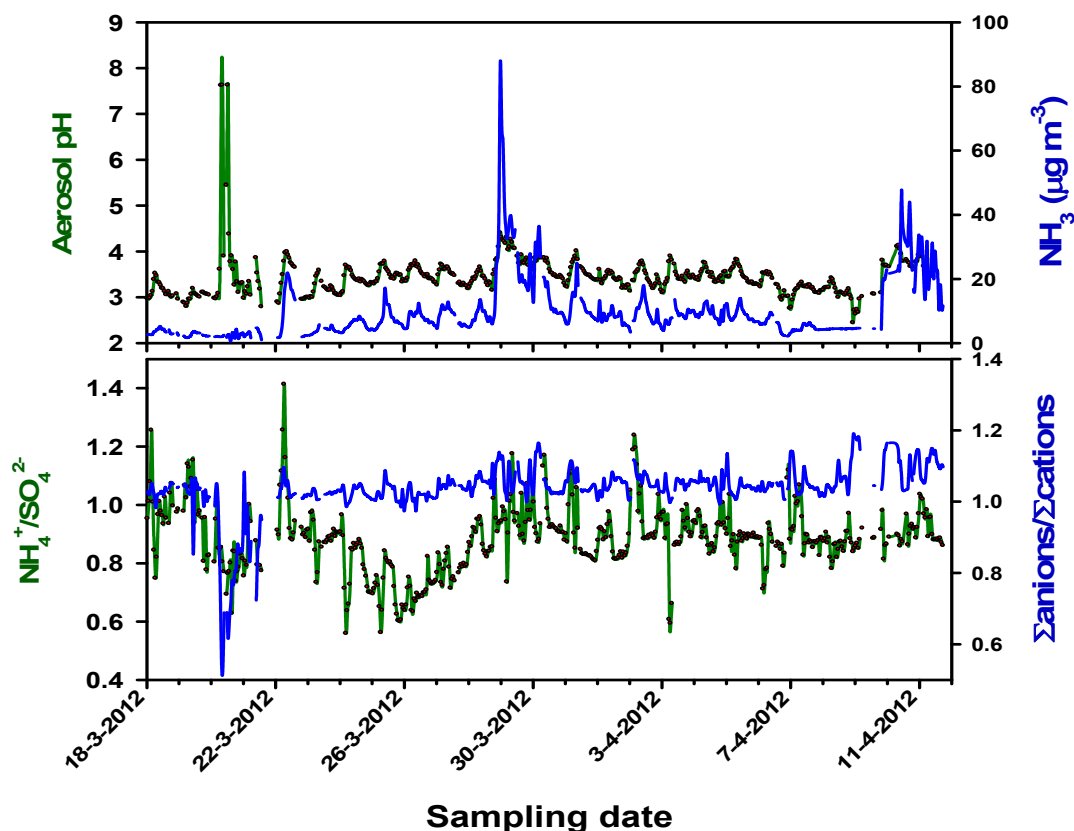


Figure 1. Temporal variation of aerosol pH estimated from thermodynamic equilibrium model and ambient NH_3 concentration along with other aerosol acidity parameters.

Figure 1 depicts the temporal variation of aerosol pH during our study period. In general, the pH was varying between 3 and 4. The elevated pH above 7 was during high levels of crustal elements like Ca^{2+} or Na^+ . The temporal trend of both NH_3 and aerosol pH suggest the variability in ambient NH_3 can influence the pH. But, it may be noted that at highest concentration of NH_3 , but still aerosol pH is less than 5. $\text{NH}_4^+/\text{SO}_4^{2-}$ ratio indicate overall deficiency of ammonia, but it provides misleading trend with respect to aerosol pH. Hence, the neutral or alkaline pH does not prevail in deliquescent particle over the study region and SO_2 oxidation mechanisms proposed and explained by Wang et al. (2016) based on laboratory experiments at pH 7 may not be a significant process for nitrogen incorporation in the particle phase. Guo et al., (2017) reported an analysis of aerosol composition and thermodynamic equilibrium results from the eastern US, Beijing and Xi'an which also suggests that it is very unlikely to attain neutral aerosol pH driven by increased NH_3 in ambient air.

CONCLUSIONS

Neutral or alkaline pH does not prevail in $\text{PM}_{2.5}$ particles over the study region even though ambient NH_3 concentration levels are high. This suggests that SO_2 oxidation process mediated by NO_2 is not a significant pathway over this region.

REFERENCES

Cheng, Y. F., Zheng, G. J., Wei, C., Mu, Q., Zheng, B., Wang, Z. B., Gao, M., Zhang, Q., He, K. B., Carmichael, G., Poschl, U., and Su, H. (2016). Reactive nitrogen chemistry in aerosol water as a source of sulfate during haze events in China. *Science Advances* 2, e1601530 DOI: 10.1126/sciadv.1601530.

Markovic, M. Z., Trevor C. Vanden Boer and Murphy J. G. (2012). Characterization and optimization of an online system for the simultaneous measurement of atmospheric water-soluble constituents in the gas and particle phases. *Journal of Environmental Monitoring* 4: 1872-1884.

Sudheer, A.K., Rengarajan, R., Deka, D., Bhushan, R., Singh, S.K. and Aslam, M.Y. (2014). Diurnal and Seasonal Characteristics of Aerosol Ionic Constituents over an Urban Location in Western India: Secondary Aerosol Formation and Meteorological Influence. *Aerosol and Air Quality Research* 14: 1701–1713. doi: 10.4209/aaqr.2013.09.0288.

Sudheer, A. K. and R. Rengarajan Time-resolved inorganic chemical composition of fine aerosol and associated precursor gases over an urban environment in western India: Gas-aerosol equilibrium characteristics, *Atmospheric Environment* 109 (2015) 217e227

Wang, G., Zhang, R., Gomez, M.E., Yang, L., Levy Zamora, M., Hu, M., Lin, Y., Peng, J., Guo, S., Meng, J., Li, J., Cheng, C., Hu, T., Ren, Y., Wang, Y., Gao, J., Cao, J., An, Z., Zhou, W., Li, G., Wang, J., Tian, P., Marrero-Ortiz, W., Secret, J., Du, Z., Zheng, J., Shang, D., Zeng, L., Shao, M., Wang, W., Huang, Y., Wang, Y., Zhu, Y., Li, Y., Hu, J., Pan, B., Cai, L., Cheng, Y., Ji, Y., Zhang, F., Rosenfeld, D., Liss, P.S., Duce, R.A., Kolb, C.E., Molina, M.J., 2016a. Persistent sulfate formation from London fog to Chinese haze. *Proc. Natl. Acad. Sci. U. S. A.*

BLACK CARBON MIXING STATE CHARACTERISATION OF CLIMATICALLY RELEVANT SIZE AEROSOLS

B. SARANGI, S. RAMACHANDRAN, T. A. RAJESH AND V. K. DHAKER

Physical Research Laboratory, Navrangpura, Ahmedabad, Gujarat – 380009, India.

KEYWORDS: Black carbon, size, mixing state

INTRODUCTION

Black carbon (BC) aerosol is produced by incomplete combustion of fossil fuels and biomass burning (Bond *et al.*, 2004). Black carbon influences the regional air quality and climate. BC is a primary aerosol and it absorbs incoming solar radiation and outgoing terrestrial radiation, which has significant implications to aerosol radiative forcing (Rajesh and Ramachandran, 2018). However, the radiative forcing and the warming effect of BC explicitly depend on its state of mixing (e.g., internally or externally) (Cappa *et al.*, 2012). External mixing (EM), in which each particle assume to be made of either hydrophilic or hydrophobic compounds and the internal mixing (IM) otherwise known as internal core-shell arrangement, in which each particles consists of hydrophobic core coated with hydrophilic shell. Therefore, optical properties of IM BC particle indicate greater absorption than the equivalent EM BC because of the Lensing effect (Bond *et al.*, 2006). BC containing particle are mostly EM and hydrophobic near emission and become IM over time by mixing with hydrophilic species through coagulation and condensation process (Moffet and Prather, 2009; Sarangi *et al.*, 2015). This process regulates the size of the particles and resulting impacts on particle hygroscopicity and optical properties (Cappa *et al.*, 2012; Laborde *et al.*, 2013; Sarangi *et al.*, 2015). Despite extensive research and significant progress achieved in understanding the hygroscopicity and optical properties of BC particles, understanding the role of mixing state in influencing the climate impacts of BC remains incomplete. It is evident that BC once reaches to climatically relevant size (i.e., 50 and 100 nm) influence climate directly or indirectly. However, size resolved BC mixing state is neglected or less investigated.

In this study, we use differential mobility analyser and a single particle soot photometer, to determine the size selective mixing state of BC containing particles over an urban environment in Ahmedabad, India. These measurements provide quantitative insight into the physico-chemical properties of size selected particles linked to its mixing states and help to improve the existing climate model and understanding the optical properties of BC containing aerosols.

METHODS

The experimental setup comprised differential mobility analyzer (DMA, MSP[®]) and a single particle soot photometer (SP2, Droplet Measurement Technologies). DMA is use to measure and segregation the size of the aerosol particles using electrical mobility principle whereas SP2 measures the size distribution, mass concentration and quantifies the mixing state of refractory BC particles using incandescence and scattering techniques. The detailed measurement techniques of DMA and SP2 are discussed elsewhere (Baumgardner *et al.*, 2012; Sarangi *et al.*, 2018). Aerosol particles are aspirated from the rooftop and dried using nafion dryer (< 5% RH). Different dried size (70, 100 and 200 nm) of the particles get selected by the DMA and fed into SP2 at a flow rate of 0.12 L min⁻¹. The detailed experimental setup is illustrated in figure 1.

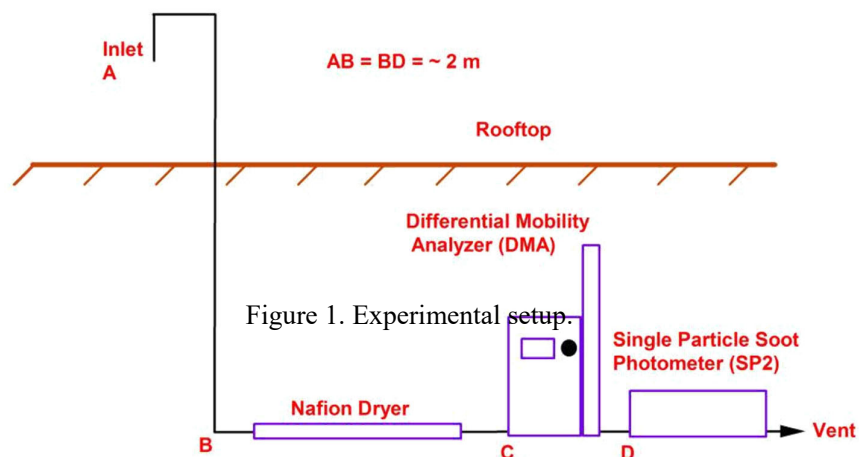


Figure 1. Experimental setup.

RESULTS & DISCUSSIONS

BC mass concentrations for each DMA sized particles are obtained using SP2. The temporal variation of BC mass concentrations for three days (November 30 to December 2, 2017) is shown in figure 2a. It is observed that BC mass concentrations for different particle size show different temporal variations. This difference is attributed to the BC mixing state. For this, we have quantified the mixing state of the particle. Based on the incandescence and scattering signals obtained from SP2 for each DMA sized particle, particles are classified as refractory, nonrefractory and coated type. A typical mixing state with respect to size for aerosol particle is shown in figure 2b. Particles in lower size (70 nm) mostly refractory BC and coated type whereas higher size (200 nm) particles are mostly nonrefractory in nature.

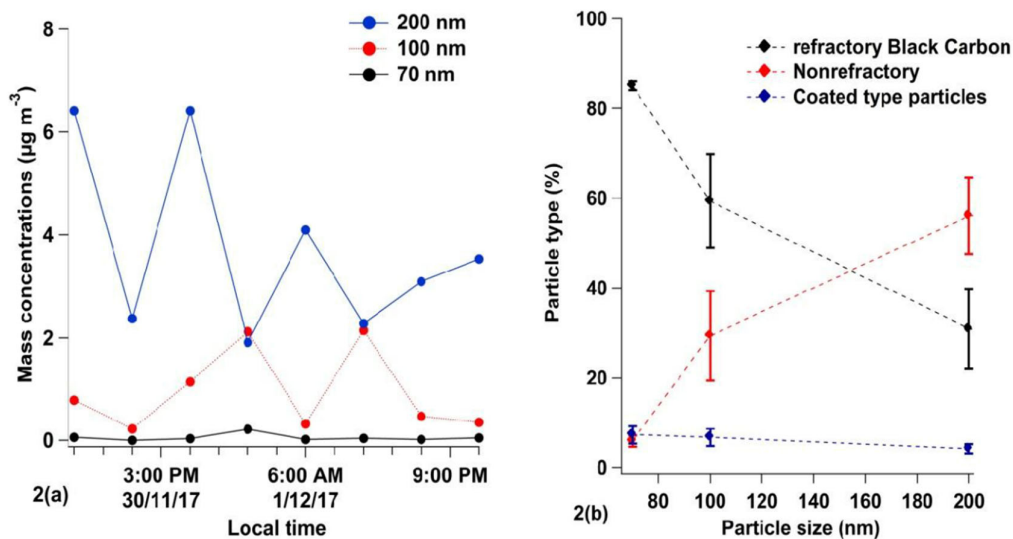


Figure 2(a). Illustrating the temporal trend of DMA sized BC mass concentration and 2(b) showing a typical mixing state of particles observed on November 31st 2017.

CONCLUSIONS

We have designed an experimental setup using differential mobility analyzer and single particle soot photometer to measured the black carbon mass concentration for size segregated (i.e., 70, 100 and 200 nm) aerosol particles. Further, we have quantified the mixing state of the particles. We observed different temporal trend in BC mass concentrations with respect to different size of the particles. The variation in BC mass concentrations with respect to size is attributed to mixing state of the particles. Our observation shows that particles containing refractory BC in lower size are both externally and internally mixed type whereas

higher size particles are mostly nonrefractory externally mixed. Our finding shows that BC mass concentrations depends on the mixing state of the particles and mixing states varies with respect to the size of the particles. These findings are important and have strong implication over regional air quality and global climate. Further, BC mixing states with respect to size information can serve as inputs in climate models for aerosol-cloud-radiation interactions studies.

REFERENCES

Baumgardner, D., Kok, G., and Raga, G. (2004). Warming of Arctic Lower Stratosphere by Light Absorbing Particles, *Geophys. Res. Lett.*, **31**, L06117.

Bond, T.C., Streets, D.G., Yarber, K.F., Nelson, S.M., Woo, J.-H., and Klimont, Z. (2004). A TechnologyBased Global Inventory of Black Carbon and Organic Carbon Emissions from Combustion, *J. Geophys. Res.*, **109**, D14203, doi: 10.1029/2003JD003967.

Bond, T.C., Habib, G., and Bergstrom, R.W. (2006). Limitations in the enhancement of visible light absorption due to mixing state, *J. Geophys. Res.*, **111**, D20211, doi:20210.21029/22006JD007315.

Cappa, C.D., Onasch, T.B., Massoli, P., Worsnop, D.R., Bates, T.S., Cross, E.S., Davidovits, P., Hakala, J., Hayden, K.L., Jobson, B.T., Kolesar, K.R., Lack, D.A., Lerner, B.M., Li, S.M., Mellon, D., Nuaaman, I., Olfert, J.S., Petaja, T., Quinn, P.K., Song, C., Subramanian, R., Williams, E.J., and Zaveri, R.A. (2012). Radiative absorption enhancements due to the mixing state of atmospheric black carbon, *Science*, **337**, 1078–1081.

Laborde, M., Crippa, M., Tritscher, T., Jurányi, Z., Decarlo, P.F., Temime-Roussel, B., Marchand, N., Eckhardt, S., Stohl, A., Baltensperger, U., Prévôt, A. S. H., Weingartner, E., and Gysel, M. (2013). Black carbon physical properties and mixing state in the European megacity Paris, *Atmos. Chem. Phys.*, **13**, 5831–5856, doi:10.5194/acp-13-5831-2013.

Moffet, R.C. and Prather, K.A. (2009). In-situ measurements of the mixing state and optical properties of soot with implications for radiative forcing estimates, *Proc. Natl. Acad. Sci.*, **106**, 11872–11877.

Rajesh, T.A. and Ramachandran, S. (2018). Black carbon aerosol mass concentration, absorption and single scattering albedo from single and dual spot aethalometers: Radiative implications, *J. Aerosol Sci.*, **119**, 77–90.

Sarangi, B., Aggarwal, S.G., and Gupta, P.K. (2015). A Simplified Approach to Calculate Particle Growth Rate Due to Self-Coagulation, Scavenging and Condensation Using SMPS Measurements during a Particle Growth Event in New Delhi, *Aerosol Air Qual. Res.*, **15(1)**, 166–179.

Sarangi, B., Aggarwal, S.G., Gupta, P.K., Kawamura, K., et al. (2018). Nighttime particle growth observed during spring in New Delhi: Evidence for the aqueous phase oxidation of SO₂, *Atmos. Environ.*, **188**, 82–96, <https://doi.org/10.1016/j.atmosenv.2018.06.018>.

DIURNAL VARIABILITY IN CHARACTERISTICS OF WATER-SOLUBLE BROWN CARBON THROUGH ONLINE MEASUREMENTS OVER NEW DELHI

N. RASTOGI¹, R. V. SATISH¹, S. N. TRIPATHI², D. GANGULY³

¹Geosciences Division, Physical Research Laboratory, Ahmedabad, India

²Department of Civil Engineering and Centre for Environmental Science and Engineering, Indian Institute of Technology, Kanpur, India

³Center for Atmospheric Sciences, Indian Institute of Technology, Delhi, India

KEYWORDS: Organic aerosol, absorption coefficient, mass absorption efficiency

INTRODUCTION

Climate forcing by various atmospheric components has been intensely investigated over a last few decades, but significant uncertainties still exist (IPCC, 2013). One of the most significant uncertainties comes from the role of carbonaceous aerosols, including black carbon (BC) and organic carbon (OC). The BC is known as the strongest light-absorbing aerosol over a broad spectral range from ultraviolet (UV) to infra-red region (Bond et al., 2013). On the other hand, OC is treated as purely scattering in most of the climate models. However, recent studies have found a class of light absorbing organics, collectively known as brown carbon (BrC). The BrC is a light-absorbing component of organic carbon (OC) and characterized by an absorption spectrum that smoothly increases from the visible to UV wavelengths (Laskin et al., 2015). Incomplete combustion and smoldering of fossil fuels (FF) and biomass burning (BB) are known to produce primary BrC (Hecobian et al., 2010; Hoffer et al., 2006). There are also evidences based on both ambient and laboratory studies that the secondary BrC chromophore form in the atmosphere through a variety of mechanisms. The climatic significance of BrC through direct radiative forcing (DRF) is currently an important issue. Further, there is a semi-direct effect that causes significant warming/heating of cloud droplets due to the presence of both BC and BrC, which could lead to cloud dissipation/evaporation. Recent global model estimates that atmospheric absorption by BrC ranges from +0.22 to +0.57 W m⁻², which corresponds to 27- 70% of that predicted due to BC (Lin et al., 2014). Despite their importance, the optical properties and chemical composition of BrC are not well characterized, mainly due to measurement limitations (Zhang et al., 2013). BrC studies are scarce over the Indian subcontinent and that too limited to filter-based measurements. High time resolved measurements help in studying detailed characteristics of species under changing sources and meteorological conditions. This study focuses on the temporal and diurnal characteristics of BrC over New Delhi during winter under the influence of various sources (BB, FFB and long-range transport) using online measurements of BrC.

METHODS

The ambient aerosol measurements were carried out at a site located on the campus of Indian Institute of Technology, Delhi (28.4 °N, 77.1°E, 230 m above mean sea level) during 10-January to 28-February, 2018. New Delhi, as a megacity, suffers from the intense pressure of urbanization, industrialization and densely populated regions. High pollutant concentrations also lead to urban and regional haze, and have a deleterious impact on the local ecosystem, crop yield and climate change. During winter, regional BB is among the significant contributors to aerosol loadings at this location. Other sources of pollution in the city include but not limited to are vehicles, bio-fuel, wood and coal burning, industrial activities, etc. Further, meteorological conditions in winter (low wind speeds and shallow boundary layer heights) favors the accumulation of pollutants over the region. The study period was characterized by high RH (up to 100%) and low-temperature conditions (lowest temperature: approximately 6 °C).

The BrC absorption spectra (300-700 nm) and WSOC mass concentration in ambient PM_{2.5} have been measured semi-continuously using an assembled system (PILS-LWCC-TOC) consists of a particle-into-liquid sampler (PILS, Model ADI 2081, Applicon Analytical) coupled to portable UV-vis spectrophotometer

(model USB-4000, Ocean Optics) with a liquid waveguide capillary cell (LWCC, World Precision Instrument, 2m path length) and total organic carbon (TOC, Sievers 900 Portable with Turbo, GE Analytical Instruments) analyser (Fig. 1). The PILS provide water-extract of ambient aerosol in real-time, which is directed through an in-line syringe filter to the LWCC where the absorbance of water extract of aerosol is measured every minute by portable UV-vis spectrophotometer (Satish et al., 2017). The outlet of LWCC is connected to the TOC analyser which measure WSOC with a 4 min integration time. Along with BrC measurements, black carbon (BC) as well as trace gases like carbon monoxide (CO) and nitrogen oxides ($\text{NO}_x = \text{Nitrogen oxide-NO} + \text{Nitrogen dioxide-NO}_2$) were measured using seven wavelengths Aethalometer, and CO and NO_x analysers respectively.

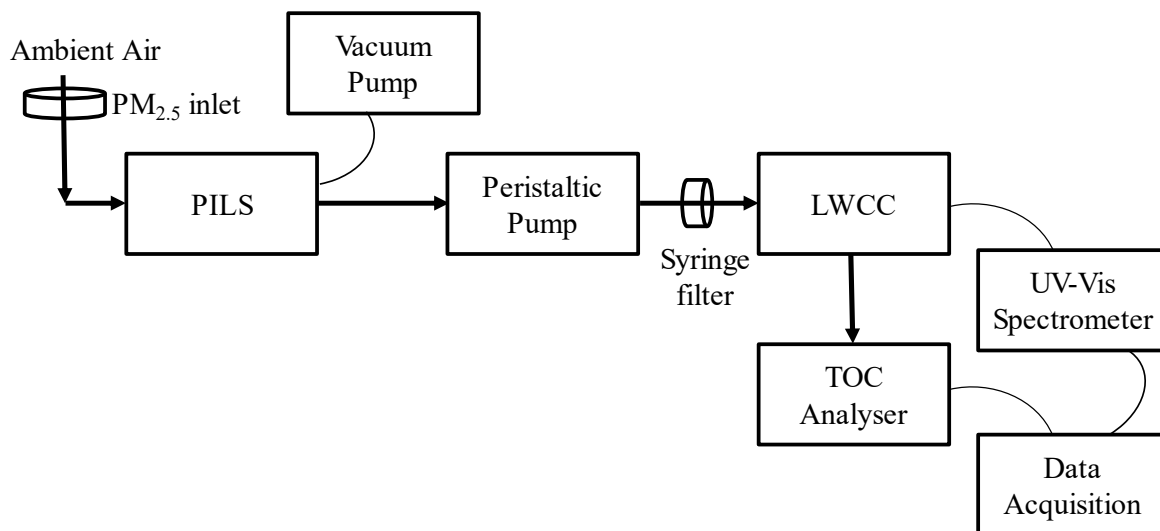


Fig. 1. Schematic diagram of assembled PILS-LWCC-TOC system used for online the measurements of BrC over New Delhi. The figure is not to scale

BrC calculations:

The light absorption coefficient at a given wavelength ($b_{abs,\lambda}$) was calculated as follows:

$$b_{abs,\lambda} = (A_{\lambda} - A_{700}) * \left(\frac{V_l}{V_a * l} \right) * \ln 10 \quad (1)$$

Where A_{λ} is the absorbance at a given wavelength, A_{700} is the absorbance at 700 nm to account for any baseline drift, V_l is the PILS liquid sample flow rate (0.7 mL min^{-1}), and V_a is air sampling flow rate (16.7 L min^{-1}), and ' l ' is the absorbing path length (2 m).

Using the $b_{abs,365}$ (Mm^{-1}) and WSOC ($\mu\text{g m}^{-3}$), mass absorption efficiency (MAE, $\text{m}^2 \text{ g}^{-1}$) of WSOC at 365 nm was calculated as follows:

$$MAE = \frac{b_{abs,365}}{WSOC} \quad (2)$$

MAE is a key parameter that describes the light absorbing ability of all the chromophores present in aerosol water extract. In this study, absorption coefficient at 365 nm ($b_{abs,365}$) was chosen as a general measure of the absorption by BrC, similar to several reported studies in literature.

RESULTS & DISCUSSIONS

A considerable diurnal and day-to-day variability was observed in WSOC concentration as well as in $b_{\text{abs}_365\text{nm}}$ values. This variability is attributable to various factors such as the dominance of specific sources (BB, FFB) and atmospheric processes. Concentrations of BC and gaseous species (CO, NO_x) also exhibited large variability, broadly similar to WSOC and $b_{\text{abs}_365\text{nm}}$. The photochemical secondary organic aerosol (SOA) formation was evident during morning hours whereas enhancement during late evening/night hours is attributed to both primary emission and secondary formation of WSOC. However, $b_{\text{abs}_365\text{nm}}$ showed high concentrations throughout the night and morning hours, which could be attributed to primary emission due to heavy-duty vehicles in the night hours. Further, the variability in $b_{\text{abs}_365\text{nm}}/\text{CO}$ ratio (a measure of secondary BrC) also suggest that secondary BrC was significant.

WSOC exhibited a strong correlation with b_{abs_365} , suggesting the presence of a significant but variable fraction of water-soluble chromophores. Further, BrC showed a strong diurnal variability due to variability in their major sources and meteorological conditions. Diurnal variability in the ratios of $b_{\text{abs}_405}/b_{\text{abs}_365}$, $b_{\text{abs}_420}/b_{\text{abs}_365}$, $b_{\text{abs}_450}/b_{\text{abs}_365}$, $b_{\text{abs}_490}/b_{\text{abs}_365}$ and $b_{\text{abs}_550}/b_{\text{abs}_365}$ suggests that BrC composition was variable throughout a day (Satish et al., 2017). The variability was ascribed to photo-bleaching/volatilization of BrC and/or rising boundary-layer height.

CONCLUSIONS

Wintertime temporal and diurnal characteristics of BrC were studied over New Delhi under the influence of various sources using the online measurements of BrC along with other species. The photochemical secondary organic aerosol (SOA) formation was evident during morning hours whereas enhancement during late evening/night hours was attributable to both primary emission and secondary formation of WSOC. The BrC ($b_{\text{abs}_365\text{nm}}$) showed high concentrations throughout the night and morning hours, which could be attributed to primary emission due to heavy-duty vehicles. Highly absorbing BrC were often found to be associated with primary emission. Observed BrC was composed of both primary and secondary light absorbing species, and they showed a strong diurnal variability due to changes in their major sources and meteorological conditions. Such studies are important in assessing the climatic effects of BrC on regional and global scale.

REFERENCES

- Bond, T. C., Doherty, S. J., Fahey, D. W., Forster, P. M., Berntsen, T., Deangelo, B. J., et al. (2013). Bounding the role of black carbon in the climate system: A scientific assessment. *Journal of Geophysical Research Atmospheres*, 118(11), 5380–5552. <https://doi.org/10.1002/jgrd.50171>
- Hecobian, A., Zhang, X., Zheng, M., Frank, N., Edgerton, E. S., & Weber, R. J. (2010). Water-soluble organic aerosol material and the light-absorption characteristics of aqueous extracts measured over the Southeastern United States. *Atmospheric Chemistry and Physics*, 10(13), 5965–5977. <https://doi.org/10.5194/acp-10-5965-2010>
- Hoffer, A., Gelencsér, A., Guyon, P., Kiss, G., Schmid, O., Frank, G. P., et al. (2006). Optical properties of humic-like substances (HULIS) in biomass-burning aerosols. *Atmospheric Chemistry and Physics*, 6(11), 3563–3570. <https://doi.org/10.5194/acp-6-3563-2006>
- IPCC. (2013). Summary for Policymakers. *Climate Change 2013: The Physical Science Basis. Contribution of Working Group I to the Fifth Assessment Report of the Intergovernmental Panel on Climate Change*, 33. <https://doi.org/10.1017/CBO9781107415324>
- Laskin, A., Laskin, J., & Nizkorodov, S. A. (2015). Chemistry of Atmospheric Brown Carbon. *Chemical Reviews*, 115(10), 4335–4382. <https://doi.org/10.1021/cr5006167>

Lin, G., Penner, J. E., Flanner, M. G., Sillman, S., Xu, L., & Zhou, C. (2014). Radiative forcing of organic aerosol in the atmosphere and on snow: Effects of SOA and brown carbon. *Journal of Geophysical Research: Atmospheres*, *119*(12), 7453–7476. <https://doi.org/10.1002/2013JD021186>

Lin, P., Bluvshstein, N., Rudich, Y., Nizkorodov, S. A., Laskin, J., & Laskin, A. (2017). Molecular Chemistry of Atmospheric Brown Carbon Inferred from a Nationwide Biomass Burning Event. *Environmental Science & Technology*, *acs.est.7b02276*. <https://doi.org/10.1021/acs.est.7b02276>

Satish, R. V., Shamjad, P. M., Thamban, N. M., Tripathi, S. N., & Rastogi, N. (2017). Temporal Characteristics of Brown Carbon over the Central Indo-Gangetic Plain. *Environmental Science & Technology*, *acs.est.7b00734*. <https://doi.org/10.1021/acs.est.7b00734>

Zhang, X., Lin, Y. H., Surratt, J. D., & Weber, R. J. (2013). Sources, composition and absorption exponent of light-absorbing organic components in aerosol extracts from the los angeles basin. *Environmental Science and Technology*, *47*(8), 3685–3693. <https://doi.org/10.1021/es305047b>

CLOUD DETECTION USING IMAGE PROCESSING

MALAIDEVAN P., RAJESH T. A. AND S. RAMACHANDRAN

Space & Atmospheric Sciences Division, Physical Research Laboratory, Ahmedabad,
Gujarat – 380009

(malaidevanp@prl.res.in)

KEYWORDS: Cloud, Sky, Image processing, Piecewise analysis

INTRODUCTION

Clouds play a major role in Earth's climate. It influences the Earth-atmosphere system by interacting with the both incoming solar shortwave radiation and outgoing terrestrial longwave radiation. Clouds absorb and re-emit longwave terrestrial radiation to space (the greenhouse effect) and scatter the shortwave solar radiation in the visible back to space (the albedo effect). The columnar aerosol measurements from the Earth's surface and satellite instruments are used for atmospheric and climate research (IPCC, 2013). The clouds exist in the line of sight between the point of observation at the Earth's surface and Sun significantly influence the columnar aerosol observation. The aim of the present study is to quantify the sky condition for cloud detection using image processing technique for the better estimation of the columnar properties of aerosols.

METHODOLOGY

The cloud detection software is based on a pattern recognition algorithm developed for the detection of clouds in the visible spectra. The primary objective of the work is to classify the sky conditions as (1) clear, (2) partially cloudy, and (3) cloudy. The high resolution vandal proof fish-eye IP camera is the heart of the present work. The hardware schematic of the work is illustrated in Figure 1. The camera is placed at the terrace of the 8-floor building to acquire the sky image. A NI Labview based data acquisition application is being developed to acquire the sky images from the camera at an interval of 15 minutes.

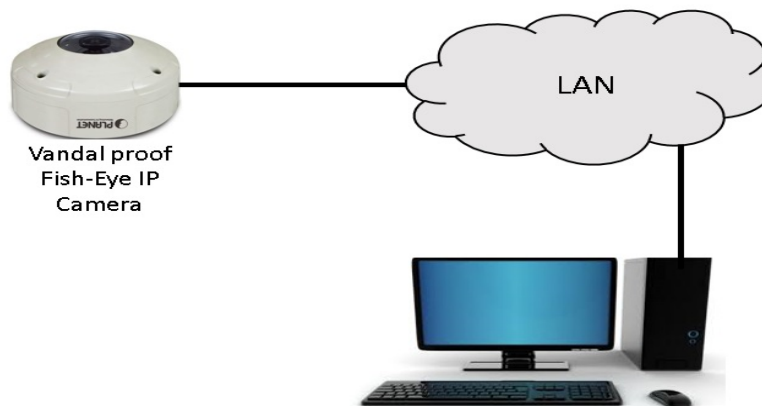


Figure 1: Schematic of the automatic sky image acquisition system.

The acquired sky image is further undergoes intensity and area analysis, and piecewise analysis using MATLAB. The following image processing parameters were utilised in order to quantify the sky condition (1) *Total Intensity*, It is the sum of all the $m \times n$ pixels, in the particular R/G/B component selected, (2) *Sun Intensity*, It is the sum of all the pixels whose value is equal to 255, (3) *Sun Intensity Percentage (SIP)*, It is the percent of Sun's intensity contribution to the total intensity, (4) *Average Intensity*, It the average value of all the pixels in the corresponding R/G/B component, (5) *Sun Area*, It is the number of pixels, which have the intensity value of the Sun, viz., 255, (6) *Sun Area Percentage (SAP)*, It is the percent of Sun's pixels

over the total no. of pixels in the image, and (7) *Piecewise analysis*, In this Analysis, we are dividing the image in to array of smaller images and studying the following properties array (piece) wise: Mean and Standard Deviation. These parameters have been implemented in the MATLAB code and tested for images taken at various times of the day.

As a case study, we will discuss the analysis of the sky image (Figure 2) acquired from the roof of PRL Main Building on 6th June 2018 @ 13:00 hrs. The computed parameters are (1) *Total Intensity*, 1.79E09 (2) *Sun Intensity*, 1.13E8, (3) SIP, 6.3%, (4) *Average Intensity*, 138.5, (5) *Sun Area*, 441374 pixels, (6) *Sun Area Percentage (SAP)*, 3.4%. The Piecewise analysis with the mean and standard deviation are illustrated in Figure 2 (right).

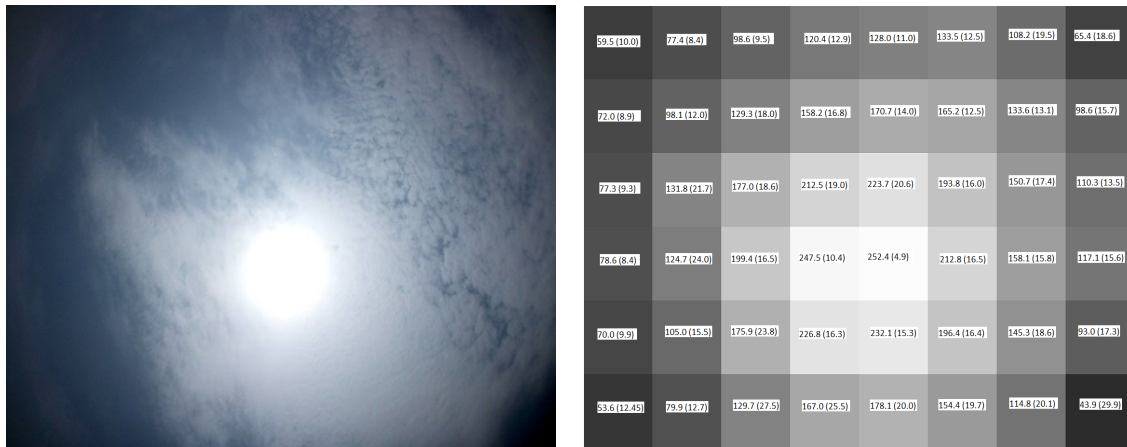


Figure 2: The sky image (left) on 6th July 2018 at 13:00 hrs and its piecewise analysis (right) indicating the mean and standard deviation.

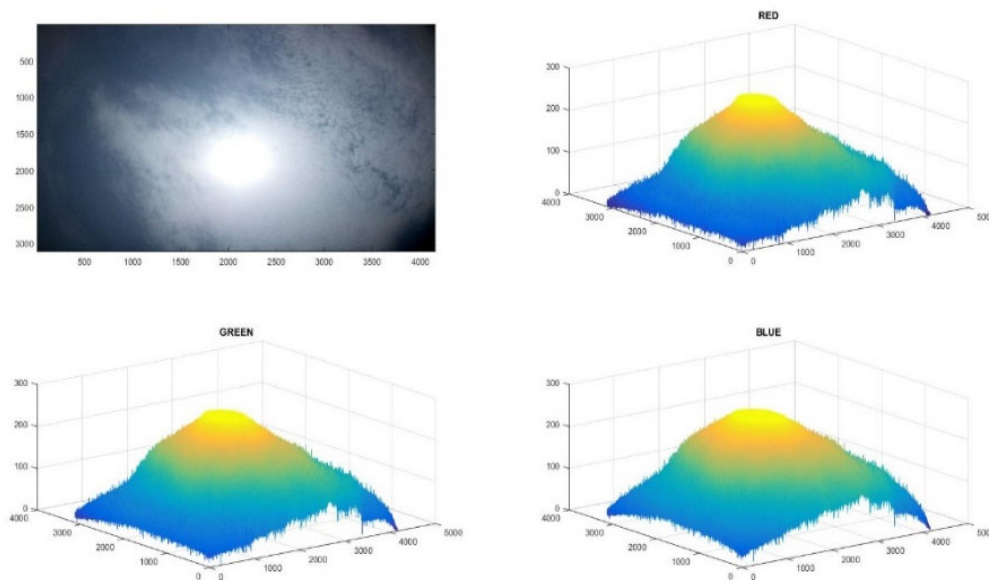


Figure 3: RGB components of the sky image on 6th July 2018 at 13:00 hrs

Every image has 3 basic color components namely Red, Green, Blue [RGB]. For the calculation of the various parameters above, we used the ‘B’ (Blue) component only. Figure 3 illustrates the RGB components of the sky image on 6th July 2018 at 13:00 hrs. The R, G, B values separately have different values, but they follow *almost* the same shape in the mesh 3-D graph. In addition, the region where the Sun is located is flat

at the top because the highest intensity value any pixel can reach is 255. The Sun is the brightest (white) object in the sky (Figure 2) with intensity value 255. The Sky is typically observed as blue colour to the observer from the Earth's surface due to scattering phenomenon (Jiebo and Stephen, 2002). The blue colour of the Sky has various spectral components and the most probable nine components are examined for the present study.

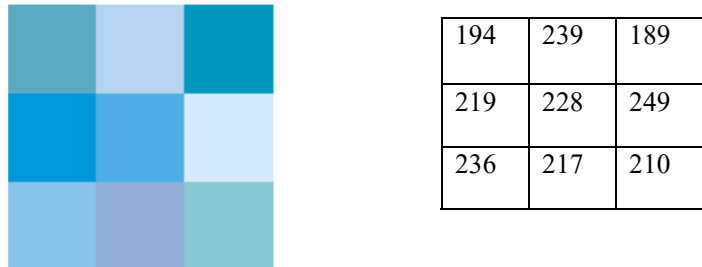


Figure 4: Sky Blue variants and their respective Blue intensities (Maerz and Paul, 1930)

The average intensity of the Sky blue turns out to be 220. Sun area percent (SAP) is $\sim 2.5\%$. The average intensity of the image with the Sun and the sky background was estimated to be 221. The intensity gradient examined for a more accurate prediction of sky non-ideality. From this a “*Cloud Factor*” was determined. From its value, a clear sky condition can be differentiated from partially cloudy condition. Various sky conditions were analysed and a threshold for discriminating them was observed as follows (1) Cloudy; SAP should be $< 2\%$, (2) Partially cloudy; cloud factor should be > 45 units, and (3) Clear sky; cloud factor should be < 45 units.

The various sources of error in the estimation of sky condition are owing to (1) Fish eye lens blackens out the edges and corners of the image, which reduces the average intensity value to a great scale, (2) intensity gradient; the image and piecewise analysis reveal that the brightest object in the frame is the sun and the darkest are the frame borders and there is a monotonous decrease in the intensity value. The cloud detection system can be used along with collocated sun photometer in order to quantify the sky condition which is required to reduce the uncertainty in the aerosol columnar properties.

SUMMARY

The quantitative and qualitative study of cloud pictures was carried out and analysed for the cloud content pixel-wise. The Experiment was carried out physically using a Vandal-proof fish-eye IP camera to acquire the sky image from an 8-floor building. An elaborate study of the captured images was done and the sky conditions (1) clear, (2) partially cloudy, and (3) cloudy were classified based on the study.

REFERENCES

IPCC, 2013: Climate Change 2013: The Physical Science Basis. Contribution of Working Group I to the Fifth Assessment Report of the Intergovernmental Panel on Climate Change [Stocker, T.F., D. Qin, G.-K. Plattner, M. Tignor, S.K. Allen, J. Boschung, A. Nauels, Y. Xia, V. Bex and P.M. Midgley (eds.)].

Cambridge University Press, Cambridge, United Kingdom and New York, NY, USA, 1535 pp, doi:10.1017/CBO9781107415324.

Maerz and Paul (1930) *A Dictionary of Color*, McGraw-Hill.

Jiebo Luo and Stephen P. Etz (2002) A Physical Model-Based Approach to Detecting Sky in Photographic Images, IEEE Transactions on Image Processing (Volume: 11, Issue: 3, Mar 2002).

IMPACTS OF DUST-ICE-CLOUD INTERACTIONS ON PRECIPITATION VARIABILITY

PIYUSHKUMAR N. PATEL¹, TAKURO MICHIBATA², RITESH GAUTAM³, HARISH GADHAVI¹

¹Space & Atmospheric Science Division, Physical Research Laboratory, India

²Research Institute for Applied Mechanics, Kyushu University, Japan

³Environmental Defense Fund, Washington, DC, USA

KEYWORDS: Aerosol-cloud interaction, dust-ice-cloud interaction, precipitation, dynamical feedback

INTRODUCTION

Mineral dust significantly perturbs hydrological and energy cycles of Earth's climate by modifying cloud microphysics and radiation budget. Although recent studies suggest a positive radiative feedback of mineral dust on precipitation variability during the Indian Summer Monsoon (ISM), the various mechanisms and feedback processes remain poorly understood. Here we investigate dust-induced changes in ice-cloud microphysics and precipitation over the ISM region, using an integrated set of year-11 multi-satellite observations and reanalysis datasets. To examine the dust-cloud-precipitation interaction and its meteorological dependency, we segregated the satellite-observed parameters into two groups with the likelihood that: (1) dust interacts with ice cloud (DII); (2) dust does not interact with ice clouds (DNI), using a thresholding analysis centered on dust in the vicinity of ice clouds based on CALIPSO observations. We show that elevated dust frequency is associated with significantly increased small ice particle concentrations in clouds observed at warmer temperatures due to heterogeneous nucleation in the thin ice-cloud regimes. On the other hand, we find that the role of dust-induced cloud invigoration in thick ice-cloud regimes is likely responsible for the further development of ice-clouds in the DII case. Additionally, the positive IWP susceptibility is greater in strong updraft regime with more humid conditions via more effective IN production. The positive IWP susceptibility further results in a positive response of precipitation intensity to AOD in an updraft regime. This "microphysical-dynamical interaction" will lead to a negative feedback, which mitigates (buffers) the aerosol effects due to enhanced wet scavenging. These observational-derived process-level understandings of dust-induced modification of clouds and precipitation variability underscore the importance of incorporating regime dependent dust-ice cloud-precipitation interactions into numerical models for more accurate climate simulations.

METHODS

Here we use an integrated set of 11-years (2006-2016) of multi-satellite observations and reanalysis data to investigate dust-induced changes in ice-cloud properties and precipitation variability during June to September over the Indian Summer Monsoon (ISM) region ($73-85^{\circ}E, 19-23^{\circ}N$). The analysis used to identify the dust and ice-cloud layers based on CAD (Cloud-Aerosol Discrimination) score" (*Liu et al., 2009*) and "Feature Classification Flags" given in CALIPSO level 2 5-km layer products (*Vaughan et al., 2009*). Once the dust and ice-cloud layers are identified, we segregated the satellite-observed parameters into two groups with the likelihood that: (1) dust interacts with ice-cloud (DII); (2) dust does not interact with ice-clouds (DNI), using a thresholding analysis based on the vicinity of dust in ice-clouds. Here, the dust and ice-cloud layers are considered well separated if the vertical distance between the top of the lower layer and bottom of the higher layer exceeds 200 meters. These cases are considered in the DNI group. On the other hand, when this vertical distance is less than 200 meters, it is assumed that the dust and ice-cloud layers are interacting and considered in the DII group. Additionally, ice-cloud properties (i.e. Cloud Effective Temperature (CET), Ice Particle Radius (IPR) and Ice Water Path (IWP) are used from CERES Single Scanner Footprint (SSF) Level 2 retrievals (*Smith et al., 2012*). These datasets were collocated in space and time to ensure that the nearest CERES pixel matchup selected with each CALIPSO footprint. Finally, we used precipitation data from the TRMM 3B42v7 merged precipitation product with spatial resolution of $0.25^{\circ} \times 0.25^{\circ}$ (*Huffman et al., 2007*). To evaluate the feedback of large-scale dynamics on dust-

ice-cloud-precipitation interactions, we analyse a number of meteorological variables from the ECMWF ERA Interim reanalysis product with $0.75^\circ \times 0.75^\circ$ and 3-hr resolutions.

RESULTS & DISCUSSIONS

We examine the dependency of ice water path (IWP) susceptibility (IWP response for AOD perturbations; defined as $d \ln(IWP)/d \ln(AOD)$) on vertical velocity at 500 hPa ($\omega_{500\text{hPa}}$) as a function of cloud effective temperature (CET) as shown in **Fig.-1**. A positive IWP susceptibility in DII is found under unstable conditions (**Fig.-1a**) because of the efficient aerosol nucleation and ice production (e.g. Sassen et al., 2003). It is interesting that there is also a positive IWP susceptibility for DII even in less favourable conditions ($\omega_{500\text{hPa}} > 0$) at warmer temperatures, which indicates the microphysical impact of dust. In this scenario, elevated dust-induced smaller ice-nuclei increase the cloud lifetime by reducing coalescence-collision efficiency, resulting in a positive response of IWP to an increased aerosol loading. In contrast, the negative IWP susceptibility at colder temperatures (i.e. high altitude) with less favourable meteorological conditions indicates that the dust-induced local heating near to cloud reduces the ice-cloud formation by evaporating the clouds in presence of lower RH (Hansen et al., 1997) and hence modifies the radiative forcing (Choobari et al., 2014). The positive susceptibility is dominant in the favourable meteorological conditions ($\omega_{500\text{hPa}} < 0$) at warmer temperatures for DII, while relatively less positive susceptibility can be seen in colder temperatures. This means that the dust aerosols tend to nucleate ice clouds at warmer CET (i.e. lower altitude) for aerosol perturbations, which is consistent with previous case study (Min & Li, 2010). This is the special feature appeared only in DII (**Fig.-1a** and **1c**), which strongly support the importance of dust aerosols in meteorological roles therein. From these results, we hypothesize that the cloud system response in ISM can be explained significantly by the dust-induced cloud invigoration depending upon the cloud geometrical scale and dynamical (thermodynamical) regime resulting in the consequent precipitation.

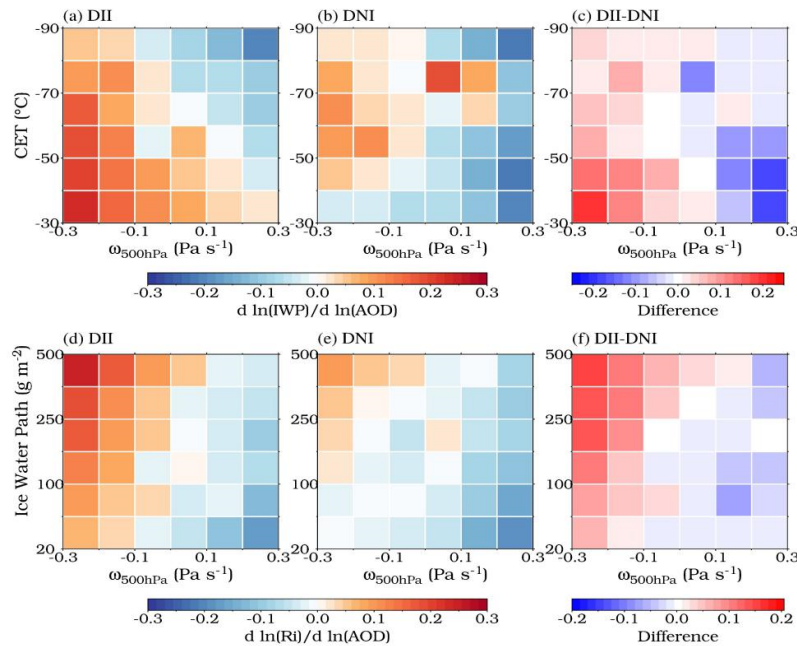


Figure 1. (a-c) Susceptibility matrix of the IWP response to AOD ($d \ln(IWP)/d \ln(AOD)$) as a function of CET and vertical velocity at 500 hPa ($\omega_{500\text{hPa}}$) for DII, DNI and the difference between DII and DNI, respectively. (d-f) Susceptibility matrix of the precipitation intensity (R_i) response to AOD ($d \ln(R_i)/d \ln(AOD)$) as a function of IWP and $\omega_{500\text{hPa}}$ for DII, DNI, and the difference of $d \ln(R_i)/d \ln(AOD)$ between DII and DNI, respectively.

Here we further investigate the precipitation susceptibility (defined as $d \ln(R_i)/d \ln(AOD)$, where R_i is precipitation intensity) as a function of IWP and $\omega_{500\text{hPa}}$, for both DII and DNI cases (Fig.-1d-f). Precipitation

susceptibility is often used to discuss the aerosol-induced precipitation modulation in warm clouds (Feingold & Siebert, 2009; Jiang et al., 2010; Sorooshian et al., 2009), but it is a great challenge to extend this analysis to ice-clouds whose microphysical behaviour will be much more complex (Glassmeier & Lohmann, 2016). In the traditional cloud lifetime hypothesis, an onset of precipitation is inhibited for incremental changes in aerosols due to less efficient collision-coalescence (Albrecht, 1989), which means negative value of $d \ln(R_i)/d \ln(AOD)$. It is therefore reasonable that the negative susceptibility is observed in almost regimes except for top-left region in the matrix, especially for DNI (Fig.-1e). This top-left regime will correspond to a larger IWP with stronger updraft regime, where aerosols ingested into the clouds operate to enhance the precipitation. This can be interpreted as the signal of the cloud invigoration (Rosenfeld, et al., 2014; Koren et al., 2010), which deepen the consequent precipitation. It is noteworthy that the positive susceptibility of precipitation variability is more evident in DII than DNI. Furthermore, the positive susceptibility is observed even in the small IWP under an updraft regime in DII case (Fig.-1d). These characteristics in other words, show that the dust aerosols simulate the onset of precipitation effectively under unstable environment. This does not contradict to prior study based on observations and modelling studies (Feingold et al., 1999; Jung et al., 2015; Levin et al., 2005; Vinoj et al., 2014), which showed a promotion of the precipitation initiation by giant CCN such the sea-salt and mineral dust aerosols.

Finally, we summarize the feedback processes for aerosol perturbations, based on the findings. Dust aerosols serve smaller ice crystals by acting as very efficient IN (Levin et al., 2005). The atmospheric instability and enhanced ice-cloud production by dust-induced modulation can enhance the precipitation via cloud invigoration (Stevens & Feingold, 2009; Koren et al., 2010; Rosenfeld et al., 2014). This provides negative feedback to the system and buffers the aerosol perturbations due to efficient wet scavenging.

Unfortunately, current global climate models (GCMs) cannot resolve such the microphysics-dynamics interactions within the subgrid-scale phenomena (Malavelle et al., 2017; Michibata et al., 2016; Mülmenstädt & Feingold, 2018). Given that GCMs are missing the bidirectional response of consequent precipitation to aerosol perturbations, aerosol effects in GCMs will be much more overestimated (Wang et al., 2012; Quaas et al., 2009) than that in the real atmosphere. We hope that the process-level understandings performed in the present paper will be a useful benchmark and thus improve the discrepancy between models and observations.

SUMMARY

Precipitation susceptibility binning by IWP also depends upon the updraft regime only in DII case. Stronger updraft enhances dust-induced cloud invigoration, and resulting in precipitation intensity for DII case, whereas DNI case shows coherent inhibition of precipitation. The cloud system response in ISM will be affected significantly by the dust-ice cloud interactions, which links to the cloud geometrical scale and (thermo-)dynamical regime resulting in the consequent precipitation. The both increase and decrease responses of hydrometeor water path and precipitation rate to aerosol perturbations is fundamentally related to buffering morphology (Rosenfeld et al., 2014; Stevens & Feingold, 2009; Wood, 2012). The dust-induced enhancement of precipitation will lead to insert a negative feedback into the aerosol-cloud interactions due to enhancement of wet scavenging of aerosols, which mitigates aerosol effects on clouds and precipitation. However, current GCMs do not have such a “bidirectional” precipitation responses to aerosols because of their coarse spatiotemporal resolution as well as lack of parameterization (Michibata et al., 2016). The observation based process-level analysis presented in this study will assist in understanding not only the aerosol-monsoon interactions but also the discrepancy between numerical models and observations.

ACKNOWLEDGEMENTS

This work is supported by Physical Research Laboratory (PRL), Department of Space, Government of India. The authors would like to express their gratitude to the CALIPSO, CERES, CloudSat, MODIS and TRMM science teams for the provision of publicly available datasets. We also thank ECMWF for providing ERA-

Interim reanalysis data in our work. Authors would like to thank their respective families for their continuous motivations.

REFERENCES

Albrecht, B. A. (1989). Aerosols, cloud microphysics, and fractional cloudiness. *Science*, 245(4923), 1227–1230. <https://doi.org/10.1126/science.245.4923.1227>

Choobari, O. A., Zawar-Reza, P., & Sturman, A. (2014). The global distribution of mineral dust and its impacts on the climate system: A review. *Atmospheric Research*. <https://doi.org/10.1016/j.atmosres.2013.11.007>

Feingold, G., Cotton, W. R., Kreidenweis, S. M., & Davis, J. T. (1999). The Impact of Giant Cloud Condensation Nuclei on Drizzle Formation in Stratocumulus: Implications for Cloud Radiative Properties. *Journal of the Atmospheric Sciences*, 56(24), 4100–4117. [https://doi.org/10.1175/1520-0469\(1999\)056<4100:TIOGCC>2.0.CO;2](https://doi.org/10.1175/1520-0469(1999)056<4100:TIOGCC>2.0.CO;2)

Feingold, G., & Siebert, H. (2009). *Cloud-Aerosol Interactions from the Micro to the Cloud Scale*. MIT Press, Cambridge, Mass, 319–338.

Glassmeier, F., & Lohmann, U. (2016). Constraining precipitation susceptibility of warm, ice- and mixed-phase clouds with microphysical equations. *Journal of the Atmospheric Sciences*, 73, JAS-D-16-0008.1. <https://doi.org/10.1175/JAS-D-16-0008.1>

Hansen, J., Sato, M., & Ruedy, R. (1997). Radiative forcing and climate response. *Journal of Geophysical Research: Atmospheres*, 102(D6), 6831–6864. <https://doi.org/10.1029/96JD03436>

Huffman, G. J., Bolvin, D. T., Nelkin, E. J., Wolff, D. B., Adler, R. F., Gu, G., ... Stocker, E. F. (2007). The TRMM Multisatellite Precipitation Analysis (TMPA): Quasi-Global, Multiyear, Combined-Sensor Precipitation Estimates at Fine Scales. *Journal of Hydrometeorology*, 8(1), 38–55. <https://doi.org/10.1175/JHM560.1>

Jiang, H., Feingold, G., & Sorooshian, A. (2010). Effect of Aerosol on the Susceptibility and Efficiency of Precipitation in Warm Trade Cumulus Clouds. *Journal of the Atmospheric Sciences*, 67(11), 3525–3540. <https://doi.org/10.1175/2010JAS3484.1>

Jung, E., Albrecht, B. A., Jonsson, H. H., Chen, Y. C., Seinfeld, J. H., Sorooshian, A., ... Russell, L. M. (2015). Precipitation effects of giant cloud condensation nuclei artificially introduced into stratocumulus clouds. *Atmospheric Chemistry and Physics*, 15(10), 5645–5658. <https://doi.org/10.5194/acp-15-5645-2015>

Koren, I., Remer, L. A., Altaratz, O., Martins, J. V., & Davidi, A. (2010). Aerosol-induced changes of convective cloud anvils produce strong climate warming. *Atmospheric Chemistry and Physics*, 10(10), 5001–5010. <https://doi.org/10.5194/acp-10-5001-2010>

Levin, Z., Teller, A., Ganor, E., & Yin, Y. (2005). On the interactions of mineral dust, sea-salt particles, and clouds: A measurement and modeling study from the Mediterranean Israeli Dust Experiment campaign. *Journal of Geophysical Research D: Atmospheres*, 110(20), 1–19. <https://doi.org/10.1029/2005JD005810>

Liu, Z., Vaughan, M., Winker, D., Kittaka, C., Getzewich, B., Kuehn, R., ... Hostetler, C. (2009). The CALIPSO lidar cloud and aerosol discrimination: Version 2 algorithm and initial assessment of performance. *Journal of Atmospheric and Oceanic Technology*, 26(7), 1198–1213. <https://doi.org/10.1175/2009JTECHA1229.1>

Malavelle, F. F., Haywood, J. M., Jones, A., Gettelman, A., Clarisse, L., Bauduin, S., ... Thordarson, T. (2017). Strong constraints on aerosol–cloud interactions from volcanic eruptions. *Nature*, 546(7659), 485–

491. <https://doi.org/10.1038/nature22974>

Michibata, T., Suzuki, K., Sato, Y., & Takemura, T. (2016). The source of discrepancies in aerosol-cloud-precipitation interactions between GCM and A-Train retrievals. *Atmospheric Chemistry and Physics*, 16(23), 15413–15424. <https://doi.org/10.5194/acp-16-15413-2016>

Min, Q., & Li, R. (2010). Longwave indirect effect of mineral dusts on ice clouds. *Atmospheric Chemistry and Physics*, 10(16), 7753–7761. <https://doi.org/10.5194/acp-10-7753-2010>

Mülmenstädt, J., & Feingold, G. (2018). The Radiative Forcing of Aerosol–Cloud Interactions in Liquid Clouds: Wrestling and Embracing Uncertainty. *Current Climate Change Reports*, 4(1), 23–40. <https://doi.org/10.1007/s40641-018-0089-y>

Quaas, J., Ming, Y., Menon, S., Takemura, T., Wang, M., Penner, J. E., ... Schulz, M. (2009). Aerosol indirect effects in a general circulation model intercomparison and evaluation with satellite data. *Atmospheric Chemistry and Physics*, 9(22), 8697–8717. <https://doi.org/10.5194/acp-9-8697-2009>

Rosenfeld, D., Sherwood, S., Wood, R., & Donner, L. (2014). Climate effects of aerosol-cloud interactions. *Science*, 343(6169), 379–380. <https://doi.org/10.1126/science.1247490>

Sassen, K., DeMott, P. J., Prospero, J. M., & Poellot, M. R. (2003). Saharan dust storms and indirect aerosol effects on clouds: CRYSTAL-FACE results. *Geophysical Research Letters*, 30(12). <https://doi.org/10.1029/2003GL017371>

Smith, G. L., Mlynczak, P. E., & Potter, G. L. (2012). A technique using principal component analysis to compare seasonal cycles of Earth radiation from CERES and model computations. *Journal of Geophysical Research Atmospheres*, 117(9). <https://doi.org/10.1029/2011JD017343>

Sorooshian, A., Feingold, G., Lebsack, M. D., Jiang, H., & Stephens, G. L. (2009). On the precipitation susceptibility of clouds to aerosol perturbations. *Geophysical Research Letters*, 36(13). <https://doi.org/10.1029/2009GL038993>

Stevens, B., & Feingold, G. (2009). Untangling aerosol effects on clouds and precipitation in a buffered system. *Nature*, 461(7264), 607–613. <https://doi.org/10.1038/nature08281>

Vaughan, M. A., Powell, K. A., Kuehn, R. E., Young, S. A., Winker, D. M., Hostetler, C. A., ... Getzewich, B. J. (2009). Fully automated detection of cloud and aerosol layers in the CALIPSO lidar measurements. *Journal of Atmospheric and Oceanic Technology*, 26(10), 2034–2050. <https://doi.org/10.1175/2009JTECHA1228.1>

Vinoj, V., Rasch, P. J., Wang, H., Yoon, J., Ma, P., Landu, K., & Singh, B. (2014). Short-term modulation of Indian summer monsoon rainfall by West Asian dust. *Nature Geoscience*, 7(April), 308–313. <https://doi.org/10.1038/NGEO2107>

Wang, M., Steven, G., Xiaohong, L., S., L. T., Kai, Z., Hugh, M., ... E., P. J. (2012). Constraining cloud lifetime effects of aerosols using A-Train satellite observations. *Geophysical Research Letters*, 39(15). <https://doi.org/10.1029/2012GL052204>

Wood, R. (2012). Stratocumulus Clouds. *Monthly Weather Review*, 140(8), 2373–2423. <https://doi.org/10.1175/MWR-D-11-00121.1>

LONG TERM TRENDS IN AEROSOL OPTICAL DEPTH OVER BAY OF BENGAL

RAJESH T. A. AND VISHNU K. DHAKER

Space & Atmospheric Sciences Division, Physical Research Laboratory, Ahmedabad,
Gujarat – 380009

(rajeshta@prl.res.in)

KEYWORDS: Aerosol optical depth, Trends, Coast, Deep Sea, Bay of Bengal

INTRODUCTION

Atmospheric aerosols are important climate agent and significantly influence regional as well as global climate. They vary considerably in size, shape, concentration and composition in the atmosphere depending on nature of production and removal mechanisms. Aerosols perturb the Earth's climate directly by scattering and absorbing incoming solar (shortwave) and outgoing terrestrial (longwave) radiations, and indirectly by acting as a cloud condensation nuclei and thus modifying the lifetime and radiative properties of clouds. Aerosols are produced by natural processes (sea salt, windblown dust, etc.) and anthropogenic (manmade) activities. Based on their production mechanisms, aerosols are divided into primary aerosols and secondary aerosols. Aerosols such as windblown dusts, pollen grains, sea salt particles, carbonaceous aerosols from combustion of fossil fuel or biomass burning emissions are directly injected into the atmosphere and are called as primary aerosols, whereas, there are several inorganic species in the atmosphere (sulfates, nitrates etc.) produced from precursor gases released into the atmosphere which gets converted into particles and these are known as secondary aerosols (IPCC, 2013). The study of spatio-temporal variabilities in aerosol optical properties is required to understand the role of aerosols on climate variability and climate change. Long-term trends in aerosol optical properties are required to understand the global and regional cycling of different aerosol species, to validate the emission inventories, and to provide aerosols input in various climate models. The columnar loading of aerosol is quantified as aerosol optical depth (AOD), which varies as a function of location. Indo-Gangetic Plain has been quantified as one of the highly polluted area and its outflow pollutes the Bay of Bengal. The present work highlights the long term trends in columnar aerosol loading near coast and deep sea over Bay of Bengal, which will provide a detailed insight into spatio-temporal variation of aerosol loading and the possible causes for it as well.

STUDY LOCATION, DATA AND METHODOLOGY

Bay of Bengal plays an important role in Indian summer monsoon system and precipitation pattern. Geographically, it is surrounded by landmasses on its east, west, and north which are densely populated and industrialized areas. Several studies over the Bay of Bengal revealed the existence of large heterogeneity in aerosol characteristics, sources and size distribution. Higher aerosol loading was reported with higher anthropogenic contribution over the Bay of Bengal as compared to the Arabian Sea (Kedia and Ramachandran, 2008). In the present study, we have selected four large regions ($2.5^\circ \times 2.5^\circ$) in the Bay of Bengal (Figure 1). Three of these regions are near to the coast in the Bay of Bengal as B1 ($87.0-89.5^\circ$ E, $19.0-21.5^\circ$ N), B2 ($83.0-85.5^\circ$ E, $15.0-17.5^\circ$ N), and B3 ($80.5-83.0^\circ$ E, $11.0-13.5^\circ$ N), and a region in the deep sea B4 ($88.0-90.5^\circ$ E, $12.0-14.5^\circ$ N) (Figure 1). The large study region ($2.5^\circ \times 2.5^\circ$) will minimize the influence of meteorological variations and long range transport.

MODerate resolution Imaging Spectroradiometer (MODIS) is a remote sensing instrument aboard Terra and Aqua satellites. The satellites operate in sun-synchronous, near-polar orbits at an altitude of 705 km. The Terra and Aqua spacecraft crosses the equator at about 10:30 LST (ascending northward) and 13:30 LST (descending southward) respectively (Remer et al., 2005). In the present work, Level 3 MODIS Collection V6 (MOD08_M3 v6 and MYD08_M3 v6) atmosphere monthly AOD data at 550 nm for $1^\circ \times 1^\circ$ grid are utilised during 2003 to 2017.

The trends in aerosol optical depth (AOD) are estimated following the weighted least square fitting method. In the weighted least square fitting method, a weight factor ($1/\sigma^2$, where σ is uncertainty) is assigned to AODs, which gives lower weight to AODs with higher uncertainty, and vice versa. The annual mean trends in AOD are expressed in terms of percentage change and are calculated as

$$\frac{\text{Slope between year and AOD} \times 15}{\text{AOD in the year 2003}} \times 100$$

The annual mean trends obtained in the study have p-values < 0.02 and the confidence level in the trends is $>95\%$. The MODIS AOD has been calculated using the combined AOD data from MODIS-Aqua and MODIS-Terra. The monthly AOD are further monthly averaged during 2003 to 2017. In the present study we have used monthly averaged 15 years of data from MODIS.

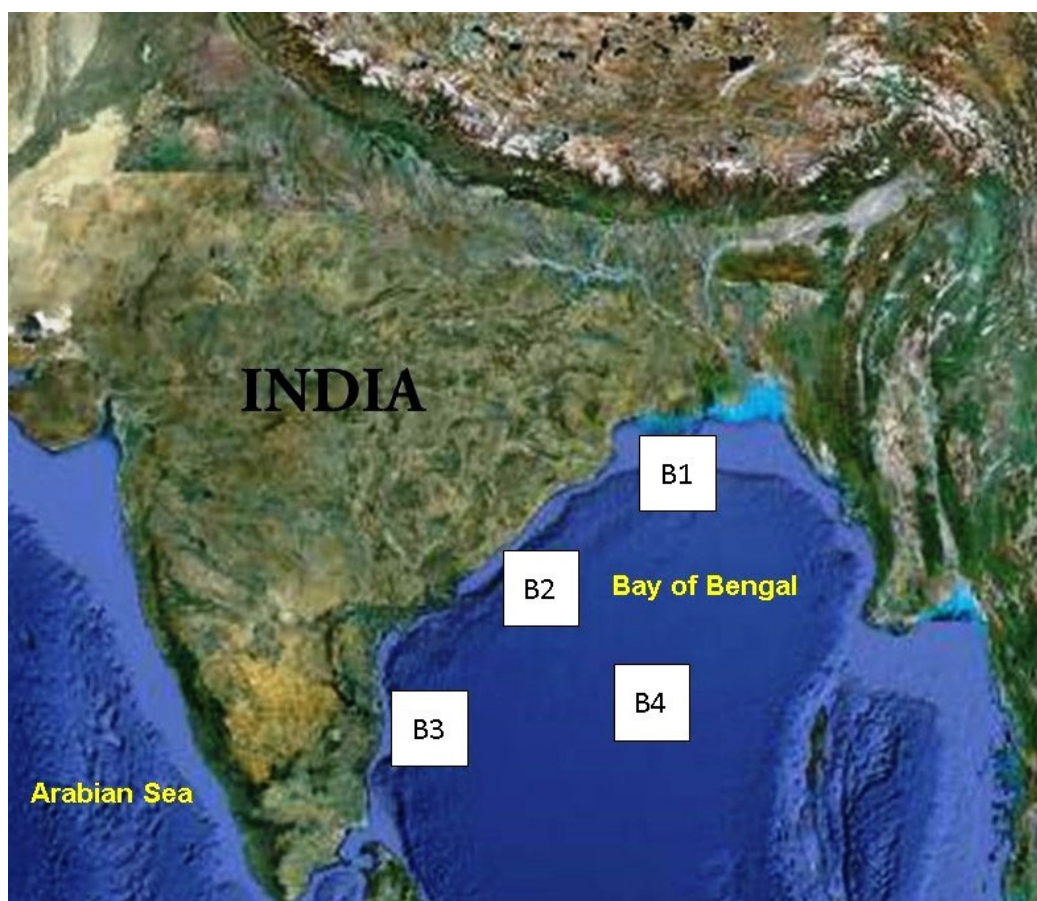


Figure 1. Study locations over the Bay of Bengal

RESULTS AND DISCUSSION

Aerosol optical depth (AOD) exhibits significant spatial variation over the Bay of Bengal (Figure 2). The maximum AOD is found over north coast (B1) of Bay of Bengal during the study period due to the significant contribution of the pollutants outflow from the Indo-Gangetic Plains (Figure 2). The AOD decreases with latitude over the Bay of Bengal (Figure 2). The deep sea (B4) AOD is found to be minimum during the study period and represents the open ocean value over Bay of Bengal.

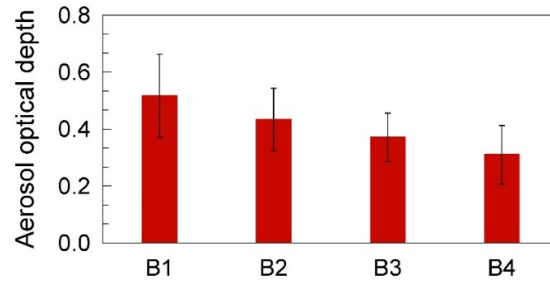


Figure 2. Annual variations of aerosol optical depth over Bay of Bengal during 2003-2017 from MODIS at 550 nm. Vertical bars represent $\pm 1\sigma$ deviation from the mean.

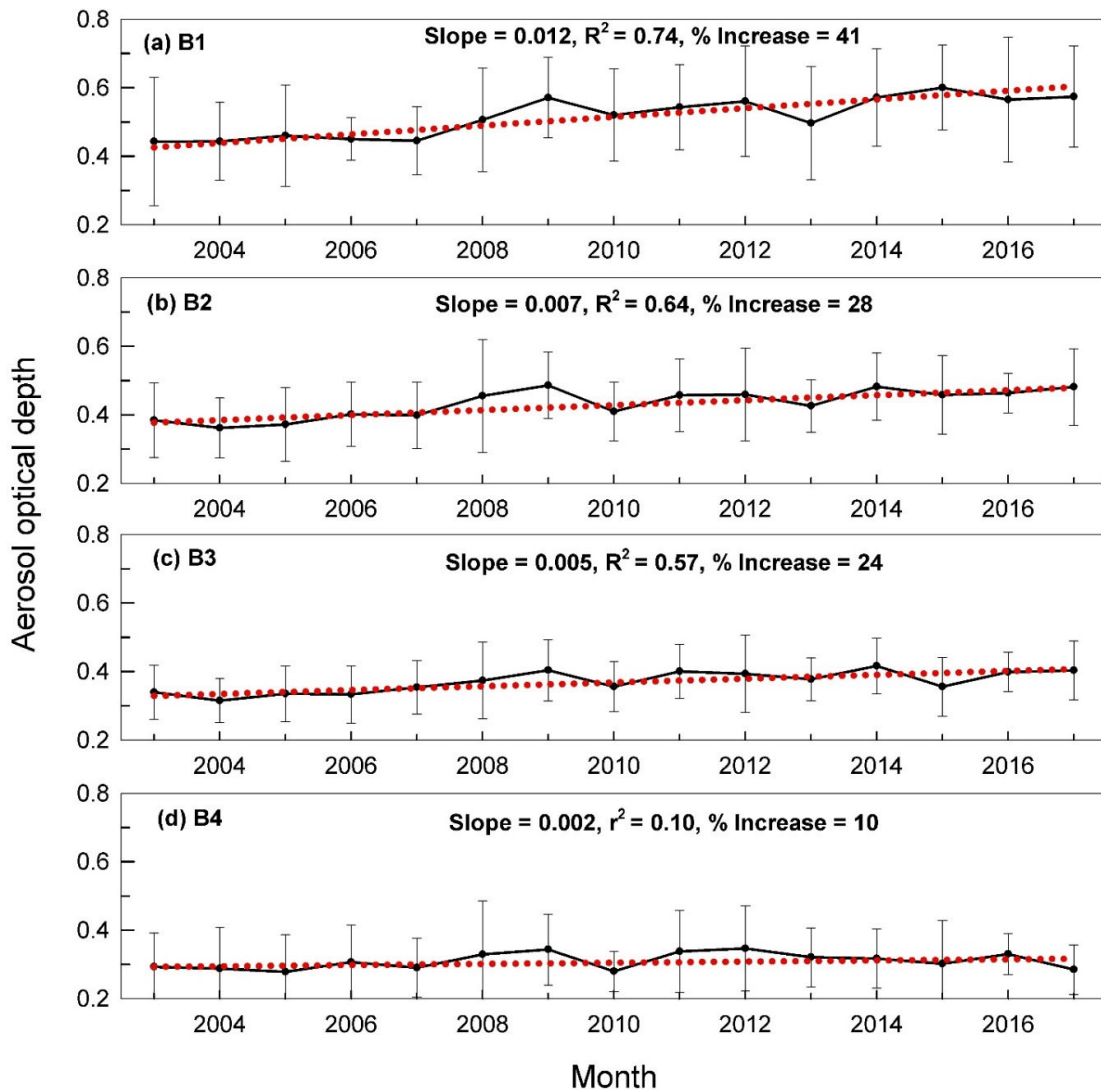


Figure 3. Annual mean trends in aerosol optical depth (AOD) over (a) B1, (b) B2, (c) B3, and (d) B4 during 2003-2017 from MODIS at 550 nm. Vertical bars represent $\pm 1\sigma$ deviation from the mean. Broken straight

lines (red) represent the trends which are obtained by weighing the annual mean AODs with their intra-annual variations using weighted least squares fitting method.

The trends in AOD show significant annual mean variations as depicted in Figure 3. The annual mean trend in AODs during 2003-2017 (15 years) over Bay of Bengal is positive (Figure 3). Annual mean AODs have increased by 41, 28, 24, and 10% during 2003-2017 over B1, B2, B3, and B4 regions in the Bay of Bengal (Figure 3). We have also found an increase in the AOD over Indo-Gangetic Plain (80.0-82.0° E, 25.0-27.0° N) during the study period (not shown in the Figures 2 and 3). The present study regions are not aerosol source regions but are influenced by the anthropogenic activities in the nearby landmass and advection processes (long range transport). The observed increase in AODs can be ascribed to the increase in urbanization, which attributes to an increase in the amount of aerosols from fossil fuel and biomass burning. On the contrary, the AOD trends over the Eastern United States and Western Europe regions show pronounced decreasing trends during 2001-2015 are resulting from the effective enforcement of emission control policies (Zhao et al, 2017). The trends in AOD over Seoul and Busan (a coastal station) in South Korea exhibit a significant decadal decrease by 22 and 19% respectively owing to reduction in anthropogenic aerosol emissions (Panicker et al., 2013). Whereas, in the Eastern and Central China AOD has been found to increase during 2001 to 2006 and decreases after 2011 due to the implementation of the emission control policies (Zhao et al, 2017). These findings become important and useful in the context of regional and global climate change due to aerosols.

SUMMARY

Annual mean trends in aerosol optical depth (AOD) were examined over different regions (near coast (B1, B2, B3) and deep sea (B4)) in Bay of Bengal during 2003 to 2017 using monthly averaged MODIS data at 550 nm. Annual mean AODs are found to increase by 41, 28, 24, and 10% over B1, B2, B3, and B4 respectively during 2003-2017. The increase in AOD can be attributed to the increase in urbanization, which attributes to an increase in the amount of aerosols from fossil fuel and biomass burning. The annual mean trends in AOD over Eastern United States, Western Europe, Eastern and Central China regions, Seoul, and Busan decrease because of the effective enforcement of emission control policies. Hence we also require to implement effective emission control policies to control the anthropogenic aerosol emissions over India, which will subsequently influence the adjoining oceans. Results on the long term inter annual variability in aerosol properties will be useful in modeling the radiative effects of aerosols and for assessment of their role on regional climate.

ACKNOWLEDGEMENTS

MODIS Level 3 AOD data were downloaded from GES-DISC, NASA. We also acknowledge the MODIS mission scientists and associated NASA personnel for the production of the data used in this research effort.

REFERENCES

IPCC, 2013: Climate Change 2013: The Physical Science Basis. Contribution of Working Group I to the Fifth Assessment Report of the Intergovernmental Panel on Climate Change [Stocker, T.F., D. Qin, G.-K. Plattner, M. Tignor, S.K. Allen, J. Boschung, A. Nauels, Y. Xia, V. Bex and P.M. Midgley (eds.)]. Cambridge University Press, Cambridge, United Kingdom and New York, NY, USA, 1535 pp, doi:10.1017/CBO9781107415324

Kedia, S., Ramachandran, S. (2008), Features of aerosol optical depths over the Bay of Bengal and the Arabian Sea during premonsoon season: variabilities and anthropogenic influence. *J. Geophys. Res.*, 113, doi:10.1029/2007JD009070.

Panicker A. S., D. I. Lee, Y. V. Kumkar, D. Kim, M. Maki and H. Uyeda (2013), Decadal climatological trends of aerosol optical parameters over three different environments in South Korea, *Int. J. Climatol.* 33, 1909-1916.

Remer L. A., Y. J. Kaufman, D. Tanré, S. Mattoo, D. A. Chu, J. V. Martins, R.R. Li, C. Ichoku, R. C. Levy, R. G. Kleidman, T. F. Eck, E. Vermote, and B. N. Holben (2005), The MODIS aerosol algorithm, products, and validation, *J. Atmos. Sci.*, 62, 947-973.

Zaho Bin, Jonathan H Jiang, Yu Gu, David Diner, John Worden, Kuo-Nan Liou, Hui Su, Jia Xing, Michael Garay and Lei Huang (2017), Decadal-scale trends in regional aerosol particle properties and their linkage to emission changes, *Environ. Res. Lett.* 12, 050421.

SPATIAL DISTRIBUTION OF BLACK CARBON AEROSOL: ROAD CAMPAIGN EXPERIMENT IN WESTERN INDIA

RAJESH T. A., VISHNU K. DHAKER, MALAIDEVAN P., AND S. RAMACHANDRAN
Space & Atmospheric Sciences Division, Physical Research Laboratory, Ahmedabad,
Gujarat – 380009

(rajeshta@prl.res.in)

KEYWORDS: Black carbon mass concentration, Aethalometer, Meteorological parameters, Road campaign

INTRODUCTION

Black carbon (BC) aerosol is the optically absorbing component of carbonaceous aerosols and is produced by incomplete combustion of fossil fuel (coal, diesel, petrol, etc.) and biomass (woods, shrubs, dry leaves, etc.). It absorbs incoming solar (shortwave) radiation and outgoing terrestrial (longwave) radiation, and is, therefore, an important contributor to the direct radiative forcing (IPCC, 2013). BC aerosol has a short lifetime of 7 to 10 days in the atmosphere but it has the potential to alter the Earth's radiation budget (Jacobson, 2001). The radiative forcing of BC aerosol is uncertain because BC aerosols exhibit significant spatial and temporal variabilities in its sources and emissions. The uncertainty in the radiative forcing by BC aerosols arises due to inadequate knowledge on the amount of BC mass concentration emitted into the atmosphere, its size distributions, contribution from different sources, and their mixing state (IPCC, 2013). There has been a considerable interest in studying the characteristics of black carbon aerosols and its climatic impact over different environments (Ramachandran and Rajesh, 2007; Ramachandran and Kedia, 2010; Rajesh and Ramachandran, 2017). However, most of the studies on aerosol characteristics are restricted to either urban/semi-urban regions or oceans adjacent to densely populated coastal regions. Studies over a remote high altitude region which is away from the potential sources represent regional background conditions. High altitude locations are pristine and aerosol characteristics over these locations are influenced by the long-range transport (advection and convection processes). Hence aerosol characteristics over high altitude remote locations can serve as the background representative of the nearby urban source regions as a function of meteorology. A scientific road campaign experiment in western India has been conceived to study the spatial distribution of aerosol characteristics in the Aravalli range of mountains in western India. The present study will discuss the spatial/vertical distribution of black carbon aerosol in western India.

STUDY LOCATION, DATA AND METHODOLOGY

The scientific road campaign spans from the foothills of Mt. Abu (Abu road, 280 m above mean sea level (AMSL)) to one of the peaks of Mt. Abu (Gurushikhar, 1680 m AMSL) (Figure 1), which provides an opportunity to investigate the vertical distribution of aerosol characteristics. Gurushikhar is the highest point of the Aravalli Range in the Arbud Mountains of Rajasthan. The observational peak is influenced by the transport of mineral dust from the Thar Desert (northwestern part of the Indian subcontinent), sea salt from the Arabian Sea (southwestern part of the Indian subcontinent) and anthropogenic aerosols mainly black carbon aerosols from the Indo-Gangetic Plain (north-northeastern part of the Indian subcontinent). The Mount Abu city (1180 m AMSL) lies downhill from Gurushikhar at a distance of 15 km on a high rocky plateau and surrounded by forests (Figure 1). The city is a hill station (tourist destination) in the Aravalli range in western India. To the northwest of the Gurushikhar location lies the Abu road city (280 m AMSL) at a distance of 40 km in the hills of the Aravalli range and has significant anthropogenic activity. During premonsoon, the winds originate and travel from the western Indian region, while during monsoon the winds are stronger and moist, and are from the marine (Arabian Sea) and western regions surrounding India. During postmonsoon, the wind pattern starts shifting in direction from southwest to northeast, whereas during winter the surface winds are calm and north-northeasterly over this region.

An instrumented vehicle fitted with aethalometer (Magee Scientific AE33; for black carbon mass concentration and absorption coefficient measurements), nephelometer (Air Photon IN101; for scattering

coefficient measurement), aerosol spectrometer (GRIMM Spectrometer WRAS; for aerosol number concentration measurement), meteorological data logging system (measures and logs timestamped temperature, pressure, humidity, manifold temperature, manifold humidity, latitude, longitude, and altitude) and 3 KVA UPS is being used in the campaign. The air sample inlet is mounted 10 feet above the ground in the front side of the vehicle. The vehicle is operated at a speed of 30 KMPH and always maintained a minimum distance of 10-15 feet from the front vehicle (to minimise the direct sampling of the exhaust from the vehicle in the front). The campaigns were conducted during early morning (05-07 HRS) and afternoon time (13-16 HRS). The minimum vehicular activity is observed during early morning as compared to afternoon time. In the present study, we will only discuss the variations in black carbon aerosol obtained from the campaign conducted during March 2018.

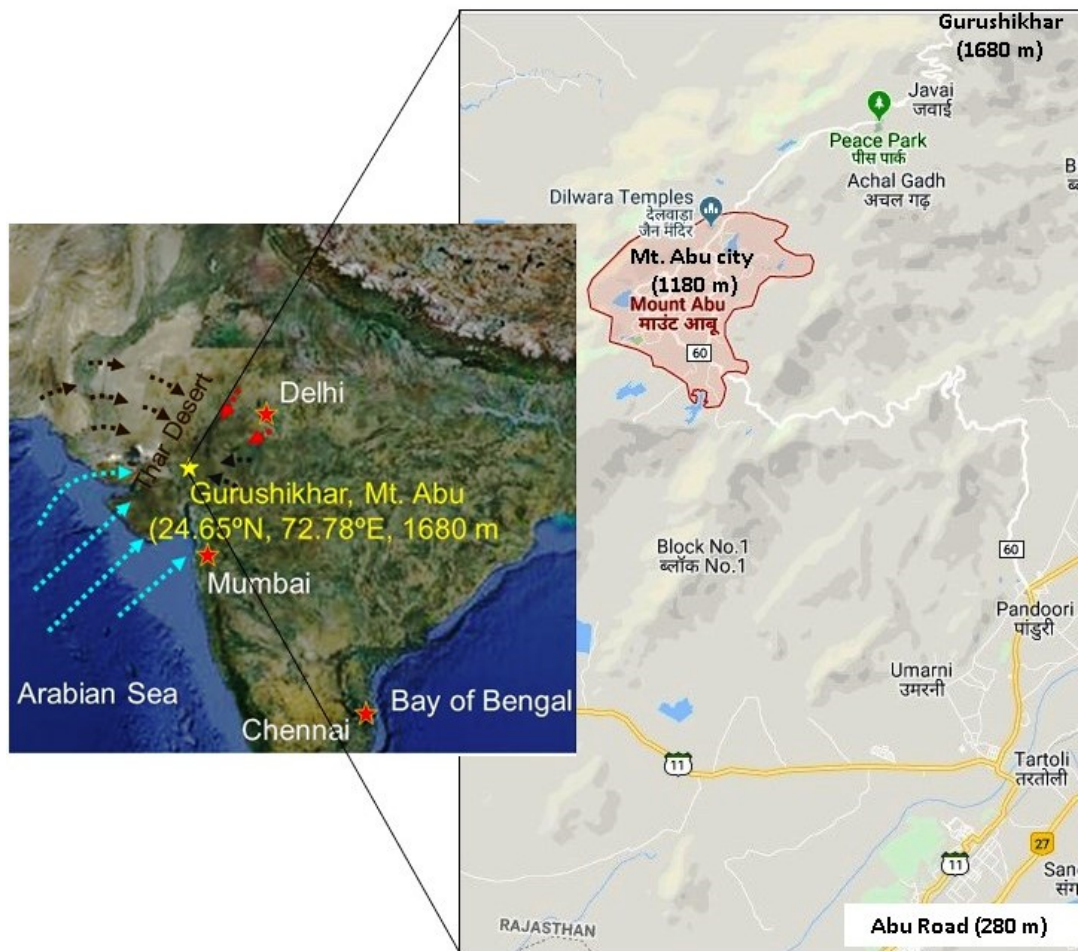


Figure 1. The high altitude observational site in western India – Gurushikhar, Mt. Abu and a few other metro cities (Delhi, Mumbai and Chennai) in India (Google Earth image). The blue arrows represent the wind patterns during monsoon with high wind speed ($>10\text{ms}^{-1}$). Brown arrows denote the synoptic wind pattern during premonsoon. Black arrows indicate the typical winds during postmonsoon. Red arrows represent the wind pattern during winter. Latitude, longitude and altitude (above mean sea level (AMSL)) of Gurushikhar are given. Google map image shows the spatial layout of Abu road (280 m), Mount Abu city (1180 m) and Gurushikhar (1680 m).

Aethalometer (AE33) is operated at a mass flow rate of 3 litres per minute and time base of 1 minute. BC measurements by aethalometer (AE33) are corrected for the variations in ambient pressure and temperature as

$$BC = BC(raw) \frac{P T_0}{P_0 T}$$

where $BC(raw)$ is the aethalometer measured raw BC mass concentration, P_0 is the standard atmospheric pressure (1017 hPa), T_0 is the standard temperature (293 K), P is the ambient atmospheric pressure, and T is the ambient temperature (Aethalometer manual, Magee Scientific Company Berkeley, California, USA, 2005.07). The ambient pressure and temperature were measured in real time using meteorological data logging system.

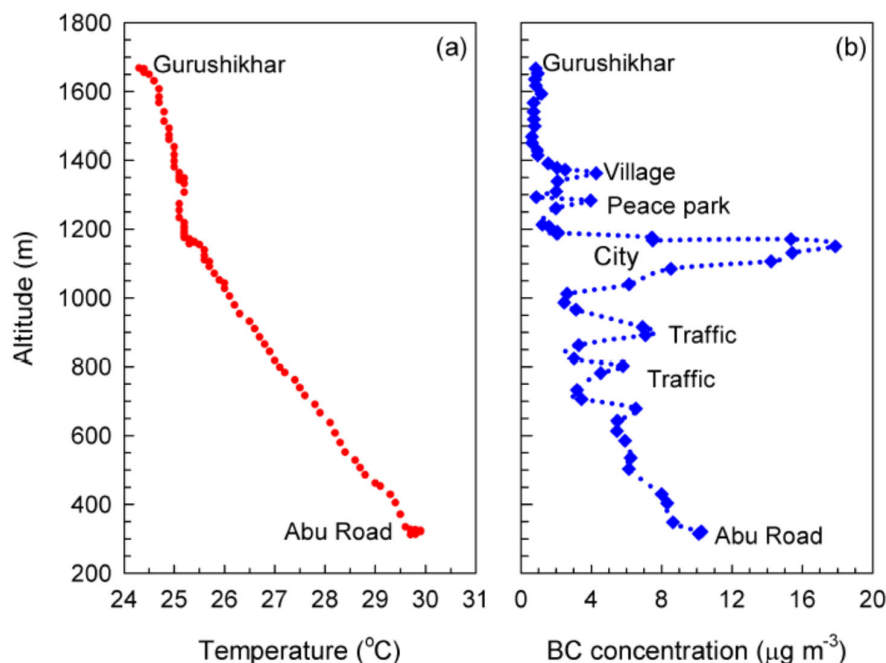


Figure 2. Altitude profiles of (a) temperature and (b) black carbon mass concentration measured during a road campaign from Abu Road (280 m AMSL) to up to Gurushikhar (1680 m AMSL) during March 2018.

RESULTS AND DISCUSSION

The surface temperature decreases from 30° C (Abu Road, 280 m) to 24° C (Gurushikhar, 1680 m) during the road campaign study (Figure 2a). The preliminary result shows the decrease in ambient temperature with altitude at an average adiabatic lapse rate of 5° C/km during March 2018 (Figure 2a). The pressure compensated black carbon mass concentration also reveals the decrease with altitude but with enhancements in the intermittent altitudes due to vehicular traffic and domestic emissions (Figure 2b). During the road campaign the maximum (18 μgm⁻³) black carbon mass concentration is found over the Mt. Abu city which is situated at an altitude of 1180 m (Figure 2b), due to the significant anthropogenic emissions from the fossil fuel and biomass burning. The minimum black carbon mass concentration (1 μgm⁻³) is observed at Gurushikhar (1680 m) (Figure 2b). The road campaign started from Abu Road (280 m) where the black carbon mass concentration was observed to be 10 μgm⁻³. The surface black carbon mass concentration decreases with altitude with intermittent peaks occurring due to the encountered vehicular traffic, and the anthropogenic emissions from the city and village (Figure 2b). The altitudinal profile of black carbon aerosol decreases exponentially following the hydrostatic equilibrium in the atmosphere during the campaign neglecting the anthropogenic emissions. A year-round measurements are envisaged to understand the relative influence of manmade emissions and transport effects on a variety of aerosol characteristics, and apportion these as a function of lower troposphere and seasons.

SUMMARY

A scientific road campaign experiment in western India has been conceived to investigate the spatial distribution of aerosol characteristics in the Aravalli range of mountains in western India. The preliminary result reveals the decrease in the surface temperature from Abu Road (280 m) to Gurushikhar (1680 m). The altitudinal profile of black carbon mass concentration also found to decrease exponentially following the hydrostatic equilibrium in the atmosphere during the campaign neglecting the anthropogenic emissions. The study illustrates that Gurushikhar is influenced by the locally and long-range transported aerosols through convection and advection processes. Long term measurements are envisaged to examine the relative influence of anthropogenic emissions and transport effects on a variety of aerosol characteristics, and apportion these as a function of lower troposphere and seasons.

ACKNOWLEDGEMENTS

We acknowledge the help and support rendered by the staff of PRL Infrared Observatory, Gurushikhar, Mt. Abu in the smooth operation of the road campaign. We acknowledge the support received from Shri J. T. Vinchhi and Shri Mitesh Bhavsar in the development and implementation of the meteorological data logging system. We thank Shri Bankim Pandya for the development of multiport glass manifold. We also acknowledge the support and contribution received from PRL Workshop and Carpentry Department in mounting the various instruments, UPS, and air inlet assembly in the vehicle. We also thank the PRL CISF unit in the smooth operation of the road campaign.

REFERENCES

- IPCC, 2013: Climate Change 2013: The Physical Science Basis. Contribution of Working Group I to the Fifth Assessment Report of the Intergovernmental Panel on Climate Change [Stocker, T.F., D. Qin, G.-K. Plattner, M. Tignor, S.K. Allen, J. Boschung, A. Nauels, Y. Xia, V. Bex and P.M. Midgley (eds.)]. Cambridge University Press, Cambridge, United Kingdom and New York, NY, USA, 1535 pp, doi:10.1017/CBO9781107415324.
- Jacobson, M. Z. (2001), Strong radiative heating due to the mixing state of black carbon, *Nature*, 409, 695–697.
- Rajesh, T. A., and S. Ramachandran (2017), Characteristics and source apportionment of black carbon aerosols over an urban site, *Environ. Sci. and Pollut. Res.*, 24(9), 8411–8424.
- Ramachandran, S., and T. A. Rajesh (2007), Black carbon aerosol mass concentrations over Ahmedabad, an urban location in western India: Comparison with urban sites in Asia, Europe, Canada, and the United States, *J. Geophys. Res.*, 112(D6), doi:10.1029/2006JD007488.
- Ramachandran, S., and S. Kedia (2010), Black carbon aerosols over an urban region: Radiative forcing and climate impact, *J. Geophys. Res.*, 115(D10), doi:10.1029/2009JD013560.

IONIC EFFECT ON CLOUD FORMATION AND ELECTRIC FIELD OF THUNDERCLOUDS

M. CHANDRA

Poornima Institutes of Engineering & Technology (Rajasthan)

e-mail: mksh.rpt@gmail.com

KEYWORDS: nucleation, condensation, ionization, conductivity, CCN.

INTRODUCTION

The ion induced nucleation has been found to be more effective at low supersaturation (even $S_{v,w} < 1$) and the effect decreases for larger nuclei. It has been shown that in ion induced nucleation, even the smaller nuclei ($< 10^{-8}$ cm) are stable at $S_{v,w} < 1$ while in homogeneous cases they cannot exist. The rate of nucleation in the presence of an electric field is found to increase by more than 100 times at electric field near breakdown for dry air and varies linearly with the electric field. The effect of electric charge on the collection efficiency for scavenging of aerosol particles by droplets was extensively modeled by Pruppacher and his group. In recent years it has been realized that even in weakly electrified clouds it is sufficient to affect contact ice nucleation and CCN concentrations (Tinsley et.al. 2010).

METHODS

In the descending air parcels, due to entrainment of air at cloud top, there is a depletion of small cloud particles and consequent enhancement of free ions. It is found that conductivity of these air parcels may be of one order of magnitude higher than the conductivity of the surrounding cloud at the same altitude. The rate of growth of electric field has been calculated for actual cloud condition using

$$\frac{dE}{dt} = \frac{\delta\sigma E^2}{3T} \left(V_0 - \frac{8\varepsilon_0 R \sigma E^2}{3T} \right)^{\frac{1}{2}} - \frac{\lambda_3 E}{\varepsilon_0}$$

The results show that if the ionization rate above the thundercloud increases the rate of electrification of the thundercloud is faster.

RESULTS & DISCUSSIONS

The calculated values of variation of conductivity σ and max, electric field E has been shown in Table 1.

Table-1: Variation of conductivity (σ) and maximum electric field (E) as the function of altitude (Z)

S.No.	Height (Z) Km	Conductivity (σ) s/m	Electric Field (E) Kv/m
1	1.5	2.223×10^{-15}	168.51
2	2.5	2.226×10^{-15}	149.39
3	3.5	2.228×10^{-15}	132.31

4	4.5	2.231×10^{-15}	117.48
5	5.5	2.233×10^{-15}	104.19
6	6.5	2.236×10^{-15}	92.33
7	7.5	2.238×10^{-15}	81.93

CONCLUSION

Theoretical analysis and calculation show that the blob conductivity decreases exponentially with increasing electric field.

REFERENCES

A.Mohan, N.Singh & G.K.Johri (2003) Sci.Lett. 26(1)23-25

N.Singh & Singh, (2004) J. Radio and Space Phys, 32, 379-381

B.K.Sapkota & N.C. Varshneya, (1988) Meteorol, Atmos. phys, 39, 213-222

C.Barthe. et al, (2016) Atmospheric Research Volume 180, 1, Pages 297-309

SIMULTANEOUS MEASUREMENTS OF NUMBER, MASS AND CHEMICAL COMPOSITIONAL CHARACTERISTICS OF AEROSOL EMISSIONS DURING FIREWORKS

MANISH JOSHI¹, AMRUTA NAKHWA¹, PALLAVI KHANDARE¹, MARIAM¹, ASHOK RANADE², ARSHAD KHAN¹ AND B. K. SAPRA¹

¹Radiological Physics and Advisory Division, ²Director's office
Bhabha Atomic Research Centre
Mumbai, 400 085, India.

KEYWORDS: Fireworks, diwali, aerosol, signature.

INTRODUCTION

Emission of particulates during fireworks possess capability to enhance number and mass concentration of atmospheric aerosol particles. In contrast to the display of fireworks at mass gatherings, multipoint source term of firecracker burning makes Diwali festival an unique event. Studies on mass loadings, chemical tracers and number concentration evolution try to establish signatures attributable to particle emissions during fireworks. Particulate matter concentration has been shown to be increasing at the times of fireworks in several studies. Emission of trace and heavy metals has been correlated to the fireworks. Increase of number concentration of particles in different size ranges have been demonstrated in studies focused on number based features. There are issues while relating changes in gross parameters in a straight forward way to emissions during fireworks. Integral features of aerosol characteristics during events (episodic and background) have been shown to be fluctuating for a longer time-period (Joshi et al. 2016). Gross value of a characteristic such as mass concentration could be similar for different kind of events as well (Nicolás et al. 2009). A measure drawback of studies conducted during fireworks pertains to not performing simultaneous measurements of mass loadings, number characteristics and chemical composition of emitted particles. This study presents the results of a campaign performed for 17 days in the year 2013 including the day of Diwali (3rd November) festival. Features of simultaneously measured aerosol characteristics have been interpreted in order to discuss appropriateness of signatures attributable to emission during fireworks.

EXPERIMENTAL METHODS

Measurements were performed in a residential building of Mumbai city via a sampling station set-up at a height of approximately 50 m. Separate sampling tubes (length 1.5 m and internal diameter 10 mm) were taken out of the window of the room to open atmosphere and used as probe for measurement of number and mass (+chemical composition) based parameters. Sampling days include 'Diwali festival days (Nov. 2-4)' with main celebration on the night of 3rd Nov. Number concentration (size distribution in the diameter range of 11-1083 nm) of aerosol particles were measured by GRIMM Scanning Mobility Particle Sizer (SMPS). It was operated at a frequency of 7 minutes continuously except at the times of maintenance activities. Gross filtration sampler was used for the measurements of Total Suspended Particulate Matter (TSPM) concentration. Filter papers employed for gravimetric estimations were analysed for mass concentration of specific elements (Cu, Fe, Zn, Ba, Ca, Sr, Al, Mg, Na and K) using Atomic absorption spectroscopy (AAS).

RESULTS & DISCUSSIONS

Diurnal variations of air temperature and relative humidity (RH) during the study period were found to be more or less similar. RH varied between 30-90 % during a typical sampling day but could not be correlated to evolution history of aerosol characteristics (specifically number concentration). Patterns of wind speed and wind direction during Diwali and non-Diwali times were observed to be similar. Average mass concentration (evening to night times) for Diwali days (2nd, 3rd and 4th Nov.) was found to be $\approx 275 \mu\text{gm}^{-3}$, $364 \mu\text{gm}^{-3}$ and $160 \mu\text{gm}^{-3}$, respectively. However, mass concentration of atmospheric aerosol particles was also found to be comparable (for instance $\approx 300 \mu\text{gm}^{-3}$ on Oct. 28-30 and 6th Nov.) on other days as well.

The highest mass concentration for the study period was measured on 25th Oct. at 493 $\mu\text{g m}^{-3}$. Afterwards, filter paper samples were analyzed for mass concentration of 10 different elements. Fe, Zn and Al was observed in all the samples representing crustal elements. Ba, K, Sr and Cu was found in Diwali samples but also in few other samples. Ca, Na and Mg was not found in the samples taken during festival days. Out of these 10 elements, {Ba, Cu, Sr, Al} could be tracer group representing the fireworks. K was removed due to the observance of high concentration values on background days. Box-whisker plot for number characteristic data for all sampling days is shown in fig. 1. As can be seen, daily maximum number concentration was highest ($\approx 1.6 \times 10^5 \text{ No. cm}^{-3}$) on the day of Diwali. This daily maximum value was found to be close to that measured on other days (e.g. 28th Oct.) as well. However, average values (mean and median) for Diwali day were found to be higher on several other days. Skewness of the distribution reflected as the difference between mean and median was found to be distinct for Diwali day. This is due to the impact of burst releases in ultrafine size ranges affecting the size distribution.

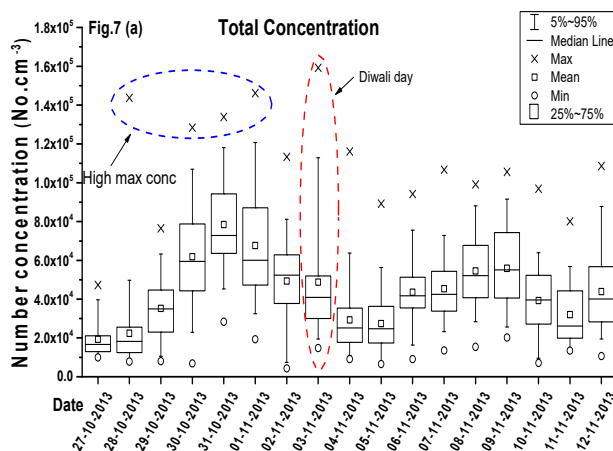


Figure 1. Number size distribution for all sampling days

Size distribution evolution for the Diwali day is depicted in fig. 2. As represented, size distribution features in entire size range got perturbed in evening times and continued evolving afterwards. Increase of particles in ultrafine size range has been observed in few other studies (Joshi et al. 2016; Zhao et al. 2014). This feature results in a sharp drop of geometric mean in evolution profile of integrated number concentration. Significant increase of particles in accumulation mode (0.1-1 μm) size-range has constantly been observed in studies performed worldwide. The figure also hints at the the possibility of ‘New Particle Formation’ signified as an increase of particles in nuclei mode (particle diameter lesser than 0.02 μm) size ranges. Variations of number concentration in nuclei mode were found to be following those for the entire size range while comparing the respective Box-whisker plots for all sampling days.

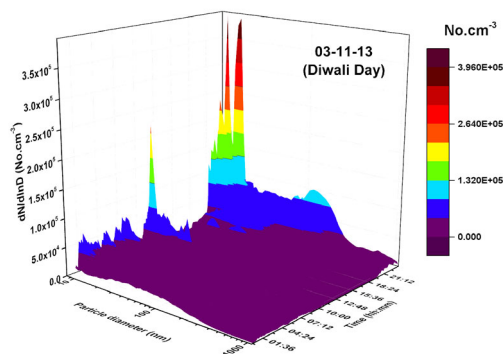


Figure 2. Size distribution evolution on Diwali day

CONCLUSIONS

This study interpreted the measurements of mass, number and chemical compositional characteristics during the festival days of Diwali 2013. Mass concentration of particles at the times of fireworks was found to be not very different with that measured for other times. Ba, Sr, Cu and Al were identified as tracers for firework induced emissions based on the time series and correlation analysis performed for all sampling days. Increase of particles in ultrafine size ranges and shifting of accumulation mode was observed at the times of fireworks. For urban environmental conditions, the approach of linking changes in single aerosol parameter with episodic events could be incorrect. Simultaneous size segregated measurements of mass and number concentration needs to be performed for proper identification of signatures of aerosol emissions during fireworks. This information is crucial in order to differentiate various events and non-events in terms of conclusive inferences. Long term background database for chemical composition of ambient aerosol particles needs to be related to the samples taken during fireworks. Most appropriate tracer group could be site specific as well.

REFERENCES

- Joshi M., Khan A., Anand S. and Sapra B. K. (2016). Size evolution of ultrafine particles: Differentia signatures of normal and episodic events. *Environ Pollut* **208**, 354-360.
- Nicolás J., Yubero E., Galindo N., Giménez J., Castañer R., Carratalá A., Crespo J. and Pastor C. (2009). Characterization of events by aerosol mass size distributions. *J Environ Monit* **11(2)**, 394-399.
- Zhao S. P., Yu Y., Yin D. Y., Liu N., He J. J. (2014). Ambient particulate pollution during Chinese Spring Festival in urban Lanzhou, Northwestern China. *Atmos Pollut Res* **5(2)**, 335-343.

. SIZE DIFFERENTIATED ATMOSPHERIC AEROSOLS DURING FIRECRACKERS BURNING AT RAIPUR

M. MAHILANG¹, M.K. DEB² AND J. NIRMALKAR

¹School of Studies in Chemistry, Pt. Ravishankar Shukla University, Raipur, Chhattisgarh, 492010, India

²Indian Institute of Science Education & Research, Bhaury, Bhopal, Madhya Pradesh, 462066, India

mithleshkumarchem@gmail.com

KEYWORDS: Deepawali festival, Pearson correlation, Size distribution, Percentage contribution.

INTRODUCTION

Deepawali, a great Indian festival, marked with enormous firecracker burning, is celebrated during the month of October and November every year (Nirmalkar *et al.* 2013). Massive firecracker burning during Deepawali festival, leads to deteriorating air quality as well as increase human health risk. During fireworks emission there is a drastic increase in aerosol mass concentration and ambient air is also contaminated with detrimental atmospheric particulate matters (PM). The mass concentration of submicron particulate matter, also increases severely which can penetrate into the deeper region of the human respiratory system. Enormous inhalable PMs have been released due to firecracker burning during Deepawali festival (Godri *et al.* 2010; Nirmalkar *et al.* 2013). Regardless of extreme firecrackers emissions, there are only few research articles available, although there is no attempt in investigation of size distribution in urban region of eastern central India. This study provides sufficient data that will be useful to explain actual size distribution atmospheric particles in three different events i.e., before Deepawali period (BDP), throughout Deepawali period (TDP) and after Deepawali period (ADP). Aerosols samples collection was done in nine different size ranges and a comparison of mass loading between above mentioned three events were done at Raipur, Chhattisgarh. Present study also gives comparative study of particulate matter concentration data with National ambient air quality standards.

METHODS

The collection of atmospheric aerosols were demonstrated at an urban site of Raipur situated between 22°33' N to 21°14' N Latitude and 82°6' to 81°38' E Longitude, throughout three different cases i.e., during fireworks emission, before fireworks emission and after fireworks emission for comparative study. Aerosol collection was done at 15 m above the ground level at Raipur. Sampling location is also under the influence of vehicular emission, industrial pollutants, road dust, from construction activities and biomass burning. Sampling was done using Anderson cascade impactor air sampler (TE 20-800, USA), which was installed on the rooftop of Department of Chemistry, Pt. Ravishankar Shukla University Raipur, Chhattisgarh, India. The sampling of size-resolved aerosols was performed during three events i.e., BDP (October 2015, n=5), TDP (November 2015, n=5) and ADP (December 2015, n=5) flow rate was set to be 28.3±0.3 Lmin⁻¹ to collect the atmospheric particles. Total 15 sets of size-resolved aerosol samples were collected on daily basis each for 24h. All samples were collected using pre-combusted quartz fiber filters. Field blank was collected before and after the sampling by keeping the filters onto the sampler without sucking any air. After sampling, the sample and field blank filters were transported to the laboratory for gravimetric analysis. The mass concentration of size-resolved aerosols was determined by gravimetric analysis.

RESULTS & DISCUSSIONS

Size Distribution

Aerosols in nine different size fractions are shown in Fig. 1. We observed significant difference between size distribution of atmospheric aerosols during BDP, TDP and ADP. During TDP, event size distribution of aerosols shows a bimodal distribution with two peaks at 0.65-1.1 µm and at in 4.7-5.8 µm which must be due to emission of smaller particles along with coarse particles during burning of firecrackers. The peak at

0.65-1.1 μm was minimized during ADP and not found BDP event. Wide distribution towards the coarse size fractions during BDP and ADP found the reason for such distribution must be constructions activities around the sampling location. High mass loading of aerosol resulted mostly due to frequent construction activates in Beijing (Han *et al.*, 2007).

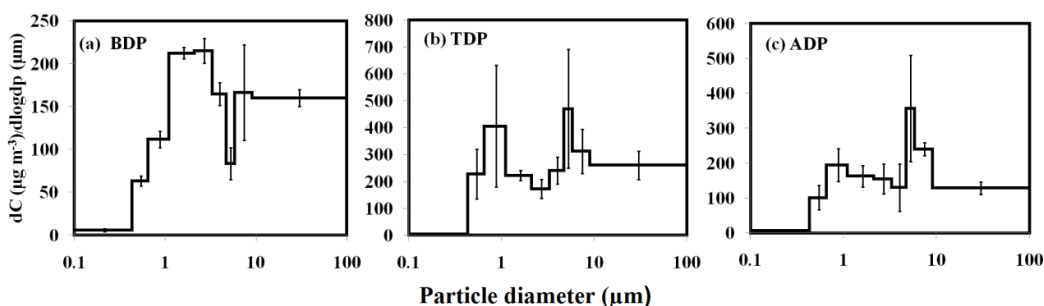


Fig. 1 Average size distributed atmospheric aerosols collected during three different events: BDP (a), TDP (b) and ADP (c)

Size Segregated Aerosols

Mass loading of size-segregated aerosols, i.e., $\text{PM}_{>9}$, $\text{PM}_{2.1->9}$, $\text{PM}_{2.1}$ and PM_1 during BDP, TDP and ADP period are given in Table 1. As shown in Table, $\text{PM}_{>9}$ and $\text{PM}_{2.1->9}$ values vary from 255.1 to 282.9 $\mu\text{g m}^{-3}$ (avg. $269.9 \pm 10.8 \mu\text{g m}^{-3}$) and 120.4 to 126.7 $\mu\text{g m}^{-3}$ (avg. $120.1 \pm 9.4 \mu\text{g m}^{-3}$) during BDP, from 481.6 to 547.8 $\mu\text{g m}^{-3}$ (avg. $520.3 \pm 30.8 \mu\text{g m}^{-3}$) and 231.0 - 270.3 $\mu\text{g m}^{-3}$ (avg. $251.8 \pm 17.1 \mu\text{g m}^{-3}$) during TDP, and 286.9 to 307.7 $\mu\text{g m}^{-3}$ (avg. $294.4 \pm 8.6 \mu\text{g m}^{-3}$) and 129.3 - 149.3 $\mu\text{g m}^{-3}$ (avg. $143.2 \pm 8.5 \mu\text{g m}^{-3}$) during ADP, respectively.

Table 1. Mass concentrations ($\mu\text{g m}^{-3}$) of PM_{10} , $\text{PM}_{2.1->9}$, $\text{PM}_{2.1}$ and PM_1 aerosols during BDP (n = 5), TDP (n = 5) and ADP (n = 5) period sampling period at Raipur in eastern central India

	PM_1	$\text{PM}_{2.1}$	$\text{PM}_{2.1->9}$	$\text{PM}_{>9}$
Study period	Mean \pm SD ^a			
	Range	Range	Range	Range
BDP	47.9 ± 2.7	150 ± 5.3	120 ± 9.4	270 ± 10.8
	43.9 - 50.3	143 - 156	120 - 127	255 - 283
TDP	174 ± 43.1	268 ± 44.9	252 ± 17.1	520 ± 30.8
	129 - 219	217 - 310	231 - 270	482 - 548
ADP	75.1 ± 14.8	151 ± 10.0	143 ± 8.5	294 ± 8.6
	72.1 - 92.1	137 - 159	129 - 149	287 - 308

^aStandard deviation

Correlation

For the determination of relation between the size resolved aerosols, Pearson correlation analysis performed in three events i.e., TDP, BDP and ADP are given in Table 2. There is strong correlation between $\text{PM}_{2.1}$, PM_1 with $\text{PM}_{>9}$ was found during TDP, the reason for this correlation must be emission of smaller particles and their tendency to accumulate together or absorb with one another (Nirmalkar *et al.*, 2015), this is due to similar sources of emission. During TDP $\text{PM}_{2.1}$, PM_1 are strongly correlated with PM_{10} reason might be

similar sources of origin and coarse size particles are negatively correlated with fine size fraction because of different sources this type of correlations were not observed during ADP and BDP. Burning activities release freshly bourn fine and submicron size fractions in the atmosphere. Significant correlation were labeled as ^a and ^b for $r < 0.01$ and $r < 0.05$ respectively in the table. Strong correlation between fine and coarse particles observed this indicates that fine particles contribute more to the coarse particles because of extreme fireworks activities.

Table 2. Pearson correlation analysis of aerosols with different size fractions

BDP				
	PM _{>9}	PM _{2.1->9}	PM _{2.1}	PM ₁
PM _{>9}				
PM _{2.1->9}	0.87			
PM _{2.1}	0.49 ^b	0.01		
PM ₁	0.19	-0.22	0.78	
TDP				
PM _{>9}				
PM _{2.1->9}	-0.74			
PM _{2.1}	0.97 ^a	-0.89		
PM ₁	0.94 ^a	-0.93 ^a	0.99 ^a	
ADP				
PM _{>9}				
PM _{2.1->9}	0.32			
PM _{2.1}	0.59 ^b	-0.58		
PM ₁	-0.64	-0.82	0.15	

^a Correlation is significant at the 0.01 level (2-tailed)

^b Correlation is significant at the 0.05 level (2-tailed).

CONCLUSION

The bimodal patterns of size distribution with two peaks at 0.65-1.1 and 4.7-5.8 μm were observed during TDP event although the peak at 0.65-1.1 μm was not observed during ADP and BDP events, the reason must be freshly borne particles due to extreme fire-crackers burning event during Deepawali celebration. When compared with environmental standards, it has been observed that the pollution level had exceeded the limits with highest during Deepawali day's coarse and fine particles was five and four times higher than the standards. Particles with size <0.43 and $0.43-0.65$ μm are strongly correlated with 1.1-2.1 and 4.7-5.8 μm during TDP these correlations was not found in other event i.e., BDP and ADP this must be due to emissions from firecrackers burning activity.

ACKNOWLEDGEMENT

Authors are thankful to the Head of the department, School of Studies in Chemistry, Pt. Ravishankar Shukla University Raipur, India for providing laboratory supports.

REFERENCES

- pollution and child respiratory health: A case-crossover study in Australia and New Zealand. *Am. J. Respir. Crit. Care. Med.* **171**, 1272
- CPCB (2009) Central pollution control board, India. National ambient air quality standards (NAAQS). Gazette notification, New Delhi, 18 November 2009
- Godec, R., Cackovic, M., Sega, K., Beslic, I. (2012) Winter mass concentrations of carbon species in PM₁₀, PM_{2.5} and PM₁ in Zagreb air, Croatia. *Bull. Environ. Contam. Toxicol.* **89**:1087.
- Godri, K., Green, D., Fuller, G., Osto, M. D., Beddows, D., Harrison, R., Mudway, I. (2010). Particulate oxidative burden associated with fireworks activity. *Environ. Sci. Technol.* **44**, 8295.
- Han, L., Zhuang, G., Cheng, S., Wang, Y. and Li, J. (2007). Characteristics of re-suspended road dust and its impact on the atmospheric environment in Beijing. *Atmos Environ* **41**, 7485.
- Hirai, K., Yamazaki, Y., Okada, K., Furuta, S. and Kubo, K. (2000). Acute eosinophilic pneumonia associated with smoke from fireworks. *Intern. Med.* **39**, 401.
- Joly, A., Smargiassi, A., Kosatsky, T., Fournier, M., Zlotorzynska, E.D., Celo, V., Mathieu, D., Servranckx, R., Damours, R., Malo, A., Brook, J. (2010). Characterization of particulate exposure during fireworks displays. *Atmos. Environ.* **44**, 4325.
- Nirmalkar, J., Deb, M.K., Deshmukh, D.K., Verma, S.K. (2013). Mass loading of size-segregated atmospheric aerosols in the ambient air during fireworks episodes in Eastern Central India. *Bull Environ Contam Toxicol*, **90**, 434.
- Nirmalkar J., Deb, M.K. (2015). Impact of intense field burning episode on aerosol mass loading and its possible health implications in rural area of Central India, *Air Qual. Atmos. Health* **9**, 241.

SHORT TERM PERTURBATION IN AEROSOL CHARACTERISTICS OVER NORTHWESTERN PART OF INDIA: CASE STUDY DURING A SEVERE DUST STORM

ONAM BANSAL AND DARSHAN SINGH

Department of Physics, Punjabi University Patiala, 147002, Punjab, India.

KEYWORDS: Particulate matter, Aerosol optical depth, Fine mode fraction, Dust storm.

INTRODUCTION

Atmospheric aerosols perturb the Earth's radiative balance directly by extinction of incoming solar radiation and indirectly by acting as cloud condensation nuclei (CCN) that affects cloud albedo, cloud lifetime, precipitation rate and hydrological cycle. As the Earth's surface is composed of large number of minerals; dust particles are the fine airborne soil or transported rock particles which are removed from the Earth's surface as a result of wind erosion under certain climatic, meteorological and soil conditions. Analysis of various properties of dust aerosols is, therefore, important to determine aerosol sources, mixing processes and transport pathways. Dust storms are common feature in the northwestern part of India, during pre-monsoon season (April–June). During long range transport, dust is mixed with locally generated anthropogenic aerosols resulting in the modification of their physical and optical characteristics and hence their radiative forcing over major part of the Indo-Gangetic Plain (IGP) (Ramanathan *et al.* 2001; Singh *et al.* 2016; Tiwari *et al.* 2015). The present study has been focused on examining the detailed characteristics of the severe dust storm that occurred from 12th June–20th June 2018 and emphasis has been made to study the day-to-day variation of physical and optical properties of aerosols over Patiala, Punjab in the northwest region of India during this period.

METHODS

Ground Based measurements

On line measurements of particles mass concentration (PM₁₀) and number density at 15 different channels (0.35–22.5 μm) were made using GRIMM Aerosol Spectrometer (Model 1.108). Details of this instrument and working principle associated errors are given in Grimm and Eatough (2009). MICROTOSPS-II (MT) sun photometer (Morys *et al.* 2001) was used to measure the spectral AOD at 380, 440, 500, 675 and 870 nm wavelengths. AOD measurements were taken at 1 h time intervals from 0900 to 1700 hours on a clear day. These hourly observations were used for obtaining daily mean AOD. Net SW flux in spectral range of 310–2800 nm has been measured with Pyranometer (Kipp & Zonen). Observations of pyranometer from 0900 IST to 1700 IST have been utilized to derive daily mean net SW flux.

Satellite Based measurements

MODIS Terra observations

In the present study, aerosol optical depth (AOD₅₅₀) is obtained from MODIS level -3 (1°×1°) gridded data on board Terra satellite. It measures the radiance at 36 spectral bands in the visible to thermal IR spectral range of 0.41–14 μm. It has a swath of 2330 km which makes it possible to observe global data in a single day and passes over Indian region at 10:30 AM (Terra) local solar time (Remer *et al.* 2005).

Ozone monitoring instrument (OMI) observation

The ozone monitoring instrument (OMI) aboard Aura is a nadir viewing, wide swath 20 hyper-spectral imaging spectrometer that provides daily global coverage with high spectral resolution and spatial resolution of 13 km × 24 km at nadir (Levelt *et al.* 2006). In the present study, we have used level 3 OMI UV aerosol index (AI) and SSA₅₅₀ using OMAERUV retrieval algorithm products during the study period.

RESULTS & DISCUSSIONS

During the study period meteorological parameters like; temperature varied from 40°C to 26°C, humidity changes from 29% to 80% and wind speed varied from 4 to 11 Km^h⁻¹ remains mostly south-westerly. Backward trajectory analysis using NOAA HYSPLIT model revealed that long range transport of air mass carried the dust aerosols from the southwest Asia to the northwest region of the IGP (figure 1(a,b)). The dust storm hit study site on 13th June and whole observation period is divided into two parts; Non dusty days (12th, 17th, 18th, 19th & 20th June), Dusty days (13th, 14th, 15th and 16th).

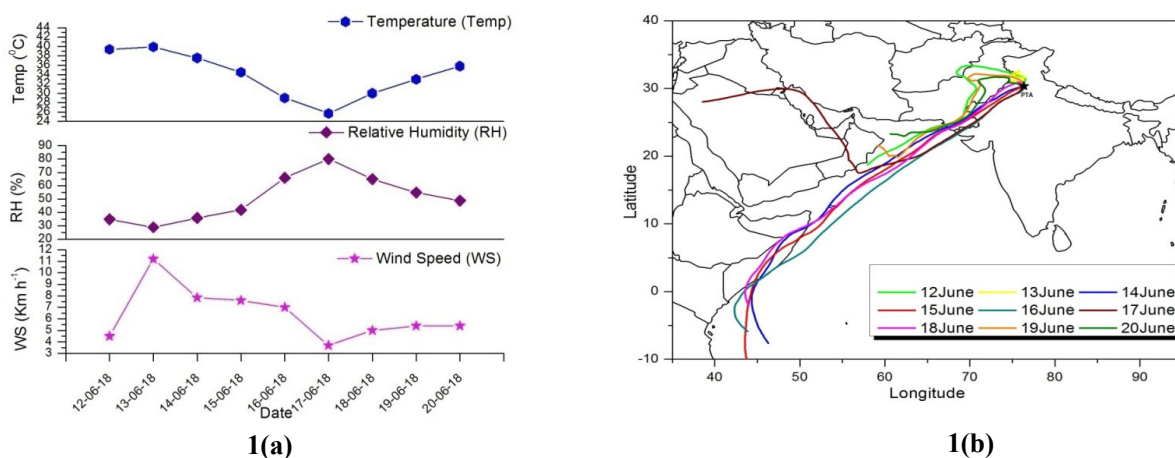


Figure 1(a,b):(a) Variation in Temperature, Relative Humidity, Wind Speed during study period (b) 5-day air mass backward trajectory at the altitude of 500m during study period.

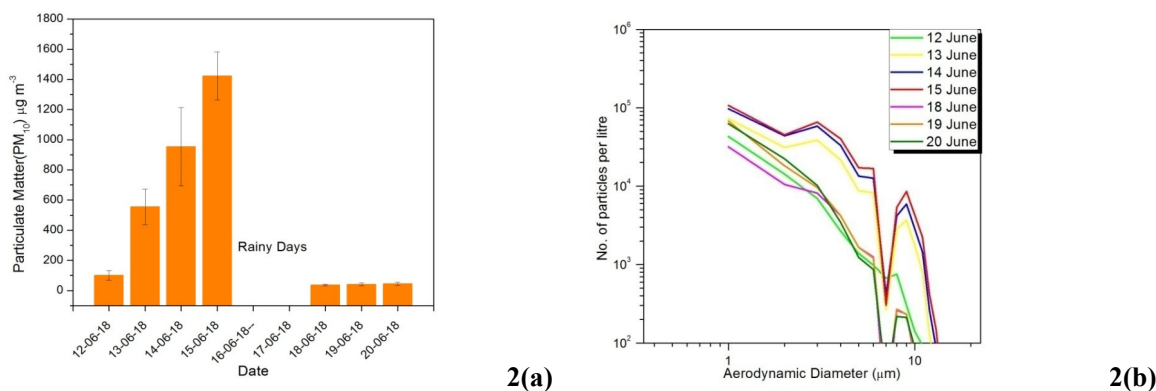


Figure 2 (a,b): (a) Variation in Particulate matter (PM₁₀) during study period with error bar represents standard deviation (b) Variation in particles density with aerodynamic diameter.

During non dusty days, PM₁₀ mass concentration varied from 37 to 100 µg m⁻³ and sudden jump in mass concentration of PM₁₀ was observed during dusty days (13th, 14th & 15th June) reaching highest value of 1422±160 µg m⁻³ on 15th June as revealed from figure 2a. Similarly, in figure 2b it is seen that number density of fine particles (0.35-0.45 µm) decreases while that of coarse particles (>0.45) increases after onset of dust storm on 13th June. Due to rain on 16th & 17th June, there is decrease in mass concentration

as well as number density of particles especially of the coarse mode over the study site from 18th to 20th June.

Table1. The variation of Aerosol Optical Depth (AOD; 550nm), Aerosol Index (AI), Single Scattering Albedo (SSA; 550), Angstrom Exponent (AE), Fine-mode Fraction (FMF) and Net Short Wave Flux (SW; 310-2800nm)

Date	MT AOD ₅₅₀	TERRA AOD ₅₅₀	AI	OMI SSA ₅₅₀	AE	FMF (PM _{2.5} /PM ₁₀)	Net SW (Wm ⁻²)
12-06-18	0.568	0.487	2.8	0.933	0.5	0.3	680
13-06-18	1.043	1.459	3.0	0.953	0.2	0.1	550
14-06-18	2.570	2.207	3.8	0.954	0.0	0.1	438
15-06-18	Cloudy	3.337	5.1	0.953	Cloudy	0.1	213
16-06-18	Rain (26.8mm)	2.810	3.8	0.951	Rain	Rain	336
17-06-18	Rain (23.6mm)	N.A	N.A	N.A	Rain	Rain	396
18-06-18	Cloudy	N.A	N.A	N.A	Cloudy	0.3	439
19-06-18	0.663	0.523	2.2	0.943	0.5	0.3	681
20-06-18	0.531	0.696	1.3	0.930	0.5	0.3	683

Ground based AOD₅₅₀ values increases from 0.568 to a maximum of 2.570 on 14th June while Satellite based AOD₅₅₀ values also depict same increment pattern showing maximum value of 3.337 on 15th June and decreases afterwards (Table1). Since variations in AOD are consistent with the variations of surface mass concentration of particulate matter, hence significant jump in AOD₅₅₀ is attributed to high loading of dust aerosols in the atmosphere over the study site. In conjunction with high value of AOD₅₅₀, increase of Aerosol Index (3.0-5.1), decrease of Angstrom Exponent (0.0 to 0.5) and Fine mode fraction (0.1 to 0.3) during dusty days demonstrates the impact of dust event due to high loading of coarse mode dust particles. OMI derived SSA₅₅₀ increases from 0.933 (12th June) to 0.953 (15th June) indicating the abundance of scattering type aerosols during dust event. In addition to this, surface reaching net short wave flux decreases by more than 50% from 13th onwards and attains a minimum value on 15th June indicating a severe dust storm hit the study region. In similar study of dust storm in year 2012 during 20th -23rd March Singh *et al* 2016 observed a decrease of ~20% in net short wave flux over the study region.

CONCLUSIONS

Significant increment in mass concentration of PM₁₀ and AOD₅₅₀ values indicate abundance of coarse mode particles and low SSA values attributes to scattering nature of dust aerosols over the study region. Significant decrease in SW flux due to severe dust storm resulted in significant decrease in visibility, air quality and may have the potential of affecting the regional climate.

ACKNOWLEDGEMENT

Authors would like to thank ISRO- Geosphere Biosphere Programme for providing the financial support to carry out this study. Meteorological Data from IMD station is highly acknowledged.

REFERENCES

- Grimm, H. and Eatough D. J. (2009), Aerosol measurement: the use of optical light scattering for the determination of particulate size distribution, and particulate mass, including the semi-volatile fraction, *J. Air. Waste. Manage.*, **59**:101–107.
- Levelt, P. F. et al (2006), The ozone monitoring instrument, *IEEE T Geosci. Remote*, **44**:1093–1101.
- Morys, M., Mims, F.M, III., Hagerup, S., Anderson, S.E., Baker, A., Kia, J. and Walkup, T. (2001), Design, calibration, and performance of MICROTOPS II handheld ozone monitor and Sun photometer, *J Geophys Res*, **106**:14573–14582.
- Ramanathan, V., Crutzen, P.J., Kiehl, J.T. and Rosenfeld, D. (2001), Aerosol, climate, and the hydrological cycle, *Science*, **294**:2119-2124.
- Remer, L.A. et al (2005) ,The MODIS aerosol algorithm, products and validation, *J Atmos Sci*, **62**:947–973. doi:10.1175/JAS3385.1.
- Singh, A., Tiwari, S., Sharma, D., Singh, D., Tiwari, S., Srivastava, A. K., Rastogi, N. and Singh, A. K. (2016), Characterization and radiative impact of dust aerosols over northwestern part of India: A case study during a severe dust storm, *Meteorol. Atmos. Phys.*,doi 10.1007/s00703-016-0445-1
- Tiwari, S., Srivastava, A.K., Singh, A.K. and Singh, S. (2015), Identification of aerosol types over Indo-Gangetic Basin: Implications to optical properties and associated radiative forcing, *Environ. Sci. Pollut. Res.*, doi: 10.1007/s11356-015-4495-6.

MEASUREMENT OF CARBONACEOUS AEROSOL WITH HIGH TIME RESOLUTION: EQUIVALENCE of TC-BC and OC/EC

M. RIGLER¹, I. JEŽEK¹, L. DRINOVEC^{1,2}, J. TURŠIČ³, I. KRANJC³, K. GLOJEK⁴, M. OGRIN⁴, J.-P. PUTEAUD⁵, V. GROS⁶, O. FAVEZ⁷, D. GREEN⁸, A. VLACHOU⁹, T. YANDONG⁹, G. STEFENELLI⁹, J.G. SLOWIK⁹, A.S.H. PRÉVÔT⁹, C. HÜGLIN¹⁰, I. STAVROULAS¹¹, J. SCIARE¹¹, A.D.A. HANSEN¹²,
G. MOČNIK^{1,2}

¹Aerosol d.o.o., R&D Dept., Ljubljana, Slovenia.

²Jozef Stefan Institute, Ljubljana, Slovenia.

³Slovenian Environment Agency, Ljubljana, Slovenia.

⁴ Dept. of Geography, Faculty of Arts, University of Ljubljana, Ljubljana, Slovenia.

⁵ EC Joint Research Centre, Institute for Environment and Sustainability, Ispra, Italy.

⁶Lab. des Sciences du Climat et de l'Environnement, CEA-CNRS-UVSQ, Gif sur Yvette, France.

⁷Institut National de l'Environnement Industriel et des Risques, Verneuil en Halatte, France. .

⁸ Environmental Research Group, King's College London, UK.

⁹Paul Scherrer Institut, Laboratory of Atmospheric Chemistry, Villigen PSI, Switzerland.

¹⁰Empa, Swiss Federal Laboratories for Materials Science and Technology, Dübendorf, Switzerland.

¹¹Energy Environment and Water Research Center, Cyprus Institute, Nicosia, Cyprus.

¹²Magee Scientific Corp., Berkeley, USA.

KEYWORDS: total carbon, black carbon, organic carbon, elemental carbon.

INTRODUCTION

Measurements of carbonaceous aerosols are of vital importance for local, regional and global air quality monitoring, regional and global climate change investigations. The approach to the measurement of organic carbon (OC) and elemental carbon (EC) has been recently standardized in Europe (CEN, 2017). We show an equivalent method and a new and innovative instrument, capable of highly time resolved measurement of total carbon (TC), which, combined with black carbon (BC) measurements, provides an equivalent of OC and EC. We call this approach TC-BC.

METHODS

The Total Carbon Analyzer (TCA-08, Aerosol d.o.o.) instrument uses a thermal method for the determination of TC. The instrument has two parallel flow channels with two chambers, which can be used either for sampling either for thermal analysis. While one channel is collecting its sample for the next time-base period, the other channel is analysing the sample collected during the previous period. The instrument collects a sample of atmospheric aerosols on a 47-mm diameter quartz fibre filter enclosed in a small stainless-steel chamber, at a controlled sampling flow rate. The sampling time used in these studies was 1 h, but may be pre-set from 15 minutes to 24 hours. For sampling, a standard flow rate of 16.7 SLPM is used, provided by closed-loop stabilized internal pump.

After collection on the filter, heating modules heat the sample almost instantaneously in a small flow of filtered ambient air. This produces almost complete combustion of all carbonaceous compounds into CO₂, which creates a short-duration, but large-amplitude pulse of CO₂ passed to a detector. The CO₂ concentration over baseline is accurately measured and integrated to give the TC content of the sample. Simplicity of the analysis allow us to have high time resolution measurement and easier field deployment of the instrument as no high purity gases are needed.

Ambient samples were collected on 24 h filters and OC/EC analysis was performed. During the same period TC analyser was operated along with an Aethalometer (AE33, Aerosol d.o.o.; Drinovec et al., 2015) to provide TC and BC concentrations. The relationship between EC and BC is expected to be linear with the slope *b*, but may be site and sample dependent. Once this relationship is established during a sampling/on-line measuring campaign, the TC and BC measurements can be combined to give the equivalent EC (eEC) and equivalent OC (eOC) values:

$$\text{eEC} = b \text{ BC}, \quad (1)$$

$$\text{eOC} = \text{TC} - b \text{ BC}. \quad (2)$$

RESULTS & DISCUSSIONS

We present measurements and analysis for the online speciation of carbonaceous aerosol with a high time resolution. Equivalence of a new online method to the standardized offline thermo-optical OC/EC methods was evaluated within winter field campaigns at different sites around the world. The determined proportionality parameter *b* is region/site specific and depends to a large extent on a thermal protocol used to determine the EC fraction with the conventional OC/EC method.

TC-BC method was validated by comparing averaged high time resolved data to the conventional OC/EC analysis on 24h filters using different thermal protocols (EUSAAR2, IMPROVE, NIOSH) in the winter campaigns in Europe, Asia and N. America: Ljubljana (Slovenia), urban background site; Loški Potok (Slovenia), rural; Ispra/Milano (Italy), urban background, Paris (France), urban background; London (United Kingdom), urban background; Zurich (Switzerland), urban background; Magadino (Switzerland), rural; Beijing (China), urban; New Delhi (India), urban; Los Angeles (United States of America), urban; Additionally, at some sites parallel measurements with aerosol mass spectrometry (AMS or ACSM) allowed us to obtain hourly comparison of OM (AMS) to OC (TC-BC) and determine the OM/OC ratio.

CONCLUSIONS

We show the equivalence of the standardized OC/EC approach with the time resolution 24 hours and the highly time resolved TC-BC measurements.

ACKNOWLEDGEMENTS

This work was supported by the the Slovenian Ministry for Economic Development and EUREKA Eurostars under grant E!8296.

REFERENCES

CEN (2017). *EN 16909:2017 Ambient air. Measurement of elemental carbon (EC) and organic carbon (OC) collected on filters*, European Committee for Standardisation.

Drinovec, L., Močnik, G., Zotter, P., Prévôt, A. S. H., Ruckstuhl, C., Coz, E., Rupakheti, M., Sciare, J., Müller, T., Wiedensohler, A., and Hansen, A. D. A. (2015). The "dual-spot" Aethalometer: an improved measurement of aerosol black carbon with real-time loading compensation, *Atmos. Meas. Tech.*, **8**, 1965.

MEASUREMENT OF CARBONACEOUS AEROSOL: HIGH TIME RESOLUTION MEASUREMENT AND SOURCE APPORTIONMENT OF TC, BC and OC, EC

M. RIGLER¹, I. JEŽEK¹, L. DRINOVEC^{1,2}, J. TURŠIČ³, I. KRANJC³, K. GLOJEK⁴, M. OGRIN⁴, J.-P. PUTEAUD⁵, V. GROS⁶, O. FAVEZ⁷, D. GREEN⁸, A. VLACHOU⁹, T. YANDONG⁹, G. STEFENELLI⁹, J.G. SLOWIK⁹, A.S.H. PRÉVÔT⁹, C. HÜGLIN¹⁰, I. STAVROULAS¹¹, J. SCIARE¹¹, A.D.A. HANSEN¹², G. MOČNIK^{1,2}

¹Aerosol d.o.o., R&D Dept., Ljubljana, Slovenia.

²Jozef Stefan Institute, Ljubljana, Slovenia.

³Slovenian Environment Agency, Ljubljana, Slovenia.

⁴Dept. of Geography, Faculty of Arts, University of Ljubljana, Ljubljana, Slovenia.

⁵EC Joint Research Centre, Institute for Environment and Sustainability, Ispra, Italy.

⁶Lab. des Sciences du Climat et de l'Environnement, CEA-CNRS-UVSQ, Gif sur Yvette, France.

⁷Institut National de l'Environnement Industriel et des Risques, Verneuil en Halatte, France. .

⁸Environmental Research Group, King's College London, UK.

⁹Paul Scherrer Institut, Laboratory of Atmospheric Chemistry, Villigen PSI, Switzerland.

¹⁰Empa, Swiss Federal Laboratories for Materials Science and Technology, Dübendorf, Switzerland.

¹¹Energy Environment and Water Research Center, Cyprus Institute, Nicosia, Cyprus.

¹²Magee Scientific Corp., Berkeley, USA.

KEYWORDS: total carbon, black carbon, organic carbon, elemental carbon.

INTRODUCTION

Carbonaceous aerosols have recently become one of the most favourite topics in the field of atmospheric sciences because they account for a large and often dominant fraction of fine particulate matter (PM_{2.5}) and are extremely diverse. They impact air quality, visibility, the climate, cloud nucleation, the planetary radiation balance, and public health (Pöschl, 2005). The carbonaceous fractions are frequently separated into organic carbon (OC) and elemental carbon (EC) based on their volatility using thermal-optical methods. While the results for OC and especially EC concentrations vary significantly for different thermal evolution protocols, the total carbon (TC) concentration is very consistent between methods (Karanasiou et al., 2015). Therefore, a new TC-BC method is presented which combines an optical method for measuring black carbon (BC), by the Aethalometer AE33 (Drinovec et al., 2014; Hansen et al., 1982), and a thermal method for TC determination, by the newly developed Total Carbon Analyzer (TCA).

METHODS

Recently developed TC-BC online method, which combines an optical method for measuring BC by the Aethalometer AE33, and a thermal method for TC determination by the Total Carbon Analyzer TCA08 is used for source apportionment of carbonaceous aerosols with high time resolution at several measuring sites around the world. TC-BC method determines organic carbon (OC) fraction of carbonaceous aerosols as $OC = TC - b \cdot BC$, where $b \cdot BC$ is equivalent to elemental carbon (EC). The determined proportionality parameter b is region/site specific and depends to a large extent on a thermal protocol used to determine the EC fraction with the conventional OC/EC method.

TCA08 measures concentration of TC by a rapid combustion of carbonaceous matter (CM) collected on a quartz filter. Pulse of CO₂ which is created during combustion phase of the analysis is detected as a large transient increase above the CO₂ level in the ambient air used as the carrier gas. Simplicity of the analysis allow us to have high time resolution measurement and easier field deployment of the instrument as no high purity gases are needed.

RESULTS & DISCUSSIONS

TC-BC method was validated by comparing averaged high time resolved data of AE33 and TCA08 to a conventional OC/EC analysis on 24h filters using different thermal protocols (IMPROVE, NIOSH, EUSAAR2) in the following winter campaigns in Europe, Asia and N. America: Ljubljana (SI), urban background site; Loški Potok (SI), rural; Milano (IT), urban background, Paris (FR), urban background; London (UK), urban background; Zurich (CH), urban background; Magadino (CH), rural; Beijing (CN), urban; New Delhi (IN), urban; Los Angeles (CA, US), urban; Additionally, parallel measurements with aerosol mass spectrometry (AMS) allowed us to obtain hourly comparison of OM_{AMS} to OC_{TC-BC}.

CONCLUSIONS

We show high time resolution measurements and source apportionment of TC, BC, OC, EC and CM and comparison to aerosol mass spectrometry.

ACKNOWLEDGEMENTS

This work was supported by the the Slovenian Ministry for Economic Development and EUREKA Eurostars under grant E!8296.

REFERENCES

Drinovec, L., Močnik, G., Zotter, P., Prévôt, A. S. H., Ruckstuhl, C., Coz, E., Rupakheti, M., Sciare, J., Müller, T., Wiedensohler, A. and Hansen, A. D. A.: The “dual-spot” Aethalometer: an improved measurement of aerosol black carbon with real-time loading compensation, *Atmospheric Measurement Techniques Discussions*, 7(9), 10179–10220, doi:10.5194/amtd-7-10179-2014, 2014.

Hansen, A. D. A., Rosen, H. and Novakov, T.: Real-time measurement of the absorption coefficient of aerosol particles, *Applied Optics*, 21, 3060, 1982.

Karanasiou, A., Minguillón, M. C., Viana, M., Alastuey, A., Putaud, J.-P., Maenhaut, W., Panteliadis, P., Močnik, G., Favez, O. and Kuhlbusch, T. A. J.: Thermal-optical analysis for the measurement of elemental carbon (EC) and organic carbon (OC) in ambient air a literature review, *Atmospheric Measurement Techniques Discussions*, 8(9), 9649–9712, doi:10.5194/amtd-8-9649-2015, 2015.

Pöschl, U.: *Atmospheric Aerosols: Composition, Transformation, Climate and Health Effects*, *Angewandte Chemie International Edition*, 44(46), 7520–7540, doi:10.1002/anie.200501122, 2005.

STUDY OF RELATIONSHIP BETWEEN DUST STORMS AND AEROSOL CONCENTRATION OVER THAR DESERT REGION OF INDIA USING SATELLITE IMAGERIES

P. R. SUJITHA, A. K. BERA, M. K. VERMA AND S. S. RAO

Regional Remote Sensing Centre (West)

NRSC/ISRO, Jodhpur, Rajasthan – 342003, India.

KEYWORDS: Dust storms, aerosol, thar desert, satellite imageries.

INTRODUCTION

The Thar Desert covering parts of Rajasthan, Gujarat, Haryana and Punjab is a hot and arid region with intense aeolian activity. Prevailing aridity, strong summer winds and the existence of loose sands in this region act together to transport the dust (Yadav and Rajamani, 2004). The dust transported to the atmosphere degrades the air quality and affect the human health. An intense international interest in dust storms have been shown due to its influences on regional and global climate as well as its potential to impair health and welfare. The main objective of the study is to analyse dust storm events with reference to aerosol concentration. This paper addresses the study of dust storm event occurred on 04 - 05 June, 2017 over India.

METHODS

Imageries from Indian National Satellite System INSAT-3D were used for the present study. It is an advanced weather satellite of India launched on 26 July 2013 with improved imaging system and atmospheric sounder. The data used includes INSAT-3D Imager LIC (map projected) & L2G Aerosol Optical Depth (AOD) whereas meteorological parameters such as wind speed, temperature, humidity & visibility were obtained from National Climatic Data Centre (NCDC). Based on various published literatures (Mishra *et al.*, 2015 and Hu *et al.*, 2008), the combination of split window algorithm, mid infrared technique, infrared difference dust index (IDDI), spatial coherence techniques are used to identify the spatial extent of the dust storm. The temporal AOD values are extracted over dust storm area by random sampling for comparison. The AOD values and meteorological observations obtained during dust storm and clear sky were compared.

RESULTS & DISCUSSIONS

Present analysis reveals that during pre-monsoon period the dust storm occasionally originates over the Thar Desert region results in increase in aerosol loadings, reducing the visibility and affecting the concentration of aerosols. The spatial extent of dust storm occurred over Thar Desert region during 04 – 05 June 2017 was derived from analysis of satellite imageries is given in figure 1.

It shows that the dust storm originated in Thar Desert moved towards the Indo-Gangetic plain with time. In addition to spatial extent, the concentration of dust storms were indirectly identified using infrared difference dust index. The high concentrations were observed near the sources and get decreased when it is moving away from the source. The observations shows that the AOD value exceeded 1.0 during dust storm events as shown in figure 2. It is also observed that the AOD is positively correlated to the concentration of dust storm.

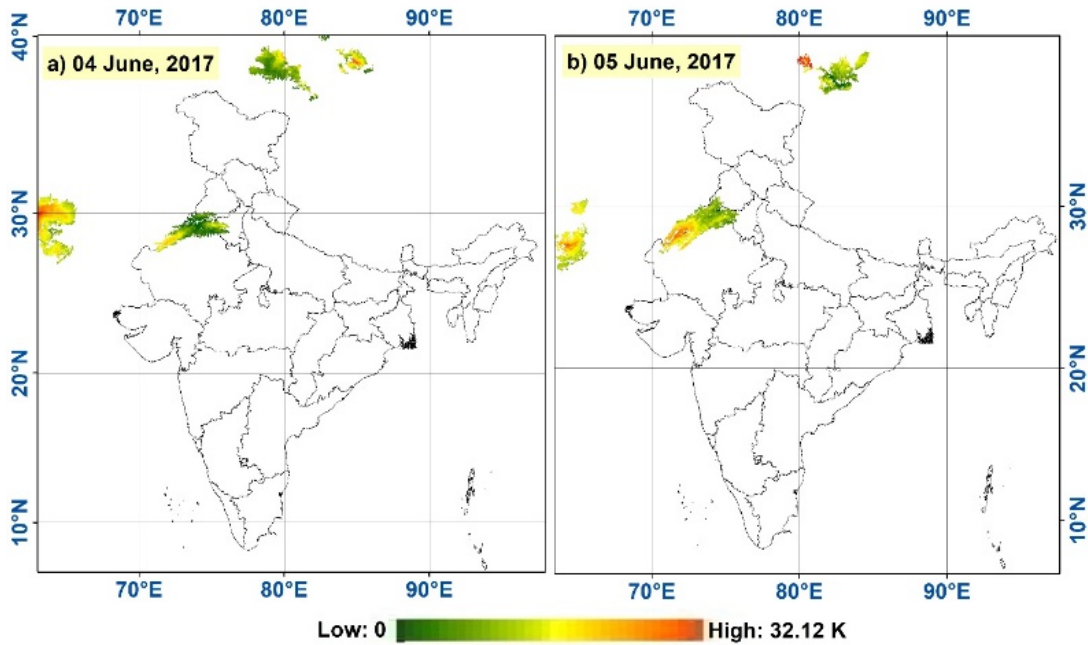


Figure 22: Dust loading in terms of IDDI. a) 04 June, 2017 and b) 05 June, 2017

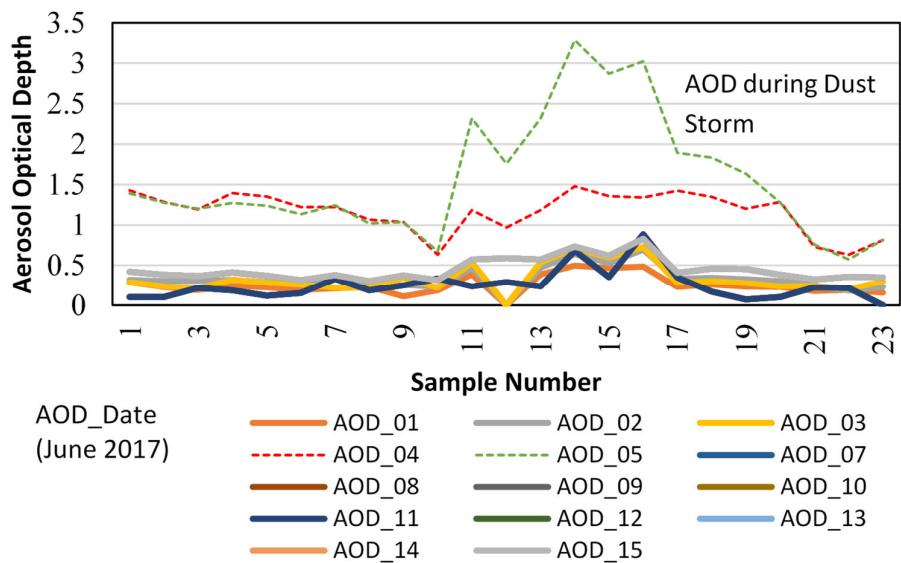


Figure 23: Analysis of AOD data showing higher value during dust storm day (greater than 1.0) and lesser value during normal days (lesser than 1.0)

The analysis of meteorological data shows that the wind speed exceeded 5 knots (Fig. 3) and visibility reduced to 0.4 miles (Fig. 4) during dust storm event, temperature raised to 44⁰ Celsius and humidity decreased to 20% (Fig. 5) on a day before dust storm occurs.

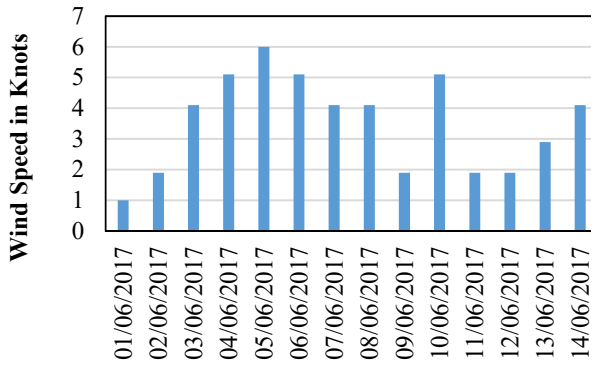


Figure 24: Wind speed data showing higher values at Ganganagar during dust storm event

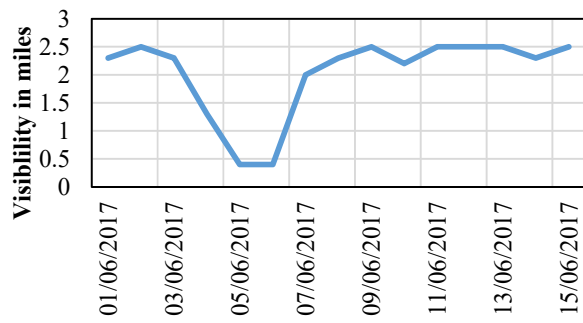


Figure 25: Visibility data showing lesser value at Ganaganagar during dust storm event

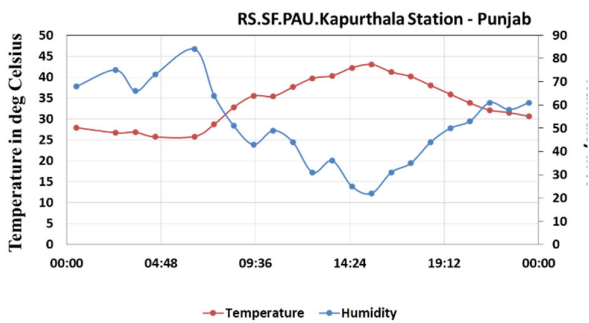


Figure 26: Temperature and humidity obtained on a day before dust storm occurs (03 June 2017)

CONCLUSIONS

The results obtained over Thar desert region have shown reasonably good agreement with various other published works (Prasad and Singh, 2007; Badrinath *et al.*, 2007; Miller and Tegen, 1999). The following conclusions have been drawn out of the present study:

- The aerosol optical depth increases with the concentration of the dust over Thar desert region.
- The visibility decreased considerably with increase in dust loadings.
- The temperature suddenly increases one day before the dust storm event.
- The combination of aerosol optical depth data and meteorological data are found to be necessary to validate the dust storm product derived using satellite imagery.

ACKNOWLEDGEMENTS

This work is a part of ongoing technology development project at RRSC-W, NRSC/ISRO, Jodhpur.

REFERENCES

- Yadav, S. and Rajamani, V. (2004). Geochemistry of aerosols of north western part of India adjoining the Thar desert, *Geochimica et Cosmochimica Acta* **68** (9), 1975-1988. ISSN 0016-7037.
- Mishra M. K., Chauhan, Prakash and Sahay, Arvind (2015). Detection of Asian dust storms from geostationary satellite observations of the INSAT-3D imager. *International Journal of Remote Sensing* **36**:18, 4668-4682.
- Hu X. Q., Lu N. M, Niu T. and Zhang P. (2008). Operational Retrieval of Asian Sand and Dust Storm from FY-2C Geostationary Meteorological Satellite and Its Application to Real Time Forecast in Asia. *Atmospheric Chemistry and Physics* **8**, 1649-2008.
- Prasad A. K. and Singh R.P. (2007). Changes in aerosol parameters during major dust storm events (2001–2005) over the Indo-Gangetic Plains using AERONET and MODIS data. *Journal of Geophysical Research* **112**, D09208, doi:10.1029/2006JD007778.
- Badarinath K. V. S., Kharol, S. K., Kaskaoutis, D. G. and Kambezidis, H. D. (2007). Case Study of Dust Storm Over Hyderabad, India: Its Impact on Solar Radiation Using Satellite Data and Ground Measurements. *Science of the Total Environment* **384**, 316–322.
- Miller, R. L. and Tegen, I. (1999). Radiative forcing of a tropical direct circulation by soil dust aerosols. *Journal of Atmospheric Sciences* **56**, 2403–2433.

STUDY OF ATMOSPHERIC AEROSOL OVER SEMI-ARID URBAN REGION RAJKOT USING MULTI-WAVELENGTH SOLAR RADIOMETER

NIMIT GODHANI, POOJA BHIMAJIYANI, CHINTAN JETHVA, H. P. JOSHI

Department of Physics, Saurashtra University, Rajkot - 360005, India.

nimitgodhani@gmail.com

KEYWORDS: AOD, Angstrom Exponent, MWR

INTRODUCTION

Aerosols are tiny particles suspended in the atmosphere which may in solid or liquid form and may be a mixture of both. Aerosols of different sizes, magnitude, and composition play a vital role in many atmospheric processes such as visibility, radiation balance, air pollution, human health, cloud formation etc. (Rajesh 2013). Also, aerosol particles have a substantial influence on global and regional climate change by absorbing and scattering solar radiation (Charlson et al. 1992). These are produced by natural or anthropogenic sources or can be transported from different regions depending upon the meteorological conditions. These aerosol have size ranging from $0.001\mu\text{m}$ to $100\mu\text{m}$, these can be further divided into 1) Nucleation mode ($0.001\ \mu\text{m} < r < 0.1\ \mu\text{m}$), 2) Accumulation mode ($0.1\ \mu\text{m} < r < 1.0\ \mu\text{m}$), 3) Coarse mode ($r > 1.0\ \mu\text{m}$)(Seinfeld and Pandis 2006).

Aerosol optical depth (AOD) is an important parameter of aerosol's optical properties, indicating the aerosol concentration over the entire vertical column of the atmosphere(Gupta, Gadhavi, and Jayaraman 2003). The presence of aerosols in the atmosphere contributes to the total optical depth, which is a measure of the transparency of the atmosphere due to the extinction of solar radiation. The amount of solar radiation extinction relates to the number of aerosols in the atmosphere. The presence of aerosols affects the transparency of the atmosphere which is referred to as aerosol optical depth, the major contributor to the extinction of solar radiation. Hence, environmental scientists are concerned about the effects of aerosols due to their capacity to warm and/or cool the planet. The focus here is to calculate optical parameters of aerosols by measuring the radiation at the surface (direct irradiance) with respect to time and wavelength using a Multi-Wavelength Sola Radiometer (MWR).

METHODS

The measurements of spectral aerosol optical depths at ten different wavelengths (380 – 1025 nm) were conducted using multi-wavelength solar radiometer (MWR) at semi-arid region Rajkot ($22^{\circ}29'$ N, $70^{\circ}74'$ E, 142 m above MSL) for the period of October 2017 to May 2018. The Multi-Wavelength Solar Radiometer (MWR), designed and developed in the Space Physics Laboratory, VSSC, Thiruvananthapuram(Moorthy et al. 1999) has been extensively used by several research institutions across the country for estimating columnar spectral aerosol optical depth (AOD), the most important parameter needed for assessing the impact of aerosols on regional aerosol forcing. Aerosol optical depths is defined as the attenuation of direct solar radiation passing through the atmosphere by scattering and absorption due to aerosols. The AODs were calculated using lambert-beer law

$$V(\lambda) = V_0(\lambda)\exp\{-(\tau_{total})am\}$$

Wavelength (Angstrom) Exponent and atmospheric turbidity are related through Angstrom turbidity formula, given by (Angstrom 1961), which are calculated using (400, 450, 500, 600, 650, 750, 850nm) wavelengths.

$$\tau_{Aerosol} = \beta\lambda^{-\alpha}$$

The AOD 500nm from MWR is converted to 550nm using the following formula (Sun et al. 2018)

$$\tau_{(550)} = \exp(\ln(\tau_{(500)} - \alpha \ln 1.1))$$

RESULTS & DISCUSSIONS

Rajkot is a semi-arid urban region near the Arabian Sea. Rajkot is the 35th-largest urban agglomeration in India, with 22th fastest-growing city in the world .and one of the prime industrial center of Gujarat which directly points towards the dominant in atmospheric pollution.

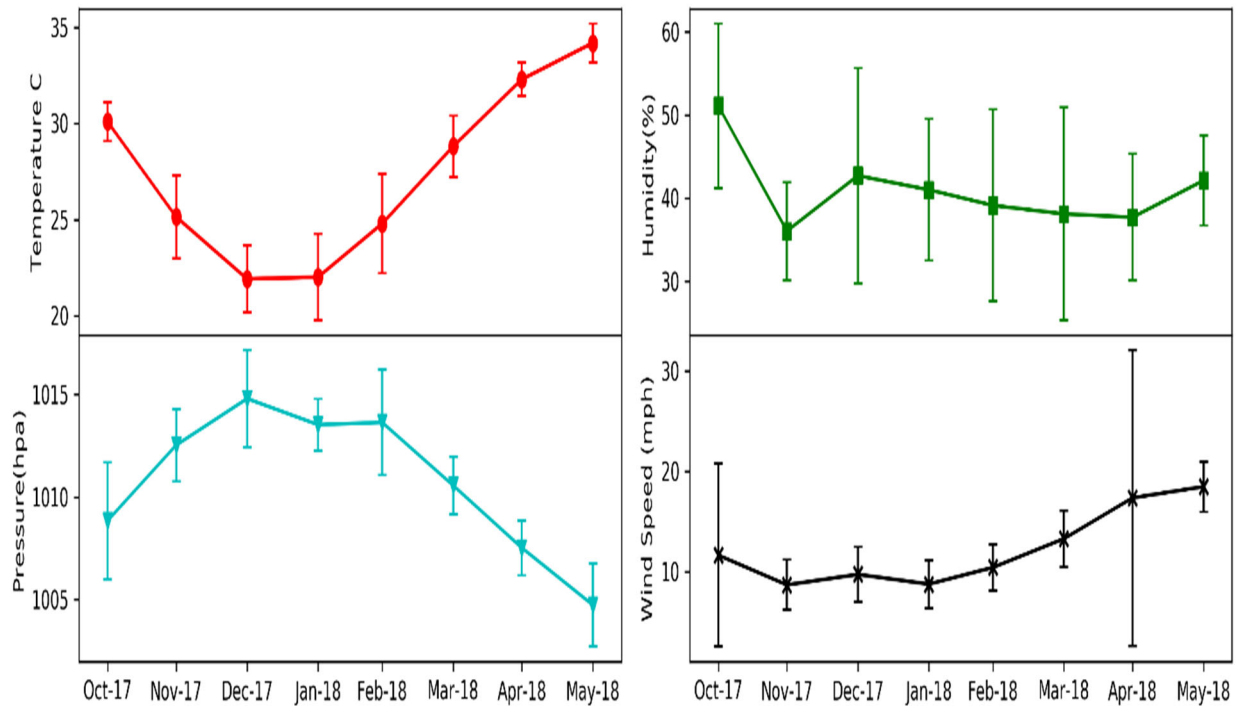


Figure 27 Monthly variation of meteorological parameters over Rajkot (Oct-2017 to May-2018).

Figure 1 shows the monthly mean metrological parameter over Rajkot, derived from daily mean value. The max average temp is 34.1 C in May, Humidity is 51.1% in Oct and Pressure is 1014.8 hPa in Dec is found.

Monthly averaged values of AOD for the entire period of observation (Oct-2017 to May-2018) for all ten wavelengths are shown in fig. 2. The AOD value shows more or less similar behavior for all wavelengths.

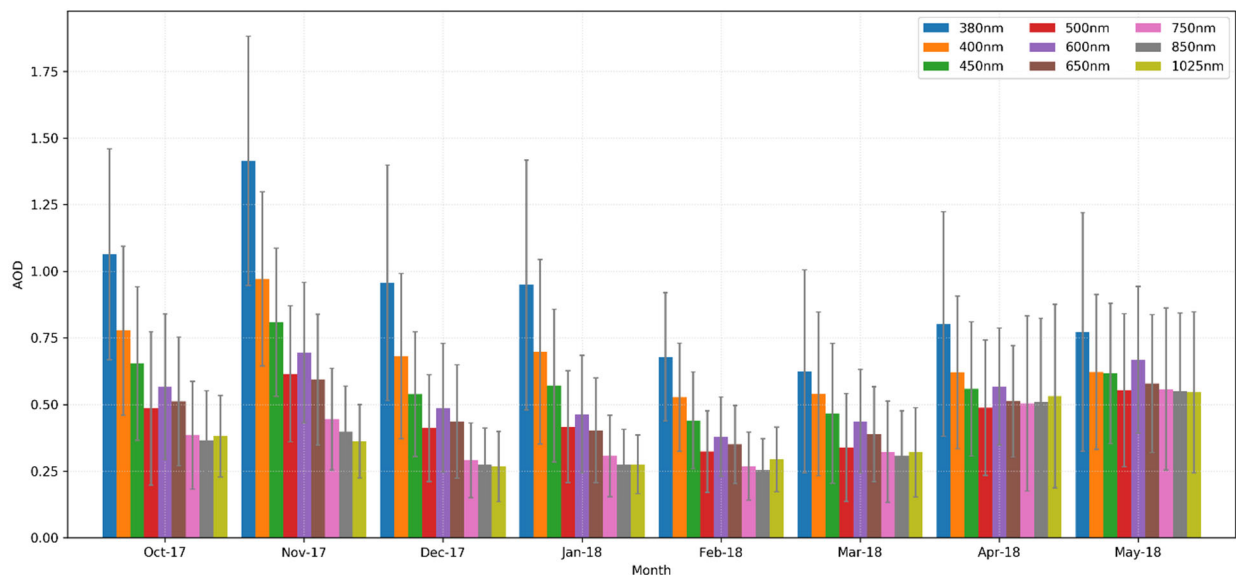


Figure 28 Monthly variation of AOD (380-1025 nm) (Oct-2017 to May-2018).

The results show that the mean AOD at a shorter wavelength (380-450nm) is maximum (~1.24 at 380nm) during the post-monsoon season and minimum during winter (~0.52 at 450nm). On the other hand longer wavelength (650-850nm) the AOD is higher during pre-monsoon months (~0.46 at 850nm) as compared to other seasons.

Table 5 Seasonal variation of AOD over Rajkot (Oct-2017 to May-2018)

Season	380nm	400nm	450nm	500nm	600nm	650nm	750nm	850nm	1025nm
Post Monsoon	1.24	0.87	0.73	0.55	0.63	0.55	0.41	0.38	0.37
Winter	0.86	0.64	0.52	0.38	0.44	0.40	0.29	0.27	0.28
Pre Monsoon	0.73	0.59	0.55	0.46	0.56	0.49	0.46	0.46	0.47

It is shown that AOD value for shorter wavelength is high in the month of Post monsoon season because of more scattering/absorption by fine mode aerosols. While it is decreased in months of Pre Monsoon season, which shows Fine mode dominance in Post Monsoon. Where at longer wavelengths higher AOD is found in Pre Monsoon, which indicates that course mode particles are dominant. In contrast, the high value in the month of April-May is mainly because of transported dust and local contribution from occasional dust raising winds over Rajkot.

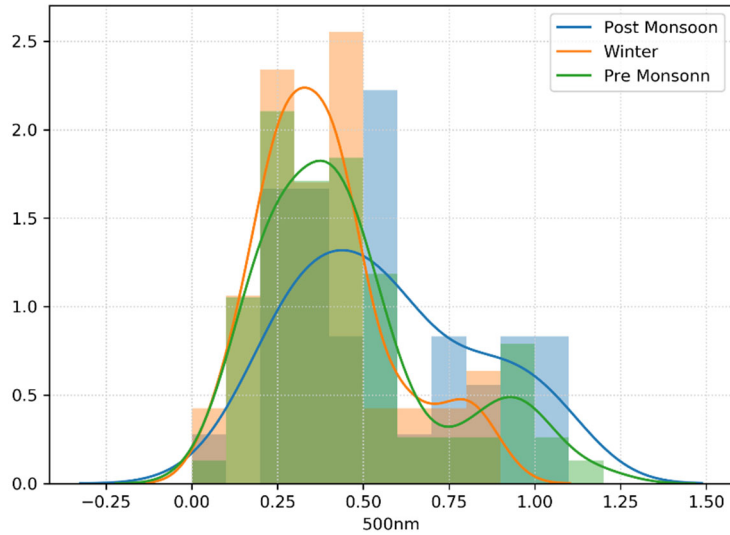


Figure 29 Seasonal Frequency Distribution of AOD_(500nm).

Figure 3 shows the seasonal frequency distribution of AOD_(500nm). It indicates that in the winter and Pre-Monsoon it shows the bimodal distribution.

Figure 4 shows the comparison of AOD at 550nm between ground based and satellite observations during the period. For this comparison AOD from MWR (500nm) is converted into 550nm AOD for comparison. The AOD values are well correlated within the range of standard deviation, except for the Apr - May with slightly high difference.

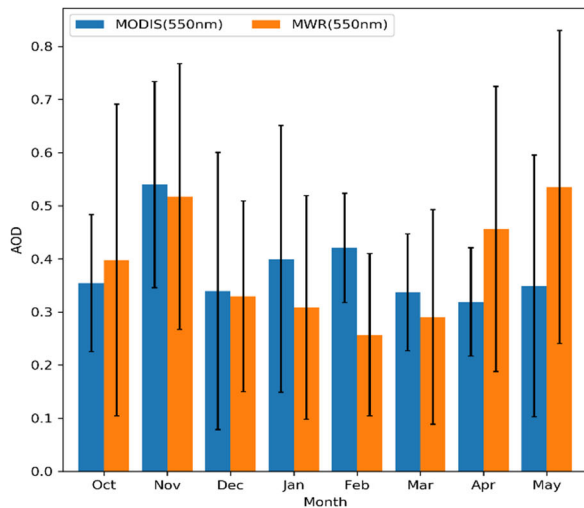


Figure 4 Comparison of MWR and MODIS AOD (550nm)

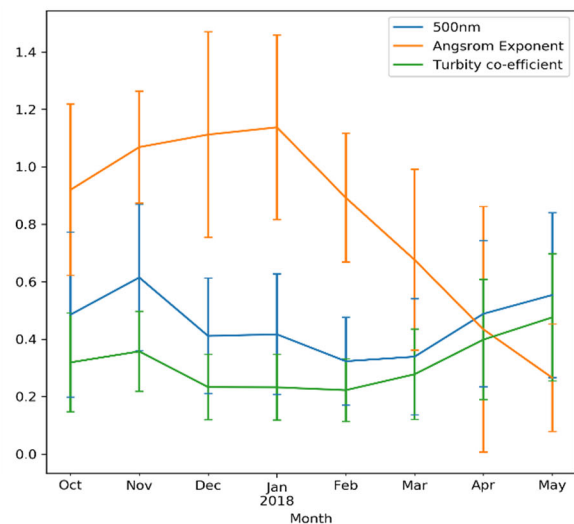


Figure 5 Monthly Variation of Angstrom Exponent and Turbidity Co-efficient and AOD 500nm

Figure 5 shows the monthly variation of Angstrom Exponent (α) and Turbidity Co-efficient (β). The wavelength exponent is high during the month of Dec-Jan and lower in Apr-May compared to other months. Wavelength exponent shows the inverse relation with Turbidity Co-efficient as well as the AOD (500nm).

AOD at 500nm shows the similar pattern of variation with β during the period of observation. From the figure 5, it is evident that high values of ($\alpha > 1$) are consistent feature over most of the Indian region during the dry season that is because of local effects from industrial or urban activities.

CONCLUSIONS

The results show that the mean AOD at shorter wavelength is higher during the post-monsoon season and minimum during winter season, which shows the fine mode particles are dominant. Where at the longer wavelength the AOD is higher during pre-monsoon, which indicate the coarse mode particles are dominant. The frequency distribution of AOD_(500nm) shows a bimodal distribution in winter and pre-monsoon season. AOD from MWR and MODIS are well correlated within the range of standard deviation. Wavelength exponent shows the inverse relation with Turbidity Co-efficient as well as the AOD (500nm). The values of ($\alpha > 1$) are high in winter months because of the dry season and other urban activities.

ACKNOWLEDGMENTS

The authors are thankful to ISRO-ARFI for providing financial assistance to this project, MODIS for providing the required datasets and Python for data processing.

REFERENCES

- Angstrom, Anders. 1961. "Techniques of Determining the Turbidity of the Atmosphere." *Tellus* 13 (2): 214–23. <https://doi.org/10.1111/j.2153-3490.1961.tb00078.x>.
- Charlson, R. J., S. E. Schwartz, J. M. Hales, R. D. Cess, J. A. Coakley, J. E. Hansen, and D. J. Hofmann. 1992. "Climate Forcing by Anthropogenic Aerosols." *Science* 255 (5043): 423–30. <https://doi.org/10.1126/science.255.5043.423>.
- Gupta, Pawan, Harish Gadhavi, and A. Jayaraman. 2003. "Aerosol Optical Depth Variation Observed Using Sun-Photometer over Indore." *IJRSP Vol.32(4) [August 2003]*, August. <http://nopr.niscair.res.in/handle/123456789/25800>.
- Moorthy, KK, K Niranjan, B Narasimhamurthy, VV Agashe, and BV Krishna Murthy. 1999. "Aerosol Climatology over India; 1–ISRO GBP MWR Network and Database." *ISRO GBP SR-03 99*.
- Rajesh, T A. 2013. "Software Package for Aerosol Size Distribution." *International Journal of Scientific Engineering and Technology* 2 (4): 7.
- Seinfeld, John H., and Spyros N. Pandis. 2006. *Atmospheric Chemistry and Physics: From Air Pollution to Climate Change*. 2nd ed. Hoboken, N.J: J. Wiley.
- Sun, Enwei, Huizheng Che, Xiaofeng Xu, Zhenzhu Wang, Chunsong Lu, Ke Gui, Hujia Zhao, et al. 2018. "Variation in MERRA-2 Aerosol Optical Depth over the Yangtze River Delta from 1980 to 2016." *Theoretical and Applied Climatology*, May. <https://doi.org/10.1007/s00704-018-2490-9>.

ABSORBING AEROSOLS OVER A SEMI ARID RAIN SHADOW LOCATION IN INDIA

P.S. SOYAM^{1*}, P.D. SAFAI², K.TODEKAR², S.BANKAR², D. GURNULE² AND T. PRABHAKARAN²

¹ Department of Environmental Sciences, Savitribai Phule Pune University, Pune, ² Indian Institute of Tropical Meteorology, Pune, India.

ABSTRACT

Using multi-wavelength MAGEE Scientific, model AE33 aethalometer black carbon aerosols concentrations and source apportionment study was carried out at Solapur, a rain shadow area of Maharashtra, India from April 2017 to March 2018. BC exhibits a strong seasonal variability during the winter with high BC value of 6.40 $\mu\text{g}/\text{m}^3$ and low BC concentration of 1.01 $\mu\text{g}/\text{m}^3$ during monsoon season. Seasonal diurnal variation of BC mass concentration showed the significant trend with two maxima and two minima during the winter and summer months. Annual means percentage contribution of fossil fuel (BC_{ff}) and wood biomass burning (BC_{wb}) to total mass concentration of BC was found to be 66% and 34% respectively over the study region. The results indicates the dominance of fossil fuel burning as compared to wood biomass burning at the study location.

KEYWORDS: Black carbon aerosols, Source Apportionment, Rain shadow location.

INTRODUCTION:

Atmospheric aerosols are the solid and liquid particles in the atmosphere. Aerosols have natural as well as anthropogenic origin and contain many different compounds depending upon their source of origin. For example, pollen, spores, sea salts, nitrates, sulfates, mineral dust and soot. The microphysical properties of the aerosols influence the atmospheric radiation balance as well as precipitation formation mechanism. Black carbon (BC) aerosols are the product of incomplete combustion of fossil fuels and biomass. Black carbon aerosols can influence the environment in various ways on local, regional, and global scales. These aerosols influence the attenuation of solar radiation by reflection and scattering based on their size and chemical characteristics. So far, studies on BC from semi arid regions are very few (Kumar et al, 2011).

METHODS AND STUDY LOCATION:

Sampling Location

Under the CAIPEEX ground observational campaign, continuous monitoring of black carbon (BC) aerosol was carried out at the Sinhgad College of Engineering, Solapur, Maharashtra, India (17°43'45.4332" N, 75°51'24.4476" E) during April 2017 to March 2018 using a multi-wavelength Aethalometer (MAGEE Scientific, model AE33) at 1 min interval and 5 LPM flow rate. Solapur falls under a rain shadow zone and the climate is dry with mean seasonal rainfall of about 540 mm.

Aethalometer

The multi-wavelength aethalometer measures the light absorbing BC mass concentration across 7 optical wavelengths viz. 370, 470, 520, 590, 660, 880 and 950 nm. It measures the light beam attenuation (ATN)

transmitted through the sample laden quartz fiber filter which is directly proportional to the concentration of BC on the filter paper tape (Hansen et al. 1984). In order to account for Spot-loading effect, the model AE-33 Aethalometer employs the dual-spot technique in which the two attenuation results are combined to eliminate non-linearity, providing compensated particle light absorption and hence corrected BC mass concentration (Drinovec et al., 2015).

Source Apportionment of BC

BC source apportionment is obtained based on the Sandradewi et al.(2008a) model where relative occurrence of fossil fuel and biomass burning fraction is calculated by measuring light absorption coefficient at ultraviolet (370 nm) to infrared (880 nm) wavelengths. The total aerosol absorption coefficient (b_{abs}) (Sandradewi et al.2008a) is represented as:

$$b_{abs\ Total}(\lambda) = b_{abs}(\lambda_{ff}) + b_{abs}(\lambda_{bb}) \quad (1)$$

$$\frac{b_{abs}(470nm)_{ff}}{b_{abs}(950nm)_{ff}} = \left(\frac{470}{950}\right)^{-\alpha_{ff}} \quad (2)$$

$$\frac{b_{abs}(470nm)_{bb}}{b_{abs}(950nm)_{bb}} = \left(\frac{470}{950}\right)^{-\alpha_{bb}} \quad (3)$$

where $b_{abs\ Total}(\lambda)$ is total absorption coefficient, λ is the wavelength, $b_{abs}(\lambda)_{ff}$ is fossil fuel fraction and $b_{abs}(\lambda)_{bb}$ is biomass burning fraction. In the present study, we have used 1 and 1.8 as α_{ff} and α_{bb} values.

RESULTS & DISCUSSIONS:

Seasonal Variation in BC mass concentration

Seasonal variation in the black carbon mass concentrations is observed to determine the behavior of BC along the different seasons of the year (Fig.1). Lower BC concentrations of $1.01\mu\text{g}/\text{m}^3$ are observed during the monsoon season due to the rain removal process. However, post-monsoon BC concentrations showed equally low concentration of $1.21\mu\text{g}/\text{m}^3$ as NE rains further continue the removal of BC during the months of post-monsoon. Solapur receives about 25 % of its annual rain in this period. Higher BC values are observed during the winter months with mean BC concentrations of $6.40\mu\text{g}/\text{m}^3$.

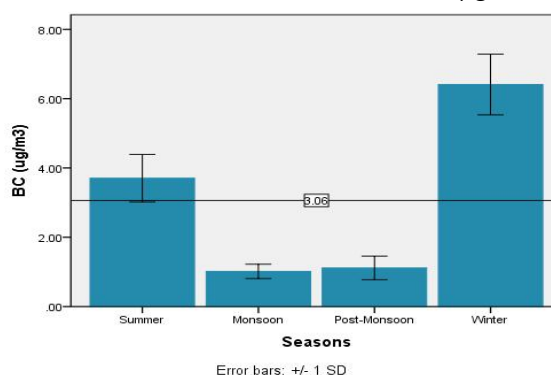


Figure 1. Seasonal variation in BC mass concentration as a function of time with $\pm\sigma$ (April 2017 – March 2018)

Season-wise diurnal variation in BC mass concentration

Season-wise diurnal variation are observed during the whole year show in Fig 2, which shows significant diurnal variation with two maxima and two minima for the winter and summer months. The first maxima observed during morning around 07:00 – 11:00 hr with BC mass concentration of $10.95\mu\text{g}/\text{m}^3$ with a gradual decrease with second minima of $3.70\mu\text{g}/\text{m}^3$ during the afternoon hours. The second maxima are

observed during the night around 20:00 – 00:00 followed by first minima during early morning hours. The seasonal diurnal variation is due to the variation in the mixing layer height and the strength of the sources.

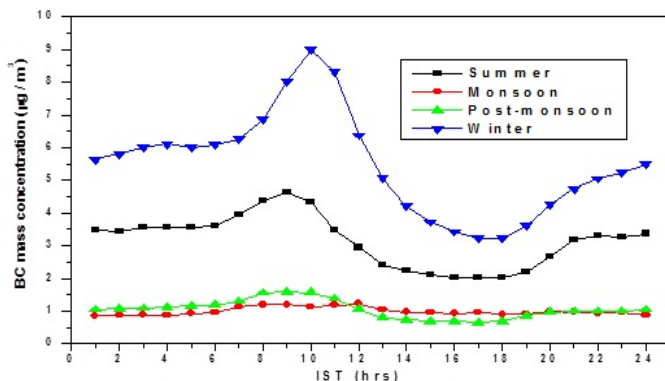


Figure 2. Variation in mean season-wise diurnal BC mass concentrations (April 2017 – March 2018).

Contribution of Fossil Fuel and Biomass Burning BC

The mean monthly contribution of fossil fuel component of BC increased during the monsoon (JJAS) and post-monsoon (ON) months and a declining trend was observed during the winters (DJF) and summers (MAM) months shown in Fig. 3 (a & b). Biomass burning (BC_{wb}) significantly contributes during the winter and summer (~ 40 %) as a result of increased crop residue burning activities. Annual mean of fossil fuel (BC_{ff}) and wood biomass burning (BC_{wb}) to total mass concentration of BC was found to be 66% and 34% over the study region throughout the year.

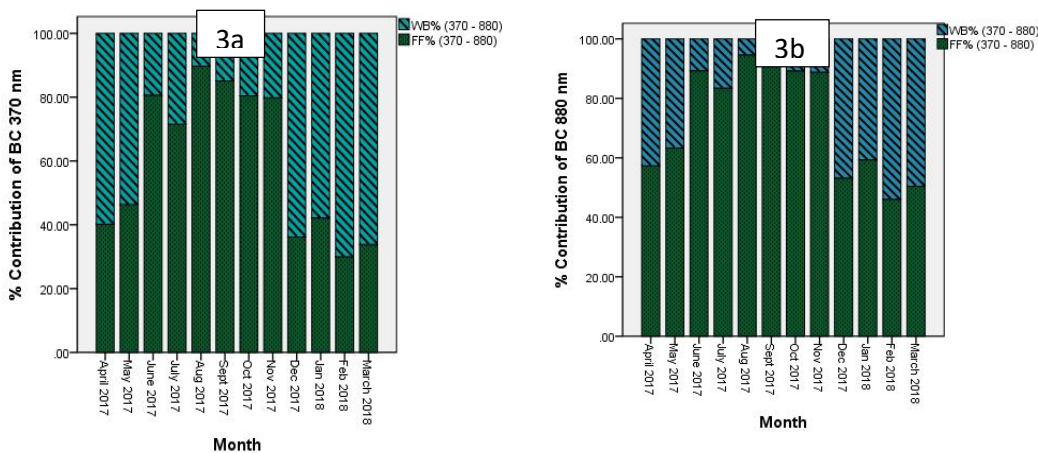


Figure 3(a&b). Percentage contribution of BC_{ff} & BC_{wb} at 370 nm and 880 nm (April 2017–March 2018).

CONCLUSIONS:

Mean BC mass concentration was maximum ($6.40 \mu\text{g}/\text{m}^3$) and minimum ($1.01 \mu\text{g}/\text{m}^3$) during monsoon and winter season, respectively. Strong seasonal gradient in BC mass concentration with lowest values during June to November mainly due to scavenging by rains and highest values during December to May as a result of low mixing heights in winter and more biomass burning in summer.

Scavenging effect of NE monsoon during the post-monsoon resulted in the lower BC mass concentration of $1.21 \mu\text{g}/\text{m}^3$ during the season.

Diurnal BC mass concentration showed strong seasonal variability with two maxima and two minima due to variation in mixed layer height and strength of sources during winter and summer.

Dominance of BC_{ff} was observed during monsoon and post-monsoon, and BC_{wb} dominance observed during winter and summer season of the year. Annual mean of fossil fuel (BC_{ff}) and wood biomass burning (BC_{wb}) to total mass concentration of BC was found to be 66% and 34% over the study region throughout the year.

ACKNOWLEDGEMENTS:

Authors are thankful to the Director of IITM for his support and encouragement during the entire CAIPEEX ground campaign. Thanks are also due to the Head, Environmental Sciences Department, SPPU for his support and guidance. Authors are grateful to all the team members of CAIPEEX at Solapur.

REFERENCES:

Drinovec L, Močnik G, Zotter P, Prévôt ASH, Ruckstuhl C, Coz E, Rupakheti M, Sciare J, Müller T, Wiedensohler A, Hansen ADA (2015). The "dual-spot" Aethalometer: an improved measurement of aerosol black carbon with real-time loading compensation. *Atmos Meas Tech* 8, 1965-1979.

Hansen ADA, Rosen H, Novakov T (1984) The Aethalometer—an instrument for the real-time measurement of optical absorption by aerosol particles. *Sci Total Environ* 36:191–196.

Kumar, K. R., Narasimhulu, K., Balakrishnaiah, G., Reddy, B. S. K., Gopal, K. R., Reddy, R. R., Babu, S. S. (2011). Characterization of aerosol black carbon over a tropical semi-arid region of Anantapur, India. *Atmospheric Research*, 100(1), 12–27.

Sandradewi J, Prevot A, Weingartner E, Schmidhauser R, Gysel M, Baltensperger U (2008a) A study of wood burning and traffic aerosols in an Alpine valley using a multi-wavelength Aethalometer. *Atmos Environ* 42(1):101–112.

Sandradewi J, Prevot AS, Szidat S, Perron N, Alfarra MR, Lanz VA, Weingartner E, Baltensperger U (2008b) Using aerosol light absorption measurements for the quantitative determination of wood burning and traffic emission contributions to particulate matter. *Environ Sci Technol* 42(9):3316–3323.

SEASONAL VARIABILITY OF SUSPENDED PARTICULATE MATTER IN AMBIENT ATMOSPHERE OVER SIKKIM HIMALAYA, INDIA

SHARMA, K^{1*} AND RANJAN, R.K.¹

¹Department of Geology, Sikkim University, Gangtok, Sikkim, India 737102

*ksharma01@sikkimuniversity.ac.in

KEYWORDS: Aerosols, Suspended Particulate Matter (SPM), Vehicular Emission, Eastern Himalaya.

INTRODUCTION

Suspended particulate matter (SPM) in the ambient atmosphere was measured at Gangtok, Sikkim, India, located at 1650 meters above mean sea level. This work is the first attempt to study the ambient SPM characteristics in the Eastern part of Himalaya. SPM has been collected on Whatman QMA 47 mm fiber filter in different seasons with the help of aerosols sampler as per US-EPA prescribed method having a flow rate of 15 liters per minute (lpm) near Pani House, NH-10, Gangtok (27°19'25.52"N 88°36'34.58"E, 1504 m). SPM concentration at this altitude of Eastern Himalayan region has shown a high seasonal variability ranging from $94.43 \pm 40.23 \mu\text{g}/\text{m}^3$ during winter to $76.63 \pm 18.52 \mu\text{g}/\text{m}^3$ during summer. The maximum SPM concentration is found to be $176.15 \mu\text{g}/\text{m}^3$ in the month of January and minimum concentration is $50.29 \mu\text{g}/\text{m}^3$ in the month of March.

METHODS

SPM has been collected on Whatman QMA 47 mm fiber filter in different seasons with the help of aerosols sampler as per US-EPA prescribed method having a flow rate of 15 liters per minute (lpm) near Pani House, NH-10, Gangtok (27°19'25.52"N 88°36'34.58"E, 1504m). The sampler was placed on the roof top of a residential building at a height of about 10 m above the road level which is located at the side of National Highway. Sampling of an aerosol was carried out for 8 months from January 2018 to August 2018. Sampler was operated continuously for two days at an interval of 7days. For conditioning, the filter papers were placed in desiccators for 24 h before and after sampling. The desiccated filter papers were weighed using Sartorius weighing balance (CPA26P) having 2 μg m resolution. Aerosol concentrations were determined gravimetrically by dividing the difference in weight of the filter paper before and after the sampling with the volume of air sampled.

RESULTS & DISCUSSIONS

The monthly mean concentration of ambient SPM in Gangtok has shown a high monthly variability (table 1 and figure 1).

Table 1. Monthly mean concentration of SPM

Month	SPM ($\mu\text{g}/\text{m}^3$)
January	154.18
February	75.34
March	87.92
April	88.89
May	97.92
June	76.43

July	62.65
August	57.25

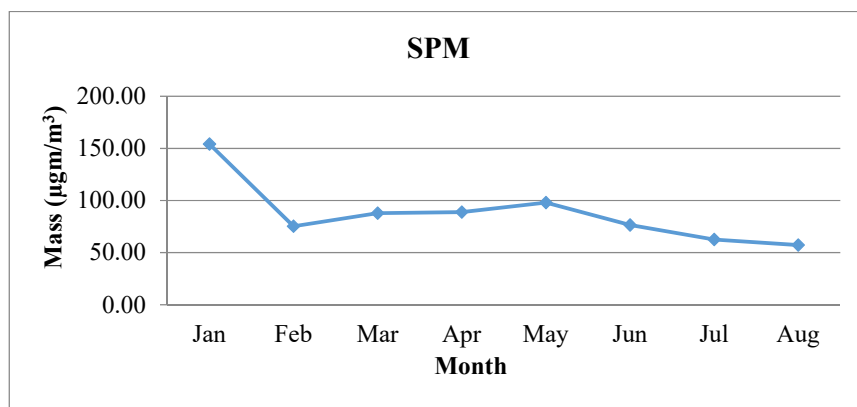


Figure 1: Monthly mean variability of SPM

CONCLUSIONS

SPM concentration in Gangtok is less than the prescribed standard of CPCB-NAAQS (140 annually and 200 Daily-24 hrs) all throughout the season. The SPM concentration during winter season (Jan-March) is significantly higher than summer. The higher concentration of SPM during winter may be attributed to higher vehicular emission due to high tourist influx, biomass burning and stable atmospheric condition. Whereas, the low concentration of SPM during summer may be accredited to high precipitation in the latter half of the season, and unstable atmospheric condition.

REFERENCES

- Ahirwar . A. V and Bajpai. S, (2017). *Seasonal Variability of TSPM, PM₁₀ and PM_{2.5} in Ambient Air at an Urban Industrial area in Eastern Central Part Of India*. International Journal of Civil Engineering and Technology (IJCIET), Volume 8, Issue 3, pp. 252–261 Article ID: IJCIET_08_03_026
- Dumka, UC et al. (2011). *Altitude variation of aerosol properties over the Himalayan range inferred from spatial measurements*. Journal of Atmospheric and Solar-Terrestrial Physics, Vol. 73, 1747-1761
- Gadi R, Sarkar A K, Gera B S, Mitra A P, and Parashar D C (2001). *Chemical Composition of Atmospheric Aerosols at New Delhi*. Indian Journal of Radio & Space Physics, Vol. 31, pp 93-97
- P. Pant et al. (2016). *Analysis of size-segregated winter season aerosol data from New Delhi, India* Atmospheric Pollution Research, Vol. 7 pp100-109
- Poschl U., et al (2005). *Atmospheric Aerosols: Composition, Transformation, Climate and Health Effects*. Angew. Chem. Int. Ed, 44, 7520-7540
- Ramachandran. S., and R. Cherian (2008). *Regional and seasonal variations in aerosol optical characteristics and their frequency distributions over India during 2001–2005*, J. Geophys. Res., 113, 1-16
- Sharma, V.K, and Patil, R.S (1992). *Size distribution of atmospheric aerosols and their source identification using factor analysis in Bombay, India*. Atmos. Environ. 26B, 135e140.
- Srivastava, A. and Jain, V.K. (2007c). *Size Distribution and Source Identification of Suspended Particulate Matters in Atmospheric Aerosols Over Delhi*. Chemosphere. 68: 579-589.

ANALYSIS OF SURFACE OZONE (O₃) AND ITS CHEMISTRY AT A SEMI-ARID REGION, ANANTAPUR, SOUTHERN INDIA

B. ELIJABETHAMMA¹, G. BALAKRISHNAIAH¹, S. PAVANKUMARI¹, K. RAMA GOPAL¹ AND R.R. REDDY¹

¹Aerosol & Atmospheric Research Laboratory, Department of physics, Sri Krishnadevaraya University, Anantapur 515003, A.P, India.

KEYWORDS: surface ozone, photochemical production, uv radiation and carbon monoxide.

INTRODUCTION

Ozone is an important precursor of hydroxyl radical of trace gases species and plays a key role in the lower atmospheric chemistry. The relationship between O₃ and its precursors represents one of the major scientific challenges associated with urban pollution (Rama Gopal et al., 2014). Tropospheric ozone is the one of the important greenhouse gases and contributes to global warming and climate change. Moreover, it is also one of the key species affecting the human health, vegetation and chemical properties of the atmosphere. Variations in ozone concentration are controlled by a number processes including photochemistry, physical or chemical removal, and transport which occur on local and regional and global scales (Naja and Lal 2002).

Many studies have shown that rural areas have huge O₃ concentration compared with urban Areas. Two mechanisms have been proposed to account for the enhanced rural O₃. One is the transport of its precursors like NO_x, CO, non-methyl hydrocarbons followed by the photochemical ozone production and another is transport of O₃ from urban areas to the downwind site. The concentration of O₃ is always recorded higher in the afternoon due to the high intensity of UV radiation from sun light. Many investigations have reported that higher O₃ concentrations are noticed due to high photochemical activity in summer and lower concentrations are observed due to rain washout process during the monsoon (David et al., 2011).

Trace gases concentration is low in the atmosphere, but they play a crucial role in determining the ambient air quality over a location. The increasing anthropogenic activities have led to increasing emissions of air pollutants such as sulfur oxides (SO_x), nitrogen oxides (NO_x), carbon monoxide (CO), volatile organic compounds (VOCs), metal oxides, and VOC are included into organic matter (Nishanth et al., 2012). Carbon Mon-oxide is said to be one of the most important precursors of ozone. Due to its considerable longer life time than NO_x, it plays a significant role in deciding the budget of surface ozone on regional as well as global scale.

EXPERIMENTAL SITE AND GENERAL METEOROLOGY

The measurements are carried out at the department of physics, Sri Krishnadevaraya University (14.62°N, 77.65°E, 331 m asl), Anantapur, India. Anantapur is a very dry semi arid and rain shadow region. This region gets very little rain that form during South-west monsoon and North- east monsoon periods. The national high ways (NH7&NH 205) pass this region and the brick making units, some factories and cement plants located in the north and southwest ward measurement site within a radius of 50 km, and diesel vehicles and biomass burning to cause air pollution. Further wind pattern is also favored enhancement of pollutant concentration over the sampling site. The site is located just 10 km from Anantapur is about 200 km from Bangalore and 350 km from Hyderabad. And heavy traffic of vehicles is being passed the site to produce more air pollution.

Based on the annual changes in meteorological parameters four seasons are identified – monsoon (June – August), post-monsoon (September – November), winter (December – February) and summer (March – May).

INSTRUMENTATION

Surface ozone is measured using an analyzer (model APOA -370, HORIBA, Germany ambient O₃ monitor). The ultraviolet absorption method is based on ozone's characteristic of absorbing ultraviolet rays of specific wavelength. The measurement cell is exposed to direct radiation by a low pressure mercury lamp which produces ultraviolet rays with central wavelength of 253.7 nm. For accurate measurements, the filter has been replaced for every three weeks. In order to acquire stable, accurate data, calibration at regular interval has been performed. The O₃ analyzer was zero calibrated with dry air and span calibration was carried out by multipoint calibrator, scheduled quality control procedures included daily zero checks, biweekly precision checks and monthly multipoint calibration (Suresh Kumar Reddy et al., 2012). Surface carbon monoxide was measured using an analyzer (Model APMA-370, HORIBA, Germany ambient CO monitor). The cross modulation type non-dispersive infrared absorption method was used for CO measurement. This analyzer uses an AS-type (antishock) interference compensating detector, and a purified reference gas. The reference gas is generated by purifying the sample through an oxidation process. These features eliminate interference from other elements, resulting in highly accurate measurements. We were replaced the filter for every month on time basis to get accurate measurements. In order to acquire stable and accurate data, calibration at regular interval was performed. The CO analyzer was zero calibrated with zero air generator and span calibration was performed by multipoint calibrator (Lingaswamy et al., 2017).

RESULTS AND DISCUSSION

DIURNAL VARIATION OF O₃, CO AND UV

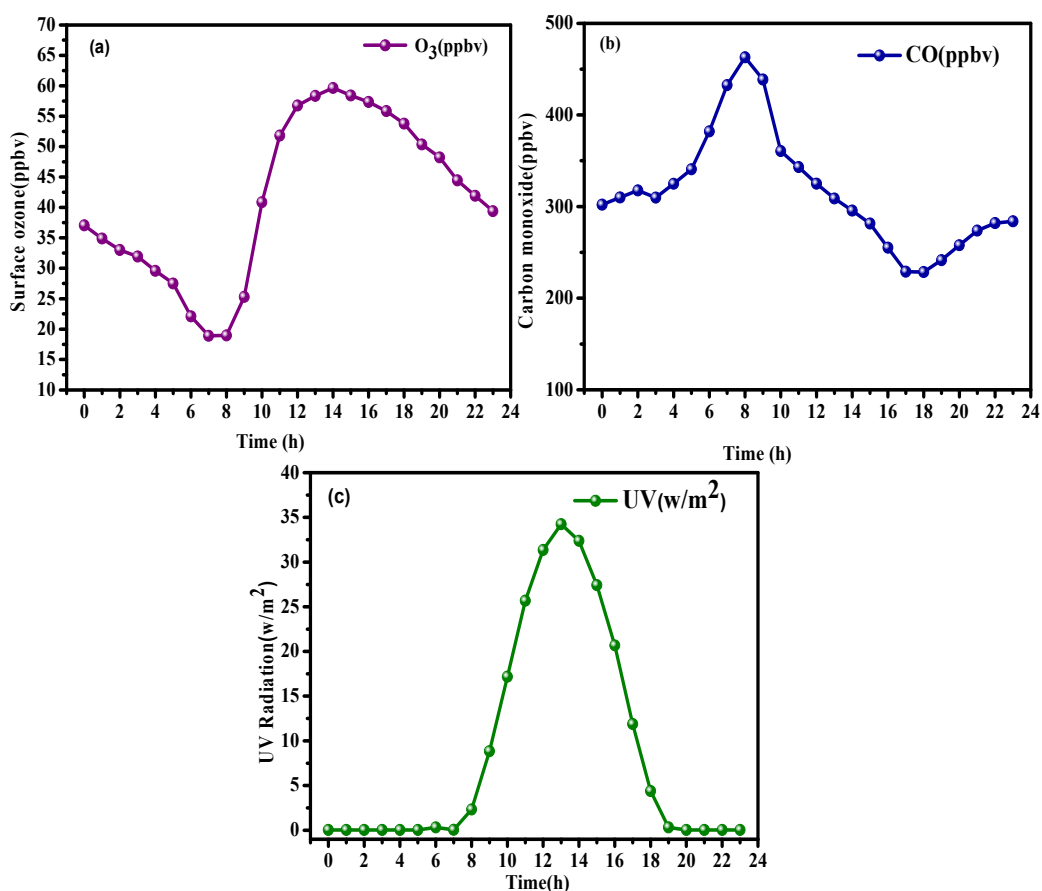
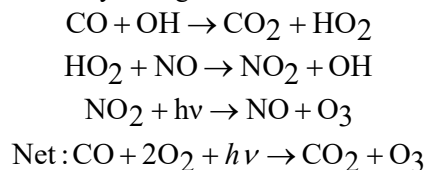


Figure 1. Diurnal variation of (a) O₃, (b) CO and (c) UV over Anantapur during the study period.

The diurnal variations of O₃ concentration is illustrated respectively in figure 1(a). In the diurnal O₃ profile, a declined peak is observed in the morning (07:00 - 09:00h). This is attributed to O₃ titration

with freshly emitted NO. After 09:00h, O₃ concentration gradually increases to reach a maximum value at around (12:00 - 16:00h) in the afternoon and due to its photochemical formation through the photolysis of NO₂. The low concentration of O₃ observed at night is due to the absence of photochemical oxidation and titration with NO in the residual boundary layer. The continuous measurements of surface ozone present, the diurnal average minimum concentration of O₃ (7:00h) is 18.8 ppbv. And the maximum concentration of O₃ (14:00h) is 59.6 ppbv. This increase strongly supported by the highest intensity of UV-A radiation observed during those hours while different trace gas precursors are getting mixed up in the mixed layer.

Figure 1(b) shows the average diurnal variations of CO. Results suggest a bimodal distribution with peaks at 7:00 - 09:00h and 18:00 - 20:00h (462.9 ppbv), due to the large number of vehicles and the pollutants get trapped in the shallow surface layer. The concentration of CO starts decreasing from 12:00 to 13:00h (228.4 ppbv) everyday, which indicates that the greater height of the boundary layer provides a large mixing region; hence the pollutants get diluted. High levels of CO during morning and late evening over the study region attributed to combined effect of anthropogenic emissions, chemistry as well as local sources and wind patterns. Major sources for CO over the site were fossil fuel burning and biogenic emissions. Diurnal variation with concentration during afternoon could partly be attributed to the less anthropogenic activities, photo oxidation process and high mixed layer height.



The diurnal variation of UV-A radiation (W/m²) is as shown in the figure 1(c). It is observed that O₃ concentration pattern is similar to that of UV (w/m²). The maximum of UV flux was present during the 12:00-14:00h (34.2 W/m²). While low values were recorded at night (3 W/m²). The maximum concentration was observed at 16:00 h, which is about 2:00-3:00 h after the maximum UV flux.

MONTHLY MEAN VARIATION OF O₃ AND CO

The monthly mean O₃ concentrations are shown in the figure 2(a). The monthly mean ozone measurements shows a maximum about 45.5 ± 16.2 ppbv during November due to transportation and photochemical production with presents the sufficient solar radiation. The minimum average ozone at about 20.9 ± 4.7 ppbv is noticed in the month of August due to intense cloud formation and rain washed out process.

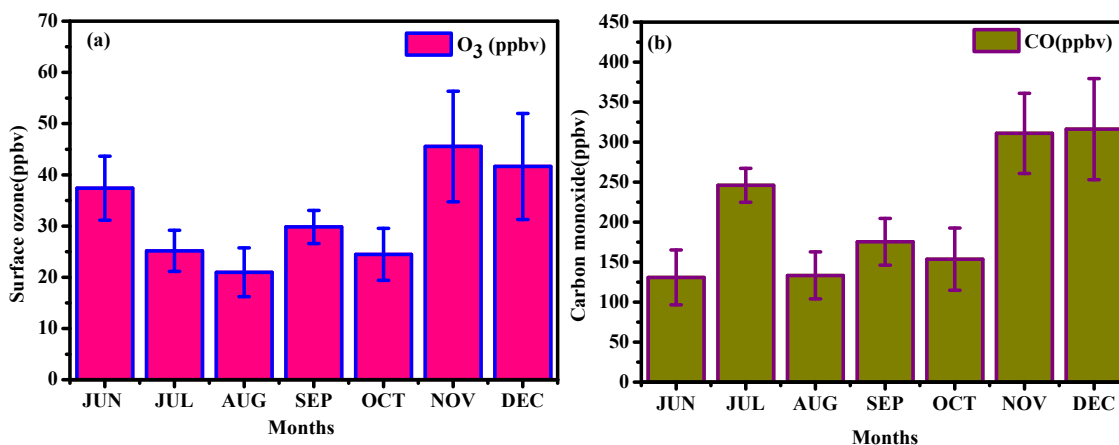


Figure 2. Monthly variation of (a) O₃ and (b) CO over Anantapur.

The monthly mean CO concentration is as shown in the figure 2(b). The maximum CO concentration was observed in the month of December (316.1 ± 63.2 ppbv) due to anthropogenic emissions, boundary layer process, chemistry as well as local sources and wind patterns. The minimum concentration was observed in the month of August (133.2 ± 29.3 ppbv). The concentration of CO was very low during August month,

which can be ascribed to the large amount of precipitation prevailed, high wind velocities, and change in general wind direction.

CORRELATION BETWEEN [O₃] VS [UV] AND [O₃] VS [CO]

Among the measurements of diurnal patterns of O₃ and CO during the study period, it is observed that O₃ concentration pattern similar to that of UV radiation (W/m²) is shown in figure 3.

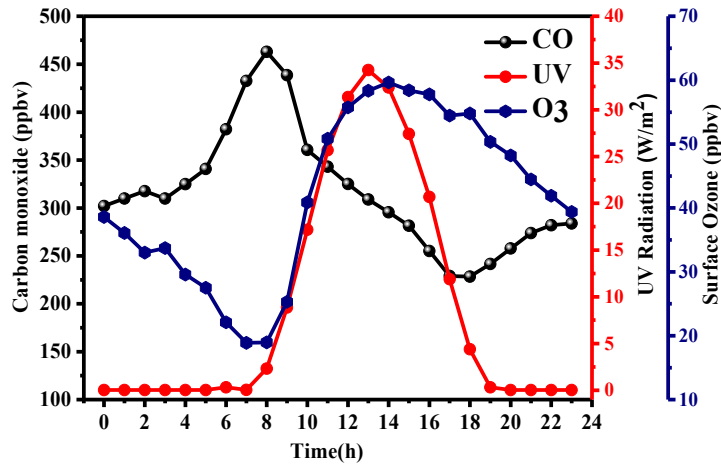


Figure 3. Diurnal variation of O₃, CO with

The maximum of UV flux was present during the 12:00-14:00h (34.2 W/m²), while low values were recorded at night (3 W/m²). The maximum O₃ concentration was observed at 16:00h, which is about 2-3h after the maximum UV flux.

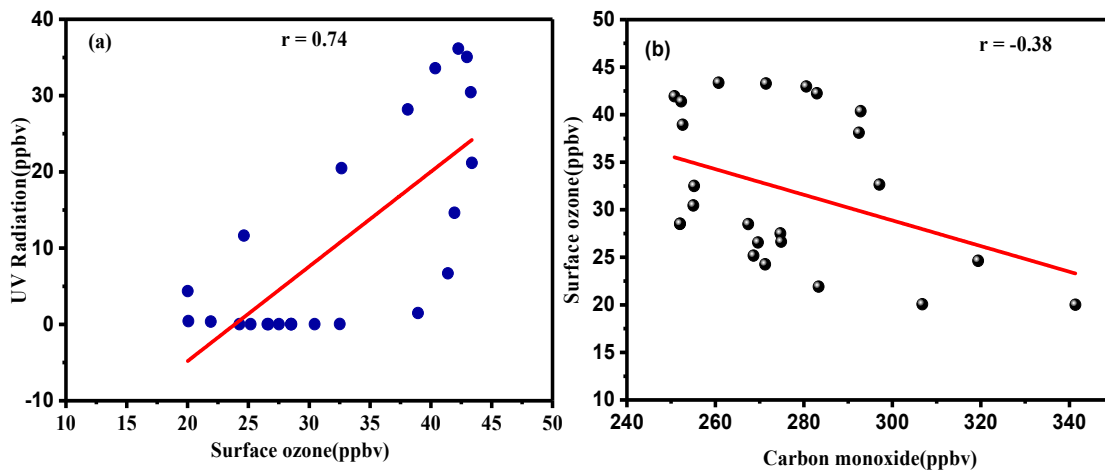


Figure 3 highlights two features associated with the diurnal variation of O₃ and CO with UV radiation. The first one is similar diurnal pattern between O₃ and UV, and the later opposite pattern of CO with O₃. In the mid afternoon the UV flux is maximum, and at the same time CO follows the lower levels, which shows a clear indication that the CO anti-correlated ($r = -0.38$) with O₃ figure 4(a) was observed. The same diurnal and monthly patterns was observed between O₃ and UV during the observation period. This variation strongly suggested that O₃ concentration is closely correlated to the UV flux with a correlation coefficient $r = 0.74$ (figure 4(b)) was observed.

CONCLUSIONS:

Simultaneous and continuous measurements of surface ozone (O₃) and its precursor CO were carried out at a semi arid rural site, Anantapur in southern India during June 2016 – December 2016. This study can contribute to a better understanding of the variations in O₃ with Carbon monoxide and UV radiation. The important findings in to be recalled from the present study are given below.

1. The diurnal variation of O₃ shows the highest concentration during noontime and the lowest concentration during the night and early morning hours, whereas, the precursor CO shows high concentration during early morning and nighttime hours and low concentration during the noontime.
2. The monthly average minimum (maximum) of O₃ observed in August (November) was 20.9 ± 4.7 (45.5 ± 16.9) ppbv. Whereas, the monthly average variation of CO was found to be high (316.2 ± 63.2 ppbv) in December and noticed low (133.2 ± 29.3) concentration in August.
3. The O₃ concentration shows significant positive correlation with UV radiation and negative correlation with CO.

ACKNOWLEDGEMENT

The authors wish to thank the Indian Space Research Organization (ISRO), Bangalore through its ISRO-GBP (AT–CTM) project for their financial assistance in the form of research project.

REFERENCES

- David, L.M. and Prabha R. Nair (2011). Diurnal and seasonal variability of surface ozone and NO_x at a tropical coastal site: Association with mesoscale and synoptic meteorological conditions, *J. Geophys. Res.*, 116.
- Lingaswamy A.P., S.Md. Arafath, G. Balakrishnaiah, K. Rama Gopal, N. Siva Kumar Reddy, K. Raja Obul Reddy, R.R. Reddy and T. Chakradhar Rao (2017). Observations of trace gases, photolysis rate coefficients and model simulations over Semi-arid region, India, *Atmos. Environ.*, 158, 1352-2310.
- Naja, M. and S. Lal (2002). Surface ozone and precursor gases at Gadanki (13.5° N, 79.2° E), a tropical rural site in India, *J. Geophys. Res.*, D14, 4197.
- Nishanth, T., K.M. Praseed, M.K. Sathish Kumar and K.T. Valsaraj (2012). Analysis of Ground Level O₃ and NO_x measured at Kannur, India, *J. Earth. Sci. Clim. Change.*, 3(1), 111.
- Rama Gopal, K., A.P. Lingaswamy, S.Md. Arafath, G. Balakrishnaiah, S. Pavan Kumari, K. Umadevi, N. Siva Kumar Reddy, K. Raja Obul Reddy, R.R. Reddy, P. Abdul Azeem, and Shyam Lal (2014). Seasonal heterogeneity in ozone and its precursors (NO_x) by in-situ and model observations on semi-arid station in Anantapur (A.P), South India, *Atmos. Environ.*, 84, 294-306.
- Suresh kumar Reddy, B., K. Raghavendra Kumar, G. Balakrishnaiah, K. Rama Gopal, R.R. Reddy, V. Sivakumar, A.P. Lingaswamy, S.Md. Arafath, K. Umadevi, S.Pavan Kumari, Y. Nazeer Ahammed and Shyam Lal (2012). Analysis of Diurnal and Seasonal Behavior of surface ozone and its Precursors (NO_x) at a Semi - Arid Rural Site in Southern India, *Aerosol and Air Quality Res.*, 12, 1081-1094.

VARIATIONS IN SCATTERING PROPERTIES OF SURFACE AEROSOLS DURING MONSOON SEASON AT SEMI-ARID REGION, ANANTAPUR, SOUTHERN INDIA.

C. MANJUNATHA¹, G. BALAKRISHNAIAH¹, S. PAVANKUMARI¹, K. RAMA GOPAL¹, R.R. REDDY¹ AND G. PULLAIAH²

¹Aerosol and Atmospheric Research Laboratory, Department of Physics, Sri Krishnadevaraya University, Anantapur – 515 003, A.P., India.

²Department of Physics, Rayalaseema University, Kurnool – 518002, A.P., India.

KEYWORDS: nephelometer, scattering coefficient, back scattering coefficient, scattering angstrom exponent.

INTRODUCTION

Non-gaseous solid or liquid phase particles that are suspended in ambient atmosphere, ranging from 0.001 to 100 μm are referred as atmospheric aerosols. The aerosol forced to climate change directly or indirectly, and also affects entire living and non-living organism. When electromagnetic radiation passes through the gaseous media, the solar radiation gets altered due to scattered, absorbed and reflected by clouds, aerosols and molecules in the atmosphere which affects radiation budget of the planet earth. The contribution of aerosol in this extinction process led to introduce important parameter called “Extinction coefficient of aerosols”. In order to estimate the extinction coefficient, it is necessary to quantify the optical properties of aerosols (scattering coefficient, absorption coefficient etc.). The present work is intended to study the Scattering Properties (scattering coefficient, Backscattering coefficient and Scattering Angstrom Exponent) of surface aerosols over the experimental site during monsoon season (Jun, July, August and September) in the year 2016.

SITE DRICRIPTION

Anantapur district in Rayalaseema region (14⁰ 62' E, 77⁰ 65' N, 331m asl) in Andhra Pradesh is geographically located in a semi-arid zone and occupies the second place to the Rajasthan. Approximately 85% of the population is affected by drought in this district, due to low rainfall, high temperature and dry winds during the monsoon periods (Balakrishnaiah et al., 2011a, Kumar et al., 2010).

METHODS

Poly-disperse nature of atmosphere aerosols in their size and composition, widely variety aerosol monitoring techniques and instrumentation are available. In this Present work we employed nephelometry principles and an instrument named Integrating Nephelometer (TSI Model 3563) which was operated at 3 different visible wavelengths (450, 550 and 700 nm) of electromagnetic radiation. It contains two temperature sensors and one humidity sensor. The humidity sensor and one temperature sensor are placed near sample and remaining temperature sensor kept at the sample inlet. Halogen lamp was used as primary source for Nephelometer real time measurements of scattering properties. Three photo multiplier tubes were used for detecting the scatter light at three different wavelengths (450, 550 and 700nm). In addition to backscattering shutter was provided which gives additional information regarding to the backscattering of surface aerosols.

The instrument placed in temperature controlled room which located at terrace of the three floor building. The instrument was calibrated with filtered air as low span gas and CO₂ as high span gas twice for a year, reported by Gopal et al., (2014). In this study, truncation errors were corrected using the method described by Anderson and Ogren (1998). The scattering angstrom exponent was measured by using following relation,

$$\sigma_{sp} \propto \frac{1}{\lambda^{\alpha_{sp}}} \Rightarrow \alpha_{sp} = -\left(\frac{\log(\sigma_{sp}^{\lambda_1}) - \log(\sigma_{sp}^{\lambda_2})}{\log(\lambda_1) - \log(\lambda_2)} \right)$$

where

σ_{sp} = Scattering coefficient of aerosols, λ_1 and λ_2 are wavelengths at 450 and 700 nm respectively.

α_{sp} = Scattering angstrom exponent at (450/700 nm).

$\sigma_{sp}^{\lambda_1}$ and $\sigma_{sp}^{\lambda_2}$ are scattering coefficients at 450 and 700nm respectively.

RESULTS & DISCUSSIONS

DIURNAL VARIATIONS OF SCATTERING COEFFICIENT (σ_{sp}) AND BACK SCATTERING COEFFICIENT (σ_{bsp})

Figure 1. shows similar diurnal variations of α_{sp} and α_{bsp} of surface aerosols at three different wavelengths (450, 550 and 700 nm). Lower values were observed at early morning hours and gradually increases with increasing of time and attained sharp peak at time interval 6:00 to 7:00h LT. Again the curve gradually decreases with increasing of time and attained minimum values around time 10:00 h to 14:00 h. After that the values of both coefficients are gradually increases and shows the secondary peak (Moderate peak) around 18:00 to 19:00 h LT.

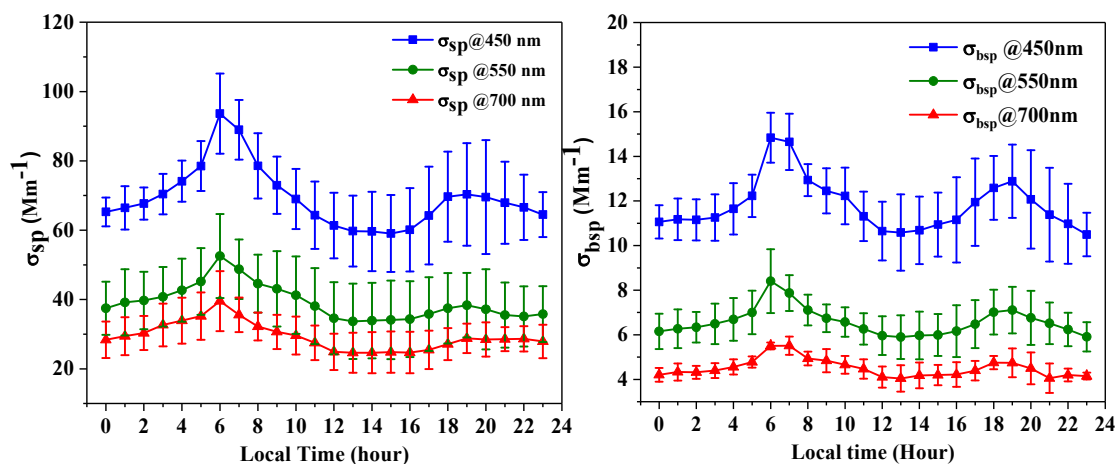


Figure 1. Diurnal variations of σ_{sp} and σ_{bsp} during the monsoon season-

The morning sharp peak occurring due to subsidence of boundary layer, low vertical mixing and wind speeds, emissions from traffic and increasing of anthropogenic activities. Lower values appeared at afternoon time due to increasing of boundary layer height, vertical mixing, high wind speeds and decreasing of anthropogenic activities, the moderate peak attained due to increasing of evening traffic, shallowness of boundary layer, again decreasing of manmade activities and presence of lower wind speeds. The secondary peak is appeared as moderately mainly due to presence of high temperature at evening time than early morning time.

Monthly variations of scattering coefficient (σ_{sp}) and back scattering coefficient (σ_{bsp})

Figure 2 shows the monthly patterns of σ_{sp} and σ_{bsp} during monsoon season at three different wavelengths (450, 550 and 700nm) respectively. The monthly variations of both coefficients at 550nm were gradually decreases with increasing months with slightly differ in their magnitudes. The maximum values of σ_{sp} and σ_{bsp} were observed in the month of June in the order of $53.27 \pm 13.71 \text{ Mm}^{-1}$ and $7.30 \pm 2.28 \text{ Mm}^{-1}$ whereas minimum values were observed in the month of September $29.08 \pm 6.49 \text{ Mm}^{-1}$ and $5.41 \pm 1.35 \text{ Mm}^{-1}$ respectively. The mean values of σ_{sp} and σ_{bsp} for entire monsoon season is found to be $39.36 \pm 8.28 \text{ Mm}^{-1}$ and $6.33 \pm 1.59 \text{ Mm}^{-1}$ respectively. The magnitudes of σ_{sp} and σ_{bsp} indirectly suggest that existence of Mie scattering theory over an experimental site (troposphere). The monthly variations in scattering properties mainly aroused due to variations in prevailing meteorological conditions over the experimental site. The slightly maximum values of both coefficients in June indirectly infers that , presence of greater aerosol

loading over experimental site as compare with remaining months of monsoon. Low cloud precipitation, less wash out process, low wind speeds and other prevailing meteorological conditions causes greater aerosol. Minimum values of σ_{sp} and σ_{bsp} observed during the September month, the reason is that September is almost ending month of monsoon season which has clear atmospheric condition due to cloud precipitation scavenging, aerosol wash out process and less anthropogenic activities were causes effective reduction of coarse mode particles.

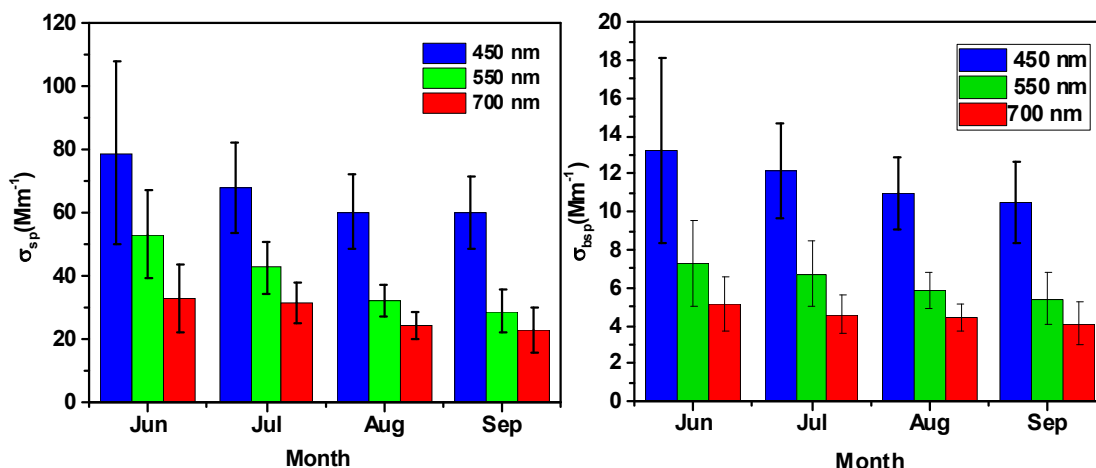


Figure 2. Monthly variations of σ_{sp} and σ_{bsp} during the monsoon-

Diurnal and Monthly variations of scattering angstrom exponent (α_{sp})

Figure 3(a) represents the diurnal variations in α_{sp} and shows two dips, one is regarding to morning during the period of time interval between 6 :00 to 7:00h LT and another is evening time at 18:00 to 19:00h LT. The higher values of α_{sp} were attained at early morning hours and afternoon hours. The variations in α_{sp} Mainly due to diurnal variation in boundary layer, Hourly concentrations of aerosol loading(traffic emissions and anthropogenic activities) and prevailing meteorological conditions.

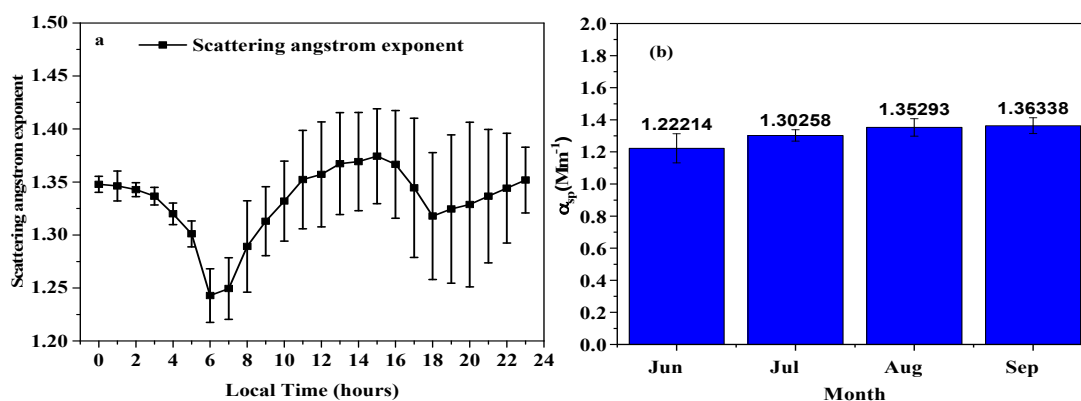


Figure 3(b) shows variations in monthly mean values of α_{sp} that infers, gradually growth with slightly differ in their in magnitudes among the months. It remained larger than unity, throughout the season and the quantified values are 1.222, 1.302, 1.352 and 1.363 for months June, July, August and September respectively. The mean value of season in the order of 1.31 which strongly suggests that the scattered light dominated by particles within the range size range about $0.1 \leq D_p \leq 1\mu m$ (accumulation mode). Little variations in magnitudes of monthly mean values mainly due to prevailing meteorological conditions over the sampling site.

Spectral variations of scattering coefficient over the experimental site

Following figure 4 illustrates the spectral variations of scattering coefficient throughout the monsoon season that inferred to consistency of Mie scattering theory over an experimental site. The mean seasonal quantified magnitudes of both back scattering and forward scattering coefficients are also suggests existence of Mie scattering theory. According to the Mie scattering theory, particle size abundance over a sampling site between the range 0.05 to 0.55 μm (mostly accumulation mode particles). The main sources for presented particles are gas to particle conversion process of reactive species, the accumulation mode particles mainly originating from coagulated particles from Aitkin mode and combustion generated Particles. An accumulation mode particle has longer residence time as compare to the nucleation and coarse mode particles mainly due to least efficiency of removal mechanisms.

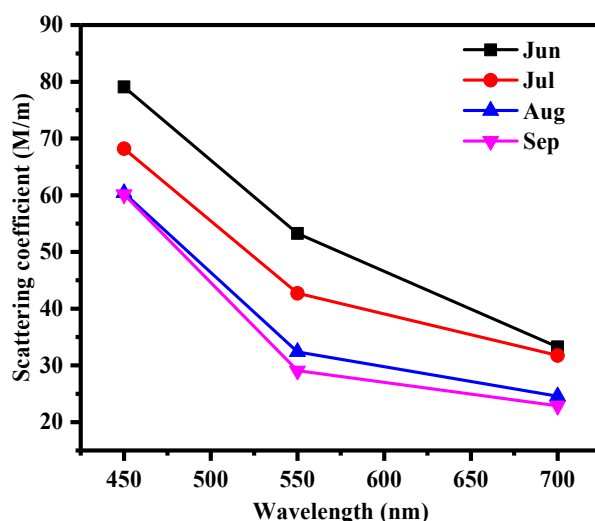


Figure 4. Spectral variations of scattering coefficient (σ_{sp}) during the monsoon season

CONCLUSIONS

The surface aerosol scattering properties were quantified during monsoon season in the year 2016 at a semi-arid region Anantapur. All parameters investigated in this present work shows well defined diurnal and monthly variations (intra seasonal variations). The main conclusions drawn from our study are summarized as below.

- 1) The measured seasonal mean values of σ_{sp} , σ_{bsp} (at 550 nm) and α_{sp} (at 450/700 nm) were found to be 39.36 ± 8.28 , 6.33 ± 1.59 and 1.31 ± 0.06 respectively.
- 2) Diurnal variations in σ_{sp} , σ_{bsp} and α_{sp} concluded that bi-peak patterns corresponding morning and evening sessions.
- 3) Monthly variations in σ_{sp} , σ_{bsp} and α_{sp} all most consistent and shows seasonal homogeneity and slightly differ in their magnitudes due to change in prevailing meteorology conditions.
- 4) Mean value of α_{sp} at (450/700nm) during the monsoon season in the order of 1.31 which strongly suggests that the scattered light dominated by particles within the range size about $0.1 \leq D_p \leq 1 \mu\text{m}$.
- 5) Spectral dependency of scattering coefficient reveals that existence of Mie scattering theory over the experimental site and dominance of accumulation mode particles.

ACKNOWLEDGEMENTS

The authors wish to thank the Indian Space Research Organization, Bangalore for the financial support is provided by ISRO-GBP under ARFI Project.

REFERENCES

- Balakrishnaiah, G., K. Raghavendra Kumar, B. Suresh Kumar Reddy, C. Swamulu, K. Rama Gopal, R.R. Reddy, L.S.S. Reddy, Y. Nazeer Ahammad, K. Narasimhulu, K.K. Murthy and S. Suresh Babu (2011). Anthropogenic impact on the temporal variations of black carbon and surface aerosol mass concentrations at a tropical semi-arid station in southeastern region of india, *J. Asian Earth Sci.*, **42**, 1297-1308.
- Kumar, K.R., K. Narasimhulu, G. Balakrishnaiah, B. Suresh Kumar Reddy, K. Rama Gopal, R.R. Reddy, S.K. Satheesh, K.K. Murthy and S. Suresh Babu (2010). A study on the variations of optical and physical properties of aerosols over a tropical semi- arid station during grassland fire, *J. Atmos. Res.*, **95**, 77-87.
- Gopal, K.R., S.Md. Arafath, A.P. Lingaswamy, G. Balakrishnaiah, S. Pavan kumari, K. Uma Devi, N. Siva Kumar Reddy, K. Raju Obul Reddy, M. Penchal Reddy, R.R. Reddy and S. Suresh Babu (2014). In-situ measurements of atmospheric aerosols by using Integrating Nephelometer over a semi-arid station southern India, *J. Atmos. Environ.*, **86**, 228-248.
- Ruby, M.G. and A.P. Waggoner (1981). Intercomparison of integrating nephelometer measurements, *J. Environ. Sci. Technol.*, **15**, 109-113.
- Gopal, K.R., G. Balakrishnaiah, S.Md. Arafath, K. Raja Obul Reddy, N. Siva Kumar Reddy, S. Pavan kumari, K. Raghavendra Kumar, T. Chakradhara Rao, T. Lokeswara Reddy, R.R. Reddy, S. Nazeer Hussain, M. Vasudevara Reddy, S. Suresh Babu and P. Mallikarjuna Reddy (2016). Measurements of scattering and absorption properties of surface aerosols at semi-arid site Anantapur, *J. Atmos. Res.*, **183**, 84-93.
- Anderson, T.L. and J.A. Ogren (1998). Determining Aerosol Radiative Properties Using the TSI 3563 Integrating Nephelometer, *J. Aerosol Sci. Technol.*, **29**, 57-69.

AEROSOL BLACK CARBON: ITS CHARACTERISTICS OVER SEMI-ARID REGION, ANANTAPUR

P. RAMANJANEYA REDDY¹, G. BALAKRISHNAIAH¹, S. PAVANKUMARI¹, K. RAMA GOPAL¹
and R.R. REDDY¹

¹Aerosol and Atmospheric Research Laboratory, Department of Physics, Sri Krishnadevaraya University, Anantapur – 515 003, A.P., India.

KEYWORDS: black carbon mass concentration, absorption coefficient, atmospheric boundary layer.

INTRODUCTION

Aerosol black carbon is a light-absorbing aerosol which strongly attenuates the incoming solar radiation. Black carbon (BC) particles are primary particles emitted into the atmosphere as a product of incomplete combustion of hydrocarbon-containing materials including bio fuel/biomass and fossil fuels. BC is one of the significant refractory components of carbonaceous particles (categorized as black/graphitic carbon and organic carbon) in atmospheric aerosols. This is the most powerful climate forcing agent and is ahead of methane and just inferior to carbon dioxide (Safai et al., 2014). The study of black carbon aerosols is important for a number of reasons. Aerosols can alter the radiation budget of the Earth-Atmosphere system directly by absorbing solar and terrestrial radiation and as a result to contribute to global warming (Ramanathan et al., 2008). BC aerosols not only enhance warming of the lower atmosphere but also increasing atmospheric instability. Recently atmospheric Black carbon has received considerable attention because of its adverse effects on human health. It is virtually certain that there will be more frequent hot and fewer cold temperature extremes over most land areas on daily and seasonal timescales, as global mean surface temperature increases due to absorption effects of Black carbon. The characterization of BC is attracting considerable interest in recent years due to its environmental and climate significance, as well as anthropogenic nature of its origin (Hansen et al., 2000).

The atmospheric BC directly accounts for the reduction of the incoming short-wave solar radiation, leading to heating of the atmosphere. BC causes serious health problems too; as it can get easily deposited into the respiratory system through inhalation because of its fine sub-micron size. Recently, BC has been used as an indicator of exposure to diesel soot. These results are obtained from Aethalometer (model AE-42, Magee scientific, USA) during the period Jan- Dec 2015. The diurnal and monthly variations of absorption properties of atmospheric aerosols have been studied and analyzed.

INSTRUMENTATION AND OBSERVATIONAL SITE

Real-time and continuous measurements of BC aerosol mass concentration were made using a seven channel Aethalometer (Model AE-42 of Magee Scientific, California, USA) operates at a flow rate of 3 LPM and observations were recorded at the time base of 5 min interval. The high intensity LED lamps operating at 370,470,520,590,660,880 and 950nm are used as light sources in Aethalometer. Details of the Aethalometer principle, operation and uncertainties involved and error budget were reported by several earlier authors (Weingartner et al., 2003; Arnott et al., 2005; Nazeer Hussain et al., 2017). The Aethalometer was installed at ~12m height from ground level at the Department of Physics, Sri Krishnadevaraya University (SKU) campus; Anantapur [14.62°N, 77.65°E, 331 m above sea level].

Anantapur located in Southeast India represents a very dry semi-arid, rain shadow and continental region of Rayalaseema, Andhra Pradesh, India. Within a 50 km radius, this region is surrounded by a number of cement plants, lime kilns, slab polishing and brick making units. These industries, the national highways (NH 44 and NH 205) and the town area are situated in the north to southwest side of the sampling site. They continuously emitted pollutants (Kumar et al., 2009).

RESULTS AND DISCUSSIONS

DIURNAL AND MONTHLY VARIATION OF BLACK CARBON (BC) MASS CONCENTRATION

The diurnal variations of black carbon (BC) mass concentration for different seasons over Anantapur were shown in figure 1(a). The vertical lines indicate the standard deviations. In all seasons, there are two prominent peaks of BC concentration a primary peak at around 07:00 LT and a secondary peak at 20:00 LT. The concentration of BC was observed to be lowest in the afternoon hours. BC was found to exhibit strong diurnal variability with sharp morning and evening peaks. The gradual build-up of BC in the early morning hours between (7:00 - 9:00 hrs) almost one hour after sunrise. This enhanced variation mainly from boundary layer dynamics and anthropogenic activities. During the early morning hour's boundary layer height very less which leads which leads black carbon particles conflict near to earth surface. Second maximum peak (19:00 – 22:00 hrs) was found to be during night hours which are contributes from increases anthropogenic activities such as vehicular emission and less boundary layer height due to lack of solar radiation (nocturnal boundary layer), this effect is known as fumigation. The morning peak in the BC arises from the combined effects of fumigation effect in the boundary layer which brings in aerosol from the nocturnal residual layer shortly after the sunrise and builds up of local anthropogenic activities in the urban area (Stull, 1998). Low values of BC during afternoon hours have been attributed to the dispersion of aerosols, due to increase in boundary layer height in addition to the low traffic density (Babu and Moorthy, 2002). The diurnal mean BC mass concentration was around $2.59 \pm 0.89 \mu\text{g m}^{-3}$ in winter, $1.65 \pm 0.29 \mu\text{g m}^{-3}$ in summer, $1.38 \pm 0.15 \mu\text{g m}^{-3}$ in monsoon and $1.95 \pm 0.15 \mu\text{g m}^{-3}$ during the post-monsoon season.

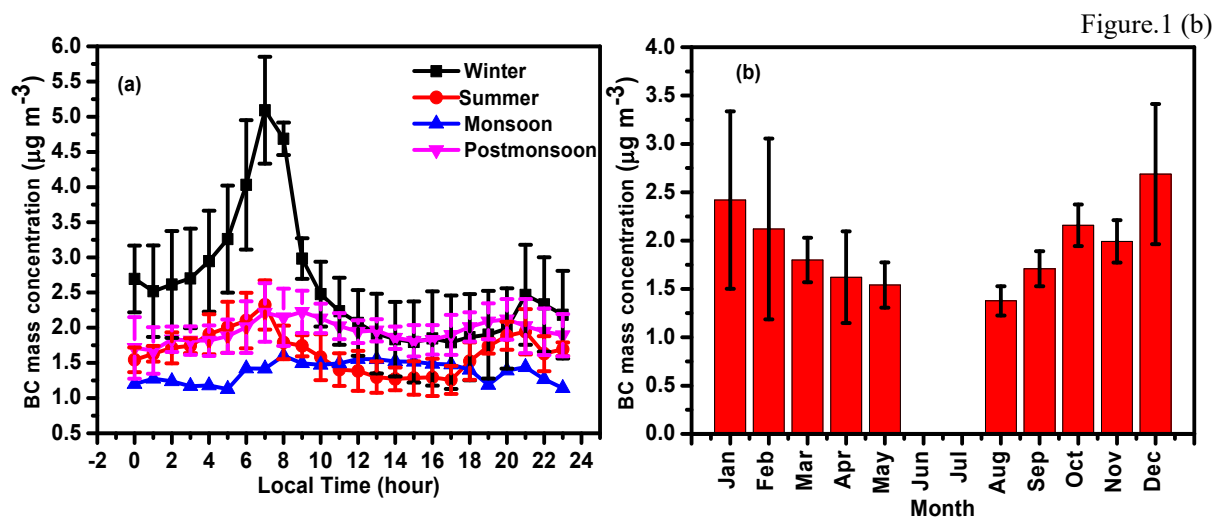


Figure 1(a). Diurnal variation of BC mass concentration for different seasons, (b). Monthly variation of BC mass concentration during the period Jan 2015- Dec 2015.

shows the monthly variation of BC mass concentration over the study period. The monthly variations of BC mass concentrations were mainly attributed to the synoptic meteorology, bio mass burning, boundary layer dynamics and transport of air mass from the surrounding regions. The highest BC is observed in the month of December ($2.78 \pm 0.79 \mu\text{g m}^{-3}$) due to the transport of air mass from the continental regions and increase in fossil fuel consumption for road transportation (Kumar et al., 2011). The lowest BC mass concentration is observed in the month of August ($1.31 \pm 0.15 \mu\text{g m}^{-3}$) due to scavenging effect and washout process. The annual mean BC concentration of ($1.94 \pm 0.34 \mu\text{g m}^{-3}$) was observed for entire data period.

DIURNAL AND MONTHLY VARIATION OF ABSORPTION COEFFICIENT (B_{ABS})

Figure 2(a) represents the diurnal variation of absorption coefficient for different wavelengths. The observed morning peak (07:00 – 08:00 h) might be associated with the fumigation effect in the boundary layer, which

brings aerosols from the nocturnal residual layer shortly after the sunrise and the severe emission of particle pollutants during morning traffic rush hours. As the day advances, increased solar heating leads to increase turbulent effects and a deeper boundary layer, leading to faster dispersion of aerosols and hence a dilution of BC concentration occurs near to the surface during the late-afternoon (16:00 h). After 16:00 h, the evening rush hour, cooking and residential heating commences during the winter. Soon after sunset, the surface inversion begins to form, trapping more primary pollutants related to BC. The wavelength 370nm shows highest peak over all wavelengths, which represents organic matter present during morning hours due to fresh diesel and biomass burning emissions.

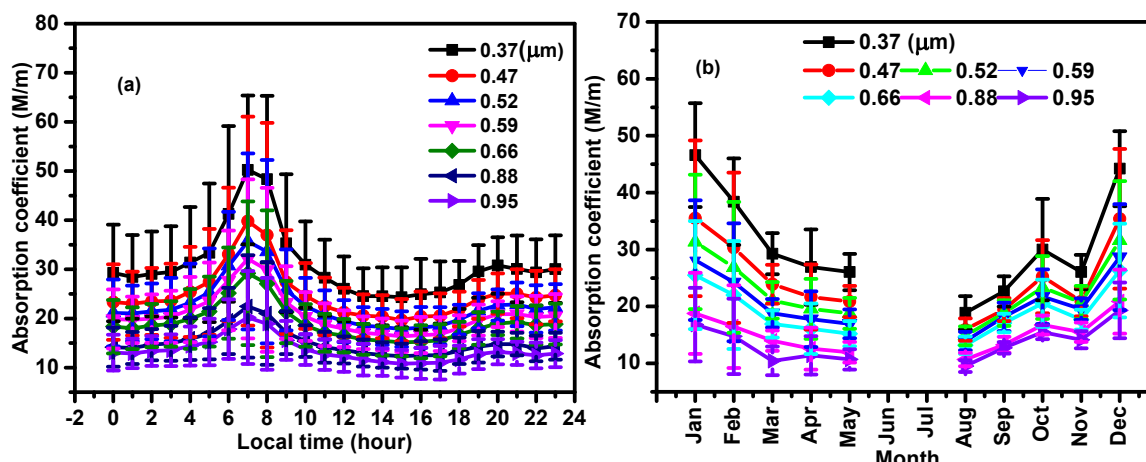


Figure 2(a). Diurnal variation of absorption coefficient for different wavelengths, **(b)** Monthly variations of absorption coefficient.

The monthly variations of absorption coefficient for study period are shown in figure 2(b). Monthly mean values of b_{abs} peaks for 370nm in the months of January (46.59 Mm^{-1}), February (38.41 Mm^{-1}), and December (44.29 Mm^{-1}) while the minima during August (18.89 Mm^{-1}) and months of 2015 at all the wavelengths.

CONCLUSIONS

The diurnal mean BC mass concentration was around $2.59 \pm 0.89 \mu\text{g m}^{-3}$ in winter, $1.65 \pm 0.29 \mu\text{g m}^{-3}$ in summer, $1.38 \pm 0.15 \mu\text{g m}^{-3}$ in monsoon and $1.95 \pm 0.15 \mu\text{g m}^{-3}$ during the post-monsoon season. The lowest BC mass concentration is observed in the month of August ($1.31 \pm 0.15 \mu\text{g m}^{-3}$) due to scavenging effect and washout process. The wavelength 370nm shows highest peak over all wavelengths, which represents organic matter present during morning hours due to fresh diesel and biomass burning emissions.

ACKNOWLEDGEMENTS

The authors wish to thank the Indian Space Research Organization (ISRO), Bangalore for carrying out this work through its Geosphere Biosphere Programme (GBP) under ARFI project and DST INSPIRE program for financial support.

REFERENCES

- Arnott, W.P., K. Hamasha, H. Moosmuller, P.J. Sheridan and J.A. Ogren (2005). Towards aerosol light-absorption measurements with a 7-wavelength aethalometer: evaluation with a photoacoustic instrument and 3-wavelength Nephelometer, *Aerosol Sci. Technol.*, **39**(1), 17–29.
- Babu, S.S. and K.K. Moorthy (2002). Aerosol Black Carbon over a Tropical Station in India, *Geophys. Res. Lett.* **29**: L2098, doi: 10.1029/2002GL015662.

- Hansen, J., M. Mato, R. Reudy, A. Lacis and V. Oinas (2000). Global warming in the 21st Century: an alternative scenarios, *Proc. National Acad. Sci.*, **97**, 9875–9880.
- Kumar, K.R., K. Narasimhulu, G. Balakrishnaiah, B.S.R. Reddy, K.R. Gopal, R.R. Reddy, S.K. Satheesh, K.K. Moorthy and S.S. Babu (2011). Characterization of Aerosol Black Carbon over a Tropical Semi-arid Region of Anantapur, India, *Atmos. Res.*, **100**, 12-27.
- Kumar, K.R., K. Narasimhulu, R.R. Reddy, K.R. Gopal, L.S.S. Reddy, G. Balakrishnaiah, K.K. Moorthy and S.S. Babu (2009). Temporal and Spectral Characteristics of Aerosol Optical Depths in a Semi-arid Region of Southern India, *Sci. Total Environ.*, **407**, 2673–2688.
- Nazeer Hussain S., T. Chakradhar Rao, G. Balakrishnaiah, K. Rama Gopal, K. Raja Obul Reddy, N. Siva Kumar Reddy, T. Lokeswara Reddy, S. Pavan Kumari, P. Ramanjaneya Reddy and R. Ramakrishna Reddy (2018). Investigation of black carbon aerosols and their characteristics over tropical urban and semi-arid rural environments in peninsular India, *J. Atmos. Sol. Terr. Phys.*, **167**, 48–57.
- Ramanathan, V. and G. Carmichael (2008). Global and regional climate changes due to black carbon, *Nature Geosci.*, **1**, 221–227.
- Safai P.D., P.C.S. Devara, M.P. Raju, K. Vijaykumar and P.S.P. Rao (2014). Relationship between black carbon and associated optical, physical and radiative properties of aerosols over two contrasting environments, *Atmos. Res.*, **149**, 292 – 299.
- Wiengartner, E., H. Saathoff, M. Schnaiter, N. Streit, B. Bitnar and U. Baltensperger (2003). Absorption of light by soot particles: determination of the absorption coefficient by means of aethalometers, *J. Aerosol Sci.*, **34**, 1445–1463.

INVESTIGATING THE CHARACTERISTICS OF MINERAL DUST OVER ARABIAN SEA THROUGH MODIS OBSERVATIONS

T. CHAKRADHAR RAO¹, K. RAJA OBUL REDDY², G. BALAKRISHNAIAH¹, K. RAMA GOPAL¹,
R. RAMAKRISHNA REDDY¹

¹Aerosol & Atmospheric Research Laboratory, Department of Physics, Sri Krishnadevaraya University,
Anantapur – 515003.

²School of Earth sciences, Zhejiang University, Hangzhou, China.

KEYWORDS: Arabian Sea, Dust Aerosol Optical Depth, Dust Fraction

INTRODUCTION

Aerosols, a tiny suspended matter in air plays a vital role in modify the atmospheric radiative properties by scattering and absorption the short wave solar radiation. The continental aerosols over remote oceanic environments were due to the long-range transport, those originated from natural (mineral dust) and anthropogenic sources have been recognized as major sources. In atmospheric aerosol budget, mineral dust is considered as the one of the dominant compound with the factor of 36% of the global aerosol emissions. Its increase in the influence of the regional and global atmospheric chemistry and radiation budget was observed since few decades (Ooki and Uematsu, 2005; Rastogi and Sarin, 2006). These dust particles acts as cloud condensation nuclei and have a strong affinity for water, even though dust is insoluble in water (Rosenfeld et al., 2001).

The Arabian Sea is considered as one of the most biologically productive oceanic regions. It is surrounded by the hyper-arid regions (vast Arabian Desert on the west), arid regions (Iranian arid regions on the north) and semi-arid (the Thar Desert on the north-east) continental regions. Since, this marine environment has the direct outflow of the natural and anthropogenic continental chemical constituents from the above mentioned regions. It provides a perfect region to study the impact on the surface ocean biogeochemistry along with the Radiative properties of the marine environment.

With its unique geographical setting and well-known annual reversal in the wind regimes, SW winds at the onset of SW monsoon (June - August), NE winds during winter months (December–February) and easterly winds during (March-May) are expected to impart characteristic changes to the aerosol composition in the Arabian Sea marine boundary layer. In the present study, Satellite remote sensing technique is used to study the characteristics of mineral dust over the Arabian Sea with MODIS is the active platform. Aerosol optical depth (AOD), dust optical depth (DOD) and dust fraction (DF) are derived from the MODIS-Aqua satellite (MYD08).

METHODOLOGY AND DATASETS

The MODIS onboard Aqua, A-train satellite (figure 1), provides column AOD in seven wavelength channels (0.47, 0.55, 0.66, 0.86, 1.24, 1.64, and 2.12 μm) retrieved from cloud-free pixels (Remer et al., 2005). The MODIS cloud-masking algorithm identifies different domains of information on surfaces illuminated by the solar radiation (land, water, snow/ice, desert, and coast). The radiance in both shortwave and longwave channels are used to identify the state of the pixel and generate a cloud mask product (MYD35) (Ackerman et al., 1998), which is used to eliminate the cloudy pixels before the process of retrieval of aerosols. Details on the retrieval process are given by Ackerman et al. (1998) and Remer et al. (2005). Nair, et al., 2013 and Babu, et al., 2013 reported Extensive comparison of MODIS level 3 aerosol optical depth (AOD) data (at 0.55 μm) with ship-borne Sun photometer measurements over oceanic regions surrounding the Indian peninsula showed good agreement with a correlation coefficient of 0.91 and slope of 0.95 (Nair, et al., 2013; Babu, et al., 2013). The present study made use of level 3 MODIS collection 6 (MYD08_M3) QA weighted data product over the ocean to obtain aerosol optical depth over the study region (Levy et al., 2013). Based on the AOD derived from MODIS the present study region is classified into 3 regions; Northern Arabian Sea (NAS), Central Arabian Sea (CAS) and Southern Arabian Sea (SAS) as shown in the figure 1.

The dust AOD is estimated from MODIS measurements of the AOD (τ) at 550 nm and the fraction of AOD contributed by the fine mode aerosol, fine mode fraction (f), based on Kaufman et al. (2005). Over marine environments under the continental influence, AOD is composed of maritime, (τ_{marine}), dust (τ_{dust}) and anthropogenic (τ_{anthro}) aerosols as described in Lakshmi et al. (2017). The dust aerosol optical depth is given by

$$\tau_{\text{dust}} = \frac{\tau(f_{\text{anthro}} - f) - \tau_{\text{marine}}(f_{\text{anthro}} - f_{\text{marine}})}{f_{\text{anthro}} - f_{\text{dust}}}$$

where f is bounded by $f_{\text{anthro}} \geq f \geq \min\{f_{\text{anthro}}, f_{\text{dust}}\}$. The f_{anthro} , f_{dust} , and f_{marine} are the fine mode fraction that corresponds to the anthropogenic, dust, and maritime aerosols, respectively. We used a priori information on the fine mode fraction of these aerosol types as follows $f_{\text{anthro}} = 0.889$, $f_{\text{dust}} = 0.309$ and $f_{\text{marine}} = 0.475$ (Kaufman et al., 2005; Lakshmi et al., 2017).

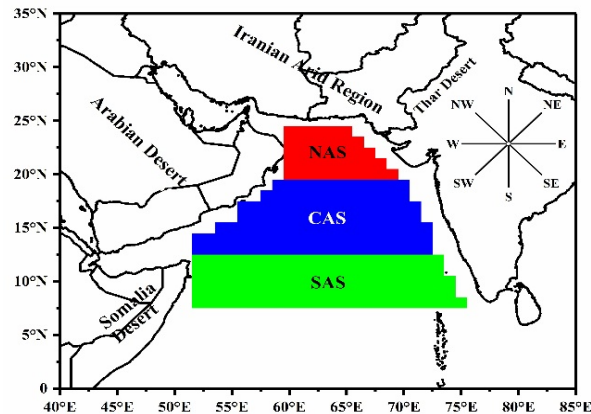


Figure 1 Classification of the study region and the important desert regions surrounded to the Arabian Sea.

RESULTS AND DISCUSSION

SPATIAL DISTRIBUTION OF AOD

The mean spatial variation of 11-years averaged MODIS AOD at 550 nm over the Arabian Sea during 2006 – 2017 winter (Win), summer (Sum), monsoon (Mon) and post monsoon (PoM) is shown in figure 2. The spatial heterogeneity of total aerosols has been illustrated clearly, with high AOD close to the continental coast line and observed a deep sweep with distance away from the source. This leads to the large AOD spatial gradients from the source regions to the remote oceanic regions. The highest AOD values were observed over northern parts of the Arabian Sea, while AOD shows large decrease towards south of 8°N.

Climatological mean value of AOD over the entire Arabian Sea is high during Mon (0.68 ± 0.17) followed by Sum (0.34 ± 0.04), PoM (0.31 ± 0.02) and low during Win (0.25 ± 0.01). The extreme high AOD (> 0.6) over the Arabian Sea during Mon is caused due to the advection of dust aerosols originating from the Arabian Peninsular, transported by the strong north - westerly offshore winds. These results are similar to those reported in the literature (Husar et al., 1997; Li and Ramanathan, 2002).

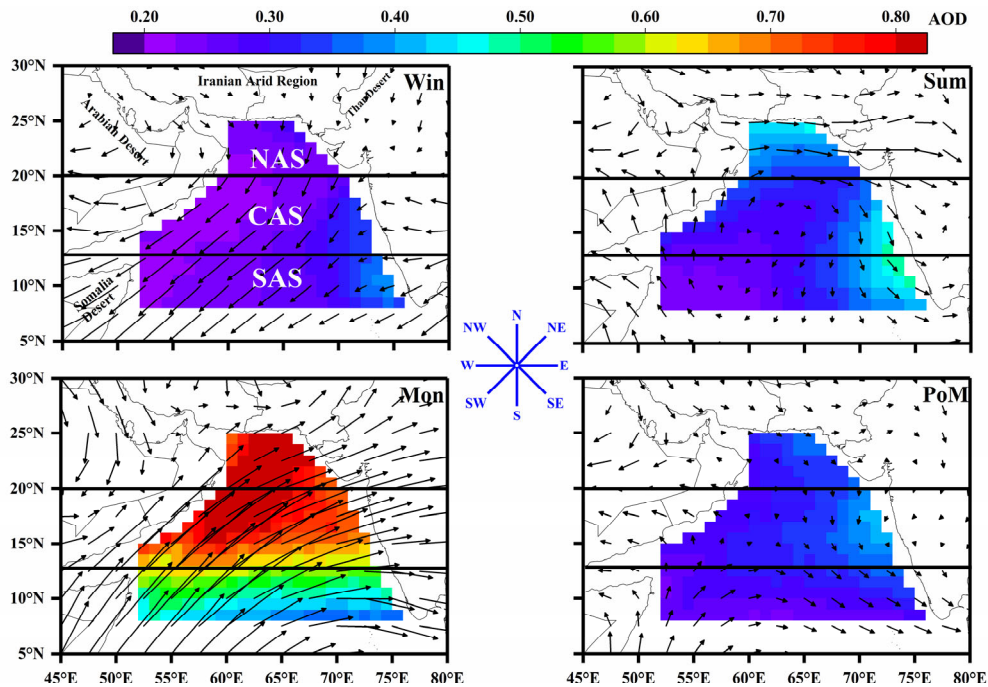


Figure 2. Seasonal mean spatial variation of AOD over Arabian Sea from June 2006 to November 2017 overlaid by the NCEP reanalysis synoptic winds at 925 hPa.

SPATIAL DISTRIBUTION OF DOD AND DF

Figure 3 and Figure 4 show the DOD and DF derived using MODIS measurements during the period of study. Both DOD and DF follow almost all same patterns as described earlier. These parameters showed higher values over NAS, moderate on CAS and lowest over SAS.

Spatial distribution of dust during this study resembles that of total AOD pattern (figure 2) with a similar latitudinal variation, which indicates that dust aerosols significantly modulate the aerosol extinction over the Arabian Sea. Most of the dust aerosols were concentrated at western side of the Arabian Sea i.e., the coastal line of the Arabian Desert regions. The highest DOD was observed during the Mon months followed by Sum, PoM and Win in the view of the entire Arabian Sea. Indeed, this domination of the dust aerosols towards the western Arabian Sea is due to the advection of dust from the massive desert areas by the action of the winds. With the view of the seasonal variation Mon was the dominated over all the three reasons with DF over NAS was 0.88, followed by CAS 0.83 and found lowest over SAS with 0.71. Moreover, Win being the lowest of all the seasons in all respective regions with 0.27, 0.20 and 0.18 of DF over NAS, CAS and SAS respectively.

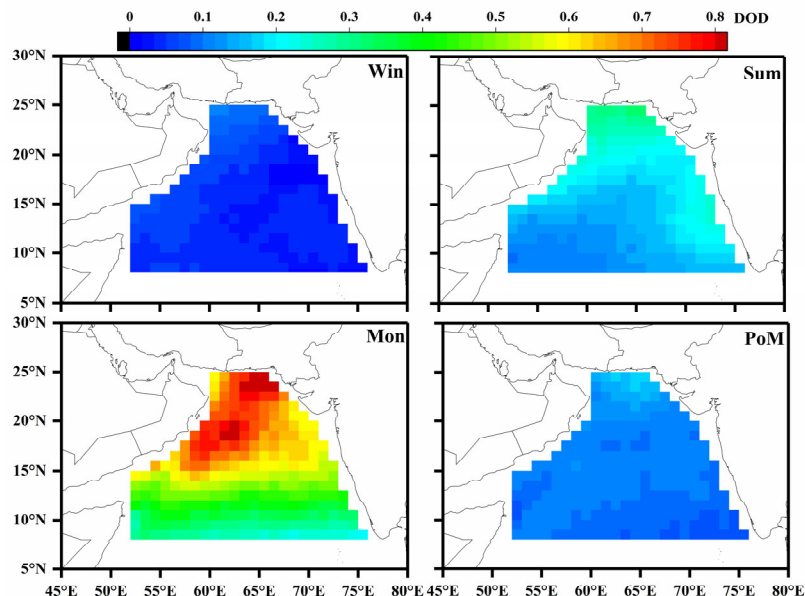


Figure 3. Seasonal mean spatial variation of DOD over Arabian Sea from June 2006 to November 2017.

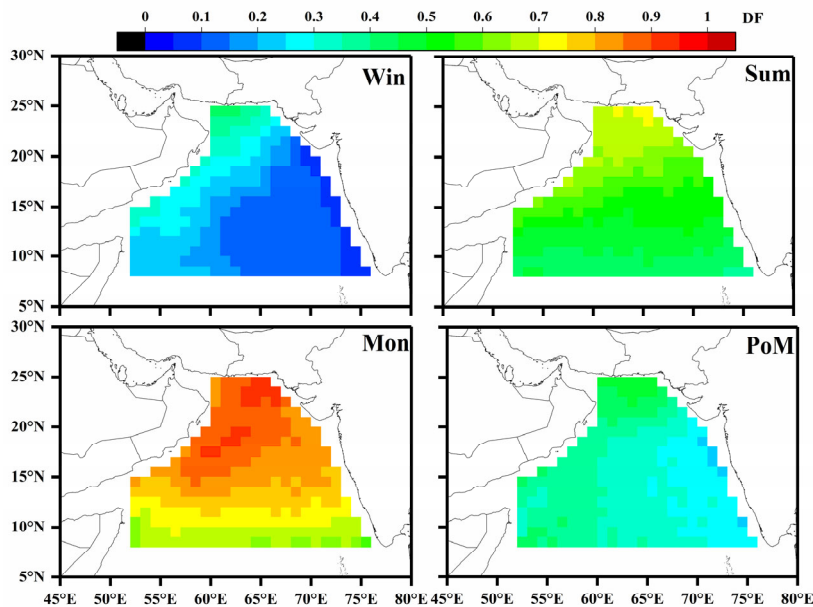


Figure 4. Seasonal mean spatial variation of DF over Arabian Sea from June 2006 to November 2017.

SEASONAL VERTICAL WINDS

Study of the vertical winds is significant which gives proper information of the source regions. The seasonal mean vertical winds from 0.1 km to 5.6 km. Triangle indicates NAS, Sphere indicates CAS and Square indicates SAS, with respective colour indicating the altitude as shown in the figure 5. During Win, almost all the winds are from N to NE over all the regions and altitudes except at high altitudes of NAS which are predominately higher wind speeds from the west of NAS. It is clearly observed that at lower altitudes weak wind speeds were observed during all the seasons and regions except during Mon where extreme high wind speeds at low altitudes from SW to W regions of the respective sites. It is clearly observed that SW to W regions of the Arabian Sea is covered with the Arabian Desert and Somalia Deserts which are said to be the dominant dust contributors to the Arabian sea during Mon to the Arabian Sea. Due to this reason the DF was found to be higher during Mon over the entire western part of the Arabian Sea.

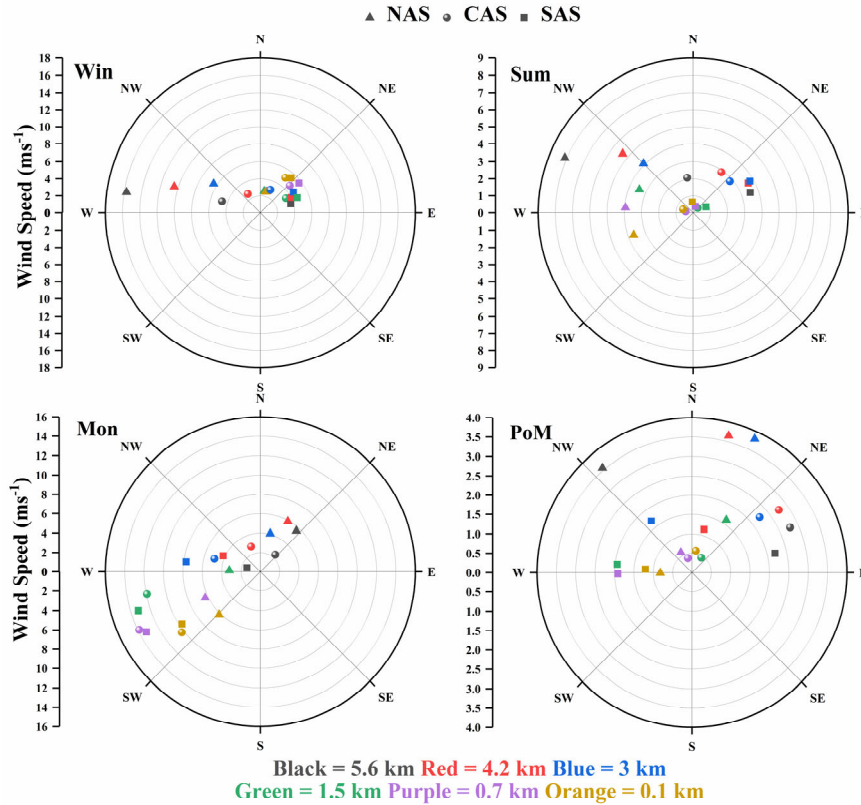


Figure 5. Seasonal mean vertical winds over Arabian Sea from June 2006 to November 2017.

CONCLUSION

Characteristics of mineral dust aerosol over the Arabian Sea are examined using MODIS-derived AOD.

- Strong latitudinal heterogeneity and seasonality is observed in the DOD as well as DF over the Arabian Sea.
- Significant contribution of dust is observed over the northern Arabian Sea during Mon season where 88% of the total aerosol extinction is contributed by dust aerosols transported from the nearby continental regions.
- During Win, dust transport is found to be less significant with fractional contribution of ~15% – 22% to the total aerosol optical depth over the Arabian Sea.
- During Sum, continental dust out flow from the arid regions of Iran, Afghanistan and Pakistan, this leads the high aerosol loading over Arabian Sea.

ACKNOWLEDGEMENTS

This work has been carried out as a part of ISRO-GBP (ARFI, AT-CTM) projects. The MODIS data were provided by NASA through the website at <http://ladsweb.nascom.nasa.gov/>.

REFERENCES

- Ackerman, S.A., K.L. Strabala, W.P. Menzel, R.A. Frey, C.C. Moeller and L.E. Gumley (1998). Discriminating clear sky from clouds with MODIS, *J. Geophys. Res.*, **103(D24)**, 32,141–32,157.
- Babu, S.S., M.R. Manoj, K.K. Moorthy, M.M. Gogoi, V.S. Nair, S.K. Kompalli and D. Singh (2013). Trends in aerosol optical depth over Indian region: Potential causes and impact indicators, *J. Geophys. Res. Atmos.*, **118**, 11,794–11,806.
- Husar, R.B., et al. (2001). Asian dust events of April 1998, *J. Geophys. Res.*, **106**, 18,317– 18,330.
- Kaufman, Y.J., I. Koren, L.A. Remer, D. Tanré, P. Ginoux and S. Fan (2005). Dust transport and deposition observed from the Terra-Moderate Resolution Imaging Spectroradiometer (MODIS) spacecraft over the Atlantic Ocean, *J. Geophys. Res.*, **110**, D10S12.
- Lakshmi, N.B., V.S. Nair and S. Suresh Babu (2017). Vertical structure of aerosols and mineral dust over the Bay of Bengal from multisatellite observations, *J. Geophys. Res. Atmos.*, **122**, 12,845–12,861.
- Li, F., and V. Ramanathan (2002). Winter to summer monsoon variation of aerosol optical depth over the tropical Indian Ocean, *J. Geophys. Res.*, **107(D16)**, 4284, doi: 10.1029/2001JD000949.
- Nair, V.S., S.S. Babu, K.K. Moorthy and S.S. Prijith (2013). Spatial gradients in aerosol-induced atmospheric heating and surface dimming over the oceanic regions around India: Anthropogenic or natural, *J. Clim.*, **26(19)**, 7611–7621.
- Ooki, A., and M. Uematsu (2005). Chemical interactions between mineral dust particles and acid gases during Asian dust events, *J. Geophys. Res.*, **110**, D03201, doi: 10.1029/2004JD004737.
- Rastogi, N. and M.M. Sarin (2006). Chemistry of aerosols over a semi-arid region: Evidence for acid neutralization by mineral dust, *Geophys. Res. Lett.*, **33** L23815, doi: 10.1029/2006GL027708.
- Remer, L.A., Y.J. Kaufman, D. Tanré, S. Mattoo, D.A. Chu, J.V. Martins and B.N. Holben (2005). The MODIS aerosol algorithm, products, and validation, *J. Atmos. Sci.*, **62(4)**, 947–973.
- Rosenfeld, D., Y. Rudich and R. Lahav (2001). Desert dust suppressing precipitation - A possible desertification feedback loop, *Proc. Natl. Acad. Sci.*, **98**, 5975– 5980

VARIABILITY OF SURFACE ENERGY BALANCE OVER SEMI-ARID STATION ANANTAPUR USING GLDAS MODEL DATA

T. LOKESWAR REDDY¹, G. BALAKRISHNAIAH¹, N. SIVAKUMAR REDDY¹, K. RAMA GOPAL¹
AND R.R. REDDY¹

¹Aerosol and Atmospheric Research Laboratory, Department of Physics, Sri Krishnadevaraya University,
Anantapur – 515 003, A.P., India.

KEYWORDS: energy balance, semi-arid, gldas, net radiometer, Anantapur.

INTRODUCTION

The variations in the surface climate and Atmospheric Boundary Layer are driven by the surface energy balance, which describes the net result of exchange of mass, momentum and energy between the earth surface and the atmosphere by conduction, convection and radiation between the land surface and the atmosphere. It is strongly influenced by the downward solar radiation (Allison et al., 2013). The energy available (R_{net}) can be quantified by balancing the downward and upward shortwave, longwave radiation and ground heat flux (Allen et al., 1998). The relevant earth energy flux densities at an urban or non-urban land surface are: the net radiation (R_{net}), the ground heat flux that transfers sensible heat by conduction to the substrate (G); and that exchange energy between the surface and atmosphere by two turbulent heat fluxes that are the latent heat flux (L_vE) and the sensible heat flux (H). At surface energy conservation means those fluxes must balance by equation 1.

$$R_{net} = G + H + L_vE \quad (1)$$

where R_{net} is the net radiation, G is the soil heat flux at the surface, H is the sensible heat flux and L_vE is the latent heat flux. These four terms represent the major earth energy components in the surface energy balance.

We count all incoming fluxes as “positive (+ve)” and all outgoing fluxes as “negative (-ve)”. Positive values of the vertical divergence mean then formally a “convergence” of radiant energy in the atmosphere, leading to its heating. On the other side, the negative values of the divergence describe a net loss of radiant energy, cooling the atmosphere to space. The process of evapo-transpiration depends upon, also other aspects, the heat availability to satisfy the latent heat flux requirements. Various studies are conducted to investigate the nature of earth energy balance at the earth surface. Several studies are confined to the infra-red and solar radiation components (Roxy et al., 2014). Remainder on the different soil surfaces also blocks the downward radiation that would otherwise reach the soil and affects transfer of water vapor and heat loss by evaporation, convection, and conduction (Steiner, 1994; Horton et al., 1994). In particular, terrestrial stores of energy and water modulate fluxes between the earth and atmosphere and exhibit persistence on interannual, seasonal and diurnal time scales (Rodell et al., 2004).

The objectives of this paper is to describe the seasonal mean diurnal and monthly variation of surface energy balance over semi-arid station during four seasons using model derived net radiation, ground heat flux, sensible and latent heat fluxes. The obtained shortwave and long-wave radiations results are well correlated with ground based net radiometer.

DATA AND SITE DESCRIPTION

A Global Land Data Assimilation System (GLDAS) has been developed jointly by scientists at the National Aeronautics and Space Administration (NASA) Goddard Space Flight Center (GSFC) and the National Oceanic and Atmospheric Administration (NOAA) National Centers for Environmental Prediction (NCEP) in order to produce such fields (Rodell et al., 2004). GLDAS makes use of the new generation of ground and space-based observation systems, which provide data to constrain the modeled land surface states. The GLDAS data is downloadable from <http://disc.sci.gsfc.nasa.gov/hydrology/data-holdings>. The data used in this study is subset from GLDAS-CLM, with a temporal resolution of 3 hours and a spatial resolution of 25km. The in-situ measurements of shortwave and long-wave radiation were taken by net radiometer, (Kipp-Zonen) model CNR1, with 0.2 Hz sampling frequency and 2-minute averages using in a datalogger. Here

we are providing measurements of surface energy balance components over four different seasons from December 2014 to November 2015.

The study was conducted at Sri Krishnadevaraya University, Anantapur (14.62 °N and 77.65 °E, 331 m above sea level) from December 2014 to November 2015 and the region gets very little rain that from during South-West monsoon and North-East monsoon periods. The climate here is primarily hot and dry in the summer, hot and humid during the monsoon and post monsoon and dry in winter season.

RESULTS AND DISCUSSION:

SEASONAL MEAN DIURNAL VARIATION OF ENERGY BALANCE COMPONENTS

In this section, the seasonal mean diurnal variation of the earth energy balance components (G, H, L_vE and R_{net}) over Anantapur were analysed. The three hourly values of G, H, L_vE and R_{net} were estimated by using GLDAS model data during December 2014 to November 2015 and the obtained results are shown in figure 1 and data are displayed in table 1. (Ferreira et al., 2013).

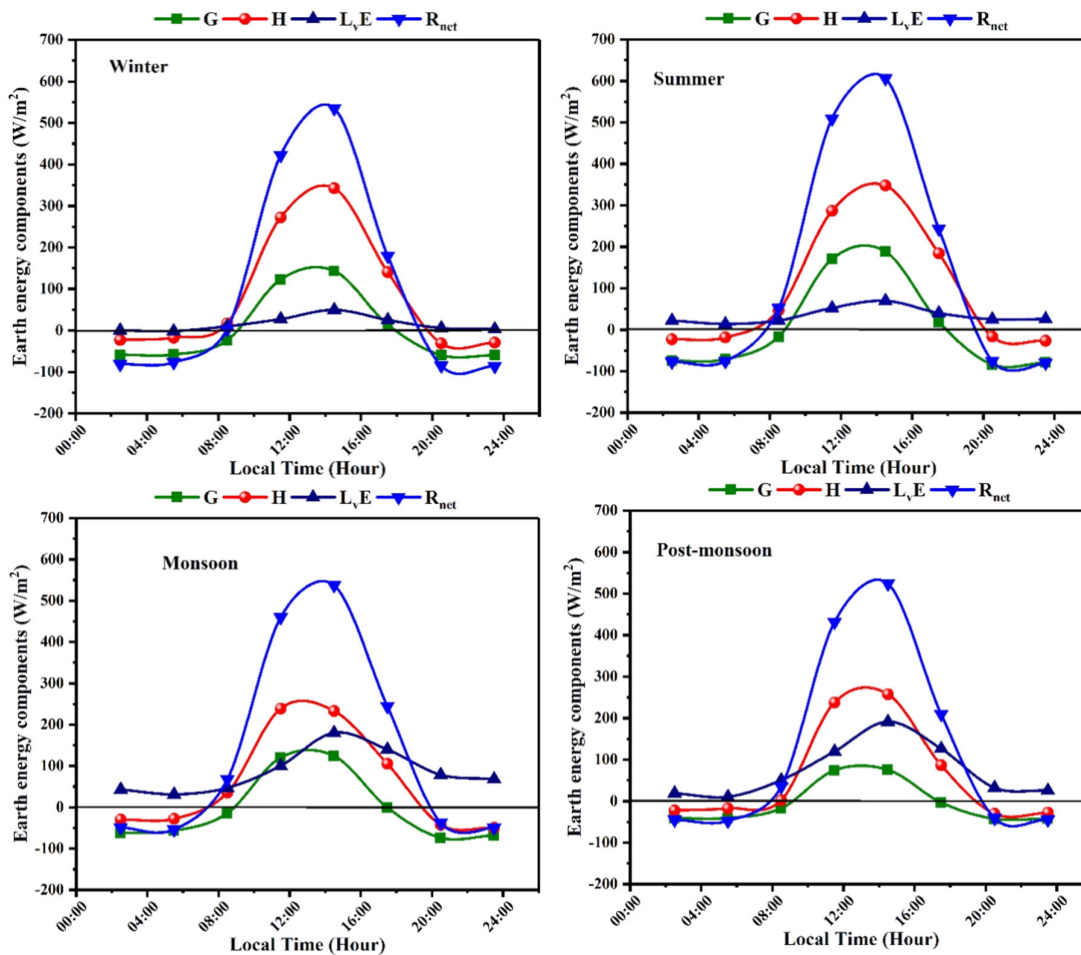


Figure 1. Seasonal mean diurnal evolution of the main components of the surface energy balance. The R_{net} = net radiation, G = ground heat flux, H = sensible heat flux, L_vE = latent heat flux.

Figure 1 shows the seasonal mean diurnal variation of earth energy components (ground heat flux, net radiation, sensible and latent heat fluxes) in Anantapur, most of the energy flux available at the surface of earth during the day and it is transferred to the urban canopy by conduction (i.e., ground heat flux); a

smaller fraction goes to the atmosphere through convection by turbulence (i.e., the sensible heat flux) and as latent heat flux by evapo-transpiration at the earth surface (Ferreira et al., 2013).

The minimum value of ground heat flux (G) occurred after sunset and its minimum value occurred after afternoon. In midnight still has the minimum value and it is constant until sunrise. During night the ground heat flux becomes negative in magnitude. At night, the energy lost by the surface, indicated by a net radiation (R_{net}), is almost totally offset by the release of heat stored in the urban canopy (Ferreira et al., 2013). The maximum energy flux of sensible heat occurs in noon time. During night the H become negative at 20:00 LT and it remains negative in magnitude and minimum until sunrise. The diurnal variation in L_vE is closely related to the available moisture and energy at the earth surface. During daytime the maximum value of L_vE occurs at same time as the maximum H. During night, the L_vE becomes minimum but always positive in magnitude and also the L_vE remains positive at night times over urban areas. (Oke et al., 1999).

The results high values r_{net} were found during summer where as low value in monsoon. Warming of Surface occurring after sunrise in the morning causes vertical temperature gradients to encourage and develops the turbulent mixing at earth surface. In the absence of solar input via downward solar radiation, H decreases at night and the atmosphere continuously to cool until the morning. After sunrise, energy is directly transferred into the substrate at the observation site and ground heat flux is the dominant heat flux in the morning. The maximum values of G were found in the summer and the minimum value in winter followed by monsoon and post-monsoon seasons. The latent heat flux representing fluxes of latent heat is lower in magnitude compare to values of G and H. The L_vE was very low during wintertime and the values are increases in summer followed by monsoon and post-monsoon seasons respectively. During the day time other fluxes are more dominant compare to L_vE . Fluxes of L_vE are influenced by availability of water, and the presence and density of natural surface cover which in turn determines the available surface for evapo-transpiration.

Earth energy components	Winter		Summer		Monsoon		Post-monsoon	
	Max (LT)	Min (LT)						
G	143.31 (14:30)	-59.74 (23:30)	188.75 (14:30)	-83.76 (20:30)	123.90 (14:30)	-73.60 (20:30)	75.39 (14:30)	-42.73 (20:30)
H	342.33 (14:30)	-31.23 (20:30)	347.45 (14:30)	-26.50 (23:30)	238.74 (11:30)	-49.57 (23:30)	257.60 (14:30)	-30.38 (20:30)
L_vE	49.32 (14:30)	-1.66 (05:30)	69.71 (14:30)	13.89 (05:30)	180.18 (11:30)	31.16 (05:30)	191.09 (14:30)	10.31 (05:30)
R_{net}	534.96 (14:30)	-86.16 (23:30)	605.90 (14:30)	-80.05 (23:30)	536.92 (14:30)	-53.70 (05:30)	524.06 (14:30)	-47.66 (05:30)

*G=Ground Heat Flux, H=Sensible Heat Flux, L_vE =Latent Heat Flux, R_{net} =Net Radiation, Max=Maximum, Min=Minimum, LT=Local Time (Hours). Note: (All the parameters in Wm^{-2})

Table 1. Maximum and minimum values of the surface energy balance components at S.K. University, Anantapur

MONTHLY MEAN VARIATION OF ENERGY BALANCE COMPONENTS

The monthly mean variation of the earth energy components (R_{net} , G, H and L_vE) are illustrated in figure 2. The values of net radiation (R_{net}) and latent heat flux (L_vE) have been found to be high around

150.26, 102.28 Wm^{-2} respectively in the month of August; with low values 96.38, 6.17 Wm^{-2} in the month of December and February respectively. A similarly trend were found in ground heat flux (G) and sensible heat flux (H) with higher values in the month of march and lower values in the of December. From figure it clearly observed that L_vE is in anti correlation with G and H. The magnitude of R_{net} flux significantly higher than all other fluxes.

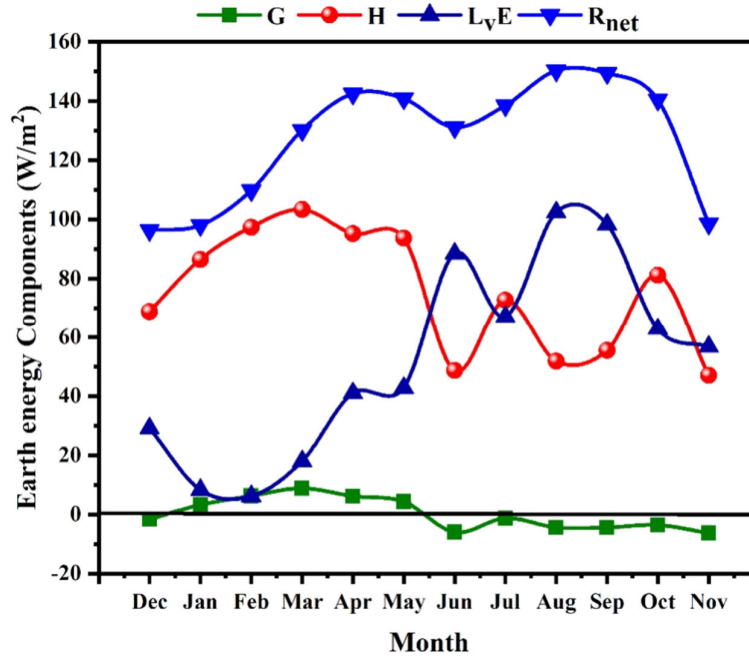


Figure 2. Monthly mean cycle of radiative and turbulent fluxes during the study period.

VALIDATION OF MODEL DATA WITH IN-SITU DATA

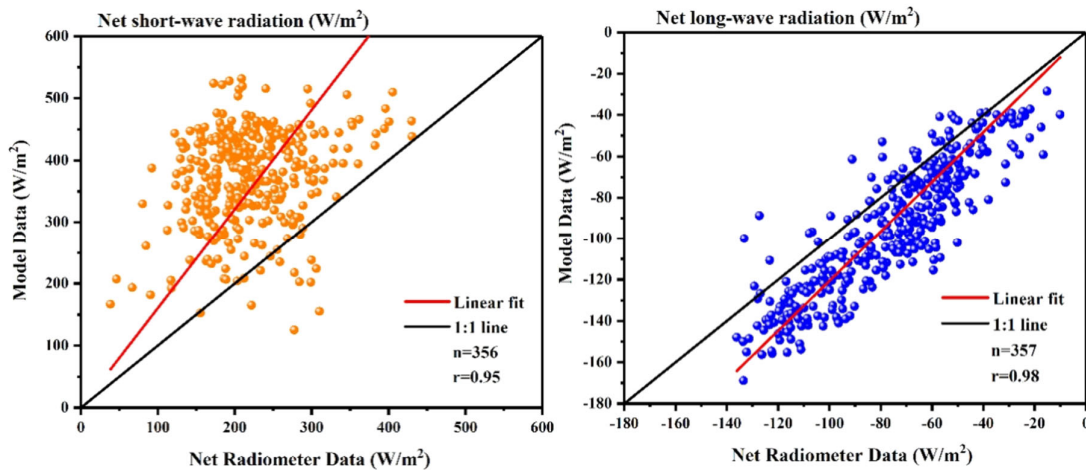


Figure 3. Comparison of net shortwave and net long-wave radiation of model data with net radiometer.

The daily mean net shortwave and net long-wave radiation from the model is compared with in-situ net radiometer is shown in figure 3. From figure the correlation coefficient for shortwave radiation and long-wave radiation are found to be $r=0.95$ ($n = 356$) and $r=0.98$ ($n=357$) respectively. It shows that the model represents over estimation in the shortwave radiation and under estimation in the long-wave radiation compared to in-situ data.

CONCLUSIONS:

The seasonal mean diurnal and monthly means of the earth energy balance components (G , H , L_vE and R_{net}) are studied. The highest values of R_{net} was found in summer followed by winter, post-monsoon and lowest value in monsoon. The higher (lower) values of L_vE was found in the month of August (February) respectively. It clearly observed that L_vE is in anti correlation with G and H . The derived parameters were well correlated with the insitu measurements over study area.

ACKNOWLEDGEMENTS

The authors are indebted to Indian Space Research Organisation (ISRO), Bangalore for carrying out this study through its Geosphere Biosphere Programme (GBP) under NOBLE project and aslo thankful to Global Land Data Assimilation System (GLDAS) model development team for providing the data used in this study.

REFERENCES

- Allen, R.G., L.S. Pereira, D. Raes and M. Smith (1998). Crop evapotranspiration guidelines for computing crop water requirements. FAO Irrigation and Drainage Paper 56, FAO, Rome; 300: 6541.
- Allison, L.S., M. Dori, J.C. Susan, E.T. Tracy and O. Andrew (2013). Observed Impact of Atmospheric Aerosols on the Surface Energy Budget, *Earth Interact.*, **17(14)**, 1-22.
- Ferreira, M.J., P. de O. Amauri and J. Soares (2013). Diurnal variation in stored energy flux in São Paulo city, Brazil, *Urban Clim.*, **5**, 36–51.
- Horton, R., G.J. Kluitenberg and K.L. Bristow (1994). *Surface crop residue effects on the soil surface energy balance*, In P. W. Unger (Ed.), *Managing Agricultural Residues* (pp. 143-162), Boca Raton, Fla.: CRC Press.
- Oke, T.R., R.A. Spronken-Smith, E. Jáuregui and C.S.B. Grimmond (1999). The energy balance of central Mexico city during the dry season, *Atmos. Environ.*, **33**, 3919–3930.
- Rodell, M., P.R. Houser, U. Jambor, J. Gottschalck, K. Mitchell, C.J. Meng, K. Arsenault, B. Cosgrove, J. Radakovich, M. Bosilovich, J.K. Entin, J.P. Walker, D. Lohmann and D. Toll (2004). The Global Land Data Assimilation System, *Bull. Amer. Meteor. Soc.*, **85**, 381–394.
- Roxy, M.S., V.B. Sumithranand and G Renuka (2014). Soil heat flux and day time surface energy balance closure at astronomical observatory, Thiruvananthapuram, south Kerala. *J. Earth Syst. Sci.*, **123(4)**, 741–750.
- Steiner, J.L. (1994). *Crop residue effects on water conservation*. In P. Unger (Ed.), *Managing Agricultural Residues* (pp. 41-76), Boca Raton, Fla.: CRC Press.

COMPARISON OF AOD OVER AHMEDABAD CITY USING SATELLITE AND GROUND DATA

HARISH SEN¹, DR. RAJESH IYER² AND TEJAS TURAKHIA²

^{1,2}Department of Physics, St. Xavier's College (Autonomous), Navrangpura, Ahmedabad – 380 009, India.

KEYWORDS: Aerosol optical Depth, MODIS, Sunphotometer, Regression

INTRODUCTION

Aerosols are small particles suspended in the atmosphere. They may have profound effects on human health. Their effects on the physical environment can also be of importance as they have the ability to both scatter and absorb incident solar radiation. The ability of aerosols to deplete solar radiation can be quantified in terms of aerosol optical depth (AOD). In this study level 2, Collection 6 aerosol products retrieved from the MODerate-Resolution Imaging Spectroradiometer (MODIS) on board the Aqua and Terra satellite were compared with Microtops II sun photometric data collected on ground to analyse their applicability at Ahmedabad (23.125 N, 72.938 S, 72.691 E and 72.492 W). AOD data from these sites was collected over a period of four seasons and were used in the comparison. The results suggest that MODIS AQUA AOD products show good agreement with ground observations, with correlation factor R is 0.69 and 0.8 for Terra and Aqua respectively. Time series graph between ground AOD and satellite derived AOD data shows similar trend. This study can be used to generate ground AOD from satellite data.

METHODS

The comparison of AOD for Ahmedabad city has been done based on the data collected for the field campaigns i.e., (i) 10th February to 13th February, 2017 (ii). 26th to 31st May, 2017 (iii). 9th October to 22nd October, 2017 and (iv). 21st to 28th February, 2018.

MODerate resolution Imaging Spectroradiometer (MODIS) is a passive remote sensing instrument aboard two Earth Observing System (EOS) Terra and Aqua satellites. The satellites operate in sun synchronous, near-polar orbits at an altitude of 705 km with a swath of 2330 km (cross track) by 10 km (along track of nadir). The Terra spacecraft crosses the equator at about 10:30 IST (ascending northwards) while Aqua spacecraft crosses the equator at around 13:30 IST (descending southwards). MODIS derived aerosol products over land and oceans have been validated and are being extensively used to investigate spatiotemporal variations in aerosol optical characteristics (Remer et al., 2005). We have used MODIS (AQUA and TERRA) Level 2, 3km resolution Collection 6 satellite data to compare with the ground data of the above-mentioned campaigns. MODIS has been selected because it has daily two passes over Indian region and due to its data availability.

To compare the AOD values of ground and satellite, the satellite data was downloaded from NASA's site EARTHDATA SEARCH (<https://search.earthdata.nasa.gov/>). The image is then geo-referenced and locations are collocated. Using different grid masks (mainly 3 by 3 and if necessary 5 by 5) satellite AOD data values are extracted for each location, if over a pixel more than one location falls then average value is taken. Further time at which the ground AOD was taken and the time of satellite data was synchronized for most of the locations and thus database for satellite AOD was created. Linear regression analysis relation between ground AOD and satellite AOD data was obtained and comparative graph between satellite acquired data and in-situ AOD measurements was plotted.

RESULT AND DISCUSSION

Figure 3 and 4 depicts the scatter plot of MODIS (Aqua and Terra) AOD versus ground AOD data during the study period. It is clear from the figure that the MODIS AOD correlated well with the ground AOD. From the figure 4 and 3 it is seen that the correlation coefficient of linear regression fit (R) is 0.68 and 0.79 for Terra and Aqua respectively. The highly variable tropical climate, weather patterns, cloud conditions and also local sources may be influenced on these correlations or the differences. The regression shows slopes

2.79 and 1.53 for Terra and Aqua respectively which is greater than unity. Here the intercept shows non-zero values. The difference in the values occurs possibly due to presence of clouds or due to computation. As we know satellite data are spreaded over large region this may lead to error when compared with insitu data.

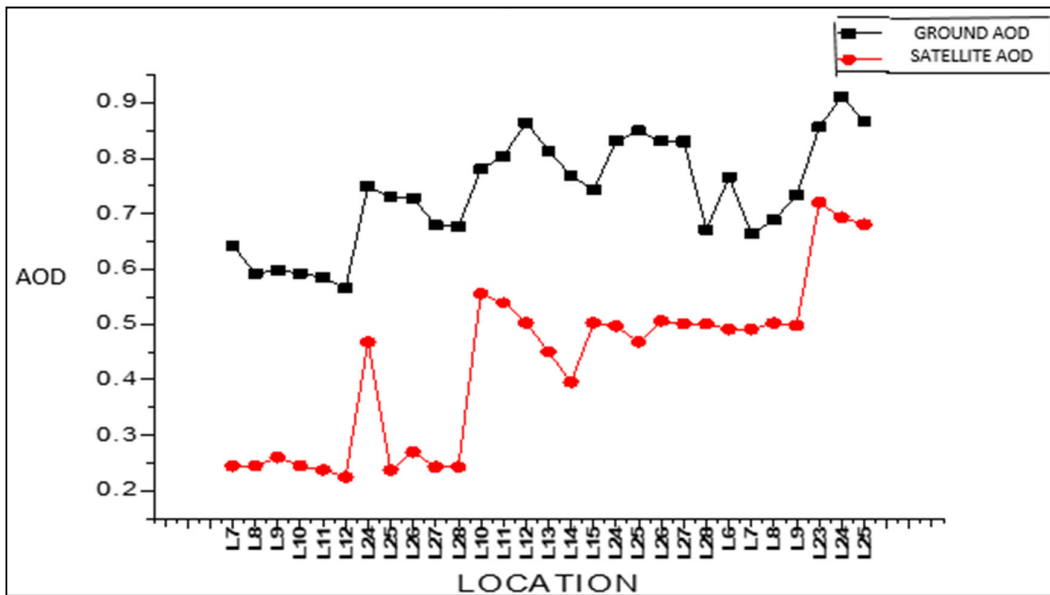


Figure 1: Time series graph of AQUA MODIS and Microtops II Sunphotometer AOD AT 500 nm.

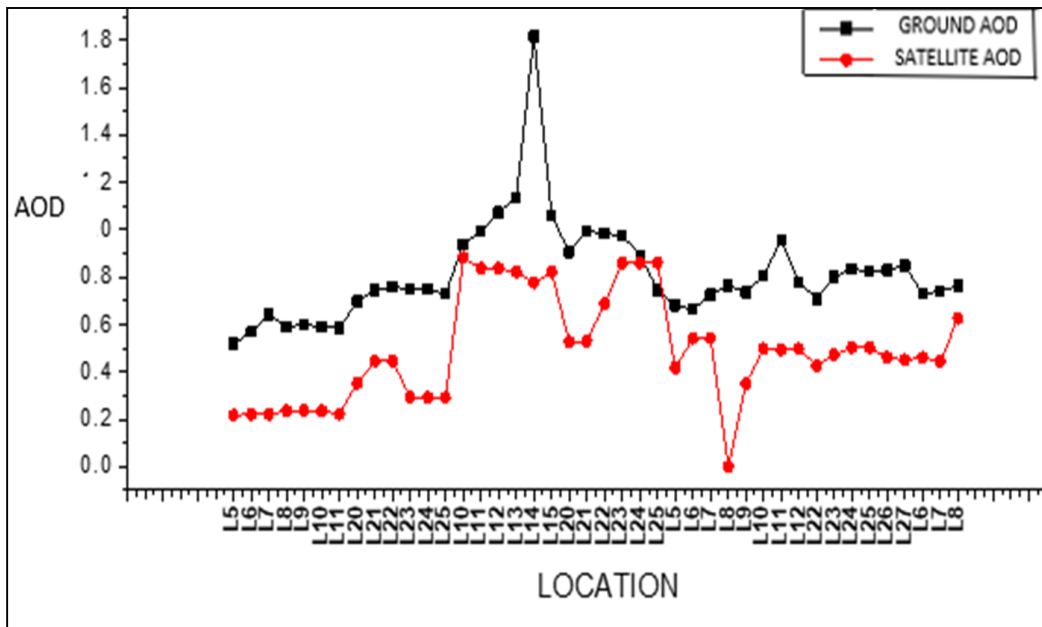


Figure 2: time series graph of TERRA MODIS and Microtops II Sunphotometer AOD AT 500 nm.

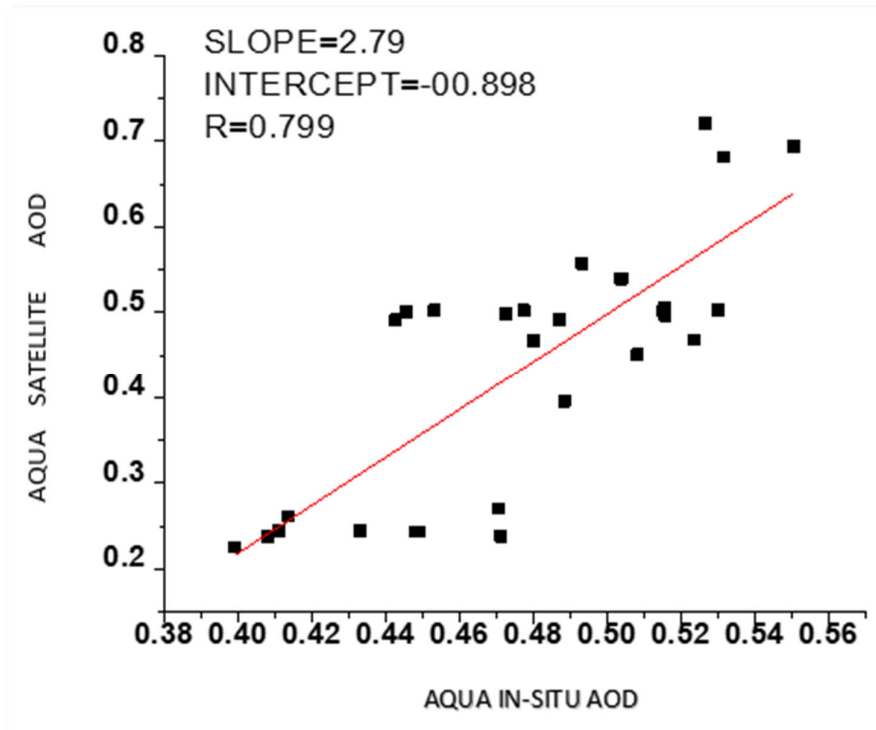


Figure 3: Scatter plot of AQUA (MODIS) AOD versus In-situ AOD

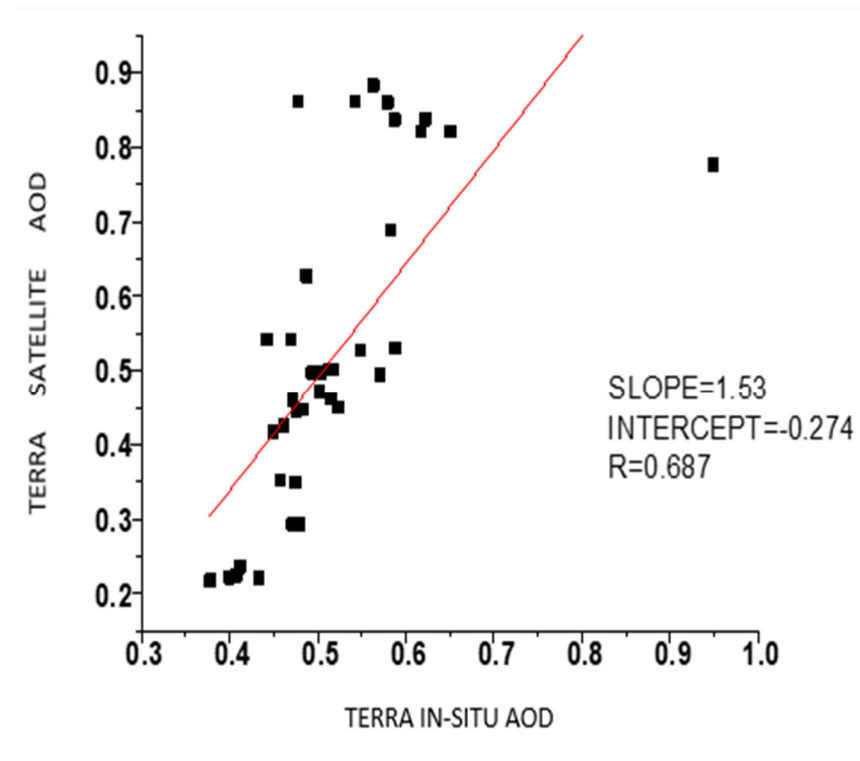


Figure 4: Scatter plot of Terra (MODIS) AOD versus In-situ AOD

CONCLUSIONS

The study highlights that (i) the correlation coefficients for the linear regression fits, R are 0.79 for AQUA and 0.69 for TERA. (ii) Terra and Aqua overestimate the AOD retrieval to the ground AOD data, as the regressed slopes are 2.79 and 1.53 for Terra and Aqua respectively which is greater than unity. (iii) Time series graph clearly shows that the AOD trend followed is nearly same for both satellite and ground AOD. Many times we are unable to collect in-situ AOD readings due to hazy or cloudy conditions or due to events like dust storm, this study can help in extrapolating AOD values on the basis of Satellite AOD. Similarly during Monsoon season the AOD values are not available through Satellite at that time this relation can be used to calculate AOD.

ACKNOWLEDGEMENTS

My project would not have been accomplished without the support, guidance & encouragement of following mentioned mentors:

1. Dr. Abha Chhabra (SAC-ISRO) for guidance in response.
2. Dr. (Fr) Robert Arockiasamy S.J. (Principal, St. Xavier's College Autonomous, Ahmedabad) without whose support this project would not have been possible. And special thanks to my parents and colleagues.

REFERENCES

Shen Y., Zhang L., Fang X., Zhao Z., Li X., Wang J. and Chai Q. “*Long-Term Analysis of Aerosol Optical Depth over the Huaihai Economic Region (HER): Possible Causes and Implications*”,

Atmosphere, 2018, 9(3), 93; <https://doi.org/10.3390/atmos9030093>

He, Q.; Li, C.; Tang, X.; Li, H.; Geng, F.; Wu, Y. Validation of modis derived aerosol optical depth over the Yangtze River Delta in China. Remote Sens. Environ. 2010, 114, 1649– 1661.

T. Jantarach, I. Masiri, S. Janjai, Comparison of MODIS aerosol optical depth retrievals with ground-based measurements in the tropics, 2012.

A FRAMEWORK FOR EXPOSURE ASSESSMENT IN RURAL INDIAN HOUSEHOLDS: A CASE STUDY OF RAJASTHAN

SNEHLATA TIGALA¹, ANU RANI SHARMA², KAMNA SACHDEVA³

¹ PhD Scholar, Department of Natural Resources, TERI School of Advanced Studies

² Assistant Professor, Department of Natural Resources, TERI School of Advanced Studies

³ Associate Professor, Department of Energy and Environment, TERI School of Advanced Studies

Address: TERI School of Advanced Studies, 10, Institutional Area, Vasant Kunj, New Delhi (110070), India

Email: ¹ snehlataigala@gmail.com, ² anu.sharma@terisas.ac.in, ³ kamna.sachdeva@terisas.ac.in
Contact: Tel. +91 11 71800222, Fax +91 11 26122874

KEYWORDS: Indoor Environment; Rural; Household Air Pollution; Kitchen Area Exposure

ABSTRACT

INTRODUCTION

Household air pollution results in approximately 3.7 million premature deaths every year. The presented study focuses on development of a framework for exposure assessment in rural Indian households.

METHODS

The framework builds up on three major drivers of exposure: air quality assessment, area exposure, and health analysis. The air quality assessment includes perception-based survey questionnaires (source and contribution), and pollutant characterization (elemental composition, morphology). The area exposure includes site monitoring for microenvironment assessment and satellite datasets for additive ambient aerosol load. The health assessment component evaluates the individual health indicators.

RESULTS AND DISCUSSION

The synergy of these components establish the health risks associated with exposure within the household (microenvironment) and the ambient environment. The results showcased high aerosol load with presence of fine range absorbing species in the ambient air. Further, condition is worsened with excessive burning of solid biomass fuel for cooking and heating purposes. The SEM-EDAX analysis showed high carbon content while cooking with biomass as compared to LPG-based cooking. The level of particles emitted during combustion also varied among the different types of solid biomass fuels. The population exclusively exposed to biomass combustion within semi-open type kitchen were found to be most vulnerable. The time-activity pattern highlights the drudgery of middle aged women and threat to young children accompanying their mothers.

CONCLUSION

The study highlights the predicament of women exposed to ambient and indoor air pollution. The study reflects upon the gender bias in the level of exposure within the subject population. The preference of household energy is directed by socio-cultural dimensions and economic rationale.

OBSERVED RELATION BETWEEN AEROSOL OPTICAL PROPERTIES WITH RELATIVE HUMIDITY

BHARATI PAUL¹, A.K.DAS¹, S.S.KUNDU², N.BARMAN²

¹Department of Environmental Science, Tezpur University Assam- 784028

²North-East Space Applications Centre Government of India, Department of Space Umiam, Meghalaya- 793103

KEYWORDS: AOD, Angstrom Exponent, MODIS, AIRS

INTRODUCTION

The hygroscopic behavior is one of the important physical properties of aerosol. This property directly influences the size distribution and mass concentration of aerosol particles at ambient relative humidity (Cheng *et al.*, 2008; Randles *et al.*, 2004; Malm *et al.*, 2003), also influences the climate system by modifying the scattering capability and residence time of these particles in the atmosphere (Ogren *et al.*, 1992).

Aerosol hydration can be studied by analyzing the behaviour of its optical properties and size characteristics as a function of RH (Randriamiarisoa *et al.*, 2006). This study is aimed at understanding the relationship between aerosol optical properties, viz., Aerosol Optical Depth (AOD) and Angstrom Exponent (AE) and RH over the high humid region of Assam India. The study has been carried out using 15 years of data covering the time period 2003 - 2018.

METHODS:

Study area: The study focuses on the state of Assam (Fig. 1) bounded by the longitudinal coordinates of 89.73 and 95.97 degree decimal and by the latitudinal coordinates of 24.15 and 27.97 degree decimal. The river Brahmaputra flows through east to west along the entire length of the state. This river valley receives high aerosol loading carried by the strong westerly wind from the Indo-Gangetic plains during the winter and pre-monsoon season. (Pathak *et al.*, Gogoi *et al.*, Kundu *et al.*, 2014; Pathak, et.al., 2015) .

DATA & METHODS:

Records of AOD 550nm, RH and AE (470nm - 870 nm) for the period 2003-2018 obtained from AIRS, MODIS and MERRA-2 is utilized in this study. The details of datasets are presented in Table-1

Parameter	Sensor	Spatial Resolution	Product level	Temporal resolution
Aerosol Optical depth 550nm	MODIS	1° × 1°	3	Monthly
Relative Humidity	AIRS	1° × 1°	3	Monthly
Angstrom Exponent (470nm - 870 nm)	MERRA-2	0.5° x 0.625°	Version 5.12.4	Monthly

Table 1. Details of datasets used.

Pearson Correlation Analysis is used to identify the temporal and seasonal relationship between the AOD at 550 nm and the relative humidity, AE (470nm - 870 nm) and relative humidity on a monthly scale for the period of 2003 Jan-2018 July. Additionally, correlations are identified at seasonal scale.

RESULTS & DISCUSSIONS:

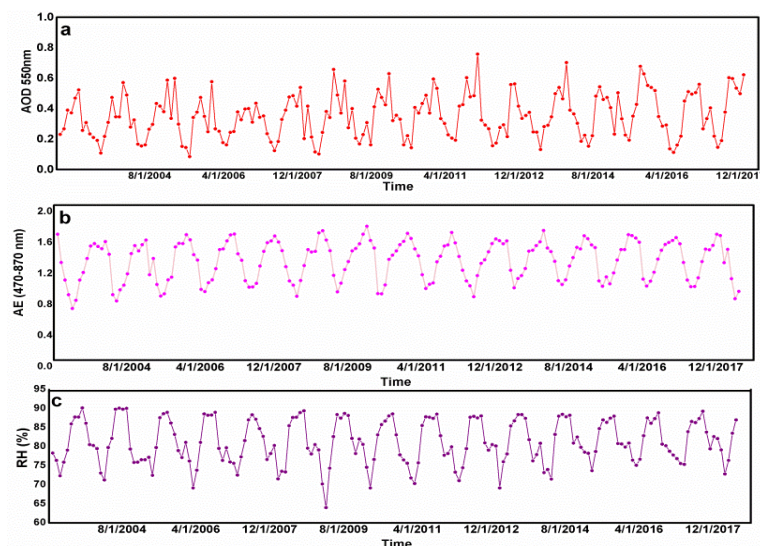


Figure 2. The monthly mean variation of (a) AOD 550nm (b) AE (470nm - 870nm) and (c) RH (%) respectively for year 2003- 2018 for Assam.

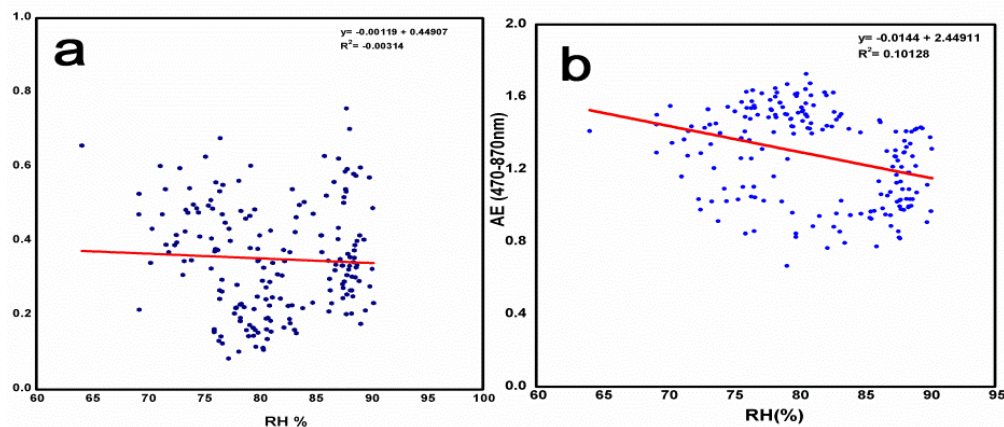


Figure 3. The (monthly) correlation between (a) AOD 550nm and Relative humidity (RH) and (b) AE (470nm - 870nm) and Relative Humidity (RH) for time period of 2003-2018 for Assam.

The weak correlation between AOD and RH {Fig 3(a)} denotes increasing relative humidity have no significant effect on AOD indicating the dominance of hydrophobic aerosol (soot, BC) particles than hydroscopic (OC, dust) aerosol in the atmosphere over the study region. These hydrophobic aerosols are mainly soot particles induced from biomass burning (Badarinath *et al.*, 2004) and black carbon from fossil fuel combustion (Pathak *et al.*, Gogoi *et al.*, Kundu *et al.*, 2014). The negative correlation between AE and relative humidity {Fig 3(b)} signifies high atmospheric humidity reduces AE value over the study area. Lower AE value shows the presence of coarse mode particles in the atmosphere

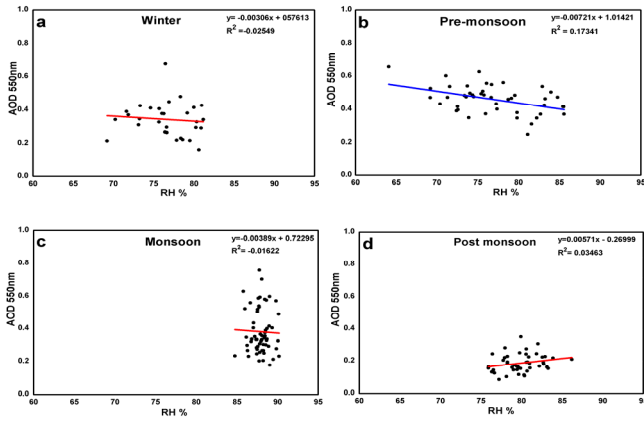


Figure 4: The correlation between AOD 550nm and Relative Humidity (RH) for different seasons– (a) Winter (b) Pre-monsoon (c) Monsoon and (d) Post Monsoon for year 2003 to 2018 respectively for Assam.

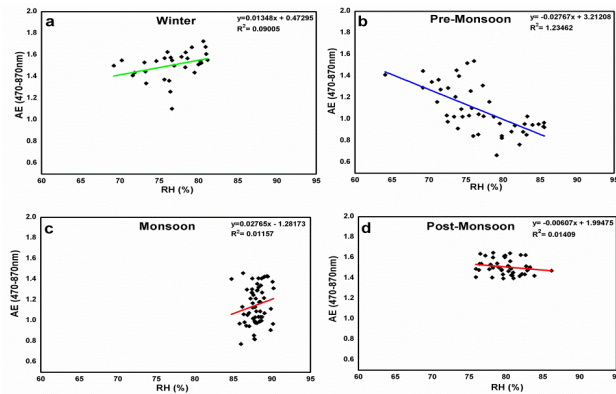


Figure 5: The correlation between AE (470nm - 870nm) and Relative Humidity (RH) for different seasons- (a) Winter (b) Pre-monsoon (c) Monsoon and (d) Post Monsoon for year 2003 to 2018 respectively for Assam.

The strongest negative correlation is observed during the pre-monsoon season between AOD and RH, AE and RH for the time period of 2003 to 2018 {Fig 4(b), 5(b)}. Highest aerosol loading over the NE region has been reported during pre-monsoon season (Pathak *et al.*, 2015) predominate by anthropogenic aerosols coming from fossil fuel or biomass/biofuel burning (Pathak *et al.*, 2014).

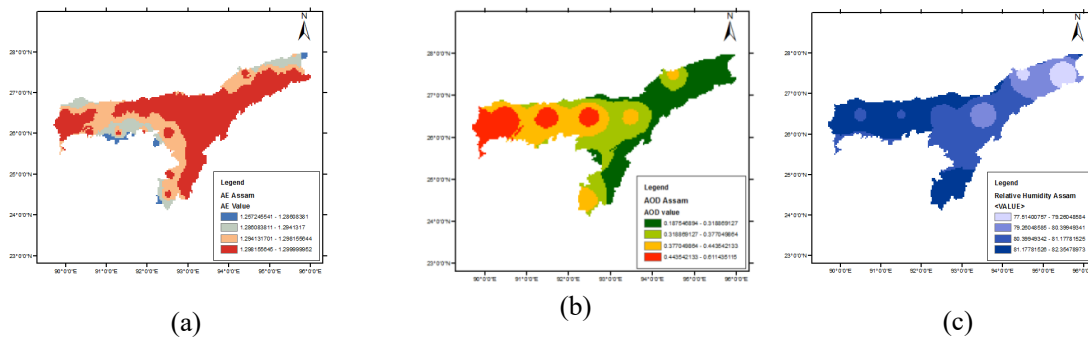


Figure 6: Time averaged map of (a) Angstrom Exponent (470-870nm) (b) AOD 550nm (c) Relative Humidity for the period of 2003-2018 for Assam.

High AOD and AE value is observed over the Lower and Middle Assam region {Fig 6(a-c)} than Upper Assam which indicates the presence of high aerosol concentration and coarse mode particles in the atmosphere of this region.

CONCLUSION:

From the above study, it can be concluded that the concentration of hydrophobic aerosol particles- smoke and BC is more than hydroscopic particle over the region. Further investigation work is required for the same.

ACKNOWLEDGEMENTS

This work was supported by the Tezpur University and North-East Space Applications Centre Government of India, Department of Space Umiam, Meghalaya

REFERENCE:

Engelhart, G. J., L. Hildebrandt, E. Kostenidou, N. Mihalopoulos, N. M. Donahue, and S. N. Pandis (2011). Water content of aged aerosol, *Atmos. Chem. Phys.***11**,911–920.

Malm, W. C., D. E. Day, S. M. Kreidenweis, J. L. Collett, and T. Lee (2003). Humidity-dependent optical properties of fine particles during the Big Bend Regional Aerosol and Visibility Observational Study, *J. Geophys. Res***108**, 4279.

Ogren, J. A., K. J. Noone (1992). Measurements of the Size Dependence of the Concentration of Nonvolatile Material in Fog Droplets, *Tellus* **44**, 570-580.

Pathak, B., A. Borgohain, P. K. Bhuyan, S. S.Kundu, S Sudhakar, M. M Gogoi and T. Takemura (2014). Spatial heterogeneity in near surface aerosol characteristics across the Brahmaputra valley, *J. Earth Syst. Sci* **123**,651–663.

Pathak, B., T. Subba, P. Dahutia, P.K. Bhuyan, K. Krishna Moorthy, M.M. Gogoi, S. Suresh Babu, L. Chutia, P. Ajay, J. Biswas, C. Bharali, A. Borgohain, P. Dhar, A. Guha, B.K. De, T. Banik, M. Chakraborty, S.S. Kundu, S. Sudhakar, S.B. Singh (2015). Aerosol characteristics in north-east India using ARFINET spectral optical depth measurements, *Atmos. Environ*1-13.

Pilinis, C., J. H. Seinfeld, and D. Grosjean (1989). Water content of atmospheric aerosols, *Atmos. Environ.***23**,1601–1606.

Randles, C., L. Russell, and V. Ramaswamy (2004). Hygroscopic and optical properties of organic sea salt aerosol and consequences for climate forcing, *Geophys. Res. Lett***31**, 16108.

Randriamiarisoa, H., P. Chazette1, P. Couvert, J. Sanak, and G. M'egie, (2006). Relative humidity impact on aerosol parameters in a Paris suburban area, *Atmos. Chem. Phys***6**, 1389–1407.

SOURCES AND ORIGIN OF AEROSOLS AT A RECEPTOR SITE IN THE WORLD'S MOST POLLUTED MEGACITY

SAHIL BHANDARI¹, SHAHZAD GANI², KANAN PATEL¹, SARAH SERAJ², DONGYU S. WANG¹, PRASHANT SONI³, ZAINAB ARUB³, GAZALA HABIB³, JOSHUA APTE², AND LEA HILDEBRANDT RUIZ¹

¹Department of Chemical Engineering, The University of Texas at Austin,
Austin, TX, USA.

²Department of Civil, Architectural and Environmental Engineering, The University of Texas at Austin,
Austin, TX, USA.

³Department of Civil Engineering, Indian Institute of Technology Delhi, Delhi, India

KEYWORDS: aerosol sources, aerosol monitoring and characterization, pmf source apportionment, Delhi.

INTRODUCTION

Exposure to fine particulate matter (PM) poses significant health risks, especially to residents in densely populated areas (Chow et al., 2006; Cohen et al., 2017). Delhi, India is the second most populated city in the world with extremely high winter PM concentrations and frequent severe pollution episodes. However, the current understanding of the sources and dynamics of PM pollution in cities of developing countries as Delhi, India is limited (Pant et al., 2016). The Delhi Aerosol Supersite (DAS) campaign provides the first long-term chemical characterization of ambient submicron aerosol in India, with near-continuous online measurements of aerosol composition. Here we report on source apportionment conducted on 1.5 years of highly time resolved speciated submicron non-refractory PM₁ (NR-PM₁, includes organics, chloride, ammonium, sulphate and nitrate) and black carbon (BC). This work improves upon the low time resolution of filter measurements previously employed in Delhi, with the ACSM sampling at a time resolution of about 1 minute. Further, this work has collected PM₁ data starting January 2017 through the end of 2018 and therefore has sampled for a period longer than most previous global ACSM-AMS campaigns that have lasted only for a few weeks.

METHODS

Our research team is filling important knowledge gaps by conducting continuous measurements of submicron (PM₁) particle concentration and composition at the Indian Institute of Technology (IIT) Delhi. An Aerodyne Aerosol Chemical Speciation Monitor (ACSM, Aerodyne Research, Billerica MA) provides data on bulk composition and the aerosol mass spectrum for non-refractory submicron aerosols (NRPM₁), an Aethalometer (Magee Scientific Model AE33, Berkeley, CA) provides information on concentrations of black carbon (BC), and a Scanning Mobility Particle Sizer (SMPS, TSI, Shoreview, MN) gives data on particle concentrations and size distributions. We have conducted source apportionment of the measured particulate matter using organic and inorganic mass spectra by Positive Matrix Factorization (PMF), a bilinear unmixing model that apportions data (here, mass spectra) in linear combinations of fixed factor profiles with variable time series. We have also employed back trajectories and inorganic thermodynamic model E-AIM (E-AIM Website; Friese and Ebel, 2010) to identify the nature of sources of PM. We have analysed seasonal differences, interannual variability, as well as studied the effects of weekdays versus weekends and regional and national holidays. While several studies have looked at PMF chloride-containing factors, identified their potential sources and developed source specific profiles, no study has focused exclusively on the presence of the exceptional chloride levels in Delhi. We have conducted a thorough literature review and validated our PMF factors containing chloride to address this knowledge gap. We have also compared results from the Sandradewi model (Sandradewi et al., 2008) apportioning black carbon to

fossil fuel and biomass burning components to black carbon apportionment based on PMF results. We have combined back trajectory analyses in HYSPLIT with factor and species concentrations to generate probability distribution contribution function (PSCF) and conditional probability function (CPF) rose plots identifying the local and regional nature of respective sources. We have also compared full PMF results for organic mass spectra with the tracer based organic component analysis to yield a real-time source apportionment approach curated for Delhi.

RESULTS & DISCUSSION

We have observed marked seasonal and diurnal variability in the concentration and composition of PM₁ owing to the interactions of sources, thermodynamics and atmospheric mixing. Winter is the most polluted period of the year with average PM₁ (NR-PM₁ + BC) mass concentrations of ~210 µg m⁻³ and the hot and rainy monsoon are the least polluted (PM₁ ~50 µg m⁻³). Organics make up more than half of the PM₁ for all seasons and times of day. While ammonium, chloride and nitrate each are ~10% of the PM₁ for the cooler months, BC and sulphate contribute ~5% each. For the warmer periods, the fractional contribution of BC and sulphate to PM₁ increases and the chloride contribution decreases to less than 2%, suggesting its volatile nature. The seasonal and diurnal variations in absolute mass loadings are generally consistent with changes in ventilation coefficients, with higher concentrations for periods with unfavourable meteorology — low planetary boundary layer height and low wind speeds. However, varying sources and thermodynamics influence the variations in fractional contributions of PM₁. During cool periods when winds are from the northwest, we have observed episodic particulate chloride concentrations reaching up to 150 µg m⁻³, some of the highest chloride concentrations reported anywhere in the world. We have also detected several episodic events associated with substantially higher concentrations compared to seasonal averages and performed PMF analyses for those periods.

For non-refractory organics, oxidized organic aerosol (OOA) is the most important factor, contributing about 60% in all seasons. Combined organic-inorganic mass spectra (MS) PMF analyses attributes chloride almost completely to ammonium chloride. This ammonium chloride factor's concentrations drop systematically from winter to summer, consistent with its volatile nature. Our literature review and PMF results points to a likely industrial source contributing high chloride emissions. We have captured multiple biomass burning events during the course of the campaign, as indicated by BBOA factor profiles obtained using episodic PMF analyses. Heavy rainfall and monsoon events are associated with a large drop in hydrocarbon-like organic aerosol (HOA) and OOA concentrations and a complete absence of BBOA. PMF results show that OOA time series correlated well with nitrate (NO₃⁻) and sulfate (SO₄²⁻), and that HOA time series correlated well with concentrations of carbon monoxide (CO) and nitrogen oxides (NO_x) from nearby monitoring stations. Preliminary results indicate strong directionality of the oxidized organics factor and the ammonium chloride factor. It is also clear that while almost 50–70% of Delhi's PM₁ is secondary in nature for the winter and spring months, up to 60–80% was secondary for the warmer summer and monsoon months. Thus, secondary aerosols are important contributors year round. Nevertheless, primary sources, including HOA, BBOA and chloride have high fractional contributions during the highest pollution episodes. When adjusted for mass closure, tracer based HOA-BBOA and OOA factors perform remarkably well compared to the organic only PMF analysis. This indicates the possibility of a real time source apportionment approach for Delhi using measurements from the ACSM.

CONCLUSIONS

Overall, these findings point to the important effects of both primary emissions and regional atmospheric chemistry on influencing the extreme particle concentrations that affect the Delhi megacity region. Future strategies considering Delhi's situation in a regional context will be more effective than policies targeting only local, primary air pollutants.

REFERENCES

Chow, J. C., Watson, J. G., Mauderly, J. L., Costa, D. L., Wyzga, R. E., Vedal, S., Hidy, G. M., Altshuler, S. L., Marrack, D., Heuss, J. M., Wolff, G. T., Arden Pope III, C., and Dockery, D. W. (2006). Health

Effects of Fine Particulate Air Pollution: Lines that Connect, *Journal of the Air & Waste Management Association*, 56, 1368–1380.

Cohen, A. J., Brauer, M., Burnett, R., Anderson, H. R., Frostad, J., Estep, K., Balakrishnan, K., Brunekreef, B., Dandona, L., Dandona, R., Feigin, V., Freedman, G., Hubbell, B., Jobling, A., Kan, H., Knibbs, L., Liu, Y., Martin, R., Morawska, L., Pope, C. A., Shin, H., Straif, K., Shaddick, G., Thomas, M., van Dingenen, R., van Donkelaar, A., Vos, T., Murray, C. J. L., and Forouzanfar, M. H. (2017). Estimates and 25-year trends of the global burden of disease attributable to ambient air pollution: an analysis of data from the Global Burden of Diseases Study 2015, *The Lancet*, 389, 1907–1918.

Friese, E. and Ebel, A. (2010). Temperature dependent thermodynamic model of the system H^+ - NH_4^+ - Na^+ - SO_4^{2-} - NO_3^- - Cl^- - H_2O . *J. Phys. Chem. A*, 114, 11595-11631.

Pant, P., Guttikunda, S. K., and Peltier, R. E. (2016) Exposure to particulate matter in India: A synthesis of findings and future directions, *Environmental Research*, 147, 480–496.

Sandradewi, J., Prévôt, A.S., Szidat, S., Perron, N., Alfarra, M.R., Lanz, V.A., Weingartner, E. and Baltensperger, U. (2008). Using aerosol light absorption measurements for the quantitative determination of wood burning and traffic emission contributions to particulate matter. *Environmental science & technology*, 42(9), pp.3316-3323.

IMPROVED DIFFUSION LOSS CORRECTION DOWN TO 1 NM PARTICLES FOR SMPS MEASUREMENTS

JACOB H.T SCHECKMAN¹, MODI CHEN¹, HEE-SIEW HAN¹, JUERGEN SPIELVOGEL¹, AXEL ZERRATH¹, NISHANT MITTAL², RAMAKRISHNA RAMISETTY²

¹ TSI Incorporated, Shoreview, Minnesota, USA

² TSI India, Bangalore, India

KEYWORDS: SMPS (Scanning Mobility Particle Sizer), CPC (Condensation Particle Counter)

INTRODUCTION

After introducing the 1 nm SMPS (Scanning Mobility Particle Sizer) at IASTA in 2016 thorough studies of particle losses in the particle sizer have led to improvements in the algorithm to correct for those losses.

As particle size decreases, diffusion loss rates increase dramatically. Less than 10% of 20 nm particles are lost in a 1 L/min laminar flow through a straight 3 m tube. For the same conditions, the loss rate of 2 nm particles is nearly 95%, and greater than 99% at 1.5 nm. Further, because of the size-dependent nature of diffusion losses, the mode of a monodisperse ($\sigma_g=1.15$) size distribution shifts from 1.5 nm entering the 3 m tube to 1.8 nm on exit.

METHODS

In the compact 1 NM SMPS configuration the 1 NM DMA model 3086 is directly installed onto the inlet of the 1 NM CPC. The aerosol neutralizer model 3088 is directly mounted on the DMA inlet instead of placing it in the classifier platform. This configuration eliminates Electrostatic Classifier internal plumbing, and neutralizer-to-DMA and DMA-to-CPC transport tubing. This configuration maximizes particle penetration through the system and minimizes uncertainties in the final corrected concentrations.

RESULTS & DISCUSSIONS

Diffusion losses in the components have been assessed experimentally. The resulting diffusion correction for the system has been tested against a stand-alone 1 NM CPC model 3757-50. The experimental results will be presented.

CONCLUSIONS

Losses through the TSI 1 nm SMPS system were characterized. An improved diffusion correction for this configuration was derived and applied to SMPS data. As shown, the diffusion corrected, integrated total number concentration from the SMPS was compared to a CPC with excellent agreement.

A QUARTZ CRYSTAL CASCADE IMPACTOR FOR REAL-TIME AMBIENT MEASUREMENT

M. CHEN¹, F. ROMAY¹, J. SPIELVOGEL¹, R. ANDERSON¹, AND D. FELTON²

¹TSI Incorporated, Minnesota – 55126, USA.

²New York State Department of Environmental Conservation, New York – 12233, USA.

KEYWORDS: real-time, qcm, cascade impactor, ambient measurement.

INTRODUCTION

A Quartz crystal microbalance cascade impactor (QCM MOUDI) has been developed for aerosol mass distribution measurements (Chen *et al.*, 2016). The QCM MOUDI has been evaluated in the laboratory with monodisperse aerosol of known materials. It was found that the mass collected on each QCM plate calculated from the Sauerbrey equation (Sauerbrey, 1959) agreed very well with the total mass calculated from the particle number concentration measured by a condensation particle counter for monodisperse aerosols. The mass discrepancy between these two methods was smaller than 10% (Chen *et al.*, 2016). In this work, the performance of the QCM MOUDI in the ambient environment was evaluated in the New York State Department of Environmental Conservation's Queens College II site. The QCM MOUDI sampled the ambient PM_{2.5} concentration for a month (i.e. June 2018). Daily PM_{2.5} concentration values were compared with those measured by a tapered element oscillating microbalance (TEOM 1405DF) Federal Equivalent Method and the filter-based US Federal Reference Method (FRM). Very good agreement was observed. When compared with the TEOM, the QCM MOUDI measured about 6% more mass on average. When plotting QCM MOUDI PM_{2.5} data against FRM data, the slope was 1.076 with R² of 0.798.

METHODS

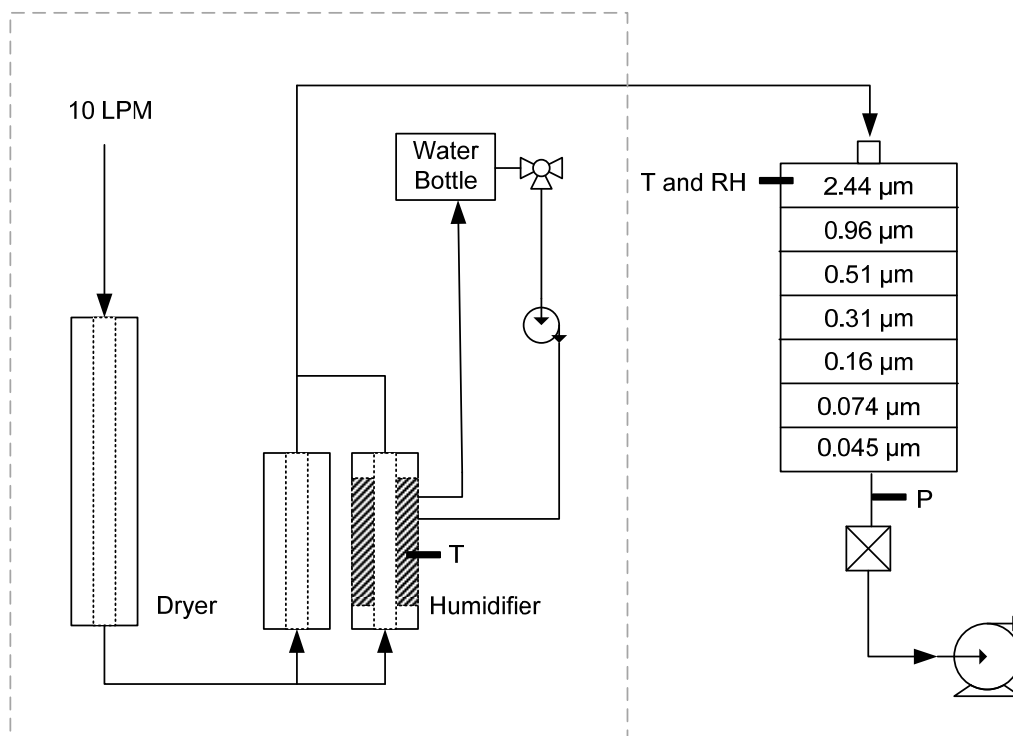


Figure 1. Schematic of the QCM MOUDI.

Figure 1 is the schematic of the QCM MOUDI. The dashed-line box indicates the relative humidity (RH) conditioner upstream of the cascade impactor. It consists of three Nafion tubes. Two of them are used as dryers, and one is filled with water and used as a humidifier. The temperature of the humidifier is controlled according to the RH sensor signal at the inlet of the impactor stack. Downstream RH of the conditioner is controlled within 1% of the set point using an active feedback control loop.

At the Queens College II site, the QCM MOUDI sampled ambient particles at the conditioned RH of 65%. This RH value was chosen to minimize particle bounce on the impactor stages. Collected particles also couple well with the QCM under this condition. The TEOM sampled aerosol on a filter maintained at 30 °C and recorded the PM_{2.5} mass as “base” value. Every six minutes, the TEOM switched the flow path and particle-free air at -20 °C dew point passed through the filter and a mass difference called a “reference” value was determined. The total PM_{2.5} concentration was calculated as the “base” minus the “reference” (Thermo scientific, 2009). FRM filters sampled aerosol at ambient conditions with a 16.7 L/min sampling flow rate for 24 hours from midnight to midnight. Filters remained on the roof in a closed container for 2-6 days depending on the pickup schedule. Prior to pre and post sampling weighing, filters were conditioned in a 20 °C to 23 °C, 30% to 40% RH laboratory environment for more than 24 hours.

RESULTS & DISCUSSIONS

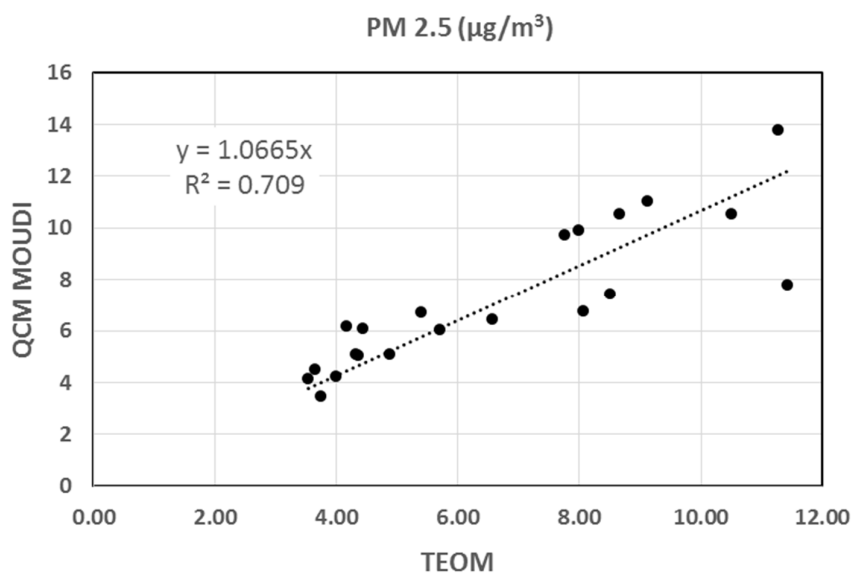


Figure 2. Comparing PM 2.5 measured by the QCM MOUDI and the TEOM

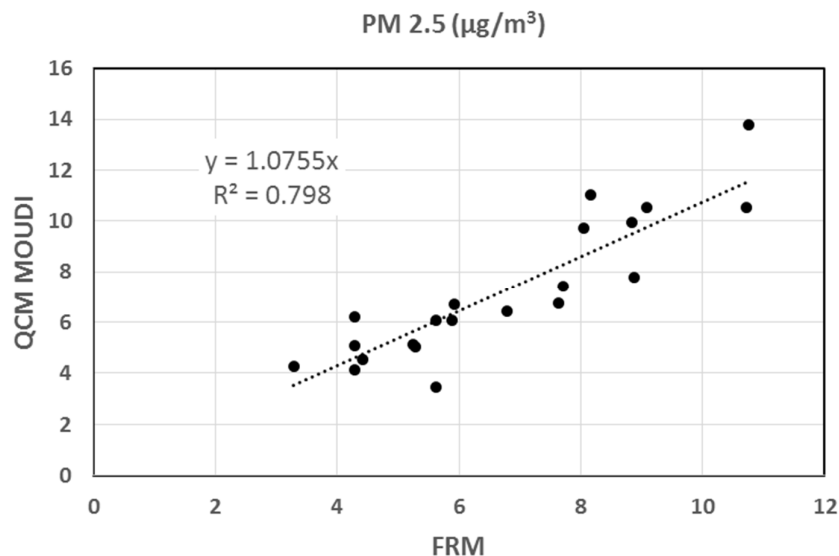


Figure 3. Comparing PM 2.5 measured by the QCM MOUDI and the FRM.

Figure 2 shows the integrated PM2.5 comparison between the QCM MOUDI and the TEOM. They agreed with each other pretty well overall except for one day. Figure 3 shows the comparison between PM2.5 measured by the QCM MOUDI and by the US FRM. The overall agreement was very good, with the QCM MOUDI measuring about 7.5% more mass on average. The QCM MOUDI sampled aerosol at higher RH than both the TEOM and the FRM filter weighing conditions. This leads to more water content in the particles, which resulted in the slightly larger PM2.5 mass fraction.

CONCLUSIONS

The QCM MOUDI was developed for real-time mass distribution measurements. It was evaluated in the Queens College II site for one month. Very good agreement was achieved among the PM2.5 mass concentrations measured by the QCM MOUDI, by the TEOM, and by the US FRM. In addition, the QCM MOUDI provides the distribution of the PM2.5 fraction in six size channels, giving users additional information on the aerosol mass as a function of particle size. The result shows that the QCM MOUDI performs very reliably in the field and can provide accurate mass concentration distribution measurements over time. The aerosol sample collected by the QCM MOUDI can also be recovered and used for further analysis.

REFERENCES

- Chen, M., Romay, F. J., Li, L., Naqwi, A., and Marple, V. A. (2016). A novel quartz crystal cascade impactor for real-time aerosol mass distribution measurement. *Aerosol Science and Technology*, 50(9), 971-983.
- Sauerbrey, G. (1959). Verwendung von Schwingquarzen zur Wägung dünner Schichten und zur Mikrowägung, *Zeitschrift für physik* 155.2: 206-222.
- Thermo scientific (2009). TEOM® 1405-DF: Dichotomous Ambient Particulate Monitor with FDMS® Option. <https://assets.thermofisher.com/TFS-Assets/LSG/manuals/EPM-manual-1405DF.pdf>

IMPACT OF CALIFORNIA FIRES ON LOCAL AND REGIONAL AIR QUALITY: THE ROLE OF A LOW-COST SENSOR NETWORK AND SATELLITE OBSERVATIONS

P. GUPTA^{1,2}, P. DORAISWAMY³, R. LEVY², O. PIKELNAYA⁴, J. MAIBACH¹, B. FEENSTRA⁴,
ANDREA POLIDORI⁴, F. KIROS³, AND K. MILLS³

¹STI-Universities Space Research Associations, AL, USA

²NASA Goddard Space Flight Center, MD, USA

³RTI International, NC, USA

⁴South Coast Air Quality Management District, CA, USA

KEYWORDS: Air Quality, Aerosols, Fires, Low-cost Sensors.

INTRODUCTION

PM_{2.5}, or fine particulate matter, is a category of air pollutant consisting of particles with effective aerodynamic diameter equal to or less than 2.5 microns. These particles have been linked to human health impacts as well as regional haze, visibility, and climate change issues. Due to cost and space restrictions, the standard monitoring network remains spatially sparse. To increase the spatial resolution of monitoring, previous studies have used satellite data to estimate ground-level PM concentrations, despite these estimates being associated with moderate to large uncertainties when relating a column measure of aerosol (aerosol optical depth or AOD) with surface measurements. In this paper, we will discuss the role of low-cost PM_{2.5} sensor and satellite observations in monitoring air quality.

METHODS

The low-cost sensors for making PM_{2.5} measurements in real-time have been deployed in the field during summer of 2017 in the California. The sensors were deployed as an independent network and also paired with existing EPA standard FEM network. Some of the sensors were also tested in the Lab under controlled conditions. During the fires season of 2017, we utilized data from these sensors, EPA network and integrated with satellite observations to map the PM_{2.5} across the CA and quantify the impact of fires on local and regional air quality.

RESULTS & DISCUSSIONS

We will present results from the lab and field evaluations of the sensor measurements with those obtained from standard measurements. We will also present a frame work to integrate low-cost sensor data with NASA satellite observations for real time air quality monitoring. Application of low-cost sensor and satellite data for quantifying the impact of wildfires in CA during October 2017 will be demonstrated. The impacts of fires on PM_{2.5} concentration at varying temporal (hourly, daily, weekly) and spatial (local to regional) scales have been evaluated. Finally, we will highlight lessons learnt and challenges associated with both low-cost sensors and satellite-based PM_{2.5} measurements around the globe.

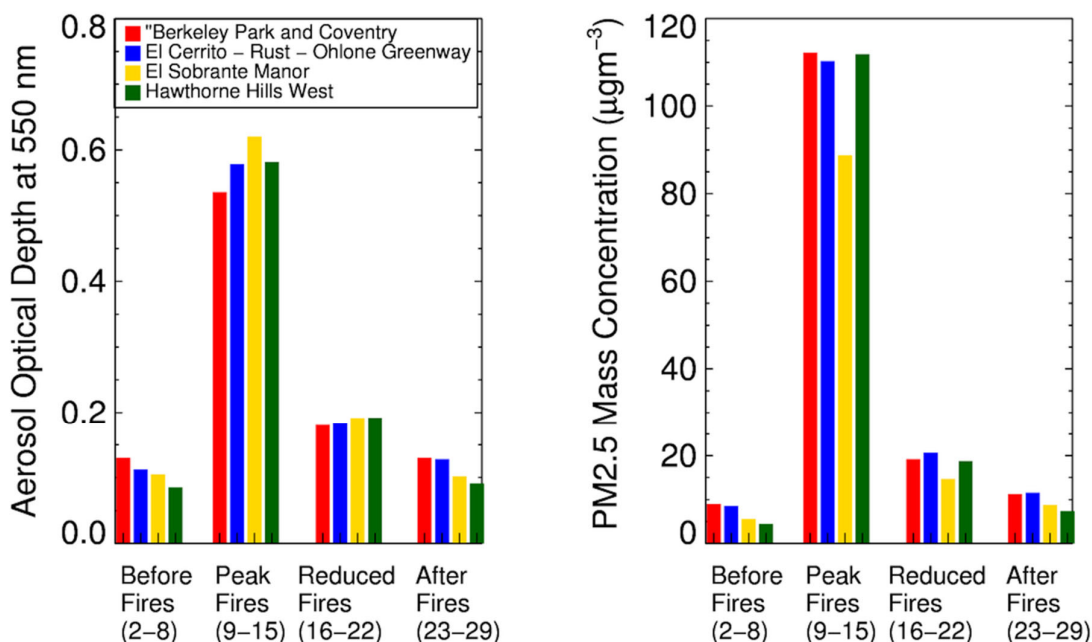


Figure 1. The impact of fires on local air quality conditions at weekly scale. The bar charts show weekly-averaged AOD (left) and PM_{2.5} (right) at selected LCAQM locations close to fires in Northern CA. These stations are located southeast of fires.

CONCLUSIONS

While the current network of FRM and FEM PM monitors across the US provide quality measurements for determining regional attainment and regulatory decision making, a dense network of low-cost air quality monitors can provide measurements for exceptional events, such as the fires in Northern California.

ACKNOWLEDGEMENTS

This work was supported by the NASA ROSES program NNH16ZDA001N-CSESP: Citizen Science for Earth Systems Program managed by Kevin Murphy under co-operative agreement number NNX17AG68A.

REFERENCES

Gupta, P., Doraiswamy, P., Levy, R., Pikelnaya, O., Maibach, J., Feenstra, B., et al. (2018). Impact of California fires on local and regional air quality: The role of a low-cost sensor network and satellite observations. *GeoHealth*, 2, 172–181. <https://doi.org/10.1029/2018GH000136>

THE USE OF A SIZE SCANNING NEPHELOMETER TO CONSTRAIN PARTICLE SIZE-DISTRIBUTION AND THEIR SCATTERING PROPERTIES

J.V. Martins¹, R.G. Kleidman², J. Hall² AND M. D. Gibson³

¹Department of Physics, University of Maryland Baltimore County, Baltimore, MD – 21250, USA.

²AirPhoton LLC, Baltimore, MD - 21227, USA.

³Department of Civil and Resource Engineering, Dalhousie University, Halifax, NS B3H 4R2, Canada

Keywords: Nephelometer, Particulate Matter, PM2.5, Size-Distribution.

INTRODUCTION

The AirPhoton IN102 integrating nephelometer is used globally by the SPARTAN network to obtain real time data on bulk particulate matter based on their light scattering properties. This instrument uses a variable air flow rate and a sharp cut off cyclone in order to sample and analyse particles in several size bins ranging from PM 2.5 to PM 10. The IN102 Ex (Extended range) goes even further and measures between PM1 and PM10 particles. Separated forward and back scatter measurements provide additional information which together with the aerodynamic size binning information, are used to constrain the size distribution of ambient particulate measurements.

An intercomparison between the AirPhoton IN102, a TSI DRX DustTrak and two Dylos light scattering instruments was conducted. The TSI DRX DustTrak has long been used for occupational, indoor and ambient monitoring of PM1/2.5/4/10 and TSP (Wheeler et. al., 2014; MacNeill et. al., 2013). The low cost Dylos instruments are typically used by the public to measure their indoor exposure to particulate number and mass concentrations in the fine and coarse size fractions (Semple et. al., 2013). We were also interested in determining the accuracy and precision of the low cost Dylos instruments when compared to the TSI DRX and the highly accurate and precise AirPhoton IN102.

The intrinsic difference in the physical variables measured by these instruments makes a direct comparison unfeasible but, nevertheless we will show some differences and similarities on their time series.

Aerodynamic particle size distributions are the most relevant for health effects and should be assessed directly. On the other hand, the effective interaction between particles and solar radiation leads to optical size distributions that may differ from the aerodynamic sizes. A combination between optical and aerodynamic sizing provides a comprehensive way to combine the main advantages from both methods. The AirPhoton IN102Ex size scanning nephelometer explore these capabilities in a single instrument.

METHODS

An AirPhoton IN102 Ex (Extended range) integrating nephelometer was deployed at BWTech in Baltimore Maryland from August 29, 2018 to September 14, 2018 and collected information on light scattering properties of particulates ingested into the tube under ambient conditions. Running continuously measurements are recorded every 15 seconds in three wavelengths (450, 532 and 650 nm). Approximately 16 days of continuous data were obtained. The instrument is equipped with a Cyclone Inlet with a PM2.5 cutoff at a flow rate of ~5.0 lpm. The instrument is operated using a feedback flow control system that allows it to select a particle cut-off size between PM1 and PM10 by varying the flow rate. In addition, the instrument measures forward and backscattering completely independently. Combining information on forward and backscattering within each of the collected size ranges is used to set size constraints and approximate a particle size distribution. A TSI (500 Cardigan Road, Shoreview, MN 55126) DRX DustTrak capable of measuring PM1/2.5/10 and TSP was also co-located with the AirPhoton IN102. The DRX measures particulate mass concentration via a time-of-flight twin beam optical scattering technique. In addition, a Dylos (Dylos Corporation, 2900 Adams St., Unit C38,

Riverside, CA 92504) DC1700 laser particle counter measuring in the small (0.5-2.5 μm) and large (>2.5 μm) particle size fractions and a Dyls DC1700-PM measuring PM2.5 and PM10 mass concentration were also co-located with the AirPhoton IN102. The DRX and Dyls instruments were deployed on August 29, 2018 to September 14, 2018.

RESULTS & DISCUSSIONS

The following panel shows total scattering coefficient, backscattering coefficients, and angstrom exponent results from the AirPhoton IN102 Ex size scanning integrating nephelometer set to aerodynamically separate particles in the PM1, PM2.5 and PM10 size ranges.

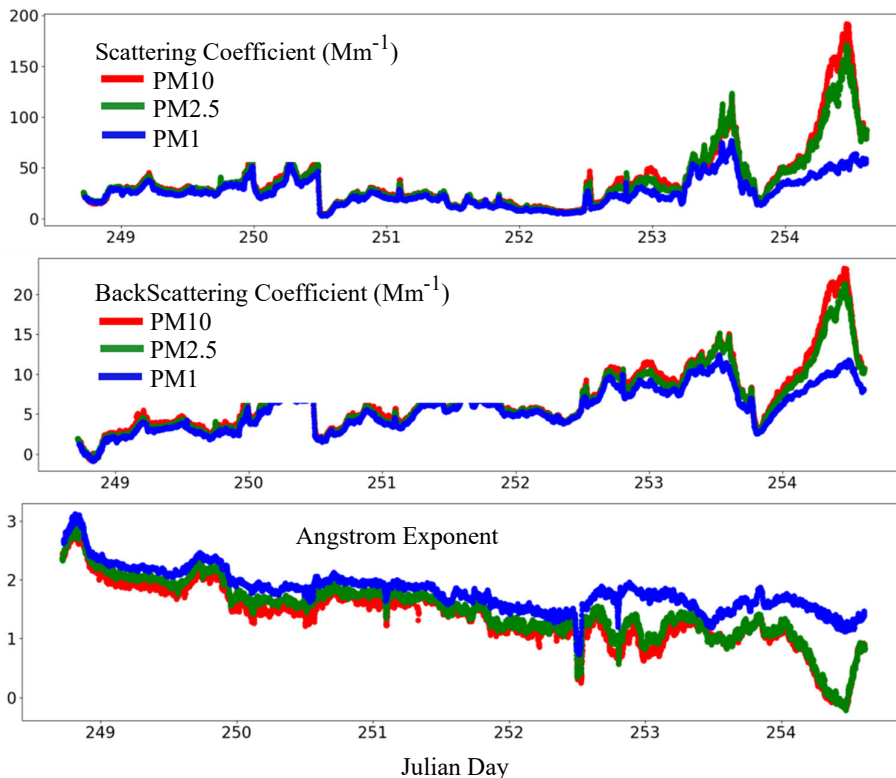


Figure 1 –Total Scattering (panel A) and backscattering coefficients measured by the Airphoton IN102 Ex instrument for the PM1, PM2.5 and PM10 size ranges. Only the green wavelength is show here to simplify the data interpretation. Panel C shows the Angstrom coefficient between the Blue and Red wavelengths in order to illustrate the variation in the optical measurement as function of the particle size ranges.

The scattering measurements of the AirPhoton Nephelometer show interesting variation in the particle sizes during the period of sampling. First, it is important to notice that for most of the experiment there was very little contribution to the scattering from particles larger than 2.5 μm (represented in red). As expected, most of the scattering came from particles smaller than 1 μm . Nevertheless, the last two days of the experiment shows large contribution to the scattering by particles between 1 and 2.5 μm . The spectral dependence of the aerosol particles also shows an interesting trend in the size of the particles throughout the experiment. A lower angstrom exponent corresponds to larger particle sizes and it is clear form the results that the particles were growing as function of time throughout the experiment. It is also important to notice that the Angstrom exponent shows larger particle sizes within all the size ranges (PM1, PM2.5 and PM10).

The following figures show similarities and differences on the parallel measurements performed in ambient conditions by the four instruments tested in this study. Figure 2 shows a comparioson between the

DustTrak and the AirPhoton Integrating nephelometer. Notice that both instruments are measuring completely different variables (mass concentration and green scattering coefficient) and the comparison is shown only for illustration of how these two variables correlated or not with each other.

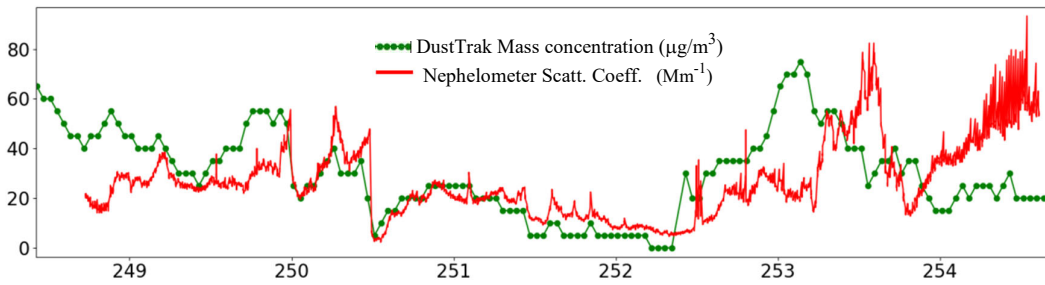


Figure 2 – Time series from the DusTrak mass concentration ($\mu\text{g}/\text{m}^3$) and green scattering coefficient ($5\times \text{Mm}^{-1}$) from the AirPhoton Nephelometer.

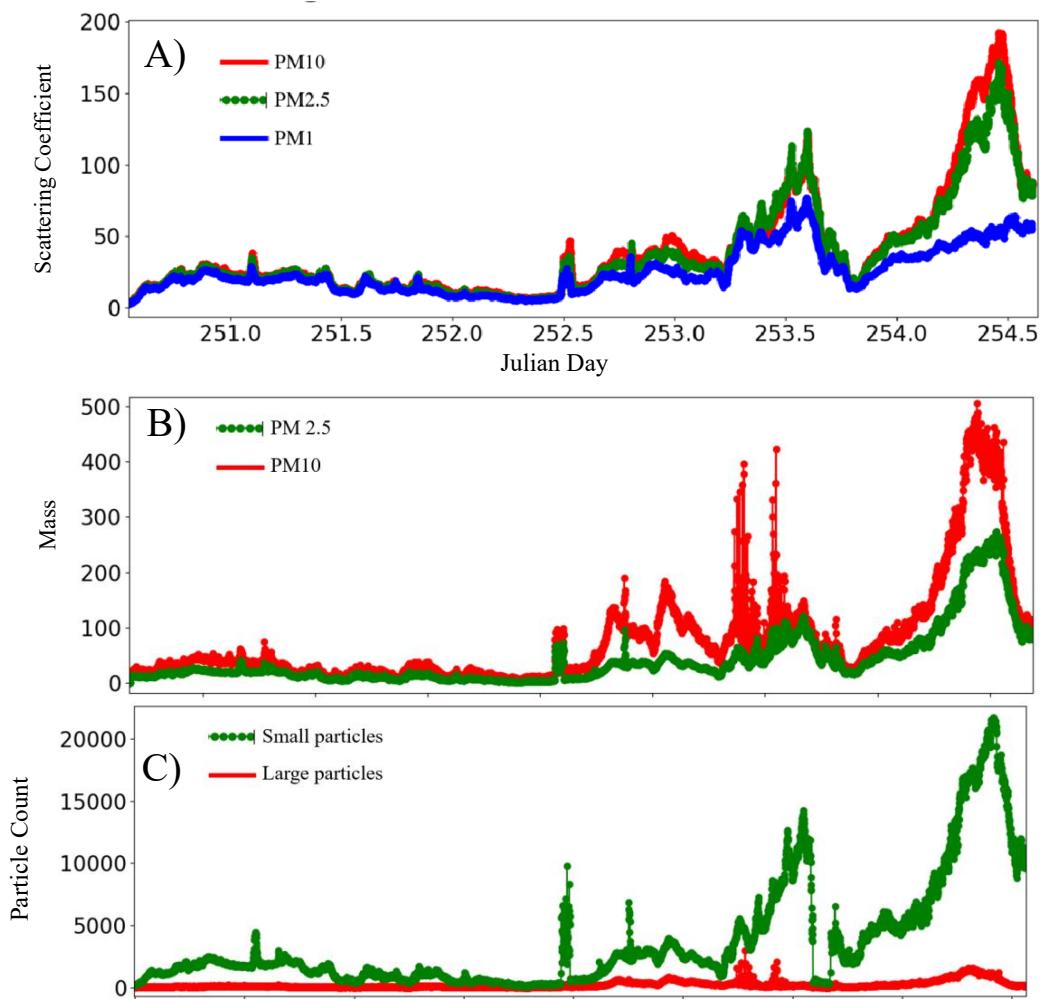


Figure 3 – Panel A) shows the results form the Airphoton IN102 Ex green scattering coefficient during the same period of the data shown in panels B) and C) collected by the Dylos monitor. Panel B) shows the Dylos estimation of Particle mass, while panel C) shows the Dylos result for particle counts in two size ranges.

Figure 3 show a comparison between the green scattering coefficient of the Airphoton Nephelometer and the mass concentration and particle counting results from the Dylos instrument. The correlation between the Dylos results and the Airphoton data set is larger than the correlation found with the DustTrak instrument. Nevertheless, there are also important difference between both instruments. It is important to emphasize that the difference in the measurement methodology of both instruments will always produce important difference in the direct comparison of their measurements. While the Dylos instrument is attempting to measure the aerosol mass concentration in different size ranges, the AirPhoton IN102 is directly measuring the contribution of the different aerosol size ranges to light scattering in the measured wavelength ranges. Nevertheless, this first comparison is important to explore the difference between the multiple methodologies to measure aerosol load in the atmosphere and the complementarity between the different techniques.

CONCLUSIONS

The AirPhoton IN102 Ex size scanning integrating nephelometer show a unique capability to aerodynamically separate particle diameters into several size ranges (e.g. PM1, PM2.5, PM4, PM10, etc.) and measure their scattering properties separately. In addition to the aerodynamic separation, the IN102Ex can also produce information on the optical particle sizing via the Angstrom exponent calculated from the measurements of scattering in three wavelengths. These results are important for estimates of the effect of the ambient aerosol on the radiative balance and radiative forcing of atmospheric aerosols.

The comparison between the different real time aerosol monitors show important differences that are related to the fact that that measured quantities by these instruments are intrinsically different.

ACKNOWLEDGEMENTS

Gibson's work was supported by All-Tech Environmental Services Ltd, 20 Duke Street, Suite 109, Bedford, Nova Scotia, B4A 2Z5, Canada AND by Thermo Fischer Scientific, 168 Third Avenue, Waltham, MA USA 02451.

REFERENCES

Thielke, J.F., R.J. Charlson, J.W. Winter, N.C. Ahlquist, K.T. Whitby, R.B. Husar, B.Y.H. Liu (1972). Multiwavelength nephelometer measurements in Los Angeles smog aerosols. II. Correlation with size distributions, volume concentrations, *J. Colloid and Interface Science* **39**, 252-259.

Snyder, G. et. al. (2016). Variation in global chemical composition of PM 2.5: emerging results from SPARTAN, *Atmos. Chem. Phys.* **16**, 9629-9653.

Wheeler, A.J., Gibson, M.D., MacNeill, M., Ward, T.J., Kuchta, J., Seaboyer, M., Dabek, E., Guernsey, J.R. and Stieb, D. (2014) Impacts of Air Cleaners on Indoor Air Quality in Residences Impacted by Wood Smoke. *Environmental Science and Technology* **48(20)**, 12157.

MacNeill, M.; Kearney, J.; Wallace, L.; Gibson, M.D.; Héroux, M.E.; Kutcha, J.; Guernsey, J.; and Wheeler, A.J. (2013) Quantifying the Contribution of Ambient and Indoor-generated Fine Particles to Indoor Air in Residential Environments. *Indoor Air*. doi:10.1111/ina.12084.

Semple, S., Apsley, A., MacCalman, L. (2013) An inexpensive particle monitor for smoker behaviour modification in homes. *Tobacco Control* **22(5)** 295.

Wheeler, A.J. (2013) Quantifying the Contribution of Ambient and Indoor-generated Fine Particles to Indoor Air in Residential Environments. *Indoor Air*. doi:10.1111/ina.12084.

SEASONAL VARIABILITY OF AEROSOL AND ITS IMPACT ON CLOUD PROPERTIES OVER GANGETIC WEST BENGAL

ISHITA SARKAR, JAYANTI PAL, RITUPARNA CHOWDHURY AND SUTAPA CHAUDHURI
Department of Atmospheric Sciences, University of Calcutta, Kolkata – 700 019, India

KEYWORDS: aerosol, cloud parameters, coarse particle.

ABSTRACT

The endeavour of the present study is to assess the impact of aerosols on cloud microphysics over Kolkata and its surroundings for the time period 2003 to 2015. For that purpose, cloud and aerosol properties are collected from MODIS. Aerosol Index has been collected from TOMS EP (2003-2004) and OMI (2005-2015). Cloud fraction has been considered from ARIS. The annual and seasonal variation shows that AOD and CERL have considerable increasing trend over Kolkata and its surroundings during the study period of 13 years. The aerosol has been classified based on regional AE and AOD through frequency distribution. The classification of the concentration of pollutants as low, moderate, high and very high and the types of pollutants are made through AOD. The classification of the size and types of aerosol particles are made through AE. The result reveals the dominance of coarse absorbing particle over Kolkata. The result also depicts that in the presence of coarse particles moderate ($0.3 < \text{AOD} < 0.6$) and high pollution ($0.6 < \text{AOD} < 0.9$) condition are found to be more favourable for altering the behaviours of cloud properties. The absorbing aerosols show direct effect in the presence of coarse particle while it shows indirect effect in presence of fine particles. The result further shows that absorbing aerosol under moderate and high pollution condition is not favourable for formation of high clouds as CTT decreases.

INTRODUCTION

It has been known for many decades that aerosols influence cloud properties. Clouds play a key role in Earth's radiation budget, and aerosols serve as the seeds i.e. cloud condensation nuclei (CCN) and ice nuclei (IN) upon which cloud droplets and ice crystals form. Changes in CCN have the potential to influence cloud macrostructure. So, aerosols have a significant impact on the Earth's climate both directly, by scattering and absorbing the incoming radiation from the Sun, and indirectly, by altering the size and density of cloud droplets thereby modifying the cloud formation, cloud albedo, cloud life-time and probability of precipitation (Lohmann and Feichter, 2005; Kosmopoulos et al., 2008). Aerosols can be of natural or anthropogenic origin. The Cloud Aerosol Interaction and Precipitation Enhancement Experiment (CAIPEEX) was carried out over northeast (NE) India to study the characteristics of aerosols and clouds in a highly polluted environmental condition and to investigate how the cloud microphysics is altered under such conditions. During pre-monsoon (April to early June) period, prevailing westerly air mass brings in mineral dust aerosols originating over the arid regions of Middle East to Thar Desert into northern India and IGP region. Bollasina et al. (2008) demonstrated that increased aerosol concentration over IGP during pre-monsoon period leads to cloud inhibition (semi-direct effect), increased shortwave reaching the surface and hence strengthen the land-sea gradient in addition to tropospheric warming during pre-monsoon season (April to early June). Over the past two decades, the rapid growth in industrialization as well as in increasing intense anthropogenic activities lead to the degradation in solar radiation, visibility and air quality. Thus, it is essential to investigate the characteristics of the aerosols, micro-physical properties of clouds and their impact on climate change. Satellite measurements can provide global observations for statistical studies of the relationships between aerosol and cloud properties. MODIS aerosol products have been applied to analyze regional trends in different locations over India by numerous scientists (Ramachandran et al., 2012; Sreekanth, 2013). The present study attempts to evaluate the cloud aerosol interaction over Kolkata and its surroundings during the period 2003-2015. For this purpose, annual and seasonal variations of cloud and aerosol properties have been investigated over Kolkata and its surrounding. Also the trend of AOD, AI & AE on a long-term scale has been observed.

METHODOLOGY

Cloud and aerosol properties are collected from MODIS that ride on board both the Terra and Aqua platforms. Aerosol Index (AI) has been collected from TOMS EP (2003-2004) and OMI (2005-2015). Cloud fraction has been considered from ARIS rides on board the Aqua platform. The conventional statistical method of Box – Whisker plot is used for the analyses of the data. The Mann–Kendall, non-parametric statistical analysis has been implemented to observe the trends in the data series of the cloud and aerosol parameters.

RESULTS & DISCUSSIONS

Aerosol properties are analyzed using aerosol optical depth (AOD), Aerosol Index (AI) and angstrom Exponent (AE). 11-point moving average of monthly AOD, AI and AE has been estimated. The result depicts a clear increasing trend in AOD with random variation. It also shows that the value of AI was quite above 0.2 indicating dominance of absorbing aerosol over Kolkata and its surroundings. The value of AE was mainly below 0.8 indicating dominance of coarse mode particle over Kolkata and its surroundings (fig 1a). Man-Kendall trend test reveals positive tau value of AOD and AE indicating increasing trend while negative tau value for AI depicts decreasing trend. Trend observed in AOD, AE and AI are statistically significant at 95% confidence level (fig 1b).

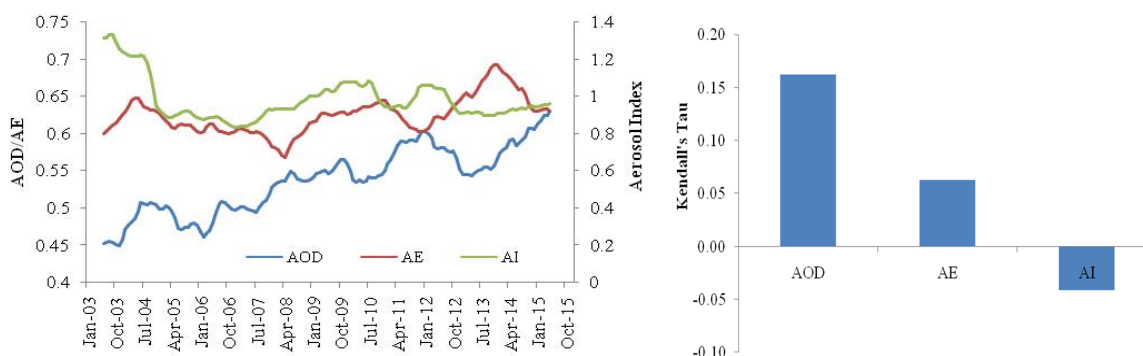


Figure 1. (a) 11-point moving average monthly variation of AOD, AE and AI and (b) Man-Kendall Tau trend analysis of AOD, AE and AI

Annual and seasonal variation shows that AOD has considerable increasing trend over Kolkata and its surroundings over 13 years. Trend analysis for cloud parameters reveals that CERL and LWP have an increasing trend while CODI, CTT and IWP have decreasing trend. All are statistically significant at 95% confidence level (Table 1). Annual and seasonal variation also shows that CERL has considerable increasing trend over Kolkata. Correlation between aerosol and cloud parameters depicts that cloud parameters are more correlated with AE and AI rather than AOD. To understand how aerosol interacts with cloud, frequency distribution has been done and aerosol has been classified based on regional AE and AOD. Low, moderate, high and very high –four type of pollution condition has been framed from AOD classification. Coarse and fine particle – two category of aerosol particle has been framed based on AE. Pre-dominance of coarse absorbing particle are obvious over Kolkata. To understand how cloud parameters are related with absorbing aerosol, categorical scatter plot for difference aerosol condition obtained from AE and AI has been analysed.

Cloud parameter	Kendall's Tau	p-value
CERI	0.005	0.659
CERL	0.069	< 0.0001
CODI	-0.024	0.026
CODL	0.007	0.482
CTP	-0.006	0.546
CTT	-0.021	0.028
IWP	-0.025	0.025
LWP	0.021	0.033
CF	0.009	0.331

Table 1. Man-Kendall Trend Analysis of Cloud Parameters

CERL shows negative correlation in presence of coarse particle for every pollution condition while for fine particle correlation becomes positive (Fig 2). But correlation is statistically significant at moderate and high pollution condition in presence of coarse particle and only at high pollution condition in presence of fine particle. Also absorbing aerosol under moderate and high pollution condition is not favourable for formation of high cloud hence CTT decreases. IWP and LWP both decreases in presence of coarse particle under moderate and high pollution condition.

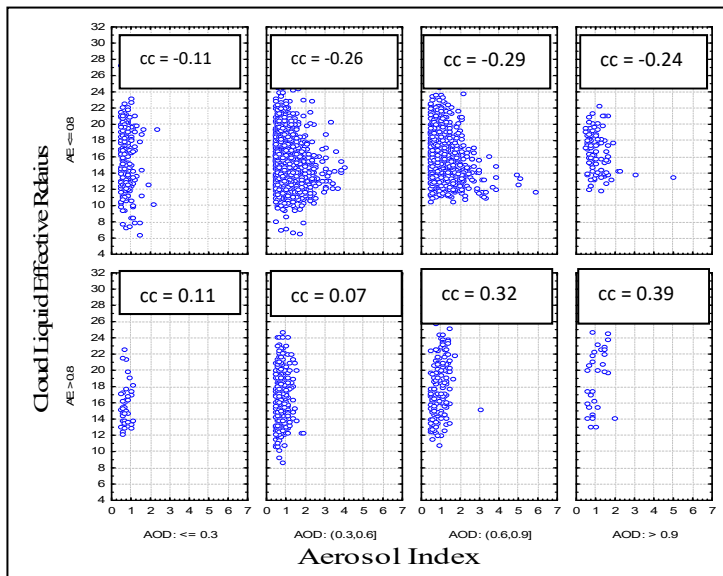


Figure 2. Correlation between CERL and AI for (a) $AE \leq 0.8$ and $AOD \leq 0.3$ (b) $AE \leq 0.8$ and $0.3 < AOD < 0.6$ (c) $AE \leq 0.8$ and $0.6 < AOD < 0.9$ (d) $AE \leq 0.8$ and $AOD > 0.9$ (e) $AE > 0.8$ and $AOD \leq 0.3$ (f) $AE > 0.8$ and $0.3 < AOD < 0.6$ (g) $AE > 0.8$ and $0.6 < AOD < 0.9$ (h) $AE > 0.8$ and $AOD > 0.9$.

CONCLUSIONS

Study finds that absorbing aerosol in presence of coarse particle prevails over Kolkata throughout a year. Cloud parameters are also more correlated with AE and AI rather than AOD as observed from correlation analysis. In presence of coarse particle, moderate ($0.3 < \text{AOD} < 0.6$) and high pollution ($0.6 < \text{AOD} < 0.9$) condition are found to be more conducive for altering behaviours of cloud properties. Absorbing aerosols shows direct effect in presence of coarse particle while it shows indirect effect in presence of fine particle. Also absorbing aerosol under moderate and high pollution condition is not favourable for formation of high cloud.

REFERENCES

- Bollasina, M., S. Nigam and K. M. Lau(2008). Absorbing aerosols and summer monsoon evolution over south Asia: an observational portrayal. *J.Clim*21: 3221–3239.
- Kosmopoulos, P., D. Kaskaoutis, P. Nastos and H. Kambezidis(2008). Seasonal variation of columnar aerosol optical properties over Athens, Greece, based on MODIS data. *Remote Sens. Environ.* 112, 2354–2366.
- Lohmann, U. and J. Feichter(2005). Global indirect aerosol effects: a review, *Atmos. Chem. Phys.* 715–737.
- Ramachandran, S., S. Kedia and R. Srivastava(2012). Aerosol optical depth trends over different regions of India. *Atmos. Environ.* 49, 338–347.
- Sreekanth, V. (2013). Satellite derived aerosol optical depth climatology over Bangalore, India. *Adv. Space Res.* 51, 2297–2308.

**SPATIO - TEMPORAL VARIABILITY OF CLOUD AND AEROSOL PROPERTIES
ASSOCIATED WITH INTER - ANNUAL VARIATION OF SUMMER MONSOON ONSET
OVER GANGETIC WEST BENGAL**

FATEMA KHAN, DEBANJANA DAS AND SUTAPA CHAUDHURI

Department of Atmospheric Sciences, University of Calcutta,
51/2 Hazra Road, Kolkata -700 019, India.

KEYWORDS: ISM, Cloud properties, AOD, GWB.

ABSTRACT

The intra seasonal and inter annual variability of Indian summer monsoon rainfall is known to be linked with aerosol - cloud interactions. In the present research an attempt has been made to identify the impact of contrasting onset of Indian summer monsoon (ISM) over Gangetic West Bengal (GWB) on cloud properties and aerosol optical depth (AOD). The categories of onset of ISM over GWB are considered to be early, normal and delayed onset. The spatial variation of cloud top temperature (CTT), combined cloud optical thickness (CCOT), liquid water cloud optical thickness (LWCOT), ice cloud optical thickness (ICOT), ice cloud effective particle radius (ICEPR), liquid water cloud effective radius (LWCER), cloud top pressure (CTP), cloud ice water path (CIWP) and cloud liquid water path (CLWP) and AOD are estimated on the onset day of ISM over GWB for all the categories of onset. The types of cloud during the period from pre to post onset of ISM over GWB have also been tracked. The result shows that the cloud parameters normally possess greater values in the northern parts of India for early onset years. The result further shows that the cloud parameters have highest value on the onset days of early onset years and lowest values for normal onset years. The values reside in between for delayed onset years except for cloud liquid effective radius which has lowest value for delayed onset and cloud top temperature and pressure have minimum value for early and maximum value for delayed onset with intermediate values for normal onset year. The result reveals that the high clouds are observed for normal and delayed onset years and medium clouds are observed for early onset years.

INTRODUCTION

The onset of summer monsoon is of immense significance over Indian states. The normal, advanced and delayed onset of monsoon rain has colossal impact on Indian agriculture as well as economy. The normal onset of SM over GWB is around 10th June. There are occasions when BOB branch takes longer time to reach GWB even with a standard deviation of 8 days with normal onset. The onset and withdrawal process of summer monsoon comprise number of stages accompanied with specific changes in the large scale atmospheric and oceanic circulation in the Indo-pacific region. Various scientists have investigated on dynamic and thermodynamic characteristics of Asian summer monsoon to predict the onset and its variability. The variability in the onset of summer monsoon over Gangetic West Bengal, India has been observed with climatology of tropopause characteristics (Mondal et al. 2017). Aerosols, clouds, and their interaction with climate is still the one of the most important area of research. To assess the regional and global climate change caused by aerosols on clouds, detailed information is required on the atmospheric concentrations of aerosol in the region (Dutkiewicz et al., 2009). A number of studies on aerosol-cloud interactions have been conducted in the south and east parts of Asian continent to address the spatial and temporal variability of aerosols and clouds (e.g., Alam et al., 2010; Balakrishnaiah et al., 2012). In the present investigation the variations of AOD and cloud properties associated with the transition from pre-monsoon to monsoon onset have been estimated.

METHODS

In the present study Moderate resolution Imaging Spectrometer (MODIS) MODIS level-3 atmosphere daily global data of cloud parameters, such as, CTT, CTP, CCOT, LWCOT, ICOT ICEPR LWCER CIWP CLWP and AOD from both the Aqua and Terra satellites has been used for the period from 2003 to 2015 at $1^\circ \times 1^\circ$ grid resolution. The dates of the onset of summer monsoon over GWB have been collected from the India Meteorological Department (IMD).

For the present study we have taken three categories of monsoon onset over GWB that is early onset, normal onset and delayed onset. According to IMD the normal date of onset of summer monsoon over GWB is 10th June (considering 8 days standard deviation in this study). Using the above criteria the monsoon onset dates over GWB are divided into three categories normal, delayed and early onset of summer monsoon. Then we have categorized the onset phase into three Sub phases, viz. pre-onset, onset and post-onset periods in each annual cycle. The onset period is considered as 2 days before and 2 days after the reported date of onset (5 days). Pre-onset and post-onset periods are considered respectively for 5 days before and 5 days after the onset period. For the analysis we have examined the spatial variation of CTT, CTP, CCOT, LWCTT, ICOT ICEPR LWCER CIWP CLWP and AOD. The types of cloud found during the period from pre-onset to post-onset are also studied. The clouds are classified following the ISCCP's cloud classification, clouds are grouped into three major types, namely, high clouds with $CTP < 440$ hPa, middle clouds with $440 \text{ hPa} < CTP < 680$ hPa and low clouds with $CTP > 680$ hPa.

RESULTS AND DISCUSSION

The spatial variation of the cloud parameters and AOD over GWB during pre-onset, onset and post-onset period for early onset, normal onset and delayed onset year has been studied. Figures 1 (a), (b) and (c) shows the spatial variation of ice cloud water path for the pre-onset, onset and post onset period in the early, normal and delayed onset years over GWB respectively. In the pre-onset period the CIWP shows maximum value in the interior parts of GWB for early years while for normal onset years the value of CIWP is lower than the early onset year and for delayed year the value is minimum in the interior parts but more in the coastal regions. In the onset period the CIWP shows the maximum value for the delayed onset year and minimum value of ice water path is observed for normal onset years. In the post-onset period the value CIWP is more for normal years and least for the early onset years. The CLWP for early year and normal onset for the pre-onset period is low as compared to the delayed onset years. In the onset period the early onset years shows the maximum CLWP values while the normal onset years has the minimum value. In the post-onset period the CLWP is minimum for early onset year when compared to normal and delayed onset year. The CTP for early onset year is highest for the pre-onset period. The CTP is greatest for onset period in the delayed onset year. In the post-onset period the CTP is maximum for the early onset year and for normal onset and delayed onset year shows a similar pattern, minimum in the southern part and increasing as going towards the north. CTP for normal and delayed onset is less than the early onset years. CTT shows similar variation as CTP. The ICEPR shows a maximum value for pre-onset period in the normal years. In the onset period the normal onset years has the least ICEPR among the three cases while in the early onset year the maximum values lies in the southern part. For the post onset period overall ICEPR is less in the early and delayed onset years than normal onset years except at few places.

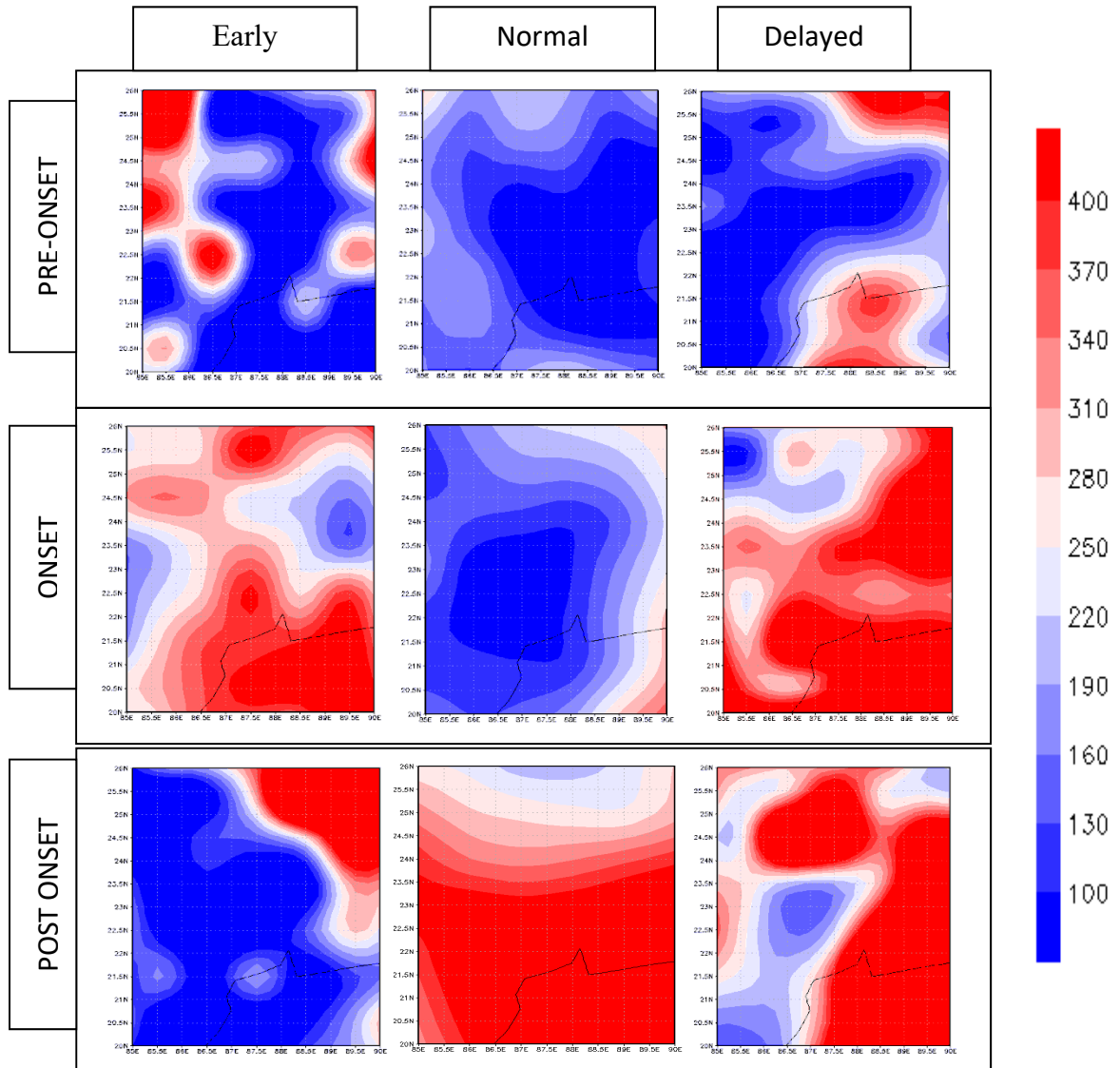


Figure 1 (a), (b) and (c) represents the cloud ice water path (g/m^2) for the pre-onset, onset and post-onset period over GWB respectively.

For the early onset years in the pre-onset period the LWCER is minimum and it is maximum for delayed onset year. In the onset period the early onset year has maximum value while the normal and delayed onset year has almost similar values in most of the regions. In the post-onset period the LWCER for early onset year is minimum and both normal and delayed onset years has maximum value in the southern part and minimum in the northern part. The pre-onset period in the early onset year has more ICOT. For the onset period, the delayed onset year has the maximum value in the southern and northern part. For delayed onset year the maximum ICOT is found in the northern part and minimum in the southern part. The onset period of delayed year has the maximum ICOT. LWCOT in the early pre-onset period the maximum value is observed for delayed onset year. In the onset period the early onset year has the maximum value. In the post-onset period the early onset year has the minimum values and delayed onset year has the maximum value in most of the regions. In the pre-onset period the CCOT is low in all the three cases. For the onset period the delayed onset year has maximum optical thickness in the southern part and CCOT is minimum for normal onset year. For the post onset period the minimum CCOT is observed for early onset year and for normal and delayed onset year maximum CCOT is observed in the southern GWB. The AOD for the pre-

onset period in the early onset year is lowest in the southernmost part. For the post-onset period in the early onset year minimum AOD is found in the western part and increases gradually moving towards the west. For the normal onset year the aerosol concentration is more in the southern side and less as moving towards the north. For the delayed onset year there was no data available.

SUMMARY AND CONCLUSION

During the pre-onset period the CIWP, CTT, CTP, ICEPR shows maximum value for early onset year. Generally the value is higher in the northern parts. The CTT and CTP is more for normal onset year as compared to delayed onset year while for other parameters no definite pattern is observed in the pre-onset period for example ICEPR is maximum in pre-onset period for normal onset years while AOD is more for delayed onset year in the pre-onset period. In the onset period delayed onset year experiences more values of CIWP, CTP, and CTT than early and normal onset except CLWP which has maximum value for early onset year. Overall the normal onset year has minimum values for all the parameters around the central part for all the parameters except for AOD which is lowest for early onset year and more for normal onset years. The values of most of the parameters are more in the northern part except for ICOT and CCOT which is more in the southern part. For the post-onset period the studied cloud parameters show minimum value for early onset year except for CTP and CTP. The variability in the cloud properties on the onset day displays an interesting pattern. The LWCOT, ICOT, CCOT, ICEPR, ICWP and CLWP has the highest value during the early onset year and minimum values of these parameters are observed for normal onset years while for delayed onset year intermediate values are observed. The CTT, and CTP has minimum value for early and maximum value for delayed with intermediate values for normal onset year. The LWCER has again highest value for early onset year but minimum value is observed for delayed onset year. The type of cloud during the whole period is also studied. For delayed and normal onset years mostly high clouds are observed in the GWB region during the onset while for early onset year mostly medium clouds exist in the region. The amount of low cloud is minimum for early and normal onset and no low cloud is observed for delayed onset year. Clouds are generally formed by upward atmospheric motions that cool the air and characteristics of these motions with different dynamical modes produces different types of clouds. So it is important to study and understand how the different atmospheric circulation affects the cloud properties and vertical structure of the clouds also needs to be examined to seek correlation between the cloud parameters and atmospheric features and find what leads to variability in the cloud properties during different cases of onset.

REFERENCES

- Alam, K., J. Iqbal, T. Blaschke, S. Qureshi and G. Khan. (2010). Monitoring Spatio-temporal Variations in Aerosols and Aerosol Cloud Interaction over Pakistan Using MODIS Data. *Adv. Space Res.* 46: 1162–1176.
- G. Balakrishnaiah, K. R. Kumar, B. S. K. Reddy, K. R. Gopal, R. R. Reddy, L. S. S. Reddy and S. S. Babu (2012). Spatio-temporal Variations in Aerosol Optical and Cloud Parameters over Southern India Retrieved from MODIS Satellite Data. *Atmos. Environ.* 47: 435–445.
- Mondal P, S. Chaudhuri, J. Pal, F. Khan, A. Roy Chowdhury, I. Sarkar (2017). Variability in the onset of summer monsoon over Gangetic West Bengal, India: An investigation with climatology of tropopause characteristics, *International Journal of Climatology (JOC)*, DOI: 10.1002/joc.5012 .
- Dutkiewicz, V. A., S. Alvi, B. M. Ghauri, M. I. Choudhary, L. Husain (2009). Black carbon aerosols in urban air in South Asia. *Atmos. Environ.* 43: 1737–1744.

GROUND BASED AND SPACE BORNE LIDAR REMOTE SENSING OF THE INTENSE FOREST FIRE AT SESHACHALA FOREST RANGE DURING MARCH 2014: A CASE STUDY

M. ROJARAMAN¹, P. PRASAD¹, M.VENKAT RATNAM², V. RAVIKIRAN, WEI NAI CHEN³
AND S. VIJYA BHASKARA RAO¹

¹Department of Physics, Sri Venkateswara University,
Tirupati – 517 502, India.

²National Atmospheric Research Laboratory, Dept. of Space, Gadanki, Tirupati – 517 502, India.

³Research Centre for Environmental Changes, Academia Sinica, Taipei-115, Taiwan.

KEYWORDS: Forest fires, Lidar remote sensing, MODIS fire, Black carbon.

INTRODUCTION

Aerosols produced by natural disasters like forest fires, dust storms and volcanic eruptions may cause severe air pollution and hence degrade the visibility of the atmosphere and adversely affect the human health (Kaufman *et al.*, 1998; Li, 1998). According to Forest Survey of India (FSI) 2017 assessment, about 21.54% of the geographic area of the country is covered with Forests. In India, January-June is considered as the fire period and during this period North eastern states are known for the highest number of fire detections. When these fires are out of control, they destroy millions of hectares depending on prevailing weather conditions and produce more black carbon than the anthropogenic sources. Early identification of forest fires using suitable techniques is necessary to control the damage caused by fires. Aerosols generated from biomass burning are mainly composed of organic carbon and black carbon, which causes significant impact on cloud process, and biological process by scattering (direct effect) and absorbing (indirect effect) the incoming solar radiation (Allen *et al.*, 2004) thereby modulate the radiative properties of the earth's climate system. Therefore, the investigation of the dispersion and optical properties of smoke aerosols generated from forest fires has got great attention (Fiebig *et al.*, 2002). As the average lifetime of emitted BC particles in the atmosphere is of about one-week (Bond *et al.*, 2013), satellite borne techniques are less efficient in monitoring the evolution and transport of fire plumes which requires high temporal resolutions. The ground based Lidars are being effectively used to monitor the small smoke plumes including their transport and dispersion caused by forest fires with high sensitivity and good spatial resolution (Amaridis *et al.*, 2008; O'Neill *et al.*, 2008; Pershin *et al.*, 1999). Further, numerical modelling was implemented by Vilar & Lavrov (1999, 2000) to increase the detection efficiency of forest fires and give early warnings. The present study, reports the observation of the intense forest fire plumes noticed using single wavelength Nd:YAG Micro Pulse Lidar (MPL) at S. V. University, Tirupati during historic fire event over Seshachala forest range (13.7°N, 79.35°E), India in March, 2014.

METHODS

An eye safe, compact, diode pumped Micro Pulse Lidar (MPL) for profiling atmospheric aerosol and cloud scattering has been operational at S.V. University, Tirupati (13.6° N, 79.4°E), 182m above mean sea level (amsl) since August 2013. The geographical location of S. V. University, Tirupati, is shown in Fig.1a. The fire event happened at Tirumala up hills which is at about 8km areal distance from the observation site.

The MPL has been operated daily during 1900 to 2100 hrs local time under clear sky condition only. The lidar backscatter signals are recorded with 1 minute integration and with 30m vertical resolution. Data during dense cloud conditions are avoided by visual observations. The quality checked range corrected signals are averaged for 15min intervals to improve the signal detectability and then used to derive the aerosol backscatter and extinction profiles are estimated following Fernald inversion method (Fernald,

1984). The MPL observations during 14-28 March, 2014 has been utilized for the present study. Further the total attenuated backscatter and the aerosol sub-type obtained from the space borne lidar (CALIPSO) overpass on 25 March 2014 over the fire region is considered. In addition, daily MODIS fire counts over this region are taken to understand the intensity of the forest fire.

RESULTS & DISCUSSIONS

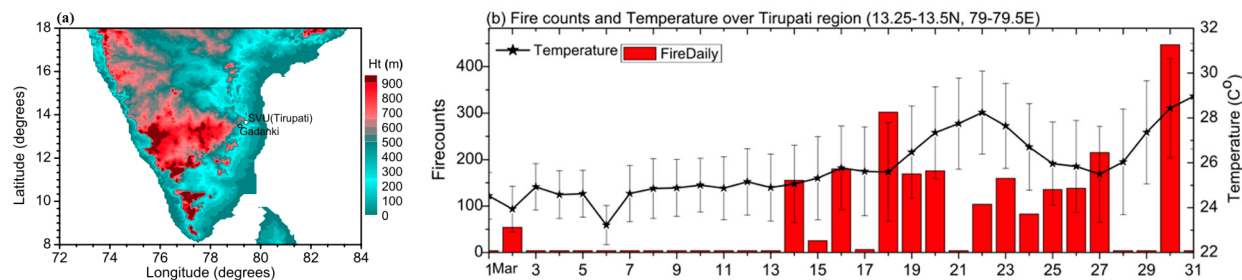


Figure 1. (a) Geographic location of observation site SVU, Tirupati and NARL, Gadanki. (b) MODIS estimated daily fire counts over Seshachala hill range during March 2014. ERA-interim daily mean surface temperature (black line) is also shown. Error bars indicate standard error.

As reported by NASA web portal and as evidenced from Fig.1b, the forest fire started on 14 March and intensified on 18 March. Due to the intense fire, the surface air temperature over this region was increased (Fig.1b, black line). The buoyancy forces caused due to large amount of heating on surface leads to generation of plumes in the lower atmosphere around 2-3 kilometres (Banta *et al.*, 1992). Possibly the elevated forest fire plumes spread over the lidar site during these events. As a result, a thin smoke plume at 3km altitude is observed in MPL signals on 18 March and the depth of the plume intensified further (Fig. 2). Note that due to the presence of clouds, the lidar observations are not available during 15-17 and on 23 March. These fires were extinguished on 20 March, however the higher concentrations of aerosols up to 3km shows the presence of smoke residues in the local environment. Further, the fire raged again on 22 March and generated 3.5km deep intense aerosol concentration. The fire continued till the end of the month in several spans and then subsided. Note that though the fire count is relatively less on 22 March compared to other days, the aerosol concentration is much higher and deeper. This might be due to the mixing of the fire smoke aerosols with the long range transported smoke or other aerosol types. This can only be verified with the simultaneous satellite observations covering the surrounding regions centered with observation site.

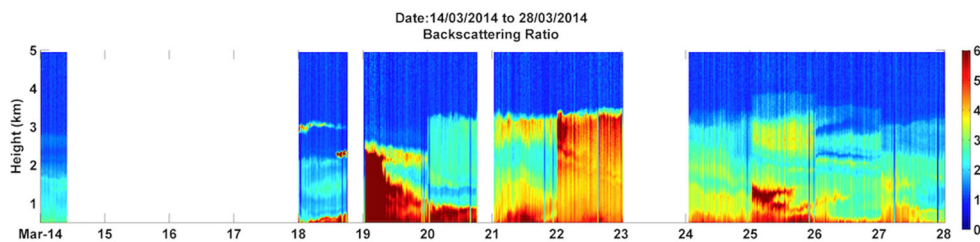


Figure 2. Nocturnal observations of Lidar back scatter at SVU showing the fire smoke plumes during 14 March – 28 March, 2014. Note that as there are no day time observations, all nocturnal observations are stitched together to show continuous variation.

The total attenuated backscatter observed with the space borne lidar (CALIPSO) overpass on 25 March confirms the presence of higher concentration of aerosols up to about 4km over the observation site. In addition to that, one can notice the deep layer of higher aerosol concentration present along the CALIPSO path in the North-East (NE) direction (Fig. 3a). Further, the aerosol subtype shown in Fig. 3b confirms the presence of smoke aerosols spread deep in the lower troposphere as observed with the MPL observations (Fig.2). Interestingly, the deep layers of smoke aerosols are spread along the CALIPSO path in the NE direction. As the background wind flows from NE during this season, the lidar observed deep layers of smoke aerosols might be mixture of forest fire smoke and long-range transport smoke aerosols.

Further, the particle dispersion from the fire location is estimated using NOAA Hysplit model for the day initialized on 0000UTC of 24 March and it is interesting to see the particles emitted from fire were elevated up to 4km in the surrounding regions (Fig.3c) and advected along the wind to few tens of kilometres in the North West direction and then dissipated to the lower levels. These smoke plumes spread to the surrounding locations might affect the local air quality.

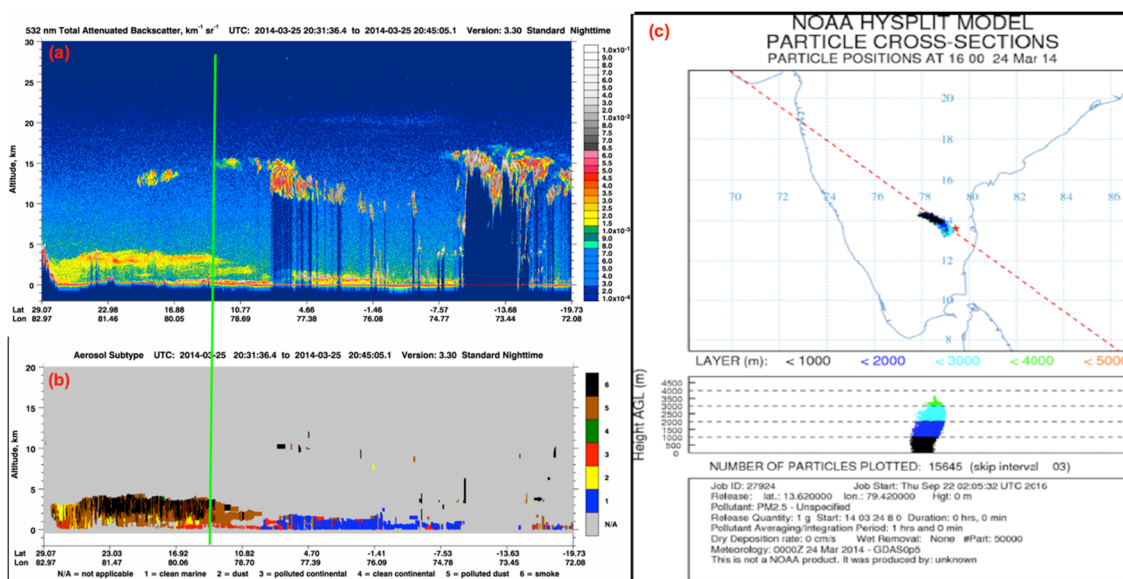


Figure 3: CALIPSO observed (a) Total attenuated back scatter and (b) aerosol subtype showing the dense smoke plumes on 25 March 2014 over the observation site. Green line shows the location of SVU lidar observations. (c) NOAA Hysplit particle dispersion from the fire location observed on 24 March 2014.

CONCLUSIONS

In this study, the intense forest fire raged in March, 2014 over Seshachala forest range (13.7°N, 79.35°E) in the South-eastern India that lasted for several days devastating rare species of flora and fauna in around two thousand hectares of forest land has been analysed using the Micro Pulse Lidar (MPL) observations made at S. V. University, Tirupati located at the foot hills of the forest range. An intense thin smoke plume has been observed on 18 March at 3 km altitude in the lidar back scatter signal on the day when wide spread fire was identified. These fires have been extinguished on 20 March and again the fire raged on 22 March. About 3.5km deep layer of intense lidar back scatter is noticed on 22 March after which it continued till 27 March. The spaceborne lidar (CALIPSO) overpass during fire clearly shows the elevated smoke aerosols around this region. In addition, the ground based in-situ observations of aerosol physical and optical properties and the Black Carbon (BC) concentrations measured at nearby station NARL, Gadanki (13.5°N, 79.2°E) is combined to investigate the environmental impact of this forest fire. MODIS observed active fire counts show significant enhancement during this event coinciding with the lidar observations. The back-ground wind circulation in the lower troposphere has been analysed using the high-

resolution GPS based radiosonde data available at NARL during the fire event to understand the dispersion of the fire smoke and possibility of long range transported dust/smoke toward observation site.

ACKNOWLEDGEMENTS

Authors are thankful to University Grants Commission for providing financial support to procure the MPL used in this study. One of the author M. R. Raman is thankful to UGC for providing RC position in CPEPA program.

REFERENCES

Allen, A. G., A. A. Cardoso, and G. O. da Rocha (2004). Influence of sugar cane burning on aerosol soluble ion composition in South eastern Brazil. *Atmospheric Environment*, 38, 5025–5038.

Amiridis, V., Balis, D. S., Giannakaki, E., Stohl, A., Kazadzis, S., Koukouli, M. E., and Zanis, P.: Optical characteristics of biomass burning aerosols over Southeastern Europe determined from UV Raman lidar measurements, *Atmos. Chem. Phys.*, 9, 2431–2440, doi:10.5194/acp-9-2431-2009, 2009.

Banta, R. M., L. D. Oliver, E. T. Holloway, R. A. Kropfli, B. W. Bartram, R. E. Cupp, and M. J. Post (1992). Smoke-column observations from two forest fires using Doppler lidar and Doppler radar, *J. Appl. Meteorol.* 31 No. (11), 1328–1349.

Fiebig, M., A. Petzold, U. Wandinger, M. Wendisch, C. Kiemle, A. Stifter, M. Ebert, T. Rother, and U. Leiterer (2002). Optical closure for an aerosol column: Method, accuracy, and inferable properties, applied to a biomass-burning aerosol and its radiative forcing. *J. Geophys. Res.*, 107, 8130, doi:10.1029/2000JD000192.

FSI, State of the Forest Report, Forest Survey of India, Ministry of Environment and Forests, GoI, 2017.

Kaufman, Y. J., P.V. Hobbs, V.W.J.H. Kirchhoff et al. (1998). Smoke, Clouds, and Radiation-Brazil (SCAR-B) experiment. *J. Geophys. Res.*, 103, no.24, 31783–31808.

Z. Li (1998). Influence of absorbing aerosols on the inference of solar surface radiation budget and cloud absorption. *J. Climate*, 11, 5–17.

O'Neill, N. T., O. Pancrati, K. Baibakov, E. Eloranta, R. L. Batchelor, J. Freemantle, L. J. B. McArthur, K. Strong, and R. Lindenmaier (2008). Occurrence of weak, sub-micron, tropospheric aerosol events at high Arctic latitudes, *Geophys. Res. Lett.*, 35, L14814, doi:10.1029/2008GL033733.

Pershin, S., W.M. Hao, R.A. Susott, R.E. Babbitt, and A. Riebau (1999). Estimation of Emission from Idaho Biomass Fires Using Compact Eye-Safe Diode Lidar. In Proc. SPIE, 3757, 60-66.

Reid, J. S., P. V. Hobbs, R. J. Ferek et al., (1998). Physical, chemical, and optical properties of regional hazes dominated by smoke in Brazil, *J. Geophys. Res.*, 103, no. 24, JD00458, 32059–32080.

Vilar, R., and A. Lavrov (2000). Estimation of Required Parameters for Detection of Small Smoke Plumes by Lidar at 1.54 μm . *Appl. Phys. B* 71, 225-228.

LONG-TERM CLIMATOLOGY OF AEROSOLS OVER TIRUPATI: A STUDY USING SATELLITE AND MODEL SIMULATIONS

K. VIJAYAKUMAR^{1*}, P.P. LEENA², S. VIJAYA BHASKARA RAO¹,
P.C.S. DEVARA³ AND C.K. JAYASANKAR¹

¹Department of Physics, Sri Venkateswara University (SVU), Tirupati – 517 502, India.

²Physics and Dynamics of Tropical Clouds, Indian Institute of Tropical Meteorology (IITM),
Dr. Homi Bhabha Road, Pune – 411 008, India.

³Amity Centre for Ocean Atmospheric Science and Technology & Amity Centre for Environmental
Science and Health, Amity University Haryana (AUH), Gurgaon – 122 413, India.

(*CORRESPONDENCE TO: KVKSUVU@GMAIL.COM)

KEYWORDS: Aod, angstrom exponent, type of aerosols, satellite data.

INTRODUCTION

Aerosols play an important role in atmospheric mechanisms relevant to climate change. They have a large impact on the radiative balance of the Earth through the scattering and absorption of incoming sunlight and cloud formation (Ramanathan *et al.*, 2001; Pöschl, 2005). Generally, aerosols are dominant in the troposphere. The lifetime of aerosols varies from minutes to days in the troposphere, due to the prevailing precipitation and interactions with the Earth's surface, depending on aerosol size and chemistry and the height of the atmosphere. Regional distributions of aerosols, their inter-annual variability and detailed descriptions of spectral aerosol optical properties are needed to understand the influences of aerosols on the climate of the region (Vijayakumar and Devara, 2013). These local and regional studies are fundamental in filling these gaps and supporting future global analysis. In this study, for the first the time, we used long-term combined data sets of satellite and model simulations over the study region.

STUDY SITE

Tirupati, a holy pilgrimage town for devotees of Lord Sri Venkateswara, is situated in Chittoor district of southern Andhra Pradesh State in India at an altitude of 182.9 m (13.05°N latitude; 79.05°E longitude). Tirupati, as a study site, represents an urban area surrounded by major industrial and agricultural activities. The town owes its existence to the sacred temple of Lord Sri Venkateswara situated on the seven hills (Tirumala) adjoining it. This town is a high-profile centre for education, tourism (mainly due to pilgrimage) and specialties in health and medical facilities attracting migrant population. This make it the ninth most populous city in the State. Industrial activities and concentration of air pollutants due to petrol and diesel operated vehicles contribute to ambient air quality of Tirupati. The long-range transport of pollutants also can influence the air quality. Thus, it becomes essential to investigate the long-term climatology of aerosols over Tirupati using satellite and model simulations from 2003 to 2017 in the present case.

DATA AND METHODOLOGY

MODIS

The Aerosol Optical Depth (AOD) data (at 550nm) and Angstrom Exponent (AE) (at 412-470nm) used for analysis in the present study are a part of MODIS Terra (MOD08_D3) and Aqua (MYD08_D3) level-3, 1°×1° Collection 6.1 daily gridded atmospheric data product and are acquired from the website <https://giovanni.gsfc.nasa.gov/giovanni/>. The first MODIS instrument was launched onboard the Terra satellite on 18 December 1999, with daytime equator crossing at 1030 LT, as part of the NASA's Earth Observing System (EOS) mission and the second one on 4 May 2002 onboard the Aqua platform with

daytime equator crossing at 1330 LT. The MODIS_L3 AOD product was created by averaging the available retrievals from the MODIS_L2 AOD product at every $1^{\circ} \times 1^{\circ}$ latitude/longitude grid.

ECMWF

The ECMWF models provide high-resolution global weather forecasts up to 10 days; Ensemble Prediction System forecasts up to 30 days; and seasonal forecast for 12 months ahead. This model has developed a reanalysis of global atmospheric composition since 2003, which includes the five main tropospheric aerosol species such as sea salt (SS), desert dust (DD), organic carbon (OC), black carbon (BC), and sulphate (SO_4) aerosols, which are advected by the model dynamics and interact with the model physics. In this study, the above parameters from 2004 to 2017 over Tirupati region are used.

RESULTS & DISCUSSION

AOD is representative of the aerosol loading in the atmospheric column, while AE gives useful information for the aerosol size and constitutes an important parameter for aerosol-type identification. The temporal variability of the monthly-averaged (mean of daily values of Terra and Aqua) AOD at 550nm values during the study period is shown in Figure 1. The results attest to the high variability of AOD, with most values ranging between 0.10 and 0.35, and several peaks higher than 0.45. For example, the time pattern during 2016 exhibited a value of AOD greater than 0.45 during the month of June and with AOD close to 0.57, which is the highest value measured during the overall period. Winter was the period that presents the lowest turbidity conditions, being characterized by values of AOD (550nm) of around 0.21, which can be assumed as the background value for the urban area of Tirupati. The climatology of AOD shows 5.58% of aerosol increase per year, and the statistical significance of AOD is 99.9%.

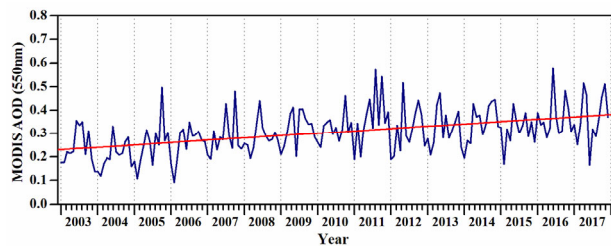


Figure 1. Long-term climatology of AOD and AE observations from MODIS satellite.

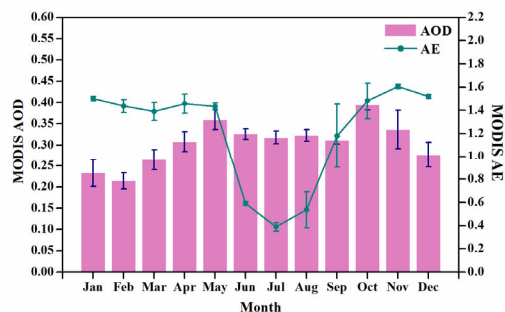


Figure 2. Month-to-month variation of AOD and AE.

Figure 2 shows month-to-month variation of AOD and AE. The high variability in both AOD and AE indicates a variety of aerosol types over the region due to transported airmasses of different origin and characteristics. There is a clear differentiation between the high and low AE values since the high values are found during the November–January period (fine-mode aerosols), while the AE exhibits low from June to August (coarse-mode aerosols). Figure 2 also reveals that the larger month-to-month variability in both AOD and AE from June to August, indicating significant changes in air-mass origin and characteristics, while the much lower variability from November to January indicates more stable atmospheric conditions and aerosol characteristics. However, cases associated with high AOD and AE may also exist during October month corresponding to increase the anthropogenic pollution plumes due to the annual Brahmotsavam. During this period, most of the pilgrims travelled by buses, two- and four- wheeled vehicles etc. For example; in 2016, it was reported that 27.3 million pilgrims visited the temple, which may have influenced the hygroscopic growth of aerosols during these months, resulting in larger particles and higher AODs.

The lowest AE values during June–August indicate a clear dominance of coarse-mode aerosols i.e., the influence of the south-westerly winds blowing in from the Arabian Sea (Vijayakumar *et al.*, 2012) or mixing of dust with marine aerosols produced by the strong sea-surface monsoon winds over the Arabian Sea (Vijayakumar *et al.*, 2014). The highest AE values during November–January reveal a rather mixing of fine with coarse mode aerosols resulting in a bimodal size distribution with equal contribution from fine and coarse particles (Bhawar and Devara, 2010). During the whole period, the mean values of AOD and AE were found to be 0.31 ± 0.05 and 1.22 ± 0.44 , respectively.

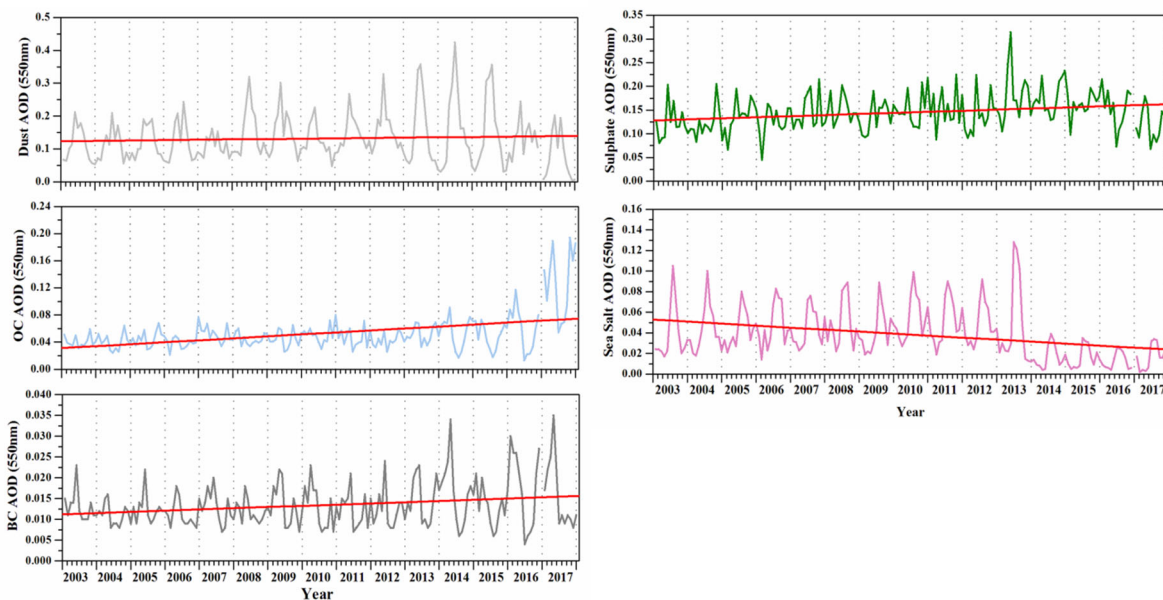


Figure 3. Long-term variation of different AODs like Dust AOD, OC AOD, BC AOD, Sulphate AOD, and Sea Salt AOD data sets from ECMWF model simulations.

The long-term variation of different types of aerosols clearly shows (Figure 3), the dust AOD shows little bit slightly variation (0.96% per year increasing); but the OC, BC, and Sulphate AODs clearly shows increasing trend due to long-range transport of dust and biomass burning due to uncertainties in the emissions inventory. The OC, BC and Sulphate AODs clearly shows 12.35%, 2.42% and 2.06% per year increasing. But the Sea salt AOD shows decreasing trend (4.12% per year) from 2003 to 2017, resulting decreasing of rainfall (1.45% per year) over this region (Figure 5), and the correlation of Sea salt AOD and rainfall is 0.20. The statistical significance of Dust AOD is 60%; while OC, BC, Sulphate and Sea salt AODs is 99.9%, 99.9%, 99% and 99% for Tirupati during 2003 to 2017. Figure 4 shows percentage of different type AODs over this region. Throughout the entire study period, sulphate optical depth accounts for the largest fraction of the total optical depth at 38.06% of the average annual aerosol with highest levels during May. The main source of sulphate aerosol is via SO₂ emissions from fossil fuel burning, and with a small contribution from biomass burning. At current production levels, the concentration of human-made sulphate aerosols are outweigh the naturally produced sulphate aerosols. Dust optical depth (which includes coarse and fine dust), contributes the next highest fraction with an annual average of 34.54% with little variability through the year. Black carbon, organic carbon, and sea salt aerosols are responsible for a relatively small fraction of the total AOD at 3.52%, 13.85% and 10.03%, respectively.

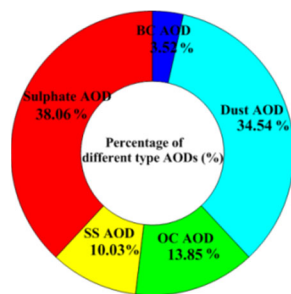


Figure 4. Doughnut diagram of percentage of different type AODs over Tirupati region.

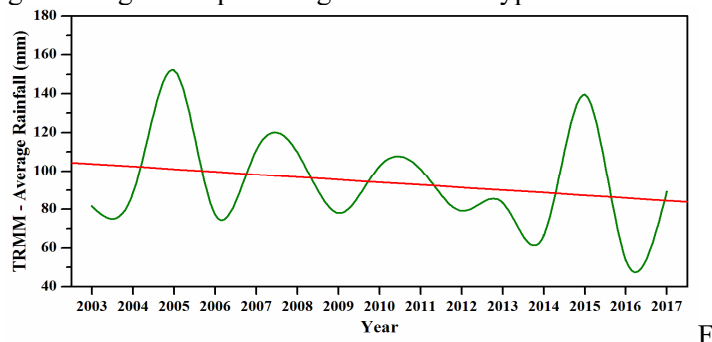


Figure 5. Long-term variation of average rainfall (mm), observed from TRMM satellite.

CONCLUSIONS

In conclusion, the urbanization and increased anthropogenic activities have contributed particulates load into the atmosphere over Tirupati. The highlights of the study indicated the following:

- (i) The climatology of AOD shows 5.58% increase of aerosols per year, (ii) Larger month-to-month variability in both AOD and AE exists from June to August, indicating significant changes in air-mass origin and characteristics, while the much lower variability from November to January indicates more stable atmospheric conditions and aerosol characteristics, (iii) The climatology of different types of AODs i.e., Dust, BC, OC, Sulphate clearly shows increasing trend, (iv) The Sea salt AOD shows decreasing trend (4.12% per year) from 2003 to 2017, resulting decreasing of rainfall (1.45% per year) over the region, (v) Sulphate AODs dominate other types of AODs.

ACKNOWLEDGEMENTS

The authors are grateful to the authorities at Sri Venkateswara University (SVU), Tirupati, Indian Institute of Tropical Meteorology (IITM), Pune and Amity University Haryana (AUH), Gurgaon (Manesar-Panchgaon). One of the authors, K. Vijayakumar gratefully acknowledges Council of Scientific and Industrial Research (CSIR), Government of India, New Delhi for providing the Research Associate (RA) Fellowship. We would like to thank the MODIS, ECMWF Science Team for providing excellent E-data products that made this study possible.

REFERENCES

Bhawar, R.L. and P.C.S. Devara (2010). Study of successive contrasting monsoons (2001–2002) in terms of aerosol variability over a tropical station Pune, India, *Atmos. Chem. Phys.*, **10**, 29.

Pöschl, U. (2005). Atmospheric aerosols: Composition, transformation, climate and health effects, *Angew. Chem. Int. Ed.*, **44**, 7520, doi:10.1002/anie.200501122.

Ramanathan, V., P.J. Crutzen, J.T. Kiehl and D. Rosenfeld (2001). Aerosols, climate, and the hydrological cycle, *Science* **294**, 2119, doi:10.1126/science.1064034.

Vijayakumar, K., P.C.S. Devara and C.P. Simha (2012). Aerosol features during drought and normal monsoon years: A study undertaken with multi-platform measurements over a tropical urban Site, *Aerosol and Air Qua. Res.*, **12**, 1444.

Vijayakumar, K. and P.C.S. Devara (2013). Study of aerosol optical depth, ozone, and precipitable water vapour content over Sinhad, a high-altitude station in the Western Ghats, *Int. J. Remote Sens.*, **34**, 613.

Vijayakumar, K., P.C.S. Devara and S.M. Sonbawne (2014). Type-segregated aerosol effects on regional monsoon activity: A study using ground-based experiments and model simulations, *Atmos. Environ.*, **99**, 650.

ONE-DECADE PRE-MONSOON AND POST-MONSOON TRENDS OF AEROSOL OPTICAL DEPTH IN RELATION TO METEOROLOGICAL PARAMETERS OVER INDIAN SUBCONTINENT

¹G.BARIK, ¹P.ACHARYA

¹Department of Geography and Environment Management, Vidyasagar University, Midnapore, West Bengal- [721102](#)

KEYWORDS: AOD, Anomaly, MODIS, MISR, IMD, Mann Kendal Tau

INTRODUCTION

Aerosol is a crucial factor in global climate diagnostic and become a major uncertainty in global climate simulation. AOD is a measure of the aerosol column concentration, of the vertical integral through the entire height of the atmosphere of the fraction of incident light either scattered or absorbed by aerosol particles (Chin Kahn., 2009). The source of aerosols and their optical, physio-chemical properties, transformation and atmospheric residence time vary with spatio-temporal scale based on seasonal meteorological conditions. Indian Meteorological Department (IMD) reported that over the last two decades there has been a 14.8% decrease in average pre-monsoon rainfall, whereas a 6.4% decrement occurred in the average monsoon rainfall.

METHODS

In this study, we analysed one-decade (2007 to 2016) of pre-monsoon and post-monsoon aerosol optical depth (AOD) trends (distribution, anomaly and regression slope) over Indian subcontinent using Moderate Resolution Imaging Spectroradiometer (MODIS) derived level-3 monthly aerosol product. The monthly data from Multi-angle Imaging Spectroradiometer (MISR) was also used in this duration to compare the results. IMD gridded rainfall (0.25° resolution) and temperature (1° resolution) products were used to represent the linear relationship with AOD. AOD was analysed for the month of pre-monsoon (March, April and May) and post-monsoon season (October and November). Mann-Kendall trend test (MK-test) was used to extract the long term spatio-temporal trend. The space-time variation of AOD anomaly was also computed followed by its relationship with rainfall and temperature anomaly.

RESULTS & DISCUSSIONS

The results in both the seasons show a high concentration of AOD (~ 0.7) in Gangetic basin. The year wise anomaly in AOD concentration during pre-monsoon and post monsoon months shows no definite spatial pattern over the year. However, the MK-test for the months in these season shows an increasing trend for southern and eastern India, whereas, central and north-west India experience a decreasing trend. The results of the linear regression in pre-monsoon and post-monsoon months show a decrease of AOD predominantly in all over India with increase of rainfall ($\beta \sim -0.25$ to -0.5). The relationship with temperature, however, shows an overall increase of AOD with increase of temperature in pre-monsoon months ($\beta \sim 0.05$ to 0.2). During post-monsoon months, the spatial clusters of increase of AOD with a β coefficient of 0.05 to 0.25 are observed in northern plains and southern India.

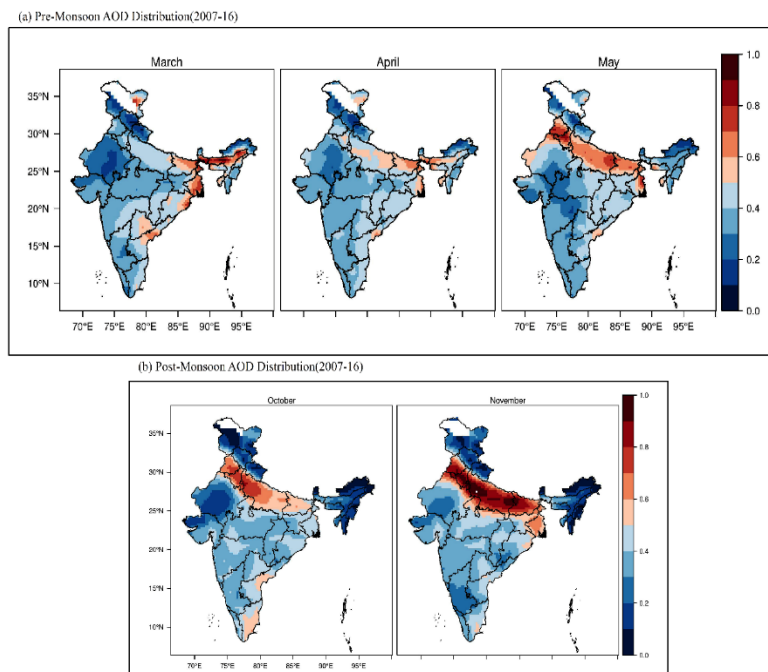


Figure 1. Pre-Monsoon and Post-Monsoon AOD distribution (2007-16). (a) March, April and May average AOD distribution. (b) October and November average AOD distribution.

CONCLUSIONS

Although, rainfall and temperature are the two major meteorological parameters in controlling AOD concentration and anomaly distribution but diverse physiographic conditions, different climatic region, heterogeneity of spatial anthropogenic activities etc are important in causing spatio-temporal variability of AOD.

ACKNOWLEDGEMENT

This work was supported by the UGC fellowship and our Departmental help.

REFERENCES

- Acharya, P. and Sreekesh, S. (2013) 'Seasonal variability in aerosol optical depth over India: A spatio-temporal analysis using the MODIS aerosol product', *International Journal of Remote Sensing*. Taylor & Francis, 34(13), pp. 4832–4849. doi: 10.1080/01431161.2013.782114.
- Ali, M. A. *et al.* (2015) 'MODIS Dark Target and Deep Blue aerosol optical depth validation over Bangladesh', *Malaysian Journal of Society and Space*, 11(11), pp. 74–83.
- Chin Kahn, R. A., Remer, L. A., Yu, H., Rind, D., Feingold, G., Quinn, P. K., Schwartz, S.E., Streets, D. G., Decola, P., and Halthore, R., M. (2009) 'Atmospheric Aerosol Properties and Climate Impacts', (January).
- Gopal, K. R. *et al.* (2016) 'Regional trends of aerosol optical depth and their impact on cloud properties over Southern India using MODIS data', *Journal of Atmospheric and Solar-Terrestrial Physics*. Elsevier, 146(February), pp. 38–48. doi: 10.1016/j.jastp.2016.05.005.
- Guo, J. *et al.* (2014) 'Trend analysis of the aerosol optical depth from fusion of MISR and MODIS retrievals over China', *IOP Conference Series: Earth and Environmental Science*, 17(1). doi:

10.1088/1755-1315/17/1/012036.

Makokha, J. W., Odhiambo, J. O. and Godfrey, J. S. (2017) 'Trend Analysis of Aerosol Optical Depth and τ_{246m} Exponent Anomaly over East Africa', *Atmospheric and Climate Sciences*, 07(04), pp. 588–603. doi: 10.4236/acs.2017.74043.

Mamun, M. I., Islam, M. and Rasel, A. H. (2014) 'An observational study of aerosol optical properties and their relationships with meteorological parameters over Bangladesh', 2(6), pp. 75–84.

Mehta, M. *et al.* (2016) 'Recent global aerosol optical depth variations and trends - A comparative study using MODIS and MISR level 3 datasets', *Remote Sensing of Environment*. Elsevier Inc., 181, pp. 137–150. doi: 10.1016/j.rse.2016.04.004.

Panicker, A. S. *et al.* (2013) 'Decadal climatological trends of aerosol optical parameters over three different environments in South Korea', *International Journal of Climatology*, 33(8), pp. 1909–1916. doi: 10.1002/joc.3557.

Roy, S. Sen (2008) 'Impact of aerosol optical depth on seasonal temperatures in India: A spatio-temporal analysis', *International Journal of Remote Sensing*, 29(3), pp. 727–740. doi: 10.1080/01431160701352121.

Sano, I. (no date) *Aerosol Remote Sensing*. doi: 10.1007/978-3-642-17725-5.

Shalin, S. and Sanilkumar, K. V. (2013) 'Climatic oscillations in aerosol optical depth over tropical oceanic regions pertaining to genesis of the Indian Ocean Dipole', *International Journal of Remote Sensing*, 34(1), pp. 86–95. doi: 10.1080/01431161.2012.706721.

EFFECT OF AEROSOL CHEMISTRY ON TEMPERATURE PATTERN IN NORTH-WESTERN INDIA DURING RICE AND WHEAT CROP RESIDUE BURNING

P. ACHARYA¹, S SREEKESH², UC KULSHRESTHA³

¹Department of Geography and Environment Management, Vidyasagar University, Midnapore, West Bengal, India

²Centre for the Study of Regional Development, School of Social Science, Jawaharlal Nehru University, New Delhi, India

³School of Environmental Sciences, Jawaharlal Nehru University, New Delhi, India

KEYWORDS: Crop Residue Burning; Particle Chemistry; AOD; Temperature Response; MODIS.

INTRODUCTION

Agricultural residue burning is one of the major sources of air pollution in South/Southeast Asia (Kant et al., 2000; Prasad et al., 2000; Gupta et al., 2001; Badarinath et al., 2006; Lasko and Vadrevu, 2018). Although the emission from vegetation fire and its effect on radiance flux are well studied (Reid et al., 2004; Giglio et al., 2006) the possible effect of crop residue burning on temperature pattern is not investigated at the same scale. Few studies have shown the evidence of lowering of temperature at the peak burning period (Zhang et al., 2016). However, it is quite unclear if the same pattern holds for the Indian sub-continent. Thus, in this study, we focused on the chemistry of the aerosol particles emitted from the rice and wheat residue burning along with its effect on temperature at north-west India.

METHODS

We used APM-821 handy air sampler to collect the sample of the aerosol particles during residue burning. The particles were analysed under scan electron microscopy (SEM) for their size and ion-chromatograph (IC) for their cation and anion composition. The time series moderate resolution imaging spectroradiometer (MODIS) derived aerosol optical depth (AOD) was also used for the period of 2002-2012. The monthly AOD from MODIS and monthly temperature and relative humidity (RH) from IMD stations (Ambala and Hisar) at the neighbouring region of cropland fire were analysed using linear regression to explore their relationship.

RESULTS & DISCUSSIONS

The results show that the median size of the aerosol particles is 1.8 μm ($\sigma = 12.17 \mu\text{m}$). The ionic composition, derived from the chromatographic analysis shows (Table 1) an abundances of metallic cations ($\text{Na}^+ > \text{Ca}^+ > \text{Mg}^+ > \text{K}^+$) and anions of inorganic salt ($\text{Cl}^- > \text{SO}_4^- > \text{F}^-$). The increase of AOD is attributed to these inorganic salts and metallic oxides which are sensitive in visible to infrared region of electromagnetic spectrum. The AOD-temperature relationship shows (Figure 1) a significant decrease in maximum temperature in May (-3.8°C) and October (-3.1°C).

Ions	Mean ($\mu\text{g m}^{-3}$)	Standard Deviation (σ)
Na ⁺	286.83	169.91
K ⁺	19.21	12.54
Ca ⁺	30.56	24.24
Mg ⁺	19.50	17.62
F ⁻	4.75	3.89
Cl ⁻	119.05	81.06
SO ₄ ⁻	18.63	29.51

Table 1. Cation and anion concentrations of aerosol particles derived from the chromatographic analysis.

A significant decrease in minimum temperature is also observed during the peak burning time (-2.9°C in May and -3.1°C in October). The comparison of burning with the pre-burning ambient conditions (March and September) manifests contradictory findings at the pre-burning situations. The maximum and minimum temperatures increase significantly with increasing AOD. Such contradictory results imply changes in atmospheric chemistry that allow alteration of optical property, i.e. increase in single scattering albedo (SSA). The results also reveal that the estimated mean aerosol load in October remains higher as compared to May. However, the estimated decrease in temperature is higher in May. It may happen due to the increased depth of the boundary layer coupled with the high thermal condition.

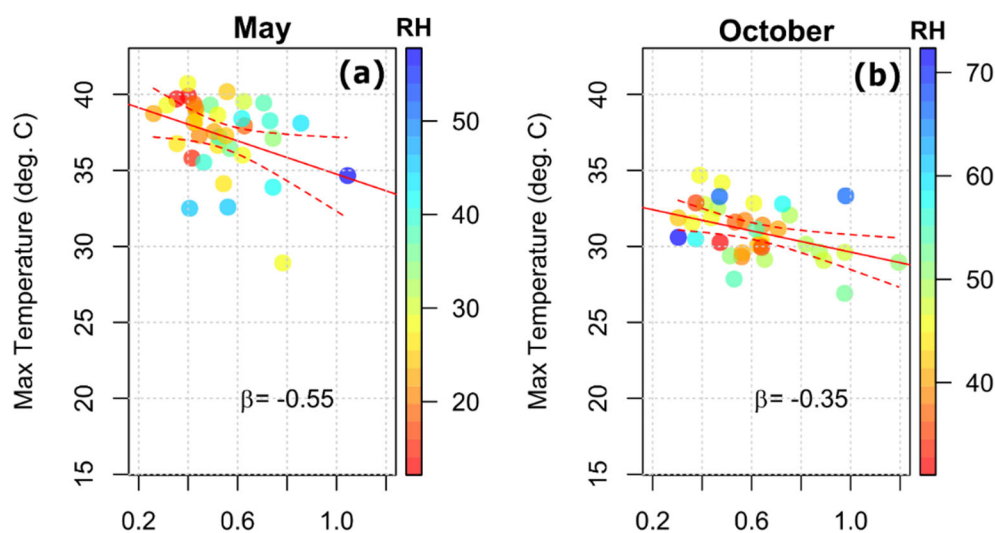


Figure 1. The relationship between AOD and maximum temperature. The x-axis is defining the variation of AOD.

CONCLUSIONS

The analysis suggests that the emission from crop residue burning alters the atmospheric optical behaviour by significantly increasing the SSA. The high proportion of SSA reduces the incoming energy

at the surface that resulted in a lowering of surface temperature. Such low thermal condition leads to boundary layer depth and in turn keeps the pollutant close to the surface which resulted in low visibility in and around the national capital region, New Delhi.

ACKNOWLEDGEMENTS

The work was supported by the CSIR fellowship, GoI.

REFERENCES

- Badarinath, K.V.S., Kiran Chand, T.R. and Krishna Prasad, V. (2006). Agriculture crop residue burning in the Indo-Gangetic Plains - A study using IRS-P6 AWiFS satellite data. *Curr. Sci.* 91: 1085–1089.
- Giglio, L., Csiszar, I. and Justice, C.O. (2006). Global distribution and seasonality of active fires as observed with the Terra and Aqua Moderate Resolution Imaging Spectroradiometer (MODIS) sensors. *J. Geophys. Res. Biogeosciences.* 111: 1–12. doi:10.1029/2005JG000142
- Gupta, P.K., Prasad, V.K., Sharma, C., Sarkar, A.K., Kant, Y., Badarinath, K.V.S. and Mitra, A.P. (2001). CH₄ emissions from biomass burning of shifting cultivation areas of tropical deciduous forests—experimental results from ground-based measurements. *Chemosphere-Global Change Science*, 3(2): 133-143.
- Kant, Yogesh, A. B. Ghosh, M. C. Sharma, Prabhat K. Gupta, V. Krishna Prasad, K. V. S. Badarinath, and Mitra, A. P. (2000). Studies on aerosol optical depth in biomass burning areas using satellite and ground-based observations. *Infrared physics & technology.* 41(1): 21-28.
- Lasko, K. and Vadrevu, K. (2018). Improved rice residue burning emissions estimates: Accounting for practice-specific emission factors in air pollution assessments of Vietnam. *Environ. Pollut.* 236: 795-806.
- Prasad, V.K., Gupta, P.K., Sharma, C., Sarkar, A.K., Kant, Y., Badarinath, K.V.S., Rajagopal, T. and Mitra, A.P. (2000). NO_x emissions from biomass burning of shifting cultivation areas from tropical deciduous forests of India—estimates from ground-based measurements. *Atmos. Environ.* 34(20): 3271-3280.
- Reid, J.S., Eck, T.F., Christopher, S. a., Koppmann, R., Dubovik, O., Eleuterio, D.P., Holben, B.N., Reid, E. a. and Zhang, J. (2004). A review of biomass burning emissions part III: intensive optical properties of biomass burning particles. *Atmos. Chem. Phys. Discuss.* 4: 5201–5260. doi:10.5194/acpd-4-5201-2004
- Zhang, J., Reid, J.S., Christensen, M. and Benedetti, A. (2016). An evaluation of the impact of aerosol particles on weather forecasts from a biomass burning aerosol event over the Midwestern United States: Observational-based analysis of surface temperature. *Atmos. Chem. Phys.* 16: 6475–6494. doi:10.5194/acp-16-6475-2016

SOURCE APPORTIONMENT OF BLACK CARBON OVER AGARTALA IN THE NORTHEASTERN INDIA

PARMINDER KAUR^{1*}, PRASANTH S.¹, PRANAB DHAR¹, BARIN KUMAR DE¹, S. SURESH BABU², M.M. GOGOI², ANIRBAN GUHA^{1*}

¹Department of Physics, Tripura University, Agartala, 799022, Tripura, India

² Space Physical Laboratory, Vikram Sarabhai Space Centre, Thiruvananthapuram, 695002 India

KEYWORDS: Aerosols; Black Carbon; Fossil Fuels; Biomass Burning;

INTRODUCTION

Atmospheric black carbon (BC) aerosol is an important constituent of particulate matter. Black carbon (BC) particles impact Earth's climate and air quality. BC is a graphitic form of carbon particles with unique physical properties. Two main sources of BC particles in the atmosphere are combustion process involving fossil fuel and biomass burning. During biomass burning several other organic materials are emitted which condense over black carbon particles and change their optical properties. In this study we explore difference in optical properties of black carbon particles as a mean to source apportion black carbon particles.

BC emission from India due to fossil fuel, biomass burning and biofuel combustion is a significant fraction of total global emissions (**Shamitaksha Talukdar, Soumyajyoti Jana and Animesh Maitra, 2014**). BC is getting much attention as climate warming agent of comparable strength as anthropogenic CO₂ (**IPCC, 2013**). There is a rapid increase in fuel demand with increases in the daily energy needs for domestic, industrial and transport sectors. This change in fuel utilization has caused a historical change in BC emissions in the past decades.

METHODS

Sampling Site:

The sampling site Agartala (23.76°N and 91.26°E), located in the Northeastern part of India in the state of Tripura. The site is a rural and continental site. The continuous measurement of BC mass concentrations has been carried out at Department of Physics, Tripura University.

Instrumentation:

The contributions of FF and BB emissions to BC have been investigated in the recent past years by analysis of multi-wavelength Aethalometer data. Aethalometer is one of the popular instruments worldwide for measuring black carbon particles. A 7-wavelength Aethalometer (Model: AE-31, Make: Magee Scientific, USA) is used to measure the BC mass concentrations at 370, 470, 520, 590, 660, 880, and 950 nm. Assuming that BC is the only absorbing component in the atmospheric aerosols, a linear relationship of BC mass concentration with the change in attenuation of light is used to determine the BC mass concentration. In this study, the attenuation signal has been integrated for 5 minutes and flow rate was maintained at 3.9 L min⁻¹.

Methodology:

The approach of determining the contribution of BB and FF to BC utilizes the stronger light absorption of BB aerosols in the near ultraviolet compared to the light absorption of aerosols from FF combustion. The contribution of BB and FF to BC was directly determined from the aerosol absorption coefficients (which were calculated by using aerosol light absorption cross-section from Aethalometer) and Angstrom exponents. Here we have presented the results of the present analysis from a rural site in Tripura measured during the year 2011.

RESULTS AND DISCUSSIONS

The monthly mean values of BC mass concentration during year 2011 have been determined and shown in figure 1. BC concentrations are higher during winter months and lower during monsoon months. Maximum BC concentrations were recorded during month of January were $28.6 \pm 5.4 \mu\text{g m}^{-3}$ and minimum during the month of July were $4.07 \pm 2.31 \mu\text{g m}^{-3}$.

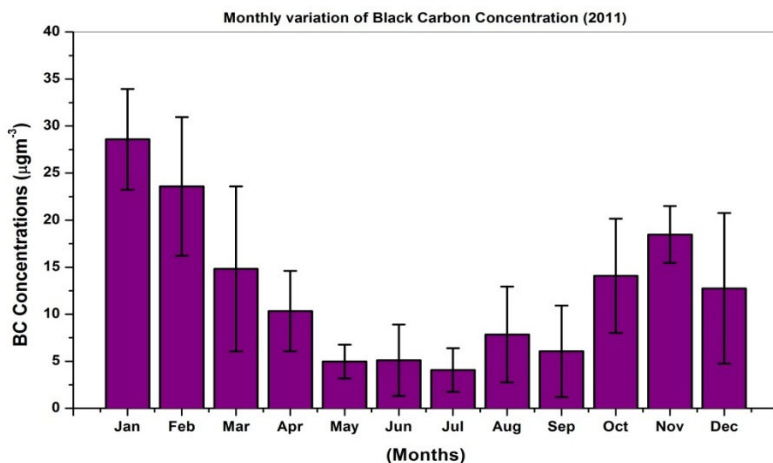


Fig. 1. Monthly mean variation of black carbon concentration observed at Agartala.

The contribution of fossil fuel and biomass burning in absorption coefficient have been determined by assuming exponent value (α) 1.7-2.6 for BB and 1.0 for FF. We tested an algorithm for year 2011 over Agartala and our results are encouraging (shown in figure 2). The annual average contribution of FF combustion sources to BC concentrations was 79%, with the remaining 21% corresponding to local and regional BB. Observational site is mainly originated from fossil fuels. However being a rural site, morning and evening times, people burn wood, dry leaves and other biomass for cooking purpose and for some other household activities. So, the local biomass burning is also a major contributor of BC. It is observed that, during the monsoon months, biomass burning is less as compare to winter months.

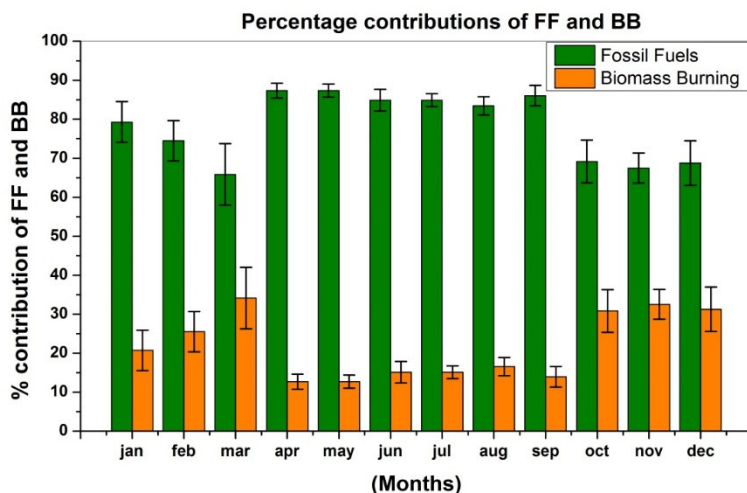


Fig. 2. Monthly mean variation of FF and BB in total BC mass concentrations over Agartala during 2011.

CONCLUSION

1. The present study shows the monthly variation of BC concentration during the year 2011 in Agartala, a rural site in the North-Eastern India.
2. The seasonal variation of BC concentration shows maximum concentrations in winter and minimum concentrations observed during the monsoon months.
3. The variations are observed on the basis of geographical location, meteorological parameters and long range transport.
4. It is found that BC at observational site is mainly originated from fossil fuels and the other source is biomass burning.
5. The observed Biomass Burning percentage is more during the winter months and less during the monsoon months.
6. It has been noticed that there is a significant difference in α value for soot generated from fossil fuel and from biomass burning.

ACKNOWLEDGEMENTS

The present work is supported by the ARFI Project of ISRO-GBP.

REFERENCES

IPCC 2013, In: Climate Change 2013: The Physical Science Basis. Contribution of Working Group I to the Fifth Assessment Report of the Intergovernmental Panel on Climate Change. Cambridge University Press, Cambridge, United Kingdom and New York, NY, USA.

Shamitaksha Talukdar, Soumyajyoti Jana and Animesh Maitra, Variation of black carbon concentration associated with rain events at a tropical urban location. *Current Science* Vol. 107, no. 1, 10 July 2014.

H. Gadhavi and A. Jayaraman (2010), Absorbing aerosols, contribution of biomass burning and implications for radiative forcing, *Ann. Geophys.*, 28, 103-111, 2010

The Aethalometer TM, A.D.A. Hansen (2005), Magee Scientific Company Berkeley, California, USA, 2005.07.

Guha, A., De, B.K., Dhar, P., Banik, T., Chakraborty, M., Roy, R., Choudhury, A., Gogoi, M.M., Babu, S.S., Moorthy, K.K., 2015. Seasonal characteristics of aerosol black carbon in relation to long range transport over Tripura in Northeast India. *Aerosol Air Qual. Res.*:1–13 <http://dx.doi.org/10.4209/aaqr.2014.02.0029>.

SUMMERTIME AEROSOL CHARACTERISTICS AT A FREE-TROPOSPHERIC SITE HIMANSH (4080 m a.s.l) IN THE WESTERN HIMALAYAS

B. S. ARUN, A. R. ASWINI, MUKUNDA M GOGOI, SOBHAN K KOMPALLI, PRASHANT HEGDE, AND S SURESH BABU

Space Physics Laboratory, Vikram Sarabhai Space Centre, Thiruvananthapuram-695022, India.

KEYWORDS: Himalayas, Climate change, Mineral dust, Carbonaceous aerosols

INTRODUCTION

Atmospheric aerosols play an integral part of the earth-atmosphere system by influencing the radiative balance through direct, indirect and semi direct effect (2013). Recent studies indicate that long-range transport from the pollution hotspot of south Asia has significant influence on the seasonality in abundance, chemistry, spatial distribution of aerosols over the pristine high-altitude Himalayas. Being close to the polluted populated landmasses, the Himalayas in the north of Indo-Gangetic Plains experiences the influence of distinct source processes unlike the air pollution in the remote Arctic and Antarctic. The increasing concern of scientific and social importance is about the possible impacts of absorbing aerosols on glaciers and the projected consequences of the changes in the snow albedo forcing on the Asian monsoon circulation, regional climate and hydrological cycles. In this regard, the source processes and impact of BC and mineral dust deposition toward darkening of snow in western Himalayas with potential implications to accelerated seasonal snowmelt and regional snow albedo feedbacks need thorough investigation. So far, there are very limited number of simultaneous in-situ observations of optical, physical and chemical composition of aerosols over the high-altitude Himalayas due to its remoteness, dynamic regimes and topographical complexity. In view of the importance of the aerosol studies in the Himalayas and in view to its importance to regional and global climate, this is the first-time approach on the characterization of aerosols over the Lahaul and Spiti valley (32.4°N, 77.6°E, 4080 m a.s.l), located close to major glaciers in the western Himalayan region. The measurements were carried out from the 'Himansh' observatory at an altitude of 4080 m a.s.l., covering a period of three months during Aug-Oct 2017.

METHODS

In this experiment, a suite of instrument was deployed at the observational site for the measurement of physical, optical and chemical properties of aerosols. Measurements of columnar spectral aerosol optical depth (AOD) were made at five wavelengths centered 340, 380, 550, 675 and 870 nm using a Microtops II Sunphotometer (Solar light company, USA). Measurements of composite aerosol mass concentrations and size distributions were carried out using a Quartz Crystal Microbalance (QCM; Model-PC-2HX, California Measurements Inc.) impactor. In addition, the mass concentration of the total suspended particulates (TSP) was also estimated using high-volume sampling (HVS, Model no: Staplex, USA). The samples collected using the HVS were used for the chemical analysis using appropriate techniques suitable with minimum uncertainty to determine various chemical components. The techniques include, OC-EC analyser (Model 5L, Sunset Laboratory Inc. USA, an Ion chromatograph (Make: Metrohm, model: 882 (cation) and 883 (anion)) and an inductively coupled plasma-mass spectrometer (ICP-MS; Make: Thermo Scientific, Model: iCAP Qc). In addition to this, near real time measurements of aerosol black carbon (BC) mass concentrations (M_{BC}) were carried out using the *new generation* Aethalometer (Model: AE33; Make: Magee Scientific, USA) operated with a sampling interval of 1 minute. Detailed description of the instrument is found elsewhere (Drinovec et al., 2015).

RESULTS & DISCUSSIONS

During the period of summer, columnar AOD varied from 0.05 to 0.11 with a mean value of $\sim 0.07 \pm 0.01$. The lower values of AOD represents a very clean atmosphere, representing a perfect background site.

The temporal variation of the mass concentrations of total suspended particulates (TSP), mineral fraction (composed of Si, Al, Fe, Ti, Ca), total carbonaceous aerosols (TC, which is sum of OC and EC), major ions (water soluble inorganic ions; combination of Mg^{2+} , Na^+ , K^+ , Cl^- , NO_3^- , SO_4^{2-}) and trace elements (combination of Li, V, Cr, Mn, Ni, Cu, Zn, As, Sr, Mo, Sn, Sb, Ti and Pb) are shown in Figure.1. TSP showed large day to day variations between $5 \mu g m^{-3}$ to $40 \mu g m^{-3}$, having dominance of mineral dust components. This was followed by carbonaceous aerosols, where the ratio of organic carbon (OC) to elemental carbon (EC) having a mean value of $OC/EC \sim 12.5 \pm 2.95$, suggesting possibly of biomass burning sources. On the other hand, the fraction ($\sim 0.56 \pm 0.20$) of water soluble OC (WSOC) on total OC component indicated the aged nature of the carbonaceous species. The average ratio of WSOC/OC is comparatively similar to the reported value from NCOP (0.65 ± 0.15) situated at an altitude of 5079 m a.s.l (Decesari et al., 2010). Analysis of air mass back-trajectories indicated that the regions located west and northwest of the measurement site, which include the regional hot-spots of Indo-Gangetic plains, west Asia and the Middle East, are possible source regions to perturb the observational site through long range transport.

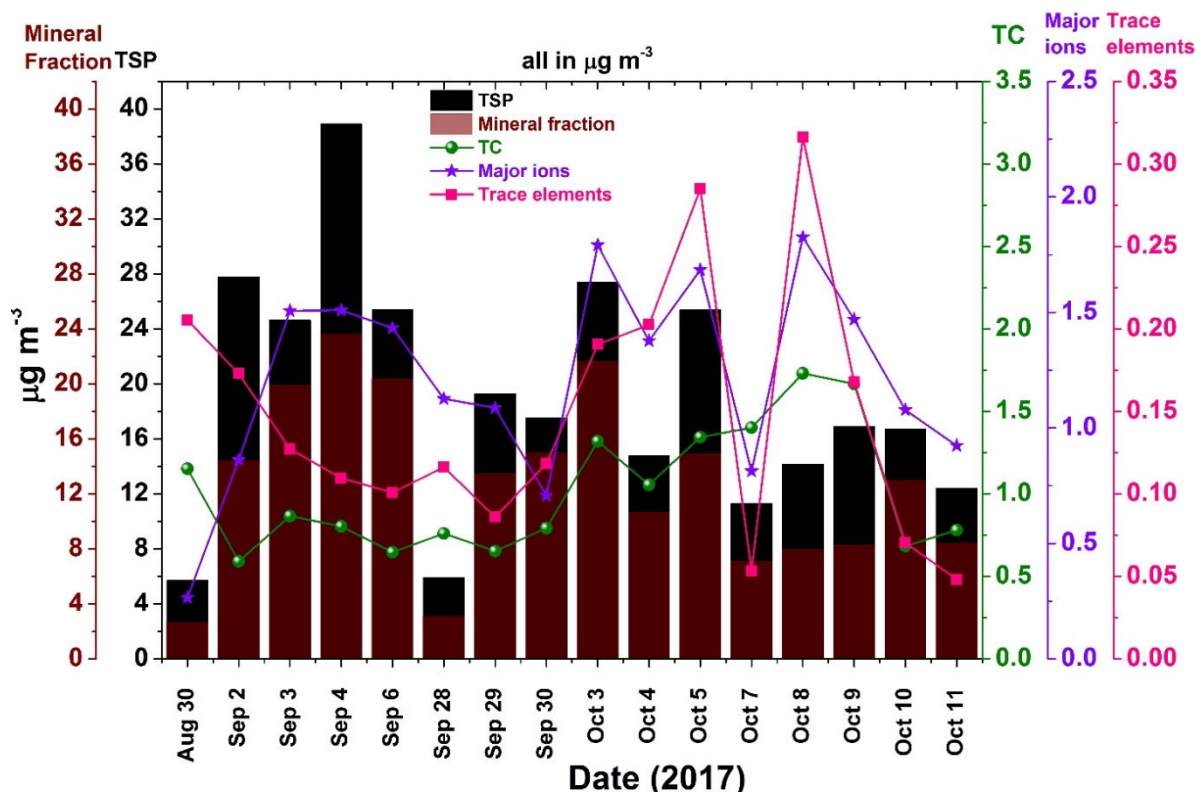


Figure 1: Temporal variation of mass concentration of Total suspended particles (TSP), Mineral fraction (in the left y-axis), total carbonaceous aerosols (TC = OC + EC), major ions and trace elements (in the right y-axis) during the study period.

With a view to examining the share of black carbon on composite aerosol loads, BC mass concentrations (M_{BC}) were measured. M_{BC} varied from a minimum of $50 ng m^{-3}$ to a maximum of $350 ng m^{-3}$ with a mean value of $M_{BC} \sim 168 \pm 58 ng m^{-3}$ during the entire study period. Interestingly, M_{BC} during August and September ($\sim 152 \pm 93 ng m^{-3}$) is lower than M_{BC} during October ($\sim 208 \pm 120 ng m^{-3}$). Similarly, high M_{BC} in October is reported over Nepal Climate Observatory Pyramid (NCOP, located at an altitude of 5079 m a.s.l) by Marinoni et al., (2010), which is attributed to increased biomass burning in the adjacent valleys.

Significant amount of black carbon (BC) mass concentrations ($M_{BC} \sim 168 \pm 58 \text{ ng m}^{-3}$) contributing as high as $\sim 4\%$ to PM₁₀ (particulate matter $< 10 \mu\text{m}$ in diameter) mass concentrations. Aerosol mass size distributions indicate the dominance of coarse mode ($> 1 \mu\text{m}$) aerosols in the size spectra, possibly originated due to local aeolian processes.

CONCLUSIONS

In the present study, we examined aerosol optical, physical and chemical properties during a field experiment carried out over a high-altitude observatory, Himansh in the western Himalayas. Our observations reveal that the overall mass loading is dominated by the mineral dust and carbonaceous species. Significantly higher OC/EC ratio prevailed over this location with dominant contribution of WSOC suggesting influence of biomass burning sources through long range transport. Our results have also clearly revealed that the western parts of the high Himalayas are heavily loaded with mineral dust, primarily of local origin. Along with this, considerable presence of the anthropogenic carbonaceous species are significant in influencing the hydrology in this region via snow albedo feedback processes.

ACKNOWLEDGEMENTS

This study was conducted as part of Geosphere Biosphere Program (ISRO-GBP) under Aerosol Radiative Forcing over India (ARFI) project of Indian Space Research Organization (ISRO).

REFERENCES

IPCC, 2013: IPCC (2013), Climate Change 2013, Working group I contribution to the fifth assessment report of the Intergovernmental Panel on Climate Change, Cambridge University press.

Decesari, S., Facchini, M. C., Carbone, C., Giulianelli, L., Rinaldi, M., Finessi, E., Laj, P. (2010). Chemical composition of PM₁₀ and PM₁ at the high-altitude Himalayan station Nepal Climate Observatory-Pyramid (NCO-P) (5079 m a.s.l.). *Atmos.Chem.Phys.*, 10(10), 4583–4596.

Drinovec, L., Močnik, G., Zotter, P., Prévôt, A. S. H., Ruckstuhl, C., Coz, E., Rupakheti, M., Sciare, J., Müller, T., Wiedensohler, A., and Hansen, A. D. A. (2015). The "dual-spot" Aethalometer: an improved measurement of aerosol black carbon with real-time loading compensation, *Atmos. Meas. Tech.*, 8, 1965-1979.

Marinoni, A., Cristofanelli, P., Laj, P., Duchi, R., Calzolari, F., Decesari, S., Bonasoni, P. (2010). Aerosol mass and black carbon concentrations, a two year record at NCO-P (5079 m, Southern Himalayas). *Atmos. Chem. Phys.*, 10(17), 8551–8562.

CHARACTERIZATION OF THE 'AEROSOL HUMIDOGRAPH INSTRUMENT' FOR AEROSOL OPTICAL GROWTH STUDIES

A. VAISHYA¹, S. K. KOMPALLI¹, P. S. AJEESHKUMAR, AND S. SURESH BABU¹

¹Space Physics Laboratory, Vikram Sarabhai Space Centre, Indian Space Research Organisation, ISRO
P.O., Thiruvananthapuram – 695 022, India.

KEYWORDS: Aerosols, Relative humidity, Hygroscopicity, Instrumentation.

INTRODUCTION

Knowledge of the hygroscopic properties of aerosols is critical in order to understand the aerosol-radiation interaction and reduce the uncertainties in quantification of associated forcing. A hand full of studies on aerosol optical growth are available globally (Titos et al., 2016). Over the Indian region the physical and optical properties of aerosols are studied extensively under the Aerosol Radiative Forcing over India (ARFI) project of ISRO-GBP using a network of observatories. But the information on the aerosol hygroscopic properties is sparse due to lack of suitable experimental facilities. Studies using such setup offer a unique opportunity to explore and couple aerosol radiative properties with aerosol chemistry and meteorology, and hence, will advance our understanding of the complex climate system. In order to quantify *RH* influence on aerosol radiative properties an experimental setup, Aerosol Humidograph Instrument (AHI) (Vaishya et al., 2014, 2016a, 2016b) is under development. AHI simultaneously conditions the incoming aerosol flow to a desired RH level, RH_{wet} and RH_{dry} . This enables measurement of aerosol optical properties at two different RH levels using aerosol optical measurement instruments. Here we present results for the characterization of the AHI in terms of dryer efficiency, aerosol losses, and flow optimization.

AEROSOL HUMIDOGRAPH INSTRUMENT - AHI

The AHI (Vaishya et al., 2016a) has three major modules viz., the dryer-I module, the humidifier module, and the dryer-II module. Besides this, there are various sub-modules and accessories. Overall flow through the AHI is maintained by two pumps and the flow rate controlled by two mass flow controllers. Sheath air flows are maintained by auxiliary pumps and limited by a critical orifice. Dryer-I conditions the incoming air flow to a low RH state. This enables measurement of aerosol properties at a reference dry state. A part of this flow is fed to a humidifier module which conditions the flow to a desired set RH, upwards between 40% and 90% and then aerosol properties are measured at a variable RH state. The measurements, dry RH and variable RH, together provide crucial information on the aerosol hygroscopic properties. For study of the aerosol hysteresis properties a ball valve controller (Ajeeshkumar et al., 2017) switches the humidified flow to a second dryer for downward RH scanning. A detailed electrical and software layout the AHI is given by Ajeeshkumar et al. (2016).

CHARACTERIZATION

AHI (Vaishya et al., 2016a) consist of a Nafion based dryer unit, responsible for preconditioning the incoming aerosol flow to a desired low RH state, RH_{dry} , and a membrane based humidifier unit for conditioning the aerosols to a RH between 40% and 90%, also termed as RH_{wet} . There are two dryers in the AHI: one for bringing the RH of aerosol flow to a reference dry state, $RH \leq 40\%$, and other for bringing the RH down from 90% to a desired low RH level. This is done to study the hysteresis properties of aerosols. A combination of incoming flow rates, sheath air flow rate, and sheath air pressure were tested to arrive at optimum values for efficient performance of the dryer module. Figure 1 shows the same with two different sheath air flow and pressure combinations. It was found that for an aerosol flow rate of 8 LPM and sheath flow rate of 2 LPM at 400 mbar the dryer performance was best with a drying capability of $\sim 40\%$ RH with respect to incoming RH. For achieving this efficiency a combination of membrane drying, vacuum purge, and partial reflux method was used. It was also found that for a given incoming aerosol flow increasing the

sheath air flow has little influence on the drying efficiency. Pressure of purge air i.e. degree of vacuum with respect to main aerosol flow is more critical.

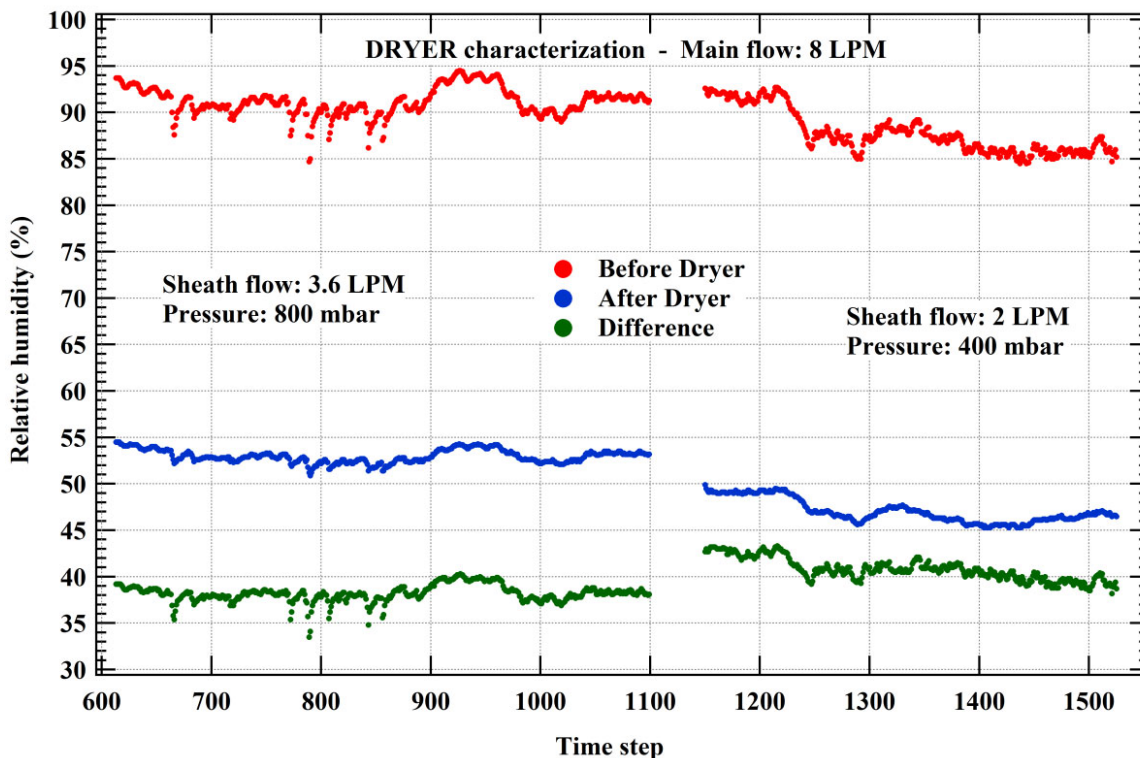


Figure 30: Performance of the Nafion based dryer module at a flow rate of 8 LPM, sheath flow rate of 3.6 and 2 LPM, and sheath flow pressure of 800 and 400 mbar, respectively. The colors indicate relative humidity before dryer (red), after dryer (blue), and the difference (green). Dryer is capable of lowering the incoming RH by ~40% RH unit.

The flow in the AHI is controlled and maintained by two mass flow controllers working at equal flow rates in the range 5 - 8 LPM each. The flow rates selected ensure minimal aerosol loss within the AHI by maintaining a laminar flow regime (Vaishya et al., 2016a). Also, adequate residence time is given to aerosols to respond to any change in RH due to drying or humidifying action.

In order to minimize the aerosol losses within the AHI due to sedimentation, impaction, and diffusion a detailed simulation of the same was performed (Vaishya A., 2017) after due consideration of various tube lengths, diameters, flow regimes and bends in the tube. Figure 2 depicts the simulated aerosol losses due to sedimentation, diffusion, and inertial impaction within the AHI for fine mode, accumulation mode, and coarse mode aerosols. Total aerosol losses are estimated to be < 5% in the submicron size range and ~ 30% for aerosols larger than 4 μm . In any case the aerosol loss percentage reported are minimum and indicate that AHI can be utilized within the aerosol size range 0.01 μm - 10 μm without crossing the 50% cut-off limit.

Arboledas (2016). Effect of hygroscopic growth on the aerosol light-scattering coefficient: A review of measurements, techniques and error sources, *Atmos. Environ.*, 141, 494-507, doi: 10.1016/j.atmosenv.2016.07.021.

Vaishya, A., S. Suresh Babu (2014). A Humidity Controlled Instrument to Measure Aerosol Radiative Properties, Indian Aerosol Science and Technology Association (IASTA), IASTA - 2014 Conference Proceedings, Volume 21, ID 14IA210.

Vaishya, A., S. K. Kompalli, P. S. Ajeeshkumar (2016a). Development of an Experimental Setup for the Study of Aerosol Hygroscopic Properties (Design Overview and Technical Details), Space Physics Laboratory, Vikram Sarabhai Space Centre, ISRO-VSSC-TR-0434-0-16 & SPL-TR-01-2016.

Vaishya, A., S. K. Kompalli, S. Suresh Babu (2016b). Aerosol Humidograph Instrument for the Study of Aerosol Hygroscopic Properties, Indian Aerosol Science and Technology Association (IASTA), IASTA - 2016 Conference Proceedings, Volume 22, pages 11-13.

Vaishya, A. (2017). Development of an Experimental Setup for the Study of Aerosol Hygroscopic Properties (Particle Loss Simulation in the AHI), Space Physics Laboratory, Vikram Sarabhai Space Centre, ISRO-VSSC-TR-0559-0-17 & SPL-TR-02-2017.

DIURNAL VARIABILITY OF INTEGRATED WATER VAPOUR CONTENT (IWC) IN THE ATMOSPHERIC BOUNDARY LAYER (ABL) AND ITS TRANSPORT TO THE FREE TROPOSPHERE DURING FAIR WEATHER AND CLOUDY CONDITIONS

EDWIN V DAVIS AND C. SURESH RAJU

Space Physics Laboratory, Vikram Sarabhai Space Centre, Thiruvananthapuram, India

KEYWORDS: Water vapour, Atmospheric boundary layer, Microwave radiometer profiler, temporal coherence technique.

INTRODUCTION

Atmospheric water vapour is a predominant greenhouse gas that critically influences the hydrological cycle and climate [louf *et al.*, 2015]. The radiative effects and moist dynamics of water vapour makes it an important feedback parameter in the atmosphere [Trenberth *et al.*, 2005]. It is a highly variable gas that undergo substantial variations over a large range of temporal scales [Bock *et al.*, 2007]. It has significant effects on many of the geophysical phenomena and its temporal, spatial and vertical distribution is necessary to understand weather and climate [Renju *et al.*, 2015]. Different techniques for measuring water vapour include satellites, GPS receivers, microwave radiometers, Raman lidar systems, radiosondes, sun photometry and Fourier transform spectrometers [Pérez-Ramírez *et al.*, 2012]. Microwave remote sensing finds advantage over the other techniques as microwaves can penetrate clouds and some extent to rain [Ulaby *et al.*, 1981], which enables us to determine water vapour in all weather conditions. Water vapour measurements with high temporal and vertical resolution can be best carried out using ground based passive multi-frequency microwave radiometer profiler (MRP). The potential of MRP to capture evolution of convective events has been reported over the tropical coastal station Thiruvananthapuram [Raju *et al.*, 2013]. Integrated water vapour content (IWC) is one of the representations of atmospheric water vapour which denotes the water vapour loading in the entire vertical column of the atmosphere as an outcome of the equilibrium between evaporation, precipitation and humidity convergence [Fontaine *et al.*, 2003], also it acts as an indicator of water vapour variability. Diurnal, intra-seasonal and inter-annual characteristics of total IWC has been established over the tropical coastal station Thiruvananthapuram using ground based Microwave radiometer profiler (MRP) during the period 2010-2013 [Renju *et al.*, 2015]. However the diurnal variation of IWC in atmospheric boundary layer (ABL) and layers in the free troposphere including its magnitude and phase change during cross boundary layer transport are the least understood areas. This study brings out the mean diurnal evolution of the IWC in the ABL and its transport to the free troposphere during fair-weather and cloudy conditions using multi-year (2011-2015) observations of water vapour from ground based passive multi-frequency MRP over a tropical coastal station Thiruvananthapuram (TVM, 8.5°N, 76.9°E). The fair-weather and cloudy conditions are differentiated by the methodologies suggested for satellite observations using spatial coherence [COAKLEY *et al.*, 1982]. Here in this study we use the temporal coherence technique for the determination of cloud and cloud-free conditions.

METHODS

A multi-frequency ground based passive MRP has been working at Thiruvananthapuram (TVM, 8.5°N, 76.9°E) since 2010. It measures atmospheric thermal radiation in two bands namely K band (22-30 GHz) and V band (51-59 GHz) with 21 and 14 frequency channels having 5-6° and 2-3° of beam width respectively. A rain detector that provides rain flag and a zenith looking infrared (IR) radiometer for measuring cloud base height are mounted on the radiometer. Details of radiometer profiler [Cimini *et al.*, 2011], configuration and its mode of operation were well explained [Raju *et al.*, 2013]. Water vapour profiles are retrieved from MRP by making use of atmospheric thermal emissions at K band (22-30 GHz). A history of radiosonde profiles from Indian Meteorological Department (IMD) at TVM are used to derive a neural network for the retrieval of humidity, cloud liquid water and temperature profiles from radiometric

measurements [Güldner and Spankuch, 2001]. MRP thus provides the profiles of humidity and temperature up to an altitude of 10 km. The accuracies of temperature and water vapour profiles derived from MRP are determined by comparing it with corresponding parameters derived from collocated radiosonde ascents [Cimini et al., 2011; Güldner and Spankuch, 2001].

To assess the variability of water vapour, time-altitude cross sections of it derived from MRP during the period of 5 years (2011-2015) has been analysed. In order to study the diurnal variability of IWC in ABL, boundary layer height (BLH) has to be determined. This is done by means of parcel method by making use of MRP data. The altitude at which the actual virtual potential temperature (θ_v) profile and dry adiabatic ascent at surface θ_v intersects is considered as the BLH [Renju et al., 2017; Seibert et al., 2000] in this method. Fair weather and cloudy conditions are determined by analysing cloud base temperature (T_b) (derived from zenith-looking infrared sensor mounted on MRP) based on temporal coherence technique. Running mean of time series of T_b is plotted against its root mean square (σ_{T_b}) for each half hour window. This method suggests that the conditions with $T_b \leq 265$ K and $\sigma_{T_b} \leq 3$ K and also with $275 \leq T_b < 265$ and $\sigma_{T_b} \leq 1.5$ K can be considered as fair-weather conditions. All the points which fall outside this limit can be considered as totally or partially cloudy. In order to bring out the mean diurnal variability of IWC in ABL and free-tropospheric layers, an “equivalent day analysis” of the IWC in each layer (surface to day time peak of ABL, ABL-3 km, 3-5 km, 5-7 km and 7-10 km) has been performed by combining the data for the same local time from the respective layers of all days during each month. The same analysis is done for fair-weather and cloudy conditions.

RESULTS & DISCUSSIONS

Time-altitude structure of water vapour (figure 1) shows clear diurnal variations that extended up to middle troposphere. These variations are more prominent during winter, pre-monsoon and post-monsoon seasons. BLH reaches its minimum (~200-300 m) during midnight to ~8 LT and it grows rapidly along with the convective boundary layer (CBL) reaching a maximum value of ~1.4-1.5 km at ~12-13 LT. ABL gradually decays after ~14 LT reaching its minimum value during midnight. Day time peak of BLH is found to be in the range of ~1.5-1.6 km during winter season and it gets reduced to ~1.2-1.3 km in pre-monsoon season. Summer monsoon season is characterized by the low value of BLH (~0.8-1 km) whereas it reaches ~1-1.2 km during post-monsoon season. Monthly mean day time peak of BLH in the cloudy conditions is consistently lower by ~200-300 metres compared to that in fair-weather conditions whereas the mean structure remains the same. Figure 2 depicts how the diurnal variation of IWC is association with the evolution of ABL. Lower value of IWC in ABL is observed at ~9-10 LT 2 hours after the minimum of BLH. As the ABL evolves rapidly, IWC gradually increases and maximizes at ~18 LT. This variability of IWC in the ABL is extended to the upper layers also. Phase of the diurnal variation in IWC at different layers shows small but systematic delay and is more evident during fair-weather conditions. Diurnal variability in IWC and its phase difference is barely observed in partial and cloudy conditions. Though the

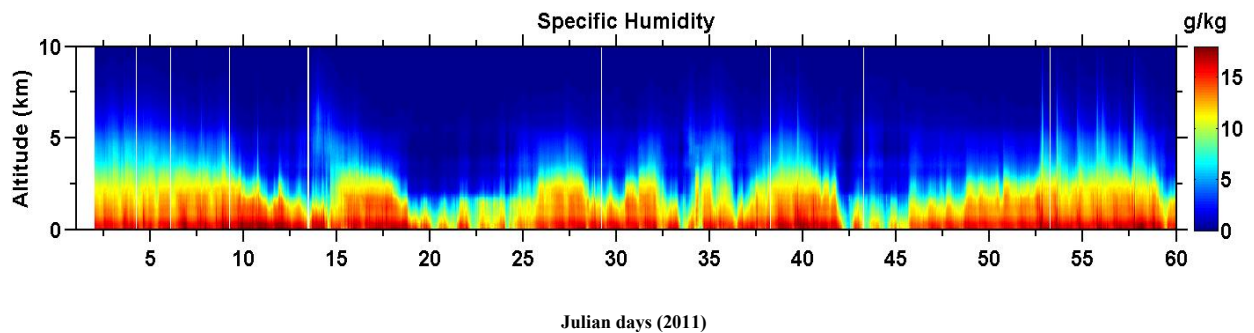


Figure 1. Time- altitude cross section of specific Humidity.

magnitude of IWC is quite small in the 2-6 km altitude layer compared to 0-2 km, magnitude of its diurnal variation is quite significant ($\sim 15-20\%$ of the mean value) throughout 0-6 km altitude band.

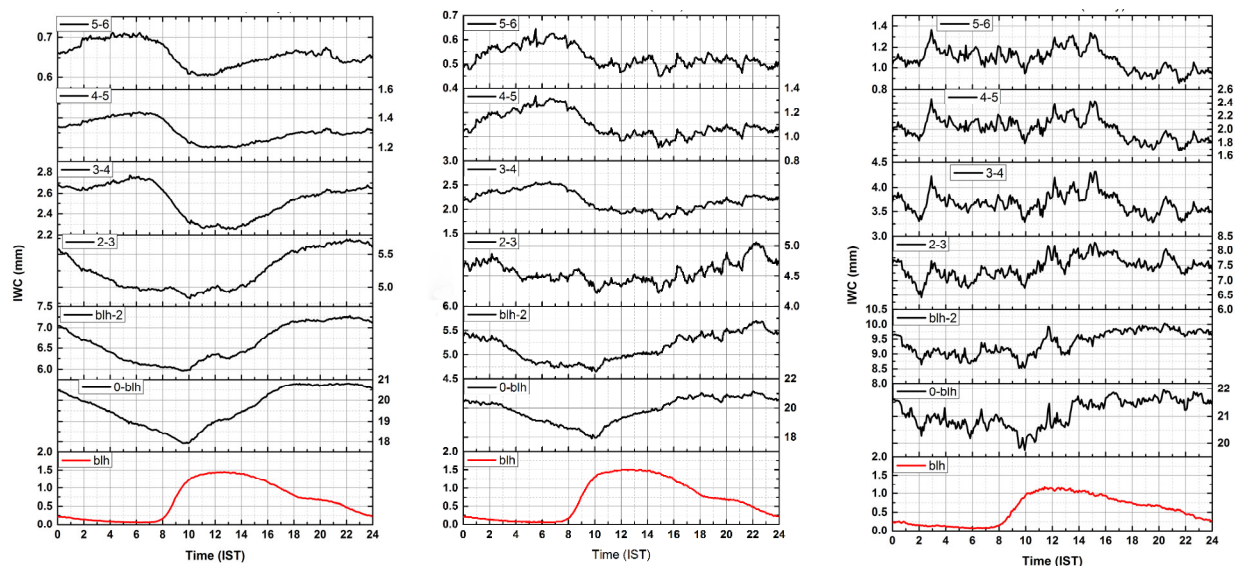


Figure 2. Monthly mean (January) diurnal evolution of BLH (red curve) and IWC (black curve) at different layers for all sky (left panel), clear (middle panel) and cloudy conditions (right panel) for the years 2011-2015.

CONCLUSIONS

Diurnal variation in the IWC associated with the diurnal evolution of ABL is investigated for all sky, clear sky and cloudy conditions using high temporal and vertical resolution multi-year (2011-2015) MRP observations. The diurnal evolution of ABL is studied for fair-weather and cloudy conditions. The variations in the magnitude and phase of the diurnal cycle of IWC at different altitude layers are examined. Systematic phase delay is observed in the diurnal cycle of IWC from surface to ~ 6 km. The percentage diurnal variations in IWC are comparable in the altitude layers from surface to ~ 6 km. This study shows the potential of MRP in capturing the high frequency variations of water vapour in the lower troposphere with better vertical resolution for studying the ABL evolution and its characteristics.

ACKNOWLEDGEMENTS

This work was supported by the ISRO Research Fellowship program.

REFERENCES

- Bock, O., F. Guichard, S. Janicot, J. Lafore, M. N. Bouin, and B. Sultan (2007), Multiscale analysis of precipitable water vapor over Africa from GPS data and ECMWF analyses., *Geophys. Res. Lett.*, 5 (L09705).
- Cimini, D., E. Campos, R. Ware, S. Albers, G. Graziano, J. Oreamuno, P. Joe, S. Koch, S. Cober, and E. R. Westwater (2011), Thermodynamic Atmospheric Profiling during the 2010 Winter Olympics Using Groundbased Microwave Radiometry, *IEEE Trans. Geosci. Remote Sens.*, 49(12), 4959-4969.

COAKLEY, J. A., JR., and F. P. BRETHERTON (1982), Cloud Cover From High-Resolution Scanner Data: Detecting and Allowing for Partially Filled Fields of View, *JOURNAL OF GEOPHYSICAL RESEARCH*, 87, 4917-4932.

Fontaine, B. P. Roucou, and S. Trzaska (2003), Atmospheric water cycle and moisture fluxes in the West African Monsoon: Mean annual cycles and relationship using NCEP/NCAR reanalysis, *Geophys. Res. Lett.*, 30.

Güldner, J., and D. Spankuch (2001), Remote sensing of the thermodynamic state of the atmospheric boundary layer by microwave radiometry, *J. Atmos. Oceanic Technol.*, 18, 925-933.

loouf, V., O. Pujol, H. Sauvageot, and J. Riedi (2015), Seasonal and diurnal water vapour distribution in the Sahelian area from microwave radiometer profiling observations, *Royal Meteorological Society*, doi:10.1002/qj.2550.

Pérez-Ramírez, F. N.-G. D., H. Lyamani, J. Fernández-Gálvez, F. J. Olmo, and L. Alados-Arboledas (2012), Retrievals of precipitable water vapor using star photometry: assessment with Raman lidar and link to sun photometry, *Journal of Geophysical Research*, 117(D05202).

Raju, C. S., R. Renju, T. Antony, N. Mathew, and K. K. Moorthy (2013), Microwave radiometric observation of a waterspout over coastal Arabian sea, *IEEE Geoscience and Remote Sensing Letters*, 10(5), 1075-1079, doi:doi:10.1109/LGRS.2012.2229960.

Renju, R., C. S. Raju, N. Mathew, T. Antony, and K. KrishnaMoorthy (2015), Microwave radiometer observations of interannual water vapor variability and vertical structure over a tropical station, *J. Geophys. Res. Atmos.*, 120, doi:10.1002/2014JD022838.

Renju, R., C. S. Raju, M. K. Mishra, N. Mathew, K. Rajeev, and K. K. Moorthy (2017), Atmospheric Boundary Layer Characterization Using Multiyear Ground-Based Microwave Radiometric Observations Over a Tropical Coastal Station, *IEEE Transactions on Geoscience and remote sensing*, 55(12).

Seibert, P., F. Beyrich, S. E. Gryning, S. Joffre, A. Rasmussen, and P. Tercier (2000), Review and intercomparison of operational methods for the determination of the mixing height, *Atmospheric Environment*, 34, (7), 1001-1027.

Trenberth, K. E., J. Fasullo, and L. Smith (2005), Trends and variability in column-integrated atmospheric water vapor, *Climate Dynamics*, doi:10.1007/s00382-005-0017-4.

Ulaby, F. T., R.K.Moore, and A.K.Fung (1981), *Microwave Remote Sensing - Active and Passive, Volume I: Microwave Remote Sensing Fundamentals and Radiometry*, Reading, MA: Addison-Wesley.

CHARACTERISTICS OF CARBONACEOUS AEROSOLS OVER A TROPICAL COASTAL LOCATION IN SOUTHERN PENINSULAR INDIA

A. R. ASWINI, PRASHANT HEGDE AND PRABHA R NAIR

Space Physics Laboratory, Vikram Sarabhai Space Centre, ISRO,

Thiruvananthapuram – 695022, Kerala, India.

KEYWORDS: carbonaceous aerosols, seasonality, coastal, trend analysis.

INTRODUCTION

Carbonaceous aerosols constituting of organic carbon (OC) and elemental carbon (EC) contributes significantly to the aerosol mass loading and play major role in influencing radiation budget, cloud formation, visibility, hydrological cycle and climate through direct as well as indirect effects (Jacobson et al., 2000). Organic compounds are emitted directly into the atmosphere as primary organic carbon (POC) mainly from biomass burning and fossil fuel combustion. Secondary organic carbon (SOC) forms through oxidation of gas phase volatile organic compounds and their subsequent conversion to particle phase (Lewandowska et al., 2010). Elemental carbon is directly emitted through incomplete combustion of carbon containing materials and is found to strongly absorb solar radiation predominantly in the visible spectrum (Bond et al., 2013). The physical and chemical characteristics of carbonaceous species are highly significant to understand their impact on radiation, air quality, atmospheric chemistry and climate.

Study of carbonaceous components of near-surface atmospheric aerosols (PM₁₀) over the tropical coastal location of Thiruvananthapuram, in south-west peninsular India for the periods 2005-09 and 2012-18 has been carried out. The study has revealed information regarding the major sources contributing to their abundance over this region, variability in the abundance pattern over different time scales, physical processes associated with the observed variability and meteorological factors controlling these processes.

METHODS

Study location Thumba (8.55°N, 77°E, 3m amsl) (TVM) is located in Thiruvananthapuram district over south-west coast of peninsular India in the state of Kerala. The aerosol samples were collected using a respirable aerosol sampler (model: Envirotech APM 460 BL), operating at a set flow rate of 1.1 m³ min⁻¹ and collecting particulate matter less than 10µm in diameter (PM₁₀) on pre-combusted quartz microfiber fibre filters (WhatmanTM, QMA, 20.3 cm×25.4 cm). In total 461 samples were collected from June 2012 to January 2018 at the rate of about 2 samples per week that included daytime (sea-breeze) and night-time (land breeze). For the period 2012-18, OC and EC were analysed using OC-EC analyser (Model 5L, Sunset Laboratory Inc., USA) with NIOSH-5040 (National Institute of Occupational Safety and Health) method based on thermal-optical transmittance (TOT) (Birch and Cary, 1996). Water-soluble organic carbon (WSOC) was analysed using Total Organic Carbon analyser (Model TOC-L_{CPH} Shimadzu, Japan). Water-insoluble organic carbon (WIOC) was estimated from the difference between OC and WSOC. Primary OC was estimated using the widely accepted EC tracer method (Castro et al., 1999) by taking minimum OC/EC ratio for each season. Secondary OC was estimated from the difference between OC and EC. Organic Matter (OM) that accounts for the total mass of organic compound was estimated by multiplying a constant factor of 1.6 for pre-monsoon, post-monsoon and monsoon periods, while using a ratio of 2.8 for winter. During the period 2005-09, an on-line OC-EC analyser, Ambient Carbon Particulate Monitor (Series 5400, Rupprecht & Patashnick, Co., Inc.) that quantifies the amount of OC and EC (in µg m⁻³) present in the collected particulate sample by direct, automatic thermal-CO₂ technique was used for OC-EC analysis.

RESULTS & DISCUSSIONS

Carbonaceous aerosols were found to constitute 36% (31.5% OC and 4.5% EC) of the PM₁₀ mass loading. They were found to exhibit consistent seasonal characteristics that persevered for the entire observation period of 2012-18 (Figure 1). Their highest contribution to total aerosol mass loading was found during winter (57±20%) followed by post-monsoon (31±15%), pre-monsoon (29±16%) and monsoon (27±15%). OC and EC were found to have annual average concentrations of 8.6±5 μg m⁻³ and 2.0±1.5 μg m⁻³ respectively. OC was found to be dominated by WIOC (62% of OC) and SOC (53% of OC) compared to WSOC and POC respectively. Seasonal characteristics were found to be mainly affected by prevailing synoptic circulation and changing sources/source strengths. For monsoon and post-monsoon period, anthropogenic influence is mostly from local/nearby sources (motor-vehicular exhaust, cooking emissions etc) while for pre-monsoon and winter period, biomass emissions substantially contributes to the carbon fraction, that are transported from north-east Asian and central parts of Indian region (evident from concentration weighted trajectory and fire count emissions). During monsoon, influence from organics of marine origin that have undergone secondary production and aging during its long range transport by the prevailing synoptic winds has been observed over this region. Diurnal characteristics were controlled by sea-breeze and land-breeze circulations. During land breeze period (night-time), air-mass advected from land, rich in anthropogenic emissions substantially increases the anthropogenic part of carbonaceous aerosols (e.g EC, POC and lower OC/EC ratio) while during sea-breeze period (daytime), the marine/secondary contribution to organic aerosols was found to be significant (SOC and higher OC/EC ratio). Based on the measurements of OC and EC during 2005-09 and 2012-18 (for more than a decade), a trend analysis has been carried out for the total carbon (TC) (Fig. 2). The overall trend for TC using linear regression analysis revealed slight decreasing trend over the years the magnitude being 0.02 μg m⁻³ per year. It can also be noticed from Fig. 2 that the increasing trend in TC is till 2013 (which is estimated as 0.3 μg m⁻³ per yr) after which TC shows a decline exhibiting a negative trend (-0.6 μg m⁻³ per yr).

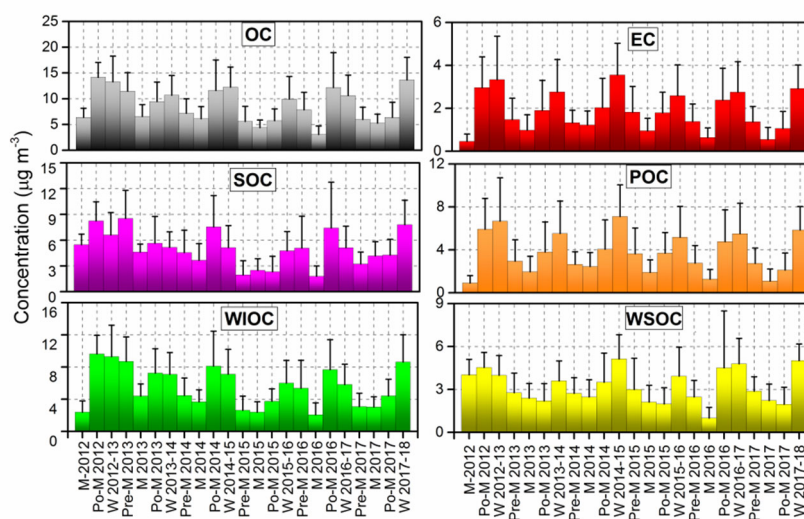


Figure 1. Inter-annual seasonal variations of carbonaceous components in near-surface PM₁₀ aerosols over the study location during the period 2012-18 for the seasons Monsoon (M), Post-Monsoon (Po-M), Winter (W) and Pre-Monsoon (Pre-M).

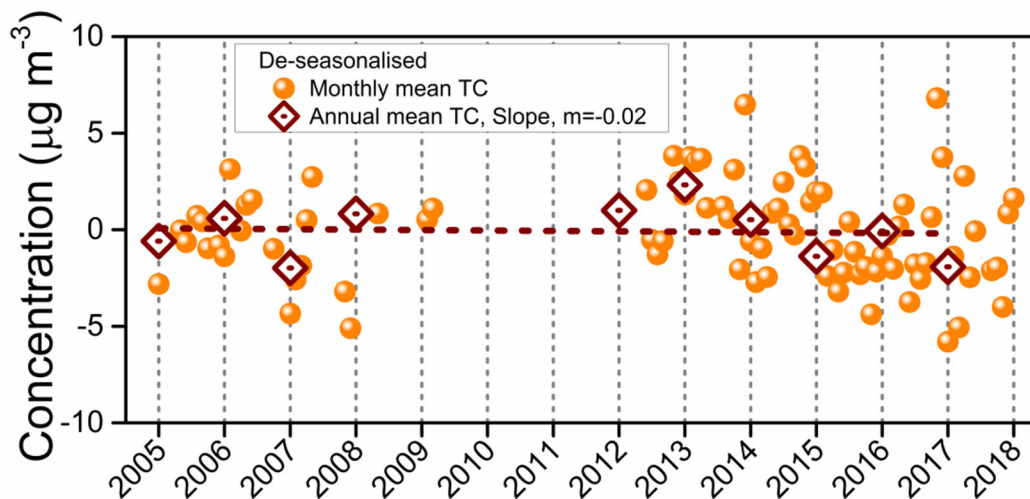


Figure 2. Monthly mean and annual mean concentrations (de-seasonalised) of TC in near surface PM₁₀ aerosols for the period 2005-17 for the study location.

CONCLUSIONS

Carbonaceous aerosols constituting 36% of the collected aerosol mass loading, exhibited well defined seasonal characteristics of winter high followed by post-monsoon, pre-monsoon and monsoon. Varying sources and source strengths combined with local meteorology, synoptic/mesoscale circulations and long range transported air-mass exhibited strong seasonal/diurnal variability that has played a crucial role in modulating the abundance pattern and characteristics of carbonaceous aerosols over this coastal location. Systematic long term observation of carbonaceous aerosols from this coastal station in peninsular India reveals that the atmospheric abundance of these aerosols does not reverberate the reported increasing trend over north-central parts of India. This can be presumed to be due to the large scale monsoon phenomenon and proximity to oceanic environment that helps in the effective dispersion of pollutants over these coastal peninsular regions.

ACKNOWLEDGEMENTS

Ms. Aswini is thankful to ISRO for her research fellowship.

REFERENCES

- Jacobson M.C., Hansson H.C., Noone K.J., Charlson R.J (2000). Organic atmospheric aerosols: review and state of the science. *Reviews of Geophysics* 38, 267–294.
- Lewandowska, A., Falkowska, L., Murawiec, D., Pryputniewicz, D., Burska, D., Bełdowska, M (2010). Elemental and organic carbon in aerosols over urbanized coastal region (southern Baltic Sea, Gdynia). *Science of the Total Environment* 408, 4761–4769.
- Birch, M.E., Cary, R.A (1996). Elemental Carbon-Based Method for Monitoring Occupational Exposures to Particulate Diesel Exhaust. *Aerosol Sci. Technol.* 25, 221–241.
- Bond, T.C., Doherty, S.J., Fahey, D.W., Forster, P.M., Berntsen, T., DeAngelo, B.J., Flanner, M.G., Ghan, S., Karche, B., Koch, D., Kinne, S., Kondo, Y., Quinn, P.K., Sarofim, M.C., Schultz, M.G., Schulz, M., Venkataraman, C., Zhang, Z., Zhang, S., Bellouin, N., Guttikunda, S.K., Hopke, P.K., Jacobson, M.Z.,

Kaiser, J.W., Klimont, Z., Lohmann, U., Schwarz, J.P., Shindell, D., Storelvmo, T., Warren, S.G., Zender, C.S (2013). Bounding the role of black carbon in the climate system: a scientific assessment. *J. Geophys. Res. D. Atmos.* 118, 5380 - 5552.

VERTICAL STRUCTURE OF OPTICAL AND RADIATIVE EFFECTS OF AEROSOLS ACROSS THE INDO-GANGETIC PLAIN

ADITYA VAISHYA¹, S. SURESH BABU¹, V. JAYACHANDRAN¹, MUKUNDA M. GOGOI¹, N. B. LAKSHMI¹, K. KRISHNA MOORTHY², S. K. SATHEESH^{2,3}

¹Space Physics Laboratory, Vikram Sarabhai Space Centre, ISRO PO, Thiruvananthapuram, India.

²Centre for Atmospheric and Oceanic Sciences, Indian Institute of Science, Bangalore, India.

³Divecha Centre for Climate Change, Indian Institute of Science, Bangalore, India.

KEYWORDS: Aerosols, Radiative properties, Atmospheric Heating, Vertical profile, Aircraft.

INTRODUCTION

The Indo-Gangetic plain (IGP), in the Southeast Asia region, spreading from Thar Desert in the far north-west to eastern boundaries of the Indian subcontinent, is a hotspot for atmospheric aerosol research for well over a decade [Ramanathan and Ramana, 2005]. During the pre-monsoon season (PMS) in the IGP significant amount of aerosols are pumped to altitudes as high as 4 Km [Prijiith et al., 2016], due to strong thermal convection driven by enhanced solar insolation. Elevated aerosol layers, depending upon their relative position with respect to clouds may heat or cool the surrounding [Satheesh et al., 2008] thus influencing cloud properties. Work presented here deliberates upon the altitudinal profile of aerosols in the IGP prior to onset of the Indian summer monsoon. Further it also ascertains role of aerosols in modulating the heating rate of the atmosphere and thus influencing properties of cloud precursors.

CAMPAIGN

With a view to understanding the vertical distribution of aerosols and estimating the radiative impacts of elevated aerosols in the lower free troposphere, extensive profiling of the vertical variation of the optical properties, namely the extinction/ scattering and absorption coefficients (respectively σ_{ext} / σ_{scat} / σ_{abs}) have been carried out from three base stations in the Indo-Gangetic Plain (IGP) using an instrumented aircraft, prior to onset of the Indian Summer Monsoon. These stations, as shown in Figure 1, represented the semiarid western IGP (Jodhpur, JDR), the anthropogenically affected central IGP (Varanasi, VNS), and the industrialized coastal location in the eastern end of the IGP, close to the northern Bay of Bengal (Bhubaneswar, BBR). A minimum of 4 profiles were taken at each station and at 6 vertical levels with each level representing minimum 20 minutes of measurements totaling over 80 minutes. Figure 1 shows the base stations with flight track superimposed on them. In the background are the mean pre-monsoon wind fields at 850hPa.

RESULTS AND DISCUSSIONS

Aerosol extensive optical properties viz. σ_{ext} , σ_{scat} , σ_{abs} showed high variability in the central IGP owing to proximity to the diverse source regions beneath. While column integrated σ_{scat} values were comparable for the west and central IGP, $\sim 64 \text{ Mm}^{-1}$, column integrated σ_{abs} values were maximum in central IGP leading to highly absorbing aerosol atmosphere over the region. A shift in the aerosol size distribution, indicated by Ångström exponent (α_{scat}), is observed in the IGP with aerosol population changing from super-micron mode dominant natural aerosols (dessert dust, $\alpha_{\text{scat}} \sim 0.9$), in the west to sub-micron mode dominant anthropogenic aerosols (mix of aerosols from industrial sources, fossil fuel and biomass burning, $\alpha_{\text{scat}} \sim 2.0$), in the east IGP.

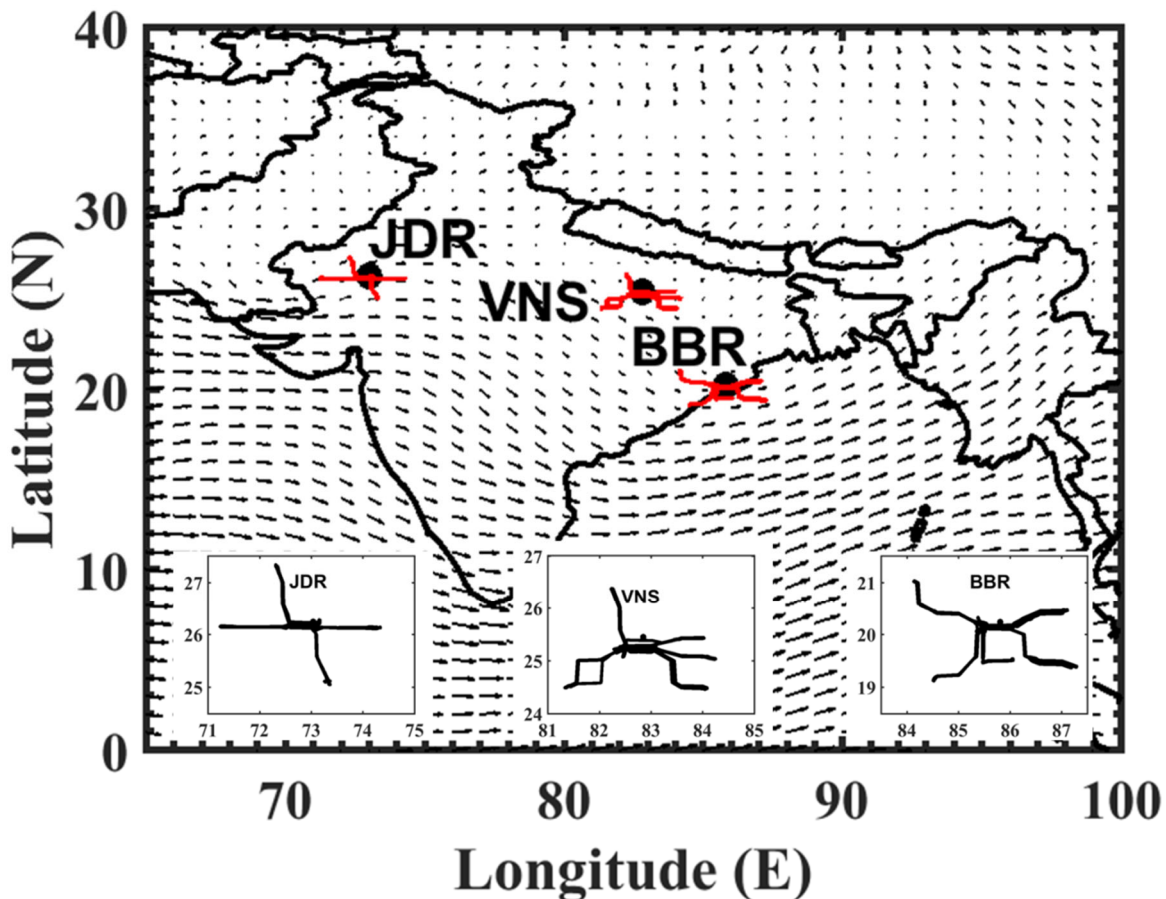


Figure 32: Geographical location of the base stations in the Indo Gangetic Plain superimposed on the mean pre-monsoon wind field. JDR, VNS & BBR stands for Jodhpur, Varanasi and Bhubaneswar, respectively. The three inset-figures show the flight track on all the measurement days for the stations JDR, VNS and BBR from left to right, respectively.

A system of highly absorbing aerosols, with single scattering albedo (SSA) values as low as ~ 0.69 , prevails over the entire IGP prior to monsoon onset. West IGP is least influenced by anthropogenic aerosols with SSA values ~ 0.81 . While SSA in central IGP increases vertically that in east IGP decreases. Comparison of SSA prior to monsoon onset to that with winter and spring values indicates that the aerosol population over the entire IGP systematically becomes highly absorbing in nature prior to onset of the Indian summer monsoon. The use of single SSA value for the entire column overestimates the heating at higher levels in western IGP and largely underestimates, by as much as $0.2 \text{ K}\cdot\text{day}^{-1}$, in the eastern IGP. In the central IGP it underestimates the heating rates at lower altitudes, specifically at layers with significant absorbing aerosol loading. Significantly low values of SSA, ~ 0.69 , prior to monsoon onset combined with the fact that there exists a gradient in the altitude at which maximum heating occurs across the IGP, has implications to atmospheric stability and regional precipitation patterns.

Figure 2 summarizes the findings of the campaign schematically.

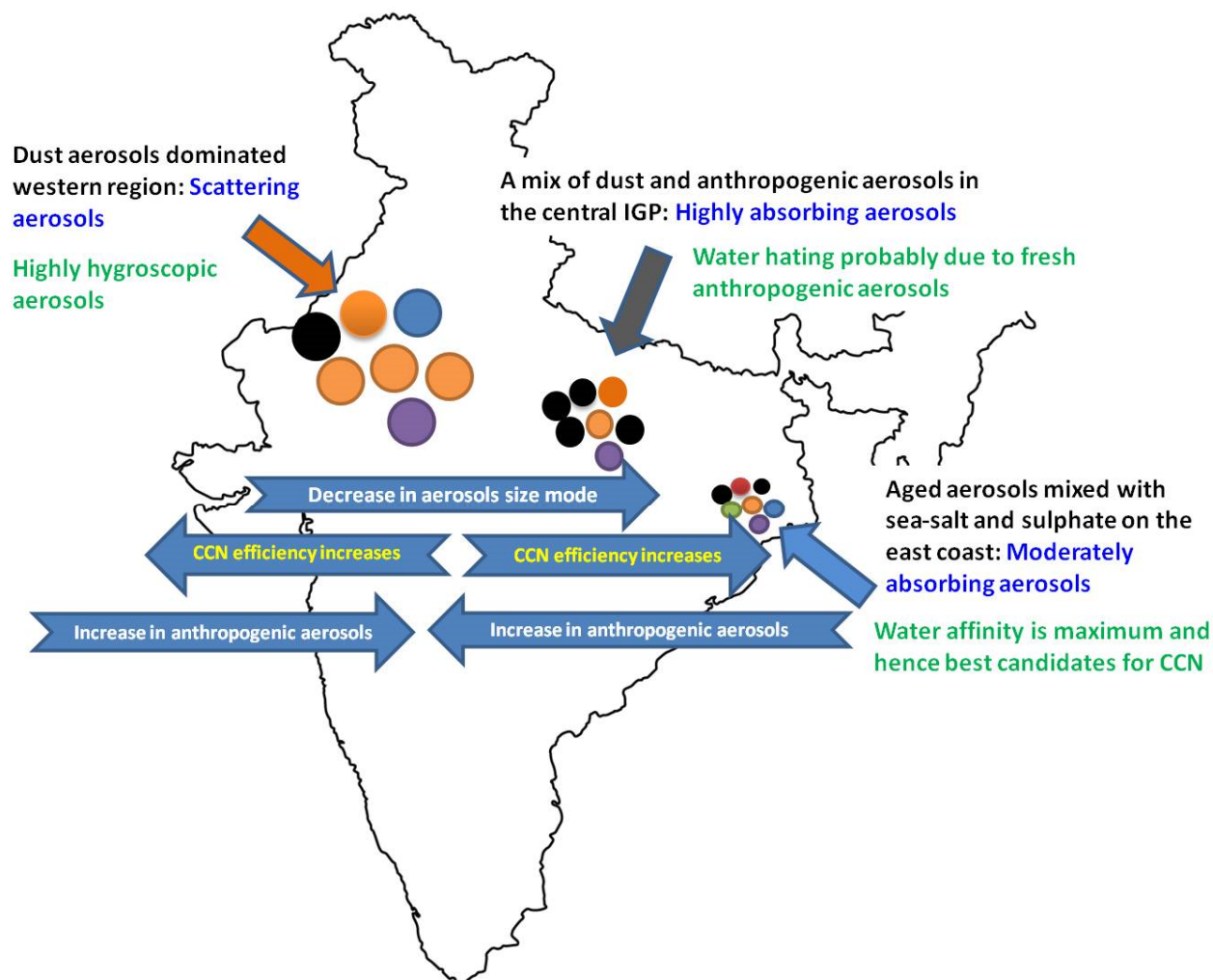


Figure 33: Graphical representation of the east-west contrast in aerosol optical and radiative properties.

CONCLUSIONS

- Vertical profiles of aerosol optical properties, prior to onset of the Indian summer monsoon, differed significantly across the IGP and resulted in a regionally significant heating rate gradient.
- While the integrated (ground to 3 km altitude) scattering coefficient remained quite comparable across the IGP, the highest absorption coefficient and hence the lowest single scattering albedo (SSA) occurred in the central IGP (Varanasi).
- Size distribution, inferred from the spectral variation of the scattering coefficient, showed a gradual shift from coarse particle dominance in the western IGP to strong accumulation dominance in the eastern coast, with the central IGP coming in-between.
- Source speciation of aerosol, using spectral aerosol properties, revealed aerosol system in the west IGP is predominantly natural (dust and sea-salt) and that in the east IGP is highly anthropogenic type (industrial emissions, fossil fuel and biomass combustion). The central IGP exhibited a mixture of both.
- Atmospheric heating rate profiles with layer resolved SSA and column averaged SSA differed significantly for highly absorbing/scattering aerosol layers.

ACKNOWLEDGEMENTS

This study was carried out as part of the SWAAMI-RAWEX campaigns. We thank Director, National Remote Sensing Centre (NRSC), Hyderabad and the Aerial Services and Digital Mapping Area (AS & DMA) for providing the aircraft support for this experiment. The authors wish to thank the crew of the aircraft for their help throughout the field campaign and the wholehearted support of the NRSC aircraft team. Aditya Vaishya is supported by the Department of Science & Technology (DST), Government of India through its INSPIRE Faculty program (award grant number DST/INSPIRE Faculty Award/2013/DST/INSPIRE/04/2013/000881). The SWAAMI project was supported by MoES.

REFERENCES

- Prijith, S. S., S. Suresh Babu, N. B. Lakshmi, S. K. Satheesh, and K. Krishna Moorthy (2016), Meridional gradients in aerosol vertical distribution over Indian Mainland: Observations and model simulations, *Atmos. Environ.*, 125, 337-345, doi:10.1016/j.atmosenv.2015.10.066.
- Ramanathan, V., and M. V. Ramana (2005), Persistent, widespread, and strongly absorbing haze over the Himalayan foothills and the Indo-Gangetic Plains, *Pure Appl. Geophys.*, 162(8-9), 1609-1626, doi:10.1007/s00024-005-2685-8.
- Satheesh, S. K., K. K. Moorthy, S. S. Babu, V. Vinoj, and C. B. S. Dutt (2008), Climate implications of large warming by elevated aerosol over India, *Geophys. Res. Lett.*, 35(19), doi:10.1029/2008GL034944.

SOURCES AND TRANSPORT OF AEROSOL SPECIES CONTRIBUTING TO AEROSOL OPTICAL DEPTH MEASURED OVER THE BAY OF BENGAL AND THE ARABIAN SEA FROM SOURCE AND RECEPTOR ORIENTED MODELLING APPROACHES

SAUVIK SANTRA, SUNNY KUMAR, SHUBHA VERMA

Department of Civil Engineering, Indian Institute of Technology Kharagpur, India

KEYWORDS: Aerosol Sources, Aerosol transport, Aerosol characterisation over the oceanic region, Species wise contribution to aerosol optical depth.

INTRODUCTION

The effects of atmospheric aerosols on the Earth-Atmosphere radiative balance, clouds, hydrological cycle and precipitation are major sources of uncertainty in quantifying the impact of human activities on climate change (IPCC, 2013). Aerosols arising from human activities, thus alter the earth's energy balance by changing radiative fluxes and hence exert radiative forcing of climate. Aerosols concentrated regionally can significantly alter the gradient of absorbed radiation, which consequently can have impacts on the hydrological cycle which connects directly to the availability and quality of fresh water.

In order to characterise physical and chemical properties and radiative effects of atmospheric aerosols and trace gases over India mainland and the surrounding oceanic regions (the Indian Ocean (IO), the Bay of Bengal (BOB) and the Arabian Sea (AS)), a number of observational campaigns have been carried out (such as 'Arabian Sea Monsoon Experiment, ARAMEX', 'Indian Ocean Experiment, INDOEX', 'Integrated Campaign for Aerosols, gases and Radiation Budget, ICARB', 'Winter ICARB, W-ICARB', 'Tigerz experiment'). These campaigns revealed a sizeable spatial heterogeneity in aerosol properties including total aerosol concentration, black carbon (BC) mass concentration, and AOD. Aerosol total mass concentration over the BOB region was two to three times higher than over the AS region with a relative predominance of fine mode over the BoB compared to the coarse mode over the AS (Kedia and Ramachandran, 2009). A significant difference in regionally averaged aerosol-induced atmospheric forcing efficiency between the oceanic regions of the BoB ($31 \pm 6 \text{ W m}^{-2}$ per unit AOD) and the AS ($18 \pm 7 \text{ W m}^{-2}$ per unit AOD) during March to May 2006 was also revealed.

Presence of high AOD over the oceanic regions as observed during the experiments indicates a significant role of aerosol transport from the adjacent continental regions of high anthropogenic emission flux. Sources of aerosol contributing to the measured AOD over the oceanic regions at a fine grid resolution is required to be resolved. In the present study, we have carried out a combined source-receptor analysis to examine the potential source regions and aerosol constituents over oceanic regions of the Bay of Bengal (BOB) and the Arabian Sea (AS). Source regions are identified through application of fuzzy c-mean clustering to back-trajectory data corresponding to ship-cruise expedition during the ICARB and W-ICARB experiments. In order to examine the relative extent of anthropogenic aerosol emissions contributing to AOD observed and the over the AS and BoB, we also evaluate the aerosol species distribution from the Free running aerosol simulations in general circulation model (GCM) and constrained aerosol simulation approach corresponding to ship-cruise measurements during the ICARB and W-ICARB experiments.

METHODS

The present study consists of the determination of potential source regions which were responsible for high AOD observed during ICARB and W-ICARB experiments. A hybrid source-receptor analysis is carried out to evaluate potential source regions having high emission flux of aerosols. The seven-day air mass back trajectories for the air parcels coming over the oceanic region during the ICARB and W-ICARB experiment are calculated using the Hybrid Single Particle Lagrangian Integrated Trajectory (HYSPLIT)

model. The back trajectories of air parcel for each day location of ship cruise are calculated at surface layer (at 10m, 100m and 500m) and elevated layer (at 1000m and 5000m).

A multivariate statistical tool, Fuzzy C-mean (FCM) clustering analysis (Kumar and Verma, 2016) of back trajectory endpoints is carried out to identify the source regions. The clustering algorithm calculates grouping by resemblance or distance among the centroids and their neighbouring elements (back trajectory endpoints for the present case). The clusters are homogeneous and distinctly different from each other. After obtaining the cluster centroids of each cluster, probable membership value (between 0 to 1) is allotted to each end-point based on their Euclidean distance from the cluster centroids. The endpoint is then assigned to the cluster, for which its probable membership value is highest. At first (PHASE-I) the number of cluster centroids are chosen, which lead to obtaining a broad distribution of centroids over the regions of interest including the Indian subcontinent, nearby and far-off regions. Further, to produce a region-specific cluster comprising of elements having a higher degree (>0.9) of membership value, the FCM clustering algorithm is simulated in an iterative process within the elements of the specific set of clusters obtained in phase 1. This is done to re-define cluster centroids (phase 2) among a selected group of cluster data points obtained in phase 1. The region-specific clusters of interest are decided based on information of emission flux composition of source regions (Indo-Gangetic plain (IGP), central India (CNI), south India (SI), northwest India (NWI), southeast Asia (SEA), Africa–west Asia (AFWA), and rest of the world (ROW)). The flowsheet consisting of alternating optimisation scheme to the fuzzy c-mean algorithm and subjective interpretation for region-specific clusters is shown in Figure:1. FCM clustering is done at the surface and elevated layer for Bay of Bengal and Arabian sea region for both ICARB and W-ICARB ship cruise locations. Combined clustering of the surface and the elevated layer is also carried out.

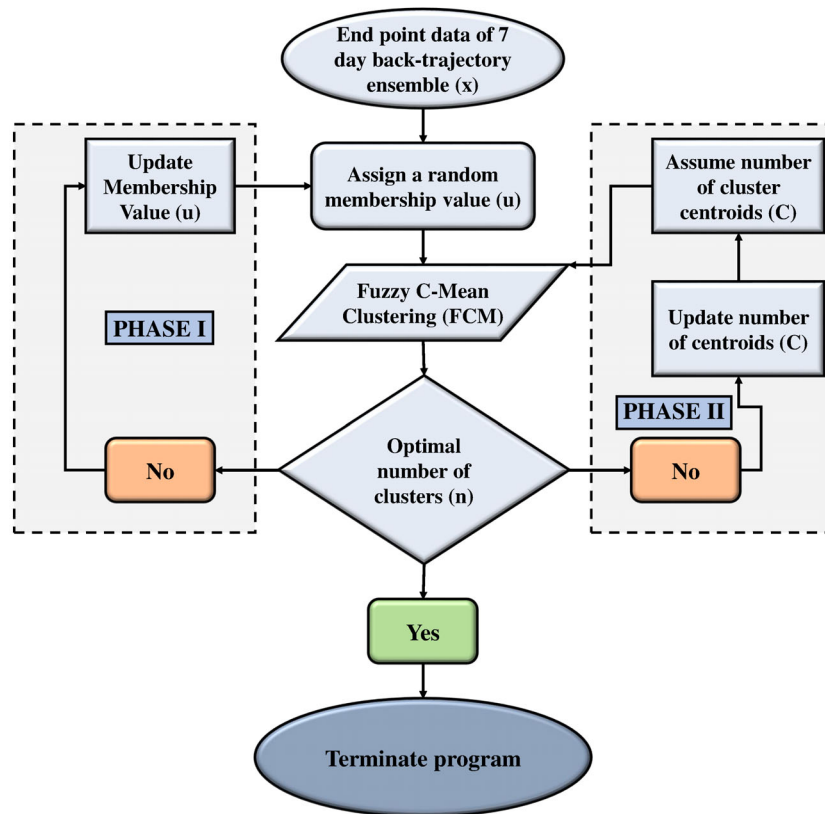


Figure 1: Flow Diagram of Fuzzy C-mean clustering algorithm as used in clusterisation of air parcel back trajectory endpoints.

To compare with the FCM clustering results source and region-tagged simulation using Laboratoire de Météorologie Dynamique atmospheric General Circulation Model (LMD-ZT GCM) (Verma et al., 2011) is evaluated. Aerosol species estimated from free running aerosol simulations in LMD-ZT GCM and that from constrained aerosol simulation approach are evaluated to examine the aerosol species-wise contribution to AOD corresponding to ship-cruise expedition over the BoB and the AS.

RESULTS & DISCUSSIONS

Analysis of clusters and cluster centroids of back trajectory end-points of the air parcel over the BOB region during W-ICARB, segregated using FCM algorithm revealed that most of the clusters for both lower and higher elevation are located over the Indo Gangetic Plain (IGP), Thar desert, North-East Indian region, South-East Asian countries (Thailand, Myanmar) and East Asia (Figure:2a).

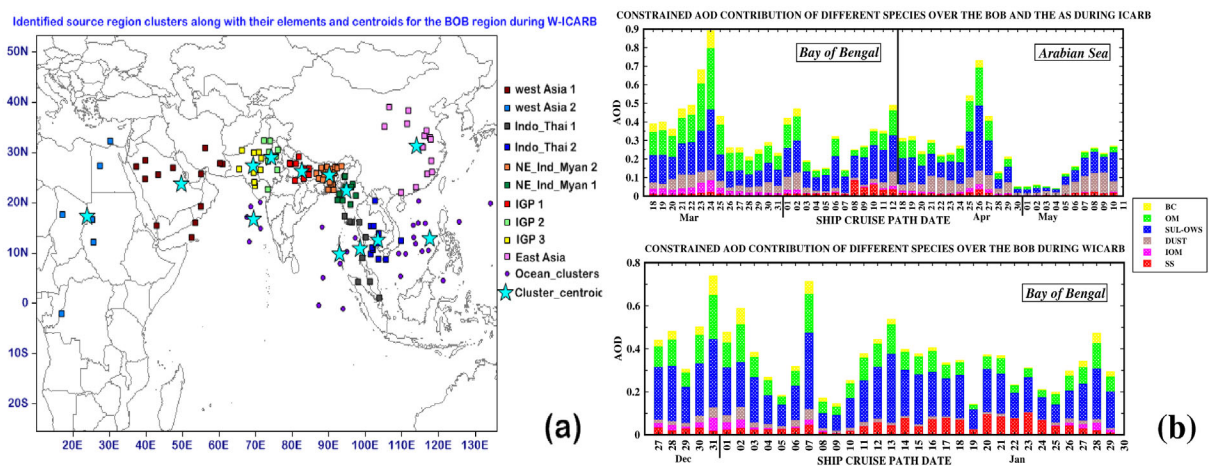


Figure 2: (a) FCM identified source region clusters along with their elements and centroids (Marked as star) for the BOB region during W-ICARB; (b) AOD contribution of different species (black carbon (BC), organic matter (OM), sulphate and other water solubles (SUL-OWS), dust, other inorganic matter (IOM) and sea salt (SS)) over the BOB and the AS during ICARB as obtained from constrained simulation.

Source regions identified using the LMD-ZT GCM simulation compares well with that from FCM cluster analysis approach. It can be seen from the simulation that during ICARB experiment, the contribution of emissions from IGP and CNI region towards high AOD is dominant over BOB region. In the second phase of ICARB experiment which was conducted over the AS region, it is seen that contribution of emissions from the IGP region to AOD is less while the contribution of emissions from Africa-west Asia is dominant. During W-ICARB experiment it can be seen that the contribution of emissions from East Asia and North-East region is also very high. When the ship moves towards the Indian landmass, the contribution of emissions from IGP increases whereas when it moves away from Indian landmass contribution of emissions from East Asia and North-East region increases while IGP and CNI decrease.

Species-wise AOD values, as obtained from constrained simulation approach (Figure:2b) indicate the predominant contribution of sulphate and other water solubles (SUL-OWS) (41%) and organic matter (OM) (29%) to the AOD over the BoB during ICARB (March-May). The relative contribution of OM to AOD is lower over the AS (19%) than that over the BoB. In contrast, dust is relatively predominant over the AS (27%) compared to the BoB (10%). For W-ICARB (December-January) over the BoB, main AOD contributor is found to be SUL-OWS (51%) followed by OM (23%) and sea salt (SS) (12%).

BC mass concentration values obtained from constrained simulation is found to be comparing well with the measured values near the coastal region. It is also found that as the ship moves in the northern part of BOB

region, the surface concentration of BC obtained from constrained simulation underestimates the measured values whereas when the ship moves in the southern part of the BOB region, model overestimates BC surface concentration. Difference between the rainfall data from the Global Precipitation Climatology Project (GPCP) and European Centre for Medium-range Weather Forecast (ECMWF) shows harmony with the difference between the modelled and measured values. LMD-ZT GCM has been nudged with ECMWF the meteorological data. This indicates the role of a possible discrepancy in aerosol scavenging attributed to wet deposition with rainfall behind the performance variation of the model.

CONCLUSIONS

Analysis of the results from the combined source-receptor cluster simulation over the oceanic regions during ICARB and W-ICARB shows that for BoB six clusters are located over the IGP region, central India, southeast Asian countries and West Asia including some parts of Africa. In contrast to that over the BOB region, for the AS region, four clusters are located over the AS region itself and only two clusters over the far-off regions of Africa, this contradicting feature indicates lesser anthropogenic invasion over the AS than the BOB. From the constrained simulation, it is observed that during ICARB, sulphate, organic carbon and dust were dominant species contributing to the total AOD over the BOB and the AS region. However, during W-ICARB, sulphate, organic carbon and sea-salt were dominant species contributing to AOD. The contribution of sulphate aerosol to the AOD found to be more during WICARB as compared to during ICARB. Estimates of the black carbon (BC) surface concentration from constrained simulation approach found to be comparing well with the measured values during W-ICARB near the coastal regions. However, BC concentration from constrained simulation approach found to be overpredicting the measured values when the ship was moving in southern BOB region and underpredicting when the ship was moving in northern BOB region attributed to possible discrepancy identified in aerosol wet deposition with rainfall nudging with the ECMWF data over the remote part of the oceanic regions.

REFERENCES

- IPCC, 2013: Climate Change 2013: The Physical Science Basis. Contribution of Working Group I to the Fifth Assessment Report of the Intergovernmental Panel on Climate Change [Stocker, T.F., D. Qin, G.-K. Plattner, M. Tignor, S.K. Allen, J. Boschung, A. Nauels, Y. Xia, V. Bex and P.M. Midgley (eds.)]. Cambridge University Press, Cambridge, United Kingdom and New York, NY, USA, 1535 pp, doi:10.1017/CBO9781107415324.
- Kedia, S., Ramachandran, S., 2009. Variability in aerosol optical and physical characteristics over the bay of bengal and the arabian sea deduced from ångström exponents. *Journal of Geophysical Research Atmospheres* 114 (D14).
- Kumar, D. B., Verma, S., 2016. Potential emission flux to aerosol pollutants over bengal gangetic plain through combined trajectory clustering and aerosol source fields analysis. *Atmospheric Research* 178, 415–425.
- Kumar, D. B., Verma, S., Boucher, O., and Wang, R.: Constrained simulation of aerosol species and sources during pre-monsoon season over the Indian subcontinent, *Atmospheric Research*, 214, 91–108, 2018.
- Verma, S., Venkataraman, C., Boucher, O., 2008. Origin of surface and columnar indian ocean experiment (indoex) aerosols using source-and region-tagged emissions transport in a general circulation model. *Journal of Geophysical Research: Atmospheres* 113 (D24).
- Verma, S., Venkataraman, C., and Boucher, O.: Attribution of aerosol radiative forcing over India during the winter monsoon to emissions from source categories and geographical regions, *Atmos. Environ.*, 45, 4398–4407, <https://doi.org/10.1016/j.atmosenv.2011.05.048>, 2011

ESTIMATION OF SHORT-WAVE AEROSOL DIRECT RADIATIVE FORCING OVER A SEMI-ARID REGION-KADAPA, ANDHRA PRADESH.

C. VISWANATHA VACHASPATI, G. RESHMA BEGAM AND Y. NAZEER AHAMMED

Atmospheric Science Laboratory, Department of Physics, Yogi Vemana University, Kadapa. (A.P.)

E-mail:ynahammed@gmail.com

KEYWORDS: Multi Wavelength Solar Radiometer, Aerosol Optical Depth (AOD), Angstrom exponent, BC concentration, Radiative forcing.

INTRODUCTION

Atmospheric aerosols cause climate forcing by altering the Earth's radiation budget, directly by scattering or absorbing solar and terrestrial radiations and indirectly by modifying the physical and microphysical properties of clouds. The greatest uncertainty to global climate forcing is due to the indirect effects of aerosols on clouds (Intergovernmental panel on climate change, 2007). Aerosols originate both from natural and anthropogenic sources. Out of numerous species of aerosols, black carbon (BC) aerosols play a major role in changing the optical properties as it is highly absorbing type aerosols (Bond and Bergstrom, 2006) and consequently to the radiation budget. The atmospheric heating and surface cooling introduced by these aerosols have been demonstrated and they can able to interact with dynamical processes in various scales to alter atmospheric circulation, and hence clouds and precipitation. The effect of aerosols on climate is normally quantified in terms of radiative forcing. Aerosols are potentially strong to perturb the surface reaching solar radiation. This would lead to distinct spectral variation of AODs and consequent impacts on the optical properties and radiative forcing of aerosols.

Site description and Instrumentation

Observations were carried out on the roof top of Sir C.V. Raman Science building at Yogi Vemana University Campus (14.47°N, 78.82°E, 138 m above mean sea level) regularly which is located 16 Km away from Kadapa town of Andhra Pradesh. The spectral dependent column integrated aerosol optical depth (AOD) in the wavelength range 380 nm-1025 nm (preferably at 10 different wavelengths) has been collected from a ground based Multi-Wavelength solar Radiometer (MWR). 7-channel Aethalometer has been used for the measurement of Black Carbon (BC) concentration during the study period i.e., December, 2013 to November, 2016 over the observational site Kadapa. The above-mentioned aerosol optical properties along with the other optical properties derived from the OPAC model have been used in the SBDART model proposed by Ricchiazzi et al. (1998) and estimated radiative fluxes (down-up) at Kadapa in the shortwave region of 0.25–4.0 μm . The above estimated radiative fluxes have been used and calculated aerosol radiative forcing values. Temporal variations in aerosol radiative forcing have been discussed.

RESULTS AND DISCUSSIONS

Temporal variations in BC mass concentration

The diurnal variation of BC mass concentration for different seasons is shown in Fig.1. It shows a gradual increasing pattern from early morning hours and attains a maximum peak at around 06:00–08:00 h LT (local time) which went on decreasing and reach its minimum at around 13:00–16:00 h LT. Thereafter again, it increases more rapidly and reaches its second maximum peak between 19:00 and 21:00 h LT for all the seasons. The diurnal variation of BC was closely related with the boundary layer height (BLH) dynamics and as well as local meteorology (Begam et al., 2016). The sharp build up in the BC mass concentration during the post dawn period arises due to the fumigation effect in the boundary layer (Stull, 1988) closely related to the time of sun rise. Due to decadence of the local boundary layer, this leads to

rapidly reduction in the ventilation, which leads to evening peak in BC concentration. Morning peak of winter season is dominant than the nocturnal peak and also amplitude of winter peaks is very high compared to other peaks of different seasons. Minima concentration was observed in the noon time during the study period.

Monthly high and low BC was found during December ($3.31 \pm 0.76 \mu\text{g m}^{-3}$) and July ($1.05 \pm 0.28 \mu\text{g m}^{-3}$) respectively. The Seasonally high BC was observed for winter season ($2.91 \pm 0.63 \mu\text{g m}^{-3}$) followed by pre monsoon ($2.45 \pm 0.73 \mu\text{g m}^{-3}$) and post monsoon ($1.56 \pm 0.45 \mu\text{g m}^{-3}$) and low was observed during monsoon ($1.18 \pm 0.38 \mu\text{g m}^{-3}$) seasons. The high BC during winter was attributed to vehicular transport and agriculture waste burning.

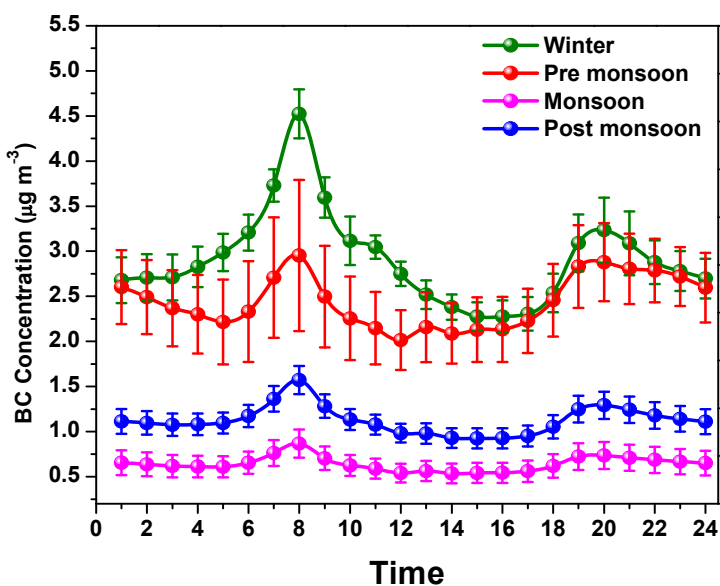


Fig.1. Diurnal variations of (BC) in different seasons.

Spectral variations in Aerosol Optical Depth (AOD)

The spectral variation of AOD is a key parameter in the modeling studies of radiative properties of aerosols. AOD measurements collected during clear sky conditions were averaged to obtain the daily mean values. Further, these daily averaged values were used to estimate the monthly and seasonal mean values. Fig.2. represents the spectral variations of AOD for different seasons and the monthly and seasonal variations of mean AOD at different wavelengths observed at Kadapa. The annual mean AOD noticed at 500 nm during the study period was 0.35 ± 0.09 . The monthly variation in AOD showed increasing trend from December

(0.32 ± 0.12) to May (0.50 ± 0.14), and then decreasing with a low value during August month (0.21 ± 0.08). Further it started increasing and attains a peak value (0.47 ± 0.09) in the month of November. The seasonal variation of mean AOD at 500 nm and found to be high during pre monsoon (0.39 ± 0.14) followed by post monsoon (0.37 ± 0.16) and winter (0.35 ± 0.17) seasons, and comparatively low was observed during the monsoon season (0.27 ± 0.09).

Optical properties derived from the OPAC model

The values of Single scattering Albedo (SSA) and Asymmetry parameter (g) are derived from OPAC model. SSA is the good indicator of radiative effects of particles and Asymmetry parameter (g) is a spectral dependent quantity. The monthly mean SSA (ASY) and value estimated from OPAC model and is varied in between 0.80(0.65) and 0.94 (0.75) with the mean value of 0.87 ± 0.03 (0.7 ± 0.03) over Kadapa. Seasonal SSA (at 500 nm) was found to be high during post monsoon (0.91 ± 0.02) and monsoon (0.89 ± 0.02) seasons revealed that the region is experienced with highly scattering type of particles during the study period. Whereas comparatively low SSA values were recorded during winter (0.86 ± 0.01) and pre monsoon (0.87 ± 0.03) due to strong absorbing nature (low scattering) of aerosol particles. High ASY values were observed during post monsoon (0.73 ± 0.01) followed by monsoon (0.72 ± 0.02) and pre monsoon season (0.72 ± 0.01). Whereas low values during winter (0.7 ± 0.01) season at 500 nm indicates the relatively more abundant of anthropogenic aerosols.

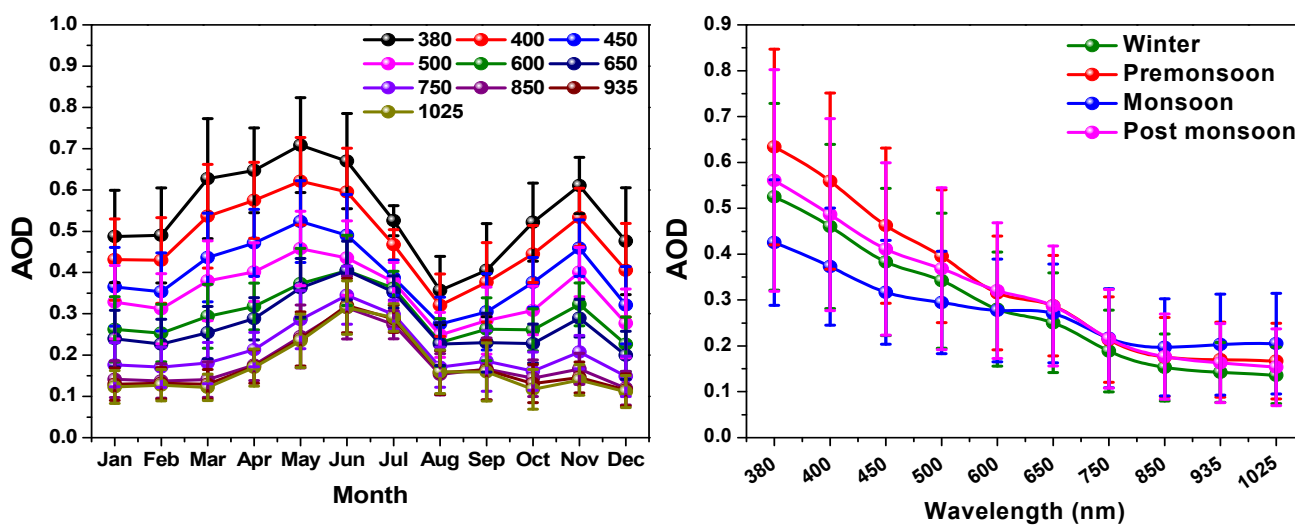


Fig.2. Monthly and seasonal spectral variation of AOD during the study period.

Direct aerosol radiative forcing

The assessment of AOD values estimated from the OPAC model and measured MWR AOD are within the uncertainty error ($\pm 5\%$). Monthly estimated mean top of the atmospheric forcing was found in between -9.9 and -2.1 W m^{-2} , with the surface forcing varied from -36.3 W m^{-2} to -17.8 W m^{-2} . The atmospheric aerosol radiative forcing which is the difference between top of the atmosphere and surface forcing varied from $+14.7$ to $+32.0 \text{ W m}^{-2}$. High values of direct atmospheric aerosol radiative forcing were noticed during pre monsoon $29.1 \pm 2.3 \text{ W m}^{-2}$ and winter ($26.0 \pm 1 \text{ W m}^{-2}$), whereas low value noticed during monsoon ($17 \pm 3.9 \text{ W m}^{-2}$) and post monsoon ($18.3 \pm 2.6 \text{ W m}^{-2}$) seasons for the study period over Kadapa.

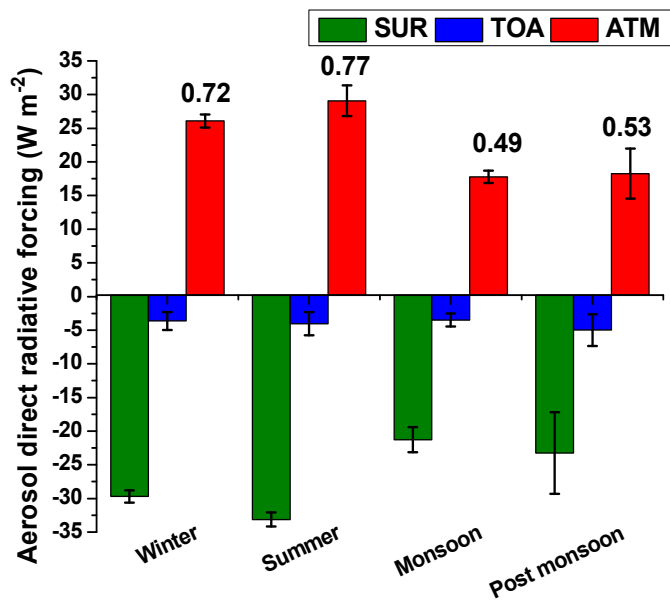


Fig.3 Seasonal estimated atmospheric radiative forcing (ARF) at Kadana during the study period

ACKNOWLEDGEMENTS

Authors are thankful to ISRO-GBP for their financial assistance in the form of Research project under ARFI Network stations.

REFERENCES

- Ricchiazzi, P., Yang, S., Gautier, C., Sowle, D., 1998. SBDART, A research and teaching tool for plane-parallel radiative transfer in the Earth's atmosphere. *Bull. Am. Meteorol. Soc.* 79, 2101-2114.
- Stull, (1988): *An Introduction to Boundary Layer Meteorology*, Kluwer Academic Publisher.
- Begam, G.R., Vachaspati, C.V., Ahammed, Y.N., Kumar, K.R., Babu, S.S., Reddy, R.R., 2016. Measurement and analysis of black carbon aerosols over a tropical semi-arid station in Kadapa, India. *Atmos. Res.* 171, 77-91.
- Bond, T.C. and Bergstrom, R.W., 2006. Light absorption by carbonaceous particles: An investigative review. *Aerosol science and technology*, 40(1), pp.27-67.

AEROSOL AND POLLUTANT ASSESSMENT DURING WINTER TIME IN DELHI: THE WIFEX CAMPAIGN

U. C. DUMKA¹, SURESH TIWARI², D. G. KASKAOUTIS³, S.D. ATTRI⁴, V. K. SONI⁴, P.D. SAFAI⁵
AND NARENDRA SINGH¹

¹Aryabhata Research Institute of Observational Sciences, Nainital, 263 001, India

²Indian Institute of Tropical Meteorology, New Delhi Branch, New Delhi -110 060, India

³Institute for Environmental Research and Sustainable Development, National Observatory of Athens, 118 10, Athens, Greece

⁴Indian Metrological Department, Lodhi Road, New Delhi – 110 003, India

⁵Indian Institute of Tropical Meteorology, Pune – 411 008, India

KEYWORDS: black carbon, Delhi, boundary-layer dynamics, aethalometer model.

INTRODUCTION

During the last decades, the carbonaceous aerosol [such as elemental carbon, (EC); black carbon (BC); organic carbon, (OC)] emissions exhibit an increasing trend over the globe, particularly in the developing south and east Asian countries, pointing out the need for detailed assessment of the levels and source apportionment close to the source. In the present work, we analyse experimental datasets consisted of continuous measurements of BC mass concentration, scattering, absorption and extinction aerosol coefficients, along with intensive aerosol properties [e.g single scattering albedo (SSA), extinction and absorption Ångström exponents (SAE and AAE, respectively)], air pollutants (CO, NO_x, O₃) and meteorological observations carried out during the winter fog experiment (WIFEX) that had been taken place in Delhi during wintertime (December 2015 to February 2016).

EXPERIMENTAL SITE AND MEASUREMENT DETAILS

The measurement sites were located in the greater Delhi region, with a total population of ~17 million, which is among the most polluted cities over the globe due to very high emissions from industries, automobiles, power plants, brick-kilns, domestic heating and cooking, open biomass burning and transported plumes of dust and agricultural burning. Except for the high emission rates from various sources, the aerosol and pollution levels in Delhi are strongly impacted by the local and regional meteorology and, especially during winter, the dry conditions, calm winds and shallow mixing layer favor very large concentrations near the ground. Therefore, the current campaign took place during wintertime to assess the sources of the BC mass concentration along with aerosol properties and several other pollutants. Further details of the experimental site and measurements protocol for the WIFEX is presented elsewhere (Bisht et al., 2016; Guide et al., 2017)

RESULTS & DISCUSSIONS

The temporal variation of Aethalometer (AE-33; Magee Scientific USA) measured BC, BC_{ff}, BC_{wb} (fossil-fuel and wood burning components of BC, respectively), along with the monochromatic Photoacoustic Extinctionmeter (PAX; Droplet Measurement Technologies, Inc., CO, USA) measurements of the extinction, scattering, absorption and single scattering albedo, PM₁₀ and PM_{2.5} mass concentrations and trace gas pollutants such as NO_x, CO and O₃ are analysed. High values of PM₁₀ ($245.5 \pm 109.8 \mu\text{g m}^{-3}$) and PM_{2.5} ($145.5 \pm 69.5 \mu\text{g m}^{-3}$) concentrations were recorded during the campaign (Figure 1a), composed of a large (~10% to PM₁₀ and ~17% to PM_{2.5}) BC fraction. During the same period, the daily BC mass concentrations varied from 3 to 60 $\mu\text{g m}^{-3}$ (with mean of $24.4 \pm 12.2 \mu\text{g m}^{-3}$), mostly affected by changes in meteorological

conditions, in mixing layer height and dispersion, and by differences in carbonaceous emission rates, with highest concentrations during night and early morning hours (Figure 1b). The fossil-fuel combustions from traffic, industries and domestic use of natural gas dominated when compared to burning of wood, waste material, dung cakes and agricultural crop residue. The BC_{ff}/BC was found to be 73% at 880 nm and 56% at 370 nm, exhibiting large daily and diurnal variability, while the relative contributions of BC_{ff} and BC_{wb} depend on wavelength. Furthermore, the average NO, NO₂, O₃ and CO concentrations were found to be 7.9 ± 2.3 ppb, 12.9 ± 1.9 ppb, 31.3 ± 18.4 ppb and 1.7 ± 0.5 ppm, respectively, while high levels of b_{sca} and b_{abs} coefficients were also recorded. Nearly all the examined parameters exhibited more or less prominent peaks around 08:00 - 09:00 LST indicating the influence of the morning rush-traffic emissions associated with a generally low MLH. The aerosol and primary air-pollutant concentrations were progressively decreasing towards midday, closely following the increase in MLH, thus allowing for vertical mixing and dilution processes. The increase in the concentrations after ~17:00 LST was coinciding with the increased domestic cooking and gradual formation of a surface inversion prohibiting vertical mixing. Later on, the evening traffic rush hour and open fires of waste material in the roads for heating purposes (especially in the slams) further increased the PM and BC concentrations and maintained them at high levels throughout the night. BC_{ff} and BC_{wb} were found to be strongly related to CO and NO emissions indicating common local sources of primary combustions, while the BC_{ff}/BC_{wb} ratio was not found to be related to CO/NO_x.

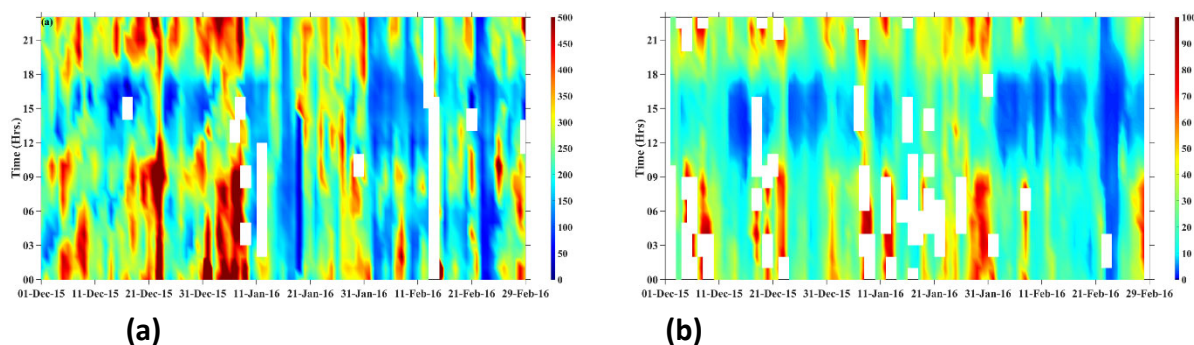


Figure 1: Temporal variation of PM₁₀ (a) and BC (b) mass concentration during the whole campaign period.

CONCLUSIONS

The main findings from the analysis can be summarized in the following:

5. Very high pollution levels were recorded over Delhi during wintertime.
6. A large BC variation (3 to 60 $\mu\text{g m}^{-3}$ on daily basis) was observed.
7. The BC_{ff}/BC was found to be 73% at 880 nm and 56% at 370 nm.
8. The boundary layer dynamics control the diurnal variations of BC, PM and trace gas concentrations.

ACKNOWLEDGEMENTS

The authors are grateful to Director IITM Pune, Director General IMD, Secretary MoES, Govt. of India and Director IARI, New Delhi for their constant encouragement and continuous support for carrying the Fog Experiment over Delhi.

REFERENCES

Bisht, D.S., Tiwari, S., Dumka, U.C. et al., (2016). Tethered balloon-born and ground-based measurements of black carbon and particulate profiles within the lower troposphere during the foggy period in Delhi, India. *Sci. Total Environ.*, 573, 894-905.

Ghude, S.D., Chate, D.M., Jena, C., et al., (2016). Premature mortality in India due to PM2.5 and ozone exposure. *Geophys. Res. Lett.* 43, 4650 – 4658.

MASS DISTRIBUTION OF SIZE SEGREGATED PARTICULATE MATTER AT DIFFERENT TRAFFIC SITES OF AGRA REGION

RAHUL TIWARI^{1,2}, PRABAL PRATAP SINGH¹ and AJAY TANEJA²

¹Department of Chemistry, GLA University, Mathura-281406, India

²Department of Chemistry, Dr. B R Ambedkar University, Agra-282001, India

KEYWORDS: Size Segregated Particulate Matter, Cascade Impactor, Traffic Junctions, Agra Region

INTRODUCTION

Road transport is worldwide known as an important and constantly increasing source of air pollution. Pollution levels are universally higher in India compared to levels reported in Europe and North America, due to their meager economy and not enough financial investment for the control of urban air pollution. Over some years there has been an increase in urbanization and industrialization in India, by means of this it has a remarkable boost in the number and density of motor vehicles in India (Taneja et al., 2008). Amplified traffic has resulted in increased pollutant emissions and the corrosion of environmental quality and human health. It has been found that urban residents living near roadways experience higher exposure to motor vehicle emitted pollutants. Vehicles are estimated to account for 70% of the respective total pollution loads in major cities of India (Sharma et al., 2004). A number of pollutants such as Ozone, Nitrogen Dioxide (NO₂) and Carbon Monoxide (CO), Polycyclic Aromatic Hydrocarbons (PAHs), Volatile Organic Compounds (VOCs) and Particulate Matter (PM) are found in ambient air due to vehicle emission. Traffic being potential sources of both coarse and fine particles is often found to be more brutal than urban areas. Resuspended road dust generally augments the source of PM. The combustion process in diesel and gasoline engine contributes significantly to particulate matter, specially to particles with diameters smaller than 2.5 µm. Several epidemiological studies have suggested a statistical association between health effect and ambient fine particle concentrations. Exposure to air pollution is considered to be the world's largest environment health risk, causing an estimated seven million deaths each year, equivalent to one in eight deaths across the globe (World Health Organization, 2016). Information on pollutant load of size segregated study of particulate matter (PM_{2.5-1.0} and PM_{1.0-0.5}) is still sparse. The present study is aimed to providing information on the concentration level of PM at three different traffic junctions of Agra region.

METHODOLOGY

SITE DESCRIPTION

Sampling was carried out at traffic site on National Highway-2 (Agra-Delhi), to explore the trend of concentration on highway at GLA University, Mathura intersection (Highway traffic only). Khandari crossing, Agra (Mixture of city traffic as well as highway) and Iradatnagar (rural traffic) in Agra region.

SAMPLING AND ANALYSIS

PM Samples were collected in the month of December and January 2017-18 using Leland Legacy pump (SKC Inc. Eighty Four PA USA) with a two stage Sioutas Cascade Impactor with particle size cut points of 2.5 µm and 0.5µm. Calibration of the instrument was performed using a Drycal DC-2 calibrator (Bios International Corporation, NJ USA). In the study, PM samples were collected on 25 mm PTFE (Poly Tetra Fluor Ethylene) filters with pore size 0.5 µm in two stage fractions (PM_{2.5-1.0}& PM_{1.0-0.5}). The instrument was mounted at six feet height above the ground level on tripod photographic stand. Pump was operated at 9 liters per minute. Total of fifty-four samples were collected as per the guidelines of National Ambient Air Quality Standards. Utmost care was taken for filter preparation, sample collection, and gravimetric analysis

of the filter papers. The standard procedures (USEPA, 1998) were followed for handling and preparation of filters for sampling and analysis. The pre- and post-weights of the filters were recorded using a microbalance (Contech analytical balance Model No CAI-35). The PM concentration was calculated by dividing the difference in pre- and post-weight of filters by the sampled air volume (Rohra et al., 2018). The ambient parameters like carbon dioxide and temperature were measured on the sampling site using Handy Air Quality monitor (TELAIRE).

RESULTS & DISCUSSIONS

The average mass concentrations at all three different traffic junctions are shown in Fig 1. The size fraction of PM_{2.5-1.0} was found higher at Iradatnagar (Rural traffic site) (518.55±205µg/m³) followed by Khandari Site (Urban site) (493.28±205.11µg/m³) and GLA traffic site (NH-2) (421.92±171.28µg/m³) respectively. In rural areas, combustion of agricultural residue and wood burning during winter season is an important source of exposure to air pollutants. Whereas average mass concentration for size fraction

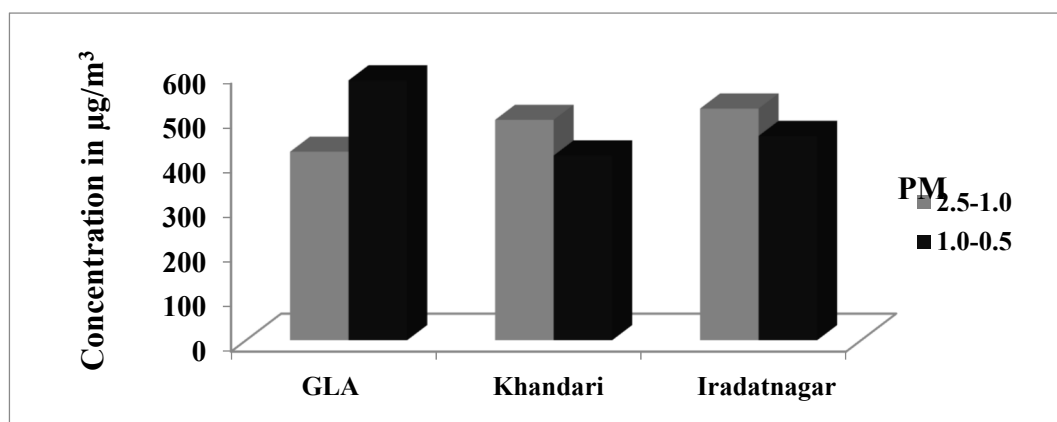


Fig 1: Comparison of Average Mass concentration of PM in different sampling site.

PM_{1.0-0.5} was found higher at Khandari (581.65±70.08µg/m³) in comparison to GLA (457.41±225.48µg/m³) and Iradatnagar (413.47±141.51µg/m³). The high levels of PM are due to vehicular traffic, industrial emissions, road and soil dust, ongoing constructional activities, municipal wastes incinerations and other industrial activities. The average PM_{2.5} concentration at all sampling sites were found higher 7-8 times than National Ambient Air Quality Standards (NAAQS) (60 µg/m³). Our results were approximate 1.2 times higher than other earlier studies 361.1±251.8µg/m³ (Goyal and Khare 2009), 313±181µg/m³ (Das et al., 2011) done at traffic intersections.

CONCLUSIONS

Highest average value for size fraction of PM_{2.5-1.0} was found higher at Iradatnagar (Rural traffic site) followed by Khandari Site (Urban site) and GLA traffic site (NH-2). Whereas highest average value for size fraction of PM_{1.0-0.5} was found higher at Khandari traffic site followed by GLA site and Iradatnagar traffic site. This study presented very high average concentration of PM at all ambient sampling sites, depicting the severity of particulate pollution at road site which has direct implications to high exposure and related health effect.

REFERENCES

Das, R., Khezri, B., Srivastava, B., Datta, S., Sikdar, P. K., Webster, R. D., & Wang, X. (2015). Trace element composition of PM_{2.5} and PM₁₀ from Kolkata-a heavily polluted Indian metropolis. *Atmospheric Pollution Research*, 6(5), 742-750.

Goyal, R., & Khare, M. (2009). Indoor-outdoor concentrations of RSPM in classroom of a naturally ventilated school building near an urban traffic roadway. *Atmospheric Environment*, 43(38), 6026-6038.

Rohra, H., Tiwari, R., Khandelwal, N., Taneja, A (2018). Mass distribution and health risk assessment of size segregated particulate in varied indoor microenvironments of Agra, India – A case study. *Urban Climate* 24 139-152.

Sharma, N., Chaudhary, K.K., Chalapati Rao, C.V., (2004). Vehicular pollution prediction modeling: a review of transport dispersion models. *Transp. Rev.* 24 (4), 409-435.

Taneja, A., Saini, R., Masih, A., (2008). Indoor air quality of houses located in the urban environment of Agra, India. *Ann. N. Y. Acad. Sci.* 1140(1),228-245.

USEPA (U.S. Environmental Protection Agency), (1998) Quality assurance guidance document 2.12: monitoring PM_{2.5} in ambient air using designated reference or class I equivalent methods. National Exposure Research Laboratory, Research Triangle Park, NC.

WHO, (2016). 7 million premature deaths annually linked to air pollution. World Health Organization, Geneva, Switzerland Access at. <http://www.who.int/mediacentre/news/releases/2014/air-pollution>.

RESPONSE OF INDIAN SUMMER MONSOON RAINFALL TO DUST AEROSOLS OF WEST ASIAN ORIGIN AT CLIMATOLOGICAL SCALE

CHARU SINGH¹, DILIP GANGULY², PUNEET SHARMA², SHIWANSHA MISHRA²

¹Indian Institute of Remote Sensing, ISRO, Dehradun - 248001, India

²Centre for Atmospheric Sciences, IIT Delhi, Hauz Khas, New Delhi-110016, India

KEYWORDS: ISM, ENSO, IOD, aerosols, dust, west Asia

INTRODUCTION

Indian summer monsoon (ISM) is one of the most important climatological phenomenon in tropical region, which hosts one of the most populated regions of the world and substantially affect the economy of this region because of the direct relationship of amount of rainfall during monsoon season with the agriculture yield. ISM rainfall substantially modulated by various factors such as sea surface temperature (SST), El Nino Southern Oscillation (ENSO), Indian Ocean Dipole (IOD), Eurasian snow cover (ESC) and North Atlantic oscillation (NAO). Previous studies have shown that the aerosol loading in and around Indian subcontinent region modify the variability of ISM rainfall (Ramanathan et al., 2005; Lau et al., 2006; Wang et al., 2009; Ganguly et al., 2012 a & b etc). Amongst all aerosol species dust is one of the most abundant sources of the suspended atmospheric particles. Gautam et al. (2009) and Kuhlmann and Quaas (2010) suggested that during the pre-monsoon and monsoon seasons Arabian sea witnesses high aerosol loading due to the presence of suspended dust particles in the atmosphere, which transported from western regions through long range transport. Later on Ginoux et al. (2012) concluded the fact that natural dust contributes about 75% of the total aerosol emission across the globe. Some of the recent studies have brought out the fact that the dust aerosols substantially modulated the rainfall over the Indian region (Vinoj et al, 2014; Jin et al., 2014, 2015 Singh et al. 2017 Singh et al., 2018a & b). West Asian regions such as Saudi Arabia, Arabian Peninsula, middle East, Iraq and Iran etc are amongst some of the potential dust source regions and reportedly have strong relationship with the ISM rainfall at short term scale of about two weeks or less (Vinoj et al, 2014; Jin et al., 2014, 2015), during JJAS (Singh et al. 2017, Singh et al., 2018a & b and references therein). In the present study role of dust aerosols emitted over the west Asian region in modulating ISM rainfall is studied using a climate slab ocean model CESM-SOM at climatological scale.

DATA SETS

Community Earth System Model (CESM 1.1.2) developed by National Centre of Atmospheric Research (NCAR) is used in this study in a coupled Atmosphere slab ocean mode (denoted as CESM-SOM). For the purpose to address only dust aerosols, CESM-SOM simulations are carried out for pre- industrial (PI) time period. Century long CESM-SOM simulations for three different experiments viz; control experiment (PI-CNT), zero dust emissions over west Asia (DST0X-WA) and double dust emission over west Asia (DST2X-WA) have been carried out to unravel the response of ISM rainfall to variable dust emissions over west Asia. For the analysis purpose model simulated data sets are analysed for dust suppression and enhancement experiments in comparison to PI control experiments (PI-CNT). Results are analysed both qualitatively and quantitatively. Central Indian (CI) region is selected to analyse response of ISM rainfall to west Asian dust aerosols considering the fact that the central Indian region is one of the sufficiently large homogenous regions wherein mean monsoon rainfall and standard deviation of rainfall during monsoon season do not vary considerably (Goswami et al., 2006).

RESULTS

Figure 1 shows the difference in the total precipitation (PRECT) pattern obtained after subtracting PI-CNT from the different dust experiments respectively. It is noted from the Figure 1 that the suppression of the dust emission over the west Asia (WA) region, substantially reduces the monsoon season rainfall over the land and oceanic regions of India in comparison to the PI-CNT experiment, whereas increase of the dust emission by double fold over the west Asia results in an increase of 0.20 to 0.40 mm/day (i.e. equivalent to 24.4 to 48.8 mm in a season) in rainfall during the monsoon season over the parts of the Southern Peninsula of India, central India (Madhya Pradesh (MP), Chhattisgarh, Bihar, Jharkhand, and Uttar Pradesh (UP)), West Bengal (WB), Uttarakhand (UK), and surrounding oceanic regions. It is also noted that the increased (decreased) dust emission over the WA region suppresses (reduces) the rainfall over the North-East Indian (NEI) region.

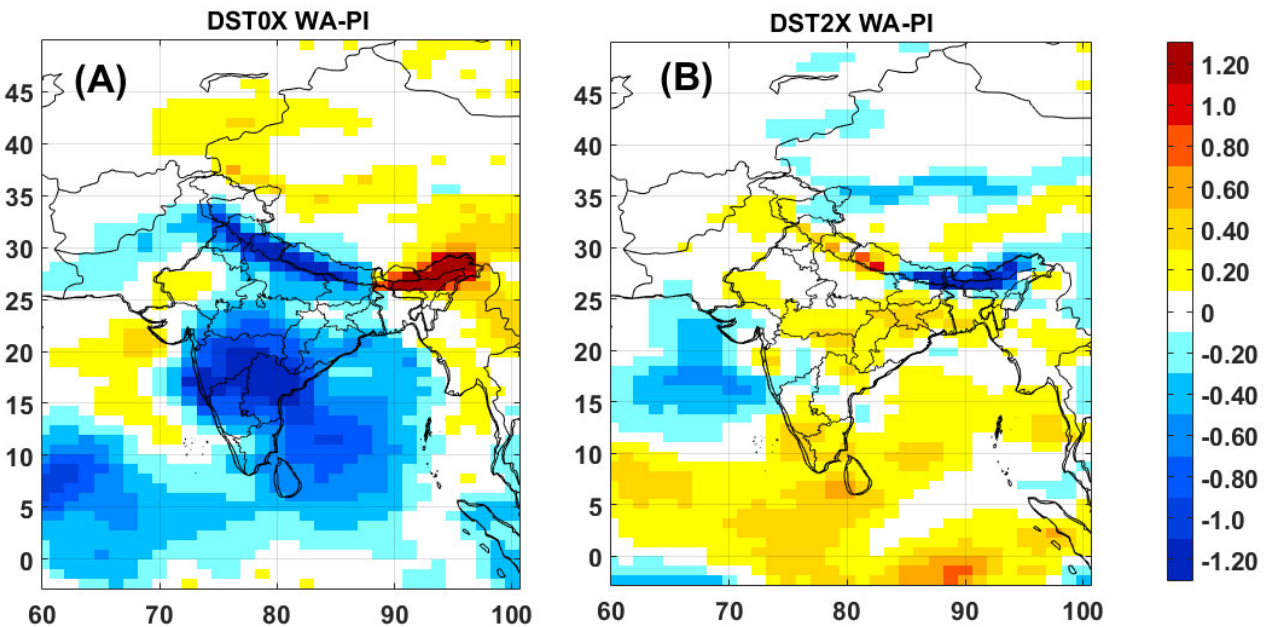


Figure 1: Difference in the precipitation during monsoon season (JJAS). (A) Difference in precipitation between the dust zero on the West Asia experiment and the PI-CNT experiment. (b) Same as (A) but for the dust double over the West Asia experiment. Difference is plotted for the long term mean rainfall during monsoon season. Colorbar indicates difference in precipitation in mm/day.

Present results suggest a strong relationship of the ISM rainfall with the amount of dust available in the atmosphere of the west Asia. These results are in concurrence with the extensive study carried out by Singh et al. (Jin et al, 2014; Singh et al., 2017 Singh et al., 2018 a & b). It is also noted from Figure 1 that the suppression of dust over the WA also affects the intensity of rainfall over the China region. Vinoj et al. (2014) based on the model simulations with dust emission on and off across the study region suggested that the dust induced increase in the rainfall primarily noted on the south and central India. Whereas Jin et al. (2015) mentioned that the maximum impact of dust on the Indian summer monsoon rainfall is noted over the Indo-Gangetic Plane (IGP) followed by Pakistan region and all India except South India. Lagged correlation between the dust load over the west Asian region (WA) for all the three experiments and the rainfall over the central Indian region (the same as taken in Singh et al. (2017) for JJAS are estimated separately and shown in the Figure 2. It is noted from the figure that in PI-CNT experiment dust load over the WA leads rainfall over central India by 20 days. When the dust emission over the WA region suppressed to zero (DST0X-WA) the lagged relationship between dust emission over WA and rain over central India

gets slow down to 40 days with reduced correlation. Lagged relationship between dust load over WA and rainfall over central India under the dust doubling experiment over the AP region (DST2X-AP) found to be same as that of the PI-CNT experiment.

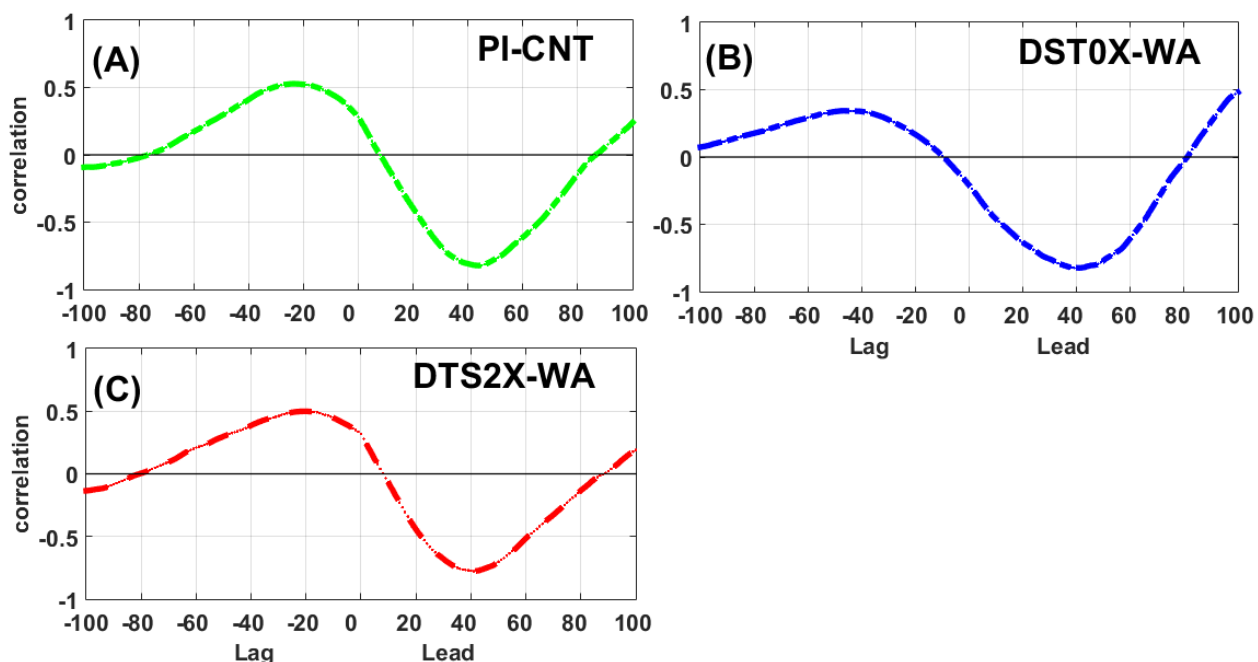


Figure 2: (A) Lagged correlation estimated for the dust load over the West Asia (WA) with the rainfall over the central Indian region during monsoon season for the PI-CNT experiment. (B) Same as (A) but for zero dust emission experiment over the West Asia (WA). (C) Same as (A) but for double dust emission experiment over the West Asia (WA). X-axis indicates lead –lag at daily scale and Y-axis shows the correlation coefficient

CONCLUSIONS

Using climate model CESM1-SOM dedicated simulations are carried out to study the response of the ISM rainfall to west Asian dust aerosols at climatological scale. Three different experiments are designed for pre-industrial time period to bring out the impact of natural dust aerosols only on ISM rainfall. Unlike previous studies, dust emissions over west Asia are perturbed by changing the dust emissions to zero and double for the completeness of the ongoing research on this theme. As reported earlier there is a strong relationship between the dust emission over the West Asia region and ISM rainfall variability, present study strongly supports the same based on the present set of the model simulations. Dust suppression over WA region slow down the temporal relationship between the dust aerosols over WA and rainfall over CI. Results obtained from the present study are encouraging, detailed analysis of the microphysical and radiative impact of dust aerosols on the ISM rainfall will be carried out in future to bring out the physical mechanism to explain this observed relationship.

ACKNOWLEDGEMENTS

First author acknowledged the support and encouragement provided by Group Head, MASD, Dean Academics and Director IIRS to carry out the present research work. CESM-SOM model simulations are carried out on High Performance Computing (HPC) facility of IIT Delhi. We thankfully acknowledged HPC facility of IIT Delhi.

REFERENCES

Ganguly, D., Philip J. Rasch, Hailong Wang, and Jin-ho Yoon (2012a), Fast and slow responses of the South Asian monsoon system to anthropogenic aerosols, *Geophys. Res. Lett.*, 39, L18804, doi:10.1029/2012GL053043.

Ganguly, D., Philip J. Rasch, Hailong Wang, and Jin-ho Yoon (2012b), Climate response of the South Asian monsoon system to anthropogenic aerosols, *J. Geophys. Res.*, 117, D13209, doi:10.1029/2012JD017508.

Gautam R., Hsu N. C., Lau K. M., and Kafatos, M. (2009). Aerosol and rainfall variability over the Indian monsoon region: distributions, trends and coupling. *Ann. Geophys.*, 27, 3691–3703.

Goswami B. N., Venugopal, V., Sengupta, D., Madhusoodanan, M. S., and Xavier, P. K (2006). Increasing trend of Extreme Rain Events over India in a Warming Environment, *Science*, 314, 1442–1445.

Jin, Q., Wei, J., Yang, Zong-Liang (2014). Positive response of Indian summer rainfall to Middle East dust. *Geophys. Res. Lett.* Doi: 10.1002/2014GL059980.

Jin, Q., Wei, J., Yang, Zong-Liang, Pu, B., and J. Huang (2015). Consistent response of Indian summer monsoon to Middle East dust in observations and simulations. *Atmos. Chem. Phys.*, 15, 9897–9915, 2015. doi:10.5194/acp-15-9897-2015

Kuhlmann, J., and Quaas, J. (2010). How can aerosols affect the Asian summer monsoon? Assessment during three consecutive pre-monsoon seasons from CALIPSO satellite data, *Atmos Chem Phys*, 10 (10), 4673-4688, doi:10.5194/acp-10-4673-2010.

Lau, K. M., Kim, M. K., and Kim, K.M. (2006). Asian summer monsoon anomalies induced by aerosol direct forcing: the role of the Tibetan Plateau, *Clim Dynam*, 26, 855-864, doi:10.1007/s00382-006-0114-z.

Ramanathan, V., et al. (2005). Atmospheric brown clouds: Impacts on South Asian climate and hydrological cycle, *Proceedings of the National Academy of Sciences of the United States of America*, 102 (15), 5326-5333, doi:10.1073/pnas.0500656102.

Singh, C., Ganguly, D., Dash, S. K., 2017a. Dust load and rainfall characteristics and their relationship over the South Asian monsoon region under various warming scenarios. *J. Geophys. Res. Atmos.*, 122, doi:10.1002/2017JD027451.

Singh, C., Ganguly, D., Dash, S. K., 2018a. On the dust load and rainfall relationship in South Asia: an analysis from CMIP5. *Climate Dynamics*, 50, pp. 403-422. <https://doi.org/10.1007/s00382-017-3617-x>.

Singh, C., Ganguly, D., Dash, S. K., 2018b. Investigation of the relationship between natural aerosols and Indian summer monsoon rainfall using a climate model, *Climate Change Impacts (Chapter -11)*, Water Sci. Technol. Library, Springer, Vol -82, Springer, Singapore, ISBN-978-981-10-5713-7.

Vinoj, V. et al. (2014). Short-term modulation of Indian summer monsoon rainfall by West Asian dust. *Nature Geoscience*, 7, 308–313, doi:10.1038/ngeo2107.

Wang, C., D. Kim, A. M. L. Ekman, M. C. Barth, and P. J. Rasch (2009), Impact of anthropogenic aerosols on Indian summer monsoon, *Geophys. Res. Lett.*, 36, L21704, doi:10.1029/2009GL040114.

AEROSOL VERTICAL TRANSPORT STUDIES DURING THE PRE-MONSOON OF 2011 OVER KANPUR

DAVENDER SETHI^{1,2}, CHHEMENDRA SHARMA², RADHAKRISHNAN S. R², JASWANT^{1,2},
SUMIT KUMAR MISHRA²

Academy of scientific and innovative research (acsir) at campus of CSIR-NPL, New Delhi 110012.

Council of scientific and industrial research (CSIR), National Physical Laboratory (NPL), New Delhi
110012.

KEYWORDS: Dust, IGP, Backscatter Coefficient, Extinction Coefficient, AOD, AAE

INTRODUCTION

In pre-monsoon repeated dust storms have been experienced in Central Indo- Gangatic Plain (IGP) mainly Kanpur. Numerous studies have been done for optical and chemical properties of aerosols over the IGP and Kanpur Region using the in-situ and remote sensing techniques. The studies on vertical profile of aerosols over the IGP are sparse. The range resolved values of the parameters like extinction coefficient, and backscatter coefficient are usually used in various atmospheric and numerical models for the estimation of radiative forcing. The lidar gives high spatially and temporally resolved data of various optical properties of aerosols and clouds. This data further helps in reducing the uncertainty involved in the radiative forcing. We can investigate various turbulent processes and the long range transport using Lidar. Through this technique atmospheric stability, thermodynamics of the lower troposphere can be studied. In the present study micro pulse lidar (MPL) has been used at 532nm wavelength channel. Ghosh et al. had studied the aerosols chemical properties during the summer 2011. Present study has been carried out to fill gap in line with earlier study of (Ghosh et al. 2014) during pre-monsoon 2011 over Kanpur. Gosh et al ., 2014 has reported (1 May ,25 May and 28 May) as high dust load days .

Earlier(Gautam, Hsu, and Lau 2010; Komppula et al. 2012; Sarangi et al. 2016; Srivastava et al. 2014, 2018) had studied the vertical profile of aerosols over IGP. Studies the vertical profiles of the aerosols are still sparse over IGP.

In the present work, aerosol backscatter profiles for the month of May in 2011 has been analysed . The variations of the backscatter coefficient of Lidar profile indicates that there was strong dust event on 25 May 2011. In this study the daily average half hourly profile for May 2011 (total 13 profiles) has been analysed. As the representative profile for the month of May, average half hourly monthly profile has been analysed. Various aerosols optical properties such as aerosols optical depth (AOD), aerosols angstrom exponent (AAE) with aerosol size distribution for the dust period has been studied. For the aerosol source identification study, back trajectory analysis has been done. Results shows that dust was originating from desert region of the country.

METHODS

MPLNET level 2 data is quality assured and calibrated data obtained from strict screening criteria. Data from MPLNET are available only during daytime because it uses the AERONET AOD product as a constraint in its algorithm.

In the present work, total 13profiles has been analysed for Micro-pulse lidar network version 2.0 data available from <https://mplnet.gsfc.nasa.gov> for the period May during 2011 over the Kanpur site. Further the aerosol optical depth, and aerosol angstrom exponent has also been analysed during month taken from AERONET site. Lastly, aerosol size distribution data has been used to study modes of aerosols during event.

RESULTS AND DISSCUSION

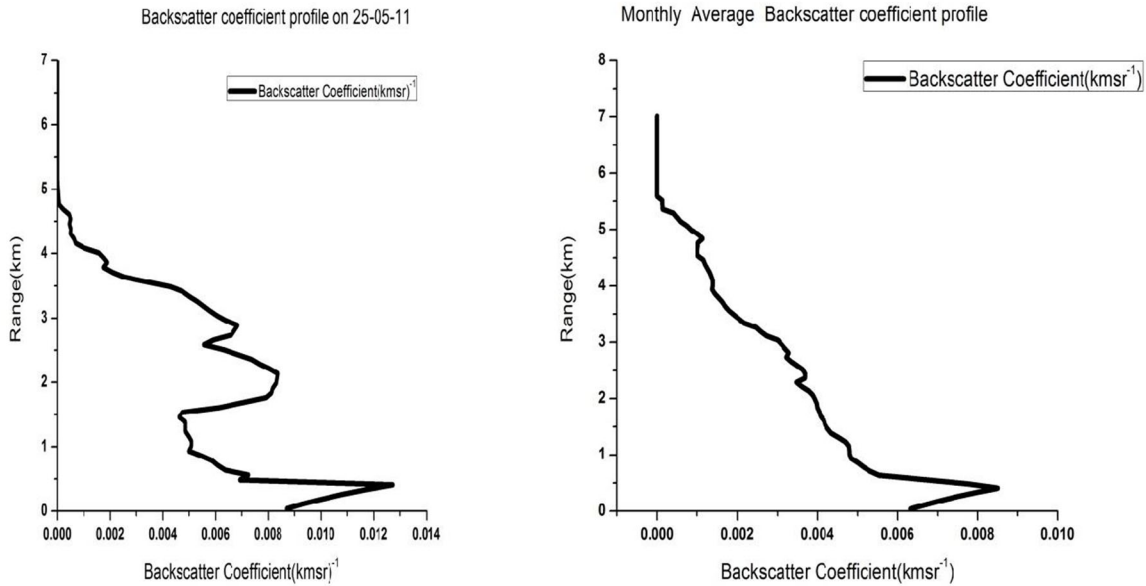


Figure 1. (a) Backscatter Profile for dust storm day (b) Monthly average backscatter profile of MAY,2014

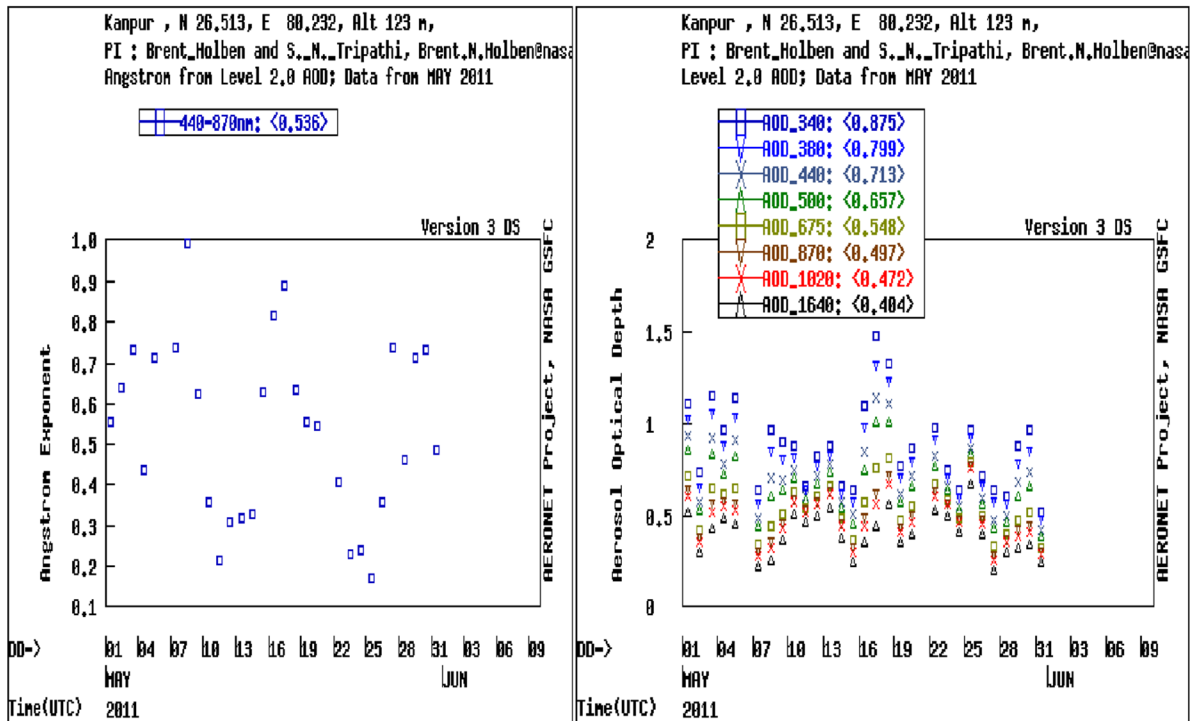


Figure 2 . Daily average variation of (a) Angstrom Exponent (b) Aerosol optical depth

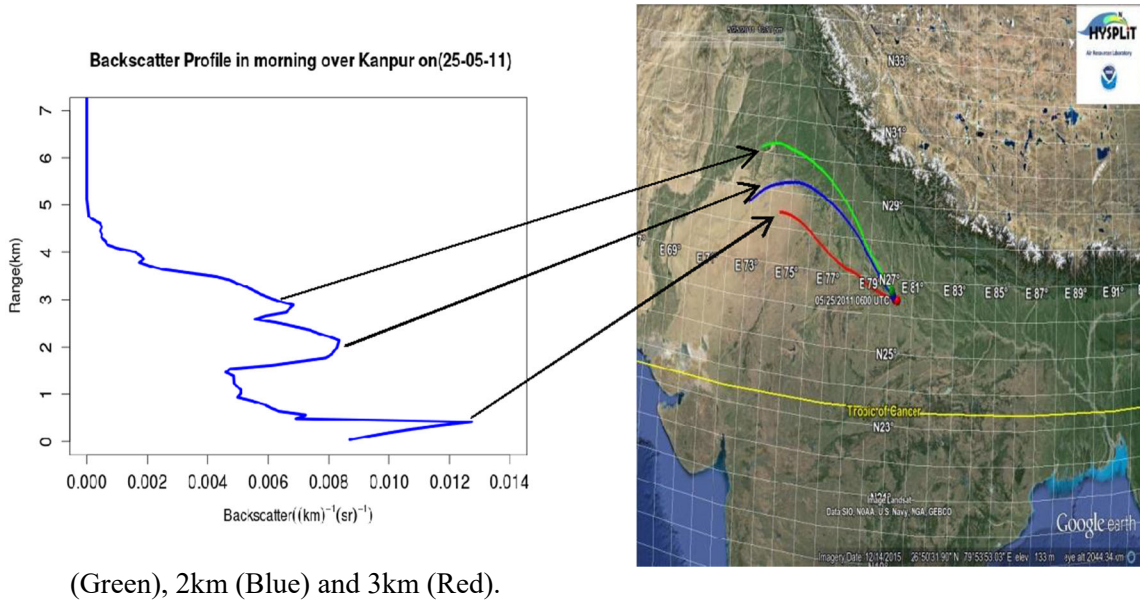


Figure 3.(a) Backscatter profile during the high dust load day (b) HYSPLIT 72 hourly back trajectory at 3km

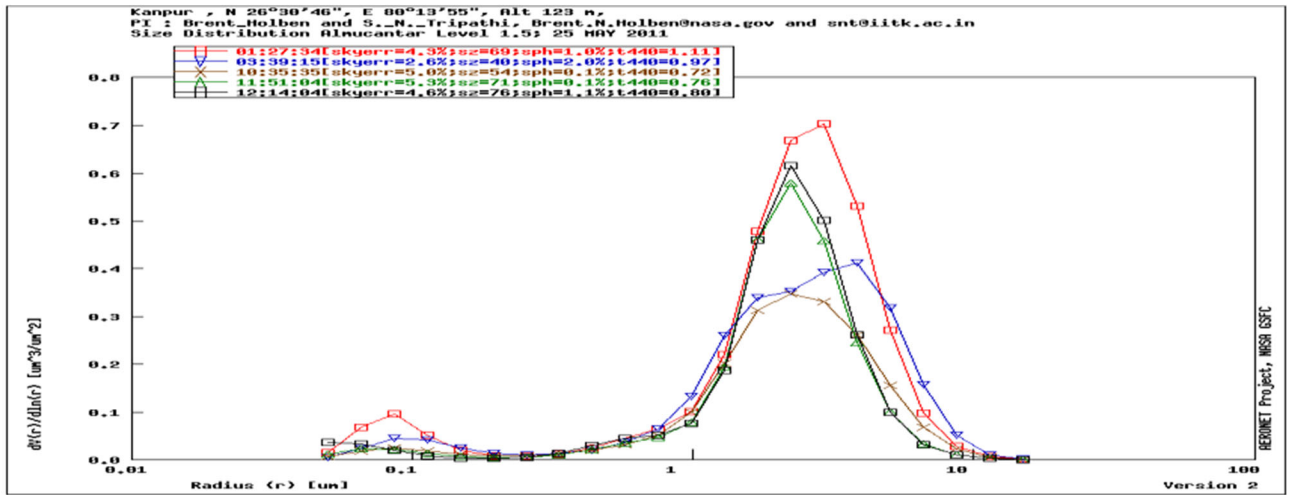


Figure 4 Shows the aerosol size distribution during the dust storm day

The results in figure 1(b) shows the backscatter profile of the particles during the May, 2011 over Kanpur. The results shows that backscatter values are high i.e. $0.008 \text{ (kmsr)}^{-1}$ in lower altitude ($\sim 500\text{m}$) . The value reaches to its half between 3-4 km. Figure (a) shows the high dust load day i.e. 25th May, 2011. During dust storm day aerosol optical depth also reaches to significant value of 0.7 in figure 2(b). The aerosol angstrom coefficient in figure 2(a) also reaches to very low value of 0.3 which indicated presence of coarse type particle during dust storm day. Aerosol size distribution further shows the clear bump in figure 4(a) variation indicates coarse mode of the particles during the high dust load day. Back trajectory analysis shows that transport from the desert part of the country. From the above study we can conclude the various aerosol properties changes significantly during dust storm day. The variation in the profile indicates the long range transport from the desert area of the country.

ACKNOWLEDGEMENTS

This work was supported by Council of Scientific and Industrial Research the CSIR Network Project under IGPHIM grant PSC-0112. Authors kindly acknowledge the AERONET data site PI's Dr. S.N Tripathi and Dr Holben for providing the useful lidar and aerosol optical properties data. The authors kindly acknowledge the financial support from CSIR Network Project PSC-0112 for project fellowship to DS. We are very thankful for the NOAA online software for providing HYSPLIT back trajectory analysis results.

REFERENCES

- Gautam, Ritesh, N. Christina Hsu, and K. M. Lau. 2010. "Premonsoon Aerosol Characterization and Radiative Effects over the Indo-Gangetic Plains: Implications for Regional Climate Warming." *Journal of Geophysical Research Atmospheres* 115(17):1–15.
- Ghosh, Subhasish, Tarun Gupta, Nikhil Rastogi, Abhishek Gaur, Amit Misra, Sachchida N. Tripathi, Debajyoti Paul, Vinod Tare, Om Prakash, Deepika Bhattu, Anubhav K. Dwivedi, Daya S. Kaul, Rosalin Dalai, and Sumit K. Mishra. 2014. "Chemical Characterization of Summertime Dust Events at Kanpur: Insight into the Sources and Level of Mixing with Anthropogenic Emissions." *Aerosol and Air Quality Research* 14(3):879–91.
- Sarangi, Chandan, S. N. Tripathi, A. K. Mishra, A. Goel, and E. J. Welton. 2016. "Elevated Aerosol Layers and Their Radiative Impact over Kanpur during Monsoon Onset Period." *Journal of Geophysical Research* 121(13):7936–57.
- Srivastava, Parul, Sagnik Dey, P. Agarwal, and George Basil. 2014. "Aerosol Characteristics over Delhi National Capital Region: A Satellite View." *International Journal of Remote Sensing* 35(13):5036–52.
- Srivastava, Parul, Sagnik Dey, Atul Kumar Srivastava, Sachchidanand Singh, and Suresh Tiwari. 2018. "Most Probable Mixing State of Aerosols in Delhi NCR, Northern India." *Atmospheric Research* 200(October 2017):88–96.

POLYCLIC AROMATIC HYDROCARBONS (PAHs): CHARACTERIZATION, DISTRIBUTION AND SOURCE MARKERS FOR AGRA (TAJ CITY), U.P., INDIA

J. DUBEY, P. K. VERMA, D. SHAH, K. M. KUMARI, A. LAKHANI*

Department of Chemistry, Faculty of Science, Dayalbagh Educational Institute, Dayalbagh, Agra (U.P.).

KEYWORDS: AGRA, PM_{2.5}, TRAFFIC, PAHs, SOURCE APPORTIONMENT, SUMMER SEASON

INTRODUCTION:

Nowadays pollution is a great problem over the world. Pollutants exist as gas and particulate phase in form of particulate matter, NO_x, SO_x, CO, NH₃, OC, EC and PAHs etc. Fine particles have more adverse health effects than coarse particles for living being. One of these pollutants, Polycyclic aromatic hydrocarbon (PAHs) have great mutagenic and carcinogenic potential with a fused ring structure containing at least two benzene rings. PAHs are also entered in atmosphere by incomplete combustion and or pyro-synthesis of organic material including natural and anthropogenic emissions. United States Environmental Protection Agency (USEPA) has already identified some PAHs as possible or probable carcinogens. In particular, Benzo(a)pyrene (BaP) has been identified as probable carcinogenic for human and animal. The carcinogenic potential of BaP has been frequently studied through epidemiological findings and animal testing. Toxic equivalency factors (TEFs) for PAHs were purposed by Nisbet and Lagoy, 1992. Several other studies reveal that urban areas are more polluted due to increasing industrialization, vehicular traffic and low dispersion of the atmospheric pollutants. So this study for fine particulate (PM_{2.5}) was carried out at traffic dominated site of Agra with aimed to:

Determination of mass concentration and distribution of PM associated PAHs in PM_{2.5}.

PAH source identification, which helps as tool of pollution emission sources.

MATERIAL AND METHODS:

Agra is situated on 26° 44'N to 27° 25'N and 77° 26'E to 78° 32'E at the banks of river Yamuna in Indo Gangetic plain of India. PM_{2.5} samples were collected on glass microfiber filters (47 mm diameter) on the roof of Queen Victoria Girls Inter College, Agra using fine particulate sampler (APM 550). The site was situated at junction of Raja Ki Mandi, Agra to Lucknow railway track and Mahatma Gandhi road, Agra. All collected samples were again desiccated and weighed till constant weight. All samples were placed in polyethylene zip-lock bags to avoid any contamination. Before analysis, the filters were extracted ultrasonically in Dichloromethane (DCM) and cleaned through column chromatography. Rotary evaporator was used for concentrate and reduces of extracts. All reduced extracts were stored in a Teflon vial at a low temperature until analysis. PAHs were analyzed by Gas Chromatograph (GC, Shimadzu 17AATF, version 3.0) equipped with a Flame Ionization detector (FID) and capillary column. Nitrogen was used as carrier gas. Standard solution of 16 PAH compounds (Supelco EPA 610 PAH mixture) was used for calibration of GC. Regression analysis was applied by five point calibration curves. The compounds Phenanthrene and Anthracene, Chrysene and benzo(A)anthracene, Benzo(b)fluranthrene (BbF) and Benzo(k)fluranthrene (BkF), co-elute. Therefore in the present study these pair of compounds has been reported as their sums. Results were depicted by computational interpretation.

RESULTS AND DISCUSSION:

MASS CONCENTRATION:

Table 1 depicts the mean (geometric) concentrations of PM_{2.5} mass and associated PAHs observed at this site during summer period along with a comparison with National Ambient Air Quality Standards (NAAQS) and the World Health Organization guidelines. The average PM_{2.5} was 46.52±0.8 µg/m³, almost three times higher than the annual average NAAQ standard of 15 µg/m³ for PM_{2.5} mass (NAAQS, 2009;

www.cpcb.nic.in) while the 24-h PM_{2.5} mass concentration ranged from 8.1 to 217.9 µg/m³ with 40% of the values exceeding the 24-h average NAAQ standard of 65µg/m³ (<http://www.cpcb.nic.in/National Ambient Standard.php>). PM_{2.5} concentration was found lower than Chennai (50 µg/m³, Bathamanabhan & Mandanayak., 2010), Agra (100.5±1.6 µg/m³, Dubey et al., 2015) and higher than Zonguldak, Turkey (15.9 µg/m³, Akyuz and Cabuk., 2009) for summer season. Local primary emissions, meteorological parameters, wet and dry depositions, low level convergence *caused by surface heating*, rain fall and long ranged transport also responsible for lower particulate loadings in summer. A strong relationship was observed between PM_{2.5} and related ΣPAHs (R²=0.90). The concentrations of PAHs increased effectively with increasing PM_{2.5} mass concentrations. The same trend was observed by Dubey et al., 2015 for Agra.

DISTRIBUTION OF PAH

The mean concentrations value for individual PAH with % contribution at traffic site for Agra is present in Table 1. The average concentrations of PAHs associated with the particulate matter ranged from 11.5 to 335.9ng/m³ with an average of 2341.3±9.7ng/m³. The average value of ΣPAH was observed to be high with Agra (866.5±3.7 for Summer, Dubey et al., 2015), Delhi (1049.3 (Okhla), 1344.37 (Daryaganj), 1117.14 (Dhaulakuan), Sharma et al., 2008) and low with Riyadh, Saudi Arabia (5871±2830, El-Mubarak et al., 2014). In general, smaller particles have a higher PAH content. High concentration depends on nature of compound, available binding site on particle and numbers of particles. Abundance of Nap, Pyr, Fla and BbF+BkF was 54.91% of the total ΣPAHs. Present study reveals that Fla has maximum 14.3% contribution of ΣPAHs. Nap has 14.2% part of ΣPAHs. A keen attention reveals that 14.2, 29.6, 33.9, 21.8 and 0.5% of total ΣPAHs was accounted for 2, 3, 4 and 5 ringed PAHs respectively. Ravindra et al., 2006 have reported that 4 ringed PAHs are generated by coal combustion. Coal and wood are commonly used in leather and Petha industries at Agra which support to higher % contribution of 4 ringed PAHs. The abundance of 5 & 6 ring PAHs was also observed by Rajput & Lakhani., 2009 in ambient atmosphere of Nunhai, Agra. The presence of 5&6 ring PAH i.e. BaP, DbA, BghiP attribute to petrogenic source i.e. vehicular, diesel, gasoline and industrial emissions. IP was below detection limit (BDL).

PAHs	No of Rings	Mean ± SD	% Contribution
Naphthalene (Nap)	2	333.4±5.8	14.23
Acenaphthylene (Acy)	3	98.5±4.2	4.20
Acenaphthene (Ace)	3	169.1±7.3	7.22
Fluorene (Flu)	3	168.8±1.9	7.20
Phenanthrene + Anthracene (Phen +Anth)	3	257.9±2.7	11.01
Pyrene (Pyr)	4	296.3±5.6	12.65
Fluoranthene (Fla)	4	335.9±4.7	14.34
Benzo(a)anthracene + Chrysene (BaA +Chy)	4	160.5±3.4	6.85
Benzo(b)fluranthrene+Benzo(k)fluranthene(BbF+BkF)	5	320.6±2.9	13.69
Benzo(a)pyrene (BaP)	5	81.27±1.9	3.47
Indeno (1,2,3-c,d)pyrene (IP)	5	BDL	-
Dibenzo(a,h) anthracene (DbA)	5	107.6±1.1	4.59

Benzo(ghi)perylene (BghiP)	6	11.5±1.3	0.49
ΣPAH		2341.3±9.7	
PM_{2.5}		46.52±0.83*	

Table 1: Concentration (ng/m³) of PAHs in Fine Particles (PM_{2.5}). (SD =Standard Deviation, *µg/m³)

On other hand BaA, BaP, BbF, BkF, Chy, DbA and IP were investigated as probable carcinogens (CANPAHs) by IARC2006. In the same way Flu, Pyr, BaA, BaP, BbF, BkF, Chy, IP and BghiP are known as combustion derived PAHs (COMPAH) (Bourotte et al., 2005). % contribution for CANPAHs and COMPAHs was 28.6 and 44.3, respectively. 4, 5 and 6 ringed PAHs are dangerous to human health due to their carcinogenic nature. Among the PAHs, PM_{2.5}-related BaP was ranged from 12.0 to 484.6ng/m³ with an average of 81.27ng/m³ which exceeded 1ng/m³, the recommended Polish national standard and NAAQs. High BaP concentration was also observed for Nunhai (140ng/m³, Rajput and Lakhani, 2009), Delhi (86.61ng/m³ (Okhla), 86.50ng/m³ (Daryaganj), 88.26ng/m³ (Dhaulakuan), Sharma et al., 2008) and Riyadh, Saudi Arabia (400ng/m³, El-Mubarak et al., 2014).

SOURCE ESTIMATION

Diagnostic Ratios are used to characterize possible emission sources of PAHs. The presence of Ace, Pyr, Chy, Phen prove to coal combustion and occurrence of BbF supports to vehicular emission sources or heavy duty diesel vehicles. Acy, Ace, Flu, Phen and Anth are typically markers for coke production and presence of Pyr, BaA, Chy, BbF, BkF indicate to pyrogenic sources. Besides these IP, DbA and BghiP also marker of vehicular sources. The calculated value for Fla/(Fla+Pyr) and Fla/pyr ratio was 0.53 (>0.4) and 1.24(>1) which indicate towards pyrogenic sources (Yunker et al., 2002). Fla/(Pyr+Flu), LMW/HMW and ΣCOMPAH/ΣPAH also support to pyrogenic source. Here, the value for Flu/(Flu+Pyr) ratio was 0.36 (<0.5), indicates to gasoline contribution. The value for Pyr/Bap (3.64, in between of 2-6) and Flu/Pyr 0.57 (<1) ratios suggest traffic releasing, petroleum and wood burning as sources of PAHs (Yang et al., 2012). Different types of ratio conclude that this site is adversely affected by multiple and mixed sources i.e. pyrogenic and petrogenic sources like Gasoline, diesel oil burning and burning of fossil fuel. The contribution from vehicular exhaust and emission from combustion of domestic fuel like coal & wood is already reported for Agra by Singla et al., 2012 and Dubey et al., 2014b & 2015.

CONCLUSION

This study concludes that the sum of PAHs (2341.3±9.7 ng/m³) was observed higher than Agra, Delhi and lowers than Riyadh. It is an alarm and challenge for upcoming fearful future. The present observation shows that BaP concentration was 81 fold higher than the NAAQS standard limit of 1ng/m³. The LMW (2&3 ringed) PAHs accounted for 43.9% of the total PAHs while HMW PAHs (4, 5&6 ringed) accounted for only 56.1% of the total PAHs in PM_{2.5}. 4 ring PAHs i.e. Pyr, Fla and BaA+Chy contribute maximum part of total PAHs (33.9%). IP was not identified. A strong relationship was observed between PM and PM bounded PAHs. The ratios of individual PAH species i.e. Fla/Pyr, Flu/Pyr, Pyr/BaP, Fla/(Fla+Pyr), Flu/(Flu+Pyr), Fla/(Pyr+Flu), LMW/HMW and ΣCOMPAH/ΣPAH indicate Pyrogenic and petrogenic sources i.e. vehicle exhaust, gasoline and coal & wood combustion as possible sources at this site.

ACKNOWLEDGEMENT

The authors are grateful to the Director, Dayalbagh Educational Institute, Dayalbagh, Agra; Head, Department of Chemistry for facilities provided and Department of Science and Technology, DST project No.: SR/S4/AS:282/ 07, New Delhi, for financial assistance. Mr. Jitendra Dubey acknowledges UGC for Research fellowship for Meritorious students. We all are thankful to Principal, Queen Victoria Girls Inter College for providing a safe, convenient, suitable place for sampling and other facility at this site.

REFERENCES

- Akyuz, M. and H. Cabuk (2009). Meteorological variations of PM_{2.5}/PM₁₀ concentrations and particle-associated polycyclic aromatic hydrocarbons in the atmospheric environment of Zonguldak, Turkey. *Journal of Hazardous Materials*, **170**:13–21.
- Bathmanabhan, S. and S.N.S., Mandanayak (2010). Analysis and interpretation of particulate matter-PM₁₀, PM_{2.5} and PM₁ emission from the heterogeneous traffic near an urban roadways. *Atmospheric Pollution Research* **1**:184-194.
- Bourotte C., M.C., Fortic, S., Taniguchi, M.C., Bicego, P.A., Lotufo (2005). A winter time study of PAHs in fine and coarse aerosols in Sao Paulo city, Brazil. *Atmospheric Environment*, **39**:3799–3811.
- Dubey J., K.M., Kumari, A., Lakhani (2015). Chemical characteristics and mutagenic activity of PM_{2.5} at a site in the Indo-Gangetic plain, India. *Ecotoxicology and Environmental Safety* **114**:75–83.
- Dubey J., V., Singla, K.M., Kumari, A., Lakhani (2014b). Identification of Polycyclic Aromatic Hydrocarbons in Atmospheric Particles of PM₁₀ at Agra, India. *International Journal of Engineering and Technical Research* **2(8)**:210-215.
- El-Mubarak A.H., A.I., Rushdi, K.F., Al-Mutlaq, A.Y., Bazeyad, S.L.M., Simonich and B.R.T., Simoneit (2014). Identification and source apportionment of PAHs in ambient air particulate matter of Riyadh, Saudi Arabia. *Environmental Science and Pollution Research*, **21**:558–567.
- IARC (International Agency for Research on Cancer) (2006). IARC Monographs on the Evaluation of Carcinogenic Risks to Humans. 88. Formaldehyde, 2-Butoxyethanol and 1-tert-Butoxypropan-2-ol.
- NAAQS (National Ambient Air Quality Standards), (2009). *Ministry of Forest and Environment. Government of India, New Delhi.*
- Nisbet ICT. and PK., LaGoy (1992). Toxic equivalency factors (TEFs) for polycyclic aromatic hydrocarbons (PAHs). *Regulatory Toxicology and Pharmacology*, **16**:290–300.
- Rajput, N., and A., Lakhani, (2009). Particle associated Polycyclic Aromatic hydrocarbons (PAHs) in urban air of Agra. *Indian Journal of Radio & Space Physics*, **38**: 98-104.
- Ravindra K., L., Bencs, E., Wauters, J., Hoog, F., Deutsch, E., Roekens, N., Bleux, P., Berghmans, R., Grieken (2006a). Seasonal and site-specific variation in vapour and aerosol phase PAHs over Flanders (Belgium) and their relation with anthropogenic activities. *Atmospheric Environment*, **40**:771–785.
- Ravindra K, E., Wauters, S.K., Taygi, S., Mor, R., Van Grieken (2006b). Assessment of air quality after the implementation of CNG as fuel in public transport in Delhi, India. *Environmental Monitoring and Assessment*, **115**: 405–417.
- Sharma H., V.K., Jain & Z.H., Khan (2008). Atmospheric polycyclic aromatic hydrocarbons (PAHs) in the urban air of Delhi during 2003. *Environmental Monitoring and Assessment*, **147**:43–55.
- Singla V., T., Pachauri, A., Satsangi, K.M., Kumari and A., Lakhani (2012). Characterization and Mutagenicity Assessment of PM_{2.5} and PM₁₀ PAH at Agra, India *Polycyclic Aromatic Compounds*, **32**: 199–220.

Yang D., Q.I., Shihua, N.L., Devi, TIAN., Fang , HUO., Ziping, ZHU., Qingyuan, WANG., Jing, (2012). Characterization of polycyclic aromatic hydrocarbons in PM_{2.5} and PM₁₀ in Tanggu District, Tianjin Binhai New Area, China. *Front. Earth Sci.* **6(3)**: 324–330.

Yunker, M.B., R.W., Macdonald, R., Vingarzan, R.H., Mitchell, D., Goyette, S., Sylvestre (2002). PAHs in the Fraser River basin: a critical appraisal of PAH ratios as indicators of PAH source and composition. *Organ. Geochem.* **33**:489–515.

SIMULATION OF AN EXTREME DUST EPISODE USING WRF-CHEM

ANIMESH CHOUDHURY¹, SACHIN BUDAKOTI², CHARU SINGH¹

¹Indian Institute of Remote Sensing, ISRO, Dehradun – 248001, India

²IDP in climate science, IIT Bombay, Mumbai, India

KEYWORDS: Dust storm, Air quality, Arabian Peninsula, WRF-CHEM, dust emission

INTRODUCTION

Dust storms are natural phenomena that occur very frequently in the arid and semi-arid regions extending from 20°N to 30°N. This region usually experience low annual rainfall, low vegetation density, high solar radiation (Kalenderski et al., 2013; Namdari et al., 2018). Dust storm has several negative impacts on the human life as well as the environment such as reduced visibility, poor air quality, reduced solar radiation, reduced soil fertility etc. Arabian Peninsula is the second largest dust source after Sahara desert (Prospero, 2002; Washington et al., 2003). The major dust sources of the Arabian Peninsula are Tigris and Euphrates river valleys, the alluvial plain in Iraq and Kuwait, the low lying flat lands in the east of the peninsula along the Persian Gulf, Ad-Dahna desert, Rub-Al-Khali desert, An Nafud desert are the major sources of dust of the Arabian peninsula (Jish Prakash et al., 2015; Middleton, 1985). Better understanding and forecasting can minimize the adverse effects of the dust storm. In the present study, one of the extreme dust event occurred from 18 to 20 March 2012 over the Middle East region has been studied based on the model simulation so as to assess the potential of Weather Research Forecasting fully coupled with chemistry (WRF-Chem) in forecasting such an event well in advance. Model simulation has been carried out for 15 days with spatial resolution of 30 Km. It is noted from the model simulation that the storm has its effect over a larger area consisting Middle East, northern Africa, Afghanistan, Pakistan and some parts of northern India. Dust emission and its transportation both are well simulated by WRF-Chem. Simulated results are compared with the satellite and ground based observations (such as MODIS, MISR, AERONET and IIRS aerosol product) and show a good match. However, in some of the cases, over estimation of AOD and wind speed is noted. Time series analysis of the data sets reveals that the increased AOD values over different locations are due to the impact of dust storm over. Results also shows that the impact of this event over northern India (which is hundreds of kilometer away from its origin) are nicely captured, and air quality over this region was substantially affected due to the transportation of dust particles from Middle East to Indian region. Results from the present work are encouraging and model configuration may be utilized for dust forecasting well in advance.

METHOD

In this study a severe dust storm event that occurred during 17th to 20th march in the Arabian Peninsula has been chosen for the simulation. The study region selected for this work is shown in the Figure 1. We chose the extent of our study region keeping in mind the extent of the dust event. The study region confined the total movement of the dust particles. The model domain is centered on 25.18416°N and 60.3088°E extending from 5.45.74°N to 42.185°N (165 grid points) and from about 36.0069°E to 84.6107°E (140 grid points) with 24 vertical levels on a Mercator projection. Spatial resolution of the model is 30 km. NCEP final analysis (FNL) 6- hourly data with a spatial resolution of 1°×1° are used to provide the meteorological initial and boundary condition. The simulation is conducted from 15th March 2012 to 30th March 2012. In this study we have chosen Yonsei University (YSU) planetary boundary scheme to parameterize the boundary layer process. We have used RRTMG to represent longwave and shortwave transfer within the atmosphere and land surface. In the model we have used Lin microphysics scheme (Lin et al., 1983) which accounts for the non-convective precipitation process and the Grell convective scheme (Grell and Devenyi., 2002) which captures the cumulous cloud parameterization. 5 bin sizes has been used in our study which are 0.5-1 μm, 1.4-2 μm, 2.4-3 μm, 4-4.5 μm, 5-8.0 μm (Table 1) For biogenic emission MEGAN, for anthropogenic emission EDGAR, and for fire emission FINN emission inventories are used in this study.

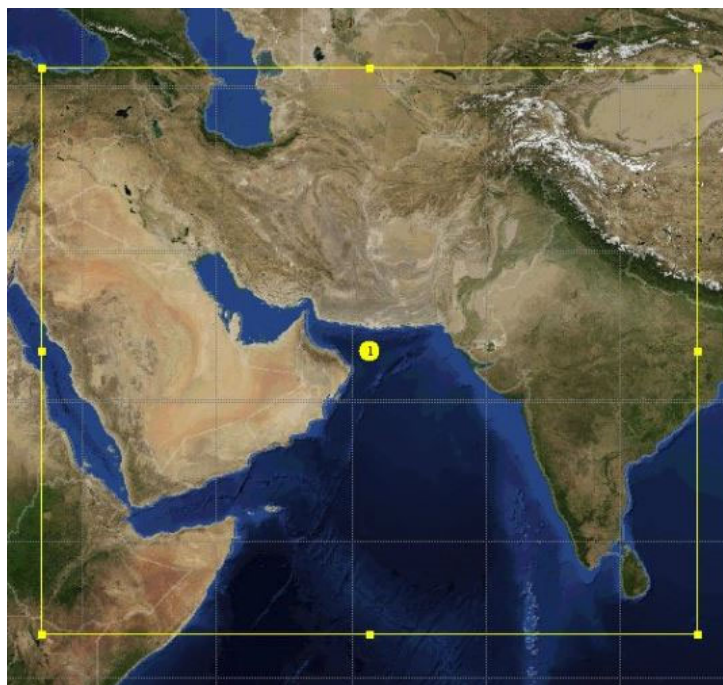


Figure 1: Study area

Horizontal resolution	30km
Centre lat/lon	25.18416N,60.3088E
Dimension (X,Y)	165,140
Vertical levels	24
Initial and boundary condition	NCEP final analysis FNL ($1^0 \times 1^0$)
Simulation period	15-30 March
Map projection	Mercator
Chemistry option	RADM2 chemistry with GOCART aerosol
Emission option	GOCARD RACM KPP emission
Biomass burn option	Include biomass burning emission and plume rise for MOZART
Dust option	AFWA dust scheme
Physical schemes	Microphysics: Lin et al. Schème (Lin et al., 1983)
	Cumulus convection: new Grell scheme (Grell and Devvenyi., 2002)
	Shortwave radiation option: RRTMG schème Longwave radiation option: RRTMG schème
	PBL:Yonsei University(YSU) planetary boundary layer scheme (Hong and Pan.1996)
Bin sizes	0.5-1 μm , 1.4-2 μm , 2.4-3 μm , 4-4.5 μm , 5-8.0 μm .

Table 1: Model configuration

RESULTS & DISCUSSIONS

Comparison between different AOD product and Model simulated AOD

Model simulated AOD has been compared with the combined (deep blue and dark target) aerosol product of MODIS Terra satellites, MISR AOD product and the merged aerosol product (IIRS). For all the datasets used for comparison, AOD is highest at the Arabian Peninsula region and it also shows its affects in the northern India (Figure 2). The model simulated AOD also shows its peak in the Arabia region and it also shows a high value over the northern India. Though the model overestimated the aerosol value at certain places but it captures the pattern very well.

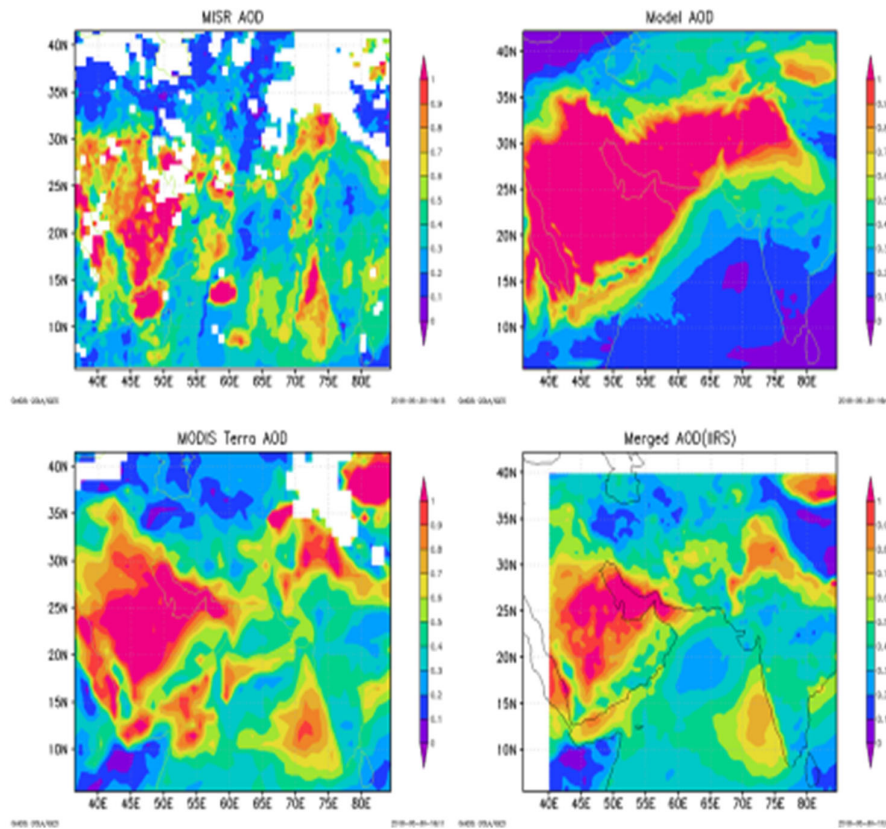


Figure 2: averaged aerosol product from 17th march to 27th march. top left-MISR AOD, top right-model AOD, bottom left-MODIS AOD, bottom right-merged AOD (IIRS)

Comparison between Model simulated wind and NCEP wind

The model simulated wind at 850hpa is compared with the NCEP wind of the same level. The direction of the wind is well matched but model overestimated the magnitude of the wind for most of the cases (figure 3). The reason behind the difference in magnitude of winds could be the difference in spatial resolution of the two data sets. It has been observed that the winds are approaching from the west directions and moving towards the east. From the figures it is evident that winds show persistent westerly flow with high magnitude over northern Arabian Peninsula and weak over the south part of Arabian Sea and Indian Ocean.

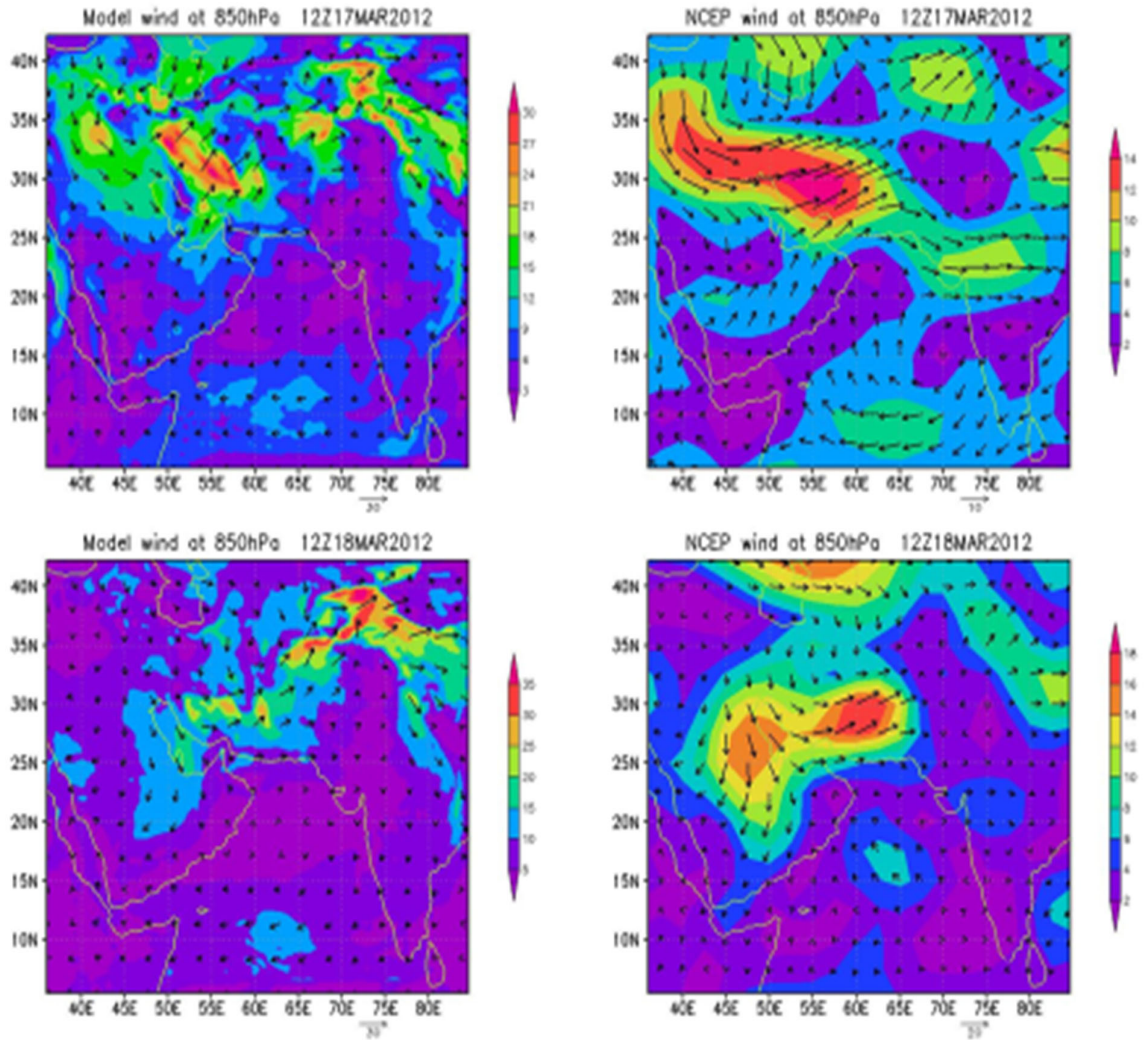


Figure 3: top left- model derived wind on 17th march, top right- NCEP wind on 17th march, bottom left- model derived wind on 18th march, bottom right- NCEP wind on 18th march. Winds are plotted at 12 UTC and at 850hPa. The arrows show the direction and shades show the magnitude.

Comparison between AERONET AOD and model AOD

AERONET data of Kaust Campus and Mezaira within our study region is compared with the model simulated AOD of that region. The change in AOD value in the month of March from AERONET observation and model derived AOD from 17th to 27th march for different places are shown in the Figure 4. The dust event hits the observation sites on different dates. Model captures the dust event quite well as it shows same pattern as shown by the AERONET observations. The best result is found at Kaust Campus where both the magnitude and the pattern are very close to the ground observation. In Mezaira the model

captures the pattern very well but it overestimates the magnitude of AOD.

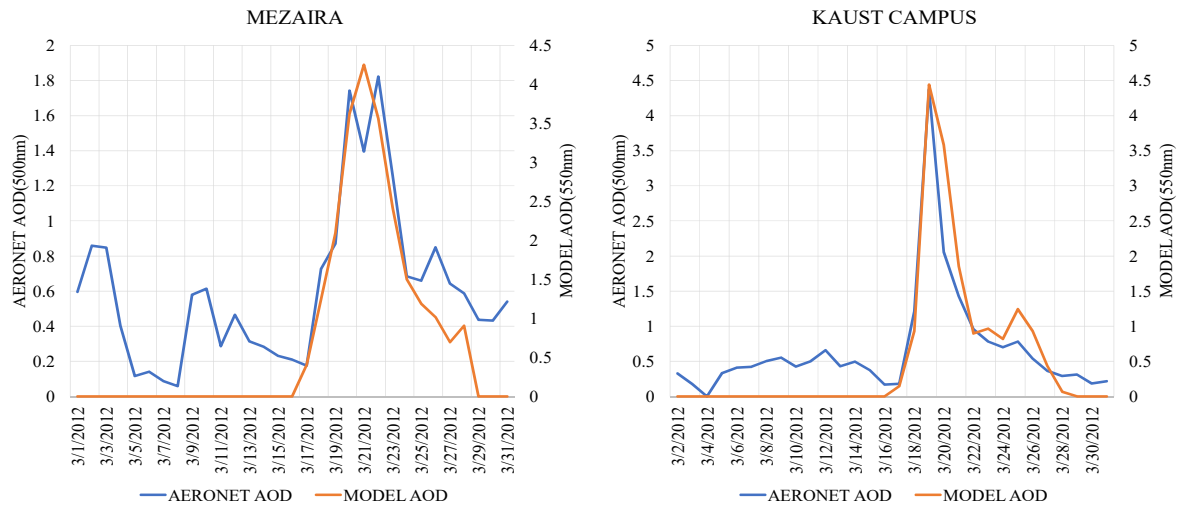


Figure 4: comparison between AERONET AOD and model derived AOD.

Comparison of pm2.5 between the Model and the CPCB observation

To understand the effect of the dust event on the air quality of Indian subcontinent, model simulated PM_{2.5} is compared with the Central Pollution Control Board (CPCB) PM_{2.5} of Mandir Marg, delhi (28.7041° N, 77.1025° E)(Figure 5). From the temporal variation of PM_{2.5}, it has been observed that the model overestimates the concentration of PM_{2.5} but able to capture the trend of change in the concentration of PM_{2.5} with respect to time. High value of PM_{2.5} has been observed for both of the datasets. The overestimation of the model simulated values may be due to the overestimation of the simulated winds.

CONCLUSION

Present study is based on the simulation of an extreme dust episode which was originated over the Middle East region. From the result, it is noted that WRF-Chem has a great potential to simulate severe dust events well in advance. Transportation of the dust particles is nicely captured by WRF-Chem. It is noted that the dust storm approached the Indian subcontinent and substantially affect the air quality over different locations throughout its path. Increased AOD values over different locations are attributed to the increased amount of dust in the atmosphere. Based on the comparison of NCEP winds with the model derived winds, it is noted that the direction of the model simulated winds matches well with NCEP winds, but the magnitude of the winds is not well matched. Model simulated winds appears to be overestimated in comparison to NCEP winds. Model derived AOD and dust load patterns show good match with the ground based and satellite observations. However, overestimation in simulated AOD is also noted, which may be due to the overestimation of the wind speed, as dust emission is a function of wind speed. Higher the wind speed, more will be the dust emission. Further to this poor air quality (increased PM_{2.5}) over the Delhi region is also noted due to the impact of dust storm over the Indian region. In case of quantitative analysis of AOD, the model shows its capability to capture both the pattern and the magnitude.

In future following suggestions may be implemented

- Better comparison of model simulated AOD with ground based AOD is possible if we convert the AOD values with respect to the AERONET wavelength (500nm).

- More dust storm events may be studied in future based on model simulations so as to establish the potential of WRF-Chem in simulating those dust events which have larger spatial extent.
-

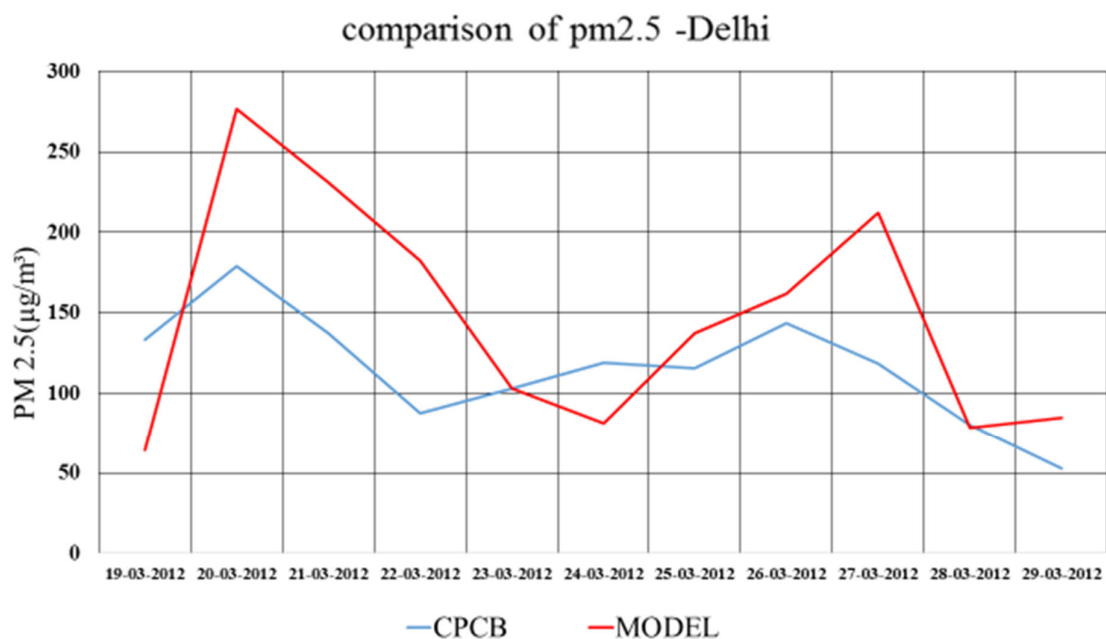


Figure 5: Comparison of PM_{2.5} from CPCB and MODEL simulated data for DELHI

ACKNOWLEDGEMENTS

Authors thankfully acknowledged the support provided by Group Head MASD, Dean Academics and Director IIRS. Model simulations are performed on High Performance Computing (HPC) facility of IIRS. Authors would like to acknowledge the use of WRF model, which is supported by the Mesoscale and Microscale Meteorology Division at the National Center for Atmospheric Research (NCAR). The NCEP final analysis data were obtained from <ftp.dss.ucar.edu>.

REFERENCES

- Grell, G. A., Dévényi, D., 2002. A generalized approach to parameterizing convection combining ensemble and data assimilation techniques. *Geophysical Research Letters*, 29(14), 38–1–38–4. <https://doi.org/10.1029/2002gl015311>
- Jish Prakash, P., Stenchikov, G., Kalenderski, S., Osipov, S., Bangalath, H., 2015. The impact of dust storms on the Arabian Peninsula and the Red Sea. *Atmos. Chem. Phys.* 15, 199–222. <https://doi.org/10.5194/acp-15-199-2015>
- Kalenderski, S., Stenchikov, G., Zhao, C., 2013. Modeling a typical winter-time dust event over the Arabian Peninsula and the Red Sea. *Atmos. Chem. Phys.* 13, 1999–2014. <https://doi.org/10.5194/acp-13-1999-2013>
- Namdari, S., Karimi, N., Sorooshian, A., Mohammadi, G.H., Sehatkashani, S., 2018. Impacts of climate and synoptic fluctuations on dust storm activity over the Middle East. *Atmos. Environ.* 173, 265–276. <https://doi.org/10.1016/j.atmosenv.2017.11.016>
- Prospero, J.M., 2002. Environmental characterization of global sources of atmospheric soil dust identified with the NIMBUS 7 Total Ozone Mapping Spectrometer (TOMS) absorbing aerosol product. *Rev.*

Geophys. 40, 1002. <https://doi.org/10.1029/2000RG000095>

Washington, R., Todd, M., Goudie, A., Middleton, N., 2003. Global dust storm source areas determined by the total ozone monitoring spectrometer and ground observations. *Ann. Assoc. Am. Geogr.* 93, 297–313. <https://doi.org/10.1111/1467-8306.9302003>

Middleton, N.J., 1985. Effect of drought on dust production in the Sahel. *Nature* 316, 431–434. <https://doi.org/10.1038/316431a0>

Hong, S.Y., Pan, H.L., 1996. Nonlocal Boundary Layer Vertical Diffusion in a Medium-Range Forecast Model. *Monthly Weather Review*, 124(10), 2322–2339. [https://doi.org/10.1175/1520-0493\(1996\)124<2322:nblvdi>2.0.co;2](https://doi.org/10.1175/1520-0493(1996)124<2322:nblvdi>2.0.co;2)

Lin, Y.L., Farley, R. D., Orville, H. D., 1983. Bulk Parameterization of the Snow Field in a Cloud Model. *Journal of Climate and Applied Meteorology*, 22(6), 1065–1092. [https://doi.org/10.1175/1520-0450\(1983\)022<1065:bpotsf>2.0.co;2](https://doi.org/10.1175/1520-0450(1983)022<1065:bpotsf>2.0.co;2)

ANALYSIS OF A DUST STORM ORIGINATED OVER WEST ASIA USING NWP MODEL

CHARU SINGH¹, SANJEEV KUMAR SINGH¹, SACHIN BUDAKOTI², RANDHIR SINGH³

¹Indian Institute of Remote Sensing, ISRO, Dehradun, India

²IDP in Climate Science, IIT Bombay, Mumbai, India

³Space Applications Centre, ISRO, Ahmedabad, India

KEYWORDS: Dust storm, West Asia, visibility, air quality, Indian subcontinent, WRF-CHEM

INTRODUCTION

In the recent years, dust episodic events have increased over the West Asian region and subsequent their impact on North Indian region air quality. Dust storm originated over west Asia (Iraq and Saudi Arabia) in last week of October 2017 is one of such events which is used as a case study in the present work. West Asia and Sahara desert are the regions which contribute most to global aerosol loading (Ginoux et al., 2012). Over the southern Arabian Peninsula, dust storms occur more frequently during summer season, whereas the northern Arabian Peninsula witnesses more dust storms during the spring season (Prakash et al., 2015). It has been documented in several previous studies that dust emanated over the dust source regions such as Arabia, Iraq, Iranian Plateau is pumped towards the Indian subcontinent through the long range transport (Ganguly, 2012a & b; Manoj et al., 2011, 2012; Singh et al., 2017) and subsequently degrade the air quality of this region (Dey et al., 2004; Prasad and Singh, 2007; Prasad et al., 2007; Sharma et al., 2012). In October 2017, a severe dust storm originated over the Iraq and Saudi Arabia, and on October 30, the storm notably reduced visibility in parts of Iraq. Further dust particles were transported over engulfed Kuwait and the Persian Gulf region on October 31. This dust storm was so severe, that it entered into the Indian subcontinent region, causing low visibility over the Delhi region. Present study is intended to investigate the contribution of the dust storm in degrading air quality which was originated over gulf region and transported dust particles in Delhi, which subsequently reduced the visibility of the region considerably. Numerical weather prediction model fully coupled with chemistry (WRF-CHEM) is employed here to explore the forecasting skills of such a severe dust storm well in advance.

METHODOLOGY AND DATA USED

WRF version 3.9 coupled with chemistry and Goddard Global Ozone Chemistry Aerosol Radiation and Transport (GOCART) dust scheme is used to simulate the dust storm. Details of GOCART scheme is documented in Ginoux et al. (2001). WRF-chem model is tuned with various suitable parameterization schemes for the simulation of dust. The configuration of the model for the present study is listed in the Table 1 and the flow chart of WRF modeling system is illustrated in Figure 1. Model has run for single domain covering the area from longitude 45° E to 100° E and latitude 5° N to 45° N. To evaluate the performance of WRF model in predicting the dust event, the 6-hourly National Centre for Environmental Prediction (NCEP) FNL (Final) global analysis datasets with 1° × 1° resolution were used for the model initial and boundary conditions. For updating the suitable configured chemical species MOZART data has been used. Concentration of dust induced PM₁₀ and PM_{2.5} has been validated with the *in-situ* measurements taken from Central Pollution Control Board (CPCB) web portal.

Initial and Boundary conditions	NCEP Final Analysis FNL (1°)
Horizontal resolution	25 km
Vertical levels	36
Simulation period	120 Hours starting from 00 UTC November 01, 2017
Height of lowest layer	50 m
Physical schemes	Microphysics: WSM6 graupel scheme PBL: Yonsei University (YSU) planetary boundary layer scheme (Hong and Pan, 1996) Surface: unified Noah land-surface model Cumulus convection: New Kain Fritsch (Kain 2004) Longwave radiation : RRTM (Mlawer et al., 1997) Shortwave radiation : Dudhia (1989)
Emission scheme	Ginoux et al. (2001)
Number of dust bins	Total 5 size bins
Dust particle size range	0.5, 1.4, 2.4, 4.5 and 8.0 μm effective radius

Table 1: Model configuration used for the experiment

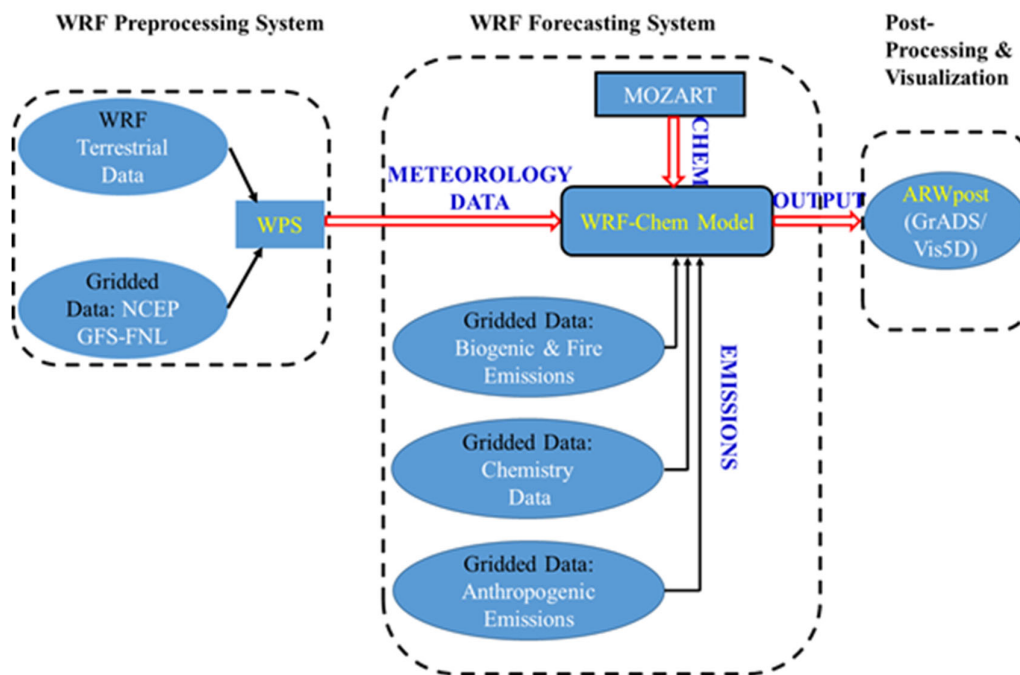


Figure 1: Flow chart for WRF-CHEM simulation for dust and particulate matter

RESULTS AND DISCUSSION

The skill of the WRF coupled with chemistry, to forecast the dust originated at Iraq and Saudi Arabia and its transportation towards the Indian subcontinent has been tested in the present study. For this purpose, 120 hours forecast from the WRF coupled with chemistry with incorporation of GOCART dust scheme has been generated from 00 UTC of November 01 to November 6, 2017 00 UTC. NCEP analysis winds have been used to initialize the model.

Figure 2a-e and 3a-e illustrate the forecasted winds and total dust load for different forecasts length. In the present study dust forecasts have been generated at every 6-hourly interval. However, results have been shown only at 24-hour interval. At 00 UTC of 02 November, 2017 high winds was present over the Iraq and some parts of Saudi Arabia region (figure 2a) and a small patch of high dust loading (integrated all size ranges) was visible over Saudi Arabia region (shown in figure 3a). In the 48 and 72-hour forecasts valid at 00 UTC of 03 and 04 November, 2017 respectively, high wind speed was present over the Iraq and Saudi Arabia regions (shown in figure 2b-c) which was favorable for dust lifting into the atmosphere, resulting high dust loading was visible over the same regions (shown in figure 3b-c). On 05 November, 2017 wind speed slightly decreased over Iraq region (shown if figure 2d) and slow down the dust transporting. Further to this, on November 06, 2017 wind speed is again strengthen over Iraq region (shown in figure 2e) and dust loading was observed all over the Delhi region (shown in figure 3e). In all the wind forecasts, a broad anti-cyclonic circulation was visible over the north-west part the Indian subcontinent extended up to Saudi Arabia and Iraq, which continuously transporting the dust towards the Indian region.

In order to validate the forecasts, the forecasted dust induced PM₁₀ and PM_{2.5} are compared with the PM₁₀ and PM_{2.5} concentration which was obtained from CPCB (<http://cpcb.nic.in>). The daily PM₁₀ and PM_{2.5} are compared with the daily averaged WRF-CHEM forecasted PM₁₀ and PM_{2.5} at Indira Gandhi International (IGI) Airport, Delhi location and shown in figure 4a-b. It is depicted in the figure that WRF-CHEM is able to capture the trend for 120 hours forecasts, however, values are slightly under estimated as compared to the CPCB observed values.

CONCLUSIONS

This study focuses on the dust storm originated at the Iraq and Saudi Arabia region in the end of October, 2017. First of all, the analysis of the dust storm activity has been performed based on the MODIS natural-color image and INSAT-3D generated aerosol product. MODIS image well capture the origin of dust storm and INSAT-3D aerosol product illustrates a well-defined dust patch across the north-west part of the India on November 6, 2017. For the purpose to analyse the dynamical process of the dust emission and to assess the skill of the NWP model, 120 hours forecast from the WRF coupled with chemistry and GOCART dust scheme has been generated from 00 UTC of November 01, 2017. The present study suggest that WRF-Chem simulated high wind speed was the trigger for the dust out break over the Iraq and Saudi Arabia region which further transported dust towards the Indian subcontinent region. Validation of particular matter (PM) shows that WRF-Chem is able to capture the temporal evaluation of the PM values, however, slight under estimation has been observed. This particular observation warrants further study. Present study reveals that the WRF coupled with chemistry is able to forecast the dust storm event and further dust transportation from the dust source region towards the Indian subcontinent well in advance.

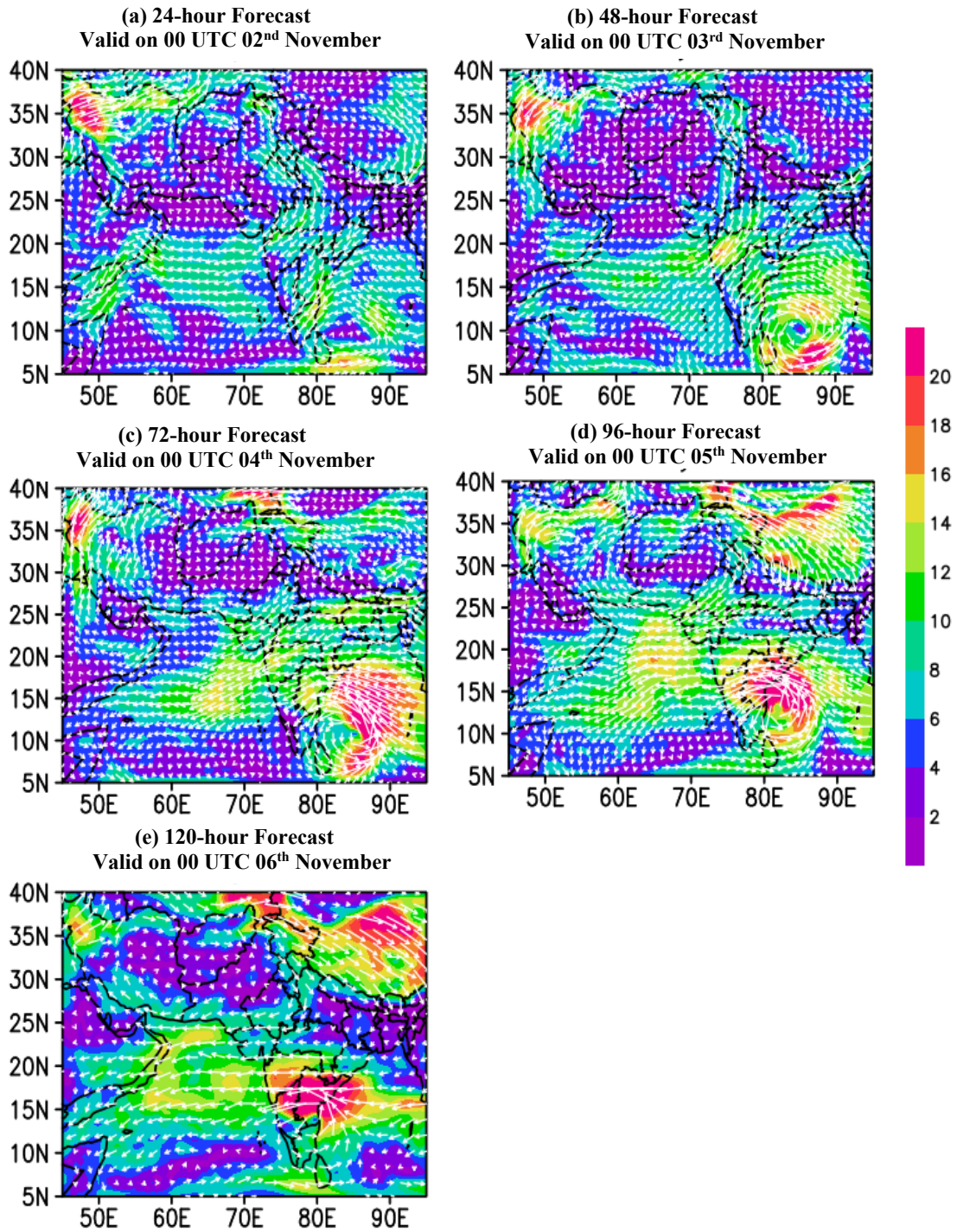


Figure 2: Spatial pattern of the forecasted wind speed and wind vectors based on WRF simulations. (a) For 00 UTC on November 02, 2017 (b) For 00 UTC November 03, 2017. (c) For 00 UTC November 04, 2017. (d) For 00 UTC November 05, 2017. (e) For 00 UTC November 06, 2017. Color bar indicates wind speed in m/s.

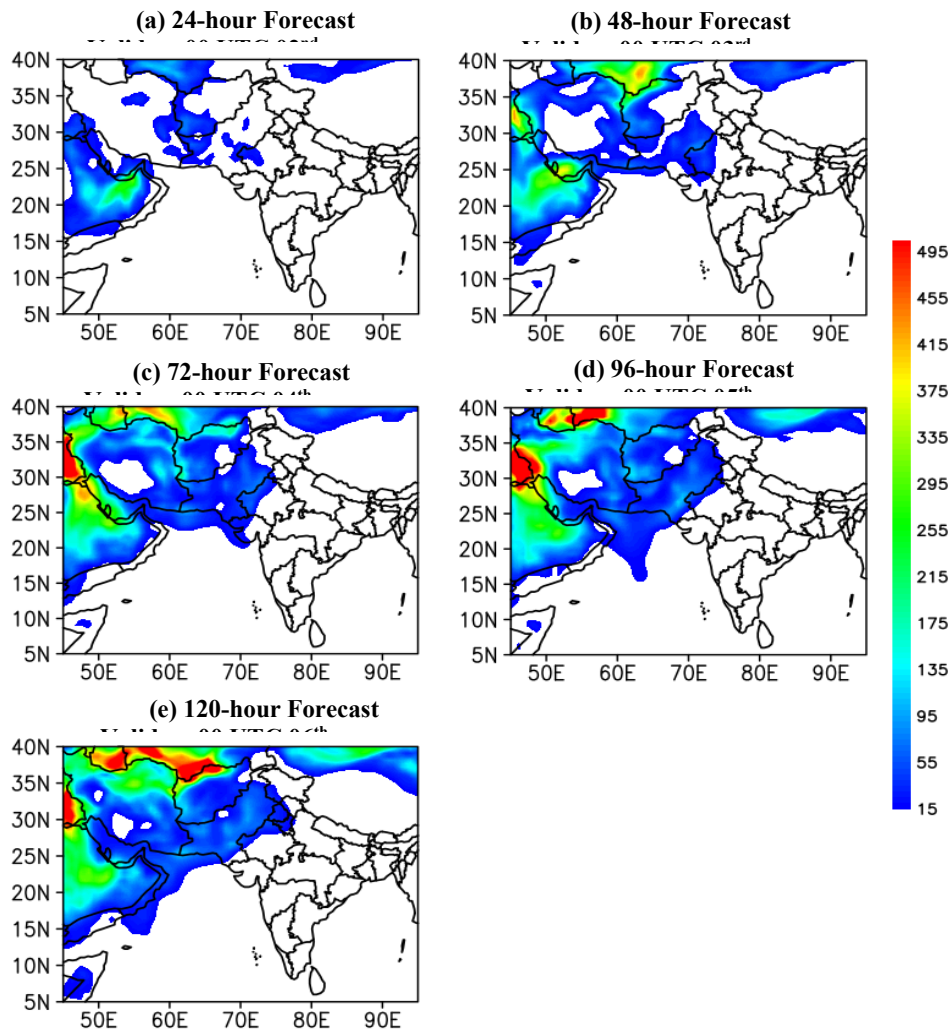


Figure 3: Spatial pattern of the forecasted dust loading based on WRF simulations. (a) For 00 UTC on November 02, 2017 (b) For 00 UTC November 03, 2017. (c) For 00 UTC November 04, 2017. (d) For 00 UTC November 05, 2017. (e) For 00 UTC November 06, 2017. Color bar indicates total dust loading in mg/m^2 .

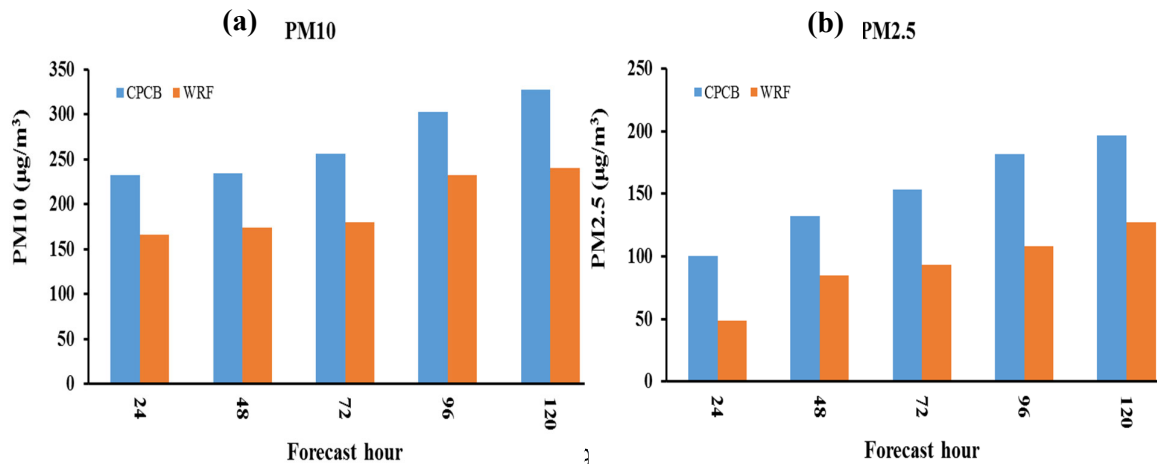


Figure 4. Comparison of PM10 and PM2.5 concentration between WRF simulation initiated on 01 November, 2017 and CPCB Observations at IGI Airport, Delhi location.

ACKNOWLEDGEMENT

Authors thankfully acknowledged the support provided by Group Head MASD, Dean Academics and Director IIRS. Model simulations are performed on High Performance Computing (HPC) facility of IIRS. Authors would like to acknowledge the use of WRF model, which is supported by the Mesoscale and Microscale Meteorology Division at the National Center for Atmospheric Research (NCAR). The NCEP final analysis data were obtained from <ftp.dss.ucar.edu>.

REFERENCES

Dey, S., Tripathi, S.N., Singh, R.P., Holben, B.N., 2004. Influence of dust storms on aerosol optical properties over the Indo-Gangetic basin. *J. Geophys. Res.* 109, D20211. <http://dx.doi.org/10.1029/2004JD004924>.

Ganguly, D., Philip J. Rasch, Hailong Wang, and Jin-ho Yoon (2012a), Fast and slow responses of the South Asian monsoon system to anthropogenic aerosols, *Geophys. Res. Lett.*, 39, L18804, doi:10.1029/2012GL053043.

Ganguly, D., Philip J. Rasch, Hailong Wang, and Jin-ho Yoon (2012b), Climate response of the South Asian monsoon system to anthropogenic aerosols, *J. Geophys. Res.*, 117, D13209, doi:10.1029/2012JD017508.

Ginoux et al., 2001. Sources and distributions of dust aerosols simulated with the GOCART model,” *Journal of Geophysical Research D*, vol. 106, no. 17, pp. 20255–20273, 2001.

Manoj MG, Devara PCS, Safai PD, Goswami BN (2011) Absorbing aerosols facilitate transition of Indian monsoon breaks to active spells. *Clim Dyn* 37:2181–2198.

Manoj MG, Devara PCS, Joseph S, Sahai AK (2012) Aerosol indirect effect during the aberrant Indian Summer Monsoon breaks of 2009. *Atmos Environ* 60:153–163

Prakash, P. J., Stenchikov, G., Kalenderski, s., Osipov, S., and Bangalath, H., 2015. The impact of dust storms on the Arabian Peninsula and the Red Sea. *Atmos. Chem. Phys.*, 15, 199–222, 2015. www.atmos-chem-phys.net/15/199/2015/ doi:10.5194/acp-15-199-2015.

Prasad, A.K., Singh, R.P., 2007. Changes in aerosol parameters during major dust storm events (2001–2005) over the Indo-Gangetic Plains using AERONET and MODIS data. *J. Geophys. Res.* 112, D09208. <http://dx.doi.org/10.1029/2006JD007778>.

Prasad, A.K., Singh, S., Chauhan, S.S., Srivastava, M.K., Singh, R.P., Singh, R., 2007. Aerosol radiative forcing over the Indo-Gangetic Plains during major dust storms. *Atmos. Environ.* 41, 6289–6301.

Sharma, D., Singh, D., Kaskaoutis, D.G., 2012. Impact of two intense dust storms on aerosol characteristics and radiative forcing over Patiala, northwestern India. *Adv. Meteorol.* 956814, 2012. <http://dx.doi.org/10.1155/2012/956814>.

Singh Charu, Litty Thomas, and K. Kishore Kumar, 2017b. Impact of aerosols and cloud parameters on Indian summer monsoon rain at intraseasonal scale: a diagnostic study. *Theoretical and Applied Climatology*, 127.1-2, 381-392.

FINDING THE POSSIBLE FACTS OF SPATIO-TEMPORAL VARIATION OF AOD OVER THE LOWER PART OF GANGES PLAIN OF WEST BENGAL, INDIA

DEBJANI DUTTA¹, SHARADIA DEY², SRIMANTA GUPTA¹, C.M. KISTAWAL³

¹Department of Environmental Science, The University of Burdwan, ²St. Xavier's College, Kolkata,

³Space Application Centre, ISRO, Ahmedabad

KEYWORDS: Land use change, Aerosol monitoring, Atmospheric effects, Health effects, Lower Gangetic plain

INTRODUCTION

A good air quality is very much a matter of concern for healthy living. Diseases generated from inhalation of polluted air is possessing more and more population day by day. This pollution is sometimes caused by human activities e.g. industrial emission, traffic emission, biomass burning (Murty,2004) or, otherwise, by natural phenomenon like dust storm and wind transport (Che *et al.*,2013, Yang *et al.*,2016). Indian population, influenced by both the two causes, are at high risk of mortal danger, especially in urban environments. Recurring smog incidents of Delhi, the capital city of India, has drawn this matter into international concern. A no. of researches is carried out on air quality of the metro cities like Delhi (around 19 RSA studies are corroborated in last decade), Agra and Kanpur with some studies in Ahmedabad, Nagpur, Mumbai, Chennai, Hyderabad, Vishakhapatnam, Durg, Raipur and Kolkata (Garaga *et al.*,2018). Though, the region mostly studied is the northern India, where the agglomeration of industries and high traffic are spotted as the cause (Garaga *et al.*,2018), the rest of India, including the lower Gangetic plain, also show a high level of pollution, even over the rural agricultural areas (Dutta and Gupta,2017).

This study focuses on the air quality status of lower Gangetic plain of West Bengal including urban cities like Kolkata, Durgapur and Asansol, semi urban areas like Burdwan city, Raniganj, coal mining zone of western Burdwan district, arid land of Purulia district, forest area of Sunderbans and a huge area of agricultural land covering eleven districts of Gangetic West Bengal. It will highlight how different human activities in different land use types of Gangetic West Bengal influence the air quality of that area and in turns the people get affected by the pollution.

The study uses ground air quality data from several stations and the remotely sensed aerosol data along with the observations of meteorological parameters which describes the natural influence on the air quality status of any area.

MATERIALS AND METHODS

Particulate matters and black carbon (for Burdwan city, Pandaveswar and Durgapur station from 2016 to 2018) concentrations over several stations like Kolkata, Burdwan city, Durgapur, Asansol, Raniganj, Pandaveswar are gathered as ground data; some from ground observations done by the authors (2016-18), some from the WBPCB website (2008-18), and others from the archived research papers (Reddy and Ruj, 2002, Mondal *et al.*,2011, Spiroska *et al.*,2011, Haque and Singh,2017). Remotely sensed AOD level 2 data (AOD dark target deep blue combined 8-day product of 3 km resolution) from collection 6 products of MODIS TERRA and AQUA platform is used in the time span of ten years (2008-18) over the whole lower Gangetic plain. To identify the land use classes, LANDSAT images (LANDSAT 4-5 TM, LANDSAT 7 ETM+ and LANDSAT 8) are downloaded from the earth explorer website and classified following a modified USGS classification. The accuracy of the classification is assessed through kappa analysis in ERDAS IMAGINE software. Wind rose diagram and NOAA HYSPLIT model are used to identify the transportation of pollutants from different places.

To carry out the study, the aerosol concentration is critically analyzed over the study area with time and then, is correlated with land use types to point out specific human activities behind the scenario. The air pollution related diseases in those areas are then discussed with the pollution episodes.

RESULTS AND DISCUSSIONS

Land use classification

Most of the parts of lower Gangetic plain is covered with agricultural areas (almost eleven districts), others are cities like Kolkata, Durgapur, mining areas, arid regions, forests, water bodies etc. The land use type has not changed much in the agricultural regions from past three decades, but a rapid progression is noticed in and outside of urban, semi urban and mining areas (tested by Mann-Kendal test at $p > 0.5$). The kappa values for each class has exceeded 0.8 with an accuracy level more than 81%.

Aerosol concentration and air quality status over lower Gangetic plain

The spatial distribution of AOD not only show dependence on its land use pattern but also largely depend on seasons. In early summer and post-monsoon seasons, the urban, mining and industrial patch show higher value than the agricultural side whereas in winter and late summer, the agricultural area shows higher AOD value than the non-agricultural land use part. The value of AOD in non-agricultural regions ranges between 0.5 to 0.9 which is quite normal for any industrial region but the agricultural area, also reflects a value range of 0.4 to 0.85. The reason may be the dust and loose soil generated by intensive agricultural techniques (Xin *et al.*,2007), application of nitrogenous pesticides, crop residue burning and use of bio fuels in cooking in the agriculture areas (Hou *et al.*,2014). These types of activities are frequent to found in rural West Bengal (Mondal *et al.*,2011, Chakraborty *et al.*,2014). The paddy-cutting dust and the crop residue burning in the cropping areas may increases the AOD of winter time (<https://nfsm.gov.in/nfmis/rpt/calenderreport.aspx>) so high that it surpluses the industrial area's AOD value of that time.

Over the mining regions in the north-western part of lower Gangetic plain, the value of $PM_{2.5}$ is more than 460 microgram/ m^3 in all the seasons. In the urban-industrial city Durgapur, the seventh polluted city of India, this value ranges from 300-450 microgram/ m^3 , excluding the monsoon season. In industrial city Asansol, the value ranges from 300-500 microgram/ m^3 (Reddy and Ruj,2002), excluding the monsoon season. In Raniganj mining-industrial city, where the coal transport is very high, the value ranges between 250-400 microgram/ m^3 (Reddy and Ruj,2002), excluding monsoon season. In Kolkata, the present value of $PM_{2.5}$ is on an average 400-550 microgram/ m^3 in winter season (Spiroska *et al.*,2011, <https://in.usembassy.gov/embassy-consulates/kolkata/air-quality-data>). The total pollution of Kolkata comes from vehicular emissions (51.4%), industrial emission (24.5%) and dust particles (21.1%) mainly (Haque and Singh,2017). The source of other polluted cities are the mines, industries, vehicles and domestic as well. Kolkata, other than in monsoon season, levels the pollution range of a heavy mining area Pandaveswar with its urban activities and sometimes surpluses the pollution level of Delhi, the most polluted city of India (TOI report, 03.05.2018). The pollution has increased significantly over all the stations with time (tested at $p < 0.5$) with an R^2 value of 0.6 and above. The rate of increase is highest in the semi-urban regions (R^2 0.85), followed by mining (R^2 0.77), industrial (R^2 0.72) and urban (R^2 0.65) areas.

The value of black carbon (excluding the monsoon season) ranges between 4 to 24 microgram/ m^3 in Burdwan city, Durgapur and Pandaveswar (a mining area) seasonally. Surprisingly, these three areas with different degree of urbanization do not differ much in the case of black carbon level. May be this is an effect of its origin, which is the incomplete combustion of fossil fuels. The traffic level and cooking may be the major contributor of black carbon in these areas, which pulls these places in same category, even a rural place of Burdwan district (Kalanabagram) also showed same level of black carbon with Pandaveswar.

Air quality and health hazards

Studies carried out by Chittaranjan National Cancer Research Institute have found that ~70% of the residents in the city suffer from respiratory disorders and more than 60 per cent children in Kolkata with lung function impairments compared to 24 per cent in cleaner areas. Almost 5 million people of Kolkata are exposed to very high air pollution which is gradually transforming Kolkata into second most polluted metro city in India (TOI report, 03.05.2018). In Burdwan municipality, there are 16 deaths recorded in 2008 due to respiratory problems (Chattopadhyay *et al.*,2010). In Kolkata, the death due to respiratory diseases (85.1%)

has far outnumbered the death due to waterborne (14.9%) and other diseases (Haque and Singh,2017). In Haldia, 67% of the population has serious respiratory problems (Gupta *et al.*, 2017).

Atmospheric effects

Aerosol concentration of any place does not only depend on the origin of the aerosols but also on the dispersion. Following the wind trajectory, it is found that, the wind trajectory over the southern Bengal is prevailing from the upper Gangetic plains. This observation was also corroborated by Prasad *et al.*, 2004. Most of the industries in Ganges plain are situated besides the Ganga river. The pollution exerted by them may be is transported by this wind trajectory which subsides or stretches over the southern West Bengal pulling up the AOD high even over the agricultural fields. In the contrary, there are also small isolated patches over the mining, urban and industrial areas influenced by the human activity receiving less from the wind transport.

CONCLUSION

There is no doubt in the raising danger with bad air quality in India; in some places it is severe, and others may be less vulnerable. Because of wind transport, urban sprawl and coal-cooking, the non-urban areas also compete with the cities in the case of air pollution. Elongation of highways through the agricultural fields and forests also contributes the vehicular emissions to the air quality status of the vegetative areas. Because of all these causes, every land use pattern is now a part of rising air pollution trend. But, the main thrust in Indian air pollution study is still on the metro cities. In West Bengal, there is a severe lack of documentation in air pollution status all over the state, so in the Gangetic plane. No reliable data are there about the mortality and morbidity status caused by bad air quality, even most of the Gangetic plain does not have any continuous air quality monitoring station. To defend the rising mortal danger of bad air quality in West Bengal, at the very first, measures should be taken to monitor the air quality status, then the defense against the death will also be easy.

ACKNOWLEDGEMENTS

This research is funded by ISRO SAC (grant no. ISRO/RES/4/625/2016-17).

REFERENCES

- Chakraborty, D., Mondal, N.K. and J.K. Dutta (2014). Indoor pollution from solid biomass fuel and rural health damage: a micro-environmental study in rural area of Burdwan, West Bengal, *International Journal of Sustainable Built Environment* **3**(2014): 262-271.
- Chattopadhyay, S., Gupta, S. and R.N. Saha (2010). Spatial and temporal variation of urban air quality: a GIS approach, *Journal of Environmental Protection* **1**(2010): 264-277.
- Che, H., Y. Wang, J. Sun, X. Xang, X. Zang and J. Guo (2013). Variation of aerosol optical properties over the Taklimakan desert in china, *Aerosol and Air Quality Research* **13** 777–785.
- Dutta, D. and S. Gupta (2017). Interactive phenomenon of crop burning activity and aerosol optical depth: a case study from a part of Gangetic basin of West Bengal, *Third International Conference on Mother Earth (ICME III)*, Department of Environmental Science, The University of Burdwan, January 11-13, 2018.
- Garaga, R., Sahu, S.K. and S.H. Kota (2018). A review of air quality modelling studies in India: local and regional scale, *Current Pollution Reports* doi: 10.1007/s40726-018-0081-0.
- Gupta, B.G., Biswas, J.K. and K.M. Agarwal (2017). Air pollution from bleaching and dyeing industries creating severe health hazards in Maheshtala textile cluster, West Bengal, India. *Air, Soil and Water Research* **10**: 1-10.

- Haque, M.S., and R.B. Singh (2017). Air pollution and human health in Kolkata, India: a case study, *Climate* **5** (2017) 77, doi: 10.3390/cli5040077.
- Hou, H., H. Jiang, X. Wang and H. Pei (2014). The spatial-temporal evolution of aerosol optical depth and the analysis of influence factors in Bohai Rim, 35th International Symposium on Remote Sensing of Environment, doi:10.1088/1755-1315/17/1/012035.
- Mondal, N.K., Saha, S.K., Datta, J.K. and A. Banerjee (2011). Indoor air pollution: a household study in the village Faridpur and Ranchi colony, Durgapur, Burdwan district, West Bengal, *World Journal of Environmental Pollution* **1(1)**: 5-7.
- Mukhopadhyay, K. (03.05.2018), Kolkata is 2nd most polluted metro, air quality worsening faster than Delhi's. Times of India <https://timesofindia.indiatimes.com/city/kolkata/kolkata-is-2nd-most-polluted-metro-air-quality-worsening-faster-than-delhis/articleshow/64007600.cms>.
- Murty, B.P. (2004), Environmental Meteorology (I.K. International Pvt. Ltd., New Delhi).
- Prasad, A.K., R.P. Singh and A. Singh (2004). Variability of aerosol optical depth over Indian Subcontinent using MODIS data, *Journal of Indian Society of Remote Sensing* **32** (4).
- Reddy, R.S. and B. Ruj (2002). Ambient air quality status in Raniganj-Asansol area, India, *Environmental Monitoring and Assessment* **89(2003)**: 153-163.
- Spiroska, J., Rahman, M.A. and S. Pal (2011). Air pollution in Kolkata: an analysis of current status and interrelation between different factors, *SEEU Review* **8(1)**: 182-214.
- Xin *et al.* (2007). Aerosol optical depth (AOD) and Angstrom exponent of aerosols observed by the Chinese Sun Hazemeter Network from August 2004 to September 2005, *Journal of Geophysical Research* **112** D05203.

DIURNAL VARIATION OF PM_{2.5} OVER THE INDIAN REGION USING MERRA-2 REANALYSIS DATASET

KUNAL BALI AND SAGNIK DEY

Centre for Atmospheric Sciences, Indian Institute of Technology Delhi, India

INTRODUCTION

Because of the rapid urbanization and industrialization, the Indian subcontinent is considered as one of the highly polluted region in the world especially north India. Here, the dominating sources of PM_{2.5} are the mineral dust, incomplete combustion of fossil fuel, biomass-biofuel burning and traffic exhausts (Yadav et al., 2014; Tiwari et al., 2009). So it has become an essential concern to understand the spatiotemporal variability of different aerosol species to further distinguish the direct and indirect impact of aerosols on the environment and human health. In our study, we focused on the diurnal pattern of particulate matter (PM_{2.5}) over India. The diurnal study of PM_{2.5} has been described in several studies using in-situ measurements and different modelling work. But these studies are confined to a few sampling sites at a given time and also limited to a short period of time. Apart from that, satellite studies are also restrict to the daily variation of aerosols. So this is a first study to anyone to present the long-term (2000-2017) diurnal variation of PM_{2.5} using Modern-Era Retrospective analysis for Research and Application (MERRA-2) data at each grid cell of Indian region.

DATASET

NASA provides the MERRA-2 reanalysis datasets that used the GEOS-5 model to assimilate the different aerosols products over the globe using the GOCART module (Bali et al., 2017; Buchard et al., 2016). The model used in reanalysis dataset individually computed the hourly PM_{2.5} of different aerosol species such as black carbon, organic carbon, dust, sulfate and sea salt with different size bins. Here, we added each bin of individual aerosol PM_{2.5} species at each grid cells over India so that we can access the total PM_{2.5} at each grid cell. MERRA-2 provides the aerosols species data with the resolution of 0.50 x 0.6250 in latitude and longitude. Additionally, the resulted MERRA-2 total PM_{2.5} has also been validating with CPCB in-situ PM_{2.5} dataset of different 80 sites (2009-2017) all over the Indian region.

RESULT

Figure (1) shows the hourly climatology of MERRA-2 PM_{2.5} at every 6 hour UTC time interval (00:30, 06:30, 12:30, 18:30) for the period of 2000-2017. In this figure, the PM_{2.5} easily observed over the IGP region. However, the high concentration of PM_{2.5} (> 80 µg/m³) noticed over northwestern part of the India (Rajasthan) and Pakistan during early morning (00:30) and late evening (18:30), that may be related to the low boundary layer height because of the less availability of solar radiation at that time period. As the day proceed, the high PM_{2.5} start decreasing over northwestern region because of the increase in the boundary layer height. The high PM_{2.5} values in figure 1 represented by red spot indicate the presence of mineral dust aerosols. On the other hand, it is observed that the green color spread over the IGP region that represents the anthropogenic PM_{2.5} (~50-70 µg/m³) such as black carbon, organic carbon from biomass burning, incomplete combustion etc. Considering the middle, south and northeastern part of Indian region that covers in blue color shows the less concentration of PM_{2.5} (<40 µg/m³) as compared to the red and green region. Here, the less PM_{2.5} concentration gives the indication of less population density area, less biomass burning activities, and less dust loading as compared to green and red domains respectively.

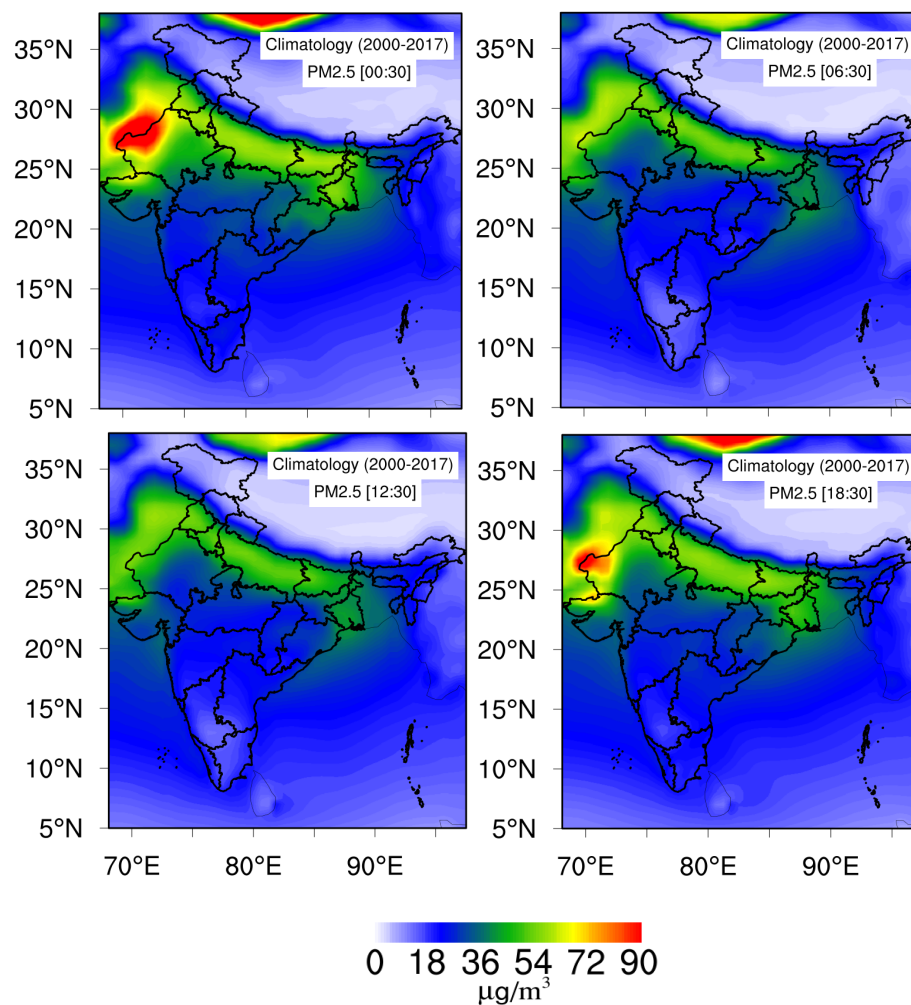


Figure 1: Spatiotemporal diurnal variation of MERRA-2 PM_{2.5} (µg/m³) 00:30, 06:30, 12:30, and 18:30 over Indian region.

CONCLUSION

MERRA-2 reanalysis dataset can easily be used to analyze the total PM_{2.5} concentration at each grid cells over the Indian region. The high PM_{2.5} concentration observed during early morning and late evening indicates the poor air quality during that particular time. Our results provide a comprehensive study of diurnal variation of the PM_{2.5} concentration over India and can be used for further climate and health implication.

ACKNOWLEDGEMENT

The first author would like to acknowledge the National Carbonaceous Aerosol Programme (NCAP) research fund under Ministry of Environment, Forest and Climate Change, Govt. of India. We also like to thank MERRA-2 reanalysis datasets provided by NASA.

REFERENCES

Bali, K., Mishra, A.K. and Singh, S., 2017. Impact of anomalous forest fire on aerosol radiative forcing and snow cover over Himalayan region. *Atmospheric Environment*, 150, pp.264-275.

Buchard, V., da Silva, A.M., Randles, C.A., Colarco, P., Ferrare, R., Hair, J., Hostetler, C., Tackett, J. and Winker, D., 2016. Evaluation of the surface PM_{2.5} in Version 1 of the NASA MERRA Aerosol Reanalysis over the United States. *Atmospheric Environment*, 125, pp.100-111.

Tiwari, S., Srivastava, A.K., Bisht, D.S., Parmita, P., Srivastava, M.K. and Attri, S.D., 2013. Diurnal and seasonal variations of black carbon and PM_{2.5} over New Delhi, India: influence of meteorology. *Atmospheric Research*, 125, pp.50-62.

Yadav, R., Sahu, L.K., Jaaffrey, S.N.A. and Beig, G., 2014. Temporal variation of particulate matter (PM) and potential sources at an urban site of Udaipur in western India. *Aerosol and Air Quality Research*, 14(6), pp.1613-1629.

5.

BUILD-UP OF AMBIENT PM_{2.5} IN DELHI NCT USING HIGH RESOLUTION SATELLITE DATASET

SOURANGSU CHOWDHURY^{1,2}, SAGNIK DEY¹, LARRY DI GIROLAMO³, KIRK R. SMITH^{2,4},
AJAY PILLARISSETTI² AND ALEXEI LYAPUSTIN⁵

¹Centre for Atmospheric Sciences, Indian Institute of Technology Delhi, New Delhi, India

²School of Public Health, University of California, Berkeley, California, USA

³Department of Atmospheric Sciences, University of Illinois at Urbana-Champaign, Urbana, Illinois, USA

⁴Collaborative Clean Air Policy Centre, Delhi, India

⁵NASA Goddard Space Flight Center, Greenbelt, Maryland, USA

KEYWORDS: MAIAC, weekly PM_{2.5}, fire count

INTRODUCTION

Exposure to ambient particulate matter less than 2.5 µm in aerodynamical diameter (PM_{2.5}) is causally associated with diseases like chronic obstructive pulmonary diseases (COPD), ischemic heart diseases (IHD), stroke, lung cancer, diabetes, pregnancy related complications, and low birth weight among other outcomes (Chowdhury and Dey 2016, Silva *et al* 2013, Pedersen *et al* 2013). The National Capital Territory (NCT) of Delhi is recognized as one of the most polluted areas in the world (Guttikunda and Calori, 2013; Tiwari *et al.*, 2012). Delhi NCT is home to about 16.7 million people and the larger Delhi National Capital Region (NCR), which includes several districts of Haryana and Uttar Pradesh has a population of 46 million. Several studies have estimated that annual PM_{2.5} concentration in the NCT exceeds India's annual national ambient air quality standard of 40 µg/m³ by more than 200%. In this study we attempt to estimate PM_{2.5} in Delhi NCT in the dry season (starting from end of September to end of June in the subsequent year) for the period 2001-2016 using 1 km resolution satellite aerosol data. We identify the peak episodes of ambient PM_{2.5} concentrations over the NCT and its changing pattern over time.

METHODS

We use a new aerosol optical depth (AOD) dataset at high resolution (1 km × 1 km) retrieved using the Multi-Angle Implementation of Atmospheric Correction (MAIAC) algorithm (Lyapustin *et al.*, 2011; 2018) applied to the MODIS (Moderate Resolution Imaging Spectroradiometer) data. The MAIAC AOD is retrieved as a combined Aqua and Terra product. We estimate PM_{2.5} from MAIAC-AOD by multiplying against a spatially and temporally varying conversion factors at 0.1° × 0.1° spatial resolution obtained from GEOS-Chem chemical transport model. A detailed description of deriving the conversion factor is provided elsewhere (van Donkelaar *et al.*, 2014, 2010a). We downscale the conversion factor to 1 km resolution using spline interpolation. We validate the estimated PM_{2.5} against in-situ measurement data archived by the Central Pollution Control Board (CPCB). Henceforth, we average all valid 1 km² PM_{2.5} that are bias corrected within the NCT for each day and present the analysis at weekly scale by then averaging over 7 days to ensure enough samples for robust statistics. We also analyse MODIS Fire Information for Resources Management System (FIRMS) data which captures fire activities at 1 km × 1 km spatial resolution. Only observations with high confidence level (>70% confidence) are included in our analysis. We compute weekly aggregates of all fire occurrences within a box which includes Punjab and Haryana, at weekly scale to understand its variability vis-à-vis PM_{2.5} variability in the NCT.

RESULTS & DISCUSSIONS

Weekly time series of PM_{2.5} concentration averaged over the 16-years period in Delhi NCT is depicted in Figure 1. Ambient PM_{2.5} concentration starts rising in October 15-21, coinciding with the increase in open biomass burning in the upwind regions of Punjab and Haryana. Prevailing north-westerly winds transport

the resulting pollution into the NCT and stable atmospheric condition indicated by low boundary layer depth and low wind speed entrap the pollution close to the ground. PM_{2.5} concentration continues to rise over the next three weeks reaching $494 \pm 250 \mu\text{g}/\text{m}^3$ in November 5-11 over Delhi NCT. Note that this estimate is a 16-year average and therefore such massive rise in pollution level over a long period of time is expected to have huge health impacts (both acute and chronic). Once the fire count starts decreasing after October 29-November 4 and wind speed strengthens, PM_{2.5} concentration falls. However, shallow boundary layer keeps pollution level above $200 \mu\text{g}/\text{m}^3$. PM_{2.5} concentration again starts rising from December 16-22 reaching a second peak ($350 \pm 130 \mu\text{g}/\text{m}^3$) during December 31-January 6. We attribute this peak to rise in local emissions from solid-waste and open biomass burning (for heating), enhancement in secondary aerosol formation (Nagar et al., 2017) and transport of pollution from adjoining states by converging winds. Hence after PM_{2.5} concentration falls and stabilizes in the range of $50\text{-}80 \mu\text{g}/\text{m}^3$

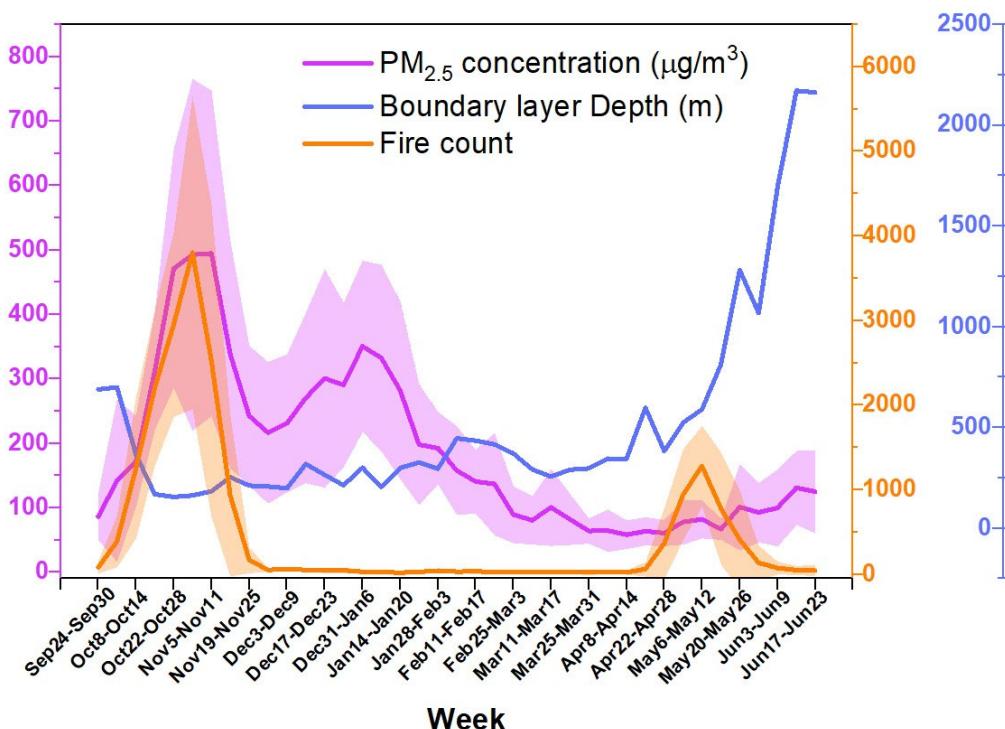


Figure 1: Weekly PM_{2.5} concentration over Delhi NCT. The blue and orange lines depict mean (shade represents $\pm 1\text{SD}$) PM_{2.5} concentration and boundary layer depth. the number of fire events in the upwind region (demarcated by magenta box in Figure S2 in SI) in red with shades showing $\pm 1\text{SD}$.

CONCLUSIONS

Despite all the mitigation policies (Chowdhury *et al* 2017, Narain and Krupnick 2007) implemented in Delhi, ambient PM_{2.5} concentration in the NCT remains almost three times higher than the longterm NAAQS. Multiple factors explain the lack of success of these policies to curb ambient air pollution, the primary being the geographic location of the NCT and the prevalent meteorological conditions. Long-range transport of pollution due to biomass burning from the upwind rural regions during the crop burning season, dust transport during the summer and transport of pollution emitted from brick kilns throughout the year (Cusworth *et al* 2018) adds to the local sources such as transport, construction, diesel generators, power plants, industries, residential use etc. Our results call for significant effort to design and implement policies within the entire NCR to curb ambient PM_{2.5} concentration. The initial pollution episode may be mitigated

by controlling open biomass burning in the upwind states, which is a priority to the Government of India and more rapid expansion of the substitution of biomass by LPG in households. Incentives for in-situ and on field straw management techniques are initiated. To ensure proper implementation of this scheme, the government will need a strong verification mechanism and new awareness campaigns among the farmers to educate them about options for crop residues uses including transfer of technologies towards higher end. The second pollution episode can be curbed by reducing local emissions during this period. Recent efforts by the government include implementation of an odd-even traffic intervention policy for few days within NCT, however, returned minimal dividends in terms of mitigating PM_{2.5} levels. This may be attributed to the remaining sources of PM_{2.5} in NCR where similar mitigation policies need to be enforced.

ACKNOWLEDGEMENTS

The work is partially supported by a grant from Department of Biotechnology under Indo-UK Program on ‘Air Pollution and Human Health’ (BT/IN/UK/APHH/41/KB/2016-17). SC and SD acknowledge the Fulbright-Nehru Doctoral Fellowship and Fulbright-Nehru Academic and Professional Excellence Fellowship, respectively. MODIS 1 km AOD data are archived at LP DAAC

REFERENCES

- Chowdhury S and Dey S 2016 Cause-specific premature death from ambient PM_{2.5} exposure in India: Estimate adjusted for baseline mortality *Environ. Int.* **91** 283–90 Online: <http://linkinghub.elsevier.com/retrieve/pii/S0160412016300848>
- Chowdhury S, Dey S, Tripathi S N, Beig G, Mishra A K and Sharma S 2017 “Traffic intervention” policy fails to mitigate air pollution in megacity Delhi *Environ. Sci. Policy* **74**
- Chudnovsky A, Lyapustin A, Wang Y, Schwartz J and Koutrakis P 2013 Analyses of high resolution aerosol data from MODIS satellite: a MAIAC retrieval, southern New England, US 87951E Online: <http://proceedings.spiedigitallibrary.org/proceeding.aspx?doi=10.1117/12.2030278>
- Cusworth D H, Mickley L J, Sulprizio M P, Liu T, Marlier M E, DeFries R S, Guttikunda S K and Gupta P 2018 Quantifying the influence of agricultural fires in northwest India on urban air pollution in Delhi, India. Supplementary Information *Environ. Res. Lett.* **13**
- Dey S, Di Girolamo L, van Donkelaar A, Tripathi S N, Gupta T and Mohan M 2012 Variability of outdoor fine particulate (PM_{2.5}) concentration in the Indian Subcontinent: A remote sensing approach *Remote Sens. Environ.* **127** 153–61 Online: <http://dx.doi.org/10.1016/j.rse.2012.08.021>
- van Donkelaar A, Martin R V., Brauer M and Boys B L 2014 Use of satellite observations for long-term exposure assessment of global concentrations of fine particulate matter *Environ. Health Perspect.* **110** 135–43 Online: <http://ehp.niehs.nih.gov/1408646>
- van Donkelaar A, Martin R V., Brauer M, Kahn R, Levy R, Verduzco C and Villeneuve P J 2010 Global estimates of ambient fine particulate matter concentrations from satellite-based aerosol optical depth: Development and application *Environ. Health Perspect.* **118** 847–55
- Guttikunda S K and Calori G 2013 A GIS based emissions inventory at 1 km Å 1 km spatial resolution for air pollution analysis in Delhi , India **67**
- Kloog I, Chudnovsky A., Just A C, Nordio F, Koutrakis P, Coull B a., Lyapustin A, Wang Y and Schwartz J 2014 A new hybrid spatio-temporal model for estimating daily multi-year PM_{2.5} concentrations across northeastern USA using high resolution aerosol optical depth data *Atmos. Environ.* **95** 581–90
- Lyapustin A, Wang Y, Laszlo I, Kahn R, Korkin S, Remer L, Levy R and Reid J S 2011 Multiangle implementation of atmospheric correction (MAIAC): 2. Aerosol algorithm *J. Geophys. Res. Atmos.* **116**

Online: <http://doi.org/10.1029/2010JD014986>

Narain U and Krupnick A 2007 The Impact of Delhi 's CNG Program on Air

Pedersen M, Giorgis-Allemand L, Bernard C, Aguilera I, Andersen A-M N, Ballester F, Beelen R M J, Chatzi L, Cirach M, Danileviciute A, Dedele A, Eijdsden M van, Estarlich M, Fernández-Somoano A, Fernández M F, Forastiere F, Gehring U, Grazuleviciene R, Gruziova O, Heude B, Hoek G, de Hoogh K, van den Hooven E H, Håberg S E, Jaddoe V W V, Klümper C, Korek M, Krämer U, Lerchundi A, Lepeule J, Nafstad P, Nystad W, Patelarou E, Porta D, Postma D, Raaschou-Nielsen O, Rudnai P, Sunyer J, Stephanou E, Sørensen M, Thiering E, Tuffnell D, Varró M J, Vrijkotte T G M, Wijga A, Wilhelm M, Wright J, Nieuwenhuijsen M J, Pershagen G, Brunekreef B, Kogevinas M and Slama R 2013 Ambient air pollution and low birthweight: a European cohort study (ESCAPE). *Lancet. Respir. Med.* **1** 695–704
Online: <http://www.sciencedirect.com/science/article/pii/S2213260013701929>

Silva R a, West J J, Zhang Y, Anenberg S C, Lamarque J-F, Shindell D T, Collins W J, Dalsoren S, Faluvegi G, Folberth G, Horowitz L W, Nagashima T, Naik V, Rumbold S, Skeie R, Sudo K, Takemura T, Bergmann D, Cameron-Smith P, Cionni I, Doherty R M, Eyring V, Josse B, MacKenzie I a, Plummer D, Righi M, Stevenson D S, Strode S, Szopa S and Zeng G 2013 Global premature mortality due to anthropogenic outdoor air pollution and the contribution of past climate change *Environ. Res. Lett.* **8** 34005 Online: <http://stacks.iop.org/1748-9326/8/i=3/a=034005?key=crossref.4619a48f65a5bc77307c00cf38f9299f>

Tiwari S, Chate D M, Srivastava A, Bisht D S and Padmanabhamurty B 2012 Assessment of PM₁, PM_{2.5} and PM₁₀ Concentrations in Delhi at different mean cycles *Geofizika* **29** 125–41

QUANTIFICATION OF HEALTH BENEFITS DUE TO REDUCTION IN ANTHROPOGENIC PM_{2.5} RESULTING FROM MITIGATION OF KEY EMITTING SECTORS THROUGH CHEMICAL TRANSPORT MODEL

¹ABHISHEK UPADHYAY, ¹SAGNIK DEY, ¹SOURANGSU CHOWDHURY AND ^{1,2}PRAMILA GOYAL

¹Centre for Atmospheric Sciences, IIT Delhi, Hauz Khas, New Delhi, India

²Now at The Northcap University, HUDA Sector 23 A, Gurgaon, India

KEYWORDS: PM_{2.5}, WRF-Chem, Emission Inventory.

INTRODUCTION

Air pollution is one of the leading health risk in world especially in developing nation like India and China and measures are being taken to tackle this severe problem. Effective air quality mitigation policy needs information about polluting sources, this information will enable the agencies to make the preferences of sectors to be targeted. Lelieveld et al. (2015), Silva et al. (2016) has carried out global studies to determine share of different sectors in total ambient PM_{2.5}. Conibear et al., (2018) and GBD-MAPS., (2018) have performed studies over India to find impact of each sector. All these studies have shown even with varying statistics residential sector is highest PM_{2.5} contributors over India. In this work we are using WRF-Chem model to estimate PM_{2.5} contributions from each key emitting sectors. Then the reduction in health burden upon complete mitigation of each source has been estimated.

METHODOLOGY

Online Chemical transport model WRF-Chem (Grell et al, 2005) at a fine resolution of 10 km has been used in this study. Model has 345 grids in North – South as well as West – East direction and 31 vertical levels are there with the 50 hPa pressure at the top, domain is shown in Figure 1. FNL data which is available at a resolution of 1°×1° for each 6-hour interval has been used as meteorological input parameters. EDGAR-HTAP emission for year 2010 at 0.1 ° × 0.1° resolution is emission input used in the model. EDGAR emission inventory consists of key emitting sectors like Residential, Industrial, Transportation, Power and Agriculture, where agriculture sector has emissions for ammonia only. YSU scheme for planetary boundary layer, RRTM for long wave and Dudhia for short wave has been used as physics scheme whereas GOCART aerosol chemistry along with RADM2 gas phase chemistry has been used in the model setup. Four different sets of simulations have been performed by subtracting one of key emitting sector in each simulation for year 2010 with this setup. Health burden has been estimated using an established method in terms of premature mortality for each district and disease like COPD, IHD, Stroke and Lung Cancer (Chowdhury and Dey, 2016) with the concentration obtained from each sectors.

$$\sum_{i,j=1}^N \Delta M_{i,j} = \sum_{i,j=1}^N Y_{i,j} \times \frac{\sum_{i=1}^N RR_{ij} - 1}{\sum_{i=1}^N RR_{i,j}} \times \sum_{i=1}^N P_i$$

Here ΔY represents baseline mortality for the disease j at district i , P is the adult population above the age of 25 for each district i (taken from the Indian census 2011) and RR is relative risk for the disease j at district i and is estimated using IERs for the annual PM_{2.5} exposures.

RESULTS

Spatial distribution of simulated anthropogenic PM_{2.5} shown in figure 1, is depicting high concentration over North and East part of India, dominantly in IGB region. Model has simulated share of PM_{2.5} concentrations for each of mentioned sectors, which shows residential sector as major contributor. Total premature mortality attributed to PM_{2.5} for all disease is 0.79 million over India. Reduction in premature mortality from complete mitigation of residential emission is 0.37 million. Whereas complete mitigation of Industrial,

Transportation and Power are showing 46000, 28000 and 18000 reductions in mortality respectively. State-wise analysis of life saved due to complete mitigation of particular emission sources is showing highest benefits from residential mitigation in most of the states.

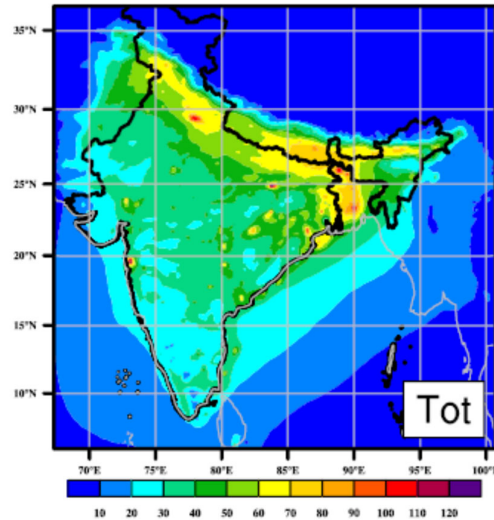


Figure1: Spatial distribution of anthropogenic simulated PM2.5 over India.

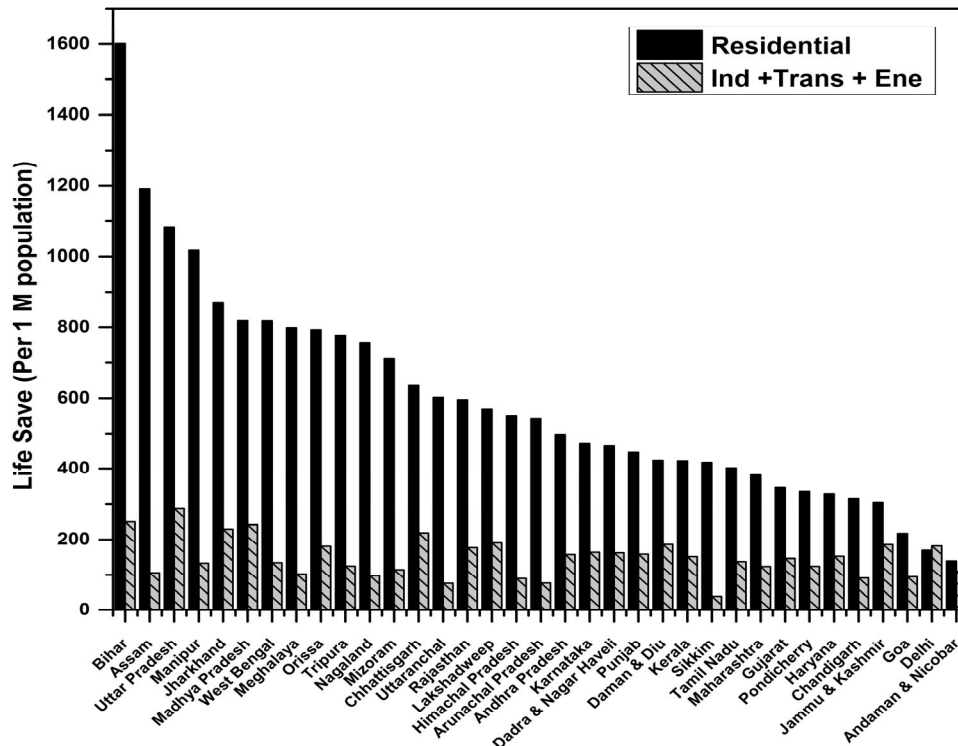


Figure2: Reduction in premature death per 100,000 populations on complete mitigation of emission from (a) Residential. (b) Industrial. (c) Transportation. (d) energy sectors

CONCLUSIONS

The impact of residential is distributed in wide region whereas the impact of Industrial, transport and power are localized. Thus different approach is required to deal with these sources. Widely spread establishments especially rural area will primary target to mitigate residential emission and this can be easily achieved by replacing high emitting fuels with less emitting fuels and combustion technique. Health benefits obtained in this experiment follows non-linear exposure response function which gets flattened at higher concentration. State wise analysis is showing highly populated states like Bihar and Uttar Pradesh have high health benefits on mitigating residential emission, where Delhi has equal impact from complete mitigation of residential as well as other three sectors.

REFERENCES

Conibear, L., Butt, E.W., Knote, C., Arnold, S.R., Spracklen, D. V., 2018. Residential energy use emissions dominate health impacts from exposure to ambient particulate matter in India. *Nat. Commun.* 9, 1–9.

Grell, G.A., Peckham, S.E., Schmitz, R., McKeen, S.A., Frost, G., Skamarock, W.C., Eder, B., 2005. Fully coupled “online” chemistry within the WRF model. *Atmos. Environ.* 39, 6957–6975. Silva, R.A., Adelman, Z., Fry, M.M., West, J.J., 2016. The impact of individual anthropogenic emissions sectors on the global burden of human mortality due to ambient air pollution. *Environ. Health Perspect.* 124, 1776–1784.

Lelieveld, J., Evans, J.S., Fnais, M., Giannadaki, D., Pozzer, A., 2015. The contribution of outdoor air pollution sources to premature mortality on a global scale. *Nature* 525, 367–371.

Lelieveld, J., Evans, J.S., Fnais, M., Giannadaki, D., Pozzer, A., 2015. The contribution of outdoor air pollution sources to premature mortality on a global scale. *Nature* 525, 367–371.

Upadhyay, A., Dey, S., Chowdhury, S., Goyal, P., 2018. Expected health benefits from mitigation of emissions from major anthropogenic PM 2.5 sources in India: Statistics at state level . *Environ. Pollution.* 242, 1817–1826.

ICE NUCLEATING PARTICLE PROPERTIES OF AEROSOLS IN THE HIMALAYAN REGION

S. YADAV^{1,2} AND M. D. PETERS²

¹Department of Environmental Sciences, Central University of Jammu, Bagla, Rahya Suchani, Samba, Jammu and Kashmir 181143, India.

²Department of Marine Earth and Atmospheric Sciences, North Carolina State University, Raleigh, North Carolina 27695-8208, United States of America.

KEYWORDS: Aerosol-Cloud Interaction, Ice Nucleating Particle (INP), The Himalayan region

INTRODUCTION

The current understanding of aerosol-cloud interaction reveals that they have net cooling effect but the large uncertainty factor remains due to the limited knowledge of global Cloud Condensation Nuclei (CCN) and Ice Nuclei distribution (Seinfeld and Pandis, 2006). One of the uncertainties is related to glaciation aerosol effects on climate (Lohmann, 2002; Lohmann and Feichter, 2004). Ice nucleating particles (INP) have potential to initiate ice formation at warmer temperatures. The important contributing sources of INP include combustion particles, mineral dust and primary bioaerosols (DeMott et al., 2003; Hoose and Möhler, 2012; Prenni et al., 2009). INP are responsible for most of the global precipitation and thus play crucial role in understanding global hydrological cycle (Mülmenstädt et al., 2015). The absence of good INP database for the Himalayan region limits modelling studies. This work includes measurement of INP from precipitation samples collected in rural and urban locations of Northern India including the Himalayan region.

METHODS

SAMPLING DETAILS

The sampling campaign includes collection of precipitation samples in clean glass dishes. The collected samples were transferred into cryovials and kept frozen until analysis. Sampling was conducted in two phases: In first phase (August, 2017 to September, 2017), total 25 samples were collected in Jammu urban, Jammu rural, and Dharamshala. In second phase (November, 2017 to March, 2018), 26 winter samples were collected at Jammu rural, Dharamshala, New Delhi and Lucknow.

DROP-FREEZING ASSAY

The precipitation samples were analyzed on the NC State Cold Stage facility using the established methodology for INP analysis and the details of the method are described elsewhere (DeMott et al., 2017; Hader et al., 2014; Petters and Wright, 2015). This procedure is based on the drop freezing assay technique (Bigg, 1953). Sample drops were placed on hydrophobic slides and the pictures were recorded every 5 s using time lapse photography. The change in brightness of the image indicated the fraction of unfrozen monodisperse droplets. Cumulative INP (C_{INP}) L^{-1} water was calculated using the method of Vali (Vali, 1971):

$$C_{INP}(T) = \frac{-\ln(F_{uf})}{V_{drop}} \quad (1)$$

where V_{drop} is the volume of the drop and F_{uf} is the fraction of unfrozen droplets at supercooling temperature T . Figure 1 shows the example of INP spectrum for a precipitation sample. Experiments were repeated thrice and the data was collated and binned into 1 °C intervals. Mean INP concentration L^{-1} air was calculated from INP concentrations L^{-1} water using the assumption of condensed water content of 0.4 $g\ m^{-3}$ (Petters and Wright, 2015).

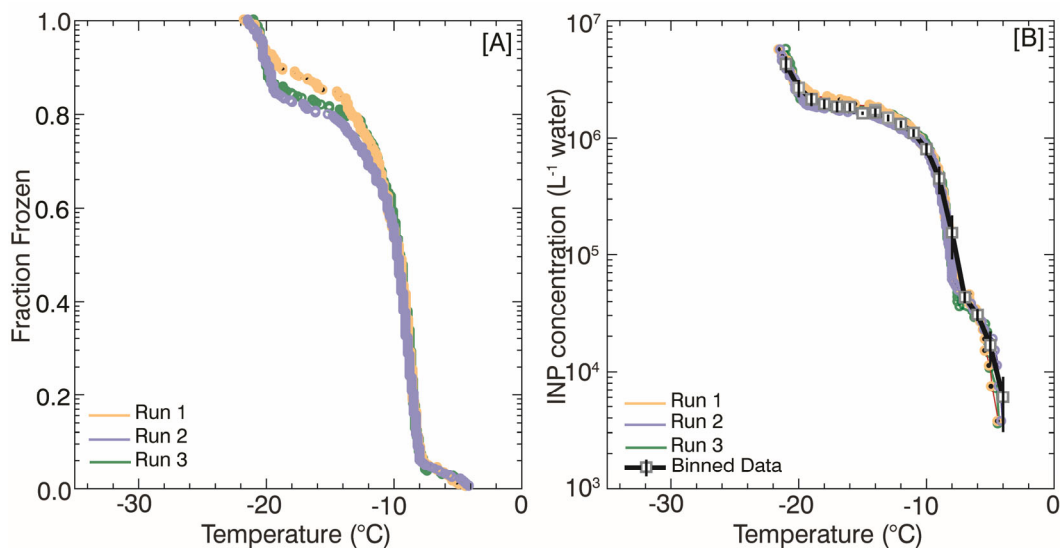


Figure 1: Panel [A] shows the fraction frozen versus temperature and Panel [B] show the cumulative INP versus temperature for three individual repeats of a precipitation sample from Dharamshala. Dark grey squares show binned data and the black vertical bars show ± 1 standard deviation of C_{INP} within the bin.

RESULTS & DISCUSSIONS

The INP concentration observed in precipitation samples, collected at five locations in Northern India is shown in Figure 2. The grey shaded area is depiction of INP observations from other parts of the world (Petters and Wright, 2015). In the monsoon season, most observations were found near or below the lower bound of the grey shaded area, while in winter season relatively larger spread was observed. In this study, the INP concentration ranged from 10^4 to $5 \times 10^6 \text{ L}^{-1}$ water or 5×10^{-3} to 100 L^{-1} air.

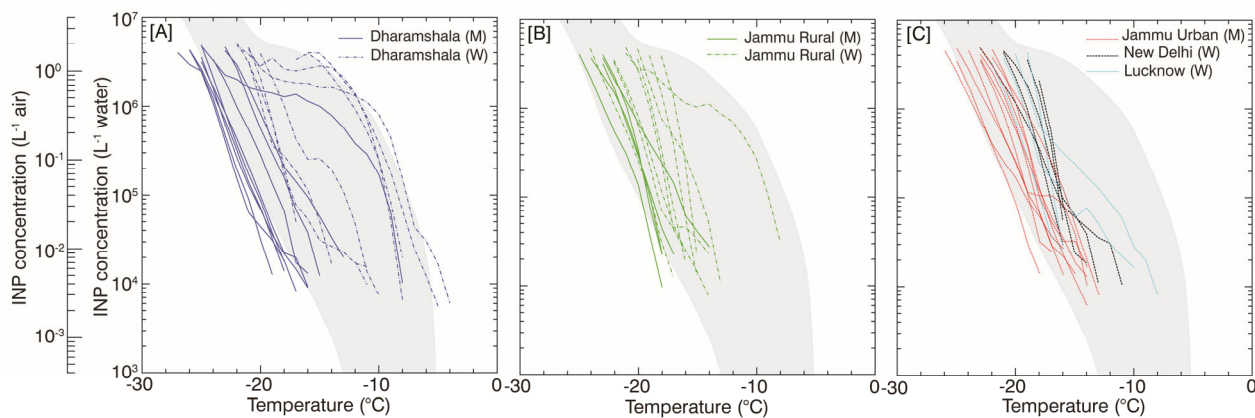


Figure 2: The mean C_{INP} for samples collected in Monsoon (M) and Winter (W) seasons is shown: Panel [A] Dharamshala, Panel [B] Jammu Rural and Panel [C] Jammu Urban, New Delhi and Lucknow. The grey shaded area shows the envelope of INP observations in precipitation taken from Petters and Wright, 2015.

The INP activity in Dharamshala samples was observed over the widest temperature range. Samples collected from relatively polluted locations of New Delhi and Lucknow did not show any distinct feature in terms of observed INP.

Six out of total 51 samples showed distinct active INP at warmer temperatures. Freezing events at temperatures warmer than -10°C suggests a biological contribution to INP concentration. The results from this study reaffirm that INP concentration ranges over a wide range.

CONCLUSIONS

This study provides circumstantial evidence that pollution is not a strong source of INP. With few exceptions most observations were found near the lower bound of previous observations. The high INP concentrations are likely biological in origin and were mostly found in the samples collected from the Himalayan region. More comprehensive studies on simultaneous quantitative assessment of bioaerosols and INP are needed to understand the sources and characteristics of INP in the region.

ACKNOWLEDGEMENTS

SY thanks United States-India Educational Foundation (USIEF) for Fulbright Kalam Climate Fellowship award for Postdoctoral Research (Award No. 2225/FKPDR/2017) and Central University of Jammu for granting study leave. Acknowledgement is due for Sarita Bamotra and Deepika Kaushal for their help with precipitation sample collection.

REFERENCES

- Bigg, E.K., 1953. The formation of atmospheric ice crystals by the freezing of droplets. *Q. J. R. Meteorol. Soc.* 79, 510–519. <https://doi.org/10.1002/qj.49707934207>
- DeMott, P.J., et al., 2017. Comparative measurements of ambient atmospheric concentrations of ice nucleating particles using multiple immersion freezing methods and a continuous flow diffusion chamber. *Atmos. Chem. Phys.* 17, 11227–11245. <https://doi.org/10.5194/acp-17-11227-2017>
- DeMott, P.J., Sassen, K., Poellot, M.R., Baumgardner, D., Rogers, D.C., Brooks, S.D., Prenni, A.J., Kreidenweis, S.M., 2003. African dust aerosols as atmospheric ice nuclei. *Geophys. Res. Lett.* 30, 26–29. <https://doi.org/10.1029/2003GL017410>
- Hader, J.D., Wright, T.P., Petters, M.D., 2014. Contribution of pollen to atmospheric ice nuclei concentrations. *Atmos. Chem. Phys.* 14, 5433–5449. <https://doi.org/10.5194/acp-14-5433-2014>
- Hoose, C., Möhler, O., 2012. Heterogeneous ice nucleation on atmospheric aerosols: a review of results from laboratory experiments. *Atmos. Chem. Phys.* 12, 9817–9854. <https://doi.org/10.5194/acp-12-9817-2012>
- Lohmann, U., 2002. A glaciation indirect aerosol effect caused by soot aerosols. *Geophys. Res. Lett.* 29, 1052. <https://doi.org/10.1029/2001GL014357>
- Lohmann, U., Feichter, J., 2004. Global indirect aerosol effects: a review. *Atmos. Chem. Phys. Discuss.* 4, 7561–7614. <https://doi.org/10.5194/acpd-4-7561-2004>
- Mülmenstädt, J., Sourdeval, O., Delanoë, J., Quaas, J., 2015. Frequency of occurrence of rain from liquid-, mixed-, and ice-phase clouds derived from A-Train satellite retrievals. *Geophys. Res. Lett.* 42, 6502–6509. <https://doi.org/10.1002/2015GL064604>
- Petters, M.D., Wright, T.P., 2015. Revisiting ice nucleation from precipitation samples. *Geophys. Res. Lett.* 42, 8758–8766. <https://doi.org/10.1002/2015GL065733>
- Prenni, A.J., Petters, M.D., Kreidenweis, S.M., Heald, C.L., Martin, S.T., Artaxo, P., Garland, R.M.,

Wollny, A.G., Pöschl, U., 2009. Relative roles of biogenic emissions and Saharan dust as ice nuclei in the Amazon basin. *Nat. Geosci.* 2, 402–405. <https://doi.org/10.1038/ngeo517>

Seinfeld, J.H., Pandolfi, S.N. 2006. *Atmospheric Chemistry and Physics*, John Wiley and Sons Inc, New York.

Vali, G., 1971. Quantitative Evaluation of Experimental Results on the Heterogeneous Freezing Nucleation of Supercooled Liquids. *J. Atmos. Sci.* 28, 402–409. [https://doi.org/10.1175/1520-0469\(1971\)028<0402:QEOERA>2.0.CO;2](https://doi.org/10.1175/1520-0469(1971)028<0402:QEOERA>2.0.CO;2)

AEROSOL ASSOCIATED WATER SOLUBLE INORGANIC IONS IN THE DHAULADHAR REGION OF NORTH-WESTERN HIMALAYA: SEASONAL VARIATION IN CONCENTRATION, SOURCES AND PROCESSES

D. KAUSHAL¹ AND A. TANDON¹

¹School of Earth and Environmental Sciences, Central University of Himachal Pradesh, Dharamshala, Kangra – 176206, India.

KEYWORDS: Aerosol Characterization, Water-soluble Inorganic Ions, North-Western Himalaya

INTRODUCTION

Water soluble inorganic ions (WSII) constitute a major fraction of ambient aerosols (Heitzenberg, 1989). These ionic species have been used as potential markers for different source(s) and underlying process(es) for the formation of ambient aerosols (Safai et al., 2010). Study of aerosol associated WSII has also been crucial to understand direct and indirect effects of aerosols on regional climate and human health (Forster et al., 2007; Isaksen et al., 2009). Water soluble inorganic ions are either emitted directly as particles or are produced through gas to particle conversion (Seinfeld and Pandis, 2006). Moreover, local and regional meteorology, geography and strength of various natural and anthropogenic emission sources viz. agricultural activities, industries and traffic etc. have influence on the composition of ambient aerosols and associated WSII (Rajput et al., 2016 and references therein). North-Western Himalayan region (NWHHR) with sizable population and attractive tourist destinations have been facing ever increasing problem of gaseous and particulate air pollution from exponential increase in vehicular traffic and other anthropogenic emissions (Gajananda et al., 2005). Though, several studies focusing on chemical characterization and source identification of aerosols have already been conducted over various urban and rural locations in India and worldwide (Singh et al., 2016 and references therein), but, very few studies based on long-term systematic measurement of ionic composition of atmospheric aerosols over NWHHR are available (Kuniyal et al., 2015). The present study has been planned to perform simultaneous measurement of ionic composition of ambient aerosols at an urban (Dharamshala) and a rural (Pohara) location over the Dhauladhar region in North-Western Himalaya leading to investigate the nature and the strength of various source(s) and different atmospheric process(es) responsible for the formation of WSII.

METHODS

24-hourly PM₁₀ aerosol samples were collected every week on pre-baked and pre-weighed quartz-microfiber filter paper (Whatman) using Respirable Dust Sampler (Envirotech, model APM 460 BL) simultaneously at an urban location Dharamshala (32°20'N, 76°32'E; 1350 m amsl) and a rural site Pohara (32°22'N, 76°25'E; 750 m amsl) in Dhauladhar region of North-Western Himalaya from January 2015 to January 2016. A portion (81 cm² area) was cut from the sampled filter paper and dissolved in 20ml of Milli Q water (18.2 MΩ.cm resistivity) and ultra-sonicated for 40 minutes. The extracted water samples were filtered through 0.22 μm pore size PVDF membrane filter papers. The extracted samples were stored at 4 °C until the analysis. Major anions (F⁻, Cl⁻, NO₃⁻, PO₄³⁻ and SO₄²⁻) and cations (Na⁺, NH₄⁺, K⁺, Ca²⁺ and Mg²⁺) were analyzed using Metrohm Ion Chromatograph (IC) model 883 basic IC plus with conductivity detector.

RESULTS & DISCUSSIONS

On annual average basis, WSII accounted for 15.6% and 14.2% of PM₁₀ aerosols load at urban location Dharamshala and at rural location Pohara, respectively. At Dharamshala, SO₄²⁻ ions contribute maximum (52%) followed by NO₃⁻ (12%) and NH₄⁺ (11%) to the total concentration of WSII analyzed. Similarly, at Pohara SO₄²⁻ dominated among all WSII analyzed, contributing 56% followed by NO₃⁻ and NH₄⁺ each contributing 12%. Seasonal average concentrations of PM₁₀ and associated WSII were observed to be higher at rural location Pohara than urban location Dharamshala in all the seasons. This could be due to the low altitude and proximity with a National Highway of the sampling site at the rural location Puhara. The total

WSII concentration was noted to be the highest during winter season over both the locations, plausibly due to lowering of mixing height coupled with the increase in the activity of source(s) viz. coal and biomass combustion for surrounding heating.

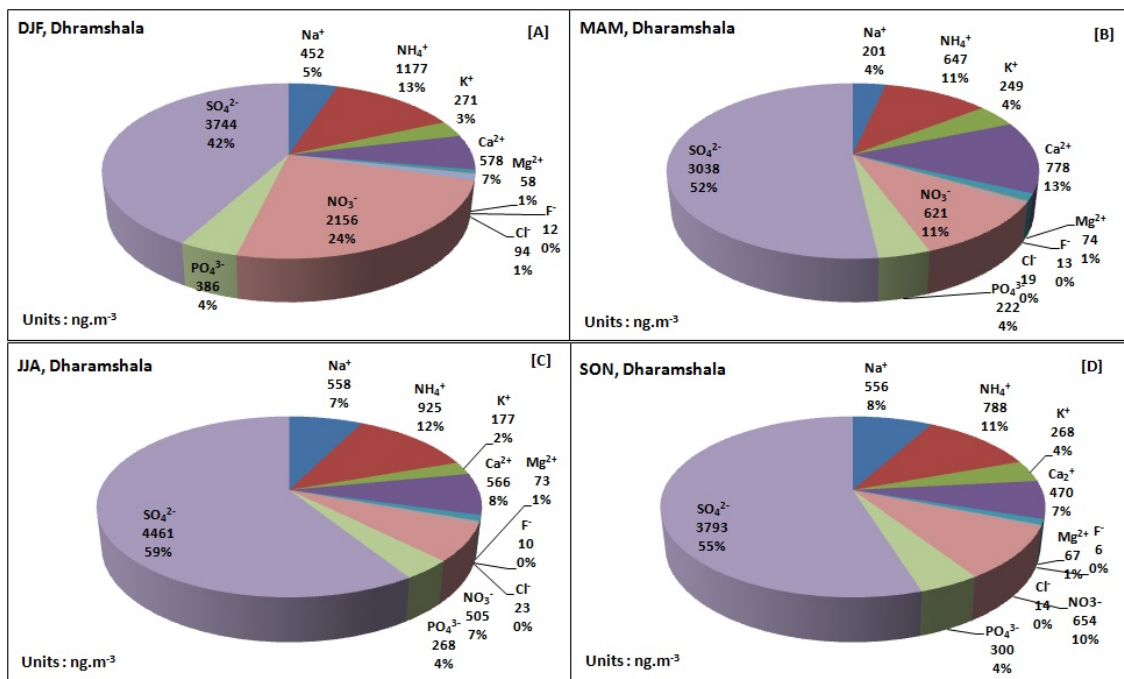


Figure 1. Seasonal distribution of Water Soluble Inorganic Ions associated with PM₁₀ over urban location Dharamshala.

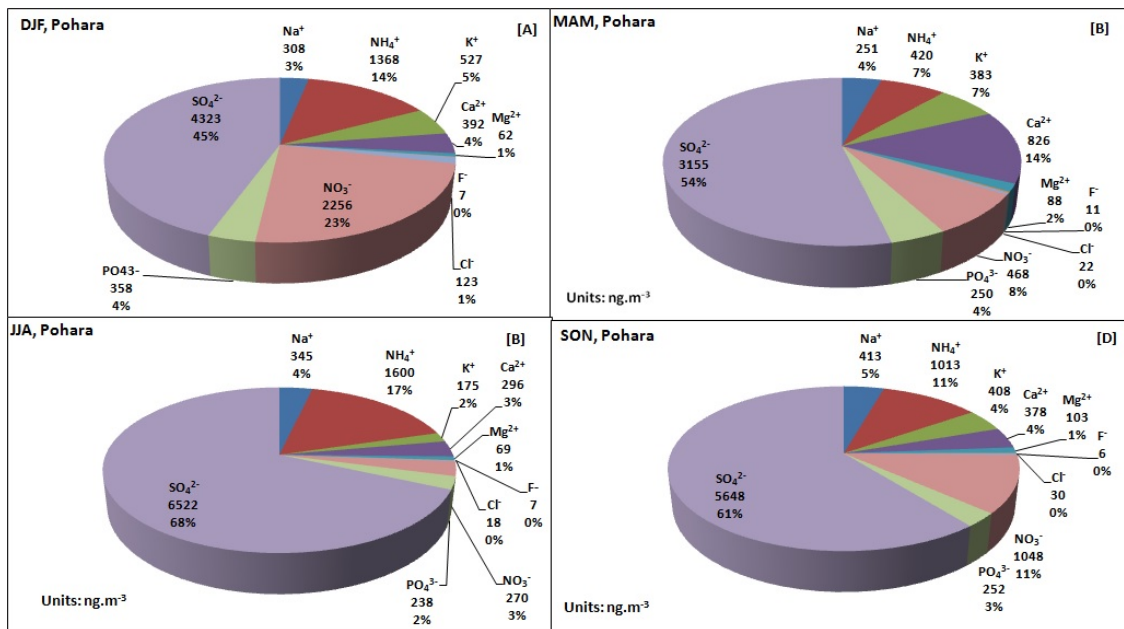


Figure 2. Seasonal distribution of Water Soluble Inorganic Ions associated with PM₁₀ over rural location Pohara.

At Dharamshala, strong correlation between NH_4^+ and SO_4^{2-} , in all the seasons, indicates the formation of Secondary Inorganic Aerosols (SIA). Their high proportions in WSII and considerable thermodynamic stability at ambient temperatures, made $(\text{NH}_4)_2\text{SO}_2$ the major contributor to SIA over NH_4NO_3 and NH_4Cl at this urban location. Moreover, low ambient temperature in winter season favoured formation of NH_4NO_3 with significant contribution to SIA. Good correlations were observed between NO_3^- , PO_4^{3-} and K^+ during winter and autumn season over both the locations. This observation suggests contribution of inorganic (NPK) fertilizers that could be re-suspended along with the loose soil from the agricultural fields present in the vicinity.

Table 1. Varimax rotated principal component loadings of different WSII present in PM_{10} at Dharamshala and Pohara

Varimax rotated principal component loadings							
Ions analyzed	Dharamshala			Pohara			
	S1	S2	S3	S1	S2	S3	S4
F^-	0.76	-0.15	0.40	-0.08	-0.32	0.65	-0.22
Cl^-	0.15	0.00	0.90	0.92	0.07	-0.05	0.08
NO_3^-	0.12	0.30	0.88	0.91	0.26	0.05	0.02
PO_4^{3-}	0.05	0.63	0.55	0.92	0.11	-0.11	0.12
SO_4^{2-}	0.51	0.81	-0.10	0.08	0.95	0.14	0.13
Na^+	-0.17	0.69	0.05	0.10	0.20	-0.11	0.86
NH_4^+	0.15	0.83	0.28	0.42	0.81	-0.17	-0.03
K^+	0.65	0.37	0.21	0.65	0.06	0.51	-0.12
Ca^{2+}	0.91	-0.16	0.10	-0.01	-0.43	0.38	0.59
Mg^{2+}	0.88	0.28	-0.08	0.03	0.32	0.76	0.31
Variance Explained (%)	40.7	20.7	15.8	37.1	16.8	14.5	11.2

The results of the Principal Component Analysis (PCA) performed on the concentration of different WSII analyzed suggested three major sources of aerosol associated WSII over the urban location of Dharamshala viz. re-suspension of soil or local sediments; conversion of pollutant gases (SO_x , NO_x and NH_3) to particles i.e. SIA formation and re-suspension of inorganic (NPK) fertilizers' residues. In addition to these three sources, biomass-burning emissions are also contributing to aerosol associated WSII over the rural location of Pohara in the Dhauladhar region of North Western Himalaya.

CONCLUSIONS

In the Dhauladhar region of North Western Himalaya, WSII constitutes ~ 15% of PM_{10} aerosols load. SO_4^{2-} contributes maximum (~50%) followed by NO_3^- (~12.5%) and NH_4^+ (~12.5%) to the total concentration of

WSII analyzed. In all the seasons, average concentrations of PM₁₀ and associated WSII were observed to be higher over low altitude rural location than mid altitude urban location. The total concentration of WSII was found to be maximum during the winter season. The results of PCA suggested four major sources of aerosol associated WSII viz. re-suspension of soil or local sediments; conversion of pollutant gases (SO_x, NO_x and NH₃) to particles i.e. SIA formation; re-suspension of inorganic (NPK) fertilizers' residues and biomass-burning emissions over the Dhauladhar region of North Western Himalaya.

ACKNOWLEDGEMENTS

Authors are thankful to Prof. Arun K. Attri, Jawaharlal Nehru University for extending facilities available in his laboratory for the processing of samples. DK acknowledges University Grants Commission, India for the financial support in the form of Non-NET Scholarship.

REFERENCES

- Forster, P., V. Ramaswamy and Co-authors (2007). Changes in atmospheric constituents and in radiative forcing, in Solomon, S., D. Qin, M. Manning, Z. Chen, M. Marquis, K.B. Averyt, M. Tignor and H.L. Miller (Eds.), Contribution of Working Group I to the Fourth Assessment Report of the Intergovernmental Panel on Climate Change, (Cambridge University Press, Cambridge, United Kingdom and New York, NY, USA).
- Gajananda, K., J.C. Kuniyal, G.A. Momin, P.S.P. Rao, P.D. Safai, S. Tiwari K. Ali (2005). Trend of atmospheric aerosols over the north western Himalayan region, India, *Atmos. Environ.* **39**, 4817–4825.
- Heintzenberg, J. (1989). Fine particles in the global troposphere A review. *Tellus B* **41**, 149-160.
- Isaksen, I.S.A., and Co-authors (2009). Atmospheric composition change: Climate–Chemistry interactions, *Atmos. Environ.* **43**, 5138–5192
- Kuniyal, J.C., M. Sharma, K. Chand and C.S. Mathela (2015). Water soluble ionic components in particulate matter (PM₁₀) during high pollution episode days at Mohal and Kothi in the north-western Himalaya, India, *Aerosol Air Qual. Res* **15**, 529-543.
- Pope III, C.A. (2000). Review: epidemiological basis for particulate air pollution health standards, *Aerosol Sci Technol* **32**, 4–14.
- Rajput, P., A. Mandaria, L. Kachawa, D.K. Singh, A.K. Singh and T. Gupta (2016). Chemical characterisation and source apportionment of PM₁ during massive loading at an urban location in Indo-Gangetic Plain: impact of local sources and long-range transport. *Tellus B* **68:1**, 30659.
- Safai, P.D., K.B. Budhavant, P.S.P. Rao, K. Ali, K. and A. Sinha (2010). Source characterization for aerosol constituents and changing roles of calcium and ammonium aerosols in the neutralization of aerosol acidity at a semi-urban site in SW India, *Atmos. Res.* **98**, 78–88.
- Seinfeld, J.H. and S.N. Pandis (2006). *Atmospheric Chemistry and Physics: From Air Pollution to Climate Change*, (John Wiley, New York, USA).
- Singh, A., N. Rastogi, A. Patel, D. Singh (2016). Seasonality in size-segregated ionic composition of ambient particulate pollutants over the Indo-Gangetic Plain: Source apportionment using PMF, *Environ Poll* **219**, 906-915.

SPATIAL AND TEMPORAL VARIATION ASPECTS OF AEROSOL BLACK CARBON CONCENTRATION OVER INDIA

*RAVI RANJAN KUMAR^{1,2}, V. K. SONI¹, M. K. JAIN², ARPIT TIWARI¹

¹India Meteorological Department, New Delhi

²Indian Institute of Technology(ISM), Dhanbad

KEYWORDS: Equivalent Black Carbon(EBC), Biomass Burning(BB)

INTRODUCTION

Black Carbon is one of the very important short term climate forcing agents and a little change in its concentration can considerably affect the climate. Considering its importance India Meteorological Department has established a network of 16 Aethalometers (AE-33) for continuous measurement of equivalent black carbon (EBC) concentration and spectral absorption coefficient over India. Biomass burning (BB) component of EBC aerosol is also estimated at the stations. In the present study, EBC and BB aerosol concentration data have been analyzed for Amini, Bhuj, Chandigarh, Guwahati, Jodhpur, Kolkata, New Delhi, Nagpur, Pune, PortBlair, Ranchi, Ranichauri, Srinagar, Thiruvananthapuram, Varanasi and Vishakhapatnam stations for the year 2016.

METHODS

The variation of BC concentrations was examined with ANOVA (analysis of variance) and F-test. ANOVA and F-tests assess the amount of variability between the group means in the context of the variation within groups to determine whether the mean differences are statistically significant. There is a significant variation in the daily mean data of different stations. F values were also calculated for monthly, seasonal and diurnal variations among all 16 stations and it is 8.6, 5.2 and 47.2 respectively. On comparing these F values according to their degree of freedom, significant monthly, seasonal and diurnal variation of EBC concentration is observed.

RESULTS & DISCUSSIONS

North Indian stations showed higher concentration of EBC than coastal stations of southern India. Mega cities like New Delhi and Kolkata have very high concentration of EBC and apart from these other stations located in Indo-Gangetic Plane also show high EBC concentration. The annual mean EBC concentration (ngm^{-3}) is depicted on geographical map of India (figure 1). Most of the north Indian stations show high BC concentration during month of November, December and January and minimum during rainy season. Seasonal variation of EBC concentration is also discussed.

CONCLUSIONS

- Highest EBC concentration was found in New Delhi and Kolkata followed by other north Indian stations.
- IGP region stations showing high EBC concentration in November, December and January.
- South Indian stations showing very low EBC concentration throughout the year.
- Diurnal variation pattern showing high concentration in the evening hours

2016 [eBC]

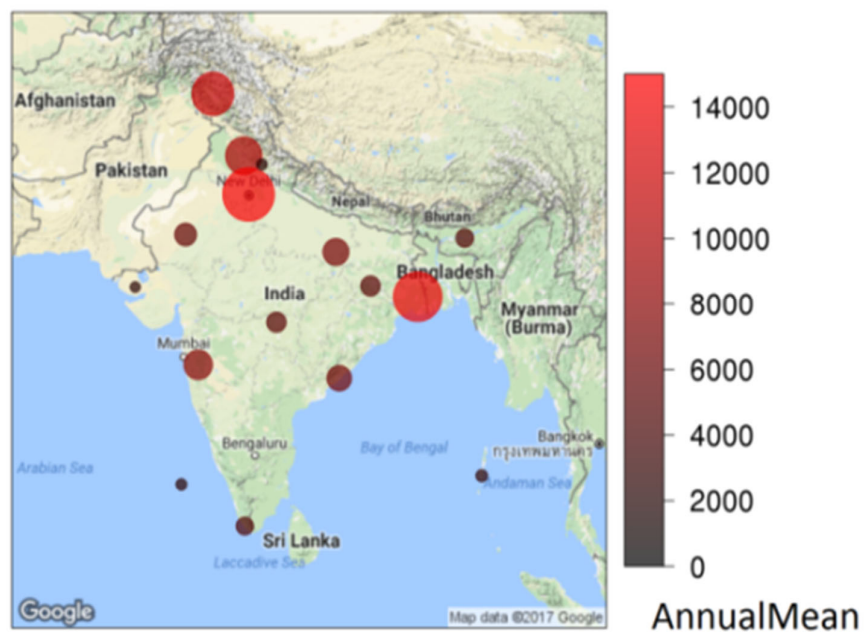


Figure 1. Annual average equivalent black carbon concentrations at different stations.

ACKNOWLEDGEMENTS

We are thankful to EMRC, India Meteorological Department for providing Black carbon data.

EFFECT OF AEROSOL COAGULATION ON HOMOGENITY IN A REACTION CHAMBER

ARSHAD KHAN¹, P. S. RAJAGOPAL², MANISH JOSHI¹, JANKI SHINDE², MADHUKAR M. RAO²
B. K. SAPRA¹ AND D. DATTA¹

¹Radiological Physics and Advisory Division, Bhabha Atomic Research Centre, Mumbai, 400 085, India.

²CFDVRi, Mount View Complex, McLeod Ganj, Himachal Pradesh-176219, India

KEYWORDS: cfd, coagulation, mixing, chamber.

INTRODUCTION

Aerosol size distribution gets evolved due to various processes which modify the parameters of the distribution function. Processes involved in such evolution include nucleation, coagulation and condensation/evaporation. Collision between two particles is characterized by a coagulation kernel which is defined for various colliding processes. The form of the kernel is the function of particle sizes (Knudsen number), colliding process and thermodynamic parameters. As analytical solutions are available for approximated cases, numerical schemes are developed for solving general coagulation equation. The strategy is important as its coupling to other process equations characterize general dynamic equation of aerosol particles. There are different ways to numerically solve the coagulation equation viz. method of moments, sectional method, nodal method and incorporation of drift fluxes. In recent times, Computation fluid dynamics (CFD) has also been employed for simulating aerosol flow and transport. Due to mathematical complexities related to coagulation equation, only few attempted coupling of Navier-Stokes equations with aerosol coagulation scheme. Rajagopal et al. 2017 discussed the development of coupling of aerosol dynamics equation (incorporated coagulation, gravitational settling, thermophoresis and diffusion) with a computational fluid dynamics code. Transport and fate of aerosol particles in closed chamber depends on mixing patterns and dynamical processes. The role of coagulation towards particle homogeneity inside the chamber is a vital aspect. This study discusses the results of simulations performed with ANSWER-CFD code (Rajagopal et al. 2017) focused on aerosol transport and coagulation in closed chamber conditions.

METHODS

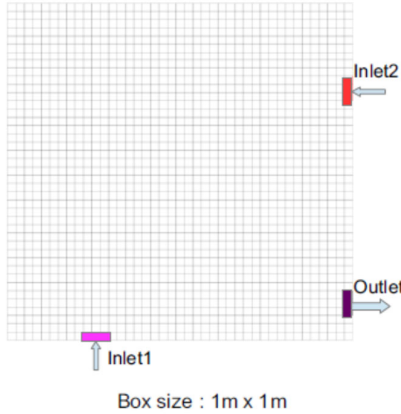
ANSWER-CFD code simulates dynamics and transport of aerosols by General dynamic equation (GDE) written as

$$\begin{aligned} \frac{\partial n(d_p, r, t)}{\partial t} + \nabla \cdot [U n(d_p, r, t)] \\ = \nabla \cdot \{D(r, t) \nabla n(d_p, r, t)\} + \frac{1}{2} \int_0^{d_p} K(d'_p, d_p - d'_p) n(d'_p, r, t) n(d_p - d'_p, r, t) d(d'_p) \\ - n(d_p, r, t) \int_0^\infty K(d_p, d'_p) n(d'_p, r, t) d(d'_p) + S(d_p, r, t) - \lambda n(d_p, r, t) \\ - \nabla \cdot [U_{drift} n(d_p, r, t)] \end{aligned}$$

Where d_p and d'_p are particle diameters; $n(d_p, r, t)$ is the spatially (r) and temporally (t) varying number concentration distribution function for particle diameter d_p ; U is the gas phase velocity; D is the particle diffusivity; K is the collision frequency between particles of different sizes; S is the source term arising from nucleation and direct emission; λ is the decay rate of the species; U_{drift} is the total drift velocity of the aerosol particles due to various mechanisms like gravitational settling, thermophoresis, turbophoresis etc. In this work, Fuchs kernel (Fuchs 1964, Jacobson 2005) was employed for coagulation collision frequency. Integration terms of coagulation were dealt using nodal approach (Prakash et al. 2003) segregating the particle size range (logarithmically equally spaced) into a finite number of zero width nodes. Validation of coagulation module of ANSWER-CFD code has been discussed elsewhere (Rajagopal et al. 2017).

RESULTS & DISCUSSIONS

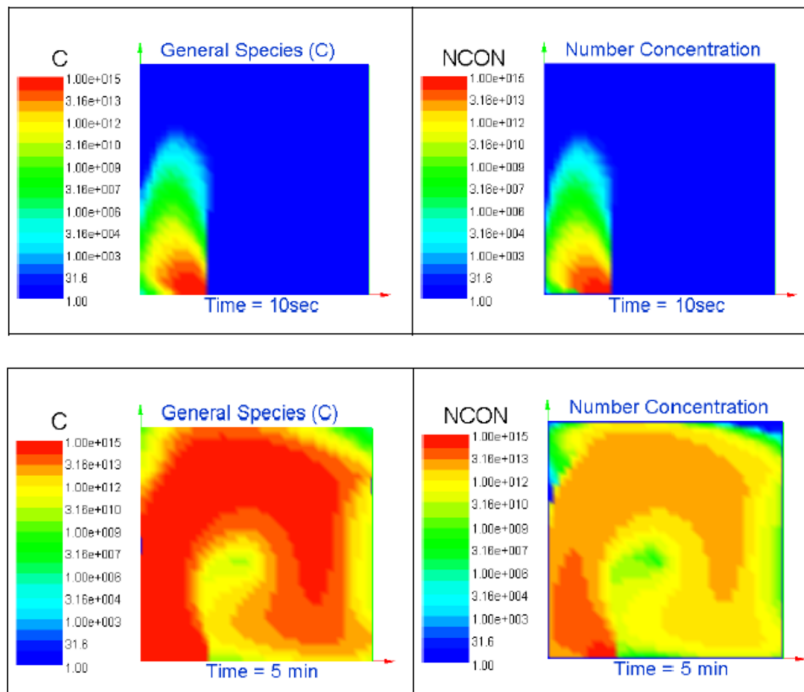
Reactor chambers are employed for aerosol experiments under controlled conditions with targeted outcomes. In this problem, a square box of dimensions 1 m x 1 m with two inlets and one outlet is used for simulations (Fig. 1). Multiple inlet flows are provided for enhanced particle mixing.



Uniform grid sizing approach (1849 nodes for grid size 43 x 43) was adopted for simulations. Two dimensional air flow ($U=-0.01$ m/s, $V=0.01$ m/s) at inlet 1 and one dimensional air flow ($U=-0.01$ m/s) at inlet 2 was used for mixing. The inlet number concentration of aerosol particles at inlet 1 was fixed as 10^{15} #/m³. These particles are assumed to have a lognormal size distribution with count median diameter of 15 nm and geometric standard deviation of 1.3. A total of 15 size bins were used for covering size spectrum from 1 nm to 10 μ m. Particle density was assumed to be 1500 kg/m³. Air exchange rate under the given conditions came out to be 5.26 h⁻¹. A generic species with the same number concentration was also injected in test domain and the behaviour of evolution profile of number concentration was studied. Aerosol particles were allowed to undergo coagulation in contrast to generic species.

Figure 1. Box specifications

Both the particles and generic species also undergo convective and diffusive transport within the domain. Diffusion coefficient for aerosol particles is computed based on their sizes. Fig. 2 compares the spatial distribution of number concentration for general species and aerosol particles in similar mixing conditions.



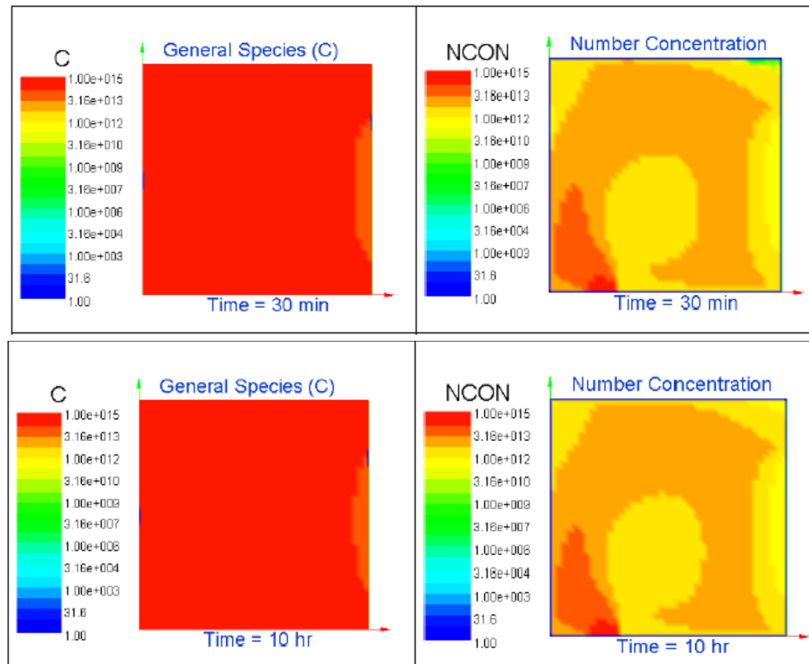


Figure 2. Spatial profile of number concentration for general species and aerosol particles at 10 sec, 5 min, 30 min and 10 h

At 10 seconds, number concentration can be seen to be injected through inlet 1 for both the cases. Except at nearby jet regions, species as well as particles could not fill the test domain for the given flow conditions. As time progresses, number concentration lob ejected through inlet 1 evolves and propagates covering the test domain. Magnitude of number concentration becomes different for species and particles, as expected (as shown for 5 min). As the time passes on, number concentration of generic species becomes uniform in entire domain whereas the profile of particles remain inhomogeneous. This inhomogeneity was found to be preserved for particles as shown for the results obtained at long times.

CONCLUSIONS

This study compared the spatial profile of number concentration in a square box generated for a generic species and aerosol particles. Both of these were allowed to undergo convective and diffusive transport but only particles coagulated. Simulations were performed by ANSWER-CFD code incorporating aerosol dynamics mainly Fuchs kernel for coagulation. It was found that number concentration generic species become homogeneous whereas steady state inhomogeneity results for aerosol particles. This kind of inhomogeneity challenges the assumption of well mixed concentration required for unbiased sampling.

REFERENCES

- Fuchs, N. A. (1964). *The Mechanics of Aerosols* 1964. Pagamon, New York.
- Jacobson, M. Z. (2005). *Fundamentals of atmospheric modeling*. Cambridge university press.
- Rajagopal P.S. et al. (2018). Numerical Modeling of Aerosol Transport and Dynamics. In: Runchal A., Gupta A., Kushari A., De A., Aggarwal S. (eds) *Energy for Propulsion. Green Energy and Technology*. Springer, Singapore DOI https://doi.org/10.1007/978-981-10-7473-8_14

EFFECT OF SOLUTE STRENGTH AND CHEMICAL NATURE OF ATOMISED AEROSOL PARTICLES ON CHARGE SIZE DISTRIBUTIONS

MARIAM, MANISH JOSHI, AMRUTA NAKHWA, PALLAVI KHANDARE, ARSHAD KHAN,
B. K. SAPRA

Radiological Physics and Advisory Division, Bhabha Atomic Research Centre, Mumbai -400085

KEYWORDS: aerosol monitoring and characterization, charge distribution, atomisation, elpi

INTRODUCTION

Effect of aerosol particles on various aspects such as human health, air quality, climate etc, depends on particle size, shape, concentration and charge. Among them charge on aerosol has a major impact on its dynamics (e.g. affecting nucleation, coagulation), transport and deposition, micro-contamination control, particle collection characteristics of air filters, deposition of particles in the human lung etc.

Different generation methods can impart different charge levels to aerosols. The charge magnitude and its distribution is function of particle size, particle's properties (such as conductivity etc.) and properties of the dispersing or generation medium (such as dielectric constant etc.). Even with same generation method different level of charging occurs for different materials, for e.g. atomised Di-octyl-sebacate (DOS) particles are almost entirely uncharged, while sodium chloride (NaCl) particles are highly charged, and polystyrene latex particles possess the highest charge (Kousaka et al., 1981), though all three have been generated by atomisation.

Earlier studies used Electrical Analyzer or Dual Mobility Particle Sizer to measure the charge in terms of number concentration which was then converted to charge fractions using charge equilibrium theories (Rodrigues et al., 2006; Sahu et al., 2012). Recently available commercial instrument which can be used for such measurements is the Electrical Low Pressure Impactor (ELPI) (Keskinen et al., 1992) which is a real time particle spectrometer for measuring airborne particle size distribution (number and charge) at high sampling frequencies. Charge measurement has become direct and easier with ELPI. Its operating principle can be divided into three parts; Particle charging, Size classification in a cascade impactor and Electrical detection with sensitive electrometers.

Charge measurement of atomizer is motivating study in view of its direct applications in asthmatic inhalers, medicine delivery, in spray dryer installations, fuel injection systems etc. In this study, the effect of solution strength (%w/v) on charge size distribution for the atomized aerosols of two chemicals with different bond nature viz., NaCl and silica were measured and interpreted.

EXPERIMENTAL METHODOLOGY

Experiments were carried out in 0.5 m³ stirred chamber (see Fig. 1) which was fed with dried atomized particles. ELPI and Condensation particle counter (CPC) were used to measure the charge distribution and the total particle concentrations respectively in the chamber. Charge being an extremely sensitive parameter, a minor sampling diversion can affect results and interpretation. Therefore, all measurements were interpreted only under steady conditions ensured by CPC, which served as a reference instrument. The essential measurement of net charge per particle (size based) was obtained using ELPI, by keeping charger ON and OFF for 20 seconds alternatively. Under charger ON condition, ELPI measures number concentration using calibrated penetration function while it measured current over all stages for charger OFF condition.

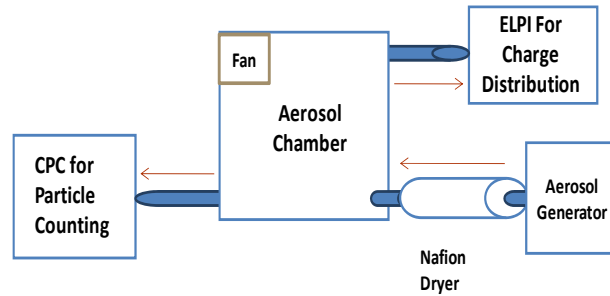


Figure 1: Experimental Set up

Results and discussion:

With same generation method i.e. atomization, two species with different bond nature viz., NaCl and silica were chosen to study the charge level acquired by them along with effect of particle size and solute strength.

NaCl

Three different concentrations of NaCl viz., 0.1%, 1% and 10% w/v were used to generate aerosols using atomiser and then analysed for acquired charge. Charge/particle was seen to be increasing from 0.116 to 11.974 within the particle diameter range of 0.01-1.1 μm (Fig. 2). As evident from the figure 2, charge/particle increases with decrease in solute concentration which is in agreement with literature (Tsai et al., 2005 and Forsyth et al., 1998 etc).

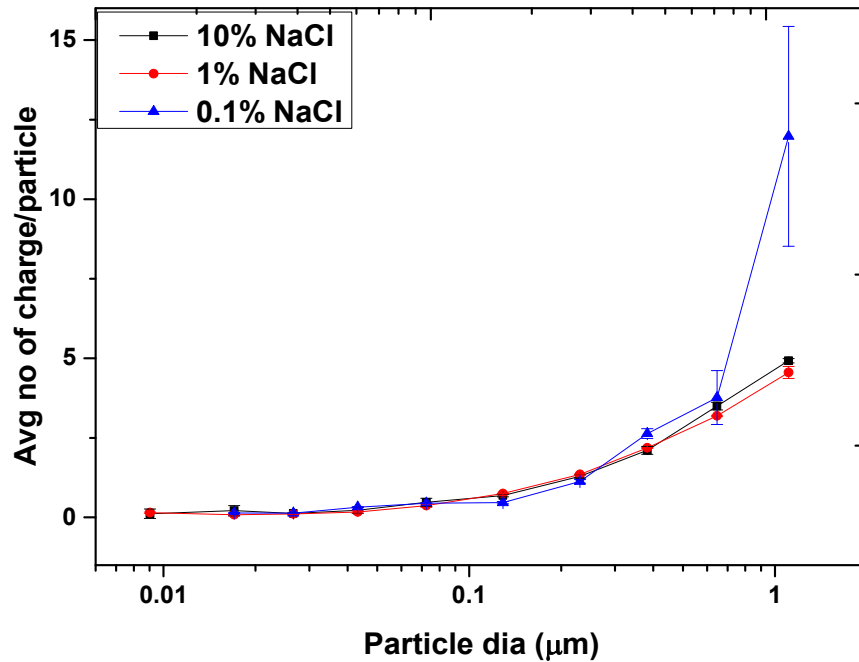


Figure 2: Combined Charge size distribution of atomized aerosols for 0.1%, 1% and 10% NaCl

Generation of aerosols by atomization promotes spray electrification, resulting in formation of electrical double layer (EDL). Impurities or additional ions may enter and interact with the EDL, causing an electrical potential change in the inner charge region. The relationship between charges on particle generated by atomizer with ion concentration can be stated as:

$$\text{Charge} \propto \frac{1}{\text{ion concentration}} \propto \text{Dielectric constant}$$

A theoretical analysis based on the theory of Smoluchowski (1912) models spray electrification as the statistical charge fluctuation occurring on sprayed droplets. The root mean square particle charge, n_{rms} is evaluated from the expression

$$n_{rms} = \left[\frac{2NVakT\kappa}{akT\kappa + 2e^2NV} \right]^{1/2} \quad (1)$$

Where, V= droplet volume (cm³), A= droplet radius (cm), κ = liquid dielectric constant, N= concentration of ionized molecules of either polarity in the liquid (particles/cm³)

When the return flow of charge from the droplet is neglected, this expression becomes a symmetrical charge distribution. As N approaches infinity Eq. (1) can be written as

$$\lim_{N \rightarrow \infty} n_{rms} = \left[\frac{akT\kappa}{e^2} \right]^{1/2} \quad (2)$$

Theoretical plots were generated using equation 2 for 0.1%, 1% and 10% NaCl which are represented in Figure 3. With increase in concentration (molarity) of NaCl, dielectric constant (κ) decreases hence the particle charge increases.

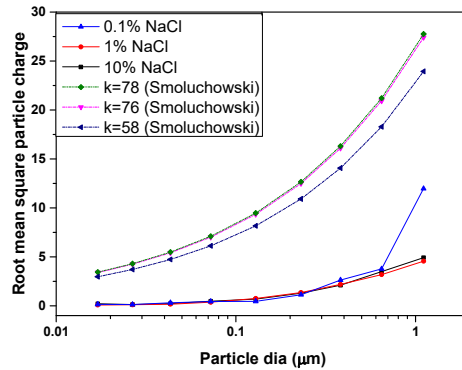


Figure 3: Experimental and theoretical plot for nebulization of NaCl

The experimental results were found to be following similar increasing trend but over-predicted by theory. The reasons for difference of experimental measurements with theory could be due to incomplete homogenization of ions (Forsyth et al., 1998) and measurement of only net current on ELPI stages, whereas Smoluchowski equation gives root mean square particle charge.

Silica

Similarly, silica aerosols were generated using four different concentrations of solution viz. 0.1%, 0.5%, 1%, and 10% (w/v). Combined results obtained are plotted in Figure 4. In this case, charge/particle was found to be increasing from 0.252 to 4.995 within the particle diameter range of 0.02-0.76 μm .

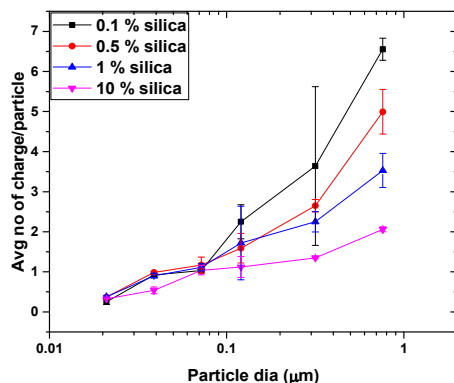


Figure 4: Charge size distribution of atomised aerosols for 0.5%, 0.1%, 1% and 10% silica

The effect of particle size on acquired charge was similar to as observed for NaCl. However in contrast, the degree of change in acquired charge/particle with solute concentration was more. The difference in NaCl and silica arises due to the difference in their chemical character and polar activity, former is ionic in nature and latter is having covalent bonding. NaCl molecule dissociates in water, therefore statistical fluctuation can be expected in disruptive dipole behaviour. Whereas, Silica being extended structure will have less fluctuation giving better results in term of concentration effect. For each concentration, charge acquired by silica is higher than NaCl (Fig. 5), which might be due to the highly polar Si-O bond affecting the water interactions and charge acquisition during spray electrification. To further elaborate the results and interpretation, a detailed study will be required to fully understand behaviour of silica upon atomisation.

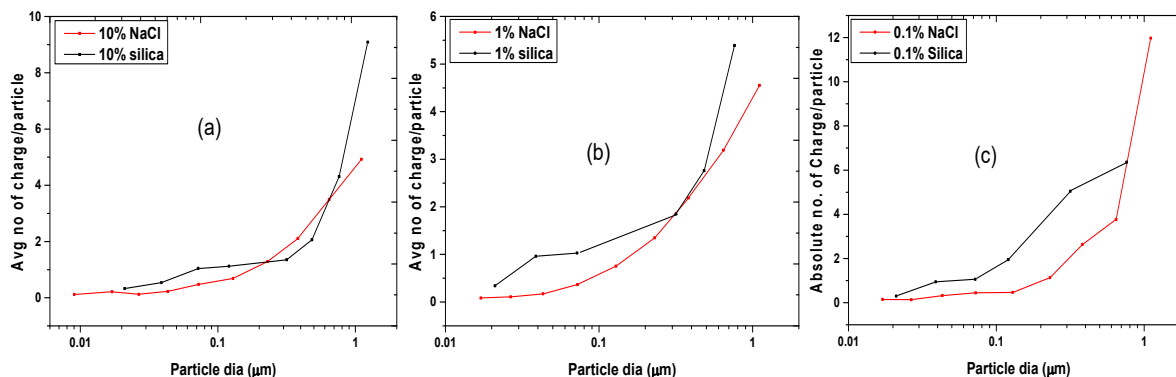


Figure 5: Comparison between charge size distribution of nebulized aerosols of silica and NaCl for a) 10%, b) 1% and c) 0.1%

CONCLUSION

Experiments were carried out to study the effect of chemical nature and solution strength on charge acquired by aerosol particles generated by same generation method i.e., atomisation. Two species of different chemical nature viz., NaCl (0.1%, %1 and 10%) and Silica (0.1%, 0.5%, %1 and 10%) were generated by atomisation and charge/particle was measured using ELPI. Experimental results were studied in terms of understanding the mechanism of charge generation. Charge/particle was found to increase with increase in particle diameter and decrease in the solute concentration. The concentration effect on charge acquired was seen to be better for silica compared to NaCl nebulisation probably due to stable structure of the former. For each concentration, charge acquired by silica is higher than NaCl, which might be due to the highly polar Si-O bond. A detailed study is required to fully understand behaviour of silica upon atomisation.

Theoretical analysis using Smoluchowski equation (spray electrification) was done for NaCl. Although capturing the trend of increase of charge with increase in particle size and decrease in solute strength, the charge levels were found to be over-predicted by theory. The reasons for this discrepancy could be because of incomplete homogenization of ions, measurement of net current on ELPI stages.

REFERENCES

Forsyth, B., Liu, B.Y.H. and Romay, F.J. (1998). Particle charge distribution measurement for commonly generated laboratory aerosols. *Aerosol Sci. Technol.*, **28**, 489-501.

Keskinen, J., Pietarinen, K. and Lehtimäki, M. (1992). Electrical low pressure impactor. *J. Aerosol Sci.*, **23**, 353–360.

Kousaka, Y., Okuyama, K., Adachi, M. and Ebie, K. (1981). Measurement of Electric Charge of Aerosol Particles Generated by Various Methods. *J. Chem. Eng. Jpn.*, **14**, 54–58.

Rodrigues, M.V., Marra, Jr. W.D., Almeida, R.G. and Coury, J.R. (2006). Measurement of the electrostatic charge in airborne particles: II – particle charge distribution of different aerosols. *Braz. J. Chem. Eng.*, **23**, 125-133.

Sahu, M., Park, J. and Biswas, P. (2012). In situ charge characterization of TiO₂ and Cu–TiO₂ nanoparticles in a flame aerosol reactor. *J. Nanoparticle Res.*, **14**, 678.

Smoluchowski, M.V. (1912). Experimentally Demonstrable Molecular Phenomenon, *Physics Z.*, **13**, 1069

Tsai, C.J., Lin, J.S., Deshpande, C.G. and Liu, L.C. (2005). Electrostatic charge measurement and charge neutralization of fine aerosol particles during the generation process. *Part. Part. Syst. Char.*, **22**, 293–298.

DEAD TIME ESTIMATION OF LICEL TRANSIENT DIGITIZER OF RAMAN LIDAR SYSTEM

JASWANT^{1,2}, RADHAKRISHNAN S. R¹, SHISHIR KUMAR SINGH^{1,2}, D. K. SHUKLA¹,
DAVENDER SETHI^{1,2}, C. SHARMA¹

¹Environmental Sciences & Biomedical Metrology Division, CSIR-National Physical Laboratory, Dr. K. S. Krishnan Marg, New Delhi-110012, India.

²Academy of Scientific and Innovative Research, CSIR Campus, CSIR Road, Taramani, Chennai, India, 600 113.

KEYWORDS: photon counting, dead time, licel transient digitizer, scaled analog.

INTRODUCTION

A lidar system can provide the vertical distribution of optical properties of aerosols or clouds with high temporal and spatial resolution (Ansmann et al 2012). With the introduction of Licel transient digitizers in Raman Lidar systems, it has become possible to simultaneously measure both the photomultiplier output in analog voltage and photon counts. A combination of both these signals provide an improved signal and can increase the dynamic range of the system [Newsom et al., 2009]. Before gluing, it is required to correct the photon count signal for the dead time in order to reduce the pulse-pile up effect [Whiteman et al., 1992]. The dead time of the system or transient recorder, depends on the high voltage setting and PMT characteristics. These properties may change with time [Newsom et al., 2009]. Thus, it is required to periodically monitor the system dead time and apply dead time correction accordingly.

METHODS

The approach used in this study involves estimating the dead time by minimizing the root-mean squared difference between the measured analog and the virtual analog data. The process of estimating τ using this method begins by selecting several days with little or no cloud cover. This typically results in very large data points which are reduced by determining a relationship between analog and photon counts data. We can obtain the shrunked data set by calculating the median value of analog voltage, photon counts and standard deviation of analog signal. Thus, a curve is obtained between the analog and photon counts values. The next step involves the minimization of equation 3 with respect to dead time. The calculation of scaled analog signal and dead time corrected photon signal is performed using equation 1 and 2 respectively.

$$a'_k = s'c'_k + o' \quad (1)$$

$$c'_k = \frac{c_k}{1 - c_k * \tau} \quad (2)$$

$$J(\tau) = N^{-1} \sum_{k=0}^{N-1} (a_k - a'_k)^2 \delta a_k^{-2} \quad (3)$$

The minimum of $J(\tau)$ is obtained by varying τ from 0 to 10 ns in steps of 0.1 ns. The minimization is estimated by fitting a parabola to the smallest value of $J(\tau)$ and its two neighbours. The minimum value of the parabola fit corresponds to the dead time of the system.

RESULTS & DISCUSSIONS

We obtained the dead time of the system using multiple profile fit method for non cloudy days in the month of June and November 2016. We obtained the minimum value of $J(\tau)$ at $\tau = 4.22\text{ns}$ for the data of November 2016. The dead time calculation for the other days in the month of June and November are given in table 1. It can be observed from the table that dead time of the system is being increased with the time. Therefore, we can say that it is mandatory to periodically monitor the dead time of the Raman lidar system.

Date	Dead Time (ns)
07.06.2016	4.12
10.06.2016	4.12
20.06.2016	4.12
21.06.2016	4.13
22.06.2016	4.13
09.11.2016	4.22
10.11.2016	4.22
11.11.2016	4.22

Table 1. Temporal evolution of the dead time of the lidar system

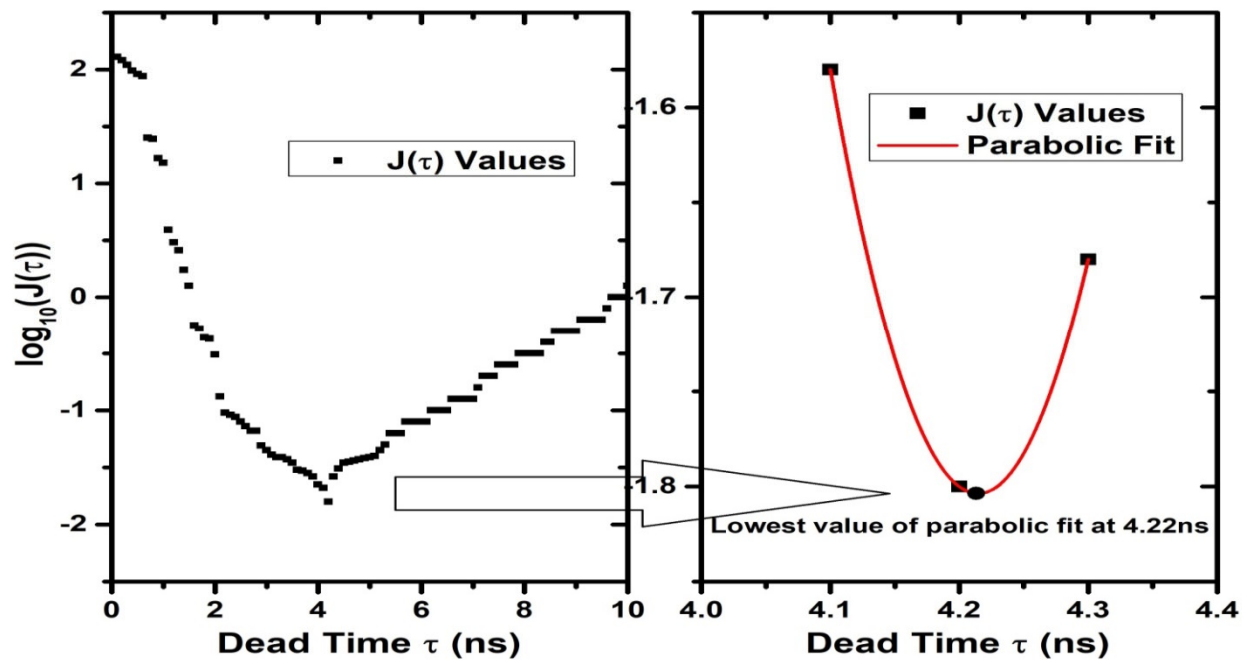


Figure 1(a). shows the behaviour of $J(\tau)$ versus τ (b) shows the parabolic fit on the smallest value of $J(\tau)$ and its two neighbouring values.

CONCLUSIONS

The dead time of the system was estimated using the multiple profile method, we have observed the system dead time approximated to 4.2 ns which is slightly higher than the value prescribed by the manufacturer. After dead time correction, the relationship between analog and photon counts was found linear. The temporal evolution of dead time was also observed and it was found that dead time of system is increasing with time. The dead time corrected signal with dead time = 4.2ns, was used to obtain the glued signal.

ACKNOWLEDGEMENTS

Authors are grateful to Director, NPL and Head Environmental Sciences & Biomedical Metrology Division (ESBMD) for necessary support. Authors are thankful to CSIR network project PSC-0112 for necessary financial support. Mr. Jaswant is thankful to Council of Scientific and Industrial Research (CSIR) for providing research fellowship and also to Academy of Scientific and Industrial Research (AcSIR) for facilitating as its PhD student.

REFERENCES

- Ansmann, A., Seifert P., Tesche M. and Wandinger U. (2012). "Profiling of fine and coarse particle mass: case studies of Saharan dust and Eyjafjallajökull/Grimsvötn volcanic plumes," *Atmospheric Chem. Phys.*, vol. 12, no. 20, pp. 9399–9415.
- Whiteman D. N., Melfi S. H. and Ferrare R. A. (1992). "Raman lidar system for the measurement of water vapor and aerosols in the Earth's atmosphere," *Appl. Opt.*, vol. 31, no. 16, p. 3068.
- Newsom R. K., Turner D. D., Mielke B., Clayton M., Ferrare R. and Sivaraman C. (2009). "Simultaneous analog and photon counting detection for Raman lidar," *Appl. Opt.*, vol. 48, no. 20, pp. 3903–3914.
- Zhang Y., Yi F., Kong W. and Yi Y. (2014). "Slope characterization in combining analog and photon count data from atmospheric lidar measurements," *Appl. Opt.*, vol. 53, no. 31, p. 7312.

SIMULATION OF VOLATILE ORGANIC COMPOUNDS AND SECONDARY ORGANIC AEROSOLS OVER THE INDIAN REGION BY THE CAM4-CHEM MODEL USING CMIP5 AND CMIP6 EMISSIONS

P. VATS¹, D. GANGULY¹, A. BISWAS¹, AND A. K. SHARMA¹

¹Centre for Atmospheric Sciences, Indian Institute of Technology Delhi, New Delhi, India

Email: pawanvats5086@gmail.com

KEYWORDS: Secondary organic aerosols (SOA), Volatile organic compounds (VOC), Coupled Model Intercomparison Project Phase 6 (CMIP6).

INTRODUCTION

Organic aerosols (OA) is an important contributor (20 to 90%) to the fine aerosols particles over land areas across the globe (Zhang et al., 2007). Previous researches on OA also suggest that it comprises of nearly 50% of surface level PM 2.5 mass concentrations over most locations across the globe (Pandis et al., 2013; Rengarajan et al., 2011). The OA consists of both primary organic aerosols (POA) and secondary organic aerosols (SOA). It has also been reported that sometimes SOA contributes a significant fraction of around 60% (Jimenez et al., 2009) of OA. SOA plays an important role in nucleation and the scattering of incoming solar radiation (Kanakidou et al., 2005; Tsigaridis & Kanakidou, 2007). However, there is a large uncertainty associated with the formation mechanisms of SOA, due to complex chemical reactions involving oxidation, reduction, photochemical, free radical with distinct organic compounds (e.g. Griffin et al., 2002; Kroll and Seinfeld, 2008; Hallquist et al., 2009; Langmann et al., 2014). These complex formation mechanism of SOA is a major hurdle in the implementation of these processes in the atmospheric chemistry models (Langmann et al., 2014). Among other major causes of uncertainty in simulation of OA by models include the incorrect emissions of POA, uncertainty associated with the volatility distribution of POA and their chemical reaction capability (Robinson et al., 2007), and uncertainty in the emissions of volatile organic compounds (VOC) which are the precursors for the formation of SOA. In the present study, we compare the simulation of VOCs, SOA, and Organic carbon over the Indian region by the CAM4-Chem model using Coupled Model Intercomparison Project phase 5 and phase 6 (CMIP5 and CMIP6) emissions. We evaluate the performance of CAM4-Chem model using these two different emission data with the available observations of OA over the Indian region. We find that although there is a slight improvement in the simulation of VOCs and SOA over the Indian region using CMIP6 emissions over CMIP5 emissions, our model results still underestimates the observations available locally from India. In this work we also discuss some of the modelling challenges involved and scope for possible improvements in the simulation of OA over the Indian region.

METHODS

We use a global climate model called the Community Earth System Model (CESM1, released version 1.2) for simulating the SOA, VOC and OC over the Indian region. The atmospheric component of CESM1 used here is the Community Atmospheric Model version 4 with coupled extensive interactive atmospheric chemistry for troposphere and stratosphere (CAM4-Chem), which consist of detailed representation of atmospheric chemistry and aerosol processes in addition to all other features of the standard CAM4 model (Lamarque et al. 2012; Tilmes et al., 2015, 2016). The interactive chemistry module in the CAM4-Chem is borrowing from the Model for Ozone and Related Chemical Tracers (MOZART), version 4. We have performed simulations of CAM4-Chem for a period of 6 years (2010-2015) with the “specified dynamics” mode, enabling us to constrain the model meteorology to agree with the meteorological analysis from MERRA-2 through prescribing winds, temperature, and surface heat and moisture fluxes, while aerosol mass concentration evolves according to the model’s governing equations. Both the simulations are

performed at the same horizontal resolution of 0.90 latitude x 1.250 longitudes and with 56 vertical pressure levels from the surface to top of the atmosphere (TOA). We use the Representative Concentration Pathways (RCP) 8.5 emission data as part of the CMIP5 emissions used in this study. The CMIP6 emissions data of anthropogenic GHGs, radiatively active gases and aerosols used here are described by Hoesly et al. (2018). Both CMIP5 and CMIP6 emissions data used here are generated using the Community emission data system (CEDS) developed at NCAR (National Centre for Atmospheric Research).

RESULTS & DISCUSSIONS

We perform two simulations using the CAM4-Chem model for the period 2010 to 2015 with identical model configuration in the “specified dynamics” mode, but first using the CMIP5 and next using the CMIP6 emissions. Hence any change in model results indicate effect of change in emission data, as chemical mechanisms, meteorology, other mechanisms involved in the life cycle of aerosols remain identical in both the simulations. We note significant differences in the distribution and concentrations of OA, VOC, OC and oxidants over Indian region due changes in emissions of anthropogenic aerosols & precursors. In both simulations, the CAM-Chem model underestimates the values of aerosol optical depth (AOD), volatile organic compounds (VOC), OC, and SOA concentrations over the Indian region and especially over the Indo-Gangetic plain with respect to available observations.

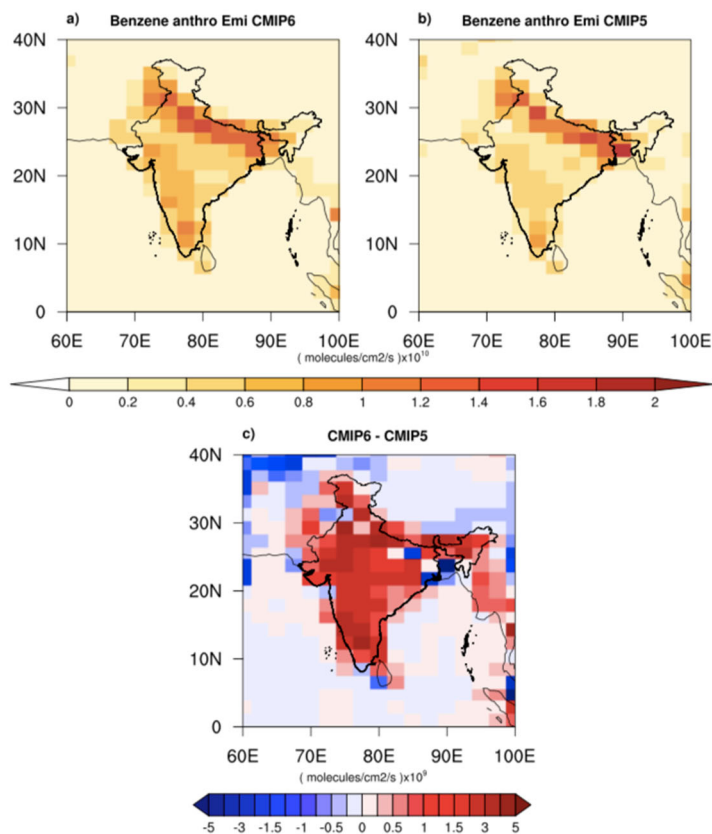


Figure 1: Annual mean surface emission of benzene from anthropogenic sources in (a) CMIP6 and (b) CMIP5 and (c) difference between CMIP6 and CMIP5 emissions. Annual mean emissions of six years (2010 to 2015) are used to generate these plots.

Figure 1 shows the spatial distribution of annual mean surface emission of benzene based on CMIP6 and CMIP5 emissions data and their differences between the two data sets. Previous literature have already reported about the underestimation of emissions of aerosols and their precursors over the Indian region in

CMIP5 data. Clearly, the emissions of Benzene from the Indian region is higher in CMIP6 data compared to CMIP5 data, particularly over the Indo-Gangetic Plain.

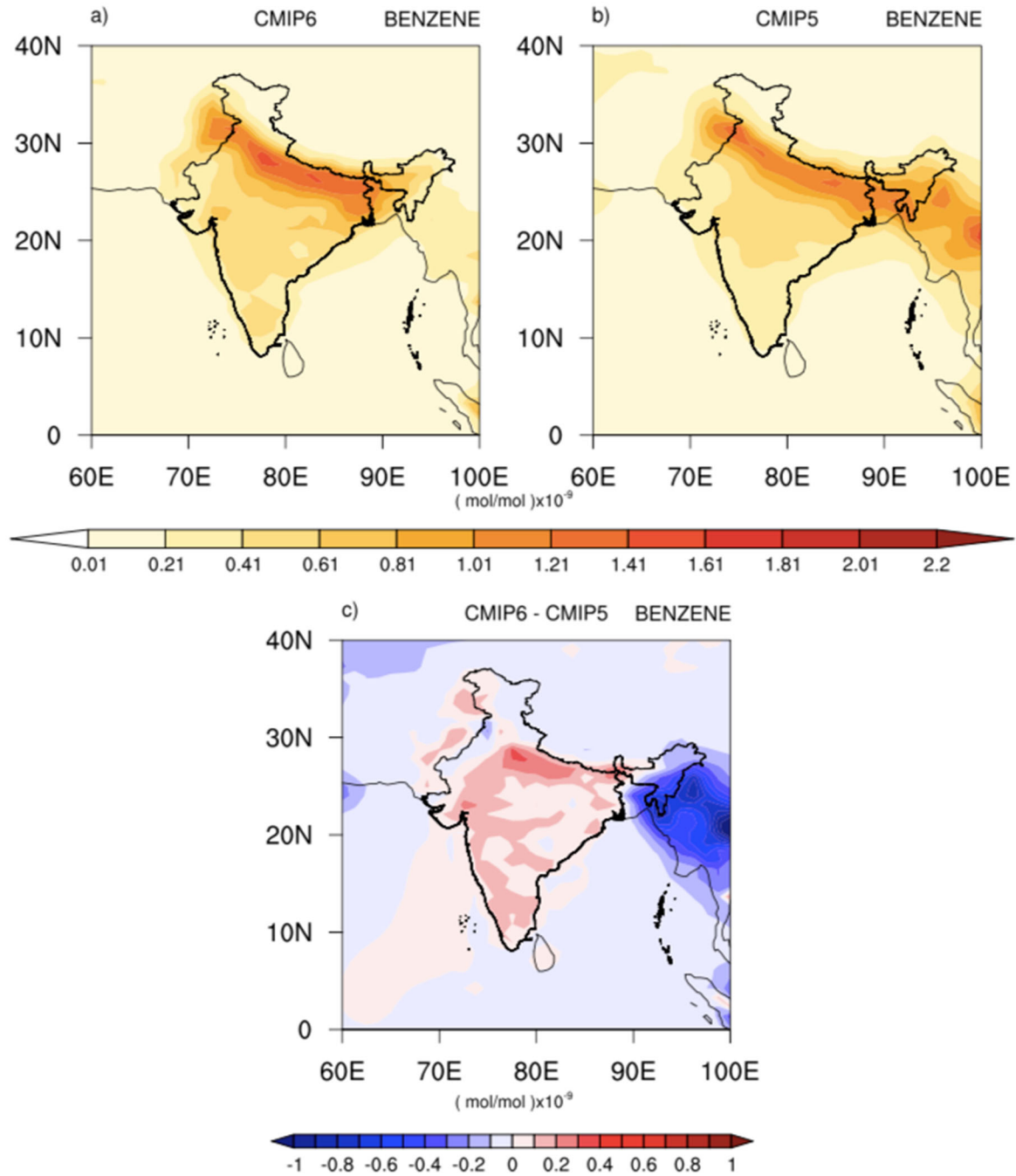


Figure 2 same as figure 1 expect shown simulated surface concentration of SOAB from two simulations for the period of 2010 to 2015 and having unit mol/mol with spatial resolution of 1 degree.

The increase in emission of benzene across the Indian region suggests that CMIP6 data incorporated rise in anthropogenic activity due increases in population across the region.

Figure 2 shows the spatial distribution of annual mean climatology (2010 to 2015) of surface concentration of SOA produced from benzene (SOAB) as simulated by the two simulations using CMIP6 and CMIP5 emissions. This difference in surface concentration of SOAB shows that how differences in the emission of benzene leads to differences in simulated SOA concentration. The noted increases in simulated concentration of SOA is a result of increases in emission of benzene as well as other oxidants such as NOx involved in the production of SOA from precursor VOCs. It is also interesting to note the decreases in the simulated concentrations of SOAB over the Myanmar region in the simulation involving the CMIP6 emissions compared to CMIP5 emissions which is partly due to lower emissions of benzene from this part of the world in CMIP6 compared to CMIP5 emissions.

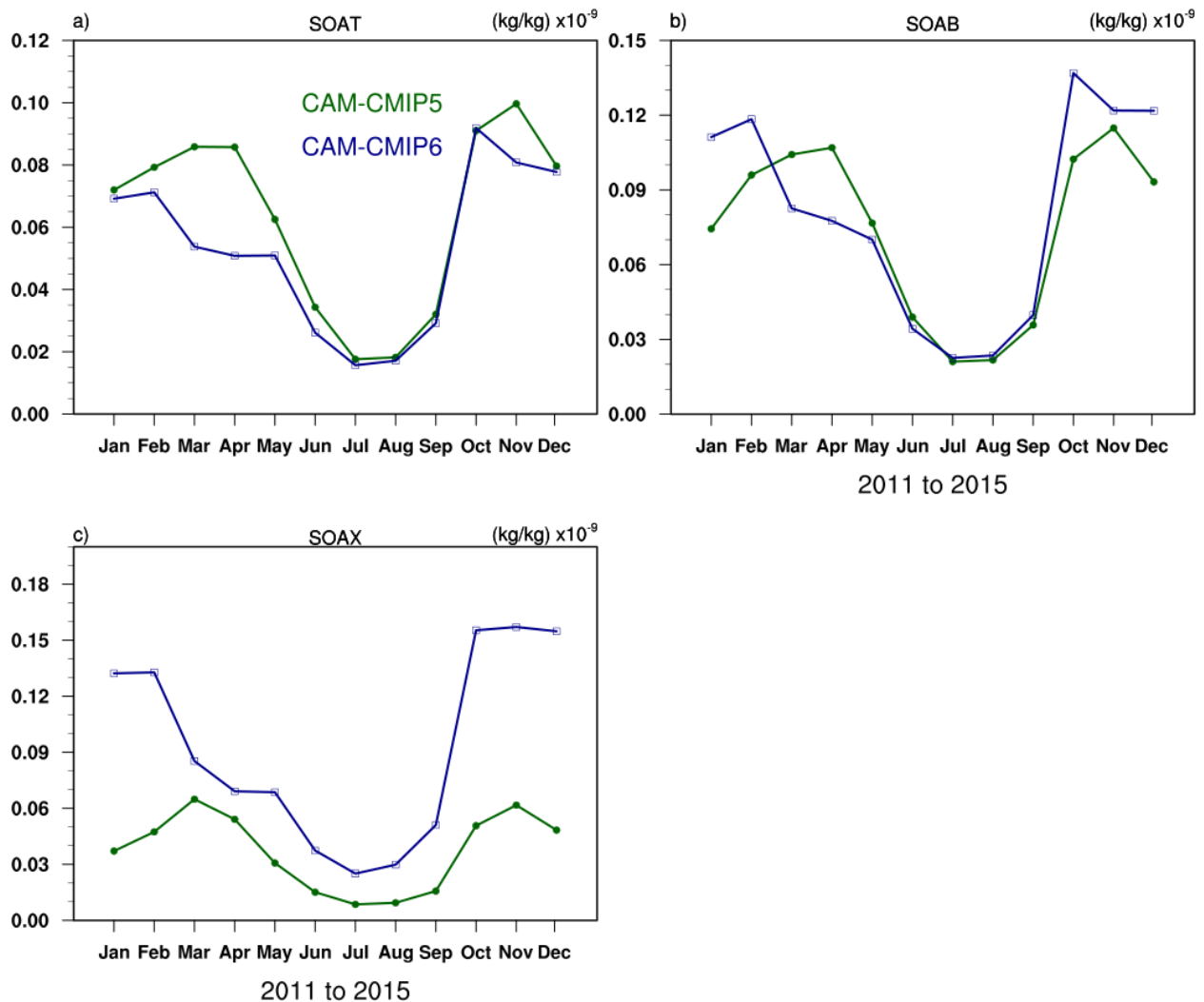


Figure 34 Annual cycle of monthly mean climatology of simulated surface concentration of SOAs from major aromatic VOCs namely (a) Tolene, (b) Benzene, and (c) Xylene from the two simulations for the period 2010 to 2015 over India.

Figure 3 shows the annual cycle of monthly mean climatology of surface concentration of SOAs from three major aromatic VOCs namely (a) Toluene, (b) Benzene, and (c) Xylene as obtained from the two simulations involving CMIP5 and CMIP6 emissions. Interestingly, although there is a significant increase in the simulation of SOA produced from Xylene (SOAX) throughout the year, we notice a decrease in concentration of SOA produced from Toluene (SOAT) during all months when we use CMIP6 emissions compared to CMIP5 emissions data. Although as we have seen earlier that there is an increase in annual mean SOAB concentrations when CMIP6 emissions are used as compared to CMIP5 emissions, however, the SOAB concentrations averaged over India based on CMIP6 emissions remains lower than the SOAB concentrations obtained using CMIP5 emissions during October to February months. Our examination of sectorwise emissions data reveal that although there is an increase in emissions of various VOCs from transportation and energy sector, there is a drop in the emissions from forest and grassland fires as well as agricultural waste burning in CMIP6 emissions compared to CMIP5 emissions data from the Indian region (Marle et al., 2017). We compare the simulated concentration of different VOCs with available measurements from two locations namely Mohali and Udaipur to confirm the underestimation of VOC emissions in both CMIP5 & CMIP6 data sets. We further evaluate the performance of CAM4-Chem model using these two different emission data with the available observations of OA over the Indian region. We find that although there is a slight improvement in the simulation of VOCs and SOA over the Indian region using CMIP6 emissions over CMIP5 emissions, our model results still underestimates the observations available locally from India. Our comparison of simulated results with available in-situ observations from six different locations suggests that CAM4-Chem is not able to capture the observed concentration of OA over the Indian region. More results with greater details will be presented during the conference.

CONCLUSIONS

In the present study, we compare the simulation of VOCs, SOA, and Organic carbon over the Indian region by the CAM4-Chem model using Coupled Model Intercomparison Project phase 5 and phase 6 (CMIP5 and CMIP6) emissions. We evaluate the performance of CAM4-Chem model using these two different emission data with the available observations of OA over the Indian region. We find that overall the simulated concentrations of VOCs, SOA, and OA have increased with the use of newly released CMIP6 emissions data compared to previous CMIP5 data, but our model results are still underestimating the concentrations of these organic gases and aerosols available from observations made locally within India. Our results suggests that over the Indian region, CMIP6 emission is relatively better than the CMIP5 emission data due to better representation emissions from transportation and energy sectors and few other anthropogenic activities over IGP region. We believe that it may be possible to further improve the simulation of SOA over the Indian region through the inclusion of new volatility basis set and fragmentation mechanism in our model for the treatment of VOC and other precursors that play an important role in SOA formation mechanism. We also need to regularly update the local emission inventory of VOCs and other primary emissions over the Indian region to improve the simulation of OA and SOA using any chemistry-climate model.

ACKNOWLEDGEMENTS

One of the authors (P. Vats) would like to thank the Council of scientific and Industrial Research (CSIR) for providing him fellowship to pursue this research work at IIT Delhi. We also thank the High-Performance Computing facility at IIT Delhi for providing the necessary computing resources for performing these numerical simulations. We also thank the developers of NCL and UV-CDAT for providing us free software for data analysis and plotting. I also want to thanks to my research group under supervision of Prof. Dilip Ganguly for their help.

REFERENCES

- Hoesly, R. M., et al., (2018), Historical (1750–2014) anthropogenic emissions of reactive gases and aerosols from the Community Emissions Data System (CEDS), *Geosci. Model Dev.*, 11, 369–408, <https://doi.org/10.5194/gmd-11-369-2018>.
- Henze, D. K., Seinfeld, et al., (2008), Global modeling of secondary organic aerosol formation from aromatic hydrocarbons: high-vs. low-yield pathways. *Atmospheric Chemistry and Physics*, 8(9), 2405–2420.
- Jimenez, J.L., et al., (2009), Evolution of Organic Aerosols in the Atmosphere, doi:10.1126/ science.1180353 *Science* 326, 1525.
- Kanakidou, M., Seinfeld, et al., (2005), Organic aerosol and global climate modelling: a review. *Atmospheric Chemistry and Physics*, 5(4), 1053–1123. Retrieved from <http://www.atmos-chem-phys.net/5/1053/2005/acp-5-1053-2005.pdf>
- Langmann, B., Sellegri, K. and Freney, E., (2014), Secondary organic aerosol formation during June 2010 in Central Europe: measurements and modelling studies with a mixed thermodynamic-kinetic approach, *Atmospheric Chem. Phys.*, 14(8), 3831–3842, doi:10.5194/acp-14-3831-2014.
- Lamarque, J.-F. et al. (2010), Historical (1850–2000) gridded anthropogenic and biomass burning emissions of reactive gases and aerosols: methodology and application, *Atmospheric Chem. Phys.*, 10(15), 7017–7039, doi:10.5194/acp-10-7017-2010.
- Lamarque, J.-F., et al. (2012), CAM-chem: description and evaluation of interactive atmospheric chemistry in the Community Earth System Model, *Geosci. Model Dev.*, 5, 369–411, doi: 10.5194/gmd-5-369-2012.
- Marle, M. J. E., et al., (2017), Historic global biomass burning emissions for CMIP6 (BB4CMIP) based on merging satellite observations with proxies and fire models (1750–2015), *Geosci. Model Dev.*, 10, 3329–3357, <https://doi.org/10.5194/gmd-10-3329-2017>.
- Pandis, S. N., et al., (2013), Introductory lecture: Atmospheric organic aerosols: insights from the combination of measurements and chemical transport models. *Faraday Discussions*, 165, 9. <https://doi.org/10.1039/c3fd00108c>
- Rengarajan, R., A. K. Sudheer, and M. M. Sarin (2011), Aerosol acidity and secondary organic aerosol formation during wintertime over urban environment in western India, *Atmos. Environ.*, 45(11), 1940–1945, doi:10.1016/j.atmosenv.2011.01.026
- Tilmes, S., et al., (2015), Description and evaluation of tropospheric chemistry and aerosols in the Community Earth System Model (CESM1.2) *Geosci. Model Dev.*, 8, 1395–1426, doi:10.5194/gmd-8-1395-2015.
- Tilmes, S., et al., (2016), Representation of the Community Earth System Model (CESM1) CAM4-chem within the Chemistry-Climate Model Initiative (CCMI), *Geosci. Model Dev.*, 9, 1853–1890, doi:10.5194/gmd-9-1853-2016.
- Tsigaridis, K. et al. (2014), The AeroCom evaluation and intercomparison of organic aerosol in global models, *Atmospheric Chem. Phys.*, 14(19), 10845–10895, doi:10.5194/acp-14-10845-2014.
- Tsimpidi, A. P., V. A. Karydis, A. Pozzer, S. N. Pandis, and J. Lelieveld (2014), ORACLE (v1.0): module to simulate the organic aerosol composition and evolution in the atmosphere, *Geosci. Model Dev.*, 7(6), 3153–3172, doi:10.5194/gmd-7-3153-2014.

Zhang, Q. et al. (2007), Ubiquity and dominance of oxygenated species in organic aerosols in anthropogenically-influenced Northern Hemisphere midlatitudes: UBIQUITY AND DOMINANCE OF OXYGENATED OA, *Geophys. Res. Lett.*, 34(13), n/a-n/a, doi:10.1029/2007GL029979.

EFFECT OF HEAT AND COLD WAVES ON ALL-CAUSE MORTALITY IN AN URBAN POLLUTION HOTSPOT OVER CENTRAL INDO-GANGETIC BASIN: IMPLICATIONS OF PM₁₀ EXPOSURE

NIDHI SINGH^{1,2}, ALAA MHAWISH², SANTU GHOSH³, TIRTHANKAR BANERJEE^{1,2}, RAJESH KUMAR MALL^{1,2}

¹DST-Mahamana Centre of Excellence in Climate Change Research, Institute of Environment and Sustainable Development, Banaras Hindu University, Varanasi, India

²Institute of Environment and Sustainable Development, Banaras Hindu University, Varanasi, India

³Department of Biostatistics, St Johns Medical College, Koramangala, Bangalore, India

KEYWORDS: Temperature extreme; PM₁₀, Mortality, Relative Risk, Health.

INTRODUCTION

Epidemiological research on possible influence of extreme temperature on mortality varies considerably with space and time (Guo et al., 2017). Impact of extreme temperature in the form of heat waves and cold waves have been a topic of extensive research among the developed countries but was scarcely been systematically investigated among the developing nations, like in India (Carreras et al., 2015). Heat and/or cold events are known to exacerbate premature mortality particularly due to cardiovascular diseases (CVD), cerebrovascular and chronic respiratory diseases (Gosling et al., 2017; Hajat et al. 2014). Additionally, heat and cold waves may bring adverse changes in various physiological processes, especially to susceptible population and people with some pre-existing conditions (Yu et al., 2011; Woodhouse et al. 1993). Beside temperature stress, another important and considerable threat to population appears from the increasing level of air pollution. Increasing levels of air pollution, especially in terms of air borne particulates has been recognized causing 7.6% of all deaths in 2016 worldwide (WHO, 2018). There are studies that exhibit the role of air pollution in further aggravating the symptoms in combination with humidity (Yang et al., 2015), meanwhile physiologic acclimatization, socio-economic resilience and population demographics also regulate the severity of the effects (Knowlton et al., 2009; Stedman 2004; Benmarhnia et al. 2014; Buckley et al. 2014).

The entire Indo-Gangetic Basin (IGB) has long been exposed to high ambient particulate matter concentration with aerodynamic diameter <10 µm (PM₁₀) (Pande et al., 2018; Dey and Girolamo 2011; Singh et al., 2017). A zone of accumulated and persisting airborne particulates has especially been recognized over central IGB (Kumar et al., 2018). The long-term impact of high ambient PM₁₀ has a potential health risks to local inhabitants particularly through cardiovascular and respiratory diseases (Carreras et al., 2015). However, there is only limited research on the association on extreme temperature and PM₁₀ on mortality over the region (Mazdiyasi et al., 2017). Therefore, in present submission we have quantified the percent increase in mortality on exposure to extreme temperature and PM₁₀ for an urban pollution hotspot located at central Indo-Gangetic basin between 2008 and 2017. Briefly, the results indicate that PM₁₀ is a strong modifier of the association between extreme temperature and mortality, thus it should be considered in further risk assessments and regional policy developments

METHODS

Daily non-accidental all-cause mortality data for 2009-2016 (inclusive) was collected from the office of Municipal Corporation of Varanasi (ICD-10 codes A00–R99; I00–I99; J00–J98). Daily mean temperature and relative humidity (RH) were obtained from the India Meteorological Department, New Delhi. Ambient

air quality at Varanasi (PM₁₀) was assessed from Central Pollution Control Board (<https://app.cpcbcr.com/ccr>).

Heat wave was defined as an event during summer with daily mean temperature remain equal or above the 95th percentile of annual mean (≥ 34.5 °C) for at least 3 consecutive days. A cold wave was defined for an event during winter with daily mean temperatures equal to or below the 5th percentile of annual mean (≤ 14.7 °C) for at least 3 consecutive days [moving average lag (0-2)].

The effects of extreme temperature such as heat wave and cold wave and PM₁₀ on daily mortality were estimated using following quasi-Poisson semi-parametric regression model:

$$\text{Log}\{E[(mortality)_t]\} = \alpha + \beta_{hw}I_t^{(hw)} + \beta_{cw}I_t^{(cw)} + \sum_{j=1}^p f_j(x_{jt}) + \sum_{k=2}^7 \alpha_k I_t^{(k)}$$

where, β_{hw} & β_{cw} are the regression coefficients corresponding to heat wave and cold wave, $I_t^{(hw)} = \begin{cases} 1, & \text{if heat wave on } t^{\text{th}} \text{ day} \\ 0, & \text{otherwise} \end{cases}$, similarly, $I_t^{(cw)}$ for cold wave; $f_j(x_{jt})$ is the j^{th} smoothed function (penalized cubic smoothing spline) of x_{jt} 's-nonlinear confounders such as time, relative humidity, PM₁₀ ($p=6$); α_k is the intercept for k^{th} day of week (starting from Monday to Saturday, Sunday is reference category), $I_t^{(k)} = \begin{cases} 1, & \text{if } k^{\text{th}} \text{ dow} \\ 0, & \text{otherwise} \end{cases}$. Further, we carried out stratified analyses by gender and age for total mortality.

RESULTS & DISCUSSIONS

Descriptive statistics of meteorology and air quality are summarized in Table 1. A distinguished seasonal pattern was observed in daily non-accidental mortality, with slightly excess mortality during winter (28%) compared to rest of the seasons (Fig.1). The monthly distribution of PM₁₀, mean temperature and relative humidity is represented in Fig. 1. The annual mean (\pm SD) PM₁₀ concentration was 219 (\pm 136) $\mu\text{g}/\text{m}^3$, varying between 188 and 320 ($\mu\text{g}/\text{m}^3$), well exceeding World Health Organization standard (20 $\mu\text{g}/\text{m}^3$) and the Indian national ambient air quality standard (60 $\mu\text{g}/\text{m}^3$) (NAAQS). The severity of PM₁₀ in deteriorating air quality in Varanasi can be assessed in a manner that 87% of the study period (n =1905 days) exhibited PM₁₀ concentration above the NAAQS standard, creating substantial adversity to the exposed population.

Using time-series adjusted Poisson regression we have quantified the relative risk (RR) associated with cold waves (RR 1.06, 95% CI 1.1-1.4) and heat waves (RR 1.13, 95% Confidence Intervals, CI 1.0-1.2) where it was evident that the mortality was amplified by exposure to temperature extremes (Fig 2). Females (RR 1.22, 95% CI 1.1-1.4) and population of age <4 years (RR 1.38, 95% CI 1.1-1.7) were found more susceptible to overall heat wave effects while population between 45-64 years' age group (RR 1.17, 95% CI 1.0-1.4) were most sensitive to the cold wave (Fig 2). The observations were supported by studies from Europe, USA, Latin America and China that reported increased risks from temperature stress for the elderly and socioeconomically deprived individuals (Guo et al., 2017; Åström et al., 2013). We observed that the associations between mortality and extreme temperature are substantially confounded by air pollution. The estimated effect of extreme temperature on total mortality was increased during heat wave for children (11%; Age: 0-4 years) and female (8%) when controlled for PM₁₀ (Table 2). Importantly, the period of cold waves showed obvious hike in all-cause mortality (8%) when the model was controlled for airborne pollutants (PM₁₀), particularly for the age group 45-64 years (54%) unaltered by difference in gender (9%; Female, 8%; Male). The result brings forth a general finding that age $\geq 0-4$ years and $\geq 45-64$ years are the most vulnerable on exposure to extreme temperature associated with air pollution. The results are in agreement with Stedman (2004), Benmarhnia et al. (2014) and Buckley et al. (2014).

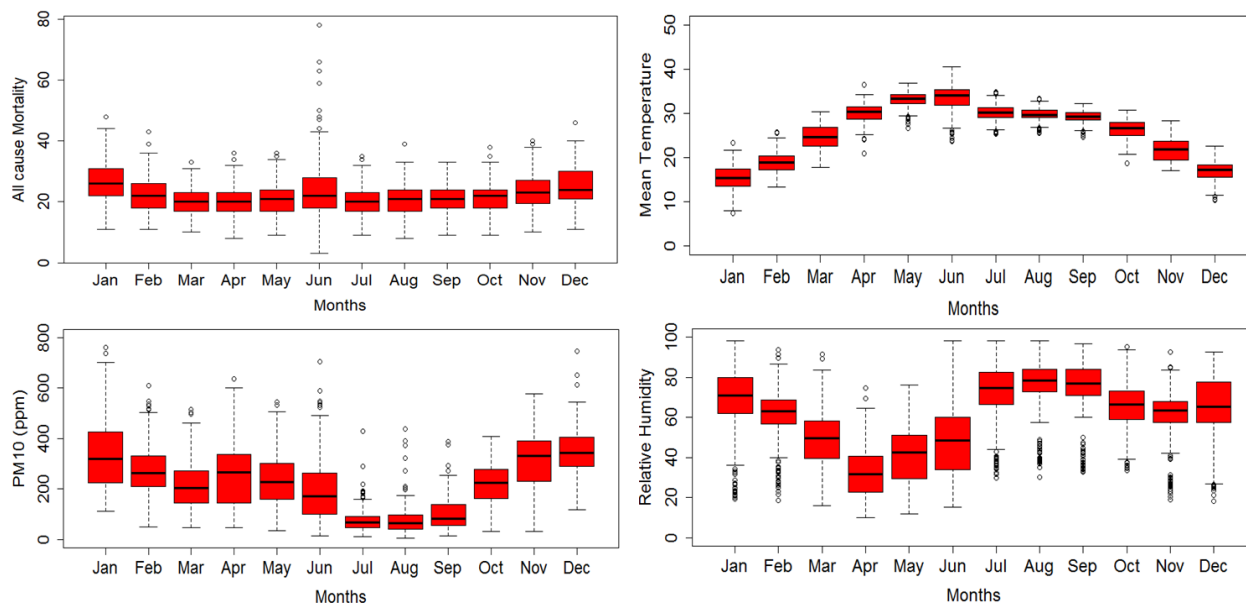


Fig.1 Boxplot representing distribution of mortality, weather parameters and gaseous pollutants across twelve months. The boxes mark the 25% and 75% quartiles while the whiskers give the minimum and maximum values. Values above the whiskers represent outliers,

Table 1. Summary of the daily number of deaths, weather conditions and air pollution in Varanasi, India, 2009–2016

Variable	No. of Obs.	Mean	SD	Median	Maximum	25th Percentile	75th Percentile
Meteorological Parameters							
T.max (°C)	2922	31.56	6.6	32.4	46.2	27.0	35.8
T.min (°C)	2922	20.05	7.0	21.8	39.6	13.8	26.2
T.mean (°C)	2922	25.81	6.4	27.7	40.6	20.1	30.7
RH (%)	2922	63.75	20.1	63.0	98.0	44.0	75.0
AT (°C)	2365	28.56	7.4	26.4	47.7	20.5	31.0
Air Pollution Parameters							
PM10 (µg/m3)	2181	219.21	135.7	208.2	901.6	97.3	317.6

SO ₂ (µg/m ³)	2344	3.93	4.9	3.1	102.6	2.2	4.4
NO ₂ (µg/m ³)	2278	20.64	11.8	19.4	132.0	12.2	28.4
O ₃ (µg/m ³)	2368	23.03	16.0	18.2	151.1	11.3	31.1

CONCLUSIONS

The study establishes the general fact that temperature extreme has lethal impact to human health and supports the possible association of air pollution in increasing the risk to ill health and mortality. The study found 30% excess mortality during extreme temperature days and 8 % hike during winter with exposure to air particulates (PM₁₀). Children and elderly were the most vulnerable group. The limitation of the study is that it didn't consider individual characteristics (age, gender) and habits (alcohol consumption and smoking) along with socio-economic condition are known to alter the relationship that must be taken in to consideration (Bravo et al., 2015). The key finding in the study will help to formulate a risk assessments model that reduce the underestimation in overall mortality burden and will be useful in policy making.

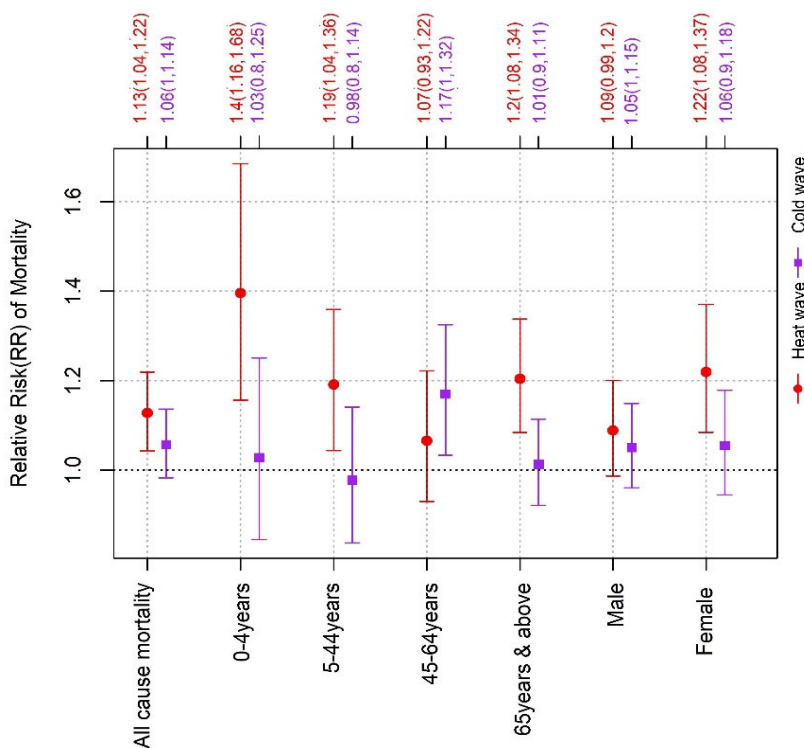


Fig.2 Rate ratios of cold spells and heat waves on daily number of deaths. The filled circle and square represent the average relative risk and whiskers represent the 95% confidence intervals (***) $p < 0.001$).

Table 2. Percent increase (95% CI) in all-cause mortality during Heat wave (HW)and Cold spell (CW) with and without adjustment for PM10 (mg/m3).

Model	Categories	Heat Wave			Cold Wave		
		% increase in Mortality	LCL	UCL	% increase in Mortality	LCL	UCL
HW+CW	All-cause mortality	14.0	6.7	21.4	5.1	-1.6	11.8
adjusted for PM10		12.0	4.2	19.8	5.5	-1.7	12.8
HW+CW	0-4years	30.1	12.7	47.4	6.0	-12.5	24.5
adjusted for PM10		33.3	14.5	52.2	2.8	-16.9	22.4
HW+CW	5-44years	20.5	8.3	32.7	-5.8	-20.3	8.7
adjusted for PM10		17.5	4.3	30.7	-2.3	-17.7	13.2
HW+CW	45-64years	10.2	-1.1	21.5	10.2	-0.6	20.9
adjusted for PM10		6.4	-7.2	20.0	15.7	3.2	28.1
HW+CW	≥65years	19.4	9.6	29.2	3.5	-5.1	12.2
adjusted for PM10		18.6	8.0	29.1	1.3	-8.2	10.8
HW+CW	Male	12.5	3.5	21.5	4.5	-3.6	12.7
adjusted for PM10		8.5	-1.3	18.2	4.9	-4.0	13.9
HW+CW	Female	18.4	7.5	29.2	5.0	-5.0	15.0
adjusted for PM10		19.8	8.1	31.5	5.4	-5.7	16.4

ACKNOWLEDGEMENTS

We thankfully acknowledge India Meteorological Department New Delhi and Municipal Corporation of Varanasi for providing the data used in this study. The authors thank the Climate Change Programme, Department of Science and Technology, New Delhi, for financial support (DST/CCP/CoE/80/2017(G))

REFERENCES

- Åström, D.O., Forsberg, B., Ebi, K.L., Rocklöv, J., 2013. Attributing mortality from extreme temperatures to climate change in Stockholm, Sweden. *Nature climate change* 3, 1050.
- Benmarhnia, T., Sottile, M.-F., Plante, C., Brand, A., Casati, B., Fournier, M., Smargiassi, A., 2014. Variability in temperature-related mortality projections under climate change. *Environmental health perspectives* 122, 1293.

- Bravo, M.A., Son, J., De Freitas, C.U., Gouveia, N., Bell, M.L., 2016. Air pollution and mortality in Sao Paulo, Brazil: Effects of multiple pollutants and analysis of susceptible populations. *Journal of Exposure Science and Environmental Epidemiology* 26, 150.
- Buckley, J.P., Samet, J.M., Richardson, D.B., 2014. Commentary: Does air pollution confound studies of temperature? *Epidemiology* 25, 242-245.
- Carreras, H., Zanobetti, A., Koutrakis, P., 2015. Effect of daily temperature range on respiratory health in Argentina and its modification by impaired socio-economic conditions and PM10 exposures. *Environmental pollution* 206, 175-182.
- Dey, S., Di Girolamo, L., 2011. A decade of change in aerosol properties over the Indian subcontinent. *Geophysical Research Letters* 38.
- Gosling, S.N., Hondula, D.M., Bunker, A., Ibarreta, D., Liu, J., Zhang, X., Sauerborn, R., 2017. Adaptation to climate change: a comparative analysis of modeling methods for heat-related mortality. *Environmental health perspectives* 125.
- Guo, Y., Gasparini, A., Armstrong, B.G., Tawatsupa, B., Tobias, A., Lavigne, E., Coelho, M.d.S.Z.S., Pan, X., Kim, H., Hashizume, M., 2017. Heat wave and mortality: a multicountry, multicomunity study. *Environmental health perspectives* 125.
- Hajat, S., Vardoulakis, S., Heaviside, C., Eggen, B., 2014. Climate change effects on human health: projections of temperature-related mortality for the UK during the 2020s, 2050s and 2080s. *J Epidemiol Community Health* 68, 641-648.
- Knowlton, K., Rotkin-Ellman, M., King, G., Margolis, H.G., Smith, D., Solomon, G., Trent, R., English, P., 2008. The 2006 California heat wave: impacts on hospitalizations and emergency department visits. *Environmental health perspectives* 117, 61-67.
- Kumar, M., Parmar, K., Kumar, D., Mhawish, A., Broday, D., Mall, R., Banerjee, T., 2018. Long-term aerosol climatology over Indo-Gangetic Plain: Trend, prediction and potential source fields. *Atmospheric Environment* 180, 37-50.
- Mazdiyasn, O., AghaKouchak, A., Davis, S.J., Madadgar, S., Mehran, A., Ragno, E., Sadegh, M., Sengupta, A., Ghosh, S., Dhanya, C., 2017. Increasing probability of mortality during Indian heat waves. *Science advances* 3, e1700066.
- Pande P, Dey S, Chowdhury S, Choudhary P, Ghosh S, Srivastava P, Sengupta B (2018) Seasonal transition in PM₁₀ exposure and associated all-cause mortality risks in India. *Environ Sci Technol* 52(15):8756–8763
- Singh, N., Murari, V., Kumar, M., Barman, S., Banerjee, T., 2017. Fine particulates over South Asia: review and meta-analysis of PM_{2.5} source apportionment through receptor model. *Environmental pollution* 223, 121-136.
- Stedman, J.R., 2004. The predicted number of air pollution related deaths in the UK during the August 2003 heatwave. *Atmospheric Environment* 38, 1087-1090.
- WHO 2018. Mortality and burden of disease from ambient air pollution. Global Health Observatory (GHO) data, world health Organization. Available at- https://www.who.int/gho/phe/outdoor_air_pollution/burden/en/
- Woodhouse, P.R., Khaw, K.-T., Plummer, M., 1993. Seasonal variation of blood pressure and its relationship to ambient temperature in an elderly population. *Journal of hypertension* 11, 1267-1274.

Yang, J., Ou, C.-Q., Guo, Y., Li, L., Guo, C., Chen, P.-Y., Lin, H.-L., Liu, Q.-Y., 2015. The burden of ambient temperature on years of life lost in Guangzhou, China. *Scientific reports* 5, 12250.

Yu, W., Hu, W., Mengersen, K., Guo, Y., Pan, X., Connell, D., Tong, S., 2011. Time course of temperature effects on cardiovascular mortality in Brisbane, Australia. *Heart, hrt.* 2010.217166.

IMPROVEMENTS IN THE SIMULATION OF AEROSOLS OVER THE INDIAN REGION USING CAM5 MODEL AND THE SMOG-INDIA (SPECIATED MULTIPOLLUTANT GENERATOR) EMISSIONS INVENTORY DEVELOPED AS PART OF THE NCAP-COALESCE PROJECT COMPARED TO CMIP6 EMISSIONS

A. K. SHARMA¹, AND D. GANGULY¹

¹ Centre for Atmospheric Sciences, Indian Institute of Technology Delhi, New Delhi, India

Email: amit.jiname04@gmail.com

KEYWORDS: Carbonaceous aerosols, Coupled Model Intercomparison Project Phase 6 (CMIP6).

INTRODUCTION

Aerosols, with their direct and indirect radiative forcing effects, are capable of influencing the climate as well as clouds in response to their changing concentration and hence are one of the most important factors which affect the earth's radiation budget. The emissions of aerosols not only can affect the atmosphere indirectly by changing the cloud droplet size and precipitation, but also can interact with the solar radiation directly (like black carbon). Studies had suggested several possibilities in response to the changing atmospheric aerosol concentration namely, the presence of aerosols like black carbon over Tibetan Plateau which is an elevated land area had an effect on strengthening Indian summer monsoon by acting like 'an elevated heat pump' [Lau et al. 2006], whereas a study by Ramanathan et al., 2005 states that, large reduction in solar radiation reaching the surface leads to less atmospheric warming and hence slowing the hydrological cycle by increasing the atmospheric stability thereby reducing the rainfall in monsoon. Thus these effects of black carbon aerosols are contrary and highly uncertain. Therefore it is crucial to keep the track of the changing aerosol emissions, especially anthropogenic, within the climate models as accurate as possible. Though, the latest released CMIP6 emissions (Coupled Model Intercomparison Project version 6) for the aerosols have proved to be more accurate in climate models compared to the previous versions (in CMIP5; as suggested in IPCC Assessment Report 5 in 2013), there is still scope of improving these emissions. Thus National Carbonaceous Aerosols Programme (NCAP) was started by Ministry of Environment, Forest and Climate Change in order to monitor and understand the role implications of aerosols in changing the climate over Indian sub-continent region.

SMOG-India (Speciated Multipollutant Generator) Emissions developed by Indian Institute of Technology, Bombay under NCAP-COALESCE project over Indian region along with the CMIP6 emissions for the rest of the globe has been used as an input in CESM-1.2.2 (CAM5) in order to perform the simulations. The SMOG emissions over Indian region is more sound and realistic compared to the CMIP6 emissions over India. The goal is to analyze several parameters like temperature, surface pressure, precipitation, reference temperature, relative humidity, winds patterns, Aerosol optical depth (AOD), geopotential height, etc. and to compare it with the simulations based on CMIP6 and CMIP5 aerosol emissions. The analysis of all these parameters and their comparison with the assimilated data (MERRA2) will help in having more elaborated understanding of their induced effects and the changes on the climate over Indian region. This can also help us to have enhanced knowledge that can lead to more explicit regional climate prediction. It is beneficial since having more precise emission dataset of the different types of aerosol species will lead to lower the initial condition uncertainty during simulations and hence to the reliable results.

METHODS

The 3 sets of simulations were performed using the aerosol emissions namely from CMIP5 (RCP8.5 for 2015), CMIP6 (for 2015) and then replacing CMIP6 data over India by SMOG emissions for 2015

(Prepared by IIT- Bombay under NCAP-COALESCE project). All the simulations are equilibrium simulations performed for 11 years with 1 year spin up time. Apart from aerosol emissions, all the other parameters like trace gases, GHGs, ozone gases were taken from RCP 8.5 emissions for the year 2015. All these experiments were performed by keeping other environments same (for eg. CAM5.3 model physics, solar constant, etc.).

The effects of carbonaceous aerosols especially black carbon, organic carbon along with the sulfate aerosols are of most important concern for the analysis since they are either highly underestimated (black carbon and sulfate) or over estimated as in case of organic carbon in the recent CMIP6 emissions.

RESULTS & DISCUSSIONS

The results from the simulations shows that in terms of annual mean surface concentration of aerosols there is significant underestimation of the black carbon, whereas organic carbon is being over estimated over the entire Indo-Gangatic plane, whereas sea salt is being over estimated in Arabian sea in CMIP 6 datasets as compared to the SMOG emissions. The emission of the dust is however nearly the same in both SMOG and CMIP6. While in comparison with the simulation from CMIP5 emissions it is observed that except for the sea-salt the surface concentration of the aerosol species (namely, Black carbon, organic carbon, sulfate SO_4 and dust) were highly underestimated in RCP 8.5 scenario.

Similar to the surface concentration, comparison of AOD from CAM5 SMOG and CAM5 CMIP6 shows that there is a increase in total AOD of about 10% in most of the central India (specially in Indo-Gangatic planes) in SMOG experiments and that is mostly contribute by sulfate (SO_4), whereas the AOD for black carbon dust and sea-salt in almost same in both. On the contrary CAM5 SMOG suggests AOD due to Organic Carbon is less almost by 12-15% as compared with CAM5 CMIP6.

Though the improvement of surface concentration and the aerosol optical depth (AOD) due to different types of aerosols are compared among these experiments, their effects on radiative forcing are equally important. Monthly mean variation shows that the net Shortwave radiation flux at the surface is slightly over predicted by CMIP5 emissions of aerosols for whole year except in december, reaching maximum about 230W/m^2 in the month of april, whereas there is significant underestimation of the same by CMIP 6 emissions from the period of march to august. CMIP6 emissions shows large variation in the solar flux during the monsoon period i.e. on june and july, which was closely captured in CMIP5 emissions.

Further it is analyzed that annual mean of net shortwave flux at the surface is almost 10W/m^2 less over entire India compared to SMOG emissions, however changes become significant when the mean over JJAS is considered. There is high underestimation of shortwave flux to the east of the western ghats and also to the other parts of central India in CMIP6 dataset, whereas in CMIP5 these fluxes are overestimated. Also fluxes in most of the northeastern states are underestimated in CMIP6 during the monsoon period.

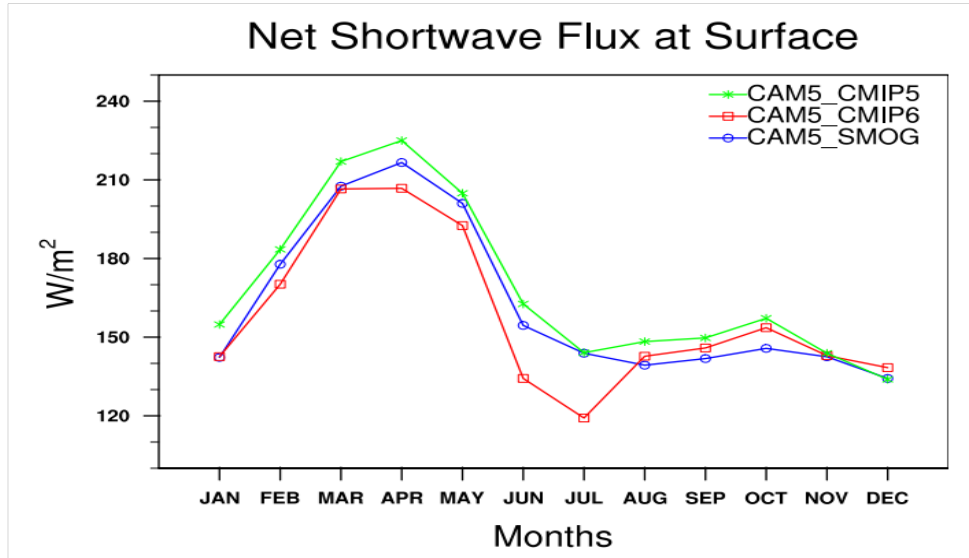


Figure1. Net Shortwave flux at the surface as simulated by all three experiments

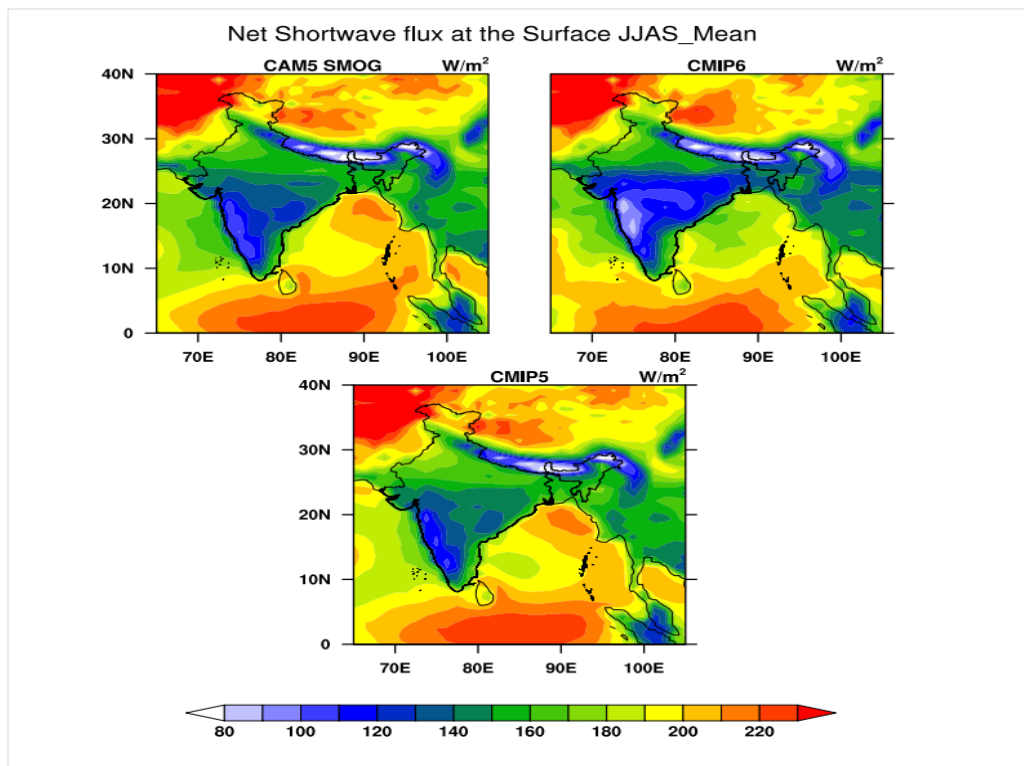


Figure2. Mean of Net Shortwave flux at surface during monsoon season in June, July, August and September

CONCLUSIONS

These experiments show that the aerosol emissions for the Indian region are not very well captured in either of CMIP5, CMIP6 emissions. Especially the concentrations of organic carbon and sulfate are mostly uncertain (OC is highly overestimated whereas sulfate SO_4 I is highly underestimated) in CMIP 6

emissions. Therefore in order to get accurate results SMOG emissions are proved to be better alternate for the Indian region.

REFERENCES

Lau, K.-M., and K.-M. Kim, Observational relationships between aerosol and Asian monsoon rainfall, and circulation. *Geophys. Res. Lett.*, 33 (L21810), doi:10.1029/2006GL027546, 2006.

Lau, K.-M., et al., Asian summer monsoon anomalies induced by aerosol direct forcing: The role of the Tibetan Plateau. *Climate Dyn.*, 26, 855–864, 2006.

Ramanathan, V., et al., Atmospheric brown clouds: Impacts on South Asian climate and hydrological cycle, *Proc. Natl. Acad. Sci. U.S.A.*, 102, 5326-5333, 2005.

FOG DROPLETS AND AEROSOLS INTERACTION: CHARACTERIZATION OF TRACE ELEMENTS AND SECONDARY ORGANIC AEROSOLS

A. CHAKRABORTY^{1*}, T. GUPTA^{1,2} AND S.N. TRIPATHI^{1,2}

¹Department of Civil Engineering, Indian Institute of Technology, Kanpur, UP-208016 India.

²Center for Environmental Science and Engineering, Indian Institute of Technology, Kanpur, UP-208016 India.

*Currently at Indian Institute of Technology (IIT), Ropar, Punjab - 140001

KEYWORDS: Aerosol-cloud (fog) interaction, trace elements, aqueous SOA, AMS.

INTRODUCTION

Trace elements and secondary OA (SOA) are an integral part of the Earth's atmosphere and present in every environment. Trace elements can enter into atmosphere from different natural and anthropogenic activities and some of the elements are toxic to human health even at minute concentrations and can penetrate deep into our lungs when associated with fine particulate matter (PM_{2.5}) and fog droplets (Abernethy, 1968; Bowes et al., 1989). SOA has several impacts on PM properties and can influence Earth's radiation budget. SOA formed inside the cloud and fog droplets are reported to be highly oxidized with very different hygroscopic and optical properties compared to gas phase SOA (Ervens et al., 2011). Aqueous SOA (aqSOA) also has the capacity to affect human health by inducing oxidative stress via production of ROS (reactive oxygenation species) (Decesari et al., 2017). Fogs formed in polluted locations especially have the potential to produce highly pollutants enriched fog droplets that can have implications for human health and climate. Kanpur, the sampling location for this study is situated in the centre of Indo-Gangetic Plain (IGP) and often counted among one of the most polluted cities of India and world (Kaul et al., 2011). Several studies have been carried out at this site and in other places of India to characterize the fog water composition and most of them reported very high levels of different trace elements and organic carbon (OC) (Chakraborty et al., 2017; Chakraborty and Gupta, 2010; Gupta and Mandariya, 2013; Singh et al., 2014; Yadav et al., 2013). However, detailed size resolved fog droplet characterization and contribution to aqSOA has rarely been studied in actual environment. So, the objectives of this study are to examine the trace elements and aqSOA concentration and enrichment inside the fog droplets in a size resolved manner and to compare the same with ambient aerosol properties. Study of the health risk enhancement has also been carried out due to inhalation of fog droplets for the exposed population.

METHODS

Aerosol sampling (online & offline) was carried out during winter 2014-15 (Dec – Feb) in IIT Kanpur campus. Several (n = 21) fog events were observed during the study period and size resolved fog droplets were collected using a Caltech 3 stage fog water collector (Raja et al., 2008). An HR-ToF-AMS (High Resolution-Time of Flight-Aerosol Mass Spectrometer; AMS) (DeCarlo et al., 2006) was deployed to measure total submicron aerosol mass concentration and characteristics in real time (with 2 min resolution). Offline PM₁ and PM_{2.5} sampling were collected on quartz filters using the medium (200 lpm) and high volume (1000 lpm) samplers (Kumar and Gupta, 2015). Mostly nighttime (9 pm – 8 am) offline sampling was done as fog generally occurs during late night to early morning time frame. A total of 110 filters (50 PM_{2.5} + 50 PM₁ + 10 Blank) were collected and later, filters were extracted via ultrasonication in water and analyzed via ICP-OES for trace elements along with fog droplets. Fog droplets were atomized via a nebulizer and analyzed in AMS to characterize organic aerosols (OA) and identification of sources.

RESULTS & DISCUSSIONS

Campaign average $PM_{2.5}$ concentration is found to be $225 \mu\text{g}/\text{m}^3$ (9 times higher than WHO guideline of $25 \mu\text{g}/\text{m}^3$, World Health Organization, 2015). However, night time average $PM_{2.5}$ concentration of $212 \mu\text{g}/\text{m}^3$ is higher than the daytime concentration of $180 \mu\text{g}/\text{m}^3$, as observed from E-BAM data. During foggy nights, this concentration is $266 \mu\text{g}/\text{m}^3$, while during non foggy nights (NFN), the same is $193 \mu\text{g}/\text{m}^3$. Mostly crustal elements (Ca, Mg, Fe) were found in abundance ($\sim 1 \mu\text{g}/\text{m}^3$) but concentrations of several toxic trace elements were also found to be very high ($> 0.2 \mu\text{g}/\text{m}^3$ and 0.1 ppm) in both aerosols and fog droplets compared to other studies reported from other parts of the world (Boman et al., 2009; Xia and Gao, 2011). Fine droplets were found to be more concentrated with trace elements than other coarser droplets, most likely due to their higher surface area and less liquid water content (LWC). Enrichment factor (EF) analysis revealed that elements in PM_1 were more enriched than in $PM_{2.5}$, indicating that anthropogenic contributions to trace elements in PM_1 were higher than in $PM_{2.5}$, in line with the smaller size of PM_1 than $PM_{2.5}$. However, EF values in fog droplets were found to be an order of magnitude higher (10 to 100 times) than observed in aerosol samples, clearly indicating much higher enrichment of toxic trace elements inside fog droplets.

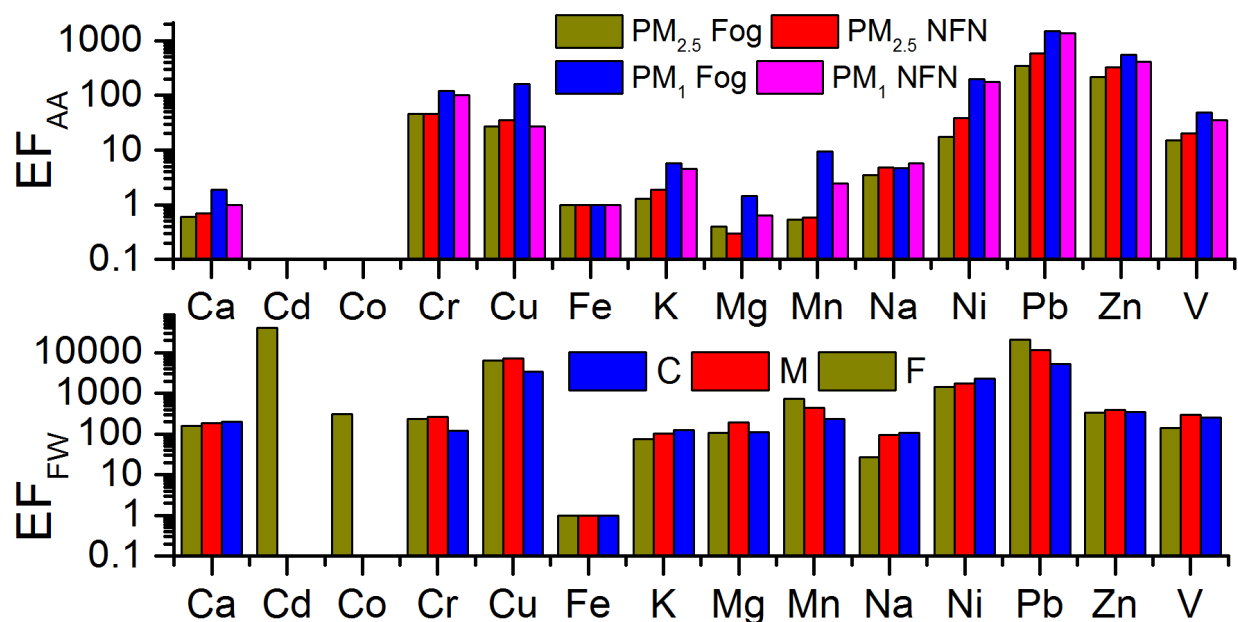


Figure 1: Enrichment factor (EF) values of different elements in ambient aerosols (AA) and fog water (FW) samples. F, M, C denotes fine, medium and coarse droplets respectively.

This observation possibly resulted from a combination of compositional differences in condensation nuclei over which fog has formed and solubility differences of different elements. Organics present inside fog droplets also showed size resolved enhancement in concentrations and oxidation efficiency; fine droplets were more enriched in oxidized organics than coarser droplets. Source apportionment of organics present inside the fog droplets using PMF revealed that some portion of primary OAs (biomass burning OA & Hydrocarbon like OA) were water soluble but fog water OA was mostly dominated by secondary/oxidized OA. Detailed calculation based on PMF revealed that aqSOA can contribute upto 30% to total SOA and fine droplets contribute maximum aqSOA in spite of having lowest water content. Risk analysis based on

aerosol and fog droplet toxic trace elemental concentrations revealed that during foggy period diurnal carcinogenic risk can be substantially enhanced (~ 20%) due to inhalation of fog droplets. Also, overall CR was much higher than the acceptable limit (1 in a million populations) for both foggy and non-foggy days.

CONCLUSIONS

This study reveals that toxic trace elements were present in significant quantity in the study site and most of the toxic trace elements were much enriched indicating their anthropogenic origin. Enrichment factors were higher for PM₁ than PM_{2.5} and in fog droplets EF values were an order of magnitude higher than aerosols, clearly indicating pollution influence on fog water characteristics. Fog processing adds significant SOA significantly to ambient background SOA with fine droplets being the main contributor. This indicates that in polluted locations fog dominated by smaller droplets can add more secondary OA to existing OA thus significantly influencing their optical and hygroscopic properties. Risk assessment analysis highlighted the impact of fog droplets inhalation which was highly concentrated with toxic trace elements. These findings indicate that only considering bulk fog/cloud droplet composition may lead to substantial underestimation of SOA quantity and oxidation properties and polluted fog droplets further enhance the risk due to air pollution.

ACKNOWLEDGEMENTS

We acknowledge the support of IIT Kanpur for providing us with HR-ToF-AMS.

REFERENCES

- Abernethy, J.D., 1968. Effects of inhalation of an artificial fog Atmospheric fog plays some role in the production of symptoms in chronic bronchitis, but hitherto the blame has rested with pollutants rather than with the water droplet content itself. An investigation of the ef. *Thorax* 421. <https://doi.org/10.1136/thx.23.4.421>
- Boman, J., Gatari, M.J., Janhäll, S., Shannigrahi, A.S., Wagner, A., 2009. Elemental content of PM_{2.5} aerosol particles collected in Göteborg during the Göte-2005 campaign in February 2005. *Atmos. Chem. Phys.* 9, 2597–2606. <https://doi.org/10.5194/acp-9-2597-2009>
- Bowes, S.M., Laube, B.L., Links, J.M., Frank, R., 1989. Regional Deposition of Inhaled Fog Droplets: Preliminary Observations, *Environmental Health Perspectives*.
- Chakraborty, A., Gupta, T., 2010. Chemical Characterization and Source Apportionment of Submicron (PM₁) Aerosol in Kanpur Region, India. *Aerosol Air Qual. Res.* 10, 433–445. <https://doi.org/10.4209/aaqr.2009.11.0071>
- Chakraborty, A., Rajeev, P., Rajput, P., Gupta, T., 2017. Water soluble organic aerosols in indo gangetic plain (IGP): Insights from aerosol mass spectrometry. *Sci. Total Environ.* 599–600. <https://doi.org/10.1016/j.scitotenv.2017.05.142>
- DeCarlo, P.F., Kimmel, J.R., Trimborn, A., Northway, M.J., Jayne, J.T., Aiken, A.C., Gonin, M., Fuhrer, K., Horvath, T., Docherty, K.S., Worsnop, D.R., Jimenez, J.L., 2006. Field-deployable, high-resolution, time-of-flight aerosol mass spectrometer. *Anal. Chem.* 78, 8281–8289. <https://doi.org/10.1021/ac061249n>
- Decesari, S., Sowlat, M.H., Hasheminassab, S., Sandrini, S., Gilardoni, S., Facchini, M.C., Fuzzi, S., Sioutas, C., 2017. Enhanced toxicity of aerosol in fog conditions in the Po Valley, Italy. *Atmos. Chem. Phys.* 17, 7721–7731. <https://doi.org/10.5194/acp-17-7721-2017>

- Ervens, B., Turpin, B.J., Weber, R.J., 2011. Secondary organic aerosol formation in cloud droplets and aqueous particles (aqSOA): a review of laboratory, field and model studies. *Atmos. Chem. Phys.* 11, 11069–11102. <https://doi.org/10.5194/acp-11-11069-2011>
- Gupta, T., Mandariya, A., 2013. Sources of submicron aerosol during fog-dominated wintertime at Kanpur. *Environ. Sci. Pollut. Res.* 20, 5615–5629. <https://doi.org/10.1007/s11356-013-1580-6>
- Kaul, D.S., Gupta, T., Tripathi, S.N., Tare, V., Collett Jr., J.L., 2011. Secondary Organic Aerosol: A Comparison between Foggy and Nonfoggy Days. *Environ. Sci. Technol.* 45, 7307–7313. <https://doi.org/10.1021/es201081d>
- Kumar, A., Gupta, T., 2015. Development and Field Evaluation of a Multiple Slit Nozzle-Based High Volume PM_{2.5} Inertial Impactor Assembly (HVIA). *Aerosol Air Qual. Res.* 15, 1188–1200. <https://doi.org/10.4209/aaqr.2015.01.0050>
- Raja, S., Raghunathan, R., Yu, X.Y., Lee, T., Chen, J., Kommalapati, R.R., Murugesan, K., Shen, X., Qingzhong, Y., Valsaraj, K.T., Collett, J.L., 2008. Fog chemistry in the Texas-Louisiana Gulf Coast corridor. *Atmos. Environ.* 42, 2048–2061. <https://doi.org/10.1016/j.atmosenv.2007.12.004>
- Singh, D.K., Lakshay, Gupta, T., 2014. Field performance evaluation during fog-dominated wintertime of a newly developed denuder-equipped PM₁ sampler. *Environ. Sci. Pollut. Res.* 21, 4551–4564. <https://doi.org/10.1007/s11356-013-2371-9>
- World Health Organization, 2015. WHO Air quality guidelines for particulate matter, ozone, nitrogen dioxide and sulfur dioxide: global update 2015: summary of risk assessment, WHO (Geneva).
- Xia, L., Gao, Y., 2011. Characterization of trace elements in PM_{2.5} aerosols in the vicinity of highways in Northeast New Jersey in the US East Coast. *Atmos. Pollut. Res.* 2, 34–44. <https://doi.org/10.5094/APR.2011.005>
- Yadav, S., Tandon, A., Attri, A.K., 2013. Characterization of aerosol associated non-polar organic compounds using TD-GC-MS: A four year study from Delhi, India. *J. Hazard. Mater.* 252, 29–44. <https://doi.org/10.1016/j.jhazmat.2013.02.024>

AIR QUALITY MODELLING OF CO USING AERMOD: CONTRIBUTION OF VARIOUS SOURCES IN THE CITY OF VARANASI

ARPIT KATIYAR¹, MUKESH SHARMA² AND SRI HARSHA KOTA¹

¹Department of Civil Engineering, Indian Institute of Technology Delhi, New Delhi – 110016, India

² Department of Civil Engineering, Indian Institute of Technology Kanpur, Kanpur – 208016, India.

KEYWORDS: Air pollution, emission inventory, air quality modelling, aermოდ.

INTRODUCTION

Air pollution is a matter of serious concern and it is rightly termed a local as well as a global issue. It is mainly attributed to rapid industrialisation and urbanisation. Indian cities are no exception to this serious issue. The Indian cities have experienced a phenomenal growth in population, industry and vehicles. Given the current rapid rate of economic development of India, the further degradation of air quality is likely to occur in future and hence preventive measures become imperative. It becomes extremely necessary to make use of scientific tools available for decision making. Some of these tools are air pollutant emission inventory and air quality modelling. Emission inventory provides the fundamental knowledge for understanding local and regional air pollution, its transport and impacts. It also provides a reliable estimate of total emissions of different pollutants, their spatial, temporal distribution; and characterization of main sources.

Carbon monoxide (CO) is a toxic air pollutant which is colourless and odourless. It is mainly produced in atmosphere due to incomplete combustion of carbon containing fuel etc. (Arellano, Kasibhatla, Giglio, van der Werf, & Randerson, 2004). It also affects oxidising capability of troposphere because of its sink effect on OH radical, thereby indirectly creating a greenhouse gas (GHG) effect (Seinfeld, Pandis, 2012). The increasing levels of CO is majorly contributed by anthropogenic activities as against natural emissions (Zhong et al., 2017). Also, exposure to the large concentrations of CO has detrimental health effects like chronic headaches etc. (Kampa and Castanas, 2008). CO is a conservative and relatively non-reactive pollutant with high residence time in the atmosphere and can represent the harmful combustion sources which may sometimes be more harmful than the inorganic component of PM_{2.5} and PM₁₀.

A lot of studies have already been done in India on source apportionment and preparation of emission inventory for metro cities (Tier-1). Some of these studies have tried to model the important sources also. The air dispersion models which are commonly used are ISCST3 and ISC-PRIME. However, significant attention needs to be given in Tier-2 cities as pollution in these cities is growing to alarming levels. Similarly, studies focussing on the estimation of contribution of different sources outside city boundary in the domain of the background concentration are also few. This can be significant in Indian context as most of Indian cities are closely located thereby affecting each other's environment.

The city of Varanasi (25.3176° N latitude, 82.9739° E longitude) is the world's oldest living city of vivid historical importance. It is rightly referred to as 'religious capital of India' and is a place of attraction for tourists and pilgrimage. The city has a continuous air quality monitoring station (CAAQMS) installed in a busy road of Ardali bazar, in the city where various pollutants viz. CO, SO₂, NO_x, PM_{2.5}, PM₁₀, etc. are measured continuously. This continuous air quality data can assist in validating air quality models for developing an action plan. Hence, this study focuses on preparation of a GIS-based, sector wise emission inventory of 2 km x 2 km resolution for the city of Varanasi taking into account various sources like vehicular, domestic cooking, hotels and restaurants, municipal solid waste (MSW) burning for the year of 2014. The study also applies and validates state-of-the-art dispersion model AERMOD, for pollutant CO for four critical months of winter viz. February, October, November, and December. AERMOD has been applied for the first time in the context of CO for a tier-2 city.

METHODS

The methodology adopted for AERMOD is displayed in Figure 1.

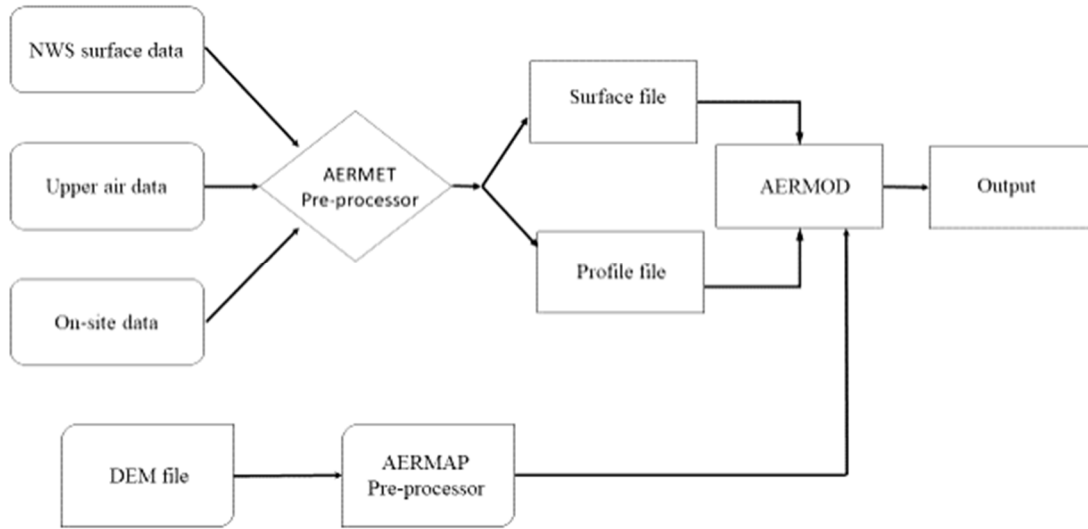


Figure 1: Data flow in AERMOD

RESULTS AND DISCUSSION

The first part of this study focuses on the preparation of a 2 km×2 km GIS based emission inventory of CO for the city of Varanasi for year 2014. The total load of CO contributed by all the emission sources being considered is estimated to be 91 tons/day. Nearly 84 % emission of total CO is from vehicles followed by 7.5 % from domestic sources and 6.6% from MSW burning. However, it is found that contributions towards CO concentration from other sources like Hotels, DG and aircrafts are very small. Thus, the study clearly indicates that the vehicular sector should primarily be the main target while considering measures for abatement of CO concentration for city of Varanasi.

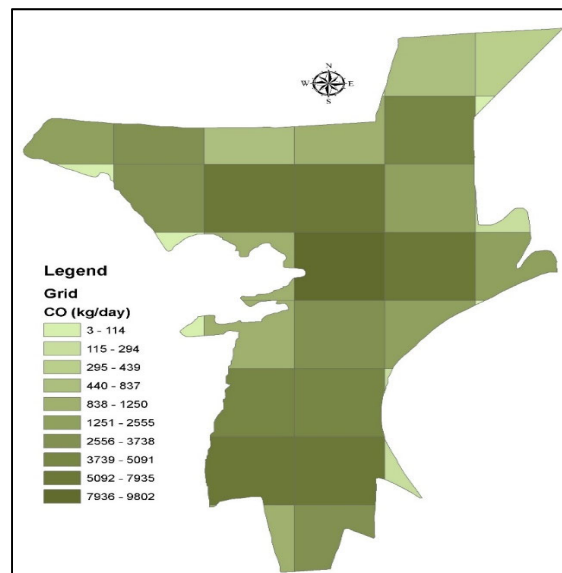


Figure 2: Spatial Distribution of total CO Emissions

The later part of study tries to fit a linear regression model between the observed and modelled values and parameters C, m and R² are obtained (Table 1). The general equation of the model is of the form:

$$y = mx + C$$

Where,

mx: contribution of the local emissions

C: contribution from outside the city boundary

The C-value is the contribution from outside city boundaries which may be either because of any one or a combination of the following:

- Emission from brick kilns. Towards the south of Varanasi, 303 brick kilns have been running regularly and we have not taken the contribution of brick kilns in our emission inventory.
- Because of long-range transport of CO as it is non-reactive, conservative specie and can travel for a long distance unaltered. The sinks of CO are found to be very less when it is in atmosphere.
-

Month	Modelled Equation	m-value	C-value	R ²
February	$y = 0.41x + 619$	0.41	619	0.64
October	$y = 0.42x + 395$	0.42	395	0.78
November	$y = 0.2x + 1073$	0.2	1073	0.46
December	$y = 0.7x + 891$	0.7	891	0.74

Table 1: Values of modelled parameters

The graph for month of October is shown:

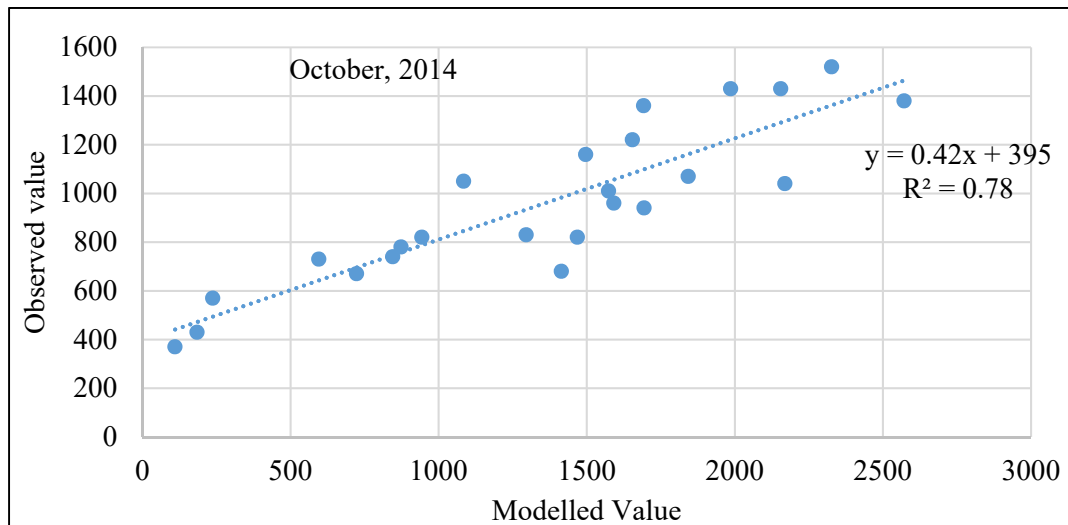


Figure 3: Modelled vs. Observed Values for October

CONCLUSIONS

Some of the conclusions from the study are listed:

1. Emission inventory shows there is maximum contribution from vehicles, largely two wheelers
 - Out of 84% contribution from vehicles, 87% is from 2 wheelers
 - Second largest contribution is from domestic sources, such as restaurants or eateries
2. Emission is found to be the largest in the centre of the city, which is the hub of all activities

3. MSW burning is also a significant source of emission (about 7%), which is preventable if burning is stopped or regulated
4. The model has performed well and can be interpreted to estimate contribution largely from outside
 - The month of November typically shows massive biomass burning in Punjab, Haryana, Uttar Pradesh and total IGP
 - Significant contribution of CO from outside city clearly seen from modelling results

REFERENCES

Kampa, M., & Castanas, E. (2008). Human health effects of air pollution. *Environmental Pollution*, 151(2), 362–367.

Seinfeld JH; Pandis SN. (2012). *Atmospheric chemistry and physics: from air pollution to climate change*(2012th ed.). John Wiley & Sons, Hoboken.

Zhong, Q., Huang, Y., Shen, H., Chen, Y., Chen, H., Huang, T., ... Tao, S. (2017). Global estimates of carbon monoxide emissions from 1960 to 2013. *Environmental Science and Pollution Research*, 24(1), 864–873.

AEROSOL INDIRECT RADIATIVE FORCING ON MARINE CLOUDS OVER INDIAN OCEAN

SOFIYA RAO & SAGNIK DEY

Centre for Atmospheric Sciences, Indian Institute of Technology Delhi, New Delhi – 110016, India.

KEYWORDS: Aerosol-cloud interaction, aerosol indirect effect, radiative forcing.

INTRODUCTION

Aerosol-cloud interaction is one of the least understood and largest sources of uncertainty in quantifying climate forcing (Boucher et al., 2013). Marine clouds are susceptible to aerosol-cloud interaction. However, most of the previous studies on aerosol-cloud interaction over the Indian Ocean (including INDOEX, CAIPEEX campaign etc.) are limited to either one particular season or short period. Here we examine aerosol impacts on marine cloud microphysics by analyzing multi-sensor data for 15 years (2000-2015) period. Influence of aerosols on liquid water path (LWP) – cloud effective radius (R_{eff}) relation is quantified. Cloud albedo (R_c) dependency on LWP and R_{eff} is examined in view of changing aerosol load. Further, the possible impacts of absorbing aerosols on marine cloud microphysics are examined. The results provide robust observational evidence of aerosol-cloud interaction in the Indian Ocean region that can be helpful in evaluating the climate model performance in representing such complex interaction.

METHODS

For this study cloud and aerosol parameters are obtained from Moderate Resolution Imaging Spectroradiometer (MODIS) and Modern-Era Retrospective analysis for Research and Applications Version 2 (MERRA-2) reanalysis products are analysed for fifteen years (Mar 2000 – Feb 2015). MODIS instrument is onboard NASA's Terra and Aqua platform and its cloud (Platnick *et al.*, 2006) and aerosol products (Remer *et al.*, 2008) are well validated and used globally. In this study, the MODIS daily level 3 at a spatial resolution of $1^\circ \times 1^\circ$ data are analyzed. We quantify each of these terms using the MODIS data over the Arabian Sea (AS), Bay of Bengal (BOB) and South Indian Ocean (SIO) for all the four seasons, the Postmonsoon and winter (when pollution is transported from the land to ocean), pre monsoon (when majorly dust particles are spread over Ocean specially over the Arabian Sea, monsoon (least anthropogenic aerosol over the ocean) seasons.

R_{eff} variation with LWP is examined for three aerosol regimes – 'clean' ($\tau < 0.1$, $0.1 < \tau < 0.2$), 'moderately polluted' ($0.2 < \tau < 0.4$), and 'highly polluted' ($\tau > 0.4$). The same dependency is examined in view of changing absorbing aerosol index derived from OMI ($AI < 1$, $1 < AI < 3$, $AI > 3$). Further, a framework is developed which relies on the observationally constrained estimate of aerosol-induced change in cloud albedo.

RESULTS & DISCUSSIONS

Cloud drop growth is facilitated in presence of high moisture content. This is evident from the fact that R_{eff} is found to broadly increase with an increase in LWP in all the seasons. It is also noted that R_{eff} is larger across a wide range of LWP in 'clean' condition ($\tau < 0.2$) and it decreases in the 'moderately polluted' condition ($0.2 < \tau < 0.4$) and decreases further in the 'highly polluted' condition and ($\tau > 0.4$). This clearly indicates that in more polluted conditions, growth of cloud drops is restricted. This is the evidence of classic aerosol indirect effect. However, we also note that the changes in R_{eff} across the three aerosol regimes are not uniform across LWP . In fact, in the low and very high LWP , the changes are not uniform. This suggests that the aerosol signal is more prominent in the mid-range of LWP . Another important observation is that the range of variation of R_{eff} across a widely ranging LWP is lower in the winter season relative to the other

seasons. This is because of the larger role of aerosols in modulating cloud microphysics than meteorology while during monsoon seasons more meteorological forcing is observed over the Indian ocean.

Further, we portioned the change in cloud albedo (R_c) into change in LWP and R_{eff} in response to an Aerosol Optical depth (τ). Cloud albedo response to an increase in τ is more sensitive in the range of LWP between 120-300 gm/m² for a range of R_{eff} varying from 8-28 μ m. Using this framework, the separation between the microphysical and macrophysical anthropogenic aerosol indirect radiative forcing is calculated using anthropogenic aerosol optical depth (τ_{an}) type. The aerosol indirect radiative forcing over the Arabian sea is in the range of -8 ± 5 w/m² for all the seasons. While the forcing values are comparatively low over BOB and SIO from AS.

CONCLUSIONS

Aerosols are playing very important role in changing cloud parameters. In clear condition R_{eff} is positively correlated with LWP for all the seasons. Rate of increase in R_{eff} wrt LWP in polluted condition is the clear hint of semi direct effect discovered first over this region during the INDOEX in the winter season. Our analysis demonstrates its evidence throughout the year.. Cloud drop growth is facilitated in presence of high moisture condition. Change in cloud albedo in response to aerosols is most sensitive in the LWP range 60-300 gm/m² throughout the year, while the sensitivity reduces at higher R_{eff} values. A theoretical framework is proposed to estimate aerosol indirect radiative forcing using observations. The analysis shows best outputs over the Arabian Sea in comparison with Bay of Bengal and the South Indian Ocean.

ACKNOWLEDGEMENT

The MODIS data sets used in this study were acquired as part of NASA's Earth Science Enterprise. The authors would like to thank the data distribution centers for their support. I also thank IIT Delhi for providing financial support to do this research.

REFERENCES

Boucher et al., Clouds and Aerosols. In: Climate Change 2013: The Physical Science Basis. Contribution of Working Group I to the Fifth Assessment Report of the Intergovernmental Panel on Climate Change (IPCC 5) Cambridge University Press, Cambridge, United Kingdom and New York, NY, USA.

Ramanathan, V. et al. (2001), The Indian Ocean Experiment: An integrated assessment of the climate forcing and effects of the Great Indo-Asian haze, *J. Geophys. Res.*, 106, 28371- 28399.

Platnick, S., M. King, S. Ackerman, et al. 2003. "The MODIS cloud products: Algorithms and examples from Terra." *IEEE Trans Geosci Remote Sens* 41 (2): 459-473

Remer.L., et al., 2008: *An emerging aerosol climatology from the MODIS satellite sensors*, *Journal of Geophysical Research*, 113, D14SO1, doi:10.1029/2007JD009661.

This page is intentionally left blank